Methods in Molecular Biology 1170

Springer Protocols

Eishi Noguchi
Mariana C. Gadaleta *Editors*

Cell Cycle Control

Mechanisms and Protocols

Second Edition

Humana Press

METHODS IN MOLECULAR BIOLOGY

Series Editor
John M. Walker
School of Life Sciences
University of Hertfordshire
Hatfield, Hertfordshire, AL10 9AB, UK

For further volumes:
http://www.springer.com/series/7651

Cell Cycle Control

Mechanisms and Protocols

Second Edition

Edited by

Eishi Noguchi and Mariana C. Gadaleta

Department of Biochemistry and Molecular Biology, Drexel University College of Medicine, Philadelphia, PA, USA

Humana Press

Editors
Eishi Noguchi
Department of Biochemistry
and Molecular Biology
Drexel University College of Medicine
Philadelphia, PA, USA

Mariana C. Gadaleta
Department of Biochemistry
and Molecular Biology
Drexel University College of Medicine
Philadelphia, PA, USA

ISSN 1064-3745 ISSN 1940-6029 (electronic)
ISBN 978-1-4939-0887-5 ISBN 978-1-4939-0888-2 (eBook)
DOI 10.1007/978-1-4939-0888-2
Springer New York Heidelberg Dordrecht London

Library of Congress Control Number: 2014938993

Printed on acid-free paper

Humana Press is a brand of Springer
Springer is part of Springer Science+Business Media (www.springer.com)

Preface

Modern cell cycle research began by elucidating the functions of cyclin-dependent kinases (CDKs). Subsequent investigations have revealed that the cell cycle is coordinated through a complex network of various cellular processes. Defects in this control system can lead to genetic instability and drive an array of genetic disorders, most notably, cancer. It is thus essential to holistically understand how the cell cycle is governed and how this regulation affects other cellular processes and homeostasis. It is noteworthy that much of what is known about cell cycle regulation depends heavily on enormous research efforts using a variety of model organisms, from yeast to mammals. The basic knowledge and techniques used in these model systems have been well documented in the previous cell cycle protocol book. In this new volume, *Cell Cycle Control: Mechanisms and Protocols, Second Edition*, which consists of a completely new set of reviews and protocols, we provide a comprehensive guide to technical and theoretical advancements in the field. Beginning with the overviews of various cell cycle regulations, we present the most current protocols and state-of-the-art techniques used to generate latest findings in cell cycle regulation. We believe that this title will be a valuable resource for a wide audience, ranging from the experienced cell cycle researchers looking for new approaches to the junior graduate students giving their first steps in cell cycle research.

Philadelphia, PA, USA

Eishi Noguchi
Mariana C. Gadaleta

Contents

Contributors

Vincent Archambault • *Department of Biochemistry, Institut de recherche en immunologie et en cancérologie, Université de Montréal, Montréal, QC, Canada*

Edgar Asiimwe • *Department of Pharmacology and Physiology, Drexel University College of Medicine, Philadelphia, PA, USA*

Jane Azizkhan-Clifford • *Department of Biochemistry and Molecular Biology, Drexel University College of Medicine, Philadelphia, PA, USA*

Sumedha Bagga • *Department of Biochemistry and Molecular Biology, Drexel University College of Medicine, Philadelphia, PA, USA*

Kevin J. Barnum • *Department of Oncological Sciences, Icahn School of Medicine at Mount Sinai, New York, NY, USA; Graduate School of Biological Sciences, Icahn School of Medicine at Mount Sinai, New York, NY, USA*

Kate Beishline • *Department of Biochemistry and Molecular Biology, Drexel University College of Medicine, Philadelphia, PA, USA*

Karen M. Berkowitz • *Department of Biochemistry and Molecular Biology, Drexel University College of Medicine, Philadelphia, PA, USA; Department of Obstetrics and Gynecology, Drexel University College of Medicine, Philadelphia, PA, USA*

James R. Birkenstamm • *Department of Pharmacology and Physiology, Drexel University College of Medicine, Philadelphia, PA, USA*

Alessandro Bitto • *Department of Pathology, University of Washington, Seattle, WA, USA*

Michael J. Bouchard • *Department of Biochemistry and Molecular Biology, Drexel University College of Medicine, Philadelphia, PA, USA*

Sara L. Bristow • *Department of Biology, Duke University, Durham, NC, USA; Duke Center for Systems Biology, Duke University, Durham, NC, USA*

Amanda S. Brooker • *Department of Biochemistry and Molecular Biology, Drexel University College of Medicine, Philadelphia, PA, USA*

Robertus A.M. de Bruin • *MRC Laboratory for Molecular Cell Biology, University College London, London, UK*

Minh Bui • *Chromatin Structure and Epigenetic Mechanisms Unit, Laboratory of Receptor Biology and Gene Expression, Center for Cancer Research, National Cancer Institute, NIH, Bethesda, MD, USA*

Paul M. Campbell • *Department of Pharmacology and Physiology, Drexel University College of Medicine, Philadelphia, PA, USA*

Matthew J. Cecchini • *London Regional Cancer Program, London, ON, Canada; Department of Biochemistry, Western University, London, ON, Canada*

Ya-Ting Chang • *Department of Biochemistry and Molecular Genetics, College of Medicine, University of Illinois at Chicago, Chicago, IL, USA*

Bruna Corominas-Faja • *Metabolism and Cancer Group, Translational Research Laboratory, Catalan Institute of Oncology (ICO), Girona, Catalonia, Spain*

Elizabeth P. Crowe • *Department of Pathology, Drexel University College of Medicine, Philadelphia, PA, USA*

Elisabet Cuyàs • *Metabolism and Cancer Group, Translational Research Laboratory, Catalan Institute of Oncology (ICO), Girona, Catalonia, Spain*
Pier Paolo D'Avino • *Department of Pathology, University of Cambridge, Cambridge, UK*
Yamini Dalal • *Chromatin Structure and Epigenetic Mechanisms Unit, Laboratory of Receptor Biology and Gene Expression, Center for Cancer Research, National Cancer Institute, NIH, Bethesda, MD, USA*
John R. Daum • *Cell Cycle and Cancer Biology Research Program, Oklahoma Medical Research Foundation, Oklahoma City, OK, USA*
Frederick A. Dick • *London Regional Cancer Program, London, ON, Canada; Children's Health Research Institute, Western University, London, ON, Canada; Department of Biochemistry, Western University, London, ON, Canada*
Nikola S. Dzhindzhev • *Department of Genetics, University of Cambridge, Cambridge, UK*
Sarah Farmer • *MRC Laboratory for Molecular Cell Biology, University College London, London, UK*
Katherine M. Feeney • *School of Cancer Sciences, University of Birmingham, Edgbaston, Birmingham, UK*
Wenyi Feng • *Department of Biochemistry and Molecular Biology, SUNY Upstate Medical University, Syracuse, NY, USA*
David M. Glover • *Department of Genetics, University of Cambridge, Cambridge, UK*
Gary J. Gorbsky • *Cell Cycle and Cancer Biology Research Program, Oklahoma Medical Research Foundation, Oklahoma City, OK, USA*
Rhys Grant • *Department of Genetics, University of Cambridge, Cambridge, UK*
Steven B. Haase • *Department of Biology, Duke University, Durham, NC, USA; Duke Center for Systems Biology, Duke University, Durham, NC, USA*
Akiyo Hayashi • *Graduate School of Life Science, University of Hyogo, Hyogo, Japan*
Nicole Hustedt • *Friedrich Miescher Institute for Biomedical Research, Basel, Switzerland*
Jorge Joven • *Unitat de Recerca Biomèdica (URB-CRB), Institut d'Investigació Sanitaria Pere i Virgili (IISPV), Universitat Rovira i Virgili, Reus, Catalonia, Spain*
Dong-Hwan Kim • *Department of Genetics, Cell Biology and Development, University of Minnesota, Minneapolis, MN, USA*
Su Yeon Kim • *Department of Pharmacology and Physiology, Drexel University College of Medicine, Philadelphia, PA, USA*
Steffi Klier • *MRC Laboratory for Molecular Cell Biology, University College London, London, UK*
Deanna M. Koepp • *Department of Genetics, Cell Biology and Development, University of Minnesota, Minneapolis, MN, USA*
Andres Kriete • *School of Biomedical Engineering, Science and Health Systems, Bossone Research Center, Drexel University, Philadelphia, PA, USA*
Adam R. Leman • *Department of Biology, Duke University, Durham, NC, USA; Duke Center for Systems Biology, Duke University, Durham, NC, USA*
Chad Lerner • *Department of Environmental Medicine, Lung Biology, and Disease Program, Pulmonary and Critical Care Division, University of Rochester Medical Center, Rochester, NY, USA*
Catherine Lindon • *Department of Genetics, University of Cambridge, Cambridge, UK*
Zoltan Lipinszki • *Department of Genetics, University of Cambridge, Cambridge, UK*

Takeshi Maeda • *Graduate School of Life Science, University of Hyogo, Hyogo, Japan*
Marcos Malumbres • *Spanish National Cancer Research Centre (CNIO), Madrid, Spain*
Hisao Masai • *Department of Genome Medicine, Tokyo Metropolitan Institute of Medical Science, Tokyo, Japan*
Laura McFarlane-Majeed • *School of Cancer Sciences, University of Birmingham, Edgbaston, Birmingham, UK*
Javier A. Menendez • *Metabolism and Cancer Group, Translational Research Laboratory, Catalan Institute of Oncology (ICO), Girona, Catalonia, Spain*
Masayuki Morino • *Graduate School of Life Science, University of Hyogo, Hyogo, Japan*
Bettina A. Moser • *Department of Biochemistry and Molecular Genetics, College of Medicine, University of Illinois at Chicago, Chicago, IL, USA*
Yusuke Murakami • *Graduate School of Life Science, University of Hyogo, Hyogo, Japan*
Timothy Nacarelli • *Department of Pathology, Drexel University College of Medicine, Philadelphia, PA, USA*
Toru M. Nakamura • *Department of Biochemistry and Molecular Genetics, College of Medicine, University of Illinois at Chicago, Chicago, IL, USA*
Hideo Nishitani • *Graduate School of Life Science, University of Hyogo, Hyogo, Japan*
Eishi Noguchi • *Department of Biochemistry and Molecular Biology, Drexel University College of Medicine, Philadelphia, PA, USA*
Matthew J. O'Connell • *Graduate School of Biological Sciences, Icahn School of Medicine at Mount Sinai, New York, NY, USA; Department of Oncological Sciences, Icahn School of Medicine at Mount Sinai, New York, NY, USA*
Joanna L. Parish • *School of Cancer Sciences, University of Birmingham, Edgbaston, Birmingham, UK*
Jie Peng • *Department of Biochemistry and Molecular Biology, SUNY Upstate Medical University, Syracuse, NY, USA*
Marcin R. Przewloka • *Department of Genetics, University of Cambridge, Cambridge, UK*
Delphine Quénet • *Chromatin Structure and Epigenetic Mechanisms Unit, Laboratory of Receptor Biology and Gene Expression, Center for Cancer Research, National Cancer Institute, NIH, Bethesda, MD, USA*
M.K. Raghuraman • *Department of Genome Sciences, University of Washington, Seattle, WA, USA*
Miguel A. Rodríguez-Gabriel • *Universidad Autónoma de Madrid-Consejo Superior de Investigaciones Científicas (UAM-CSIC), Cantoblanco, Madrid, Spain*
Christian Sell • *Department of Pathology, Drexel University College of Medicine, Philadelphia, PA, USA*
Kenji Shimada • *Friedrich Miescher Institute for Biomedical Research, Basel, Switzerland*
Yasushi Shiomi • *Graduate School of Life Science, University of Hyogo, Hyogo, Japan*
Sushama Sivakumar • *Cell Cycle and Cancer Biology Research Program, Oklahoma Medical Research Foundation, Oklahoma City, OK, USA*
Matthew C. Stout • *Department of Pharmacology and Physiology, Drexel University College of Medicine, Philadelphia, PA, USA*
Naohiro Suenaga • *Graduate School of Life Science, University of Hyogo, Hyogo, Japan*
Miyuki Tanaka • *Graduate School of Life Science, University of Hyogo, Hyogo, Japan*
Michael J. Thwaites • *London Regional Cancer Program, London, ON, Canada; Department of BiochemistryWestern University, London, ON, Canada*

Claudio Torres • *Department of Pathology, Drexel University College of Medicine, Philadelphia, PA, USA*
Marcin P. Walkiewicz • *Chromatin Structure and Epigenetic Mechanisms Unit, Laboratory of Receptor Biology and Gene Expression, Center for Cancer Research, National Cancer Institute, NIH, Bethesda, MD, USA*
Bin Wang • *Department of Genetics, The University of Texas M.D. Anderson Cancer Center, Houston, TX, USA*
Peng Wang • *Department of Biochemistry, Institut de recherche en immunologie et en cancérologie, Université de Montréal, Montréal, QC, Canada*
Naoko Yoshizawa-Sugata • *Department of Genome Medicine, Tokyo Metropolitan Institute of Medical Science, Tokyo, Japan*

Part I

Reviews: Cell Cycle Regulations

Chapter 1

Cell Cycle-Regulated Transcription: Effectively Using a Genomics Toolbox

Sara L. Bristow, Adam R. Leman, and Steven B. Haase

Abstract

The cell cycle comprises a series of temporally ordered events that occur sequentially, including DNA replication, centrosome duplication, mitosis, and cytokinesis. What are the regulatory mechanisms that ensure proper timing and coordination of events during the cell cycle? Biochemical and genetic screens have identified a number of cell-cycle regulators, and it was recognized early on that many of the genes encoding cell-cycle regulators, including cyclins, were transcribed only in distinct phases of the cell cycle. Thus, "just in time" expression is likely an important part of the mechanism that maintains the proper temporal order of cell cycle events. New high-throughput technologies for measuring transcript levels have revealed that a large percentage of the *Saccharomyces cerevisiae* transcriptome (~20 %) is cell cycle regulated. Similarly, a substantial fraction of the mammalian transcriptome is cell cycle-regulated. Over the past 25 years, many studies have been undertaken to determine how gene expression is regulated during the cell cycle. In this review, we discuss contemporary models for the control of cell cycle-regulated transcription, and how this transcription program is coordinated with other cell cycle events in *S. cerevisiae*. In addition, we address the genomic approaches and analytical methods that enabled contemporary models of cell cycle transcription. Finally, we address current and future technologies that will aid in further understanding the role of periodic transcription during cell cycle progression.

Key words *Saccharomyces cerevisiae*, Cell cycle, Periodic transcription, Transcription factor network, Cyclins, Cyclin-dependent kinases (CDKs)

1 Introduction

Successful cell division requires complete duplication of genetic material followed by equal segregation into two cell bodies, resulting in two identical daughter cells. Historically, the cell cycle has been divided into four phases—Gap 1 (G1), Synthesis (S), Gap 2 (G2), and Mitosis (M)—that describe the chronological order of different events observed in normally cycling cells. The bulk of duplication and segregation events occur in S and M phases. During S phase, both DNA and centrosomes are duplicated (Fig. 1). Duplicated centrosomes separate in order to form the poles of the mitotic spindle responsible for segregating sister

Eishi Noguchi and Mariana C. Gadaleta (eds.), *Cell Cycle Control: Mechanisms and Protocols*, Methods in Molecular Biology, vol. 1170, DOI 10.1007/978-1-4939-0888-2_1,

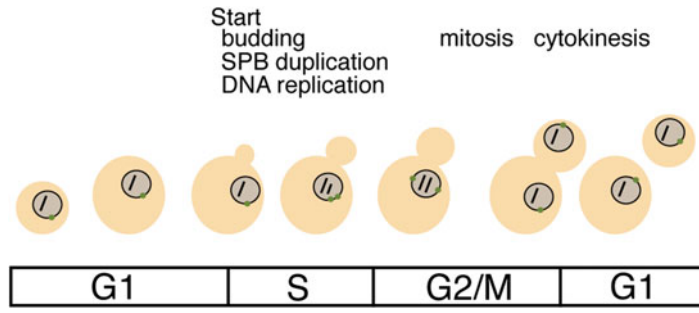

Fig. 1 Cell-cycle progression in *Saccharomyces cerevisiae*. Budding yeast serves as an excellent model system to study the cell cycle. Timing and regulation of events are conserved across species. More importantly, the phase of the cell cycle can be deduced by observing the state and size of the bud, the future daughter cell

chromatids (Fig. 1). Sister chromatid segregation is initiated during M phase, or mitosis (Fig. 1).

G1 and G2 were termed "gap" phases, as they separate the visibly observable events of S and M phase. Although no overt cellular changes or events are observed during G1 and G2, cells are interpreting signals from their extracellular and intracellular environments to ensure that conditions are appropriate for cellular division events. In early G1, cells interpret extracellular signals (e.g., nutrient abundance, mating pheromone) to decide whether to commit to a new cell cycle. Following this point of commitment (called START in *Saccharomyces cerevisiae*), cells prepare for entry into S phase by activating the expression of genes required for duplicating DNA and centrosomes (Fig. 1). In G2, cells interpret intracellular signals from checkpoint pathways that monitor whether duplication events have been completed with fidelity, and whether the mitotic spindle apparatus is functional.

Each cell cycle event—such as DNA replication, centrosome duplication, and chromosome segregation—is a complex process that requires the coordination of many different proteins acting together to complete the task at hand. In turn, each of these complex events must be coordinately controlled with the other events. What, then, are the mechanisms that orchestrate the complex set of events required for cellular division? Over the past three decades, an overwhelming number of studies have identified and characterized two proteins that act in a complex to trigger cell cycle events: cyclins and cyclin-dependent kinases (CDKs). Both biochemical and genetic approaches have shown that, throughout the cell cycle, CDKs are activated by different cyclins, whose role is to activate and inhibit different events at the proper time and in the proper order (reviewed in [1–3]). More recently, it has been shown that up to a fifth of the *S. cerevisiae* genome, including cyclins themselves,

is transcribed once per cell cycle [4–7]. This set of genes is often referred to as the cell cycle-regulated transcriptional program. The precise nature of this temporal transcriptional program may serve as another mechanism to ensure proper timing and ordering of cell cycle events.

Historical models of cell-cycle regulation have proposed that cyclin/CDK activity directs transcription factors to initiate gene expression at the proper time [8] (reviewed in [9–11]). However, recent studies have shown that cell cycle-regulated transcription has the capacity to occur largely in the absence of CDKs [5, 12]. These findings suggest that some other regulatory mechanism is responsible for controlling periodic transcription and coordinating cell cycle events. To better understand and characterize this control module, single gene studies have given way to genome-wide experimental approaches that measure global gene expression dynamics [4–7]. These studies require unbiased quantitative analyses tailored both to the experimental method and to the overarching biological question. Here, we will discuss both current and future experimental and analytical methods used to address the seemingly simple questions: What portion of the genome is cell cycle-regulated? And how is this transcription program coordinated with other cell cycle events?

2 Cell Cycle-Regulated Transcription

2.1 Identifying Periodic Transcripts

With the advent of modern molecular biology, measuring mRNA levels in cells became a regular test to address whether genes are regulated at the transcriptional level. For genes involved in the cell cycle, understanding gene regulation at the transcriptional level requires measuring mRNA abundance over time in synchronous populations of cells as they progress through the cell cycle. Histones were the first genes identified whose expression oscillates periodically during the cell cycle [13]. Classifying histone gene expression as cell cycle-regulated was done by correlating the timing of histone mRNA expression with the timing of DNA replication over the course of several cell cycles [13]. Over the following decade, ten more genes involved in cell cycle events were also identified as being expressed in a periodic manner—*HO* [14], *CDC21* [15], *CDC9* [16], *RAD6* [17], *SWI5* [18], *CDC8* [19], *POL1* [20], *DBF4* [21], *PRI1* [22], and *DBF2* [23]. For each of these genes, the definition of periodic is anchored to the correlation of gene expression with an observable cell cycle event that is known to occur only once per cycle. The periodic expression of these genes was discovered while investigating the function of each gene during cell cycle events. Is periodic expression of cell cycle genes a global phenomenon or specific to just a small set of genes? In total, approximately 100 periodically expressed budding yeast genes were identified one

at a time using northern blots. However, a technology that is able to measure transcript dynamics at a genome-wide level was necessary not only to quantify the proportion of genes that is periodically transcribed but also to understand how cell cycle-regulated transcription is coordinated with cell cycle progression.

The microarray is one method developed to measure mRNA levels of many genes in an organism [24]. Several genome-wide studies utilizing microarrays have been reported that focus on identifying periodic genes with respect to the cell cycle in synchronized populations of budding yeast cells. Cho and colleagues identified 416 genes as being cell cycle-regulated at the transcriptional level by visual inspection of transcript dynamics [4]. Spellman and colleagues identified 800 genes that demonstrate oscillations in transcript levels during the cell cycle using quantitative methods including a Fourier transform and Pearson correlation [7]. Pramila and colleagues found 991 cell cycle-regulated transcripts using a permutation-based method developed by de Lichtenberg and colleagues [6, 25]. Orlando and colleagues identified 1,275 periodically expressed genes also using a permutation-based method [5, 25]. Overall, between the three studies using quantitative methods to identify periodic genes, 440 cell cycle-regulated genes are shared [5–7].

Although each study identifies slightly different sets of periodic genes, it is clear that many more genes are regulated at the transcriptional level during the cell cycle than previously thought. Differences between periodic gene lists from each study result from a combination of experimental design and quantitative analysis. Further discussion of these differences is addressed in a later section.

Is the phenomenon of cell cycle-regulated transcription specific only to budding yeast? Additional studies in fission yeast and human cells have measured gene expression dynamics in synchronized cells to determine the scope of periodic transcription in these organisms. In fission yeast, three genome-wide studies identified a limited number of periodic genes [26–28]. Unlike budding yeast, fewer genes were classified as cell cycle-regulated; less than 800 genes were identified by each study. Similar to budding yeast, the consensus between studies is very low, with only 171 genes shared between all analyses [26–28]. Two studies in human cell lines have classified fewer than 1,000 periodic genes [29, 30]. The low numbers of periodic genes may be due to the larger genome size, undetected alternative splicing of introns, or the difficulty involved in synchronizing fission yeast or human cell lines. While budding yeast has the largest number of identified periodic genes, cell cycle-regulated transcription is also clearly observed in fission yeast and human cell lines, suggesting that this phenomenon is conserved between organisms. Moreover, the transcriptional regulation of some orthologs in the evolutionarily diverged yeast species *S. cerevisiae* and *S. pombe* have been shown to be conserved [31]. With improved experimental approaches and mRNA measuring technology, the

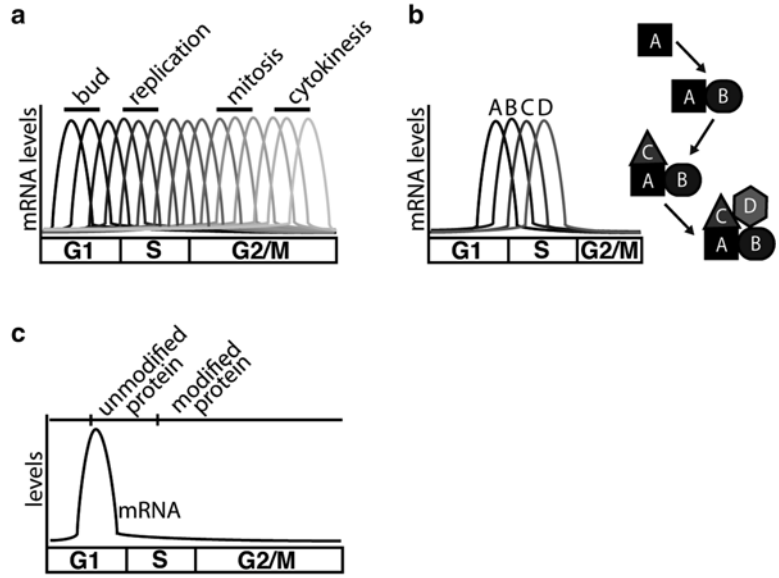

Fig. 2 Significance of the periodic transcription program. (**a**) Genes are expressed only during the cell-cycle phase needed. Genes required for DNA replication are expressed during S phase. (**b**) The temporal order of gene expression may aid in the construction of a protein complex only needed once per cycle. (**c**) While protein levels of cell-cycle regulators may remain constant, posttranslational modifications may alter the activity of the proteins

characterization of periodic gene expression will become more tractable in other model systems.

Two questions arise from the finding that the transcriptional program is conserved across eukaryotes: (1) what is the significance of cell cycle-regulated transcription and (2) what mechanisms coordinate this large transcriptional program with cell cycle progression?

2.2 Significance of Cell Cycle-Regulated Transcription

Many hypotheses have been posed to explain the importance of cell cycle-regulated transcription. The explanations can be generalized into three categories. While all are plausible reasons for regulating gene expression timing during the cell cycle, it is not currently possible to discriminate between the multiple hypotheses. Moreover, each potential hypothesis is not mutually exclusive and may be true for only a subset of cell cycle-regulated genes.

The first category postulates that cell cycle-regulated transcription is a mechanism to expend energy resources efficiently, as transcription and translation are energetically expensive. This concept is often referred to as "just in time" transcription, in which gene products that function at a specific cell cycle interval are expressed only when needed (Fig. 2a) (reviewed in [10, 32, 33]). A variation on this first explanation has been referred to as the "Sleeping Beauty" situation, which takes into account the full lifetime of a

cell or tissue, rather than the completion of a single cell cycle ([7], reviewed in [9]). Whether it is a single budding yeast or a population of cells that form tissues in an organism, active cellular division occurs during only a portion of a cell's overall life cycle. Microorganisms are subject to environmental constraints and will divide when conditions (nutrients, temperature, growth factor signaling, etc.) permit, but not when the local environment is not amenable to cell division. Therefore, much of the life of a single cell is spent outside the cell cycle, in a state of rest or quiescence. However, once a signal is received to initiate cellular division, the cells are poised to complete cell cycle events with the proper genes expressed at the correct time.

A second proposal for the importance of cell cycle-regulated transcription centers on building a required structure only once per cell cycle (Fig. 2b) (reviewed in [32, 33]). For example, proteins required for DNA replication are loaded onto DNA in different stages. The components of the replication complex are periodically transcribed themselves, lending to the temporal events that are required for DNA replication. A pre-initiation complex first binds to DNA replication origins and is only activated when elements are phosphorylated by S-phase cyclin/CDK. Other components required for replication are then synthesized, recruited to origins, and replicate DNA (reviewed in [34]). Further, mitotic cyclin/CDK activity inhibits the reformation of pre-initiation complexes until the following cell cycle [35]. This mechanism ensures that the complex required to trigger DNA replication is only built once and thus acts as a layer of control to prevent re-replication.

A third category of hypotheses centers on renewing pools of unmodified protein. Gene products that are posttranslationally modified may no longer be active or be responsive to additional signaling. Therefore, periodic transcription provides a pool of unmodified product that is able to carry out cell cycle events (Fig. 2c) (reviewed in [9]). For example, Swi6, a component of transcription factor complexes SBF and MBF, is phosphorylated in S phase after START to localize it to the cytoplasm [36]. Periodic transcription of *SWI6* may provide a new pool of the Swi6 protein to induce transcription at START.

Despite varying hypotheses on the physiological importance of the cell cycle-regulated transcriptional program, the underlying requirement for proper expression timing during the cell cycle has led to the development of a sophisticated program for cell cycle transcription control. Additionally, transcriptional regulation of these genes may represent only a single layer of control; post-translational modifications such as cyclin/CDK phosphorylation have also been shown to play a critical role in proper coordination of cell cycle events. Understanding how periodic transcription is

Table 1
Transcription factors that are known to play a role in activating or repressing periodic transcription during the cell cycle

TF	Phase	Function	Representative target	CDK target?	CDK regulation
SBF	G1/S	Activator	*CLN1*	Yes [52]	Inhibitory
MBF	G1/S	Activator	*POL1*	Yes [98]	Unknown
Yhp1	G1/S	Repressor	*CLN3*	No	N/A
Yox1	G1/S	Repressor	*SWI4*	No	N/A
Nrm1	G1/S	Co-repressor	N/A	Yes [99]	Unknown
Hcm1	S	Activator	*NDD1*	No	N/A
SFF	G2/M	Activator	*CLB2*	Yes [61, 63]	Activating
Ace2	M/G1	Activator	*NIS1*	Yes [64]	Inhibitory
Swi5	M/G1	Activator	*SIC1*	Yes [65]	Inhibitory

regulated and is coordinated with other cell cycle events may lead to insight into the importance of such a substantial periodic transcriptional program.

2.3 What Are the Regulators of Periodic Transcription?

How does the cell generate a large and continuous program of temporally ordered gene transcription throughout the cell cycle? In order to understand how this is done, we need to understand the transcriptional regulators. As more and more transcripts were identified as periodic during the cell cycle, focus turned to the regulators that activated or inhibited transcription—transcription factors (TFs). To identify the regulators that control activation or repression of periodic transcription in budding yeast, researchers utilized genetic tools, promoter sequence information, and physical localization studies [37–39]. Not surprisingly, a number of TFs were found to regulate distinct subsets of periodic genes throughout the cell cycle (reviewed in [9–11, 33]). A list of known TFs involved in cell cycle-regulated transcription and relevant information on their activation timing and regulation by cyclin/CDKs is shown in Table 1.

The TFs identified possess three striking qualities that suggest potential modes of regulation for the periodic transcription program. First, many of the TFs that play a role in controlling cell cycle-regulated transcription are themselves periodically transcribed (reviewed in [11]). For TFs that act in complexes, at least one TF is periodically expressed. This observation suggests that a portion of genes may be cell cycle-regulated due to the periodic expression of their regulators. Second, cyclin/CDK activity has been found to affect the activity of many of these transcription factors.

In these cases, cyclins that are expressed during any of these phases have the capacity to affect TF activity (Table 1). Additionally, this regulation can be either activating or inhibitory depending on the TF (Table 1). These findings, coupled with cyclin deletion experiments, imply that cell cycle-regulated gene expression is also modulated by cyclin/CDK activity [40–42]. Finally, genome-wide binding data have shown that these TFs also bind to the promoters of other TFs shown to regulate periodic gene expression [8, 43, 44]. In fact, TFs expressed late in the cell cycle have been shown to bind to the promoters of TFs responsible for early periodic gene expression [45]. This finding demonstrates that the TFs controlling the last wave of periodic transcription may also activate the first TFs in the following cycle. Taken together with global views of transcript dynamics from microarray experiments [7], it was proposed that a TF network could account for the periodic nature of the TFs themselves and the entire periodic transcription program ([8, 44], reviewed in [9–11]). Models for how the TF network is integrated with cyclin/CDK activity and cell cycle events will be discussed below.

Several versions of TF networks that control cell cycle-regulated transcription have been proposed [5, 6, 8, 12, 44]. Understanding which TFs are included in the network is an important outstanding question. For the purposes of this review, we will focus on how a transcriptional signal is transmitted through a version of the transcription network (Fig. 3).

Concurrent with passage through START and the commitment to the cell cycle, the heterodimeric TFs SBF and MBF activate a large program of periodic genes involved in budding, centrosome duplication, and DNA replication. SBF and MBF share a trans-activating subunit, Swi6 [46], and each have a distinct DNA-binding subunit, Swi4 and Mbp1, respectively [47, 48]. Activation of SBF and MBF centers on feedback loops that include G1 cyclin/CDKs and the transcriptional co-repressor Whi5 [40, 41, 49, 50] (Fig. 3). Activation begins when Cln3/Cdk1 phosphorylates Whi5, triggering its dissociation from SBF complexes and the activation of transcription of SBF targets. Two of these targets are the genes encoding the G1-cyclins; Cln1 and Cln2. Cln1/Cdk1 and Cln2/Cdk1 kinase complexes also phosphorylate Whi5, triggering further dissociation from SBF complexes and export from the nucleus. Following activation, a series of transcriptional repressors and B-type cyclins inactivate SBF and MBF in a series of negative feedback loops. SBF activates the *YOX1* and *YHP1* genes, and in turn, their gene products repress the transcription of the gene encoding the SBF component, Swi4 [51]. Moreover, SBF transcriptional activity is repressed by Clb2 [52], after a cascade of transcriptional activation that triggered the expression of the *CLB2* gene (Fig. 3). The transcriptional activity of MBF is modulated by its direct target and co-repressor *NRM1* [53] (Fig. 3). Thus, positive feedback loops contribute to the full activation of SBF and MBF, while negative feedback loops serve as the "OFF switch" for their activity.

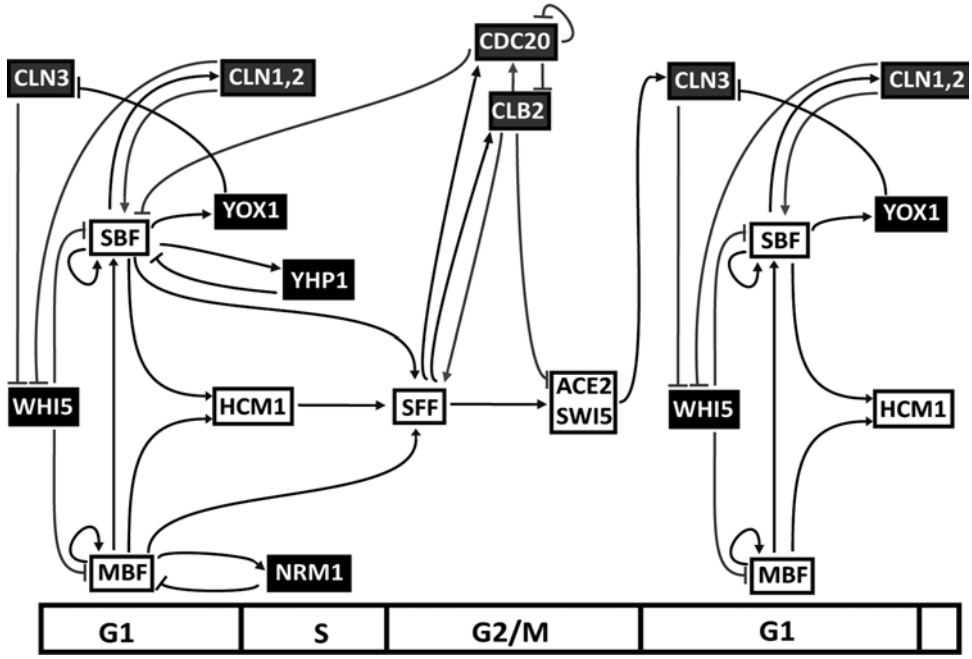

Fig. 3 Cell-cycle transcription network. An interconnected network of transcription factors that demonstrate how a transcriptional signal could be passed through the cell cycle. Note that this is just one representation of a TF network. Based on significance cutoffs and TFs included, different networks may be constructed. *Boxes* are nodes. *Green*, transcriptional activators; *red*, transcriptional repressors; *blue*, posttranslational modifications. *Arrows* signify either an upstream promoter binding to the promoter of the downstream target (*black arrows*) or a posttranslational modification that affects the activity of the TF (*blue arrows*). Nodes are placed on a cell-cycle timeline based on time of peak expression in wild-type cells (Color figure online)

SBF and MBF transmit a transcriptional signal to activator Hcm1 [54] that is responsible for expression of genes required for chromosome segregation, centrosome dynamics, and budding during late S phase [6] (Fig. 3). *HCM1* is periodically transcribed, and its protein levels are also periodic, closely mirroring the behavior of *HCM1* mRNA [6]. Moreover, Hcm1 activates the synthesis of the SBF co-repressor *WHI5* and Swi-five factor (SFF) subunit *NDD1* [6] (Fig. 3). SFF, a TF complex composed of Fkh1, Fkh2, Ndd1, and Mcm1 [55–59], activates a set of periodic genes referred to as the "*CLB2* cluster" during G2/M phase ([7, 60], reviewed in [9–11]). SFF activity is modulated through a positive feedback loop with the B-type cyclin Clb2 [52]. SFF activates *CLB2* gene transcription [60], which in turn binds CDK and further stimulates components of SFF to increase its transcriptional activity [61–63] (Fig. 3). SFF transmits the periodic transcriptional signal by activating transcription of genes encoding TFs *ACE2* and *SWI5* [60] (Fig. 3). Ace2 and Swi5 share a number of targets (Ace2 also activates a number of unique targets only in daughter cells) and activate periodic transcripts involved in the transition between late M phase and the beginning of early G1 of the subsequent cell cycle.

While Ace2 and Swi5 are transcribed during G2/M, their activity is inhibited by Clb2/CDK-dependent cytoplasmic sequestration [64, 65]. Mitosis triggers the destruction of Clb2, and thus, Swi5 and Ace2 can return to the nucleus and bind to the promoters of their target genes. Swi5 and Ace2 bind to the promoter of *CLN3* to activate *CLN3* expression and thus begin a new cycle of transcription [45] (Fig. 3). Currently, these TFs, in addition to other TFs that potentially regulate periodic transcription, are being further studied to better understand the connections with each other and with cyclin/CDKs.

2.4 Roles of Cyclin/CDKs and a Transcription Factor Network in Controlling the Periodic Transcriptional Program

Although the periodic transcriptional program during the cell cycle could be explained by a network of sequentially activated transcription factors, cyclin/CDK regulation of network TF activities could be critical for the proper execution of the program.

A series of studies have been carried out to determine the relative contributions of cyclin/CDKs and the transcription factor network on periodic transcription during the cell cycle. The first study to address this question measured the effect of S phase and mitotic cyclin/CDKs on periodic transcription by deleting all six of these cyclins (*clb1,2,3,4,5,6*) in budding yeast. These cells are kept alive by the inducible overexpression of Clb1; in the absence of Clb1, cells arrest due to the absence of all S-phase and mitotic cyclin/CDK activity, resulting in their inability to initiate DNA replication, centrosome duplication, or mitosis. However, the arrested cells continue to carry out G1 events, including budding and G1-specific transcription [66]. What happens to the rest of the periodic transcriptional program in these cells? In a synchronous population of early G1 cells lacking all S-phase and mitotic cyclins (synchronized by centrifugal elutriation), global gene expression dynamics were measured by microarray. Strikingly, compared to the expression dynamics of genes normally periodic in wild-type cells, 70 % of genes remain periodic in the absence of both S-phase and mitotic cyclins and in the absence of cell cycle progression, with a period very similar to normally cycling cells [5]. These findings suggest that S-phase and mitotic CDKs are not required for the execution of the majority of the cell cycle-transcriptional program, and that this program can continue to oscillate even in arrested cells.

How then is the periodic transcriptional program maintained in arrested cells? Included in the 70 % of genes that remain periodic in these cells are many of the TFs involved in modulating periodic transcription throughout the cell cycle [5, 8, 44]. Using these periodic TFs and binding information, Orlando and colleagues were able to construct a mathematical model of the TF network. Model simulations indicated that the TF network itself could sustain oscillation independent of S-phase and mitotic cyclin/CDKs and cell cycle progression [5]. This finding led to the proposal that a TF

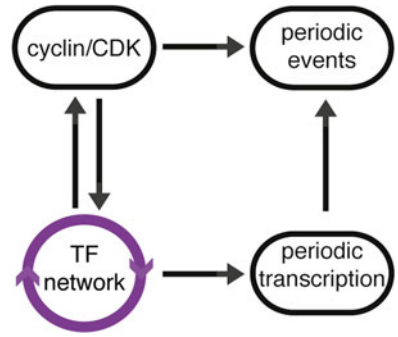

Fig. 4 Model of cell-cycle regulation. A transcription factor network is responsible for regulating the timing of the periodic transcriptional program, including cyclins. Cyclins, in complex with CDKs, then act as effectors to trigger events at the proper time after periodic synthesis

network may function as an underlying cell cycle oscillator that controls the periodic transcriptional program ([5], reviewed in [33]).

In yeast and somatic cells, several experiments have shown that cyclin/CDKs have the capacity to alter TF activity. What is the effect that cyclin/CDK feedback acting on TF activity has on transcriptional oscillations? Comparing transcriptional dynamics reveals that the overall amplitude of periodic gene expression dynamics decreases as cyclin/CDK activity is removed [12]. Additionally, the period of transcriptional oscillations also increase with decreasing cyclin/CDK activity [12]. These observations suggest that cyclin/CDK activity plays an important role in regulating the amplitude and period of transcriptional oscillations. In addition to cyclin/CDK feedback on the TF network, cyclins themselves are periodically transcribed (reviewed in [9–11, 33]). Yet in the absence of CDK activity, cell cycle progression is halted. A study showed that in the absence of all S-phase and mitotic cyclins, except for a single S-phase cyclin, periodic cycles of DNA replication occur together with transcriptional activation of the S-phase cyclin [12]. This observation implies that cyclin/CDK activity also acts as an effector of the TF network oscillator.

Taken together, these results led to the proposal of a new model of cell-cycle regulation (Fig. 4) [12]. A TF network acts as an oscillator that drives the timing of periodic transcription, including transcription of cyclin genes. Cyclins (in complex with CDKs) then feedback onto the TF network via phosphorylation to contribute robust transcriptional oscillations. Phosphorylation of a TF is capable of enhancing or reducing transactivation of the TF's target genes, thus "fine-tuning" the TF network output during the cell cycle. Additionally, cyclin/CDKs also act as effectors of the TF network to trigger cell cycle events in the proper order (Fig. 4). This model is different from previous cell cycle models in that a TF

network, rather than cyclin/CDK activity, acts as the oscillator that keeps the timing and ordering of cell cycle progression, and functions to control the temporal program of transcription. Although the mechanism by which the timing of cell cycle oscillations is different, the process by which cell cycle events are triggered by cyclin/CDKs is not different. The activation of different events in the proper order is dependent both on transcriptional oscillations and cyclin/CDK activity. However, it remains to be determined how a TF network oscillator is coupled to other cell cycle events and cyclin/CDK activity.

An important factor in designing experiments to address still-open questions is the use of technologies and analytical tools available to measure periodic transcription. Here we will discuss many of the technologies that have been used in the past as well as the computational tools that exist to identify periodic behaviors. Each technology and analytical tool has its own advantages and drawbacks, and it is critical to choose the right combination of the two in order to most completely distinguish between the models described above.

3 Assaying Cell Cycle-Regulated Transcription

Over the past three decades, we have learned that periodic gene transcription is not simply a phenotype of a small subset of cell cycle-regulated genes. In fact, a large portion of the budding yeast genome is periodically transcribed [4–7]. Models of cell cycle-regulated transcription have evolved over the years and this evolution was enabled by new experimental approaches and analytical methods. First, single gene approaches demonstrated that a handful of genes were transcribed periodically. Then, with the advent of genome-wide approaches, a global view of transcript dynamics demonstrated that many more genes have the capacity to oscillate. The analytical methods used to define periodicity also changed with each of these experimental approaches. Here, we will discuss the strengths and limitations of each.

3.1 Single Gene Approaches

The first sets of periodic genes were identified in budding yeast by northern blotting [67] (reviewed in [68, 69]). Although this method was able to classify a number of genes as periodically transcribed, the major limitation of northern blotting is scalability. Northern blotting is limited to testing only a handful of genes at a time. So while it was useful for asking whether any specific gene might be cell cycle-regulated, it was not a particularly useful tool for discovering new periodic genes. Additionally, because only a small number of genes could be assayed on each blot, the temporal and quantitative relationships between all periodic genes could not be determined. Thus, a global view of the program and the regulatory

mechanisms that governed them could not be easily discerned by this approach. Often, a gene was defined as periodically transcribed if dynamics matched the period of observable events. For example, histones were shown to be transcribed in concert with DNA replication during every cell cycle [13].

Quantitative real time PCR (qRT-PCR) is a more recent technology developed to measure mRNA levels at a single gene level. While not many studies have utilized qRT-PCR to measure mRNA dynamics during the cell cycle, this approach is also able to provide transcript dynamics.

3.2 Transcription Microarrays

Transcription microarrays have proven to be very useful in revealing genome-wide transcriptional behaviors in a variety of different systems. Microarray approaches facilitated the discovery of new cell cycle-regulated genes. In fact, several studies demonstrated that a substantial portion of the budding yeast genome is periodically transcribed ([4–7], reviewed in [32]). This approach also revealed that transcripts rise and fall in a continuum throughout the budding yeast cell cycle, and that clusters of genes with similar behaviors were likely to be co-regulated [7].

However, the substantial differences in periodic gene lists generated by these studies demonstrate that even global studies must be analyzed critically to understand methods used to define cell cycle-regulated transcription. Several factors, including experimental methods and definition of periodicity, play a role in the different periodic gene lists generated by each report.

A series of differences in experimental approach may contribute to low agreement between the results of these studies. First, the methods to synchronize populations of cells varied between each study, resulting in starting populations that were released from a variety of cell cycle phases. Depending on the starting population, periodic mRNAs expressed during cell cycle phases immediately following release may be more synchronous than those mRNAs in later cell-cycle phases as populations become more asynchronous. This observation may be due to the following factors: (1) normally cycling cells complete cellular division at different rates and (2) different synchronizations result in starting populations that vary in level of synchrony [31]. Second, each research group used different microarrays with different sets of oligos to represent the budding yeast genome. These differences may play a role in discrepancies between mRNA measurements. Third, the method of labeling and hybridizing mRNAs to the chips varied between the groups, which may result in differences in the quantification of mRNA levels. Fourth, Spellman and colleagues and Pramila and colleagues hybridized mRNA from an asynchronous population of cells labeled with a different fluorescent probe to each chip as a control in addition to the synchronized pools of labeled mRNA [6, 7]. This was meant as a way to control for

differences across different microarray chips. Alternatively, Cho and colleagues and Orlando and colleagues only hybridized the synchronized pools of mRNA to each chip [4, 5]. This approach generates a direct measure of mRNA levels relative to other time points from the synchronized time course. Finally, each group used different methods to normalize the microarrays with each other for consistent measures of gene expression both within and across microarrays, which can affect the resulting dynamic range of expression measurements. An important factor to consider is the differences in experimental approaches that measure and quantify gene expression dynamics when comparing the various studies centered on identifying cell cycle-regulated transcription.

In addition to differences in experimental approaches, each study utilized different methods to classify genes as periodically transcribed. Similar yet distinct definitions of periodic are embedded within each of the different methods applied to identify cell cycle-regulated transcripts. As described in Subheading 2.1, these four groups exploited different methods to classify a set of periodic genes. Two features play prominent roles in describing periodicity; each method integrates these features differently. The first feature addresses the oscillatory nature of gene expression dynamics. Whether by visual inspection or by some quantitative approach, a necessary component of any of these analyses requires identifying genes that are expressed once per cell cycle across multiple cycles. The second feature addresses the dynamic range of the queried genes. This attribute is much more subjective in nature, as it is unclear what minimum dynamic range is above stochastic noise within a synchronous population of cells. Additional quantitative methods exist to measure the periodicity of gene expression dynamics and define periodic behavior in a variety of ways [70]. Therefore, it is important to have an understanding of how you want to define periodic genes and select a computational algorithm that best matches your assumptions.

3.3 RNA Sequencing

A more recent experimental approach to measuring gene expression in cells is RNA-Sequencing (RNA-seq). This method provides a new way to measure transcript levels in cells and can benefit many biological systems when gene expression microarrays are not efficient [71]. First, RNA-seq requires much less starting RNA. This is advantageous when studying a system in which cells are in short supply. Second, RNA-seq allows for measuring the abundance of multiple transcript isoforms. This benefit is especially helpful in organisms that possess introns because microarrays usually do not distinguish between different splice variants of the same transcribed gene. Finally, RNA-seq has a much larger dynamic range compared to gene expression microarrays [71]. A major drawback of current RNA-seq methodologies is the lack of standardized normalization approaches, especially in time-series experiments.

Table 2
A summary of approaches used to determine cell-cycle transcript abundance

Approach	Detection	Population/ single cell	Target measurement	Target amplification
Northern blot	RNA	Population	Preselected probes	No
Microarray	RNA	Population	Preselected ORFs (all annotated genes)	Yes
RNA-sequencing	RNA	Population	Unbiased	Yes/no
RNA-FISH	RNA	Single cells	Preselected probes	No
Reverse transcription PCR	RNA	Population	Preselected primers	Yes

This drawback is critical when comparing time points across the cell cycle. While few groups have used RNA-seq to study cell cycle-regulated transcription, with continued development of experimental and analytical techniques, this technology may provide a way to gain a better insight into the scope of periodic gene expression.

3.4 Mapping Relationships Between Transcription Factors and Their Targets by Physical Interaction Approaches

The past 15 years have seen massive strides in the characterization of cell cycle gene expression. Many techniques have allowed us to elucidate the dynamics of cell cycle transcription (Table 2). However, much still needs to be done to understand the molecular mechanisms governing transcription dynamics during the cell cycle.

One important method for developing regulatory models involves detecting the physical interaction between a TF and a target gene promoter. Using Chromatin Immunoprecipitation approaches (ChIP) coupled with microarray or RNA-sequencing (ChIP-chip or ChIP-seq) provides information on where a particular TF binds genome-wide. Such localization studies enable the construction of global transcription factor networks that describe the regulatory interactions of the cell cycle transcription program [8, 39, 43, 44, 54, 72, 73].

Most publicly available large-scale ChIP-chip datasets were derived from asynchronous populations of cells. Thus, these experiments lack any temporal information about dynamic TF binding. Moreover, TFs that bind very strongly to a target gene promoter for only a short amount of time yield a "low" signal that resembles a regulator that only binds weakly to a promoter throughout the cell cycle. Thus, it is likely that short-lived TF/promoter interactions are under-represented in these data sets. Both of these issues could be rectified by performing ChIP approaches on synchronized cells. However, performing a single replicate of a ChIP-chip or ChIP-seq experiment over 10 time points for all *S. cerevisiae* TFs

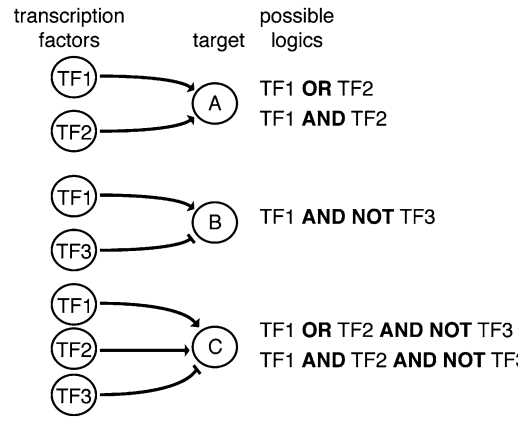

Fig. 5 Logics of multiple transcription factors regulating a single target affect its synthesis. Depending on the combinations of transcription factors that bind to the promoter of a single target, they may work together (AND logic) or may work separately (OR logic). Repressors most likely override any activators that may be bound at the same time (AND NOT logic). Depending on the number and combination of potential regulators, other logics may be possible

would require ~2,000 ChIP experiments followed by the same number of microarray hybridizations or sequencing runs. Presently, this is an effort that is currently beyond the capacity of most labs.

In budding yeast, ChIP-chip and associated computational studies have shown that many different TFs can bind within the promoter region of a single gene [8, 39, 43, 44, 54, 72, 73]. While ChIP studies have been informative in determining the physical association of a DNA-binding protein with a given promoter, these studies do not reveal the degree to which multiple TFs bind in a coordinated or exclusive fashion. Furthermore, binding studies do not reveal the functional relationships between multiple TFs bound at the same promoter. Since transcriptional regulators can promote or repress transcription (some TFs can perform both tasks), there are several different logical combinations that can define the transcription of a given gene (Fig. 5).

A primary goal of the field is to understand the functional targets of cell cycle transcription factors. However, physical interaction data can only predict binding, and binding does not predict function. Therefore, to determine the downstream targets of TFs in vivo, one can use genetic approaches to observe changes in target gene behavior directly.

3.5 Genetic Approaches to Transcriptional Target Discovery

Gene knockout experiments are straightforward methods to begin characterizing TF-target relationships in budding yeast. Nonessential TFs may be deleted and, in theory, their targets should have altered expression. This method had been used successfully to identify gene targets with altered expression upon deletion of cell cycle TFs [74]. The method can even be combined with microarray or

other whole-genome analysis to determine expression changes among large numbers of genes [75]. However, this method does not necessarily demonstrate direct TF-target relationships between the deleted TF and gene expression. In some instances, the deletion of TF1 could alter the expression of another TF2, resulting in expression changes for the targets of TF2. Therefore, these methods are often tied to physical interaction data to strengthen the argument for a direct relationship [74, 75].

An alternative method to TF deletion is conditional TF expression. Using an inducible TF, one can determine the state of transcription prior to and post TF induction, while controlling and monitoring the timescale of gene activation/repression. Budding yeast researchers have long relied on inducible promoter constructs to turn on gene expression and monitor the outcome. The replacement of an endogenous promoter with the GAL promoter has allowed for induction of transcription via a shift to galactose-containing medium [76]. The use of the GAL-inducible promoter, among others, allows a researcher to turn on gene expression of a TF and then monitor the effect on target genes. However, after the shift to galactose medium, the TF must be expressed, translated, and then activate/repress gene expression of its targets. Thus, there is a desire to shorten the time from induction to the activation/repression of target genes.

Instead of inducing TF expression, one can induce TF localization to the nucleus using a hormone-induced localization. To construct an estradiol-induction system, a Gal4-DNA binding domain was fused to the human estrogen receptor [77, 78]. The addition of estradiol hormone results in the localization of the fusion protein to the nucleus and binding to Gal4 transcriptional targets. This massive shift in localization leads to the rapid binding of Gal4 targets without concern for protein level thresholds for transactivation. McIsaac and colleagues employed microarrays to monitor temporal changes in global transcription in asynchronous populations and found that the targets of Gal4 transactivation were quickly upregulated, as soon as 5 min after estradiol treatment [79]. By sampling mRNA levels at several time points after induction, one can determine direct transcriptional targets and observe the activation/repression dynamics. Using a similar system, one can identify the targets of many of the yeast cell-cycle TFs employing an induction system in asynchronous populations of cells and monitoring the first genes to respond, thus identifying the direct targets of the TF. The forced expression of these targets should be readily detectable over the background expression in an asynchronous population (low amplitude changes may require cell cycle synchronization to be observed).

As mentioned for physical interactions in Subheading 3.4, temporal dynamics are important for determining first-order targets of a TF. A systematic analysis of cell cycle TFs would be possible, using 4–5 time points after induction, thus reducing the time and cost of

such an experiment compared to ChIP analysis of TFs throughout the cell cycle. Combining the identification of TF targets with existing data on expression dynamics of the TFs themselves will help to build a temporal network of transcription regulation during the cell cycle.

Ideally, data from physical interaction studies can be combined with data from genetic experiments in order to develop high confidence molecular models. Additional information can be gained by approaches that identify global changes in chromatin structure, such as nucleosome dynamics. Nucleosome positioning experiments identify chromatin that is accessible to TFs. However, recent work on temporal dynamics of nucleosome binding at promoters suggests that TFs can actually induce nucleosome position changes once they bind a site, while some sites which are "accessible" to TFs remain transcriptionally inactive [80]. These experiments help to build a model describing the transactions at a promoter. By correlation, this information can be associated with expression timing and provide additional information to describe mechanisms of gene activation and repression during the cell cycle. As these experiments do not directly probe the activation/repression of genes, expression analysis upon induction of TF localization to the nucleus remains a more direct observation of transcriptional activity at TF targets.

Much stands to be gained from leveraging both physical and genetic approaches. The data eventually yielded from these approaches will ultimately allow us to develop quantitative methods to integrate and interpret present and future "big data." Designing future experiments in the context of cell cycle dynamics and with the understanding that several regulators may contribute to target gene regulation will provide the information necessary for the challenging analyses to come. The use of genetic experiments may direct the strategic implementation of physical interaction studies that may prove too costly on a larger scale (or vice versa). Thus, collection of physical and genetic data will only strengthen our ability to understand cell-cycle TF regulation.

3.6 Gaps in Knowledge and the Future

The ability to quantify the levels of RNA in a cell at any given moment, in an unbiased manner, is the Holy Grail for developing a precise understanding of cell cycle-regulated transcription. The field has come a long way from original expression studies, and new technologies are continuously being developed to address issues with sensitivity, noisy data, and population effects. However, in overcoming some of the current obstacles, one must understand potential pitfalls and biases introduced by the various methods used to measure transcript levels, which are especially important while implementing methods that measure expression over time. Improving current approaches and developing novel assays will allow the field to continue to move forward.

One of the key improvements needed in cell cycle gene expression analysis is the removal of amplification bias. Microarray analysis and RNA sequencing protocols typically use a reverse transcription step to produce a complementary DNA or RNA, which is then amplified to add a fluorophore to the nucleic acid. The introduction of these amplification steps during any RNA detection assay increases the risk that some RNA species are preferentially amplified over others. To prepare libraries representing an mRNA population, the use of poly-thymidine primers to amplify cDNA from purified RNA leads to a preference for mRNAs with longer poly-adenine tails, altering the representative population in the amplified pool.

One possible solution is the use of single-molecule sequencing technologies to eliminate the amplification steps of RNA-seq and microarray methods [71]. So-called third-generation single-molecule sequencing removes the requirement for RNA amplification from the assay [81, 82]. These sequencing technologies have longer read lengths than current deep-sequencing technologies, making sequencing of an entire mRNA possible. Critically, a formidable problem for these technologies is the improvement of the sequencing accuracy which currently sits at ~85 % for PacBio sequencing and ~75–90 % for Nanopore sequencing [83, 84]. With these accuracy rates, the possibility that a read does not identify the correct gene is substantial. Recently, it has been shown that aligning single molecule sequencing with reads from amplification based sequencing (such as Illumina) greatly enhances the accuracy of single molecule sequencing while still allowing for quantitation to be performed in a no-amplification manner, increasing the viability of the technology, but increasing the cost and effort involved [85, 86]. With the introduction of these technologies to RNA-Seq, the biases of amplification-based methods should be greatly reduced.

While great advances have been made in removing artifacts and biases from microarray and sequencing methods, they do not address a main concern that many researchers harbor: the fact that these methods detect average transcript levels in a population. To eliminate this problem, many have made use of RNA fluorescence in situ hybridization, or RNA-FISH [87]. RNA-FISH uses a fluorophore-conjugated nucleotide probe to detect target RNAs in fixed cells. The foci generated by the probe are visualized by microscopy, and each focus represents an mRNA contained within a cell at that moment. Barcoding FISH probes and ultraresolution microscopy has lead to the potential for identifying and quantifying more transcripts than available fluorophore colors [88, 89]. Using RNA-FISH, one can determine the actual number of transcripts at a time point in a single cell. Observing multiple cells, one can determine the range of transcript abundance at a given time in a collection of single cells, which helps understand the distribution

of RNA abundance in a population in a way that cannot be determined using methods that rely on purified RNA from a population of cells (microarray, RNA-seq, etc.).

The drawbacks to this method are also inherent to working with single cells. For each time point, many cells must be labeled and analyzed to obtain statistically significant results. Furthermore, the method requires cells to be fixed. Hence, transcript dynamics cannot be measured in the same cells over a period of time. Therefore, a time course using an RNA-FISH approach still samples a population, albeit in a manner that allows for individual mRNA molecules to be quantified. The ability to determine the number of mRNA transcripts in cells at a time point serves as a complementary approach to the whole transcriptome approaches described above.

Methods for tracking RNA in live cells have been developed to expand temporal observations and localization behavior [90]. These methods rely on inserting hairpin-forming sequences to the noncoding regions of the mRNA. These hairpin constructs are recognized by virus-derived hairpin-recognition proteins. The best characterized of these systems is the MS2 reporter [91, 92]. The hairpin-binding protein domain can be detected as they are typically fused to a fluorescent reporter. MS2 stem-loop repeats are integrated into the mRNA of interest and co-expressed in a cell with the bacteriophage derived MS2-binding protein fused to a fluorescent reporter. When the mRNA is expressed, the stem-loop structures fold and are recognized by the MS2-binding domain, generating fluorescent foci that can be tracked within a living cell.

The system was originally described in yeast, where it was used to follow *ASH1* mRNA as it was trafficked from the nucleus to the bud [93]. Since the introduction of the system, it has been effectively used in a variety of eukaryotes and expanded to a two-color system [94, 95]. Still, live-cell imaging using reporters has typically shied away from quantitation and has been used more extensively for localization experiments. The RNA hairpin-binding approach is, so far, relatively unproven in systems where mRNA levels are dynamically regulated over time (though some efforts have been made to quantify mRNA by foci in prokaryotes [96, 97]). For example, the *ASH1* experiment described above observed mRNA localization dynamics, not abundance. A major limitation of probing mRNAs by FISH or by hairpin-binding proteins is the introduction of bias to the analysis while limiting scale. Using these methods, an experimenter can only determine the transcript levels of the specific mRNAs that they have targeted for analysis. Therefore, examining correlation or coherence with other transcripts is not yet possible with this approach. In time, the ability to multiplex probes may expand the experimental arsenal of probe targets. Certainly, with advances in fluorescent probe development and live cell imaging, the potential remains for RNA binding

probes to yield fruitful results in the field of cell cycle transcription. Currently, the field still benefits from data collected at the population level as well as in single cells.

Presently, there does not appear to be a "cure-all" experiment that generally addresses the concerns of those studying cell-cycle transcription. The most benefit appears to come from integrating the data the field has already collected. Using a growing body of correlative data can increase the confidence in understanding the coordination of periodic transcription with other cell cycle events and the coordination of two major regulators: a TF network and cyclin/CDKs. Quantitative methods that integrate existing data with an understanding of all possible limitations will greatly increase our current knowledge and help direct specific experiments to address new hypotheses in cell-cycle transcription.

Acknowledgement

Members of the Haase Lab are thanked for their critical reading and comments.

References

1. Morgan DO (1997) Cyclin-dependent kinases: engines, clocks, and microprocessors. Annu Rev Cell Dev Biol 13:261–291
2. Morgan DO (2007) The cell cycle: principles of control. Primers in biology. New Science Press in association with Oxford University Press, London, Distributed inside North America by Sinauer Associates Publishers Sunderland, MA
3. Murray AW, Kirschner MW (1989) Dominoes and clocks: the union of two views of the cell cycle. Science 246(4930):614–621
4. Cho RJ, Campbell MJ, Winzeler EA, Steinmetz L, Conway A, Wodicka L, Wolfsberg TG, Gabrielian AE, Landsman D, Lockhart DJ, Davis RW (1998) A genome-wide transcriptional analysis of the mitotic cell cycle. Mol Cell 2(1):65–73
5. Orlando DA, Lin CY, Bernard A, Wang JY, Socolar JE, Iversen ES, Hartemink AJ, Haase SB (2008) Global control of cell-cycle transcription by coupled CDK and network oscillators. Nature 453(7197):944–947
6. Pramila T, Wu W, Miles S, Noble WS, Breeden LL (2006) The Forkhead transcription factor Hcm1 regulates chromosome segregation genes and fills the S-phase gap in the transcriptional circuitry of the cell cycle. Genes Dev 20(16):2266–2278
7. Spellman PT, Sherlock G, Zhang MQ, Iyer VR, Anders K, Eisen MB, Brown PO, Botstein D, Futcher B (1998) Comprehensive identification of cell cycle-regulated genes of the yeast Saccharomyces cerevisiae by microarray hybridization. Mol Biol Cell 9(12):3273–3297
8. Simon I, Barnett J, Hannett N, Harbison CT, Rinaldi NJ, Volkert TL, Wyrick JJ, Zeitlinger J, Gifford DK, Jaakkola TS (2001) Serial regulation of transcriptional regulators in the yeast cell cycle. Cell 106(6):697–708
9. Breeden LL (2003) Periodic transcription: a cycle within a cycle. Curr Biol 13(1): R31–R38
10. McInerny CJ (2011) Cell cycle regulated gene expression in yeasts. Adv Genet 73:51–85
11. Wittenberg C, Reed SI (2005) Cell cycle-dependent transcription in yeast: promoters, transcription factors, and transcriptomes. Oncogene 24(17):2746–2755
12. Simmons Kovacs LA, Mayhew MB, Orlando DA, Jin Y, Li Q, Huang C, Reed SI, Mukherjee S, Haase SB (2012) Cyclin-dependent kinases are regulators and effectors of oscillations driven by a transcription factor network. Mol Cell 45(5):669–679
13. Hereford LM, Osley MA, Ludwig TR 2nd, McLaughlin CS (1981) Cell-cycle regulation of yeast histone mRNA. Cell 24(2):367–375

14. Nasmyth K (1983) Molecular analysis of a cell lineage. Nature 302(5910):670–676
15. Storms RK, Ord RW, Greenwood MT, Mirdamadi B, Chu FK, Belfort M (1984) Cell cycle-dependent expression of thymidylate synthase in *Saccharomyces cerevisiae*. Mol Cell Biol 4(12):2858–2864
16. White JHM, Barker DG, Nurse P, Johnston LH (1986) Periodic transcription as a means of regulating gene-expression during the cell-cycle – contrasting modes of expression of DNA-ligase genes in budding and fission yeast. EMBO J 5(7):1705–1709
17. Kupiec M, Simchen G (1986) Regulation of the RAD6 gene of *Saccharomyces cerevisiae* in the mitotic cell cycle and in meiosis. Mol Gen Genet 203(3):538–543
18. Nasmyth K, Seddon A, Ammerer G (1987) Cell cycle regulation of SW15 is required for mother-cell-specific HO transcription in yeast. Cell 49(4):549–558
19. White JHM, Green SR, Barker DG, Dumas LB, Johnston LH (1987) The Cdc8 transcript is cell-cycle regulated in yeast and is expressed coordinately with Cdc9 and Cdc21 at a point preceding histone transcription. Exp Cell Res 171(1):223–231
20. Johnston LH, White JH, Johnson AL, Lucchini G, Plevani P (1987) The yeast DNA polymerase I transcript is regulated in both the mitotic cell cycle and in meiosis and is also induced after DNA damage. Nucleic Acids Res 15(13):5017–5030
21. Chapman JW, Johnston LH (1989) The yeast gene, DBF4, essential for entry into S phase is cell cycle regulated. Exp Cell Res 180(2):419–428
22. Johnston LH, White JH, Johnson AL, Lucchini G, Plevani P (1990) Expression of the yeast DNA primase gene, PRI1, is regulated within the mitotic cell cycle and in meiosis. Mol Gen Genet 221(1):44–48
23. Johnston LH, Eberly SL, Chapman JW, Araki H, Sugino A (1990) The product of the *Saccharomyces cerevisiae* cell cycle gene DBF2 has homology with protein kinases and is periodically expressed in the cell cycle. Mol Cell Biol 10(4):1358–1366
24. Ramsay G (1998) DNA chips: state-of-the art. Nat Biotechnol 16(1):40–44
25. de Lichtenberg U, Jensen LJ, Fausboll A, Jensen TS, Bork P, Brunak S (2005) Comparison of computational methods for the identification of cell cycle-regulated genes. Bioinformatics 21(7):1164–1171
26. Rustici G, Mata J, Kivinen K, Lio P, Penkett CJ, Burns G, Hayles J, Brazma A, Nurse P, Bahler J (2004) Periodic gene expression program of the fission yeast cell cycle. Nat Genet 36(8):809–817
27. Peng X, Karuturi RK, Miller LD, Lin K, Jia Y, Kondu P, Wang L, Wong LS, Liu ET, Balasubramanian MK, Liu J (2005) Identification of cell cycle-regulated genes in fission yeast. Mol Biol Cell 16(3):1026–1042
28. Oliva A, Rosebrock A, Ferrezuelo F, Pyne S, Chen H, Skiena S, Futcher B, Leatherwood J (2005) The cell cycle-regulated genes of *Schizosaccharomyces pombe*. PLoS Biol 3(7): e225
29. Cho RJ, Huang M, Campbell MJ, Dong H, Steinmetz L, Sapinoso L, Hampton G, Elledge SJ, Davis RW, Lockhart DJ (2001) Transcriptional regulation and function during the human cell cycle. Nat Genet 27(1):48–54
30. Whitfield ML, Sherlock G, Saldanha AJ, Murray JI, Ball CA, Alexander KE, Matese JC, Perou CM, Hurt MM, Brown PO, Botstein D (2002) Identification of genes periodically expressed in the human cell cycle and their expression in tumors. Mol Biol Cell 13(6): 1977–2000
31. Orlando DA, Lin CY, Bernard A, Iversen ES, Hartemink AJ, Haase SB (2007) A probabilistic model for cell cycle distributions in synchrony experiments. Cell Cycle 6(4):478–488
32. Futcher B (2000) Microarrays and cell cycle transcription in yeast. Curr Opin Cell Biol 12(6):710–715
33. Simmons Kovacs LA, Orlando DA, Haase SB (2008) Transcription networks and cyclin/CDKs: the yin and yang of cell cycle oscillators. Cell Cycle 7(17):2626–2629
34. Barberis M, Spiesser TW, Klipp E (2010) Replication origins and timing of temporal replication in budding yeast: how to solve the conundrum? Curr Genomics 11(3):199–211
35. Dahmann C, Diffley JF, Nasmyth KA (1995) S-phase-promoting cyclin-dependent kinases prevent re-replication by inhibiting the transition of replication origins to a pre-replicative state. Curr Biol 5(11):1257–1269
36. Sidorova JM, Mikesell GE, Breeden LL (1995) Cell cycle-regulated phosphorylation of Swi6 controls its nuclear localization. Mol Biol Cell 6(12):1641–1658
37. Abdulrehman D, Monteiro PT, Teixeira MC, Mira NP, Lourenco AB, dos Santos SC, Cabrito TR, Francisco AP, Madeira SC, Aires RS, Oliveira AL, Sa-Correia I, Freitas AT (2011) YEASTRACT: providing a programmatic access to curated transcriptional regulatory associations in *Saccharomyces cerevisiae* through a web services interface. Nucleic Acids Res 39(Database issue):D136–D140

38. Monteiro PT, Mendes ND, Teixeira MC, d'Orey S, Tenreiro S, Mira NP, Pais H, Francisco AP, Carvalho AM, Lourenco AB, Sa-Correia I, Oliveira AL, Freitas AT (2008) YEASTRACT-DISCOVERER: new tools to improve the analysis of transcriptional regulatory associations in *Saccharomyces cerevisiae*. Nucleic Acids Res 36(Database issue): D132–D136
39. Teixeira MC, Monteiro P, Jain P, Tenreiro S, Fernandes AR, Mira NP, Alenquer M, Freitas AT, Oliveira AL, Sa-Correia I (2006) The YEASTRACT database: a tool for the analysis of transcription regulatory associations in *Saccharomyces cerevisiae*. Nucleic Acids Res 34(Database issue):D446–D451
40. Cross FR, Tinkelenberg AH (1991) A potential positive feedback loop controlling CLN1 and CLN2 gene expression at the start of the yeast cell cycle. Cell 65(5):875–883
41. Dirick L, Nasmyth K (1991) Positive feedback in the activation of G1 cyclins in yeast. Nature 351(6329):754–757
42. Marini NJ, Reed SI (1992) Direct induction of G1-specific transcripts following reactivation of the Cdc28 kinase in the absence of de novo protein synthesis. Genes Dev 6(4):557–567
43. Harbison CT, Gordon DB, Lee TI, Rinaldi NJ, Macisaac KD, Danford TW, Hannett NM, Tagne JB, Reynolds DB, Yoo J, Jennings EG, Zeitlinger J, Pokholok DK, Kellis M, Rolfe PA, Takusagawa KT, Lander ES, Gifford DK, Fraenkel E, Young RA (2004) Transcriptional regulatory code of a eukaryotic genome. Nature 431(7004):99–104
44. Lee TI, Rinaldi NJ, Robert F, Odom DT, Bar-Joseph Z, Gerber GK, Hannett NM, Harbison CT, Thompson CM, Simon I, Zeitlinger J, Jennings EG, Murray HL, Gordon DB, Ren B, Wyrick JJ, Tagne JB, Volkert TL, Fraenkel E, Gifford DK, Young RA (2002) Transcriptional regulatory networks in *Saccharomyces cerevisiae*. Science 298(5594):799–804
45. Di Talia S, Wang H, Skotheim JM, Rosebrock AP, Futcher B, Cross FR (2009) Daughter-specific transcription factors regulate cell size control in budding yeast. PLoS Biol 7(10): e1000221
46. Dirick L, Moll T, Auer H, Nasmyth K (1992) A central role for SWI6 in modulating cell cycle Start-specific transcription in yeast. Nature 357(6378):508–513
47. Andrews BJ, Herskowitz I (1989) The yeast SWI4 protein contains a motif present in developmental regulators and is part of a complex involved in cell-cycle-dependent transcription. Nature 342(6251):830–833
48. Koch C, Moll T, Neuberg M, Ahorn H, Nasmyth K (1993) A role for the transcription factors Mbp1 and Swi4 in progression from G1 to S phase. Science 261(5128):1551–1557
49. Costanzo M, Nishikawa JL, Tang X, Millman JS, Schub O, Breitkreuz K, Dewar D, Rupes I, Andrews B, Tyers M (2004) CDK activity antagonizes Whi5, an inhibitor of G1/S transcription in yeast. Cell 117(7):899–913
50. de Bruin RA, McDonald WH, Kalashnikova TI, Yates J 3rd, Wittenberg C (2004) Cln3 activates G1-specific transcription via phosphorylation of the SBF bound repressor Whi5. Cell 117(7):887–898
51. Pramila T, Miles S, GuhaThakurta D, Jemiolo D, Breeden LL (2002) Conserved homeodomain proteins interact with MADS box protein Mcm1 to restrict ECB-dependent transcription to the M/G1 phase of the cell cycle. Genes Dev 16(23):3034–3045
52. Amon A, Tyers M, Futcher B, Nasmyth K (1993) Mechanisms that help the yeast cell cycle clock tick: G2 cyclins transcriptionally activate G2 cyclins and repress G1 cyclins. Cell 74(6):993–1007
53. de Bruin RA, Kalashnikova TI, Chahwan C, McDonald WH, Wohlschlegel J, Yates J 3rd, Russell P, Wittenberg C (2006) Constraining G1-specific transcription to late G1 phase: the MBF-associated corepressor Nrm1 acts via negative feedback. Mol Cell 23(4):483–496
54. Iyer VR, Horak CE, Scafe CS, Botstein D, Snyder M, Brown PO (2001) Genomic binding sites of the yeast cell-cycle transcription factors SBF and MBF. Nature 409(6819): 533–538
55. Kumar R, Reynolds DM, Shevchenko A, Shevchenko A, Goldstone SD, Dalton S (2000) Forkhead transcription factors, Fkh1p and Fkh2p, collaborate with Mcm1p to control transcription required for M-phase. Curr Biol 10(15):896–906
56. Pic A, Lim FL, Ross SJ, Veal EA, Johnson AL, Sultan MR, West AG, Johnston LH, Sharrocks AD, Morgan BA (2000) The forkhead protein Fkh2 is a component of the yeast cell cycle transcription factor SFF. EMBO J 19(14): 3750–3761
57. Maher M, Cong F, Kindelberger D, Nasmyth K, Dalton S (1995) Cell cycle-regulated transcription of the CLB2 gene is dependent on Mcm1 and a ternary complex factor. Mol Cell Biol 15(6):3129–3137
58. Lim FL, Hayes A, West AG, Pic-Taylor A, Darieva Z, Morgan BA, Oliver SG, Sharrocks AD (2003) Mcm1p-induced DNA bending regulates the formation of ternary transcription

factor complexes. Mol Cell Biol 23(2): 450–461

59. Koranda M, Schleiffer A, Endler L, Ammerer G (2000) Forkhead-like transcription factors recruit Ndd1 to the chromatin of G2/M-specific promoters. Nature 406(6791):94–98
60. Althoefer H, Schleiffer A, Wassmann K, Nordheim A, Ammerer G (1995) Mcm1 is required to coordinate G2-specific transcription in *Saccharomyces cerevisiae*. Mol Cell Biol 15(11):5917–5928
61. Darieva Z, Pic-Taylor A, Boros J, Spanos A, Geymonat M, Reece RJ, Sedgwick SG, Sharrocks AD, Morgan BA (2003) Cell cycle-regulated transcription through the FHA domain of Fkh2p and the coactivator Ndd1p. Curr Biol 13(19):1740–1745
62. Pic-Taylor A, Darieva Z, Morgan BA, Sharrocks AD (2004) Regulation of cell cycle-specific gene expression through cyclin-dependent kinase-mediated phosphorylation of the forkhead transcription factor Fkh2p. Mol Cell Biol 24(22):10036–10046
63. Reynolds D, Shi BJ, McLean C, Katsis F, Kemp B, Dalton S (2003) Recruitment of Thr 319-phosphorylated Ndd1p to the FHA domain of Fkh2p requires Clb kinase activity: a mechanism for CLB cluster gene activation. Genes Dev 17(14):1789–1802
64. O'Conallain C, Doolin MT, Taggart C, Thornton F, Butler G (1999) Regulated nuclear localisation of the yeast transcription factor Ace2p controls expression of chitinase (CTS1) in *Saccharomyces cerevisiae*. Mol Gen Genet 262(2):275–282
65. Moll T, Tebb G, Surana U, Robitsch H, Nasmyth K (1991) The role of phosphorylation and the CDC28 protein kinase in cell cycle-regulated nuclear import of the S. cerevisiae transcription factor SWI5. Cell 66(4):743–758
66. Haase SB, Reed SI (1999) Evidence that a free-running oscillator drives G1 events in the budding yeast cell cycle. Nature 401(6751): 394–397
67. (2005) Northern blotting: transfer of denatured RNA to membranes. Nat Methods 2(12):997–998
68. Koch C, Nasmyth K (1994) Cell cycle regulated transcription in yeast. Curr Opin Cell Biol 6(3):451–459
69. Johnston LH (1990) Periodic events in the cell cycle. Curr Opin Cell Biol 2(2):274–279
70. Deckard A, Anafi RC, Hogenesch JB, Haase SB, Harer J (2013) Design and analysis of large-scale biological rhythym studies: a comparison of algorithms for detecting periodic signals in biological data. Bioinformatics 29(24):3174–3180
71. Wang Z, Gerstein M, Snyder M (2009) RNA-Seq: a revolutionary tool for transcriptomics. Nat Rev Genet 10(1):57–63
72. Ren B, Robert F, Wyrick JJ, Aparicio O, Jennings EG, Simon I, Zeitlinger J, Schreiber J, Hannett N, Kanin E, Volkert TL, Wilson CJ, Bell SP, Young RA (2000) Genome-wide location and function of DNA binding proteins. Science 290(5500):2306–2309
73. Horak CE, Luscombe NM, Qian J, Bertone P, Piccirrillo S, Gerstein M, Snyder M (2002) Complex transcriptional circuitry at the G1/S transition in *Saccharomyces cerevisiae*. Genes Dev 16(23):3017–3033
74. Ogas J, Andrews BJ, Herskowitz I (1991) Transcriptional activation of CLN1, CLN2, and a putative new G1 cyclin (HCS26) by SWI4, a positive regulator of G1-specific transcription. Cell 66(5):1015–1026
75. Zhu G, Spellman PT, Volpe T, Brown PO, Botstein D, Davis TN, Futcher B (2000) Two yeast forkhead genes regulate the cell cycle and pseudohyphal growth. Nature 406(6791): 90–94
76. Bitter GA (1998) Function of hybrid human-yeast cyclin-dependent kinases in *Saccharomyces cerevisiae*. Mol Gen Genet 260(1):120–130
77. Gao CY, Pinkham JL (2000) Tightly regulated, beta-estradiol dose-dependent expression system for yeast. Biotechniques 29(6):1226–1231
78. Louvion J-F, Havaux-Copf B, Picard D (1993) Fusion of GAL4-VP16 to a steroid-binding domain provides a tool for gratuitous induction of galactose-responsive genes in yeast. Gene 131(1):129–134
79. McIsaac RS, Silverman SJ, McClean MN, Gibney PA, Macinskas J, Hickman MJ, Petti AA, Botstein D (2011) Fast-acting and nearly gratuitous induction of gene expression and protein depletion in *Saccharomyces cerevisiae*. Mol Biol Cell 22(22):4447–4459
80. Huebert DJ, Kuan PF, Keles S, Gasch AP (2012) Dynamic changes in nucleosome occupancy are not predictive of gene expression dynamics but are linked to transcription and chromatin regulators. Mol Cell Biol 32(9): 1645–1653
81. Ozsolak F, Platt AR, Jones DR, Reifenberger JG, Sass LE, McInerney P, Thompson JF, Bowers J, Jarosz M, Milos PM (2009) Direct RNA sequencing. Nature 461(7265):814–818
82. Eid J, Fehr A, Gray J, Luong K, Lyle J, Otto G, Peluso P, Rank D, Baybayan P, Bettman B, Bibillo A, Bjornson K, Chaudhuri B, Christians F, Cicero R, Clark S, Dalal R, Dewinter A, Dixon J, Foquet M, Gaertner A, Hardenbol P, Heiner C, Hester K, Holden D, Kearns G, Kong X, Kuse R, Lacroix Y, Lin S, Lundquist

P, Ma C, Marks P, Maxham M, Murphy D, Park I, Pham T, Phillips M, Roy J, Sebra R, Shen G, Sorenson J, Tomaney A, Travers K, Trulson M, Vieceli J, Wegener J, Wu D, Yang A, Zaccarin D, Zhao P, Zhong F, Korlach J, Turner S (2009) Real-time DNA sequencing from single polymerase molecules. Science 323(5910):133–138

83. Cherf GM, Lieberman KR, Rashid H, Lam CE, Karplus K, Akeson M (2012) Automated forward and reverse ratcheting of DNA in a nanopore at 5-A precision. Nat Biotech 30(4): 344–348
84. Quail MA, Smith M, Coupland P, Otto TD, Harris SR, Connor TR, Bertoni A, Swerdlow HP, Gu Y (2012) A tale of three next generation sequencing platforms: comparison of Ion Torrent, Pacific Biosciences and Illumina MiSeq sequencers. BMC Genomics 13:341
85. Koren S, Schatz MC, Walenz BP, Martin J, Howard JT, Ganapathy G, Wang Z, Rasko DA, McCombie WR, Jarvis ED, Adam MP (2012) Hybrid error correction and de novo assembly of single-molecule sequencing reads. Nat Biotechnol 30(7):693–700
86. Au KF, Underwood JG, Lee L, Wong WH (2012) Improving PacBio long read accuracy by short read alignment. PLoS One 7(10): e46679
87. O'Connor C (2008) Fluorescence in situ hybridization (FISH). Nat Educ 1(1):171
88. Cai L (2013) Turning single cells into microarrays by super-resolution barcoding. Brief Funct Genomics 12(2):75–80
89. Lubeck E, Cai L (2012) Single-cell systems biology by super-resolution imaging and combinatorial labeling. Nat Meth 9(7):743–748
90. Querido E, Chartrand P (2008) Using fluorescent proteins to study mRNA trafficking in living cells. Methods Cell Biol 85:273–292
91. Witherell GW, Gott JM, Uhlenbeck OC (1991) Specific interaction between RNA phage coat proteins and RNA. Prog Nucleic Acid Res Mol Biol 40:185–220
92. Stockley PG, Stonehouse NJ, Murray JB, Goodman ST, Talbot SJ, Adams CJ, Liljas L, Valegard K (1995) Probing sequence-specific RNA recognition by the bacteriophage MS2 coat protein. Nucleic Acids Res 23(13): 2512–2518
93. Bertrand E, Chartrand P, Schaefer M, Shenoy SM, Singer RH, Long RM (1998) Localization of ASH1 mRNA particles in living yeast. Mol Cell 2(4):437–445
94. Hocine S, Raymond P, Zenklusen D, Chao JA, Singer RH (2013) Single-molecule analysis of gene expression using two-color RNA labeling in live yeast. Nat Meth 10(2):119–121
95. Tyagi S (2009) Imaging intracellular RNA distribution and dynamics in living cells. Nat Meth 6(5):331–338
96. Golding I, Cox EC (2004) RNA dynamics in live Escherichia coli cells. Proc Natl Acad Sci U S A 101(31):11310–11315
97. Golding I, Paulsson J, Zawilski SM, Cox EC (2005) Real-time kinetics of gene activity in individual bacteria. Cell 123(6):1025–1036
98. Ubersax JA, Woodbury EL, Quang PN, Paraz M, Blethrow JD, Shah K, Shokat KM, Morgan DO (2003) Targets of the cyclin-dependent kinase Cdk1. Nature 425(6960):859–864
99. Ostapenko D, Burton JL, Solomon MJ (2012) Identification of anaphase promoting complex substrates in S. cerevisiae. PLoS One 7(9):e45895

Chapter 2

Cell Cycle Regulation by Checkpoints

Kevin J. Barnum and Matthew J. O'Connell

Abstract

Cell cycle checkpoints are surveillance mechanisms that monitor the order, integrity, and fidelity of the major events of the cell cycle. These include growth to the appropriate cell size, the replication and integrity of the chromosomes, and their accurate segregation at mitosis. Many of these mechanisms are ancient in origin and highly conserved, and hence have been heavily informed by studies in simple organisms such as the yeasts. Others have evolved in higher organisms, and control alternative cell fates with significant impact on tumor suppression. Here, we consider these different checkpoint pathways and the consequences of their dysfunction on cell fate.

Key words Checkpoint, DNA damage, Cell cycle, Genome stability, Mitosis

1 Introduction

The cell cycle is the series of events in which cellular components are doubled, and then accurately segregated into daughter cells. In eukaryotes, DNA replication is confined to a discrete Synthesis or S-phase, and chromosome segregation occurs at Mitosis or M-phase. Two Gap phases separate S phase and mitosis, known as G1 and G2. These are not periods of inactivity, but rather periods where cells obtain mass, integrate growth signals, organize a replicated genome, and prepare for chromosome segregation.

The central machines that drive cell cycle progression are the cyclin-dependent kinases (CDKs). These are serine/threonine protein kinases that phosphorylate key substrates to promote DNA synthesis and mitotic progression. The catalytic subunits are in molar excess, but lack activity until bound by their cognate cyclin subunits, which are tightly regulated at both the levels of synthesis and ubiquitin-dependent proteolysis. Cyclin-binding allows inactive CDKs to adopt an active configuration akin to monomeric and active kinases. Layered on top of this regulation, CDK activity can also be negatively regulated by the binding of small inhibitory

Eishi Noguchi and Mariana C. Gadaleta (eds.), *Cell Cycle Control: Mechanisms and Protocols*, Methods in Molecular Biology, vol. 1170, DOI 10.1007/978-1-4939-0888-2_2,

proteins, the CKIs, or by inhibitory tyrosine phosphorylation which blocks phosphate transfer to substrates.

Checkpoints emerged as a series of cell cycle dependencies. In seminal studies in the fission yeast *Schizosaccharomyces pombe*, Mitchison and colleagues determined that cell size was a determinant of cell division [1–4]. Further, Rao and Johnson used human cell fusion experiments [5–8], and determined a dependency between S phase and mitosis. That is, nuclei undergoing S phase could delay mitotic entry of a G2 nucleus, whereas mitotic cells stimulated nuclei to prematurely enter mitosis. In addition, studies in oocytes had determined a similar relationship between S phase and mitosis [9, 10]. In addition, Weinert and Hartwell utilized the cell cycle arrest induced by DNA damage in the budding yeast *Saccharomyces cerevisiae* to identify the first DNA damage checkpoint genes [11, 12], which has subsequently been expanded in several systems into a detailed signaling pathway, with significant overlap of signals making mitosis dependent on the completion of DNA replication [13–16]. Similarly, the mitotic arrest caused by microtubule inhibitors was utilized to identify the first spindle checkpoint genes in *Saccharomyces cerevisiae* [17, 18], again leading to a highly conserved checkpoint pathway that governs chromosome segregation [19]. It is these checkpoints acting as feed-forward signalers that give the cell cycle its remarkable fidelity, and ensure normal development and tissue homeostasis.

2 The Checkpoints

There has been enormous progress in the molecular dissection of various cell cycle checkpoint pathways. In many cases, this is very detailed with close dissection of posttranslational modifications, structural biology, enzyme kinetics, and so on. It would take a textbook to adequately detail all these events, which we do not attempt to do here. Rather, we will focus on the key concepts and regulatory events, and refer the reader to excellent articles that describe the molecular details of these pathways [19–25].

2.1 Cell Size Control

In order to maintain cell size and ensure that each daughter cell is endowed with the appropriate amount of genetic and biosynthetic material, cells must, on average, exactly double their contents before division. Control of cell size is critical for regulating nutrient distribution for the cell and for regulating organ size and function in multicellular organisms. The existence of cell size checkpoints has been proposed for allowing cells to coordinate cell size with cell cycle progression. Cell size checkpoints have been observed in G1 and G2. Early evidence for these checkpoints came from observations that the size of new daughter cells after mitosis affects cell cycle progression: large daughter cells speed up progression

through G1 and/or G2, and small daughter cells delay exit from these growth phases [26, 27]. However, different species and cell types vary widely in the location of these checkpoints within the cell cycle, and thus in how the cell cycle is affected in response to change in cell size.

Not surprisingly, much of what is known about size checkpoints at the molecular level is based on regulation of the proteins involved in G1 and G2/M progression. Control of the G1 cell size checkpoint has been studied most extensively in budding yeast, where the cyclin Cln3, which activates Start, regulates cell size [28, 29]. Control of the G2/M cell size checkpoint has been studied most extensively in fission yeast, where Cdc25 and Wee1 respond to cell size and nutritional status in their control of the Cdc2-cyclin B complex [30, 31].

One proposed mechanism for control of cell size is via the monitoring of protein translation. Ribosomal mass, and thus translational activity, should correlate with the size of the cell, so it is thought that there is some product of translation called a "translational sizer" that increases in abundance with cell size and that exerts control over the cell cycle after a certain amount has accumulated [32]. Cln3 and Cdc25 are both proposed translational sizers. This hypothesis also offers an explanation for how cell size and the cell cycle respond to nutritional status. In yeast, several signaling pathways, including the PKA and TOR pathways, are proposed to mediate nutrient control of the cell cycle, and the unifying characteristic of these pathways is that they control ribosome biogenesis, such that translational activity serves as a cellular indicator of nutritional status.

Another mechanism by which cells may coordinate cell size with cell cycle progression is via monitoring of cell geometry. The fission yeast *S. pombe* is shaped like a cylinder and grows lengthwise prior to division. A protein called Pom1 localizes to the tips of the cell and halts cell cycle progression via regulation of the Cdr1-Cdr2-Wee1-Cdc2 axis, which is centrally placed in a region called the interphase node. At longer cell lengths, Pom1 can no longer influence this complex, and the cell cycle can progress to M phase [33, 34]. Though this system may depend on the relatively unique cell shape of *S. pombe*, it raises the question of whether similar mechanisms exist in other species.

While a number of explanations for coordination of cell cycle and cell size have been offered, it is possible that any number of them function simultaneously in a cell. How they are all integrated, however, remains unclear.

2.2 DNA Damage Responses

Throughout interphase, DNA damage elicits a cell cycle arrest that allows time for repair pathways to operate prior to commitment to subsequent phases of the cell cycle. The source of DNA damage may be intrinsic, such as intermediates of metabolism, attrition of

telomeres, oncogene overexpression, and DNA replication errors. Alternatively, there are many extrinsic sources of DNA damage ranging from sunlight, to carcinogens, ionizing radiation or other anticancer therapeutics. While there are many lesion-specific responses for DNA repair, different lesions in genomic DNA activate common checkpoint pathways whose goal is to maintain CDKs in an inactive state until the lesion is removed. Broadly speaking, DNA damage checkpoints can be separated into those controlled by the tumor suppressor and transcription factor p53, and those ultimately under the control of the checkpoint kinase Chk1, and we will consider the latter first.

The Chk1 pathway is highly conserved from yeast to man. The components of the pathway have come largely from genetic screens in the yeasts among damage-sensitive mutants [11, 14, 35–38], with some additional components identified in mammalian cells [39–42]. Chk1 is activated by all known forms of DNA damage, though this is more efficient in S- and G2-phase than in G1, and restricted to post-replicative lesions [15, 36, 43]. The diversity of activating lesions suggested a common intermediate, which is single-stranded DNA coated by Replication Protein A (RPA), and containing a primer template junction [13, 44]. Complexes of checkpoint proteins assemble on the RPA-coated DNA, including a protein kinase known as ATR (Ataxia Telangiectasia and Rad3-Related) in humans that is targeted by its interacting protein ATRIP, and a PCNA-related clamp called the 9-1-1 complex (Rad9-Rad1-Hus1) that is loaded by a variant Replication Factor C (RFC) complex. Following phosphorylation by ATR, BRCT-domain mediator proteins are recruited to these sites. There are more mediators in mammals than in the yeasts, but they serve the same purpose: the recruitment of Chk1, which undergoes activating phosphorylation by ATR, and is then released to maintain the mitotic CDK Cdc2 in its Y15 phosphorylated and inactive state. Chk1 phosphorylates both the kinase (Wee1) and phosphatase (Cdc25) that regulate Y15 phosphorylation. This leads to increased Wee1 stability and decreased Cdc25 activity and/or protein levels. Subsequently, Chk1 is subject to dephosphorylation by type 1 phosphatases [45–47], and the cells resume cycling into mitosis.

In *S. cerevisiae,* the upstream signaling events are identical to those described above, but the effector kinase is different. Although Chk1 is conserved, the major effector is an unrelated kinase known as Rad53 [48, 49]. Moreover, the point of cell cycle arrest is not the G2–M transition, but the metaphase to anaphase transition. This is brought about by Rad53 controlling the activity of the cohesin protease, separase, through phosphorylation of its regulator securin [50]. This damage-induced mitotic arrest is not seen in other species including fission yeast, and notably human mitotic cells are unable to mount a delay to mitotic progression [51]. Further, another kinase known as Dun1 is activated in budding

yeast [52], which controls transcriptional responses to DNA damage including activation of ribonucleotide reductase, the enzyme required for dNTP synthesis.

In higher organisms, the transcription factor p53 is a critical component of DNA damage checkpoints [25], particularly in G1 phase. p53 is regulated by a plethora of posttranslational modifications, including N-terminal phosphorylation on serine-15, which is catalyzed by ATR and its cousins ATM (Ataxia Telangiectasia Mutated) and DNA-PKcs (DNA-dependent protein kinase, catalytic subunit). Similar to ATR, these kinases are targeted to double-strand DNA breaks by interacting proteins: the MRN (Mre11-Rad50-Nbs1) complex for ATM, and the Ku70-Ku80 complex for DNA-PKcs. Activated p53 is stabilized through protection from its E3 ubiquitin ligase Mdm2, and as a tetramer transactivates the expression of a large number of genes, including the cyclin-dependent kinase inhibitor (CKI) p21. Through this mechanism, G1 CDKs are inhibited, and DNA damage is repaired prior to DNA replication. However, p53 can also repress the expression of genes, and is required for prolonged G2 arrest in the face of persistent DNA damage [53, 54]. Moreover, p53 can direct the alternative cell fates of apoptosis or senescence [55]. Indeed, the cell cycle arrest function of p53 seems to be a later adopted function, as *Drosophila* p53 regulates apoptosis, but not cell cycle progression [56].

2.3 Monitoring DNA Replication

S phase marks a particularly vulnerable time for cells to cope with DNA damage. Not only must lesions be repaired as in G1 and G2 cells, but they also act as a physical impediment to the replicative polymerases. DNA replication is initiated at specific sites, the replication origins. These are epigenetically defined by a number of proteins that ensure they fire (start replicating) once and only once per cell cycle. Replication origin firing is controlled by the phosphorylation of two proteins, Cdt1 and Cdc6, which is catalyzed by both CDKs and the Dbf4-dependent protein kinase (DDK) Cdc7. Such phosphorylation not only initiates replication but also leads to degradation of these proteins, and hence the origin cannot refire [57].

When the polymerase and its associated proteins (the replisome) encounter a blockade to progression, it is imperative that the replisome remains stably associated with the replicating chromatid so that replication can resume once the blockade is removed. Such blockades can be modified dNTPs, abasic sites, protein–DNA complexes, or result from the depletion of dNTPs. This replisome stabilization is the function of the intra-S-phase checkpoint.

The effector kinase of the intra-S-phase checkpoint is known as Cds1 in fission yeast or Chk2 in humans. Despite its related name, Chk2 is not biochemically or functionally related to Chk1. Cds1/Chk2 has an N-terminal phospho-S/T-binding Forkhead-Associated (FHA) domain followed by a kinase domain. Upon replication stalling, the replisome component Mrc1 (Mediator of the replication

checkpoint) is phosphorylated by ATR. This creates a binding site for Cds1/Chk2, which is then phosphorylated by ATR, and then fully activated by autophosphorylation [58]. Activated Cds1/Chk2 then stabilizes the stalled replisome by phosphorylation of several subunits, notably the MCM helicase [59, 60]. In budding yeast, the Rad53 kinase serves the function of Cds1/Chk2. Like Cds1/Chk2, Rad53 has an N-terminal FHA domain followed by a kinase domain. However, Rad53 has an additional C-terminal FHA domain not seen in Cds1 that is important in its activation by DNA damage [61].

2.4 S–M Dependency

Upon stabilization, the replisome may stay in position until the blockade is removed or dNTPs restored. Alternatively, the cell can employ post-replication repair pathways to bypass the lesion, either by recruiting mutagenic bypass polymerases, or switching templates by recombination and then replicate using the other nascent strand as a template [62]. In either case, checkpoints must be employed to ensure mitosis is not attempted until replication is complete, or else cells run the risk of reduced ploidy. It is clear that mitotic entry is blocked via Y15 phosphorylation of Cdc2, and that the checkpoint components that act upstream of mediator recruitment are required for this [36, 37, 63]. How this leads to cell cycle delay remains less than clear.

If the source of the blockade is DNA damage, then the Chk1 pathway is activated as described above. However, if the blockade is due to dNTP depletion only, for example by hydroxyurea treatment, Chk1 is not activated and yet the cells will not enter mitosis [64]. Some studies have concluded that Cds1 also regulates cell cycle progression [65, 66]. However, if cells lack Cds1, then the stalled replisome disassociates from its template, a process known as fork collapse, and this is seen as DNA damage that activates Chk1. Consequently, it is difficult to experimentally separate the phenomena of replication fork stability and function for the effector kinases.

A more extreme uncoupling of the dependency of mitosis on prior replication can be seen when fission yeast cells lack both Y15 kinases (Wee1 and Mik1), or when origin firing proteins are deleted [67]. In these cases, cells enter lethal mitoses from G1, a process originally termed mitotic catastrophe, a moniker that has subsequently been used to describe mitotic death in mammalian cells.

In order to maintain ploidy, there is an equally important dependency relationship to ensure one round of replication per cell cycle. This can be uncoupled when degradation of Cdt1 and Cdc6 is defective [68], and replication origin firing becomes constitutive. Complete rounds of S phase without mitosis can also be observed in fission yeast when the CKI Rum1 is overproduced [69]. Similarly, cells devoid of mitotic cyclins bypass mitosis [70],

suggesting these confer knowledge of a G2 state [71]. In each of these situations, mitosis is completely bypassed, and ploidy continues to increase.

2.5 The Mitotic Spindle Checkpoint

The segregation of sister chromatids at anaphase is under the mechanical control of the mitotic spindle. The spindle is comprised of microtubules and several motor proteins at both the centrosomal and kinetochore ends, plus additional motors that provide force between overlapping microtubules that do not attach to kinetochores [72]. It is essential that spindle attachment occurs in a bi-oriented fashion such that sister chromatids are under tension at metaphase, and attached to both poles of the spindle. Once all kinetochores are attached and aligned at the metaphase plate, anaphase can proceed as is promoted by the activity of a large E3 ubiquitin ligase known as the Anaphase-Promoting Complex or Cyclosome (APC/C). This ligase targets a number of proteins, but most essential are the mitotic cyclins, which abolishes CDK activity, and securin, the degradation of which allows separase to be released and cleave cohesin complexes at the kinetochores. APC activity is controlled by two accessory proteins: Cdc20, which functions up to the metaphase–anaphase, and Cdh1, which continues to facilitate APC-mediated ubiquitination once cyclin and separase degradation has begun [73]. Once sister chromatid cohesion is released, spindle tension and the associated motor proteins enable sister chromatids to move apart and form identical daughter nuclei.

The spindle checkpoint functions to prevent activation of APC^{Cdc20} under conditions where kinetochores are not occupied by spindle microtubules, or are attached but not under tension (for example, when attached to the same pole, known as a merotelic attachment). Under these conditions, the spindle checkpoint protein Mad2 (Mitotic Arrest Deficient) inhibits Cdc20 activity both in the context of Cdc20 at unattached kinetochores, where it forms a mitotic checkpoint complex, and at APC-bound molecules. Cdc20 is also regulated by the mitotic checkpoint kinase Bub1 in yeast (Budding uninhibited by benomyl) and its cousin Bub1R in mammals. As Cdc2 is inactive, so is APC, and hence, cells cannot enter anaphase.

The spindle checkpoint includes a number of other proteins, with the list growing with evolutionary complexity. In addition, the formation of the spindle and the detection and correction of spindle defects are under the control of the Polo, Aurora, and NIMA-related (Nek) kinases [74, 75]. In this regard, the spindle checkpoint shares the same basic premise as those controlling DNA integrity discussed above—prevent a cell cycle transition while other effectors correct a genome-altering defect. However, the mitotic checkpoint is unique in that it functions to maintain CDK activity, whereas those functioning in interphase aim to maintain CDK inactivity.

3 The Fate of Checkpoint Dysfunction in Human Disease

Depending on the severity of the cell cycle defect, checkpoint dysfunction can result in outcomes ranging from cell death to cell cycle reprogramming, which can lead to cancer. In the case of p53 loss, arguably the most common genetic defect in cancer, several cell fate decisions are affected. Among these are a lack of CDK control by p21, and hence a loss of the G1 checkpoint. However, p53 can also direct cells into apoptosis and/or senescence, and so the physiological consequence of p53 in cancer is both at the level of cancer etiology and the ability for therapies to kill cells [25]. Interestingly, p53 loss presents a heightened requirement for the Chk1 pathway, which is often up-regulated in cancer cells, and required for the viability of many cancer cells [15, 16, 76]. Hence, there has been a lot of interest in targeting Chk1 [77] and its substrate Wee1 [78] as a therapeutic regimen in the clinic.

Loss of the Chk1 pathway in a fission yeast only manifests a significant phenotype with extrinsic DNA damage, or when combined with DNA repair defects [79]. Entry into mitosis with fragmented or incompletely repaired chromosomes does not trigger the spindle checkpoint, which only measures kinetochore attachment. Therefore, such mitoses are either immediately lethal or result in a significant loss of chromosomal fragments. In mouse and in *Drosophila,* the Chk1 pathway is essential for passage through early embryogenesis [80, 81]. However, this is a bottleneck of rapid cell cycling, and the S–M dependency is critical for genome integrity. Similarly, conditional Chk1 loss is lethal in some tissues and cell lines [82–84], though not others [76, 82, 85, 86], where again proliferation rates may be critical. Nevertheless, mutations in Chk1 pathway genes in human cancers are extremely rare (if at all existent). While cancers exhibit genome instability, they cannot survive in the complete absence of genome integrity checkpoints.

A characteristic of most solid tumors is highly aneuploid karyotypes. Chromosome loss and rearrangement is a rapid means to tumor suppressor loss and oncogene activation. However, while mutations in the spindle checkpoint genes have been reported, they are comparatively rare [87]. Still, with the complexity of the mitotic apparatus and extreme consequence of whole chromosome loss or gain, modest dysfunction can have profound consequences. As with the DNA integrity checkpoints, where high level DNA damage tends to induce cell death, altering the dynamic instability of spindle microtubules can also be lethal, with the advantage that spindles are only present in cycling cells.

4 Conclusions

We have described here the basic principles behind the common cell cycle checkpoints. They share the feature of detecting a defect in the division program, and then sending signals forward to alter the oscillations of CDK activity and therefore cell cycle events. Some aspects of checkpoint signaling remain to be clarified or determined (known unknowns), either as a simple principle, or in the context of human development and disease. Doubtless, we will uncover unforeseen aspects of checkpoint signaling (unknown unknowns), and the ever-growing arsenal of highly sophisticated experimental tools and technologies will enable a more complete picture of the remarkable fidelity of the cell cycle.

Acknowledgements

We thank our colleagues and collaborators for a stimulating discussion. This work was supported by NIH grants RO1-GM087326 (M.J.O.) and T32-CA078207 (K.J.B.).

References

1. Mitchison JM (1990) The fission yeast, Schizosaccharomyces pombe. Bioessays 12(4): 189–191
2. Mitchison JM, Nurse P (1985) Growth in cell length in the fission yeast Schizosaccharomyces pombe. J Cell Sci 75:357–376
3. Mitchison JM (1957) The growth of single cells. I. Schizosaccharomyces pombe. Exp Cell Res 13(2):244–262
4. Fantes PA (1977) Control of cell size and cycle time in Schizosaccharomyces pombe. J Cell Sci 24(51):51–67
5. Rao PN, Johnson RT (1971) Mammalian cell fusion. IV. Regulation of chromosome formation from interphase nuclei by various chemical compounds. J Cell Physiol 78(2):217–223
6. Johnson RT, Rao PN, Hughes HD (1970) Mammalian cell fusion. 3. A HeLa cell inducer of premature chromosome condensation active in cells from a variety of animal species. J Cell Physiol 76(2):151–157
7. Johnson RT, Rao PN (1970) Mammalian cell fusion: induction of premature chromosome condensation in interphase nuclei. Nature 226(5247):717–722
8. Rao PN, Johnson RT (1970) Mammalian cell fusion: studies on the regulation of DNA synthesis and mitosis. Nature 225(5228): 159–164
9. Maller JL (1990) MPF and cell cycle control. Adv Second Messenger Phosphoprotein Res 24:323–328
10. Masui Y (2001) From oocyte maturation to the in vitro cell cycle: the history of discoveries of Maturation-Promoting Factor (MPF) and Cytostatic Factor (CSF). Differentiation 69(1): 1–17
11. Weinert T, Hartwell L (1988) The RAD9 gene controls the cell cycle response to DNA damage in Saccharomyces cerevisiae. Science 241: 317–322
12. Hartwell L, Weinert T (1989) Checkpoints: controls that ensure the order of cell cycle events. Science 246:629–634
13. O'Connell MJ, Cimprich KA (2005) G2 damage checkpoints: what is the turn-on? J Cell Sci 118(Pt 1):1–6
14. O'Connell MJ, Walworth NC, Carr AM (2000) The G2-phase DNA-damage checkpoint. Trends Cell Biol 10(7):296–303
15. Tapia-Alveal C, Calonge TM, O'Connell MJ (2009) Regulation of Chk1. Cell Div 4(1):8
16. Kuntz K, O'Connell MJ (2009) The G(2) DNA damage checkpoint: could this ancient

regulator be the achilles heel of cancer? Cancer Biol Ther 8(15):1433–1439

17. Hoyt MA, Totis L, Roberts BT (1991) *S.cerevisiae* genes required for cell cycle arrest in response to loss of microtubule function. Cell 66:507–517
18. Li R, Murray AW (1991) Feedback control of mitosis in budding yeast. Cell 66:519–531
19. Lara-Gonzalez P, Westhorpe FG, Taylor SS (2012) The spindle assembly checkpoint. Curr Biol 22(22):R966–R980
20. Goodarzi AA, Jeggo PA (2013) The repair and signaling responses to DNA double-strand breaks. Adv Genet 82:1–45
21. Grallert B, Boye E (2008) The multiple facets of the intra-S checkpoint. Cell Cycle 7(15): 2315–2320
22. Errico A, Costanzo V (2012) Mechanisms of replication fork protection: a safeguard for genome stability. Crit Rev Biochem Mol Biol 47(3):222–235
23. Lambert S, Carr AM (2013) Replication stress and genome rearrangements: lessons from yeast models. Curr Opin Genet Dev 23(2): 132–139
24. Lambert S, Carr AM (2005) Checkpoint responses to replication fork barriers. Biochimie 87(7):591–602
25. Giono LE, Manfredi JJ (2006) The p53 tumor suppressor participates in multiple cell cycle checkpoints. J Cell Physiol 209(1):13–20
26. Killander D, Zetterberg A (1965) A quantitative cytochemical investigation of the relationship between cell mass and initiation of DNA synthesis in mouse fibroblasts in vitro. Exp Cell Res 40(1):12–20
27. Killander D, Zetterberg A (1965) Quantitative cytochemical studies on interphase growth. I. Determination of DNA, RNA and mass content of age determined mouse fibroblasts in vitro and of intercellular variation in generation time. Exp Cell Res 38:272–284
28. Cross F (1988) DAF1, a mutant gene affecting size control, pheromone arrest and cell cycle kinetics of S. cerevisiae. Mol Cell Biol 8: 4675–4684
29. Nash R, Tokiwa G, Anand S, Erickson K, Futcher AB (1988) The WHI1+ gene of Saccharomyces cerevisiae tethers cell division to cell size and is a cyclin homolog. EMBO J 7(13):4335–4346
30. Moreno S, Nurse P, Russell P (1990) Regulation of mitosis by cyclic accumulation of p80cdc25 mitotic inducer in fission yeast. Nature 344(6266):549–552
31. Nurse P (1975) Genetic control of cell size at cell division in yeast. Nature 256:547–551
32. Jorgensen P, Nishikawa JL, Breitkreutz BJ, Tyers M (2002) Systematic identification of pathways that couple cell growth and division in yeast. Science 297(5580):395–400
33. Martin SG, Berthelot-Grosjean M (2009) Polar gradients of the DYRK-family kinase Pom1 couple cell length with the cell cycle. Nature 459(7248):852–856
34. Moseley JB, Mayeux A, Paoletti A, Nurse P (2009) A spatial gradient coordinates cell size and mitotic entry in fission yeast. Nature 459(7248):857–860
35. Al-Khodairy F, Carr AM (1992) DNA repair mutants defining G2 checkpoint pathways in Schizosaccharomyces pombe. EMBO J 11(4): 1343–1350
36. Al-Khodairy F, Fotou E, Sheldrick KS, Griffiths DJF, Lehman AR, Carr AM (1994) Identification and characterisation of new elements involved in checkpoint and feedback controls in fission yeast. Mol Biol Cell 5:147–160
37. Enoch T, Carr A, Nurse P (1992) Fission yeast genes involved in coupling mitosis to completion of DNA replication. Genes Dev 6:2035–2046
38. Enoch T, Gould K, Nurse P (1991) Mitotic checkpoint control in fission yeast. Cold Spring Harbor Symp Quant Biol 56:409–416, CSH Laboratory Press
39. Wang B, Matsuoka S, Carpenter PB, Elledge SJ (2002) 53BP1, a mediator of the DNA damage checkpoint. Science 298(5597):1435–1438
40. Goldberg M, Stucki M, Falck J, D'Amours D, Rahman D, Pappin D, Bartek J, Jackson SP (2003) MDC1 is required for the intra-S-phase DNA damage checkpoint. Nature 421(6926): 952–956
41. Stewart GS, Wang B, Bignell CR, Taylor AM, Elledge SJ (2003) MDC1 is a mediator of the mammalian DNA damage checkpoint. Nature 421(6926):961–966
42. Kumagai A, Dunphy WG (2000) Claspin, a novel protein required for the activation of Chk1 during a DNA replication checkpoint response in Xenopus egg extracts. Mol Cell 6(4):839–849
43. Latif C, Elzen NR, O'Connell MJ (2004) DNA damage checkpoint maintenance through sustained Chk1 activity. J Cell Sci 117(Pt 16): 3489–3498
44. MacDougall CA, Byun TS, Van C, Yee MC, Cimprich KA (2007) The structural determinants of checkpoint activation. Genes Dev 21(8):898–903

45. Lu X, Nannenga B, Donehower LA (2005) PPM1D dephosphorylates Chk1 and p53 and abrogates cell cycle checkpoints. Genes Dev 19(10):1162–1174
46. den Elzen N, Kosoy A, Christopoulos H, O'Connell MJ (2004) Resisting arrest: recovery from checkpoint arrest through dephosphorylation of Chk1 by PP1. Cell Cycle 3(5): 529–533
47. den Elzen NR, O'Connell MJ (2004) Recovery from DNA damage checkpoint arrest by PP1-mediated inhibition of Chk1. Embo J 23(4): 908–918
48. Allen JB, Zhou Z, Siede W, Friedberg E, Elledge S (1994) The *SAD1/Rad53* protein kinase controls multiple checkpoints and DNA damage-induced transcription in yeast. Genes Dev 8:2416–2428
49. Sun Z, Hsiao J, Fay DS, Stern DF (1998) Rad53 FHA domain associated with phosphorylated Rad9 in the DNA damage checkpoint. Science 281(5374):272–274 [see comments]
50. Cohen-Fix O, Koshland D (1997) The anaphase inhibitor of Saccharomyces cerevisiae Pds1p is a target of the DNA damage checkpoint pathway. Proc Natl Acad Sci U S A 94(26): 14361–14366
51. Rieder CL, Cole RW (1998) Entry into mitosis in vertebrate somatic cells is guarded by a chromosome damage checkpoint that reverses the cell cycle when triggered during early but not late prophase. J Cell Biol 142(4):1013–1022
52. Zhou Z, Elledge S (1993) *DUN1* encodes a protein kinase that controls the DNA damage response in yeast. Cell 75:1119–1127
53. Carvajal LA, Hamard PJ, Tonnessen C, Manfredi JJ (2012) E2F7, a novel target, is up-regulated by p53 and mediates DNA damage-dependent transcriptional repression. Genes Dev 26(14):1533–1545
54. St Clair S, Giono L, Varmeh-Ziaie S, Resnick-Silverman L, Liu WJ, Padi A, Dastidar J, DaCosta A, Mattia M, Manfredi JJ (2004) DNA damage-induced downregulation of Cdc25C is mediated by p53 via two independent mechanisms: one involves direct binding to the cdc25C promoter. Mol Cell 16(5): 725–736
55. Carvajal LA, Manfredi JJ (2013) Another fork in the road–life or death decisions by the tumour suppressor p53. EMBO Rep 14(5): 414–421
56. Nordstrom W, Abrams JM (2000) Guardian ancestry: fly p53 and damage-inducible apoptosis. Cell Death Differ 7(11):1035–1038
57. Nishitani H, Lygerou Z (2004) DNA replication licensing. Front Biosci 9:2115–2132
58. Xu YJ, Davenport M, Kelly TJ (2006) Two-stage mechanism for activation of the DNA replication checkpoint kinase Cds1 in fission yeast. Genes Dev 20(8):990–1003
59. Bailis JM, Luche DD, Hunter T, Forsburg SL (2008) Minichromosome maintenance proteins interact with checkpoint and recombination proteins to promote s-phase genome stability. Mol Cell Biol 28(5):1724–1738
60. Stead BE, Brandl CJ, Sandre MK, Davey MJ (2012) Mcm2 phosphorylation and the response to replicative stress. BMC Genet 13:36
61. Sweeney FD, Yang F, Chi A, Shabanowitz J, Hunt DF, Durocher D (2005) Saccharomyces cerevisiae Rad9 acts as a Mec1 adaptor to allow Rad53 activation. Curr Biol 15(15):1364–1375
62. Lee KY, Myung K (2008) PCNA modifications for regulation of post-replication repair pathways. Mol Cells 26(1):5–11
63. Rhind N, Furnari B, Russell P (1997) Cdc2 tyrosine phosphorylation is required for the DNA damage checkpoint in fission yeast. Genes Dev 11:504–511
64. Lindsay HD, Griffiths DJF, Edwards RJ, Christensen PU, Murray JM, Osman F, Walworth N, Carr AM (1998) S-phase-specific activation of Cds1 kinase defines a subpathway of the checkpoint response in Schizosaccharomyces pombe. Genes Dev 12:382–395
65. Zeng Y, Forbes KC, Wu Z, Moreno S, Piwnica-Worms H, Enoch T (1998) Replication checkpoint requires phosphorylation of the phosphatase cdc25 by cds1 or chk1. Nature 395:507–510
66. Furnari B, Blasina A, Boddy MN, McGowan CH, Russell P (1999) Cdc25 inhibited in vivo and in vitro by checkpoint kinases Cds1 and Chk1. Mol Biol Cell 10(4):833–845
67. Lundgren K, Walworth N, Booher R, Dembski M, Kirschner M, Beach D (1991) mik1 and wee1 cooperate in the inhibitory tyrosine phosphorylation of cdc2. Cell 64(6):1111–1122
68. Nishitani H, Nurse P (1995) $p65^{cdc18}$ plays a major role controlling the initiation of DNA replication in fission yeast. Cell 83:397–405
69. Moreno S, Nurse P (1994) Regulation of progression through the G1 phase of the cell cycle by the *rum1*$^{+}$ gene. Nature 367:236–242
70. Hayles J, Fisher D, Woollard A, Nurse P (1994) Temporal order of S-phase and mitosis in fission yeast is determined by the state of the $p34^{cdc2}$/mitotic B cyclin complex. Cell 78: 813–822
71. O'Connell MJ, Nurse P (1994) How cells know they are in G1 or G2. Curr Opin Cell Biol 6(6):867–871

72. Wittmann T, Hyman A, Desai A (2001) The spindle: a dynamic assembly of microtubules and motors. Nat Cell Biol 3(1):E28–E34
73. McLean JR, Chaix D, Ohi MD, Gould KL (2011) State of the APC/C: organization, function, and structure. Crit Rev Biochem Mol Biol 46(2):118–136
74. O'Connell MJ, Krien MJ, Hunter T (2003) Never say never. The NIMA-related protein kinases in mitotic control. Trends Cell Biol 13(5):221–228
75. Malumbres M, Barbacid M (2007) Cell cycle kinases in cancer. Curr Opin Genet Dev 17(1):60–65
76. Koniaras K, Cuddihy AR, Christopolous H, Hogg A, O'Connell MJ (2001) Inhibition of Chk1-dependent G2 DNA damage checkpoint radiosensitises p53 mutant human cells. Oncogene 20:7453–7463
77. Maugeri-Sacca M, Bartucci M, De Maria R (2013) Checkpoint kinase 1 inhibitors for potentiating systemic anticancer therapy. Cancer Treat Rev 39(5):525–533
78. Stathis A, Oza A (2010) Targeting Wee1-like protein kinase to treat cancer. Drug News Perspect 23(7):425–429
79. Walworth N, Davey S, Beach D (1993) Fission yeast *chk1* protein kinase links the rad checkpoint pathway to *cdc2*. Nature 363:368–371
80. Liu Q, Guntuku S, Cui XS, Matsuoka S, Cortez D, Tamai K, Luo G, Carattini-Rivera S, DeMayo F, Bradley A, Donehower LA, Elledge SJ (2000) Chk1 is an essential kinase that is regulated by Atr and required for the G(2)/M DNA damage checkpoint. Genes Dev 14(12): 1448–1459
81. Fogarty P, Campbell SD, Abu-Shumays R, Phalle BS, Yu KR, Uy GL, Goldberg ML, Sullivan W (1997) The Drosophila grapes gene is related to checkpoint gene chk1/rad27 and is required for late syncytial division fidelity. Curr Biol 7(6):418–426
82. Greenow KR, Clarke AR, Jones RH (2009) Chk1 deficiency in the mouse small intestine results in p53-independent crypt death and subsequent intestinal compensation. Oncogene 28(11):1443–1453
83. Smith J, Larue L, Gillespie DA (2013) Chk1 is essential for the development of murine epidermal melanocytes. Pigment Cell Melanoma Res 26(4):580–585
84. Lam MH, Liu Q, Elledge SJ, Rosen JM (2004) Chk1 is haploinsufficient for multiple functions critical to tumor suppression. Cancer Cell 6(1):45–59
85. Petermann E, Maya-Mendoza A, Zachos G, Gillespie DA, Jackson DA, Caldecott KW (2006) Chk1 requirement for high global rates of replication fork progression during normal vertebrate S phase. Mol Cell Biol 26(8): 3319–3326
86. Zachos G, Rainey MD, Gillespie DA (2003) Chk1-deficient tumour cells are viable but exhibit multiple checkpoint and survival defects. EMBO J 22(3):713–723
87. Kops GJ, Weaver BA, Cleveland DW (2005) On the road to cancer: aneuploidy and the mitotic checkpoint. Nat Rev Cancer 5(10):773–785

Chapter 3

Interplay Between the Cell Cycle and Double-Strand Break Response in Mammalian Cells

Kate Beishline and Jane Azizkhan-Clifford

Abstract

The cell cycle is intimately associated with the ability of cells to sense and respond to and repair DNA damage. Understanding how cell cycle progression, particularly DNA replication and cell division, are regulated and how DNA damage can affect these processes has been the subject of intense research. Recent evidence suggests that the repair of DNA damage is regulated by the cell cycle, and that cell cycle factors are closely associated with repair factors and participate in cellular decisions regarding how to respond to and repair damage. Precise regulation of cell cycle progression in the presence of DNA damage is essential to maintain genomic stability and avoid the accumulation of chromosomal aberrations that can promote tumor formation. In this review, we discuss the current understanding of how mammalian cells induce cell cycle checkpoints in response to DNA double-strand breaks. In addition, we discuss how cell cycle factors modulate DNA repair pathways to facilitate proper repair of DNA lesions.

Key words Checkpoint, Chk2, Chk2, ATM, ATR, Double-strand breaks, Homologous recombination

1 Introduction

Ataxia telangiectasia mutated kinase (ATM), ataxia telangiectasia-Rad3 related kinase (ATR), and DNA-protein kinase (DNA-PK) are phosphatidyl-inositol 3 kinase-like kinases (PI3KKs), which are essential signaling molecules for activation of the cellular response to DNA lesions (*see* reviews in refs. 1–3). The PI3KKs function by responding to sensor proteins that detect various DNA lesions and activating a cascade of events to facilitate repair processes. The PI3KKs are essential for stalling cell cycle progression and promoting DNA repair. Downstream targets of the damage response kinases have proven to be important in activation of cell cycle checkpoints; most notably, the checkpoint kinases, Chk1 and Chk2. Chk2 activation can take place throughout the cell cycle [4]. In contrast, Chk1 activation and phosphorylation occurs primarily in S and G2, when ATR is activated in response to the formation of single stranded DNA products. Chk1 and Chk2 modify

Eishi Noguchi and Mariana C. Gadaleta (eds.), *Cell Cycle Control: Mechanisms and Protocols*, Methods in Molecular Biology, vol. 1170, DOI 10.1007/978-1-4939-0888-2_3,

a number of downstream targets important for maintaining cell cycle arrest in the presence of DNA damage.

This review briefly discusses cell cycle dynamics, specifically the preparation for DNA replication during G1, initiation of DNA replication during S phase, and the progression from G2 into mitosis (M phase). The factors discussed are those known to be associated with the DNA damage-induced cell cycle response, with a focus on studies using mammalian cells. We then discuss in detail the current understanding of damage-induced cell cycle checkpoints. Due to the absolute necessity for cell cycle regulation in double-strand break repair, discussion will focus specifically on double-strand breaks (DSBs). DSBs are recognized and repaired primarily by homologous recombination (HR) or non-homologous end joining (NHEJ), which repair DSBs resulting from direct damage or damage arising from replication-associated lesions. Other types of DNA lesions can activate damage-induced arrest through activation of Chk1 and Chk2, but these are not the main focus of this review. It is important to note that a large volume of literature has addressed these processes in model systems, specifically in yeast, and these data fully support the similarity of the pathways among eukaryotes [5]. In addition, we discuss what is known about cell cycle-regulated DNA repair, and the relevance of this regulation in oncogenic signaling.

2 Cell Cycle Progression

2.1 G1–S Transition

Progression through the G1 phase of the cell cycle involves coordinated regulation of Cyclin–Cdk complexes and key transcriptional regulators (reviewed in refs. 6, 7). Following mitosis, mitogen-activated signaling increases Cyclin D expression. There are three D type cyclins, which seem to be regulated in a cell type-dependent manner (reviewed in ref. 7). Cyclin D1, discussed here, associates with Cdk4 or Cdk6, and as a complex they phosphorylate a number of important factors required for progression through G1. The initial progression through G1 is considered to be mitogen-dependent due to the requirement for mitogenic stimulation of cyclin D1 transcription. The most important target of the active Cyclin D1–Cdk4/6 complex is retinoblastoma protein (pRB). Hypo-phosphorylated pRB interacts with hypo-phosphorylated E2F1, which blocks its transcriptional activity; E2F1 transcriptionally upregulates a number of factors that are needed for progression from G1 to S phase. Phosphorylation of pRB by active Cyclin D1–Cdk4/6 complex results in the release of E2F1, which transcriptionally activates Cyclin E, and thereby promotes additional phosphorylation of pRB by Cyclin E–Cdk2. Once a threshold of pRB phosphorylation is reached, E2F1 levels are sufficient to promote mitogen-independent progression through G1 into S. The transition from mitogen dependence to independence is called the restriction point.

The Cyclin E–Cdk2 complex requires the removal of inhibitory phosphorylation on Cdk2 to reach full activity. Cdc25 phosphatases remove phosphate groups on the Cdk molecules allowing for full activation of the Cyclin–Cdk complexes. There are three mammalian Cdc25 proteins, Cdc25A, B, and C; Cdc25A likely functions as the primary phosphatase, as it is the only family member whose gene knockout is embryonic lethal. Cdc25A is required throughout the cell cycle, while Cdc25B/C are preferentially important for the entrance into mitosis ([8], reviewed in refs. 9, 10). Along with the phosphorylation of other factors, Cyclin E–Cdk2 primes the cells for S-phase entry and is essential for the formation of active pre-initiation complexes at origins of replication. Prior to the entry into S phase, origins of replication (ORIs) must be licensed and loaded with the replication initiation machinery to ensure proper firing of replication origins (reviewed in ref. 11). During early G1, pre-replication complexes associate with ORI sequences. First, Orc1 binds to the ORI and recruits Cdc6 and Cdt1, which are responsible for recruiting the helicases, MCM2-7. DDK (Dbf4/Drf1-dependent kinase) directly phosphorylates the MCMs and Cdc45. These modifications facilitate the loading of Cdc45 onto origins, the critical step in activation of MCMs. These events then facilitate downstream phosphorylation of the MCMs by active Cyclin E–Cdk2 in late S phase.

2.2 G2–M Transition

The transition from G2 into M phase involves a number of checks and balances and is regulated primarily by Cyclin B1–Cdk1 (reviewed in refs. 7, 12). Cyclin B1 relies on the activation of Cyclin A–Cdk2 and its modification of transcription factors that transcriptionally upregulate Cyclin B1. This provides an activation loop where Cyclin B1, which solely controls the entry into mitosis, can only be activated in the presence of Cyclin A. Upregulation of Cyclin B1 then begins in late S phase and peaks in G2. Cdk1 levels are kept high to ensure that Cyclin B1 is the rate-limiting factor in the activation of mitosis. During interphase, Cyclin B1–Cdk1 complex is held in its inactive state at centrosomes. Wee1 and Myt1 kinases maintain inhibitory phosphorylation of the Cyclin B1–Cdk1 complex. To initiate entry into mitosis, Cdc25A is required to dephosphorylate Cdk1 and allow for activation of the Cyclin B1–Cdk1 complex. Once activated, Cdk1 phosphorylates its negative and positive regulators Wee1 and Cdc25A, respectively, to maintain activation. Phosphorylation of Wee1 by Cdk1 facilitates the recruitment of Plk1, which further phosphorylates Wee1, leading to its polyubiquitination and degradation. In addition, Plk1 phosphorylates Cdc25A during mitosis, which facilitates its nuclear accumulation to enhance its activity on essential substrates. All these events allow for maximal activation of Cyclin B1 and the progression into mitosis. The APC complex then degrades Cyclin B1 at the end of mitosis to ensure that its activity is lost prior to entry into a new G1 phase.

3 Damage-Activated Cell Cycle Arrest

As discussed earlier, ATM and ATR are the two main activator kinases that function in damage-induced cell cycle arrest. Their activity suppresses cell cycle progression, supports activation of repair pathways, promotes the open chromatin structure required for repair, facilitates repair, and also may promote programmed cell death in the context of excessive or sustained DNA damage (for review *see* refs. 1, 3). Which kinase functions during damage recognition is dependent on when in the cell cycle damage occurs, and how the damage is recognized (Fig. 1).

3.1 Damage-Induced G1–S Checkpoint

The cell has both transcriptional and non-transcriptional mechanisms that prevent S-phase entry in the presence of DNA damage, specifically double-strand breaks. All G1 arrest pathways are initiated by the activation of ATM (reviewed in refs. 13–16). Initially, ATM stalls the cell cycle through the phosphorylation and activation of cell cycle checkpoint protein, Chk2. Chk2 kinase will directly exert control over the cell cycle by modulating the activation of Cdks (Fig. 2). In addition, Chk2 and ATM can target transcription factors themselves to modulate downstream activation of cell cycle inhibitory factors (Fig. 3).

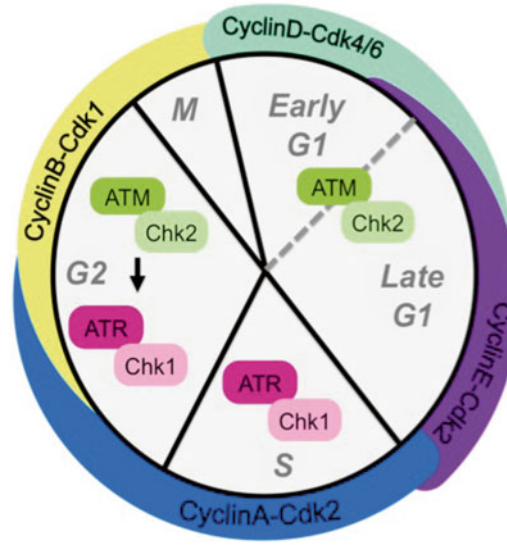

Fig. 1 ATM–Chk2 and ATR–Chk1 cell cycle regulation. ATM and Chk2 are the primary kinases responsible for checkpoint activation in G1 and G2 phases of the cell cycle. ATR and Chk1 kinases are activated by ssDNA substrates and, for this reason, are the primary responders to DNA replication-associated double-strand breaks and stalled replication forks. They are also activated downstream of ATM during G2 phase by recognition of processed ssDNA ends of double-strand breaks

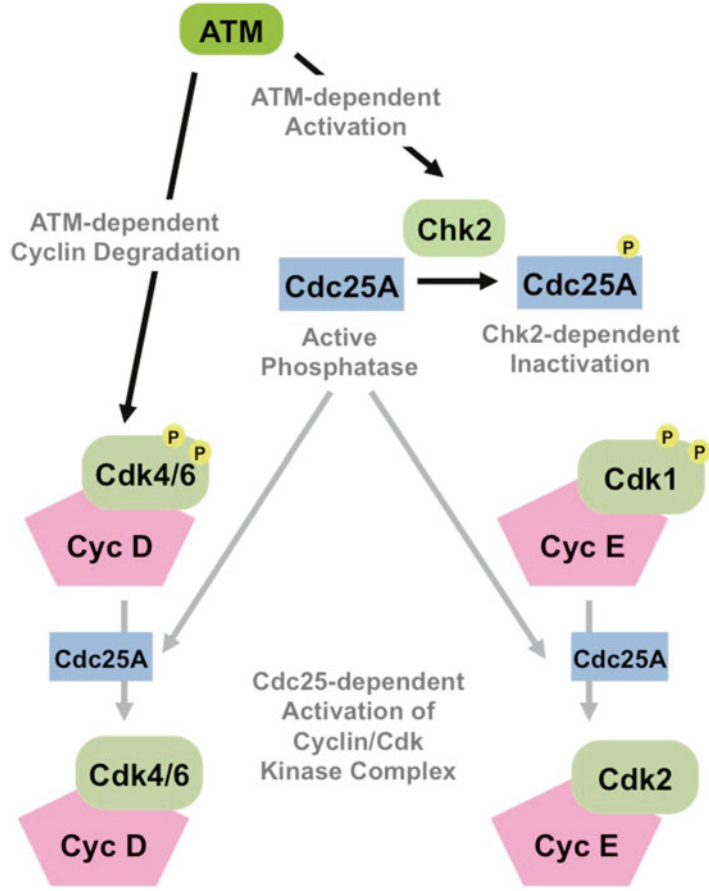

Fig. 2 Transcription-independent G1 arrest. The initial suppression of G1 progression is mediated by posttranslational modification of Cdc25A by Chk2. Chk2 is activated by ATM. Phosphorylation of Cdc25A suppresses its phosphatase activity, which is required for proper Cdk activation (*grey arrows*). In the absence of Cdk activity, cells cannot progress through G1 phase and into S phase

ATM functions directly upstream of Chk2, phosphorylating it on Thr68, allowing for Chk2 auto-phosphorylation, oligomerization, and activation [17]. During the G1–S checkpoint, Chk2 phosphorylates Cdc25A, thereby mediating its degradation. This allows for key inhibitory residues on Cdk2 to remain phosphorylated, thereby inhibiting the transition into S phase [18, 19], which requires the activity of the Cyclin E–Cdk2 complex. This inhibition of Cdk2 relies entirely on posttranslational modifications and the proteasomal degradation pathway. Compared to other mechanisms that require transcriptional upregulation of factors, this response is rapid but is limited by the fact that the Chk2-Cdc25A pathway is only capable of inhibiting further activation of Cdk2. Experiments have shown that in cells damaged during late G1, inhibition of progression into S phase is not strong, allowing cells

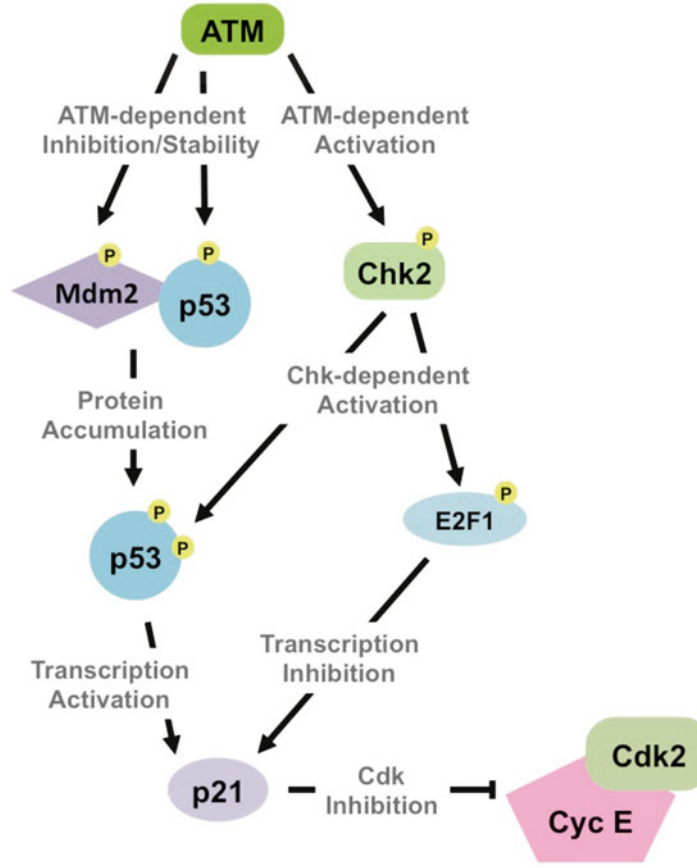

Fig. 3 Transcription-dependent G1 arrest. ATM indirectly modulates transcriptional regulation of cell cycle progression through direct modification of transcription factors, e.g., p53, other factors, e.g., Mdm2, or indirectly through activation of Chk2, which can further modulate transcription factors e.g., p53, E2F1. The downstream consequence of these events is the up regulation of factors such as p21, which inhibit Cdk2 activity

to enter S phase regardless of checkpoint activation and thereby resulting in accumulation of chromosomal breaks in the subsequent G2 phase [20]. This likely represents the cell's inability to suppress the Cdk2 pathway in the face of a high level of Cyclin E–Cdk2 activation. Supportive of this notion, once cells have passed the G1 restriction point, E2F1 initiates a positive feedback loop to further activate Cyclin E–Cdk2 [16].

Additionally, Cyclin D1 has been shown to be a direct target of ATM through phosphorylation of Thr286 [21]. This residue is critical for the suppression of Cyclin D1 in normal S phase. This phosphorylation likely modulates its ubiquitin-mediated degradation, since degradation is dependent on ATM and another unrelated kinase, GSK3β, in response to genotoxic stress [22].

This suppression would likely only function in checkpoint activation in cells that have undergone DNA damage early in G1 phase, when Cyclin D1 is most active.

Cells damaged early in G1, prior to or at the restriction point, are capable of activating a stronger checkpoint response. It has been shown that these cells move more slowly into S phase than cells damaged in late G1; however, the ability to progress into S phase in the presence of DNA damage suggests a general inefficiency of the G1–S checkpoint response, regardless of where in G1 the damage is incurred [23].

In addition to direct modulation of the cell cycle regulators, progression into S phase is transcriptionally regulated through an ATM–p53-mediated response (Fig. 3). The transcription factor p53 and its negative regulator Mdm2 are both phosphorylated by ATM [24, 25]. In addition, Chk2 further phosphorylates p53 in response to DNA damage signaling [26–28]. These modifications stabilize p53 through blocking Mdm2-mediated degradation [26]. Active p53 can then transcriptionally upregulate the Cdk inhibitor, p21 (WAF1/CIP1), which inhibits S-phase entry through its binding to Cyclin E and Cyclin D complexes and inhibiting their Cdk-mediated activities [29, 30]. Evidence suggests the phosphorylation of p53 is also dependent on the activation of other damage response complexes, such as the BRCA1–BARD1 complex [31]. These factors are required for p53-dependent G1–S arrest, and their depletion compromises the p53-dependent upregulation of p21 induced by ionizing radiation [31]. Due to the requirement for transcription, p53-mediated cell cycle arrest is a much slower process, but is essential for complete inhibition of S-phase entry [23, 32, 33]. Transcriptional modulation is likely secondary to the modification of the Cyclin–Cdk complexes themselves, possibly to sustain arrest.

In parallel to the p53 modulation, progression into S phase can be controlled through the modification of E2F1. E2F1 is phosphorylated by Chk2 in response to damage, which results in its stabilization, increased transcriptional activation, and downstream apoptotic signaling [34]. Early studies showed that Chk1 and Chk2 phosphorylate pRb to enhance its interaction with E2F1, and inhibit E2F1-dependent transcription [35]. More recent reports suggest that DNA damage results in multiple pools of post-translationally modified E2F1 molecules that promote or inhibit specific E2F1 functions differentially [36]. There is evidence of cross-talk between p53 and E2F1; E2F1 can bind p53 at promoters such as p21 and BAX, and attenuate p53-dependent induction of transcription, thereby blocking p53-mediated cell cycle arrest [37]. A full understanding of how the different pools of E2F1 may be participating in its conflicting activities during DNA damage checkpoint activation is needed to fully appreciate how this factor modulates checkpoint activation during G1.

Other factors have been shown to be essential for the ATM-mediated cell cycle arrest during G1. p53-binding protein 1 (53BP1) associates with chromatin around DNA double-strand breaks throughout the cell cycle [38]. It has been shown to associate with topoisomerase-binding protein 1 (TopBP1) during the G1 phase of the cell cycle, and this interaction is associated with inhibition of progression from G1 into S phase [38], likely through maintaining ATM-mediated signaling. TopBP1 has also been shown to be associated with intra-S phase checkpoint responses resulting from replication stress, but in this case, it acts downstream of ATR, not ATM [39, 40]. In addition, the MRN complex (Mre11–Rad50–-Nbs1) is necessary for full and sustained ATM activation in G1 and throughout the rest of the cell cycle. The MRN complex may affect modification of specific downstream targets, which suggests that it is also required for full G1–S checkpoint arrest [41].

3.2 Intra-S Phase Checkpoint

Once the cell passes through G1 and enters S phase, DNA damage can interfere with normal replicative processes. The intra-S phase checkpoint is hypothesized to function in two ways: the first and seemingly primary function is to decrease the firing of late origins; secondarily, the elongation process itself is slowed, by the pausing and slowing of replication fork progression (reviewed in refs. 42, 43). ATR is the primary kinase functioning during the intra-S phase checkpoint. ATR and its downstream target Chk1 can modify origin complexes, as well as stabilize the components of the replication fork during stalling (Fig. 4). These events allow for slow progression through S phase to permit repair of lesions that could otherwise cause genetic changes during replication.

Replication stress is thought to increase the ssDNA around replication forks. Uncoupling may occur when the replication machinery runs into DNA lesions, and the replicative helicases continue to unwind the DNA without further DNA synthesis, creating ssDNA substrates for RPA. Increased binding of RPA to ssDNA recruits ATR via its accessory factor ATRIP [44–46]. Through a separate mechanism, the 9-1-1 complex, composed of Rad9–Hus1–Rad1, is recruited to the replication fork and supports ATR activation [47, 48]. TopBP1 is also recruited to the lesion, where it can interact with ATRIP and facilitate the activation of ATR through its auto-phosphorylation [40, 49]. ATR can then activate its substrates, most importantly Chk1, phosphorylating it on two main serine residues, S317 and S345 [50, 51]. Chk1 acts similarly to Chk2 in G1 arrest, suppressing Cyclin–Cdk-dependent activities through inhibition of Cdc25A phosphatase, as well as suppressing other replication-promoting functions. Canonical ATR signaling suggests that, unlike ATM, ATR must be recruited to damaged DNA (RPA-bound ssDNA) for activation.

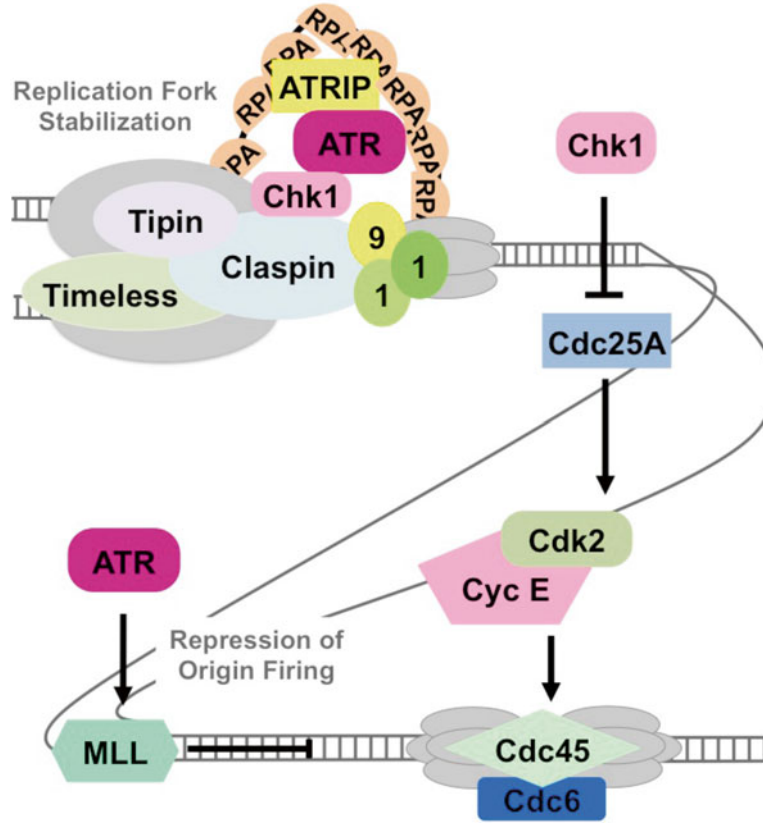

Fig. 4 Intra-S phase checkpoint. Evidence suggests that the ATR–Chk1 cascade can function at the origin to stabilize replication intermediates and promote fork progression. ATR binds directly to replication forks, promoting stabilization when the forks meet a DNA lesion. ATR may function distal to progressing replication forks to suppress late origin firing. In addition, Chk1 can signal directly to S-phase Cyclin E–CDK2 complex to inhibit origin firing

ATR signaling can inhibit firing of origins when DNA damage occurs in S phase. Origin firing is regulated by the loading and activation of the MCM helicase complex and Cdc45. This process requires decreasing trimethylation of histone H3 on lysine 4 (H3K4me3), a modification known to inhibit Cdc45 binding. In response to DNA damage, the enzyme responsible for the H3K4me3 modification, the lysine methyltransferase MLL, is stabilized through phosphorylation by ATR [52]. During S phase, MLL is normally degraded by the SCF^{skp2} ubiquitin ligase [53]; ATR phosphorylation prevents this degradation to maintain H3K4me3 modification and thereby inhibit Cdc45 activity at origins. In addition, inhibition of Cdc25A phosphatase by Chk1 prevents the dephosphorylation and inactivation of Cdk2 [54]. This supports the suppression of Cyclin E–Cdk2 and Cyclin A–Cdk2 complexes, which are required for firing of replication origins and progression

through S phase into G2. Cyclin E–Cdk2 is vital for association of the initiation factor Cdc45 with chromatin at origins; suppression of Cdk activation by Cdc25A actively prevents Cdc45 association and origin firing [55].

Conversely, there is some evidence that ATR can support origin firing. When replication forks stall at regions of DNA damage, dormant origins nearby can fire to promote replication progression. ATR can phosphorylate the MCM2 helicase subunit at origins, a phosphorylation event that supports PLK1 recruitment and origin firing [56–59]. This was shown to support firing only of dormant origins, and not unfired late origins, suggesting that ATR may also function in the recovery of replication after recognition and repair of damaged forks.

In addition to preventing origin firing in the presence of DNA damage, the ATR checkpoint pathway can stabilize the replication fork machinery to promote proper repair or damage bypass when forks meet DNA lesions. During fork stalling, the replication machinery must be maintained stably associated with the replication fork. Dissociation of the replication machinery, can lead to fork reversal and formation of aberrant DNA structures that can be targeted by nucleases, leading to further damage. There is evidence indicating that factors of the replication pausing complex or fork protection complex (FPC), which include Timeless and Tipin, help maintain replication fork structure and support ATR checkpoint signaling in the presence of DNA damage in S phase [60]. Under normal cellular conditions, the FPC helps in coordinating helicase and polymerase activities at replication forks to ensure that the enzymatic functions of fork machinery stay coupled during fork slowing or stalling [61–66]. Timeless, Tipin, and Claspin, members of the FPC, have all been shown to be important in ATR–Chk1 activation in response to DNA damage in S phase [67–70]. Claspin is thought to participate in the regulation of fork progression speed and was shown to directly participate in the recruitment of Chk1. Claspin-dependent recruitment of Chk1 allows it to associate with ATR at replication forks and be activated [71–74]. Timeless and Tipin likely participate by stabilizing the binding of Claspin at replication forks, in addition to maintaining DNA polymerase α association with stalled forks, making participation of these factors in Chk1 activation less direct but still important [67, 68, 75].

Other complexes support ATR–Chk1 signaling in response to S-phase DNA damage. Fanconi anemia (FANC) factors and other related factors form complexes that respond to replication forks that have stalled or collapsed at DNA crosslinks. Independently of the other nine FANC family members, FANCM localizes to replication forks to stabilize and maintain fork progression [76]. FANCM helps to support repair and proper replication in response to DNA damage. Chk1 seems to function upstream by stabilizing FANCM to promote its activities, but additional evidence suggests

that FANCM may provide some stabilization of Chk1 as well [76], making it important for suppressive signaling during S phase.

Coordinated checkpoint responses during S phase help support the completion of S phase and full replication of the cell's genetic material. Release from the checkpoint likely occurs in several ways; most obvious among these is the suppression of ATR activity by the shortening of ssDNA stretches that result from progressing replication. Checkpoint inactivation can also occur through proteasomal degradation of Chk1, which is favored by the same phosphorylation events that promote Chk1 activity [77]. In addition, Claspin can be targeted for degradation to promote Chk1 inactivation [78–80]. This regulation of Chk1 activity and stability suggests tight regulation of the activity of Chk1 during S phase in order to maintain proper but reversible cell cycle arrest. Additional repair factors including Mre11, Brca2, and Rad51 have been shown to be important for proper S phase checkpoint functions, which is likely due to their participation in recombination-dependent repair [81–85].

3.3 G2–M Checkpoint

Cell cycle arrest during G2 is essential to prevent cells with unresolved DNA lesions from progressing into mitosis, when cells are most sensitive to damage due to suppressed repair. Evidence suggests that cell cycle arrest during G2 is complex and requires a large amount of damage. Chk2 and Chk1 are activated by the same factors during G2–M as during G1 and S (reviewed in refs. 16, 62). ATM seems to be the initial kinase activated by damage in G2, and provides downstream activation of Chk2 (reviewed in refs. 13, 62). This occurs immediately, but is unable to sustain cell cycle arrest during G2 on its own. Activation of ATR and its subsequent activation of Chk1 occurs downstream of ATM–Chk2 signaling and seems to be necessary for sustained arrest during G2 (reviewed in ref. 62) (Fig. 5).

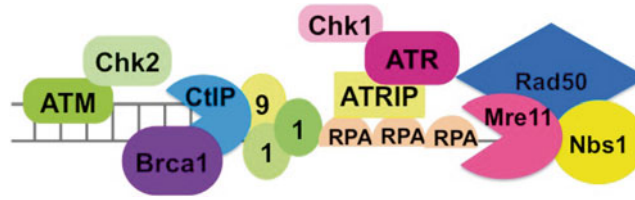

Fig. 5 G2–M checkpoint arrest. Both the ATM and the ATR pathways of damage-induced checkpoint arrest can function during the G2 phase. Evidence suggests that ATM acts primarily to stall the cell cycle in the presence of double-strand breaks. Further suppression is maintained by downstream activation of ATR–Chk1 in the presence of ssDNA intermediates processed for HR-based repair. The downstream consequence of ATM/ATR and Chk2/Chk1 activation is the suppression of Cyclin B–Cdk1 activity, which is required for entry into M phase

In response to DSBs in G2, there is coordinate activation of ATM, the MRN complex, and Brca1–CtIP to allow for DSB processing and the formation of RPA-coated ssDNA, which is then bound by ATR to initiate the downstream activation of Chk1. This processing and activation of the ATR–Chk1 pathway functions to sustain cell cycle arrest in G2 phase to allow for the slower DNA repair by homologous recombination [86–90]. The processing of the ssDNA ends requires the nuclease activity of Mre11 [91, 92], as well as the phosphorylation of Brca1 on S1423 and binding of the nuclease CtIP [93–96]. Similar to S phase checkpoint activation, recruitment of the 9-1-1 complex is also needed for proper suppression of the G2–M transition by ATR [97, 98].

In G2, Cyclin B1–Cdk1 activity, which is required for progression from G2 into mitosis as well as to inhibit entrance into M phase, must be suppressed. Initial Cdc25C phosphorylation by Chk1 and Chk2 increases interaction between Cdc25C and 14-3-3, which impedes its nuclear localization and decreases protein levels, leading to rapid G2 arrest in a dose-independent manner [18, 19, 99, 100]. Sustained arrest is dose dependent and is most easily seen when making comparisons between wild-type cells and cells depleted of ATM, Nbs1, or Brca1 [65]. Studies have shown that 20 or more double-strand breaks are required for prolonged G2 arrest [66, 101, 102].

Cdk2 interacts with Cyclin A throughout the S and G2 phases and can function to positively regulate G2–M checkpoint arrest. Active Cdk2 is maintained through S phase into G2 phase. Cdk2 that is activated in S phase would not be subject to inhibition by Cdc25C, which is induced by damage occurring in the G2 phase. Cells lacking Cdk2 are unable to exclude Cdk1 from the nucleus, and have impaired activation of Chk1 in response to radiation [103]. In addition, Cdk2 participates in stabilizing Cdc6, a factor that binds to the ATR–Chk1–Cdc25A complex and contributes to arrest [103]. Cdc6 functions in the loading of replicative helicases during preparation for S phase; however, depletion of Cdc6 causes aberrant entrance into mitosis and its over-expression induces G2–M arrest [104–109]. Cdc6 modulates anaphase progression by binding to and inhibiting Cdk1, thereby participating in the G2–M checkpoint [103].

The importance of other factors, such as MDC1 and 53BP1, for G2–M checkpoint activation and maintenance is likely through their activities at DSBs where they amplify the ATM/ATR signaling cascades [110]. Although a role for p53-dependent regulation of G2–M arrest has been proposed, how p53 promotes checkpoint activation or maintains checkpoint signaling during G2 is not fully understood.

4 Cell Cycle Factors and Double-Strand Break Repair

In addition to stalling the cell cycle to accommodate the time needed to repair damaged DNA, the cell cycle checkpoint proteins, as well as the Cdks can facilitate activation of repair path-

ways to ensure that the cell utilizes the appropriate repair mechanisms. This allows for the highest fidelity repair possible during each portion of the cell cycle. The strongest evidence seems to suggest that the homologous recombination factors are activated in S and G2–M to allow HR only during these portions of the cell cycle when homologous sister chromatids are available as repair templates.

The earliest example of cell cycle regulation of HR is the modification of the nuclease CtIP by the Cdks, specifically Cdk2. Two independent groups have identified conserved sites CtIP-S327 [111] and CtIP-T847 as sites phosphorylated by Cdks [112, 113]. These modifications modulate CtIP's interaction with its binding partner Brca1 and its ability to promote end resection, an essential priming event in HR repair [111–114]. Secondarily, the Cdk modification of CtIP helps enhance the interaction between CtIP–Brca1 and the MRN complex, helping stimulate the nuclease activity of Mre11 [115]. Cdk2, the S-phase Cdk, modifies CtIP to enhance its activity during S and G2 phases of the cell cycle, when resection and HR repair are optimal [116]. End resection, driven by Mre11 and CtIP is a key event in the process of HR and is irreversible, suggesting that the choice to repair by HR over NHEJ is highly regulated by the cell cycle checkpoints.

In addition to the upstream factors, cell cycle regulatory proteins modulate a number of downstream HR repair enzymes. RPA, the single-strand-binding protein, is phosphorylated on multiple serine residues, by ATR and Cdks, which optimize RPA binding to ssDNA [117, 118]. Downstream of RPA, both Rad51 and its binding partner Brca2 are modulated by checkpoint kinases and Cdks to facilitate events in HR. Both Chk2 and Chk1 have been shown to phosphorylate Rad51 and modulate its interaction with Brca2, an interaction that is required for Rad51 recruitment to and loading onto RPA-coated ssDNA [119]. In addition, Cdk-dependent phosphorylation of Brca2 inhibits the Brca2–Rad51 interaction and, in the context of the cell cycle, has been shown to inhibit HR upon entry into M phase [120]. Finally, there is some evidence that 53BP1, a key factor in the decision to repair by HR or NHEJ in G2 phase, is a target of Cdks in yeast and vertebrates; however, there is an incomplete understanding of how these modifications may affect 53BP1 function [121].

5 Concluding Remarks

There is strong and growing evidence for critical and highly regulated interplay between cell cycle progression and the DNA damage response. Many DNA damage factors are directly involved in normal cell cycle progression, such as BRCA1 and MRN. Moreover, cell cycle factors control repair pathways to ensure high fidelity repair. It is likely that there are a number of yet undiscovered

factors that will prove to be essential for activating and maintaining checkpoints, as well as controlling reentry into the cell cycle. In addition, we know very little about how cell cycle factors influence the choice between repair pathways, and further studies are needed to elucidate these processes and their contribution to genomic stability.

Acknowledgements

The authors are indebted to Oleg Alekseev for editing and to members of the Clifford and Noguchi laboratories for helpful discussions and to W.W. Smith Foundation and the PA Tobacco Settlement Funds for research support. We apologize to colleagues whose research we have failed to cite due to the breadth of the topics.

References

1. Nam EA, Cortez D (2011) ATR signalling: more than meeting at the fork. Biochem J 436(3):527–536
2. Neal JA, Meek K (2011) Choosing the right path: does DNA-PK help make the decision? Mutat Res 711(1–2):73–86
3. Shiloh Y, Ziv Y (2013) The ATM protein kinase: regulating the cellular response to genotoxic stress, and more. Nat Rev Mol Cell Biol 14(4):197–210
4. Chan EH, Santamaria A, Sillje HH, Nigg EA (2008) Plk1 regulates mitotic Aurora A function through betaTrCP-dependent degradation of hBora. Chromosoma 117(5):457–469
5. Langerak P, Russell P (2011) Regulatory networks integrating cell cycle control with DNA damage checkpoints and double-strand break repair. Philos Trans R Soc Lond B Biol Sci 366(1584):3562–3571
6. Donjerkovic D, Scott DW (2000) Regulation of the G1 phase of the mammalian cell cycle. Cell Res 10(1):1–16
7. Satyanarayana A, Kaldis P (2009) Mammalian cell-cycle regulation: several Cdks, numerous cyclins and diverse compensatory mechanisms. Oncogene 28(33):2925–2939
8. Ray D, Kiyokawa H (2008) CDC25A phosphatase: a rate-limiting oncogene that determines genomic stability. Cancer Res 68(5): 1251–1253
9. Kristjansdottir K, Rudolph J (2004) Cdc25 phosphatases and cancer. Chem Biol 11(8): 1043–1051
10. Donzelli M, Draetta GF (2003) Regulating mammalian checkpoints through Cdc25 inactivation. EMBO Rep 4(7):671–677
11. Sacco E, Hasan MM, Alberghina L, Vanoni M (2012) Comparative analysis of the molecular mechanisms controlling the initiation of chromosomal DNA replication in yeast and in mammalian cells. Biotechnol Adv 30(1): 73–98
12. Ohi R, Gould KL (1999) Regulating the onset of mitosis. Curr Opin Cell Biol 11(2): 267–273
13. Abraham RT (2001) Cell cycle checkpoint signaling through the ATM and ATR kinases. Genes Dev 15(17):2177–2196
14. Falck J, Mailand N, Syljuasen RG, Bartek J, Lukas J (2001) The ATM-Chk2-Cdc25A checkpoint pathway guards against radioresistant DNA synthesis. Nature 410(6830): 842–847
15. Bartek J, Lukas J (2001) Mammalian G1- and S-phase checkpoints in response to DNA damage. Curr Opin Cell Biol 13(6):738–747
16. Deckbar D, Jeggo PA, Lobrich M (2011) Understanding the limitations of radiation-induced cell cycle checkpoints. Crit Rev Biochem Mol Biol 46(4):271–283
17. Brown EJ, Baltimore D (2003) Essential and dispensable roles of ATR in cell cycle arrest and genome maintenance. Genes Dev 17(5): 615–628
18. Peng CY, Graves PR, Thoma RS, Wu Z, Shaw AS, Piwnica-Worms H (1997) Mitotic and G2 checkpoint control: regulation of 14-3-3 protein binding by phosphorylation of Cdc25C on serine-216. Science 277(5331): 1501–1505
19. Sanchez Y, Wong C, Thoma RS, Richman R, Wu Z, Piwnica-Worms H, Elledge SJ (1997) Conservation of the Chk1 checkpoint pathway in mammals: linkage of DNA damage to Cdk

regulation through Cdc25. Science 277(5331): 1497–1501

20. Deckbar D, Stiff T, Koch B, Reis C, Lobrich M, Jeggo PA (2010) The limitations of the G1-S checkpoint. Cancer Res 70(11): 4412–4421
21. Hitomi M, Yang K, Stacey AW, Stacey DW (2008) Phosphorylation of cyclin D1 regulated by ATM or ATR controls cell cycle progression. Mol Cell Biol 28(17):5478–5493
22. Pontano LL, Aggarwal P, Barbash O, Brown EJ, Bassing CH, Diehl JA (2008) Genotoxic stress-induced cyclin D1 phosphorylation and proteolysis are required for genomic stability. Mol Cell Biol 28(23):7245–7258
23. Di Leonardo A, Linke SP, Clarkin K, Wahl GM (1994) DNA damage triggers a prolonged p53-dependent G1 arrest and long-term induction of Cip1 in normal human fibroblasts. Genes Dev 8(21):2540–2551
24. Maya R, Balass M, Kim ST, Shkedy D, Leal JF, Shifman O, Moas M, Buschmann T, Ronai Z, Shiloh Y, Kastan MB, Katzir E, Oren M (2001) ATM-dependent phosphorylation of Mdm2 on serine 395: role in p53 activation by DNA damage. Genes Dev 15(9):1067–1077
25. Zhang Y, Xiong Y (2001) A p53 amino-terminal nuclear export signal inhibited by DNA damage-induced phosphorylation. Science 292(5523):1910–1915
26. Chehab NH, Malikzay A, Appel M, Halazonetis TD (2000) Chk2/hCds1 functions as a DNA damage checkpoint in G(1) by stabilizing p53. Genes Dev 14(3):278–288
27. Hirao A, Kong YY, Matsuoka S, Wakeham A, Ruland J, Yoshida H, Liu D, Elledge SJ, Mak TW (2000) DNA damage-induced activation of p53 by the checkpoint kinase Chk2. Science 287(5459):1824–1827
28. Shieh SY, Ahn J, Tamai K, Taya Y, Prives C (2000) The human homologs of checkpoint kinases Chk1 and Cds1 (Chk2) phosphorylate p53 at multiple DNA damage-inducible sites. Genes Dev 14(3):289–300
29. Sherr CJ, Roberts JM (1999) CDK inhibitors: positive and negative regulators of G1-phase progression. Genes Dev 13(12):1501–1512
30. Agami R, Bernards R (2000) Distinct initiation and maintenance mechanisms cooperate to induce G1 cell cycle arrest in response to DNA damage. Cell 102(1):55–66
31. Fabbro M, Savage K, Hobson K, Deans AJ, Powell SN, McArthur GA, Khanna KK (2004) BRCA1-BARD1 complexes are required for p53Ser-15 phosphorylation and a G1/S arrest following ionizing radiation-induced DNA damage. J Biol Chem 279(30):31251–31258
32. Wahl GM, Linke SP, Paulson TG, Huang LC (1997) Maintaining genetic stability through TP53 mediated checkpoint control. Cancer Surv 29:183–219
33. Yamauchi M, Oka Y, Yamamoto M, Niimura K, Uchida M, Kodama S, Watanabe M, Sekine I, Yamashita S, Suzuki K (2008) Growth of persistent foci of DNA damage checkpoint factors is essential for amplification of G1 checkpoint signaling. DNA Repair (Amst) 7(3):405–417
34. Stevens C, Smith L, La Thangue NB (2003) Chk2 activates E2F-1 in response to DNA damage. Nat Cell Biol 5(5):401–409
35. Inoue Y, Kitagawa M, Taya Y (2007) Phosphorylation of pRB at Ser612 by Chk1/2 leads to a complex between pRB and E2F-1 after DNA damage. EMBO J 26(8):2083–2093
36. Carnevale J, Palander O, Seifried LA, Dick FA (2012) DNA damage signals through differentially modified E2F1 molecules to induce apoptosis. Mol Cell Biol 32(5):900–912
37. Yoshihara Y, Wu D, Kubo N, Sang M, Nakagawara A, Ozaki T (2012) Inhibitory role of E2F-1 in the regulation of tumor suppressor p53 during DNA damage response. Biochem Biophys Res Commun 421(1):57–63
38. Cescutti R, Negrini S, Kohzaki M, Halazonetis TD (2010) TopBP1 functions with 53BP1 in the G1 DNA damage checkpoint. EMBO J 29(21):3723–3732
39. Kumagai A, Lee J, Yoo HY, Dunphy WG (2006) TopBP1 activates the ATR-ATRIP complex. Cell 124(5):943–955
40. Mordes DA, Glick GG, Zhao R, Cortez D (2008) TopBP1 activates ATR through ATRIP and a PIKK regulatory domain. Genes Dev 22(11):1478–1489
41. Girard PM, Riballo E, Begg AC, Waugh A, Jeggo PA (2002) Nbs1 promotes ATM dependent phosphorylation events including those required for G1/S arrest. Oncogene 21(27): 4191–4199
42. Labib K, De Piccoli G (2011) Surviving chromosome replication: the many roles of the S-phase checkpoint pathway. Philos Trans R Soc Lond B Biol Sci 366(1584):3554–3561
43. Grallert B, Boye E (2008) The multiple facets of the intra-S checkpoint. Cell Cycle 7(15): 2315–2320
44. Rouse J, Jackson SP (2002) Interfaces between the detection, signaling, and repair of DNA damage. Science 297(5581):547–551
45. Zou L, Elledge SJ (2003) Sensing DNA damage through ATRIP recognition of RPA-ssDNA complexes. Science 300(5625):1542–1548
46. Namiki Y, Zou L (2006) ATRIP associates with replication protein A-coated ssDNA

through multiple interactions. Proc Natl Acad Sci U S A 103(3):580–585

47. Kondo T, Wakayama T, Naiki T, Matsumoto K, Sugimoto K (2001) Recruitment of Mec1 and Ddc1 checkpoint proteins to double-strand breaks through distinct mechanisms. Science 294(5543):867–870
48. Melo JA, Cohen J, Toczyski DP (2001) Two checkpoint complexes are independently recruited to sites of DNA damage in vivo. Genes Dev 15(21):2809–2821
49. Matsuno K, Kumano M, Kubota Y, Hashimoto Y, Takisawa H (2006) The N-terminal non-catalytic region of Xenopus RecQ4 is required for chromatin binding of DNA polymerase alpha in the initiation of DNA replication. Mol Cell Biol 26(13):4843–4852
50. Liu Q, Guntuku S, Cui XS, Matsuoka S, Cortez D, Tamai K, Luo G, Carattini-Rivera S, DeMayo F, Bradley A, Donehower LA, Elledge SJ (2000) Chk1 is an essential kinase that is regulated by Atr and required for the G(2)/M DNA damage checkpoint. Genes Dev 14(12): 1448–1459
51. Zhao H, Watkins JL, Piwnica-Worms H (2002) Disruption of the checkpoint kinase 1/cell division cycle 25A pathway abrogates ionizing radiation-induced S and G2 checkpoints. Proc Natl Acad Sci U S A 99(23):14795–14800
52. Liu H, Takeda S, Kumar R, Westergard TD, Brown EJ, Pandita TK, Cheng EH, Hsieh JJ (2010) Phosphorylation of MLL by ATR is required for execution of mammalian S-phase checkpoint. Nature 467(7313):343–346
53. Liu H, Cheng EH, Hsieh JJ (2007) Bimodal degradation of MLL by SCFSkp2 and APCCdc20 assures cell cycle execution: a critical regulatory circuit lost in leukemogenic MLL fusions. Genes Dev 21(19):2385–2398
54. Sorensen CS, Syljuasen RG, Falck J, Schroeder T, Ronnstrand L, Khanna KK, Zhou BB, Bartek J, Lukas J (2003) Chk1 regulates the S phase checkpoint by coupling the physiological turnover and ionizing radiation-induced accelerated proteolysis of Cdc25A. Cancer Cell 3(3):247–258
55. Liu P, Barkley LR, Day T, Bi X, Slater DM, Alexandrow MG, Nasheuer HP, Vaziri C (2006) The Chk1-mediated S-phase checkpoint targets initiation factor Cdc45 via a Cdc25A/Cdk2-independent mechanism. J Biol Chem 281(41):30631–30644
56. Deckbar D, Birraux J, Krempler A, Tchouandong L, Beucher A, Walker S, Stiff T, Jeggo P, Lobrich M (2007) Chromosome breakage after G2 checkpoint release. J Cell Biol 176(6):749–755
57. Trenz K, Errico A, Costanzo V (2008) Plx1 is required for chromosomal DNA replication under stressful conditions. EMBO J 27(6): 876–885
58. Yoo HY, Shevchenko A, Shevchenko A, Dunphy WG (2004) Mcm2 is a direct substrate of ATM and ATR during DNA damage and DNA replication checkpoint responses. J Biol Chem 279(51):53353–53364
59. Ge XQ, Blow JJ (2010) Chk1 inhibits replication factory activation but allows dormant origin firing in existing factories. J Cell Biol 191(7):1285–1297
60. Leman AR, Noguchi C, Lee CY, Noguchi E (2010) Human Timeless and Tipin stabilize replication forks and facilitate sister-chromatid cohesion. J Cell Sci 123(Pt 5):660–670
61. Nedelcheva MN, Roguev A, Dolapchiev LB, Shevchenko A, Taskov HB, Stewart AF, Stoynov SS (2005) Uncoupling of unwinding from DNA synthesis implies regulation of MCM helicase by Tof1/Mrc1/Csm3 checkpoint complex. J Mol Biol 347(3):509–521
62. Lobrich M, Jeggo PA (2007) The impact of a negligent G2/M checkpoint on genomic instability and cancer induction. Nat Rev Cancer 7(11):861–869
63. Errico A, Costanzo V, Hunt T (2007) Tipin is required for stalled replication forks to resume DNA replication after removal of aphidicolin in Xenopus egg extracts. Proc Natl Acad Sci U S A 104(38):14929–14934
64. Katou Y, Kanoh Y, Bando M, Noguchi H, Tanaka H, Ashikari T, Sugimoto K, Shirahige K (2003) S-phase checkpoint proteins Tof1 and Mrc1 form a stable replication-pausing complex. Nature 424(6952):1078–1083
65. Smith KD, Fu MA, Brown EJ (2009) Tim-Tipin dysfunction creates an indispensible reliance on the ATR-Chk1 pathway for continued DNA synthesis. J Cell Biol 187(1):15–23
66. Gambus A, van Deursen F, Polychronopoulos D, Foltman M, Jones RC, Edmondson RD, Calzada A, Labib K (2009) A key role for Ctf4 in coupling the MCM2-7 helicase to DNA polymerase alpha within the eukaryotic replisome. EMBO J 28(19):2992–3004
67. Leman AR, Noguchi E (2012) Local and global functions of Timeless and Tipin in replication fork protection. Cell Cycle 11(21): 3945–3955
68. Yao G, Lee TJ, Mori S, Nevins JR, You L (2008) A bistable Rb-E2F switch underlies the restriction point. Nat Cell Biol 10(4):476–482
69. Shimmoto M, Matsumoto S, Odagiri Y, Noguchi E, Russell P, Masai H (2009) Interactions between Swi1-Swi3, Mrc1 and S

phase kinase, Hsk1 may regulate cellular responses to stalled replication forks in fission yeast. Genes Cells 14(6):669–682

70. Yoshizawa-Sugata N, Masai H (2007) Human Tim/Timeless-interacting protein, Tipin, is required for efficient progression of S phase and DNA replication checkpoint. J Biol Chem 282(4):2729–2740
71. Szyjka SJ, Viggiani CJ, Aparicio OM (2005) Mrc1 is required for normal progression of replication forks throughout chromatin in S. cerevisiae. Mol Cell 19(5):691–697
72. Tourriere H, Versini G, Cordon-Preciado V, Alabert C, Pasero P (2005) Mrc1 and Tof1 promote replication fork progression and recovery independently of Rad53. Mol Cell 19(5):699–706
73. Hodgson B, Calzada A, Labib K (2007) Mrc1 and Tof1 regulate DNA replication forks in different ways during normal S phase. Mol Biol Cell 18(10):3894–3902
74. Lou H, Komata M, Katou Y, Guan Z, Reis CC, Budd M, Shirahige K, Campbell JL (2008) Mrc1 and DNA polymerase epsilon function together in linking DNA replication and the S phase checkpoint. Mol Cell 32(1):106–117
75. Chou DM, Elledge SJ (2006) Tipin and Timeless form a mutually protective complex required for genotoxic stress resistance and checkpoint function. Proc Natl Acad Sci U S A 103(48):18143–18147
76. Luke-Glaser S, Luke B, Grossi S, Constantinou A (2010) FANCM regulates DNA chain elongation and is stabilized by S-phase checkpoint signalling. EMBO J 29(4):795–805
77. Zhang YW, Otterness DM, Chiang GG, Xie W, Liu YC, Mercurio F, Abraham RT (2005) Genotoxic stress targets human Chk1 for degradation by the ubiquitin-proteasome pathway. Mol Cell 19(5):607–618
78. Mailand N, Bekker-Jensen S, Bartek J, Lukas J (2006) Destruction of Claspin by SCFbetaTrCP restrains Chk1 activation and facilitates recovery from genotoxic stress. Mol Cell 23(3): 307–318
79. Mamely I, van Vugt MA, Smits VA, Semple JI, Lemmens B, Perrakis A, Medema RH, Freire R (2006) Polo-like kinase-1 controls proteasome-dependent degradation of Claspin during checkpoint recovery. Curr Biol 16(19): 1950–1955
80. Peschiaroli A, Dorrello NV, Guardavaccaro D, Venere M, Halazonetis T, Sherman NE, Pagano M (2006) SCFbetaTrCP-mediated degradation of Claspin regulates recovery from the DNA replication checkpoint response. Mol Cell 23(3):319–329
81. Kramer A, Mailand N, Lukas C, Syljuasen RG, Wilkinson CJ, Nigg EA, Bartek J, Lukas J (2004) Centrosome-associated Chk1 prevents premature activation of cyclin-B-Cdk1 kinase. Nat Cell Biol 6(9):884–891
82. Loffler H, Lukas J, Bartek J, Kramer A (2006) Structure meets function–centrosomes, genome maintenance and the DNA damage response. Exp Cell Res 312(14):2633–2640
83. Bryant HE, Petermann E, Schultz N, Jemth AS, Loseva O, Issaeva N, Johansson F, Fernandez S, McGlynn P, Helleday T (2009) PARP is activated at stalled forks to mediate Mre11-dependent replication restart and recombination. EMBO J 28(17):2601–2615
84. Hashimoto Y, Ray Chaudhuri A, Lopes M, Costanzo V (2010) Rad51 protects nascent DNA from Mre11-dependent degradation and promotes continuous DNA synthesis. Nat Struct Mol Biol 17(11):1305–1311
85. Schlacher K, Christ N, Siaud N, Egashira A, Wu H, Jasin M (2011) Double-strand break repair-independent role for BRCA2 in blocking stalled replication fork degradation by MRE11. Cell 145(4):529–542
86. Lindqvist A, van Zon W, Karlsson Rosenthal C, Wolthuis RM (2007) Cyclin B1-Cdk1 activation continues after centrosome separation to control mitotic progression. PLoS Biol 5(5): e123
87. Adams KE, Medhurst AL, Dart DA, Lakin ND (2006) Recruitment of ATR to sites of ionising radiation-induced DNA damage requires ATM and components of the MRN protein complex. Oncogene 25(28):3894–3904
88. Cuadrado M, Martinez-Pastor B, Fernandez-Capetillo O (2006) ATR activation in response to ionizing radiation: still ATM territory. Cell Div 1(1):7
89. Warmerdam DO, Kanaar R (2010) Dealing with DNA damage: relationships between checkpoint and repair pathways. Mutat Res 704(1–3):2–11
90. Shiotani B, Zou L (2009) Single-stranded DNA orchestrates an ATM-to-ATR switch at DNA breaks. Mol Cell 33(5):547–558
91. Jazayeri A, Falck J, Lukas C, Bartek J, Smith GC, Lukas J, Jackson SP (2006) ATM- and cell cycle-dependent regulation of ATR in response to DNA double-strand breaks. Nat Cell Biol 8(1):37–45
92. Myers JS, Cortez D (2006) Rapid activation of ATR by ionizing radiation requires ATM and Mre11. J Biol Chem 281(14):9346–9350
93. Taylor WR, Stark GR (2001) Regulation of the G2/M transition by p53. Oncogene 20(15): 1803–1815

94. Yarden RI, Pardo-Reoyo S, Sgagias M, Cowan KH, Brody LC (2002) BRCA1 regulates the G2/M checkpoint by activating Chk1 kinase upon DNA damage. Nat Genet 30(3): 285–289
95. Xu B, Kim S, Kastan MB (2001) Involvement of Brca1 in S-phase and G(2)-phase checkpoints after ionizing irradiation. Mol Cell Biol 21(10):3445–3450
96. Cortez D, Wang Y, Qin J, Elledge SJ (1999) Requirement of ATM-dependent phosphorylation of brca1 in the DNA damage response to double-strand breaks. Science 286(5442): 1162–1166
97. Pandita TK (2006) Role of mammalian Rad9 in genomic stability and ionizing radiation response. Cell Cycle 5(12):1289–1291
98. Pandita RK, Sharma GG, Laszlo A, Hopkins KM, Davey S, Chakhparonian M, Gupta A, Wellinger RJ, Zhang J, Powell SN, Roti Roti JL, Lieberman HB, Pandita TK (2006) Mammalian Rad9 plays a role in telomere stability, S- and G2-phase-specific cell survival, and homologous recombinational repair. Mol Cell Biol 26(5):1850–1864
99. Dalal SN, Schweitzer CM, Gan J, DeCaprio JA (1999) Cytoplasmic localization of human cdc25C during interphase requires an intact 14-3-3 binding site. Mol Cell Biol 19(6): 4465–4479
100. Takizawa CG, Morgan DO (2000) Control of mitosis by changes in the subcellular location of cyclin-B1-Cdk1 and Cdc25C. Curr Opin Cell Biol 12(6):658–665
101. Marples B (2004) Is low-dose hyperradiosensitivity a measure of G2-phase cell radiosensitivity? Cancer Metastasis Rev 23 (3–4):197–207
102. Marples B, Wouters BG, Collis SJ, Chalmers AJ, Joiner MC (2004) Low-dose hyperradiosensitivity: a consequence of ineffective cell cycle arrest of radiation-damaged G2-phase cells. Radiat Res 161(3):247–255
103. Chung JH, Bunz F (2010) Cdk2 is required for p53-independent G2/M checkpoint control. PLoS Genet 6(2):e1000863
104. Borlado LR, Mendez J (2008) CDC6: from DNA replication to cell cycle checkpoints and oncogenesis. Carcinogenesis 29(2):237–243
105. Clay-Farrace L, Pelizon C, Santamaria D, Pines J, Laskey RA (2003) Human replication protein Cdc6 prevents mitosis through a checkpoint mechanism that implicates Chk1. EMBO J 22(3):704–712
106. Lau E, Zhu C, Abraham RT, Jiang W (2006) The functional role of Cdc6 in S-G2/M in mammalian cells. EMBO Rep 7(4): 425–430
107. Liu L, Choi JH, Yim H, Choi JS, Park BD, Cho SJ, Lee SK (2009) ATR (AT mutated Rad3 related) activity stabilizes Cdc6 and delays G2/M-phase entry during hydroxyurea-induced S-phase arrest of HeLa cells. Int J Biochem Cell Biol 41(6):1410–1420
108. Oehlmann M, Score AJ, Blow JJ (2004) The role of Cdc6 in ensuring complete genome licensing and S phase checkpoint activation. J Cell Biol 165(2):181–190
109. Fersht N, Hermand D, Hayles J, Nurse P (2007) Cdc18/CDC6 activates the Rad3-dependent checkpoint in the fission yeast. Nucleic Acids Res 35(16):5323–5337
110. Shibata A, Barton O, Noon AT, Dahm K, Deckbar D, Goodarzi AA, Lobrich M, Jeggo PA (2010) Role of ATM and the damage response mediator proteins 53BP1 and MDC1 in the maintenance of G(2)/M checkpoint arrest. Mol Cell Biol 30(13): 3371–3383
111. Yu X, Wu LC, Bowcock AM, Aronheim A, Baer R (1998) The C-terminal (BRCT) domains of BRCA1 interact in vivo with CtIP, a protein implicated in the CtBP pathway of transcriptional repression. J Biol Chem 273(39):25388–25392
112. Huertas P, Jackson SP (2009) Human CtIP mediates cell cycle control of DNA end resection and double strand break repair. J Biol Chem 284(14):9558–9565
113. Huertas P, Cortes-Ledesma F, Sartori AA, Aguilera A, Jackson SP (2008) CDK targets Sae2 to control DNA-end resection and homologous recombination. Nature 455 (7213):689–692
114. Sartori AA, Lukas C, Coates J, Mistrik M, Fu S, Bartek J, Baer R, Lukas J, Jackson SP (2007) Human CtIP promotes DNA end resection. Nature 450(7169):509–514
115. Chen L, Nievera CJ, Lee AY, Wu X (2008) Cell cycle-dependent complex formation of BRCA1.CtIP.MRN is important for DNA double-strand break repair. J Biol Chem 283(12):7713–7720
116. Wu-Baer F, Baer R (2001) Effect of DNA damage on a BRCA1 complex. Nature 414(6859):36
117. Din S, Brill SJ, Fairman MP, Stillman B (1990) Cell-cycle-regulated phosphorylation of DNA replication factor A from human and yeast cells. Genes Dev 4(6):968–977
118. Anantha RW, Vassin VM, Borowiec JA (2007) Sequential and synergistic modification of

human RPA stimulates chromosomal DNA repair. J Biol Chem 282(49):35910–35923

119. Bahassi EM, Ovesen JL, Riesenberg AL, Bernstein WZ, Hasty PE, Stambrook PJ (2008) The checkpoint kinases Chk1 and Chk2 regulate the functional associations between hBRCA2 and Rad51 in response to DNA damage. Oncogene 27(28): 3977–3985
120. Esashi F, Christ N, Gannon J, Liu Y, Hunt T, Jasin M, West SC (2005) CDK-dependent phosphorylation of BRCA2 as a regulatory mechanism for recombinational repair. Nature 434(7033):598–604
121. Wang G, Tong X, Weng S, Zhou H (2012) Multiple phosphorylation of Rad9 by CDK is required for DNA damage checkpoint activation. Cell Cycle 11(20):3792–3800

Chapter 4

Cell Cycle Regulation by Protein Degradation

Deanna M. Koepp

Abstract

Cell division is controlled by a highly regulated program to accurately duplicate and segregate chromosomes. An important feature of the cell cycle regulatory program is that key cell cycle proteins are present and active during specific cell cycle stages but are later removed or inhibited to maintain appropriate timing. The ubiquitin–proteasome system has emerged as an important mechanism to target cell cycle proteins for degradation at critical junctures during cell division. Two key E3 ubiquitin ligase complexes that target key cell cycle proteins are the Skp1–Cul1–F-box protein complex and the anaphase-promoting complex/cyclosome. This chapter focuses on the role of these E3 ubiquitin ligases and how ubiquitin-dependent degradation of central cell cycle regulatory proteins advances the cell cycle.

Key words Cell cycle, Ubiquitin, Proteasome, Ubiquitin ligase, Anaphase-promoting complex, Cyclosome, Skp1/Cul1/F-box protein complex, Cyclin, Cyclin-dependent kinase

1 Introduction

Cells are driven to grow and divide by a coordinated series of events collectively called the cell cycle. An important feature of the cell cycle regulatory program is that specific proteins are present and active during critical cell cycle stages but then are removed or inhibited to maintain appropriate timing. The ubiquitin–proteasome system has emerged as an important regulatory mechanism to target cell cycle proteins for degradation at critical junctures during cell division.

Progression through the cell cycle is accomplished primarily by the activity of a family of kinases, the cyclin-dependent kinases (CDKs). The ubiquitin–proteasome system is key to regulating the activity of CDKs and other cell cycle factors, many of which are CDK targets. The activity of CDKs is controlled such that specific kinase complexes are active only during critical cell cycle transitions. CDK activity is regulated by access to partner proteins, cyclins, and inhibitory complexes, the cyclin-dependent kinase inhibitors (CKIs). Many key cell cycle factors in addition to those that

Eishi Noguchi and Mariana C. Gadaleta (eds.), *Cell Cycle Control: Mechanisms and Protocols*, Methods in Molecular Biology, vol. 1170, DOI 10.1007/978-1-4939-0888-2_4,

directly affect CDK activity are also targeted for ubiquitin-mediated proteolysis. Moreover, pathways that intersect with the cell cycle regulatory program, such as checkpoint systems, stress responses, and nutrient sensing and signaling pathways are regulated by the ubiquitin–proteasome system, thus indicating the wide impact this system has on cell proliferation in general. However, this chapter focuses on the role of ubiquitin-dependent degradation in the core cell cycle regulatory program.

2 The Ubiquitin–Proteasome System

The formation of ubiquitin conjugates requires the activity of three enzymes (Fig. 1a). A ubiquitin-activating enzyme (E1) covalently attaches to the small polypeptide ubiquitin [1] and transfers it to an E2 or ubiquitin-conjugating enzyme [2]. The E2 transfers ubiquitin to a substrate protein, often with a third enzyme, the ubiquitin ligase (E3) [3]. Multiple rounds of this cycle lead to polyubiquitination of the substrate protein [4]. Because ubiquitin contains multiple lysine residues, there are different types of linkages that can be used to generate ubiquitin chains. To be recognized and destroyed by the 26S proteasome, a protein is frequently modified with a chain of at least four ubiquitins, typically using lysine 48 (K48) chain linkages [5]. Ubiquitin receptor proteins recognize ubiquitin chains and target the modified protein to the regulatory subunit of the 26S proteasome (reviewed in ref. 6). At the proteasome, ubiquitin chains are trimmed and cleaved by the action of de-ubiquitination enzymes and the substrate protein is unfolded to enter the central core of the proteasome, which is composed of proteases that sever peptide bonds [6, 7]. The substrate protein is digested to short stretches of amino acids and released from the proteasome; these short peptides are eventually cleaved to free amino acids by isopeptidases in the cytosol [6, 8].

The primary means of specificity in this process is provided by the E3 ubiquitin ligase. As such, ubiquitin ligases are prime targets for regulation themselves. Restricting access to E3 ubiquitin ligases or controlling their activities has significant impacts on the ubiquitination of their respective substrate proteins. Two types of ubiquitin ligases have substantial roles in regulating cell cycle transitions, the Skp1–Cul1–F-box protein (SCF) complex family and the anaphase-promoting complex/cyclosome (APC/C) (reviewed in refs. 9–11). The SCF and APC/C complexes belong to a broader family of cullin–RING ubiquitin ligases (CRLs). RING domain-containing proteins are important for interacting with E2 enzymes, whereas cullin proteins often serve as scaffolds to assemble multicomponent E3 complexes [10].

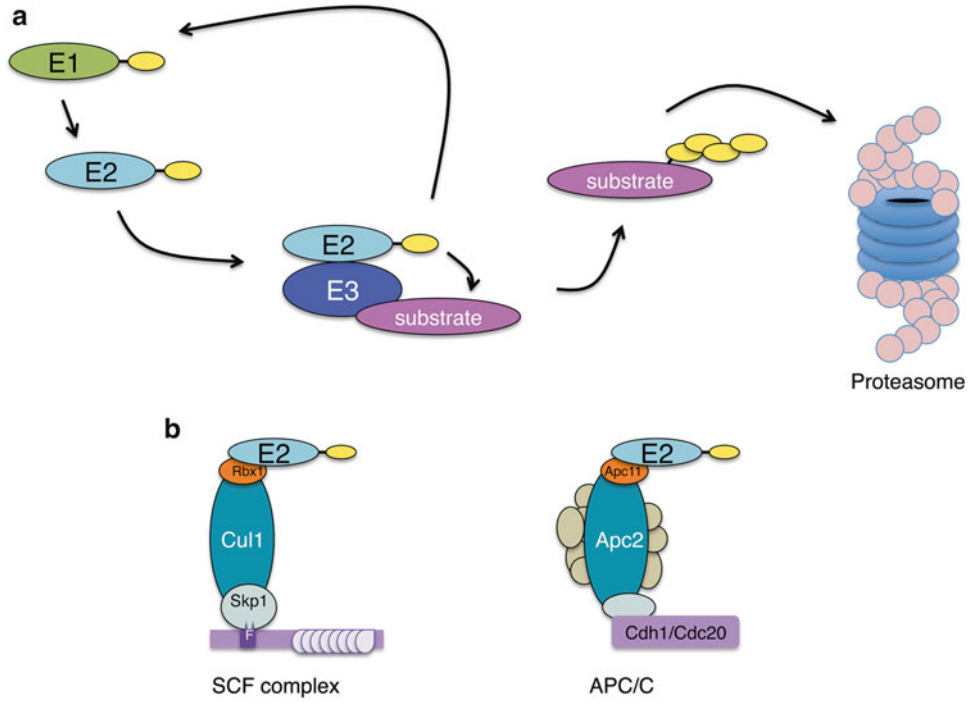

Fig. 1 (**a**) Schematic diagram of the ubiquitination of a substrate protein targeted for degradation by the proteasome. Ubiquitin (*ovals*) is first attached to the E1 ubiquitin-activating enzyme and then is transferred to the E2 ubiquitin-conjugating enzyme. The E3 ubiquitin ligase recognizes and binds the substrate protein. The coordinated effort of the E2 and E3 enzymes transfers ubiquitin to a lysine side chain on the substrate protein. Multiple rounds of this cycle can produce polyubiquitin chains on the substrate, which is then targeted to the proteasome. (**b**) The architecture of the APC/C and SCF E3 ubiquitin ligases, two E3 complexes in the CRL family that target many cell cycle factors for ubiquitin-mediated destruction. Each complex contains a RING protein (Rbx1 in SCF, Apc11 in APC/C) and a cullin scaffold protein (Cul1 in SCF, Apc2 in APC/C). There are many substrate adaptor proteins called F-box proteins in the SCF complex, which interact with the Skp1 bridging protein via the F-box domain, whereas the APC/C has two substrate adaptors (Cdc20 and Cdh1). The APC/C contains a number of other proteins that contribute to its function and regulation that are not conserved with the SCF complex

2.1 The SCF Ubiquitin Ligase Complex

The SCF family is one of the largest groups of E3 ubiquitin ligases and has many targets throughout the cell cycle, but a substantial number of core cell cycle components during the G1-to-S phase transition. The SCF has four components, Skp1, Cdc53/Cul1 (the cullin protein), an F-box-containing protein, and the RING protein Rbx1/Roc1/Hrt1 [12–18] (Fig. 1b). Skp1 and F-box proteins interact with each other via the F-box domain. F-box proteins act as adapters between substrates and the rest of the E3 complex [12]. There are multiple SCF complexes, and the F-box protein that is bound determines the specificity of the complex. Many F-box proteins contain repeat domains in their C-termini, which are involved in binding the substrate protein (reviewed in ref. 19).

Access to F-box proteins is often regulated to control ubiquitination of substrates. For example, in many SCF complexes, phosphorylation of the target protein is required for interaction with its cognate F-box protein [19]. Furthermore, F-box proteins themselves are often unstable and targeted for degradation, either through autoubiquitination or distinct E3 ubiquitin ligases [20–22].

2.2 The APC/C Ubiquitin Ligase Complex

The APC/C is a large, multicomponent ubiquitin ligase complex composed of more than a dozen individual proteins and is active during mitosis through G1. The RING-containing protein Apc11 interacts with E2 enzymes, and the cullin protein Apc2 serves as a scaffold (reviewed in ref. 11) (Fig. 1b). Substrate adaptor proteins for the APC/C include Cdh1 (Hct1/Ste9/Fzr) and Cdc20 (Slp1/Fzy) [23], which interact with substrate proteins by recognizing specific degradation domains called degrons (reviewed in refs. 24–27). The degrons recognized by the APC/C include the D-box and KEN box, each of which is a short conserved sequence (6–9 amino acids) [28, 29].

The activity of the APC/C is regulated by CDK phosphorylation of core APC/C components [30] and pseudo-substrate inhibitors [31–33], which help to limit the function of the complex to mitosis and G1. Interestingly, recent work suggests that in higher eukaryotes, the APC/C functions with an E2 enzyme that preferentially builds lysine 11 (K11) ubiquitin chain linkages to target substrates for degradation by the proteasome [34].

3 Major Cell Cycle Transitions

Each cell cycle must accomplish two key steps: the accurate duplication of genetic material during S phase and the precise segregation of chromosomes into two daughter cells during mitosis. These processes are highly conserved, and the role of ubiquitin-dependent proteolysis is critical to each step. The periodicity of CDK activity, low at the end of mitosis through early G1 and then high during the remainder of the cell cycle, is accomplished in part by the proteolysis of cyclins and CKIs at specific transitions.

3.1 Progression from G1 Phase Through DNA Replication

Both the APC/C and the SCF complexes have important roles in the regulation of the G1-to-S phase transition (Fig. 2). Moreover, these two complexes control each other's activities, thus enforcing another level of periodicity in the cell cycle.

During G1 phase, CDK activity is kept in check by the accumulation of CKIs. In budding yeast, the key CKI that must be degraded at the G1-to-S phase transition to initiate S phase is Sic1 and was the initial substrate that led to the identification of SCF complexes. The SCF^{Cdc4} complex recognizes Sic1 phosphorylated

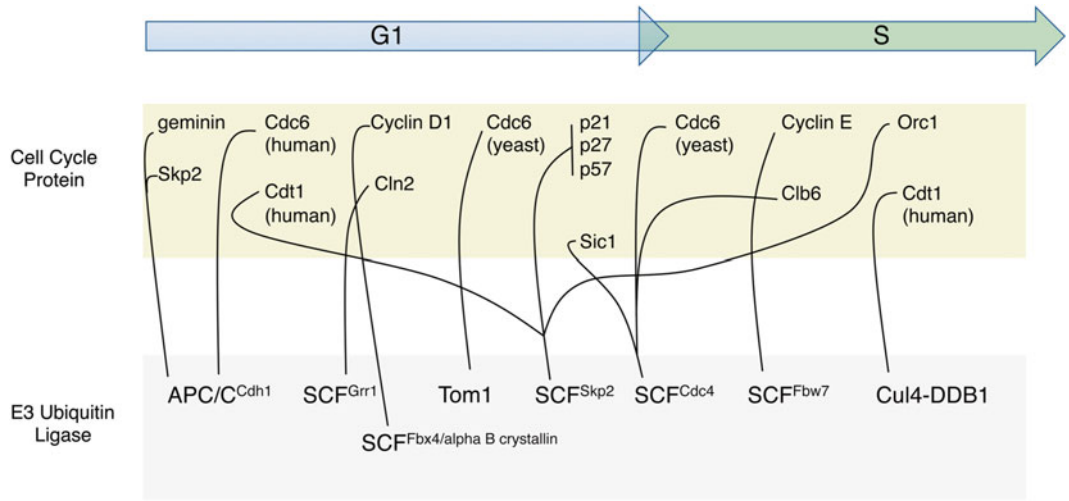

Fig. 2 Ubiquitin-mediated degradation of key cell cycle proteins during G1 and S phases of the cell cycle. A *line* matches the cell cycle protein with the E3 ubiquitin ligase that targets it for ubiquitination and subsequent degradation by the proteasome. For details, please see text

by G1-CDKs, leading to degradation of Sic1 and accumulation of CDK activity required for S-phase entry [12, 35–38]. In higher eukaryotes, CKIs $p21^{Cip1}$, $p27^{Kip1}$, and $p57^{Kip2}$ are recognized by a different SCF complex, SCF^{Skp2} [39–42]. Skp2 contains a leucine-rich repeat (LRR) domain that binds phosphorylated targets. For example, $p27^{Kip1}$ is phosphorylated by the G1/S CDK cyclin E/Cdk2 on threonine 187 prior to recognition by Skp2 [40, 41]. In addition, the SCF^{Skp2} complex often requires the small cofactor Cks1 to associate with specific substrates, including $p27^{Kip1}$ [43, 44]. Interestingly, the APC/C^{Cdh1} complex plays a role in maintaining the accumulation of CKIs in G1 phase by targeting Skp2 for ubiquitin-mediated degradation [21, 22], but this is overcome in late G1 by the transcription of S-phase cyclins that leads to increased CDK activity. One phosphorylation target of S-CDKs is Cdh1, which reduces its association with the APC core complex and contributes to inactivation of the APC/C ubiquitin ligase as cells progress into S phase [30, 45, 46].

The G1- and S-phase cyclins are also targeted for degradation by the proteasome. In yeast, the G1 cyclin Cln2 undergoes autophosphorylation, leading to recognition and ubiquitination via the SCF^{Grr1} complex and subsequent proteolysis by the proteasome [13, 47–49]. This mechanism helps to keep G1 cyclin levels in balance for subsequent cell cycles. In human cells, cyclin D1, a G1 cyclin, is phosphorylated on threonine 286 by GSK-3β and subsequently targeted for ubiquitination and degradation by the $SCF^{Fbx4\text{-alpha B crystallin}}$ complex [50–52]. In this complex, alpha B crystallin functions as a cofactor in substrate recognition [52].

A critical CDK in the G1-to-S phase transition is the cyclin E/Cdk2 complex, which has roles in the promotion of S phase and centrosome duplication (reviewed in ref. 53). Cyclin E is targeted for ubiquitin-mediated destruction by the $SCF^{Fbw7\ (hCdc4/Ago)}$ complex after the combined action of Cdk2 and GSK-3β phosphorylation [54–57]. Fbw7 is a highly regulated F-box protein, with its activity modulated by dimerization, isoform-specific activation, and de-ubiquitination enzymes [58–61]. The budding yeast homolog of Fbw7, Cdc4, targets the S-phase cyclin Clb6 for ubiquitination after phosphorylation by CDKs Cdc28 or Pho85 [62]. In contrast, a second S-phase cyclin in yeast, Clb5, is targeted for ubiquitin-mediated turnover by the APC/C^{Cdc20} complex during mitosis [63].

In addition to the regulation of CDK activity, progression through G1 into S phase is a critical time for cells to prepare chromatin for the initiation of DNA synthesis. During early G1, replication origins are "licensed" by the assembly of pre-replicative (pre-RC) complexes (reviewed in ref. 64). Two proteins that are key to this process are Cdc6 and Cdt1, which work to load the MCM replicative helicase onto origins [65–70]. In higher eukaryotes, components of the origin recognition complex (ORC) must first bind to origin DNA to begin pre-RC assembly, whereas in yeast, ORC remains bound to chromatin throughout the cell cycle [71, 72]. These processes are regulated to limit DNA replication to once per cell cycle, and one mechanism used to accomplish this is ubiquitin-mediated proteolysis.

There are multiple degradation mechanisms that control Cdc6 and Cdt1 levels. In budding yeast, Cdc6 is unstable throughout the cell cycle, but the best studied proteolytic pathway involves SCF^{Cdc4} recognition of Cdc6 after CDK phosphorylation beginning at the G1-to-S phase transition and continuing into mitosis [73, 74]. During G1, Cdc6 is targeted by a distinct ubiquitin ligase in the HECT family called Tom1 [75]. In humans, Cdc6 is degraded in early G1 via the action of the APC/C^{Cdh1} complex, but as G1 progresses, phosphorylation by CDK protects Cdc6 from degradation by shielding it from interaction with Cdh1 [76, 77]. During G1, Cdt1 is targeted for ubiquitination by the SCF^{Skp2} complex [78], but a more efficient degradation mechanism involves another CRL family member, CUL4-DDB1, and PCNA as a necessary cofactor after initiation of DNA synthesis [79–81]. In addition, the Orc1 subunit of the origin recognition complex is also degraded after the start of the DNA replication in part via the action of the SCF^{Skp2} complex in human cells [82].

Another mechanism used to limit DNA replication to once per cycle involves the inhibitor geminin. Geminin is a small protein in higher eukaryotes that binds and inhibits the activity of Cdt1 after initiation of DNA replication to restrict origin licensing to early in the cell cycle [83, 84]. At the end of mitosis and throughout G1,

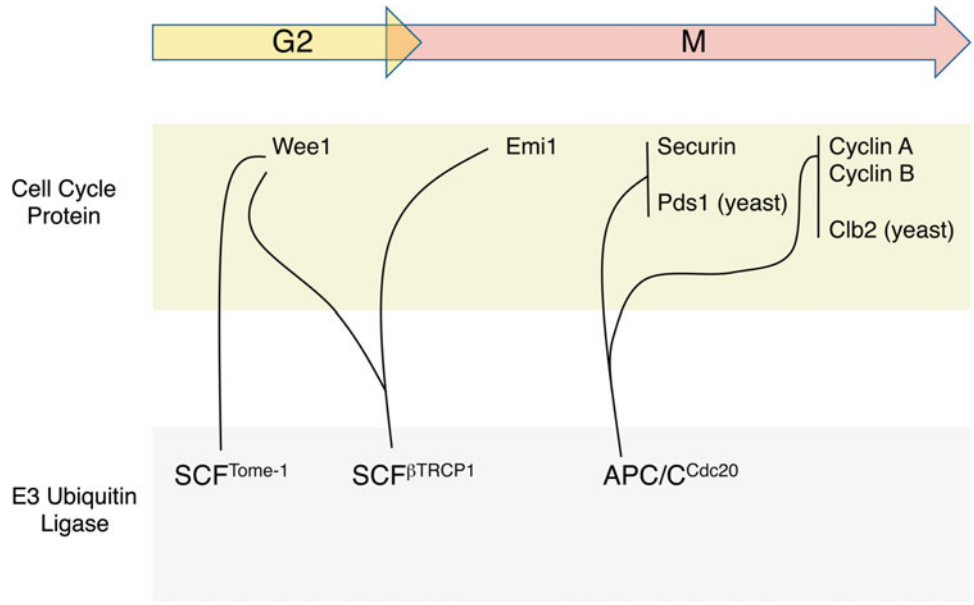

Fig. 3 Ubiquitin-mediated degradation of key cell cycle proteins during G2 and M phases of the cell cycle. A *line* matches the cell cycle protein with the E3 ubiquitin ligase that targets it for ubiquitination and subsequent degradation by the proteasome. For details, please see text

degradation of geminin is accomplished by the activity of the APC/C^{Cdh1} complex [83]. In this way, Cdt1 is released from inhibition during G1 to contribute to pre-RC assembly.

3.2 Progression Through G2 into Mitosis and Mitotic Exit

The identification of mitotic cyclins and the mechanisms that control their periodicity have provided key insights into the nature of cell cycle progression (Fig. 3). During S and G2 phases, mitotic cyclins are transcribed, but mitotic CDKs are held inactive by the action of an inhibitory kinase, Wee1 [85]. This allows the pool of mitotic CDKs to grow in number; these complexes are then rapidly activated as cells transition from G2 to M phase. One mechanism that contributes to the rapid activation of mitotic CDKs is the degradation of Wee1 [86]. In response to phosphorylation by cyclin B/Cdk1, Wee1 is recognized by one of the two SCF complexes, SCFβ^{TRCP} and SCF^{Tome-1}, in higher eukaryotes [87, 88]. The regulation of the budding yeast homolog of Wee1 by ubiquitin-dependent degradation is conserved, but the mechanisms are more complex and involve a separate family of ubiquitin ligases [89, 90]. Such divergences are commonly observed in cell cycle proteolytic pathways in that the general degradation profiles are conserved but the specific ubiquitin ligases involved may be distinct.

As previously mentioned, the APC/C is inactive during S and G2 phases of the cell cycle and this is accomplished via multiple mechanisms. In metazoans, the inhibitor Emi1 binds to APC/C

and prevents association with other APC/C substrates [31]. Interestingly, Emi1 is an F-box protein that is not part of a functional SCF ubiquitin ligase [31]. As cells enter M phase, cyclin B/Cdk1 and polo-like kinases phosphorylate Emi1, targeting it to $SCF\beta^{TRCP}$ for ubiquitin-mediated degradation [91–94]. The removal of Emi1 allows the activation of APC/C^{Cdc20} by cyclin B/Cdk1. Key cell cycle substrates of APC/C^{Cdc20} are mitotic cyclins (cyclins A and B in higher eukaryotes, Clb2 in yeast) and securin (Pds1 in yeast) [95–97].

Ubiquitination and degradation of mitotic cyclins are critical to mitotic exit and resetting the cell cycle by reducing CDK activity. Indeed, the recognition that the mitotic cyclin B was degraded by the ubiquitin–proteasome system was the first insight into the regulation of the cell cycle by proteolysis [95, 96, 98–100], thus opening a new and ever-growing field. As mitotic cyclin levels drop, CDK activity levels fall. The metaphase-to-anaphase transition is accomplished by the degradation of securin [97], which up until this point has held the protease separase inactive. When the APC/C^{Cdc20} becomes active, securin is recognized and degraded, leading to the release of separase, which cleaves the cohesin complexes holding sister chromatids together [101–104]. In late mitosis, APC/C^{Cdc20} is inactivated by a number of mechanisms, including ubiquitin-mediated proteolysis of Cdc20, via autoubiquitination in yeast or APC/C^{Cdh1} in metazoans [105, 106]. APC/C^{Cdh1} remains active through mitotic exit and into G1, keeping mitotic cyclin levels low and helping to regulate G1 progression as described in the previous section.

4 Concluding Remarks

The periodicity of the cell cycle program is an integral feature necessary for cell growth and proliferation. The ubiquitin proteasome system is critical to maintaining the periodic nature of the cell cycle program by targeting specific core cell cycle factors for degradation. This chapter focused only on our current understanding of the role ubiquitin-mediated proteolysis plays in the degradation of central cell cycle factors and in contributing to key cell cycle transitions, but the ubiquitin–proteasome system influences many other pathways that directly regulate the cell cycle, including spindle assembly, chromatin condensation, DNA replication checkpoint signaling, and DNA damage checkpoint signaling. The complexity of the role of the ubiquitin–proteasome system and how it intersects with cell cycle programming are only beginning to be understood.

Acknowledgments

The author's research has been supported by the National Institutes of Health (R01 GM076663).

References

1. Wilkinson KD, Urban MK, Haas AL (1980) Ubiquitin is the ATP-dependent proteolysis factor I of rabbit reticulocytes. J Biol Chem 255(16):7529–7532
2. Ciechanover A, Elias S, Heller H, Hershko A (1982) "Covalent affinity" purification of ubiquitin-activating enzyme. J Biol Chem 257(5):2537–2542
3. Hershko A, Heller H, Elias S, Ciechanover A (1983) Components of ubiquitin-protein ligase system. Resolution, affinity purification, and role in protein breakdown. J Biol Chem 258(13):8206–8214
4. Hershko A (1983) Ubiquitin: roles in protein modification and breakdown. Cell 34(1):11–12
5. Piotrowski J, Beal R, Hoffman L, Wilkinson KD, Cohen RE, Pickart CM (1997) Inhibition of the 26 S proteasome by polyubiquitin chains synthesized to have defined lengths. J Biol Chem 272(38):23712–23721
6. Finley D (2009) Recognition and processing of ubiquitin-protein conjugates by the proteasome. Annu Rev Biochem 78:477–513
7. Tomko RJ Jr, Hochstrasser M (2013) Molecular architecture and assembly of the eukaryotic proteasome. Annu Rev Biochem 82:415–445
8. Hershko A, Ciechanover A (1998) The ubiquitin system. Annu Rev Biochem 67:425–479
9. Page AM, Hieter P (1999) The anaphase-promoting complex: new subunits and regulators. Annu Rev Biochem 68:583–609
10. Deshaies RJ, Joazeiro CAP (2009) RING domain E3 ubiquitin ligases. Annu Rev Biochem 78:399–434
11. Teixeira LK, Reed SI (2013) Ubiquitin ligases and cell cycle control. Annu Rev Biochem 82:387–414
12. Bai C, Sen P, Hofmann K, Ma L, Goebl M, Harper JW, Elledge SJ (1996) SKP1 connects cell cycle regulators to the ubiquitin proteolysis machinery through a novel motif, the F-box. Cell 86(2):263–274
13. Skowyra D, Craig KL, Tyers M, Elledge SJ, Harper JW (1997) F-box proteins are receptors that recruit phosphorylated substrates to the SCF ubiquitin-ligase complex. Cell 91(2):209–219
14. Feldman RM, Correll CC, Kaplan KB, Deshaies RJ (1997) A complex of Cdc4p, Skp1p, and Cdc53p/cullin catalyzes ubiquitination of the phosphorylated CDK inhibitor Sic1p. Cell 91(2):221–230
15. Kamura T, Koepp DM, Conrad MN, Skowyra D, Moreland RJ, Iliopoulos O, Lane WS, Kaelin WG Jr, Elledge SJ, Conaway RC, Harper JW, Conaway JW (1999) Rbx1, a component of the VHL tumor suppressor complex and SCF ubiquitin ligase. Science 284(5414):657–661
16. Ohta T, Michel JJ, Schottelius AJ, Xiong Y (1999) ROC1, a homolog of APC11, represents a family of cullin partners with an associated ubiquitin ligase activity. Mol Cell 3(4):535–541
17. Tan P, Fuchs SY, Chen A, Wu K, Gomez C, Ronai Z, Pan ZQ (1999) Recruitment of a ROC1-CUL1 ubiquitin ligase by Skp1 and HOS to catalyze the ubiquitination of I kappa B alpha. Mol Cell 3(4):527–533
18. Seol JH, Feldman RM, Zachariae W, Shevchenko A, Correll CC, Lyapina S, Chi Y, Galova M, Claypool J, Sandmeyer S, Nasmyth K, Deshaies RJ, Shevchenko A, Deshaies RJ (1999) Cdc53/cullin and the essential Hrt1 RING-H2 subunit of SCF define a ubiquitin ligase module that activates the E2 enzyme Cdc34. Genes Dev 13(12):1614–1626
19. Skaar JR, Pagan JK, Pagano M (2013) Mechanisms and function of substrate recruitment by F-box proteins. Nat Rev Mol Cell Biol 14(6):369–381
20. Zhou P, Howley PM (1998) Ubiquitination and degradation of the substrate recognition subunits of SCF ubiquitin-protein ligases. Mol Cell 2(5):571–580
21. Bashir T, Dorrello NV, Amador V, Guardavaccaro D, Pagano M (2004) Control of the SCF(Skp2-Cks1) ubiquitin ligase by the APC/C(Cdh1) ubiquitin ligase. Nature 428(6979):190–193
22. Wei W, Ayad NG, Wan Y, Zhang GJ, Kirschner MW, Kaelin WG Jr (2004) Degradation of the SCF component Skp2 in cell-cycle phase G1 by the anaphase-promoting complex. Nature 428(6979):194–198

23. Visintin R, Prinz S, Amon A (1997) CDC20 and CDH1: a family of substrate-specific activators of APC-dependent proteolysis. Science 278(5337):460–463
24. Peters JM (2006) The anaphase promoting complex/cyclosome: a machine designed to destroy. Nat Rev Mol Cell Biol 7(9):644–656
25. Sullivan M, Morgan DO (2007) Finishing mitosis, one step at a time. Nat Rev Mol Cell Biol 8(11):894–903
26. Pesin JA, Orr-Weaver TL (2008) Regulation of APC/C activators in mitosis and meiosis. Annu Rev Cell Dev Biol 24:475–499
27. Barford D (2011) Structural insights into anaphase-promoting complex function and mechanism. Philos Trans R Soc Lond B Biol Sci 366(1584):3605–3624
28. Glotzer M, Murray AW, Kirschner MW (1991) Cyclin is degraded by the ubiquitin pathway. Nature 349(6305):132–138
29. Pfleger CM, Kirschner MW (2000) The KEN box: an APC recognition signal distinct from the D box targeted by Cdh1. Genes Dev 14(6): 655–665
30. Zachariae W, Schwab M, Nasmyth K, Seufert W (1998) Control of cyclin ubiquitination by CDK-regulated binding of Hct1 to the anaphase promoting complex. Science 282(5394): 1721–1724
31. Reimann JD, Freed E, Hsu JY, Kramer ER, Peters JM, Jackson PK (2001) Emi1 is a mitotic regulator that interacts with Cdc20 and inhibits the anaphase promoting complex. Cell 105(5):645–655
32. Reimann JD, Gardner BE, Margottin-Goguet F, Jackson PK (2001) Emi1 regulates the anaphase-promoting complex by a different mechanism than Mad2 proteins. Genes Dev 15(24):3278–3285
33. Martinez JS, Jeong DE, Choi E, Billings BM, Hall MC (2006) Acm1 is a negative regulator of the CDH1-dependent anaphase-promoting complex/cyclosome in budding yeast. Mol Cell Biol 26(24):9162–9176
34. Jin L, Williamson A, Banerjee S, Philipp I, Rape M (2008) Mechanism of ubiquitin-chain formation by the human anaphase-promoting complex. Cell 133(4):653–665
35. Mendenhall MD, Jones CA, Reed SI (1987) Dual regulation of the yeast CDC28-p40 protein kinase complex: cell cycle, pheromone, and nutrient limitation effects. Cell 50(6): 927–935
36. Schneider BL, Yang QH, Futcher AB (1996) Linkage of replication to start by the Cdk inhibitor Sic1. Science 272(5261):560–562
37. Tyers M (1996) The cyclin-dependent kinase inhibitor p40SIC1 imposes the requirement for Cln G1 cyclin function at start. Proc Natl Acad Sci U S A 93(15):7772–7776
38. Verma R, Feldman RM, Deshaies RJ (1997) SIC1 is ubiquitinated in vitro by a pathway that requires CDC4, CDC34, and cyclin/CDK activities. Mol Biol Cell 8(8):1427–1437
39. Yu ZK, Gervais JL, Zhang H (1998) Human CUL-1 associates with the SKP1/SKP2 complex and regulates p21(CIP1/WAF1) and cyclin D proteins. Proc Natl Acad Sci U S A 95(19):11324–11329
40. Tsvetkov LM, Yeh KH, Lee SJ, Sun H, Zhang H (1999) p27(Kip1) ubiquitination and degradation is regulated by the SCF(Skp2) complex through phosphorylated Thr187 in p27. Curr Biol 9(12):661–664
41. Carrano AC, Eytan E, Hershko A, Pagano M (1999) SKP2 is required for ubiquitin-mediated degradation of the CDK inhibitor p27. Nat Cell Biol 1(4):193–199
42. Kamura T, Hara T, Kotoshiba S, Yada M, Ishida N, Imaki H, Hatakeyama S, Nakayama K, Nakayama KI (2003) Degradation of p57Kip2 mediated by SCFSkp2-dependent ubiquitylation. Proc Natl Acad Sci U S A 100(18):10231–10236
43. Ganoth D, Bornstein G, Ko TK, Larsen B, Tyers M, Pagano M, Hershko A (2001) The cell-cycle regulatory protein Cks1 is required for SCF(Skp2)-mediated ubiquitinylation of p27. Nat Cell Biol 3(3):321–324
44. Spruck C, Strohmaier H, Watson M, Smith AP, Ryan A, Krek TW, Reed SI (2001) A CDK-independent function of mammalian Cks1: targeting of SCF(Skp2) to the CDK inhibitor p27Kip1. Mol Cell 7(3):639–650
45. Jaspersen SL, Charles JF, Tinker-Kulberg RL, Morgan DO (1998) A late mitotic regulatory network controlling cyclin destruction in Saccharomyces cerevisiae. Mol Biol Cell 9(10): 2803–2817
46. Lukas C, Sorensen CS, Kramer E, Santoni-Rugiu E, Lindeneg C, Peters JM, Bartek J, Lukas J (1999) Accumulation of cyclin B1 requires E2F and cyclin-A-dependent rearrangement of the anaphase-promoting complex. Nature 401(6755):815–818
47. Barral Y, Jentsch S, Mann C (1995) G1 cyclin turnover and nutrient uptake are controlled by a common pathway in yeast. Genes Dev 9(4):399–409
48. Willems AR, Lanker S, Patton EE, Craig KL, Nason TF, Mathias N, Kobayashi R, Wittenberg C, Tyers M (1996) Cdc53 targets phosphorylated G1 cyclins for degradation by the ubiquitin proteolytic pathway. Cell 86(3):453–463
49. Li FN, Johnston M (1997) Grr1 of Saccharomyces cerevisiae is connected to the ubiquitin

proteolysis machinery through Skp1: coupling glucose sensing to gene expression and the cell cycle. Embo J 16(18):5629–5638

50. Diehl JA, Zindy F, Sherr CJ (1997) Inhibition of cyclin D1 phosphorylation on threonine-286 prevents its rapid degradation via the ubiquitin-proteasome pathway. Genes Dev 11(8):957–972
51. Diehl JA, Cheng M, Roussel MF, Sherr CJ (1998) Glycogen synthase kinase-3beta regulates cyclin D1 proteolysis and subcellular localization. Genes Dev 12(22):3499–3511
52. Lin DI, Barbash O, Kumar KG, Weber JD, Harper JW, Klein-Szanto AJ, Rustgi A, Fuchs SY, Diehl JA (2006) Phosphorylation-dependent ubiquitination of cyclin D1 by the SCF(FBX4-alphaB crystallin) complex. Mol Cell 24(3):355–366
53. Siu KT, Rosner MR, Minella AC (2012) An integrated view of cyclin E function and regulation. Cell Cycle 11(1):57–64
54. Koepp DM, Schaefer LK, Ye X, Keyomarsi K, Chu C, Harper JW, Elledge SJ (2001) Phosphorylation-dependent ubiquitination of cyclin E by the SCFFbw7 ubiquitin ligase. Science 294(5540):173–177
55. Strohmaier H, Spruck CH, Kaiser P, Won KA, Sangfelt O, Reed SI (2001) Human F-box protein hCdc4 targets cyclin E for proteolysis and is mutated in a breast cancer cell line. Nature 413(6853):316–322
56. Moberg KH, Bell DW, Wahrer DC, Haber DA, Hariharan IK (2001) Archipelago regulates Cyclin E levels in Drosophila and is mutated in human cancer cell lines. Nature 413(6853): 311–316
57. Welcker M, Singer J, Loeb KR, Grim J, Bloecher A, Gurien-West M, Clurman BE, Roberts JM (2003) Multisite phosphorylation by Cdk2 and GSK3 controls cyclin E degradation. Mol Cell 12(2):381–392
58. Zhang W, Koepp DM (2006) Fbw7 isoform interaction contributes to cyclin E proteolysis. Mol Cancer Res 4(12):935–943
59. Welcker M, Clurman BE (2007) Fbw7/hCDC4 dimerization regulates its substrate interactions. Cell Div 2:7
60. Van Drogen F, Sangfelt O, Malyukova A, Matskova L, Yeh E, Means AR, Reed SI (2006) Ubiquitylation of cyclin E requires the sequential function of SCF complexes containing distinct hCdc4 isoforms. Mol Cell 23(1):37–48
61. Popov N, Herold S, Llamazares M, Schulein C, Eilers M (2007) Fbw7 and Usp28 regulate Myc protein stability in response to DNA damage. Cell Cycle 6(19):2327–2331
62. Jackson LP, Reed SI, Haase SB (2006) Distinct mechanisms control the stability of the related S-phase cyclins Clb5 and Clb6. Mol Cell Biol 26(6):2456–2466
63. Shirayama M, Zachariae W, Ciosk R, Nasmyth K (1998) The Polo-like kinase Cdc5p and the WD-repeat protein Cdc20p/fizzy are regulators and substrates of the anaphase promoting complex in Saccharomyces cerevisiae. Embo J 17(5):1336–1349
64. Sclafani RA, Holzen TM (2007) Cell cycle regulation of DNA replication. Annu Rev Genet 41:237–280
65. Tanaka T, Knapp D, Nasmyth K (1997) Loading of an Mcm protein onto DNA replication origins is regulated by Cdc6p and CDKs. Cell 90(4):649–660
66. Donovan S, Harwood J, Drury LS, Diffley JF (1997) Cdc6p-dependent loading of Mcm proteins onto pre-replicative chromatin in budding yeast. Proc Natl Acad Sci U S A 94(11): 5611–5616
67. Liang C, Stillman B (1997) Persistent initiation of DNA replication and chromatin-bound MCM proteins during the cell cycle in cdc6 mutants. Genes Dev 11(24):3375–3386
68. Aparicio OM, Weinstein DM, Bell SP (1997) Components and dynamics of DNA replication complexes in S. cerevisiae: redistribution of MCM proteins and Cdc45p during S phase. Cell 91(1):59–69
69. Maiorano D, Moreau J, Mechali M (2000) XCDT1 is required for the assembly of pre-replicative complexes in Xenopus laevis. Nature 404(6778):622–625
70. Nishitani H, Lygerou Z, Nishimoto T, Nurse P (2000) The Cdt1 protein is required to license DNA for replication in fission yeast. Nature 404(6778):625–628
71. Diffley JF, Cocker JH, Dowell SJ, Rowley A (1994) Two steps in the assembly of complexes at yeast replication origins in vivo. Cell 78(2): 303–316
72. Mendez J, Stillman B (2000) Chromatin association of human origin recognition complex, cdc6, and minichromosome maintenance proteins during the cell cycle: assembly of prereplication complexes in late mitosis. Mol Cell Biol 20(22):8602–8612
73. Drury LS, Perkins G, Diffley JF (1997) The Cdc4/34/53 pathway targets Cdc6p for proteolysis in budding yeast. Embo J 16(19): 5966–5976
74. Drury LS, Perkins G, Diffley JFX (2000) The cyclin-dependent kinase Cdc28p regulates distinct modes of Cdc6p proteolysis during the budding yeast cell cycle. Curr Biol 10(5): 231–240
75. Kim DH, Zhang W, Koepp DM (2012) The Hect domain E3 ligase Tom1 and the F-box

protein Dia2 control Cdc6 degradation in G1 phase. J Biol Chem 287(53):44212–44220

76. Petersen BO, Wagener C, Marinoni F, Kramer ER, Melixetian M, Lazzerini Denchi E, Gieffers C, Matteucci C, Peters JM, Helin K (2000) Cell cycle- and cell growth-regulated proteolysis of mammalian CDC6 is dependent on APC-CDH1. Genes Dev 14(18):2330–2343
77. Mailand N, Diffley JF (2005) CDKs promote DNA replication origin licensing in human cells by protecting Cdc6 from APC/C-dependent proteolysis. Cell 122(6):915–926
78. Li X, Zhao Q, Liao R, Sun P, Wu X (2003) The SCF(Skp2) ubiquitin ligase complex interacts with the human replication licensing factor Cdt1 and regulates Cdt1 degradation. J Biol Chem 278(33):30854–30858
79. Arias EE, Walter JC (2006) PCNA functions as a molecular platform to trigger Cdt1 destruction and prevent re-replication. Nat Cell Biol 8(1):84–90
80. Senga T, Sivaprasad U, Zhu W, Park JH, Arias EE, Walter JC, Dutta A (2006) PCNA is a cofactor for Cdt1 degradation by CUL4/DDB1-mediated N-terminal ubiquitination. J Biol Chem 281(10):6246–6252
81. Nishitani H, Sugimoto N, Roukos V, Nakanishi Y, Saijo M, Obuse C, Tsurimoto T, Nakayama KI, Nakayama K, Fujita M, Lygerou Z, Nishimoto T (2006) Two E3 ubiquitin ligases, SCF-Skp2 and DDB1-Cul4, target human Cdt1 for proteolysis. Embo J 25(5):1126–1136
82. Mendez J, Zou-Yang XH, Kim SY, Hidaka M, Tansey WP, Stillman B (2002) Human origin recognition complex large subunit is degraded by ubiquitin-mediated proteolysis after initiation of DNA replication. Mol Cell 9(3):481–491
83. McGarry TJ, Kirschner MW (1998) Geminin, an inhibitor of DNA replication, is degraded during mitosis. Cell 93(6):1043–1053
84. Wohlschlegel JA, Dwyer BT, Dhar SK, Cvetic C, Walter JC, Dutta A (2000) Inhibition of eukaryotic DNA replication by geminin binding to Cdt1. Science 290(5500):2309–2312
85. Russell P, Nurse P (1987) Negative regulation of mitosis by wee1+, a gene encoding a protein kinase homolog. Cell 49(4):559–567
86. Michael WM, Newport J (1998) Coupling of mitosis to the completion of S phase through Cdc34-mediated degradation of Wee1. Science 282(5395):1886–1889
87. Watanabe N, Arai H, Nishihara Y, Taniguchi M, Watanabe N, Hunter T, Osada H (2004) M-phase kinases induce phospho-dependent ubiquitination of somatic Wee1 by SCFbeta-TrCP. Proc Natl Acad Sci U S A 101(13):4419–4424
88. Ayad NG, Rankin S, Murakami M, Jebanathirajah J, Gygi S, Kirschner MW (2003) Tome-1, a trigger of mitotic entry, is degraded during G1 via the APC. Cell 113(1):101–113
89. Raspelli E, Cassani C, Lucchini G, Fraschini R (2011) Budding yeast Dma1 and Dma2 participate in regulation of Swe1 levels and localization. Mol Biol Cell 22(13):2185–2197
90. King K, Kang H, Jin M, Lew DJ (2013) Feedback control of Swe1p degradation in the yeast morphogenesis checkpoint. Mol Biol Cell 24(7):914–922
91. Guardavaccaro D, Kudo Y, Boulaire J, Barchi M, Busino L, Donzelli M, Margottin-Goguet F, Jackson PK, Yamasaki L, Pagano M (2003) Control of meiotic and mitotic progression by the F box protein beta-Trcp1 in vivo. Dev Cell 4(6):799–812
92. Margottin-Goguet F, Hsu JY, Loktev A, Hsieh HM, Reimann JD, Jackson PK (2003) Prophase destruction of Emi1 by the SCF (betaTrCP/Slimb) ubiquitin ligase activates the anaphase promoting complex to allow progression beyond prometaphase. Dev Cell 4(6):813–826
93. Moshe Y, Boulaire J, Pagano M, Hershko A (2004) Role of Polo-like kinase in the degradation of early mitotic inhibitor 1, a regulator of the anaphase promoting complex/cyclosome. Proc Natl Acad Sci U S A 101(21):7937–7942
94. Hansen DV, Loktev AV, Ban KH, Jackson PK (2004) Plk1 regulates activation of the anaphase promoting complex by phosphorylating and triggering SCFbetaTrCP-dependent destruction of the APC Inhibitor Emi1. Mol Biol Cell 15(12):5623–5634
95. King RW, Peters JM, Tugendreich S, Rolfe M, Hieter P, Kirschner MW (1995) A 20S complex containing CDC27 and CDC16 catalyzes the mitosis-specific conjugation of ubiquitin to cyclin B. Cell 81(2):279–288
96. Sudakin V, Ganoth D, Dahan A, Heller H, Hershko J, Luca FC, Ruderman JV, Hershko A (1995) The cyclosome, a large complex containing cyclin-selective ubiquitin ligase activity, targets cyclins for destruction at the end of mitosis. Mol Biol Cell 6(2):185–197
97. Cohen-Fix O, Peters JM, Kirschner MW, Koshland D (1996) Anaphase initiation in Saccharomyces cerevisiae is controlled by the APC-dependent degradation of the anaphase inhibitor Pds1p. Genes Dev 10(24):3081–3093
98. Holloway SL, Glotzer M, King RW, Murray AW (1993) Anaphase is initiated by proteolysis rather than by the inactivation of maturation-promoting factor. Cell 73(7):1393–1402

99. Hershko A, Ganoth D, Sudakin V, Dahan A, Cohen LH, Luca FC, Ruderman JV, Eytan E (1994) Components of a system that ligates cyclin to ubiquitin and their regulation by the protein kinase cdc2. J Biol Chem 269(7): 4940–4946
100. Seufert W, Futcher B, Jentsch S (1995) Role of a ubiquitin-conjugating enzyme in degradation of S- and M-phase cyclins. Nature 373(6509):78–81
101. Uhlmann F, Lottspeich F, Nasmyth K (1999) Sister-chromatid separation at anaphase onset is promoted by cleavage of the cohesin subunit Scc1. Nature 400(6739):37–42
102. Ciosk R, Zachariae W, Michaelis C, Shevchenko A, Mann M, Nasmyth K (1998) An ESP1/PDS1 complex regulates loss of sister chromatid cohesion at the metaphase to anaphase transition in yeast. Cell 93(6):1067–1076
103. Jager H, Herzig A, Lehner CF, Heidmann S (2001) Drosophila separase is required for sister chromatid separation and binds to PIM and THR. Genes Dev 15(19):2572–2584
104. Waizenegger IC, Hauf S, Meinke A, Peters JM (2000) Two distinct pathways remove mammalian cohesin from chromosome arms in prophase and from centromeres in anaphase. Cell 103(3):399–410
105. Fang G, Yu H, Kirschner MW (1998) Direct binding of CDC20 protein family members activates the anaphase-promoting complex in mitosis and G1. Mol Cell 2(2): 163–171
106. Prinz S, Hwang ES, Visintin R, Amon A (1998) The regulation of Cdc20 proteolysis reveals a role for APC components Cdc23 and Cdc27 during S phase and early mitosis. Curr Biol 8(13):750–760

Chapter 5

Linking Chromosome Duplication and Segregation via Sister Chromatid Cohesion

Adam R. Leman and Eishi Noguchi

Abstract

DNA replication during S phase generates two identical copies of each chromosome. Each chromosome is destined for a daughter cell, but each daughter must receive one and only one copy of each chromosome. To ensure accurate chromosome segregation, eukaryotic cells are equipped with a mechanism to pair the chromosomes during chromosome duplication and hold the pairs until a bi-oriented mitotic spindle is formed and the pairs are pulled apart. This mechanism is known as sister chromatid cohesion, and its actions span the entire cell cycle. During G1, before DNA is copied during S phase, proteins termed cohesins are loaded onto DNA. Paired chromosomes are held together through G2 phase, and finally the cohesins are dismantled during mitosis. The processes governing sister chromatid cohesion ensure that newly replicated sisters are held together from the moment they are generated to the metaphase–anaphase transition, when sisters separate.

Key words Sister chromatid cohesion, SMC proteins, Cohesin, Adherin/kollerin, DNA replication, Cohesinopathy, Replication fork, Genomic integrity, S phase, Chromosome segregation

1 Introduction

During the cell cycle, new organelles, membranes, cytosol, and genetic materials are all generated to give rise to two new cells. Even during processes that promote asymmetrical cell divisions, arguably, the most important cell-cycle processes revolve around duplication and segregation of the entire genome, so that both daughter cells inherit the exact same genetic material.

During S phase, genomic DNA is replicated and packaged into chromatin. The identical copies of each chromosome are known as sister chromatids, and they are tightly associated together through G2 phase and early mitosis. During metaphase of mitosis, sister chromatids are associated with the mitotic spindle, aligned along the central axis of the cell, and one sister from each pair is associated with a separate spindle pole under tension. At the metaphase–anaphase transition, sister chromatid cohesion is relieved, and the

Eishi Noguchi and Mariana C. Gadaleta (eds.), *Cell Cycle Control: Mechanisms and Protocols*, Methods in Molecular Biology, vol. 1170, DOI 10.1007/978-1-4939-0888-2_5,

microtubule spindle-pulling forces separate each sister chromatid pair and move one copy of the entire genome to one pole. The spindle-pulling forces continue until the cell is divided, and two separate cells are generated at cytokinesis.

Sister pairing calls for the physical tethering of the sister chromatids to each other. The primary proteins responsible for this tethering comprise the cohesin complex. Cohesins are well conserved throughout eukaryotes, and the processes governing cohesion are generally conserved as well. The cohesin complex must be loaded onto DNA during G1 phase prior to DNA replication. For sister chromatid cohesion to be established, the newly replicated DNA copies are encircled by the cohesin complex in S phase. Finally, owing to the elaborate regulation during mitosis, cohesin-mediated sister chromatid-pairing ends, allowing for equal segregation of the genome to each daughter cell. In this review, we discuss the structure of the cohesin complex, how it is loaded onto DNA, the link between DNA replication and cohesion establishment, and finally how the cohesin is released from sister chromatids during mitosis.

2 The Cohesion Complex

Cohesin is a four-subunit complex comprising "structural maintenance of chromosomes (SMC)"-type proteins and non-SMC-type proteins. SMC-type proteins exist in all three domains of life (eukaryota, prokaryota, and archaea), and eukaryotic cells have several SMC proteins that help govern a variety of cellular processes [1]. Smc1 and Smc3 form the cohesin complex with non-SMC subunits, Scc1 and Scc3, and function in sister chromatid cohesion [2]. We focus on this cohesin complex in this review; however, various other complexes containing SMC proteins are involved in the preservation of genome integrity. The Smc2–Smc4 complex is known as condensin and works during mitosis to compact chromosomes [3, 4]. The Smc5–Smc6 complex contributes to various genome maintenance processes including homologous recombination [5–7]. Furthermore, Rad50, a component of the MRN complex, is also an SMC family member and initiates DNA double-strand break processing [8]. While these SMC family proteins are involved in diverse roles in genomic integrity, their structures are remarkably similar (reviewed in ref. 9).

These proteins are characterized by a conserved modular structure, possessing a long coiled-coil region interrupted by a dimerization domain (also known as a hinge domain) and the amino (N)- and carboxyl (C)-termini domains that contain Walker A and Walker B ATP-binding motifs, respectively. Because the coiled-coil region folds at the hinge domain, and the N- and C-termini are brought together to create a nucleotide-binding domain (NBD), each monomer of SMC proteins forms a structure

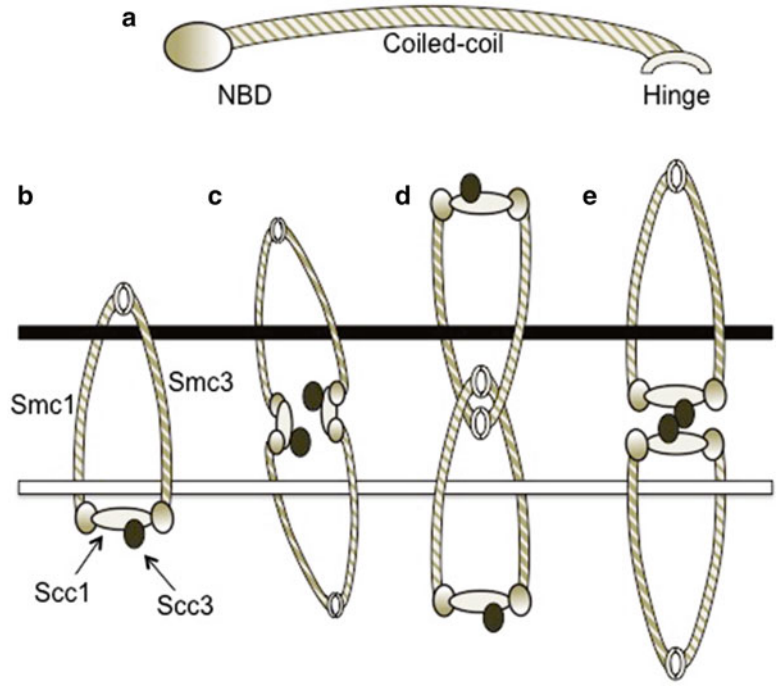

Fig. 1 Models of cohesin structure. (**a**) The general structure of the Smc1/3 proteins. A nucleotide-binding domain with ATPase activity (NBD) connected by a coiled-coil domain to a hinge domain. (**b**) The cohesin complex as a ring. (**c**) The cohesin ring as a 2:2:2 complex of Smc1/Smc3/Scc1. (**d**) The cohesin complex as a bracelet or links in a chain. (**e**) The cohesin complex "handcuff" model. The *black* and *white bars* denote the sister chromatids

reminiscent of two spheroid objects connected by a flexible chain (Fig. 1a) [10, 11].

The overall structure of the cohesion SMC proteins helps to define the function of the cohesin complex and its role in tethering sister chromatids. While the precise shape of the cohesion complex has yet to be fully sorted out (discussed below), the structures of the major components of the cohesion complex have been determined. The cohesin SMC proteins exist as an Smc1–Smc3 heterodimer in the cell, with two 50-nm extensions protruding from the interacting hinge domain (Fig. 1a) [2]. The heterodimer is brought to a closed form by Scc1, which is a member of kleisin protein family [2, 12, 13]. Scc1 interacts with NBD domains of both Smc1 and Smc3, generating a ring with a diameter of approximately 45–50 nm (Fig. 1b) [2, 13, 14]. Within this tripartite complex, paired sister chromatids are trapped and physically kept in close proximity. The cohesins then keep the sister chromatids juxtaposed within multiple complexes loaded on every chromosome. Localization analyses place the cohesin complex at intervals of ~20 kb throughout the genome [15, 16].

Apart from the core ring-forming subunits, the functional cohesin complex requires the Scc3 subunit [17, 18]. In vertebrates, there are two Scc3 homologs, known as stromal antigen (SA) or STAG proteins, SA1/STAG1 and SA2/STAG2 [19]. Although Scc3 is not a structural subunit of cohesin, it is essential for cell growth in yeast and is required for proper cohesion processes [18, 20]. Scc3 binds directly to Scc1, and together these proteins mediate cohesin interaction with other proteins required for regulation of sister chromatid cohesion throughout the cell cycle [2, 21].

The structure of the cohesin complex in vivo is still a topic for discussion in the field. Several different models of cohesin complex entrapment of DNA have been proposed, and each has different implications for the overall cohesin complex stoichiometry. The most prominent model of cohesin complex structure is that of a tripartite ring made of Smc1–Smc3–Scc1 [2, 22]. This ring encircles sister chromatid pairs within its diameter with a 1:1:1 stoichiometry (Fig. 1b). As an alternative possibility, it has been proposed that these rings could be concatenated to increase the ring diameter. In this model, the interacting faces each still associates with the same subunit, but on a different molecule (with a stoichiometry of 2:2:2, 3:3:3, etc.) (Fig. 1c) [23]. Instead of one ring holding two chromosomes, another model posits that the rings can form links such as on a chain. In this model, each ring holds one chromosome and also another cohesin ring (Fig. 1d) [24]. Finally, a handcuff model has been proposed in which closed cohesin rings are bridged by an Scc3 molecule, a shape reminiscent of handcuff around two arms [25, 26] (Fig. 1e). The strongest evidence so far has been for 1:1:1 tripartite rings forming cohesin complexes in vivo on circular minichromosomes in yeast, but further work will define whether this conformation is universal [27].

3 Loading Cohesin Prior to DNA Replication

To properly pair chromosomes and to reduce pairing errors, sister chromosomes need to be held together as soon as they are duplicated. Rather than loading cohesin complexes after DNA replication, the rings are loaded onto the parental DNA prior to DNA replication. Vertebrates perform this process almost immediately after the parental DNA is separated from its sister copy, during telophase at the end of mitosis. In fungi, the cohesin loading occurs during G1 phase. In both cases, a conserved protein complex performs the loading. In yeast, two proteins, Scc2 and Scc4, form a complex and are responsible for cohesin loading (Fig. 2) [28]. In mammals, orthologs of these proteins are known as NIPBL and MAU2, respectively, and form a cohesin-loading complex. In the literature, this complex is often referred to as adherin, but it

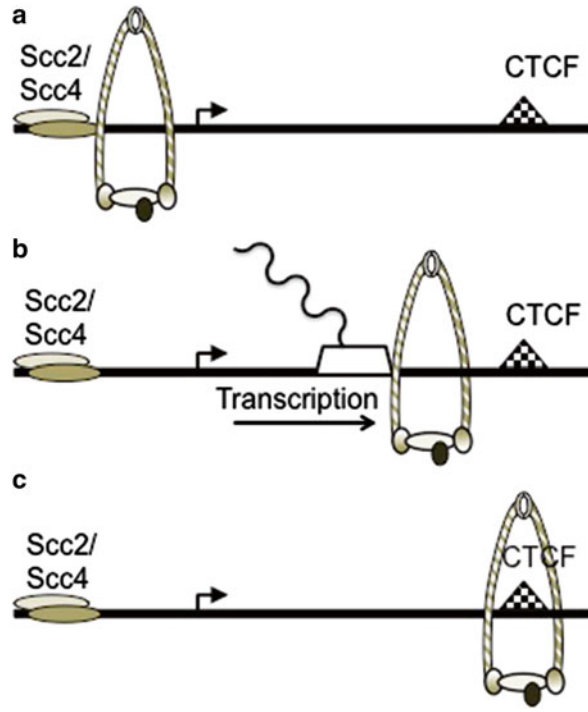

Fig. 2 Redistribution of cohesins by transcription. (**a**) The Scc2/Scc4 complex loads cohesin complexes onto chromatin. (**b**) The transcription machinery pushes some cohesin complexes to the end of open reading frames. (**c**) Cohesins interact with CTCF proteins bound at the edge of open transcription

was recently proposed to rename the complex kollerin to avoid confusion with cadherin proteins [23]. Neither subunit in the loading complex has enzymatic function. It is thought that the function of the adherin/kollerin complex is to facilitate or stimulate the ATPase activity of the Smc1 and Smc3 proteins to load them onto DNA. The ATPase activity of the Smc1/3 proteins is involved in loading of cohesin rings onto DNA [29, 30]. However, an ATPase mutation, which permits ATP binding but ATP hydrolysis, in Smc1 and Smc3 still allows for the loading of the cohesin ring complex onto DNA, although the association is not stable. This indicates that the cohesin complex can be recruited to chromatin without ATPase activity, but likely not in the conformation required for proper chromosome cohesion [31]. Strikingly, the localization of these mutant cohesin complexes is similar to that of Scc2/4, suggesting that ATP binding by SMCs is involved in initial recruitment and association of cohesins with chromatin, but transition to a stable cohesin loading on DNA and subsequent relocalization of cohesins require ATP hydrolysis.

What might the hydrolysis of ATP do to load cohesin rings onto DNA? Interestingly, the answer may come at the opposite

ends of Smc1/3 molecules, the hinge domain. There are several lines of evidence that the complex opens at the Smc1–Smc3 hinge domains to trap or encircle chromatin. Gruber et al. fused Smc1 and Smc3 hinge domains. This fusion construct was lethal to budding yeast, whereas fusion constructs that permanently connect SMC subunits and Scc1 (Smc1–Scc1 and Smc3–Scc1) were not [32]. These experiments suggest that the ring opens at the hinge domain. How then could ATP hydrolysis at the NBD, which is at the opposite end of each SMC subunit, affect the hinge domain interface? Investigation of Rad50, an SMC family protein involved in DNA double-strand break processing, revealed that ATP hydrolysis at the NBD induces a conformational change of the entire protein [33]. The dimerization- and nucleotide-binding domains of Rad50 are separated by a long coiled coil of about 50 nm [34]. In spite of this long distance, upon ATP hydrolysis at its NBD, Rad50 undergoes a conformational change that rotates and releases Rad50 from dimerization at the hinge-domain equivalent [35]. Therefore, a similar conformational change may occur in the Smc1–Smc3 hinge interaction upon ATP hydrolysis at the NBD, leading to ring opening. Once the ring is opened, the next step is to trap sister chromatids and close the ring. The dimerization of two hinges from Smc1 and Smc3 is dependent on two independent interaction surfaces of each hinge. This configuration creates a small donut-like structure at the hinge [2]. Mutational analysis of the hinge domains of Smc1/3 has shown that the interaction between two separate faces on each hinge domain is required for stable association of cohesin with chromatin. Mutations within either interface resulted in lethal defects of sister chromatid cohesion, presumably due to the inability to close the ring and stably load cohesins onto chromatin [36]. Therefore, cohesin loading involves two processes: ATP hydrolysis to open the complex at the hinge interface, followed by securing interactions of the hinge domains of Smc1/3 to close the ring for stable chromatin association.

To successfully tether sister chromatids together, cohesin complexes must be loaded at many sites on each chromosome. Therefore, cohesin loading occurs throughout the genome. However, the loading sites are species specific, although there is no major difference in the quality of sister chromatid cohesion. In yeast, cohesin loading is especially concentrated at centromeres and telomeres [37]. Interestingly, in *Xenopus*, the pre-replication complexes (pre-RCs) forming at replication origins recruit the Scc2–Scc4 complex [38, 39]. This recruitment links origins of replication to cohesin loading. Other factors at both origin and cohesin-loading sites facilitate the loading of cohesins. In yeast, kinetochore proteins as well as replication fork proteins are required for proper loading of cohesins at the centromere and for subsequent stability of pericentromeric cohesion [40]. Strikingly, kinase activity known to regulate origin firing is also required for cohesin loading in *Xenopus*. The recruitment of the adherin/kollerin

complex to the pre-RC is dependent upon the DDK (Dbf4–Cdc7) kinase, which acts on pre-RCs [41]. It appears that mechanisms linking cohesin loading to other processes have somewhat diverged in evolution; however, each leads to successful loading of cohesin complexes.

Although cohesins are loaded at Scc2–Scc4 sites, some cohesins do not stay localized at the same sites for the duration of the cell cycle. In yeast, large numbers of cohesin rings can be "pushed" or "slid" away from their original loading sites and moved into intergenic regions (Fig. 2) [37, 42]. Since these sites are often at the end of open reading frames or at regions of convergent transcription, the model is that the transcription elongation complex facilitates the translocation of cohesins away from transcriptionally active sites to heterochromatin regions, usually proximal to euchromatin. In mammalian cells, the outcome is the same, but the mechanism may be different. The majority of NIPBL/Scc2-binding sites colocalize with cohesin rings; however, the cohesin ring sites far outnumber NIPBL sites, and most cohesin ring sites do not have coincident NIPBL binding [43, 44]. These results are consistent with the model that mammalian cohesin can be loaded at NIPBL/Scc2–Mau2/Scc4 sites and then relocated elsewhere (Fig. 2). However, in higher eukaryotes, cohesin rings might not be displaced by transcription machinery as seen in yeast. For example, *Drosophila* genes contain cohesins even when actively transcribed [45]. Therefore, the relocation of cohesin rings after loading may occur by a different process. In metazoans, the transcriptional repressor CTCF uses its zinc-finger domains to recognize DNA sequences containing CCCTC repeats. CTCF is found in numerous sites on the genome and has a variety of roles in chromatin architecture and transcription regulation (reviewed in ref. 46). Interestingly, CTCF has a role in determining cohesin ring sites on DNA (Fig. 2). Cohesin loading is not dependent on CTCF, but the localization of a large subset of cohesin complexes is dictated by CTCF [16]. The tethering of cohesin rings to CTCF appears to act through SA2 (Scc3), which binds the CTCF C-terminus, and this interaction appears to contribute to CTCF functions in transcription insulation [47]. Although this study explains how cohesin complexes are associated with CTCF sites, no clear mechanism has been found for translocating cohesin rings from NIPBL sites to CTCF sites.

4 Establishment of Sister Chromatid Cohesion During DNA Replication

Sister chromatid cohesion is established during DNA replication and maintained until the two sisters separate in mitosis. Cohesin complexes are loaded onto DNA and associated with chromatin prior to DNA replication. However, these cohesins are not yet engaged in sister chromatid cohesion. Initially, it was unclear

whether cohesin paired chromatids during DNA replication or after replication was completed. To test whether sister chromosome cohesion could be established during S phase or during G2 (after the genome has been duplicated), Uhlmann and Nasmyth placed the *SCC1* gene under an inducible promoter and restricted Scc1 production to G1 or G2 phase in budding yeast [48]. When Scc1 was expressed in G1 phase (before DNA replication), the cells paired their chromosomes properly. However, when Scc1 expression was turned on only in G2 (after DNA replication), cells failed to pair their chromosomes, leading to chromosome missegregation and cell death [48]. The temporal requirement for Scc1 is consistent with the requirement of the adherin/kollerin cohesin loader complex, which is dispensable after G1 [49]. Thus, the cohesin ring subunits must be present when Scc2–Scc4 mediates their loading. Further, mutation in a critical arginine finger within the ATPase-active site suggests that Smc1/3-mediated ATP hydrolysis only occurs during cohesin loading during G1 in yeast [49]. Thus, the complete cohesin complex must be loaded onto chromatin prior to DNA replication to establish sister chromatid cohesion [48]. In addition, cohesion establishment requires involvement of replication factors moving with the replication fork in order to pair the sister chromosomes during S phase without displacing the cohesin ring from the chromatin [49]. Therefore, cohesin complexes are loaded prior to DNA replication, remain associated with chromatin during DNA replication, and then fully establish sister chromatid cohesion during DNA replication. Because sister chromatids are in close proximity immediately after DNA replication at the replication fork, cells are able to eliminate the need to search for sister chromatids, thus increasing the fidelity of sister chromatid cohesion.

Upon DNA replication, the cohesin complex undergoes a transition, leading to a more secure association with chromatin. Fluorescent recovery after photobleaching (FRAP) experiments show that, after cohesion is established during S phase in mammalian cells, cohesin complexes are far more stably associated with DNA [50]. One of the major S-phase factors involved in establishment of sister chromatin cohesion is the acetyltransferase Eco1, which is also known as Ctf7 [18, 51]. In animals, two genes encode for the acetyltransferase. In humans, the Eco1 homologs are known as Esco1/2 (or EFO1/2), and in *Drosophila*, they are called san and deco; both acetyltransferases are required for cohesion in animals [52–54]. In yeast, Eco1 appears to progress with the replication fork during DNA replication [37]. Although the Eco1 acetyltransferase activity leads to the establishment of cohesion, Eco1 does not promote a direct interaction of cohesin and DNA. Instead, it appears that Eco1-dependent acetylation leads to a stabilization of cohesin complexes on chromatin. The target of Eco1/Ctf7 acetylation activity is known to be two lysine residues near the NBD on the Smc3 [55–57].

The exact mechanism by which Eco1/Ctf7-dependent Smc3 acetylation stabilizes cohesion is unknown, but several models have been put forward. In the first model, Smc3 acetylation negatively regulates ATP binding by Smc3 and breaks the ATP-loading and -hydrolysis cycle of cohesin loading. This leads to stabilization of the cohesin complex on chromatin while preventing oligomerization of SMC proteins that could negatively affect sister chromatid cohesion. This is supported by the fact that acetyl-mimetic mutations of Smc3 restore viability of cells with lethal ATP-hydrolysis mutations of the same molecule [58]. In the second model, Smc3 acetylation appears to have an effect on suppressing anti-cohesion factors, such as Wapl and Pds5, that bind to the cohesin complex [59, 60]. Mutations in budding yeast Wpl1 (Wapl homolog) rescue a mutant allele of Eco1 (*eco1-1*), demonstrating that these proteins have counteracting activities in cohesion [55]. Furthermore, when Wpl1 and Pds5 are deleted in yeast, the requirement for Eco1-dependent acetylation of Smc3 is abolished, and cells remain viable. This is presumably due to the suppression of the anti-cohesion establishment activity of the Wpl1–Pds5 complex during S phase [61, 62]. Interestingly, Eco1/Ctf7 activity is continuously required to maintain Smc3 acetylation, but it is dispensable after DNA replication, further supporting the model that the acetylated form of Smc3 is only required for cohesion establishment during S phase, but not for cohesion maintenance after DNA replication has been completed [18, 51, 61]. Thus, Smc3 acetylation by Eco1/Ctf7 may counteract an antiestablishment activity of Wapl and Pds5 in order to establish cohesion. In vertebrate animals, this appears to occur through recruitment of an essential cohesion protein, Sororin, which stabilizes cohesin on chromatin [63, 64]. Sororin is required only in the presence of Wapl, suggesting that Sororin counteracts Wapl after it is recruited to acetylated cohesins [65]. However, this mechanism may not be universal, because no Sororin homolog has been identified in yeast.

5 Establishing Cohesion at the Replication Fork

The establishment of cohesion at the replication fork is, as mentioned previously, a clever mechanism to pair sister chromatids as soon as they are generated. While most work has focused on how replication fork proteins impact chromosome cohesion phenotypes, proper establishment of cohesion also plays an important role in DNA replication. It has been shown that by restricting Smc3 acetylation, DNA replication speed is reduced [66]. Eco1 is a replisome-associated acetyltransferase and travels with the replisome during DNA replication (Fig. 3) [49, 67, 68]. Overexpression of the polymerase clamp PCNA rescues temperature-sensitive mutants of Eco1 in budding yeast [51]. PCNA is a heterotrimeric

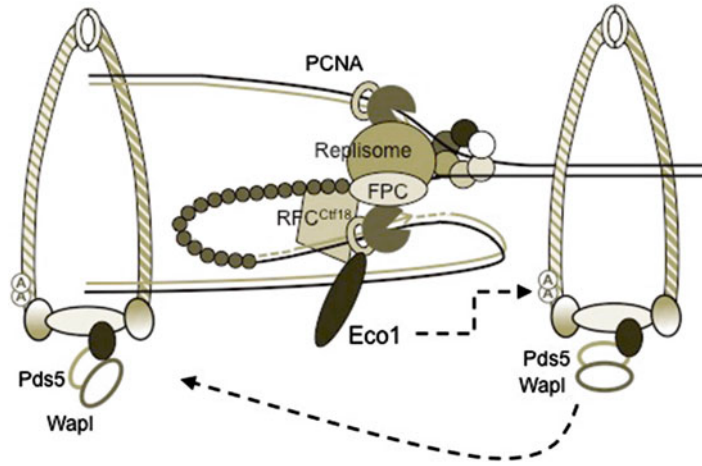

Fig. 3 Interactions between the cohesins and the replisome establish sister chromatid cohesion. Localizing the Eco1 acetyltransferase to the replisome through PCNA interaction allows for cohesion establishment at the replication fork. Factors such as the FPC and RFC^{Ctf18} stabilize the replisome and ensure that the replisome structure is amenable to cohesion establishment

clamp that coordinates a myriad of interactions between replication and other processes [69]. Eco1 binds PCNA at its PCNA-interacting protein (PIP) box domain. The PIP box domain is conserved throughout Eco1 homologs, including the human variant Esco2 [68]. Since Eco1 interacts with PCNA, one can imagine a model in which Eco1 travels with the replication fork and acetylates Smc3 subunits of cohesin complexes as they are encountered by the replication fork, establishing cohesion as the replisome progresses (Fig. 3).

During DNA replication, PCNA is loaded onto DNA continuously by a five-subunit clamp loader known as replication factor C (RFC) complex [70]. An alternative RFC complex containing Ctf18 (RFC^{Ctf18}) is capable of loading PCNA onto DNA and is required for proper sister chromatid cohesion [49, 66, 71–75]. Indeed, PCNA localization to chromatin is dramatically reduced in *ctf18* mutants, rendering these cells more sensitive to genotoxic agents [49]. However, replication and cohesion establishment still occur in *ctf18* cells, indicating that this function is not essential for cohesion establishment. An open question is how RFC^{Ctf18}-mediated PCNA loading enhances cohesin establishment in a manner different from the canonical RFC complex. It is possible that RFC^{Ctf18} loads PCNA specifically at sites of cohesin localization or loads a modified PCNA that interacts more efficiently with Eco1. RFC^{Ctf18}-dependent promotion of cohesion establishment may be indirect, in which RFC^{Ctf18} might serve to increase replisome integrity or maintain the replisome in a confirmation in such a way that the replisome can smoothly progress through cohesin-associated chromosome sites.

Proteins involved in replisome structure and stability also play a role in proper cohesion establishment during DNA replication (Fig. 3). Representative of these include Mrc1/Claspin, Ctf4/And-1, and the replication fork protection complex (FPC). Mrc1/Claspin, which interacts with DNA polymerase ε and the MCM helicase, moves with the replication fork and mediates the signal of stalled replication forks to activate the replication checkpoint [76–78]. The Ctf4/And-1 protein acts as a linker between the MCM helicase and the DNA polymerase α-primase complex while promoting proper cohesion establishment [79–82]. The FPC, which consists of the Timeless and Tipin proteins in metazoans, plays a critical role in replisome stabilization and replication checkpoint signaling and is also involved in promoting sister chromatid cohesion (reviewed in ref. 83). Although it is still largely unknown how this complex serves as a cohesion-promoting factor, depletion or mutation of FPC components in a variety of eukaryotic organisms leads to a cohesion defect [84–91]. It has been proposed that the FPC coordinates leading- and lagging-strand DNA synthesis processes at the replication fork [92, 93]. Inefficient lagging-strand synthesis may cause a long stretch of single-stranded DNA, generating a large loop structure at the replication fork. Such a large replication fork structure with the replisome components would render the replisome unable to pass through the cohesin ring complex [49]. Consistent with this notion, lagging-strand processing has been linked with Smc3 acetylation. Eco1 interacts with Fen1, a flap endonuclease required for Okazaki fragment maturation, possibly positioning the acetyltransferase to act on Smc3 as it localizes to the lagging-strand processing machinery [94, 95].

As mentioned above, efficient lagging-strand synthesis appears to be a key determinant of sister chromatid cohesion establishment. In both mammalian cells and budding yeast, Fen1 associates with the ChlR1 (Chl1 in yeast) protein, a member of the FANCJ DNA helicase family [95, 96]. The loss of ChlR1 leads to sister chromatid cohesion defects in yeast and mammalian cells [97–101]. Biochemical studies revealed that ChlR1 stimulates Fen1 flap endonuclease activity in vitro, and loss of Fen1 itself also leads to cohesion defects with striking similarity to the cohesion defects associated with ChlR1 depletion [96], indicating the intimate link between lagging-strand processing at the replication fork and sister chromatid cohesion. It appears that ChlR1 and FPC operate in the same pathway to promote sister chromatid cohesion. Studies in human cells show that ChlR1 co-purifies with the FPC and that both the FPC and ChlR1 are found to interact with cohesin complexes by immunoprecipitation [89, 101]. ChlR1 overexpression rescues cohesion defects caused by FPC depletion, while Chl1 overexpression suppresses the sensitivity of FPC mutants to genotoxic agents in fission yeast [86, 89]. Furthermore, downregulation of FPC or ChlR1 causes profound defects in replication

recover after replication stress [89, 102]. Considering that ChlR1 interacts with Fen1 [96], it is highly possible that the FPC and ChlR1 act together to facilitate lagging-strand synthesis to accommodate proper establishment of sister chromatid cohesion at the replication fork.

In addition to the direct involvement of lagging-strand synthesis in sister chromatid cohesion, the replisome itself may also need to be stabilized when it passes through the cohesin-bound chromosome regions. It is proposed that the fork stalls transiently at the sites of cohesin complexes, necessitating fork stabilization [103, 104]. Indeed, the FPC and ChlR1/Chl1 are involved in maintaining replisome stability when the replication fork stalls, probably at the lagging strand [83, 102]. It is also important to note that RFC^{Ctf18} is involved in both fork stabilization and sister chromatid cohesion [86]. Interestingly, loss of RFC^{Ctf18} results in reduced levels of Smc3 acetylation [66]. In addition, RFC^{Ctf18} stimulates the helicase activity of ChlR1, suggesting the role of RFC^{Ctf18} in lagging-strand processing. Therefore, it is possible that fork stabilization and efficient lagging-strand synthesis are required for efficient acetylation of Smc3 by Eco1 acetyltransferase at the replication fork. Since Eco1 physically associates with PCNA [68], the localization of Eco1 at the fork may be dependent on PCNA loaded by RFC^{Ctf18} and also on Fen1 engaged at the lagging strand. Such a molecular configuration may provide a condition for efficient Smc3 acetylation that promotes fork progression through cohesin-bound chromosome regions. An alternative explanation is that uncoupling the lagging strand from the leading strand creates a structure that is incompatible with passage through the cohesin complex. Additional studies are needed to disentangle these possibilities and determine the relationship between replisome progression and cohesion establishment.

6 G2/M Phase: Maintaining and Disassembling Chromosome Cohesion

Once sister chromatid cohesion is established, it must be maintained until cells segregate sister chromosomes at anaphase. Upon the completion of DNA replication in budding yeast, cohesion establishment is ended by the Clb2–Cdk1 complex-dependent phosphorylation of Eco1 [105]. This phosphorylation greatly enhances the targeting of Eco1 to the SCF^{Cdc4} ubiquitin ligase complex, leading to the degradation of Eco1 [106]. There is one notable exception: in response to DNA damage, Eco1 is stabilized, and cohesin complexes need to be loaded at the sites of DNA damage for a proper DNA damage response [107–109]. Therefore, in the absence of DNA damage, chromosome cohesion must be maintained on chromosomes after DNA replication, since Eco1 is not available to reestablish cohesion.

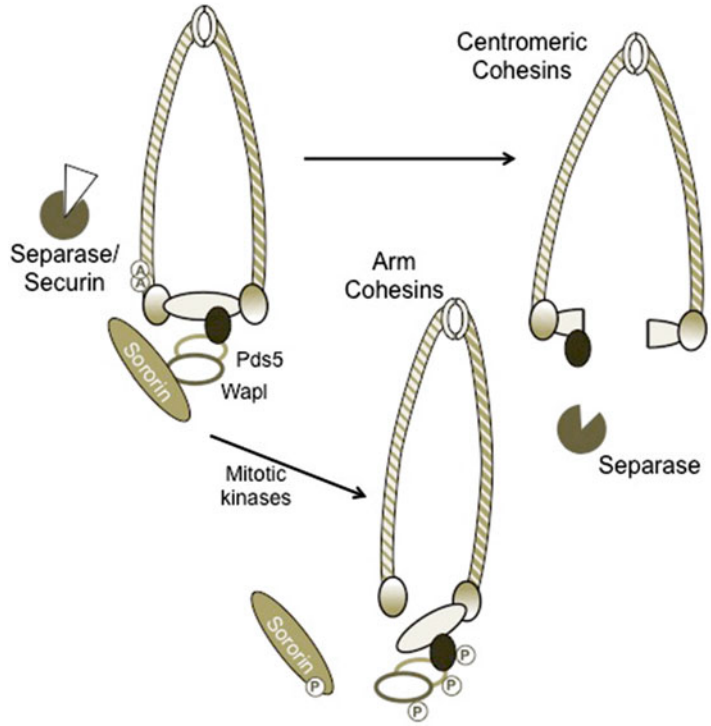

Fig. 4 The cohesin complex is opened by two mechanisms at mitosis. G2 cohesins are stabilized and protected from dissociation and complex opening. On chromosome arms, mitotic kinases phosphorylate multiple targets, reducing Sororin inhibition of Wapl and opening the cohesion complex at the Smc3–Scc1 interface. At centromeres and pericentromeres, the APC destroys securin, activating separase and leading to Scc1 degradation and complex opening

After DNA replication, cohesin complexes are rendered far more stable on chromatin than prior to S phase. FRAP studies in both yeast and humans show that the turnover of cohesin complexes on chromatin is greatly reduced in G2 [36, 50, 110]. In human cells perhaps one-third of cohesin complexes are stably associated with chromatin for the duration of G2 phase, a dramatic increase from the ~25-min residence time of G1 cohesin complexes [50]. In this state, cohesins stably pair sister chromatids until mitosis where the process of removing cohesin complexes is highly regulated (Fig. 4).

How is then cohesion maintained? It appears that Smc3 acetylation has a key role in this mechanism. Major factors involved in cohesion maintenance include Scc3 and Pds5. In the absence of functional Scc3 or Pds5, the levels of cohesin on DNA are reduced [18, 111]. As described below, Pds5 appears to protect Smc3 from deacetylation by Hos1/HDAC8 deacetylase during G2 phase through early mitosis. Since cohesion maintenance and subsequent cohesin removal are tightly coordinated,

the mechanisms that stabilize cohesin complexes on chromatin must be efficiently deactivated to facilitate removal of cohesin complexes during mitosis.

Cohesin complexes distributed over each chromatid pair in the eukaryotic genome must be disassembled at the proper time every cell cycle. The dismantling of cohesion completes the task of the cohesin complexes that pair the sister chromatids until they are separated equally to two daughter cells. Two distinct processes are initiated during mitosis to remove cohesin complexes (Fig. 4). First, during prophase and metaphase much of the cohesin complexes localized to chromosome arms are released. This action is followed by destroying cohesin complexes at pericentromeric regions at the metaphase–anaphase transition, allowing the segregation of sister chromatids to opposing poles. Together, these processes remove all functional cohesin complexes from the DNA.

First, removal of cohesin complexes from the chromosome arms requires the antiestablishment factor Wapl [59, 60]. Interestingly, Wapl-mediated alleviation of cohesion does not require degradation of cohesins, whereas later stage cohesin removal does. Instead, Wapl-associated cohesin removal involves opening of the cohesin complex at the Smc3–Scc1 interface [112]. This is counteracted by Smc3 acetylation, which represses Wapl-mediated cohesin opening [112, 113]. Therefore, maintaining Smc3 acetylation is vital to preserving cohesion until prometaphase. By preventing the Wapl-dependent cohesin opening, Pds5, in concert with Scc3, protects Smc3 acetylation from a deacetylase known as HDAC8 (Hos1 in budding yeast) [114].

It appears that the concerted effort of several kinases on cohesin complexes effectively deactivate the protective activity of Pds5 and Sororin, the latter of which stabilizes acetylated cohesins by counteracting Wapl activity [63, 65, 115, 116]. Consistent with this idea, phosphorylation of SA2 (Scc3 ortholog) is required for the dissociation of cohesins during prophase and prometaphase [117]. Mitotic cyclin–CDK complexes phosphorylate *Xenopus* XSA1/2 (Scc3 orthologs) in vitro [19]. Plk1 activity is required for alleviation of cohesion during mitosis, where *Xenopus* Scc3 orthologs are phosphorylated in a Plk1-dependent manner [118]. Furthermore, proteomics approaches indicate that both Pds5 and Wapl are phosphorylated by mitotic kinases [116]. Sororin-dependent antagonization of Wapl is also regulated by mitotic kinases. During mitosis, aurora B and cyclin–CDK complexes phosphorylate Sororin, thus freeing Wapl from its inhibition [119]. From these studies, one could imagine a mechanism by which mitotic kinases further stimulate Wapl activity (by removal of Sororin) while deactivating Pds5 to allow deacetylation of Smc3 and opening of cohesin complexes. It is also possible that phosphorylation of cohesin complexes promotes Smc3 deacetylation (Fig. 4). These actions lead to robust cohesin complex release from DNA on chromosome arms.

Interestingly, the process of cohesin removal at centromeric/pericentromeric regions is Wapl independent. The centromeric regions of sister chromosomes are protected during metaphase by the Shugoshin (Sgo1) protein [120]. When SA2 mitotic phosphorylation-site mutants were expressed, cohesion defects and the mitotic arrest phonotype of Sgo1-deficient cells were alleviated, suggesting that Shugoshin prevents phosphorylation of Scc3 to preserve cohesion until Shugoshin is destroyed [121]. Indeed, Shugoshin is activated by mitotic cyclin–CDK activity and associates with centromeres during mitosis [122]. At the centromere, Shugoshin recruits PP2A, a phosphatase that prevents the phospho-regulation of cohesin subunits [123]. The localization of PP2A to centromeres prevents the Wapl-mediated mechanism of cohesin removal by preventing phosphorylation of key cohesin components. Therefore, another mechanism must control cohesin removal at the centromeric and pericentromeric regions of chromosomes.

Sister chromatid separation should ideally occur during anaphase as this is when sister chromosomes migrate to opposite poles of the mitotic spindle. Cohesion of chromosome arms is removed before the metaphase–anaphase transition, leaving only centromeric cohesion to tether sister chromatids to each other. This leaves a relatively small area of each chromosome held by cohesins left to remove. At the onset of anaphase, the Scc1 subunit of the tripartite cohesin complex undergoes a proteolytic cleavage by a protein known as separin or separase [124, 125]. The separin protein is bound and rendered inactive by securin, preventing premature activity [126, 127]. Securin is a target of the anaphase-promoting complex (APC), a ubiquitin ligase complex that becomes active at the metaphase–anaphase transition [128, 129]. Securin has been characterized as one of the major targets (along with the mitotic cyclin) for the APC^{Cdc20} complex in yeast cell-cycle regulation [130]. Once securin is degraded, separin/separase is free to cleave Scc1 and relieve chromosome cohesion, allowing sister chromatids to be pulled to their respective poles by the mitotic microtubule spindle (Fig. 4). At this point, chromosomes are unpaired and free of cohesin complexes. Prior to the next DNA replication round, cohesins are loaded again and the cycle is iterated.

7 Cohesinopathies: Broken Rings That Compromise Genomic Integrity

The regulation of genetic inheritance is critical for the reproductive and cellular health of humans. Although not discussed in this review, meiotic chromosome cohesion uses a similar mechanism to that of mitotic sister chromatid cohesion, and failure to properly pair chromosomes during meiosis can lead to trisomy disorders such as Downs, Edwards, or Patau syndromes [131]. However, most types of aneuploidy are incompatible with development.

In analyses of human spontaneous abortions, it has been observed that over 35 % are trisomic or monosomic [132]. It has been proposed that this high rate of chromosomal abnormalities is due to chromosome cohesion defects during meiosis, probably due to the fact that cohesion must be maintained for many years in human oocytes (reviewed in ref. 133).

Autosomal or spontaneous mutations in the cohesion establishment and maintenance pathways can also lead to syndromes in humans that are collectively known as cohesinopathies. The severity of these disorders underlines the importance of maintaining proper sister chromosome cohesion during development and cell proliferation in tissue maintenance. Cornelia de Lange syndrome (CdLS) is a human disease characterized by short stature, craniofacial/limb abnormalities, seizures, and mental retardation. In addition, many CdLS patients die of gastrointestinal problems or pneumonia, suggesting immune-system problems in these patients [134]. CdLS is caused by mutations in cohesion proteins NIPBL (the human Scc2 homolog), Smc1, or Smc3 [135–138]. Mutations in NIPBL, the cohesin loader, have a stronger effect and lead to a more serious form of CdLS. Recently, mutations in HDAC8, the Smc3 deacetylase, have also been identified in some CdLS patients with previously uncharacterized mutations [139].

Interestingly, cells derived from CdLS patients display strong sensitivity to DNA-damaging agents [140]. This suggests that some phenotypes of the disease could result from improper DNA repair responses, yet most CdLS patients do not have increased tumor incidence. Roberts syndrome has a similar clinical presentation to CdLS, although it is caused by mutations in Esco2 acetyltransferase [141].

A recently characterized disease, Warsaw breakage syndrome (WABS), has been attributed to the loss of functional DDX11/ChlR1 DNA helicase, which plays a critical role during S phase to establish proper sister chromatid cohesion [101, 102, 142, 143]. Mutations to both alleles of the *DDX11/CHLR1* gene lead to WABS, which is characterized by severe developmental defects, including microcephaly, growth and mental retardation, and facial dysmorphy [143]. The first WABS patient was reported to carry biallelic mutations in the *DDX11/CHLR1* gene, including a splice-site mutation and a carboxyl-terminal deletion [143]. More recently, a new homozygous mutation in *DDX11/CHLR1* was identified in siblings with many of the symptoms associated with WABS, confirming the role of *DDX11/CHLR1* mutations in WABS [144]. Interestingly, the phenotypic presentation of WABS is a combination of those seen in patients with mutations in cohesion establishment proteins (such as Roberts syndrome or CdLS) and in Fanconi anemia pathway, which plays a critical role in the repair of DNA interstrand cross-links during DNA replication [145], further confirming the role of DDX11/ChlR1 in sister chromatid cohesion during S phase.

The processes of cohesin establishment, maintenance, and dissolution are tightly regulated through the cell cycle. The ability to coordinate chromosome cohesion with DNA replication is critical for proper sister chromatid pairing during S phase, thereby allowing for their equal segregation at mitosis. Unlocking these mechanisms is an important research focus of genome maintenance mechanisms. However, much work remains to understand how the processes occurring at the replication fork are linked to cohesin complexes. Importantly, CdLS cells have increased genotoxic sensitivity [140], and WABS cells show combined phenotypes of Fanconi anemia and the cohesinopathies, including abnormal chromosome segregation and sensitivities to interstrand crosslinking agents [143]. These findings indicate the inseparable connection between sister chromatid cohesion and DNA replication/repair pathways. By studying the mechanisms of these diseases and developing possible therapeutic strategies, we will have a unique opportunity to further characterize the complicated interplay between DNA replication and cohesion processes.

Acknowledgments

This work was supported in part by NIH grants (AG035480 to A.R.L. and GM0776043 to E.N.).

References

1. Hirano T (2002) The ABCs of SMC proteins: two-armed ATPases for chromosome condensation, cohesion, and repair. Genes Dev 16(4): 399–414
2. Haering CH, Lowe J, Hochwagen A, Nasmyth K (2002) Molecular architecture of SMC proteins and the yeast cohesin complex. Mol Cell 9(4):773–788
3. Hirano T, Mitchison TJ (1994) A heterodimeric coiled-coil protein required for mitotic chromosome condensation in vitro. Cell 79(3): 449–458
4. Hirano T, Kobayashi R, Hirano M (1997) Condensins, chromosome condensation protein complexes containing XCAP-C, XCAP-E and a Xenopus homolog of the Drosophila Barren protein. Cell 89(4):511–521
5. Fousteri MI, Lehmann AR (2000) A novel SMC protein complex in *Schizosaccharomyces pombe* contains the Rad18 DNA repair protein. EMBO J 19(7):1691–1702
6. Taylor EM, Moghraby JS, Lees JH, Smit B, Moens PB, Lehmann AR (2001) Characterization of a novel human SMC heterodimer homologous to the *Schizosaccharomyces pombe* Rad18/Spr18 complex. Mol Biol Cell 12(6): 1583–1594
7. Verkade HM, Bugg SJ, Lindsay HD, Carr AM, O'Connell MJ (1999) Rad18 is required for DNA repair and checkpoint responses in fission yeast. Mol Biol Cell 10(9):2905–2918
8. Usui T, Ohta T, Oshiumi H, Tomizawa J, Ogawa H, Ogawa T (1998) Complex formation and functional versatility of Mre11 of budding yeast in recombination. Cell 95(5): 705–716
9. Cobbe N, Heck MM (2000) Review: SMCs in the world of chromosome biology—from prokaryotes to higher eukaryotes. J Struct Biol 129(2–3):123–143
10. Hirano M, Hirano T (2006) Opening closed arms: long-distance activation of SMC ATPase by hinge-DNA interactions. Mol Cell 21(2): 175–186
11. Melby TE, Ciampaglio CN, Briscoe G, Erickson HP (1998) The symmetrical structure of structural maintenance of chromosomes (SMC) and MukB proteins: long,

antiparallel coiled coils, folded at a flexible hinge. J Cell Biol 142(6):1595–1604

12. Furuya K, Takahashi K, Yanagida M (1998) Faithful anaphase is ensured by Mis4, a sister chromatid cohesion molecule required in S phase and not destroyed in G1 phase. Genes Dev 12(21):3408–3418
13. Haering CH, Schoffnegger D, Nishino T, Helmhart W, Nasmyth K, Lowe J (2004) Structure and stability of cohesin's Smc1-kleisin interaction. Mol Cell 15(6):951–964
14. Schleiffer A, Kaitna S, Maurer-Stroh S, Glotzer M, Nasmyth K, Eisenhaber F (2003) Kleisins: a superfamily of bacterial and eukaryotic SMC protein partners. Mol Cell 11(3):571–575
15. Parelho V, Hadjur S, Spivakov M, Leleu M, Sauer S, Gregson HC, Jarmuz A, Canzonetta C, Webster Z, Nesterova T, Cobb BS, Yokomori K, Dillon N, Aragon L, Fisher AG, Merkenschlager M (2008) Cohesins functionally associate with CTCF on mammalian chromosome arms. Cell 132(3):422–433
16. Wendt KS, Yoshida K, Itoh T, Bando M, Koch B, Schirghuber E, Tsutsumi S, Nagae G, Ishihara K, Mishiro T, Yahata K, Imamoto F, Aburatani H, Nakao M, Imamoto N, Maeshima K, Shirahige K, Peters JM (2008) Cohesin mediates transcriptional insulation by CCCTC-binding factor. Nature 451(7180):796–801
17. Klein F, Mahr P, Galova M, Buonomo SB, Michaelis C, Nairz K, Nasmyth K (1999) A central role for cohesins in sister chromatid cohesion, formation of axial elements, and recombination during yeast meiosis. Cell 98(1):91–103
18. Toth A, Ciosk R, Uhlmann F, Galova M, Schleiffer A, Nasmyth K (1999) Yeast cohesin complex requires a conserved protein, Eco1p (Ctf7), to establish cohesion between sister chromatids during DNA replication. Genes Dev 13(3):320–333
19. Losada A, Yokochi T, Kobayashi R, Hirano T (2000) Identification and characterization of SA/Scc3p subunits in the Xenopus and human cohesin complexes. J Cell Biol 150(3):405–416
20. Kurlandzka A, Rytka J, Gromadka R, Murawski M (1995) A new essential gene located on *Saccharomyces cerevisiae* chromosome IX. Yeast 11(9):885–890
21. Zhang N, Jiang Y, Mao Q, Demeler B, Tao YJ, Pati D (2013) Characterization of the interaction between the cohesin subunits Rad21 and SA1/2. PLoS One 8(7):e69458
22. Gruber S, Haering CH, Nasmyth K (2003) Chromosomal cohesin forms a ring. Cell 112(6):765–777
23. Nasmyth K (2011) Cohesin: a catenase with separate entry and exit gates? Nat Cell Biol 13(10):1170–1177
24. Huang CE, Milutinovich M, Koshland D (2005) Rings, bracelet or snaps: fashionable alternatives for Smc complexes. Philos Trans R Soc Lond B Biol Sci 360(1455):537–542
25. Zhang N, Kuznetsov SG, Sharan SK, Li K, Rao PH, Pati D (2008) A handcuff model for the cohesin complex. J Cell Biol 183(6):1019–1031
26. Zhang N, Pati D (2009) Handcuff for sisters: a new model for sister chromatid cohesion. Cell Cycle 8(3):399–402
27. Haering CH, Farcas AM, Arumugam P, Metson J, Nasmyth K (2008) The cohesin ring concatenates sister DNA molecules. Nature 454(7202):297–301
28. Ciosk R, Shirayama M, Shevchenko A, Tanaka T, Toth A, Shevchenko A, Nasmyth K (2000) Cohesin's binding to chromosomes depends on a separate complex consisting of Scc2 and Scc4 proteins. Mol Cell 5(2):243–254
29. Arumugam P, Gruber S, Tanaka K, Haering CH, Mechtler K, Nasmyth K (2003) ATP hydrolysis is required for cohesin's association with chromosomes. Curr Biol 13(22):1941–1953
30. Weitzer S, Lehane C, Uhlmann F (2003) A model for ATP hydrolysis-dependent binding of cohesin to DNA. Curr Biol 13(22):1930–1940
31. Hu B, Itoh T, Mishra A, Katoh Y, Chan KL, Upcher W, Godlee C, Roig MB, Shirahige K, Nasmyth K (2011) ATP hydrolysis is required for relocating cohesin from sites occupied by its Scc2/4 loading complex. Curr Biol 21(1):12–24
32. Gruber S, Arumugam P, Katou Y, Kuglitsch D, Helmhart W, Shirahige K, Nasmyth K (2006) Evidence that loading of cohesin onto chromosomes involves opening of its SMC hinge. Cell 127(3):523–537
33. Anderson DE, Trujillo KM, Sung P, Erickson HP (2001) Structure of the Rad50×Mre11 DNA repair complex from *Saccharomyces cerevisiae* by electron microscopy. J Biol Chem 276(40):37027–37033
34. Williams GJ, Lees-Miller SP, Tainer JA (2010) Mre11-Rad50-Nbs1 conformations and the control of sensing, signaling, and effector responses at DNA double-strand breaks. DNA Repair (Amst) 9(12):1299–1306

35. Hopfner KP, Karcher A, Shin DS, Craig L, Arthur LM, Carney JP, Tainer JA (2000) Structural biology of Rad50 ATPase: ATP-driven conformational control in DNA double-strand break repair and the ABC-ATPase superfamily. Cell 101(7):789–800
36. Mishra A, Hu B, Kurze A, Beckouet F, Farcas AM, Dixon SE, Katou Y, Khalid S, Shirahige K, Nasmyth K (2010) Both interaction surfaces within cohesin's hinge domain are essential for its stable chromosomal association. Curr Biol 20(4):279–289
37. Lengronne A, Katou Y, Mori S, Yokobayashi S, Kelly GP, Itoh T, Watanabe Y, Shirahige K, Uhlmann F (2004) Cohesin relocation from sites of chromosomal loading to places of convergent transcription. Nature 430(6999): 573–578
38. Gillespie PJ, Hirano T (2004) Scc2 couples replication licensing to sister chromatid cohesion in Xenopus egg extracts. Curr Biol 14(17):1598–1603
39. Takahashi TS, Yiu P, Chou MF, Gygi S, Walter JC (2004) Recruitment of Xenopus Scc2 and cohesin to chromatin requires the pre-replication complex. Nat Cell Biol 6(10): 991–996
40. Fernius J, Marston AL (2009) Establishment of cohesion at the pericentromere by the Ctf19 kinetochore subcomplex and the replication fork-associated factor, Csm3. PLoS Genet 5(9):e1000629
41. Takahashi TS, Basu A, Bermudez V, Hurwitz J, Walter JC (2008) Cdc7-Drf1 kinase links chromosome cohesion to the initiation of DNA replication in Xenopus egg extracts. Genes Dev 22(14):1894–1905
42. Schmidt CK, Brookes N, Uhlmann F (2009) Conserved features of cohesin binding along fission yeast chromosomes. Genome Biol 10(5):R52
43. Kagey MH, Newman JJ, Bilodeau S, Zhan Y, Orlando DA, van Berkum NL, Ebmeier CC, Goossens J, Rahl PB, Levine SS, Taatjes DJ, Dekker J, Young RA (2010) Mediator and cohesin connect gene expression and chromatin architecture. Nature 467(7314):430–435
44. Schmidt D, Schwalie PC, Ross-Innes CS, Hurtado A, Brown GD, Carroll JS, Flicek P, Odom DT (2010) A CTCF-independent role for cohesin in tissue-specific transcription. Genome Res 20(5):578–588
45. Misulovin Z, Schwartz YB, Li XY, Kahn TG, Gause M, MacArthur S, Fay JC, Eisen MB, Pirrotta V, Biggin MD, Dorsett D (2008) Association of cohesin and Nipped-B with transcriptionally active regions of the *Drosophila melanogaster* genome. Chromosoma 117(1): 89–102
46. Lee BK, Iyer VR (2012) Genome-wide studies of CCCTC-binding factor (CTCF) and cohesin provide insight into chromatin structure and regulation. J Biol Chem 287(37):30906–30913
47. Xiao T, Wallace J, Felsenfeld G (2011) Specific sites in the C terminus of CTCF interact with the SA2 subunit of the cohesin complex and are required for cohesin-dependent insulation activity. Mol Cell Biol 31(11):2174–2183
48. Uhlmann F, Nasmyth K (1998) Cohesion between sister chromatids must be established during DNA replication. Curr Biol 8(20): 1095–1101
49. Lengronne A, McIntyre J, Katou Y, Kanoh Y, Hopfner KP, Shirahige K, Uhlmann F (2006) Establishment of sister chromatid cohesion at the *S. cerevisiae* replication fork. Mol Cell 23(6):787–799
50. Gerlich D, Koch B, Dupeux F, Peters JM, Ellenberg J (2006) Live-cell imaging reveals a stable cohesin-chromatin interaction after but not before DNA replication. Curr Biol 16(15): 1571–1578
51. Skibbens RV, Corson LB, Koshland D, Hieter P (1999) Ctf7p is essential for sister chromatid cohesion and links mitotic chromosome structure to the DNA replication machinery. Genes Dev 13(3):307–319
52. Hou F, Zou H (2005) Two human orthologues of Eco1/Ctf7 acetyltransferases are both required for proper sister-chromatid cohesion. Mol Biol Cell 16(8):3908–3918
53. Williams BC, Garrett-Engele CM, Li Z, Williams EV, Rosenman ED, Goldberg ML (2003) Two putative acetyltransferases, san and deco, are required for establishing sister chromatid cohesion in Drosophila. Curr Biol 13(23):2025–2036
54. Bellows AM, Kenna MA, Cassimeris L, Skibbens RV (2003) Human EFO1p exhibits acetyltransferase activity and is a unique combination of linker histone and Ctf7p/Eco1p chromatid cohesion establishment domains. Nucleic Acids Res 31(21):6334–6343
55. Ben-Shahar T, Heeger S, Lehane C, East P, Flynn H, Skehel M, Uhlmann F (2008) Eco1-dependent cohesin acetylation during establishment of sister chromatid cohesion. Science 321(5888):563–566
56. Unal E, Heidinger-Pauli JM, Kim W, Guacci V, Onn I, Gygi SP, Koshland DE (2008) A molecular determinant for the establishment

of sister chromatid cohesion. Science 321 (5888): 566–569

57. Zhang J, Shi X, Li Y, Kim BJ, Jia J, Huang Z, Yang T, Fu X, Jung SY, Wang Y, Zhang P, Kim ST, Pan X, Qin J (2008) Acetylation of Smc3 by Eco1 is required for S phase sister chromatid cohesion in both human and yeast. Mol Cell 31(1):143–151
58. Heidinger-Pauli JM, Onn I, Koshland D (2010) Genetic evidence that the acetylation of the Smc3p subunit of cohesin modulates its ATP-bound state to promote cohesion establishment in *Saccharomyces cerevisiae*. Genetics 185(4):1249–1256
59. Kueng S, Hegemann B, Peters BH, Lipp JJ, Schleiffer A, Mechtler K, Peters JM (2006) Wapl controls the dynamic association of cohesin with chromatin. Cell 127(5): 955–967
60. Gandhi R, Gillespie PJ, Hirano T (2006) Human Wapl is a cohesin-binding protein that promotes sister-chromatid resolution in mitotic prophase. Curr Biol 16(24):2406–2417
61. Rowland BD, Roig MB, Nishino T, Kurze A, Uluocak P, Mishra A, Beckouet F, Underwood P, Metson J, Imre R, Mechtler K, Katis VL, Nasmyth K (2009) Building sister chromatid cohesion: smc3 acetylation counteracts an antiestablishment activity. Mol Cell 33(6): 763–774
62. Sutani T, Kawaguchi T, Kanno R, Itoh T, Shirahige K (2009) Budding yeast Wpl1 (Rad61)-Pds5 complex counteracts sister chromatid cohesion-establishing reaction. Curr Biol 19(6):492–497
63. Rankin S, Ayad NG, Kirschner MW (2005) Sororin, a substrate of the anaphase-promoting complex, is required for sister chromatid cohesion in vertebrates. Mol Cell 18(2):185–200
64. Schmitz J, Watrin E, Lenart P, Mechtler K, Peters JM (2007) Sororin is required for stable binding of cohesin to chromatin and for sister chromatid cohesion in interphase. Curr Biol 17(7):630–636
65. Nishiyama T, Ladurner R, Schmitz J, Kreidl E, Schleiffer A, Bhaskara V, Bando M, Shirahige K, Hyman AA, Mechtler K, Peters JM (2010) Sororin mediates sister chromatid cohesion by antagonizing Wapl. Cell 143(5): 737–749
66. Terret ME, Sherwood R, Rahman S, Qin J, Jallepalli PV (2009) Cohesin acetylation speeds the replication fork. Nature 462(7270): 231–234
67. Ivanov D, Schleiffer A, Eisenhaber F, Mechtler K, Haering CH, Nasmyth K (2002) Eco1 is a novel acetyltransferase that can acetylate proteins involved in cohesion. Curr Biol 12(4):323–328
68. Moldovan GL, Pfander B, Jentsch S (2006) PCNA controls establishment of sister chromatid cohesion during S phase. Mol Cell 23(5):723–732
69. Moldovan GL, Pfander B, Jentsch S (2007) PCNA, the maestro of the replication fork. Cell 129(4):665–679
70. Majka J, Burgers PM (2004) The PCNA-RFC families of DNA clamps and clamp loaders. Prog Nucleic Acid Res Mol Biol 78: 227–260
71. Formosa T, Nittis T (1999) Dna2 mutants reveal interactions with Dna polymerase alpha and Ctf4, a Pol alpha accessory factor, and show that full Dna2 helicase activity is not essential for growth. Genetics 151(4): 1459–1470
72. Hanna JS, Kroll ES, Lundblad V, Spencer FA (2001) *Saccharomyces cerevisiae* CTF18 and CTF4 are required for sister chromatid cohesion. Mol Cell Biol 21(9):3144–3158
73. Mayer ML, Gygi SP, Aebersold R, Hieter P (2001) Identification of RFC(Ctf18p, Ctf8p, Dcc1p): an alternative RFC complex required for sister chromatid cohesion in *S. cerevisiae*. Mol Cell 7(5):959–970
74. Naiki T, Kondo T, Nakada D, Matsumoto K, Sugimoto K (2001) Chl12 (Ctf18) forms a novel replication factor C-related complex and functions redundantly with Rad24 in the DNA replication checkpoint pathway. Mol Cell Biol 21(17):5838–5845
75. Bermudez VP, Maniwa Y, Tappin I, Ozato K, Yokomori K, Hurwitz J (2003) The alternative Ctf18-Dcc1-Ctf8-replication factor C complex required for sister chromatid cohesion loads proliferating cell nuclear antigen onto DNA. Proc Natl Acad Sci U S A 100 (18):10237–10242
76. Xu H, Boone C, Klein HL (2004) Mrc1 is required for sister chromatid cohesion to aid in recombination repair of spontaneous damage. Mol Cell Biol 24(16):7082–7090
77. Katou Y, Kanoh Y, Bando M, Noguchi H, Tanaka H, Ashikari T, Sugimoto K, Shirahige K (2003) S-phase checkpoint proteins Tof1 and Mrc1 form a stable replication-pausing complex. Nature 424(6952):1078–1083
78. Lou H, Komata M, Katou Y, Guan Z, Reis CC, Budd M, Shirahige K, Campbell JL (2008) Mrc1 and DNA polymerase epsilon function together in linking DNA replication and the S phase checkpoint. Mol Cell 32(1): 106–117

79. Gambus A, van Deursen F, Polychronopoulos D, Foltman M, Jones RC, Edmondson RD, Calzada A, Labib K (2009) A key role for Ctf4 in coupling the MCM2-7 helicase to DNA polymerase alpha within the eukaryotic replisome. EMBO J 28(19):2992–3004
80. Zhu W, Ukomadu C, Jha S, Senga T, Dhar SK, Wohlschlegel JA, Nutt LK, Kornbluth S, Dutta A (2007) Mcm10 and And-1/CTF4 recruit DNA polymerase alpha to chromatin for initiation of DNA replication. Genes Dev 21(18): 2288–2299
81. Tanaka H, Katou Y, Yagura M, Saitoh K, Itoh T, Araki H, Bando M, Shirahige K (2009) Ctf4 coordinates the progression of helicase and DNA polymerase alpha. Genes Cells 14(7): 807–820
82. Bermudez VP, Farina A, Tappin I, Hurwitz J (2010) Influence of the human cohesion establishment factor Ctf4/AND-1 on DNA replication. J Biol Chem 285(13):9493–9505
83. Leman AR, Noguchi E (2012) Local and global functions of Timeless and Tipin in replication fork protection. Cell Cycle 11(21):3945–3955
84. Mayer ML, Pot I, Chang M, Xu H, Aneliunas V, Kwok T, Newitt R, Aebersold R, Boone C, Brown GW, Hieter P (2004) Identification of protein complexes required for efficient sister chromatid cohesion. Mol Biol Cell 15(4): 1736–1745
85. Warren CD, Eckley DM, Lee MS, Hanna JS, Hughes A, Peyser B, Jie C, Irizarry R, Spencer FA (2004) S-phase checkpoint genes safeguard high-fidelity sister chromatid cohesion. Mol Biol Cell 15(4):1724–1735
86. Ansbach AB, Noguchi C, Klansek IW, Heidlebaugh M, Nakamura TM, Noguchi E (2008) RFC^{Ctf18} and the Swi1-Swi3 complex function in separate and redundant pathways required for the stabilization of replication forks to facilitate sister chromatid cohesion in *Schizosaccharomyces pombe*. Mol Biol Cell 19(2):595–607
87. Errico A, Cosentino C, Rivera T, Losada A, Schwob E, Hunt T, Costanzo V (2009) Tipin/Tim1/And1 protein complex promotes Pol alpha chromatin binding and sister chromatid cohesion. EMBO J 28(23):3681–3692
88. Tanaka H, Kubota Y, Tsujimura T, Kumano M, Masai H, Takisawa H (2009) Replisome progression complex links DNA replication to sister chromatid cohesion in Xenopus egg extracts. Genes Cells 14(8):949–963
89. Leman AR, Noguchi C, Lee CY, Noguchi E (2010) Human Timeless and Tipin stabilize replication forks and facilitate sister-chromatid cohesion. J Cell Sci 123(Pt 5):660–670
90. Dheekollu J, Wiedmer A, Hayden J, Speicher D, Gotter AL, Yen T, Lieberman PM (2011) Timeless links replication termination to mitotic kinase activation. PLoS One 6(5): e19596
91. Smith-Roe SL, Patel SS, Simpson DA, Zhou YC, Rao S, Ibrahim JG, Kaiser-Rogers KA, Cordeiro-Stone M, Kaufmann WK (2011) Timeless functions independently of the Tim-Tipin complex to promote sister chromatid cohesion in normal human fibroblasts. Cell Cycle 10(10):1618–1624
92. Sommariva E, Pellny TK, Karahan N, Kumar S, Huberman JA, Dalgaard JZ (2005) *Schizosaccharomyces pombe* Swi1, Swi3, and Hsk1 are components of a novel S-phase response pathway to alkylation damage. Mol Cell Biol 25(7):2770–2784
93. Noguchi E, Noguchi C, McDonald WH, Yates JR 3rd, Russell P (2004) Swi1 and Swi3 are components of a replication fork protection complex in fission yeast. Mol Cell Biol 24(19):8342–8355
94. Liu Y, Kao HI, Bambara RA (2004) Flap endonuclease 1: a central component of DNA metabolism. Annu Rev Biochem 73: 589–615
95. Rudra S, Skibbens RV (2012) Sister chromatid cohesion establishment occurs in concert with lagging strand synthesis. Cell Cycle 11(11):2114–2121
96. Farina A, Shin JH, Kim DH, Bermudez VP, Kelman Z, Seo YS, Hurwitz J (2008) Studies with the human cohesin establishment factor, ChlR1. Association of ChlR1 with Ctf18-RFC and Fen1. J Biol Chem 283(30): 20925–20936
97. Wu Y, Suhasini AN, Brosh RM Jr (2009) Welcome the family of FANCJ-like helicases to the block of genome stability maintenance proteins. Cell Mol Life Sci 66(7):1209–1222
98. Holloway SL, Poruthu J, Scata K (1999) Chromosome segregation and cancer. Exp Cell Res 253(2):308–314
99. Petronczki M, Chwalla B, Siomos MF, Yokobayashi S, Helmhart W, Deutschbauer AM, Davis RW, Watanabe Y, Nasmyth K (2004) Sister-chromatid cohesion mediated by the alternative RF-CCtf18/Dcc1/Ctf8, the helicase Chl1 and the polymerase-alpha-associated protein Ctf4 is essential for chromatid disjunction during meiosis II. J Cell Sci 117(Pt 16):3547–3559
100. Skibbens RV (2004) Chl1p, a DNA helicase-like protein in budding yeast, functions in sister-chromatid cohesion. Genetics 166(1):33–42
101. Parish JL, Rosa J, Wang X, Lahti JM, Doxsey SJ, Androphy EJ (2006) The DNA helicase

ChlR1 is required for sister chromatid cohesion in mammalian cells. J Cell Sci 119(Pt 23): 4857–4865

102. Shah N, Inoue A, Woo Lee S, Beishline K, Lahti JM, Noguchi E (2013) Roles of ChlR1 DNA helicase in replication recovery from DNA damage. Exp Cell Res 319(14): 2244–2253
103. Sherwood R, Takahashi TS, Jallepalli PV (2010) Sister acts: coordinating DNA replication and cohesion establishment. Genes Dev 24(24):2723–2731
104. Onn I, Heidinger-Pauli JM, Guacci V, Unal E, Koshland DE (2008) Sister chromatid cohesion: a simple concept with a complex reality. Annu Rev Cell Dev Biol 24:105–129
105. Lyons NA, Morgan DO (2011) Cdk1-dependent destruction of Eco1 prevents cohesion establishment after S phase. Mol Cell 42(3):378–389
106. Lyons NA, Fonslow BR, Diedrich JK, Yates JR 3rd, Morgan DO (2013) Sequential primed kinases create a damage-responsive phosphodegron on Eco1. Nat Struct Mol Biol 20(2):194–201
107. Unal E, Heidinger-Pauli JM, Koshland D (2007) DNA double-strand breaks trigger genome-wide sister-chromatid cohesion through Eco1 (Ctf7). Science 317(5835): 245–248
108. Strom L, Karlsson C, Lindroos HB, Wedahl S, Katou Y, Shirahige K, Sjogren C (2007) Postreplicative formation of cohesion is required for repair and induced by a single DNA break. Science 317(5835):242–245
109. Strom L, Lindroos HB, Shirahige K, Sjogren C (2004) Postreplicative recruitment of cohesin to double-strand breaks is required for DNA repair. Mol Cell 16(6):1003–1015
110. Kurze A, Michie KA, Dixon SE, Mishra A, Itoh T, Khalid S, Strmecki L, Shirahige K, Haering CH, Lowe J, Nasmyth K (2011) A positively charged channel within the Smc1/Smc3 hinge required for sister chromatid cohesion. EMBO J 30(2):364–378
111. Panizza S, Tanaka T, Hochwagen A, Eisenhaber F, Nasmyth K (2000) Pds5 cooperates with cohesin in maintaining sister chromatid cohesion. Curr Biol 10(24): 1557–1564
112. Chan KL, Roig MB, Hu B, Beckouet F, Metson J, Nasmyth K (2012) Cohesin's DNA exit gate is distinct from its entrance gate and is regulated by acetylation. Cell 150(5): 961–974
113. Lopez-Serra L, Lengronne A, Borges V, Kelly G, Uhlmann F (2013) Budding yeast Wapl controls sister chromatid cohesion maintenance and chromosome condensation. Curr Biol 23(1):64–69
114. Chan KL, Gligoris T, Upcher W, Kato Y, Shirahige K, Nasmyth K, Beckouet F (2013) Pds5 promotes and protects cohesin acetylation. Proc Natl Acad Sci U S A 110: 13020–13025
115. Albuquerque CP, Smolka MB, Payne SH, Bafna V, Eng J, Zhou H (2008) A multidimensional chromatography technology for in-depth phosphoproteome analysis. Mol Cell Proteomics 7(7):1389–1396
116. Hegemann B, Hutchins JR, Hudecz O, Novatchkova M, Rameseder J, Sykora MM, Liu S, Mazanek M, Lenart P, Heriche JK, Poser I, Kraut N, Hyman AA, Yaffe MB, Mechtler K, Peters JM (2011) Systematic phosphorylation analysis of human mitotic protein complexes. Sci Signal 4(198):rs12
117. Hauf S, Roitinger E, Koch B, Dittrich CM, Mechtler K, Peters JM (2005) Dissociation of cohesin from chromosome arms and loss of arm cohesion during early mitosis depends on phosphorylation of SA2. PLoS Biol 3(3):e69
118. Sumara I, Vorlaufer E, Stukenberg PT, Kelm O, Redemann N, Nigg EA, Peters JM (2002) The dissociation of cohesin from chromosomes in prophase is regulated by Polo-like kinase. Mol Cell 9(3):515–525
119. Nishiyama T, Sykora MM, Huis In 't Veld PJ, Mechtler K, Peters JM (2013) Aurora B and Cdk1 mediate Wapl activation and release of acetylated cohesin from chromosomes by phosphorylating Sororin. Proc Natl Acad Sci U S A 110:13404–13409
120. Salic A, Waters JC, Mitchison TJ (2004) Vertebrate shugoshin links sister centromere cohesion and kinetochore microtubule stability in mitosis. Cell 118(5):567–578
121. McGuinness BE, Hirota T, Kudo NR, Peters JM, Nasmyth K (2005) Shugoshin prevents dissociation of cohesin from centromeres during mitosis in vertebrate cells. PLoS Biol 3(3):e86
122. Liu H, Rankin S, Yu H (2013) Phosphorylation-enabled binding of SGO1-PP2A to cohesin protects sororin and centromeric cohesion during mitosis. Nat Cell Biol 15(1):40–49
123. Kitajima TS, Sakuno T, Ishiguro K, Iemura S, Natsume T, Kawashima SA, Watanabe Y (2006) Shugoshin collaborates with protein phosphatase 2A to protect cohesin. Nature 441(7089):46–52
124. Hauf S, Waizenegger IC, Peters JM (2001) Cohesin cleavage by separase required for

anaphase and cytokinesis in human cells. Science 293(5533):1320–1323

125. Uhlmann F, Lottspeich F, Nasmyth K (1999) Sister-chromatid separation at anaphase onset is promoted by cleavage of the cohesin subunit Scc1. Nature 400(6739):37–42
126. Waizenegger I, Gimenez-Abian JF, Wernic D, Peters JM (2002) Regulation of human separase by securin binding and autocleavage. Curr Biol 12(16):1368–1378
127. Hornig NC, Knowles PP, McDonald NQ, Uhlmann F (2002) The dual mechanism of separase regulation by securin. Curr Biol 12(12):973–982
128. Cohen-Fix O, Peters JM, Kirschner MW, Koshland D (1996) Anaphase initiation in *Saccharomyces cerevisiae* is controlled by the APC-dependent degradation of the anaphase inhibitor Pds1p. Genes Dev 10(24): 3081–3093
129. Yamamoto A, Guacci V, Koshland D (1996) Pds1p, an inhibitor of anaphase in budding yeast, plays a critical role in the APC and checkpoint pathway(s). J Cell Biol 133(1): 99–110
130. Thornton BR, Toczyski DP (2003) Securin and B-cyclin/CDK are the only essential targets of the APC. Nat Cell Biol 5(12): 1090–1094
131. Hunt P, Hassold T (2010) Female meiosis: coming unglued with age. Curr Biol 20(17): R699–R702
132. Hassold T, Abruzzo M, Adkins K, Griffin D, Merrill M, Millie E, Saker D, Shen J, Zaragoza M (1996) Human aneuploidy: incidence, origin, and etiology. Environ Mol Mutagen 28(3):167–175
133. Nagaoka SI, Hassold TJ, Hunt PA (2012) Human aneuploidy: mechanisms and new insights into an age-old problem. Nat Rev Genet 13(7):493–504
134. Liu J, Zhang Z, Bando M, Itoh T, Deardorff MA, Clark D, Kaur M, Tandy S, Kondoh T, Rappaport E, Spinner NB, Vega H, Jackson LG, Shirahige K, Krantz ID (2009) Transcriptional dysregulation in NIPBL and cohesin mutant human cells. PLoS Biol 7(5): e1000119
135. Musio A, Selicorni A, Focarelli ML, Gervasini C, Milani D, Russo S, Vezzoni P, Larizza L (2006) X-linked Cornelia de Lange syndrome owing to SMC1L1 mutations. Nat Genet 38(5):528–530
136. Tonkin ET, Wang TJ, Lisgo S, Bamshad MJ, Strachan T (2004) NIPBL, encoding a homolog of fungal Scc2-type sister chromatid cohesion proteins and fly Nipped-B, is mutated in Cornelia de Lange syndrome. Nat Genet 36(6):636–641
137. Krantz ID, McCallum J, DeScipio C, Kaur M, Gillis LA, Yaeger D, Jukofsky L, Wasserman N, Bottani A, Morris CA, Nowaczyk MJ, Toriello H, Bamshad MJ, Carey JC, Rappaport E, Kawauchi S, Lander AD, Calof AL, Li HH, Devoto M, Jackson LG (2004) Cornelia de Lange syndrome is caused by mutations in NIPBL, the human homolog of *Drosophila melanogaster* Nipped-B. Nat Genet 36(6):631–635
138. Deardorff MA, Kaur M, Yaeger D, Rampuria A, Korolev S, Pie J, Gil-Rodriguez C, Arnedo M, Loeys B, Kline AD, Wilson M, Lillquist K, Siu V, Ramos FJ, Musio A, Jackson LS, Dorsett D, Krantz ID (2007) Mutations in cohesin complex members SMC3 and SMC1A cause a mild variant of cornelia de Lange syndrome with predominant mental retardation. Am J Hum Genet 80(3):485–494
139. Deardorff MA, Bando M, Nakato R, Watrin E, Itoh T, Minamino M, Saitoh K, Komata M, Katou Y, Clark D, Cole KE, de Baere E, Decroos C, di Donato N, Ernst S, Francey LJ, Gyftodimou Y, Hirashima K, Hullings M, Ishikawa Y, Jaulin C, Kaur M, Kiyono T, Lombardi PM, Magnaghi-Jaulin L, Mortier GR, Nozaki N, Petersen MB, Seimiya H, Siu VM, Suzuki Y, Takagaki K, Wilde JJ, Willems PJ, Prigent C, Gillessen-Kaesbach G, Christianson DW, Kaiser FJ, Jackson LG, Hirota T, Krantz ID, Shirahige K (2012) HDAC8 mutations in Cornelia de Lange syndrome affect the cohesin acetylation cycle. Nature 489(7415):313–317
140. Vrouwe MG, Elghalbzouri-Maghrani E, Meijers M, Schouten P, Godthelp BC, Bhuiyan ZA, Redeker EJ, Mannens MM, Mullenders LH, Pastink A, Darroudi F (2007) Increased DNA damage sensitivity of Cornelia de Lange syndrome cells: evidence for impaired recombinational repair. Hum Mol Genet 16(12):1478–1487
141. Vega H, Waisfisz Q, Gordillo M, Sakai N, Yanagihara I, Yamada M, van Gosliga D, Kayserili H, Xu C, Ozono K, Jabs EW, Inui K, Joenje H (2005) Roberts syndrome is caused by mutations in ESCO2, a human homolog of yeast ECO1 that is essential for the establishment of sister chromatid cohesion. Nat Genet 37(5):468–470
142. Suhasini AN, Brosh RM Jr (2013) Disease-causing missense mutations in human DNA helicase disorders. Mutat Res 752(2): 138–152
143. Van der Lelij P, Chrzanowska KH, Godthelp BC, Rooimans MA, Oostra AB, Stumm M,

Zdzienicka MZ, Joenje H, de Winter JP (2010) Warsaw breakage syndrome, a cohesinopathy associated with mutations in the XPD helicase family member DDX11/ChlR1. Am J Hum Genet 86(2):262–266

144. Capo-Chichi JM, Bharti SK, Sommers JA, Yammine T, Chouery E, Patry L, Rouleau GA, Samuels ME, Hamdan FF, Michaud JL, Brosh RM Jr, Megarbane A, Kibar Z (2013) Identification and biochemical characterization of a novel mutation in DDX11 causing Warsaw breakage syndrome. Hum Mutat 34(1):103–107
145. Deans AJ, West SC (2011) DNA interstrand crosslink repair and cancer. Nat Rev Cancer 11(7):467–480

Chapter 6

The Greatwall–PP2A Axis in Cell Cycle Control

Peng Wang, Marcos Malumbres, and Vincent Archambault

Abstract

Cell cycle progression is largely controlled by reversible protein phosphorylation mediated by cyclically activated kinases and phosphatases. It has long been known that cyclin B–Cdk1 activation triggers mitotic entry, and the enzymatic network controlling its activation and inactivation has been well characterized. Much more recently protein phosphatase 2A (PP2A) together with its B55 regulatory subunit has been recognized as the major activity dephosphorylating Cdk1 targets. Moreover, PP2A-B55 activity is high in late M phase and interphase, but low at mitotic entry. A series of discoveries in the fly and frog model systems have uncovered the molecular mechanism mediating this regulation. The Greatwall (Gwl) kinase activates endosulfines, which become specific inhibitors of PP2A-B55. Cdk1-dependent activation of Gwl at mitotic entry leads to PP2A-B55 downregulation, which synergizes with Cdk1 activation to promote the phosphorylated states of several mitotic substrates. Much less is known on the mechanisms inactivating Gwl and endosulfines at mitotic exit. Recent reports show the importance of spatiotemporal regulation of Gwl, endosulfines, and PP2A-B55 for cell cycle progression. The various systems and cell types differ in their dependence on the Gwl–PP2A axis for cell cycle progression. Moreover, this pathway also regulates gene expression in yeast, and this function could be conserved in metazoans.

Key words Cell cycle, Mitosis, Mitotic exit, Greatwall, PP2A, B55, Endosulfine, Cdk1

1 Cyclin B–Cdk1 Commands Mitotic Entry

Activated cyclin B–Cdk1, also known as maturation-promoting factor (MPF), triggers mitotic or meiotic entry by phosphorylating a large number of substrates [1]. These phosphorylation events promote the reorganization of the cellular architecture, including mitotic spindle assembly, chromosome condensation, and nuclear envelope breakdown (NEB). This large-scale phosphorylation campaign is highly coordinated. Before mitotic entry, Cdk1 is inhibited by the Wee1 and Myt1 kinases by phosphorylation at Thr14 and Tyr15. As cyclin B levels rise, partially active cyclin B–Cdk1 contributes to the activation of the Cdc25 phosphatase, which removes inhibitory phosphates on Cdk1. Meanwhile, with the reinforcement of Plk1, active Cdk1 launches counterattacks on its inhibitory kinases Wee1/Myt1 through direct

Eishi Noguchi and Mariana C. Gadaleta (eds.), *Cell Cycle Control: Mechanisms and Protocols*, Methods in Molecular Biology, vol. 1170, DOI 10.1007/978-1-4939-0888-2_6,

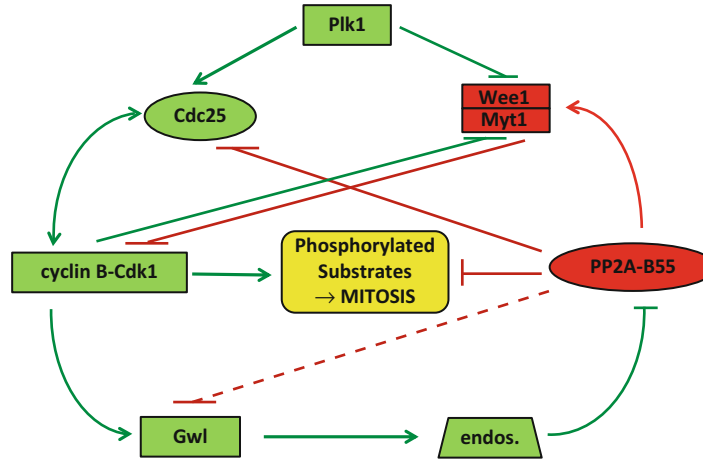

Fig. 1 Wiring model for the control of mitotic entry. *Rectangles* are kinases, and *ovals* are phosphatases. Activation events are indicated by *pointed arrows*, and inhibition events are indicated by *blunt-ended arrows*. Cyclin B–Cdk1, Cdc25, Plk1, Gwl, and endosulfines promote mitotic entry, whereas PP2A-B55, Wee1, and Myt1 repress mitotic entry. See text for more details

phosphorylation to initiate their inactivation. These mechanisms contribute to a switch-like activation of MPF, leading to a rapid mitotic entry [2] (Fig. 1).

The decisive effect of cyclin B–Cdk1 activity on mitotic entry is the result of the phosphorylation of a plethora of substrates, perhaps hundreds of them. It has been difficult to ascribe essential roles to individual phosphorylation sites on Cdk1 substrates in the major cellular changes occurring at mitotic entry. In addition to its effect on other enzymatic regulators of mitotic entry and exit, cyclin B–Cdk1 phosphorylates several effectors, including proteins involved in cellular rearrangements. For example, Cdk1-dependent phosphorylation of lamins appears to be important for NEB [3], phosphorylation of condensin promotes chromosome condensation [4], and phosphorylation of several microtubule-associated proteins contributes to the alteration of microtubule dynamics and helps the formation and proper function of the mitotic spindle [5]. Most cyclin B–Cdk1 substrates are not degraded but are dephosphorylated at mitotic exit.

2 PP2A-B55 Opposes Cyclin B–Cdk1

The importance of periodical cyclin–Cdk activity for cell cycle progression was recognized early on, already from the identification of the first cyclin as a cyclically appearing protein in sea urchin embryos [6]. Different types of cyclins were subsequently identified, with differences in the cell cycle events they regulate.

Much investigation then explored to what extent different cyclin subunits confer molecular substrate specificity to the Cdks or whether total Cdk activity levels were responsible for ordering the cell cycle events [7, 8]. However, it was generally assumed that constitutive phosphatase activity would suffice in reversing Cdk substrate phosphorylation at mitotic exit.

Discoveries in budding yeast profoundly altered this view. In this system, the phosphatase Cdc14 was shown to dephosphorylate several Cdk1 substrates at mitotic exit [9]. Moreover, Cdc14 was regulated in the cell cycle by an elegant mechanism. Upon completion of anaphase through the bud neck, a signalling cascade, the mitotic exit network (MEN) was triggered, leading to its pancellular release from a nucleolar sequestration [10]. Because there are Cdc14 sequence orthologs in higher eukaryotes, many expected that the role of Cdc14 in reversing phosphorylation by Cdk1 at mitotic exit would be conserved. So often before, budding yeast had been bringing understanding of conserved mechanisms of cell cycle control. However, strong evidence for such a role for Cdc14 orthologs in animals is still lacking [11].

Results obtained in flies and frogs suggested that protein phosphatase 2A (PP2A) played an important role in this process. PP2A is a heterotrimeric protein composed of a structural subunit (A), a catalytic phosphatase subunit (C), and a regulatory or an adaptor subunit (B) [12]. At least four subtypes of regulatory subunits exist (B55/B, B56/B′, B″, and B‴), with several members of each subtype in humans. Drosophila mutants in *twins* (*tws*), the sole subunit of the B55 subtype, showed a strongly reduced ability to dephosphorylate Cdk1 substrates [13]. Moreover, Tws was required for anaphase [14]. Forms of PP2A had been found to oppose cyclin B–Cdk1 in human cell extracts [15] and in cycling Xenopus egg extracts [16]. In human cells, immunostaining experiments revealed that a pool of PP2A-B55 localized to microtubules and that its phosphatase activity was low in G2 and M but high in interphase [17]. The authors tried to imagine the possible mechanisms of regulation at play.

More recently, it was shown that PP2A-B55δ is cell cycle regulated in Xenopus egg extracts, following an opposite pattern to cyclin B–Cdk1 (high in interphase and low in M phase), and that this regulation is crucial for mitotic entry and exit [18, 19]. Moreover, PP2A-B55δ was relatively specific for a model Cdk1 substrate [18]. In mammalian cells, an RNAi screen coupled to live-cell imaging of cell division identified PP2A-B55α as the major phosphatase needed for mitotic exit events, including spindle disassembly and nuclear envelope reformation [20]. In parallel, both PP2A-B55α and PP2A-B55δ activities, the two ubiquitous isoforms of the B55 mammalian family, were shown to be required for mitotic exit in mouse cells [21]. Other phosphatases, including

PP1, are likely to contribute to mitotic exit, and this is being investigated [21, 22]. But the role of PP2A-B55 enzymes in antagonizing Cdk1 in higher eukaryotes is clear.

However, in *S. cerevisiae*, PP2A-Cdc55 (B55) promotes mitotic entry [23] and represses mitotic exit by promoting the nucleolar sequestration of the Cdc14 phosphatase [24, 25]. The localization and enzymatic activity of PP2A-Cdc55 are regulated in the cell cycle partly by Zds1 and Zds2, two paralogs that appear to lack orthologs in higher eukaryotes [23, 25, 26]. At face value, the roles of phosphatases in cell cycle regulation of the budding yeasts and animals show shocking discrepancies in the cell cycle machinery of otherwise highly similar molecular systems.

3 Greatwall Assists Cyclin B–Cdk1 by Antagonizing PP2A-B55

Two independent genetic screens in Drosophila and one RNAi screen in S2 cells identified Greatwall (Gwl) as an important mitotic kinase [27–30]. Its name comes from initial phenotypic observations that suggested that the gene acted to protect the structure of mitotic chromosomes [28]. The authors recognized that the chromosome condensation defects observed in *gwl* mutant flies' neuroblasts could reflect a reduction in cyclin B–Cdk1 function. A gain of Gwl function in syncytial embryos caused mitotic defects when the activity of Polo kinase was reduced [29]. Yet, the downstream substrate and molecular process controlled by Gwl remained unknown. Sequence alignments showed that the Gwl kinase was conserved from yeasts to vertebrates [28] (*see* Table 1 for names of components of the Gwl–PP2A axis in different organisms). The single kinase domain of Gwl is interrupted by a very long stretch of protein sequence that we now know to serve in the spatial regulation of Gwl (discussed below).

Biochemical experiments in Xenopus egg extracts provided some crucial clues regarding the regulation of Gwl. Immunodepletion of Gwl from M phase-arrested egg extracts induced

Table 1
Names of proteins of the Gwl–PP2A axis in different organisms

Protein function	*D. melanogaster*	*X. laevis*	*H. sapiens*	*S. cerevisiae*
Kinase	Gwl	Gwl	MASTL (Gwl)	Rim15
Phosphatases	PP2A-Tws	PP2A-B55α PP2A-B55δ	PP2A-B55α PP2A-B55δ	PP2A-Cdc55
Phosphatase inhibitors	Endos	Endosulfine (ENSA) Arpp19	Endosulfine (ENSA) Arpp19	Igo1 Igo2

mitotic exit despite high cyclin B–Cdk1 activity [31]. Moreover, the addition of low concentrations of okadaic acid, known to inhibit PP2A, restored the M-phase state when Gwl was depleted, suggesting that the function of Gwl was to inhibit PP2A [32]. It was quickly shown that PP2A-B55 was the specific downstream phosphatase antagonized by Gwl [19, 32], but the molecular mechanism of this function remained unknown.

A major breakthrough came from the identification by two independent groups of endosulfine (ENSA) and Arpp19, two small homologous proteins, as substrates of Gwl in Xenopus extracts [33, 34]. These proteins provided the missing link between Gwl and PP2A-B55. Once phosphorylated, endosulfine and Arpp19 (here together referred to as endosulfines) become specific inhibitors of PP2A-B55 (and not other forms of PP2A). These findings led to a model whereby activation of Gwl at mitotic entry leads to inhibition of PP2A-B55, promoting the accumulation of phosphorylated forms of Cdk1 substrates [35].

The identification of endosulfines as Gwl substrates is the result of heroic biochemical screens. The determination of ENSA as a key substrate of Gwl [33] was also aided by the observation made earlier in Drosophila mutants of *endosulfine* (*endos*), where female meiosis fails to progress to the normal metaphase I arrest, despite normal cyclin B–Cdk1 activity [36], a situation reminiscent of the mitotic exit observed in Xenopus extracts depleted of Gwl [31]. While this biochemical work in Xenopus extracts was being conducted, two independent genetic screens for enhancers and suppressors of a gain-of-function allele of Gwl in Drosophila eggs identified mutation in PP2A-B55/Tws subunit genes and in *endos*, respectively [37, 38]. The two studies went on to show that the Gwl–endosulfine–PP2A-B55 mechanism proposed in frogs was conserved in flies and was important for mitosis and meiosis. Experiments in human cells and in mice also confirmed that the pathway contributes to cell cycle regulation in mammals, where Gwl is also known as microtubule-associated serine threonine-like kinase (Mastl) [21, 39, 40].

4 Importance of the Gwl–PP2A Axis for Cell Cycle Regulation in Various Systems

Unlike Cdk1, Gwl is not essential for mitotic entry in all systems. In Drosophila, *gwl* null mutants mostly die during development but occasionally develop to adulthood, albeit with various morphological defects [29]. Examination of *gwl* mutant neuroblasts or Gwl RNAi-depleted cells in culture shows chromosome and spindle defects, but cells do enter mitosis [28–30]. In addition, a recent genetic model in the mouse has shown that the kinetics of mitotic entry are not altered in the absence of Gwl, whereas most Gwl-null cells display mitotic aberrations and defective

chromosome segregation [41]. Gwl-deficient mouse embryos also display an accumulation of aberrant mitotic cells in vivo [41]. Previous results from Gwl silencing in mammalian cells described a delay in G2, accompanied by increases in anaphase bridges and multinucleation, but not a highly penetrant cell cycle arrest [39, 40]. Cells in these studies were synchronized by different protocols that result in certain levels of DNA damage, and the delays in G2 may therefore be a consequence of the requirements for Gwl in checkpoint recovery [42, 43]. Therefore, the inhibition of PP2A-B55 by the Gwl pathway is not essential for mitotic entry in unperturbed cell cycles but may have a critical role in the recovery from stress conditions. However, to what extent other members of the Mastl kinase family (Mast1–4) can compensate for the absence of Gwl needs to be explored.

Only a fraction of mitotic phosphorylation substrates may require protection from PP2A-B55 in mitosis, and their identity remains to be established. One of these crucial substrates appears to be PRC1, a protein required for microtubule bundling and central spindle function during cytokinesis. Cdk1 phosphorylates PRC1 in early mitosis to prevent its interaction with microtubules [44]. It was recently shown that PP2A-B55 is responsible for dephosphorylating PRC1 at the Cdk1 site and that Gwl and ENSA activities are required to delay PP2A-B55 activity towards PRC1 until late anaphase [45]. Failure to delay PP2A-B55 activation causes premature PRC1 recruitment to microtubules and central spindle contraction before sister chromatids have completed segregation. It remains to be seen whether the proposed Gwl-dependent delay between the onset of cyclin B and securin degradation and PP2A-B55 activation in mitotic exit is reflected on a majority of PP2A-B55 substrates.

While inactivation of Gwl does not prevent mitotic entry in Drosophila or vertebrate cells, depletion of Gwl from mitotic Xenopus egg extracts causes inactivation of cyclin B–Cdk1 and complete exit from the mitotic state [31]. This result alone suggests an essential role for Gwl in the maintenance of M phase, at least in eggs. It has even been shown that Gwl is an essential component of the MPF (together with cyclin B–Cdk1) as originally defined as a biochemical activity necessary and sufficient for M-phase entry [46]. A Drosophila mutant allele of Gwl that disrupts its function specifically in the female germline has been shown to cause sterility and a failure to maintain the normal metaphase I arrest in eggs [29]. Thus, meiosis could depend more heavily on Gwl than could mitosis [47]. As Gwl is also required for meiotic maturation in pig oocytes [48], it is very likely to be essential for female meiosis in humans.

The components of the Gwl–PP2A axis are conserved in yeasts. In *S. cerevisiae*, Rim15 (Gwl) and Igo1/2 (endosulfines) are not required for unperturbed cell cycles. Yet, they are needed for

timely mitotic entry under temperature stress [49]. That Rim15 and Igo1/2 promote mitotic entry may appear surprising because inhibition of PP2A-Cdc55 is known to promote mitotic exit [24]. Although phosphorylation of Igo1 and Igo2 by Rim15 enables them to bind and inhibit PP2A-Cdc55 in vitro, genetic results suggest that Igo1 and Igo2 positively regulate PP2A-Cdc55 [49]. Therefore, although the Gwl–PP2A axis does contribute to cell cycle regulation in yeast, its mechanism may differ from that in higher eukaryotes. Alternatively, some aspects of the Gwl–PP2A pathway may be more complex than proposed in our current simple models and conserved between animals and yeast.

5 Spatiotemporal Regulation of the Gwl–PP2A Axis

In vitro experiments have shown that Gwl activation depends on its phosphorylation by cyclin B–Cdk1 at mitotic entry and by an unprecedented mechanism involving an intramolecular rearrangement of Gwl [31, 50, 51]. The identity of the phosphatases that inactivate Gwl and endosulfines and precisely when this occurs in the cell cycle is currently unknown. Neither Gwl nor endosulfines or PP2A-B55 has been shown to be cell cycle regulated by ubiquitin-dependent proteolysis. Yet, other levels of control can contribute to regulate the pathway. Our tendency to interpret genetic and biochemical results as simple wiring diagrams (Fig. 1) can lead us to forget that enzymes and substrates alike are organized heterogeneously in the cell, sometimes even sequestered away in different compartments. It is therefore paramount to carefully examine the spatiotemporal dynamics of mitotic entry and exit regulators if we are to truly understand cell cycle regulation (Fig. 2).

Spatial regulation is clearly important for cyclin B–Cdk1 activation. As it begins to become active in the cytoplasm, cyclin B–Cdk1 promotes its autophosphorylation on cyclin B and its nuclear import [52–54]. This mechanism allows a sharp transition at mitotic entry that promotes proper coordination of subsequent mitotic events. Meanwhile, B55 regulatory subunits (likely contained in PP2A-B55 holoenzymes) are suspiciously cytoplasmic [55]. Because cyclin B is phosphorylated by Cdk1, it could be a target for dephosphorylation by PP2A-B55, thus imposing the need to physically separate cyclin B–Cdk1 and PP2A-B55 at mitotic entry [54].

At the time of its initial identification in Drosophila, Gwl was observed to be nuclear in interphase and to become dispersed in the cytoplasm after NEB [28]. We have recently found that Drosophila and human Gwl become cytoplasmic and excluded from the nucleus for a few minutes in prophase, before NEB [41, 56]. The enigmatic central region of the Gwl protein, interrupting the

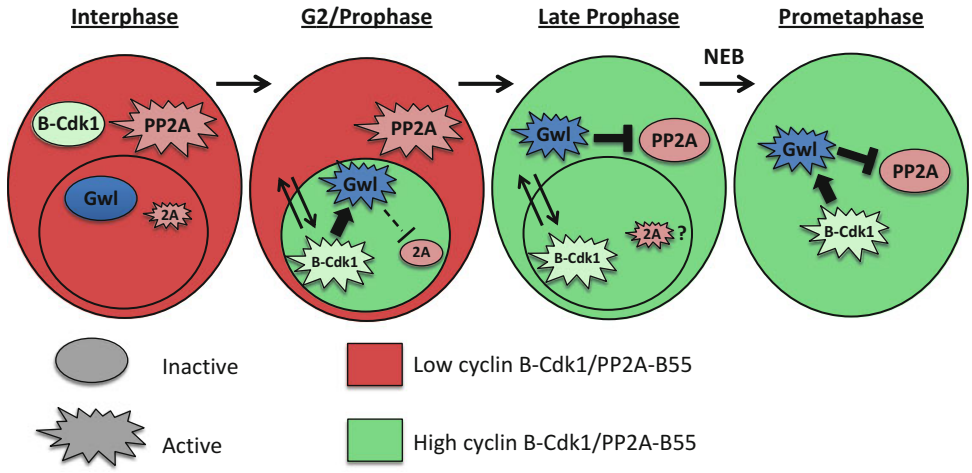

Fig. 2 Spatial model for the Gwl–PP2A axis in the control of mitotic entry. In interphase, cyclin B–Cdk1 is largely inactive, while PP2A-B55 is active. Both cyclin B–Cdk1 and PP2A-B55 are mostly cytoplasmic, while Gwl is nuclear. In early prophase, cyclin B–Cdk1 begins to shuttle into the nucleus and becomes active through the auto-amplification loop (not shown). In the nucleus, cyclin B–Cdk1 activates Gwl. Gwl then translocates to the cytoplasm, where it is positioned to antagonize PP2A-B55 by phosphorylating endosulfines (not shown). As a result, the cyclin B–Cdk1/PP2A-B55 ratio is high throughout the cell before NEB

kinase domain, turned out to serve as a platform for this spatial regulation. It contains nuclear localization signals (NLSs) and is the target of multiple phosphorylation events. In Drosophila, phosphorylation of Gwl by Polo and cyclin B–Cdk1 in the central region of Gwl promotes its cytoplasmic localization in prophase [56]. Murine Gwl exhibits a similar behavior in cell culture, and its nuclear exclusion in prophase has been shown to require its own kinase activity and its activation by cyclin B–Cdk1-dependent phosphorylation in its kinase domain [41]. Drosophila Gwl kinase-dead mutants also fail to become excluded from the nucleus in prophase (unpublished observations). Therefore, multiple mechanisms appear to collaborate to ensure the efficient translocation of Gwl from the nucleus to the cytoplasm before NEB, suggesting the functional importance of Gwl translocation. In yeast, the nucleocytoplasmic localization of Rim15 is regulated by phosphorylation, although this process has not been finely dissected [57]. The precise mechanisms mediating the translocation of Gwl may differ between organisms, especially events associated with the central region of Gwl, which is poorly conserved in sequence.

Rescue experiments in flies and mammalian cells in culture showed that both the nuclear localization of Gwl and its nuclear exclusion in prophase are required for its function [41, 56], indicating the importance of the spatiotemporal regulation of this kinase during the cell cycle. We have proposed that the nuclear localization of Gwl may poise it for efficient and timely activation by cyclin B–Cdk1 in the nucleus in prophase [41, 56]. It will be

interesting to determine to what extent Gwl's relocalization to the cytoplasm helps antagonize PP2A-B55 in prophase. Endosulfines are small enough proteins to diffuse freely through the nuclear pores, and therefore the nucleocytoplasmic localization of Gwl should have little effect on the localization of phosphorylated endosulfines, unless their diffusion is restricted in some way. Unphosphorylated Drosophila Endos can interact with Tws (B55) in vitro [47], suggesting that its nucleocytoplasmic diffusion may be restricted by PP2A-Tws. Intriguingly, expression of mutant forms of Gwl that fail to be excluded from the nucleus in prophase prolonged mitosis, even in the presence of endogenous Gwl, suggesting that nuclear PP2A-B55 activity in prophase is required for mitotic progression. Additional work is required to test these models.

In yeast, like in animals, Rim15 phosphorylation of Igo1 and Igo2 at mitotic entry promotes their interaction with PP2A-Cdc55 and inhibition of its phosphatase activity [49, 58]. However, yeast PP2A-Cdc55 promotes mitotic entry and inhibits mitotic exit, unlike its animal orthologs. Recently, surprising genetic results suggested that Igo1 and Igo2 positively regulate the function of PP2A-Cdc55 at mitotic entry, and phosphorylation of Igo1 and Igo2 by Rim15 helped the nuclear export of PP2A-Cdc55 [49]. The cytoplasmic pool of PP2A-Cdc55 is known to promote mitotic entry, and it also depends on Zds1/2 [23]. Whether PP2A-B55 is also subject to changes in nucleocytoplasmic localization at cell cycle transitions in metazoans is unknown.

6 Other Functions of the Gwl–PP2A Pathway

In yeast, the Rim15–Igo1/2 pathway was first recognized for its requirement for entry into quiescence, partly by promoting the stability of mRNAs important for the G0 program [57, 59]. The role of endosulfines in inhibiting PP2A-B55 found later in higher eukaryotes suggested that Igo1/2 might act through PP2A-Cdc55 in promoting quiescence. This has been confirmed genetically. The Rim15–Igo1/2–PP2A-Cdc55 pathway is required for transcriptional regulation and mRNA stabilization leading to entry into quiescence (G0) [58]. The transcription factor Gis1 was identified as an important effector in this process; its dephosphorylation by PP2A-Cdc55 is inhibited by Igo1/2 [58].

While the Rim15 pathway can contribute to cell cycle progression in yeast, conversely, the Gwl pathway could function in the regulation of transcription and mRNA stability in higher eukaryotes. Drosophila *endos* mutant oocytes show reduced levels of Twine phosphatase (Cdc25) and Polo kinase, two positive regulators of meiotic entry, but how this occurs is unknown [36]. In Drosophila, *gwl* and *endos* mutant oocytes show morphological

abnormalities [29, 60] that could be partly due to misregulation of transcription and mRNA stability, two crucial processes as the maternal contribution is being synthesized in oogenesis. Alternatively, the *endos* mutant oocyte phenotypes could reflect a role in osmotic regulation at the level of ion channels based on reports showing such functions for endosulfine in mammalian systems [61]. Whether endosulfines require phosphorylation by Gwl in these other physiological functions is unknown. However, we note that while a lack of Gwl in Drosophila oocytes causes a failure to maintain a metaphase I arrest [29], a lack of Endos causes a failure to reach metaphase I [36]. Thus, Endos may fulfill functions independently of Gwl. Interestingly, Endos is conserved in *C. elegans*, but Gwl is not, and no effect on mitosis or meiosis could be detected in *endos* mutants [47]. The function and regulation of endos in this system are still unclear.

7 Perspective

The discovery of the Gwl–PP2A axis and its role in the regulation of mitosis has revealed the existence of a major battleground in the enzymatic war that takes place in the cell cycle. Much remains to be investigated before we can get a full picture of the molecular actors and how they function together in this process. If the Gwl–endosulfine and Rim15–Igo1/2 pathways seemed at first to control completely different processes in animals and in yeasts, it should be no surprise that they now appear increasingly similar in function. Deeper biochemical and cell biological investigations of the Gwl–PP2A module and its relationship to other mitotic regulators would lead to a better understanding of the spatiotemporal control of the cell cycle as a whole.

Acknowledgements

Work on the Gwl–PP2A axis in V.A.'s lab is supported by the Canadian Institutes of Health Research (CIHR). V.A. also holds a New Investigator Award from the CIHR. P.W. holds a studentship from the Fonds de recherche du Québec—Santé (FRQ-S). IRIC is supported in part by the Canadian Center of Excellence in Commercialization and Research, the Canada Foundation for Innovation, and the FRQ-S. Work in M.M.'s laboratory was funded by grants from Bayer Pharma AG, Fundación Ramón Areces, MINECO (SAF2012-38215), the OncoCycle Programme (S2010/BMD-2470) from the Comunidad de Madrid, and the European Union Seventh Framework Programme (MitoSys project; HEALTH-F5-2010-241548).

References

1. Morgan DO (2007) The cell cycle: principles of control, Primers in Biology. New Science, London
2. Lindqvist A, Rodriguez-Bravo V, Medema RH (2009) The decision to enter mitosis: feedback and redundancy in the mitotic entry network. J Cell Biol 185(2):193–202
3. Dessev G, Iovcheva-Dessev C, Bischoff JR, Beach D, Goldman R (1991) A complex containing p34cdc2 and cyclin B phosphorylates the nuclear lamin and disassembles nuclei of clam oocytes in vitro. J Cell Biol 112(4):523–533
4. Kimura K, Hirano M, Kobayashi R, Hirano T (1998) Phosphorylation and activation of 13S condensin by Cdc2 in vitro. Science 282(5388):487–490
5. Glotzer M (2009) The 3Ms of central spindle assembly: microtubules, motors and MAPs. Nat Rev Mol Cell Biol 10(1):9–20
6. Evans T, Rosenthal ET, Youngblom J, Distel D, Hunt T (1983) Cyclin: a protein specified by maternal mRNA in sea urchin eggs that is destroyed at each cleavage division. Cell 33(2):389–396
7. Stern B, Nurse P (1996) A quantitative model for the cdc2 control of S phase and mitosis in fission yeast. Trends Genet 12(9):345–350
8. Bloom J, Cross FR (2007) Multiple levels of cyclin specificity in cell-cycle control. Nat Rev Mol Cell Biol 8(2):149–160
9. Visintin R, Craig K, Hwang ES, Prinz S, Tyers M, Amon A (1998) The phosphatase Cdc14 triggers mitotic exit by reversal of Cdk-dependent phosphorylation. Mol Cell 2(6):709–718
10. Bardin AJ, Amon A (2001) Men and sin: what's the difference? Nat Rev Mol Cell Biol 2(11):815–826
11. Mocciaro A, Schiebel E (2010) Cdc14: a highly conserved family of phosphatases with non-conserved functions? J Cell Sci 123 (Pt 17):2867–2876
12. Lambrecht C, Haesen D, Sents W, Ivanova E, Janssens V (2013) Structure, regulation, and pharmacological modulation of PP2A phosphatases. Methods Mol Biol 1053:283–305
13. Mayer-Jaekel RE, Ohkura H, Ferrigno P, Andjelkovic N, Shiomi K, Uemura T, Glover DM, Hemmings BA (1994) Drosophila mutants in the 55 kDa regulatory subunit of protein phosphatase 2A show strongly reduced ability to dephosphorylate substrates of p34cdc2. J Cell Sci 107(Pt 9):2609–2616
14. Mayer-Jaekel RE, Ohkura H, Gomes R, Sunkel CE, Baumgartner S, Hemmings BA, Glover DM (1993) The 55 kd regulatory subunit of Drosophila protein phosphatase 2A is required for anaphase. Cell 72(4):621–633
15. Ferrigno P, Langan TA, Cohen P (1993) Protein phosphatase 2A1 is the major enzyme in vertebrate cell extracts that dephosphorylates several physiological substrates for cyclin-dependent protein kinases. Mol Biol Cell 4(7):669–677
16. Lee TH, Turck C, Kirschner MW (1994) Inhibition of cdc2 activation by INH/PP2A. Mol Biol Cell 5(3):323–338
17. Sontag E, Nunbhakdi-Craig V, Bloom GS, Mumby MC (1995) A novel pool of protein phosphatase 2A is associated with microtubules and is regulated during the cell cycle. J Cell Biol 128(6):1131–1144
18. Mochida S, Ikeo S, Gannon J, Hunt T (2009) Regulated activity of PP2A-B55 delta is crucial for controlling entry into and exit from mitosis in Xenopus egg extracts. EMBO J 28(18):2777–2785
19. Castilho PV, Williams BC, Mochida S, Zhao Y, Goldberg ML (2009) The M phase kinase Greatwall (Gwl) promotes inactivation of PP2A/B55delta, a phosphatase directed against CDK phosphosites. Mol Biol Cell 20(22):4777–4789
20. Schmitz MH, Held M, Janssens V, Hutchins JR, Hudecz O, Ivanova E, Goris J, Trinkle-Mulcahy L, Lamond AI, Poser I, Hyman AA, Mechtler K, Peters JM, Gerlich DW (2010) Live-cell imaging RNAi screen identifies PP2A-B55alpha and importin-beta1 as key mitotic exit regulators in human cells. Nat Cell Biol 12(9):886–893
21. Manchado E, Guillamot M, de Carcer G, Eguren M, Trickey M, Garcia-Higuera I, Moreno S, Yamano H, Canamero M, Malumbres M (2010) Targeting mitotic exit leads to tumor regression in vivo: modulation by Cdk1, Mastl, and the PP2A/B55alpha, delta phosphatase. Cancer Cell 18(6):641–654
22. Wurzenberger C, Gerlich DW (2011) Phosphatases: providing safe passage through mitotic exit. Nat Rev Mol Cell Biol 12(8):469–482
23. Rossio V, Yoshida S (2011) Spatial regulation of Cdc55-PP2A by Zds1/Zds2 controls mitotic entry and mitotic exit in budding yeast. J Cell Biol 193(3):445–454
24. Queralt E, Lehane C, Novak B, Uhlmann F (2006) Downregulation of PP2A(Cdc55) phosphatase by separase initiates mitotic exit in budding yeast. Cell 125(4):719–732

25. Queralt E, Uhlmann F (2008) Separase cooperates with Zds1 and Zds2 to activate Cdc14 phosphatase in early anaphase. J Cell Biol 182(5):873–883
26. Wicky S, Tjandra H, Schieltz D, Yates J 3rd, Kellogg DR (2010) The Zds proteins control entry into mitosis and target protein phosphatase 2A to the Cdc25 phosphatase. Mol Biol Cell 22(1):20–32
27. White-Cooper H, Carmena M, Gonzalez C, Glover DM (1996) Mutations in new cell cycle genes that fail to complement a multiply mutant third chromosome of Drosophila. Genetics 144(3):1097–1111
28. Yu J, Fleming SL, Williams B, Williams EV, Li Z, Somma P, Rieder CL, Goldberg ML (2004) Greatwall kinase: a nuclear protein required for proper chromosome condensation and mitotic progression in Drosophila. J Cell Biol 164(4): 487–492
29. Archambault V, Zhao X, White-Cooper H, Carpenter AT, Glover DM (2007) Mutations in Drosophila Greatwall/Scant reveal its roles in mitosis and meiosis and interdependence with polo kinase. PLoS Genet 3(11):e200
30. Bettencourt-Dias M, Giet R, Sinka R, Mazumdar A, Lock WG, Balloux F, Zafiropoulos PJ, Yamaguchi S, Winter S, Carthew RW, Cooper M, Jones D, Frenz L, Glover DM (2004) Genome-wide survey of protein kinases required for cell cycle progression. Nature 432(7020):980–987
31. Yu J, Zhao Y, Li Z, Galas S, Goldberg ML (2006) Greatwall kinase participates in the Cdc2 autoregulatory loop in Xenopus egg extracts. Mol Cell 22(1):83–91
32. Vigneron S, Brioudes E, Burgess A, Labbe JC, Lorca T, Castro A (2009) Greatwall maintains mitosis through regulation of PP2A. EMBO J 28(18):2786–2793
33. Mochida S, Maslen SL, Skehel M, Hunt T (2010) Greatwall phosphorylates an inhibitor of protein phosphatase 2A that is essential for mitosis. Science 330(6011):1670–1673
34. Gharbi-Ayachi A, Labbe JC, Burgess A, Vigneron S, Strub JM, Brioudes E, Van-Dorsselaer A, Castro A, Lorca T (2010) The substrate of Greatwall kinase, Arpp19, controls mitosis by inhibiting protein phosphatase 2A. Science 330(6011):1673–1677
35. Lorca T, Castro A (2012) The Greatwall kinase: a new pathway in the control of the cell cycle. Oncogene 32(5):537–543
36. Von Stetina JR, Tranguch S, Dey SK, Lee LA, Cha B, Drummond-Barbosa D (2008) alpha-Endosulfine is a conserved protein required for oocyte meiotic maturation in Drosophila. Development 135(22):3697–3706
37. Rangone H, Wegel E, Gatt MK, Yeung E, Flowers A, Debski J, Dadlez M, Janssens V, Carpenter AT, Glover DM (2011) Suppression of scant identifies Endos as a substrate of greatwall kinase and a negative regulator of protein phosphatase 2A in mitosis. PLoS Genet 7(8): e1002225
38. Wang P, Pinson X, Archambault V (2011) PP2A-twins is antagonized by greatwall and collaborates with polo for cell cycle progression and centrosome attachment to nuclei in drosophila embryos. PLoS Genet 7(8):e1002227
39. Burgess A, Vigneron S, Brioudes E, Labbe JC, Lorca T, Castro A (2010) Loss of human Greatwall results in G2 arrest and multiple mitotic defects due to deregulation of the cyclin B-Cdc2/PP2A balance. Proc Natl Acad Sci U S A 107(28):12564–12569
40. Voets E, Wolthuis RM (2010) MASTL is the human orthologue of Greatwall kinase that facilitates mitotic entry, anaphase and cytokinesis. Cell Cycle 9(17):3591–3601
41. Alvarez-Fernandez M, Sanchez-Martinez R, Sanz-Castillo B, Gan PP, Sanz-Flores M, Trakala M, Ruiz-Torres M, Lorca T, Castro A, Malumbres M (2013) Greatwall is essential to prevent mitotic collapse after nuclear envelope breakdown in mammals. Proc Natl Acad Sci U S A 110(43):17374–17379
42. Peng A, Yamamoto TM, Goldberg ML, Maller JL (2010) A novel role for greatwall kinase in recovery from DNA damage. Cell Cycle 9(21):4364–4369
43. Peng A, Wang L, Fisher LA (2011) Greatwall and Polo-like kinase 1 coordinate to promote checkpoint recovery. J Biol Chem 286(33): 28996–29004
44. Mollinari C, Kleman JP, Jiang W, Schoehn G, Hunter T, Margolis RL (2002) PRC1 is a microtubule binding and bundling protein essential to maintain the mitotic spindle midzone. J Cell Biol 157(7):1175–1186
45. Cundell MJ, Bastos RN, Zhang T, Holder J, Gruneberg U, Novak B, Barr FA (2013) The BEG (PP2A-B55/ENSA/Greatwall) pathway ensures cytokinesis follows chromosome separation. Mol Cell 52(3):393–405
46. Hara M, Abe Y, Tanaka T, Yamamoto T, Okumura E, Kishimoto T (2012) Greatwall kinase and cyclin B-Cdk1 are both critical constituents of M-phase-promoting factor. Nat Commun 3:1059
47. Kim MY, Bucciarelli E, Morton DG, Williams BC, Blake-Hodek K, Pellacani C, Von Stetina

JR, Hu X, Somma MP, Drummond-Barbosa D, Goldberg ML (2012) Bypassing the Greatwall-endosulfine pathway: plasticity of a pivotal cell-cycle regulatory module in *Drosophila melanogaster* and *Caenorhabditis elegans*. Genetics 191(4):1181–1197

48. Li YH, Kang H, Xu YN, Heo YT, Cui XS, Kim NH, Oh JS (2013) Greatwall kinase is required for meiotic maturation in porcine oocytes. Biol Reprod 89(3):53
49. Juanes MA, Khoueiry R, Kupka T, Castro A, Mudrak I, Ogris E, Lorca T, Piatti S (2013) Budding yeast greatwall and endosulfines control activity and spatial regulation of PP2A(Cdc55) for timely mitotic progression. PLoS Genet 9(7):e1003575
50. Vigneron S, Gharbi-Ayachi A, Raymond AA, Burgess A, Labbe JC, Labesse G, Monsarrat B, Lorca T, Castro A (2011) Characterization of the mechanisms controlling Greatwall activity. Mol Cell Biol 31(11):2262–2275
51. Blake-Hodek KA, Williams BC, Zhao Y, Castilho PV, Chen W, Mao Y, Yamamoto TM, Goldberg ML (2012) Determinants for activation of the atypical AGC kinase greatwall during M phase entry. Mol Cell Biol 32(8):1337–1353
52. Gavet O, Pines J (2010) Activation of cyclin B1-Cdk1 synchronizes events in the nucleus and the cytoplasm at mitosis. J Cell Biol 189(2):247–259
53. Gavet O, Pines J (2010) Progressive activation of CyclinB1-Cdk1 coordinates entry to mitosis. Dev Cell 18(4):533–543
54. Santos SD, Wollman R, Meyer T, Ferrell JE Jr (2012) Spatial positive feedback at the onset of mitosis. Cell 149(7):1500–1513
55. Janssens V, Goris J (2001) Protein phosphatase 2A: a highly regulated family of serine/threonine phosphatases implicated in cell growth and signalling. Biochem J 353(Pt 3): 417–439
56. Wang P, Galan JA, Normandin K, Bonneil E, Hickson GR, Roux PP, Thibault P, Archambault V (2013) Cell cycle regulation of Greatwall kinase nuclear localization facilitates mitotic progression. J Cell Biol 202(2):277–293
57. Pedruzzi I, Dubouloz F, Cameroni E, Wanke V, Roosen J, Winderickx J, De Virgilio C (2003) TOR and PKA signaling pathways converge on the protein kinase Rim15 to control entry into G0. Mol Cell 12(6):1607–1613
58. Bontron S, Jaquenoud M, Vaga S, Talarek N, Bodenmiller B, Aebersold R, De Virgilio C (2013) Yeast endosulfines control entry into quiescence and chronological life span by inhibiting protein phosphatase 2A. Cell Rep 3(1):16–22
59. Talarek N, Cameroni E, Jaquenoud M, Luo X, Bontron S, Lippman S, Devgan G, Snyder M, Broach JR, De Virgilio C (2010) Initiation of the TORC1-regulated G0 program requires Igo1/2, which license specific mRNAs to evade degradation via the 5'-3' mRNA decay pathway. Mol Cell 38(3):345–355
60. Drummond-Barbosa D, Spradling AC (2004) Alpha-endosulfine, a potential regulator of insulin secretion, is required for adult tissue growth control in Drosophila. Dev Biol 266(2):310–321
61. Bataille D (2000) Endosulfines: novel regulators of insulin secretion. Drug News Perspect 13(8):453–462

Chapter 7

Cell Cycle Regulation by the Nutrient-Sensing Mammalian Target of Rapamycin (mTOR) Pathway

Elisabet Cuyàs, Bruna Corominas-Faja, Jorge Joven, and Javier A. Menendez

Abstract

Cell division involves a series of ordered and controlled events that lead to cell proliferation. Cell cycle progression implies not only demanding amounts of cell mass, protein, lipid, and nucleic acid content but also a favorable energy state. The mammalian target of rapamycin (mTOR), in response to the energy state, nutrient status, and growth factor stimulation of cells, plays a pivotal role in the coordination of cell growth and the cell cycle. Here, we review how the nutrient-sensing mTOR-signaling cascade molecularly integrates nutritional and mitogenic/anti-apoptotic cues to accurately coordinate cell growth and cell cycle. First, we briefly outline the structure, functions, and regulation of the mTOR complexes (mTORC1 and mTORC2). Second, we concisely evaluate the best known ability of mTOR to control G1-phase progression. Third, we discuss in detail the recent evidence that indicates a new genome stability caretaker function of mTOR based on the specific ability of phosphorylated forms of several mTOR-signaling components (AMPK, raptor, TSC, mTOR, and S6K1), which spatially and temporally associate with essential mitotic regulators at the mitotic spindle and at the cytokinetic cleavage furrow.

Key words Cell cycle, mTOR, mTORC, Nutrients, Energy status, Mitosis, AMPK, Raptor, S6K1

1 Introduction

Cell division in mammals involves ordered and controlled molecular events, which are structured in four distinct phases: two gap phases, G1 and G2, where cells typically grow and protein synthesis occurs; the S phase, during which DNA is replicated; and the M phase, during which cells undergo mitosis, followed by a final cytokinesis. There is also a G0 phase, in which cells remain in a quiescent or a resting state until the necessary conditions are present to enter the cycle. Progress through each phase of the cell cycle is under the strict control of different molecules, e.g., cyclins, cyclin-dependent kinases (CDKs), and CDK inhibitors (CDKIs), all of which play crucial roles in the regulation of the multiple cell cycle events. Furthermore, to ensure the correct order of events

Eishi Noguchi and Mariana C. Gadaleta (eds.), *Cell Cycle Control: Mechanisms and Protocols*, Methods in Molecular Biology, vol. 1170, DOI 10.1007/978-1-4939-0888-2_7,

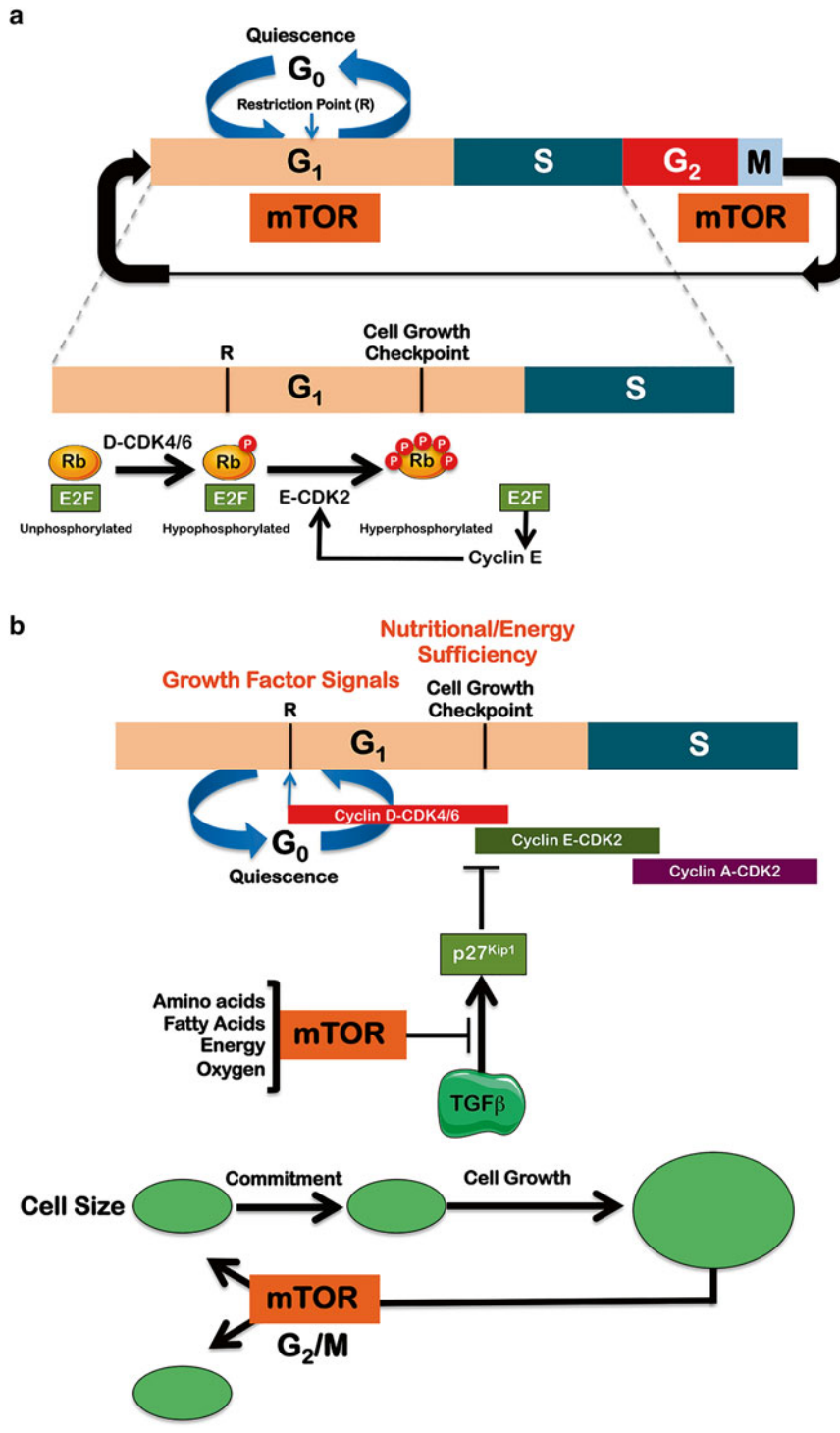

Fig. 1 mTOR and the mammalian cell cycle. (**a**) G1 and G2 are the gaps between mitosis and S phase and between S phase and mitosis, respectively. G1 is where critical decisions are made as to whether to enter a resting quiescent stage (G0) or to continue cycling and commit to replicating the genome and mitosis. Rb exists in different phosphorylation stages, i.e., unphosphorylated (G1–postmitotic, before the restriction point), hypophosphorylated (at the point in G1 where the growth factor-dependent cycling decision is made [R]), and hyperphosphorylated (G1/pre-S). The Rb hypophosphorylated state occurs after phosphorylation by cyclin D–CDK4/6, and this process leaves Rb associated with E2F such that E2F is unable to activate transcription.

and to guarantee that cells complete the cell cycle, there are three major checkpoints: (1) the entry into S phase (G1/S checkpoint), known as the restriction (R) point; (2) the entrance of mitosis (G2/M checkpoint); and (3) a final spindle checkpoint to ensure that conditions remain suitable for the cell to complete cell division (cytokinesis). Importantly, the progression through the cell cycle must ensure that a proliferating cell has captured enough energy and cell mass (protein, lipid, and nucleic acid content) to give rise to two daughter cells. Indeed, cell cycle progression demands a large supply of nutrients to ensure that the energy supply and protein synthesis are adequate to support cell growth (i.e., increase in cell size), proliferation, and accumulation of biomass. Most cells respond to these changing needs by altering the balance between energy-producing (catabolic) and energy-consuming (anabolic) processes, which require the coordination of complex metabolic pathways. The signaling network that regulates cell metabolism, growth, proliferation, and survival is controlled by the mammalian target of rapamycin (mTOR), which responds to a variety of stimuli, such as energy status, nutrients, stress, or growth factors. Indeed, the mTOR cascade serves a unique function in coordinating nutrient availability and energy metabolism by cell responses to growth factors. Here, we review how the nutrient-sensing mTOR-signaling cascade molecularly integrates nutritional and mitogenic/anti-apoptotic cues to accurately coordinate cell growth and cell cycle (Fig. 1).

Fig. 1 (continued) Rb becomes hyperphosphorylated after the activation of cyclin E–CDK2 such that E2F can dissociate from Rb and can initiate the transcription of genes that are required for progression into S phase such as cyclin E, thus generating a positive feedback loop to aid in the progression through G1/pre-S. Suppressing mTOR results in arrest late in G1, and cells arrested with rapamycin are smaller than the untreated cells, which is consistent with a role of mTOR as a nutritional sensor that restricts cell growth in the absence of nutrients [98, 149]. (**b**) The mTOR-dependent checkpoint that senses whether there is sufficient nutrition for a cell to double size prior to committing to replicate the genome and divide could more appropriately be referred to as a "cell growth" checkpoint [96, 97]. Signals that regulate mTOR and cell growth need to be deregulated in proliferative disorders such as tumorigenesis. In this regard, genetic studies that have revealed a requirement for elevated mTOR signaling in cell transformation to suppress TGFβ signals, which suppresses cell cycle progression late in G1 and also increases levels of cyclin E–CDK2 inhibitor $p27^{Kip1}$, strongly indicate that this late G1, mTOR-driven cell growth checkpoint is clearly distinguishable from the early (R) G1 site regulated by cyclin D, which is elevated in response to growth factor signals and activation of the Ras–MEK–MAPK pathway. The connection between cyclin E and mTOR via TGFβ signaling links cyclin E to nutritional sensing in that mTOR is activated by amino acids and is suppressed by an inadequate energy status (e.g., low ATP levels). Indeed, the commitment model for G1 cell cycle progression is consistent with a need to pass through a growth factor cyclin D-dependent R and an mTOR and cyclin E-dependent cell growth checkpoint. Recent findings have disclosed a novel regulatory network (*see* Fig. 3) for mTOR that is active during mitosis, important for G2/M progression and for maintaining genomic integrity during cell division

2 A Brief Overview of the Cell Cycle

Mitogenic signals, such as the binding of growth factors to their cell surface receptors, stimulate several signaling pathways, e.g., the Ras-dependent mitogen-activated protein kinase (MAPK) cascade (Ras-MAPK), which leads to the entrance into G1 phase. In the absence of growth-promoting signals, the cell undergoes a reversible, non-proliferating state of quiescence (i.e., the G0 phase). Once entry into the cell cycle is triggered, D-type cyclins are activated, and, together with the CDKs CDK4 and CDK6, form the essential complexes that are necessary for the progression through the G1 phase [1]. Later, retinoblastoma (Rb) and the related pocket proteins p107 and p130, also known as RBL1 and RBL2, respectively, are phosphorylated, thus remaining inactive and allowing Rb to dissociate from the E2F-DP1 transcription factor, which permits the transcription of target genes, such as E-type cyclins (E1 and E2), CDK2, cyclin A, phosphatase CDC25A, or CDK1, which are required for DNA replication and for further events. Subsequently, cyclin E activates CDK2 and forms the CDK2–cyclin E complex, thus completing Rb hyper-phosphorylation and inactivation as well as the promotion into the S-phase entry and the initiation of DNA replication [2, 3] (Fig. 1).

To control the G1/S transition, cells must overcome the restriction point (R), which is controlled by different mechanisms. First, two families of cyclin kinase inhibitors (CKIs) control the formation of CDK–cyclin complexes: the INK4 family of CKIs ($p16^{INK4A}$, $p15^{INK4B}$, $p18^{INK4C}$, $p19^{INK4D}$), which inhibits cyclin D activity by preventing complex formation with CDK4 and CDK6, and the CIP/KIP family ($p21^{CIP1/WAF1}$, $p27^{KIP1}$, $p57^{KIP2}$), which impedes the formation of the CDK2–cyclin E complex [1, 4]. Of particular interest are $p21^{CIP1/WAF1}$ and $p27^{KIP1}$ because the overexpression of the former induces cell cycle arrest in G1, and high levels of $p21^{CIP1/WAF1}$ are induced as a result of p53 activation in response to DNA damage [5]. Furthermore, once CDK2 is fully activated by the action of CDK-activating kinase (CAK) and the phosphatase CDC25, $p27^{KIP1}$ is phosphorylated and marked for polyubiquitination and destruction, thus ensuring progress through G1 [6]. The Ras–MEK–ERK kinase cascade can also promote CDK activation once ERK phosphorylates and stabilizes c-Myc, which is a transcription factor that induces the expression of cyclin D1 and suppresses that of CDK inhibitors, thereby promoting S-phase entry [7]. Another example is the activation of AKT (protein kinase B), which contributes to CDK activation by two different processes: (1) the inhibition of GSK3β and the prevention of this kinase to phosphorylate and destabilize cyclin D (2) and the inhibition of forkhead box protein O (FOXO) transcription factors, which excludes them from the nucleus and thus prevents this transcription factor's association with target genes, such as $p27^{Kip1}$ and $p21^{Cip1/WAF1}$ [6].

CDK2 binds to cyclin A to promote S-phase progression by the phosphorylation of several substrates, such as ORC1 (origin recognition complex, which serves as the point for the initiation of the replication complexes) and MCM-2 or MCM-4 (mini chromosome maintenance proteins 2 and 4, which form an essential component of the DNA initiation complex) [4–6]. The G2/M phase transition is primarily driven by CDK1, which interacts first with cyclin A and finally with cyclin B, leading to the entrance into M phase. Apart from CDK1, another group of protein kinases, the polo-like kinases (PLKs), also contributes to mitotic progression [8]. At this stage of the cell cycle, cap-dependent translation is low, as a result of CDK1–cyclin B phosphorylation and inactivation of EF2 [9, 10]. Once the nuclear envelope is disrupted and A-type cyclins are degraded by anaphase-promoting complex/cyclosome (APC/C), CDK1–cyclin B complexes accumulate in the nucleus, where these complexes are involved in the initiation of many mitotic events [5, 11].

DNA damage control systems act throughout the entire cell cycle. Both damaged and unreplicated DNA activate DNA repair mechanisms to prevent their transmission to daughter cells. If the damage is too severe, then cell cycle arrest occurs, and if the damage cannot be repaired, then apoptosis is triggered. For instance, the activation of p53 occurs as a response to genotoxic stress, in part through the activation of the ataxia telangiectasia-mutated/ATM-related (ATM/ATR) kinases [12]. The activation of the ATM–p53 pathway induces the expression of $p21^{CIP1/WAF1}$ and various apoptotic factors, oxidative-stress responses, and DNA repair genes. Unreplicated DNA promotes the ATR-CHK1 cascade, which inhibits Cdc25 phosphatase, thus maintaining the phosphorylation and inhibition of CDKs and preventing premature mitosis [6]. The permanent inactivation of CDKs by $p21^{CIP1/WAF1}$ blocks DNA synthesis and mitotic entry, thereby inducing the exit from the cell cycle [13].

3 mTOR: Different mTOR Functions for Different mTOR Complexes (mTORCs)

The evolutionarily conserved mechanistic target of rapamycin (mTOR, formerly known as mammalian TOR) protein is a conserved serine/threonine kinase that belongs to the phosphoinositide 3-kinase (PI3K)-related kinase (PIKK) family. mTOR is the target of the molecule rapamycin, which is a *Streptomyces hygroscopicus-derived* macrolide antibiotic that has well-known antiproliferative properties. Early studies in yeast identified *TOR1* and *TOR2* as the genes that conferred resistance to rapamycin [14, 15], and subsequent studies in mammals led to the identification of mTOR as the target of this compound [16–18]. mTOR is the catalytic subunit of two different complexes, named mTORC1 and mTORC2, which differ in their regulation, functions, and

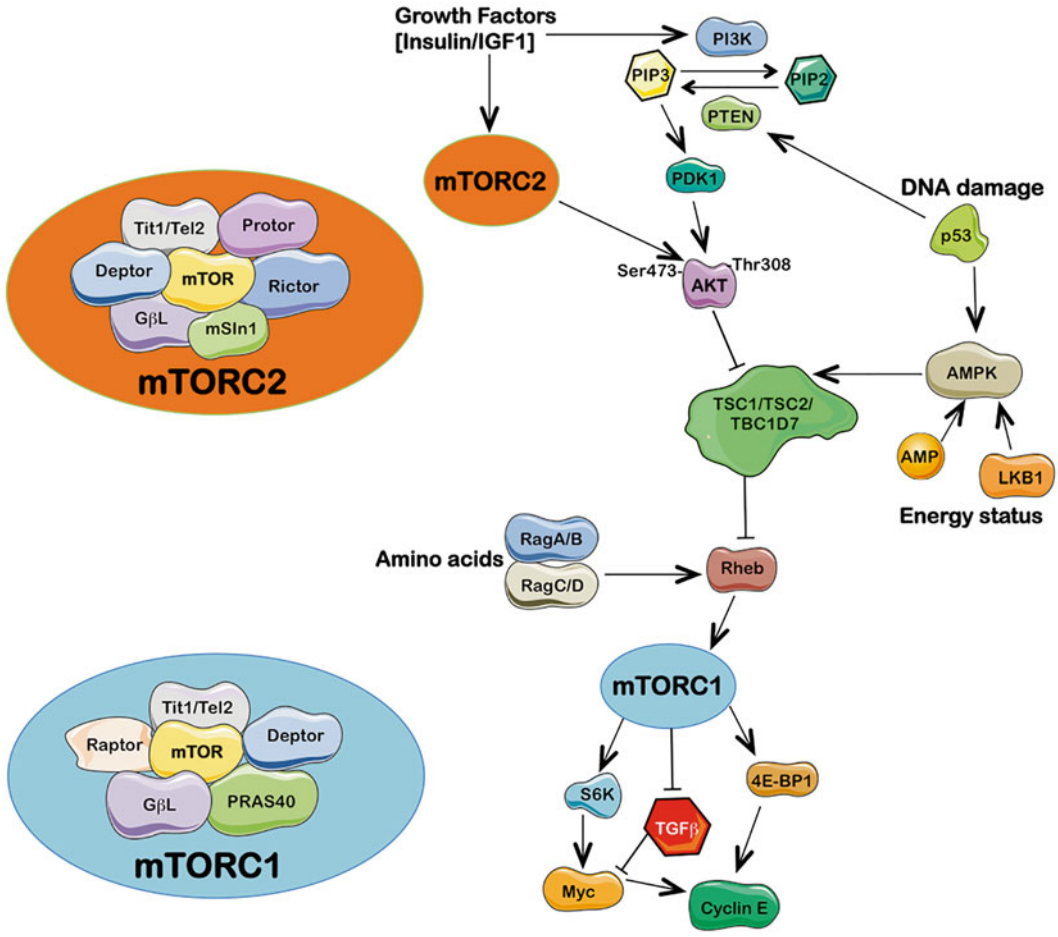

Fig. 2 The complexity of the mTOR pathway. mTOR is a serine/threonine kinase which serves as intracellular sensor for nutrients, energy, and stress, regulating cellular growth and metabolism. Although detailed molecular signaling network and regulation of mTOR signaling have been reviewed comprehensively in several articles, this figure summarizes few important biochemical features of the mTOR-signaling network. mTOR, with other molecular components, forms two structurally and functionally distinct complexes, namely, mTOR complex 1 (mTORC1) and mTOR complex 2 (mTORC2). mTOR functions as the catalytic subunit within mTORC1 and mTORC2, and its enzymatic activity is regulated and distinguished by its unique accessory proteins raptor and rictor, respectively. Raptor and rictor function as scaffold proteins for assembling mTORC1 and mTORC2 and also for binding substrates and regulator in the respective complex. Rapamycin is well known to inhibit mTORC1 but not mTORC2 activity, although prolonged treatment with rapamycin has been shown to inhibit mTORC2 in certain cell types. While mTORC2 seems to be regulated only by growth factors, mTORC1 is regulated by many stimuli including growth factors, energy status, and stressors, such as DNA damage, hypoxia, and nutrients (amino acids). The small GTPase protein Rheb can be considered the key end point for mTORC1 activity by stimulating the kinase activity of mTORC1. The GTPase-activating protein (GAP) complex TSC1–TSC2–TBC1D7 negatively modulates Rheb by converting the active form Rheb-GTP into its inactive form Rheb-GDP and thus reducing mTORC1 activity. Except nutrient amino acids, all of the abovementioned stimuli (e.g., growth factors, energy status, DNA damage) regulate mTORC1 activity through modulation of TSC1–TSC2 activity. Growth factors, through activation of the PI3K input, inactivate TSC1–TSC2 via AKT–ERK; the PI3K input involves the generation of PIP3 from PIP2, which recruits and activates PDK1, which then phosphorylates AKT at Thr308. AKT can then phosphorylate and suppress the GAP activity of TSC1–TSC2, resulting in elevated activation of the GTPase Rheb, which then leads to a complex activation of mTORC1. AMPK, in combination with the tumor-suppressor LKB1, activates TSC1–TSC2 and suppresses mTOR activity under conditions where ATP levels are low and AMP levels are high. Indeed, energy deficit, DNA damage, or

sensitivity to rapamycin (Fig. 2). mTORC1 is acutely sensitive to the compound, whereas mTORC2 is rapamycin insensitive, although it has been observed that prolonged treatment can disrupt the assembly and function of this complex [19].

3.1 Components and Functions of the mTORCs

mTORC1 consists of six proteins, and mTORC2 is composed of seven proteins (Fig. 2). Both complexes share the catalytic subunit mTOR, the DEP domain-containing mTOR-interacting protein (DEPTOR) [20], the mammalian lethal with Sec13 protein 8 (mLST8, also known as GβL) [21], and the Tti1–Tel2 complex that regulates the functional assembly of the complexes [22, 23]. The role of mLST8 in mTORC1 function is not clear because the deletion of this protein does not affect mTORC1 activity but seems to be critical to mTORC2 assembly and function [24]. The regulatory-associated protein of mammalian target of rapamycin (raptor) [25, 26] and the proline-rich AKT substrate 40 kDa (PRAS40) [27, 28] are specific to mTORC1 because the rapamycin-insensitive companion of mTOR (rictor, also known as mAVO3) [29, 30], the mammalian stress-activated map kinase-interacting protein 1 (mSIn1) [31–33], and the protein observed with rictor 1 and 2 (protor1/2, also known as PRR5) [34, 35] are only found in mTORC2. PRAS40 and DEPTOR act as negative regulators and substrates of mTORC1 [20, 28, 36]. Raptor plays an important role in mTORC1 assembly, substrate recognition, binding and phosphorylation of downstream proteins (e.g., S6Ks, 4EBPs, and STAT3), amino acid sensing, and regulation of its subcellular localization [37, 38]. Rictor is absolutely necessary for mTORC2

Fig. 2 (continued) hypoxia activates TSC1–TSC2 through activation of AMPK or REDD1 (regulated in development and DNA damage response 1), respectively, resulting in inactivation of Rheb and thus inhibition of mTORC1. Amino acids activate mTORC1 independently of TSC1–TSC2, but through action of Rag GTPases. In the presence of amino acids, Rag GTPases interact with mTORC1 and translocate the complex from cytoplasm to lysosomal membranes where Rheb activates mTORC1. mTORC1 enhances protein synthesis through 4E-BP1 and S6K1. Upon phosphorylation by mTORC1, 4E-BP1 dissociates from eIF4E, relieving its suppressing effect on mRNA translation; S6K1, when phosphorylated by mTORC1, promotes the translation of many transcripts including those for Myc. mTORC1 suppresses TGFβ signals leading to elevated cyclin E–CDK2 activity and subsequently higher levels of cyclin E. In addition, mTORC1 also induces lipogenesis in the liver through activating transcription factors SREBP1 and PPARγ, inhibits autophagy through phosphorylation of the ULK1–Atg13–FIP200 complex, and promotes mitochondrial biogenesis by activating PGC1α/YY1. In contrast to mTORC1, the regulatory mechanisms and functions of mTORC2 signaling are less well characterized; AKT is also phosphorylated by mTORC2 at Ser473 in response to insulin and IGF1 in a PLD-dependent manner. mTORC2 exerts its effects on metabolism, stress responses, apoptosis, and cytoskeleton organization through phosphorylation of many AGC kinases including AKT, serum- and glucocorticoid-induced protein kinase (SGK), protein kinase C-α (PKC-α), and Rho1 GDP-GTP exchange protein-2. Since mTORC2 activates AKT that in turn enhances mTORC1 activity through inactivation of TSC1–TSC2, mTORC2 is the upstream of mTORC1 upon stimulation by growth factors

catalytic activity and substrate recruitment, in a way similar to raptor for mTORC1 [30]. Rictor and mSIn1 stabilize each other and provide structural stability to mTORC2 [32, 33].

3.2 Upstream Regulators of mTORC1: Nutrients, Growth Factors, and Energy Status

The mTORC1 pathway integrates signals from intracellular and extracellular inputs, e.g., growth factors, energy status, amino acids, stress, and hypoxia, to regulate many processes that are involved in cell growth and proliferation, such as protein and lipid synthesis or autophagy. All of the abovementioned signals, with the exception of amino acids, activate the mTORC1 pathway through the TSC1–TSC2 complex, which is formed by the tuberous sclerosis 1 and 2 proteins (TSC1 and TSC2; also known as hamartin and tuberin, respectively), and TBC1D7 (Tre2–Bub2–Cdc16 (TBC) 1 domain family, member 7), a third component that has recently been identified [39, 40]. This complex negatively regulates mTORC1 by converting the GTP-bound active form of the small Ras-related GTPase (Rheb) to its inactive state (Fig. 2) [41].

The binding of growth factors, such as insulin and insulin-like growth factor 1 (IGF1), to its tyrosine kinase receptors promotes the recruitment of the insulin receptor substrate 1 (IRS1) and the activation of PI3K, which produces phosphoinositol (3,4,5)-triphosphate (PIP3) and recruits AKT to the cell membrane for its full activation. Once active, AKT promotes the phosphorylation and inactivation of the TSC1–TSC2 complex, thus activating mTORC1 (Fig. 2) [42, 43]. AKT can also promote mTORC1 signaling in a TSC1–TSC2-independent manner by phosphorylating raptor, which causes the dissociation of the mTORC1 inhibitor PRAS40 from raptor [27, 28, 36]. Upon activation, a regulatory negative feedback loop strongly represses the PI3K–AKT axis upstream of PI3K through the phosphorylation of IRS1 by both mTORC1 and its downstream target S6K1 (p70 ribosomal S6 kinase 1). Other regulatory mechanisms involve the S6K1-mediated phosphorylation of mTORC2, leading to the attenuation of AKT activation or to the phosphorylation of the growth receptor-bound protein 10 (Grb10) [44–46]. The Ras–ERK pathway can also promote the activation of mTORC1 in response to growth factors by phosphorylating and inhibiting the TSC1–TSC2 complex [47, 48].

The cellular energy status is indirectly sensed by mTORC1 through the AMP-dependent kinase (AMPK) in both TSC-dependent and TSC-independent manners (Fig. 2). AMPK is a serine/threonine kinase that consists of one catalytic (α) and two regulatory (β and γ) subunits (reviewed in ref. 49). Under nutrient starvation conditions that result in energy depletion and, therefore, a rise in AMP and ADP content, AMPK is activated by the binding of ADP or AMP to the γ subunit and phosphorylation at threonine 172 in the activation loop by the serine/threonine kinase LKB1 [50].

As a consequence, mTORC1 activity is reduced, either through the phosphorylation of TSC2 at serine 1345, resulting in an increment of the inactive Rheb GDP-bound state [51], or by directly phosphorylating raptor, which leads to its association with 14-3-3 [52, 53]. The phosphorylation of TSC2 by AMPK acts as a primer for the phosphorylation and activation of the TSC2 function by glycogen synthase kinase (GSK) 3β. Wnt signaling, which is a major regulator of cell growth, proliferation, polarity, differentiation, and development, promotes mTOR inhibition through the activation of GSK3β and activation of TSC1–TSC2 [54].

Amino acids, particularly leucine and arginine, are transported into the cell in a glutamine-dependent fashion [55] and must be present for any upstream signal, including growth factors, to activate mTORC1. As stated above, this activation occurs in a TSC-independent manner [56] and involves the Rag GTPase family [37, 57]. In mammals, four Rag proteins (RagA to RagD) are found in heterodimers that are formed by RagA or RagB with RagC or RagD. Each member of the heterodimer has opposite loading states; thus, when RagA/B is bound to GTP, RagC/D is bound to GDP and vice versa. Amino acids promote the loading of RagA/B with GTP, which enables the heterodimer to interact with raptor [37]. This interaction promotes the translocation of mTORC1 from its cytoplasmic location to the lysosomal surface, where it interacts with Rheb [58]. Once in the lysosomal membrane, Rag GTPases dock on Ragulator, a complex that is essential for the activation of mTORC1 by amino acids [58]. How amino acids are sensed to activate the mTORC1 pathway remains unclear; however, it has been proposed that this sensing may begin within the lysosome in an "inside-out" model in which amino acids accumulate in the lysosomal lumen and initiate signaling through a mechanism that requires the vacuolar H^+-adenosine triphosphate ATPase (v-ATPase) [59]. In addition, recent studies suggest another amino acid-sensing mechanism wherein leucine availability is sensed by the leucyl-tRNA synthetase (LRS). Hence, LRS may cause the formation of the GDP-bound form of RagD, promoting the configuration of the active Rag heterodimer complex [60].

A model has been recently proposed to explain why growth factors or amino acids cannot activate mTORC1 efficiently in the absence of each other. In accordance, signaling inputs from the amino acid–Rag pathway and the growth factor–Rheb pathway occur in parallel and converge at the lysosome to effectively promote mTORC1 activation (reviewed in refs.61, 62). Such cooperation may warrant success once energy-expensive processes, such as cell growth and proliferation, are triggered because this cooperation ensures growth factors, energy, and presence of amino acids as building blocks.

3.3 Other Upstream Regulators of mTORC1: Hypoxia, DNA Damage, Pro-inflammatory Cytokines, and Phosphatidic Acid

Low oxygen levels, or hypoxia, are also capable of inhibiting mTORC1. Under these conditions, the reduction in ATP levels activates AMPK, promoting TSC2 activation and, therefore, inhibition of mTORC1, as described above. Hypoxia also induces the expression of the hypoxia-inducible factor 1α (HIF-1α), which, in turn, induces the regulated in development and DNA damage response 1 (REDD1) gene, which in turn activates TSC2 and suppresses mTORC1 activity [63–65].

DNA damage induces the expression of p53, which, in turn, activates AMPK, leading to the activation of TSC2 and the inhibition of mTORC1 activity through a mechanism that depends on the induction of sestrin 1/2 (Sesn1/2) [66]. p53 also negatively regulates mTORC1 by activating TSC2 and phosphatase and tensin homolog deleted on chromosome 10 (PTEN), which opposes the activity of PI3K and causes the downregulation of the entire pathway (Fig. 2) [67].

Pro-inflammatory cytokines, such as TNFα, can activate mTORC1 through a mechanism similar to growth factors; that is, IκB kinase β (IKKβ) phosphorylates TSC1, causing TSC1–TSC2 inhibition and thereby activating mTORC1, in a process that is thought to be important in tumor angiogenesis and insulin resistance [68]. Finally, some reports have shown that phosphatidic acid (PA) can also act as an activator of mTORC1. Although its role is unclear, exogenous PA or overexpression of PA-producing enzymes, such as phospholipase D1 and D2 (PLD1 and PLD2), significantly increases mTORC1 activity and facilitates the assembly of mTOR complexes or its stabilization (reviewed in ref. 69).

Deficiencies in these signaling cascades may lead to the inappropriate activation of mTORC1, which causes a wide range of pathologies, including cancer, type 2 diabetes, cardiac hypertrophy, and neurodegenerative diseases [70].

3.4 Downstream Cellular Effects of the mTORC1 Complex: Protein and Lipid Synthesis, Mitochondrial Metabolism, and Autophagy

mTORC1 activates protein synthesis through the phosphorylation of the translational regulators eukaryotic translation initiation factor 4E (eIF4E)-binding protein 1 (4E-BP1) and the p70 ribosomal S6 kinase 1 (S6K1). The phosphorylation of 4E-BP1 promotes its dissociation from eIF4E, thereby recruiting the translation machinery to the 5′ cap of eukaryotic mRNAs to promote cap-dependent translation. S6K1 regulates cell size, protein translation, and cell proliferation. Its stimulation by mTORC1 leads to increased protein synthesis through the regulation of different proteins, such as S6K1 Aly/REF-like target (SKAR), programmed cell death 4 (PDCD4), eukaryotic initiation factor 4B (eIF4B), eukaryotic elongation factor 2 kinase (eEF2K), and cap-binding protein 80 (CBP80) (reviewed in ref. 71). mTORC1 activation also upregulates protein synthesis in other ways: the inactivation of the protein phosphatase 2A (PP2A) and the transcription initiation factor 1A (TIF-1A) promotes ribosome biogenesis through the interaction with RNA polymerase I (Pol I)

and the expression of ribosomal RNA (rRNA) [72] or through the inhibition of Maf1, which is an RNA polymerase III repressor that induces 5S rRNA and transfer RNA (tRNA) transcription [73].

The regulation of lipid synthesis is important for proliferating cells to generate membranes. mTORC1 promotes lipid synthesis by activating the expression of the sterol regulatory element-binding protein 1/2 (SREBP1/2) [74]. The precise molecular mechanism whereby mTORC1 regulates SREBP-1 activity remains unclear. It has been proposed that S6K1 may mediate SREBP-1 cleavage and activation [75]. Lipin-1 is also involved in SERBP-1 activation because once lipin-1 is phosphorylated by mTORC1, it is excluded from the nucleus, thus promoting the nuclear accumulation of SERBP-1 [76]. Additionally, mTORC1 promotes the expression and activity of peroxisome proliferator-activated receptor γ (PPARγ), which is a key element in adipogenesis regulation [77, 78].

Mitochondrial number and function are also regulated by mTORC1 activity. Rapamycin inhibition has been shown to decrease mitochondrial oxygen consumption and decrease oxidative capacity, whereas mTORC1 hyper-activation increases the mitochondrial DNA copy number [79]. mTORC1 activity has been shown to directly act on the expression of mitochondrial proteins by mediating the interaction of the transcriptional activity of PPARγ co-activator 1α (PGC1α) and the transcription factor Ying–Yang 1 (YY1), which regulates mitochondrial biosynthesis and oxidative function [80]. Furthermore, mTORC1 binding to the mitochondrial outer membrane proteins VDAC1 and Bcl-xl has also been reported [81].

Another important function of mTORC1 is the inhibition of autophagy, which is an evolutionarily conserved process that allows cells to obtain energy by degrading cytoplasmatic proteins and organelles during periods of nutrient starvation. In mammals, mTORC1 phosphorylates and inhibits ULK1/Atg13/FIP200 (unc-51-like kinase 1/mammalian autophagy-related gene 13/focal adhesion kinase family-interacting protein of 200 kDa), which is the complex necessary to initiate autophagy [82, 83]. Other mechanisms, such as the regulation of the autophagy-suppressor death-associated protein 1 (DAP1), also appear to operate through mTORC1 signaling [84, 85].

3.5 Regulation and Functions of mTORC2: The Great Unknown

Compared with mTORC1, little is known about mTORC2 (reviewed in ref. 86). mTORC2 is insensitive to amino acids and nutrients but responds to growth factors through a still unknown mechanism that involves PI3K [87] and ribosomes [88]. It has also been suggested that TSC1–TSC2 physically interacts with mTORC2, positively regulating its activity [89]. Once active, mTORC2 is phosphorylated on Ser2481 [90] and regulates cell survival, metabolism, and cytoskeletal organization.

mTORC2 phosphorylates protein kinase C-α (PKC-α), which regulates cell proliferation, differentiation, and cytoskeletal organization; it has been observed that the knockdown of mTORC2 components disrupts cell morphology and actin polymerization [29]. AKT, which is activated downstream of PI3K, is an important component for cell survival, metabolism, and proliferation. The full activation of AKT requires phosphorylation at Ser308 by phosphoinositide-dependent kinase (PDK1) and at Ser473 by mTORC2 [91]. Serum- and glucocorticoid-induced protein kinase 1 (SGK1) is also a target for mTORC2. SGK1 is involved in growth and in ion transport after its activation by growth factors [87].

mTORC2 phosphorylates and activates AGC kinase family members, including AKT, PKC, and SGK1, in response to insulin/IGF1. Using liver-specific rictor knockout mice, Hagiwara et al. [92] recently revealed that the mTORC2-deficient liver is unable to sense satiety because hepatic mTORC2 activates glycolysis and lipogenesis through AKT, glucokinase, and SREBP1c [92]. Using insulin-unresponsive mice that lack the essential mTORC2 component rictor in liver, Yuan et al. [93] revealed the occurrence of an AKT-independent relay from mTORC2 to hepatic lipogenesis that separates the effects of insulin on glucose and lipid metabolism. Although a central role for mTOR in lipid homeostasis, including adipogenesis, ketogenesis, lipogenesis, and lipolysis, has been recently depicted by Lamming and Sabatini [94], the ultimate mechanism(s) by which mTORC2 regulates lipogenesis and lipolysis is (are) currently unknown, although AKT may be involved in the regulation of lipogenesis.

4 mTOR Regulation of the Cell Cycle

4.1 Role of mTOR in the G1/S Transition

To grow and proliferate, cells require sufficient nutrients and growth factors. Tight coordination between cell growth and proliferation is essential to warrant proper cell cycle progress and survival because conflicting signals can induce cell death (apoptosis) or senescence. Although it is commonly said that senescence is an "exit from the cell cycle," senescence is an active arrest in the advanced points of G1, G1/S, and even G2; therefore, cell cycle arrest is not senescence [95]. Rather, the block of the cell cycle in the face of growth stimulation causes a molecular condition that is known as cellular senescence. As previously described, mTOR is the master regulator of cell metabolism and responds to intracellular and extracellular signals; therefore, mTOR is expected to be a pivotal player in the coordination of cell growth and division. The inhibition of mTOR activity, by both rapamycin and nutrient starvation, has been shown to induce cell cycle arrest at G1. Indeed, mTOR inhibition arrests cells in the late G1, strongly suggesting a role of mTOR as the final arbiter for nutrient sufficiency before

committing to replicating the genome. Recent evidence appears to confirm that growth factors, amino acids, and mTOR mediate distinct checkpoints in the mammalian G1 phase. These checkpoints include a growth factor-dependent mid-G1 restriction point (R), where cells determine whether it is appropriate to divide, and a series of late-G_1 metabolic checkpoints dictated by amino acids and mTOR, where cells determine whether they have sufficient nutrients to accomplish the task [96, 97] (Fig. 1).

A landmark study by Fingar et al. [98] revealed that activities of both the 4E-BP1 and S6K1 pathways are required for and independently mediate the mTOR-dependent G1-phase progression. First, the restoration of mTOR signaling by a rapamycin-resistant mutant form of mTOR rescues the rapamycin-inhibited G1-phase progression, whereas the restoration of signaling along the mTOR-dependent 4E-BP1–eIF4E and S6K1 pathways provides a partial rescue. Thus, the activation of either the 4E-BP1–eIF4E or S6K1 pathways partially rescues the inhibitory effect of rapamycin on the G0-to-S phase cell cycle progression and modestly accelerates cell cycle progression in the absence of drugs. Both the S6K1 and 4E-BP1–eIF4E pathways independently mediate mTOR-dependent cell cycle control in parallel because the simultaneous downregulation of these pathways additively inhibits G1-phase progression compared with the downregulation of the pathways individually. Indeed, because the simultaneous downregulation of both the 4E-BP1–eIF4E and S6K1 pathways inhibits G1-phase progression to an extent approaching that of rapamycin, these pathways likely represent the major pathways mediating mTOR-dependent cell cycle control. In addition, the overexpression of constitutively active mutants of S6K1 or wild-type 4E-BP1 accelerates serum-stimulated G1-phase progression, and the stable expression of wild-type S6K1 confers a proliferative advantage in low-serum-containing media, suggesting that the activity of each of these pathways is limiting for mTOR-regulated cell proliferation.

The control of G1/S-phase progression is mediated by the transcriptional regulation of G1 cyclins (D-type and E-type cyclins) through the mTORC1 effectors 4E-BP and S6K1 [98] or by the protein synthesis control of cyclin inhibitors $p21^{CIP1/WAF1}$ and $p27^{kip1}$ [99–102] (Fig. 1). In addition, mTORC1 influences the subcellular localization of $p27^{kip1}$. In the presence of growth factors, $p27^{kip1}$ is phosphorylated by the AGC kinase family (AKT, activated by mTORC2; SGK1, activated by mTORC1 and mTORC2; and RSK), leading to $p27^{kip1}$ cytoplasmatic sequestration that blocks its nuclear function as a CDK inhibitor, thus promoting DNA replication and cyclin D–CDK4/6 complex stabilization [103]. Furthermore, mTORC2 participates in the AKT-mediated inhibition of FOXO transcription factors, which are key players in inducing apoptosis and blocking the further transcription of $p21^{CIP1/WAF1}$ and $p27^{kip1}$ [24, 104].

Moreover, in response to DNA damage or other stresses, the activation of p53 leads to cell cycle arrest through the induction of $p21^{CIP1/WAF1}$. p53 negatively regulates mTORC1, in part, through the activation of AMPK and PTEN and the induction of TSC1–TSC2 activity [67, 105]. AMPK is activated either by the phosphorylation of sestrin 1 and 2 or directly by p53 itself. In addition, AMPK can phosphorylate and activate TSC2, which can also be directly activated by p53. Other reports suggest that mTOR can induce p53 in response to nutrient stress conditions by the activation of PP2A [106, 107].

4.2 Role of mTOR in G2/M Cell Progression: The mTOR Pathway Within the Mitotic Apparatus

The crucial energy- and nutrient-sensing proteins of the mTOR pathway (i.e., AMPK and mTOR itself; some of their regulators, e.g., TSC and raptor; and several targets of mTORC1, e.g., S6K1) have begun to be recognized as novel regulators of mitotic completion in proliferating cells (Fig. 3).

4.2.1 Mitotic Phospho-AMPK

Genetic and pharmacological ablation of AMPK leads to mitotic defects, including chromosomal misalignments in metaphase, chromosomal lagging during anaphase, as well as failures in cytokinesis and polyploidy [108–112]. Intriguingly, an equivalent impairment of mitosis progression leading to a multinucleated cellular state can also be triggered upon the pharmacological hyperactivation of AMPK [113, 114]. These observations are generally compatible with the molecular consequences of altering either the expression or the activation status of some well-known mitotic apparatus-bound proteins, including Auroras (A and B), INCENP, Mad2, or PLK, whose inhibition or activation results in mitotic defects. Accordingly, our own group was the first to report that the active form of the α-catalytic AMPK subunit transiently associates with several mitosis-specific structures, including centrosomes, spindle poles, the central spindle midzone, and the midbody throughout all of the mitotic stages and during the furrowing process in cytokinesis [115, 116]. Phospho-active AMPKα is rapidly relocated at centrosomes when cells enter mitosis and during nuclear envelope breakdown. Thereafter, phospho-$AMPK\alpha^{Thr172}$ appears to directly bind the mitotic apparatus to travel from centrosomes to the spindle midzone, overlapping with essential mitotic and cytokinetic regulators at precise locations and specific times. Indeed, although not identical, the mitotic geography of AMPKα activation toward the end of anaphase and in telophase notably overlaps the location occupied by the chromosomal passenger proteins Aurora B and INCENP [116]. Moreover, not only is the α-catalytic AMPK subunit a component of the cytokinetic apparatus, but the AMPK regulatory subunits β and γ have also been identified as mitotic proteins, suggesting that the subunit composition of activated AMPK at the spindle midzone may be α2/β2/γ2 [117, 118].

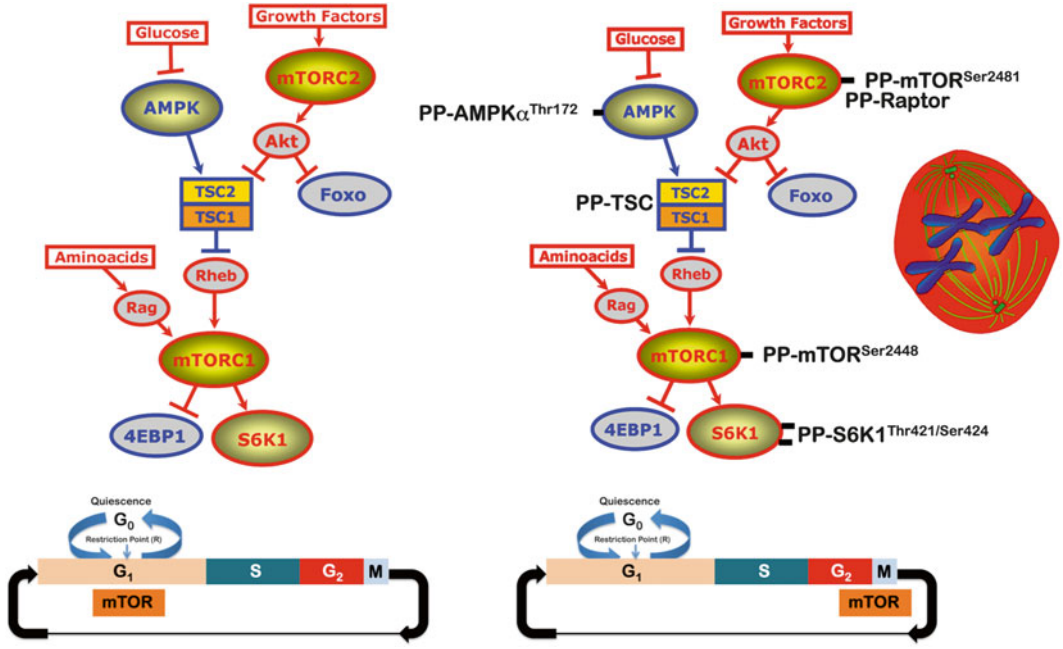

Fig. 3 The "phosphorylated mTOR pathway": a facilitator of the cell cycle through G2/M and a new caretaker of genome stability. During the G1 phase, overall protein synthesis rates increase through S phase to allow cells to grow and enter another round of cell division while maintaining cell size. As with G0, entrance into mitosis (G2/M phase) results in a global downregulation of cap-dependent mRNA translation in several types of mammalian cells. Despite the fact that the PI3K–AKT network and AKT itself (which modulate mTORC1 activity) are reportedly inactivated during late mitosis, mTORC1 remains hyperactive during mitosis and phosphorylates 4E-BP1 and S6K1 during G2/M. G2/M-specific phosphorylation of a component of mTORC1, the protein raptor, has been shown to alter mTORC1 function during mitosis; that is, mitotic phosphorylation of raptor facilitates cell cycle transit through G2/M because phosphorylation-deficient mutants of raptor cause cells to delay in G2/M, whereas depletion of raptor causes cells to accumulate in G1. It is important to note that phosphorylation of raptor during mitosis has consequences distinct from those of AMPK-mediated raptor phosphorylation. A "metabolic checkpoint" mediated by AMPK and mTORC1 could be considered part of the mTOR-regulated G1 cell growth checkpoint. In addition, growing evidence is suggesting that another layer of complexity in the mTOR regulatory network related to the dynamic compartmentalization of mTOR regulatory inputs and outputs to certain mitotic structures in a stage-dependent manner. Several studies aimed to elucidate the spatiotemporal immunolocalization of several kinase-active forms of mTOR, raptor, AMPK, TSC, and p70S6K1 during mitosis and cytokinesis have revealed specific accumulations and transient associations with several mitotic structures including centrosomes, spindle poles, the central spindle midzone, and the midbody. For instance, it has been confirmed that Thr172-phosphorylated AMPKα localizes to the mitotic spindle poles and increases when cells enter mitosis; the mitotic AMPK activity appears to be essential for normal spindle orientation, and when it is defective, mitosis does not proceed efficiently. Forthcoming studies should be designated to unambiguously establish whether the phosphorylated forms of multiple mTOR signaling components can causally contribute to the structural and/or functional integrity of centrosomes, mitotic spindle, and/or cytokinetic apparatus, thus confirming a previously unrecognized role of the phospho-mTOR pathway as a multifaceted "metabo-mitotic sensor" that precisely regulates chromosome duplication and segregation to ensure genomic stability

Functionally supporting the unexpected mitotic localization of the phospho-active AMPK, a chemical genetic screen aimed at identifying direct substrates of a catalytic subunit of the energy-sensing AMPKα2 revealed that the AMPK substrates PPP1R12C (phosphatase 1 regulatory subunit 12C) and PAK2 (p21-activated protein kinase) were directly involved in mitosis completion and chromosomal segregation [119, 120]. In this scenario, Thaiparambil et al. [121] have proposed a model in which mitotic AMPK, apparently independent of glucose deprivation, may indirectly activate the phosphorylation of Ser19 in myosin regulatory light chain (MRLC), which is a crucial phenomenon that ensures the normal recruitment of myosin molecules into the contractile ring structure to allow the proper transition from metaphase to anaphase and the completion of cytokinesis. Indeed, we recently confirmed that the deprivation of exogenous glucose fails to alter the distribution of phospho-AMPKα^{Thr172} in all of the mitotic phases and does not disrupt its apparent association with the mitotic spindle and other structures that are involved in cell division [122]. Moreover, we established for the first time that phospho-AMPKα^{Thr172} colocalizes exclusively with Ser19-phosphorylated MRLC in cleavage furrows, intercellular bridges, and the midbody during cell division. This is a previously unvisualized interaction that appears to occur irrespective of glucose availability [122].

Because AMPK is active under low-energy conditions, it appears counterintuitive that AMPK promotes cell division, given the high-energy demands of cellular division. It is possible that under low-energy conditions, AMPK activity ensures the completion of mitosis because cell cycle arrest at this stage could have disastrous consequences for the genomic stability of a cell [123]. Mao et al. [124] have recently confirmed that AMPK is phosphorylated and activated when cells enter mitosis and that AMPK activation is essential for the Golgi apparatus disassembly and subsequent mitosis entry. It should be noted that glucose starvation does not appear to alter AMPK-regulated mitotic progression, and AMPK would not promote mitosis in response to energy starvation. Therefore, given that cell cycle progression is energy consuming, one would think that the yet-to-be-discovered mitotic stimuli should specifically activate the mitotic apparatus-bound AMPK to operate independently of low cellular energy status. We initially proposed a working model in which AMPKα can be pre-activated "by default" in an LKB1-independent manner (i.e., the mitotic activation of AMPKα can occur regardless of the expression/activation status of the upstream AMPK kinase LKB1) by being directed to centrosomes and kept active throughout the entire M phase [116]. Because activation of AMPK can result in proliferation inhibition and cell cycle arrest, AMPKα must become inactivated at the cytokinetic exit to allow the proliferation of daughter cells, thus tethering the AMPK-interpreted cell bioenergetic state to the

spatiotemporal regulation of the chromosomal and cytoskeletal events during mitosis and cytokinesis.

A crucial question that remained to be elucidated in the above-mentioned working model was how AMPKα could be activated at the onset of the mitotic phase. Given that PLKs regulate many aspects of mitotic progression, including centrosome maturation, bipolar spindle assembly, chromosome congression and segregation, and cytokinesis, we recently combined an immunofluorescence microscopy analysis with a biochemical approach that employs a small-molecule PLK1 inhibitor to dissect a putative relation between PLK1 and AMPKα during G2/M transition [122, 125]. First, PLK1 and phospho-AMPKα^{Thr172} were found to exhibit largely overlapping temporal and spatial dynamics during mitosis and cytokinesis; thus, PLK1 and phospho-AMPKα^{Thr172} display a major overlap early at centrosomes, from prophase until anaphase, and late at the midbody, during telophase and cytokinesis. Whereas short-term treatment with a selective PLK1 inhibitor fully abolished the mitotic activation of AMPKα, upon the long-term inhibition of PLK1, phospho-AMPKα^{Thr172} was barely detected surrounding the spindle poles of prometaphase-like arrested cells that displayed the "polo" phenotype [122]. Similarly, phospho-AMPKαThr172 was largely inhibited in PLK1-inhibited cells that displayed cytokinesis failure and binucleate cell formation.

Because PLK1 is a well-recognized master regulatory kinase for the numerous protein substrates that are involved in mitosis, our recent description of a causal link between PLK1 activity and mitotic phosphorylation of AMPKα may provide fundamental insights into how the energy sensor AMPK is directly coupled to mitotic cell division and cell cycle exit. Interestingly, a commonly used inhibitor of AMPK activity, compound C, has no effect on the phosphorylation state of AMPK in mitotic cells. This "mitotic protection" of AMPKα phosphorylation against pharmacological inhibitors of the multimeric AMPK enzyme, together with an exquisite "mitotic sensitivity" of AMPKα phosphorylation to PLK1 inhibition, may support the notion that the transient disruption of the nucleus/cytoplasm compartmentalization in mitotic cells provides specialized microenvironments (e.g., centrosomes) in which the coordination of complex molecular interactions between many apparently unrelated enzymes (e.g., PLK1 and AMPK) is distinctly regulated [122]. In this regard, we have recently revealed that the inhibition of the mitosis-associated AMPK activity in response to the pharmacological blockade of PLK1 completely prevents the colocalization of phospho-AMPKαThr172 and phospho-MRLC^{Ser19} during the final stages of cytokinesis and midbody ring formation [122]. Forthcoming studies should clarify whether PLK1 could link the sensing of nutrient availability and cellular bioenergetics with the onset and/or completion of mitotic

cell division via AMPK and mTOR. Interestingly, PLK1 inhibition efficiently suppresses the AMPK-mediated activation of MRLC at the cytokinetic cleavage furrow regardless of the absence of glucose strongly. This fact supports a previously unrecognized role for AMPK in ensuring that cytokinesis occurs at the proper place and time by establishing a molecular dialog between PLK1 and MRLC in an energy-independent manner.

4.2.2 Mitotic Phospho-TSC

The multi-system disorder tuberous sclerosis (TSC), which is characterized by hamartomatous tumors and abnormal brain development, is associated with mutations in two genes, *TSC1* and *TSC2*, which encode hamartin and tuberin, respectively. Hamartin and tuberin form a complex and inhibit signaling by mTORC1. The *Drosophila* homolog of TSC2, gigas, was found to be required for the G2/M transition of the cell cycle [126, 127]. Using co-immunoprecipitation and confocal microscopy, Catania et al. [128] reported that tuberin interacts and colocalizes with the CDK CDK1 and its binding partner cyclin B1 to trigger the G2/M transition in multiple cell types; additionally, tuberin interacts with the other regulatory subunit of CDK1, cyclin A. Hamartin also interacts with CDK1 and cyclin B1, which suggests a direct role of tuberin and hamartin in modulating the activity of CDK1 during the G2 and G2/M transition. Indeed, endogenous hamartin is threonine-phosphorylated during the nocodazole-induced G2/M arrest and during the G2/M phase of a normal cell cycle [129]. CDK1 phosphorylates hamartin at three sites, one of which (Thr417) is the hamartin–tuberin interaction domain; thus, tuberin interacts with phospho-hamartin, and tuberin expression attenuates the phosphorylation of exogenous hamartin.

Not only does the phosphorylation of hamartin regulate the function of the hamartin–tuberin complex during the G2/M phase of the cell cycle, but also hamartin is localized to the centrosomes, and phosphorylated hamartin and phosphorylated tuberin co-immunoprecipitate with the mitotic kinase PLK1 [130]. Notably, *Tsc1* (−/−) mouse embryonic fibroblasts (MEFs) have an increased number of centrosomes and increased DNA content when compared with *Tsc1* (+/+) cells, and both phenotypes are rescued after pretreatment with the mTOR inhibitor rapamycin. These data reveal a novel subcellular localization for hamartin and a novel interaction partner for the hamartin–tuberin complex and implicate hamartin and mTOR in the regulation of centrosome duplication. Indeed, the cancer-associated centrosomal transforming acidic coiled coil-3 (TACC-3) protein, which is a central player in structures and processes connected to the centrosomes that are essential for spindle-dependent chromosome alignment and mitotic survival [131], is also necessary for the proper localization of phospho-TSC2S^{Ser939} at spindle poles and cytokinetic bridges. Accordingly, abscission alterations and an increased frequency of

binucleated cells were observed in Tacc3- and Tsc2-deficient cells relative to controls [132]. Because TACC-3 and TSC2 colocalize and copurify with components of the nuclear envelope and because their deficiency causes morphological alterations of this structure, these findings link TACC3 to novel structural and cell division functions of TSC2. Therefore, in regulating cell division, TSC2 appears to act epistatically to TACC3 and, in addition to canonical TSC-mTOR signaling and cytokinetic associations, converges to early mitotic checkpoints, which is consistent with nuclear envelope associations.

4.2.3 Mitotic Phospho-Raptor

The protein synthesis rates fluctuate throughout the cell cycle but diminish significantly during the G2/M transition. The mTORC1 pathway, which stimulates protein synthesis, is actually hyperactive during mitosis, despite decreased protein synthesis and reduced activity of mTORC1 upstream activators. Regulatory-associated protein of mTOR (raptor) and rapamycin-insensitive companion of mTOR (rictor) are unique accessory proteins that appear to distinguish mTORC1 and mTORC2, respectively (Fig. 2). As mentioned above, these mTOR companions function as scaffolds for assembling the complexes and for binding substrates and regulators. Raptor is a non-catalytic protein that functions as the substrate-binding element of mTORC1. The ability of raptor to properly present substrates, such as the translational regulators 4E-BP and p70 S6 kinase, to the mTOR catalytic domain is essential for their mTOR-catalyzed phosphorylation. Interestingly, Ramirez-Valle et al. [133] originally described a previously unknown G2/M-specific phosphorylation of raptor and demonstrated that the mitotic phosphorylation of raptor alters mTORC1 function during mitosis. The mitotic phosphorylation of raptor appears to facilitate the cell cycle transit through G2/M because phosphorylation-deficient mutants of raptor cause cells to delay in G2/M, whereas the depletion of raptor causes cells to accumulate in G1. Mitotic raptor promotes translation by internal ribosome entry sites (IRES) on mRNA during mitosis, which is a phenomenon that is associated with resistance to rapamycin.

Although Ramirez-Valle et al. [133] provided evidence that cyclin-dependent kinase 1 (CDK1/cdc2) and glycogen synthase kinase 3 (GSK3) pathways function as two probable mitosis-regulated protein kinase pathways that are involved in the mitosis-specific raptor phosphorylation that alter mTORC1 activity, Gwinn et al. [134] confirmed that the mitotic CDK CDK1/cdc2 is the kinase that is responsible for phosphorylating the two key sites in raptor during mitosis, i.e., Ser696 and Thr706. These authors further demonstrated that cyclin B, which is the mitotic partner of CDK1, efficiently co-immunoprecipitates with raptor in mitotic cells, thus sharing common mitotic partners with TSC1–TSC2.

These studies, altogether, reinforced previous studies suggesting that mTOR activity is highly regulated and important for mitotic progression; moreover, they pointed to a direct modulation of the mTORC1 complex during mitosis as the key mTOR-binding partner that raptor directly phosphorylates during mitosis by CDK1. In this scenario, we recently explored the spatiotemporal cell dynamics of five different phospho-raptor isoforms (i.e., Thr706, Ser722, Ser863, Ser792, and Ser877).

Notably, our approach revealed many remarkable events that differentially define a topological resetting of phospho-raptor^{Thr706} on interphasic and mitotic chromosomes [135]. In interphase nuclei, phospho-raptor^{Thr706} colocalizes with fibrillarin, which is a component of the nucleolar small nuclear ribonucleoprotein particle, as well as with RNA polymerase I, which is the enzyme that transcribes nucleolar rRNA. Upon actinomycin D-induced nucleolar segregation and disaggregation, phospho-raptor^{Thr706} is excluded from the nucleolus to accumulate at discrete nucleoplasmic bodies. During mitosis, the CDK1 inhibition-induced premature assembly of nucleoli relocates fibrillarin to the surrounding regions of chromosomal associated phospho-raptor^{Thr706}, suggesting that a subpopulation of mitotic phospho-raptor^{Thr706} may remain targeted at chromosomal loops of rDNA or nuclear organizer regions (NORs). Accordingly, at the end of mitosis and cytokinesis, when the reassembly of incipient nucleoli begins upon the NORs' activation of rDNA transcription, fibrillarin spatially reorganizes with phospho-raptorThr706 to give rise to daughter nucleoli. Because raptor must be continuously associated with mTOR not only to enhance its kinase activity but also to recruit substrates for its own phosphorylation by the kinase domain of mTOR, it is tempting to suggest that raptor phosphorylation could induce conformational changes in the mTORC1 complex, which would allow its nuclear import to facilitate raptor-bound nuclear substrates to access to the kinase domain of mTOR. Supporting this suggestion, the treatment of cells with IGF-1, which is known to stimulate the transcriptional activity of RNA Pol I in an mTOR-regulated manner, exclusively hyperactivates nuclear phospho-raptor^{Thr706} and concomitantly promotes the Ser2481-autophosphorylation of mTOR [135], which monitors mTORC1-associated catalytic activity.

Together, these findings are in agreement with earlier studies that demonstrate that the mTORC1 complex is hyperactive during mitosis and suggest that the entire (or at least part of the components of the) mTORC1 complex may remain physically and functionally linked during mitosis. A previously unrecognized nucleolar localization of phospho-active forms of raptor may provide a spatio-functional molecular scenario that links the growth-promoting, nutrient-sensing mTOR pathway, mTOR-regulated translation, and protein synthesis. Although nucleolar- and NOR-associated phospho-raptor^{Thr706} may physically link mTORC1

signaling to the ever-growing nucleolus plurifunctionality, including ribosome biogenesis, cell stress sensor, and cell cycle control, it remains to be demonstrated whether mitotic phospho-raptor may directly adapt mTOR to target other mitotic proteins. The exact role raptor–mTOR interaction might play in modulating the phosphorylation status of nuclear mTOR remains to be fully elucidated. The fact that raptor, which is a positive regulatory subunit of the rapamycin-sensitive mTORC1, can function as a phosphoprotein of the nucleolus and NOR of mitotic chromosomes might suggest a previously unrecognized "nucleolar mode" for mTORC1-regulated cellular physiology [135].

4.2.4 Mitotic Phospho-mTOR

Although it has been assumed that the coordination of mTORC1 function relates to cytoplasmic-nuclear shuttling phenomena, the ultimate mechanisms that are responsible for its nuclear transportation remain largely unclear. It has been suggested that the existence of a nuclear shuttling signal for mTOR could provide definitive evidence for a requirement of mTOR nuclear import in cytoplasmic signaling to the mTOR effector S6K1 [136]. Considering the role of raptor as a docking and scaffold partner of the mTORC1 complex, it is tempting to suggest that the phosphorylation of raptor at specific sites might function not only as a biochemical rheostat that modulates mTORC1 signaling but also as the mechanism that drives the mTORC1 complex to specific subcellular localizations to exert specific mTORC1 functions. In this regard, earlier studies in our laboratory first described the spatiotemporal subcellular distribution of the Ser2481-autophosphorylated form of mTOR during the G1/S-to-M phase transition, both in cultured cancer cells and in cancer tissue specimens [137, 138]. Phospho-mTOR^{Ser2481} was found to exhibit a punctate nuclear distribution in interphase cancer cells, with the number of phosho-mTOR^{Ser2481} nuclear speckles positively relating to the proliferative capacity of cancer cells [137]. Phospho-mTORSer2481 expression appeared to dynamically rearrange within the cytoplasm in a close association near and between separating chromosomes during the early stages of mitosis. Toward the end of anaphase and in telophase, phospho-mTOR^{Ser2481} drastically focused on the midzone and, ultimately, on the center of the midbody at the presumptive cleavage furrow. In cells at cytokinesis, phospho-mTOR^{Ser2481} appeared as a doublet facing each other at the apical ends of two daughter cells. Three-dimensional analyses strongly suggested that phospho-mTOR^{Ser2481} might position at a ring structure that is wrapped around by microtubule bundles to connect daughter cells [137].

Because these findings revealed for the first time that phosho-mTORSer2481 is associated near and between separating chromosomes not only during early mitotic stages but also to the midzone and to the midbody at ana/telophase through cytokinesis, we

recently performed a systematic approach to unambiguously explore the possibility that phospho-mTOR^{Ser2481} might colocalize with chromosomal passenger proteins during mammalian cell cytokinesis. In prophase, bright phospho-mTOR^{Ser2481} likewise appeared among condensed chromosomes. Although the faint punctate staining of prophasic phospho-mTOR^{Ser2481} seemed to distribute along the arms of the chromosomes, there was no evident colocalization between phospho-mTOR^{Ser2481} and the Ser10- and Ser28-phosphorylated forms of histone H3 [138]. Although the phospho-mTOR^{Ser2481}-immunopositive signals in mitotic cells continued to exhibit a diffuse pattern that partially colocalized with the mitotic spindle from prophase to telophase, phospho-mTORSer2481 was most prominent as a broad cytoplasmic signal until the chromatids were pulled apart and began to migrate toward the poles. However, a completely different picture emerged when analyzing the mitotic dynamics of phospho-mTOR^{Ser2481} from late anaphase. "PP-mTORSer2481-somes" notably and specifically accumulated at the midzone and midbody until the end of the furrowing process at the completion of telophase and cytokinesis [139].

The detection of phospho-mTOR^{Ser2481} in the intercellular bridge reached its maximum during early telophase, and at the completion of telophase, prominent staining of phospho-mTORSer2481 as a doublet was apparent on either side of the midbody within the intercellular cytokinetic bridge as mentioned above. Indeed, in the late stages of mitosis and cytokinesis, phospho-mTORSer2481 persisted near the midbody in the post-mitotic bridges connecting the dividing daughter cells. Similar to the *bona fide* chromosomal passenger proteins (CPPs) INCENP and Aurora B, phospho-mTOR^{Ser2481} displayed noteworthy accumulation in the central spindle midzone and the midbody regions, which persisted during the furrowing process; moreover, double-staining experiments confirmed that toward the end of anaphase and during telophase, phospho-mTOR^{Ser2481} and the CPP INCENP showed similar localizations at the central spindle and midbody [139]. At late anaphase, INCENP localization was mostly restricted to the central spindle. Late-anaphase phospho-mTOR^{Ser2481} began to accumulate in the spindle midzone, although some was not apparently bound to any mitotic structure. More revealing was the observation of a prominent overlap of INCENP and phospho-mTORSer2481 in the two bands on either side of the midbody at the cleavage furrow area. The localization of INCENP and phospho-mTORSer2481 continued to overlap in cells at cytokinesis, when both proteins appeared as a doublet facing each other at the apical ends connecting two daughter cells. A similar colocalization pattern occurred when we evaluated the immunofluorescence costaining of phospho-mTOR^{Ser2481} and Aurora B from late anaphase to the completion of cytokinesis [139]. At this late stage of the mitotic process, however, phospho-mTOR^{Ser2481} appeared to

position internally relative to Aurora B. Intriguingly, the CPP-like mitotic localization of phospho-mTOR^{Ser2481} was fully prevented by the microtubule-depolymerizing drug nocodazole; the mitotic traveling of phospho-mTOR^{Ser2481} to the midbody during telophase and cytokinesis, where it appears to be integrated into the CPP-driven cytokinetic machinery, may therefore require dynamic microtubules.

Taken together, these findings strongly suggest that phospho-mTORSer2481 functions as a microtubule-binding protein that translocates to the equatorial plane before cleavage furrow formation through molecular interactions requiring dynamic microtubules. Because the formation of the contractile rings is a rather late phenomenon during mitosis and because phospho-mTOR^{Ser2481} relocates to the equatorial plate at the metaphase–anaphase transition, it may be tempting to suggest that phospho-mTOR^{Ser2481} is a member of the class of CPPs. However, we should acknowledge that members of the CPP class of proteins share some traits that we failed to observe when assessing the mitotic/cytokinetic geography of phospho-mTOR^{Ser2481} in dividing cells. Indeed, CPPs associate with chromosomes during metaphase and colocalize with the microtubules of the overlap zone of the central spindle during anaphase. In contrast, phospho-mTOR^{Ser2481} does not appear to use the chromosomes to correctly position itself at the metaphase plate and at the midbodies.

The Ser2481 and Ser2448 phosphorylation sites of mTOR are absent in invertebrates but are highly conserved across vertebrate species, suggesting their recent evolution and distinctive regulation of mTOR signaling in vertebrates. However, it cannot be excluded that phospho-mTOR^{Ser2481} and phospho-mTOR^{Ser2448} did share a common function that was once acquired during early vertebrate evolution. In this regard, mTOR phosphorylation at Ser2481 and Ser2448 may behave in a similar manner to mitotic survival checkpoints. Yaba et al. [140] were pioneers in revealing that phospho-mTOR^{Ser2448} is present at high levels during M phase in ovarian granulosa cells. They further reported that phospho-mTORSer2448 is enriched on or near the mitotic spindle and near the contractile ring during cytokinesis. Using spontaneously immortalized rat granulosa cells and costaining experiments with α-tubulin, they confirmed that phospho-mTOR^{Ser2448} is expressed at higher levels during mitosis relative to neighboring interphase cells and is highly enriched in the region of the mitotic spindle [141, 142].

In our hands, the phospho-mTOR^{Ser2448} showed enriched expression that correlated strongly and specifically with the mitotic status of cultured cancer cells [139]. However, although phospho-mTORSer2448 exhibited an adjacent pattern to condensed chromatin in the early stages of mitosis, which was particularly visible when the chromosomes arranged at the metaphase plate

and was comparable to that observed with phospho-mTOR^{Ser2481}, we failed to observe any tight localization of phospho-mTOR^{Ser2448} to the CCP-positive midbody region within the intracellular bridge during the late stages of mitosis and cytokinesis [139].

4.2.5 Mitotic Phospho-p70SK1

The best characterized downstream effectors of mTOR include two signaling pathways that act in parallel to control mRNA translation: the eukaryotic translation initiation factor 4E-BP1 (also known as the PHAS-I–eIF4E pathway) and the 70-kDa ribosomal protein S6 kinase 1 (p70S6K1 or S6K1) pathway. Interestingly, the phosphorylation status of the mTOR targets 4E-BP1 and S6K1 is enhanced specifically during mitosis. 4E-BP1 is hyperphosphorylated and inactivated during mitosis [142], which correlates with the lower cap-dependent translation that has been described at this stage. S6K1, which is a downstream effector of mTOR that is linked to the translation of ribosomal protein mRNAs, is subject to regulation by CDK1 in mitosis. Indeed, S6K1 activity is highest during G2/M, consistent with the elevated activity of mTORC1 during mitosis [143]. When the activity of CDK1 is high, S6K1 is phosphorylated at multiple Ser/Thr residues, including Ser371, Ser411, Thr421, and Ser424 [144]. Concomitant with this observation, the phosphorylation of the hydrophobic motif site, Thr389, is reduced, resulting in a decrease in the specific activity of S6K1. In vitro, CDK1–cyclin B, which is the universal cell cycle regulator, readily phosphorylates the mitotic phosphorylation sites of S6K1, which are sensitive to chemical inhibitors of CDK1 but not to inhibitors of mTOR.

During the mitotic phase, the presence of the active form of S6K1 (i.e., phospho-p70S6K1$^{Thr421/Ser424}$) as immunofluorescent signals in cultured human cells and formalin-fixed tissues of rats and mice has been observed [145]. Our own group has confirmed by high-resolution confocal microscopy that phospho-p70S6K1Thr421$^{/Ser424}$ exhibits a dynamic nuclear and cytoplasmic distribution in the M phase of the cell cycle from prophase to telophase and during cytokinesis (unpublished observations). Thus, S6K1, as the final effector of the AMPK–mTOR pathway, whose activity depends on growth factors and energy and nutritional status of the cell, appears to integrate these stimuli to regulate cell division by dynamically interacting with the mitotic apparatus.

Ribosomal S6 kinase 2 (S6K2), which is a predominantly nuclear protein that acts downstream of mTOR and whose maximal activation requires an optimal cytoplasmic-nuclear distribution or shuttling rate for mTOR [146, 147], has been found to localize at the centrosome throughout the cell cycle [148]. Notably, the centrosomal location of S6K2 is unaffected by serum withdrawal or by treatment with rapamycin, wortmannin, U0126, or phorbol-12-myristate-13-acetate (PMA). Unlike S6K2, S6K1 does not appear to localize at the centrosome, suggesting that the two kinases may also have non-overlapping functions.

These findings suggest that centrosomal S6K2 may have a role in the mTOR pathway, which has also been detected in the centrosome (e.g., TSC, phospho-AMPK, phospho-mTOR).

5 Corollary

Cell division involves a series of ordered and controlled events leading to cell proliferation. Cell cycle progression implies not only demanding amounts of cell mass protein, lipid, and nucleic acid content but also a favorable energy state. mTOR, in response to the cell's energy state, nutrient status, and growth factor stimulation, plays a pivotal role in the coordination of cell growth and cell cycle. Here, we reviewed how the nutrient-sensing mTOR signaling cascade molecularly integrates nutritional and mitogenic/anti-apoptotic cues to accurately coordinate cell growth and cell cycle. Beyond the best known ability of mTOR to control the G1-phase progression, we discussed how a growing list of phospho-active forms of proteins belonging to the AMPK–mTOR–S6K1 signaling axis resides at the mitotic and cytokinetic apparatus (Fig. 3). Future studies should elucidate the specific ability of the components of the mTOR-signaling pathway to spatially and temporally signal to or from the basic machinery of mitosis and cell abscission while connecting nutrient- and energy-sensing functions with cell structure and mitotic progression.

Acknowledgements

This work was supported financially by grants CP05-00090, PI06-0778, and RD06-0020-0028 from the Instituto de Salud Carlos III (Ministerio de Sanidad y Consumo, Fondo de Investigación Sanitaria (FIS), Spain; the Fundación Científica de la Asociación Española Contra el Cáncer (AECC, Spain); and the Ministerio de Ciencia e Innovación (SAF2009-11579 and SAF2012-389134, Plan Nacional de I + D + I, MICINN, Spain).

References

1. Malumbres M, Barbacid M (2009) Cell cycle, CDKs and cancer: a changing paradigm. Nat Rev Cancer 9(3):153–166
2. Weinberg RA (1995) The retinoblastoma protein and cell cycle control. Cell 81(3):323–330
3. Cobrinik D (2005) Pocket proteins and cell cycle control. Oncogene 24 (17):2796–2809
4. Sherr CJ, Roberts JM (1999) CDK inhibitors: positive and negative regulators of G1-phase progression. Genes Dev 13(12): 1501–1512
5. Barbash O, Diehl JA (2008) Regulation of the cell cycle. In: Mendelsohn J, Howley PM, Israel MA, Gray JW, Thompson CB (eds)

The molecular basis of cancer, 3rd edn. WB Saunders, Philadelphia, PA, pp 177–188

6. Massagué J (2004) G1 cell-cycle control and cancer. Nature 432(7015):298–306
7. Santoni-Rugiu E, Falck J, Mailand N, Bartek J, Lukas J (2000) Involvement of Myc activity in a G(1)/S-promoting mechanism parallel to the pRb/E2F pathway. Mol Cell Biol 20(10):3497–3509
8. Stark GR, Taylor WR (2006) Control of the G2/M transition. Mol Biotechnol 32(3): 227–248
9. Pyronnet S, Sonenberg N (2001) Cell-cycle-dependent translational control. Curr Opin Genet Dev 11(1):13–18
10. Pyronnet S, Dostie J, Sonenberg N (2001) Suppression of cap-dependent translation in mitosis. Genes Dev 15(16):2083–2093
11. Peters JM (2006) The anaphase promoting complex/cyclosome: a machine designed to destroy. Nat Rev Mol Cell Biol 7(9):644–656
12. Horn HF, Vousden KH (2007) Coping with stress: multiple ways to activate p53. Oncogene 26(9):1306–1316
13. Baus F, Gire V, Fisher D, Piette J, Dulić V (2003) Permanent cell cycle exit in G2 phase after DNA damage in normal human fibroblasts. EMBO J 22(15):3992–4002
14. Heitman J, Movva NR, Hall MN (1991) Targets for cell cycle arrest by the immunosuppressant rapamycin in yeast. Science 253(5022):905–909
15. Kunz J, Henriquez R, Schneider U, Deuter-Reinhard M, Movva NR, Hall MN (1993) Target of rapamycin in yeast, TOR2, is an essential phosphatidylinositol kinase homolog required for G1 progression. Cell 73(3):585–596
16. Brown EJ, Albers MW, Shin TB, Ichikawa K, Keith CT, Lane WS, Schreiber SL (1994) A mammalian protein targeted by G1-arresting rapamycin-receptor complex. Nature 369(6483):756–758
17. Sabatini DM, Erdjument-Bromage H, Lui M, Tempst P, Snyder SH (1994) RAFT1: a mammalian protein that binds to FKBP12 in a rapamycin-dependent fashion and is homologous to yeast TORs. Cell 78(1):35–43
18. Sabers CJ, Martin MM, Brunn GJ, Williams JM, Dumont FJ, Wiederrecht G, Abraham RT (1995) Isolation of a protein target of the FKBP12-rapamycin complex in mammalian cells. J Biol Chem 270(2):815–822
19. Sarbassov DD, Ali SM, Sengupta S, Sheen JH, Hsu PP, Bagley AF, Markhard AL, Sabatini DM (2006) Prolonged rapamycin treatment inhibits mTORC2 assembly and Akt/PKB. Mol Cell 22(2):159–168
20. Peterson TR, Laplante M, Thoreen CC, Sancak Y, Kang SA, Kuehl WM, Gray NS, Sabatini DM (2009) DEPTOR is an mTOR inhibitor frequently overexpressed in multiple myeloma cells and required for their survival. Cell 137(5):873–886
21. Kim DH, Sarbassov DD, Ali SM, Latek RR, Guntur KV, Erdjument-Bromage H, Tempst P, Sabatini DM (2003) GbetaL, a positive regulator of the rapamycin-sensitive pathway required for the nutrient-sensitive interaction between raptor and mTOR. Mol Cell 11(4): 895–904
22. Kaizuka T, Hara T, Oshiro N, Kikkawa U, Yonezawa K, Takehana K, Iemura S, Natsume T, Mizushima N (2010) Tti1 and Tel2 are critical factors in mammalian target of rapamycin complex assembly. J Biol Chem 285(26): 20109–20116
23. Kim SG, Hoffman GR, Poulogiannis G, Buel GR, Jang YJ, Lee KW, Kim BY, Erikson RL, Cantley LC, Choo AY, Blenis J (2013) Metabolic stress controls mTORC1 lysosomal localization and dimerization by regulating the TTT-RUVBL1/2 complex. Mol Cell 49(1):172–185
24. Guertin DA, Stevens DM, Thoreen CC, Burds AA, Kalaany NY, Moffat J, Brown M, Fitzgerald KJ, Sabatini DM (2006) Ablation in mice of the mTORC components raptor, rictor, or mLST8 reveals that mTORC2 is required for signaling to Akt-FOXO and PKCalpha, but not S6K1. Dev Cell 11(6): 859–871
25. Kim DH, Sarbassov DD, Ali SM, King JE, Latek RR, Erdjument-Bromage H, Tempst P, Sabatini DM (2002) mTOR interacts with raptor to form a nutrient-sensitive complex that signals to the cell growth machinery. Cell 110(2):163–175
26. Hara K, Maruki Y, Long X, Yoshino K, Oshiro N, Hidayat S, Tokunaga C, Avruch J, Yonezawa K (2002) Raptor, a binding partner of target of rapamycin (TOR), mediates TOR action. Cell 110(2):177–189
27. Thedieck K, Polak P, Kim ML, Molle KD, Cohen A, Jenö P, Arrieumerlou C, Hall MN (2007) PRAS40 and PRR5-like protein are new mTOR interactors that regulate apoptosis. PLoS One 2(11):e1217
28. Sancak Y, Thoreen CC, Peterson TR, Lindquist RA, Kang SA, Spooner E, Carr SA, Sabatini DM (2007) PRAS40 is an insulin-regulated inhibitor of the mTORC1 protein kinase. Mol Cell 25(6):903–915

29. Jacinto E, Loewith R, Schmidt A, Lin S, Rüegg MA, Hall A, Hall MN (2004) Mammalian TOR complex 2 controls the actin cytoskeleton and is rapamycin insensitive. Nat Cell Biol 6(11):1122–1128
30. Sarbassov DD, Ali SM, Kim DH, Guertin DA, Latek RR, Erdjument-Bromage H, Tempst P, Sabatini DM (2004) Rictor, a novel binding partner of mTOR, defines a rapamycin-insensitive and raptor-independent pathway that regulates the cytoskeleton. Curr Biol 14(14):1296–1302
31. Yang Q, Inoki K, Ikenoue T, Guan KL (2006) Identification of Sin1 as an essential TORC2 component required for complex formation and kinase activity. Genes Dev 20(20): 2820–2832
32. Jacinto E, Facchinetti V, Liu D, Soto N, Wei S, Jung SY, Huang Q, Qin J, Su B (2006) SIN1/MIP1 maintains rictor-mTOR complex integrity and regulates Akt phosphorylation and substrate specificity. Cell 127(1):125–137
33. Frias MA, Thoreen CC, Jaffe JD, Schroder W, Sculley T, Carr SA, Sabatini DM (2006) mSin1 is necessary for Akt/PKB phosphorylation, and its isoforms define three distinct mTORC2s. Curr Biol 16(18):1865–1870
34. Pearce LR, Huang X, Boudeau J, Pawłowski R, Wullschleger S, Deak M, Ibrahim AF, Gourlay R, Magnuson MA, Alessi DR (2007) Identification of Protor as a novel Rictor-binding component of mTOR complex-2. Biochem J 405(3):513–522
35. Woo SY, Kim DH, Jun CB, Kim YM, Haar EV, Lee SI, Hegg JW, Bandhakavi S, Griffin TJ (2007) PRR5, a novel component of mTOR complex 2, regulates platelet-derived growth factor receptor beta expression and signaling. J Biol Chem 282(35):25604–25612
36. Vander Haar E, Lee SI, Bandhakavi S, Griffin TJ, Kim DH (2007) Insulin signalling to mTOR mediated by the Akt/PKB substrate PRAS40. Nat Cell Biol 9(3):316–323
37. Sancak Y, Peterson TR, Shaul YD, Lindquist RA, Thoreen CC, Bar-Peled L, Sabatini DM (2008) The Rag GTPases bind raptor and mediate amino acid signaling to mTORC1. Science 320(5882):1496–1501
38. Dunlop EA, Dodd KM, Seymour LA, Tee AR (2009) Mammalian target of rapamycin complex 1-mediated phosphorylation of eukaryotic initiation factor 4E-binding protein 1 requires multiple protein-protein interactions for substrate recognition. Cell Signal 21(7): 1073–1084
39. Tee AR, Manning BD, Roux PP, Cantley LC, Blenis J (2003) Tuberous sclerosis complex gene products, Tuberin and Hamartin, control mTOR signaling by acting as a GTPase-activating protein complex toward Rheb. Curr Biol 13(15):1259–1268
40. Dibble CC, Elis W, Menon S, Qin W, Klekota J, Asara JM, Finan PM, Kwiatkowski DJ, Murphy LO, Manning BD (2012) TBC1D7 is a third subunit of the TSC1-TSC2 complex upstream of mTORC1. Mol Cell 47(4): 535–546
41. Inoki K, Li Y, Xu T, Guan KL (2003) Rheb GTPase is a direct target of TSC2 GAP activity and regulates mTOR signaling. Genes Dev 17(15):1829–1834
42. Inoki K, Li Y, Zhu T, Wu J, Guan KL (2002) TSC2 is phosphorylated and inhibited by Akt and suppresses mTOR signalling. Nat Cell Biol 4(9):648–657
43. Manning BD, Tee AR, Logsdon MN, Blenis J, Cantley LC (2002) Identification of the tuberous sclerosis complex-2 tumor suppressor gene product tuberin as a target of the phosphoinositide 3-kinase/akt pathway. Mol Cell 10(1):151–162
44. Huang J, Manning BD (2009) A complex interplay between Akt, TSC2 and the two mTOR complexes. Biochem Soc Trans 37 (Pt 1):217–222
45. Dibble CC, Asara JM, Manning BD (2009) Characterization of Rictor phosphorylation sites reveals direct regulation of mTOR complex 2 by S6K1. Mol Cell Biol 29(21): 5657–5670
46. Hsu PP, Kang SA, Rameseder J, Zhang Y, Ottina KA, Lim D, Peterson TR, Choi Y, Gray NS, Yaffe MB, Marto JA, Sabatini DM (2011) The mTOR-regulated phosphoproteome reveals a mechanism of mTORC1-mediated inhibition of growth factor signaling. Science 332(6035):1317–1322
47. Ma L, Chen Z, Erdjument-Bromage H, Tempst P, Pandolfi PP (2005) Phosphorylation and functional inactivation of TSC2 by Erk implications for tuberous sclerosis and cancer pathogenesis. Cell 121(2):179–193
48. Roux PP, Shahbazian D, Vu H, Holz MK, Cohen MS, Taunton J, Sonenberg N, Blenis J (2007) RAS/ERK signaling promotes site-specific ribosomal protein S6 phosphorylation via RSK and stimulates cap-dependent translation. J Biol Chem 282(19):14056–14064
49. Hardie DG, Ross FA, Hawley SA (2012) AMPK: a nutrient and energy sensor that maintains energy homeostasis. Nat Rev Mol Cell Biol 13(4):251–262
50. Shaw RJ, Kosmatka M, Bardeesy N, Hurley RL, Witters LA, DePinho RA, Cantley LC (2004) The tumor suppressor LKB1 kinase

directly activates AMP-activated kinase and regulates apoptosis in response to energy stress. Proc Natl Acad Sci U S A 101(10): 3329–3335

51. Inoki K, Zhu T, Guan KL (2003) TSC2 mediates cellular energy response to control cell growth and survival. Cell 115(5): 577–590
52. Gwinn DM, Shackelford DB, Egan DF, Mihaylova MM, Mery A, Vasquez DS, Turk BE, Shaw RJ (2008) AMPK phosphorylation of raptor mediates a metabolic checkpoint. Mol Cell 30(2):214–226
53. Hardie DG (2008) AMPK and Raptor: matching cell growth to energy supply. Mol Cell 30(3):263–265
54. Inoki K, Ouyang H, Zhu T, Lindvall C, Wang Y, Zhang X, Yang Q, Bennett C, Harada Y, Stankunas K, Wang CY, He X, MacDougald OA, You M, Williams BO, Guan KL (2006) TSC2 integrates Wnt and energy signals via a coordinated phosphorylation by AMPK and GSK3 to regulate cell growth. Cell 126(5): 955–968
55. Nicklin P, Bergman P, Zhang B, Triantafellow E, Wang H, Nyfeler B, Yang H, Hild M, Kung C, Wilson C, Myer VE, MacKeigan JP, Porter JA, Wang YK, Cantley LC, Finan PM, Murphy LO (2009) Bidirectional transport of amino acids regulates mTOR and autophagy. Cell 136(3):521–534
56. Smith EM, Finn SG, Tee AR, Browne GJ, Proud CG (2005) The tuberous sclerosis protein TSC2 is not required for the regulation of the mammalian target of rapamycin by amino acids and certain cellular stresses. J Biol Chem 280(19):18717–18727
57. Kim E, Goraksha-Hicks P, Li L, Neufeld TP, Guan KL (2008) Regulation of TORC1 by Rag GTPases in nutrient response. Nat Cell Biol 10(8):935–945
58. Sancak Y, Bar-Peled L, Zoncu R, Markhard AL, Nada S, Sabatini DM (2010) Ragulator-Rag complex targets mTORC1 to the lysosomal surface and is necessary for its activation by amino acids. Cell 141(2):290–303
59. Zoncu R, Bar-Peled L, Efeyan A, Wang S, Sancak Y, Sabatini DM (2011) mTORC1 senses lysosomal amino acids through an inside-out mechanism that requires the vacuolar H(+)-ATPase. Science 334(6056): 678–683
60. Han JM, Jeong SJ, Park MC, Kim G, Kwon NH, Kim HK, Ha SH, Ryu SH, Kim S (2012) Leucyl-tRNA synthetase is an intracellular leucine sensor for the mTORC1-signaling pathway. Cell 149(2):410–424
61. Jewell JL, Guan KL (2013) Nutrient signaling to mTOR and cell growth. Trends Biochem Sci 38(5):233–242
62. Kim SG, Buel GR, Blenis J (2013) Nutrient regulation of the mTOR Complex 1 signaling pathway. Mol Cells 35(6):463–473
63. Brugarolas J, Lei K, Hurley RL, Manning BD, Reiling JH, Hafen E, Witters LA, Ellisen LW, Kaelin WG (2004) Regulation of mTOR function in response to hypoxia by REDD1 and the TSC1/TSC2 tumor suppressor complex. Genes Dev 18(23):2893–2904
64. Sofer A, Lei K, Johannessen CM, Ellisen LW (2005) Regulation of mTOR and cell growth in response to energy stress by REDD1. Mol Cell Biol 25(14):5834–5845
65. DeYoung MP, Horak P, Sofer A, Sgroi D, Ellisen LW (2008) Hypoxia regulates TSC1/2-mTOR signaling and tumor suppression through REDD1-mediated 14-3-3 shuttling. Genes Dev 22(2):239–251
66. Budanov AV, Karin M (2008) p53 target genes sestrin1 and sestrin2 connect genotoxic stress and mTOR signaling. Cell 134(3):451–460
67. Feng Z, Zhang H, Levine AJ, Jin S (2005) The coordinate regulation of the p53 and mTOR pathways in cells. Proc Natl Acad Sci U S A 102(23):8204–8209
68. Lee DF, Hung MC (2007) All roads lead to mTOR: integrating inflammation and tumor angiogenesis. Cell Cycle 6(24):3011–3014
69. Foster DA (2009) Phosphatidic acid signaling to mTOR: signals for the survival of human cancer cells. Biochim Biophys Acta 1791(9):949–955
70. Laplante M, Sabatini DM (2012) mTOR signaling in growth control and disease. Cell 149(2):274–293
71. Ma XM, Blenis J (2009) Molecular mechanisms of mTOR-mediated translational control. Nat Rev Mol Cell Biol 10(5):307–318
72. Mayer C, Zhao J, Yuan X, Grummt I (2004) mTOR-dependent activation of the transcription factor TIF-IA links rRNA synthesis to nutrient availability. Genes Dev 18(4):423–434
73. Kantidakis T, Ramsbottom BA, Birch JL, Dowding SN, White RJ (2010) mTOR associates with TFIIIC, is found at tRNA and 5S rRNA genes, and targets their repressor Maf1. Proc Natl Acad Sci U S A 107(26): 11823–11828
74. Porstmann T, Santos CR, Griffiths B, Cully M, Wu M, Leevers S, Griffiths JR, Chung YL, Schulze A (2008) SREBP activity is regulated by mTORC1 and contributes to Akt-

dependent cell growth. Cell Metab 8(3): 224–236

75. Düvel K, Yecies JL, Menon S, Raman P, Lipovsky AI, Souza AL, Triantafellow E, Ma Q, Gorski R, Cleaver S, Vander Heiden MG, MacKeigan JP, Finan PM, Clish CB, Murphy LO, Manning BD (2010) Activation of a metabolic gene regulatory network downstream of mTOR complex 1. Mol Cell 39(2): 171–183
76. Peterson TR, Sengupta SS, Harris TE, Carmack AE, Kang SA, Balderas E, Guertin DA, Madden KL, Carpenter AE, Finck BN, Sabatini DM (2011) mTOR complex 1 regulates lipin 1 localization to control the SREBP pathway. Cell 146(3):408–420
77. Kim JE, Chen J (2004) Regulation of peroxisome proliferator-activated receptor-gamma activity by mammalian target of rapamycin and amino acids in adipogenesis. Diabetes 53(11):2748–2756
78. Laplante M, Sabatini DM (2009) An emerging role of mTOR in lipid biosynthesis. Curr Biol 19(22):R1046–R1052
79. Schieke SM, Phillips D, McCoy JP, Aponte AM, Shen RF, Balaban RS, Finkel T (2006) The mammalian target of rapamycin (mTOR) pathway regulates mitochondrial oxygen consumption and oxidative capacity. J Biol Chem 281(37):27643–27652
80. Cunningham JT, Rodgers JT, Arlow DH, Vazquez F, Mootha VK, Puigserver P (2007) mTOR controls mitochondrial oxidative function through a YY1-PGC-1[agr] transcriptional complex. Nature 450(7170):736–740
81. Ramanathan A, Schreiber SL (2009) Direct control of mitochondrial function by mTOR. Proc Natl Acad Sci U S A 106(52): 22229–22232
82. Ganley IG, Lam DH, Wang J, Ding X, Chen S, Jiang X (2009) ULK1.ATG13.FIP200 complex mediates mTOR signaling and is essential for autophagy. J Biol Chem 284(18): 12297–12305
83. Jung CH, Ro SH, Cao J, Otto NM, Kim DH (2010) mTOR regulation of autophagy. FEBS Lett 584(7):1287–1295
84. Koren I, Reem E, Kimchi A (2010) DAP1, a novel substrate of mTOR, negatively regulates autophagy. Curr Biol 20(12):1093–1098
85. Koren I, Reem E, Kimchi A (2010) Autophagy gets a brake: DAP1, a novel mTOR substrate, is activated to suppress the autophagic process. Autophagy 6(8):1179–1180
86. Oh WJ, Jacinto E (2011) mTOR complex 2 signaling and functions. Cell Cycle 10(14): 2305–2316
87. García-Martínez JM, Alessi DR (2008) mTOR complex 2 (mTORC2) controls hydrophobic motif phosphorylation and activation of serum- and glucocorticoid-induced protein kinase 1 (SGK1). Biochem J 416(3):375–385
88. Zinzalla V, Stracka D, Oppliger W, Hall MN (2011) Activation of mTORC2 by association with the ribosome. Cell 144(5):757–768
89. Huang J, Dibble CC, Matsuzaki M, Manning BD (2008) The TSC1-TSC2 complex is required for proper activation of mTOR complex 2. Mol Cell Biol 28(12):4104–4115
90. Copp J, Manning G, Hunter T (2009) TORC-specific phosphorylation of mammalian target of rapamycin (mTOR): phospho-Ser2481 is a marker for intact mTOR signaling complex 2. Cancer Res 69(5):1821–1827
91. Sarbassov DD, Guertin DA, Ali SM, Sabatini DM (2005) Phosphorylation and regulation of Akt/PKB by the rictor-mTOR complex. Science 307(5712):1098–1101
92. Hagiwara A, Cornu M, Cybulski N, Polak P, Betz C, Trapani F, Terracciano L, Heim MH, Rüegg MA, Hall MN (2012) Hepatic mTORC2 activates glycolysis and lipogenesis through Akt, glucokinase, and SREBP1c. Cell Metab 15(5):725–738
93. Yuan M, Pino E, Wu L, Kacergis M, Soukas AA (2012) Identification of Akt-independent regulation of hepatic lipogenesis by mammalian target of rapamycin (mTOR) complex 2. J Biol Chem 287(35):29579–29588
94. Lamming DW, Sabatini DM (2013) A Central role for mTOR in lipid homeostasis. Cell Metab 18(4):465–469
95. Blagosklonny MV (2011) Cell cycle arrest is not senescence. Aging (Albany NY) 3(2): 94–101
96. Foster DA, Yellen P, Xu L, Saqcena M (2010) Regulation of G1 cell cycle progression: distinguishing the restriction point from a nutrient-sensing cell growth checkpoint(s). Genes Cancer 1(11):1123–1131
97. Saqcena M, Menon D, Patel D, Mukhopadhyay S, Chow V, Foster DA (2013) Amino acids and mTOR mediate distinct metabolic checkpoints in mammalian G1 cell cycle. PLoS One 8(8):e74157
98. Fingar DC, Richardson CJ, Tee AR, Cheatham L, Tsou C, Blenis J (2004) mTOR controls cell cycle progression through its cell growth effectors S6K1 and 4E-BP1/eukaryotic translation initiation factor 4E. Mol Cell Biol 24(1):200–216
99. Averous J, Fonseca BD, Proud CG (2008) Regulation of cyclin D1 expression by mTORC1 signaling requires eukaryotic

initiation factor 4E-binding protein 1. Oncogene 27(8):1106–1113

100. Balcazar N, Sathyamurthy A, Elghazi L, Gould A, Weiss A, Shiojima I, Walsh K, Bernal-Mizrachi E (2009) mTORC1 activation regulates beta-cell mass and proliferation by modulation of cyclin D2 synthesis and stability. J Biol Chem 284(12):7832–7842
101. Dowling RJ, Topisirovic I, Alain T, Bidinosti M, Fonseca BD, Petroulakis E, Wang X, Larsson O, Selvaraj A, Liu Y, Kozma SC, Thomas G, Sonenberg N (2010) mTORC1-mediated cell proliferation, but not cell growth, controlled by the 4E-BPs. Science 328(5982):1172–1176
102. Hong F, Larrea MD, Doughty C, Kwiatkowski DJ, Squillace R, Slingerland JM (2008) mTOR-raptor binds and activates SGK1 to regulate p27 phosphorylation. Mol Cell 30(6):701–711
103. Medema RH, Kops GJ, Bos JL, Burgering BM (2000) AFX-like Forkhead transcription factors mediate cell-cycle regulation by Ras and PKB through p27kip1. Nature 404(6779):782–787
104. Vadlakonda L, Pasupuleti M, Pallu R (2013) Role of PI3K-AKT-mTOR and Wnt Signaling Pathways in Transition of G1-S Phase of Cell Cycle in Cancer Cells. Front Oncol 3:85
105. Feng Z, Hu W, de Stanchina E, Teresky AK, Jin S, Lowe S, Levine AJ (2007) The regulation of AMPK beta1, TSC2, and PTEN expression by p53: stress, cell and tissue specificity, and the role of these gene products in modulating the IGF-1-AKT-mTOR pathways. Cancer Res 67(7):3043–3053
106. Levine AJ, Feng Z, Mak TW, You H, Jin S (2006) Coordination and communication between the p53 and IGF-1-AKT-TOR signal transduction pathways. Genes Dev 20(3): 267–275
107. Lee CH, Inoki K, Karbowniczek M, Petroulakis E, Sonenberg N, Henske EP, Guan KL (2007) Constitutive mTOR activation in TSC mutants sensitizes cells to energy starvation and genomic damage via p53. EMBO J 26(23):4812–4823
108. Brenman JE (2007) AMPK/LKB1 signaling in epithelial cell polarity and cell division. Cell Cycle 6(22):2755–2759
109. Koh H, Chung J (2007) AMPK links energy status to cell structure and mitosis. Biochem Biophys Res Commun 362(4):789–792
110. Williams T, Brenman JE (2008) LKB1 and AMPK in cell polarity and division. Trends Cell Biol 18(4):193–198
111. Bettencourt-Dias M, Giet R, Sinka R, Mazumdar A, Lock WG, Balloux F, Zafiropoulos PJ, Yamaguchi S, Winter S, Carthew RW, Cooper M, Jones D, Frenz L, Glover DM (2004) Genome-wide survey of protein kinases required for cell cycle progression. Nature 432(7020):980–987
112. Lee JH, Koh H, Kim M, Kim Y, Lee SY, Karess RE, Lee SH, Shong M, Kim JM, Kim J, Chung J (2007) Energy-dependent regulation of cell structure by AMP-activated protein kinase. Nature 447(7147):1017–1020
113. Oliveras-Ferraros C, Vazquez-Martin A, Menendez JA (2009) Genome-wide inhibitory impact of the AMPK activator metformin on [kinesins, tubulins, histones, auroras and polo-like kinases] M-phase cell cycle genes in human breast cancer cells. Cell Cycle 8(10): 1633–1636
114. Vazquez-Martin A, Oliveras-Ferraros C, Lopez-Bonet E, Menendez JA (2009) AMPK: Evidence for an energy-sensing cytokinetic tumor suppressor. Cell Cycle 8(22):3679–3683
115. Vazquez-Martin A, López-Bonet E, Oliveras-Ferraros C, Pérez-Martínez MC, Bernadó L, Menendez JA (2009) Mitotic kinase dynamics of the active form of AMPK (phospho-AMPKalphaThr172) in human cancer cells. Cell Cycle 8(5):788–791
116. Vazquez-Martin A, Oliveras-Ferraros C, Menendez JA (2009) The active form of the metabolic sensor: AMP-activated protein kinase (AMPK) directly binds the mitotic apparatus and travels from centrosomes to the spindle midzone during mitosis and cytokinesis. Cell Cycle 8(15):2385–2398
117. Pinter K, Jefferson A, Czibik G, Watkins H, Redwood C (2012) Subunit composition of AMPK trimers present in the cytokinetic apparatus: implications for drug target identification. Cell Cycle 11(5):917–921
118. Menendez JA, Vazquez-Martin A (2012) AMPK: a bona fide resident of the mitotic spindle midzone. Cell Cycle 11(5):841–842
119. Banko MR, Allen JJ, Schaffer BE, Wilker EW, Tsou P, White JL, Villén J, Wang B, Kim SR, Sakamoto K, Gygi SP, Cantley LC, Yaffe MB, Shokat KM, Brunet A (2011) Chemical genetic screen for AMPKα2 substrates uncovers a network of proteins involved in mitosis. Mol Cell 44(6):878–892
120. Robitaille AM, Hall MN (2012) Ramping up mitosis: an AMPKα2-regulated signaling network promotes mitotic progression. Mol Cell 45(1):8–9
121. Thaiparambil JT, Eggers CM, Marcus AI (2012) AMPK regulates mitotic spindle orientation through phosphorylation of myosin regulatory light chain. Mol Cell Biol 32(16):3203–3217

122. Vazquez-Martin A, Cufí S, Oliveras-Ferraros C, Menendez JA (2012) Polo-like kinase 1 directs the AMPK-mediated activation of myosin regulatory light chain at the cytokinetic cleavage furrow independently of energy balance. Cell Cycle 11(13):2422–2426
123. Rafalski VA, Mancini E, Brunet A (2012) Energy metabolism and energy-sensing pathways in mammalian embryonic and adult stem cell fate. J Cell Sci 125(Pt23):5597–5608
124. Mao L, Li N, Guo Y, Xu X, Gao L, Xu Y, Zhou L, Liu W (2013) AMPK phosphorylates GBF1 for mitotic Golgi disassembly. J Cell Sci 126(Pt 6):1498–1505
125. Vazquez-Martin A, Corominas-Faja B, Oliveras-Ferraros C, Cufí S, Dalla Venezia N, Menendez JA (2013) Serine79-phosphorylated acetyl-CoA carboxylase, a downstream target of AMPK, localizes to the mitotic spindle poles and the cytokinesis furrow. Cell Cycle 12(10):1639–1641
126. Ito N, Rubin GM (1999) gigas, a Drosophila homolog of tuberous sclerosis gene product-2, regulates the cell cycle. Cell 96(4):529–539
127. Tapon N, Ito N, Dickson BJ, Treisman JE, Hariharan IK (2001) The Drosophila tuberous sclerosis complex gene homologs restrict cell growth and cell proliferation. Cell 105(3):345–355
128. Catania MG, Mischel PS, Vinters HV (2001) Hamartin and tuberin interaction with the G2/M cyclin-dependent kinase CDK1 and its regulatory cyclins A and B. J Neuropathol Exp Neurol 60(7):711–723
129. Astrinidis A, Senapedis W, Coleman TR, Henske EP (2003) Cell cycle-regulated phosphorylation of hamartin, the product of the tuberous sclerosis complex 1 gene, by cyclin-dependent kinase 1/cyclin B. J Biol Chem 278(51):51372–51379
130. Astrinidis A, Senapedis W, Henske EP (2006) Hamartin, the tuberous sclerosis complex 1 gene product, interacts with polo-like kinase 1 in a phosphorylation-dependent manner. Hum Mol Genet 15(2):287–297
131. Schneider L, Essmann F, Kletke A, Rio P, Hanenberg H, Wetzel W, Schulze-Osthoff K, Nürnberg B, Piekorz RP (2007) The transforming acidic coiled coil 3 protein is essential for spindle-dependent chromosome alignment and mitotic survival. J Biol Chem 282(40):29273–29283
132. Gómez-Baldó L, Schmidt S, Maxwell CA, Bonifaci N, Gabaldón T, Vidalain PO, Senapedis W, Kletke A, Rosing M, Barnekow A, Rottapel R, Capellá G, Vidal M, Astrinidis A, Piekorz RP, Pujana MA (2010) TACC3-TSC2 maintains nuclear envelope structure and controls cell division. Cell Cycle 9(6):1143–1155
133. Ramírez-Valle F, Badura ML, Braunstein S, Narasimhan M, Schneider RJ (2010) Mitotic raptor promotes mTORC1 activity, G(2)/M cell cycle progression, and internal ribosome entry site-mediated mRNA translation. Mol Cell Biol 30(13):3151–3164
134. Gwinn DM, Asara JM, Shaw RJ (2010) Raptor is phosphorylated by cdc2 during mitosis. PLoS One 5(2):e9197
135. Vazquez-Martin A, Cufí S, Oliveras-Ferraros C, Menendez JA (2011) Raptor, a positive regulatory subunit of mTOR complex 1, is a novel phosphoprotein of the rDNA transcription machinery in nucleoli and chromosomal nucleolus organizer regions (NORs). Cell Cycle 10(18):3140–3152
136. Bachmann RA, Kim JH, Wu AL, Park IH, Chen J (2006) A nuclear transport signal in mammalian target of rapamycin is critical for its cytoplasmic signaling to S6 kinase 1. J Biol Chem 281(11):7357–7363
137. Vazquez-Martin A, Oliveras-Ferraros C, Bernadó L, López-Bonet E, Menendez JA (2009) The serine 2481-autophosphorylated form of mammalian Target Of Rapamycin (mTOR) is localized to midzone and midbody in dividing cancer cells. Biochem Biophys Res Commun 380(3):638–643
138. Lopez-Bonet E, Vazquez-Martin A, Pérez-Martínez MC, Oliveras-Ferraros C, Pérez-Bueno F, Bernadó L, Menendez JA (2010) Serine 2481-autophosphorylation of mammalian target of rapamycin (mTOR) couples with chromosome condensation and segregation during mitosis: confocal microscopy characterization and immunohistochemical validation of PP-mTOR(Ser2481) as a novel high-contrast mitosis marker in breast cancer core biopsies. Int J Oncol 36(1):107–115
139. Vazquez-Martin A, Sauri-Nadal T, Menendez OJ, Oliveras-Ferraros C, Cufí S, Corominas-Faja B, López-Bonet E, Menendez JA (2012) Ser2481-autophosphorylated mTOR colocalizes with chromosomal passenger proteins during mammalian cell cytokinesis. Cell Cycle 11(22):4211–4221
140. Yaba A, Bianchi V, Borini A, Johnson J (2008) A putative mitotic checkpoint dependent on mTOR function control cell proliferation and survival in ovarian granulosa cells. Reprod Sci 15(2):128–138

141. Yu J, Yaba A, Kasiman C, Thomson T, Johnson J (2011) mTOR controls ovarian follicle growth by regulating granulosa cell proliferation. PLoS One 6(7):e21415
142. Heesom KJ, Gampel A, Mellor H, Denton RM (2001) Cell cycle-dependent phosphorylation of the translational repressor eIF-4E binding protein-1 (4E-BP1). Curr Biol 11(17):1374–1379
143. Boyer D, Quintanilla R, Lee-Fruman KK (2008) Regulation of catalytic activity of S6 kinase 2 during cell cycle. Mol Cell Biochem 307(1–2):59–64
144. Shah OJ, Ghosh S, Hunter T (2003) Mitotic regulation of ribosomal S6 kinase 1 involves Ser/Thr, Pro phosphorylation of consensus and non-consensus sites by Cdc2. J Biol Chem 278(18):16433–16442
145. Schmidt T, Wahl P, Wüthrich RP, Vogetseder A, Picard N, Kaissling B, Le Hir M (2007) Immunolocalization of phospho-S6 kinases: a new way to detect mitosis in tissue sections and in cell culture. Histochem Cell Biol 127(2):123–129
146. Park IH, Bachmann R, Shirazi H, Chen J (2002) Regulation of ribosomal S6 kinase 2 by mammalian target of rapamycin. J Biol Chem 277(35):31423–31429
147. Filonenko VV, Tytarenko R, Azatjan SK, Savinska LO, Gaydar YA, Gout IT, Usenko VS, Lyzogubov VV (2004) Immuno-histochemical analysis of S6K1 and S6K2 localization in human breast tumors. Exp Oncol 26(4):294–299
148. Rossi R, Pester JM, McDowell M, Soza S, Montecucco A, Lee-Fruman KK (2007) Identification of S6K2 as a centrosome-located kinase. FEBS Lett 581(21):4058–4064
149. Fingar DC, Salama S, Tsou C, Harlow E, Blenis J (2002) Mammalian cell size is controlled by mTOR and its downstream targets S6K1 and 4EBP1/eIF4E. Genes Dev 16(12): 1472–1487

Chapter 8

The Senescence Arrest Program and the Cell Cycle

Alessandro Bitto, Elizabeth P. Crowe, Chad Lerner, Claudio Torres, and Christian Sell

Abstract

All living organisms are subject to progressive loss of function and damage to their tissues, a process known as aging. At the cellular level, the accumulation of damage to DNA, proteins, and organelles induces cellular senescence, a stress-response pathway that likely influences the aging process. Although the senescence arrest program was initially described in vitro, accumulating evidence suggests that this damage response program occurs in a variety of pathologic settings. This review discusses aspects of the senescence program, their interrelationships with damage arrest pathways, the cell cycle, and the impact of senescence in vivo.

Key words Aging, Senescence, DNA damage, Cell cycle, Chromatin, SAHF, SASP, Stress, ROS

1 Introduction

Cellular senescence is a stress response activated by mammalian cells upon exposure to several insults, such as oxidative stress, genotoxic stress, telomere attrition, or dysregulated mitogenic signaling [1, 2]. These stresses activate the senescence response by triggering two pathways: the p53/p21$^{CIP1/WAF1}$ and the p16^{INK4A}/Rb pathway, which are required to establish and maintain the senescence response [3, 4]. Senescence-inducing stimuli can cause DNA damage and trigger a sustained DNA damage response (DDR). In response to sustained, unresolved DNA damage, the ataxia telangiectasia-mutated (ATM) kinase activates p53 and its transcriptional target p21$^{CIP1/WAF1}$, which arrests cellular proliferation by inhibiting cell cycle-dependent kinases [4]. In addition, the same senescence-inducing stimuli can trigger the activation of the stress-activated protein kinase p38 MAPK independently of DNA damage [5]. p38 MAPK then can promote the arrest of the cell cycle and establish senescence by activating the transcription factor HBP1, which increases the expression of p16^{INK4A} [6]. These two pathways seem to establish senescence with different kinetics: the DDR pathway usually mediates the initial arrest by increasing

Eishi Noguchi and Mariana C. Gadaleta (eds.), *Cell Cycle Control: Mechanisms and Protocols*, Methods in Molecular Biology, vol. 1170, DOI 10.1007/978-1-4939-0888-2_8,

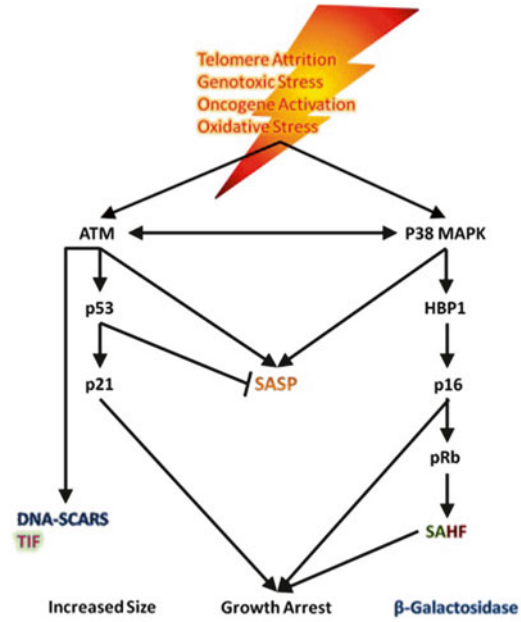

Fig. 1 Signaling pathways and phenotypical characteristics of cellular senescence

the levels of $p21^{CIP1/WAF1}$, and only at later times senescence is reinforced by expression of $p16^{INK4A}$ [3, 7]. Furthermore, the p53 and the p38 MAPK pathways appear to be mostly independent of one another and are thus redundant [8, 9], even though cross talk between them has been postulated [1] (Fig. 1).

2 Cellular Senescence

The senescence transition is characterized by several morphological and cellular changes in vitro. The initiating event is an arrest in proliferation [10] and in cell cycle progression which is triggered by an increased expression of $p21^{CIP1/WAF1}$ and $p16^{INK4A}$ [3]. Subsequent changes include increased cell size [11], increased activity of the lysosomal senescence-associated β-galactosidase (SA-β-Gal) activity [12], persistent DDR signaling foci (DNA segments with chromatin alterations reinforcing senescence, or DNA-SCARS, and telomere dysfunction-induced foci, or TIF) [4, 13, 14], chromatin rearrangements and formation of senescence-associated heterochromatin foci (SAHF) [15], increased activation of p38 mitogen-activated protein kinase (MAPK) [5, 16], loss of lamin B1 [17], and finally secretion of several cytokines, growth factors, and proteases (senescence-associated secretory phenotype, or SASP) [18, 19]. The interrelationships between these events are slowly being unraveled, and it seems that most aspects of the

senescent phenotype are under control of either senescence-establishing pathway: TIFs, DNA-SCARS, and other DNA damage foci are in fact associated with the DDR-p53/p21$^{CIP1/WAF1}$ pathway [4, 13, 14], while heterochromatin reorganization appears to be dependent on p16^{INK4A} and Rb [20]. Conversely, both pathways regulate many aspects of the SASP [9, 21], even though p38 MAPK is dispensable for the expression of matrix metallo-proteases (MMPs) [9]. Although induced by both senescence-establishing pathways, the SASP is not influenced by the effectors of the senescence arrest, p53/p21$^{CIP1/WAF1}$ and p16^{INK4A}/Rb [21, 22], and is actually induced by nuclear factor κ B (NFκB) [9], suggesting that the senescence arrest and the secretory phenotype are two separate and independent features of cellular senescence. Since cellular senescence can be established by either the p53 or the p38 MAPK pathway independently, none of the aforementioned markers of senescence is specific for all senescent cells, and senescent cells do not necessarily express all of these markers [2]. Thus, cellular senescence is usually assessed by the presence of two or more of these features in the same population of cells.

Cellular senescence has been conceptually linked to the aging process since its discovery in 1961 [10, 11, 23]. In fact, primary human cells divide only a limited number of times before going into senescence in vitro, a feature that was thought to recapitulate the aging of the whole organism and was thus termed "replicative senescence" [11]. In human cells, a major determinant of this limited proliferative potential is the continuous shortening with each round of replication of telomeres, the repeating sequences at the end of linear chromosomes [24]. When telomeres are shortened to a critical length, they are sensed as irreparable damage to the DNA and trigger senescence through the DDR/p53/p21$^{CIP1/WAF1}$ pathway [4]. In fact, replicative senescence can be bypassed by inducing the expression of telomerase, an enzyme that extends telomeres and allows human cells to proliferate indefinitely without tumorigenic transformation [25], suggesting a direct correlation between telomere length and aging. Conversely, mouse fibroblasts, which continuously express the telomerase enzyme, enter cellular senescence independently of their telomere length but because of accumulating damage to genomic DNA caused by oxidative stress [26]. It has been reported that telomere length correlates with the age of donor in human skin biopsies [27], increased telomere loss is associated with cellular senescence in fibroblasts derived from patients affected by Hutchinson–Gilford progeria syndrome [28], and senescence induced by progeroid-mutant lamin A can be delayed by ectopic expression of telomerase [29]. Nevertheless, no direct correlation was found between proliferative potential and age of donor in cultured human fibroblasts [30], suggesting that senescence and aging are not a direct function of telomere length. Indeed, individual cells in a population can

undergo senescence at very different cumulative population doubling levels (cPDL), which implies that other stochastic elements regulate senescence, in addition to the "molecular clock" of telomere shortening [31]. In fact, p38 MAPK induces cellular senescence in response to oxidative, genotoxic, and oncogenic stresses independently of telomere loss [5, 16, 32–36]. Interestingly though, telomeres appear to be particularly sensitive to oxidative and genotoxic stress [37]. Hence it is possible that stochastic events like ROS production, UV exposure, and age-dependent accumulation of dysfunctional mitochondria induce cellular senescence in vivo also through telomere loss, but independently of cPDL.

Cells bearing markers of senescence can be found in vivo in association with increasing age but also at sites of pathology [38, 39]. For example, aging primates show increasing numbers of cells with TIF and heterochromatin markers in the skin [40, 41], as well as signs of chromatin reorganization in the lungs, liver, and skeletal muscle [42], and increasing levels of $p16^{INK4A}$ are found in several tissues of old mice [43] and in the skin and brain of the elderly [44, 45]. On the other hand, more $p16^{INK4A}$-expressing cells are found in patients affected by Alzheimer's disease [45], in atherosclerotic plaques [46], and in kidneys of patients suffering from hypertension [47], than in age-matched and otherwise healthy subjects. Furthermore, $p16^{INKA}$ expression and DNA damage foci are increased upon treatment with ionizing radiation and chemotherapeutics [48]; $p21^{CIP1/WAF1}$, SA-β-Gal, and lipofuscin levels are increased upon exposure to cigarette smoke in mice lungs [49]; and senescent cells are found in association with several tumors [1]. Senescent cells are thus a common feature of both aging and diseased tissues, especially in age-related pathologies.

Importantly, senescent cells not just are a marker of aging and age-related pathologies but also likely contribute to the aging process as well as to the onset and progression of age-associated conditions. In fact, senescent cells can promote the proliferation of pre-neoplastic cell lines in vivo [50], and clearing $p16^{INK4A}$-positive senescent cells reverts nearly all aging phenotypes in a progeroid mouse model [51]; these observations suggest that accumulating senescent cells increases the incidence of these age-related conditions. In fact, senescent cells can contribute to the onset and progression of several age-related conditions through the SASP, which contains pro-inflammatory cytokines, matrix metalloproteases, and growth factors that can easily disrupt the local homeostasis of the tissue and contribute to cancer progression, metastasis, neurodegenerative disorders, inflammatory diseases, metabolic dysfunction, and other conditions that preferentially affect the elderly [1, 38]. For example, senescent cell-derived interleukin 6, interleukin 8, and matrix metallo-proteases promote migration, invasion, and epithelial-to-mesenchymal transition in tumor cells [18, 19] and can contribute to Alzheimer's disease [45], atherosclerosis [52], osteoarthritis [53], insulin resistance,

and type 2 diabetes [54] by increasing inflammation in the brain, the vasculature, and the adipose tissue, respectively. Furthermore, senescent fibroblasts increase tumor vascularization in mouse by secreting vascular endothelial growth factor [55], can stimulate the growth of prostate and breast cancer cells by secreting amphiregulin and other growth factors [56, 57], and can even disrupt normal mammary epithelium [57], thus contributing to the progression of age-related tumors. Lastly, the SASP can affect tissue homeostasis by inducing senescence in neighboring cells [58] and potentially disrupting the stem cell niche, thereby promoting death and senescence of stem cells and impairing tissue regeneration. The SASP factors interleukin 6, interleukin 8, and secreted frizzled-related protein 1 can induce cellular senescence in stem cells by promoting inflammation and altering the Wnt signaling pathway [59–64]. In addition, the SASP could inhibit the differentiation of progenitor cells and thus directly impair tissue regeneration, although no direct evidence of this mechanism has been provided yet.

Age-related decline can be triggered by accumulating senescent cells and by the increasingly deleterious effects of the secretory phenotype. Notably though, cellular senescence also suppresses tumorigenesis and promotes healing in determinate circumstances, contributing to tissue homeostasis instead of disrupting it. In fact, cellular senescence inhibits the proliferation of damaged and potentially tumorigenic cells [65] and can recruit the immune system to clear malignant lesions [66]. Furthermore, senescent cells appear to promote wound healing and tissue remodeling, reducing fibrosis and scarring in several settings [1, 67]. Indeed, several components of the SASP are known to recruit the immune system, which is required for efficient wound healing and tissue regeneration [68]. Senescent cells are removed by the immune system themselves, after the injury has been repaired [66, 69]. This observation suggests that transient activation of cellular senescence can actually preserve tissue homeostasis, while chronic, sustained signaling from accumulating senescent cells damages the tissue microenvironment in aging organisms. Intriguingly, senescent cells may accumulate with age because of the progressive loss of function of the immune system [70], which is subject to replicative senescence itself [71], but also because of increasing exposure to senescence-inducing stresses with age, such as oxidative stress, organelle dysfunction, and oncogenic mutations, especially in long-lived cells.

3 Cell Cycle Arrest During Senescence

The primary phase of cell cycle arrest during senescence is the G1/S transition [72]. Formal demonstration of the G1 nature of the senescent arrest was provided by cell cycle analysis of primary human fibroblasts with increasing population doublings, which revealed a progressive increase in the length of G1 in late-passage cultures [73].

The presence of a G1/S block during replicative senescence was demonstrated in a classic experiment in which the simian virus 40 large T antigen was introduced into senescent cells in order to abrogate both p53- and pRb-mediated cell cycle arrest. The introduction of T antigen into cell populations that were stringently selected to be fully senescent allowed a single round of full genomic DNA synthesis to occur [74]. These results demonstrated that senescence induced by exhaustive replication leading to telomere erosion induces a G1 arrest. Similarly, the introduction of an activated Ras gene into primary human fibroblasts induces an abortive DNA synthesis that appears to initiate DNA damage response due to replication fork collapse causing a late G1/S arrest [75]. The cell cycle arrest in cells lacking key G1 cell cycle regulatory genes indicates that there is redundancy in senescence-inducing pathways. For example, Li–Fraumeni cells lacking p53 undergo senescence and, similar to cells expressing SV40 T antigen, only rarely undergo immortalization [76], while direct targeting of both alleles of p21 in human fibroblasts does not abrogate senescence [77].

Although senescent cells appear to make the initial exit from the cell cycle in G1, a significant population of G2-arrested cells can be found in a stable population of senescent human cells. This population can be substantially greater in rodent cells, and direct experimental evidence suggests that the S/G2 arrest is substantially more stable in human cells than in rodent cells [78]. Based on this data, it has been postulated that the stability of cell cycle arrest may be a determinant of species life-span [79].

4 Detection of Senescence In Vivo

No single method for the detection of senescent cells in vivo is absolutely definitive due to the fact that cellular events unique to senescence have not been identified. Rather, the senescence program involves quantitative changes in gene expression and markers of differentiation. For example, the senescence-associated beta-galactosidase (SA-β-gal), a lysosomal enzyme described in a landmark study that provided the first evidence that senescent cells can be detected in vivo [12, 80], has been used successfully to identify senescent cells in vivo although it has been demonstrated that the assay does not distinguish between cells in crisis and true senescent cells [81]. The detection of senescent cells is an evolving area of aging research that will become more precise as new markers, tools, and molecular cell type-specific events are evaluated both in vitro and in vivo. One molecular change that appears to have potential to provide specific markers for senescent cells is the chromatin remodeling which occurs as a result of the senescence program. Areas of facultative heterochromatin occur in senescent cells.

These areas of chromatin remodeling are referred to as SAHF [82]. The formation of SAHF appears to occur in a stepwise fashion involving histone chaperones and histone variant macro H2A [83]. The ability to quantify chromatin changes and the use of multiple markers for senescence-associated events are likely to provide useful approaches to the quantification of senescent cells in a variety of disease states.

Acknowledgements

This work was supported in part by NIH grant AG039799 (C.S.).

References

1. Campisi J (2013) Aging, cellular senescence, and cancer. Annu Rev Physiol 75:685–705
2. Rodier F, Campisi J (2011) Four faces of cellular senescence. J Cell Biol 192(4):547–603
3. Stein G, Drullinger L, Soulard A, Dulić V (1999) Differential roles for cyclin-dependent kinase inhibitors p21 and p16 in the mechanisms of senescence and differentiation in human fibroblasts. Mol Cell Biol 19(3): 2109–2117
4. Herbig U, Jobling W, Chen B, Chen D, Sedivy J (2004) Telomere shortening triggers senescence of human cells through a pathway involving ATM, p53, and p21(CIP1), but not p16(INK4a). Mol Cell 14(4):501–513
5. Iwasa H, Han J, Ishikawa F (2003) Mitogen-activated protein kinase p38 defines the common senescence-signalling pathway. Genes Cells 8(2):131–144
6. Li H, Wang W, Liu X, Paulson K, Yee A, Zhang X (2010) Transcriptional factor HBP1 targets P16(INK4A), upregulating its expression and consequently is involved in Ras-induced premature senescence. Oncogene 29(36): 5083–5094
7. Alcorta DA, Xiong Y, Phelps D, Hannon G, Beach D, Barrett JC (1996) Involvement of the cyclin-dependent kinase inhibitor p16 (INK4a) in replicative senescence of normal human fibroblasts. Proc Natl Acad Sci U S A 93(24):13742–13747
8. Naka K, Tachibana A, Ikeda K, Motoyama N (2004) Stress-induced premature senescence in hTERT-expressing ataxia telangiectasia fibroblasts. J Biol Chem 279(3):2030–2037
9. Freund A, Patil C, Campisi J (2011) p38MAPK is a novel DNA damage response-independent regulator of the senescence-associated secretory phenotype. EMBO J 30(8):1536–1548
10. Hayflick L, Moorhead P (1961) The serial cultivation of human diploid cell strains. Exp Cell Res 25:585–621
11. Hayflick L (1965) The limited *in vitro* lifetime of human diploid strains. Exp Cell Res 37:614–636
12. Dimri G, Lee X, Basile G, Acosta M, Scott G, Roskelley C, Medrano E, Linskens M, Rubelj I, Pereira-Smith O (1995) A biomarker that identifies senescent human cells in culture and in aging skin in vivo. Proc Natl Acad Sci U S A 92(20):9363–9367
13. d'Adda di Fagagna F, Reaper P, Clay-Farrace L, Fiegler H, Carr P, Von Zglinicki T, Saretzki G, Carter N, Jackson S (2003) A DNA damage checkpoint response in telomere-initiated senescence. Nature 426(6963):194–198
14. Rodier F, Munoz DP, Teachenor R, Chu V, Le O, Bhaumik D, Coppe JP, Campeau E, Beausejour CM, Kim SH, Davalos AR, Campisi J (2011) DNA-SCARS: distinct nuclear structures that sustain damage-induced senescence growth arrest and inflammatory cytokine secretion. J Cell Sci 124(Pt 1):68–81
15. Adams PD (2007) Remodeling of chromatin structure in senescent cells and its potential impact on tumor suppression and aging. Gene 397(1–2):84–93
16. Wang W, Chen JX, Liao R, Deng Q, Zhou JJ, Huang S, Sun P (2002) Sequential activation of the MEK-extracellular signal-regulated kinase and MKK3/6-p38 mitogen-activated protein kinase pathways mediates oncogenic ras-induced premature senescence. Mol Cell Biol 22(10):3389–3403

17. Freund A, Laberge R-M, Demaria M, Campisi J (2012) Lamin B1 loss is a senescence-associated biomarker. Mol Biol Cell 23(11):2066–2075
18. Coppe JP, Boysen M, Sun CH, Wong BJ, Kang MK, Park NH, Desprez PY, Campisi J, Krtolica A (2008) A role for fibroblasts in mediating the effects of tobacco-induced epithelial cell growth and invasion. Mol Cancer Res 6(7): 1085–1098
19. Coppe JP, Patil CK, Rodier F, Sun Y, Munoz DP, Goldstein J, Nelson PS, Desprez PY, Campisi J (2008) Senescence-associated secretory phenotypes reveal cell-nonautonomous functions of oncogenic RAS and the p53 tumor suppressor. PLoS Biol 6(12):2853–2868
20. Narita M, Nũnez S, Heard E, Narita M, Lin A, Hearn S, Spector D, Hannon G, Lowe S (2003) Rb-mediated heterochromatin formation and silencing of E2F target genes during cellular senescence. Cell 113(6):703–716
21. Rodier F, Coppe JP, Patil CK, Hoeijmakers WA, Munoz DP, Raza SR, Freund A, Campeau E, Davalos AR, Campisi J (2009) Persistent DNA damage signalling triggers senescence-associated inflammatory cytokine secretion. Nat Cell Biol 11(8):973–979
22. Coppe JP, Rodier F, Patil CK, Freund A, Desprez PY, Campisi J (2011) Tumor suppressor and aging biomarker p16(INK4a) induces cellular senescence without the associated inflammatory secretory phenotype. J Biol Chem 286(42):36396–36403
23. Fries J (1980) Aging, natural death, and the compression of morbidity. N Engl J Med 303(3):130–135
24. Harley C, Futcher A, Greider C (1990) Telomeres shorten during ageing of human fibroblasts. Nature 345(6274):458–460
25. Bodnar A, Ouellette M, Frolkis M, Holt S, Chiu C, Morin G, Harley C, Shay J, Lichtsteiner S, Wright W (1998) Extension of life-span by introduction of telomerase into normal human cells. Science 279(5349):349–352
26. Parrinello S, Samper E, Krtolica A, Goldstein J, Melov S, Campisi J (2003) Oxygen sensitivity severely limits the replicative lifespan of murine fibroblasts. Nat Cell Biol 5(8):741–747
27. Lindsey J, McGill N, Lindsey L, Green D, Cooke H (1991) In vivo loss of telomeric repeats with age in humans. Mutat Res 256(1): 45–48
28. Huang S, Risques R, Martin G, Rabinovitch P, Oshima J (2008) Accelerated telomere shortening and replicative senescence in human fibroblasts overexpressing mutant and wild-type lamin A. Exp Cell Res 314(1):82–91
29. Kudlow B, Stanfel M, Burtner C, Johnston E, Kennedy B (2008) Suppression of proliferative defects associated with processing-defective lamin A mutants by hTERT or inactivation of p53. Mol Biol Cell 19(12):5238–5248
30. Cristofalo V, Allen R, Pignolo R, Martin B, Beck J (1998) Relationship between donor age and the replicative lifespan of human cells in culture: a reevaluation. Proc Natl Acad Sci U S A 95(18):10614–10619
31. Smith J, Whitney R (1980) Intraclonal variation in proliferative potential of human diploid fibroblasts: stochastic mechanism for cellular aging. Science 207(4426):82–84
32. Lee S, Jeong S-Y, Lim W-C, Kim S, Park Y-Y, Sun X, Youle R, Cho H (2007) Mitochondrial fission and fusion mediators, hFis1 and OPA1, modulate cellular senescence. J Biol Chem 282(31):22977–22983
33. Yoon Y-S, Yoon D-S, Lim I, Yoon S-H, Chung H-Y, Rojo M, Malka F, Jou M-J, Martinou J-C, Yoon G (2006) Formation of elongated giant mitochondria in DFO-induced cellular senescence: involvement of enhanced fusion process through modulation of Fis1. J Cell Physiol 209(2):468–480
34. Bitto A, Sell C, Crowe E, Lorenzini A, Malaguti M, Hrelia S, Torres C (2010) Stress-induced senescence in human and rodent astrocytes. Exp Cell Res 316(17):2961–2968
35. Gorbunova V, Seluanov A, Pereira-Smith O (2002) Expression of human telomerase (hTERT) does not prevent stress-induced senescence in normal human fibroblasts but protects the cells from stress-induced apoptosis and necrosis. J Biol Chem 277(41): 38540–38549
36. Toussaint O, Medrano E, von Zglinicki T (2000) Cellular and molecular mechanisms of stress-induced premature senescence (SIPS) of human diploid fibroblasts and melanocytes. Exp Gerontol 35(8):927–945
37. von Zglinicki T (2002) Oxidative stress shortens telomeres. Trends Biochem Sci 27(7): 339–344
38. Naylor R, Baker D, van Deursen J (2013) Senescent cells: a novel therapeutic target for aging and age-related diseases. Clin Pharmacol Ther 93(1):105–116
39. Jeyapalan J, Sedivy J (2008) Cellular senescence and organismal aging. Mech Ageing Dev 129(7–8):467–541
40. Herbig U, Ferreira M, Condel L, Carey D, Sedivy J (2006) Cellular senescence in aging primates. Science 311(5765):1257
41. Jeyapalan J, Ferreira M, Sedivy J, Herbig U (2007) Accumulation of senescent cells in

mitotic tissue of aging primates. Mech Ageing Dev 128(1):36–44

42. Kreiling J, Tamamori-Adachi M, Sexton A, Jeyapalan J, Munoz-Najar U, Peterson A, Manivannan J, Rogers E, Pchelintsev N, Adams P, Sedivy J (2011) Age-associated increase in heterochromatic marks in murine and primate tissues. Aging Cell 10(2):292–304
43. Krishnamurthy J, Torrice C, Ramsey M, Kovalev G, Al-Regaiey K, Su L, Sharpless N (2004) Ink4a/Arf expression is a biomarker of aging. J Clin Invest 114(9):1299–1307
44. Ressler S, Bartkova J, Niederegger H, Bartek J, Scharffetter-Kochanek K, Jansen-Dürr P, Wlaschek M (2006) p16INK4A is a robust in vivo biomarker of cellular aging in human skin. Aging Cell 5(5):379–389
45. Bhat R, Crowe E, Bitto A, Moh M, Katsetos C, Garcia F, Johnson F, Trojanowski J, Sell C, Torres C (2012) Astrocyte senescence as a component of Alzheimer's disease. PLoS One 7(9):e45069
46. Holdt L, Sass K, Gäbel G, Bergert H, Thiery J, Teupser D (2011) Expression of Chr9p21 genes CDKN2B (p15(INK4b)), CDKN2A (p16(INK4a), p14(ARF)) and MTAP in human atherosclerotic plaque. Atherosclerosis 214(2):264–270
47. Westhoff J, Hilgers K, Steinbach M, Hartner A, Klanke B, Amann K, Melk A (2008) Hypertension induces somatic cellular senescence in rats and humans by induction of cell cycle inhibitor p16INK4a. Hypertension 52(1):123–129
48. Le ON, Rodier F, Fontaine F, Coppe JP, Campisi J, DeGregori J, Laverdiere C, Kokta V, Haddad E, Beausejour CM (2010) Ionizing radiation-induced long-term expression of senescence markers in mice is independent of p53 and immune status. Aging Cell 9(3): 398–409
49. Tsuji T, Aoshiba K, Nagai A (2004) Cigarette smoke induces senescence in alveolar epithelial cells. Am J Respir Cell Mol Biol 31(6): 643–649
50. Krtolica A, Parrinello S, Lockett S, Desprez P, Campisi J (2001) Senescent fibroblasts promote epithelial cell growth and tumorigenesis: a link between cancer and aging. Proc Natl Acad Sci U S A 98(21):12072–12077
51. Baker D, Wijshake T, Tchkonia T, Lebrasseur N, Childs B, van de Sluis B, Kirkland J, van Deursen J (2011) Clearance of p16(Ink4a)-positive senescent cells delays ageing-associated disorders. Nature 479:232–236
52. Wang J, Bennett M (2012) Aging and atherosclerosis: mechanisms, functional consequences, and potential therapeutics for cellular senescence. Circ Res 111(2):245–259
53. Shane Anderson A, Loeser R (2010) Why is osteoarthritis an age-related disease? Best Pract Res Clin Rheumatol 24(1):15–26
54. Tchkonia T, Morbeck D, Von Zglinicki T, Van Deursen J, Lustgarten J, Scrable H, Khosla S, Jensen M, Kirkland J (2010) Fat tissue, aging, and cellular senescence. Aging Cell 9(5): 667–684
55. Coppe JP, Kauser K, Campisi J, Beausejour CM (2006) Secretion of vascular endothelial growth factor by primary human fibroblasts at senescence. J Biol Chem 281(40): 29568–29574
56. Bavik C, Coleman I, Dean J, Knudsen B, Plymate S, Nelson P (2006) The gene expression program of prostate fibroblast senescence modulates neoplastic epithelial cell proliferation through paracrine mechanisms. Cancer Res 66(2):794–802
57. Parrinello S, Coppe JP, Krtolica A, Campisi J (2005) Stromal-epithelial interactions in aging and cancer: senescent fibroblasts alter epithelial cell differentiation. J Cell Sci 118(Pt 3): 485–496
58. Acosta JC, Banito A, Wuestefeld T, Georgilis A, Janich P, Morton JP, Athineos D, Kang TW, Lasitschka F, Andrulis M, Pascual G, Morris KJ, Khan S, Jin H, Dharmalingam G, Snijders AP, Carroll T, Capper D, Pritchard C, Inman GJ, Longerich T, Sansom OJ, Benitah SA, Zender L, Gil J (2013) A complex secretory program orchestrated by the inflammasome controls paracrine senescence. Nat Cell Biol 15(8):978–990
59. Liu H, Fergusson M, Castilho R, Liu J, Cao L, Chen J, Malide D, Rovira I, Schimel D, Kuo C, Gutkind J, Hwang P, Finkel T (2007) Augmented Wnt signaling in a mammalian model of accelerated aging. Science 317(5839):803–806
60. D-y Z, H-j W, Y-z T (2011) Wnt/β-catenin signaling induces the aging of mesenchymal stem cells through the DNA damage response and the p53/p21 pathway. PLoS One 6(6):e21397
61. Diala I, Wagner N, Magdinier F, Shkreli M, Sirakov M, Bauwens S, Schluth-Bolard C, Simonet T, Renault V, Ye J, Djerbi A, Pineau P, Choi J, Artandi S, Dejean A, Plateroti M, Gilson E (2013) Telomere protection and TRF2 expression are enhanced by the canonical Wnt signalling pathway. EMBO Rep 14(4):356–363
62. McKay B, Ogborn D, Baker J, Toth K, Tarnopolsky M, Parise G (2013) Elevated

SOCS3 and altered IL-6 signaling is associated with age-related human muscle stem cell dysfunction. Am J Physiol Cell Physiol 304(8): C717–C728

63. Wei H, Shen G, Deng X, Lou D, Sun B, Wu H, Long L, Ding T, Zhao J (2013) The role of IL-6 in bone marrow (BM)-derived mesenchymal stem cells (MSCs) proliferation and chondrogenesis. Cell Tissue Bank 14(4):699–706
64. Elzi D, Song M, Hakala K, Weintraub S, Shiio Y (2012) Wnt antagonist SFRP1 functions as a secreted mediator of senescence. Mol Cell Biol 32(21):4388–4399
65. Prieur A, Peeper D (2008) Cellular senescence in vivo: a barrier to tumorigenesis. Curr Opin Cell Biol 20(2):150–155
66. Kang T-W, Yevsa T, Woller N, Hoenicke L, Wuestefeld T, Dauch D, Hohmeyer A, Gereke M, Rudalska R, Potapova A, Iken M, Vucur M, Weiss S, Heikenwalder M, Khan S, Gil J, Bruder D, Manns M, Schirmacher P, Tacke F, Ott M, Luedde T, Longerich T, Kubicka S, Zender L (2011) Senescence surveillance of pre-malignant hepatocytes limits liver cancer development. Nature 479(7374):547–551
67. Jun J-I, Lau L (2010) The matricellular protein CCN1 induces fibroblast senescence and restricts fibrosis in cutaneous wound healing. Nat Cell Biol 12(7):676–685
68. Park J, Barbul A (2004) Understanding the role of immune regulation in wound healing. Am J Surg 187(5A):11S–16S
69. Krizhanovsky V, Yon M, Dickins R, Hearn S, Simon J, Miething C, Yee H, Zender L, Lowe S (2008) Senescence of activated stellate cells limits liver fibrosis. Cell 134(4):657–667
70. Shaw A, Joshi S, Greenwood H, Panda A, Lord J (2010) Aging of the innate immune system. Curr Opin Immunol 22(4):507–513
71. Chou J, Effros R (2012) T cell replicative senescence in human aging. Curr Pharm Des 19(9):1680–1698
72. Dulic V, Drullinger LF, Lees E, Reed SI, Stein GH (1993) Altered regulation of G1 cyclins in senescent human diploid fibroblasts: accumulation of inactive cyclin E-Cdk2 and cyclin D1-Cdk2 complexes. Proc Natl Acad Sci U S A 90(23):11034–11038
73. Grove GL, Cristofalo VJ (1977) Characterization of the cell cycle of cultured human diploid cells: effects of aging and hydrocortisone. J Cell Physiol 90(3):415–422
74. Gorman SD, Cristofalo VJ (1985) Reinitiation of cellular DNA synthesis in BrdU-selected nondividing senescent WI-38 cells by simian virus 40 infection. J Cell Physiol 125(1):122–126
75. Di Micco R, Fumagalli M, Cicalese A, Piccinin S, Gasparini P, Luise C, Schurra C, Garre M, Nuciforo PG, Bensimon A, Maestro R, Pelicci PG, d'Adda di Fagagna F (2006) Oncogene-induced senescence is a DNA damage response triggered by DNA hyper-replication. Nature 444(7119):638–642
76. Medcalf AS, Klein-Szanto AJ, Cristofalo VJ (1996) Expression of p21 is not required for senescence of human fibroblasts. Cancer Res 56(20):4582–4585
77. Brown JP, Wei W, Sedivy JM (1997) Bypass of senescence after disruption of p21CIP1/WAF1 gene in normal diploid human fibroblasts. Science 277(5327):831–834
78. Fink LS, Roell M, Caiazza E, Lerner C, Stamato T, Hrelia S, Lorenzini A, Sell C (2011) 53BP1 contributes to a robust genomic stability in human fibroblasts. Aging 3(9):836–845
79. Lorenzini A, Stamato T, Sell C (2011) The disposable soma theory revisited: time as a resource in the theories of aging. Cell Cycle 10(22):3853–3856
80. Lee BY, Han JA, Im JS, Morrone A, Johung K, Goodwin EC, Kleijer WJ, DiMaio D, Hwang ES (2006) Senescence-associated beta-galactosidase is lysosomal beta-galactosidase. Aging Cell 5(2):187–195
81. Wei W, Sedivy JM (1999) Differentiation between senescence (M1) and crisis (M2) in human fibroblast cultures. Exp Cell Res 253(2):519–522
82. Zhang R, Poustovoitov MV, Ye X, Santos HA, Chen W, Daganzo SM, Erzberger JP, Serebriiskii IG, Canutescu AA, Dunbrack RL, Pehrson JR, Berger JM, Kaufman PD, Adams PD (2005) Formation of MacroH2A-containing senescence-associated heterochromatin foci and senescence driven by ASF1a and HIRA. Dev Cell 8(1):19–30
83. Zhang R, Chen W, Adams PD (2007) Molecular dissection of formation of senescence-associated heterochromatin foci. Mol Cell Biol 27(6):2343–2358

Chapter 9

Oncogenic Ras Pushes (and Pulls) Cell Cycle Progression Through ERK Activation

Paul M. Campbell

Abstract

The Ras–Raf–MEK–ERK signaling cascade is capable of channeling a wide variety of extracellular signals into control of cell proliferation, differentiation, senescence, and death. Because aberrant regulation at all steps of this signaling axis is observed in cancer, it remains an area of great interest in the field of tumor biology. Here we present evidence of the intricate and delicate levels of control of this pathway as it pertains to cell cycle regulation and illustrate how this control is not simply a rheostat.

Key words Ras, Raf, MEK, ERK, Cell cycle, Proliferation, Cyclin

1 Introduction

While there are several phenotypes that are common to and form the basis for cancer biology [1], neoplasia can be thought of, in the most simplest of terms, as a loss of control. Essentially, the checks and balances of normal cellular functions have been dysregulated in tumors. One of the principal hallmarks of cancer is the uncontrolled proliferation of cells, governed by the entrance into and continued reiteration of, but lack of exit from, the mitotic cell cycle. There are many levels of modulation and signaling that impinge upon aberrantly controlled cell cycle, and the Ras family of oncogenes plays a large role in this and other cancer phenotypes [2, 3].

Ras proteins (H-, N-, and K-Ras are the prototypes) are associated with the inner leaflet of the plasma membrane (although they can and do signal via endomembranes [4]) where they transmit signaling initiated by an abundantly diverse group of extracellular stimuli [5]. Ras activity is regulated by cycling between inactive GDP-bound and active GTP-bound forms, and this regulation involves interaction between Ras and guanine nucleotide exchange factors (GEFs), including SOS1/2, RasGRP, and RasGRF1/2 proteins [6]. When GTP bound, Ras engages and activates a multitude

Eishi Noguchi and Mariana C. Gadaleta (eds.), *Cell Cycle Control: Mechanisms and Protocols*, Methods in Molecular Biology, vol. 1170, DOI 10.1007/978-1-4939-0888-2_9,

of effector molecules [5, 7, 8]. While Ras proteins are GTPases in their own right, the baseline hydrolysis of GTP is rather slow [9, 10]. As such, GTP hydrolysis is facilitated by GTPase-activating proteins (GAPs) such as p120GAP and NF1. Mutated variants of Ras (mutations at residues 12, 13, or 61) [11], which are found in approximately 30 % of all human cancers, are insensitive to GAP stimulation and are consequently rendered constitutively active [11, 12].

In addition to mutational activation, Ras GTPase signaling is often upregulated due to aberrant activity of cell surface receptors. In particular, members of the epidermal growth factor (EGF) family of receptor tyrosine kinases (including EGFR/ErbB/HER1 and ErbB2/Her2/Neu [13–15]) or other tyrosine kinases (e.g., Bcr-Abl) are commonly overexpressed and/or hyperactivated in cancer, leading to persistent activation of Ras even in the absence of Ras gene mutation. Thus, Ras activation is an important mediator of most aspects of tumor initiation and progression caused by these and other tyrosine kinases and extracellular signals. However, for the purpose of this review, we limit our focus to the effects of activated Ras proteins on proliferation and tumor growth.

The aberrant activation of Ras proteins has been implicated in controlling virtually all aspects of the malignant phenotype of the cancer cell, including cellular proliferation, transformation, invasion, and metastasis (reviewed in ref. 10). Over the last couple of decades, much has been uncovered regarding the mechanisms by which aberrant Ras drives unabated proliferation by deregulating cell cycle progression and promoting cell survival. The bulk of the information on oncogenic Ras signaling surrounds the activation of three downstream effector-signaling cascades, namely, Raf–MEK–ERK, PI3K–AKT, and RalGEF–RalA/RalB pathways. This review provides a brief snapshot of some of the influences from the first of these three canonical signaling axes, the Ras–Raf–MEK–ERK pathway, with respect to cancer cell proliferation.

2 Raf–MEK–ERK Activation

Mitogen-activated protein kinases (MAPKs) are a family of kinases that are aberrantly regulated in a variety of cancers and includes p38, c-Jun-N-terminal kinase (JNK), extracellular signal-related kinase 5 (ERK5), ERK1, and ERK2. Because the latter two are 85 % homologous and share substrates in vitro [16, 17], they are typically referred to jointly as ERK1/2. ERK1/2 are activated via phosphorylation by the MAPK kinases MEK1 and MEK2, which are in turn phosphorylated by the Raf family of MAPK kinase kinases. The details behind the activation of Raf kinases (A-Raf, B-Raf, c-Raf-1, etc.) are beyond the scope of this review, but it has

been demonstrated that their autoinhibition is relieved by the engagement of Ras-GTP and phosphorylated 14-3-3 regulatory proteins [18]. Thus the signaling cascade downstream of extracellular stimulation can be mostly simply diagrammed by RasGDP<> RasGTP>Raf>MEK1/2>ERK1/2.

3 ERK Phosphorylation Governs Location and Activity

Like most proteins whose activation is dependent on phosphorylation, ERK1/2 are susceptible to rapid inactivation by dual-specificity phosphatases like MKP1 [19] and others. Indeed, when inactive, ERK1/2 is often found in the cytoplasm sequestered by protein complexes that include MKPs [20]. However, upon phosphorylation, ERK1/2 translocates to the nucleus, where it phosphorylates ETS family transcription factors such as Elk-1. Phospho-Elk-1 has a greater affinity for serum response factor [21], and the interaction of these two proteins and their binding to the serum response element of a variety of gene promoter regions initiate the transcription of many cell cycle and pro-survival proteins such as $p21^{Cip1/Waf1}$, c-Fos, EGR-1, DTL, and others [22–25]. Critical for the translocation of phospho-ERK1/2 to the nucleus is an intact cytoskeleton, which is itself dependent on integrin signaling through Raf [26] and presumably to some extent Ras activation.

4 Activated ERK Has Extranuclear RSK Partners

In addition to phospho-ERK1/2 translocation to the nucleus to engage and phosphorylate transcription factors, active cytoplasmic ERK1/2 can also activate members of the ribosomal s6 kinase (RSK) family, including RSK1, RSK2, and RSK3. Once phosphorylated by ERK1/2, they too can translocate to the nucleus and stimulate the transcription factors c-Fos and cAMP response element-binding protein (CREB) [27–29]. CREB activation is responsible in part for the transcription of several anti-apoptotic genes including Bcl-2, Mcl-1, Bcl-xL, and xIAP [30] as well as the transcriptional repression of pro-apoptotic proteins such as Bad, Bak, Puma, and Bim [31, 32]. MAPK-dependent RSK kinases also phosphorylate and inhibit the CDK inhibitor Myt1, allowing for G2/M progression in oocytes [33] and mammalian cells [34]. Not to relegate Myt1 kinase to simply a role of cell cycle blockade, Nakajima et al. showed in HeLa cancer cells that proper Myt1 regulation is critical for correct telophase control and exit from the cell cycle [34].

5 ERK Directs Both the Progression and Inhibition of Cell Cycle Through Cyclin–CDK Activity

Once activated, ERK1/2 phosphorylates the protein phosphatase CDC25A, which dephosphorylates CDK4, CDK2, and CDK6 [35–37], necessary for G1 progression and G1/S transition. Once activated, CDK2 and CDK4 bind cyclins E and D, respectively. Both Chellepan et al. and Goodrich et al. showed that these cyclin–CDK complexes phosphorylate retinoblastoma (pRb), which serves to release it from the E2F transcription factors [38, 39]. Some of these transcription factors (including E2F1 and E2F3) can replace repressor-associated members (E2F4, E2F5) on promoter regions and activate the expression of several cell cycle-dependent genes to allow G1 progression, G1/S transition, and DNA replication. Some examples of these genes are *MYC*, *CCND1*, *CDC25A*, *CCNE1*, *PCNA*, *MCM2-7*, and *CDC6* (reviewed in ref. 40).

The cyclin–CDK–CDKI cell cycle mechanism remains an interesting and not completely resolved dance of time and space. Since many of these proteins share partners and substrates, when and where interaction occurs is as critical an element to the correct timing of mitotic progression as what binds to which. For example, the cell cycle-dependent kinase inhibitor (CDKI) $p27^{Kip1}$ binds both cyclin D–CDK4/6 and cyclin E–CDK2 complexes, but not at the same time, and Cooper describes some of the feed-forward and feedback loops between p27 and cyclin D1 that are fed by Ras activation [41]. As mentioned above, Ras and ERK1/2 drive the activation of cyclin D1–CDK4/6 to initially phosphorylate pRb and ultimately allow for E2F-dependent gene transcription. One of these responsive genes, *CCND1*, encodes cyclin D1, and accumulation of cyclin D1 causes a sequestration of the inhibitor $p27^{Kip1}$, in turn promoting the activity of cyclin E–CDK2. This second kinase complex is then free to further phosphorylate pRb as well as phosphorylate and target $p27^{Kip1}$ for degradation. While this Ras-dependent degradation of $p27^{Kip1}$ has been largely ascribed to PI3K activity through AKT phosphorylation (three seminal papers in 2002 [42–44]), it is becoming clear that ERK1/2 activity also plays a role [45], thereby providing another example of possible redundancies of control that cancer cells are able to exploit.

In addition to the regulation of CDK complex activity by CDKI, elements such as cyclin D1 also show interesting expression patterns that are similarly defined by time and space. As mentioned earlier, the Ras–MEK–ERK pathway induces the expression of the oncogenic transcription factor c-Fos. While it is expected, and has been shown, that c-Fos drives transcription of cyclin D1, the regulation is more complex than that simple transactivation. Depending on the timing of the cell cycle, ERK1/2 can activate the cyclin D1 promoter [46] or bind the p300 repressor to inhibit transcription [47].

Burch et al. recently showed in lung epithelia that depending on the stimuli and timing, c-Fos and its related member Fra-1 can be mutually exclusive in their nuclear translocation and recruitment to chromatin. In the case of cyclin D1 mRNA, the former is inhibitory (despite the transcription of other immediate early genes), while the latter promotes transcription [48]. This exchange of Fra-1 for c-Fos on cyclin D1 promoter AP-1 sites appears to be critical for G0–G1 entry into the cell cycle, demonstrating the importance of ERK activity at early points in the mitotic cell cycle.

Further along in the cell cycle, ERK-dependent activation of CDC25B and CDC25C acts upon CDK1 to promote its binding to cyclin B. This facilitates the progression in, and exit from, M phase [49, 50]. Active CDK1–cyclin complexes phosphorylate a wide variety of proteins in G2 and M phases, including a feed-forward activation of CDC25C demonstrated by Hoffmann et al. [51]. This triggers nuclear envelope dissolution, then chromosome condensation, and their alignment along the metaphase plate [52]. These results, coupled with the ERK-regulated activation of G0/G1 and G1/S transitions, demonstrate how sustained ERK activation is necessary to ensure cell cycle progression.

Interestingly, Massagué's group has shown that under certain circumstances, TGFβ signaling, a known stimulator of Ras, can lead to inactivation of murine Cdk4/6 but has dual roles of decreasing expression of Cdc25 and increasing activity of the tumor suppressor $p15^{Ink4b}$ [36]. This is yet another example of the paradoxical TGFβ-Ras signaling axis that on one hand can drive cell cycle progression and proliferation and on the other hand can be inhibitory to the mitotic cell cycle [53]. TGFβ-regulated cell cycle block is driven via $p27^{Kip1}$ and $p15^{Ink4b}$ [54, 55], where TGFβ signaling augments the expression of $p27^{Kip1}$ and $p15^{Ink4b}$ via ERK-dependent FOXO transcriptional activation [56–58]. At the same time, TGFβ-receptor signaling promotes $p27^{Kip1}$ nuclear accumulation by inhibiting the SCF(Skp2)-targeting complex that drives ubiquitin-mediated degradation [54].

6 Ras Activation Levels: When More Does Not Always Mean More

Finally, in addition to time and space considerations for Ras-driven ERK effects on the cell cycle, *amount* has to be accounted for. While as mentioned oncogenic Ras activity leads to a plethora of cancer phenotypes, the idea that "more Ras leads to more ERK leads to more malignancy" is not entirely realized, and additional signaling factors are required [59, 60]. There are several examples of ERK activation leading to anti-transformation effects in human and other mammalian cells, and many of these pertain to proliferation blockade, cell death, or senescence initiation. Samuels et al. used Raf–estrogen receptor chimeras to show that high lev-

els of Raf activation lead to cell cycle arrest [61]. Despite the fact that ERK activation leads to increases in cyclin D1 expression as indicated above, persistent and augmented ERK signaling also causes upregulation of the CDKI $p21^{Waf1/Cip1}$. Moderate ERK phosphorylation provides for modest $p21^{Waf1/Cip1}$ expression, which, like $p27^{Kip1}$, can be partially sequestered in G1 by cyclin D–CDK4/6 complexes [62]. This leaves cyclin E–CDK2 available to push through G1/S transition by the mechanisms detailed above. On the contrary, high levels of Ras–Raf–ERK signaling lead to a massive expression and accumulation of p21, which inhibits the kinase activity of both CDK4/6 and CDK2 and results in cell cycle arrest [63, 64].

7 Conclusions

The Ras family of small GTPases is among the most commonly mutated or aberrantly activated proteins seen in human cancer. As such, the signaling associated with these oncogenes is of great interest to cancer biologists as we strive to understand mechanism better. Even though the downstream effectors of Ras have been under scrutiny for several decades, and a wealth of knowledge has been uncovered, the complexity of Ras signaling in both normal and tumor cells is still being revealed.

Ras enzymes have a multitude of effector cascades that are initiated in response to various extracellular stimuli. This review has focused on just one of those, the Raf–MAPK axis, and only selected areas at that, to demonstrate some of the levels of regulation that impinge upon cell cycle control. The lessons learned from the plethora of experiments and data described herein suggest that despite the urge to draw the Ras-dependent pathways as linear mechanisms, the reality is that these signaling networks are nuanced and varied. Location matters, partners matter, levels matter, timing is critical, and, of course, cellular context is paramount. Continued research into how cancer is able to usurp the many levels of control to drive growth and malignancy will require a further understanding of the Ras biology.

References

1. Hanahan D, Weinberg RA (2011) Hallmarks of cancer: the next generation. Cell 144(5): 646–674
2. Campbell PM, Der CJ (2004) Oncogenic Ras and its role in tumor cell invasion and metastasis. Semin Cancer Biol 14(2):105–114
3. Campbell PM, Groehler AL, Lee KM, Ouellette MM, Khazak V, Der CJ (2007) K-Ras promotes growth transformation and invasion of immortalized human pancreatic cells by Raf and phosphatidylinositol 3-kinase signaling. Cancer Res 67(5):2098–2106
4. Choy E, Chiu VK, Silletti J, Feoktistov M, Morimoto T, Michaelson D, Ivanov IE, Philips MR (1999) Endomembrane trafficking of Ras: the CAAX motif targets proteins to the ER and Golgi. Cell 98(1):69–80
5. Shields JM, Pruitt K, McFall A, Shaub A, Der CJ (2000) Understanding Ras: 'it ain't over 'til it's over'. Trends Cell Biol 10(4):147–154

6. Quilliam LA, Rebhun JF, Castro AF (2002) A growing family of guanine nucleotide exchange factors is responsible for activation of Ras-family GTPases. Prog Nucleic Acid Res Mol Biol 71:391–444
7. Feig LA, Buchsbaum RJ (2002) Cell signaling: life or death decisions of ras proteins. Curr Biol 12(7):R259–R261
8. Wolthuis RM, Bos JL (1999) Ras caught in another affair: the exchange factors for Ral. Curr Opin Genet Dev 9(1):112–117
9. Bivona TG, Philips MR (2003) Ras pathway signaling on endomembranes. Curr Opin Cell Biol 15(2):136–142
10. Downward J (2003) Targeting RAS signalling pathways in cancer therapy. Nat Rev Cancer 3(1):11–22
11. Bos JL (1989) ras oncogenes in human cancer: a review. Cancer Res 49(17):4682–4689
12. Barbacid M (1987) ras genes. Annu Rev Biochem 56:779–827
13. Janes PW, Daly RJ, deFazio A, Sutherland RL (1994) Activation of the Ras signalling pathway in human breast cancer cells overexpressing erbB-2. Oncogene 9(12):3601–3608
14. Clark GJ, Der CJ (1995) Aberrant function of the Ras signal transduction pathway in human breast cancer. Breast Cancer Res Treat 35(1): 133–144
15. Tzahar E, Yarden Y (1998) The ErbB-2/HER2 oncogenic receptor of adenocarcinomas: from orphanhood to multiple stromal ligands. Biochim Biophys Acta 1377(1): M25–M37
16. Boulton TG, Nye SH, Robbins DJ, Ip NY, Radziejewska E, Morgenbesser SD, DePinho RA, Panayotatos N, Cobb MH, Yancopoulos GD (1991) ERKs: a family of protein-serine/threonine kinases that are activated and tyrosine phosphorylated in response to insulin and NGF. Cell 65(4):663–675
17. Sturgill TW, Ray LB, Erikson E, Maller JL (1988) Insulin-stimulated MAP-2 kinase phosphorylates and activates ribosomal protein S6 kinase II. Nature 334(6184):715–718
18. Terai K, Matsuda M (2005) Ras binding opens c-Raf to expose the docking site for mitogen-activated protein kinase kinase. EMBO Rep 6(3):251–255
19. Sun H, Charles CH, Lau LF, Tonks NK (1993) MKP-1 (3CH134), an immediate early gene product, is a dual specificity phosphatase that dephosphorylates MAP kinase in vivo. Cell 75(3):487–493
20. Karlsson M, Mathers J, Dickinson RJ, Mandl M, Keyse SM (2004) Both nuclear-cytoplasmic shuttling of the dual specificity phosphatase MKP-3 and its ability to anchor MAP kinase in the cytoplasm are mediated by a conserved nuclear export signal. J Biol Chem 279(40): 41882–41891
21. Shore P, Sharrocks AD (1994) The transcription factors Elk-1 and serum response factor interact by direct protein-protein contacts mediated by a short region of Elk-1. Mol Cell Biol 14(5):3283–3291
22. Shin SY, Kim CG, Lim Y, Lee YH (2011) The ETS family transcription factor ELK-1 regulates induction of the cell cycle-regulatory gene p21(Waf1/Cip1) and the BAX gene in sodium arsenite-exposed human keratinocyte HaCaT cells. J Biol Chem 286(30):26860–26872
23. Hipskind RA, Roa VN, Muller CGF, Raddy ESP, Nordheim A (1991) Ets-related protein Elk-1 is homologous to the c-fos regulatory factor p62TCF. Nature 354(6354):531–534
24. Patki M, Chari V, Sivakumaran S, Gonit M, Trumbly R, Ratnam M (2013) The ETS domain transcription factor ELK1 directs a critical component of growth signaling by the androgen receptor in prostate cancer cells. J Biol Chem 288(16):11047–11065
25. Reddy ES, Rao VN (1991) erg, an ets-related gene, codes for sequence-specific transcriptional activators. Oncogene 6(12):2285–2289
26. Aplin AE, Stewart SA, Assoian RK, Juliano RL (2001) Integrin-mediated adhesion regulates ERK nuclear translocation and phosphorylation of Elk-1. J Cell Biol 153(2):273–282
27. Anjum R, Blenis J (2008) The RSK family of kinases: emerging roles in cellular signalling. Nat Rev Mol Cell Biol 9(10):747–758
28. Zhao Y, Bjorbaek C, Weremowicz S, Morton CC, Moller DE (1995) RSK3 encodes a novel pp90rsk isoform with a unique N-terminal sequence: growth factor-stimulated kinase function and nuclear translocation. Mol Cell Biol 15(8):4353–4363
29. Bonni A, Brunet A, West AE, Datta SR, Takasu MA, Greenberg ME (1999) Cell survival promoted by the Ras-MAPK signaling pathway by transcription-dependent and -independent mechanisms. Science 286(5443):1358–1362
30. Cagnol S, Chambard JC (2010) ERK and cell death: mechanisms of ERK-induced cell death—apoptosis, autophagy and senescence. FEBS J 277(1):2–21
31. Versteeg HH, Borensztajn KS, Kerver ME, Ruf W, Reitsma PH, Spek CA, Peppelenbosch MP (2008) TF:FVIIa-specific activation of CREB upregulates proapoptotic proteins via protease-activated receptor-2. J Thromb Haemost 6(9): 1550–1557
32. Balmanno K, Cook SJ (2009) Tumour cell survival signalling by the ERK1/2 pathway. Cell Death Differ 16(3):368–377

33. Palmer A, Gavin AC, Nebreda AR (1998) A link between MAP kinase and p34(cdc2)/cyclin B during oocyte maturation: p90(rsk) phosphorylates and inactivates the p34(cdc2) inhibitory kinase Myt1. EMBO J 17(17): 5037–5047
34. Nakajima H, Yonemura S, Murata M, Nakamura N, Piwnica-Worms H, Nishida E (2008) Myt1 protein kinase is essential for Golgi and ER assembly during mitotic exit. J Cell Biol 181(1):89–103
35. Terada Y, Tatsuka M, Jinno S, Okayama H (1995) Requirement for tyrosine phosphorylation of Cdk4 in G1 arrest induced by ultraviolet irradiation. Nature 376(6538):358–362
36. Iavarone A, Massague J (1997) Repression of the CDK activator Cdc25A and cell-cycle arrest by cytokine TGF-beta in cells lacking the CDK inhibitor p15. Nature 387(6631):417–422
37. Hoffmann I, Draetta G, Karsenti E (1994) Activation of the phosphatase activity of human cdc25A by a cdk2-cyclin E dependent phosphorylation at the G1/S transition. EMBO J 13(18):4302–4310
38. Goodrich DW, Wang NP, Qian YW, Lee EY, Lee WH (1991) The retinoblastoma gene product regulates progression through the G1 phase of the cell cycle. Cell 67(2):293–302
39. Chellappan SP, Hiebert S, Mudryj M, Horowitz JM, Nevins JR (1991) The E2F transcription factor is a cellular target for the RB protein. Cell 65(6):1053–1061
40. Nevins JR (2001) The Rb/E2F pathway and cancer. Hum Mol Genet 10(7):699–703
41. Aktas H, Cai H, Cooper GM (1997) Ras links growth factor signaling to the cell cycle machinery via regulation of cyclin D1 and the Cdk inhibitor p27KIP1. Mol Cell Biol 17(7): 3850–3857
42. Viglietto G, Motti ML, Bruni P, Melillo RM, D'Alessio A, Califano D, Vinci F, Chiappetta G, Tsichlis P, Bellacosa A, Fusco A, Santoro M (2002) Cytoplasmic relocalization and inhibition of the cyclin-dependent kinase inhibitor p27Kip1 by PKB/Akt-mediated phosphorylation in breast cancer. Nat Med 8(10): 1136–1144
43. Shin I, Yakes FM, Rojo F, Shin N-Y, Bakin AV, Baselga J, Arteaga CL (2002) PKB/Akt mediates cell-cycle progression by phosphorylation of p27Kip1 at threonine 157 and modulation of its cellular localization. Nat Med 8(10): 1145–1152
44. Liang J, Zubovitz J, Petrocelli T, Kotchetkov R, Connor MK, Han K, Lee J-H, Ciarallo S, Catzavelos C, Beniston R, Franssen E, Slingerland JM (2002) PKB/Akt phosphorylates p27, impairs nuclear import of p27 and opposes p27-mediated G1 arrest. Nat Med 8(10): 1153–1160
45. Donovan JC, Milic A, Slingerland JM (2001) Constitutive MEK/MAPK activation leads to p27(Kip1) deregulation and antiestrogen resistance in human breast cancer cells. J Biol Chem 276(44):40888–40895
46. Albanese C, Johnson J, Watanabe G, Eklund N, Vu D, Arnold A, Pestell RG (1995) Transforming p21ras mutants and c-Ets-2 activate the cyclin D1 promoter through distinguishable regions. J Biol Chem 270(40): 23589–23597
47. Preston GA, Srinivasan D, Barrett JC (2000) Apoptotic response to growth factor deprivation involves cooperative interactions between c-Fos and p300. Cell Death Differ 7(2): 215–226
48. Burch PM, Yuan Z, Loonen A, Heintz NH (2004) An extracellular signal-regulated kinase 1- and 2-dependent program of chromatin trafficking of c-Fos and Fra-1 is required for cyclin D1 expression during cell cycle reentry. Mol Cell Biol 24(11):4696–4709
49. Draetta G, Beach D (1988) Activation of cdc2 protein kinase during mitosis in human cells: cell cycle-dependent phosphorylation and subunit rearrangement. Cell 54(1):17–26
50. Wang R, He G, Nelman-Gonzalez M, Ashorn CL, Gallick GE, Stukenberg PT, Kirschner MW, Kuang J (2007) Regulation of Cdc25C by ERK-MAP kinases during the G2/M transition. Cell 128(6):1119–1132
51. Hoffmann I, Clarke PR, Marcote MJ, Karsenti E, Draetta G (1993) Phosphorylation and activation of human cdc25-C by cdc2—cyclin B and its involvement in the self-amplification of MPF at mitosis. EMBO J 12(1):53–63
52. Malumbres M, Barbacid M (2005) Mammalian cyclin-dependent kinases. Trends Biochem Sci 30(11):630–641
53. Ravitz MJ, Wenner CE (1997) Cyclin-dependent kinase regulation during G1 phase and cell cycle regulation by TGF-beta. Adv Cancer Res 71:165–207
54. Lecanda J, Ganapathy V, D'Aquino-Ardalan C, Evans B, Cadacio C, Ayala A, Gold LI (2009) TGFβ prevents proteasomal degradation of the cyclin-dependent kinase inhibitor p27 kip1 for cell cycle arrest. Cell Cycle 8(5): 742–756
55. Hannon GJ, Beach D (1994) p15INK4B is a potential effector of TGF-beta-induced cell cycle arrest. Nature 371(6494):257–261

56. Dijkers PF, Medema RH, Pals C, Banerji L, Thomas NS, Lam EW, Burgering BM, Raaijmakers JA, Lammers JW, Koenderman L, Coffer PJ (2000) Forkhead transcription factor FKHR-L1 modulates cytokine-dependent transcriptional regulation of p27(KIP1). Mol Cell Biol 20(24):9138–9148
57. Malumbres M, Perez De Castro I, Hernandez MI, Jimenez M, Corral T, Pellicer A (2000) Cellular response to oncogenic ras involves induction of the Cdk4 and Cdk6 inhibitor p15(INK4b). Mol Cell Biol 20(8):2915–2925
58. Gomis RR, Alarcon C, Nadal C, Van Poznak C, Massague J (2006) C/EBPbeta at the core of the TGFbeta cytostatic response and its evasion in metastatic breast cancer cells. Cancer Cell 10(3):203–214
59. Franza BR Jr, Maruyama K, Garrels JI, Ruley HE (1986) In vitro establishment is not a sufficient prerequisite for transformation by activated ras oncogenes. Cell 44(3):409–418
60. Hirakawa T, Ruley HE (1988) Rescue of cells from ras oncogene-induced growth arrest by a second, complementing, oncogene. Proc Natl Acad Sci U S A 85(5):1519–1523
61. Samuels ML, Weber MJ, Bishop JM, McMahon M (1993) Conditional transformation of cells and rapid activation of the mitogen-activated protein kinase cascade by an estradiol-dependent human raf-1 protein kinase. Mol Cell Biol 13(10):6241–6252
62. LaBaer J, Garrett MD, Stevenson LF, Slingerland JM, Sandhu C, Chou HS, Fattaey A, Harlow E (1997) New functional activities for the p21 family of CDK inhibitors. Genes Dev 11(7):847–862
63. Sewing A, Wiseman B, Lloyd AC, Land H (1997) High-intensity Raf signal causes cell cycle arrest mediated by p21Cip1. Mol Cell Biol 17(9):5588–5597
64. Woods D, Parry D, Cherwinski H, Bosch E, Lees E, McMahon M (1997) Raf-induced proliferation or cell cycle arrest is determined by the level of Raf activity with arrest mediated by p21Cip1. Mol Cell Biol 17(9): 5598–5611

Chapter 10

Cell Cycle Regulation During Viral Infection

Sumedha Bagga and Michael J. Bouchard

Abstract

To replicate their genomes in cells and generate new progeny, viruses typically require factors provided by the cells that they have infected. Subversion of the cellular machinery that controls replication of the infected host cell is a common activity of many viruses. Viruses employ different strategies to deregulate cell cycle checkpoint controls and modulate cell proliferation pathways. A number of DNA and RNA viruses encode proteins that target critical cell cycle regulators to achieve cellular conditions that are beneficial for viral replication. Many DNA viruses induce quiescent cells to enter the cell cycle; this is thought to increase pools of deoxynucleotides and thus, facilitate viral replication. In contrast, some viruses can arrest cells in a particular phase of the cell cycle that is favorable for replication of the specific virus. Cell cycle arrest may inhibit early cell death of infected cells, allow the cells to evade immune defenses, or help promote virus assembly. Although beneficial for the viral life cycle, virus-mediated alterations in normal cell cycle control mechanisms could have detrimental effects on cellular physiology and may ultimately contribute to pathologies associated with the viral infection, including cell transformation and cancer progression and maintenance. In this chapter, we summarize various strategies employed by DNA and RNA viruses to modulate the replication cycle of the virus-infected cell. When known, we describe how these virus-associated effects influence replication of the virus and contribute to diseases associated with infection by that specific virus.

Key words Cell cycle, Regulation, DNA and RNA viruses, Consequences

1 Introduction

Viruses are obligate intracellular parasites that depend on the infected host cell for the resources that are required to replicate the viral genome; viruses have evolved multiple mechanisms to manipulate the environment of infected cells in order to replicate more efficiently [1]. Viral genomes can be composed of single- or double-stranded DNA or single- or double-stranded RNA, hereafter referred to as DNA or RNA viruses, respectively. While many viruses replicate their genomes by directly generating an exact DNA or RNA copy of the genome, other viruses, such as retroviruses or hepadnaviruses, use reverse transcription to generate intermediates that are required for their replication [2]. Subversion of the

Eishi Noguchi and Mariana C. Gadaleta (eds.), *Cell Cycle Control: Mechanisms and Protocols*, Methods in Molecular Biology, vol. 1170, DOI 10.1007/978-1-4939-0888-2_10,

host cell replication cycle, hereafter referred to as the "cell cycle," is a common strategy employed by many viruses to create a cellular environment that is favorable for viral replication [1]. Examples of virus-induced alterations in cellular replication processes have been identified as consequences of infection by both DNA and RNA viruses.

DNA viruses have been studied more extensively in regard to effects on cell cycle control. Many DNA viruses primarily infect quiescent or differentiated cells, which contain rate-limiting levels of deoxynucleotides and may not represent an ideal environment for viral replication. It is thought that these viruses can induce quiescent cells to enter the cell cycle in order to create an environment that generates factors, such as nucleotides, that are required for viral replication [3]. Some small DNA tumor viruses can promote entry into the S phase in order to activate the host cell DNA replication machinery and provide the resources necessary for viral replication. In contrast, some larger DNA viruses such as Herpesviruses can elicit a cell cycle arrest to limit the competition between the virus and the host for cellular DNA replication resources. Retroviruses and other RNA viruses can also interfere with the host cell cycle [1, 4–7]. There are various speculations regarding the advantages associated with regulation of the cell cycle by RNA viruses; these include increasing the efficiency of replication, translation, and virus assembly [8, 9]. Cell cycle arrest may also help delay the apoptosis of infected cells [10]. Additionally, a G2/M arrest induced by the human immunodeficiency virus (HIV) type-1 is thought to help HIV-1 avoid human immune defenses by preventing new cell production [8]. Overall, both DNA and RNA viruses manipulate the cell cycle to generate resources and cellular conditions that favor viral replication.

An unfortunate consequence of virus-mediated deregulation of normal cell cycle control mechanisms is that these effects may ultimately generate an environment that promotes disease, including the development, progression, or maintenance of certain types of cancer [11]. Some viruses encode proteins that deregulate normal cell cycle controls and manipulate cell proliferation pathways, and some of these proteins can directly influence the oncogenic potential of that virus. Viruses that cause human cancers include Hepatitis B virus (HBV), Hepatitis C virus (HCV), Human T-cell lymphotropic virus type I, Kaposi's sarcoma-associated herpesvirus (KSHV), Epstein–Barr virus (EBV), and Human papillomavirus (HPV), and viral infections may account for approximately 20 % of all human cancers worldwide [12–14]. Deregulation of the cell cycle and alteration in the expression levels and activities of the cell cycle regulatory proteins are frequently observed in transformed cells; consequently, disruption of normal mechanisms that regulate the cell cycle is thought to contribute to the development of many cancers [15]. The study of viral regulation of the cell cycle has

contributed to our understanding of viral replication processes and mechanisms that regulate the cell cycle and are altered in cancers. Moreover, analyses of the dynamic regulation of cell cycle by viruses have helped highlight key regulators of cell cycle progression. The cell cycle factors that are targeted by specific viral gene products to deregulate the cell cycle can be potential therapeutic targets for antiviral interventions and prevention of associated cancers [1, 16, 17].

In this chapter, we focus on different strategies employed by viruses to manipulate the host cell cycle in order to create an environment conducive for viral replication. A description of all viral factors that influence the cell cycle is beyond the scope of this chapter. Instead, examples of how some DNA and RNA viruses regulate different stages of the cell cycle are discussed to illustrate various viral strategies. Viral regulation of the G0/G1 transition, the G1 and S phases, and the G2/M checkpoint will be the focus of this review. In each section, we provide examples of viruses that can regulate the specific phase of the cell cycle, describe viral proteins that are involved in the virus-mediated deregulation of the cell cycle and mechanisms associated with the effects of these viral proteins, and discuss known or proposed consequences of the virus-mediated cell cycle stimulation and/or arrest for the virus life cycle and virus-associated diseases. Regulation of the cell cycle by certain viruses, such as the small DNA tumor viruses, has been studied for decades and has been reviewed extensively [18, 19]. While we briefly describe how these viruses modulate the host cell cycle, we emphasize more recently discovered effects of the Influenza A virus, HCV, HBV, and KSHV on the cell cycle. Overall, we aim to summarize key mechanisms that are used by viruses to manipulate the cell cycle and to provide insights into the consequences of these viral protein-mediated effects on the cell cycle for both the virus and the host cell.

2 The Cell Cycle

2.1 An Overview of the Cell Cycle

The eukaryotic cell cycle is composed of an ordered and tightly regulated series of events that can be controlled by intracellular and extracellular factors. The cell cycle also includes checkpoints that ensure normal cell cycle progression. The eukaryotic cell cycle consists of 4 phases: Gap 1 (G1), Synthesis (S), Gap 2 (G2), and Mitosis (M) (Fig. 1) [20, 21]. Differentiated cells are usually maintained in a nondividing state, known as the quiescent or G0 phase [22]. Quiescent cells must receive a growth signal in order to exit the G0 phase and enter the cell cycle [21, 23]. Binding of external factors such as mitogens to their cell surface receptors can activate signaling pathways, such as the Ras/mitogen-activated protein kinase (MAPK) pathway, which play a major role in cell entry into the G1 phase.

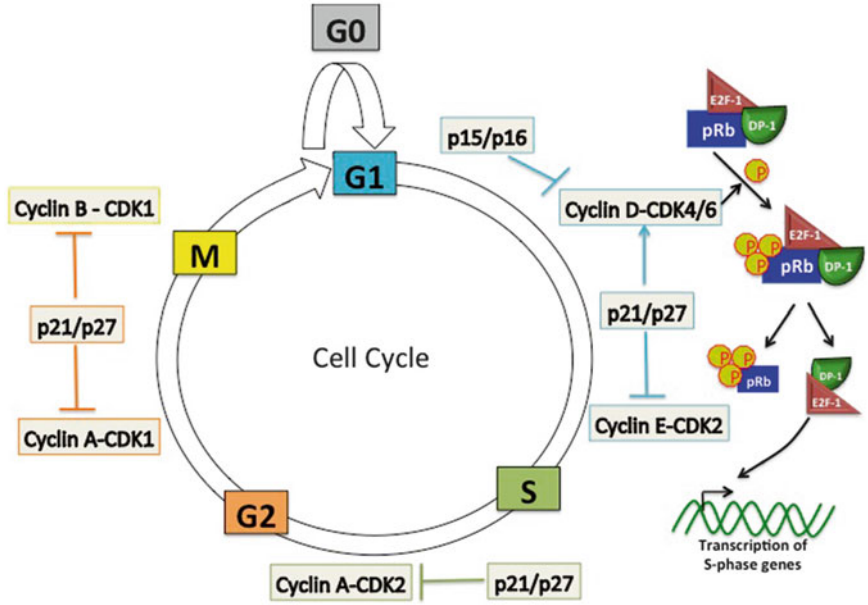

Fig. 1 Overview of the eukaryotic cell cycle. The eukaryotic cell cycle consists of 4 phases; G1, S, G2, and M. Progression through the cell cycle is tightly controlled; both positive and negative regulators of the cell cycle are shown. See text and references for details

When quiescent cells receive a growth signal, they enter into the G1 phase. During G1, the cell prepares to replicate its DNA; synthesis of the mRNAs and proteins necessary for DNA synthesis also occurs. The first major checkpoint of the cell cycle, which is present at the G1/S border, is known as the restriction point; if this checkpoint is not activated and the growth signal is still present, the cell proceeds into S phase, the stage during which DNA synthesis and duplication of the cell genome occurs. Once the cell enters S phase, DNA replication is completed regardless of the removal of the growth signal or the presence of DNA damage. After DNA replication is completed, the cell enters the G2 phase and prepares for mitosis, cell division. The G2 phase provides an opportunity for the cellular machinery to check for any DNA damage that may have accumulated during DNA replication. Therefore, cell cycle progression into the S phase and mitosis is controlled by the checkpoints at G1 and G2, respectively. Once the appropriate signals that are required for cell cycle progression are present, the cell enters into the M phase [20, 21]. A third checkpoint, referred to as the spindle checkpoint, exists after metaphase and prior to anaphase, which are steps during mitosis that are required for cell division. At this checkpoint, the cell employs strategies to detect improper alignment of chromosomes on the mitotic spindle. If improper alignment of chromosomes is detected, the cell cycle is stopped in metaphase; however, if the chromosomes

are properly attached to the spindle apparatus, the cell continues into anaphase, completes the cell cycle, and eventually generates two daughter cells [20, 24].

2.2 Mechanisms That Control the Cell Cycle

2.2.1 Positive Regulators of Cell Cycle Progression

Various cellular proteins regulate the transition from one phase of the cell cycle to the next phase. Key regulatory proteins that control cell cycle progression are cyclins and cyclin-dependent kinases (CDKs). CDKs are a family of serine/threonine protein kinases that are activated at specific points in the cell cycle. There are five CDKs that have been associated with cell cycle progression in mammalian cells: CDKs 4 and 6, which are active during the early G1 phase; CDK2, which is active in the late G1 and S phase; CDK1, which is active during the G2 and M phases; and CDK7, which acts in combination with cyclin H as a CDK-activating kinase (CAK) (Fig. 1). The activity of CDKs is highly regulated and requires the expression of activating cyclins and phosphorylation of the cyclin-CDK complex. CDK expression levels remain stable throughout the cell cycle. In contrast to CDK expression, cyclin levels rise and fall depending on the phase of the cell cycle, enabling cyclins to periodically activate the CDKs [20, 21]. The D type cyclins, cyclin D1, cyclin D2, and cyclin D3, bind to CDK4 and CDK6 to activate these CDKs. Activation of CDK4 and CDK6 is required for entry into the G1 phase [25, 26]. Cyclin D is synthesized as long as the growth factor stimulation is present [27]. Cyclin E associates with CDK2 to regulate progression from G1 into S phase [28]. During the S phase, cyclin A binds to CDK2 to regulate S-phase progression, and during the G2 and M phases, cyclin A binds to CDK1 to promote entry into the M phase [29, 30]. An additional cyclin, cyclin B, is expressed during mitosis; cyclin B binds to CDK1 to regulate the remainder of mitosis. Cyclins are rapidly degraded by proteasomes when the cell cycle has progressed beyond the phase during which their expression is required [20].

Complete CDK activity is dependent upon cyclin expression and binding to the CDK as well as the phosphorylation of the CDK by the cyclin H-CDK7 complex, also referred to as the CAK. CAK phosphorylation of the CDKs occurs on conserved threonine residues and induces conformational changes, which can enhance the binding of cyclins to further regulate CDK activity. CDK4 activation requires phosphorylation of threonine 172 of CDK4, activation of CDK2 requires phosphorylation of threonine 160 of CDK2, and CDK1 activation requires phosphorylation of threonine 161 of CDK1 [20]. Phosphorylation of the cyclin-CDK complexes can also inhibit CDK activity. The cyclin A-CDK1 complex can be inhibited by phosphorylation of CDK1 at tyrosine 15 and/or threonine 14 by the kinases Wee1 and Myt1. The enzyme Cdc25 phosphatase can remove this inhibitory phosphate, and this dephosphorylation of CDK1 is required for the full activation of CDK1 and subsequent progression through the cell cycle [31].

Active CDKs induce downstream signaling events by phosphorylating target proteins that regulate cell cycle progression [32, 33]. One of the most frequently studied CDK substrates is the retinoblastoma tumor suppressor protein (pRB), which the CDK4/6-cyclin D complex phosphorylates to inactivate (Fig. 1). In its active state, pRb is in a complex with the histone deacetylase (HDAC) protein and the transcription factors E2F-1 and DP-1. During the G1 phase, pRb is phosphorylated, which results in its inactivation and the subsequent release of E2F-1 and DP-1. E2F-1 activates transcription of genes required for S-phase progression, including the cyclin E, cyclin A, and Cdc25 genes [34–36]. E2F also regulates the expression of genes encoding enzymes that are involved in nucleotide synthesis, such as dihydrofolate reductase, thymidine kinase, and thymidylate synthetase [37]. pRb remains hyperphosphorylated for the rest of the cell cycle, and the cyclin E-CDK2 complex stabilizes this hyperphosphorylated state. During the G1/S phase, the cyclin E-CDK2 complex also phosphorylates p27, a negative regulator of CDK2-containing complexes; this phosphorylation results in degradation of p27 [38, 39]. The cyclin E-CDK2 complexes also phosphorylate histone H1, which may be important for chromosome condensation that is required during DNA replication. Histone H1 is also a substrate for cyclin B-CDK1 complexes. Finally, the cyclin A-dependent kinases regulate initiation of DNA replication by phosphorylating the DNA polymerase alpha primase [20].

2.2.2 Negative Regulators of Cell Cycle Progression

The cell cycle is also controlled by negative regulators; these typically inhibit CDK activity. CDK activity can be negatively regulated by interacting with cellular proteins referred to as CDK inhibitors, or CKIs (Fig. 1). CKIs can either bind to isolated CDKs or to the cyclin-CDK complex to prevent activation of CDKs. There are two families of CKIs, the INK4 (inhibitor of CDK4) family and the Cip (CDK-interacting protein)/Kip (kinase inhibitor protein) family. The INK4 family includes p15 (INK4b), p16 (INK4a), p18 (INK4c), and p19 (INK4d). Members of the INK4 family of CKIs inactivate the CDKs by forming stable complexes with the isolated CDKs prior to cyclin binding. Binding of INK4 family members to CDK4 and CDK6 blocks their association with cyclin D and prevents entry into the G1 phase [20, 21]. Members of the Cip/Kip family include p21 (Waf1, Cip1), p27 (Kip1), and p57 (Kip2). These inhibitors contain a conserved region that is involved in cyclin binding and kinase inhibition [21, 40]. Members of the Cip/Kip family display a broader specificity than the INK4 family and can bind and inhibit the activities of the cyclin E-CDK2, cyclin A-CDK2, and cyclin B-CDK1 complexes [20, 21]. Interestingly, members of the Cip/Kip family of CKIs can participate in activation of the G1 phase by assisting in the assembly of the cyclin D-CDK4/6 complexes in the early G1 phase and by stabilizing this complex

throughout G1 [41]. p21 expression is controlled by the transcription factor and tumor suppressor p53. In response to cellular stresses, p53 receives signals from various cellular factors such as Ataxia Telangiectasia Mutated (ATM), Ataxia Telangiectasia and Rad3-related protein (ATR), Chk1, and Chk2, members of a signaling cascade network that responds to the detection of damaged DNA, and stimulates p21 expression and associated inhibition of cell cycle progression beyond the G1 phase [42]. Finally, PP2A phosphatases can dephosphorylate pRB, thus activating pRB so that it can bind with E2F, inhibiting E2F activity and progression of the cell cycle [43].

2.2.3 Control of the G2/M Checkpoint

Additional factors not described above are involved in the control of the G2/M checkpoint. Control of the G2/M checkpoint and progression through the G2 and M phases are critical for the replication of some viruses and are therefore summarized here.

Before the cell enters mitosis, the G2 phase allows a delay in cell cycle progression to ensure that no DNA damage has occurred and that the entire cellular genome has been replicated to generate two copies. The G2/M checkpoint, which is activated in response to DNA damage and incomplete genome replication, induces a G2 arrest and prevents entry into mitosis [44–46]. The ultimate goal of the G2/M checkpoint is to inhibit the cyclin B-CDK1 complex, which is referred to as the mitosis-promoting kinase complex (Fig. 1). Progression of the cell cycle from the G2 phase to mitosis, M phase, requires the activation of CDK1. During the G2 phase, cyclin B accumulates and forms a complex with CDK1. The cyclin B-CDK1 complex, also referred to as the M-CDK complex, is kept inactivated by phosphorylation of a pair of inhibitory sites on CDK1; phosphorylation is catalyzed by the Wee1 kinase. During the late G2 phase, the dephosphorylation of CDK1 by the Cdc25C phosphatase activates the cyclin B-CDK1 complex, which triggers entry into the M phase (Fig. 1). Thus, a balance between the activities of the Wee1 kinase and the Cdc25C phosphatase can regulate the entry of cells into mitosis. Interestingly, Cdc25C can be partly activated by CDK1, and the inhibitory Wee1 kinase may be inhibited by the active M-CDK complex. Since M-CDK can activate its own activator and inhibit its own inhibitor, this suggests that the activation of M-CDK in mitosis involves positive feedback loops [42, 44]. The cyclin B-CDK1 complex must be in the nucleus to phosphorylate the substrates that are required during mitosis [47]. The cyclin B-CDK1 complex can enter the nucleus in the G2 phase; however, since its rate of nuclear export exceeds its rate of nuclear import, the cyclin B-CDK1 complex is predominantly localized in the cytoplasm. The inhibition of nuclear export of the cyclin B-CDK1 complex leads to nuclear accumulation of the active complex, which promotes entry into mitosis [8, 44]. The cyclin B-CDK1 complex can be inactivated by the E3 ubiquitin ligase

anaphase-promoting complex (APC), which targets cyclin B for degradation. The ubiquitination of cyclin B by APC, which leads to its degradation, is essential for the cells to exit mitosis [44, 48]. The activity of APC is regulated by interaction with either of two coactivator proteins, cell division cycle protein 20 (Cdc20) or Cdc20 homologue 1 (Cdh1), both of which act on different phases of the cell cycle [49–52]. PP2A can inhibit APC through its interaction with Cdc20 [53–55]. Finally, progression through mitosis requires that spindle fibers attach to chromatids via a complex of proteins called the kinetochores that help pull the sister chromatids apart, which is essential for chromosome segregation [8, 50].

Cdc25C is usually cytoplasmic but translocates to the nucleus before the M phase. However, when Cdc25C is bound to 14-3-3 proteins, Cdc25C is sequestered in the cytoplasm, which prevents it from activating the cyclin B-CDK1 complex [56]. In the presence of DNA damage or stalled DNA replication forks, it is critical for the cells to prevent mitotic entry. Depending upon the type of DNA damage, ATM or ATR is activated, which in turn phosphorylates Chk2 or Chk1, leading to their activation. Both Chk1 and Chk2 phosphorylate Cdc25C on serine residue 216 of Cdc25C, which facilitates binding of Cdc25C to 14-3-3 proteins. Thus, Chk1- and Chk2-mediated phosphorylation of Cdc25C causes cytoplasmic sequestration of Cdc25C and prevents the activation of CDK1. The checkpoint control regulators, ATM-Chk2 or ATR-Chk1, respond to conditions such as DNA damage or inhibition of DNA replication and arrest cells in the G2 phase. These checkpoint pathways can also prevent the nuclear accumulation of cyclin B-CDK1 complexes. Finally, the cyclin B-CDK1 complex can be inhibited following activation of the p53 tumor suppressor pathway. p53 upregulates the expression of p21, which can bind to cyclin B1-CDK1 complexes and inhibit their kinase activity. Further, p53 can also inhibit CDK1 through the activation of 14-3-3σ and DNA damage-inducible 45 (GADD45) [8, 42, 44, 57, 58].

3 Viral Regulation of the G0/G1 Transition

3.1 Influenza A Virus Induces a G0/G1 Phase Cell Cycle Arrest

Influenza A virus (IAV) is an important pathogenic virus that causes influenza in humans. IAV is the most virulent human pathogen among the three types of influenza viruses and causes contagious respiratory illnesses [59–61]. There have been three human IAV pandemics during the last century, with the 1918 flu pandemic, referred to as the Spanish flu pandemic, resulting in about 50–100 million deaths worldwide [62, 63]. IAV belongs to the Orthomyxovirus family; viruses in this family are enveloped and have a single-stranded, negative-sense, segmented RNA genome. Orthomyxoviruses are unique among RNA viruses because Orthomyxoviruses replicate their genomes inside the nucleus of an infected host cell [2, 64–66].

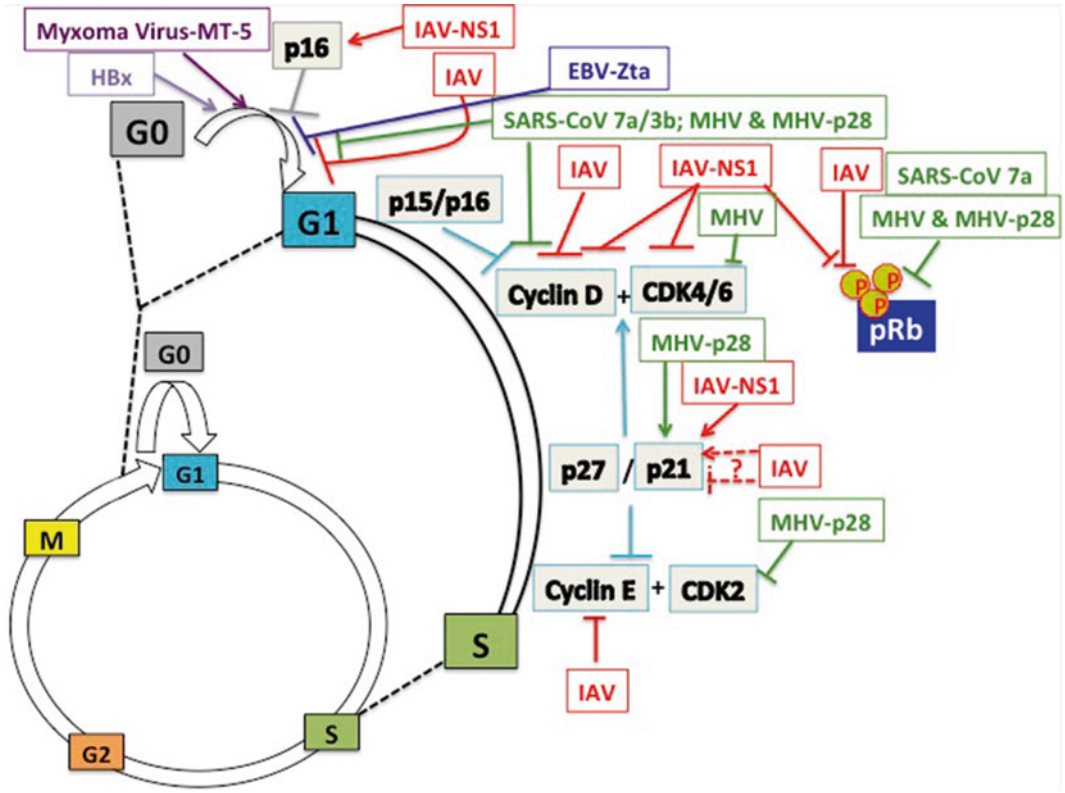

Fig. 2 Viral regulation of G0/G1 transition. Examples of viruses that can regulate the G0/G1 transition are shown. Influenza A Virus (IAV), Coronaviruses (SARS-CoA and MHV), and the Herpesvirus (EBV) encode proteins that induce a G0/G1 arrest. The mechanisms by which these viruses induce a G0/G1 arrest are shown. In contrast, some viral proteins (MT-5, encoded by the Myxoma virus and HBx, encoded by the Hepatitis B Virus (HBV)) induce progression from G0 to G1. See text and references for details

IAVs induce a G0/G1 arrest to create favorable conditions for viral replication (Fig. 2) [10, 67–69]. Influenza A H1N1 virus (a subtype of IAV) can cause a G0/G1 phase accumulation of infected A549 cells, a human lung adenocarcinoma epithelial cell line. This G0/G1-phase arrest was caused by prevention of entry of virus-infected cells into the S phase [10]. Infection with the H1N1 virus decreased the levels of hyperphosphorylated pRb, which is critical for progression of cells from late G1 to S phase. Additionally, HIN1 IAV-infected cells showed a significant increase in levels of the CDK inhibitor, p21 and a decrease in levels of the G1/S cyclins, cyclin D and cyclin E. Interestingly, cells synchronized in the G0/G1 phase and subsequently infected with H1N1 IAV had increased viral protein accumulation and progeny virus production as compared to unsynchronized cells or those synchronized in the G2/M phase. The G0/G1 arrest was also observed in cells infected with different strains of IAV, indicating that the G0/G1 arrest may be a common strategy employed by IAVs to facilitate

their own replication [10]. These results were also consistent with other studies demonstrating that influenza viruses cause an increase in the expression of the tumor suppressor, p53 [67, 69]. Since p21 expression is upregulated by p53, it was speculated that influenza virus replication might induce a G0/G1-phase arrest by regulating the p53-p21 signaling axis [10]. However, conflicting results were obtained in a different study where the p53 pathway was found to be downregulated in IAV-infected A549 cells. This study demonstrated that infection with IAV decreased the expression levels of p21 and that inhibition of p53 was important for IAV replication (Fig. 2) [70]. The reasons for these contradictory observations are unknown, and the role of p53 in IAV replication remains incompletely understood.

IAV-mediated G0/G1 arrest has also been linked to expression of the IAV nonstructural protein 1 (NS1) (Fig. 2) [68]. NS1 is a nonessential IAV protein that has a plethora of accessory functions during viral infection [71]. Of particular importance to cell cycle regulation, the NS1 protein was shown to downregulate the expression and activity of the Ras homologue gene family member A (RhoA) kinase [68]. RhoA is a small GTPase that is critical for the G1/S phase transition. RhoA inhibition can affect G1/S progression by increasing the expression levels of p21 and p27, the accumulation of p16, and decreasing cyclin D1 levels [72–75]. Overexpression of NS1 increased the levels of the CDK inhibitors, p16 and p21, whereas cyclin D1 levels decreased [68]. NS1 also decreased the phosphorylation levels of pRb, a downstream mediator of RhoA. Consistent with the observation that NS1 mediates hypophosphorylation of pRb, CDK4 and CDK6 activities were also reduced. In summary, NS1 protein was found to arrest the host cell cycle at G0/G1 via inhibition of the RhoA-pRb signaling cascade, and this was linked to the enhanced viral protein accumulation and replication [68].

While it is clear that IAV proteins can regulate the expression levels and activities of key host factors that are involved in G1/S phase transition of IAV-infected cells, precisely how the G0/G1 arrest affects IAV replication remains unclear. Although still speculative, there have been some proposed reasons for why IAV induces cells to arrest in G0/G1. For example, IAV transcription requires DNA-dependent RNA polymerase II (Pol II) [76], and the transcriptional activity of Pol II is significantly higher in the G0/G1 phase as compared to the S and G2/M phases [77]. It is therefore possible that IAV arrests cells in the G0/G1 phase to increase the transcriptional activity of Pol II, which would consequently lead to enhanced viral transcription and replication [10]. Secondly, there is evidence that the translation of influenza viral proteins is linked to host cap-dependent translation activity [78, 79]; cap-dependent translation is optimal in the G0/G1 phase and is suppressed in mitosis [80]. Therefore, a G0-G1 arrest of IAV-infected cells would prevent progression into mitosis and could enhance cap-dependent

translation of viral proteins and ultimately favor viral replication [10]. Thirdly, since cell cycle arrest can delay induction of apoptosis under certain conditions [81, 82], it is possible that IAV-mediated modulation of the G0/G1 phase prevents early death of infected cells, which would likely benefit IAV genome replication [10].

In summary, the results of many studies suggest that infection with different strains of IAV can alter initiation of the host cell cycle to maintain cells in the G0/G1 phase; retention of IAV-infected cells in the G0/G1 phase is thought to provide optimal conditions for IAV replication. In future studies, it would be interesting to determine the impact of an IAV infection on cell cycle initiation in primary human lung epithelial cells. This would provide valuable information for defining mechanisms that link IAV-dependent modulation of the cell cycle to enhanced IAV replication in the normal site of an IAV infection.

3.2 Severe Acute Respiratory Syndrome Coronavirus and the Murine Coronavirus Arrest Cells in the G0/G1 Phase of the Cell Cycle

Severe acute respiratory syndrome coronavirus (SARS-CoV) and the murine coronavirus mouse hepatitis virus (MHV) can induce a G0/G1-phase arrest of infected host cells (Fig. 2) [83–86]. SARS-CoV and MHV belong to the Coronavirus family of viruses [87]. Members of the Coronavirus family are enveloped viruses with a positive-sense, single-stranded RNA genome [2]. SARS-CoV is the causative agent of the severe acute respiratory syndrome (SARS) [87]. The genome of SARS-CoV encodes a replicase, four major structural proteins, and a number of nonstructural proteins [87–89]. The SARS-CoV 3b nonstructural protein can induce cell cycle arrest at the G0/G1 phase (Fig. 2) [83]. Additionally, the SARS-CoV 7a nonstructural protein can inhibit cell growth and induce a G0/G1-phase arrest (Fig. 2); expression of 7a was shown to decrease the levels of cyclin D3 and inhibit phosphorylation of pRb [84]. Unfortunately the effects of 3b and 7a have not been assessed in the context of SARS-CoV infection, and it remains unclear whether these effects are apparent during an authentic SARS-CoV infection. Further, the molecular mechanisms that underlie the effects of 3b and 7a on the host cell cycle remain undefined.

MHV can also modulate the cell cycle of infected cells [85, 86]. MHV causes various diseases in mice, including hepatitis and enteritis [90, 91]. The results of one study demonstrated that MHV infection inhibited cellular DNA synthesis and caused an accumulation of the infected cells in the G0/G1 phase (Fig. 2) [85]. When quiescent cells were infected with MHV and then serum stimulated, these cells failed to enter S phase. MHV infection led to a reduction in the levels of Cdk4, Cdk6, and G1 cyclins in infected cell, which led to insufficient phosphorylation of pRb and caused the cells to arrest at the G0/G1 phase [85]. Results from another study demonstrated that the MHV nonstructural protein p28 can also induce a G0/G1-phase arrest (Fig. 2) [86]. The expression of p28 induced the stabilization and accumulation

of p53, which elevated transcription of p21. The increased levels of p21 suppressed cyclin E-CDK2 activity and resulted in an accumulation of hypo- and/or unphosphorylated Rb. Whether similar effects are apparent in the context of a natural MHV infection was not determined, and future studies could focus on defining the effect of p28, in the presence of other MHV proteins and in the context of MHV replication, on the infected host cell cycle.

The effect of MHV-induced cell cycle arrest on MHV replication remains incompletely understood; however, various possibilities have been proposed [85]. The first proposed possibility is that cell cycle arrest in the G0/G1 phase may provide greater amounts of ribonucleotides for the synthesis of MHV RNA. Since ribonucleotides are precursors for synthesis of deoxyribonucleotides, an inhibition of host cellular DNA synthesis could increase the availability of ribonucleotides in cells and promote efficient MHV RNA synthesis [85]. A second proposed reason for why MHV causes cell cycle arrest is that this may prevent the induction and execution of early cell death in the MHV-infected cells [85]. MHV replication in cultured cells has been shown to lead to cell death; however, the onset of apoptosis occurs when the highest levels of MHV production are attained [92–94]. It is not yet clear how MHV can attain maximal levels of viral replication prior to cell death. In certain systems, apoptosis has been shown to follow cell cycle arrest [81, 82], but in other systems cell cycle progression is required for the induction of apoptosis [95]. It is possible that MHV-dependent inhibition of the cell cycle slows the activation of apoptotic pathways in MHV-infected cells to allow for maximum viral replication prior to apoptosis of the infected cells. A third proposed reason for why MHV may cause cell cycle arrest is that this might facilitate efficient MHV assembly [85]. Assembly of MHV occurs in the intermediate compartment between the endoplasmic reticulum (ER) and the Golgi apparatus and requires proper intracellular membrane structures [96, 97]. Since most membrane trafficking steps are disrupted during the M phase [98, 99], MHV-mediated host cell cycle arrest may lead to efficient MHV assembly [85]. A fourth proposed reason for why MHV causes cell cycle arrest is that this may be beneficial for cap-dependent translation of MHV mRNAs [85]. Due to the impaired function of the cap-binding protein, cap-dependent translation is reduced during the M phase [100]. All the mRNAs of MHV are capped at the 5′ end, and the translation of all MHV proteins, except the E protein, is cap-dependent [101]. Lastly, MHV-induced cell cycle arrest may have an important significance for MHV-induced pathogenesis [85]. Since noncycling cells are less susceptible to being killed by cytotoxic T cells [102], MHV-infected cells arrested in the G0/G1 phase may be less likely to be killed by cytotoxic T cells [85].

3.3 Additional Viruses That Regulate the G0/G1 Transition

The Zta protein of the EBV, a member of the Herpesvirus family, can induce a G0/G1 arrest [4]. Some viruses can also induce cell cycle entry in resting cells by dysregulating the G0/G1 transition. For example, the myxoma virus M-T5 protein can promote the transition of myxoma virus infected cells out of the G0 phase [103]. The HBV, a member of the Hepadnavirus family, has also been shown to induce an exit of cells from G0 into the G1 phase [104]; HBV regulation of the cell cycle will be described below.

4 Viruses That Regulate the G1 and S Phases of the Cell Cycle

4.1 Hepatitis C Virus Modulates the G1/S Checkpoint

HCV, a member of the Flavivirus family, is a small, enveloped virus with a positive-sense, single-stranded RNA genome. The HCV genome encodes a large polyprotein that is co- and posttranslationally processed to produce the mature structural core, E1 and E2 and nonstructural NS2, NS3, NS4A, NS4B, NS5A, and NS5B proteins [105, 106]. HCV infections are a global health problem that affects approximately 170 million people worldwide [107]. HCV is hepatotropic and is one of the major causes of chronic hepatitis, cirrhosis, and primary liver cancer, hepatocellular carcinoma (HCC) in humans [108]. Currently, there is no effective vaccine against HCV infection, and the standard treatment, consisting of a combination of pegylated interferon-α and a nucleoside analogue, ribavirin, produces a sustained virological response in only 50 % of the patients infected with genotype 1 and 80 % of the patients infected with genotypes 2 and 3 [109, 110]. The use of pegylated interferon-α and ribavirin has various side effects such as hematological complications. There are many new therapies for HCV infection in clinical development including Direct-Acting Antiviral Agents (DAA) and Host-Targeting Antiviral Agents. Two DAAs, the protease inhibitors boceprevir and telaprevir, which are both reversible covalent inhibitors of the HCV NS3-NS4A serine protease, have been approved for HCV treatment. Additionally, other DAAs, which are in phase III studies, include an NS5A inhibitor, NS5B polymerase inhibitors, and noncovalent NS3-NS4A protease inhibitors. Additionally, certain host-targeting antiviral agents, including inhibitors of cyclophilin A and microRNA (miR)122, have advanced to phase 2 or 3 clinical trials. The approval of boceprevir and telaprevir has led to the use of a triple therapy for HCV genotype 1 infection. A triple therapy regimen usually consists of one of these two protease inhibitors in combination with pegylated interferon and ribavirin. Although the triple therapy regimens are usually more effective than a combination of pegylated interferon and ribavirin without a protease inhibitor, they are associated with various side effects, and the combination of pegylated interferon and ribavirin remains the recommended treatment for HCV genotypes 2, 3, 4, 5, and 6 infection [109–111].

Table 1
Hepatitis C Virus (HCV) modulation of the G1/S checkpoint

HCV protein	Affect on cell cycle	Cell type	Reference
HCV core	Decreased p21 levels	Huh 7	[117]
HCV core	Increased number of cells in the S phase	HepG2	[122]
HCV core	Stimulate cell growth by downregulating p16 levels	HepG2	[113]
HCV NS3	Repress promoter activity of p21	NIH3T3	[129]
HCV NS5A	Repress transcription of p21 and increase expression of PCNA	Murine fibroblasts and HepG2 cells	[112]
HCV NS5B HCV infection	Downregulation of pRb	Huh 7.5 cells	[127]
HCV NS2	Induces cell cycle arrest in the S phase, downregulates cyclin A levels	HeLa, Huh 7, Vero	[115]
NS5B	Delays S-phase progression by interacting with CINP	U-20S, HepG2	[118]
HCV core	Arrests cell cycle progression by stabilizing p27	T cells	[131]
HCV core	Induces expression of p21	SAOS-2, HepG2	[132]
HCV core	Biphasic regulation of p21	HepG2	[130]
Full genome HCV expression	Upregulated CDK-pRb-E2F pathway, upregulated anchorage independent growth	HepG2	[114]
HCV infection	Delay in cell cycle progression	Huh7.5	[119]
Chronic HCV infection	G1-phase arrest	Patient hepatocytes	[136, 137]

Summary of the different studies that have analyzed the effect of HCV proteins on the host cell cycle. See text and references for details

HCV proteins have been shown to both promote and inhibit cell cycle progression, and it is likely that the effects of HCV on the cell cycle are influenced by the experimental system used to test HCV effects on these cellular processes. The results of several studies have suggested that one or more HCV proteins can modulate cell cycle regulatory genes to affect the G1/S checkpoint in HCV-infected cells (Table 1) [112–127]. The HCV viral core protein, which forms the viral capsid, is thought to play a vital role in the development of HCV-associated HCC [11]. The results of a recent study demonstrated that the HCV core protein decreased p21 expression in human hepatoma cells. An HCV core-induced

increase in the level of miR-345 was found to suppress endogenous p21 expression by targeting the 3′ untranslated region (UTR) of the p21 mRNA [117]. Decreases in the levels of p21 would lead to accelerated cell cycle progression, and increased p21 expression is frequently observed in human cancers [128]. Thus it is possible that the HCV core protein-induced decrease in p21 expression may contribute to HCV-induced HCC. These results are in agreement with previous studies that have shown a pro-proliferative effect of the core protein; HCV core induced S-phase progression in various cell systems and growth conditions [22, 122, 124, 125]. For example, HCV core protein expression increased the fraction of HepG2 cells, a human hepatoblastoma cell line, in the S phase by increasing the stability of the c-myc oncoprotein [122]. Additionally, the HCV core protein, expressed alone or in the context of HCV replication, promoted cell proliferation, DNA synthesis, and cell cycle progression in Huh-7 cells, a human hepatoma cell line [22]. In this system, HCV core activated the Wnt-β catenin signaling pathway, which was shown to be a major mediator of HCV core-induced cell proliferation. Results from another study in HepG2 cells also showed that the HCV core protein stimulated cell growth by decreasing the levels of the CDK inhibitor, p16 via induction of hypermethylation of the p16 transcription promoter [113]. The HCV NS3, NS5A, and NS5B proteins have also been shown to promote cell growth [126, 127]. The results of one study in NIH3T3 cells showed that NS3 mediated a p53-dependent transcriptional repression of p21 [129]. In murine fibroblasts and HepG2 cells, the NS5A protein repressed transcription of p21 and increased expression of Proliferating Cell Nuclear Antigen (PCNA), which is expressed during the S phase and required for DNA replication [112]. pRb expression was also shown to be decreased in HCV-infected hepatoma cells; decreased levels of pRb were caused by NS5B-dependent ubiquitination of pRb and subsequent proteasome-mediated degradation of pRb. Loss of pRb function in HCV-infected cells could promote hepatocyte proliferation and contribute to the development of HCC [127]. Overall, the results of these various studies suggest that HCV proteins can promote cell proliferation by affecting the cellular functions or levels of cell cycle regulatory proteins.

In contrast to the studies described above, which demonstrate a pro-proliferative effect of the HCV proteins, the results of another study demonstrated that NS2 can inhibit cell proliferation and induce cell cycle arrest in the S phase (Table 1). The induction of S-phase arrest in NS2-expressing cells was associated with decreased cyclin A expression [115]. The results of a different study also showed that the HCV RNA-dependent RNA polymerase, NS5B, delayed S-phase progression by interacting with the CDK-interacting protein (CINP) [118]. In fact, this study led to the identification of CINP and provides an example of how analyzing

viral regulation of the cell cycle may help identify novel cell cycle regulatory proteins. Similar to the NS2- and NS5B-mediated cell cycle arrest, and in contrast to studies outlined above, the results of additional studies have suggested that the HCV core protein can impair the G1 to S phase transition through various mechanisms, including induction of p21 expression and stabilization of the CDK inhibitor, p27 (Table 1) [130–132]. Interestingly, Nguyen et al. demonstrated that the HCV core protein modulates p21 expression levels in a biphasic manner [130]. The 21-kDa, immature form, of the HCV core protein can be proteolytically processed to a 19-kDa, mature form [133]. Nguyen et al. analyzed the role of the HCV core protein in cell cycle modulation by using a HepG2-derived cell line, where the expression of the HCV core protein was under the control of an inducible promoter. At early time points after induction of core protein expression, both the 21-kDa and 19-kDa forms were equally abundant in HCV core-expressing cells; however, at later time points, the 19-kDa form accumulated and became the dominant species. The 21-kDa form of the core protein was associated with an increased expression of p21 and a concomitant decrease in CDK2 activity. These changes in p21 and CDK2 activity led to a decrease in cellular proliferation. However, accumulation of the 19-kDa form caused a decline in p21 levels. These results suggest that the HCV core protein-dependent regulation of p21 expression might depend on the early presence of the immature form of the core protein or the later expression of the mature form of the core protein during an HCV infection and may provide an explanation for the conflicting observations in various studies that have analyzed the regulation of p21 by the HCV core protein. It is possible that some studies only analyzed the effect of the 19-kDa, mature form, of the core protein or that the processing kinetics of the HCV core protein may differ in the individual studies, leading to varying effects of the core protein on p21 expression [130]. Biphasic effects on cell cycle regulatory molecules have also been demonstrated for the human cytomegalovirus (HCMV), a member of the Herpesvirus family; cyclin A expression was repressed early after HCMV infection but induced at later stages of the viral infection [134]. Overall, various studies suggest that the HCV core protein modulates cell cycle regulatory proteins and plays a vital role in HCV pathogenesis; however, the exact effects of the HCV core protein on hepatocyte cell cycle modulation remain incompletely defined.

The studies described above predominantly focused on effects of HCV proteins that were expressed in isolation or outside of the context of an authentic HCV infection. The impact of expressing the entire HCV genome on the cell cycle has also been analyzed (Table 1); however, because of the lack of an efficient HCV infection system, the effects of an HCV infection on the host cell cycle

remain unclear. To begin to clarify these effects, in one study a Cre recombinase/loxP conditional system for the expression of the full-length HCV genome was generated in HepG2 cells, thus enabling the creation of a system that at least partially mimicked persistently HCV-infected hepatocytes. The results of this study showed that cells expressing the full-length HCV RNA activated the CDK-pRb-E2F pathway more effectively than observed when individual HCV proteins were expressed [114]. Full genome HCV RNA expression also enhanced anchorage-independent growth of HepG2 cells, whereas HepG2 cells only expressing HCV structural, nonstructural, or even all viral proteins showed no significant changes in anchorage-independent growth; this observation might suggest that the viral RNA itself somehow affects the cell cycle [114]. The tumor suppressor, pRb, is frequently inactivated in HCC, and HCV-mediated regulation of the CDK-pRb-E2F pathway may be one of the mechanisms responsible for the high incidence of HCC in HCV-infected patients [114, 135]. Finally, the results of a different study indicated that an HCV infection is associated with a delay in cell cycle progression. HCV-infected Huh-7.5 cells, a subline of Huh-7 hepatoma cells that can support HCV replication, showed significantly fewer cells in the S phase as compared to mock-infected cells. Further, results from gene expression analysis suggested that HCV-mediated apoptosis of Huh-7.5 cells might be a result of perturbations in cell cycle progression [119]. Interestingly, a G1 arrest was also observed in patient hepatocytes during a chronic HCV infection [121, 136, 137]. The G1 arrest was associated with increased p21 expression, which correlated with the severity of fibrosis [136]. These in vivo results suggest that the delayed cell cycle progression observed in HCV-infected Huh-7.5 cells may be physiologically relevant.

Although the studies described above provide some indications of HCV full genome effects on the cell cycle, few studies have analyzed the effects of the cell cycle status on HCV replication or the effect of the replicating virus on the cell cycle during an authentic HCV infection. Therefore, the significance of HCV-induced cell cycle arrest or proliferation for HCV replication and HCV-associated disease remains unclear. In addition, the paucity of authentic HCV replication systems, and the consequential study of HCV replication in systems that may not accurately reflect all aspects of an authentic HCV infection, has sometimes generated seemingly discrepant observations of HCV effects on the cell cycle. Although direct confirmation is lacking, various possible effects of cell cycle regulation on HCV replication have been proposed. For example, the biphasic effect of the HCV core protein on the cell cycle may be important for HCV replication, and it is possible that HCV-mediated cell cycle arrest protects cells from apoptosis during the initial stages of an HCV infection. Alternatively, during

early stages of HCV infection, the immature form of the HCV core protein may regulate the expression of proteins that are required for repressing the immune response and thus help infected cells evade immune defenses [130]. Some studies have linked the effect of the cell cycle status on the translational activity of the HCV internal ribosome entry site (IRES), which mediates cap-independent translation of the HCV RNA and is located at the 5′ end of the HCV genome. The HCV IRES-dependent translation efficiency in Huh-7 cells was highest during the G0 and G1 phases of the cell cycle but was decreased during the S phase and dramatically reduced during the G2/M phase. Therefore, it is possible that HCV proteins modulate cell cycle regulatory proteins to induce a cell cycle arrest to allow efficient HCV translation and replication [138]. It has also been proposed that HCV-mediated cell cycle arrest limits the regenerative response of the liver to ongoing injury and contributes to the progression of liver disease [121, 136, 137]. In contrast, some studies have demonstrated a positive impact of cell proliferation on HCV replication. The results of one study showed that the translational activity of the HCV IRES was greatest in cells that are actively dividing [139]. In accordance with this, findings from another study suggested that HCV replication is highly dependent on cellular proliferation, and HCV RNA synthesis was strongly enhanced in the S phase. Surprisingly, and in contrast to previous studies, the same study also showed that HCV protein expression and genome replication did not affect the cell cycle status of Huh-7 cells [120].

In summary, numerous studies have analyzed the effect of HCV infection on the cell cycle status of hepatocytes. However, most of these studies were conducted with overexpression of a single HCV protein, and the results of these studies have sometimes identified contradictory effects on cell cycle regulatory proteins. Studies involving a single HCV protein may not accurately represent the expression levels of that HCV protein in HCV-infected livers and cannot analyze the consequence of interactions between different HCV proteins that could influence the cell cycle during an HCV infection. Moreover, most HCV studies that analyzed the impact of HCV proteins on the cell cycle were conducted in immortalized or transformed cell lines. Although challenging, future studies in primary hepatocytes may help delineate the exact effects of HCV on the cell cycle during an authentic HCV infection [140]. These types of studies should also consider that HCV has several genotypes and that different disease outcomes have been reported in patients infected with different HCV genotypes [141]. Therefore, it is possible that different genotypes of HCV will have different effects on the cell cycle, which might account for some of the contradictory observations that have been reported. Recently, a genetically humanized mouse model that expresses human CD81 and human occludin and can be infected with HCV

was generated. This is the first mouse model where the entire HCV life cycle can be studied and provides new opportunities to understand the in vivo consequences of an HCV infection for hepatocyte genome replication and the cell cycle [142].

4.2 Small DNA Tumor Viruses Drive Cells into the S Phase

The small DNA tumor viruses are a group of double-stranded DNA viruses; representative examples of these viruses are papillomaviruses such as the HPV, Adenoviruses (Ad), and polyomaviruses such as the Simian virus 40 (SV40) [2, 143]. HPV infections are associated with the development of cervical, anal, and neck cancers [144]. Although SV40 and adenoviruses have not been linked to human cancers, they can immortalize and transform cells in culture [145]. The small DNA tumor viruses are dependent on the host cell DNA replication machinery for the replication of the viral genomes. These viruses typically infect differentiated, quiescent cells, which may not be an ideal environment for viral replication because the host cell DNA replication machinery is only available during the S phase [146, 147]. The small DNA tumor viruses do not encode a DNA polymerase or other enzymes that are involved in DNA synthesis [4]. Moreover, since quiescent cells have low levels of deoxynucleotides, the environment of quiescent cells may not be conducive to viral DNA synthesis. Thus, it is thought that small DNA viruses must induce S-phase entry of infected cells in order to create an environment that is favorable for viral replication. HPV, Ad, and SV40 have evolved strategies to promote unscheduled entry of infected cells into the S phase [6, 146, 147] (Fig. 3). Entry into S phase allows these viruses to use host enzymatic activities and cellular DNA precursors for their own DNA replication. Consequently, these viruses encode proteins that can affect cell cycle control mechanisms. For example, the small DNA tumor viruses encode proteins that can inhibit p53 and the Rb family members [6, 18, 19, 148–150] (Fig. 3). Inhibition of p53 and Rb family members by these virally encoded proteins induces the cells to enter S phase. Inhibition of p53 and Rb by the small DNA tumor virus proteins is also required for the cell transformation that is associated with HPV, Ad, or SV40 infections [6, 18, 145, 150, 151].

4.2.1 Small DNA Tumor Virus Oncoproteins Inhibit the Retinoblastoma Family Proteins

Transforming oncoproteins of the small DNA tumor viruses include E1A from adenovirus, E7 from HPV, and large T antigen (LTag) from SV40 [145]; these oncoproteins bind to and inactivate Rb family members, thus abrogating the need for phosphorylation by the G1 CDKs, CDK4 and CDK6 [3] (Fig. 3). The Rb family of proteins, also referred to as the pocket protein family, consists of the three proteins pRb, p107, and p130. These proteins negatively regulate the transition from the G1 to S phase [21, 152]. E1A, E7, and LTag oncoproteins contain an LXCXE (Leu-X-Cys-X-Glu, where X represents any amino acid) motif, which facilitates interaction

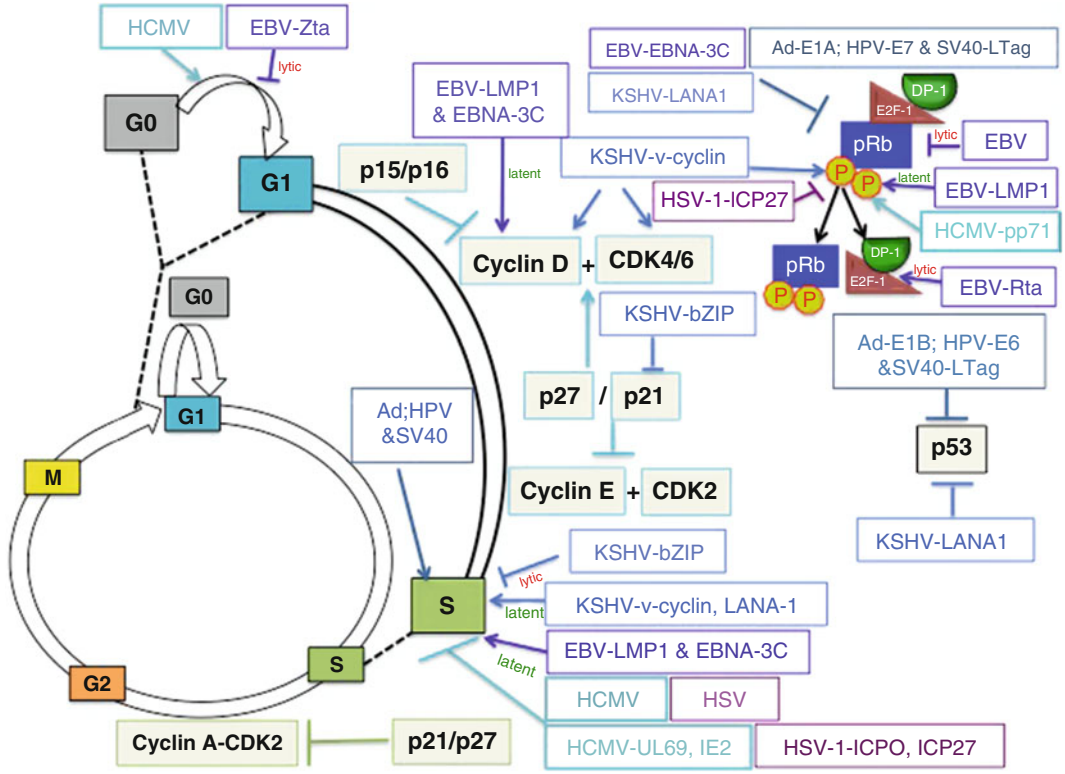

Fig. 3 Regulation of the early phases of the cell cycle by small DNA tumor viruses and the herpesviruses. Small DNA tumor viruses (Human papillomavirus (HPV), Simian virus 40 (SV40), and Adenoviruses (Ad)) and herpesviruses (Kaposi's sarcoma-associated herpesvirus (KSHV), Epstein–Barr virus (EBV), Herpes simplex virus 1 (HSV-1), and Human cytomegalovirus (HCMV)) regulate the transition from G1 to S. The mechanism used by these viruses to regulate the early phases of the cell cycle is depicted. See text and references for details

with all three members of the Rb family. The LXCXE motif interacts with a site on Rb that is referred to as the pocket region of Rb [6, 7]. The binding of E1A, E7, or the LTag to the pocket region of Rb leads to the displacement of its cellular binding partners, HDAC and E2F. The steric disruption of the E2F-Rb complexes allows the release of the S-phase transcription factor, E2F [6, 7, 146, 153–164]. In addition to disrupting the interaction of Rb with E2F, E1A and LTag can inhibit pocket protein function by inducing posttranslational modifications [146]. The results of various studies indicate that the binding of E7 to all three Rb proteins induces their degradation by the ubiquitin-proteasome pathway [7, 146, 165, 166]. Overall, the transforming oncoproteins of the small DNA tumor viruses can inactivate Rb family members and cause unscheduled progression into the S phase. Inactivation of the Rb family by E1A, E7, and LTag would lead to the induction of transcription of E2F responsive genes, which include the E2F-controlled cell cycle and DNA synthesis genes, and help establish a favorable environment for viral replication [6, 146].

4.2.2 Small DNA Tumor Virus Oncoproteins Inhibit the p53 Tumor Suppressor Pathway

The p53 tumor suppressor pathway can be activated as a response to various cellular stresses, including DNA damage. The activation of p53 either leads to the induction of cell cycle arrest to allow time for the cell to repair any DNA damage or initiates apoptosis if the DNA damage is too extensive or cannot be repaired. Infection with many different viruses has been linked to activation of p53; extensive viral DNA replication can trigger a DNA damage response that activates p53. Since the induction of cell cycle arrest or apoptosis could prevent new virus production, many viruses, including the small DNA tumor viruses, have evolved mechanisms to inactivate the p53 tumor suppressor pathway [167]. The SV40 LTag, Ad E1B, and HPV E6 oncoproteins have been shown to bind to p53 [6, 167] (Fig. 3). LTag can directly bind and inactivate p53 [168–170]. In fact, p53 was first identified as an interaction partner of the LTag and then later shown to have an important tumor suppressor activity [171, 172]. E1B and E6 can facilitate the ubiquitination and proteasome-mediated degradation of p53 via recruitment of other cellular factors that regulate this process. E1B, in conjunction with the adenovirus protein E4-ORF6, assembles into an ubiquitin ligase complex together with cellular proteins involved in ubiquitination (Cullin 5 and Elongins B/C), to target p53 for degradation [173, 174]. E6 stimulates the degradation of p53 by recruiting the cellular ubiquitin ligase E6AP-100K [175]. Overall, small DNA tumor viruses, which usually infect quiescent cells, encode proteins that bypass restriction points in the cell cycle in order to activate the host cell replication machinery and induce cell proliferation. SV40, Ad, and HPV thus create a favorable environment for viral DNA replication.

4.3 Herpesvirus Regulation of the G1 and S Phases

Whereas small DNA tumor viruses have evolved mechanisms to activate the transcription of cellular genes that generate deoxynucleotide pools for DNA replication and rely on cellular DNA polymerases, Herpesviruses encode many of these genes in their viral genomes [4, 5, 7, 148]. Members of the Herpesviruses family are enveloped viruses that contain a large, double-stranded DNA genome that typically encodes 100–200 genes. Expression of Herpesvirus genes are temporally regulated during an infection and can be classified as immediate early, early, or late genes, reflecting their relative time of expression following infection of a cell. The Herpesvirus family is subdivided into the α-, β-, and γ-herpesviruses to distinguish various biological properties including host range and speed of replication. Within an infected cell, Herpesviruses can exist in a lytic state, where most genes are expressed and the virus is actively replicating, or in a latent state where a subset of genes are expressed and the virus is not generating infectious progeny. Herpes simplex virus 1 (HSV-1) is representative of α-herpesviruses, HCMV is representative of β-herpesviruses, and EBV and KSHVs are representative of γ-herpesviruses [2, 176–179]. Several research

groups have analyzed the effects of HSV-1, HCMV, EBV, and KSHV on cell cycle regulatory pathways [4]. Here, we will describe HSV-1, HCMV, EBV, and KSHV-dependent modulation of the host cell cycle as examples of how members of the Herpesvirus family regulate the cell cycle and how this affects viral replication, cell physiology, and the development and progression of some Herpesvirus-associated diseases.

4.3.1 Kaposi's Sarcoma-Associated Herpesvirus Regulates the G1/S Checkpoint

KSHV, also referred to as human herpesvirus 8 (HHV8), is the most recently identified human oncogenic virus. KSHV is the infectious cause of Kaposi sarcoma (KS) and two lymphoproliferative disorders that are frequently found in individuals with acquired immune deficiency syndrome (AIDS); the lymphoproliferative disorders include primary effusion lymphomas (PEL) and multicentric Castleman's disease. KS is a common cancer in HIV-1 infected, untreated individuals. Although originally linked to diminished CD4 T cell levels, even HIV-infected individuals receiving anti-HIV therapy have a higher incidence of KS than is observed in the general population. Almost 20 years after the discovery of KSHV, palliative treatments for KS exist, but none are curative. Additionally, there is no vaccine against KSHV. Substantial advances have been made in understanding the pathobiology of KSHV, and potential targets for the treatment of KS have been suggested [180–183]. The KSHV genome encodes a large number of cellular orthologues that affect the cell cycle, DNA synthesis, and apoptotic pathways in KSHV-infected cells [180–182]. KSHV primarily infects endothelial and B cells [184, 185]. During the latent phase of a KSHV infection, viral gene expression is restricted to a subset of viral genes, and gene products are thought to avoid the host antiviral immune response and provide a proliferative advantage to the KSHV-infected cells. KSHV replication and transcriptional programs are fully activated upon induction of the lytic phase, where the virus progeny is produced, packaged, and released from the host cells [183, 186]. KSHV genes have been classified into three major categories: class 1 genes that are constitutively expressed, class II genes that are expressed during latency, but are upregulated during lytic replication, and class III genes that are only present during the lytic phase of a KSHV infection [186]. Most tumor cells in PEL or KS only express KSHV latent proteins, and only a small percentage of the tumor cells express lytic proteins [183].

KSHV expresses various proteins that can modulate the cell cycle of infected cells (Fig. 3); these KSHV-encoded proteins deregulate cell cycle checkpoints, promote cell cycle progression, and are thought to contribute to KSHV-mediated oncogenesis by functioning as growth factor receptors, signal transduction proteins, transcription factors, and cell cycle regulators [187].

The KSHV homologue of cellular cyclin D is known as the viral cyclin (v-cyclin). v-cyclin is expressed from the major latency

locus of the KSHV genome and is used by KSHV to hijack cell cycle control mechanisms (Fig. 3) [183, 188]. Similar to the cellular D-type cyclins, v-cyclin interacts with and activates CDK4 and CDK6 kinases; the primary target of v-cyclin is CDK6 [189]. The v-cyclin-CDK6 complex phosphorylates pRb in vitro and in vivo [189]. The interaction of v-cyclin with CDK6 causes S-phase entry and DNA replication of KSHV-infected cells [183, 188, 190, 191]. The v-cyclin-CDK6 complex can also phosphorylate other factors that are involved in the G1/S phase transition of the cell cycle. v-cyclin-CDK6 substrates include CDK2, histone H1, p27, Cdc6, and origin-recognition complex-1 [183, 191–194]. Unlike the cellular cyclin D-CDK6 complex, which usually requires CDK6 phosphorylation by a CAK for full activation, the complex of v-cyclin with CDK6 is fully active in the unphosphorylated form [195, 196]. Importantly, v-cyclin is resistant to the action of the CDK inhibitors p21, p27, and p16 [195]. v-cyclin-CDK6 complexes can phosphorylate and inactivate p21 and p27, which favors activation of the cellular cyclin-CDK2 complexes and promotes cell cycle progression [183, 197]. Although, the results of various studies demonstrate that v-cyclin can promote S-phase entry [192, 195, 198], in primary cells, v-cyclin has been shown to induce a p53-dependent growth arrest and to sensitize cells to apoptotic signals [199, 200]. The results of studies in v-cyclin-expressing transgenic mice showed that the ability of v-cyclin to promote cell survival and tumor formation was only apparent in the absence of p53 [200, 201]. Overall, these studies confirm a role of v-cyclin in regulating the cell cycle but suggest that the exact effect of v-cyclin might be influenced by experimental conditions [199].

The latency-associated nuclear antigen (LANA1) is encoded by the major latency locus of the KSHV genome. LANA1 has no homologue in the human genome [183]. LANA1 binds to the pocket region of pRb and inhibits pRB function, thereby disrupting normal G1/S checkpoint control mechanisms (Fig. 3) [202]. Similar to the oncogenic proteins of many other tumor viruses, LANA1 can inactivate the tumor suppressor, p53, highlighting the importance of evading tumor suppressor checkpoints in viral-induced oncogenesis (Fig. 3) [183].

KSHV also possesses a number of other proteins that regulate mitogenic signaling pathways to affect the cell cycle control machinery. One such KSHV mitogenic signaling protein is the KSHV G protein-coupled receptor (vGPCR). vGPCR is expressed during early phases of KSHV lytic replication [188]. This viral chemokine receptor is homologous to the human chemokine receptors CXCR1 and CXCR2 [187]. vGPCR has been shown to activate the mitogen-activated protein kinase (MAP Kinase) and AKT signal transduction pathways, which increases the expression of angiogenic factors, such as vascular endothelial growth factor (VEGF), and can contribute to cell transformation processes [107, 188, 203].

Interestingly, KSHV encodes several DNA synthesis enzymes, including thymidine kinase, dihydrofolate reductase, thymidylate synthetase, and ribonucleotide reductase. In contrast to the cellular homologues of these KSHV genes, expression of KSHV thymidine kinase, dihydrofolate reductase, thymidylate synthetase, and ribonucleotide reductase is not under the control of the S-phase transcription factor, E2F. Consequently, expression of these KSHV DNA synthesis enzymes may enable KSHV replication even when cells are not in the S phase and when pRb is active [188, 204].

All of the KSHV proteins mentioned above can modulate host cell cycle checkpoints to prevent G1/S arrest. However, the KSHV K-bZIP protein, also referred to as the replication-associated protein (RAP), can have opposite effects on cell cycle regulation (Fig. 3) [188]. K-bZIP is expressed during lytic KSHV replication and belongs to the basic region-leucine zipper family of transcription factors [188, 205]. K-bZIP causes cell cycle arrest by inducing expression of the CDK inhibitor, p21, and the CCAAT/enhancer binding protein-α [206–208]. The results of one study also demonstrated that K-bZIP directly interacts with cyclin A-CDK2 complexes and promotes G1 arrest during early phases of KSHV lytic replication [209]. The reasons for this G1 arrest are not clear, but it is possible that the KSHV-induced arrest prevents premature apoptosis during the lytic phases of replication. It is also possible that lytic-phase KSHV DNA synthesis enzymes generate a quasi-S-phase state during the cell cycle arrest, thus enabling KSHV DNA replication. Importantly, the effects of K-bZIP are apparent during lytic replication, whereas v-cyclin and LANA1 effects are typically observed during KSHV latency [188].

Overall, the results of various studies suggest that latent and lytic phases of a KSHV infection may have different effects on the host cell cycle [188]. However, it is important to note that most studies of the effect of KSHV proteins on the cell cycle were conducted when these proteins were expressed individually and not in the context of KSHV replication, and caution should be exercised when attempting to extrapolate the results of these studies to effects in KSHV-infected cells. It may be important to determine the effects of a particular KSHV protein on the host cell cycle in the context of the actual KSHV life cycle, where multiple KSHV proteins would be acting in concert [188]. Moreover, a more comprehensive understanding of the interplay of viral and cellular factors in KSHV-infected cells will shed light on the mechanism underlying KSHV-induced tumorigenesis and may enable the development-targeted therapeutic agents [180–183].

4.3.2 Epstein–Barr Virus Regulates the Early Phases of the Cell Cycle

EBV, also referred to as human herpes virus 4 (HHV4), is the causative agent of the self-limiting, lympho-proliferative disease, infectious mononucleosis. EBV infection has also been linked to the development of Burkitt's lymphoma, Hodgkin's lymphoma,

and nasopharyngeal carcinoma [210]. EBV preferentially infects B cells, and EBV-encoded latent genes can induce B-cell transformation in vitro [211].

Latent EBV infection has been associated with cellular proliferation (Fig. 3). The role of EBV latent proteins, such as Latent Membrane Protein 1 (LMP-1) and Epstein–Barr Nuclear Antigen 3C (EBNA-3C), in inducing cell cycle progression has been well characterized. LMP-1 induces the expression of cyclin D1 and phosphorylation of pRb [7, 212, 213]. EBNA-3C has also been implicated in inhibition of the pRb pathway and can bind to pRb in vitro [7]. EBNA-3C functions in a manner similar to SV40 LTag, Ad E1A, and HPV E7; EBNA-3C binds to the pocket region of pRb and inactivates its cell cycle inhibitory function [214]. EBNA-3C can also stabilize cyclin D by inhibiting its ubiquitination and subsequent degradation [215]. Viral nucleotide biosynthetic enzymes are not expressed during latency, which causes EBV to be reliant on the E2F-induced cellular gene expression for the very low level of EBV genome replication that is observed during latency. EBV might also activate the pRb-E2F pathway to facilitate cell cycle progression and division to expand the pool of latently infected cells. Unlike EBV lytically infected cells, latent EBV infection allows the long-term persistence of infected cells that can avoid the host antiviral immune response. Thus, the proliferation of latently infected EBV cells would lead to an increase of the infected B-cell population [7].

In order to study the EBV lytic replication cycle, latently EBV-infected cells are typically exposed to agents that induce a switch from latent to lytic EBV replication. EBV lytic replication has been shown to be associated with a cell cycle arrest (Fig. 3). When latently infected cells are treated with agents that induce the lytic phase of EBV replication, the EBV-infected cells stop dividing and arrest at the G0/G1 phase [4, 216–218]. The EBV immediate-early transactivator, Zta, also referred to as the lytic switch transactivator, can induce a G0/G1 arrest [218]. Zta acts at multiple distinct control points in the cell cycle regulatory machinery to mediate cell cycle arrest, including Zta induction of the CDK inhibitors p21 and p27. Expression of Zta has been shown to induce arrest in the G0 and G1 phases; however, it also induces the expression of certain S-phase genes [4, 7, 18, 217, 218]. Additionally, another EBV-encoded lytic transactivator, Rta, is thought to have a cell cycle activation function (Fig. 3). Rta can induce the expression of E2F, which would favor cell cycle progression [219]. Thus, despite the ability of EBV to cause cell cycle arrest during a lytic infection, it has also been shown to stimulate certain cell cycle activation pathways [7]. During a lytic infection, EBV inactivates pRb and expresses many EBV-encoded nucleotide biosynthetic enzymes (Fig. 3). Therefore, both cellular and viral nucleotide biosynthetic enzymes are present during an EBV lytic

infection. Since EBV encodes many nucleotide biosynthetic enzymes during a lytic infection, it is possible that EBV is relatively resistant to the changes in E2F-mediated transcription of cellular nucleotide biosynthetic enzymes [7].

Overall, EBV seems to both inhibit and stimulate cell cycle progression. The inactivation of pRb in latently EBV-infected B cells may help expand the number of infected B cells. On the contrary, since the EBV genome contains many genes required for genome replication, lytic replication in a G0 state may prevent competition from the host cell machinery for the precursors for DNA synthesis [3].

4.3.3 Human Cytomegalovirus Regulation of the Cell Cycle

HCMV, also referred to as human herpesvirus 5 (HHV5), is not generally considered an oncogenic virus; however, HCMV infection has been implicated in certain malignant diseases [220, 221]. HCMV usually infects quiescent cells in vivo, and it is therefore likely that it is beneficial for HCMV to modulate the host cell cycle to maximize viral DNA replication [222]. Some studies have shown that HCMV infection can stimulate cellular DNA synthesis; however, most of these studies were conducted in cell lines that were not permissive to HCMV replication [222–224]. The infection of quiescent fibroblasts with HCMV leads to a reentry into the cell cycle, progression through the G1 phase, and an arrest at the G1/S border (Fig. 3) [7, 222, 225–228]. Although these observations suggested that HCMV-infected cells are arrested at the G1/S border, it is important to note that these cells exhibited characteristics of early S-phase entry, including hyperphosphorylation of pRb and increased E2F transcriptional activity [222, 226, 227]. Further, infection of cycling cells with HCMV also leads to the induction of a G1/S arrest [226, 228]. It is possible that the G1/S arrest leads to an unrestricted access to the precursors of viral replication while preventing host cell DNA synthesis [227]. During lytic infection, both cell cycle arrest, mediated by the tegument protein UL69 [229] and the immediate early IE2 protein [230], and stimulatory effects, mediated by the HCMV kinase pUL97 [231], the tegument protein pp71 [232–234], and IE2 [235–237], have been observed. Since the HCMV genome does not encode nucleotide biosynthetic enzymes, it is possible that HCMV depends on cellular E2F transcriptional targets for efficiency of lytic replication. Cell cycle effects during latent HCMV infections have not been examined [7]. Thus, HCMV expresses several proteins that allow it to modulate the cell cycle towards an S-phase like environment.

4.3.4 Herpes Simplex Virus 1 Regulation of the Cell Cycle

HSV-1, also known as Human herpesvirus 1 (HHV1), is the main cause of herpes infections that occur on the mouth and lips, including cold sores and fever blisters [238]. Similar to other Herpesviruses, HSV-1 can establish both a latent and lytic infection

and can modulate the cell cycle of infected cells [4, 7]. HSV-1 cell cycle effects during latent infections remain unknown. During a lytic HSV-1 infection, HSV-1 does not stimulate the production of cellular nucleotide biosynthetic enzymes but instead induces cell cycle arrest and relies on viral nucleotide biosynthetic enzymes (Fig. 3) [7]. The results of various studies indicate that HSV-1-infected cells accumulate in the G1 phase [239–241]. Cells that are synchronized in the G0 phase and then simultaneously subjected to both serum treatment and HSV-1 infection fail to enter S phase [239–242]. HSV-1 infection also leads to an accumulation of E2F factors that are complexed with pRb and blocks cellular DNA synthesis [240, 242]. Overall, during lytic phases of HSV-1 infection, HSV-1 induces changes in cell cycle regulatory controls that are consistent with the cells arresting in the G1 phase.

The HSV-1-encoded immediate-early transcription factor, infected cell protein 0 (ICP0), can arrest cell cycle progression [243, 244]. Infected cell protein 27 (ICP27), another immediate early HSV-1 protein, has also been implicated in HSV-mediated growth arrest; ICP27 prevented phosphorylation of pRb in HSV-1-infected cells [239]. Interestingly, although pRb is hypophosphorylated in HSV-1 infected cells, the activity of CDKs that are responsible for the phosphorylation of pRb seems to be essential for HSV-1 replication, and the activity of CDKs is required for the expression of HSV-1 genes [245, 246]. Although not completely clear, it is thought that CDKs stimulate HSV-1 replication by modulating RNA Polymerase II function [247]. Further, it is possible that CDKs may enhance the ability of ICP0 to activate transcription [248]. Surprisingly, although CDK activity seems to be required for expression of HSV-1 genes, the results of two studies demonstrated that HSV-1 infection suppresses cyclin-CDK function [239, 241]. One group showed that HSV-1 infection prevents the induction of cyclin D1 and cyclin D3 following the addition of serum to serum-starved cells [239]. Additionally, results from another group showed that the infection of quiescent cells suppressed serum-induced cyclin D-CDK4/6 and cyclin E-CDK2 activity and also led to a loss of cyclin E levels [241]. However, in contrast to these studies, results of a different study showed that HSV-1 infection of serum-starved cells resulted in no change in CDK4 activity, an induction of cyclin A expression, and a transient induction of CDK2 activity [249]. These seemingly discrepant observations could be explained by a difference in the experimental systems used in these studies. The first two groups infected quiescent cells in the presence of newly replaced serum, whereas the later group infected quiescent cells in the presence of spent, not freshly replaced, medium. Thus, while the first two studies addressed the ability of HSV-1 to prevent serum-stimulated induction of cyclin-CDK function, the latter group determined whether HSV-1 infection could activate cyclin-CDK function

above the uninduced, background levels [4]. Overall, the results of these various studies suggest that HSV-1 infection may partly suppress the serum-stimulated induction of cyclin-CDK activity but probably not the basal uninduced levels. Therefore, HSV-1 infection may not completely arrest cell cycle progression, and it is possible that HSV-1 regulates cyclin-CDK activity to levels that helps support efficient HSV-1 genome replication [4].

4.3.5 Conclusions from Studies That Have Analyzed the Effect of EBV, HCMV, HSV-1 Lytic Replication on the Cell Cycle

Most of the studies that have analyzed the effect of Herpesviruses on the cell cycle have focused on lytic replication. Interestingly, similar to the small DNA tumor viruses, the human Herpesviruses can modulate pRb activity during infection [7]. Due to their restricted genome size, the small DNA tumor viruses do not encode their own DNA polymerase or other accessory factors that are required for viral DNA replication. In contrast to the small DNA tumor viruses, Herpesviruses encode a DNA polymerase and some accessory factors involved in nucleotide generation [4, 7]. During lytic replication, Herpesviruses must generate large amounts of DNA. Thus, Herpesviruses have a significant requirement for nucleotide biosynthesis, metabolic, and nucleotide polymerization enzymes. Herpesviruses can either rely on their own viral machinery for the nucleotide biosynthetic enzymes or activate cellular pathways, which leads to the accumulation of these enzymes. Since Herpesviruses encode for their own DNA polymerase, it is possible that a subset of the Herpesviruses that rely on cellular nucleotide biosynthetic enzymes modulate the pRb-E2F pathway to induce the expression of these enzymes [7]. Herpesviruses might also modulate the pRb-E2F pathway in order to synchronize infected cells in the particular cell cycle state that leads to efficient replication of the viral DNA genome [7].

Results of various studies indicate that during lytic replication, EBV, HCMV, and HSV-1 induce growth arrest [4]. Synchronization in the G1 phase is an early step in the lytic infection of these viruses [4]. These Herpesvirus-encoded growth-arrest genes are components of the infecting virion and/or immediate early genes. It appears that these viruses employ very early viral products to induce a cell cycle block, which may help ensure that the cells are arrested in G0 for EBV and G1 for HSV and HCMV before viral genome replication begins. This enables the virus to ensure that cellular DNA synthesis is blocked before the virus engages in DNA replication, which may limit competition for resources between the cellular and virus DNA replication machinery [4]. Herpesviruses also employ an additional strategy to ensure that the cell is arrested at the appropriate phase before viral replication is initiated. The immediate early gene expression of these viruses has been shown to be regulated by the cell cycle; these genes are expressed immediately before the checkpoint where the respective protein has been shown to function [4]. For example, the promoter for the Zta genes of

EBV is activated by G0 growth arrest signals [216, 217]. Furthermore, immediate-early HCMV gene expression was found to occur only when the infected cells progressed to the G1 phase [4]. Therefore, the viral cell cycle regulatory factors are activated at the appropriate point of the cell cycle where they function to induce growth arrest. Finally, HSV-1, HCMV, and EBV also encode immediate early proteins that affect the expression and function of p53. Interestingly, in addition to causing cell cycle arrest, Herpesviruses can also stimulate certain cell cycle activation signals [4]. The exact role of the cell cycle promotion signals during Herpesvirus replication is unclear. Overall, Herpesviruses appear to have evolved highly sophisticated mechanisms to regulate the cell cycle so as to favor viral replication.

4.4 Hepatitis B Virus Regulation of the Early Phases of the Cell Cycle

4.4.1 Hepatitis B Virus Replication and the Cell Cycle

The human HBV is a prototype member of the Hepadnavirus family of viruses. Hepadnaviruses are enveloped DNA viruses that predominately infect hepatocytes in their respective hosts [250]. Worldwide, there are over 350 million cases of chronic HBV infections; chronic HBV infection is the most common cause of HCC [250, 251]. Despite the availability of an HBV vaccine, HBV-related diseases remain a major worldwide health problem [252]. Although the association between chronic HBV infections and HCC is clear, there are still gaps in our understanding of how a chronic HBV infection can cause HCC.

HBV replication has been linked to modulation of cell cycle progression, and the status of cell proliferation pathways can also affect HBV replication in certain experimental systems [253]. Expression of the HBV genome in Huh7 cells caused these cells to progress through the G1 phase but inhibited entry into the S phase; similar results were seen in HepG2.215 cells, human hepatoblastoma cells that contain an integrated HBV genome and replicating HBV [254]. Additionally, the results of another study in HepG2.2.15 cells also showed decreased proliferation of HepG2.2.15 cells as compared to HepG2 cells. This study demonstrated that HBV modulates the expression levels of certain cell cycle regulatory proteins, which leads to a G1-phase arrest [255]. Alternatively, another study that examined the effect of HBV replication in Huh7 cells and primary marmoset hepatocytes demonstrated that in the context of replicating HBV, these cells stall in the G2 phase [256]. Overall, it appears that HBV regulates cell cycle progression; however, the exact effects of HBV infection on cell cycle may be influenced by the specific characteristics of the cell type used for the study [257].

A number of studies have analyzed the impact of the cell cycle phase on HBV replication. The levels of HBV DNA replication were found to vary in HepG2.2.15 cells depending on the phase of the cell cycle. HBV DNA levels were increased when HepG2.2.15 cells were arrested in either G1 or G2, whereas cell entry into the

S phase increased the levels of cellular DNA synthesis but decreased the levels of HBV replication [258, 259]. Importantly, these results were confirmed in vivo; analysis in liver specimens from HBV-infected patients showed that hepatocytes expressing the S-phase-specific marker, PCNA, contained little or no HBV-specific DNA. Similarly, most hepatocytes that contained HBV DNA were found to be negative for PCNA [259]. Overall, these results suggest that HBV replication is decreased in actively proliferating cells and is inversely correlated with cellular DNA synthesis [257, 259]. Contrary to the studies that showed that HBV replication is regulated by the cell cycle status, one group demonstrated that HBV replication is independent of the cell cycle phase in HBV-transgenic mice [260]. However, HBV-transgenic mice do not completely mimic all aspects of an authentic HBV infection; thus, it is unclear whether results from studies conducted in HBV-transgenic mice accurately reflect all the mechanisms that can regulate HBV replication [261]. Cumulatively, the results of most studies suggest that the status of the cell cycle can influence HBV replication.

4.4.2 HBx Regulation of the Cell Cycle

HBx is a multifunctional protein that is encoded by the smallest open reading frame of the HBV genome [11]. Studies of HBV replication in some cell culture systems and in various in vivo mouse models of HBV replication demonstrated that HBx has an essential role during HBV replication [11, 257, 262, 263]. HBx can modulate cytosolic calcium levels, regulate cellular signal transduction and transcription pathways, and affect numerous cellular processes such as apoptosis and cell cycle progression [262, 263]. HBx effects have sometimes varied depending on the model system and the method of HBx expression used in a particular study [11, 263]. Thus, while many functions have been attributed to HBx, these could reflect cell type-specific consequences of a limited number of upstream initiating events that are controlled by a small number of primary HBx activities [257]. This highlights the importance of analyzing HBx activities in biologically relevant systems, such as cultured primary hepatocytes, both when HBx is expressed alone and in the context of HBV replication.

We will first describe the impact of HBx expression on cell cycle progression in immortalized or transformed cell lines. The effects of HBx expression on cell proliferation pathways in cultured primary hepatocytes will be discussed in the next section. The results of studies in immortalized or transformed cells have shown that HBx can induce cells to enter the cell cycle, enter the cell cycle but stall in the S phase, or progress more rapidly through the cell cycle [264–272]. The reported variations in HBx effects may be attributed to the use of different cell lines, varying methods of HBx expression, and the experimental conditions of the study [257]. HBx expression can cause cells in the G0 phase to exit G0 but stall at the G1/S boundary; this could be interpreted as induction of

cell cycle progression beyond the G0 phase or inhibition of cell progression into the S phase. Therefore, some results that seem discrepant may actually represent varying interpretations of the same data by different researchers [257, 262]. A seminal study by the Andrisani group has provided support for the notion that HBx can have different effects on the cell cycle depending on specific cellular characteristics [268]. In these studies, two HBx-expressing cell lines were derived from the same parental AML12 liver cell line; AML12 cells are immortalized mouse hepatocytes [273]. One of the HBx-expressing cell lines displayed features consistent with that of a differentiated hepatocyte, whereas the other HBx-expressing cell line was more dedifferentiated [274, 275]. The dedifferentiated cell line displayed HBx-dependent cell cycle entry but paused early in S phase [268]. In contrast, HBx expression in the differentiated hepatocytes caused the cells to progress rapidly through the cell cycle; differentiated hepatocytes displayed HBx-dependent G1-, S-, and G2/M-phase progression [268]. Overall, the results of these studies suggest that HBx can modulate cell proliferation pathways in immortalized or transformed cells.

HBx can modulate the levels and activities of the positive regulators of the cell cycle [257]. HBx can increase the levels of cyclin D1, cyclin E, and cyclin A; activate the endogenous cyclin A promoter; promote the formation of cyclin A-CDK2 complexes; and enhance CDK1 and CDK2 activity in various immortalized and transformed cells [264, 266, 270, 276, 277]. HBx can also affect the negative cell cycle regulators, p16, p21, and p27 [257]. Results from a study in HBV-associated HCC liver sections demonstrated that the liver sections that contained high levels of methylated p16 promoters also had high expression levels of HBx. These results indicate that the expression of HBx correlates with the methylation status of the p16 promoter [278]. Similarly, HBx induced hypermethylation of the p16 promoter and downregulation of p16 protein levels in HepG2 cells [276]. Studies were also conducted in liver tissue samples from HBV-associated HCCs and corresponding HBV-infected noncancerous liver sections. HBx expression in HBV-infected noncancerous tissues correlated positively with DNA methyltransferase 1 (DNMT1) and negatively with p16 protein expression. However, in the HBV-associated HCC tissues, HBx expression still correlated positively with DNMT1 but did not correlate with the hypermethylation of the p16 promoter or with p16 protein expression. Thus, the results of this study suggest that HBx-mediated hypermethylation of p16 may play a role in the early stages of HBV-related HCC [279]. HBx has been shown to lead to both upregulation and downregulation of the Cip/Kip family members; the precise impact of HBx expression on the members of the Cip/Kip family seems to vary in different cellular contexts [257]. HBx increased p21 levels in NIH3T3 cells, a mouse embryonic fibroblast cell line, when p53 was present but

did not increase the level of p21 when p53 was knocked down [280]. However, in a different study, HBx was found to increase p21 levels in Hep3B cells, a p53 mutant HCC cell line [281]. In Huh7 cells, HBx expression increased proteasomal degradation of p27 [270]. Interestingly, the results of a study in Chinese hamster ovary cells showed that the level of HBx expression influenced its effects on p21 and p27. Low levels of HBx expression resulted in an increased activity of the p21 and p27 promoters. On the contrary, when HBx was expressed at high levels, there was an inhibition of the activity of the p21 and p27 promoters [282]. This study suggests that the observed effects of HBx on CKIs can be influenced by the experimental conditions.

4.4.3 HBx Regulation of Cell Proliferation in Primary Hepatocytes

Most of the studies described above were conducted in immortalized or transformed cell lines and when HBx was overexpressed in the absence of other HBV proteins, which could contribute to the varying HBx effects that were observed. Since cellular signaling pathways that control normal cell cycle progression are usually altered in established cell lines, the effects of HBx in these cells could reflect functions that are valid in a specific cellular context but are not present in normal hepatocytes, which are the site of an authentic HBV infection. Recent studies in cultured primary hepatocytes have analyzed the effect of HBx expression, both when HBx is expressed alone and in the context of HBV replication, on hepatocyte cell cycle regulatory pathways (Fig. 4). HBx decreased the expression level of both p15 and p16 in cultured primary rat hepatocytes. Additionally, HBx increased the expression of p21 and p27. Thus, HBx expression decreased the levels of the CDK inhibitors that maintain the quiescent status of hepatocytes but increased the levels of the CDK inhibitors that prevent cell cycle progression past the late G1 phase [104]. Similar results were apparent in primary mouse hepatocytes; HBx increased the expression of both p21 and p27 and decreased cellular DNA synthesis [283]. An increase in cyclin D1 and cyclin E expression was also observed in HBx-expressing cultured primary rat hepatocytes. However, HBx expression did not induce a change in the levels of S-phase activating proteins, including cyclin A and PCNA, indicating that HBx expression in normal hepatocytes does not induce entry into the S phase [104]. Importantly, similar effects were observed in primary rat hepatocytes when HBx was expressed in the context of the HBV genome and in the presence of other HBV proteins [104]. Further, these effects of HBx were also confirmed in cultured primary human hepatocytes [284]. Although HBx upregulated CDK4 activity in primary rat hepatocytes, the increase in cyclin E expression levels was not associated with an increase in CDK2 activity [104]. Overall, the results of these studies suggest that HBx induces quiescent hepatocytes to exit G0 but stall in the G1 phase.

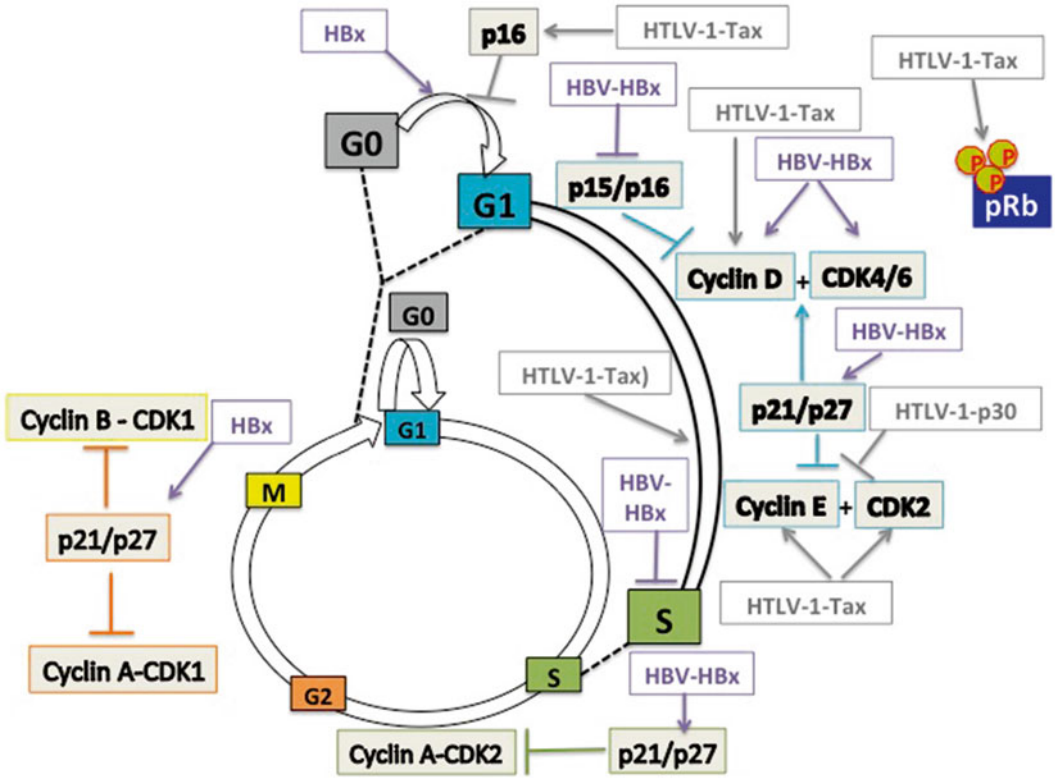

Fig. 4 Modulation of cell proliferation pathways by HBV (HBx) and HTLV-1. The effect of HBV (HBx) on cell proliferation pathways in primary hepatocytes is depicted. Human T-cell lymphotropic virus type I (HTLV-1) encodes proteins, such as Tax and p30, which regulate cell cycle progression. See text and references for details

HBx-mediated exit of hepatocytes from G0 but subsequent HBx-induced arrest of hepatocytes at the G1/S phase border was shown to be critical for HBV replication in cultured primary rat hepatocytes [104]. The entry of quiescent hepatocytes into the G1 phase was necessary for the activation of the HBV polymerase [285]. The inhibition of S-phase progression was proposed to be important for HBV replication because the stalling of the cell cycle at the G1/S border might prevent competition between the host cell DNA replication machinery and the HBV replication machinery for available deoxynucleotide triphosphates (dNTPs). Since the levels of dNTPs in quiescent cells are low [286], it is possible that HBx modulation of the cell cycle may lead to an increase in the levels of cellular dNTPs that are available to the HBV polymerase. Interestingly, HBx upregulated the expression of active ribonucleotide reductase in cultured primary rat hepatocytes [285]. Cumulatively, these observations in primary hepatocytes suggest that HBx modulation of cell proliferation is essential for HBV replication. Alterations in cell cycle proteins and their regulatory

mechanisms have been linked to cancer development [287], and HBx-induced changes in normal proliferation pathways of quiescent hepatocytes may facilitate HBV replication while ultimately proving detrimental to normal hepatocyte physiology and contributing to processes that influence the development of HBV-associated liver transformation [285].

4.4.4 HBx and Liver Regeneration

Several groups have used HBx-transgenic mouse models to analyze the effect of HBx expression on liver regeneration. However, because of differences in mouse strains and experimental protocols and because hepatocyte proliferation was analyzed at different times after a partial hepatectomy (PH), it is difficult to compare the results from the different groups [11]. Two of the studies suggested that HBx expression inhibits liver regeneration [288, 289], whereas the results of another study suggested that HBx did not affect total hepatocyte division but caused a subpopulation of HBx-expressing hepatocytes to enter the cell cycle prematurely [290]. These studies used mouse models in which HBx expression was controlled by the human antithrombin III gene promoter [288], the mouse albumin gene promoter [289], or the human α1-antitrypsin regulatory region [290]. Although these promoters function in hepatocytes, because the endogenous HBV HBx transcription promoter was not used to drive HBx expression, variations in the level of HBx expression that may not completely mimic normal levels of HBx and may vary between these different promoters could have influenced the HBx-mediated effect on hepatocyte proliferation. Recently, a novel HBx transgenic mouse model was generated; in these mice, HBx expression was under the control of endogenous HBx viral regulatory elements. In these mice, HBx caused delayed cell cycle progression and liver regeneration that was linked to HBx-induced IL-6 overexpression [291]. Thus, the results of this study were consistent with the previously described antiproliferative effects of HBx expression on liver regeneration. Although this system could be argued to more accurately reflect endogenous HBx levels during an HBV infection, unfortunately mRNA splice sites, which are not present in the HBV genome, and a foreign, non-HBx mRNA 3′ noncoding region were included, which likely affected HBx expression levels. Therefore, this system also does not completely mimic HBx expression during an authentic HBV infection. Cumulatively, the studies in HBx transgenic mice have demonstrated that HBx can regulate hepatocyte proliferation pathways; however, the exact impact seems to vary in different mouse models. Determining the impact of HBx expression on liver regeneration will likely provide a more accurate understanding of the effects of HBx on hepatocyte proliferation pathways in vivo. The impact of HBx on liver regeneration could be an important HBx activity that influences the development of HBV-associated HCC.

4.5 Human T-Cell Lymphotropic Virus Type I Regulation of Cell Cycle Progression

Human T-cell lymphotropic virus type I (HTLV-1) is a human oncogenic Retrovirus. Retroviruses are enveloped viruses containing a single-stranded positive-sense RNA genome; two copies of the genome are contained within each virion [292, 293]. HTLV-1 is the causative agent of Adult T-cell Leukemia (ATL), which is an aggressive malignancy of CD4+ T lymphocytes [294–296]. HTLV-1 infects an estimated 15–20 million people worldwide [293], and ATL can occur in approximately 2–5 % of the HTLV-1-infected individuals [297, 298]. HTLV-1 has also been implicated as the causative agent of tropical spastic paraparesis/HTLV-associated myelopathy (TSP/HAM) [293]. HTLV-1 is associated with malignancies that are characterized by excessive proliferation of T cells [299].

The HTLV-1 transactivator, regulatory protein, Tax is both necessary and sufficient for cell transformation and is considered to be a viral oncoprotein. Tax is a potent activator of HTLV-1 and cellular gene expression [297, 300]. The results of various studies suggest that Tax can prevent programmed cell death and increase the proliferation of HTLV-1-infected cells [297, 300]. Tax expression in cells can accelerate progression through the G1 phase and induce defects in the G1/S checkpoint, S phase, G2/M checkpoint, and the M phase [297, 300]. The oncogenic potential of Tax is thought to depend on its ability to modulate the expression levels of genes involved in cell proliferation pathways as well as the interaction of Tax with cell cycle regulatory proteins [300]. HTLV-1-transformed cells display genomic instability. Tax can inhibit cellular DNA repair pathways and override cell cycle checkpoints. These effects are thought to contribute to genomic instability and ultimately lead to Tax-mediated cellular transformation [300]. It is not clear if Tax directly inhibits DNA repair or if Tax inhibition of cell cycle checkpoints allows HTLV-1-infected cells to replicate damaged DNA and undergo mitosis before the damaged or altered DNA is repaired [300].

Cells expressing Tax have an accelerated progression through the G1 phase [301, 302] (Fig. 4). Several different mechanisms have been proposed to explain Tax-mediated disruption of G1 phase regulatory mechanisms and accelerated progression into the S phase [300]. Tax expression can activate transcription of cyclin E and cyclin D2 mRNAs [300, 302]. Tax also directly interacts with CDK4 and CDK6 and stabilizes cyclin D-CDK4 complexes [297, 303]. The results of one study indicated that Tax can stimulate CDK4 activity, and this activity correlated with the direct binding of Tax to CDK4. The cyclin D2-CDK4-Tax complex phosphorylated pRb in vitro, and the amount of phosphorylated pRb correlated with the degree of Tax protein binding to CDK4. Additionally, the cyclin D2-CDK4-Tax complexes were resistant to repression by the CDK inhibitor, p21 [303]. Tax can also stimulate proteasomal degradation of pRb, which would affect cell cycle

progression by promoting passage through the G1/S checkpoint [304]. Further, Tax can activate the transcription of CDK4 and CDK2 [305] and repress the transcription of the CDK inhibitors, p18 and p19 [305, 306]. Tax can directly bind to p16 and prevent it from binding and inhibiting CDK6 [307]. Finally, Tax can inhibit p53 activation [308, 309]. Overall, the results of various reports suggest that the HTLV-1 Tax protein can disrupt normal cell cycle controls.

In contrast to the studies described above, the results of other studies have suggested that infection with HTLV-1 and the expression of Tax may not be sufficient to induce cell proliferation; the accumulation of certain genetic defects, such as those induced by IL2 or somatic mutations that inactivate the CDK inhibitors p21 and p27, may be necessary to override cell cycle checkpoints and stimulate cell proliferation [310–312]. Results of one study showed that HeLa cells infected with HTLV-1 or transduced with Tax arrested in the G1 phase; HTLV-1 infected cells, similar to the cells transduced with Tax, expressed high levels of p21 and p27 [310]. On the contrary, HOS (human osteosarcoma lineage) cells continued to proliferate after HTLV-1 infection or Tax expression; however, these cells demonstrated a reduced growth rate and exhibited mitotic aberrations. Constitutive activation of the P13K/Akt pathway in HOS cells leads to a reduction in the expression of p21 and p27, which allows HTLV-1 and Tax-induced G1 arrest to be reverted. Similar to Tax effects in HeLa cells, HTLV-1 infection or Tax expression also caused human SupT1 T cells to arrest in the G1 phase [310]. The results of this study suggest that an HTLV-1 infection usually leads to a Tax-mediated G1 arrest. Alternatively, T cells containing somatic mutations that inactivate the CDK inhibitors, p21 and p27, may proliferate after an HTLV-1 infection [310]. It is thought that in the context of an HTLV-1 infection, Tax promotes cell proliferation; oligoclonal expansion of infected T cells can lead to the onset of ATL. However, this cannot completely explain the long clinical latency of ATL following an HTLV-1 infection. The results of this study suggest that the oncogenic potentials of Tax could be revealed only when HTLV-1 infects or reactivates from T cells whose p21 and p27 function and/or expression has been lost [310]. The HTLV-1 accessory protein, p30, has also been shown to interact with cyclin E, reduce the function of cyclin E-CDK2 complexes, and delay the cell cycle before entry into S phase (Fig. 4) [311]. p30 also binds to the mRNA encoding the Tax/Rex proteins to prevent its nuclear export. Since Tax and Rex are positive regulators of viral gene expression, their inhibition by p30 leads to a decrease in virus expression [313]. This is thought to be beneficial for the establishment of a latent and persistent infection [311]. Since HTLV-1 is a highly immunogenic virus and has low genetic variability, a controlled and reduced expression of the viral proteins could be

essential for viral maintenance in the course of a natural infection. The different effects of Tax and p30 on cell cycle regulation may be reflected in their different effects on HTLV-1 replication; Tax is a positive regulator of HTLV-1 replication, whereas p30 is a negative regulator [311, 314]. It is possible that rapid proliferation of cells is required at certain stages of HTLV-1 replication; however, uncontrolled proliferation of infected cells may lead to expression of viral proteins [311]. Therefore, HTLV-1 seems to have also evolved strategies that prevent rapid division of the infected cells [311]. Finally, the results of additional studies suggest that HTLV-1-encoded small proteins, such as p30 and p12, help the infected cells to evade immune defenses and prevent elimination of infected cells by host immune cells [311, 315–321]. Overall, a number of studies have analyzed the effects of various HTLV-1 proteins, particularly Tax, on the host cell cycle. However, the exact effects of these viral proteins on the cell cycle are not yet completely defined, and future studies should focus on understanding the effects of HTLV-1 proteins on the cell cycle in the context of an HTLV-1 infection and in primary T cells.

5 Viral Regulation of the G2/M Checkpoint

Some DNA and RNA viruses can induce cell cycle arrest at the G2/M phase [8]. In this section, we summarize strategies used by viruses to elicit a G2/M arrest and the potential advantages of a G2/M arrest for viral replication.

5.1 Viral Strategies for Inducing G2/M Arrest

5.1.1 Inactivation of CDK1

A number of viruses encode proteins that inhibit the activity of the cyclin B1-CDK1 complex [8] (Fig. 5). Examples include the ORF20 gene of Murine gamma herpesvirus 68 virus (MHV68), the Agnoprotein of JC human polyomavirus, ICP0 of HSV-1, E4 proteins of the HPV1, and the ς1s protein of serotype 3 reovirus, a member of the Reovirus family; members of the reovirus family are non-enveloped and contain a segmented, double-stranded RNA genome [2, 8, 322–327]. The activity of the mitosis-promoting cyclin B1-CDK1 complex can be negatively regulated by phosphorylation of CDK1 [44]. Expression of MHV68 ORF20 can induce a G2/M arrest. ORF20 expression increased CDK1 phosphorylation; the ORF20-mediated G2 arrest was a result of inactivation of the cyclin B-CDK1 complex [323]. Cells expressing Agnoprotein, which is encoded by the human neurotropic JC virus, accumulate at the G2/M phase. Agnoprotein-expressing cells showed a decrease in the expression levels and the activities of cyclins A and B. Further, Agnoprotein also stimulated p21 promoter activity, and cells continuously expressing Agnoprotein showed higher expression levels of p21 [322]. ICP0, a multifunctional HSV-1 immediate early gene product, can also induce a

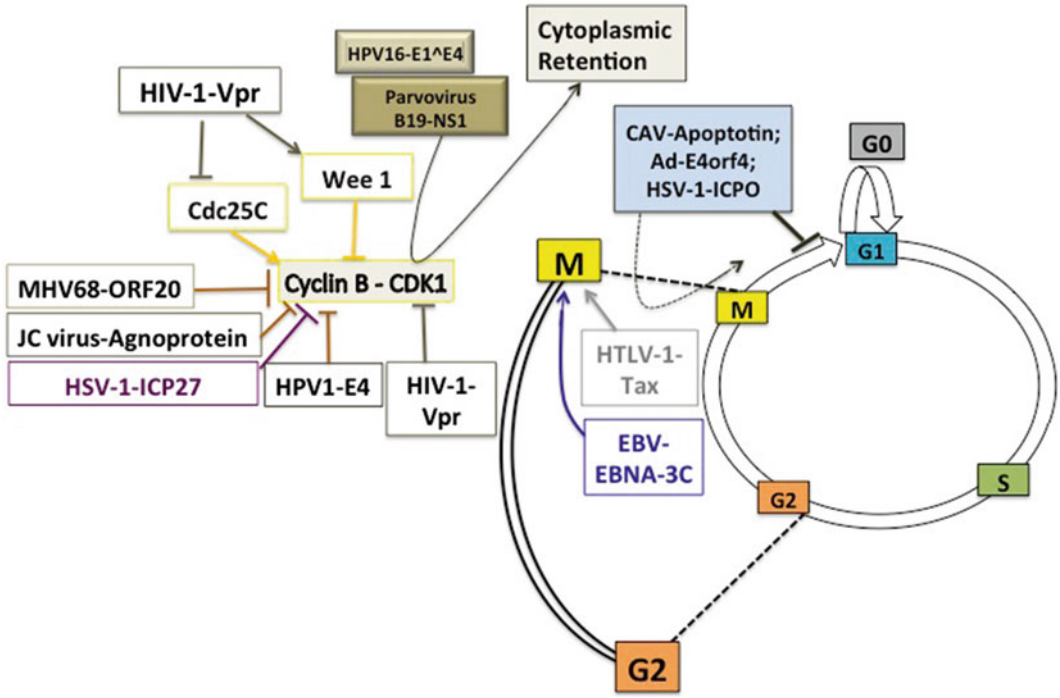

Fig. 5 Examples of viruses that regulate the G2/M checkpoint. Various strategies by which viruses can induce a G2/M arrest (Inactivation of the cyclin B-CDK1 complex, Cytoplasmic retention of cyclin B-CDK1 complexes, and Inhibition of mitotic exit) are depicted. The Vpr protein of human immunodeficiency virus type 1 (HIV-1) induces a G2/M arrest; some of the mechanisms by which Vpr induces a G2/M arrest are shown. See text and references for details

G2/M arrest. ICP0-induced G2/M arrest was shown to require ATM and Chk2 and correlated with phosphorylation of Cdc25C on serine 216 [324]. Phosphorylation of Cdc25C on Ser216 inactivates Cdc25C. Cdc25C is required for activation of CDK1, and inactivation of Cdc25C is an important event in establishment of the G2/M checkpoint [42, 44]. HPV1 E4 also elicits a G2/M arrest, and cells that expressed two E4 proteins (E4-17K/16K) contained inactive CDK1 complexes. During the infectious cycle of HPV1, a full length E1^E4 protein (E4-17K) is present, along with other smaller E4 polypeptides, including E4-16K, which arise by sequential cleavage of residues from the N-terminus of E4-17K. The inactivation of CDK1 was shown to be the result of an inhibitory phosphorylation on residue Tyr15 of CDK1, and the cells were found to contain elevated levels of Wee1. The kinase Wee1 inhibits CDK1 [42, 44]; interestingly, the depletion of Wee1 in cells co-expressing E4-17K and E4-16K alleviated the G2/M arrest [325]. Serotype 3 reoviruses-induced G2/M arrest was shown to require the viral S1 gene-encoded ς1s nonstructural protein. Serotype 3 reovirus infection caused a significant reduction in CDK1 activity and was associated with an increase in the

inhibitory phosphorylation of CDK1. The ς1s protein was required for the inhibitory phosphorylation of CDK1 [326]. The Human Herpesvirus 6A (HHV-6A) can also induce a G2/M arrest. HHV-6A infected cells had a decrease in the activity of the cyclin B1-CDK1 complex [328]. The inactivation of the cyclin B1-CDK1 complex was associated with an increase in the inhibitory phosphorylation of CDK1, which was a result of elevated Wee1 expression and inactivation of Cdc25C. Moreover, HHV-6A infected cells had increased expression of p21; this elevated p21 expression was p53-dependent [328]. p21 can bind to the cyclin B1-CDK1 complex, inhibit its activity, and prevent G2/M transition. Finally, HHV-6 infection activated the DNA damage checkpoint kinases Chk2 and Chk1. Thus, HHV-6A infection induces a G2/M arrest by reducing cyclin B1-CDK1 activity through various regulatory mechanisms [328]. SV40 and EBV have also been reported to induce a G2/M arrest [329]. SV40 infection prevents activation of the cyclin B1-CDK1 complex, and this has been linked to maintenance of CDK1 phosphorylation [329]. A recent study showed that the EBV LMP-1 induces a G2/M-phase arrest; 14-3-3 sigma and Reprimo were found to be upregulated in LMP-1 expressing cells [330]. 14-3-3 sigma and Reprimo are p53-regulated inhibitors of G2/M progression [331, 332]. Expression of 14-3-3 sigma can result in an inhibition of the activity of various CDKs, including CDK1 [333]. Further, p53 expression results in increased mRNA levels of Reprimo and leads to the induction of a G2/M arrest. In arrested cells, Reprimo can inhibit the activity of CDK1 [331]. Taken together, the various studies described here demonstrate that many viruses affect the activity of the mitosis-promoting kinase complex, cyclin B-CDK1, in order to induce a G2/M arrest.

5.1.2 Cytoplasmic Retention of Cyclin B1-CDK1 Complexes

Interestingly, even in the presence of active cyclin B1-CDK1 complexes, mitosis can be inhibited, provided these mitosis-promoting kinase complexes are prevented from accumulating in the nucleus [8] (Fig. 5). The viral E1^E4 protein of HPV16 uses a novel mechanism to induce G2 arrest. E1^E4 does not inhibit the kinase activity of the cyclin B1-CDK1 complex. Instead, E1^E4 sequesters the cyclin B1-CDK1 complexes on the cytokeratin network, which prevents the accumulation of active cyclin B1-CDK1 complexes in the nucleus and thus inhibits entry into mitosis [334]. A mutant of the E1^E4 protein of HPV16 that did not bind or colocalize with cyclin B1 failed to induce a G2 arrest [334]. Additionally, in vivo studies lend further significance to these in vitro observations; HPV-16 induced lesions showed cyclin B1-CDK1 activity on the cytokeratin filament network of the E1^E4-expressing cells [334]. The G2 arrest induced by the parvovirus B19 NS1 protein appears to use a mechanism that is similar to the HPV 16 E1^E4 protein-dependent regulation of cyclin B1-CDK1 localization. B19 virus-infected cells have enhanced

activity of the cyclin B1-CDK1 complex; however, B19 infection causes an accumulation of cyclin B1 in the cytoplasm, thereby resulting in a G2/M arrest [335].

5.1.3 Inhibition of Mitotic Exit

Some viruses induce a G2/M arrest by allowing the cells to enter but not exit mitosis [8, 336] (Fig. 5). Examples include the effects of apoptotin protein from chicken anemia virus (CAV), E4orf4 from adenovirus, high-risk HPV E2 proteins, pUL97 and pUL21A from HCMV, ICP0 from HSV-1, and EC27 from baculovirus [54, 55, 337–344]. The CAV protein Apoptotin associates with subunit 1 of the anaphase-promoting complex/cyclosome (APC10) and induces a G2/M arrest by inhibiting the function of APC10. Expression of Apoptotin caused disruption of the APC10 complex and stabilization of APC substrates [337]. The adenovirus E4orf4 can also elicit a cell cycle block at the G2/M phase. E4orf4 alters the activity of APC to either activate or inhibit the APC; E4orf4 regulates APC in a PP2A-dependent manner [54, 55]. The detailed mechanisms that underlie E4orf regulation of APC are unknown, and it has not yet been shown whether this regulation occurs during adenovirus infection [336]. The HPV E2 proteins from high-risk but not low-risk HPV strains induce a G2/M block, which is independent of E6 and E7. E2-expressing cells that escaped the mitotic block displayed genomic instability. E2 proteins from high-risk HPV strains can also bind directly to Cdh1 and Cdc20, which are APC activators, delocalize Cdh1 to insoluble cytoplasmic aggregates, and cause the accumulation of APC substrates like cyclin B. These results suggest that the high-risk HPV E2 proteins may contribute to the oncogenic potential of HPV by inducing genomic instability [338]. The HCMV viral protein kinase pUL97 also induces Cdh1 phosphorylation during HCMV infection, which prevents the binding of Cdh1 to APC [339]. Further, during HCMV infection, HCMV pUL21A interacts with APC and targets APC4 and APC5, which are two bridge subunits of APC, for proteasomal degradation and thus leads to disruption of APC [340]. Taken together, these studies suggest that HCMV uses several mechanisms to ensure that the APC is inactivated [16, 336]. HSV-1 uses a different strategy to prevent mitotic exit. HSV-1 ICP0 induces the degradation of the kinetochore proteins, centromeric protein A (CENP-A) and CENP-C, and therefore, causes kinetochore structural defects and mitotic delay [341, 342]. Finally, the baculovirus EC27 protein is thought to act as a nondegradable cyclin B1-CDK1 analogue; however, the inhibition of mitotic exit by EC27 is not well understood [343, 344]. Additional descriptions of how viruses regulate APC can be found in a series of recently published comprehensive reviews regarding this topic [53, 336]. Overall, the results of studies described here demonstrate that many viruses can induce a G2/M arrest by interfering with mitotic progression.

5.1.4 Human Immunodeficiency Virus Type 1 Viral Protein R Induces a G2/M Arrest

HIV is a lentivirus, and a member of Retrovirus family. HIV infections can cause acquired immunodeficiency syndrome (AIDS) [345]. Two types of HIV have been characterized, HIV-1 and HIV-2; HIV-1 has higher virulence and infectivity and is the causative agent of the majority of HIV infections globally [345–347]. HIV-1 viral protein R (Vpr) is a virion-associated multifunctional accessory protein that affects multiple stages of the HIV-1 life cycle [348]. Various studies have highlighted the importance of Vpr for viral replication and pathogenesis in vivo. Vpr can activate the HIV-1 long terminal repeat (LTR) promoter and can induce a G2 arrest and apoptosis [345, 348–350].

The results of several studies have shown that HIV-1 Vpr can inhibit cell proliferation by arresting HIV-1-infected cells in the G2/M phase [348, 351] (Fig. 5). Vpr induces a G2 arrest through Tyr15 hyperphosphorylation of human CDK1 [352, 353], the CDK which regulates the entry into mitosis in all eukaryotic cells [44]. Vpr can directly bind and inhibit the phosphatase activity of Cdc25 [354]. Vpr can also stabilize and promote the kinase activity of Wee1 [355, 356]. Vpr-mediated activation of Wee1 and inhibition of Cdc25 promote phosphorylation of CDK1 during induction of G2 arrest [356–358]. The results of recent studies support the involvement of the ubiquitin proteasome system in the Vpr-induced G2 arrest [359–362]. In these studies, Vpr promoted the coordination of a E3 ubiquitin ligase complex comprised of Cullin 4A, damaged DNA-binding protein 1 (DDB1), and Vpr-binding protein (VprBP) [359–362]; this ubiquitin ligase complex ubiquitinates a specific substrate that promotes G2/M transition and thus leads to its degradation [16, 348]. Interestingly, the inhibition of polyubiquitination or the suppression of proteasome-mediated degradation alleviated the Vpr-induced G2 arrest [359, 362]. The cellular substrates that are specifically targeted by the Vpr-mediated ubiquitin proteasome system for induction of a G2/M arrest are not yet known. Identifying these substrates would lend further insight into the G2/M regulation by Vpr [16, 348].

A number of studies have analyzed the cause underlying the Vpr-induced G2 arrest, and cell cycle checkpoint proteins have been shown to be involved. Vpr and the eukaryotic DNA damage or the DNA replication checkpoint controls induce G2 arrest through the inhibitory phosphorylation of CDK1 that is regulated by Wee1 or Cdc25, and it was thought that Vpr might induce G2 arrest through the DNA damage or replication checkpoint pathways [348, 351]. However, studies in human cells showed that Vpr does not induce a G2 arrest through the DNA damage checkpoint pathway [348, 351]. Two observations which support this conclusion are that Vpr can induce G2 arrest in cells from patients with ataxia telangiectasia, which is a disorder caused by a defect in the ATM gene [358] and that Vpr expression does not increase gene mutation frequencies [363]. Instead, activation of

human ATR plays a major role in the Vpr-induced G2 arrest through Ser345 phosphorylation-dependent activation of Chk1 [364–367]. Overall, the results of these studies suggest that the Vpr-induced G2 arrest may be similar to the activation of the DNA replication checkpoint rather than the DNA damage checkpoint control [348, 351]. The results of additional studies have shown that Vpr can also induce genomic instability, formation of micronuclei, and aneuploidy, which could be sensed as replication stresses that would lead to the activation of the DNA replication checkpoint [351]. Interestingly, the results of a recent study have led to the proposal of a novel mechanism underlying Vpr-induction of a G2/M arrest; the results of this study showed that the Vpr-induced G2 arrest occurs through an S-phase dependent mechanism. Although Vpr is well known to induce a G2/M arrest, the initiating event occurred in the S phase. Vpr-induced Chk1 Ser345 phosphorylation occurred in the S phase, and Vpr-expressing cells completed the S phase but arrested at the G2/M boundary. The results of this study also showed that the DNA licensing factor Cdt1 was responsible for Vpr-mediated phosphorylation of Chk1 at Ser345 and for the G2 arrest induced by Vpr. This suggests that the Vpr-induced Chk1 phosphorylation and G2/M-phase arrest may be triggered during the onset of DNA replication [365]. Finally, PP2A is also involved in the Vpr-mediated G2 arrest; okadaic acid, which is a specific inhibitor of PP2A, blocks the Vpr-induced G2/M arrest in both fission yeast and human cells [352, 368]. PP2A is a regulator of Cdc25C and G2/M checkpoint activation. Other viruses, including adenoviruses and HTLV-1, can also modulate the activity of PP2A [54, 369]. Both adenovirus E4orf4 and HTLV-1 Tax can induce a G2/M arrest [54, 370–372], and modulation of PP2A may be one of the strategies used by many viruses to induce a G2 arrest.

The results of studies with Vpr provide important examples of how viral proteins can manipulate cellular pathways at various points in order to promote efficient viral replication. The suppression of cell proliferation and G2 arrest induced by Vpr is thought to suppress human immune function by inhibiting T-cell clonal expansion [373]. Further, a Vpr-induced G2/M arrest is thought to provide an optimal cellular environment to achieve maximum levels of HIV-1 replication. The expression of HIV RNA is optimal in the G2 phase, and the ability of Vpr to manipulate the cell cycle and keep the cells in the G2 phase leads to an indirect increase in HIV LTR expression. Finally, Vpr expression leads to increased HIV-1 production, which correlated with increased LTR promoter activity in the G2 phase of HIV-1 infected cells. Overall, HIV-Vpr maximizes viral production in vivo by delaying cells in the G2 phase, where the HIV LTR is most active [349].

5.1.5 Advantages of G2/M Arrest During Virus Life Cycle

Induction of G2/M arrest by various viruses is thought to help establish a pseudo-S-phase state that may be more favorable for viral replication [8]. In this pseudo-S phase, although cellular DNA replication is complete, the cellular environment is such that the substrates and the machinery for DNA replication are available. This extends the amount of time available to DNA viruses for replication of their genomes. For some DNA viruses, this continuous replicative state can lead to an increase in viral genome copy number [8]. The levels of some viral proteins also increase in the G2/M phase [8]. For example, the results of one study demonstrated that infection with the Coronavirus, Infectious Bronchitis Virus (IBV), caused an accumulation of infected cells in the G2/M phase. Interestingly, when the effects of the cell cycle perturbations on viral replication were examined, the IBV-infected, synchronized G2/M cells showed increased viral protein expression as compared to cells in the G0 phase or the asynchronously replicating cells [9]. Some RNA viruses, such as HIV, are more transcriptionally active in G2 [349], and an increased level of transcription during G2/M may lead to production of more viral genomes [8]. Additionally, some viruses can utilize the different phases of the cell cycle to modulate protein expression via utilization of IRES-mediated translation; the IRES of HIV is upregulated in G2/M while that of HCV appears to be downregulated [8, 374, 375]. Apart from the effects on transcription and translation of viral proteins, a G2/M arrest may also impact virion assembly and release [8]. It has been proposed that the enveloped RNA viruses arrest the cell cycle prior to mitosis so as to maintain an intact intracellular organization [1]. This is beneficial to the viruses whose assembly occurs in the Golgi apparatus and ER [376]. For example, coronaviruses, such as IBV, utilize golgi and ER structures for their protein processing and assembly [377–380]. Finally, it is important to note that virus-induced G2/M arrest has been mostly studied in immortalized or transformed cell lines. Since cellular signaling pathways that regulate the cell cycle are usually altered in immortalized or transformed cell lines, the actual effect of the viral protein might be confounded in these systems [8]. Additionally, for many viruses, the consequence of a G2/M arrest for viral replication remains incompletely understood and requires further investigation, especially in systems that more accurately mimic sites of an authentic infection.

5.2 Viral Inhibition of the G2/M Checkpoint

Although all the studies described above focus on how viruses can initiate a G2 arrest, some viral proteins can also abrogate the G2/M checkpoint; examples of these viral proteins include HTLV1-Tax and EBV-EBNA3C. HTLV-1 Tax causes a G2 arrest in certain cell systems [372]; however, in some cell systems, Tax can interact with Chk1, impair Chk1 kinase activity, and inactivate Chk1-mediated phosphorylation-dependent degradation of Cdc25C,

resulting in the inhibition of the gamma-irradiation-induced G2 arrest [381]. Further, EBV-EBNA3C can release a G2/M block by manipulating Chk2 signaling [382, 383].

5.3 Viral Activation of the APC

HTLV-1 Tax and HBV-HBx can activate APC [336]. HTLV-1 binds and activates APC during the S phase [384]; however, the mechanism by which it activates APC remains unknown. Additionally, the impact of HTLV-1 Tax protein on APC in the context of infection is not known [336]. It is possible that the premature activation of APC by Tax may lead to chromosome instability and contribute to the tumorigenic ability of HTLV-1 [336]. HBx has been shown to activate APC through its interaction with BubR1, which is a component of the spindle assembly checkpoint (SAC). The binding of HBx to BubR1 prevents the interaction of the APC coactivator, Cdc20 with BubR1 and therefore, induces the release of Cdc20 from the SAC. Release of Cdc20 from the SAC allows Cdc20 to associate with the core APC subunits and causes premature activation of the APC [385]. However, studies that investigated the effect of HBx on APC were conducted when HBx was expressed in Chang cells and HeLa cells, which are human cervical cancer cells, and when HBx was expressed alone and not in the context of viral replication. Therefore, the effect of HBx on APC in context of HBV replication and in primary hepatocytes warrants further investigation.

5.3.1 Benefits of Targeting APC

Inhibition of APC could be advantageous for viral replication [336]. APC can cause the ubiquitination and degradation of multiple proteins, and inhibition of APC would lead to the stabilization of its various substrates including securin, cyclin B1, thymidine kinase (TK), and ribonucleotide reductase M2 [48, 50, 336, 386]. HCMV is the only Herpesvirus that has been found to modulate the activity of APC. HCMV does not encode its own TK and RRM2 enzymes [387], which are important for nucleotide biosynthesis. It is possible that HCMV inhibits APC to prevent the degradation of these enzymes, which would allow the production of nucleotides that can be used for viral DNA replication [336]. Additionally, several HCMV proteins contain a consensus APC recognition signal, which is commonly observed in APC substrates [339]. It is possible that APC may limit viral replication by degrading these viral proteins, and inhibition of APC could enhance the stability of these viral proteins [336]. Future studies should focus on determining the impact of viral proteins on APC in the context of infection. Additionally, for certain viruses, APC has been shown to limit viral replication; therefore, it will be important to determine whether APC regulates replication by acting on viral or cellular substrates [336].

6 Conclusions and Perspectives

Many viruses have developed strategies to alter cell cycle regulatory mechanisms. Viruses often encode proteins that modify cell cycle progression by affecting the expression levels and activities of cell cycle regulatory proteins. Manipulation of the host cell cycle by viruses is thought to promote a favorable cellular environment for viral replication; however, subversion of the host cell cycle by viruses can often pose detrimental consequences to host cell physiology and contribute to viral-induced diseases.

The study of viruses, such as the small DNA tumor viruses, has led to many fundamental discoveries that have expanded our understanding of the dynamic regulation of the cell cycle. Particularly, the studies of small DNA tumor viruses have been extremely valuable in understanding the role of p53 and pRb in cell cycle control. For many viruses, such as the small DNA viruses and some Herpesviruses, the effects of infections with the viruses on the cell cycle are well understood. However, there are still many unanswered questions in regard to the exact outcomes of viral-induced cell cycle progression and arrest during infections with viruses such as HBV, HCV, HIV, and HTLV-1. Many studies that have analyzed the effects of these viruses on the host cell cycle have, by necessity, been conducted in immortalized or transformed cells. Since signaling pathways that control normal cell cycle progression are usually altered in immortalized or transformed cell lines, the effects of the viral protein, although valid in that specific cellular context, may not necessarily be similar during the course of a natural infection in normal cells. Effects of the viral proteins may be influenced by factors that are present in the transformed or immortalized cells as compared to normal cells as well as structural alteration, as described below, that might regulate these viral proteins in specific cellular systems. Future studies should focus on understanding the effects of viral proteins on the host cell cycle in systems that closely resemble a natural infection [8]. Moreover, many studies that have analyzed the effect of a particular viral protein on the host cell cycle were conducted in systems in which individual viral proteins were overexpressed, and often out of the context of the entire viral genome. These types of systems may not accurately reflect the expression level of the viral protein during an actual infection. Therefore, it will be important in future studies to analyze the effects of viral proteins on the cell cycle when these proteins are expressed in the context of viral replication, and in the presence of other viral proteins.

As described in this chapter, the multifunctionality of many viral proteins, such as those encoded by HBV, HCV, HIV, and HTLV-I, can often lead to context-dependent activities and an

array of seemingly contradictory effects on cellular signaling pathways. Many viral proteins seem to have adopted a multifaceted approach to manipulate the host cell cycle. Because viruses have limits to their genome size and must encode many functions in a limited number of proteins, it is not surprising that many viral proteins are multifunctional. To this end, many viruses encode regulatory proteins that can each modulate multiple cellular factors, including those that regulate the cell cycle, to promote viral replication. Very recently, the results of two studies have provided insights into the multifunctionality of viral proteins. The results of one study showed that the viral matrix protein 40 (VP40) of the Ebola virus can rearrange into different structural assemblies. The highly plastic, unmodified, wild-type VP40 polypeptide assembled into distinct structures including a dimeric precursor, a hexameric structural component, and a nonstructural RNA-binding ring structure. Each of these distinct structures was shown to have unique and critical functions in the Ebola virus life cycle; the butterfly-shaped VP40 dimer was essential for cellular trafficking, the hexameric structural component was essential for matrix assembly, and viral budding and the RNA-binding structure had a critical role in regulating viral transcription [388]. Ebola virus encodes just 7 genes, and the ability of its protein, VP40, to adopt a different shape for a different function provides one possible explanation for how the virus can accomplish a multiple-step life cycle even though it encodes a small number of genes. The physical plasticity possessed by VP40 that enables it to arrange into distinct structures demonstrates how a structural rearrangement can allow the product of a single viral gene to accomplish a number of essential functions [388]. A second study analyzed the multifunctionality of the Adenovirus E1A protein. Multiple cellular proteins can interact with the E1A protein, and this was linked to dynamic changes in the intrinsically disordered portions of E1A that expand the repertoire of cellular proteins that can bind to E1A [389]. Many viruses have a small genome, and encoding proteins that form distinct structures that function at different stages of the virus life cycle would help these viruses to accomplish a large number of diverse functions with a small number of genes. Thus, it is possible that, like Ebola Virus and Adenoviruses, other viruses also encode proteins that undergo structural transformations, which help the viral proteins to perform different functions [388]. Consequently, future studies should continue to analyze the context-dependent effect of viral proteins on cell cycle progression as these may identify novel therapeutic targets for inhibiting viral replication in various cells as well as strategies for modulating cell cycle effects that contribute to diseases such as cancers. Moreover, these types of studies might also provide insights into the context-dependent effects of many viral proteins.

Finally, alterations in normal cell cycle regulatory mechanisms can lead to the development of many human cancers, and viral infections have been linked to a significant proportion of human cancers worldwide [12, 15]. Thus, a more comprehensive understanding of the mechanisms underlying virus-mediated alterations of the host cell cycle would help provide an in-depth understanding of virus-induced oncogenesis. The results of future studies that address the effects of virus-encoded proteins on the host cell cycle in authentic systems and in the context of viral replication may help generate new therapies that target viral proteins so as to inhibit viral replication and the development of virus-associated cancers. Moreover, these future studies could help identify novel cell cycle regulators and provide insights into many processes that influence cell transformation [16, 17]. Cell cycle regulatory proteins that are targeted by viruses also offer potential targets for antiviral and anticancer therapies; drugs that target cellular proteins instead of viral proteins may help limit the development of drug resistance in these viruses and thus limit both their replication and their ability to cause diseases such as cancer.

References

1. Nascimento R, Costa H, Parkhouse RM (2012) Virus manipulation of cell cycle. Protoplasma 249(3):519–528
2. Condit RC (2013) Principles of virology. In: Knipe DM, Howley PM (eds) Fields virology, vol 1, 6th edn. Lippincot Williams and Wilkins, Philadelphia, PA, pp 21–51
3. Swanton C, Jones N (2001) Strategies in subversion: de-regulation of the mammalian cell cycle by viral gene products. Int J Exp Pathol 82(1):3–13
4. Flemington EK (2001) Herpesvirus lytic replication and the cell cycle: arresting new developments. J Virol 75(10):4475–4481
5. Emmett SR, Dove B, Mahoney L, Wurm T, Hiscox JA (2005) The cell cycle and virus infection. Methods Mol Biol 296:197–218
6. Lavia P, Mileo AM, Giordano A, Paggi MG (2003) Emerging roles of DNA tumor viruses in cell proliferation: new insights into genomic instability. Oncogene 22(42):6508–6516
7. Hume AJ, Kalejta RF (2009) Regulation of the retinoblastoma proteins by the human herpesviruses. Cell Div 4:1
8. Davy C, Doorbar J (2007) G2/M cell cycle arrest in the life cycle of viruses. Virology 368(2):219–226
9. Dove B, Brooks G, Bicknell K, Wurm T, Hiscox JA (2006) Cell cycle perturbations induced by infection with the coronavirus infectious bronchitis virus and their effect on virus replication. J Virol 80(8):4147–4156
10. He Y, Xu K, Keiner B, Zhou J, Czudai V, Li T, Chen Z, Liu J, Klenk HD, Shu YL, Sun B (2010) Influenza A virus replication induces cell cycle arrest in G0/G1 phase. J Virol 84(24):12832–12840
11. Bouchard MJ, Navas-Martin S (2011) Hepatitis B and C virus hepatocarcinogenesis: lessons learned and future challenges. Cancer Lett 305(2):123–143
12. Dayaram T, Marriott SJ (2008) Effect of transforming viruses on molecular mechanisms associated with cancer. J Cell Physiol 216(2):309–314
13. Saha A, Kaul R, Murakami M, Robertson ES (2010) Tumor viruses and cancer biology: modulating signaling pathways for therapeutic intervention. Cancer Biol Ther 10(10):961–978
14. McLaughlin-Drubin ME, Munger K (2008) Viruses associated with human cancer. Biochim Biophys Acta 1782(3):127–150
15. Hanahan D, Weinberg RA (2000) The hallmarks of cancer. Cell 100(1):57–70
16. Chaurushiya MS, Weitzman MD (2009) Viral manipulation of DNA repair and cell cycle checkpoints. DNA Repair (Amst) 8(9):1166–1176
17. Howley PM, Livingston DM (2009) Small DNA tumor viruses: large contributors to biomedical sciences. Virology 384(2):256–259

18. Op De Beeck A, Caillet-Fauquet P (1997) Viruses and the cell cycle. In: Meijer L, Guidet S, Philippe M (eds) Progress in cell cycle research, vol 3. Plenum Press, New York, NY, pp 1–19
19. Vousden KH (1995) Regulation of the cell cycle by viral oncoproteins. Semin Cancer Biol 6(2):109–116
20. Vermeulen K, Van Bockstaele DR, Berneman ZN (2003) The cell cycle: a review of regulation, deregulation and therapeutic targets in cancer. Cell Prolif 36(3):131–149
21. Harper JV, Brooks G (2005) The mammalian cell cycle: an overview. Methods Mol Biol 296:113–153
22. Cooper GM (2000) The cell cycle. In: Cooper GM (ed) The cell: a molecular approach, 2nd edn. Sinauer Associates, Sunderland, MA, http://www.ncbi.nlm.nih.gov/books/NBK9839
23. Cook SJ, Balmanno K, Garner A, Millar T, Taverner C, Todd D (2000) Regulation of cell cycle re-entry by growth, survival and stress signalling pathways. Biochem Soc Trans 28(2):233–240
24. Amon A (1999) The spindle checkpoint. Curr Opin Genet Dev 9(1):69–75
25. Sherr CJ (1993) Mammalian G1 cyclins. Cell 73(6):1059–1065
26. Sherr CJ (1994) G1 phase progression: cycling on cue. Cell 79(4):551–555
27. Assoian RK, Zhu X (1997) Cell anchorage and the cytoskeleton as partners in growth factor dependent cell cycle progression. Curr Opin Cell Biol 9(1):93–98
28. Ohtsubo M, Theodoras AM, Schumacher J, Roberts JM, Pagano M (1995) Human cyclin E, a nuclear protein essential for the G1-to-S phase transition. Mol Cell Biol 15(5): 2612–2624
29. Girard F, Strausfeld U, Fernandez A, Lamb NJ (1991) Cyclin A is required for the onset of DNA replication in mammalian fibroblasts. Cell 67(6):1169–1179
30. Walker DH, Maller JL (1991) Role for cyclin A in the dependence of mitosis on completion of DNA replication. Nature 354(6351): 314–317
31. Lew DJ, Kornbluth S (1996) Regulatory roles of cyclin dependent kinase phosphorylation in cell cycle control. Curr Opin Cell Biol 8(6):795–804
32. Pines J, Hunter T (1991) Cyclin-dependent kinases: a new cell cycle motif? Trends Cell Biol 1(5):117–121
33. Morgan DO (1997) Cyclin-dependent kinases: engines, clocks, and microprocessors. Annu Rev Cell Dev Biol 13:261–291
34. Brehm A, Miska EA, McCance DJ, Reid JL, Bannister AJ, Kouzarides T (1998) Retinoblastoma protein recruits histone deacetylase to repress transcription. Nature 391(6667):597–601
35. Kato J, Matsushime H, Hiebert SW, Ewen ME, Sherr CJ (1993) Direct binding of cyclin D to the retinoblastoma gene product (pRb) and pRb phosphorylation by the cyclin D-dependent kinase CDK4. Genes Dev 7(3):331–342
36. Buchkovich K, Duffy LA, Harlow E (1989) The retinoblastoma protein is phosphorylated during specific phases of the cell cycle. Cell 58(6):1097–1105
37. Bracken AP, Ciro M, Cocito A, Helin K (2004) E2F target genes: unraveling the biology. Trends Biochem Sci 29(8):409–417
38. Hinds PW, Mittnacht S, Dulic V, Arnold A, Reed SI, Weinberg RA (1992) Regulation of retinoblastoma protein functions by ectopic expression of human cyclins. Cell 70(6):993–1006
39. Montagnoli A, Fiore F, Eytan E, Carrano AC, Draetta GF, Hershko A, Pagano M (1999) Ubiquitination of p27 is regulated by Cdk-dependent phosphorylation and trimeric complex formation. Genes Dev 13(9): 1181–1189
40. Roberts JM, Koff A, Polyak K, Firpo E, Collins S, Ohtsubo M, Massague J (1994) Cyclins, Cdks, and cyclin kinase inhibitors. Cold Spring Harb Symp Quant Biol 59:31–38
41. Sherr CJ, Roberts JM (1999) CDK inhibitors: positive and negative regulators of G1-phase progression. Genes Dev 13(12):1501–1512
42. Alberts B, Jhonson A, Lewis J, Raff M, Roberts K, Walter P (2008) The cell cycle. In: Alberts B, Jhonson A, Lewis J, Raff M, Roberts K, Walter P (eds) Molecular biology of the cell, 5th edn. GS, New York, NY, pp 1053–1092
43. Kolupaeva V, Janssens V (2013) PP1 and PP2A phosphatases—cooperating partners in modulating retinoblastoma protein activation. FEBS J 280(2):627–643
44. Stark GR, Taylor WR (2006) Control of the G2/M transition. Mol Biotechnol 32(3): 227–248
45. Branzei D, Foiani M (2008) Regulation of DNA repair throughout the cell cycle. Nat Rev Mol Cell Biol 9(4):297–308
46. Lobrich M, Jeggo PA (2007) The impact of a negligent G2/M checkpoint on genomic instability and cancer induction. Nat Rev Cancer 7(11):861–869
47. Porter LA, Donoghue DJ (2003) Cyclin B1 and CDK1: nuclear localization and upstream regulators. Prog Cell Cycle Res 5:335–347

48. Manchado E, Eguren M, Malumbres M (2010) The anaphase-promoting complex/cyclosome (APC/C): cell-cycle-dependent and -independent functions. Biochem Soc Trans 38(Pt 1):65–71
49. Barford D (2011) Structure, function and mechanism of the anaphase promoting complex (APC/C). Q Rev Biophys 44(2):153–190
50. Page AM, Hieter P (1999) The anaphase-promoting complex: new subunits and regulators. Annu Rev Biochem 68:583–609
51. Peters JM (2006) The anaphase promoting complex/cyclosome: a machine designed to destroy. Nat Rev Mol Cell Biol 7(9): 644–656
52. Acquaviva C, Herzog F, Kraft C, Pines J (2004) The anaphase promoting complex/cyclosome is recruited to centromeres by the spindle assembly checkpoint. Nat Cell Biol 6(9):892–898
53. Mo M, Shahar S, Fleming SB, Mercer AA (2012) How viruses affect the cell cycle through manipulation of the APC/C. Trends Microbiol 20(9):440–448
54. Kornitzer D, Sharf R, Kleinberger T (2001) Adenovirus E4orf4 protein induces PP2A-dependent growth arrest in Saccharomyces cerevisiae and interacts with the anaphase-promoting complex/cyclosome. J Cell Biol 154(2):331–344
55. Mui MZ, Roopchand DE, Gentry MS, Hallberg RL, Vogel J, Branton PE (2010) Adenovirus protein E4orf4 induces premature APCCdc20 activation in Saccharomyces cerevisiae by a protein phosphatase 2A-dependent mechanism. J Virol 84(9): 4798–4809
56. Smits VA, Medema RH (2001) Checking out the G(2)/M transition. Biochim Biophys Acta 1519(1–2):1–12
57. Lukas J, Lukas C, Bartek J (2004) Mammalian cell cycle checkpoints: signalling pathways and their organization in space and time. DNA Repair (Amst) 3(8–9):997–1007
58. Sancar A, Lindsey-Boltz LA, Unsal-Kacmaz K, Linn S (2004) Molecular mechanisms of mammalian DNA repair and the DNA damage checkpoints. Annu Rev Biochem 73:39–85
59. Rumschlag-Booms E, Rong L (2013) Influenza a virus entry: implications in virulence and future therapeutics. Adv Virol 2013:121924
60. La Gruta NL, Kedzierska K, Stambas J, Doherty PC (2007) A question of self-preservation: immunopathology in influenza virus infection. Immunol Cell Biol 85(2): 85–92
61. Webster RG, Bean WJ, Gorman OT, Chambers TM, Kawaoka Y (1992) Evolution and ecology of influenza A viruses. Microbiol Rev 56(1):152–179
62. Simonsen L, Clarke MJ, Williamson GD, Stroup DF, Arden NH, Schonberger LB (1997) The impact of influenza epidemics on mortality: introducing a severity index. Am J Public Health 87(12):1944–1950
63. Morens DM, Fauci AS (2007) The 1918 influenza pandemic: insights for the 21st century. J Infect Dis 195(7):1018–1028
64. Samji T (2009) Influenza A: understanding the viral life cycle. Yale J Biol Med 82(4):153–159
65. Palese P, Shaw ML (2007) Orthomyxoviridae: the viruses and their replication. In: Knipe DM, Howley PM (eds) Fields virology, 5th edn. Lippincot Williams and Wilkins, Philadelphia, PA, pp 1647–1690
66. Couch RB (1996) Orthomyxoviruses. In: Baron S (ed) Medical microbiology, 4th edn. University of Texas medical branch at Galveston, Galveston, TX, http://www.ncbi.nlm.nih.gov/books/NBK8611/
67. Zhirnov OP, Klenk HD (2007) Control of apoptosis in influenza virus-infected cells by up-regulation of Akt and p53 signaling. Apoptosis 12(8):1419–1432
68. Jiang W, Wang Q, Chen S, Gao S, Song L, Liu P, Huang W (2013) Influenza A virus NS1 induces G0/G1 cell cycle arrest by inhibiting the expression and activity of RhoA protein. J Virol 87(6):3039–3052
69. Turpin E, Luke K, Jones J, Tumpey T, Konan K, Schultz-Cherry S (2005) Influenza virus infection increases p53 activity: role of p53 in cell death and viral replication. J Virol 79(14):8802–8811
70. Terrier O, Josset L, Textoris J, Marcel V, Cartet G, Ferraris O, N'Guyen C, Lina B, Diaz JJ, Bourdon JC, Rosa-Calatrava M (2011) Cellular transcriptional profiling in human lung epithelial cells infected by different subtypes of influenza A viruses reveals an overall down-regulation of the host p53 pathway. Virol J 8:285
71. Hale BG, Randall RE, Ortin J, Jackson D (2008) The multifunctional NS1 protein of influenza A viruses. J Gen Virol 89(Pt 10):2359–2376
72. Zhang S, Tang Q, Xu F, Xue Y, Zhen Z, Deng Y, Liu M, Chen J, Liu S, Qiu M, Liao Z, Li Z, Luo D, Shi F, Zheng Y, Bi F (2009) RhoA regulates G1-S progression of gastric cancer cells by modulation of multiple INK4 family tumor suppressors. Mol Cancer Res 7(4):570–580

73. Weber JD, Hu W, Jefcoat SC Jr, Raben DM, Baldassare JJ (1997) Ras-stimulated extracellular signal-related kinase 1 and RhoA activities coordinate platelet-derived growth factor-induced G1 progression through the independent regulation of cyclin D1 and p27. J Biol Chem 272(52):32966–32971
74. Li H, Ung CY, Ma XH, Li BW, Low BC, Cao ZW, Chen YZ (2009) Simulation of crosstalk between small GTPase RhoA and EGFR-ERK signaling pathway via MEKK1. Bioinformatics 25(3):358–364
75. Croft DR, Olson MF (2006) The Rho GTPase effector ROCK regulates cyclin A, cyclin D1, and p27Kip1 levels by distinct mechanisms. Mol Cell Biol 26(12):4612–4627
76. Engelhardt OG, Fodor E (2006) Functional association between viral and cellular transcription during influenza virus infection. Rev Med Virol 16(5):329–345
77. Yonaha M, Chibazakura T, Kitajima S, Yasukochi Y (1995) Cell cycle-dependent regulation of RNA polymerase II basal transcription activity. Nucleic Acids Res 23(20): 4050–4054
78. Garfinkel MS, Katze MG (1992) Translational control by influenza virus. Selective and cap-dependent translation of viral mRNAs in infected cells. J Biol Chem 267(13): 9383–9390
79. Park YW, Wilusz J, Katze MG (1999) Regulation of eukaryotic protein synthesis: selective influenza viral mRNA translation is mediated by the cellular RNA-binding protein GRSF-1. Proc Natl Acad Sci U S A 96(12):6694–6699
80. Pyronnet S, Dostie J, Sonenberg N (2001) Suppression of cap-dependent translation in mitosis. Genes Dev 15(16):2083–2093
81. Stewart SA, Poon B, Jowett JB, Xie Y, Chen IS (1999) Lentiviral delivery of HIV-1 Vpr protein induces apoptosis in transformed cells. Proc Natl Acad Sci U S A 96(21): 12039–12043
82. Gozlan J, Lathey JL, Spector SA (1998) Human immunodeficiency virus type 1 induction mediated by genistein is linked to cell cycle arrest in G2. J Virol 72(10):8174–8180
83. Yuan X, Shan Y, Zhao Z, Chen J, Cong Y (2005) G0/G1 arrest and apoptosis induced by SARS-CoV 3b protein in transfected cells. Virol J 2:66
84. Yuan X, Wu J, Shan Y, Yao Z, Dong B, Chen B, Zhao Z, Wang S, Chen J, Cong Y (2006) SARS coronavirus 7a protein blocks cell cycle progression at G0/G1 phase via the cyclin D3/pRb pathway. Virology 346(1):74–85
85. Chen CJ, Makino S (2004) Murine coronavirus replication induces cell cycle arrest in G0/G1 phase. J Virol 78(11):5658–5669
86. Chen CJ, Sugiyama K, Kubo H, Huang C, Makino S (2004) Murine coronavirus nonstructural protein p28 arrests cell cycle in G0/G1 phase. J Virol 78(19):10410–10419
87. Weiss SR, Navas-Martin S (2005) Coronavirus pathogenesis and the emerging pathogen severe acute respiratory syndrome coronavirus. Microbiol Mol Biol Rev 69(4):635–664
88. Marra MA, Jones SJ, Astell CR, Holt RA, Brooks-Wilson A, Butterfield YS, Khattra J, Asano JK, Barber SA, Chan SY, Cloutier A, Coughlin SM, Freeman D, Girn N, Griffith OL, Leach SR, Mayo M, McDonald H, Montgomery SB, Pandoh PK, Petrescu AS, Robertson AG, Schein JE, Siddiqui A, Smailus DE, Stott JM, Yang GS, Plummer F, Andonov A, Artsob H, Bastien N, Bernard K, Booth TF, Bowness D, Czub M, Drebot M, Fernando L, Flick R, Garbutt M, Gray M, Grolla A, Jones S, Feldmann H, Meyers A, Kabani A, Li Y, Normand S, Stroher U, Tipples GA, Tyler S, Vogrig R, Ward D, Watson B, Brunham RC, Krajden M, Petric M, Skowronski DM, Upton C, Roper RL (2003) The Genome sequence of the SARS-associated coronavirus. Science 300(5624):1399–1404
89. Rota PA, Oberste MS, Monroe SS, Nix WA, Campagnoli R, Icenogle JP, Penaranda S, Bankamp B, Maher K, Chen MH, Tong S, Tamin A, Lowe L, Frace M, DeRisi JL, Chen Q, Wang D, Erdman DD, Peret TC, Burns C, Ksiazek TG, Rollin PE, Sanchez A, Liffick S, Holloway B, Limor J, McCaustland K, Olsen-Rasmussen M, Fouchier R, Gunther S, Osterhaus AD, Drosten C, Pallansch MA, Anderson LJ, Bellini WJ (2003) Characterization of a novel coronavirus associated with severe acute respiratory syndrome. Science 300(5624):1394–1399
90. Compton SR, Barthold SW, Smith AL (1993) The cellular and molecular pathogenesis of coronaviruses. Lab Anim Sci 43(1):15–28
91. Wege H, Siddell S, ter Meulen V (1982) The biology and pathogenesis of coronaviruses. Curr Top Microbiol Immunol 99:165–200
92. An S, Chen CJ, Yu X, Leibowitz JL, Makino S (1999) Induction of apoptosis in murine coronavirus-infected cultured cells and demonstration of E protein as an apoptosis inducer. J Virol 73(9):7853–7859
93. Chen CJ, Makino S (2002) Murine coronavirus-induced apoptosis in 17Cl-1 cells involves a mitochondria-mediated pathway and its downstream caspase-8 activation and bid cleavage. Virology 302(2):321–332

94. Belyavsky M, Belyavskaya E, Levy GA, Leibowitz JL (1998) Coronavirus MHV-3-induced apoptosis in macrophages. Virology 250(1):41–49
95. Zhu L, Anasetti C (1995) Cell cycle control of apoptosis in human leukemic T cells. J Immunol 154(1):192–200
96. Klumperman J, Locker JK, Meijer A, Horzinek MC, Geuze HJ, Rottier PJ (1994) Coronavirus M proteins accumulate in the Golgi complex beyond the site of virion budding. J Virol 68(10):6523–6534
97. Tooze J, Tooze S, Warren G (1984) Replication of coronavirus MHV-A59 in sac- cells: determination of the first site of budding of progeny virions. Eur J Cell Biol 33(2):281–293
98. Lowe M, Nakamura N, Warren G (1998) Golgi division and membrane traffic. Trends Cell Biol 8(1):40–44
99. Warren G (1993) Membrane partitioning during cell division. Annu Rev Biochem 62:323–348
100. Bonneau AM, Sonenberg N (1987) Involvement of the 24-kDa cap-binding protein in regulation of protein synthesis in mitosis. J Biol Chem 262(23):11134–11139
101. Thiel V, Siddell SG (1994) Internal ribosome entry in the coding region of murine hepatitis virus mRNA 5. J Gen Virol 75(Pt 11):3041–3046
102. Nishioka WK, Welsh RM (1994) Susceptibility to cytotoxic T lymphocyte-induced apoptosis is a function of the proliferative status of the target. J Exp Med 179(2):769–774
103. Johnston JB, Wang G, Barrett JW, Nazarian SH, Colwill K, Moran M, McFadden G (2005) Myxoma virus M-T5 protects infected cells from the stress of cell cycle arrest through its interaction with host cell cullin-1. J Virol 79(16):10750–10763
104. Gearhart TL, Bouchard MJ (2010) The hepatitis B virus X protein modulates hepatocyte proliferation pathways to stimulate viral replication. J Virol 84(6):2675–2686
105. Ashfaq UA, Javed T, Rehman S, Nawaz Z, Riazuddin S (2011) An overview of HCV molecular biology, replication and immune responses. Virol J 8:161
106. Lindenbach BD, Rice CM (2005) Unravelling hepatitis C virus replication from genome to function. Nature 436(7053):933–938
107. Sy T, Jamal MM (2006) Epidemiology of hepatitis C virus (HCV) infection. Int J Med Sci 3(2):41–46
108. Rosen HR (2011) Clinical practice. Chronic hepatitis C infection. N Engl J Med 364(25):2429–2438
109. Liang TJ, Ghany MG (2013) Current and future therapies for hepatitis C virus infection. N Engl J Med 368(20):1907–1917
110. Munir S, Saleem S, Idrees M, Tariq A, Butt S, Rauff B, Hussain A, Badar S, Naudhani M, Fatima Z, Ali M, Ali L, Akram M, Aftab M, Khubaib B, Awan Z (2010) Hepatitis C treatment: current and future perspectives. Virol J 7:296
111. Ray S, Bailey J, Thomas D (2013) Hepatitis C virus. In: Knipe DM, Howley PM (eds) Fields virology, 6th edn. Lippincot Williams and Wilkins, Philadelphia, PA, pp 795–824
112. Ghosh AK, Steele R, Meyer K, Ray R, Ray RB (1999) Hepatitis C virus NS5A protein modulates cell cycle regulatory genes and promotes cell growth. J Gen Virol 80(Pt 5):1179–1183
113. Park SH, Lim JS, Lim SY, Tiwari I, Jang KL (2011) Hepatitis C virus Core protein stimulates cell growth by down-regulating p16 expression via DNA methylation. Cancer Lett 310(1):61–68
114. Tsukiyama-Kohara K, Tone S, Maruyama I, Inoue K, Katsume A, Nuriya H, Ohmori H, Ohkawa J, Taira K, Hoshikawa Y, Shibasaki F, Reth M, Minatogawa Y, Kohara M (2004) Activation of the CKI-CDK-Rb-E2F pathway in full genome hepatitis C virus-expressing cells. J Biol Chem 279(15): 14531–14541
115. Yang XJ, Liu J, Ye L, Liao QJ, Wu JG, Gao JR, She YL, Wu ZH, Ye LB (2006) HCV NS2 protein inhibits cell proliferation and induces cell cycle arrest in the S-phase in mammalian cells through down-regulation of cyclin A expression. Virus Res 121(2):134–143
116. Bittar C, Shrivastava S, Bhanja Chowdhury J, Rahal P, Ray RB (2013) Hepatitis C virus NS2 protein inhibits DNA damage pathway by sequestering p53 to the cytoplasm. PLoS One 8(4):e62581
117. Shiu TY, Huang SM, Shih YL, Chu HC, Chang WK, Hsieh TY (2013) Hepatitis C virus core protein down-regulates p21(Waf1/Cip1) and inhibits curcumin-induced apoptosis through microRNA-345 targeting in human hepatoma cells. PLoS One 8(4): e61089
118. Wang Y, Wang Y, Xu Y, Tong W, Pan T, Li J, Sun S, Shao J, Ding H, Toyoda T, Yuan Z (2011) Hepatitis C virus NS5B protein delays s phase progression in human hepatocyte-derived cells by relocalizing cyclin-dependent kinase 2-interacting protein (CINP). J Biol Chem 286(30):26603–26615
119. Walters KA, Syder AJ, Lederer SL, Diamond DL, Paeper B, Rice CM, Katze MG (2009)

Genomic analysis reveals a potential role for cell cycle perturbation in HCV-mediated apoptosis of cultured hepatocytes. PLoS Pathog 5(1):e1000269

120. Scholle F, Li K, Bodola F, Ikeda M, Luxon BA, Lemon SM (2004) Virus-host cell interactions during hepatitis C virus RNA replication: impact of polyprotein expression on the cellular transcriptome and cell cycle association with viral RNA synthesis. J Virol 78(3):1513–1524
121. Sarfraz S, Hamid S, Siddiqui A, Hussain S, Pervez S, Alexander G (2008) Altered expression of cell cycle and apoptotic proteins in chronic hepatitis C virus infection. BMC Microbiol 8:133
122. Ruggieri A, Murdolo M, Harada T, Miyamura T, Rapicetta M (2004) Cell cycle perturbation in a human hepatoblastoma cell line constitutively expressing hepatitis C virus core protein. Arch Virol 149(1):61–74
123. Chen H, Pei R, Chen X (2013) Different response of two highly permissive cell lines upon HCV infection. Virol Sin 28(4): 202–208
124. Cho JW, Baek WK, Suh SI, Yang SH, Chang J, Sung YC, Suh MH (2001) Hepatitis C virus core protein promotes cell proliferation through the upregulation of cyclin E expression levels. Liver 21(2):137–142
125. Honda M, Kaneko S, Shimazaki T, Matsushita E, Kobayashi K, Ping LH, Zhang HC, Lemon SM (2000) Hepatitis C virus core protein induces apoptosis and impairs cell-cycle regulation in stably transformed Chinese hamster ovary cells. Hepatology 31(6):1351–1359
126. Banerjee A, Ray RB, Ray R (2010) Oncogenic potential of hepatitis C virus proteins. Viruses 2(9):2108–2133
127. Munakata T, Liang Y, Kim S, McGivern DR, Huibregtse J, Nomoto A, Lemon SM (2007) Hepatitis C virus induces E6AP-dependent degradation of the retinoblastoma protein. PLoS Pathog 3(9):1335–1347
128. Abbas T, Dutta A (2009) p21 in cancer: intricate networks and multiple activities. Nat Rev Cancer 9(6):400–414
129. Kwun HJ, Jung EY, Ahn JY, Lee MN, Jang KL (2001) p53-dependent transcriptional repression of p21(waf1) by hepatitis C virus NS3. J Gen Virol 82(Pt 9):2235–2241
130. Nguyen H, Mudryj M, Guadalupe M, Dandekar S (2003) Hepatitis C virus core protein expression leads to biphasic regulation of the p21 cdk inhibitor and modulation of hepatocyte cell cycle. Virology 312(1): 245–253
131. Yao ZQ, Eisen-Vandervelde A, Ray S, Hahn YS (2003) HCV core/gC1qR interaction arrests T cell cycle progression through stabilization of the cell cycle inhibitor p27Kip1. Virology 314(1):271–282
132. Otsuka M, Kato N, Lan K, Yoshida H, Kato J, Goto T, Shiratori Y, Omata M (2000) Hepatitis C virus core protein enhances p53 function through augmentation of DNA binding affinity and transcriptional ability. J Biol Chem 275(44):34122–34130
133. Lo SY, Masiarz F, Hwang SB, Lai MM, Ou JH (1995) Differential subcellular localization of hepatitis C virus core gene products. Virology 213(2):455–461
134. Salvant BS, Fortunato EA, Spector DH (1998) Cell cycle dysregulation by human cytomegalovirus: influence of the cell cycle phase at the time of infection and effects on cyclin transcription. J Virol 72(5):3729–3741
135. Burkhart DL, Sage J (2008) Cellular mechanisms of tumour suppression by the retinoblastoma gene. Nat Rev Cancer 8(9): 671–682
136. Marshall A, Rushbrook S, Davies SE, Morris LS, Scott IS, Vowler SL, Coleman N, Alexander G (2005) Relation between hepatocyte G1 arrest, impaired hepatic regeneration, and fibrosis in chronic hepatitis C virus infection. Gastroenterology 128(1):33–42
137. Marshall A, Rushbrook S, Morris LS, Scott IS, Vowler SL, Davies SE, Coleman N, Alexander G (2005) Hepatocyte expression of minichromosome maintenance protein-2 predicts fibrosis progression after transplantation for chronic hepatitis C virus: a pilot study. Liver Transpl 11(4):427–433
138. Fehr C, Conrad KD, Niepmann M (2012) Differential stimulation of hepatitis C virus RNA translation by microRNA-122 in different cell cycle phases. Cell Cycle 11(2): 277–285
139. Honda M, Kaneko S, Matsushita E, Kobayashi K, Abell GA, Lemon SM (2000) Cell cycle regulation of hepatitis C virus internal ribosomal entry site-directed translation. Gastroenterology 118(1):152–162
140. Grana X, Reddy EP (1995) Cell cycle control in mammalian cells: role of cyclins, cyclin dependent kinases (CDKs), growth suppressor genes and cyclin-dependent kinase inhibitors (CKIs). Oncogene 11(2):211–219
141. Mohd Hanafiah K, Groeger J, Flaxman AD, Wiersma ST (2013) Global epidemiology of hepatitis C virus infection: new estimates of age-specific antibody to HCV seroprevalence. Hepatology 57(4):1333–1342

142. Dorner M, Horwitz JA, Donovan BM, Labitt RN, Budell WC, Friling T, Vogt A, Catanese MT, Satoh T, Kawai T, Akira S, Law M, Rice CM, Ploss A (2013) Completion of the entire hepatitis C virus life cycle in genetically humanized mice. Nature 501(7466):237–241
143. Gaston KL (2012) Small DNA tumor viruses, 4th edn. Caister Academic Press, Bristol, UK
144. Gatza ML, Chandhasin C, Ducu RI, Marriott SJ (2005) Impact of transforming viruses on cellular mutagenesis, genome stability, and cellular transformation. Environ Mol Mutagen 45(2–3):304–325
145. Flint SJ, Enquist LW, Racaniello VR, Skalka AM (2009) Transformation and oncogenesis. In: Flint SJ, Enquist LW, Racaniello VR, Skalka AM (eds) Principles of virology, vol II, 3rd edn. ASM Press, New York, NY, pp 201–248
146. Helt AM, Galloway DA (2003) Mechanisms by which DNA tumor virus oncoproteins target the Rb family of pocket proteins. Carcinogenesis 24(2):159–169
147. Moran E (1993) DNA tumor virus transforming proteins and the cell cycle. Curr Opin Genet Dev 3(1):63–70
148. Nevins JR (1994) Cell cycle targets of the DNA tumor viruses. Curr Opin Genet Dev 4(1):130–134
149. Sherr CJ, McCormick F (2002) The RB and p53 pathways in cancer. Cancer Cell 2(2): 103–112
150. Polager S, Ginsberg D (2009) p53 and E2f: partners in life and death. Nat Rev Cancer 9(10):738–748
151. Harbour JW, Dean DC (2000) The Rb/E2F pathway: expanding roles and emerging paradigms. Genes Dev 14(19):2393–2409
152. Henley SA, Dick FA (2012) The retinoblastoma family of proteins and their regulatory functions in the mammalian cell division cycle. Cell Div 7(1):10
153. Raychaudhuri P, Bagchi S, Devoto SH, Kraus VB, Moran E, Nevins JR (1991) Domains of the adenovirus E1A protein required for oncogenic activity are also required for dissociation of E2F transcription factor complexes. Genes Dev 5(7):1200–1211
154. Liu X, Marmorstein R (2007) Structure of the retinoblastoma protein bound to adenovirus E1A reveals the molecular basis for viral oncoprotein inactivation of a tumor suppressor. Genes Dev 21(21):2711–2716
155. Ikeda MA, Nevins JR (1993) Identification of distinct roles for separate E1A domains in disruption of E2F complexes. Mol Cell Biol 13(11):7029–7035
156. DeCaprio JA, Ludlow JW, Figge J, Shew JY, Huang CM, Lee WH, Marsilio E, Paucha E, Livingston DM (1988) SV40 large tumor antigen forms a specific complex with the product of the retinoblastoma susceptibility gene. Cell 54(2):275–283
157. Zalvide J, DeCaprio JA, Stubdal H (2001) Binding of SV40 large T antigen to the retinoblastoma susceptibility gene product and related proteins. Methods Mol Biol 165: 213–218
158. Zalvide J, DeCaprio JA (1995) Role of pRb-related proteins in simian virus 40 large-T-antigen-mediated transformation. Mol Cell Biol 15(10):5800–5810
159. Zalvide J, Stubdal H, DeCaprio JA (1998) The J domain of simian virus 40 large T antigen is required to functionally inactivate RB family proteins. Mol Cell Biol 18(3): 1408–1415
160. Sullivan CS, Cantalupo P, Pipas JM (2000) The molecular chaperone activity of simian virus 40 large T antigen is required to disrupt Rb-E2F family complexes by an ATP-dependent mechanism. Mol Cell Biol 20(17): 6233–6243
161. Stubdal H, Zalvide J, DeCaprio JA (1996) Simian virus 40 large T antigen alters the phosphorylation state of the RB-related proteins p130 and p107. J Virol 70(5): 2781–2788
162. Pagano M, Durst M, Joswig S, Draetta G, Jansen-Durr P (1992) Binding of the human E2F transcription factor to the retinoblastoma protein but not to cyclin A is abolished in HPV-16-immortalized cells. Oncogene 7(9):1681–1686
163. Chellappan S, Kraus VB, Kroger B, Munger K, Howley PM, Phelps WC, Nevins JR (1992) Adenovirus E1A, simian virus 40 tumor antigen, and human papillomavirus E7 protein share the capacity to disrupt the interaction between transcription factor E2F and the retinoblastoma gene product. Proc Natl Acad Sci U S A 89(10): 4549–4553
164. Wu EW, Clemens KE, Heck DV, Munger K (1993) The human papillomavirus E7 oncoprotein and the cellular transcription factor E2F bind to separate sites on the retinoblastoma tumor suppressor protein. J Virol 67(4):2402–2407
165. Boyer SN, Wazer DE, Band V (1996) E7 protein of human papilloma virus-16 induces degradation of retinoblastoma protein through the ubiquitin-proteasome pathway. Cancer Res 56(20):4620–4624

166. Jones DL, Munger K (1997) Analysis of the p53-mediated G1 growth arrest pathway in cells expressing the human papillomavirus type 16 E7 oncoprotein. J Virol 71(4):2905–2912
167. O'Shea CC, Fried M (2005) Modulation of the ARF-p53 pathway by the small DNA tumor viruses. Cell Cycle 4(3):449–452
168. Jiang D, Srinivasan A, Lozano G, Robbins PD (1993) SV40 T antigen abrogates p53-mediated transcriptional activity. Oncogene 8(10):2805–2812
169. Segawa K, Minowa A, Sugasawa K, Takano T, Hanaoka F (1993) Abrogation of p53-mediated transactivation by SV40 large T antigen. Oncogene 8(3):543–548
170. Mietz JA, Unger T, Huibregtse JM, Howley PM (1992) The transcriptional transactivation function of wild-type p53 is inhibited by SV40 large T-antigen and by HPV-16 E6 oncoprotein. EMBO J 11(13):5013–5020
171. Lane DP, Crawford LV (1979) T antigen is bound to a host protein in SV40-transformed cells. Nature 278(5701):261–263
172. Linzer DI, Levine AJ (1979) Characterization of a 54K dalton cellular SV40 tumor antigen present in SV40-transformed cells and uninfected embryonal carcinoma cells. Cell 17(1):43–52
173. Harada JN, Shevchenko A, Shevchenko A, Pallas DC, Berk AJ (2002) Analysis of the adenovirus E1B-55K-anchored proteome reveals its link to ubiquitination machinery. J Virol 76(18):9194–9206
174. Querido E, Blanchette P, Yan Q, Kamura T, Morrison M, Boivin D, Kaelin WG, Conaway RC, Conaway JW, Branton PE (2001) Degradation of p53 by adenovirus E4orf6 and E1B55K proteins occurs via a novel mechanism involving a Cullin-containing complex. Genes Dev 15(23):3104–3117
175. Scheffner M, Huibregtse JM, Vierstra RD, Howley PM (1993) The HPV-16 E6 and E6-AP complex functions as a ubiquitin-protein ligase in the ubiquitination of p53. Cell 75(3):495–505
176. Pellet PE, Roizman B (2013) Herpesviridae. In: Knipe DM, Howley PM (eds) Fields virology, 6th edn. Lippincot Williams and Wilkins, Philadelphia, PA, pp 1802–1820
177. Sandri-Goldin RM (2006) Alpha Herpesviruses: molecular and cellular biology. Caister Academic Press, Bristol, UK
178. Flint SJ, Enquist LW, Racaniello VR, Skalka AM Patterns of infection. In: Flint SJ, Enquist LW, Racaniello VR, Skalka AM (eds) Principles of virology vol Volume II: Pathogenesis and control, vol 2, 3rd edn. ASM Press, New York, NY, pp 134–163
179. McGeoch DJ, Rixon FJ, Davison AJ (2006) Topics in herpesvirus genomics and evolution. Virus Res 117(1):90–104
180. Dittmer DP, Damania B (2013) Kaposi sarcoma associated herpesvirus pathogenesis (KSHV)-an update. Curr Opin Virol 3(3):238–244
181. Mesri EA, Cesarman E, Boshoff C (2010) Kaposi's sarcoma and its associated herpesvirus. Nat Rev Cancer 10(10):707–719
182. Cai Q, Verma SC, Lu J, Robertson ES (2010) Molecular biology of Kaposi's sarcoma-associated herpesvirus and related oncogenesis. Adv Virus Res 78:87–142
183. Jarviluoma A, Ojala PM (2006) Cell signaling pathways engaged by KSHV. Biochim Biophys Acta 1766(1):140–158
184. Cesarman E, Chang Y, Moore PS, Said JW, Knowles DM (1995) Kaposi's sarcoma-associated herpesvirus-like DNA sequences in AIDS-related body-cavity-based lymphomas. N Engl J Med 332(18):1186–1191
185. Renne R, Blackbourn D, Whitby D, Levy J, Ganem D (1998) Limited transmission of Kaposi's sarcoma-associated herpesvirus in cultured cells. J Virol 72(6):5182–5188
186. Sarid R, Flore O, Bohenzky RA, Chang Y, Moore PS (1998) Transcription mapping of the Kaposi's sarcoma-associated herpesvirus (human herpesvirus 8) genome in a body cavity-based lymphoma cell line (BC-1). J Virol 72(2):1005–1012
187. Direkze S, Laman H (2004) Regulation of growth signalling and cell cycle by Kaposi's sarcoma-associated herpesvirus genes. Int J Exp Pathol 85(6):305–319
188. Moore PS (2007) KSHV manipulation of the cell cycle and apoptosis. In: Arvin A, Campadelli-Fiume G, Mocarski E et al (eds) Human herpesviruses: biology, therapy, and immunoprophylaxis. Cambridge University Press, Cambridge
189. Chang Y, Moore PS, Talbot SJ, Boshoff CH, Zarkowska T, Godden K, Paterson H, Weiss RA, Mittnacht S (1996) Cyclin encoded by KS herpesvirus. Nature 382(6590):410
190. Li M, Lee H, Yoon DW, Albrecht JC, Fleckenstein B, Neipel F, Jung JU (1997) Kaposi's sarcoma-associated herpesvirus encodes a functional cyclin. J Virol 71(3): 1984–1991
191. Laman H, Coverley D, Krude T, Laskey R, Jones N (2001) Viral cyclin-cyclin-dependent kinase 6 complexes initiate nuclear DNA replication. Mol Cell Biol 21(2):624–635
192. Ellis M, Chew YP, Fallis L, Freddersdorf S, Boshoff C, Weiss RA, Lu X, Mittnacht S (1999) Degradation of p27(Kip) cdk inhibitor triggered by Kaposi's sarcoma virus

cyclin-cdk6 complex. EMBO J 18(3): 644–653

193. Godden-Kent D, Talbot SJ, Boshoff C, Chang Y, Moore P, Weiss RA, Mittnacht S (1997) The cyclin encoded by Kaposi's sarcoma-associated herpesvirus stimulates cdk6 to phosphorylate the retinoblastoma protein and histone H1. J Virol 71(6): 4193–4198
194. Laman H, Peters G, Jones N (2001) Cyclin-mediated export of human Orc1. Exp Cell Res 271(2):230–237
195. Swanton C, Mann DJ, Fleckenstein B, Neipel F, Peters G, Jones N (1997) Herpes viral cyclin/Cdk6 complexes evade inhibition by CDK inhibitor proteins. Nature 390(6656):184–187
196. Kaldis P, Ojala PM, Tong L, Makela TP, Solomon MJ (2001) CAK-independent activation of CDK6 by a viral cyclin. Mol Biol Cell 12(12):3987–3999
197. Sarek G, Jarviluoma A, Ojala PM (2006) KSHV viral cyclin inactivates p27KIP1 through Ser10 and Thr187 phosphorylation in proliferating primary effusion lymphomas. Blood 107(2):725–732
198. Mann DJ, Child ES, Swanton C, Laman H, Jones N (1999) Modulation of p27(Kip1) levels by the cyclin encoded by Kaposi's sarcoma-associated herpesvirus. EMBO J 18(3): 654–663
199. Ojala PM, Tiainen M, Salven P, Veikkola T, Castanos-Velez E, Sarid R, Biberfeld P, Makela TP (1999) Kaposi's sarcoma-associated herpesvirus-encoded v-cyclin triggers apoptosis in cells with high levels of cyclin-dependent kinase 6. Cancer Res 59(19): 4984–4989
200. Verschuren EW, Klefstrom J, Evan GI, Jones N (2002) The oncogenic potential of Kaposi's sarcoma-associated herpesvirus cyclin is exposed by p53 loss in vitro and in vivo. Cancer Cell 2(3):229–241
201. Verschuren EW, Hodgson JG, Gray JW, Kogan S, Jones N, Evan GI (2004) The role of p53 in suppression of KSHV cyclin-induced lymphomagenesis. Cancer Res 64(2): 581–589
202. Radkov SA, Kellam P, Boshoff C (2000) The latent nuclear antigen of Kaposi sarcoma-associated herpesvirus targets the retinoblastoma-E2F pathway and with the oncogene Hras transforms primary rat cells. Nat Med 6(10):1121–1127
203. Cannon M, Philpott NJ, Cesarman E (2003) The Kaposi's sarcoma-associated herpesvirus G protein-coupled receptor has broad signaling effects in primary effusion lymphoma cells. J Virol 77(1):57–67
204. Russo JJ, Bohenzky RA, Chien MC, Chen J, Yan M, Maddalena D, Parry JP, Peruzzi D, Edelman IS, Chang Y, Moore PS (1996) Nucleotide sequence of the Kaposi sarcoma-associated herpesvirus (HHV8). Proc Natl Acad Sci U S A 93(25):14862–14867
205. Seaman WT, Ye D, Wang RX, Hale EE, Weisse M, Quinlivan EB (1999) Gene expression from the ORF50/K8 region of Kaposi's sarcoma-associated herpesvirus. Virology 263(2):436–449
206. Wang SE, Wu FY, Yu Y, Hayward GS (2003) CCAAT/enhancer-binding protein-alpha is induced during the early stages of Kaposi's sarcoma-associated herpesvirus (KSHV) lytic cycle reactivation and together with the KSHV replication and transcription activator (RTA) cooperatively stimulates the viral RTA, MTA, and PAN promoters. J Virol 77(17): 9590–9612
207. Wang SE, Wu FY, Fujimuro M, Zong J, Hayward SD, Hayward GS (2003) Role of CCAAT/enhancer-binding protein alpha (C/EBPalpha) in activation of the Kaposi's sarcoma-associated herpesvirus (KSHV) lytic-cycle replication-associated protein (RAP) promoter in cooperation with the KSHV replication and transcription activator (RTA) and RAP. J Virol 77(1):600–623
208. Wu FY, Wang SE, Tang QQ, Fujimuro M, Chiou CJ, Zheng Q, Chen H, Hayward SD, Lane MD, Hayward GS (2003) Cell cycle arrest by Kaposi's sarcoma-associated herpesvirus replication-associated protein is mediated at both the transcriptional and posttranslational levels by binding to CCAAT/enhancer-binding protein alpha and p21(CIP-1). J Virol 77(16):8893–8914
209. Izumiya Y, Lin SF, Ellison TJ, Levy AM, Mayeur GL, Izumiya C, Kung HJ (2003) Cell cycle regulation by Kaposi's sarcoma-associated herpesvirus K-bZIP: direct interaction with cyclin-CDK2 and induction of G1 growth arrest. J Virol 77(17):9652–9661
210. Maeda E, Akahane M, Kiryu S, Kato N, Yoshikawa T, Hayashi N, Aoki S, Minami M, Uozaki H, Fukayama M, Ohtomo K (2009) Spectrum of Epstein–Barr virus-related diseases: a pictorial review. Jpn J Radiol 27(1):4–19
211. Young LS, Rickinson AB (2004) Epstein–Barr virus: 40 years on. Nat Rev Cancer 4(10):757–768
212. Arvanitakis L, Yaseen N, Sharma S (1995) Latent membrane protein-1 induces cyclin D2 expression, pRb hyperphosphorylation, and loss of TGF-beta 1-mediated growth inhibition in EBV-positive B cells. J Immunol 155(3):1047–1056

213. Dirmeier U, Hoffmann R, Kilger E, Schultheiss U, Briseno C, Gires O, Kieser A, Eick D, Sugden B, Hammerschmidt W (2005) Latent membrane protein 1 of Epstein–Barr virus coordinately regulates proliferation with control of apoptosis. Oncogene 24(10):1711–1717
214. Parker GA, Crook T, Bain M, Sara EA, Farrell PJ, Allday MJ (1996) Epstein–Barr virus nuclear antigen (EBNA)3C is an immortalizing oncoprotein with similar properties to adenovirus E1A and papillomavirus E7. Oncogene 13(12):2541–2549
215. Saha A, Halder S, Upadhyay SK, Lu J, Kumar P, Murakami M, Cai Q, Robertson ES (2011) Epstein–Barr virus nuclear antigen 3C facilitates G1-S transition by stabilizing and enhancing the function of cyclin D1. PLoS Pathog 7(2):e1001275
216. Fukuda M, Satoh TA, Takanashi M, Hirai K, Ohnishi E, Sairenji T (2000) Inhibition of cell growth and Epstein–Barr virus reactivation by CD40 stimulation in Epstein–Barr virus-transformed B cells. Viral Immunol 13(2):215–229
217. Rodriguez A, Armstrong M, Dwyer D, Flemington E (1999) Genetic dissection of cell growth arrest functions mediated by the Epstein–Barr virus lytic gene product, Zta. J Virol 73(11):9029–9038
218. Cayrol C, Flemington EK (1996) The Epstein–Barr virus bZIP transcription factor Zta causes G0/G1 cell cycle arrest through induction of cyclin-dependent kinase inhibitors. EMBO J 15(11):2748–2759
219. Swenson JJ, Mauser AE, Kaufmann WK, Kenney SC (1999) The Epstein–Barr virus protein BRLF1 activates S phase entry through E2F1 induction. J Virol 73(8):6540–6550
220. Michaelis M, Doerr HW, Cinatl J (2009) The story of human cytomegalovirus and cancer: increasing evidence and open questions. Neoplasia 11(1):1–9
221. Huang ES, Johnson RA (2000) Human cytomegalovirus—no longer just a DNA virus. Nat Med 6(8):863–864
222. Castillo JP, Kowalik TF (2004) HCMV infection: modulating the cell cycle and cell death. Int Rev Immunol 23(1–2):113–139
223. Albrecht T, Nachtigal M, St Jeor SC, Rapp F (1976) Induction of cellular DNA synthesis and increased mitotic activity in syrian hamster embryo cells abortively infected with human cytomegalovirus. J Gen Virol 30(2):167–177
224. Gonczol E, Plotkin SA (1984) Cells infected with human cytomegalovirus release a factor(s) that stimulates cell DNA synthesis. J Gen Virol 65(Pt 10):1833–1837
225. Sinclair J, Baillie J, Bryant L, Caswell R (2000) Human cytomegalovirus mediates cell cycle progression through G(1) into early S phase in terminally differentiated cells. J Gen Virol 81(Pt 6):1553–1565
226. Dittmer D, Mocarski ES (1997) Human cytomegalovirus infection inhibits G1/S transition. J Virol 71(2):1629–1634
227. Bresnahan WA, Boldogh I, Thompson EA, Albrecht T (1996) Human cytomegalovirus inhibits cellular DNA synthesis and arrests productively infected cells in late G1. Virology 224(1):150–160
228. Lu M, Shenk T (1996) Human cytomegalovirus infection inhibits cell cycle progression at multiple points, including the transition from G1 to S. J Virol 70(12):8850–8857
229. Lu M, Shenk T (1999) Human cytomegalovirus UL69 protein induces cells to accumulate in G1 phase of the cell cycle. J Virol 73(1):676–683
230. Wiebusch L, Hagemeier C (1999) Human cytomegalovirus 86-kilodalton IE2 protein blocks cell cycle progression in G(1). J Virol 73(11):9274–9283
231. Hume AJ, Finkel JS, Kamil JP, Coen DM, Culbertson MR, Kalejta RF (2008) Phosphorylation of retinoblastoma protein by viral protein with cyclin-dependent kinase function. Science 320(5877):797–799
232. Kalejta RF, Bechtel JT, Shenk T (2003) Human cytomegalovirus pp 71 stimulates cell cycle progression by inducing the proteasome-dependent degradation of the retinoblastoma family of tumor suppressors. Mol Cell Biol 23(6):1885–1895
233. Kalejta RF, Shenk T (2003) Proteasome-dependent, ubiquitin-independent degradation of the Rb family of tumor suppressors by the human cytomegalovirus pp 71 protein. Proc Natl Acad Sci U S A 100(6): 3263–3268
234. Kalejta RF, Shenk T (2003) The human cytomegalovirus UL82 gene product (pp 71) accelerates progression through the G1 phase of the cell cycle. J Virol 77(6):3451–3459
235. Hagemeier C, Caswell R, Hayhurst G, Sinclair J, Kouzarides T (1994) Functional interaction between the HCMV IE2 transactivator and the retinoblastoma protein. EMBO J 13(12):2897–2903

236. Fortunato EA, Sommer MH, Yoder K, Spector DH (1997) Identification of domains within the human cytomegalovirus major immediate-early 86-kilodalton protein and the retinoblastoma protein required for physical and functional interaction with each other. J Virol 71(11):8176–8185
237. Bresnahan WA, Albrecht T, Thompson EA (1998) The cyclin E promoter is activated by human cytomegalovirus 86-kDa immediate early protein. J Biol Chem 273(34): 22075–22082
238. Chayavichitsilp P, Buckwalter JV, Krakowski AC, Friedlander SF (2009) Herpes simplex. Pediatr Rev 30(4):119–129, quiz 130
239. Song B, Liu JJ, Yeh KC, Knipe DM (2000) Herpes simplex virus infection blocks events in the G1 phase of the cell cycle. Virology 267(2):326–334
240. de Bruyn Kops A, Knipe DM (1988) Formation of DNA replication structures in herpes virus-infected cells requires a viral DNA binding protein. Cell 55(5):857–868
241. Ehmann GL, McLean TI, Bachenheimer SL (2000) Herpes simplex virus type 1 infection imposes a G(1)/S block in asynchronously growing cells and prevents G(1) entry in quiescent cells. Virology 267(2):335–349
242. Olgiate J, Ehmann GL, Vidyarthi S, Hilton MJ, Bachenheimer SL (1999) Herpes simplex virus induces intracellular redistribution of E2F4 and accumulation of E2F pocket protein complexes. Virology 258(2):257–270
243. Hobbs WE 2nd, DeLuca NA (1999) Perturbation of cell cycle progression and cellular gene expression as a function of herpes simplex virus ICP0. J Virol 73(10): 8245–8255
244. Lomonte P, Everett RD (1999) Herpes simplex virus type 1 immediate-early protein Vmw110 inhibits progression of cells through mitosis and from G(1) into S phase of the cell cycle. J Virol 73(11):9456–9467
245. Diwan P, Lacasse JJ, Schang LM (2004) Roscovitine inhibits activation of promoters in herpes simplex virus type 1 genomes independently of promoter-specific factors. J Virol 78(17):9352–9365
246. Schang LM, Phillips J, Schaffer PA (1998) Requirement for cellular cyclin-dependent kinases in herpes simplex virus replication and transcription. J Virol 72(7):5626–5637
247. Durand LO, Roizman B (2008) Role of cdk9 in the optimization of expression of the genes regulated by ICP22 of herpes simplex virus 1. J Virol 82(21):10591–10599
248. Davido DJ, Von Zagorski WF, Maul GG, Schaffer PA (2003) The differential requirement for cyclin-dependent kinase activities distinguishes two functions of herpes simplex virus type 1 ICP0. J Virol 77(23):12603–12616
249. Hossain A, Holt T, Ciacci-Zanella J, Jones C (1997) Analysis of cyclin-dependent kinase activity after herpes simplex virus type 2 infection. J Gen Virol 78(Pt 12):3341–3348
250. Seeger C, Mason WS, Zoulim F (2007) Hepadnaviruses. In: Knipe DM, Howley PM (eds) Fields virology, 5th edn. Lippincot Williams and Wilkins, Philadelphia, PA, pp 2977–3029
251. Block TM, Mehta AS, Fimmel CJ, Jordan R (2003) Molecular viral oncology of hepatocellular carcinoma. Oncogene 22(33):5093–5107
252. Nguyen VT, Law MG, Dore GJ (2009) Hepatitis B-related hepatocellular carcinoma: epidemiological characteristics and disease burden. J Viral Hepat 16(7):453–463
253. Madden CR, Slagle BL (2001) Stimulation of cellular proliferation by hepatitis B virus X protein. Dis Markers 17(3):153–157
254. Friedrich B, Wollersheim M, Brandenburg B, Foerste R, Will H, Hildt E (2005) Induction of anti-proliferative mechanisms in hepatitis B virus producing cells. J Hepatol 43(4):696–703
255. Wang T, Zhao R, Wu Y, Kong D, Zhang L, Wu D, Li C, Zhang C, Yu Z, Jin X (2011) Hepatitis B virus induces G1 phase arrest by regulating cell cycle genes in HepG2.2.15 cells. Virol J 8:231
256. Chin R, Earnest-Silveira L, Koeberlein B, Franz S, Zentgraf H, Dong X, Gowans E, Bock CT, Torresi J (2007) Modulation of MAPK pathways and cell cycle by replicating hepatitis B virus: factors contributing to hepatocarcinogenesis. J Hepatol 47(3):325–337
257. Casciano J, Bagga S, Yang B, Bouchard M (2012) Modulation of cell proliferation pathways by the hepatitis B virus X protein: a potential contributor to the development of hepatocellular carcinoma. In: Lau JWY (ed) Hepatocellular carcinoma-basic research. InTech, Rijeka, Croatia, pp 103–152
258. Huang YQ, Wang LW, Yan SN, Gong ZJ (2004) Effects of cell cycle on telomerase activity and on hepatitis B virus replication in HepG2 2.2.15 cells. Hepatobiliary Pancreat Dis Int 3(4):543–547
259. Ozer A, Khaoustov VI, Mearns M, Lewis DE, Genta RM, Darlington GJ, Yoffe B (1996) Effect of hepatocyte proliferation and cellular DNA synthesis on hepatitis B virus replication. Gastroenterology 110(5):1519–1528

260. Guidotti LG, Matzke B, Chisari FV (1997) Hepatitis B virus replication is cell cycle independent during liver regeneration in transgenic mice. J Virol 71(6):4804–4808
261. Guidotti LG, Matzke B, Schaller H, Chisari FV (1995) High-level hepatitis B virus replication in transgenic mice. J Virol 69(10): 6158–6169
262. Bouchard MJ, Schneider RJ (2004) The enigmatic X gene of hepatitis B virus. J Virol 78(23):12725–12734
263. Benhenda S, Cougot D, Buendia MA, Neuveut C (2009) Hepatitis B virus X protein molecular functions and its role in virus life cycle and pathogenesis. Adv Cancer Res 103:75–109
264. Bouchard M, Giannakopoulos S, Wang EH, Tanese N, Schneider RJ (2001) Hepatitis B virus HBx protein activation of cyclin A-cyclin-dependent kinase 2 complexes and G1 transit via a Src kinase pathway. J Virol 75(9):4247–4257
265. Benn J, Schneider RJ (1994) Hepatitis B virus HBx protein activates Ras-GTP complex formation and establishes a Ras, Raf, MAP kinase signaling cascade. Proc Natl Acad Sci U S A 91(22):10350–10354
266. Benn J, Schneider RJ (1995) Hepatitis B virus HBx protein deregulates cell cycle checkpoint controls. Proc Natl Acad Sci U S A 92(24):11215–11219
267. Koike K, Moriya K, Yotsuyanagi H, Iino S, Kurokawa K (1994) Induction of cell cycle progression by hepatitis B virus HBx gene expression in quiescent mouse fibroblasts. J Clin Invest 94(1):44–49
268. Lee S, Tarn C, Wang WH, Chen S, Hullinger RL, Andrisani OM (2002) Hepatitis B virus X protein differentially regulates cell cycle progression in X-transforming versus non-transforming hepatocyte (AML12) cell lines. J Biol Chem 277(10):8730–8740
269. Chen HY, Tang NH, Lin N, Chen ZX, Wang XZ (2008) Hepatitis B virus X protein induces apoptosis and cell cycle deregulation through interfering with DNA repair and checkpoint responses. Hepatol Res 38(2):174–182
270. Mukherji A, Janbandhu VC, Kumar V (2007) HBx-dependent cell cycle deregulation involves interaction with cyclin E/A-cdk2 complex and destabilization of p27Kip1. Biochem J 401(1):247–256
271. Singh AK, Swarnalatha M, Kumar V (2011) c-ETS1 facilitates G1/S-phase transition by up-regulating cyclin E and CDK2 genes and cooperates with hepatitis B virus X protein for their deregulation. J Biol Chem 286(25): 21961–21970
272. Zhang JL, Zhao WG, Wu KL, Wang K, Zhang X, Gu CF, Li Y, Zhu Y, Wu JG (2005) Human hepatitis B virus X protein promotes cell proliferation and inhibits cell apoptosis through interacting with a serine protease Hepsin. Arch Virol 150(4):721–741
273. Wu JC, Merlino G, Cveklova K, Mosinger B Jr, Fausto N (1994) Autonomous growth in serum-free medium and production of hepatocellular carcinomas by differentiated hepatocyte lines that overexpress transforming growth factor alpha 1. Cancer Res 54(22): 5964–5973
274. Tarn C, Bilodeau ML, Hullinger RL, Andrisani OM (1999) Differential immediate early gene expression in conditional hepatitis B virus pX-transforming versus nontransforming hepatocyte cell lines. J Biol Chem 274(4):2327–2336
275. Wu JC, Merlino G, Fausto N (1994) Establishment and characterization of differentiated, nontransformed hepatocyte cell lines derived from mice transgenic for transforming growth factor alpha. Proc Natl Acad Sci U S A 91(2):674–678
276. Jung JK, Arora P, Pagano JS, Jang KL (2007) Expression of DNA methyltransferase 1 is activated by hepatitis B virus X protein via a regulatory circuit involving the p16INK4a-cyclin D1-CDK 4/6-pRb-E2F1 pathway. Cancer Res 67(12):5771–5778
277. Park SG, Chung C, Kang H, Kim JY, Jung G (2006) Up-regulation of cyclin D1 by HBx is mediated by NF-kappaB2/BCL3 complex through kappaB site of cyclin D1 promoter. J Biol Chem 281(42):31770–31777
278. Zhu R, Li BZ, Li H, Ling YQ, Hu XQ, Zhai WR, Zhu HG (2007) Association of p16INK4A hypermethylation with hepatitis B virus X protein expression in the early stage of HBV-associated hepatocarcinogenesis. Pathol Int 57(6):328–336
279. Zhu YZ, Zhu R, Fan J, Pan Q, Li H, Chen Q, Zhu HG (2010) Hepatitis B virus X protein induces hypermethylation of p16(INK4A) promoter via DNA methyltransferases in the early stage of HBV-associated hepatocarcinogenesis. J Viral Hepat 17(2):98–107
280. Ahn JY, Jung EY, Kwun HJ, Lee CW, Sung YC, Jang KL (2002) Dual effects of hepatitis B virus X protein on the regulation of cell-cycle control depending on the status of cellular p53. J Gen Virol 83(Pt 11):2765–2772
281. Park US, Park SK, Lee YI, Park JG, Lee YI (2000) Hepatitis B virus-X protein upregulates the expression of p21waf1/cip1 and prolongs G1→S transition via a p53-independent pathway in human hepatoma cells. Oncogene 19(30):3384–3394

282. Leach JK, Qiao L, Fang Y, Han SL, Gilfor D, Fisher PB, Grant S, Hylemon PB, Peterson D, Dent P (2003) Regulation of p21 and p27 expression by the hepatitis B virus X protein and the alternate initiation site X proteins, AUG2 and AUG3. J Gastroenterol Hepatol 18(4):376–385

283. Qiao L, Leach K, McKinstry R, Gilfor D, Yacoub A, Park JS, Grant S, Hylemon PB, Fisher PB, Dent P (2001) Hepatitis B virus X protein increases expression of p21(Cip-1/WAF1/MDA6) and p27(Kip-1) in primary mouse hepatocytes, leading to reduced cell cycle progression. Hepatology 34(5): 906–917

284. Gearhart TL, Bouchard MJ (2011) The hepatitis B virus HBx protein modulates cell cycle regulatory proteins in cultured primary human hepatocytes. Virus Res 155(1):363–367

285. Gearhart TL, Bouchard MJ (2010) Replication of the hepatitis B virus requires a calcium-dependent HBx-induced G1 phase arrest of hepatocytes. Virology 407(1):14–25

286. Yamashita M, Emerman M (2006) Retroviral infection of non-dividing cells: old and new perspectives. Virology 344(1):88–93

287. Ford HL, Parade AB (1999) Cancer and the cell cycle. J Cell Biochem 32–33(suppl): 166–172

288. Tralhao JG, Roudier J, Morosan S, Giannini C, Tu H, Goulenok C, Carnot F, Zavala F, Joulin V, Kremsdorf D, Brechot C (2002) Paracrine in vivo inhibitory effects of hepatitis B virus X protein (HBx) on liver cell proliferation: an alternative mechanism of HBx-related pathogenesis. Proc Natl Acad Sci U S A 99(10):6991–6996

289. Wu BK, Li CC, Chen HJ, Chang JL, Jeng KS, Chou CK, Hsu MT, Tsai TF (2006) Blocking of G1/S transition and cell death in the regenerating liver of Hepatitis B virus X protein transgenic mice. Biochem Biophys Res Commun 340(3):916–928

290. Hodgson AJ, Keasler VV, Slagle BL (2008) Premature cell cycle entry induced by hepatitis B virus regulatory HBx protein during compensatory liver regeneration. Cancer Res 68(24):10341–10348

291. Quetier I, Brezillon N, Duriez M, Massinet H, Giang E, Ahodantin J, Lamant C, Brunelle MN, Soussan P, Kremsdorf D (2013) Hepatitis B virus HBx protein impairs liver regeneration through enhanced expression of IL-6 in transgenic mice. J Hepatol 59(2): 285–291

292. Mahieux R, Gessain A (2007) Adult T-cell leukemia/lymphoma and HTLV-1. Curr Hematol Malig Rep 2(4):257–264

293. Jadoul M, Poignet JL, Geddes C, Locatelli F, Medin C, Krajewska M, Barril G, Scheuermann E, Sonkodi S, Goubau P, HCV Collaborative Group (2004) The changing epidemiology of hepatitis C virus (HCV) infection in haemodialysis: European multicentre study. Nephrol Dial Transplant 19(4):904–909

294. Matsuoka M, Jeang KT (2007) Human T-cell leukaemia virus type 1 (HTLV-1) infectivity and cellular transformation. Nat Rev Cancer 7(4):270–280

295. Hinuma Y, Nagata K, Hanaoka M, Nakai M, Matsumoto T, Kinoshita KI, Shirakawa S, Miyoshi I (1981) Adult T-cell leukemia: antigen in an ATL cell line and detection of antibodies to the antigen in human sera. Proc Natl Acad Sci U S A 78(10):6476–6480

296. Yoshida M, Seiki M, Yamaguchi K, Takatsuki K (1984) Monoclonal integration of human T-cell leukemia provirus in all primary tumors of adult T-cell leukemia suggests causative role of human T-cell leukemia virus in the disease. Proc Natl Acad Sci U S A 81(8): 2534–2537

297. Currer R, Van Duyne R, Jaworski E, Guendel I, Sampey G, Das R, Narayanan A, Kashanchi F (2012) HTLV tax: a fascinating multifunctional co-regulator of viral and cellular pathways. Front Microbiol 3:406

298. Goncalves DU, Proietti FA, Ribas JG, Araujo MG, Pinheiro SR, Guedes AC, Carneiro-Proietti AB (2010) Epidemiology, treatment, and prevention of human T-cell leukemia virus type 1-associated diseases. Clin Microbiol Rev 23(3):577–589

299. Franchini G, Nicot C, Johnson JM (2003) Seizing of T cells by human T-cell leukemia/lymphoma virus type 1. Adv Cancer Res 89:69–132

300. Marriot SJ, Semmes OJ (2005) Impact of HTLV-1 Tax on cell cycle progression and the cellular DNA damage repair response. Oncogene 24(39):5986–5995

301. Lemoine FJ, Marriott SJ (2001) Accelerated G(1) phase progression induced by the human T cell leukemia virus type I (HTLV-I) Tax oncoprotein. J Biol Chem 276(34): 31851–31857

302. Ohtani K, Iwanaga R, Arai M, Huang Y, Matsumura Y, Nakamura M (2000) Cell type-specific E2F activation and cell cycle progression induced by the oncogene product Tax of human T-cell leukemia virus type I. J Biol Chem 275(15):11154–11163

303. Haller K, Wu Y, Derow E, Schmitt I, Jeang KT, Grassmann R (2002) Physical interaction of human T-cell leukemia virus type 1 Tax with cyclin-dependent kinase 4 stimulates the

phosphorylation of retinoblastoma protein. Mol Cell Biol 22(10):3327–3338

304. Kehn K, Fuente Cde L, Strouss K, Berro R, Jiang H, Brady J, Mahieux R, Pumfery A, Bottazzi ME, Kashanchi F (2005) The HTLV-I Tax oncoprotein targets the retinoblastoma protein for proteasomal degradation. Oncogene 24(4):525–540
305. Iwanaga R, Ohtani K, Hayashi T, Nakamura M (2001) Molecular mechanism of cell cycle progression induced by the oncogene product Tax of human T-cell leukemia virus type I. Oncogene 20(17):2055–2067
306. Suzuki T, Narita T, Uchida-Toita M, Yoshida M (1999) Down-regulation of the INK4 family of cyclin-dependent kinase inhibitors by tax protein of HTLV-1 through two distinct mechanisms. Virology 259(2):384–391
307. Low KG, Dorner LF, Fernando DB, Grossman J, Jeang KT, Comb MJ (1997) Human T-cell leukemia virus type 1 Tax releases cell cycle arrest induced by p16INK4a. J Virol 71(3):1956–1962
308. Mulloy JC, Kislyakova T, Cereseto A, Casareto L, LoMonico A, Fullen J, Lorenzi MV, Cara A, Nicot C, Giam C, Franchini G (1998) Human T-cell lymphotropic/leukemia virus type 1 Tax abrogates p53-induced cell cycle arrest and apoptosis through its CREB/ATF functional domain. J Virol 72(11):8852–8860
309. Pise-Masison CA, Choi KS, Radonovich M, Dittmer J, Kim SJ, Brady JN (1998) Inhibition of p53 transactivation function by the human T-cell lymphotropic virus type 1 Tax protein. J Virol 72(2):1165–1170
310. Liu M, Yang L, Zhang L, Liu B, Merling R, Xia Z, Giam CZ (2008) Human T-cell leukemia virus type 1 infection leads to arrest in the G1 phase of the cell cycle. J Virol 82(17):8442–8455
311. Baydoun HH, Pancewicz J, Bai X, Nicot C (2010) HTLV-I p30 inhibits multiple S phase entry checkpoints, decreases cyclin E-CDK2 interactions and delays cell cycle progression. Mol Cancer 9:302
312. Bellon M, Baydoun HH, Yao Y, Nicot C (2010) HTLV-I Tax-dependent and -independent events associated with immortalization of human primary T lymphocytes. Blood 115(12):2441–2448
313. Nicot C, Dundr M, Johnson JM, Fullen JR, Alonzo N, Fukumoto R, Princler GL, Derse D, Misteli T, Franchini G (2004) HTLV-1-encoded p30II is a post-transcriptional negative regulator of viral replication. Nat Med 10(2):197–201
314. Bai XT, Baydoun HH, Nicot C (2010) HTLV-I p30: a versatile protein modulating virus replication and pathogenesis. Mol Aspects Med 31(5):344–349
315. Taylor JM, Brown M, Nejmeddine M, Kim KJ, Ratner L, Lairmore M, Nicot C (2009) Novel role for interleukin-2 receptor-Jak signaling in retrovirus transmission. J Virol 83(22):11467–11476
316. Fukumoto R, Dundr M, Nicot C, Adams A, Valeri VW, Samelson LE, Franchini G (2007) Inhibition of T-cell receptor signal transduction and viral expression by the linker for activation of T cells-interacting p12(I) protein of human T-cell leukemia/lymphoma virus type 1. J Virol 81(17):9088–9099
317. Albrecht B, Lairmore MD (2002) Critical role of human T-lymphotropic virus type 1 accessory proteins in viral replication and pathogenesis. Microbiol Mol Biol Rev 66(3):396–406, table of contents
318. Johnson JM, Nicot C, Fullen J, Ciminale V, Casareto L, Mulloy JC, Jacobson S, Franchini G (2001) Free major histocompatibility complex class I heavy chain is preferentially targeted for degradation by human T-cell leukemia/lymphotropic virus type 1 p12(I) protein. J Virol 75(13):6086–6094
319. Fukumoto R, Andresen V, Bialuk I, Cecchinato V, Walser JC, Valeri VW, Nauroth JM, Gessain A, Nicot C, Franchini G (2009) In vivo genetic mutations define predominant functions of the human T-cell leukemia/lymphoma virus p12I protein. Blood 113(16):3726–3734
320. Silic-Benussi M, Cavallari I, Zorzan T, Rossi E, Hiraragi H, Rosato A, Horie K, Saggioro D, Lairmore MD, Willems L, Chieco-Bianchi L, D'Agostino DM, Ciminale V (2004) Suppression of tumor growth and cell proliferation by p13II, a mitochondrial protein of human T cell leukemia virus type 1. Proc Natl Acad Sci U S A 101(17):6629–6634
321. Kim SJ, Ding W, Albrecht B, Green PL, Lairmore MD (2003) A conserved calcineurin-binding motif in human T lymphotropic virus type 1 p12I functions to modulate nuclear factor of activated T cell activation. J Biol Chem 278(18):15550–15557
322. Darbinyan A, Darbinian N, Safak M, Radhakrishnan S, Giordano A, Khalili K (2002) Evidence for dysregulation of cell cycle by human polyomavirus, JCV, late auxiliary protein. Oncogene 21(36):5574–5581
323. Nascimento R, Parkhouse RM (2007) Murine gammaherpesvirus 68 ORF20 induces cell-cycle arrest in G2 by inhibiting the Cdc2-cyclin B complex. J Gen Virol 88(Pt 5): 1446–1453

324. Li H, Baskaran R, Krisky DM, Bein K, Grandi P, Cohen JB, Glorioso JC (2008) Chk2 is required for HSV-1 ICP0-mediated G2/M arrest and enhancement of virus growth. Virology 375(1):13–23
325. Knight GL, Turnell AS, Roberts S (2006) Role for Wee1 in inhibition of G2-to-M transition through the cooperation of distinct human papillomavirus type 1 E4 proteins. J Virol 80(15):7416–7426
326. Poggioli GJ, Dermody TS, Tyler KL (2001) Reovirus-induced sigma1s-dependent G(2)/M phase cell cycle arrest is associated with inhibition of p34(cdc2). J Virol 75(16):7429–7434
327. Patton JT (2008) Segmented double-stranded RNA viruses: structural and molecular biology. Caister Academic Press, Bristol, UK
328. Li L, Gu B, Zhou F, Chi J, Wang F, Peng G, Xie F, Qing J, Feng D, Lu S, Yao K (2011) Human herpesvirus 6 suppresses T cell proliferation through induction of cell cycle arrest in infected cells in the G2/M phase. J Virol 85(13):6774–6783
329. Scarano FJ, Laffin JA, Lehman JM, Friedrich TD (1994) Simian virus 40 prevents activation of M-phase-promoting factor during lytic infection. J Virol 68(4):2355–2361
330. Yeo KS, Mohidin TB, Ng CC (2012) Epstein–Barr virus-encoded latent membrane protein-1 upregulates 14-3-3sigma and Reprimo to confer G(2)/M phase cell cycle arrest. C R Biol 335(12):713–721
331. Ohki R, Nemoto J, Murasawa H, Oda E, Inazawa J, Tanaka N, Taniguchi T (2000) Reprimo, a new candidate mediator of the p53-mediated cell cycle arrest at the G2 phase. J Biol Chem 275(30):22627–22630
332. Mhawech P (2005) 14-3-3 proteins—an update. Cell Res 15(4):228–236
333. Laronga C, Yang HY, Neal C, Lee MH (2000) Association of the cyclin-dependent kinases and 14-3-3 sigma negatively regulates cell cycle progression. J Biol Chem 275(30):23106–23112
334. Davy CE, Jackson DJ, Raj K, Peh WL, Southern SA, Das P, Sorathia R, Laskey P, Middleton K, Nakahara T, Wang Q, Masterson PJ, Lambert PF, Cuthill S, Millar JB, Doorbar J (2005) Human papillomavirus type 16 E1 E4-induced G2 arrest is associated with cytoplasmic retention of active Cdk1/cyclin B1 complexes. J Virol 79(7): 3998–4011
335. Morita E, Tada K, Chisaka H, Asao H, Sato H, Yaegashi N, Sugamura K (2001) Human parvovirus B19 induces cell cycle arrest at G(2) phase with accumulation of mitotic cyclins. J Virol 75(16):7555–7563
336. Fehr AR, Yu D (2013) Control the host cell cycle: viral regulation of the anaphase-promoting complex. J Virol 87(16):8818–8825
337. Teodoro JG, Heilman DW, Parker AE, Green MR (2004) The viral protein Apoptin associates with the anaphase-promoting complex to induce G2/M arrest and apoptosis in the absence of p53. Genes Dev 18(16): 1952–1957
338. Bellanger S, Blachon S, Mechali F, Bonne-Andrea C, Thierry F (2005) High-risk but not low-risk HPV E2 proteins bind to the APC activators Cdh1 and Cdc20 and cause genomic instability. Cell Cycle 4(11): 1608–1615
339. Tran K, Kamil JP, Coen DM, Spector DH (2010) Inactivation and disassembly of the anaphase-promoting complex during human cytomegalovirus infection is associated with degradation of the APC5 and APC4 subunits and does not require UL97-mediated phosphorylation of Cdh1. J Virol 84(20): 10832–10843
340. Fehr AR, Gualberto NC, Savaryn JP, Terhune SS, Yu D (2012) Proteasome-dependent disruption of the E3 ubiquitin ligase anaphase-promoting complex by HCMV protein pUL21a. PLoS Pathog 8(7):e1002789
341. Everett RD, Earnshaw WC, Findlay J, Lomonte P (1999) Specific destruction of kinetochore protein CENP-C and disruption of cell division by herpes simplex virus immediate-early protein Vmw110. EMBO J 18(6):1526–1538
342. Lomonte P, Sullivan KF, Everett RD (2001) Degradation of nucleosome-associated centromeric histone H3-like protein CENP-A induced by herpes simplex virus type 1 protein ICP0. J Biol Chem 276(8):5829–5835
343. Belyavskyi M, Braunagel SC, Summers MD (1998) The structural protein ODV-EC27 of Autographa californica nucleopolyhedrovirus is a multifunctional viral cyclin. Proc Natl Acad Sci U S A 95(19):11205–11210
344. Ikeda M, Kobayashi M (1999) Cell-cycle perturbation in Sf9 cells infected with Autographa californica nucleopolyhedrovirus. Virology 258(1):176–188
345. Freed EO, Martin MA (2013) Human immunodeficiency viruses: replication. In: Knipe DM, Howley PM (eds) Fields virology, 6th edn. Lippincot Williams and Wilkins, Philadelphia, PA, pp 1502–1560
346. Gilbert PB, McKeague IW, Eisen G, Mullins C, Gueye NA, Mboup S, Kanki PJ (2003) Comparison of HIV-1 and HIV-2 infectivity

from a prospective cohort study in Senegal. Stat Med 22(4):573–593

347. Sharp PM, Hahn BH (2011) Origins of HIV and the AIDS pandemic. Cold Spring Harb Perspect Med 1(1):a006841
348. Zhao RY, Li G, Bukrinsky MI (2011) Vpr-host interactions during HIV-1 viral life cycle. J Neuroimmune Pharmacol 6(2):216–229
349. Goh WC, Rogel ME, Kinsey CM, Michael SF, Fultz PN, Nowak MA, Hahn BH, Emerman M (1998) HIV-1 Vpr increases viral expression by manipulation of the cell cycle: a mechanism for selection of Vpr in vivo. Nat Med 4(1):65–71
350. Kogan M, Rappaport J (2011) HIV-1 accessory protein Vpr: relevance in the pathogenesis of HIV and potential for therapeutic intervention. Retrovirology 8:25
351. Zhao RY, Elder RT (2005) Viral infections and cell cycle G2/M regulation. Cell Res 15(3):143–149
352. Re F, Braaten D, Franke EK, Luban J (1995) Human immunodeficiency virus type 1 Vpr arrests the cell cycle in G2 by inhibiting the activation of p34cdc2-cyclin B. J Virol 69(11):6859–6864
353. He J, Choe S, Walker R, Di Marzio P, Morgan DO, Landau NR (1995) Human immunodeficiency virus type 1 viral protein R (Vpr) arrests cells in the G2 phase of the cell cycle by inhibiting p34cdc2 activity. J Virol 69(11):6705–6711
354. Goh WC, Manel N, Emerman M (2004) The human immunodeficiency virus Vpr protein binds Cdc25C: implications for G2 arrest. Virology 318(1):337–349
355. Kamata M, Watanabe N, Nagaoka Y, Chen IS (2008) Human immunodeficiency virus type 1 Vpr binds to the N lobe of the Wee1 kinase domain and enhances kinase activity for CDC2. J Virol 82(12):5672–5682
356. Yuan H, Kamata M, Xie YM, Chen IS (2004) Increased levels of Wee-1 kinase in G(2) are necessary for Vpr- and gamma irradiation-induced G(2) arrest. J Virol 78(15): 8183–8190
357. Elder RT, Yu M, Chen M, Zhu X, Yanagida M, Zhao Y (2001) HIV-1 Vpr induces cell cycle G2 arrest in fission yeast (Schizosaccharomyces pombe) through a pathway involving regulatory and catalytic subunits of PP2A and acting on both Wee1 and Cdc25. Virology 287(2):359–370
358. Bartz SR, Rogel ME, Emerman M (1996) Human immunodeficiency virus type 1 cell cycle control: Vpr is cytostatic and mediates G2 accumulation by a mechanism which differs from DNA damage checkpoint control. J Virol 70(4):2324–2331
359. DeHart JL, Zimmerman ES, Ardon O, Monteiro-Filho CM, Arganaraz ER, Planelles V (2007) HIV-1 Vpr activates the G2 checkpoint through manipulation of the ubiquitin proteasome system. Virol J 4:57
360. Belzile JP, Duisit G, Rougeau N, Mercier J, Finzi A, Cohen EA (2007) HIV-1 Vpr-mediated G2 arrest involves the DDB1-CUL4AVPRBP E3 ubiquitin ligase. PLoS Pathog 3(7):e85
361. Schrofelbauer B, Hakata Y, Landau NR (2007) HIV-1 Vpr function is mediated by interaction with the damage-specific DNA-binding protein DDB1. Proc Natl Acad Sci U S A 104(10):4130–4135
362. Tan L, Ehrlich E, Yu XF (2007) DDB1 and Cul4A are required for human immunodeficiency virus type 1 Vpr-induced G2 arrest. J Virol 81(19):10822–10830
363. Mansky LM (1996) The mutation rate of human immunodeficiency virus type 1 is influenced by the vpr gene. Virology 222(2):391–400
364. Roshal M, Kim B, Zhu Y, Nghiem P, Planelles V (2003) Activation of the ATR-mediated DNA damage response by the HIV-1 viral protein R. J Biol Chem 278(28):25879–25886
365. Li G, Park HU, Liang D, Zhao RY (2010) Cell cycle G2/M arrest through an S phase-dependent mechanism by HIV-1 viral protein R. Retrovirology 7:59
366. Li G, Elder RT, Qin K, Park HU, Liang D, Zhao RY (2007) Phosphatase type 2A-dependent and -independent pathways for ATR phosphorylation of Chk1. J Biol Chem 282(10):7287–7298
367. Zimmerman ES, Chen J, Andersen JL, Ardon O, Dehart JL, Blackett J, Choudhary SK, Camerini D, Nghiem P, Planelles V (2004) Human immunodeficiency virus type 1 Vpr-mediated G2 arrest requires Rad17 and Hus1 and induces nuclear BRCA1 and gamma-H2AX focus formation. Mol Cell Biol 24(21):9286–9294
368. Zhao Y, Cao J, O'Gorman MR, Yu M, Yogev R (1996) Effect of human immunodeficiency virus type 1 protein R (vpr) gene expression on basic cellular function of fission yeast Schizosaccharomyces pombe. J Virol 70(9): 5821–5826
369. Fu DX, Kuo YL, Liu BY, Jeang KT, Giam CZ (2003) Human T-lymphotropic virus type I tax activates I-kappa B kinase by inhibiting I-kappa B kinase-associated serine/threonine protein phosphatase 2A. J Biol Chem 278(3):1487–1493

370. Roopchand DE, Lee JM, Shahinian S, Paquette D, Bussey H, Branton PE (2001) Toxicity of human adenovirus E4orf4 protein in Saccharomyces cerevisiae results from interactions with the Cdc55 regulatory B subunit of PP2A. Oncogene 20(38):5279–5290
371. Shtrichman R, Sharf R, Barr H, Dobner T, Kleinberger T (1999) Induction of apoptosis by adenovirus E4orf4 protein is specific to transformed cells and requires an interaction with protein phosphatase 2A. Proc Natl Acad Sci U S A 96(18):10080–10085
372. Haoudi A, Daniels RC, Wong E, Kupfer G, Semmes OJ (2003) Human T-cell leukemia virus-I tax oncoprotein functionally targets a subnuclear complex involved in cellular DNA damage-response. J Biol Chem 278(39): 37736–37744
373. Poon B, Grovit-Ferbas K, Stewart SA, Chen IS (1998) Cell cycle arrest by Vpr in HIV-1 virions and insensitivity to antiretroviral agents. Science 281(5374):266–269
374. Venkatesan A, Sharma R, Dasgupta A (2003) Cell cycle regulation of hepatitis C and encephalomyocarditis virus internal ribosome entry site-mediated translation in human embryonic kidney 293 cells. Virus Res 94(2):85–95
375. Brasey A, Lopez-Lastra M, Ohlmann T, Beerens N, Berkhout B, Darlix JL, Sonenberg N (2003) The leader of human immunodeficiency virus type 1 genomic RNA harbors an internal ribosome entry segment that is active during the G2/M phase of the cell cycle. J Virol 77(7):3939–3949
376. Lin GY, Lamb RA (2000) The paramyxovirus simian virus 5 V protein slows progression of the cell cycle. J Virol 74(19):9152–9166
377. Alonso-Caplen FV, Matsuoka Y, Wilcox GE, Compans RW (1984) Replication and morphogenesis of avian coronavirus in Vero cells and their inhibition by monensin. Virus Res 1(2):153–167
378. Lim KP, Liu DX (2001) The missing link in coronavirus assembly. Retention of the avian coronavirus infectious bronchitis virus envelope protein in the pre-Golgi compartments and physical interaction between the envelope and membrane proteins. J Biol Chem 276(20):17515–17523
379. Lontok E, Corse E, Machamer CE (2004) Intracellular targeting signals contribute to localization of coronavirus spike proteins near the virus assembly site. J Virol 78(11): 5913–5922
380. Machamer CE, Mentone SA, Rose JK, Farquhar MG (1990) The E1 glycoprotein of an avian coronavirus is targeted to the cis Golgi complex. Proc Natl Acad Sci U S A 87(18):6944–6948
381. Park HU, Jeong JH, Chung JH, Brady JN (2004) Human T-cell leukemia virus type 1 Tax interacts with Chk1 and attenuates DNA-damage induced G2 arrest mediated by Chk1. Oncogene 23(29):4966–4974
382. Krauer KG, Burgess A, Buck M, Flanagan J, Sculley TB, Gabrielli B (2004) The EBNA-3 gene family proteins disrupt the G2/M checkpoint. Oncogene 23(7):1342–1353
383. Choudhuri T, Verma SC, Lan K, Murakami M, Robertson ES (2007) The ATM/ATR signaling effector Chk2 is targeted by Epstein–Barr virus nuclear antigen 3C to release the G2/M cell cycle block. J Virol 81(12):6718–6730
384. Liu B, Hong S, Tang Z, Yu H, Giam CZ (2005) HTLV-I Tax directly binds the Cdc20-associated anaphase-promoting complex and activates it ahead of schedule. Proc Natl Acad Sci U S A 102(1):63–68
385. Kim S, Park SY, Yong H, Famulski JK, Chae S, Lee JH, Kang CM, Saya H, Chan GK, Cho H (2008) HBV X protein targets hBubR1, which induces dysregulation of the mitotic checkpoint. Oncogene 27(24):3457–3464
386. Chabes AL, Pfleger CM, Kirschner MW, Thelander L (2003) Mouse ribonucleotide reductase R2 protein: a new target for anaphase-promoting complex-Cdh1-mediated proteolysis. Proc Natl Acad Sci U S A 100(7):3925–3929
387. Wiebusch L, Bach M, Uecker R, Hagemeier C (2005) Human cytomegalovirus inactivates the G0/G1-APC/C ubiquitin ligase by Cdh1 dissociation. Cell Cycle 4(10):1435–1439
388. Bornholdt ZA, Noda T, Abelson DM, Halfmann P, Wood MR, Kawaoka Y, Saphire EO (2013) Structural rearrangement of Ebola Virus VP40 begets multiple functions in the virus life cycle. Cell 154(4):763–774
389. Ferreon AC, Ferreon JC, Wright PE, Deniz AA (2013) Modulation of allostery by protein intrinsic disorder. Nature 498(7454):390–394

Chapter 11

The Roles of Cohesins in Mitosis, Meiosis, and Human Health and Disease

Amanda S. Brooker and Karen M. Berkowitz

Abstract

Mitosis and meiosis are essential processes that occur during development. Throughout these processes, cohesion is required to keep the sister chromatids together until their separation at anaphase. Cohesion is created by multiprotein subunit complexes called cohesins. Although the subunits differ slightly in mitosis and meiosis, the canonical cohesin complex is composed of four subunits that are quite diverse. The cohesin complexes are also important for DNA repair, gene expression, development, and genome integrity. Here we provide an overview of the roles of cohesins during these different events as well as their roles in human health and disease, including the cohesinopathies. Although the exact roles and mechanisms of these proteins are still being elucidated, this review serves as a guide for the current knowledge of cohesins.

Key words Cohesin, Mitosis, Meiosis, Sister chromatid cohesion, Cell cycle, Chromosome segregation, Aneuploidy, Human health, Cohesinopathies, Maternal age effect

1 Introduction

During the S phase of the cell cycle, DNA replication generates a pair of sister chromatids with identical genetic content. The sister chromatids must be physically connected through the G2 phase and will only begin to separate during the transition from metaphase to anaphase during mitosis. The separation is completed in anaphase owing to the loss of cohesion between the sister chromatids. The end result is two daughter cells that are identical to each other and to the parent cell. Separation of sister chromatids in mitosis is the most important event during the cell cycle, and this process must be monitored effectively.

Meiosis occurs strictly in germ cells and differs between males and females. The key difference between meiosis and mitosis is that meiotic cells undergo two cell divisions, meiosis I and meiosis II, without an intervening S phase. During meiosis I, the chromatin condenses as in mitosis and the sister chromatids are held together through a process called cohesion. In prophase I, however, DNA

Eishi Noguchi and Mariana C. Gadaleta (eds.), *Cell Cycle Control: Mechanisms and Protocols*, Methods in Molecular Biology, vol. 1170, DOI 10.1007/978-1-4939-0888-2_11,

crossovers form between paired homologous chromosomes, called bivalents. This involves chromosomal synapsis and formation of a tripartite protein complex, the synaptonemal complex (SC), as well as formation of chiasmata. Prophase I is divided into five distinct substages: leptonema, zygonema, pachynema, diplonema, and diakinesis. The bivalents, which are attached to microtubules through their kinetochores and centromeres, align on the metaphase plate during metaphase I. Unlike in mitosis, the sister chromatids remain attached at their centromeres by cohesion, and only the homologous chromosomes segregate during anaphase I. The second meiotic division is exactly like the division in mitosis, with separation of the sister chromatids. However, the end result is four haploid spermatids or one haploid oocyte (and two or three polar bodies) that are not identical to each other or to the parent cell.

Both mitosis and meiosis require cohesion to keep the sister chromatids together until separation is imminent at anaphase. Cohesion is established during DNA replication before both mitosis and meiosis by multiprotein subunit complexes called cohesins. Although the subunits differ slightly in mitosis and meiosis, the canonical cohesin complex is composed of four subunits. In mammals these are the following: two structural maintenance of chromosome (SMC) subunits (SMC1α or SMC1β and SMC3); one stromalin, HEAT-repeat domain subunit (STAG1 or STAG2 or STAG3 also called SA1 or SA2 or SA3, respectively); and one kleisin subunit protein (RAD21 or REC8 or RAD21L) (Fig. 1). Because these subunits are quite diverse, a wide variety of cohesin complexes with different subunit compositions exists in mitotic and meiotic cells. These cohesin complexes are important for chromosome segregation, DNA repair, gene expression, development, and genome integrity.

Although cohesins have been studied extensively, the exact roles and mechanisms of these proteins are still being elucidated. Recent interest focuses on the roles of cohesins in genome integrity during mitosis and meiosis. The role sister chromatid cohesion plays in replication fork maintenance is still unclear, but several mechanisms have been proposed. Cohesins are also important in double-strand break (DSB) repair and are implemented in cellular responses to DNA damage. Exactly how these processes occur is still unknown, but recent work is illuminating them. This review highlights the importance of cohesins during mitosis and meiosis by distinguishing different aspects of cohesin complexes and their functions. We include the structure of cohesins, the tempo-spatial association of cohesin subunits with chromosomes, recent mammalian studies involving targeted deletion of cohesin subunits, and importance of cohesins in genome integrity. We also discuss the roles and mechanisms of cohesins in human health and disease, highlighting the cohesinopathies and the maternal age effect.

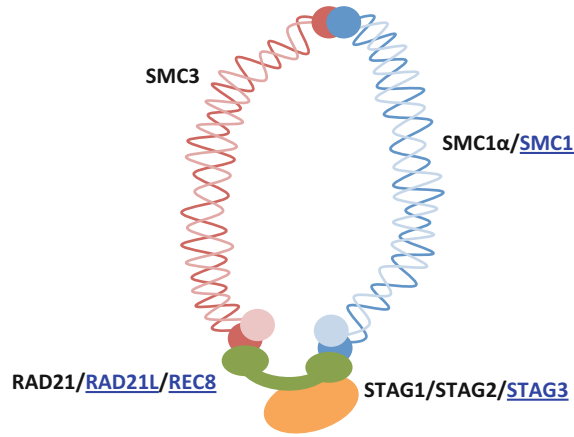

Fig. 1 Cohesin subunits form a ringlike structure. SMC1 and SMC3 form a heterodimer, interacting through their hinge regions. The SMC1 and SMC3 head domains, which contain ATPase motifs, interact with the C- and N-termini of the REC8 or RAD21 or RAD21L kleisin subunit, effectively closing the ring. The STAG1 or STAG2 or STAG3 (also called SA1/SA2/SA3) subunit interacts with RAD21 or RAD21L or REC8, contributing to maintenance of the ring structure. Mammalian subunits are shown. Meiosis-specific subunits are depicted as underlined

2 Mitosis

During somatic cell division, several key events occur before a cell can complete the cell cycle and divide into two identical cells. The specific phases of the cell cycle and its checkpoints allow healthy cells to divide and prevent abnormal cells from replicating. In some instances, however, problems occur and the regulation of the cell cycle is dysfunctional, leading to aberrant cell division. The G1 checkpoint is designed to identify these errors, halt the cell cycle, and to allow only functional cells to progress into S phase. The G2 checkpoint ensures that the cell has replicated its DNA correctly so that it can progress into mitosis and begin cell division. During S phase of the cell cycle, the chromosomes undergo DNA replication in order to produce identical sister chromatids. The sister chromatids must be held together throughout G2 phase and into mitosis by cohesin complexes, most of which are conserved among eukaryotes. During prophase, the loosely coiled chromatin begins to condense into distinct chromosomes while the spindle apparatus migrates to opposite poles of the cell. In early metaphase the condensed chromosomes align on the equatorial plate and then begin to separate in late metaphase as the cell transitions into early anaphase. Cohesion between the sister chromatids is maintained until this point, known as the metaphase-to-anaphase transition. During early anaphase, the sis-

ter chromatids begin to separate to opposite poles via kinetochore attachment to the spindle microtubules. Normally, sister kinetochores attach to microtubules with opposite orientations, known as amphitelic attachment. Attachment of kinetochores to microtubules with the same orientation is called syntelic. Failure to correct erroneous syntelic attachment during mitosis will lead to improper segregation of sister chromatids and the gain or the loss of chromosomes. Once sister chromatids have separated in late anaphase, the final steps of telophase and cytokinesis yield two daughter cells, which are identical to the parent cell.

2.1 What Is Cohesion?

It is critical that cohesion between sister chromatids be maintained until chromosome segregation occurs during both mitosis and meiosis. Disruption of cohesion can lead to genome instability, such as aneuploidy, defects in DNA repair, and chromosomal translocations. Cohesion exists along the sister chromatid arms and at centromeres. In late metaphase, the microtubules at the spindle begin to contract to opposite poles of the cell, biorienting the sister chromatids. Sister chromatid cohesion is an essential part of this process, and it also provides a force that counteracts that exerted by the microtubules [1]. Separation of sister chromatids occurs only after chromosomes have bioriented on the metaphase plate, triggering the dissolution of cohesion and subsequent migration to the spindle poles [2] (Fig. 2). Cohesion between sister chromatids results in a tight association that is not released until the metaphase-to-anaphase transition (Fig. 2). The linkage between the sister chromatids is especially crucial at centromeres because it ensures correct microtubule attachment to the kinetochores.

2.2 Cohesins Create Cohesion Between Sister Chromatids

Sister chromatids are held together by multisubunit complexes called cohesins, which were first identified in the budding yeast, *Saccharomyces cerevisiae*, and in *Xenopus* (Table 1). The cohesin complex is evolutionarily conserved among eukaryotes and consists of four main proteins. The core subunits of the cohesin complex in budding yeast contain two subunits of the SMC family, Smc1 and Smc3; a kleisin subunit protein Scc1/Mcd1; and a stromalin, HEAT-repeat domain protein Scc3/Irr1 [3–6]. Homologues of the cohesin subunits have been identified in a variety of eukaryotic organisms from yeast to humans (Table 1). Higher eukaryotes have three homologues of Scc3 termed SA1, SA2, and SA3, also known as STAG1, STAG2, and STAG3 [7]. SA1/STAG1 and SA2/STAG2 are present in mitosis, while SA3/STAG3 is specific to meiosis. Both SA1 and SA2 associate with the other cohesin subunits to create a diverse group of cohesin complexes in vertebrates [7–9]. Two mammalian homologues of Smc1 are termed SMC1α, found in both mitosis and meiosis, and SMC1β, which is specific to meiosis. Fission yeast Psc3 and Rec11 are also homologues of Scc3, but Rec11 is required for cohesion during meiosis.

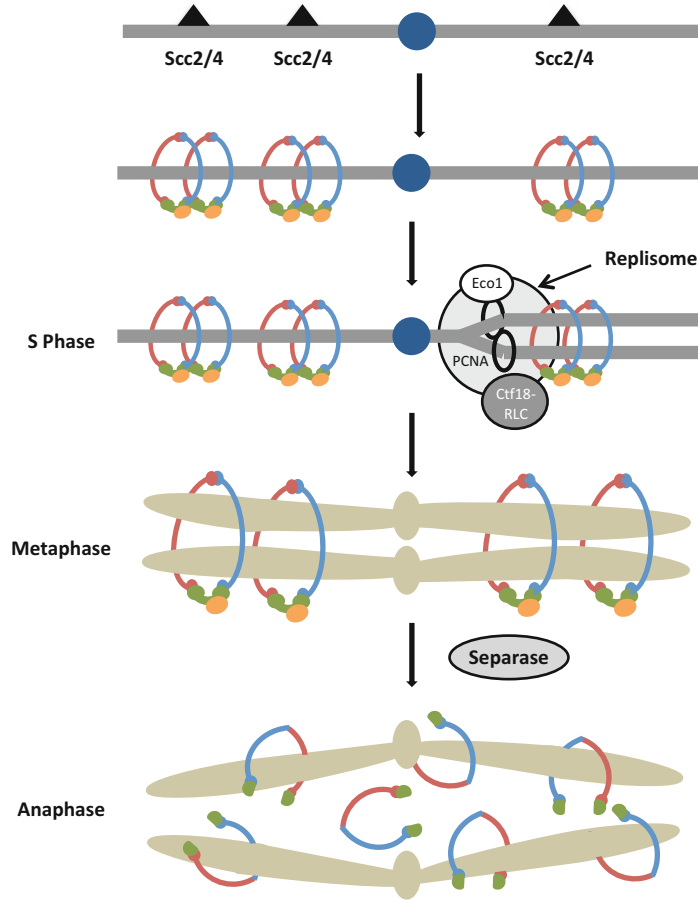

Fig. 2 Cohesion in yeast mitosis. Cohesin complexes require the Scc2/Scc4 protein complex in order to be loaded on chromosomes. Several proteins act together to establish cohesion during DNA replication. These proteins include Eco1 acetyltransferase, the CTF18–RLC complex, and the polymerase-associated protein Ctf4. Tension at centromeres is generated by the bipolar attachment of kinetochores to the mitotic spindle. Following biorientation of sister chromatids, separase is activated to cleave the Scc1 subunit resulting in removal of cohesin complexes, loss of cohesion, and separation of sister chromatids

A model of the cohesin complex has been frequently proposed in which each proteinaceous ring entraps two sister chromatids [6, 10, 11]. The Smc1 and Smc3 molecules consist of long, rod-shaped proteins that fold back on themselves at N and C terminal domains to form long stretches of intramolecular and antiparallel coiled coils [10, 12] (Fig. 1). A characteristic ATP-binding cassette (ABC)-like ATPase is found at one end of the monomer and a half-hinge domain at the other of each Smc1 and Smc3 molecule [12]. The ABC-like ATPase is a member of the protein superfamily that utilizes the energy of ATP hydrolysis to carry out certain functions.

Table 1
Mitotic, meiotic, and regulatory protein homologues

	Budding yeast	Fission yeast	Mammals	*Xenopus*	*C. elegans*	*Drosophila*
Cohesin subunits	Smc1	Psm1	SMC1α, **SMC1β**	XSMC1	Him1	DCAP
	Smc3	Psm3	SMC3	XSMC3	Smc3	Smc3
	Scc1/Mcd1	Rad21 **Rec8**	RAD21, **RAD21L REC8**	XRAD21, **XREC8**	Coh2/Scc1 **Rec8**	DRAD21 **DREC8**
	Scc3/Irr1	Psc3 **Rec11**	SA1/STAG1, SA2/STAG2, **SA3/STAG3**	XSA1, XSA2	Scc3	DSA1, **DSA2/MNM**
Loading	Scc2	Mis4	NIPBL	SCC2	Pqn-85	Nipped-B
	Scc4	Ssl3	Mau2/Scc4	XSCC4	Mau2	Mau2
Establishment	Ctf7/Eco1	Eso1	ESCO1, ESCO2	XECO1, XECO2		Deco/San
Maintenance	Pds5	Pds5	PDS5A, PDS5B	PDS5A, PDS5B	Pds5/Evl14	Pds5
	Rad61	Wpl1	WAPL			
Dissolution	Pds1	Cut2	Securin	Securin		PIM
	Esp1	Cut1	Separase	Separin		SSE/THR
	Cdc5	Plo1	PLK1	PLX1		POLO
	Sgo1	Sgo2 **Sgo1**	Shugoshin/ SGOL1 SGOL2	Shugoshin-like 1 (xSGO1)		MEI-S332

Bold denotes meiosis-specific

One Smc1 and one Smc3 molecule join together through their hinge domains to form a heterodimer [10] when ATP binds. This complex is then joined together by the Scc1/Mcd1/Rad21 subunit, effectively closing the ring [5, 6]. The Scc1 N-terminus binds Smc3, while the C-terminus of Scc1 binds Smc1. Scc3/SA1/SA2 binds to the C-terminus of Scc1 and does not make direct contact with Smc1 or Smc3. Together these cohesin proteins form a very distinct ring structure that are distinguished from other associated proteins.

Biorientation of sister chromatids is tightly regulated and requires several proteins that work in concert to allow the metaphase-to-anaphase transition to occur. Separase is a mammalian cysteine protease; it is the homologue of Esp1 in budding yeast and Cut1 in fission yeast. When the centromeres are under tension in metaphase, the mitotic checkpoint prevents separase activation through Mad2 and Aurora B (Ipl1 in budding yeast) [1]. When activated, Mad2 and Aurora B inhibit APC^{Cdc20}, a ubiquitin ligase for securin, which in turn inhibits separase [13, 14]. This tension is relaxed once all the pairs have aligned correctly on

the metaphase plate. Aurora B/Ipl1 plays a crucial role in promoting biorientation of sister chromatids [1, 15, 16]. In the absence of Ipl1, attachment of sister kinetochores is syntelic, leading both sister chromatids to segregate to the same daughter cell [16]. Aurora B plays a similar role in humans by destabilizing defective kinetochore attachments, but only when there is no tension on the kinetochores.

Several studies utilizing cohesin mutants have helped to elucidate the role of cohesins in sister chromatid cohesion; the mutants were all incapable of keeping sister chromatids together during metaphase [3–5, 17, 18]. In eukaryotic cells lacking cohesin, sister chromatids separate precociously, leading to inefficient biorientation and errors in segregation [19–21]. Mutations in cohesins have also been shown to result in an increased distance between sister centromeres [3, 4]. Cohesin function has been studied in higher eukaryotes by employing different techniques including gene deletion in *Xenopus* and chickens and RNA interference (RNAi) in *Drosophila* and humans. Scc1-deficient cells in chickens show chromosome misalignment at metaphase, resulting in mitotic arrest or delay with aberrant disjunction at anaphase [21]. Sonoda et al. also observed a significant increase in distance between sister chromatids in Scc1-deficient cells, but not full separation. Cells with separated sisters and aberrant anaphases were also observed in *Drosophila* cells depleted of DRAD21 by RNAi [22]. This phenotype, however, was not observed in cells depleted of DSA1, the *Drosophila* homologue of Scc3. These cells had cohered sisters and were able to progress through anaphase normally, despite a slight increase in distance between the sisters. In order to release the cohesin complexes from the DNA, RAD21 is cleaved by separase in mammals. When a deficiency in a cleavable form of RAD21 was expressed in human cells, no loss of centromeric cohesion was observed in prophase or prometaphase [23]. Anaphase, however, occurred aberrantly because the separation of chromosome arms was perturbed. This finding indicates that separation of the chromosome arms is promoted by RAD21 cleavage and that cohesion-independent forces maintain cohesion at centromeres until anaphase.

Although the structure of the cohesin complex forms a tripartite ring [6, 10], how the complex associates with the DNA is not well understood. Different ring models have been described, but two types are most common (Fig. 3). One ring model predicts that both sister chromatids are entrapped within a single cohesin ring [6, 24]. This model proposes that the connection between the sisters is topological rather than biochemical. The model would explain why cohesin does not bind strongly to DNA on its own [25] and why cohesin is readily released once the Scc1 subunit is cleaved [2]. Another type of ring model, the “handcuff” model, suggests that each of the two cohesin rings entraps one sister chromatid, by either binding a single Scc3 subunit or topological interconnection

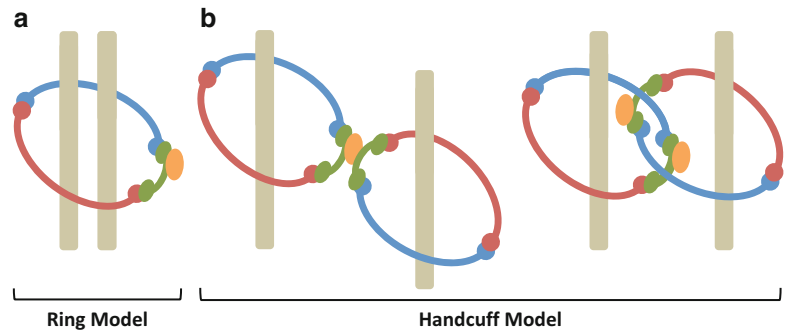

Fig. 3 Models of cohesin rings. (**a**) One ring model predicts that both sister chromatids are entrapped within a single cohesin ring. (**b**) Another type of ring model, the "handcuff" model, proposes that each of the two cohesin rings entraps one sister chromatid, by either binding a single Scc3 subunit or topological interconnection between rings

between rings [26] (Fig. 3). The exact method by which the cohesin complex associates with DNA has yet to be elucidated, but a few models have been proposed.

2.3 The Association and Dissociation of Cohesins

Sister chromatids are tightly associated through cohesion, which prevents the separation of sisters before the metaphase-to-anaphase transition (Fig. 2). As early as S phase of the cell cycle, cohesion components are present in eukaryotes. For example, Scc1 in budding yeast associates with chromosomes during S phase and remains tightly associated until the metaphase-to-anaphase transition [4] (Fig. 2). When Scc1 expression is induced experimentally during G2, it is ineffective at promoting cohesion because it is needed at the time of DNA replication to establish sister chromatid cohesion [27]. Cohesion is also needed throughout G2 to facilitate the repair of DSBs by homologous recombination between sister chromatids [28]. Cohesins are recruited to DSBs in G2 and are implicated in holding the sister chromatid with a DSB near its undamaged sister template. Preventing cohesins from localizing to the DSBs actually abolishes DNA repair [29]. The loading of cohesins is extremely important from S phase through mitosis, but the dissociation signals the beginning of segregation between the sister chromatids.

In budding yeast, the cohesin dissociation and destruction process begins with proteolytic cleavage of the Scc1 subunit at specific residues by Esp1, a separin and protease [2, 30, 31] (Fig. 2). This triggers the dissociation of cohesins from chromosomes that is essential for the segregation of the sister chromatids to opposite poles of the cell in anaphase [2]. This important step is disrupted in Scc1 mutants as demonstrated by the premature separation of sister chromatids [4]. Sister chromatids in yeast that express a non-cleavable

form of Scc1 resistant to Esp1 are unable to separate [2]. Conversely, artificially targeting a different protease to Scc1 can still result in premature separation of sister chromatids [30]. In fission yeast only a small amount of the Scc1 homologue, Rad21, is cleaved at the metaphase-to-anaphase transition to promote sister chromatid separation [32]. A bulk of Rad21 associated with the chromosomes remains during anaphase and may be necessary for the establishment of cohesion at the next S phase. In lower eukaryotes the dissociation process occurs in one step, but higher eukaryotes require additional steps.

In vertebrate cells, cohesin dissociation is regulated by two distinct pathways. A bulk of cohesins is removed from sister chromatid arms during prophase by a separase- and cleavage-independent pathway [9, 33, 34] through phosphorylation by polo-like kinases (PLK) and Aurora B [35–38]. This occurs when chromosomes begin to condense and also when they biorient on the mitotic spindle during prometaphase. Phosphorylation of SA2/STAG2 by Plk1 and Aurora B is essential for cohesion dissociation during these stages, but it is not required in the next stage of removal [39]. Hauf et al. have also shown that although RAD21 phosphorylation is not essential for cohesin dissociation in early mitosis, it enhances the ability of separase to be cleaved during the metaphase-to-anaphase transition. The cohesins remain at the centromeres and are responsible for holding the sisters together while they biorient during prometaphase. They are removed, however, at the metaphase-to-anaphase transition when all the chromosomes have correctly bioriented and the spindle assembly checkpoint has been fulfilled. This occurs through an anaphase-promoting complex or cyclosome (APC/C)- and separin-dependent pathway by cleavage of RAD21 [34]. In human cells, RAD21 is cleaved by separase, a step required to progress into anaphase [40]. Separase is also required for cleavage of the remaining cohesin complexes at sister chromatid arms during metaphase in human cells [41].

Until the metaphase-to-anaphase transition, separase is kept inactive by an inhibitory chaperone called securin [42], also known as Pds1 in budding yeast [31, 43] and Cut2 in fission yeast [44]. Securin is controlled by the ubiquitin protein ligase APC/C. It is destroyed via ubiquitination by the APC/C only after all the chromatid pairs have aligned correctly on the mitotic spindle, allowing separase to become active. Once separase is activated in vertebrate cells by the APC/C, it undergoes autocleavage, similar to that of caspases. Separase cleaves RAD21 and the cohesin ring opens, allowing the release of cohesion and separation of sister chromatids. Sister chromatids do not separate in the presence of non-cleavable Scc1, which suggests that separase may be the only mode of cohesin removal from the sister chromatid arms.

2.4 Accessory Cohesion Factor Components

Proteins that are essential for sister chromatid cohesion but not structural components of the cohesin complex are known as accessory or cofactor proteins (Table 1). Scc2 and Scc4 function together in a complex to load cohesins onto chromosomes; they are conserved among budding yeast and humans and are required for initial cohesin binding to chromosomes [45, 46]. Cohesin is initially loaded onto the Scc2–Scc4 complex at centromeres and at cohesion-associated regions along sister chromatid arms (Fig. 2). Scc2 is conserved in most eukaryotes; the fission yeast homologue is Mis4, and the *Drosophila* homologue is Nipped-B, while the Scc4 homologue in fission yeast is Ssl3. Metazoan Scc2 contains a heterochromatin protein 1 (HP1)-binding domain that has been shown to interact with HP1α, raising the possibility that Scc2 is directly involved in the establishment and maintenance of heterochromatic domains [47]. Depletion of Scc4 results in severe premature sister chromatid separation, suggesting that Scc4 is critical for chromosome cohesion in actively dividing metazoan cells [46, 48]. Both Scc2 and Scc4 are essential for cohesin loading onto chromosomes during S phase.

Pds5 [49, 50], WAPL [51], sororin [52], and haspin [53] are involved in the regulation of cohesin complex association to and dissociation from chromatin. These proteins physically associate either directly or indirectly with the cohesin complex and they are involved in cohesion maintenance. In humans, PDS5 interacts with SA1/STAG1- and SA2/STAG2-containing complexes [9], and in *Caenorhabditis elegans* PDS5 also has an important role in sister chromatid cohesion during mitosis and meiosis [54]. Two vertebrate PDS5 proteins have been characterized, PDS5A and PDS5B, and depletion of these proteins from *Xenopus* extracts results in partial defects in sister chromatid cohesion, but not in mammals [55, 56]. Human WAPL regulates the resolution of sister chromatid cohesion and promotes cohesin complex dissociation during and after anaphase by direct interaction with the RAD21 and SA/STAG subunits [51, 57]. WAPL has also been found on axial and lateral elements (AE/LE) in some prophase I stages in mouse spermatocytes and oocytes, colocalizing with SYCP2 [58, 59]. Sororin was first identified in vertebrates during a screen for substrates of the APC/C, but no homologues have been characterized in other organisms [52]. Sororin is ubiquitinated and degraded after cohesion is dissolved between sister chromatids. Recently, however, sororin has been shown to be necessary for maintaining sister chromatid cohesion in mitotic cells as well as for the stable binding of cohesin to chromatin and efficient repair of DSBs in G2 [52, 60]. Haspin is a histone H3 threonine-3 kinase that colocalizes with the cohesin complex at inner centromeres during vertebrate mitosis. Depletion of haspin in human cells results in premature separation of sister chromatids, suggesting a role in the maintenance of centromeric cohesion prior to anaphase [53]. Thus, PDS5, WAPL, sororin, and haspin are all important mediators of cohesin complex function during mitosis.

2.5 Role of Cohesins in Genome Integrity

Mutations and deletions in replication machinery components result in defects in sister chromatid cohesion, suggesting a functional relationship between processes that involve DNA replication and cohesion establishment. This requires not only the cohesin complex but also a number of accessory protein factors. Initial studies in budding yeast demonstrated that the Eco1/Ctf7 acetyltransferase is required during S phase for cohesion establishment [5, 61, 62] (Fig. 2). Eco1/Ctf7 mutations are synthetically lethal with proliferating cell nuclear antigen (PCNA) mutations. The synthetically lethal phenotype can be rescued, however, by overexpressing PCNA. Recent work has shown that Eco1/Ctf7 is also necessary to establish sister chromatid cohesion in G2/M in response to DSBs [63]. The acetyltransferase domain of Eco1/Ctf7 and its activity are required to generate cohesion during G2/M, as well as during S phase. Thus, cohesion can be generated outside of S phase. Homologues in fission yeast, *Drosophila*, and humans have been termed Eso1, deco, and Esco2, respectively (Table 1).

Another group of proteins involved in establishing cohesion in budding yeast are components of the replication machinery. Investigators have suggested that stabilization of stalled replication forks may be essential for proper establishment of cohesion. Ctf18 is a protein subunit of the alternative replication factor C-like complex (Ctf18-RLC), a seven-subunit complex (Ctf18–Ctf8–Dcc1–Rfc2–Rfc3–Rfc4–Rfc5). Ctf18–RLC establishes sister chromatid cohesion and has been shown to load and unload PCNA onto and off of DNA [64–67]. Eco1/Ctf7, Ctf4, and Ctf18-RLC all act in close proximity to the replication fork and are essential for cohesion [68] (Fig. 2). Ctf4 associates with replication origins and with DNA polymerase α and moves with the replication machinery along chromosomes [66, 67]. Recent work has suggested that Eco1/Ctf7 and Ctf18-RLC colocalize with replication forks, but it is not known whether they move with the replication machinery. In their absence, however, sister chromatid cohesion is compromised. Stabilization or "protection" of stalled replication forks and proper sister chromatid cohesion involves proteins Swi1–Swi3, Ctf18-RLC, and Chl1 in fission yeast [69]. The Swi1–Swi3 complex plays an important role in efficient activation of Cds1, a replication checkpoint kinase. The complex moves with replication forks and is required to prevent accumulation of single-stranded DNA structures near the replication fork [70]. Homologues of Swi–Swi3 exist as the Timeless–Tipin complex in humans and the Tof1–Csm3 complex in budding yeast. The DNA helicase activity of Chl1 is evolutionarily conserved and appears to be involved in sister chromatid cohesion. In fission yeast, Chl1 has been shown to stabilize replication forks and to promote proper establishment of sister cohesion [69], and in budding yeast Chl1 associates with Eco1/Ctf7 for critical involvement in chromatid cohesion [71]. ChlR1, the homologue of Chl1 in mammals, binds cohesin and is required for normal sister chromatid cohesion [72]. Depletion of

ChlR1 results in abnormal sister cohesion and a delay at prometaphase. These proteins are critical for cohesion between sister chromatids, but their functions have not been fully elucidated.

In this same context, Ctf18-RLC has been suggested to control the speed, spacing, and restart activity of replication forks in human cells and is also required for robust acetylation of SMC3 and sister chromatid cohesion [73]. Terret et al. also found that cohesin acetylation itself is a "central determinant of fork processivity," because slow-moving replication forks were found in human cells expressing a form of non-acetylatable SMC3 and in cells lacking the Eco1-related acetyltransferases, ESCO1 or ESCO2. The defect was a consequence of the strong interaction between cohesin and the regulatory cofactors WAPL and PDS5A because removal of either cofactor allowed forks to progress rapidly without ESCO1, ESCO2, or Ctf18-RLC. Although only demonstrated in human cells, these findings suggest a possible new mechanism for clamp loader-dependent fork progression, resulting from the posttranslational modification and structural remodeling of the cohesin ring [73].

Several mechanisms have been proposed for the role of replication fork maintenance in sister chromatid cohesion. One model proposes that cohesin bound to chromosomes before arrival of the replication fork is sufficient to establish sister chromatid cohesion [68]. Therefore, it is thought that the replication machinery slides through the cohesin rings. However, Lengronne et al. have also proposed that the cohesin complex may transiently dissociate upon fork passage through the rings. Fork components, such as Ctf18-RLC and/or Swi1–Swi3, may tether cohesin-related proteins to DNA when forks pass through the cohesin ring [69]. CHTF18, the gene product of the human Ctf18 homologue, has been shown to interact with several cohesin proteins, supporting this idea [64]; recent work also supports a possible interaction of CHTF18 with cohesins during mammalian meiosis [74]. Another model suggests that the cohesin ring may be an obstacle for replication fork progression and causes stalling of the fork [69]. This would require stabilizing proteins, such as Swi1–Swi3 and Ctf18-RLC, at cohesin sites. A third model proposes that Ctf18-dependent unloading of PCNA might loosen the replication fork structure in order for the forks to pass through the cohesin ring without its dissociation [65]. A very recent model proposes that sister chromatid cohesion is established simultaneously with cohesin loading behind the replication fork in close proximity to processing of the lagging strand [75]. Although several models have been proposed, the exact mechanism for replication fork maintenance in sister chromatid cohesion remains unknown.

Cohesins are also involved in cellular responses to DNA damage [76]. Mammalian cohesins are recruited to DSBs; they take part in the ataxia telangiectasia mutant (ATM) DNA damage signal

transduction pathway and are important for survival after irradiation [76]. Two different populations of cohesins contribute to the repair process: cohesins engaged in holding sisters together at the time of the break and cohesins subsequently recruited to chromatin surrounding the break itself [29, 77]. After induction of DSBs, cohesins are recruited to these sites via the DNA damage response pathway. Because recombination between sister chromatids is generally more efficient than between homologous chromosomes, cohesin might inhibit recombination between the homologues. Suppressing recombination between homologues is important in preventing chromosome instability and rearrangements such as nonallelic recombination and/or loss of heterozygosity. In budding yeast the cohesin complex encoded by *MCD1* genes plays a dual role in protecting chromosome and genome integrity [78]. Even a small reduction in the levels of cohesin subunits decreases DSB repair and significantly increases damage-induced recombination between homologous chromosomes. Thus, cohesin levels appear to be a limiting factor in controlling genome integrity [78].

Phosphorylation of cohesin SMC subunits has also been found to be implemented in the cellular response to DNA damage. In response to ionizing radiation, the phosphorylation of S957 and S966 of human SMC1 by ATM kinase is required for the activation of the S-phase checkpoint [79]. Mutant cells defective in SMC1 phosphorylation still exhibited formation of DNA damage foci after exposure to ionizing radiation [80]. However, these cells show decreased survival, chromosomal anomalies, and a defective S-phase checkpoint after DNA damage. Investigators have also reported that SMC3 is phosphorylated at two specific serine residues as well as by two different kinases [81]. Human SMC3 S1083 phosphorylation is inducible and ATM dependent by ionizing radiation, while S1067 is constitutively phosphorylated by CK2 kinase and not increased by ionizing radiation. Phosphorylation of both of these sites, however, is required for the S-phase checkpoint. The roles of cohesins in genome integrity are still being elucidated, but it is well known that cohesins play a larger role during mitosis than originally thought.

3 Meiosis

Although the process of meiosis is similar to mitosis, haploid gametes are generated instead of diploid cells. Several distinct differences between the two processes have been established, and cohesins play a vital role in many aspects of meiosis. Meiosis begins in diploid germ cells following one round of DNA replication in which maternal and paternal homologous chromosomes have been duplicated, each chromosome consisting of two sister chromatids (4C DNA content). Ultimately, these duplicated pairs of

sister chromatids are separated into four different nuclei by two rounds of cell division without any intervening DNA replication. In mammals, male meiosis gives rise to four different haploid gametes (spermatids) whereas female meiosis gives rise to ultimately one haploid gamete (oocyte) and two or three polar bodies. During the first meiotic division (meiosis I), pairs of maternal and paternal homologous chromosomes ultimately segregate in opposite directions. This reduces the chromosome number and also ensures that each gamete will inherit a complete copy of the genome. Pairs of sister chromatids then separate in the second meiotic division (meiosis II) as in mitosis.

Meiosis I is unique in the manner of chromosome segregation and in the distinct processes that occur during prophase I. Homologous recombination is an essential phenomenon during meiosis because it physically joins the maternal and paternal homologues before segregation and ultimately generates new combinations of alleles and genetic variation. Homologous recombination during meiosis I (also called meiotic recombination) results in the exchange of DNA between maternal and paternal chromatids, and the sites of DNA exchange are called crossovers. Crossovers are seen cytologically as structures called chiasmata. Chiasmata and cohesion along sister chromatid arms hold homologous chromosomes together prior to their segregation in anaphase I. Attachment of sister kinetochores to microtubules with the same polarity, called syntelic attachment, is another feature that is unique to meiosis I. This type of attachment of sister kinetochores is also known as mono-orientation, and it differs from the biorientation of sister kinetochores during mitosis. Because the chiasmata physically link homologous chromosomes, tension is generated and a new form of equilibrium is established during metaphase I. Chiasmata ensure that the tension will be generated if both maternal centromeres attach to microtubules with one orientation and both paternal centromeres attach to microtubules with the opposite orientation. The spindle machinery senses this bipolar attachment-like tension between homologous chromosomes and not sister chromatids in metaphase I. Although tension on homologues of maternal and paternal centromeres pulls them in opposite directions, they are prevented from disjoining during prophase I by the presence of chiasmata and cohesion between sister chromatids. Cells systematically suppress amphitelic attachment and promote syntelic attachment of the sister chromatids during the first meiotic division to prevent aneuploidy. During the second meiotic division sister kinetochores attach to microtubules in an amphitelic manner and the sisters are segregated to opposite poles during the metaphase-to-anaphase transition, as in mitosis. Only sister chromatid arm cohesion is destroyed during anaphase I, leaving centromeric cohesion to persist. This process, along with resolution of chiasmata, results in the separation of homologues only and not sister chromatids during

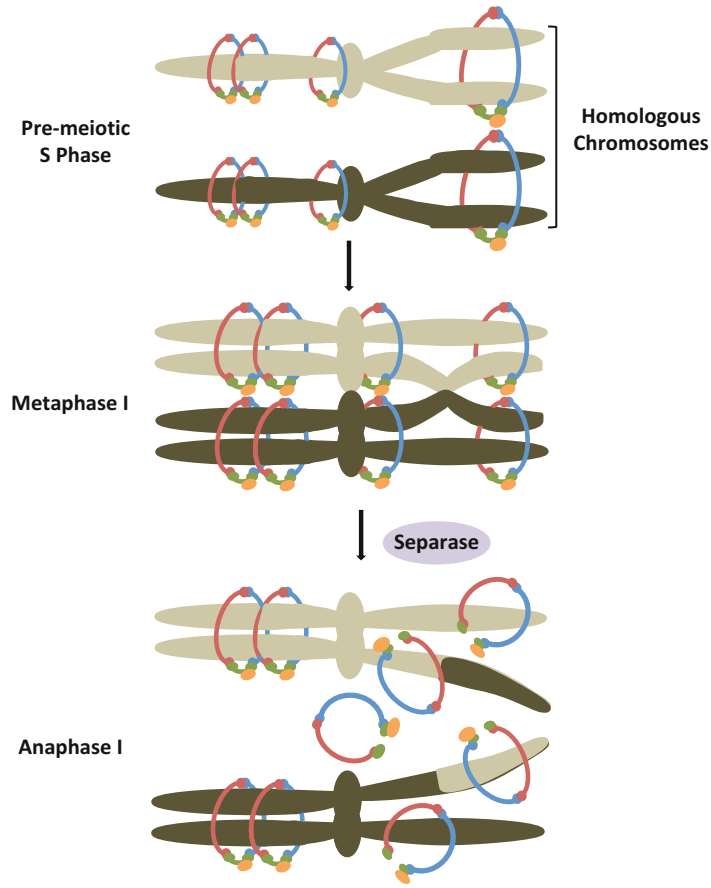

Fig. 4 Cohesion in yeast meiosis I. Rec8 replaces Scc1 of the cohesin complex in S phase. During prophase I homologous chromosomes pair and meiotic recombination leads to DNA crossovers between non-sister chromatids. In order for homologous chromosomes to segregate, kinetochores of sister chromatid pairs must each be mono-oriented to opposite poles during metaphase I. Separase cleavage of Rec8 during anaphase I, much like that during mitosis, resolves the cohesion distal to crossovers to allow segregation of homologues. In order to allow for the proper biorientation and segregation of sister chromatids during meiosis II, cohesion proximal to centromeres is preserved

anaphase I. Centromeric cohesion in meiosis II is essential to ensure the bipolar attachment of sister kinetochores as in mitosis.

Cohesion between sister chromatids is established during premeiotic DNA replication and differs from its mitotic counterparts (Fig. 4). Meiotic cohesins must participate in the recombination process as well as persist at centromeres through the first division. However, cohesion along sister chromatid arms must dissolve during meiosis I to allow the homologues, joined by chiasmata, to separate (Fig. 4). The cohesion along sister chromatid arms ensures correct chromosome alignment during the first division, and

cohesion at the centromeres ensures proper segregation at the second division [82, 83]. Once cohesion between sister chromatid arms is released, the microtubules pull maternal and paternal centromere pairs to opposite poles of the cell. These different types of cohesion are extremely important during meiosis because the chromosomes must undergo two distinct rounds of segregation. Cohesion at the centromeres ensures biorientation of chromatids on the spindle and accurate segregation during meiosis II, as in mitosis. The destruction of centromeric sister chromatid cohesion triggers their disjunction and segregation to opposite poles of the cell, yielding haploid cells. The two steps involved in cohesin removal during meiosis are similar to the steps in prophase and anaphase of mitosis.

Meiotic recombination has been most well characterized in yeast. The process begins with generation of DNA DSBs by Spo11 endonuclease [84]. This occurs in early prophase I at multiple locations along each of the four chromatids. The 5′ ends resulting from Spo11 cleavage are resected in yeast by Rad50, Mre11, and Com1/Sae2 to form single-stranded 3′ overhangs on each side of the break [85–87]. First-end capture occurs by one 3′ overhang invading the homologous non-sister chromatid [88]. The invading 3′ end becomes paired with the complementary strand from the other chromatid, creating a template for repair. The displaced strand will then pair with the second 3′ overhang on the original chromatid. The ends are ligated to the newly synthesized DNA, creating a joint molecule. At this point, the non-sister chromatids (one maternal and one paternal) will have recombined homologues and crossing over will be complete, creating a double Holliday junction (DHJ). The final step in the recombination process is the resolution of DHJs by cleaving of a pair of chromosome strands at each end and their reciprocal ligation. The cleavage can be either horizontal or vertical, but crossover occurs only when one junction is resolved horizontally and the other vertically. Most organisms create several of these exchanges per chromosome, but only one chiasma is needed to hold a pair of homologous chromosomes together.

3.1 Unique Meiotic Cohesin Characteristics

The cohesin complex in germ cells differs from somatic cells, and distinct meiosis-specific subunits have been characterized in various organisms. In both fission and budding yeast, Rad21 is involved in mitosis and Rec8 is the meiotic paralogue of Scc1 [82, 89, 90]. Fission yeast has two Scc3 homologues, Rec11 and Psc3 (Table 1). Rec11 is meiosis-specific and forms a complex with Rec8, mainly along the chromosome arm regions, and the complex is critical for recombination [91]. Psc3, however, is expressed in mitosis and meiosis and associates with Rec8 mainly at the centromeres. Although inactivation of Rec11 impairs sister chromatid cohesion specifically along the arm and reduces the rate of recombination, Psc3 is

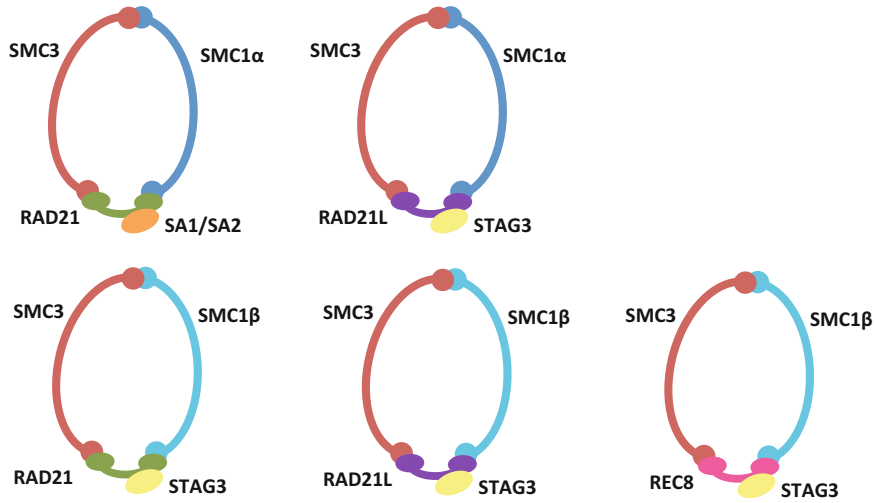

Fig. 5 Putative subunit compositions of some of the cohesin complexes in mammals. Differences in spatiotemporal distribution occur throughout the meiotic divisions

dispensable for these functions but it is required for centromeric cohesion persisting throughout meiosis I. In mammals, the meiotic paralogues of SMC1, SCC1/RAD21, and SA/STAG1/2 are SMC1β, REC8, and SA3/STAG3, respectively [92–96] (Table 1). Although these three subunits are strictly expressed in germ cells, SMC1α, RAD21, and SA2/STAG2 are also implemented in meiotic chromosome dynamics [97]. Recently, a third kleisin subunit in mammals, named RAD21L, has been identified in meiotic cells and localizes along the AE/LEs of the SC throughout meiosis I [98–101]. This subunit may be involved in synapsis initiation and crossover formation between homologous chromosomes. RAD21L has also been shown to be a functionally relevant meiotic kleisin subunit that is essential for male fertility and maintenance of fertility during natural aging in females [99]. Evidence for participation of different cohesin complexes during mammalian meiosis suggests a variety of putative cohesin complexes formed by combinations of cohesin subunits (Fig. 5). Several distinct complexes are thought to exist, showing differences in spatiotemporal distribution throughout the meiotic divisions.

3.2 Cohesins in Genome Integrity During Meiosis

In yeast Chl1, Ctf4, and Ctf18-RLC are necessary for sister chromatid cohesion in both mitosis and meiosis, and they are essential for chromosome segregation during meiosis. In fact, they contribute significantly to the establishment of cohesion in the region of centromeres. Deletion of *CTF18,* or *CHL1,* or *CTF4* in budding yeast leads to severe defects in chromosome segregation, aneuploidy in the spores, and meiosis II nondisjunction at a high fre-

quency [102]. In yeast, frequent errors in meiosis II, rather than homologue nondisjunction in meiosis I, predominantly contribute to the mis-segregation phenotype in meiotic mutant cells.

Cohesin is particularly important in meiotic cells to hold bivalents together during homologous recombination and DSB repair. Whether cohesin is actively recruited to sites of DSBs during meiosis, as it is in mitotic cells, is not well known. A conserved DNA damage checkpoint, known as the pachytene checkpoint, also monitors the efficient repair of meiotic DSBs and induces apoptosis when DSBs are not repaired in a timely fashion. The involvement of cohesin in repair of meiotic DSBs and activation of the pachytene checkpoint have been demonstrated in the *C. elegans* germline [103]. Loading of cohesin onto chromatin during S phase, and also in response to DSBs in post-replicative cells, depends on a conserved complex composed of Scc2 and Scc4 proteins. Meiotic cohesin is loaded by Scc2, and in the absence of meiotic cohesin, recombination intermediates accumulate extensively but fail to trigger the apoptotic response of the pachytene checkpoint [103]. Meiotic cohesion is required for early DSB processing and for efficient recruitment of DNA damage sensors [103]. This suggests that cohesin is involved in early events of the meiotic DNA damage response.

3.3 Specific Events in Meiosis I and II

Prophase I is prolonged in mammalian meiosis, and it is divided into substages according to chromatin changes based on cytological studies. The most important event during prophase I is formation of the SC, which forms between homologous chromosomes. This structure supports meiotic recombination, and it represents an essential difference between mitosis and meiosis. Meiosis-specific cohesin complexes are believed to form a scaffold to which components of the SC can attach.

During leptonema of prophase I, the AE form along each chromosome. SYCP2 and SYCP3 create a bipartite polymer along the bivalent axes and are the main structural protein components of the AE/LE [104–107]. Then in zygonema, homologues begin to pair and central elements (CE) are deposited between the AE (now called LE). Zip1 in yeast and SYCP1 in mammals, known as transverse filaments, form the center of the SC or the central elements. In pachynema, homologues synapse along their length, the SC fully forms, and DNA recombination takes place. This close association between maternal and paternal axes along the entire length of the bivalent is called synapsis, and it is achieved by the SC. The onset of diplonema is characterized by the disassembly of the SC and homologue desynapsis. The final stage of prophase I is diakinesis, which quickly progresses into metaphase I. Homologues remain connected at chiasmata, which can now be seen cytologically at this stage, and cohesion between sister chromatids prevents premature segregation. Immunocytological studies have helped characterize the spatiotemporal localization of cohesins during meiosis.

3.3.1 Leptonema

During prophase I in spermatocytes, cohesin subunits are observed at different stages and in different quantities. SMC1β can be observed along the asynapsed AE, and STAG3 is found along the AE during leptonema [95, 96]. REC8 is localized along asynapsed, synapsed, and desynapsed AE/LE throughout prophase I [92]. RAD21, like REC8, also appears at the AE/LE during all stages of prophase I [108, 109]. RAD21L is expressed from premeiotic S phase and localizes along the AE in leptonema, with some conflicting reports as to whether it persists to mid-pachynema or diplonema and into metaphase I [98–101].

3.3.2 Zygonema

In the zygotene stage of prophase I, *SMC1β* is found along the asynapsed AE and also the synapsed LE [96]. SMC1α and SMC3 are observed in a distinct punctate pattern along the synapsed LE in late zygonema and are found to interact with SYCP2 and SYCP3, structural protein components of the SC [110]. STAG3 is observed along the AE/LE as in leptonema [95]. RAD21L localizes along the AE/LE in zygonema in a punctate or a continuous linear pattern depending on the report [98–101].

3.3.3 Pachynema

During pachynema, SMC1α and SMC3 are still seen immunocytologically in a distinct punctate pattern along the synapsed LE and interact with SYCP2 and SYCP3 [96, 110]. SMC1β and STAG3 are also found along the synapsed LE. Although RAD21L is distributed along the SC through at least mid-pachynema, reports of its localization vary. Some groups have reported that RAD21L is evenly distributed along the AE/LE, while other groups have reported that it is discontinuous [98–101]. In addition, two groups have reported that RAD21L localizes in a mutually exclusive pattern with REC8, perhaps suggesting inherent loading sites for these cohesins [100, 101].

3.3.4 Diplonema/Diakinesis

SMC1α is lost from the desynapsed LE during diplonema and it is not detected on bivalents in diakinesis or metaphase I. SMC3, however, persists at the desynapsed LE but is progressively lost and accumulates at centromeres during diakinesis. SMC1β is found along the desynapsed LE, most of it dissociating in late diplonema, and accumulating at the centromeres during diakinesis. STAG3 is still visible along the LE but is observed as patches along the contact surface between sister chromatids, called the "interchromatid domain," during diakinesis [95, 111]. This subunit is maintained at the chromosome arms and centromeres until metaphase I [95]. During late diplonema, RAD21 appears along desynapsed LE but also accumulates in areas where it is colocalized with SYCP3. By late diplonema to diakinesis, RAD21 is partially released from the LE [108]. REC8 has been found at the interchromatid domain along chromosome arms and centromeres during diakinesis and metaphase I bivalents [92, 110]. RAD21L disappears by mid-pachynema or diplonema as it accumulates at centromeres [98–101].

Based on the studies mentioned here, several different cohesin complexes are present during mammalian prophase I (Fig. 5). The complex, SMC1α/SMC3/RAD21/SA1 or SA2, is present during premeiotic S phase. SMC1α/SMC3/RAD21L/STAG3 and SMC1β/SMC3/RAD21L/STAG3 are present along the AE/LE from premeiotic S phase through diplonema. The canonical meiotic complex, SMC1β/SMC3/REC8/STAG3, and the SMC1β/SMC3/RAD21/STAG3 complex are likely present throughout prophase I. These complexes ensure that at the end of prophase I homologous chromosomes remain connected at chiasmata despite dissolution of the SC.

3.3.5 Metaphase I

In metaphase I mammalian spermatocytes, STAG3 is seen as discontinuous bright patches lining the interchromatid domain along sister chromatid arms, but not at chiasmata [95]. STAG3 is also present at the centromere domain just below the closely associated sister kinetochores. The same pattern of labeling has also been reported for REC8 [92, 110]. SMC3 was initially reported to be concentrated at centromeres and absent from chromosome arms [96, 112]. However, recent work has suggested that SMC3, like STAG3 and REC8, is distributed along the interchromatid and centromere domains of metaphase I bivalents [113]. The distribution of RAD21 is distinctive; it accumulates at the inner centromere domain in a "double cornet-like" configuration with SYCP2 and SYCP3 and is also seen as small patches at the interchromatid domain [108]. SMC1β also localizes with SYCP2 and SYCP3 to mainly the centromeres of metaphase I spermatocytes, but the exact configuration at the inner centromere domain has not been studied [114]. Studies suggest that RAD21L remains in residual amounts, partly colocalized with SYCP3 at or near centromeres, although reports are conflicting [98–101].

3.3.6 Anaphase I to Metaphase II

The exact localization pattern of cohesin subunits from anaphase I to metaphase II is not known. REC8, STAG3, RAD21, SMC3, and SMC1β persist at centromeres during anaphase I, although their patterns differ [92, 95, 108, 109, 112]. The dynamics of these subunits are unknown during telophase I and interkinesis, but some information is known about a few of the subunits. RAD21 changes its distribution to a bar-like pattern in between sister kinetochores at telophase I centromeres [108]. These bars are also seen during interkinesis at "heterochromatic chromocenters," which represent closely associated centromeres [108, 113]. This pattern disappears at prophase II. STAG3 and REC8 have also been reported to disappear from centromeres during telophase I and are no longer seen in interkinesis nuclei [95, 113, 115].

3.3.7 Metaphase II

Reports regarding the appearance and distribution of cohesin subunits at centromeres in metaphase II are conflicting. Original

studies in rodent surface-spread spermatocytes indicated that RAD21, SMC1β, and SYCP3 appeared as rod-shaped aggregates between sister centromeres [96, 109]. However, RAD21 and SYCP3 were not visualized at centromeres in squashed spermatocytes [108, 115]. The conflicting results obtained are attributed to differences in the techniques used as well as possible differences in the ability to detect small amounts of the cohesins [108, 113, 115].

3.3.8 Female Meiosis

Although features of meiosis are similar in male and female mammals, important gender-specific differences exist in the onset, timing, duration, and outcome of meiotic processes. Female germ cells enter meiosis as oocytes during fetal development and arrest at the end of the diplotene stage of prophase I, known as dictyate. Dictyate arrest lasts from the late stages of fetal development until resumption of meiosis just prior to ovulation. Information regarding chromosome cohesion during this extended time frame and whether cohesin complexes established during fetal life are present decades later is not known. Localization patterns of several meiotic cohesins have been compared to SYCP3 during the formation and dissolution of the SC in fetal oocytes during human and murine prophase I [116]. Results from this study suggested that STAG3, REC8, SMC1β, and SMC3 associate with chromatin to form a "cohesin axis" prior to AE formation during female meiosis in mammals [116]. In human fetal oocytes STAG3 and REC8 are scattered throughout preleptotene nuclei but become more organized in leptonema and partially colocalize with SYCP3. By zygonema, however, REC8 and STAG3 colocalize with SYCP3 and persist into early diplonema. In mouse oocytes expression of STAG3, SMC3, and SMC1β first appears as fibers in leptonema prior to AE formation, similar to the timing of cohesin axis formation in human oocytes. The cohesin fibers become more prominent in zygonema with AE formation and then colocalize with SYCP3 in pachynema. During dictyate arrest in mouse oocytes there is gradual loss of both SYCP3 and the cohesin axis [116].

A recent study analyzed the distribution of SMC3, REC8, SMC1β, STAG3, and SYCP3 in human oocytes throughout meiosis [117]. As meiosis progresses into leptonema in oocytes, the cohesins appear as thin threads and their staining completely overlaps with SYCP3 and remains colocalized through diplonema. Unlike mouse oocytes, cohesins do not appear to be lost during dictyate arrest in human oocytes. REC8, STAG3, and SMC3 appear as short filaments with a diffuse pattern of distribution in the nucleoplasm and cytoplasm [117]. SMC1β, however, appears intensely all over the oocyte, including the nucleus and cytoplasm. In fully grown germinal vesicle oocytes STAG3 appears as cohesin threads all over the chromatin, including intense staining at the nucleolus. In metaphase I oocytes, cohesins are seen as bright patches along the interchromatid domain and the centromeric area of all bivalents. From early

anaphase I, cohesins are no longer seen at the arms of sister chromatids and are confined to the centromeric area. At metaphase II, REC8, STAG3, SMC1β, and SMC3 are observed in the space between sister kinetochores, and SYCP3 appears as small dots partially colocalizing with each sister kinetochore.

3.3.9 Synaptonemal Complex: Central Elements and Cohesin Function

One component of the CE unique to mammals is FK506-binding protein 6 (FKBP6), which belongs to the FKBP family of proteins and is expressed in mouse male and female germ cells during prophase I [118]. FKBP6 localizes to SYCP1 of synapsed chromosome cores and also coimmunoprecipitates with SYCP1, suggesting a role in the assembly and maintenance of the SC [118, 119]. FKBP6 appears to interact with NEK1, a never-in-mitosis A (NIMA)-related kinase 1 dual-specificity serine–threonine and tyrosine kinase [119]. NEK1 is highly expressed in spermatogonial cells and spermatocytes during prophase I in mice. SMC3 staining decreases and becomes more diffuse in spermatocytes of wild-type mice during diplonema. However, SMC3 persists in diplotene *Nek1*-deficient spermatocytes, consistent with a role of NEK1 in removal of the meiotic cohesin SMC3 from chromosome cores at the end of prophase I [119]. Similar findings are observed in *Fkbp6*-null spermatocytes, suggesting that the FKBP6–NEK1 pathway may be involved in cohesin removal at the end of prophase I. However, normal accumulation of SC and DSB repair proteins is seen in *Nek1*-deficient spermatocytes [119].

3.4 Loss of Cohesion Through Destruction of Cohesins

Destruction of cohesion distal to chiasmata is mediated by the same mechanism that triggers disjunction of chromatids in mitosis. Rec8 is present along sister chromatid arms during metaphase I but disappears from the arms at the onset of anaphase I in budding yeast and mice [82, 83, 92]. In budding yeast resolution of chiasmata and removal of Rec8 from sister chromatid arms depend on cleavage by separase, just like Scc1 in mitosis [120]. However, Rec8 remains in the area of centromeres until the onset of anaphase II in budding yeast [82], fission yeast [83], *C. elegans* [121], and mouse spermatocytes [92]. These findings suggest that eukaryotic organisms maintain sufficient cohesion around centromeres during meiosis II by protecting Rec8 from separase cleavage during meiosis I. Mutations in *rec8* result in precocious separation of sister chromatids during anaphase I. In fission yeast, Rad21 ectopically expressed at centromeres cannot rescue this defect, suggesting that Rec8 is responsible for the persisting centromeric cohesion until meiosis II and it cannot be replaced by Rad21 [89]. Protection of centromeric Rec8 is lost after anaphase I, as indicated by the dissociation of Rec8 from chromosomes with reactivation of separase at the onset of anaphase II. If the protection were to dissolve prior to inactivation of separase, premature disjunction of sister centromeres would occur. It is interesting, however, that exchange of

Scc1 for Rec8 during mitosis does not prevent cohesin cleavage at the centromere, suggesting that other meiosis-specific factors are involved [120]. In *C. elegans*, where separase is also required for meiosis I, the phosphorylation of Rec8 by the Aurora B protein Air2 might ensure that only Rec8 distal to chiasmata is cleaved at the first division [122–124]. In budding and fission yeast, the expression of a nondegradable form of Rec8 that carries mutations at the separase target sites dominantly blocks the onset of anaphase I. This phenotype is suppressed by the elimination of chiasmata, suggesting that the separase-mediated cleavage of Rec8 triggers homologue separation by resolving chiasmata on the arm regions [120, 125]. An accumulation of securin, the inhibitory chaperone of separase, has been observed not only in meiosis I but also in meiosis II, indicating separase activation at both meiotic divisions [120, 125]. The same observation has been made in *C. elegans* and in mice, where the activation of securin is crucial for the progression of meiosis I [122, 126, 127].

Identification of a protein that protects centromeric cohesion during prophase I has revealed why centromeric Rec8 is only cleaved during meiosis II and not during meiosis I. In fission yeast this protector of Rec8 centromeric cohesion is a gene product that when coexpresssed with Rec8 causes toxicity during mitotic growth [128]. The gene encodes a meiosis-specific protein named shugoshin (Sgo1), a homologue of the *Drosophila* protector Mei-S332 [129–131]. Shugoshin associates with protein phosphatase 2A (PP2A) and forms a complex at centromeres, which blocks the cohesin phosphorylation necessary for removal of cohesion and also prevents premature loss of centromere cohesion [132, 133]. Fission yeast Sgo1 localizes exclusively at the site where Rec8 is predicted to have a role in centromeric protection during meiosis I [91]. Budding yeast shugoshin is also thought to have the same effect on Rec8 during meiosis I [128, 130, 131]. Fission yeast and mammals also possess paralogues of Sgo1 called Sgo2 and SGOL2, respectively. Their proteins are ubiquitously expressed throughout the mitotic and meiotic cell cycle in yeast, [128, 129] but only SGOL2 is essential for meiosis in mammals [134]. However, both SGOL1 and SGOL2 are expressed in mouse germ cells, and SGOL1-depleted oocytes also show meiotic defects [135, 136]. During metaphase II, SGOL2 relocates in a tension-dependent way to the centromeres in mouse spermatocytes and oocytes [115, 135]. In the absence of Sgo1, fission yeast sister chromatids co-segregate to the same pole, implying that monopolar attachment is intact, but they start to separate precociously during anaphase I. Thus because Rec8 is no longer protected without Sgo1 during meiosis I, the sister chromatids separate prematurely in anaphase I.

The finding that shugoshins protect centromeric cohesion by recruiting PP2A suggests that the phosphorylation of a protein is needed for Rec8 cleavage. In mitotic yeast cells, cohesin cleavage is

promoted through phosphorylation of Scc1 by PLK (Cdc5 in yeast), which also participates in the phosphorylation of Rec8 [36]. Replacement of alanine for Rec8 residues that are thought to be phosphorylated by Cdc5 has no significant effect on the kinetics of cohesin cleavage at meiosis I [137]. Recent work has shown that casein kinase 1δ/ε (CK1δ/ε), Hrr25 in yeast, and Dbf4-dependent Cdc7 kinase (DDK) are essential for Rec8 cleavage, not Cdc5 [138]. Investigators have proposed that Hrr25- and DDK-dependent phosphorylation of Rec8 promotes cohesin cleavage in meiosis I, whereas dephosphorylation of Rec8 by PP2A bound to Sgo1 protects it from separase at centromeres.

3.5 Characterization of Cohesin Subunit Mutants

The characterization of mice deficient in meiosis-specific subunits has helped us to understand the function of these proteins in mammalian meiosis. Both male and female *SMC1β*-deficient mice are sterile and show defects in SC formation and premature loss of sister chromatid cohesion [139]. *SMC1β*-deficient spermatocytes undergo pachytene arrest, whereas mutant oocytes reveal premature loss of cohesion at metaphase II. *REC8*-deficient male and female mice are also sterile and display severe defects in synapsis and sister chromatid cohesion, but the phenotypes are different than those of *SMC1β* mutant mice [140]. SC formation occurs aberrantly in *REC8* mutant spermatocytes between sister chromatids instead of between homologous chromosomes. AE-like structures are formed, even though synapsis does not occur correctly. Rec8 deletion mutants in budding yeast and *C. elegans* also cause sister chromatids to lose cohesion and to separate early, yielding aneuploid gametes [82, 121]. However, in fission yeast Rec8 mutants lose cohesion only at centromeres because Rad21 provides cohesion along sister chromatid arms [83]. RAD21L-deficient male mice show a defect in chromosome synapsis at prophase I, which leads to meiotic arrest at a zygotene-like stage [99]. Deficient females, however, are initially fertile but develop an age-dependent sterility.

Absence of SYCP2 or SYCP3 in mice results in a sexually dimorphic phenotype: males are sterile, and females are subfertile [141, 142]. Males show a disruption in chromosomal synapsis and meiotic arrest in prophase I, but females have reduced litter size and embryo death due to chromosome mis-segregation from aneuploid oocytes. *Sycp3*-deficient male mice show defects in AE formation, chromosomal synapsis, and SC assembly [141]. A null mutation of *Sycp1* causes sterility in homozygous male and female mice. Most of *Sycp1*-deficient spermatocytes display defects in meiotic recombination and arrest at the pachytene stage, and mutant ovaries reveal a paucity of oocytes and growing follicles [143]. Male *Fkbp6*$^{-/-}$ mice are sterile, whereas mutant females are fertile. The mutant spermatocytes show severe defects in pairing and synapsis and arrest at pachytene of prophase I [118]. Similar to

Fkbp6-null mice, *Nek1*-null male mice show severely impaired fertility consistent with an absence of epididymal sperm and a reduction in testis weight and size [119]. Holloway et al. also demonstrated that *Nek1*-null mice show defects in cohesin SMC3 removal during diplonema, suggesting that NEK1 plays a role in cohesin unloading at the end of prophase I.

4 Human Health and Disease

4.1 Cohesinopathies

Human diseases caused by mutations in primary genes associated with the cohesin network are termed cohesinopathies. All the cohesinopathies that have been identified manifest as multisystem developmental disorders, but they have distinct phenotypes. Although mutations in the cohesin network might be expected to generate defects in chromosome segregation and/or the ability to repair DNA, mutations of this nature are probably lethal and have not been reported. Instead, cohesinopathies are characterized by a variety of developmental defects, including growth and mental retardation, limb deformities, and craniofacial anomalies. These phenotypes are consistent with a role for cohesins in gene expression during embryogenesis. Although downregulating cohesin sufficiently to cause significant sister chromatid cohesion defects is lethal in eukaryotes, the mechanism of action by which cohesin affects developmental processes appears to be through a noncanonical role as a regulator of gene expression and other genomic processes. The molecular mechanisms underlying the changes in gene expression that result in cohesinopathies are not well known. Mechanisms have been proposed, such as actions of cohesin in transcriptional activation, transcriptional repression, transcript termination, and long-distance enhancer–promoter interactions, none of which are mutually exclusive.

4.2 Cornelia de Lange Syndrome

Cornelia de Lange syndrome (CdLS) is a dominantly inherited, multisystem developmental disorder characterized by classic facial anomalies, upper extremity malformations, hirsutism, cardiac defects, growth and cognitive retardation, and gastrointestinal abnormalities. Behavioral and cognitive defects display a wide range of severity, as do limb malformations, which can range from small digits to both upper and lower limb defects. CdLS is caused by point mutations or small deletions/insertions in one of the two alleles of *SMC1*, SMC3, or most commonly, *NIPBL* (Nipped-B-like and the human orthologue of *SCC2*) [144–147]. Mutations in NIPBL, the vertebrate homologue of the yeast Scc2 protein and a regulator of cohesin loading and unloading, are responsible for approximately 50 % of cases of CdLS [144, 145, 148]. Two other mutations in SMC1 and SMC3 were shown to result in an X-linked form of CdLS that is milder than the syndrome caused by NIPBL mutations [146].

The mutations in the SMC proteins have been identified within the coiled coil of the ATPase head domain and near the interface of the coiled coil with the hinge domain [147]. Mutations in this region disrupt DNA binding and ATP hydrolysis involved in loading cohesins. Mutations in *NIPBL* have been identified throughout the coding and noncoding regions of the gene. Alternative splicing of *NIPBL* is consistent with multiple transcripts detected by Northern blot analysis, and some types of mutations tend to result in more severe forms of CdLS [144, 148]. Mutations have been identified only in the context of the genomic copy and may affect particular splice variants, potentially affecting the severity of the disease phenotype.

The mutations in the SMC proteins could weaken interactions between cohesin subunits or between chromatin and cohesin. However, the mutations most likely do not abolish complex formation or chromatin association completely because patients do not exhibit severe defects in chromosome cohesion, DNA damage response, or chromosome segregation [149, 150]. Sister chromatid cohesion has been reported to be mildly affected in cell lines derived from individuals with mutations in *NIPBL* [149], but no defects in precocious sister chromatid separation have been observed in cells with a mutation in *SMC1* or SMC3 [151]. CdLS mutations could affect the dynamics of cohesin subunit–chromatin interaction, resulting in mild destabilization of the complex on chromatin without affecting the overall function of the complex for cohesion. Interestingly, *NIPBL* expression in human embryonic tissue sections is consistent with affected tissues and organs seen in patients [145]. Molecular studies of cohesins in this disease will help elucidate the defects underlying the mechanism of the mutated cohesins.

A mouse model of CdLS has been developed in which the mice are heterozygous for an *Nipbl* mutation [152]. These mice show similar defects that are characteristic of the syndrome, including small size, craniofacial anomalies, delayed bone maturation, microbrachycephaly, behavioral disturbances, and high mortality during the early weeks of postnatal life. The *Nipbl* deficiency in heterozygous mice leads to small but significant transcriptional dysregulation of many genes. Expression changes at the protocadherin β locus, which encodes synaptic cell adhesion molecules for neural tube and CNS development, as well as other loci, support the notion that *NIPBL* influences long-range chromosomal regulatory interactions. Although this model has proven to be beneficial in studying CdLS, closer scrutiny of cohesins in the disease is still needed.

4.3 Roberts Syndrome/SC Phocomelia

Roberts syndrome and SC phocomelia are rare, recessively inherited, multisystem disorders involving craniofacial, cardiac, limb, other systemic abnormalities, and neurocognitive dysfunction. Roberts syndrome and SC phocomelia are similar disorders, but SC phocomelia

represents a milder phenotype of Roberts syndrome. Chromosomal features in metaphase spreads of patients with Roberts syndrome reveal a lack of cohesion in heterochromatic areas around centromeres and at the distal region on the long arm of the Y chromosome, known as heterochromatin repulsion or puffing or premature centromere separation [153, 154]. Mitotic chromosomes have a railroad track-like appearance; although this resembles a cohesion defect, it does not appear to cause chromosome segregation defects. Roberts syndrome/SC phocomelia is caused by a mutation in both alleles of *ESCO2*, the human orthologue of yeast *ECO1*. In most cases the mutations are truncating, but at least two mutations that disrupt the acetyltransferase activity of ESCO2 have been identified [155]. The majority of mutations identified result in low or undetectable levels of mRNA compared with wild-type *ESCO2* expression. Although there are two genes that encode *ECO1* paralogues, *ESCO1* and *ESCO2*, only *ESCO2* has been implicated in Roberts syndrome and SC phocomelia. This is interesting because the *ESCO1* and *ESCO2* genes share a C-terminal acetyltransferase domain and a zinc-finger motif but differ in their N-termini [156].

Although ESCO2 is required for the establishment of sister chromatid cohesion, processivity of DNA replication forks in cells from patients with Roberts syndrome is reduced, suggesting a role for *ESCO2* in replication-coupled cohesion [73]. Decreased *ESCO2* activity may lead to some loss of cohesion that manifests as heterochromatic repulsion, but there may be sufficient protection of centromeric cohesion through the activity of shugoshin and PP2A so that chromosome segregation is not disturbed. As in CdLS, *ESCO2* is expressed in human embryonic tissues in a pattern that is consistent with the systems and organs affected in patients with this syndrome [155].

4.4 PDS5 Deficiencies

Two copies of the *Pds5* gene, *Pds5A* and *Pds5B*, are found in mammals and differ in expression [55]. Both *Pds5A*- and *Pds5B-deficient* mice are born with multiple congenital abnormalities, including growth retardation, cleft palate, and congenital heart defects, similar to the abnormalities found in humans with CdLS, and they die at birth [56, 157]. Surprisingly, *Pds5B*-deficient mouse embryonic fibroblasts lack defects in sister chromatid cohesion, but expression is detected in postmitotic neurons in the brain [157], suggesting an alternate role for cohesins. This expression pattern is similar to that of *Smc1*, *Rad21*, *Pds5B*, and *Smc3* in zebrafish [158], and in conjunction with the neurological phenotypes of the mutants the pattern suggests a crucial role for cohesin in the development and migration of neurons. Because this regulatory cohesin protein has not been well characterized in the human disease, examining these deficiencies more closely would be beneficial to better understand the mechanisms underlying PDS5A and PDS5B function.

4.5 α-Thalassemia/Mental Retardation Syndrome, X-Linked

α-Thalassemia/mental retardation syndrome, X-linked (ATRX), is a multisystem disorder of postnatal growth deficiency, mental retardation, microcephaly, dysmorphic craniofacial features, genital abnormalities in males, seizures, and a mild form of hemoglobin H disease. ATRX is caused by mutations in the *ATRX* gene on the X chromosome and was recently found to also lead to a cohesion defect in ATRX-depleted mammalian cells. The *ATRX* gene encodes a chromatin remodeling enzyme that is highly enriched at pericentromeric heterochromatin in mouse and human cells and associates with heterochromatin protein 1α (HP1α), just like NIPBL [159]. In mammalian cells, defects in sister chromatid cohesion and chromosome congression at the metaphase plate and mitotic defects were described. Defects in the *ATRX* gene are thought to result from perturbed cohesin targeting or loading/unloading. ATRX is believed to play a dual role in the regulation of cohesion during mitosis and in the control of gene expression in interphase, which is reminiscent of cohesin complex function. Investigators have recently found that ATRX is required for normal recruitment of cohesin in mouse brain cells and alters expression of imprinted genes in the postnatal brain [160]. Therefore, ATRX along with cohesin may regulate expression of this imprinted gene network by controlling higher order chromatin structure. Defects in the *ATRX* gene disrupt the cohesin targeting and/or loading/unloading, resulting in ATRX syndrome phenotypes.

4.6 Warsaw Breakage Syndrome

Only one patient with Warsaw breakage syndrome has been reported who displayed severe microcephaly, pre- and postnatal growth retardation, and abnormal skin pigmentation. The patient displayed two mutations in the *ChlR1* helicase, also called DDX11: a splice-site mutation in intron 22 of the maternal allele and a three-base pair deletion in exon 26 of the paternal allele [161]. The maternal allele mutation leads to a deletion of the last 10 base pairs of exon 22 from the cDNA, and the paternal allele mutations result in deletion of a highly conserved lysine residue in the ChlR1 protein. Cells from this patient reveal chromosomal instability characterized by sister cohesion defects, chromosomal breakage, and sensitivity to DNA cross-linking agents and topoisomerase inhibitors. Investigators have suggested that Warsaw breakage syndrome represents a unique disease with cellular features of both Fanconi anemia and Roberts syndrome, but with a distinct clinical phenotype. Other patients have yet to be identified with these same characteristics, and the defects underlying the *ChlR1* mutations have yet to be revealed.

4.7 Maternal Aging and Chromosome Segregation

Chromosome abnormalities represent not only the leading cause of birth defects in humans but also the major cause of pregnancy loss. Approximately 0.2–0.3 % of newborn infants are trisomic, and a majority of these errors result from fertilization of a chromosomally

abnormal egg by a normal sperm (reviewed in ref. 162). For this reason, attention has focused on why human female meiosis is so error prone. It is widely understood that the number of pregnancies involving trisomies increases drastically among women in their 40s to 35 %, compared with women in their 20s, in whom the rate is 2–3 % (reviewed in ref. 163). Little is known about the basis of this increased frequency of aneuploidy with age, but cohesins are becoming increasingly implicated because these complexes are essential for proper chromosome segregation in mitosis and meiosis. Because S phase takes place during fetal development in the oocyte and cell division does not occur until resumption of meiosis beginning at puberty, cohesins may in part be responsible for these errors. Sites of DNA crossover are also established decades before they function as physical mediators of chromosome segregation (reviewed in ref. 163). The correlation between age and aneuploidy in humans has been postulated to result from age-related weakening of cohesion.

SMC1β-deficient female mice provided the first direct evidence of an age-related decline in chromosome cohesion in mammalian oocytes [139]. Revenkova et al. demonstrated that *SMC1β*-deficient mice in both sexes were sterile, but male meiosis was blocked in pachynema, whereas in females meiosis progressed until metaphase II. AEs are markedly shortened, chromatin extends further from the AEs, chromosome synapsis is incomplete, sister chromatid cohesion at chromosome arms and centromeres are lost prematurely, and crossovers are absent or reduced owing to this deficiency. A recent study observed that when the *SMC1β* gene is deleted in mice after the neonatal period and the protein is produced only during fetal development, fertility is not affected [164]. This finding suggests that meiotic cohesin is sufficiently robust that once cohesion is established in fetal oocytes, little or no turnover of the cohesin protein occurs until fertilization at reproductive maturity. The pronounced age effect observed in *SMC1β*-deficient mice suggests that the cause may not be related to recombination itself, but instead to defective cohesion [165]. Weakened cohesion in these mice may accelerate the normal aging process, but severe abnormalities occur if cohesin complexes are absent [139]. Loss of cohesion may explain human age-related nondisjunction, but it raises a question about the fate of cohesins during prophase I arrest in women.

The possible association between age-related degradation of cohesion and increasing rate of aneuploidy was also examined in older, naturally aged female mice [166, 167]. Centromere cohesion was assessed by examining the distances between sister kinetochores in old compared to young oocytes [166]. Studies of metaphase I and II oocytes revealed an increase in distance between sister kinetochores from old compared to young mice, suggesting an age-related loss of centromere cohesion. Immunofluorescence

staining of chromosome-associated REC8 was also analyzed, and levels were significantly reduced in old compared to young oocytes [166]. Thus, loss of cohesion with age could predispose oocytes to meiotic errors involving the premature separation of homologues and sister chromatids. In a similar study, 14-month-old female mice showed increased interkinetochore distances, reduction in REC8 staining, and increases in anaphase defects compared to 2-month-old mice [167]. An age-related depletion of SGO2, a protein necessary for preventing degradation of centromere cohesin at anaphase I, was also observed, suggesting another cause of aneuploidy. These studies provide a plausible explanation for nondisjunction events, including not only abnormalities involving homologous chromosomes at the first meiotic division but also abnormalities involving mis-segregation of sister chromatids.

Human oogenesis is an extremely error-prone process, which leads to a high percentage of aneuploid oocytes compared to spermatocytes. The percentage of aneuploid oocytes increases with age, known as the "maternal age effect," and loss of sister chromatid cohesion has been postulated as a culprit for this phenomenon [168]. A recent study has shed light on cohesins in human oocytes and provides surprising counterpoints to the mouse data above [117]. In oocytes from women aged 18 to 34 years, no age-related changes were identifiable in immunolocalization patterns of REC8, SMC3, STAG3, or SMC1β, or in levels of *SMC1β* gene expression. Direct evidence linking age-related cohesin degradation to human oogenesis is therefore lacking, and the physiological basis of maternal age-related aneuploidy is unknown, although loss of cohesion could still be an important contributing factor.

5 Conclusions

Cumulative studies from many model organisms have established that cohesins play a key role in sister chromatid cohesion and the maintenance of genome integrity during cell division. During meiosis, distinct cohesin complexes, composed of different subunits including those that are meiosis-specific, regulate chromosome dynamics and are essential for normal germ cell development and precise chromosome segregation. The recent discovery that cohesins are involved with the replication machinery and other factors necessary for proper DNA replication during mitosis and meiosis barely touches the surface in shedding light on these complex proteins. The question of how cohesin complexes associate with DNA has yet to be answered. Debate over the different models continues, and conclusive data are needed to settle the issue. Only in the past several years have cohesinopathies been recognized and mutations in the cohesin subunits characterized. The maternal age effect is unresolved, but it is thought to be due to loss of cohesion

between sister chromatids with age, leading to premature chromosome separation and ultimately to aneuploidy. Although the roles of cohesins and their mechanisms of action have yet to be fully elucidated, research continues to move forward and progress so far has been remarkable.

Acknowledgements

This work was supported in part by the NIH (1R01GM106262 to KMB). We thank Dr. Soumya Rudra for critical reading of the manuscript. We apologize to any authors/researchers whose contributions we may have overlooked.

References

1. Tanaka T, Fuchs J, Loidl J, Nasmyth K (2000) Cohesin ensures bipolar attachment of microtubules to sister centromeres and resists their precocious separation. Nat Cell Biol 2:492–499
2. Uhlmann F, Lottspeich F, Nasmyth K (1999) Sister-chromatid separation at anaphase onset is promoted by cleavage of the cohesin subunit Scc1. Nature 400:37–42
3. Guacci V, Koshland D, Strunnikov AV (1997) A direct link between sister chromatid cohesion and chromosome condensation revealed through the analysis of *MCD1* in S. cerevisiae. Cell 91(1):47–57
4. Michaelis C, Ciosk R, Nasmyth K (1997) Cohesins: chromosomal proteins that prevents premature separation of sister chromatids. Cell 91:35–45
5. Toth A, Ciosk R, Uhlmann F, Galova M, Schleiffer A, Nasmyth K (1999) Yeast cohesin complex requires a conserved protein, Eco1p(Ctf7), to establish cohesion between sister chromatids during DNA replication. Genes Dev 13:320–333
6. Gruber S, Haering CH, Nasmyth K (2003) Chromosomal cohesin forms a ring. Cell 112(6):765–777
7. Carramolino L, Lee BC, Zaballos A, Peled A, Barthelemy I, Shav-Tal Y, Prieto I, Carmi P, Gothelf Y, Gonzalez de Buitrago G, Aracil M, Marquez G, Barbero JL, Zipori D (1997) SA-1, a nuclear protein encoded by one member of a novel gene family: molecular cloning and detection in hemopoietic organs. Gene 195(2):151–159
8. Losada A, Yokochi T, Kobayashi R, Hirano T (2000) Identification and characterization of SA/Scc3p subunits in the *Xenopus* and human cohesin complexes. J Cell Biol 150(3):405–416
9. Sumara I, Vorlaufer E, Gieffers C, Peters BH, Peters J-M (2000) Characterization of vertebrate cohesin complexes and their regulation in prophase. J Cell Biol 151(4):749–761
10. Haering CH, Lowe J, Hochwagen A, Nasmyth K (2002) Molecular architecture of SMC proteins and the yeast cohesin complex. Mol Cell 9(4):773–788
11. Anderson DE, Losada A, Erickson HP, Hirano T (2002) Condensin and cohesin display different arm conformations with characteristic hinge angles. J Cell Biol 156(3): 419–424
12. Melby TE, Ciampaglio CN, Briscoe G, Erickson HP (1998) The symmetrical structure of structural maintenance of chromosomes (SMC) and MukB proteins: long, antiparallel coiled coils, folded at a flexible hinge. J Cell Biol 142(6):1595–1604
13. Biggins S, Murray AW (2001) The budding yeast protein kinase Ipl1/Aurora allows the absence of tension to activate the spindle checkpoint. Genes Dev 15(23):3118–3129
14. Tanaka TU, Rachidi N, Janke C, Pereira G, Galova M, Schiebel E, Stark MJR, Nasmyth K (2002) Evidence that the Ipl1-Sli15 (Aurora kinase-INCENP) complex promotes chromosome bi-orientation by altering kinetochore-spindle pole connections. Cell 108:317–329
15. He X, Rines DR, Espelin CW, Sorger PK (2001) Molecular analysis of kinetochore-microtubule attachment in budding yeast. Cell 106(2):195–206
16. Biggins S, Severin FF, Bhalla N, Sassoon I, Hyman AA, Murray AW (1999) The conserved protein kinase Ipl1 regulates microtubule binding to kinetochores in budding yeast. Genes Dev 13(5):532–544

17. Strunnikov AV, Larionov VL, Koshland D (1993) *SMC1*: an essential yeast gene encoding a putative head-rod-tail protein is required for nuclear division and defines a new ubiquitous protein family. J Cell Biol 123(6): 1635–1648
18. Strunnikov AV, Hogan E, Koshland D (1995) *SMC2*, a *Saccharomyces cerevisiae* gene essential for chromosome segregation and condensation, defines a subgroup within the SMC family. Genes Dev 9:587–599
19. Hoque MT, Ishikawa F (2002) Cohesin defects lead to premature sister chromatid separation, kinetochore dysfunction, and spindle-assembly checkpoint activation. J Biol Chem 277(44):42306–42314
20. Britton RA, Lin DC, Grossman AD (1998) Characterization of a prokaryotic SMC protein involved in chromosome partitioning. Genes Dev 12(9):1254–1259
21. Sonoda E, Matsusaka T, Morrison C, Vagnarelli P, Hoshi O, Ushiki T, Nojima K, Fukagawa T, Waizenegger IC, Peters J-M, Earnshaw WC, Takeda S (2001) Scc1/Rad21/Mcd1 is required for sister chromatid cohesion and kinetochore function in vertebrate cells. Dev Cell 1:759–770
22. Vass S, Cotterill S, Valdeolmillos AM, Barbero JL, Lin E, Warren WD, Heck MMS (2003) Depletion of Drad21/Scc1 in *Drosophila* cells leads to instability of the cohesin complex and disruption of mitotic progression. Curr Biol 13:208–218
23. Diaz-Martinez LA, Gimenez-Abian JF, Clarke DJ (2007) Cohesin is dispensable for centromere cohesion in human cells. PLoS One 2(3):e318
24. Chang C-R, Wu C-S, Hom Y, Gartenberg MR (2005) Targeting of cohesin by transcriptionally silent chromatin. Genes Dev 19(24): 3031–3042
25. Losada A, Hirano T (2001) Intermolecular DNA interactions stimulated by the cohesin complex in vitro: Implications for sister chromatid cohesion. Curr Biol 11(4):268–272
26. Zhang N, Kuznetsov SG, Sharan SK, Li K, Rao PH, Pati D (2008) A handcuff model for the cohesin complex. J Cell Biol 183(6): 1019–1031
27. Uhlmann F, Nasmyth K (1998) Cohesion between sister chromatids must be established during DNA replication. Curr Biol 8(20): 1095–1101
28. Sjogren C, Nasmyth K (2001) Sister chromatid cohesion is required for postreplicative double-strand break repair in *Saccharomyces cerevisiae*. Curr Biol 11:991–995
29. Strom L, Lindroos HB, Shirahige K, Sjogren C (2004) Postreplicative recruitment of cohesin to double-strand breaks is required for DNA repair. Mol Cell 16:1003–1015
30. Uhlmann F, Wernic D, Poupart M-A, Koonin EV, Nasmyth K (2000) Cleavage of cohesin by the CD clan protease separin triggers anaphase in yeast. Cell 103:375–386
31. Ciosk R, Zachariae W, Michaelis C, Shevchenko A, Mann M, Nasmyth K (1998) An ESP1/PDS1 complex regulates loss of sister chromatid cohesion at the metaphase to anaphase transition in yeast. Cell 93(6): 1067–1076
32. Tomonaga T, Nagao K, Kawasaki Y, Furuya K, Murakami A, Morishita J, Yuasa T, Sutani T, Kearsey SE, Uhlmann F, Nasmyth K, Yanagida M (2000) Characterization of fission yeast cohesin: essential anaphase proteolysis of Rad21 phosphorylated in the S phase. Genes Dev 14:2757–2770
33. Losada A, Hirano M, Hirano T (1998) Identification of *Xenopus* SMC protein complexes required for sister chromatid cohesion. Genes Dev 12(13):1986–1997
34. Waizenegger IC, Hauf S, Meinke A, Peters J-M (2000) Two distinct pathways remove mammalian cohesin from chromosome arms in prophase and from centromeres in anaphase. Cell 103:399–410
35. Sumara I, Vorlaufer E, Stukenberg PT, Kelm O, Redemann N, Nigg EA, Peters J-M (2002) The dissociation of cohesin from chromosomes in prophase is regulated by Polo-like kinase. Mol Cell 9:515–525
36. Alexandru G, Uhlmann F, Mechtler K, Poupart M-A, Nasmyth K (2001) Phosphorylation of the cohesin subunit Scc1 by Polo/Cdc5 kinase regulates sister chromatid separation in yeast. Cell 105(4): 459–472
37. Hoque MT, Ishikawa F (2001) Human chromatid cohesin component hRad21 is phosphorylated in M phase and associated with metaphase centromeres. J Biol Chem 276(7): 5059–5067
38. Gimenez-Abian JF, Sumara I, Hirota T, Hauf S, Gerlich D, de la Torre C, Ellenberg J, Peters J-M (2004) Regulation of sister chromatid cohesion between chromosome arms. Curr Biol 14(13):1187–1193
39. Hauf S, Roitinger E, Koch B, Dittrich CM, Mechtler K, Peters J-M (2005) Dissociation of cohesin from chromosome arms and loss of arm cohesion during early mitosis depends on phosphorylation of SA2. PLoS Biol 3(3): 0419–0432
40. Hauf S, Waizenegger IC, Peters J-M (2001) Cohesin cleavage by separase required for anaphase and cytokinesis in human cells. Science 293(5533):1320–1323

41. Nakajima M, Kumada K, Hatakeyama K, Noda T, Peters J-M, Hirota T (2007) The complete removal of cohesin from chromosome arms depends on separase. J Cell Sci 120:4188–4196
42. Zou H, McGarry TJ, Bernal T, Kirschner MW (1999) Identification of a vertebrate sister-chromatid separation inhibitor involved in transformation and tumorigenesis. Science 285:418–422
43. Cohen-Fix O, Peters J-M, Kirschner MW, Koshland D (1996) Anaphase initiation in *Saccharomyces cerevisiae* is controlled by the APC-dependent degradation of the anaphase inhibitor Pds1p. Genes Dev 10:3081–3093
44. Funabiki H, Yamano H, Kumada K, Nagao K, Hunt T, Yanagida M (1996) Cut2 proteolysis required for sister-chromatid separation in fission yeast. Nature 381(6581):438–441
45. Ciosk R, Shirayama M, Shevchenko A, Tanaka T, Toth A, Shevchenko A, Nasmyth K (2000) Cohesin's binding to chromosomes depends on a separate complex consisting of Scc2 and Scc4 proteins. Mol Cell 5(2):243–254
46. Watrin E, Schleiffer A, Tanaka K, Eisenhaber F, Nasmyth K, Peters J-M (2006) Human Scc4 is required for cohesin binding to chromatin, sister-chromatid cohesion, and mitotic progression. Curr Biol 16:863–874
47. Lechner MS, Schultz DC, Negorev D, Maul GG, Rauscher FJ III (2005) The mammalian heterochromatin protein 1 binds diverse nuclear proteins through a common motif that targets the chromoshadow domain. Biochem Biophys Res Commun 331(4):929–937
48. Seitan VC, Banks P, Laval S, Majid NA, Dorsett D, Rana A, Smith J, Bateman A, Krpic S, Hostert A, Rollins RA, Erdjument-Bromage H, Tempst P, Benard CY, Hekimi S, Newbury SF, Strachan T (2006) Metazoan Scc4 homologs link sister chromatid cohesion to cell and axon migration guidance. PLoS Biol 4(8):e242
49. Hartman T, Stead K, Koshland D, Guacci V (2000) Pds5p is an essential chromosomal protein required for both sister chromatid cohesion and condensation in *Saccharomyces cerevisiae*. J Cell Biol 151(3):613–626
50. Panizza S, Tanaka T, Hochwagen A, Eisenhaber F, Nasmyth K (2000) Pds5 cooperates with cohesin in maintaining sister chromatid cohesion. Curr Biol 10:1557–1564
51. Gandhi R, Gillespie PJ, Hirano T (2006) Human Wapl is a cohesin-binding protein that promotes sister-chromatid resolution in mitotic prophase. Curr Biol 16(24):2406–2417
52. Rankin S, Ayad NG, Kirschner MW (2005) Sororin, a substrate of the anaphase-promoting complex, is required for sister chromatid cohesion in vertebrates. Mol Cell 18:185–200
53. Dai J, Sullivan BA, Higgins JMG (2006) Regulation of mitotic chromosome cohesion by Haspin and Aurora B. Dev Cell 11(5): 741–750
54. Wang F, Yoder J, Antoshechkin I, Han M (2003) *Caenorhabditis elegans* EVL-14/PDS5 and SCC-3 are essential for sister chromatid cohesion in meiosis and mitosis. Mol Cell Biol 23(21):7698–7707
55. Losada A, Yokochi T, Hirano T (2005) Functional contribution of Pds5 to cohesin-mediated cohesion in human cells and *Xenopus* egg extracts. J Cell Sci 118(Pt 10):2133–2141
56. Zhang B, Chang J, Fu M, Huang J, Kashyap R, Salavaggione E, Jain S, Shashikant K, Deardorff MA, Giovannucci Uzielli ML, Dorsett D, Beebe DC, Jay PY, Heuckeroth RO, Krantz ID, Millbrandt J (2009) Dosage effects of cohesin regulatory factor PDS5 on mammalian development: implications for cohesinopathies. PLoS One 4(5):1–17
57. Kueng S, Hegemann B, Peters BH, Lipp JJ, Schleiffer A, Mechtler K, Peters J-M (2006) Wapl controls the dynamic association of cohesin with chromatin. Cell 127(5):955–967
58. Kuroda M, Oikawa K, Ohbayashi T, Yoshida K, Yamada K, Mimura J, Matsuda Y, Fujii-Kuriyama Y, Mukai K (2005) A dioxin sensitive gene, mammalian *WAPL*, is implicated in spermatogenesis. FEBS J 579(1):167–172
59. Zhang J, Hakansson H, Kuroda M, Yuan L (2008) Wapl localization on the synaptonemal complex, a meiosis-specific proteinaceous structure that binds homologous chromosomes, in the female mouse. Reprod Domest Anim 43(1):124–126
60. Schmitz J, Watrin E, Lenart P, Mechtler K, Peters J-M (2007) Sororin is required for stable binding of cohesin to chromatin and for sister chromatid cohesion in interphase. Curr Biol 17:630–636
61. Skibbens RV, Corson LB, Koshland D, Hieter P (1999) Ctf7p is essential for sister chromatid cohesion and links mitotic chromosome structure to the DNA replication machinery. Genes Dev 13:307–319
62. Ivanov D, Schleiffer A, Eisenhaber F, Mechtler K, Haering CH, Nasmyth K (2002) Eco1 is a novel acetyltransferase that can acetylate proteins involved in cohesion. Curr Biol 12(4): 323–328
63. Unal E, Heidinger-Pauli JM, Koshland D (2007) DNA double-strand breaks trigger genome-wide sister-chromatid cohesion through Eco1 (Ctf7). Science 317:245–248
64. Bermudez VP, Maniwa Y, Tappin I, Ozato K, Yokomori K, Hurwitz J (2003) The alternative

Ctf18-Dcc1-Ctf8-replication factor C complex required for sister chromatid cohesion loads proliferating cell nuclear antigen onto DNA. PNAS 100(18):10237–10242

65. Bylund GO, Burgers PM (2005) Replication protein A-directed unloading of PCNA by the Ctf18 cohesion establishment complex. Mol Cell Biol 25(13):5445–5455
66. Hanna JS, Kroll ES, Lundblad V, Spencer FA (2001) *Saccharomyces cerevisiae* CTF18 and CTF4 are required for sister chromatid cohesion. Mol Cell Biol 21(9):3144–3158
67. Mayer ML, Gygi SP, Aebersold R, Hieter P (2001) Identification of RFC(Ctf18p, Ctf8p, Dcc1p): an alternative RFC complex required for sister chromatid cohesion in *S. cerevisiae*. Mol Cell 7:959–970
68. Lengronne A, McIntyre J, Katou Y, Kanoh Y, Hopfner K-P, Shirahige K, Uhlmann F (2006) Establishment of sister chromatid cohesion at the *S. cerevisiae* replication fork. Mol Cell 23(6):787–799
69. Ansbach AB, Noguchi C, Klansek IW, Heidlebaugh M, Nakamura TM, Noguchi E (2008) RFC^{Ctf18} and the Swi1-Swi3 complex function in separate and redundant pathways required for the stabilization of replication forks to facilitate sister chromatid cohesion in *Schizosaccharomyces pombe*. Mol Biol Cell 19(2):595–607
70. Noguchi E, Noguchi C, McDonald WH, Yates JRI, Russell P (2004) Swi1 and Swi3 are components of a replication fork protection complex in fission yeast. Mol Cell Biol 24(19): 8342–8355
71. Skibbens RV (2004) Chl1p, a DNA helicase-like protein in budding yeast, functions in sister-chromatid cohesion. Genetics 166:33–42
72. Parish JL, Rosa J, Wang X, Lahti JM, Doxsey SJ, Androphy EJ (2006) The DNA helicase ChlR1 is required for sister chromatid cohesion in mammalian cells. J Cell Sci 119 (4857–4865)
73. Terret ME, Sherwood R, Rahman S, Qin J, Jallepalli PV (2009) Cohesin acetylation speeds the replication fork. Nature 462(7270): 231–234
74. Berkowitz KM, Sowash AR, Koenig LR, Urcuyo D, Khan F, Yang F, Wang PJ, Jongens TA, Kaestner KH (2012) Disruption of CHTF18 causes defective meiotic recombination in male mice. PLoS Genet 8(11):e1002996
75. Rudra S, Skibbens RV (2012) Sister chromatid cohesion establishment occurs in concert with lagging strand synthesis. Cell Cycle 11(11):2114–2121
76. Kim S-T, Xu B, Kastan MB (2002) Involvement of the cohesin protein, Smc1, in Atm-dependent and independent responses to DNA damage. Genes Dev 16(5):560–570
77. Unal E, Arbel-Eden A, Sattler U, Shroff R, Lichten M, Haber JE, Koshland D (2004) DNA damage response pathway uses histone modification to assemble a double-strand break-specific cohesin domain. Mol Cell 16: 991–1002
78. Covo S, Westmoreland JW, Gordenin DA, Resnick MA (2010) Cohesin is limiting for the suppression of DNA damage-induced recombination between homologous chromosomes. PLoS Genet 6(7):1–16
79. Yazdi PT, Wang Y, Zhao S, Patel N, Lee EY-HP, Qin J (2002) SMC1 is a downstream effector in the ATM/NBS1 branch of the human S-phase checkpoint. Genes Dev 16:571–582
80. Kitagawa R, Bakkenist CJ, McKinnon PJ, Kastan MB (2004) Phosphorylation of SMC1 is a critical downstream event in the ATM-NBS1-BRCA1 pathway. Genes Dev 18(12): 1423–1438
81. Luo H, Li Y, Mu J-J, Zhang J, Tonaka T, Hamamori Y, Jung SY, Wang Y, Qin J (2008) Regulation of intra-S phase checkpoint by ionizing radiation (IR)-dependent and IR-independent phosphorylation of SMC3. J Biol Chem 283(28):19176–19183
82. Klein F, Mahr P, Galova M, Buonomo SBC, Michaelis C, Nairz K, Nasmyth K (1999) A central role for cohesins in sister chromatid cohesion, formation of axial elements, and recombination during yeast meiosis. Cell 98(1):91–103
83. Watanabe Y, Nurse P (1999) Cohesin Rec8 is required for reductional chromosome segregation at meiosis. Nature 400(6743): 461–464
84. Keeney S, Giroux CN, Kleckner N (1997) Meiosis-specific DNA double-strand breaks are catalyzed by Spo11, a member of a widely conserved protein family. Cell 88(3):375–384
85. Alani E, Padmore R, Kleckner N (1990) Analysis of wild-type and *rad50* mutants of yeast suggests an intimate relationship between meiotic chromosome synapsis and recombination. Cell 61:419–436
86. Nairz K, Klein F (1997) *mre11S* - a yeast mutation that blocks double-strand break processing and permits nonhomologous synapsis in meiosis. Genes Dev 11:2272–2290
87. Prinz S, Amon A, Klein F (1997) Isolation of *COM1*, a new gene required to complete meiotic double-strand break induced recombination in *Saccharomyces cerevisiae*. Genetics 146:781–795
88. Hunter N, Kleckner N (2001) The single-end invasion: an asymmetric intermediate at the

double-strand break to double-Holliday junction transition of meiotic recombination. Cell 106(1):59–70

89. Yokobayashi S, Yamamoto M, Watanabe Y (2003) Cohesins determine the attachment manner of kinetochores to spindle microtubules at meiosis I in fission yeast. Mol Cell Biol 23(11):3965–3973
90. Kateneva AV, Konovchenko AA, Guacci V, Dresser ME (2005) Recombination protein Tid1p controls resolution of cohesin-dependent linkages in meiosis in *Saccharomyces cerevisiae*. J Cell Biol 171(2):241–253
91. Kitajima TS, Yokobayashi S, Yamamoto M, Watanabe Y (2003) Distinct cohesin complexes organize meiotic chromosome domains. Science 300(5622):1152–1155
92. Lee J, Iwai T, Yokota T, Yamashita M (2003) Temporally and spatially selective loss of Rec8 protein from meiotic chromosomes during mammalian meiosis. J Cell Sci 116(Pt 13): 2781–2790
93. Parisi S, McKay MJ, Molnar M, Thompson MA, van der Spek PJ, van Drunen-Schoenmaker E, Kanaar R, Lehmann E, Hoeijmakers JHJ, Kohli J (1999) Rec8p, a meiotic recombination and sister chromatid cohesion phosphoprotein of the Rad21p family conserved from fission yeast to humans. Mol Cell Biol 19(5):3515–3528
94. Pezzi N, Prieto I, Kremer L, Jurado LAP, Valero C, del Mazo J, Martinez-A C, Barbero JL (2000) *STAG3*, a novel gene encoding a protein involved in meiotic chromosome pairing and location of *STAG3*-related genes flanking the Williams-Beuren syndrome deletion. FASEB J 14(3):581–595
95. Prieto I, Suja JA, Pezzi N, Kremer L, Martinez-A C, Rufas JS, Barbero JL (2001) Mammalian STAG3 is a cohesin specific to sister chromatid arms in meiosis I. Nat Cell Biol 3:761–766
96. Revenkova E, Eijpe M, Heyting C, Gross B, Jessberger R (2001) Novel meiosis-specific isoform of mammalian SMC1. Mol Cell Biol 21(20):6984–6998
97. Prieto I, Pezzi N, Buesa JM, Kremer L, Barthelemy I, Carreiro C, Roncal F, Martinez A, Gomez L, Fernandez R, Martinez AC, Barbero JL (2002) STAG2 and Rad21 mammalian mitotic cohesins are implicated in meiosis. EMBO Rep 3(6):543–550
98. Gutierrez-Caballero C, Herran Y, Sanchez-Martin M, Suja JA, Barbero JL, Llano E, Pendas AM (2011) Identification and molecular characterization of the mammalian alpha-kleisin RAD21L. Cell Cycle 10(9): 1477–1487
99. Herran Y, Gutierrez-Caballero C, Sanchez-Martin M, Hernandez T, Viera A, Barbero JL, De Alava E, de Rooij DG, Suja JA, Llano E, Pendas AM (2011) The cohesin subunit RAD21L functions in meiotic synapsis and exhibits sexual dimorphism in fertility. EMBO J 30(15):3091–3105
100. Ishiguro K, Kim J, Fujiyama-Nakamura S, Kato S, Watanabe Y (2011) A new meiosis-specific cohesin complex implicated in the cohesin code for homologous pairing. EMBO Rep 12(3):267–275
101. Lee J, Hirano T (2011) RAD21L, a novel cohesin subunit implicated in linking homologous chromosomes in mammalian meiosis. J Cell Biol 192(2):263–276
102. Petronczki M, Chwalla B, Siomos MF, Yokobayashi S, Helmhart W, Deutschbauer AM, Davis RW, Watanabe Y, Nasmyth K (2004) Sister-chromatid cohesion mediated by the alternative RF-$C^{Ctf18/Dcc1/Ctf8}$, the helicase Chl1 and the polymerase-a-associated protein Ctf4 is essential for chromatid disjunction during meiosis II. J Cell Sci 117(16):3547–3559
103. Lightfoot J, Testori S, Barroso C, Martinez-Perez E (2011) Loading of meiotic cohesin by SCC-2 is required for early processing of DSBs and for the DNA damage checkpoint. Curr Biol 21(17):1421–1430
104. Sym M, Engebrecht J, Roeder GS (1993) ZIP1 is a synaptonemal complex protein required for meiotic chromosome synapsis. Cell 72:365–378
105. Meuwissen RLJ, Offenberg HH, Dietrch AJJ, Riesewijk A, van Iersel M, Heyting C (1992) A coiled-coil related protein specific for synapsed regions of meiotic prophase chromosomes. EMBO J 11(13):5091–5100
106. Schmekel K, Meuwissen RLJ, Dietrch AJJ, Vink ACG, van Marle J, van Veen H, Heyting C (1996) Organization of SCP1 protein molecules within synaptonemal complexes of the rat. Exp Cell Res 226:20–30
107. Schalk JAC, Dietrch AJJ, Vink ACG, Offenberg HH, van Aalderen M, Heyting C (1998) Localization of SCP2 and SCP3 protein molecules within synaptonemal complexes of the rat. Chromosoma 107:540–548
108. Parra MT, Viera A, Gomez R, Page J, Benavente R, Santos JL, Rufas JS, Suja JA (2004) Involvement of the cohesin Rad21 and SCP3 in monopolar attachment of sister kinetochores during mouse meiosis I. J Cell Sci 117:1221–1234
109. Xu H, Beasley M, Verschoor S, Inselman A, Handel MA, McKay MJ (2004) A new role for the mitotic RAD21/SCC1 cohesin in

meiotic chromosome cohesion and segregation in the mouse. EMBO Rep 5:378–384

110. Eijpe M, Heyting C, Gross B, Jessberger R (2000) Association of mammalian SMC1 and SMC3 proteins with meiotic chromosomes and synaptonemal complexes. J Cell Sci 113: 673–682
111. Suja JA, Antonio C, Debec A, Rufas JS (1999) Phosphorylated proteins are involved in sister-chromatid arm cohesion during meiosis I. J Cell Sci 112:2957–2969
112. Eijpe M, Offenberg HH, Jessberger R, Revenkova E, Heyting C (2003) Meiotic cohesin REC8 marks the axial elements of rat synaptonemal complexes before cohesins SMC1b and SMC3. J Cell Biol 160(5): 657–670
113. Suja JA, Barbero JL (2009) Cohesin complexes and sister chromatid cohesion in mammalian meiosis. Genome Dyn 5:94–116
114. Kouznetsova A, Novak I, Jessberger R, Hoog C (2005) SYCP2 and SYCP3 are required for cohesin core integrity at diplotene but not for centromere cohesion at the first meiotic division. J Cell Sci 118:2271–2278
115. Gomez R, Valdeolmillos AM, Parra MT, Viera A, Carreiro C, Roncal F, Rufas JS, Barbero JL, Suja JA (2007) Mammalian SGO2 appears at the inner centromere domain and redistributes depending on tension across centromeres during meiosis II and mitosis. EMBO Rep 8(2):173–180
116. Prieto I, Tease C, Pezzi N, Buesa JM, Ortega S, Kremer L, Martinez A, Martinez-A C, Hulten MA, Barbero JL (2004) Cohesin component dynamics during meiotic prophase I in mammalian oocytes. Chromosome Res 12:197–213
117. Garcia-Cruz R, Brieno MA, Roig I, Grossmann M, Velilla E, Pujol A, Cabero L, Pessarrodona A, Barbero JL, Garcia Caldes M (2010) Dynamics of cohesin proteins REC8, STAG3, SMC1b and SMC3 are consistent with a role in sister chromatid cohesion during meiosis in human oocytes. Hum Reprod 25(9):2316–2327
118. Crackower MA, Kolas NK, Noguchi J, Sarao R, Kikuchi K, Kaneko H, Kobayashi E, Kawai Y, Kozieradzki I, Landers R, Mo R, Hui C-C, Nieves E, Cohen PE, Osborne LR, Wada T, Kunieda T, Moens PB, Penninger JM (2003) Essential role of Fkbp6 in male fertility and homologous chromosome pairing in meiosis. Science 300(5623):1291–1295
119. Holloway K, Roberson EC, Corbett KL, Kolas NK, Nieves E, Cohen PE (2011) NEK1 facilitates cohesin removal during mammalian spermatogenesis. Genes 2(1):260–279
120. Buonomo SB, Clyne RK, Fuchs J, Loidl J, Uhlmann F, Nasmyth K (2000) Disjunction of homologous chromosomes in meiosis I depends on proteolytic cleavage of the meiotic cohesin Rec8 by separin. Cell 103(3): 387–398
121. Pasierbek P, Jantsch M, Melcher M, Schleiffer A, Schweizer D, Loidl J (2001) A *Caenorhabditis elegans* cohesion protein with functions in meiotic chromosome pairing and disjunction. Genes Dev 15:1349–1360
122. Siomos MF, Badrinath A, Pasierbek P, Livingstone D, White J, Glotzer M, Nasmyth K (2001) Separase is required for chromosome segregation during meiosis I in *Caenorhabditis elegans*. Curr Biol 11:1825–1835
123. Rogers E, Bishop JD, Waddle JA, Schumacher JM, Lin R (2002) The aurora kinase AIR-2 functions in the release of chromosome cohesion in *Caenorhabditis elegans* meiosis. J Cell Biol 157(2):219–229
124. Kaitna S, Pasierbek P, Jantsch M, Loidl J, Glotzer M (2002) The aurora B kinase AIR-2 regulated kinetochores during mitosis and is required for separation of homologous chromosomes during meiosis. Curr Biol 12:798–812
125. Kitajima T, Miyazaki Y, Yamamoto M, Watanabe Y (2003) Rec8 cleavage by separase is required for meiotic nuclear division in fission yeast. EMBO J 22(20):5643–5653
126. Herbert M, Levasseur M, Homer H, Yallop K, Murdoch A, McDougall A (2003) Homologue disjunction in mouse oocytes requires proteolysis of securin and cyclin B1. Nat Cell Biol 5(11):1023–1025
127. Terret ME, Wassmann K, Waizenegger IC, Maro B, Peters J-M, Verlhac M-H (2003) The meiosis I-to-meiosis II transition in mouse oocytes requires separase activity. Curr Biol 13:1797–1802
128. Kitajima TS, Kawashima SA, Watanabe Y (2004) The conserved kinetochore protein shugoshin protects centromeric cohesion during meiosis. Nature 427(6974):510–517
129. Rabitsch KP, Gregan J, Schleiffer A, Javerzat J-P, Eisenhaber F, Nasmyth K (2004) Two fission yeast homologs of *Drosophila* Mei-S332 are required for chromosome segregation during meiosis I and II. Curr Biol 14: 287–301
130. Marston AL, Tham W-H, Shah H, Amon A (2004) A genome-wide screen identifies genes required for centromeric cohesion. Science 303:1367–1370

131. Katis VL, Galova M, Rabitsch KP, Gregan J, Nasmyth K (2004) Maintenance of cohesin at centromeres after meiosis I in budding yeast requires a kinetochore-associated protein related to MEI-S332. Curr Biol 14(7):560–572

132. Kitajima TS, Sakuno T, Ishiguro K, Iemura S, Natsume T, Kawashima SA, Watanabe Y (2006) Shugoshin collaborates with protein phosphatase 2A to protect cohesin. Nature 441(7089):46–52

133. Ridel CG, Katis VL, Katou Y, Mori S, Itoh T, Helmhart W, Galova M, Petronczki M, Gregan J, Cetin B, Mudrak I, Ogris E, Mechtler K, Pelletier L, Buchholz F, Shirahige K, Nasmyth K (2006) Protein phosphatase 2A protects centromeric sister chromatid cohesion during meiosis I. Nature 441(7089): 53–61

134. Llano E, Gomez R, Gutierrez-Caballero C, Herran Y, Sanchez-Martin M, Vazquez-Quinones L, Hernandez T, de Alava E, Cuadrado A, Barbero JL, Suja JA, Pendas AM (2008) Shugoshin-2 is essential for the completion of meiosis but not for mitotic cell division in mice. Genes Dev 22:2400–2413

135. Lee J, Kitajima TS, Tanno Y, Yoshida K, Morita T, Miyano T, Miyake M, Watanabe Y (2008) Unified mode of centromeric protection by shugoshin in mammalian oocytes and somatic cells. Nat Cell Biol 10(1):42–52

136. Yin S, Ai J-S, Shi L-H, Wei L, Yuan J, Ouyang Y-C, Hou Y, Chen D-Y, Schatten H, Sun Q-Y (2008) Shugoshin 1 may play important roles in separation of homologous chromosomes and sister chromatids during mouse oocyte meiosis. PLoS One 3(10):1–7

137. Brar GA, Kiburz BM, Zhang Y, Kim JE, White F, Amon A (2006) Rec8 phosphorylation and recombination promote the stepwise loss of cohesins in meiosis. Nature 441(7092):532–536

138. Katis VL, Lipp JJ, Imre R, Bogdanova A, Okaz E, Habermann B, Mechtler K, Nasmyth K, Zachariae W (2010) Rec8 phosphorylation by casein kinase 1 and Cdc7-Dbf4 kinase regulates cohesin cleavage by separase during meiosis. Dev Cell 18(3):397–409

139. Revenkova E, Eijpe M, Heyting C, Hodges CA, Hunt PA, Liebe B, Scherthan H, Jessberger R (2004) Cohesin SMC1b is required for meiotic chromosome dynamics, sister chromatid cohesion and DNA recombination. Nat Cell Biol 6(6):555–562

140. Xu H, Beasley MD, Warren WD, van der Horst GTJ, McKay MJ (2005) Absence of mouse REC8 cohesin promotes synapsis of sister chromatids in meiosis. Dev Cell 8: 949–961

141. Yuan L, Liu J-G, Zhao J, Brundell E, Daneholt B, Hoog C (2000) The murine *SCP3* gene is required for synaptonemal complex assembly, chromosome synapsis, and male fertility. Mol Cell 5:73–83

142. Yang F, De La Fuente R, Leu NA, Baumann C, McLaughlin KJ, Wang PJ (2006) Mouse SYCP2 is required for synaptonemal complex assembly and chromosomal synapsis during male meiosis. J Cell Biol 173(4):497–507

143. de Vries FAT, de Boer E, van den Bosch M, Baarends WM, Ooms M, Yuan L, Liu J-G, van Zeeland AA, Heyting C, Pastink A (2005) Mouse *Sycp1* functions in synaptonemal complex assembly, meiotic recombination, and XY body formation. Genes Dev 19(11):1376–1389

144. Krantz ID, McCallum J, DeScipio C, Kaur M, Gillis LA, Yaeger D, Jukofsky L, Wasserman N, Bottani A, Morris CA, Nowaczyk MJM, Toriello H, Bamshad MJ, Carey JC, Rappaport E, Kawauchi S, Lander AD, Calof AL, Li H, Devoto M, Jackson LG (2004) Cornelia de Lange syndrome is caused by mutations in *NIPBL*, the human homolog of *Drosophila melanogaster Nipped-B*. Nat Genet 36(6):631–635

145. Tonkin ET, Wang T-J, Lisgo S, Bamshad MJ, Strachan T (2004) *NIPBL*, encoding a homolog of fungal Scc2-type sister chromatid cohesion proteins and fly Nipped-B, is mutated in Cornelia de Lange syndrome. Nat Genet 36(6):636–641

146. Musio A, Selicorni A, Focarelli ML, Gervasini C, Milani D, Russo S, Vezzoni P, Larizza L (2006) X-linked Cornelia de Lange syndrome owing to *SMC1L1* mutations. Nat Genet 38(5):528–530

147. Deardorff MA, Kaur M, Yaeger D, Rampuria A, Korolev S, Pie J, Gil-Rodriguez C, Arnedo M, Loeys B, Kline AD, Wilson M, Lillquist K, Siu V, Ramos FJ, Musio A, Jackson LG, Dorsett D, Krantz ID (2007) Mutations in cohesin complex members SMC3 and SMC1A cause a mild variant of Cornelia de Lange syndrome with predominant mental retardation. Am J Hum Genet 80(3):485–494

148. Gillis LA, McCallum J, Kaur M, DeScipio C, Yaeger D, Mariani A, Kline AD, Li H, Devoto M, Jackson LG, Krantz ID (2004) *NIPBL* mutational analysis in 120 individuals with Cornelia de Lange syndrome and evaluation of genotype-phenotype correlations. Am J Hum Genet 75(4):610–623

149. Kaur M, DeScipio C, McCallum J, Yaeger D, Devoto M, Jackson LG, Spinner NB, Krantz ID (2005) Precocious sister chromatid separation (PSCS) in Cornelia de Lange syndrome. Am J Med Genet 138A(1):27–31
150. Vrouwe MG, Elghalbzouri-Maghrani E, Meijers M, Schouten P, Godthelp BC, Bhuiyan ZA, Redeker EJ, Mannens MM, Mullenders LHF, Pastink A, Darroudi F (2007) Increased DNA damage sensitivity of Cornelia de Lange syndrome cells: evidence for impaired recombinational repair. Hum Mol Genet 16(12):1478–1487
151. Revenkova E, Focarelli ML, Susani L, Paulis M, Bassi MT, Mannini L, Frattini A, Delia D, Krantz ID, Vezzoni P, Jessberger R, Musio A (2009) Cornelia de Lange syndrome mutations in SMC1A or SMC3 affect binding to DNA. Hum Mol Genet 18(3):418–427
152. Kawauchi S, Calof AL, Santos R, Lopez-Burks ME, Young CM, Hoang MP, Chua A, Lao T, Lechner MS, Daniel JA, Nussenzweig A, Kitzes L, Yokomori K, Hallgrimsson B, Lander AD (2009) Multiple organ system defects and transcriptional dysregulation in the *Nipbl*$^{+/-}$ mouse, a model of Cornelia de Lange syndrome. PLoS Genet 5(9):1–17
153. Vega H, Waisfisz Q, Gordillo M, Sakai N, Yanagihara I, Yamada M, van Gosliga D, Kayserili H, Xu C, Ozono K, Jabs EW, Inui K, Joenje H (2005) Roberts syndrome is caused by mutations in *ESCO2*, a human homolog of yeast *ECO1* that is essential for the establishment of sister chromatid cohesion. Nat Genet 37(5):468–470
154. Schule B, Oviedo A, Johnston K, Pai S, Francke U (2005) Inactivating mutations in *ESCO2* cause SC phocomelia and Roberts syndrome: no phenotype-genotype correlation. Am J Hum Genet 77(6):1117–1128
155. Vega H, Trainer AH, Gordillo M, Crosier M, Kayserili H, Skovby F, Giovannucci Uzielli ML, Schnur RE, Manouvrier S, Blair E, Hurst JA, Forzano F, Meins M, Simola KOJ, Raas-Rothschild A, Hennekam RCM, Jabs EW (2010) Phenotypic variability in 49 cases of *ESCO2* mutations, including novel missense and codon deletion in the acetyltransferase domain, correlates with *ESCO2* expression and establishes the clinical criteria for Roberts syndrome. J Med Genet 47(1):30–37
156. Hou F, Zou H (2005) Two human orthologues of Eco1/Ctf7 acetyltransferases are both required for proper sister-chromatid cohesion. Mol Biol Cell 16(8):3908–3918
157. Zhang B, Jain S, Song H, Fu M, Heuckeroth RO, Erlich JM, Jay PY, Millbrandt J (2007) Mice lacking sister chromatid cohesion protein PDS5B exhibit developmental abnormalities reminiscent of Cornelia de Lange syndrome. Development 134:3191–3201
158. Monnich M, Banks S, Eccles M, Dickinson E, Horsfield J (2009) Expression of cohesin and condensin genes during zebrafish development supports a non-proliferative role for cohesin. Gene Expr Patterns 9:586–594
159. Ritchie K, Seah C, Moulin J, Isaac C, Dick F, Berube NG (2008) Loss of ATRX leads to chromosome cohesion and congression defects. J Cell Biol 180(2):315–324
160. Kernohan KD, Jiang Y, Tremblay DC, Bonvissuto AC, Eubanks JH, Mann MRW, Berube NG (2010) ATRX partners with cohesin and MeCP2 and contributes to developmental silencing of imprinted genes in the brain. Dev Cell 18(2):191–202
161. van der Lelij P, Chrzanowska KH, Godthelp BC, Rooimans MA, Oostra AB, Stumm M, Zdzienicka MZ, Joenje H, de Winter JP (2010) Warsaw breakage syndrome, a cohesinopathy associated with mutations in the XPD helicase family member DDX11/ChlR1. Am J Hum Genet 86:262–266
162. Hassold TJ, Jacobs PA (1984) Trisomy in man. Annu Rev Genet 18:69–97
163. Hunt PA, Hassold TJ (2010) Female meiosis: coming unglued with age. Curr Biol 20(17): R699–R702
164. Revenkova E, Hermann K, Adelfalk C, Jessberger R (2010) Oocyte cohesin expression restricted to predictyate stages provides full fertility and prevents aneuploidy. Curr Biol 20:1529–1533
165. Hodges CA, Revenkova E, Jessberger R, Hassold TJ, Hunt PA (2005) SMC1b-deficient female mice provide evidence that cohesins are a missing link in age-related nondisjunction. Nat Genet 37(12):1351–1355
166. Chiang T, Duncan FE, Schindler K, Schultz RM, Lampson MA (2010) Evidence that weakened centromere cohesion is a leading cause of age-related aneuploidy in oocytes. Curr Biol 20(17):1522–1528
167. Lister LM, Kouznetsova A, Hyslop LA, Kalleas D, Pace SL, Barel JC, Nathan A, Floros V, Adelfalk C, Watanabe Y, Jessberger R, Kirkwood TB, Hoog C, Herbert M (2010) Age-related meiotic segregation errors in mammalian oocytes are preceded by depletion of cohesin and Sgo2. Curr Biol 20(17): 1511–1521
168. Chiang T, Schultz RM, Lampson MA (2012) Meiotic origins of maternal age-related aneuploidy. Biol Reprod 86(1):1–7

Chapter 12

Introductory Review of Computational Cell Cycle Modeling

Andres Kriete, Eishi Noguchi, and Christian Sell

Abstract

Recent advances in the modeling of the cell cycle through computer simulation demonstrate the power of systems biology. By definition, systems biology has the goal to connect a parts list, prioritized through experimental observation or high-throughput screens, by the topology of interactions defining intracellular networks to predict system function. Computer modeling of biological systems is often compared to a process of reverse engineering. Indeed, designed or engineered technical systems share many systems-level properties with biological systems; thus studying biological systems within an engineering framework has proven successful. Here we review some aspects of this process as it pertains to cell cycle modeling.

Key words Cell cycle, Computer modeling, Systems biology, Biological systems, Computer simulation, Cell cycle modeling, System function

1 Introduction

The complexity of biological systems requires us to take a systems-level view in order to holistically understand the networks of cellular regulation. Such approaches involve in silico modeling of biological systems and have a remarkable similarity to reverse engineering. Indeed, designed or engineered technical systems share many systems-level properties with evolved biological systems [1]. The cell cycle, which consists of an orderly sequence of events, is an example of biological complexity and involves both positive and negative feedback regulations. Such regulations are also at the core of other major oscillating systems including circadian rhythms; thus computational systems biology has become an important area of cell cycle research [2–4]. Here we describe an introductory overview of the main steps required to develop cell cycle models.

Eishi Noguchi and Mariana C. Gadaleta (eds.), *Cell Cycle Control: Mechanisms and Protocols*, Methods in Molecular Biology, vol. 1170, DOI 10.1007/978-1-4939-0888-2_12,

2 Steps of the Modeling Process

2.1 Scope and Goals

Model development is an iterative process, whereby graphical representations, mathematical implementations, simulations, predictions, and experimental validations are continuously refined until all project goals are reached. Modeling can also help to provide consistency between different experimental efforts as well as to generate and test new hypotheses. The first step in the modeling process is to define the scope and objectives of the model, and to identify all state variables such as genes or proteins, which change their state or activity through transcription, phosphorylation, or other mechanisms. The most difficult part of a modeling process is to accurately define all necessary rates and parameters and to make a decision on the most adequate level of complexity or comprehensiveness and scale. Most likely, the modeler is faced with a situation where some parameters are available, and some not. Parameters missing can be initially estimated, and experimental research can be guided to determine more precise values. This task is greatly enhanced by focusing on the most essential items required to build the model; it is essential to discern which components of a model are absolutely necessary and have to be prioritized. Obviously, it is also important to gauge which components can be omitted in the initial model and reintroduced in future extensions. In many areas, the development of models naturally follows a pattern from simple to more complex. For instance, an early model of the MAPK pathway originally contained only nine state variables [5], but subsequently grew to a network representation with 202 proteins, and additional ions, oligomers, and genes [6]. However, the qualitative behavior of the pathway in terms of a negative feedback had already been captured correctly by the initial model. Cell cycle models are no exception. The first models published by Tysen [7] and Goldbeter [8] in 1991 have grown steadily in complexity. The Goldbeter model is the most minimalistic model featuring three state variables; however, it captures the essential behavior of the core constituents of the cell cycle. While the examples of this model discussed below assume a continuous cycling, which is a suitable assumption for embryonic development, most cell cycles are different from a continuous oscillatory system, since they depend on and are regulated by external cues and internal cell cycle checkpoints.

2.2 Model Topology

The second major step is to lay out the topology of the connectivity or network wiring in a graphical fashion. While the interactions of proteins are typically defined by biochemical reactions rates, the topology can be defined in terms of control elements or regulatory network motifs, such as feedback loops [9, 10]. In combination, rates and network topologies determine the overall dynamic of the system. Both amplifying positive and inhibitory negative feedback

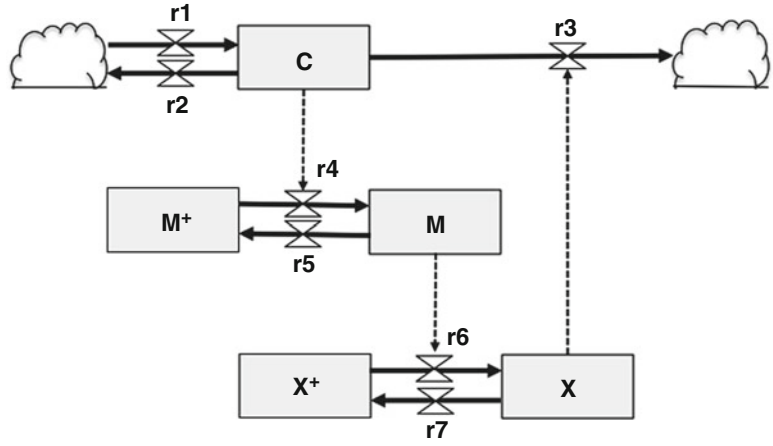

Fig. 1 Schema for the mitotic oscillator from Goldbeter [8] using Forrester diagram notations. The state variables [Cyclin (C), maturation promotion factor (M), and protease (X)] are shown by boxes, with in- and outflows denoted by valves of defined molecular reaction rates. The cloud symbols represent sources or sinks, and *dotted lines* indicate regulatory connections

motifs are relevant for cell cycle regulation, and their fine-tuned interaction gives rise to a cyclic behavior.

Using formal graphical notations, as compared to pathway cartoons, promotes model exchange and enhances the process of deriving mathematical formulations. Among the early schematic representations used in biology, specifically in ecology, are Forrester diagrams and Petri Nets with different level of abstraction [11]. Forrester diagrams make use of only one graphical element for state variables with sources and sinks limiting the representation of more complex diagrams in which state variables of different kinds have to be discerned. Another limitation is that these diagrammatic concepts were developed when computer graphics and user interfaces were still in initial development; thus no convenient computer programs were available to support the development of such diagrams, and the application was limited to simpler models.

Figure 1 shows a diagram for a simple cell cycle model using Forrester Diagram notation. This model, which is proposed by Goldbeter, is a minimalistic model of a mitotic oscillator during the cell cycle [8]. In this model, the mathematical representation uses three state variables of interest: Cyclin (C), active dephosphorylated Cdc2 (also known as CDK1) kinase (M), and active phosphorylated protease (X). The Cyclin protein (C) is a key ingredient in the cell cycle, since its periodic buildup and breakdown drives cell cycle progression. When Cyclin exceeds a certain threshold, it begins to combine with and activate a protein kinase Cdc2 to form a complex called "maturation-promoting factor (or M-phase promoting factor, MPF: M)," which stimulates mitosis.

The Cdc2 kinase stimulates degradation of Cyclin by activating a protease (X). Since Cyclin promotes its own degradation by a protease related to MPF, this constitutes a negative feedback. The biochemical reactions r1–r7 based on enzyme kinetics constitute the in- and outflows, which in combination determine the behavior of each state variable. The cloud symbols denote undefined sources and sinks; these are outside the scope of the Goldbeter model. In this circuit, Cyclin (C) is constantly synthesized (r1), while nonspecific degradation of Cyclin also occurs constantly (r2). When the concentration of Cyclin is below the threshold, Cyclin does not form a complex with Cdc2, keeping Cdc2 inactive (M^+). In r4, when Cyclin (C) concentration rises over the threshold, Cyclin activates the Cdc2 kinase by increasing the velocity of the phosphatase that activates the kinase ($M^+ \rightarrow M$). In this reaction, the phosphatase (Cdc25 protein, not modeled) converts inactive Cdc2 (M^+) to the active form (M), by removing the inhibitory phosphate groups (r4). In r5, although it is not explicitly modeled, the Wee1 kinase deactivates Cdc2 by adding the inhibitory phosphate group to Cdc2. Here, the amount of Wee1 is considered to be constant (r5). When the Cdc2 kinase is activated (M), it directly promotes r6 without other intervening factors. In this reaction, Cdc2 phosphorylates and activates Cyclin-specific protease ($X^+ \rightarrow X$), which promotes r3 that degrades Cyclin. Finally, in r7, Cyclin-specific protease is deactivated, and the amount of deactivating phosphatase (not modeled) for the cyclin protease (X) is considered to be constant. In this reaction, the activating phosphate groups are removed from the Cyclin-specific protease. Taken together, the total amounts of ($M + M^+$) and ($X + X^+$) are constant, thus completing the mitotic oscillator cycle, which is caused by negative feedback.

One instructional implementation and description of the Goldbeter model is available from Mathworks (http://www.mathworks.com). The model from Tyson [7] has also been available as an educational resource [12]. To handle the increasing complexity of molecular data several graphical modeling tools, such as CellDesigner [6], still based on the principles used in Forrester diagrams, are now available to conveniently design molecular networks graphically. Based on a Systems Biology Graphical Notation (SBGN) standard, such programs use different symbols for variables (genes, proteins, and phenotypes); they allow for entering functions and reaction rates to define the mathematical model, and subsequently support to execute the simulation. As part of these developments model sharing through using standardized formats such as Systems Biology Markup Language (SBML) and the use of model repositories (such as CellML or BioModels at EMBL-EBI) has become essential to advance the field.

2.3 Simulation and Prediction

The mathematical equations resulting from graphical models are typically linear or nonlinear ordinary differential equations (ODE).

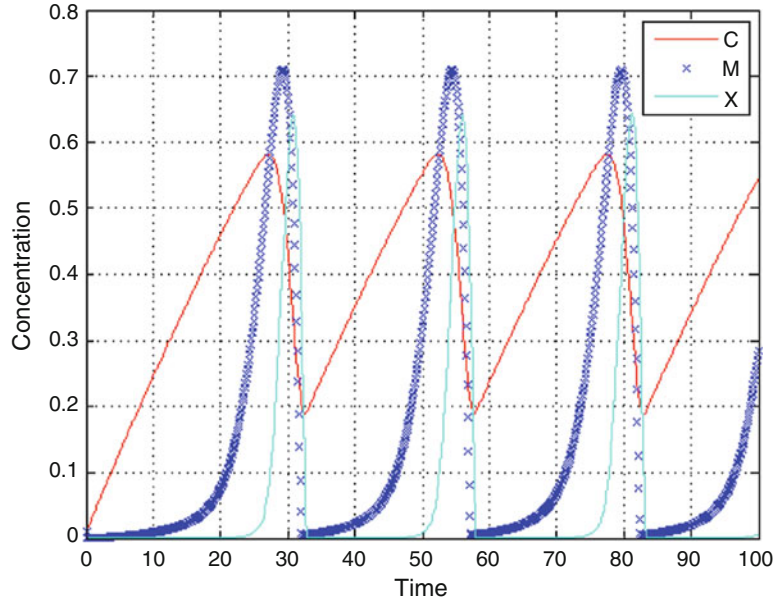

Fig. 2 Example of a cell cycle simulation using the Goldbeter model. Shown are the oscillations of Cyclin (C), the maturation promoting factor (M), and the activity of the protease (X). As C increases, it activates M and X, which subsequently degrades C. The simulation has been performed with a stiff solver of variable step size, as demonstrated for M

Each ODE represents one state variable and its change during each time step, which means for most systems several ODEs have to be solved at each time step. The connection to other state variables is expressed in any of the terms defining either an increase or decrease of the state variable, or expressed in auxiliary equations. Rate equations are solved by ODE solvers such as Euler, Runga-Kutta, or Stiff solvers. Stiff solvers with variable time steps are most adequate and computationally efficient for systems that have a fluctuating dynamic consisting of regimes of smooth change with more rapid changes. User-defined error thresholds will force the computation to take small step sizes when the system changes, and will relax the step size when the change is more linear, as demonstrated in Fig. 2 for the parameter M.

However, using classical mathematical modeling can pose limitations. Not all parameters might be available, specifically if there is an understanding about the role of other factors, external regulators, or interaction with other networks. The understanding of the topology of a network can grow more rapidly than the ability to quantify all required parameters. The two alternative approaches are Boolean logic [13] and Fuzzy-logic [14, 15]; both are used to develop rule-based representations. In these cases, the qualitative known regulatory mechanisms of interactions are

implemented as defined rules into the model. Fuzzy-logic rule-based models can be adjusted to the granularity of available quantitative data; i.e., they can start with a low resolution (ON/OFF) but can be calibrated to a higher resolution if more discernable states are provided.

2.4 Model Analysis

An objective analysis of the relevance of components and properties can be made once the model is complete. A mathematical representation has the ability to identify how defined perturbations influence the overall behavior of the model. Such a computational task can be done repeatedly and iteratively in a manner not available in the wet laboratory. One goal could be to identify state variables most amenable to experimental perturbation for the purpose of experimental model validation. Another goal could be to identify targets most suitable for intervention and drug development. In addition, it may be useful to identify unnecessary components in the overall model to reduce model complexity. A sensitivity analysis, which allows a ranking of all model parameters, is the most commonly applied. In such an analysis, each parameter is changed by a defined degree, and compared to a defined output parameter. One definition is the Sensitivity Objective Function (SOF), a ration of % change in outcome and % change of rate. An example of a sensitivity analysis for the Goldbeter model is shown in Table 1. V2 is the parameter with the greatest sensitivity out of all the parameters when the initial value is perturbed by 10 %, using the amount of C at the end of the calculation as a reference. This is the case because the V2 parameter is involved in the enzyme kinetics of reaction r5 (*see* Fig. 1), which determines the outflow or conversion of the active into the inactive form of MPF. As long as M is active, it activates the protease (r6 in Fig. 1), and herewith influences the cyclic behavior. V4, which is involved in reaction r7 and represents degradation of the active protease, has the least effect on the simulation outcome, and requires a stronger perturbation to cause a noticeable effect.

The investigation of sensitivities can lead to broader questions such as robustness of the biological system. Robustness is a systems-level property, not determined by a single factor alone, but by the overall behavior of the system, its circuitry, and connectivity. Fluctuations can arise from stochastic effects in gene transcription and protein concentrations [16], as well as environmental perturbations. A high sensitivity in certain parameters can make the system fragile to specific perturbations, while the topology of a network can contribute to an enhancement of stability. It can be assumed that the evolved design of an essential process such as cell cycle regulation is stable and provides robustness against many common fluctuations [17]. Thus, mathematical modeling has become an important tool to conveniently study and compare responses to perturbations and noise [18–21].

Table 1
Example of a sensitivity analysis using the mitotic oscillator model by Goldbeter

Perturbation target	End amount of cyclin	% Change in outcome	S.O.F
None	0.54	0	0
K1 (r4)	0.53	0.016	0.165
K2 (r5)	0.52	0.031	0.317
K3 (r6)	0.54	0.007	0.071
K4 (r7)	0.53	0.021	0.213
Kc (r4)	0.33	0.379	3.790
Kd (r3)	0.53	0.012	0.123
Kdd (r2)	0.53	0.011	0.113
V2 (r5)	0.06	0.880	8.800
V4 (r7)	0.54	0.006	0.058
Vd (r3)	0.56	0.043	0.428
VM1 (r4)	0.26	0.518	5.182
VM3 (r6)	0.51	0.050	0.496

Each parameter or constant involved in the molecular reactions is perturbed by 10 %. V2, part of the reaction r5 (*see* Fig. 1), is the most sensitive parameter, and V4, part of reaction r7, is the least sensitive.

3 Conclusions and Outlook

The reverse engineering of the cell cycle has been a successful enterprise in systems biology. The mathematical models can be executed conveniently and repeatedly to study the influence of specific or random perturbations. The model revisited here is minimalistic and had been chosen to demonstrate essential steps involved in the modeling process. The reader is referred to systems biology textbooks for an in-depth discussion of computational modeling and applications [22–25].

The growing complexity of cell cycle models is mostly driven from experimental insights, and panels of genetically engineered strains in model organisms allow validation of hundreds of model parameters [26]. Current model development strides are designed to integrate cell cycle models into a larger scope of cellular mechanisms and functions, which includes identifications of cell cycle regulators and checkpoints, which are hooks to connect other models representing signaling, transcriptional regulation, or metabolism [27, 28]. Functional and hierarchical modularity can

keep the growing model complexity manageable [29]. Finally, such aggregated models will allow studying the involvement of the cell cycle regulation in development, aging, and disease.

Acknowledgments

This work was supported in part by NIH (GM0776043 to E.N.) and Drexel University College of Medicine Aging Research Initiative.

References

1. Csete ME, Doyle JC (2002) Reverse engineering of biological complexity. Science 295(5560):1664–1669
2. Csikasz-Nagy A (2009) Computational systems biology of the cell cycle. Brief Bioinform 10(4):424–434
3. Ingolia NT, Murray AW (2004) The ups and downs of modeling the cell cycle. Curr Biol 14(18):R771–R777
4. Sible JC, Tyson JJ (2007) Mathematical modeling as a tool for investigating cell cycle control networks. Methods 41(2):238–247
5. Kholodenko BN (2000) Negative feedback and ultrasensitivity can bring about oscillations in the mitogen-activated protein kinase cascades. Eur J Biochem 267(6):1583–1588
6. Oda K, Matsuoka Y, Funahashi A, Kitano H (2005) A comprehensive pathway map of epidermal growth factor receptor signaling. Mol Syst Biol 1:2005.0010
7. Tyson JJ (1991) Modeling the cell division cycle: cdc2 and cyclin interactions. Proc Natl Acad Sci U S A 88(16):7328–7332
8. Goldbeter A (1991) A minimal cascade model for the mitotic oscillator involving cyclin and cdc2 kinase. Proc Natl Acad Sci U S A 88(20): 9107–9111
9. Tyson JJ, Chen KC, Novak B (2003) Sniffers, buzzers, toggles and blinkers: dynamics of regulatory and signaling pathways in the cell. Curr Opin Cell Biol 15(2):221–231
10. Milo R, Shen-Orr S, Itzkovitz S, Kashtan N, Chklovskii D, Alon U (2002) Network motifs: simple building blocks of complex networks. Science 298(5594):824–827
11. Jimenez E, Recalde L, Silva M (2001) Forrester diagrams and continuous Petri nets: a comparative view. In: IEEE proceedings emerging technologies and factory automation, vol 2:85–94
12. Sobie EA (2011) Computational modeling of the cell cycle. Sci Signal 4(192):tr11
13. Faure A, Naldi A, Chaouiya C, Thieffry D (2006) Dynamical analysis of a generic Boolean model for the control of the mammalian cell cycle. Bioinformatics 22(14):e124–e131
14. Bosl WJ (2007) Systems biology by the rules: hybrid intelligent systems for pathway modeling and discovery. BMC Syst Biol 1:13
15. Kriete A, Bosl WJ, Booker G (2010) Rule-based cell systems model of aging using feedback loop motifs mediated by stress responses. PLoS Comput Biol 6(6):e1000820
16. Rosenfeld N, Young JW, Alon U, Swain PS, Elowitz MB (2005) Gene regulation at the single-cell level. Science 307(5717):1962–1965
17. Cross FR, Siggia ED (2005) Shake it, don't break it: positive feedback and the evolution of oscillator design. Dev Cell 9(3):309–310
18. Barkai N, Leibler S (2000) Circadian clocks limited by noise. Nature 403(6767): 267–268
19. Vilar JM, Kueh HY, Barkai N, Leibler S (2002) Mechanisms of noise-resistance in genetic oscillators. Proc Natl Acad Sci U S A 99(9): 5988–5992
20. Gonze D, Halloy J, Goldbeter A (2002) Robustness of circadian rhythms with respect to molecular noise. Proc Natl Acad Sci U S A 99(2):673–678
21. Braunewell S, Bornholdt S (2007) Superstability of the yeast cell-cycle dynamics: ensuring causality in the presence of biochemical stochasticity. J Theor Biol 245(4):638–643
22. Alon U (2007) An introduction to systems biology: design principles of biological circuits. Chapman & Hall/CRC mathematical and computational biology series, vol 10. Chapman & Hall/CRC, Boca Raton, FL.

23. Eils R, Kriete AE (2013) Computational systems biology: from molecular mechanisms to disease, 2nd edn. Academic, New York, NY
24. Walhout AJM, Vidal M, Dekker J (2012) Handbook of systems biology concepts and insights. Academic Press, Amsterdam
25. Klipp E (2009) Systems biology: a textbook. Wiley-VCH, Weinheim
26. Chen KC, Calzone L, Csikasz-Nagy A, Cross FR, Novak B, Tyson JJ (2004) Integrative analysis of cell cycle control in budding yeast. Mol Biol Cell 15(8):3841–3862
27. Calzone L, Gelay A, Zinovyev A, Radvanyi F, Barillot E (2008) A comprehensive modular map of molecular interactions in RB/E2F pathway. Mol Syst Biol 4:173
28. Kaizu K, Ghosh S, Matsuoka Y, Moriya H, Shimizu-Yoshida Y, Kitano H (2010) A comprehensive molecular interaction map of the budding yeast cell cycle. Mol Syst Biol 6:415
29. Faure A, Naldi A, Lopez F, Chaouiya C, Ciliberto A, Thieffry D (2009) Modular logical modelling of the budding yeast cell cycle. Mol Biosyst 5(12):1787–1796

Part II

Protocols: Analyzing Cell Cycle Regulations

Chapter 13

Cell Cycle Synchronization and Flow Cytometry Analysis of Mammalian Cells

Naoko Yoshizawa-Sugata and Hisao Masai

Abstract

Analysis of cellular DNA content and measurement of pulse-labeled newly replicated DNA by flow cytometry are useful techniques for cell cycle studies. In this chapter, we describe the protocols for cell cycle synchronization of mammalian cells, including time course designs and consideration of cell types to achieve successful experiments, along with the methods for detection of DNA. Some selected applications dealing with siRNA-mediated knockdown are also presented.

Key words Cell cycle synchronization, Flow cytometry, Double-thymidine block, Mitosis, DNA replication, Cell cycle inhibitors, BrdU incorporation, Click chemistry, Embryonic stem cells, siRNA-mediated gene knockdown

1 Introduction

Analysis of cell cycle by flow cytometry is an important technique for monitoring cell proliferation, DNA replication, cell division, and checkpoint-dependent cell cycle arrest. In cancer research, detection of aneuploidy by flow cytometry is a classical but effective method [1]. Flow cytometry techniques related to cell cycle analysis have been well established and documented in the literature [2–6]. This chapter first describes basic methods for cell cycle synchronization and analysis of DNA content and then shows selected useful applications. In the following sections, we will list classical techniques useful for cell cycle analysis and describe their features. We will then provide the detailed protocols for each of them.

Eishi Noguchi and Mariana C. Gadaleta (eds.), *Cell Cycle Control: Mechanisms and Protocols*, Methods in Molecular Biology, vol. 1170, DOI 10.1007/978-1-4939-0888-2_13,

1.1 Single Staining of Cellular DNA in Asynchronous Culture: What Do We Know from Cell Cycle Profiles of Single-Staining Data?

The most basic technique would be to take a snapshot of the cell cycle profile of asynchronously growing cells. Proliferating cells replicate DNA in S phase and divide into two daughter cells in mitosis, with the two phases being separated by gap phases. The DNA content of normal mammalian cells varies from 2N in G1 to 4N in G2/M phase. It is somewhere between 2N and 4N during S phase. In contrast, quiescent cells in G0 phase show 2N DNA population. In transition from quiescence into growing phase, changes in cell cycle snapshots can indicate that cells are entering the proliferative cell cycle phase. In cancer cells, especially at a late stage, chromosomal aneuploidy may be detected by flow cytometry as cells harbor abnormal chromosome sets. DNA content can be analyzed by well-established protocols using propidium iodide (PI), a compound that intercalates into double-stranded DNA or RNA and emits strong fluorescence [3].

1.2 Single Staining of Cellular DNA in Synchronous Culture: Why Do We Have to Synchronize the Cells for Analysis?

In growing cells, most of the essential proteins required for the cell cycle regulation are expressed, activated, or degraded in a cell cycle-dependent manner. Therefore, single snapshots of the cell cycle of asynchronous cells may be insufficient to accurately describe the effect of mutations or siRNA depletion on various phenotypes. When the target protein is a cell cycle regulator, cells may tend to become arrested at specific stages of the cell cycle. This is called "cell cycle effect." Analysis of synchronized cells would circumvent this sort of complication.

There are many reagents available for synchronization. In Subheadings 3.1–3.3, the standard protocols for HeLa cells or mouse embryonic stem cells will be presented. There is no recipe that is good for all cell types, and optimization of the protocol (concentration, duration of treatment, choice, and combination of reagents) is generally required for each cell type to be analyzed. It appears that the most important is to keep cells in a good condition during the course of treatment. It should be noted that synchronization could be difficult for some cell lines due to inability of the cells to return to the cell cycle or acute cell death caused by the treatment.

1.3 Double Staining of Total DNA and Nascent DNA: What Is the Advantage of Double Staining?

The snapshot of cell cycle profile described in Subheading 1.1 is useful but is limited in its capacity to accurately estimate cell cycle states. For example, the accumulation of S-phase populations may be related to cell proliferation in most cases but it can be caused by defects in S-phase progression. The dual labeling of total and newly synthesized DNA can distinguish between these two possibilities.

The most common reagent used to label nascent DNA is 5-bromo-2′-deoxyuridine (BrdU), a deoxythymidine analog, which is readily incorporated into DNA in place of deoxythymidine by addition to the medium. BrdU is detected by a specific antibody after mild denaturation of the DNA [3]. Another thymidine analog,

5-ethynyl-2′-deoxyuridine (EdU), is also frequently used for labeling nascent DNA. EdU is detected after the covalent coupling of fluorochroms in a copper-catalyzed reaction between azide and alkyne [7]. The advantage of the use of EdU is that EdU incorporated into DNA can be detected without denaturation steps, enabling co-staining with other antibodies. Both methods will be explained in Subheadings 3.4.1 and 3.4.2, and the combination with synchronization protocols will be presented in Subheading 3.4.3. BrdU and EdU have been used to detect proliferation of tumors or cells from specific tissues in animals as well [8–10].

1.4 Multi-staining of Cellular DNA, Nascent DNA, and Proteins

Cell cycle regulating proteins are often expressed at specific stages of the cell cycle and can be detected by co-staining with DNA using flow cytometry. Data from multi-staining experiments can give useful information on the cell cycle-specificity of protein expression. Details of these procedures are not presented in this chapter but are described elsewhere [4].

More recently, single-cell mass cytometer has been developed using a mass spectrometric detector. This technology enables simultaneous detection of over 40 proteins with isotope-tagged antibodies, and expression timing of each protein can be assigned to specific cell cycle stages [11]. Nascent DNA is labeled with 5-iodo-2′-deoxyuridine (IdU) and analyzed directly by mass spectrometry. This state-of-the-art technique will not be described in this chapter but those interested may be referred to the literature [12].

2 Materials

The following is equipment and materials commonly required for the protocols described in this chapter:

1. Fluorescent flow cytometer: For cell cycle analysis, flow cytometers with at least single argon or blue laser excitation can be used. In case of analyzing EdU-labeled DNA, the manufacturer recommends the use of a cytometer with two lasers (e.g., UV and blue laser; or blue and red laser). Software for analysis is included in the cytometer system or is commercially provided from Verity Software House (for ModFit LT™), Phoenix Flow systems (for Multi cycle AV), or others.
2. Microcentrifuge: To spin down or wash cells in 1.5-mL microcentrifuge tubes, a refrigerated microcentrifuge is required. Availability of a swing rotor is preferred.
3. Culture medium: For HeLa cells, Dulbecco's Modified Eagle Medium (DMEM) containing 10 % fetal bovine serum and 2 mM glutamine is used. For mouse ES cells, DMEM supplemented with 15 % fetal bovine serum, 4 mM glutamine, 0.1 mM

2-mercaptoethanol, 1 mM sodium pyruvate, and 1,000 U/mL ESGRO® leukemia inhibitory factor (LIF, Millipore).

4. Phosphate buffered saline (PBS): 136.9 mM NaCl, 2.68 mM KCl, 8.1 mM Na_2HPO_4, and 1.47 mM KH_2PO_4, pH 7.4.

2.1 Single-Staining of DNA of HeLa Cells in Asynchronous Culture

1. 100 % ethanol.
2. 70 % ethanol.
3. RSA-PI(50) buffer: PBS supplemented with 100 μg/mL RNaseA, 2 % fetal bovine serum, 0.02 % NaN_3, and 50 μg/mL propidium iodide (PI).

2.2 Single-Staining of DNA of HeLa Cells in Synchronous Culture

1. Thymidine stock solution (100 mM): Dissolve 242 mg of thymidine in 10 mL of serum-free DMEM and filtrate with 0.22 μm pore size membrane. This can be stored at −20 °C for 6 months.
2. Nocodazole stock solution (10 mg/mL): Dissolve 10 mg of nocodazole in 1 mL of dimethysulfoxide (DMSO). This can be stored at −20 °C for at least 6 months. Just before use, dilute 1,000-fold with serum-free DMEM (10 μg nocodazole/mL). The diluted solution is not suitable for long storage.
3. L-mimosine stock solution (10 mM): Dissolve 10 mg L-mimosine ((S)-alpha-Amino-β-[1-(3-hydroxy-4-oxopyridine)]propionic acid) in 5.05 mL of serum-free DMEM and filtrate with 0.22 μm pore size membrane. Can be stored at −20 °C for 6 months.
4. 100 % ethanol.
5. 70 % ethanol.
6. RSA-PI(50) buffer (*see* Subheading 2.1).

2.3 Sequential Treatment with Two Cell Cycle Blockers and Synchronous Release

1. Thymidine stock solution (*see* Subheading 2.2).
2. Nocodazole stock solution (*see* Subheading 2.2).
3. Gelatin-coated 10-cm dishes.
4. 100 % ethanol.
5. 70 % ethanol.
6. RSA-PI(50) buffer (*see* Subheading 2.2).

2.4 Pulse-Labeling of Nascent and Cellular DNA

1. 5-bromo-2′-deoxyuridine (BrdU) stock solution (20 mM): Dissolve 61.42 mg of BrdU in 10 mL of distilled water and filtrate with 0.22 μm pore size membrane. This can be stored at −20 °C for 6 months.
2. 100 % ethanol.
3. 70 % ethanol.
4. Wash buffer containing RNaseA: PBS supplemented with 0.5 % bovine serum albumin, 0.02 % NaN_3, and 100 μg/mL RNaseA.

5. Denaturation buffer: 2N HCl and 0.5 % Triton X-100.
6. Neutralizing buffer: 0.1 N NaB_4O_7, with pH adjusted at 8.5 by boric acid-saturated solution.
7. Wash buffer (+): PBS supplemented with 0.5 % Tween 20, 0.5 % bovine serum albumin, and 0.02 % NaN_3.
8. FITC-conjugated anti-BrdU antibody (Beckton Dickinson).
9. FITC-conjugated anti-igG antibody (Beckton Dickinson).
10. SA-PI(10) buffer: PBS supplemented with 2 % fetal bovine serum, 0.02 % NaN_3, and 10 μg/mL PI.
11. Click-iT® EdU Imaging Kit (Invitrogen), containing EdU, Alexa Fluor® 488 azide, DMSO, Click-iT® EdU reaction buffer, 100 mM $CuSO_4$, and Click-iT® EdU buffer additive.
12. EdU stock solution (10 mM): Dissolve 5 mg of EdU (from the Kit shown above) in 2 mL of DMSO. This can be stored at −20 °C for up to 1 year.
13. PBS/Triton buffer: PBS supplemented with 0.5 % Triton X-100.
14. Hoechst staining solution: PBS containing 1 % bovine serum albumin, 20 μg/mL RNaseA, and 5 μg/mL Hoechst 33342.
15. Lipofectamine 2000 (Life Technologies).
16. Hydroxyurea stock solution (2 M): Dissolve 1.522 g of hydroxyurea in 10 mL of distilled water and filtrate with 0.22 μm pore size membrane. Can be stored at −20 °C for 6 months.

2.5 Analysis of Cell Cycle Profile During Differentiation

1. 100 % ethanol.
2. 70 % ethanol.
3. RSA-PI(50) buffer (*see* Subheading 2.2).
4. All-trans-retinoic acid stock solution (10 mM): Dissolve 3 mg retinoic acid in 1 mL of ethanol. Store under argon or other inert gas at −80 °C, and keep in the dark.

3 Methods

3.1 Single-Staining of DNA of HeLa Cells in Asynchronous Culture

1. Harvest cells: Culture HeLa cells in a 6-cm dish until the culture has semi-confluent density, detach cells with trypsin, and harvest to a 1.5-mL microcentrifuge tube.
2. Wash cells: Centrifuge cells at 176 × *g* for 3 min and remove the supernatant. Add 0.5–1 mL of cold PBS to wash. Repeat centrifugation and remove the PBS.
3. Fix cells: Resuspend cells in 400 μL of cold PBS. Add 1 mL (2.5 × volume) of 100 % EtOH. Immediately invert tubes upside down several times and mix by gentle vortex for 5 s. Alternatively, add 9 × volume of 70 % EtOH to the cell suspension and vortex gently. Let the tube sit at room temperature

for 5 min or at 4 °C for 30 min. Cells can be stored at 4 °C for weeks or at −20 °C for months.

4. Wash fixed cells: Centrifuge cells at 314 × *g* for 3 min at 4 °C and remove EtOH. Add 0.5–1 mL of cold PBS. Centrifuge cells at 314 × *g* for 3 min and remove the supernatant.
5. Stain DNA with PI: Suspend cells in RSA-PI(50) buffer. Keep tubes in the dark at 37 °C for 10 min or at room temperature for 30 min.
6. Analyze cells by fluorescent flow cytometer: PI signal can be detected at 617 nm, at FL2 channel for FACSCalibur and FACScan, or PE channel for FACSCantoII (Becton Dickinson Immunocytometry Systems).

3.2 Single-Staining of DNA of HeLa Cells in Synchronous Culture

Thymidine is the most commonly used S-phase blocker and its addition to the medium depletes nucleotide pools and inhibits new DNA synthesis, causing the slowdown or arrest of S-phase progression (*see* **Note 1**). As a result, cells accumulate as a broadly distributed population between 2N and 4N. For clear synchronization at early S phase, the double thymidine block procedure described in Subheading 3.3.1 is recommended.

3.2.1 Arrest at S Phase

1. Culture HeLa cells until 60–70 % confluency is achieved.
2. Add thymidine to a final concentration of 2.5 mM and incubate for 16 h.
3. Harvest cells and analyze as in Subheading 3.1.

3.2.2 Arrest at M Phase

1. Culture HeLa cells until 80 % confluency is achieved.
2. Add nocodazole to a final concentration of 20–100 ng/mL and incubate for 16 h.
3. Harvest cells by mitotic shake-off. Collect round, mitotic-arrested cells from the dish by tapping or gentle pipetting using a 5-mL pipette or a Pasteur glass pipette. Process cells for cytometric analysis as in Subheading 3.1.

3.2.3 Arrest at G1/S Boundary

Mimosine is an iron chelator and an inhibitor of initiation of DNA replication in mammalian cells, causing sharp arrest at the G1/S transition. Blocking the cell cycle with mimosine for longer time is highly cytotoxic and induces cell death.

1. Culture HeLa cells until 60–70 % confluency is achieved.
2. Add L-mimosine to a final concentration of 0.3 mM and incubate for 16 h.
3. Harvest and analyze cells as in Subheading 3.1.

3.2.4 Arrest at G0 Phase

Some cell types can be synchronized by release from G0-arrest by contact inhibition or serum deprivation. The protocols for these methods are described elsewhere [13].

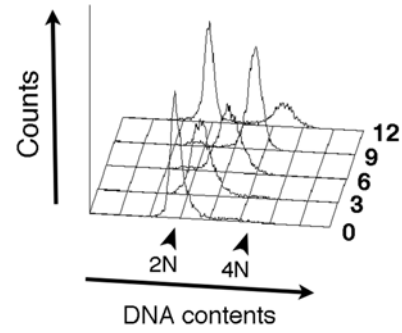

Fig. 1 Histograms of DNA contents of HeLa cells in double thymidine block and release protocol. HeLa cells were treated as in Subheading 3.3.1 and histograms were overlayed at series of time after release (0–12 h)

3.3 Sequential Treatment with Two Cell Cycle Blockers and Synchronous Release

In this protocol, HeLa cells are treated with thymidine twice sequentially with an interval in between the treatments. As shown in Fig. 1, highly synchronous cell cycle populations can be obtained with this method. For tips on the release from the first block and optimization of the protocol for other cells lines, *see* **Notes 2** and **3**.

3.3.1 Double Thymidine Block and Release of HeLa Cells

1. Culture HeLa cells in a 10-cm dish until 25–30 % confluency is achieved.
2. Add thymidine to a final concentration of 2.5 mM and incubate at 37 °C for 16 h.
3. Wash cells twice with 3 mL of pre-warmed PBS or serum-free DMEM.
4. Add pre-warmed medium with serum and release cells into cell cycle at 37 °C for 9 h.
5. Add thymidine to a final concentration of 2.5 mM and incubate at 37 °C for 14–16 h.
6. Wash cells twice with 3 mL of pre-warmed PBS or serum-free DMEM.
7. Release cells at 37 °C as in **step 4** and harvest cells at 0, 3, 6, 9, and 12 h.

3.3.2 Mitotic Release of HeLa Cells After Thymidine Block

HeLa cells can be easily arrested at mitosis by nocodazole as described in Subheading 3.2.2, although release efficiency is often unsatisfactory. To increase the efficiency of mitotic release and synchronization, nocodazole arrest is often combined with thymidine block. The method can also be combined with siRNA-mediated knockdown of a cell cycle regulator. The ideal design of this experiment is to synchronize the cell cycle at the early stage of knockdown when siRNA has little effects on cell proliferation, and then analyze cell cycle progression after the effective knockdown of the target. We usually start the first synchronization soon after the first transfection of siRNA to achieve maximum synchronization with the

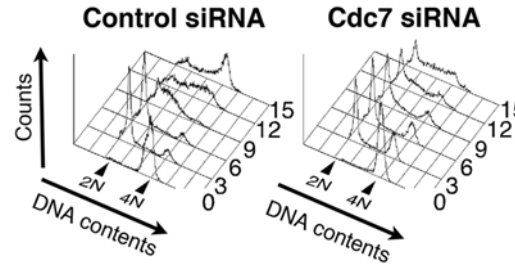

Fig. 2 Histograms of DNA contents of HeLa cells released from nocodazole block. The effect of Cdc7 kinase knockdown. Cells were treated with control siRNA (*left*) or siRNA against Cdc7 kinase (*right*)

least effect of knockdown. For details, refer to [14, 15]. Figure 2 shows that S-phase progression is inhibited by depletion of Cdc7, a kinase essential for initiation of DNA replication. For alternative mitotic blockers, *see* **Note 4** and [16].

1. Culture HeLa cells in a 10-cm dish until 60–70 % confluency is achieved.
2. Add thymidine to a final concentration of 2.5 mM and incubate at 37 °C for 16 h.
3. Wash cells twice with 3 mL of pre-warmed PBS or serum-free DMEM.
4. Add pre-warmed medium with serum and release cells at 37 °C for 8 h.
5. Add nocodazole to a final concentration of 15–50 ng/mL and incubate at 37 °C for 6–8 h (*see* **Note 5**).
6. Harvest cells by mitotic shake-off or by gentle pipetting with 10-mL pipette. Centrifuge cells at 190 × *g* at room temperature for 5 min. Wash cells twice with 5 mL of pre-warmed PBS or serum-free DMEM.
7. Resuspend cells in pre-warmed medium with serum and transfer to new dishes (*see* **Note 6**).
8. Release cells at 37 °C and harvest at 0, 3, 6, 9, 12, and 15 h.

3.3.3 Thymidine Block and Release of Mouse Embryonic Stem (ES) Cells After Mitotic Block/Release

1. Culture E14tg2a cells in a gelatin-coated 10-cm dish until 30 % confluency.
2. Add nocodazole to a final concentration of 25 ng/mL and incubate cells at 37 °C for 14 h.
3. Harvest cells by gentle pipetting with Pasteur pipettes or 1-mL tips. Centrifuge cells at 190 × *g* at room temperature for 5 min. Wash the cells once with 5 mL of pre-warmed PBS and then once with culture medium containing LIF.

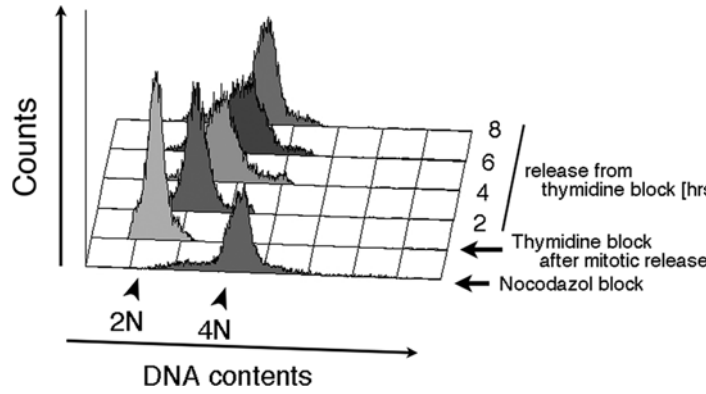

Fig. 3 Synchronous release of mouse E14tg2a ES cells from thymidine block

4. Resuspend cells in pre-warmed medium containing 1.5 mM thymidine and transfer cells to four new gelatin-coated dishes. Incubate at 37 °C for 6 h.
5. Wash cells twice with 4 mL of pre-warmed PBS or culture medium.
6. Release cells in fresh medium at 37 °C and harvest cells at 0, 2, 4, 8 h (*see* **Note 6**).
7. Analyze cells as in Subheading 3.1. A representative result is shown in Fig. 3.

3.4 Pulse-Labeling of Nascent and Cellular DNA

3.4.1 Detection of Nascent DNA Labeled with BrdU in HeLa Cells

1. Add BrdU to a final concentration of 10 μM to semi-confluent HeLa cells in two 6-cm dishes. Incubate for 30 min at 37 °C.
2. Harvest cells into two tubes. Fix and wash cells as described in Subheading 3.1, **steps 1–4**.
3. Resuspend cells in Wash buffer containing 100 μg/mL RNaseA. Keep tubes in the dark at 37 °C for 10 min or at room temperature for 30 min.
4. Centrifuge cells at 314 × *g* for 3 min and resuspend cell pellets in 0.5 mL of Denaturation buffer. Incubate for 20 min in the dark.
5. Centrifuge cells at 314 × *g* for 3 min and resuspend cell pellets in 0.5 mL of Neutralizing buffer for 2 min.
6. Wash cells with 0.5 mL of Wash buffer (+).
7. Dislodge cell pellets. Add 20 μL of FITC-labeled anti-BrdU antibody for tube 1, and add 20 μL of FITC-labeled control IgG (negative control) for tube 2. Incubate for 20 min at room temperature in the dark.
8. Add 0.5 mL of Wash buffer (+) and remove unbound antibodies.
9. Resuspend cells in 0.5 mL of SA-PI(10) buffer and incubate for a few minutes in the dark (*see* **Note 7**).

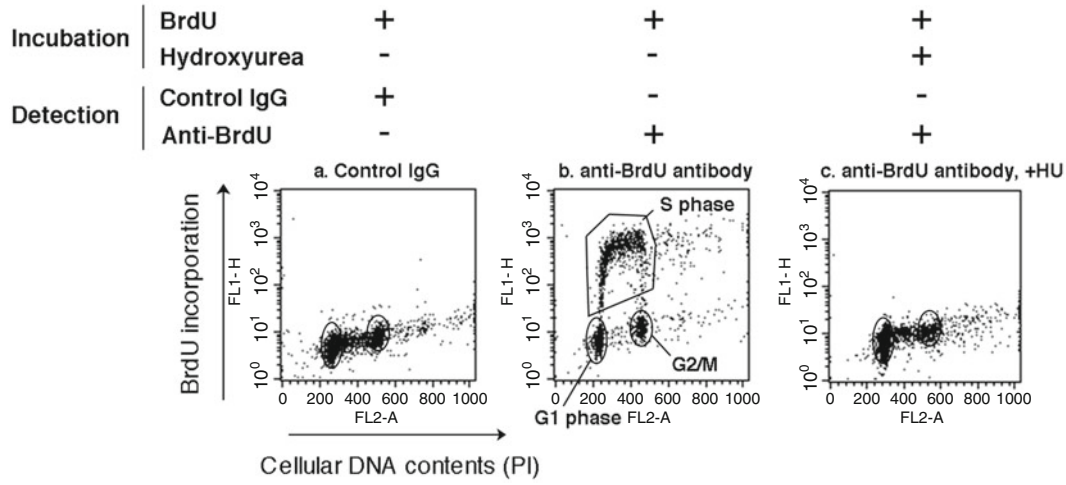

Fig. 4 Dot plots of incorporated BrdU and propidium iodide-stained cellular DNA in HeLa cells. Cells were labeled with BrdU for 30 min in this experiment. In (**c**), hydroxyurea was also added at 1 mM at **step 1** of Subheading 3.4.1. As a result, BrdU-positive cell population was abolished

10. Analyze total and pulse-labeled DNA. If you use FACScan or FACSCalibur cytometer, parameters are FL2-A channel (linearity mode) for total DNA content and FL1-H (logarithm mode) for incorporated BrdU. Representative dot plots are presented in Fig. 4a (negative control) and in Fig. 4b (anti-BrdU antibody).

3.4.2 Detection of Nascent DNA Labeled with EdU in Mouse Embryonic Stem Cells

1. Add EdU to a final concentration of 10 μM to 50 % confluent E14tg2a cells in a 6-cm dish. Incubate for 20 min (or 10–30 min).
2. Harvest cells into two tubes. Fix and wash cells as described in Subheading 3.1, **steps 1–4**.
3. Resuspend cells in PBS/Triton buffer and incubate at room temperature for 5 min.
4. Prepare Click-iT® reaction cocktail. Make 1× Reaction buffer additive by diluting Click-iT® EdU reaction buffer with distilled water. For 1 reaction, mix 10 μL of 100 mM $CuSO_4$ solution, 2.5 μL of Alexa Fluor® 488 azide, 50 μL of Click-iT® EdU reaction buffer additive, and 438 μL of PBS. Use Click-iT® reaction cocktail within 15 min.
5. Add 0.5 mL of Click-iT® reaction cocktail per tube. Incubate at room temperature for 30 min in the dark.
6. Wash cells with 0.5 mL of PBS/Triton buffer.
7. Resuspend cells in Hoechst staining solution and incubate at room temperature for 30 min in the dark.

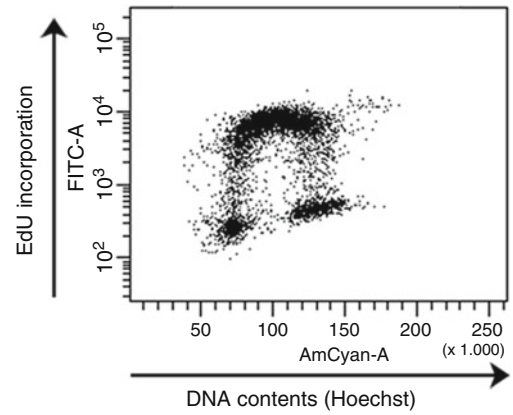

Fig. 5 A dot plot of incorporated EdU and Hoechst-stained cellular DNA in mouse E14tg2a ES cells. G1, S, G2/M populations can be mapped as in Fig. 4

8. Analyze total and pulse-labeled DNA. If you use FACSCantoII cytometer, parameters are AmCyan-A (linearity mode) for total DNA contents and PE (logarithm mode) for incorporated EdU. A representative result is shown in Fig. 5.

3.4.3 Pulse-Labeling and Time-Lapse Protocol Combined with siRNA-Mediated Knockdown

1. Transfect HeLa cells in 10-cm dishes with control or Cdc7 siRNA using Lipofectamine 2000. Incubate cells for 24 h at 37 °C.
2. Replate cells from each dish into three 6-cm dishes (dishes 1–3), and incubate cells for 24 h.
3. Add BrdU to a final concentration of 10 μM to each dish and incubate for 20 min at 37 °C.
4. Harvest dish 1 and fix as in Subheading 3.1 (sample "time 0"). For others (dishes 2 and 3), wash cells with pre-warmed PBS twice and add fresh medium for release.
5. At 4 or 8 h after the release, harvest cells from dishes 2 or 3, respectively, and fix cells (samples "time 4 and 8"). Analyze DNA as in Subheading 3.4.1. A representative result is shown in Fig. 6 (*see* **Note 8**).

3.5 Analysis of Cell Cycle Profile During Differentiation

1. Culture mouse CCE28 embryonic stem cells with medium containing LIF in three 6-cm dishes.
2. At day 0, harvest cells from dish 1 and fix as in Subheading 3.1.
3. Replace the medium in dishes 2 and 3 with LIF-free medium and add all-trans-retinoic acid solution to a final concentration of 1 μM to induce differentiation into neuronal lineage.
4. Continue to culture and subculture if needed.
5. At day 2 and 6, harvest cells from dishes 2 and 3, respectively, and fix as in Subheading 3.1. A representative result is shown in Fig. 7.

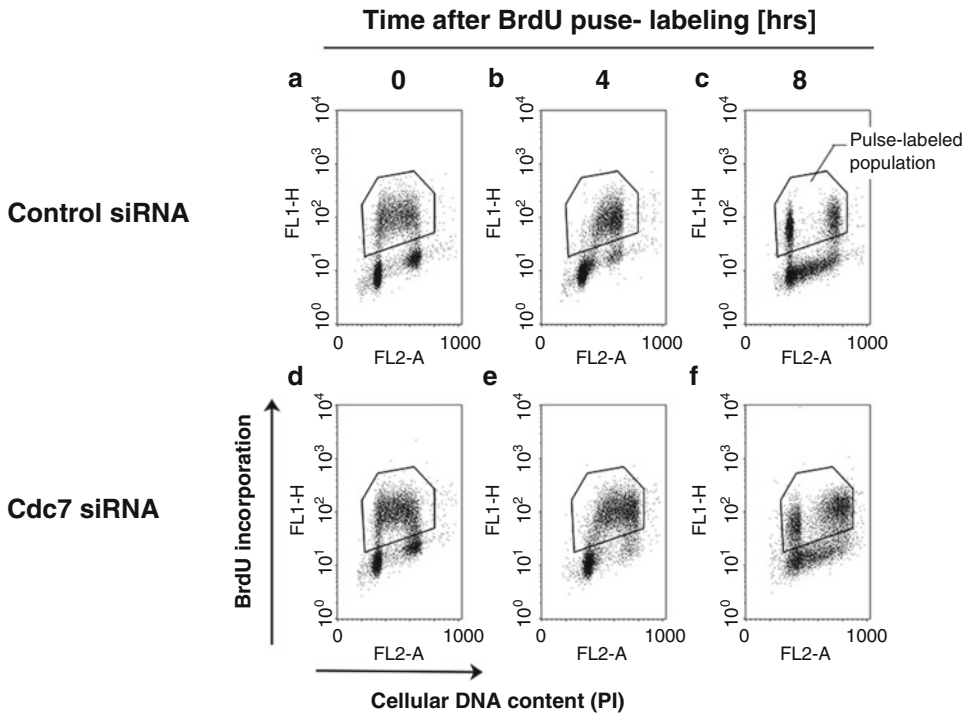

Fig. 6 Detection of S-phase progression of HeLa cells by pulse-labeling and time-lapse protocol (*see* Subheading 3.4.3 for details). In control cells, BrdU-labeled population proceeds through S phase at 4 h (**b**) and more than half moves into next G1 phase at 8 h (**c**). In contrast, the pulse-labeled fraction in Cdc7-depleted cells distributed broadly in the S-phase fraction at 4 h (**e**) and mid to late S-phase cells remained even at 8 h after release (**f**)

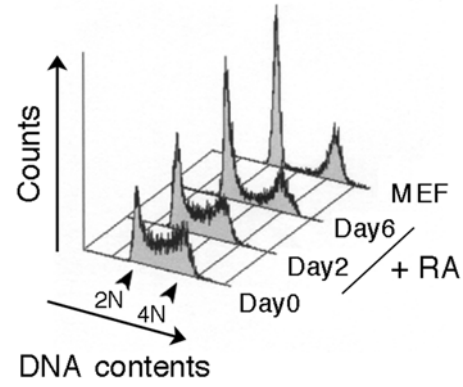

Fig. 7 Cell cycle profiles of mouse ES cells after induction of differentiation. The undifferentiated ES cells show abundant S-phase cells (Day 0), whereas G1-phase population increases after induction of differentiation (Day 2 and 6). As control, DNA content of the mouse embryonic fibroblast (MEF) cells is also shown

4 Notes

1. Choice of S-phase blocking reagents: In place of thymidine, HeLa cells can be arrested with other S-phase inhibitors such as hydroxyurea (HU; 1 mM) or aphidicolin (1 μg/mL). In our experience, thymidine is less toxic and release from thymidine block into the cell cycle works well in most cell lines. Treatment with HU or aphidicolin at higher doses or longer incubation times should be avoided since it causes severe DNA damage response and hyper-checkpoint activation or cell death. This may influence the expression levels of cell cycle-related proteins. Other drugs used for cell cycle synchronization are listed elsewhere [16].
2. Tips on the release from the first block in "double thymidine block and release" protocol: For better synchronization, keep cells warm during the wash and handle only a small number of dishes at one time (at most 4–5 dishes).
3. Optimization of the "double thymidine block and release" protocol for other cells lines: In case of working with other cell types, time for block and release should be conditioned. The time for the first release should be long enough for cells to pass through S phase and should be shorter than the sum of G2, M, and G1 phases. For slowly growing cells, a longer blocking time is required. For rapidly cycling cells such as mouse embryonic stem cells, the double thymidine block and release protocol is not generally applicable because of their short G1 phase. Other methods, such as mitotic block and release (similar to what is described in Subheading 3.3.2), or S-phase block and release after mitotic release (described in Subheading 3.3.3) or release from mimosine-induced G1/S block [17] are recommended.
4. Alternative reagents for mitotic block and release: Nocodazole inhibits assembly of microtubule reversibly and stops mitosis at metaphase under the activated spindle checkpoint. TN-16 (3-(1-Anilinoethylidene)-5-benzylpyrrolidine-2,4-dione, Sigma) is another reversible mitotic inhibitor and can be used for HeLa cells at 75–150 ng/mL for mitotic block and release experiments. In contrast, demecorcin (corcemid) is an irreversible mitotic blocker and thus not useful for synchronous release.
5. Tips for nocodazole block: For efficient release, optimization of nocodazole treatment using the cells and reagent stocks in your laboratory is recommended. The optimum concentration is the lowest that is sufficient to block most of the cells in the population (95 %<). Higher concentration and longer incubation times (>10 h) inhibit release into the cell cycle and increase cell death.
6. Tips for release from nocodazole block: Over 90 % of HeLa cells can be released into cell cycle after nocodazole treatment

under a highly optimized condition. Under an unconditioned protocol or when difficult-to-release cells are used, a fraction of the cells stops cycling and remains floating with a round shape. Removal of these uncycling cells at 2–3 h after nocodazole release may help increase the better-synchronized populations.

7. For double-staining protocols in Subheadings 3.4.1 and 3.4.3, the use of PI at a low concentration is essential to acquire FITC signal without interference by emission from DNA-bound PI. A minor adjustment of detectors for compensation may still be required to minimize overlaps. For compensation or subtraction, refer to the cytometer manuals or textbooks of basic flow cytometric analysis.
8. S-phase cells incorporating BrdU in asynchronous culture can be chased in dot plots of FL2-A and FL1-H (*see* Fig. 4). The advantage of this protocol is to circumvent the use of cell cycle blockers. When cell cycle-related genes are knocked down, cell cycle synchronization becomes less effective, or cellular toxicity is induced, making the interpretation of results difficult. Other useful applications have been described elsewhere [18].

Acknowledgments

This work was supported in part by The Naito Foundation Continuation Subsidy for Outstanding Projects (H.M.) and JSPS KAKENHI grant 23580243 (N.Y.-S.).

References

1. Wenger CR, Beardslee S, Owens MA, Pounds G, Oldaker T, Vendely P, Pandian MR, Harrington D, Clark GM, McGire WL (1993) DNA ploidy, S-phase, and steroid receptors in more than 127,000 breast cancer patients. Breast Cancer Res Treat 28(1):9–20
2. Juan G, Darzynkiewicz Z (1998) Cell cycle analysis by flow and scanning cytometry. In: Celis JE, Hunter T, Carter N, Shotton D, Small JV, Simons K (eds) Cell biology: a laboratory handbook. Cell and tissue culture and associated techniques, 2nd edn. Academic Press, San Diego, pp 261–274
3. Dolbeare F, Selden JR (1994) Immunochemical quantitation of bromodeoxyuridine: application to cell-cycle kinetics. Methods Cell Biol 41:297–316
4. Pozarowski P, Darzynkiewicz Z (2004) Analysis of cell cycle by flow cytometry. Methods Mol Biol 281:301–311
5. Davies D, Allen P (2007) DNA analysis by flow cytometry. In: Macey MG (ed) Flow cytometry: principles and applications, 2007 edn. Humana Press, New York, pp 165–180
6. Jacobberger JW, Sramkoski RM, Stefan T (2011) Multiparameter cell cycle analysis. Methods Mol Biol 699:229–249
7. Rostovtsev VV, Green LG, Fokin VV, Sharpless KB (2002) A stepwise Huisgen cycloaddition process: copper(I)-catalyzed regioselective "ligation" of azides and terminal alkynes. Angew Chem Int Ed Engl 41(14):2596–2599
8. Onda K, Davis RL, Shibuya M, Wilson CB, Hoshino T (1994) Correlation between the bromodeoxyuridine labeling index and the MIB-1 and Ki-67 proliferating cell indices in cerebral gliomas. Cancer 74(7):1921–1926
9. Kuhn HG, Dickinson-Anson H, Gage FH (1996) Neurogenesis in the dentate gyrus of the adult rat: age-related decrease of neuronal

progenitor proliferation. J Neurosci 16(6): 2027–2033

10. Perea-Martinez I, Nagai T, Chaudhari N (2013) Functional cell types in taste buds have distinct longevities. PLoS One 8(1):e53399
11. Bendall SC, Simonds EF, Qiu P, el Amir AD, Krutzik PO, Finck R, Bruggner RV, Melamed R, Trejo A, Ornatsky OI, Balderas RS, Plevritis SK, Sachs K, Pe'er D, Tanner SD, Nolan GP (2011) Single-cell mass cytometry of differential immune and drug responses across a human hematopoietic continuum. Science 332(6030):687–696
12. Behbehani GK, Bendall SC, Clutter MR, Fantl WJ, Nolan GP (2012) Single-cell mass cytometry adapted to measurements of the cell cycle. Cytometry A 81(7):552–566
13. Davis PK, Ho A, Dowdy SF (2001) Biological methods for cell-cycle synchronization of mammalian cells. Biotechniques 30(6):1322–1331
14. Yoshizawa-Sugata N, Ishii A, Taniyama C, Matsui E, Arai K, Masai H (2005) A second human Dbf4/ASK-related protein, Drf1/ASKL1, is required for efficient progression of S and M phases. J Biol Chem 280(13):13062–13070
15. Yoshizawa-Sugata N, Masai H (2007) Human Tim/Timeless-interacting protein, Tipin, is required for efficient progression of S phase and DNA replication checkpoint. J Biol Chem 282(4):2729–2740
16. Rosner M, Schipany K, Hengstschlager M (2013) Merging high-quality biochemical fractionation with a refined flow cytometry approach to monitor nucleocytoplasmic protein expression throughout the unperturbed mammalian cell cycle. Nat Protoc 8(3):602–626
17. Fujii-Yamamoto H, Kim JM, Arai K, Masai H (2005) Cell cycle and developmental regulations of replication factors in mouse embryonic stem cells. J Biol Chem 280(13):12976–12987
18. Terry NH, White RA (2006) Flow cytometry after bromodeoxyuridine labeling to measure S and G2 + M phase durations plus doubling times in vitro and in vivo. Nat Protoc 1(2):859–869

Chapter 14

Analyzing Transcription Dynamics During the Budding Yeast Cell Cycle

Adam R. Leman, Sara L. Bristow, and Steven B. Haase

Abstract

Assaying global cell cycle-regulated transcription in budding yeast involves extracting RNA from a synchronous population and proper normalization of detected transcript levels. Here, we describe synchronization of *Saccharomyces cerevisiae* cell populations by centrifugal elutriation, followed by the isolation of RNA for microarray analysis. Further, we outline the computational methods required to directly compare RNA abundance from individual time points within an experiment and to compare independent experiments. Together, these methods describe the complete workflow necessary to observe RNA abundance during the cell cycle.

Key words The cell cycle, Transcription, Microarray, RNA, Centrifugal elutriation, Gene expression, Data normalization

1 Introduction

The budding yeast *Saccharomyces cerevisiae* has over 5,000 genes. Often, gene regulation is thought of in the context of response to stimulus (e.g., changing environments, food sources, and cell fate decisions). However, few processes dynamically regulate transcription to the extent of cell cycle progression, as up to one-third of the yeast genome comes under the control of the cell cycle transcription program [1–4]. The ability to detect dynamic changes in many transcripts is a powerful tool to assay the phenotype of cell cycle mutants. Our lab has utilized a workflow similar to the one described in this chapter to measure the expression of genes in wild-type yeast as well as cyclin–CDK mutants. The use of centrifugal elutriation coupled to microarray analysis has led to the recognition and characterization of a transcription factor network capable of regulating cell cycle gene expression [2, 5]. By properly monitoring a synchronous population of budding yeast, one can determine the dynamic changes of the entire transcriptional program during the cell cycle.

Eishi Noguchi and Mariana C. Gadaleta (eds.), *Cell Cycle Control: Mechanisms and Protocols*, Methods in Molecular Biology, vol. 1170, DOI 10.1007/978-1-4939-0888-2_14,

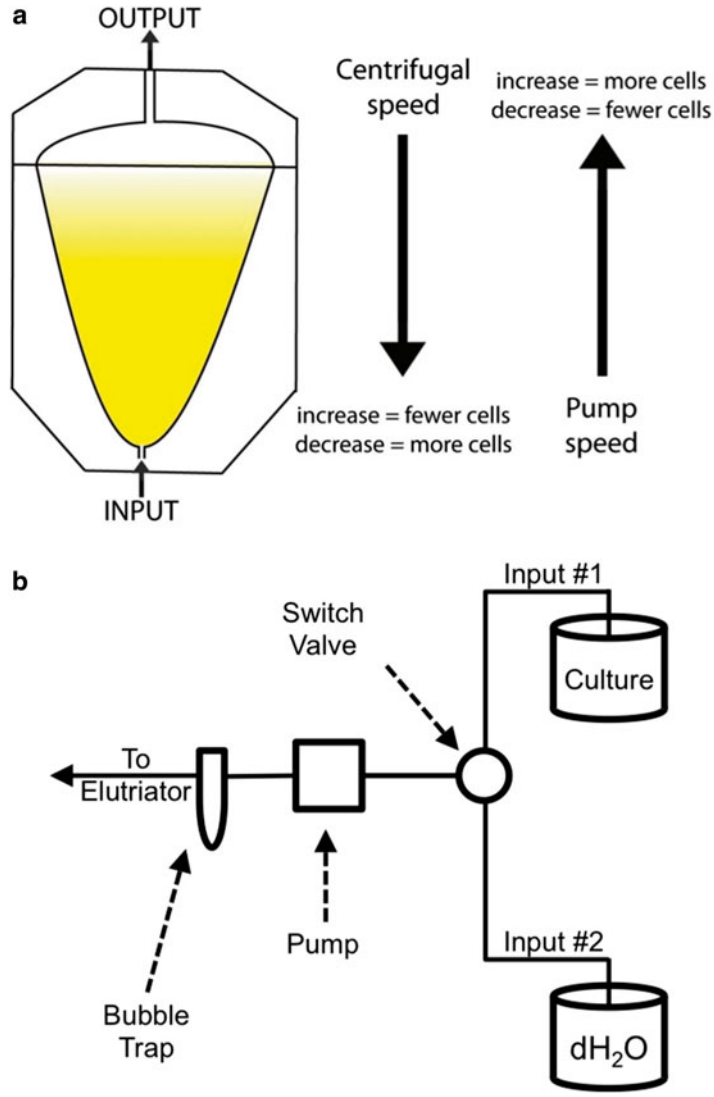

Fig. 1 Centrifugal elutriation. (**a**) *At left*, a mock-up of an elutriation chamber. *At right*, the adjustments required to change the flow of cells from the chamber and to the output for collection. (**b**) A schematic circuit of the elutriation tubing setup

Here we describe the isolation of a synchronous population of G1 cells from a logarithmically growing culture using centrifugal elutriation. We prefer centrifugal elutriation to other methods of synchronization as it is generally considered to be a minimal perturbation to cells compared to arrest [6]. A key aspect of elutriation is that there is no cell cycle arrest involved, but rather a synchronous population of unbudded (early G1) cells is removed from an asynchronous population by size fractionation (Fig. 1). This population of cells is resuspended and released into medium

to synchronously grow and progress through multiple cell cycles. Cells are periodically monitored for budding in order to follow cell cycle progression. Separately, cell aliquots are removed from the population and stored for RNA extraction. The RNA is extracted, purified, and then prepared for microarray analysis of gene expression; each time series sample is amplified, labeled, and hybridized to the microarray. The microarray is read, and the data is returned to the user.

Before any analysis of microarray data can be started, the measured raw fluorescent intensities for every probe on all chips that will be compared must be normalized to each other. The normalization process eliminates non-biological variations in gene expression across time points and/or conditions. Labeled cDNA destined for each chip may vary in mRNA isolation efficiency, fluorescent labeling, and hybridization. Thus, differences in raw values of gene expression of a single gene on a single chip and across multiple chips will be a convolution of biological and technical variance. As many different normalization methods have been developed, the user must make a choice on how to normalize the data before analysis of cell cycle transcription can be carried out. We prefer to use Affymetrix (yeast 2.0) microarrays as the data is returned in a manner that makes it simple for the user to employ their preferred normalization method. Here, we describe the implementation of several algorithms designed to normalize microarray data. After the normalization is complete, the user may commence analysis of the global periodic transcription program.

2 Materials

2.1 Yeast Culture Growth

1. Rich growth medium (YEP + 2 % sugar): 10 g/L yeast extract, 20 g/L Bacto-Peptone, 20 g/L sugar (dextrose, sucrose, galactose, etc., *see* **Note 1**), 80 mg/L adenine hemisulfate, 4 mg/L uracil.
2. Fernbach culture flask, sterile.
3. Water bath shaking incubator with adjustable temperature (from 25 to 37 °C) and shaking speed control (up to 180 rpm).
4. Compound light microscope.
5. Hemacytometer (Neubauer Improved Grid).
6. Sonicator cell disruptor with 7.5 cm microtip attachment (Misonix Model XL2000 or equivalent).

2.2 Centrifugal Elutriation to Isolate G1 Daughter Cells

1. Elutriation system: Refrigerated elutriation centrifuge such as a Beckman J-6M/E with strobe light delay control, portal, and tube access. Peristaltic pump, with adjustable pump speed capable of 5–100 mL per minute. Tubing set up with two intake tubes, a manual directional valve to change fluid supply,

and a bubble trap. The output should be long enough to switch between several different collection tubes. An appropriate elutriation rotor for the refrigerated elutriation centrifuge is the Beckman J-6M/E or equivalent. More information at https://www.beckmancoulter.com/wsrportal/techdocs?docname=JE5-IM-13.

2. 200-mL conical tubes.
3. Hemacytometer (Neubauer Improved Grid).
4. Refrigerated centrifuge with the capability of spinning 200-mL conical tubes at 3,000 × *g*.
5. Pre-warmed rich growth medium (*see* Subheading 2.1).
6. Pre-warmed 500-mL flasks.
7. 2× PBS: 274 mM NaCl, 5.4 mM KCl, 20 mM Na_2HPO_4, 3.6 mM KH_2PO_4, adjust pH to 7.2 using 10 N HCl.
8. Fixative solution: 4 % formaldehyde in 2× PBS.
9. Bleach, household use strength.
10. 190 proof ethanol.

2.3 Sampling Cells Through Time Course

1. Fixative solution: 4 % formaldehyde in 2× PBS.
2. Multichannel vacuum filtration apparatus (GE Health Sciences or equivalent).
3. 0.45 μM PVDF membrane filters, at the appropriate diameter for the multichannel vacuum filtration apparatus.
4. Flat-bladed tweezers for removal of filter membranes from apparatus.
5. 15-mL conical tubes.
6. Liquid nitrogen for flash freezing.

2.4 Determination of Cell Cycle Time

1. Compound light microscope.
2. Hemacytometer (Neubauer Improved Grid).
3. Personal computer capable of running JavaScript applets.
4. CLOCCS software.

2.5 RNA Extraction

1. Tris–EDTA–SDS (TES) buffer: 10 mM Tris–HCl pH 7.5, 10 mM EDTA, 0.5 % SDS. Warmed to 60–65 °C.
2. Water-saturated phenol, pH 4.5–5.0.
3. Microfuge.
4. Chloroform, ACS grade.
5. 3 M sodium acetate, pH 5.3.
6. 200 proof ethanol, molecular biology grade.
7. 70 % ethanol.
8. DEPC-treated distilled H_2O.

2.6 RNA Gel Electrophoresis

1. 10× MEN buffer (for dilution to 1× MEN as running buffer and for use as 10× MEN in sample loading buffer): 44.8 g MOPS, 6.8 g NaAc (anhydrous), 3.72 g EDTA (dihydrous). Add to 800 mL dH_2O, adjust pH to 7.2 using 10 N NaOH, and bring volume to 1 L. Store in the dark at room temperature.
2. Formaldehyde gel: 0.5 g agarose, 5 mL 10× MEN buffer, 37 mL dH_2O. Melt agarose, let it cool until ~55 °C, move to fume hood, and add 8 mL 100 % formaldehyde. Pour the gel into a 5 cm × 12 cm gel casting mold. If it is necessary to make a larger gel to run all samples, double the above recipe.
3. 6× Nucleic acid loading dye: 1.7 mL 0.5 M EDTA, 4.2 mL 100 % glycerol, 35 mg bromophenol blue, add ddH_2O to 14 mL.
4. Sample loading buffer: 100 µL 100 % formamide, 40 µL 100 % formaldehyde, 30 µL 10× MEN buffer, 30 µL of 6× nucleic acid loading dye, 5 µL ethidium bromide (2 mg/mL).

2.7 Sample Cleanup

1. Nanodrop Spectrophotometer.
2. RNeasy MinElute Cleanup Kit (Qiagen).
3. DEPC-treated RNase-free dH_2O.

2.8 Sample Submission

1. Agilent Bioanalyzer.
2. Ambion MessageAmp Premier kit.
3. Affymetrix GeneChip Yeast Genome 2.0 arrays.

2.9 Normalization of Time Series Microarray Data

1. Personal computer capable of running R (http://www.R--project.org).

3 Methods

3.1 Yeast Culture Growth

Using centrifugal elutriation to obtain a synchronized population of cells relies on isolating a population subset, rather than synchronizing an entire population. To observe cell cycle-transcription dynamics, we isolate early G1 cells and release them into conditions under which we monitor the cell cycle progression and gene expression. For such an approach to work, one needs to generate a large number of cells in logarithmic growth. This process takes several days to scale up. The cells must be monitored, and care must be taken to prevent overgrowth of the cultures and subsequent quiescence.

1. Begin by inoculating a 25 mL rich growth medium starter culture in a 125 mL flask for overnight growth in a shaking water bath incubator at the optimal growth temperature for the strain (*see* **Note 2**).

2. The next morning (approximately 16 h later), back dilute the culture in fresh growth medium to 50 mL at a concentration of ~5×10^6 cells/mL. Cells should not be allowed to grow to a concentration greater than 3×10^7 cells/mL to avoid cells exiting the cell cycle to G0 (quiescence) (*see* **Note 3**).
3. The night before the time course, inoculate 2.25 L of medium in a 3 L Fernbach flask. The number of cells used should be predetermined to give a density of $1.5–3.0 \times 10^7$/mL cells when the cells are removed from the incubator for the experiment the next morning (*see* **Note 4**).
4. After removing the flask from the incubator, sonicate the culture to break up cell clumps. This will facilitate movement of cells through the elutriator system tubing and reduce the possibility of clogging. Three pulses of 5 s (at 25 % power) with 1 min between each pulse are sufficient, with at least 5 cm of the probe tip submerged in the medium.
5. Remove sonicated cells from Fernbach flask to one or more beakers surrounded by ice to cool cells and prevent further cell proliferation. Cover the beaker with foil (*see* **Note 5**).

3.2 Centrifugal Elutriation to Isolate G1 Daughter Cells

Elutriation of budding yeast has been described previously in detail [6, 7]. Elutriation depends on two different separation processes occurring simultaneously, the sedimentation of cells by centrifugation countered by fluid flow, allowing for the release of the smallest particles from the elutriation chamber (Fig. 1a). Determination of the parameters required for isolating early G1 cells is highly strain dependent. The parameters are also variable according to elutriator and pump model. Therefore, it is highly recommended that the protocol for growing cells, centrifugal elutriation, sampling for time course, and determination of cell cycle time (Subheadings 3.1–3.4) are carried out at least three times before an attempt is made at a time course for microarray analysis of cell cycle transcription (*see* **Note 6**).

1. With cells on ice (Subheading 3.1, **step 5**), prepare for centrifugal elutriation. The specific details of setup vary depending on elutriator and pump model. Assemble a single elutriation chamber, fill the system with sterile dH_2O, and cool the centrifuge chamber to 4–10 °C. The system should have two inputs; input #2 will serve as a constant reservoir of sterile H_2O to ensure that when switching input #1 to a cell culture, no air is introduced (Fig. 1b). If air is introduced into the system, it may interrupt the flow of cells and increase the pressure, resulting in a tube blowoff.
2. Once the system is filled and all air bubbles are purged, turn the centrifuge on and allow the speed to reach the desired elutriation rpm setting (*see* **Note 7**).

3. Move the input #1 tube to the beaker containing the yeast culture to pump cells through the fluidics system. Leave the output tube in a liquid waste receptacle (*see* **Note 8**).
4. When medium begins to flow from the output tube, place the output into the beaker containing the cell culture. This allows for a closed system and provides the necessary fluid supply for continuous elutriation.
5. Set your elutriation conditions (pump speed and centrifuge rotor speed), and allow for a gradient to set up within the cell chamber of the elutriator (typically about 10 min). At this point, turn on the strobe light setup and adjust the delay so that the cell chamber is visible.
6. Observe the cell chamber through the elutriator portal. Wait for approximately two-thirds of the cell chamber to fill before beginning any observation of cells from the output (*see* **Note 9**).
7. Check the output medium under the microscope. Ideal conditions are found once the percentage of budded cells in the output falls below 5 % and the concentration of cells becomes sufficient to collect at least 1.5×10^6 cells/mL (*see* **Note 10**).
8. Once the cells are ready to be collected, move the output tube to a cold 200 mL conical tube surrounded by ice. Once the conical tube is filled, add 10 μL to a hemacytometer and count. Determine the total number of cells in the conical tube. Keep the conical tube on ice. Filling multiple tubes may be necessary depending on the concentration of cells collected.
9. Continuously collect cells while ensuring that sufficient fluid remains within the elutriation system (*see* **Note 11**).
10. Once all of the small unbudded cells are collected and on ice, pellet the cells in a 4 °C centrifuge set up to spin 200 mL conical tubes at $3{,}000 \times g$ for 5 min (*see* **Note 12**).
11. Remove the supernatant while taking care to retain the cell pellet.
12. Return the pellets to ice, and pool the cell pellets.
13. While cells are still cold, set up suction apparatus and liquid nitrogen-holding container before releasing cells into the cell cycle.
14. Add 3×10^9 cells to pre-warmed medium for a final concentration of 1×10^7 cells/mL in a pre-warmed 500-mL flask. Place the flask in a pre-warmed incubator at the optimal temperature/shaking settings for your strain.
15. Before you begin the time course, take a time zero budding sample. Use a P1000 micropipette to remove 200 μL of medium containing cells and add directly to 200 μL fixative solution in a 1.5 mL microfuge tube.

3.3 Sampling Cells Through Time Course

1. Determine the number of samples required for your experiment. Typically analysis is greatly enhanced by the use of greater than ten samples per cell cycle.
2. At each time point, stop the shaking water bath, use a P1000 micropipette to remove 200 μL of medium containing cells, and add directly to 200 μL fixative solution in a 1.5 mL microfuge tube.
3. Next, remove 4–16 mL of culture medium containing cells and add to a vacuum apparatus containing a pre-wetted 0.45 μM PVDF filter membrane. As cell concentration goes up, the volume of cells necessary for each time point is decreased. Open the suction valve to trap cells onto filter membrane.
4. Using tweezers, remove the filter membrane from the apparatus. Place the filter, with the cell-containing surface curved inward into a 15-mL conical tube.
5. Flash-freeze the conical tube containing the filter membrane in liquid nitrogen.
6. Move the conical tube to −80 °C freezer for long-term storage.

3.4 Determination of Cell Cycle Time

The ability to determine cell cycle time intervals by population is convolved by the differential cell cycle times of mother and daughter cells as a result of asymmetric cell division in *S. cerevisiae* [8–11]. Therefore, we have implemented a closed-form, parametric, mathematical model to better model cell cycle times in an experimental population. Characterizing loss of cell cycle synchrony (CLOCCS) models the progression of a semi-synchronous population through cell cycles to determine a cell cycle time for the population based on observance of cell cycle markers [12, 13]. This model can be applied to data from budding dynamics collected over the cell cycle experiment. A graphical user interface has been developed to implement CLOCCS and is freely available as a JavaScript application (*see* **Note 13**) (Fig. 2).

1. Using fixed cells collected at each time point, count 200 cells under a microscope at 400 times magnification.
2. Determine the number of budded and unbudded cells in the counted sample.
3. Open the CLOCCS program.
4. Provide CLOCCS with the required information, the model type (bud), experimental temperature, time points (in minutes), and the number of budded and unbudded cells.
5. Allow CLOCCS to run using the following settings: sim anneal: 10,000; burn-in: 100,000; iterations: 250,000.
6. Use the provided posterior parameters to determine the cell cycle time of the population monitored during the experiment: “mu0” gives you the recovery time after elutriation, the

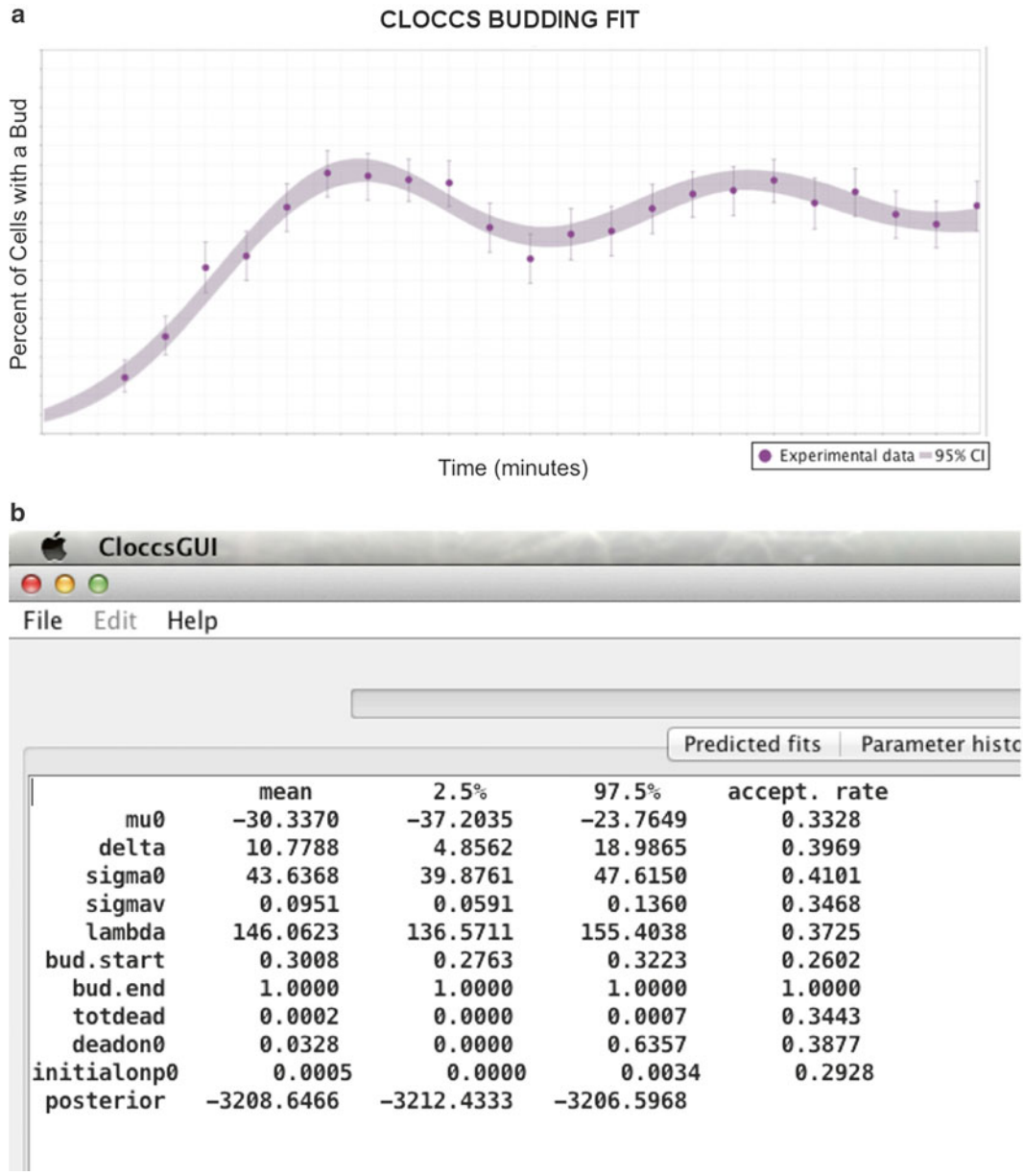

	mean	2.5%	97.5%	accept. rate
mu0	-30.3370	-37.2035	-23.7649	0.3328
delta	10.7788	4.8562	18.9865	0.3969
sigma0	43.6368	39.8761	47.6150	0.4101
sigmav	0.0951	0.0591	0.1360	0.3468
lambda	146.0623	136.5711	155.4038	0.3725
bud.start	0.3008	0.2763	0.3223	0.2602
bud.end	1.0000	1.0000	1.0000	1.0000
totdead	0.0002	0.0000	0.0007	0.3443
deadon0	0.0328	0.0000	0.6357	0.3877
initialonp0	0.0005	0.0000	0.0034	0.2928
posterior	-3208.6466	-3212.4333	-3206.5968	

Fig. 2 CLOCCS analysis of cell cycle time. Screenshots for the CLOCCS program after fitting population data from an elutriation time course. (**a**) A CLOCCS fit from data supplied from a budding, exponentially growing population of cells after elutriation and release into rich medium. These budding curves can be found under the Predicted Fits tab of the CLOCCS program. (**b**) Under the Posterior Parameters tab of the CLOCCS parameters, mu0 (corresponding to the recovery time of the population) and lambda (corresponding to the cell cycle time of the population) can be found

minutes from experimental start to the first START during the experiment. "lambda" is the cell cycle time over the time course, post-recovery.

7. Compare the recovery and cell cycle time output by CLOCCS to determine if the experimental timing is as expected from previous experiments. If the cell cycle or the recovery times are altered from preliminary experiments, it could indicate that the experiment should not be followed through to microarray analysis.

3.5 RNA Extraction

Isolation of RNA from cells requires conditions to minimize the degradation of RNA due to environmental contamination by RNase enzymes. To mitigate this potential experimental pitfall, one must prepare an appropriate workspace complete with cleaned consumable reagents and tools (*see* **Note 14**). Often, RNA is commonly extracted using a TRIzol-based reagent [14, 15]. We prefer to use an acidic (pH ~4.5) water-saturated phenol solution, preferentially retaining RNA in the aqueous phase during an aqueous/organic-phase separation [16]. This protocol is based on and modified from an existing protocol [17].

1. Working in batches of less than 12 samples to prevent samples from thawing, remove the samples from −80 °C storage and keep on ice until ready to work on the individual sample. After each sample is removed from ice, keep the sample at room temperature. The SDS in the TES buffer will precipitate out at cold temperatures.
2. Using a P1000 micropipette add 400 μL of pre-warmed TES buffer to each 15 mL conical tube containing the time course samples of intact cells.
3. Pipette up and down gently a few times to loosen cells from the filter membrane. Take care not to generate too much foam.
4. Briefly vortex the conical tube to facilitate removal of cells from the filter membrane. Again, take care not to generate too much foam in the sample.
5. Transfer the TES buffer containing the cells removed from the membrane to a 1.5 mL microfuge tube.
6. Move on to the next sample within the batch.
7. To each sample, add 400 μL (1 volume) of acid phenol. Vortex vigorously for 10 s, and place on 65 °C heat block.
8. Move on to the next batch of samples until all are incubating at 65 °C.
9. Once all samples are on the heat block at 65 °C, incubate for at least 45 min.
10. Every 15 min during the incubation, vortex each sample vigorously for 10 s.

11. After the 65 °C incubation is complete, place the samples on ice for 5 min.
12. Spin the samples in a microfuge for 5 min at max speed (>12,000 × *g*) in a 4 °C microfuge.
13. Transfer the aqueous phase to a new microfuge tube containing 400 µL of acid phenol.
14. Vortex vigorously for 10 s, and then place the samples on ice for 5 min.
15. Spin the samples in a microfuge for 5 min at max speed (>12,000 × *g*) in a 4 °C microfuge.
16. Transfer the aqueous phase to a new microfuge tube containing 400 µL of chloroform.
17. Vortex vigorously for 10 s, and then place the samples on ice for 5 min.
18. Spin the samples in a microfuge for 5 min at max speed (>12,000 × *g*) in a 4 °C microfuge.
19. Transfer the aqueous phase to a new microfuge tube containing 40 µL of 3 M sodium acetate (pH 5.3) and 1,000 mL of ice-cold 100 % ethanol. Mix well by inversion.
20. Place the samples on ice for 5–10 min.
21. Spin the samples at max speed for 5 min in a 4 °C microfuge.
22. Completely remove the supernatant, taking care not to disturb the pellet containing RNA.
23. Gently wash the pellet with ice-cold 70 % ethanol, immediately followed by spinning the samples at max speed for 5 min in a 4 °C microfuge.
24. Completely remove the supernatant, taking care not to disturb the pellet containing RNA.
25. Resuspend the pellet in 100 µL of DEPC-treated RNase-free dH_2O.
26. At this point, RNA samples can be stored at –80 °C or moved to the next step.

3.6 RNA Gel Electrophoresis (Optional)

Checking the RNA integrity before the samples leave the lab is a potential time- and money-saving measure. Using an agarose formaldehyde gel, one can prevent RNA secondary structure formation while protecting the RNA sample from degradation. Detecting the structural ribosomal RNA bands at 28S and 18S is typically sufficient to ensure that the sample mRNA is intact.

1. Prepare a 1 % agarose formaldehyde gel (*see* Subheading 2.6).
2. Add 5 µL of RNA sample to 10 µL of RNA sample loading buffer.

3. Incubate samples at 65 °C for 5 min. Briefly centrifuge at RT to gather condensation.
4. Run the gel in a fume hood. Using 1× MEN running buffer, load samples to gel and run at 100–120 V until dye front has reached about 75 % of the way down the gel.
5. Using a UV light source, check for the presence of the 28S and 18S ribosomal RNA bands. A separate 5/5.8S band may be present if it has not run off the gel.
6. If these bands are present, the RNA integrity is intact and the samples can be processed further.

3.7 Sample Cleanup

RNA extracted by acid-phenol extraction in Subheading 3.5 may still have some level of impurities such as salts. These impurities are incompatible with amplification and labeling for microarray analysis, so they must be removed. Here we describe desalting and purification using a commercially available silica-membrane column.

1. To determine the approximate RNA concentration in each sample, load 2 μL of 1:10 diluted RNA onto a NanoDrop spectrophotometer.
2. Determine the RNA concentration of the original samples.
3. Remove 45 μg of RNA from the original sample for RNA cleanup and desalting. Using the Qiagen RNeasy Minelute cleanup kit, more than 45 μg of RNA will hinder the purification process.
4. Process samples according to the manufacturer's protocols.
5. Elute RNA using 14 μL of DEPC-treated RNase-free dH_2O.

3.8 Sample Submission

At this point, many labs are able to hand off their samples for post-process quality checking, generation of labeled RNA, hybridization, and finally array detection of RNA. Samples are quality checked and post-processed at the Duke Microarray Core Facility (*see* **Note 15**) in the following way.

1. Two microfuge tubes of RNA are required: one sample of at least 3 μL (>50 ng/μL, total 150–500 ng of RNA) for amplification/labeling for array hybridization, and the other sample is 3 μL for quality control.
2. For quality control, samples are checked for RNA integrity via an Agilent Bioanalyzer.
3. Once samples have passed quality control, they are amplified and labeled using the Ambion MessageAmp Premier kit, according to the manufacturer's instructions.
4. Samples are hybridized to Affymetrix GeneChip Yeast Genome 2.0 arrays.
5. Arrays are read, and the data is disseminated back to the lab.

3.9 Normalization of Time Series Microarray Data

The entire process of normalizing microarrays occurs in three main steps: (1) background adjustment, (2) normalization, and (3) summarization [18]. The background adjustment takes into account any hybridization artifacts. Normalization accounts for variation in overall chip fluorescence intensities across all chips. This step will alter fluorescence intensities of the probes on each chip to ensure that the overall fluorescence of each chip is similar. Summarization takes all of the probes that correspond to a single gene in the genome and combine the fluorescence intensities into a combined value. A variety of normalization approaches have been developed specifically for the Affymetrix gene expression microarrays, which can be found in the *affy* package available through Bioconductor in R [19–21]. Each normalization approach makes different assumptions about the fluorescent intensities and the types of non-biological variations that are present on the chips that are to be compared. It is important to understand the methods used for each different approach before carrying out this critical pre-processing step.

1. Download R onto your computer from the R project website http://www.r-project.org [21]. Install Bioconductor [20] within the R environment (http://www.bioconductor.org) using the following commands: (a) source("http://bioconductor.org/biocLite.R")—This command accesses the Bioconductor website. (b) biocLite()—This command downloads all packages into R.
2. Open the *affy* [19] package from Bioconductor, which contains the information for normalizing Affymetrix gene expression microarrays: (a) library("affy").
3. Import CEL files for all Affymetrix gene expression microarray chips that will be compared into R. To do this, you enter the command Data<- ReadAffy(widget=T). A GUI will appear on the screen. Identify the folder(s) with the data of interest in the left column. Highlight the individual files and add to the right column. Continue adding data from folders until all data to be normalized is in the right column (*see* **Note 16**).
4. The Yeast 2.0 arrays contain probes for both *S. cerevisiae* and *Schizosaccharomyces pombe*. Mask the *S. pombe* probes to prevent using these probes for the normalization process. To do this, first download the masking file from Affymetrix. Log into the Affymetrix website (http://www.affymetrix.com, free account). From the home screen, select Products → Microarray Solutions → RNA Analysis Solutions → 3′ IVT Expression Analysis → Arrays → Other Organisms → Yeast Genome 2.0 Array. Under the Mask Files in the Technical Documentation Tab, download the Yeast Genome 2.0 Array: *S. cerevisiae*, which will mask the *S. pombe* probes.

5. Three distinct approaches for normalizing CEL files: The dChip [22], Robust Multichip Average (RMA) [23], and MAS5 [24] methods are explained further in **Note 17(a)**. To implement the dChip method, use the following command: out<- expresso (Data, normalize.method="invariantset", bgcorrect.method= "none", pmcorrect.method="pmonly", summary.method= "liwong"). **Note 17(b)** To implement the RMA method, use the following command: out<- expresso(Data, bgcorrect. method="rma",normalize.method="quantiles",pmcorrect. method="pmonly",summary.method="medianpolish"). **Note 17(c)** To implement the MAS5 method, use the following command: out<- mas5(Data).
6. Export the newly normalized data. This command will create a tab-delimited file with the rows referencing a gene and each column referencing a different microarray chip you added in **step 3**. The first column will have the probe IDs, the second column will have the first CEL file input, and so on: (a) write. exprs(out, file="filename.txt").
7. Begin analyses to address your biological question.

4 Notes

1. Depending on the genetic background of the yeast strain and the desired growth rate, different sugars may be used as carbon source. Additionally, the percentage of sugar as a carbon source in the media can be varied. Elutriations have even been performed on cells growing in nonsugar carbon sources such as ethanol/glycerol [4].
2. Cells from a freshly grown plate may be used to inoculate the 25 mL starter culture. However, depending on the strain, cells from a 5 mL starter culture may be used to inoculate the 25 mL.
3. The time it takes for cells to reenter the cell cycle from quiescence is variable and will negatively affect doubling time growth calculations.
4. For the larger volume of the Fernbach flask, the cells should be grown using gentle shaking at the optimal temperature for the strain. Gentle shaking denotes a setting with sufficient force to mix the sample and allow for aeration without splashing the sample near the mouth of the flask.
5. Once cells are removed from their Fernbach flask, they are no longer in a sterile environment. Care must be taken to prevent contamination of the culture. Ensure that vessels where cells are kept in are clean. Any vessel containing cells should be covered with new aluminum foil. Clean practices must be utilized to keep the elutriator clean (*see* **Note 12**). Pipettes used to collect samples for observation during elutriation should not be reused.

Contamination of the culture can occur during the elutriation process, and if this does happen, the experiment should be abandoned.

6. Elutriating cells to determine a cell cycle time before performing a microarray experiment is highly recommended. We recommend at least three time courses before a microarray experiment. Doing so will allow the user to determine the conditions necessary for a successful centrifugal elutriation isolation of early G1 cells. As important, doing several experiments prior to microarray will allow the user to determine the range of cell cycle duration of a specific strain after centrifugal elutriation. Cells have variable recovery times from the centrifugal elutriation, and cell cycle time may vary from a "doubling time" assessed before a time course with synchronized cells.
7. We typically start at 3,400 rpm. Optimal centrifuge rotor speed will depend upon the size of cells in the population.
8. We typically begin with a pump speed of 30–40 mL/min. Optimal pump speed will depend upon the size of cells in the population. The speed can be adjusted before elutriation begins or even during the protocol.
9. Before this point, conditions are changing too rapidly to reliably assess the cell fraction being collected.
10. Cells collected should be consistently small-sized and unbudded. Both phenotypic markers indicate that the population is newly divided daughter cells. If the population contains a distribution of differentially sized unbudded cells, they will not be synchronous upon release. If this occurs in an experiment, elutriation conditions should be adjusted for better selection of small cells: typically an increase in centrifuge speed and/or decrease in pump speed.
11. If more than several 200 mL conical tubes are filled with the cells required for the experiment, the overall fluid level in the system is reduced. To maintain a sufficient amount of liquid in the centrifugal elutriation system, it may be necessary to pellet synchronized cells and add the medium back to the input medium. Use a 4 °C centrifuge to keep cells from entering the cell cycle.
12. Once the elutriator is no longer needed, clean and turn off the machine. Cleaning the elutriation fluidics and chamber immediately after performing a centrifugal elutriation is vital for the upkeep of the devices as well as for minimizing contamination that might develop within the fluidics or the chambers of the apparatus. To clean the elutriator (after the centrifuge has stopped rotating), first we flow double-distilled H_2O through the machine until the chamber is free of remaining cells (~300 mL). Next, we flow 300 mL of a weak bleach (about 1:100 in H_2O, measured by eye) solution through the machine to kill the remaining cells.

To complete the disinfection, we flow 300 mL of 70 % ethanol in H_2O. Disassemble the cell chamber, and connect the tubing to close the system without the cell chamber. The system should be dried as best as possible by keeping the pump on at full speed until fluid is no longer observed coming out of the output tube. The cell chamber should also be rinsed with dH_2O and dried.

13. The CLOCCS program is available at http://www.cs.duke.edu/~amink/software/cloccs/.
14. Working with RNA requires diligence to maintain a clean, RNase-free environment. We have separate microfuge tubes and tips that are used only for RNA work. These tubes and tips are only handled with clean gloves and then autoclaved before use. We use a spray RNase-decontamination solution to clean the benchtop, pipettors, tube racks, lab markers, and vortex surface (as well as any other surface required to perform the steps in Subheading 3.5). To minimize contamination and also for personal protection, clean lab coats, protective gloves, and safety glasses should be used during this protocol. Additionally, phenol should be handled in a ventilated fume hood.
15. Use of a core facility or an RNA microarray service to perform the labeling and hybridization is a cost-effective and reliable method to obtain high-quality microarray data. For further information on submission to the Duke University Microarray Core Facility: Website, http://www.genome.duke.edu/cores/microarray; E-mail, microarraylab@duke.edu; Phone, 1-919-684-8224.
16. It is important to remember the order in which you add the data to the right-side window in the widget pop-up. This is the order that will be output after the normalization.
17. The following are summaries of normalization approaches:
    (a) dChip does not perform any background correction. The normalization step is completed by choosing the chip with the median level of overall fluorescence and uses this as a baseline to adjust the overall fluorescence levels of all other chips. The summarization step utilizes a model-based expression index that will down-weight probes for a gene with high variability. The output is a set of absolute values that can be compared to each other.
    (b) RMA background corrects using a closed-form transformation with an exponential signal and normalized noise. The normalization step is done using a quantile normalization, and the probes are summarized with median polish. The output of RMA pre-processing is a set of log-change values.
    (c) MAS5 background corrects by subtracting out the fluorescence from the corresponding mismatch probe. Normalization is completed by scaling the intensity of

each chip to a target intensity (default is 500). Summarization uses Tukey's biweight method. The output of MAS5 pre-processing is a set of log-change values.

(d) The background correction, normalization, and summarization steps are completed after you specify the type of normalization approach you want to use in Subheading 3.9, **step 5**. The variations in the command used will change the type of background correction, normalization, and summarization. The exported data from Subheading 3.9, **step 6**, will have the fully normalized data according to your choices.

Acknowledgements

Members of the Haase Lab are thanked for their critical reading and comments.

References

1. Cho RJ, Campbell MJ, Winzeler EA, Steinmetz L, Conway A, Wodicka L, Wolfsberg TG, Gabrielian AE, Landsman D, Lockhart DJ, Davis RW (1998) A genome-wide transcriptional analysis of the mitotic cell cycle. Mol Cell 2(1):65–73
2. Orlando DA, Lin CY, Bernard A, Wang JY, Socolar JE, Iversen ES, Hartemink AJ, Haase SB (2008) Global control of cell-cycle transcription by coupled CDK and network oscillators. Nature 453(7197):944–947
3. Pramila T, Wu W, Miles S, Noble WS, Breeden LL (2006) The Forkhead transcription factor Hcm1 regulates chromosome segregation genes and fills the S-phase gap in the transcriptional circuitry of the cell cycle. Genes Dev 20(16):2266–2278
4. Spellman PT, Sherlock G, Zhang MQ, Iyer VR, Anders K, Eisen MB, Brown PO, Botstein D, Futcher B (1998) Comprehensive identification of cell cycle-regulated genes of the yeast *Saccharomyces cerevisiae* by microarray hybridization. Mol Biol Cell 9(12):3273–3297
5. Simmons Kovacs LA, Mayhew MB, Orlando DA, Jin Y, Li Q, Huang C, Reed SI, Mukherjee S, Haase SB (2012) Cyclin-dependent kinases are regulators and effectors of oscillations driven by a transcription factor network. Mol Cell 45(5):669–679
6. Walker GM (1999) Synchronization of yeast cell populations. Methods Cell Sci 21(2–3): 87–93
7. Johnston LH, Johnson AL (1997) Elutriation of budding yeast. Methods Enzymol 283: 342–350
8. Hartwell LH, Unger MW (1977) Unequal division in *Saccharomyces cerevisiae* and its implications for the control of cell division. J Cell Biol 75(2 Pt 1):422–435
9. Lord PG, Wheals AE (1980) Asymmetrical division of *Saccharomyces cerevisiae*. J Bacteriol 142(3):808–818
10. Lord PG, Wheals AE (1981) Variability in individual cell cycles of *Saccharomyces cerevisiae*. J Cell Sci 50:361–376
11. Woldringh CL, Huls PG, Vischer NO (1993) Volume growth of daughter and parent cells during the cell cycle of *Saccharomyces cerevisiae* a/alpha as determined by image cytometry. J Bacteriol 175(10):3174–3181
12. Orlando DA, Lin CY, Bernard A, Iversen ES, Hartemink AJ, Haase SB (2007) A probabilistic model for cell cycle distributions in synchrony experiments. Cell Cycle 6(4):478–488
13. Orlando DA, Iversen ES Jr, Hartemink AJ, Haase SB (2009) A branching process model for flow cytometry and budding index measurements in cell synchrony experiments. Ann Appl Stat 3(4):1521–1541
14. Chomczynski P, Sacchi N (2006) The single-step method of RNA isolation by acid guanidinium thiocyanate-phenol-chloroform extraction: twenty-something years on. Nat Protoc 1(2): 581–585

15. Chomczynski P, Sacchi N (1987) Single-step method of RNA isolation by acid guanidinium thiocyanate-phenol-chloroform extraction. Anal Biochem 162(1):156–159
16. Perry RP, La Torre J, Kelley DE, Greenberg JR (1972) On the lability of poly(A) sequences during extraction of messenger RNA from polyribosomes. Biochim Biophys Acta 262(2):220–226
17. Collart MA, Oliviero S (2001) Preparation of yeast RNA. Curr Protoc Mol Biol Chapter 13:Unit13.12
18. Lim WK, Wang K, Lefebvre C, Califano A (2007) Comparative analysis of microarray normalization procedures: effects on reverse engineering gene networks. Bioinformatics 23(13):i282–i288
19. Gautier L, Cope L, Bolstad BM, Irizarry RA (2004) affy—analysis of Affymetrix GeneChip data at the probe level. Bioinformatics 20(3): 307–315
20. Gentleman RC, Carey VJ, Bates DM, Bolstad B, Dettling M, Dudoit S, Ellis B, Gautier L, Ge Y, Gentry J, Hornik K, Hothorn T, Huber W, Iacus S, Irizarry R, Leisch F, Li C, Maechler M, Rossini AJ, Sawitzki G, Smith C, Smyth G, Tierney L, Yang JY, Zhang J (2004) Bioconductor: open software development for computational biology and bioinformatics. Genome Biol 5(10):R80
21. R Core Team (2012) R: A language and environment for statistical computing. R Foundation for Statistical Computing, Vienna, Austria. ISBN 3-900051-07-0. http://www.R-project.org/
22. Li C, Wong WH (2001) Model-based analysis of oligonucleotide arrays: expression index computation and outlier detection. Proc Natl Acad Sci U S A 98(1):31–36
23. Irizarry RA, Hobbs B, Collin F, Beazer-Barclay YD, Antonellis KJ, Scherf U, Speed TP (2003) Exploration, normalization, and summaries of high density oligonucleotide array probe level data. Biostatistics 4(2): 249–264
24. Hubbell E, Liu WM, Mei R (2002) Robust estimators for expression analysis. Bioinformatics 18(12):1585–1592

Chapter 15

Analyzing Cell Cycle Checkpoints in Response to Ionizing Radiation in Mammalian Cells

Bin Wang

Abstract

Exposure of cells to DNA-damaging agents, such as ionizing radiation (IR), results in perturbation of cell cycle progression. IR activates cell cycle checkpoints that arrest the cell cycle at the G1/S, S, and G2/M phases. The DNA damage-signaling network involves a number of important DNA damage response factors that are required for maintaining genome stability and prevention of cancer. These factors are involved in the regulation of cell cycle checkpoints and include ATM, NBS1, BRCA1, Chk2, and p53. Here we describe a series of assays that are often used to analyze cell cycle checkpoints after IR. These assays include a G1/S checkpoint assay that measures 5-bromodeoxyuridine incorporation into DNA, an S-phase checkpoint assay that measures DNA synthesis at a very early time point after IR, and a G2/M checkpoint assay that quantitates histone H3 phosphorylation. This collection of assays allows us to investigate the specific functions of proteins involved in regulating different cell cycle checkpoints in mammalian cells as a response to IR.

Key words Cell cycle checkpoints, BrdU, Ionizing radiation, DNA synthesis, Flow cytometry, Histone H3 phosphorylation

1 Introduction

Ionizing radiation (IR) induces DNA double-strand breaks (DSBs), which are the most deleterious form of DNA damage. Cells have evolved an intricate network of complex mechanisms for the signaling and repair of DSBs in response to IR [1]. One of the mechanisms developed is the activation of cell cycle checkpoints that arrest cell cycle progression, presumably to facilitate DNA repair, thereby ensuring genetic stability and preventing tumorigenesis. Mutations in checkpoint proteins, such as ATM, BRCA1, p53, and Chk2, lead to predisposition to cancer [1].

IR causes cell cycle arrest at the G1/S, S, and G2/M phases. The assays used for measuring cell cycle checkpoints utilize DNA synthesis, DNA content, immunofluorescence, and flow cytometry to monitor percentage of cells positioned in each cell cycle phase. Defects in cell cycle checkpoints are detected by comparing cell

Eishi Noguchi and Mariana C. Gadaleta (eds.), *Cell Cycle Control: Mechanisms and Protocols*, Methods in Molecular Biology, vol. 1170, DOI 10.1007/978-1-4939-0888-2_15,

cycle profile of cells treated and untreated with IR. The G1/S checkpoint assay uses flow cytometry analysis to measure 5-bromodeoxyuridine (BrdU) incorporation into DNA in order to monitor the progression of cells from G1 to S phase. The S-phase checkpoint assay measures $^{3}H/^{14}C$ thymidine incorporation to monitor DNA synthesis at a very early time point after IR. The G2/M checkpoint assay quantitates histone H3 phosphorylation shortly after IR treatment in order to detect cells entering M phase from G2 phase. A number of key DNA damage response proteins have been reported to regulate different cell cycle checkpoints after IR. For example, ATM is required for G1/S, S, and G2/M checkpoints [2, 3] in response to irradiation. p53 regulates the G1/S checkpoint [4, 5], and BRCA1 and 53BP1 are critical for the intra-S-phase and the G2/M checkpoint after IR [6, 7].

2 Materials

2.1 G1/S Checkpoint Assay

1. Mammalian cell growth medium (e.g., DMEM with 10 % fetal bovine serum, FBS).
2. 1× DPBS: Dulbecco's phosphate-buffered saline, 0.2 g/L KCl, 0.2 g/L KH_2PO_4, 8 g/L NaCl, 2.16 g/L $Na_2HPO_4{\cdot}7H_2O$, pH 7.0–7.2.
3. 0.25 % Trypsin–EDTA: 0.25 % trypsin, 2.21 mM EDTA in HBSS without sodium bicarbonate, calcium, and magnesium.
4. 10 mM BrdU (1,000× BrdU).
5. 100 % ethanol.
6. 4 N HCl.
7. 0.5 % BSA/0.25 % Tween-20/DPBS: 0.5 % BSA, 0.25 % Tween-20 in 1× DPBS.
8. Alexa Fluor 488-conjugated anti-BrdU antibody (Invitrogen).
9. 10 mg/mL propidium iodide.
10. 100 mg/mL RNase A.

2.2 S-Phase Checkpoint Assay

1. Mammalian cell growth medium (e.g., DMEM containing 10 % FBS).
2. 1× DPBS.
3. 0.25 % Trypsin–EDTA.
4. Thymidine [methyl-^{3}H] (specific activity 2 Ci/mmol).
5. Thymidine [2-^{14}C] (specific activity 50 mCi/mmol).
6. 21-mm Whatman glass microfiber filters GF/C circles (Whatman).
7. 70 % methanol/DPBS: 70 % methanol, 30 % 1× DPBS.
8. 95 % methanol/DPBS: 95 % methanol, 5 % 1× DPBS.

9. Pyrex No. 36060 fritted funnel, 15-mL fine.
10. Scintillation fluid.
11. Beckman Scintillation counter.

2.3 G2/M Checkpoint Assay

1. Mammalian cell growth medium (e.g., DMEM with 10 % FBS).
2. 1× DPBS.
3. 0.25 % Trypsin–EDTA.
4. 100 % ethanol.
5. 0.25 % Triton X-100/DPBS: Add 0.625 mL 20 % Triton X-100 to 49.375 mL 1× DPBS.
6. 1 % BSA/DPBS: Dissolve 0.5 g BSA in 50 mL 1× PBS.
7. Rabbit anti-phospho-histone H3 Ser10 antibody (Upstate).
8. Alexa 488-conjugated goat anti-rabbit antibody (Invitrogen).
9. 10 mg/mL propidium iodide.
10. 100 mg/mL RNase.

3 Methods

3.1 G1/S Checkpoint Assay

The G1/S-phase checkpoint assay detects a decrease in the number of cells entering S phase after DNA damage. In response to IR, cells in G1 do not continue to enter S phase, whereas cells that are already in S phase at the time of DNA damage appear to continue to progress into G2/M phase [4, 5]. The assay is carried out 12–24 h after IR when the proliferation of irradiated cells is maximally inhibited [4]. Cells that are still proliferating with DNA synthesis are pulse labeled by 5-bromo-2′deoxyuridine 14 h after IR treatment. The relative amount of cells in each phase of the cell cycle can be assessed by measuring the overall DNA content with propidium iodide staining. The percentage of cells synthesizing DNA can be calculated by measuring the incorporation of fluorescence-conjugated anti-BrdU antibody in the flow cytometry analysis. Cells with the intact G1/S checkpoint show a marked decrease of BrdU-labeled S-phase cells in response to IR when compared to untreated cells [4, 5].

1. Seed cells 1 day before the experiment in appropriate cell culture medium at 37 °C such that cells grow to exponential phase the next day. Aim about 50–60 % confluency at the time of the experiment.
2. Treat cells with 5 Gy of IR. Include a plate of cells for mock treatment (untreated cells) in the analysis. Return cells to the 37 °C incubator to grow for an additional 14 h.
3. Pulse label cells with BrdU by adding BrdU (10 mM stock) to the medium for a final concentration of 10 μM BrdU. Incubate at 37 °C for 60 min.

4. Remove the labeling medium by aspiration and wash twice with 1× DPBS.
5. Trypsinize cells with 0.25 % trypsin–EDTA, and harvest cells by centrifugation at 220 × *g* for 5 min.
6. Wash cells with 5 mL of 1× DPBS twice to further remove unincorporated BrdU.
7. Resuspend cells in 300 μL of cold 1× DPBS and transfer into a 2 mL Eppendorf tube.
8. Fix cells by adding 700 μL of ice-cold ethanol (stored at −20 °C) dropwise to make a final concentration of 70 % ethanol (*see* **Note 1**). Mix it well by inverting the tube a couple of times. Incubate at −20 °C for at least 1 h.
9. Centrifuge fixed cells at 2,000 rpm in a microfuge for 5 min. Wash once with cold 1× DPBS, and centrifuge at 2,000 rpm in a microfuge for 5 min.
10. Denature by adding 500 μL of 4 N HCl to the pellet (*see* **Note 2**). Incubate at room temperature for 15 min.
11. After denaturation, add 1.5 mL of 1× DPBS and centrifuge at 3,500 rpm in a microfuge for 5 min. Wash the pellet two more times with 2 mL of 1× DPBS (*see* **Note 3**).
12. Resuspend the pellet with 100 μL of 0.5 % BSA/0.1 % Tween20/PBS and incubate for 20 min at room temperature to block unspecific binding.
13. Centrifuge at 3,500 rpm in a microfuge for 5 min.
14. Resuspend the pellet in 100 μL of 0.5 % BSA/0.1 % Tween20/PBS containing Alexa 488-conjugated anti-BrdU antibody (1:20 dilution). Incubate for 45 min at 37 °C in a humid chamber in the dark.
15. Centrifuge at 3,500 rpm in a microfuge for 5 min. Wash the pellet twice with 500 μL of 1× DPBS.
16. Resuspend the pellet in a 0.5–1 mL of 1× DPBS containing propidium iodide (25 μg/mL) and RNaseA (0.1 mg/mL). Incubate at room temperature for 30 min.
17. Analyze on a flow cytometer.

3.2 S-Phase Checkpoint Assay

The IR-induced intra-S-phase checkpoint in mammalian cells represents an inhibition of DNA synthesis in response to IR-induced damage [3]. It is measured as a transient decrease in [^{3}H]thymidine incorporation to cells at an early time point (30 min) after irradiation [2, 6]. Cells are pre-labeled in growth medium containing [^{14}C]thymidine. This pre-labeling provides an internal control for cell number by allowing normalization for total DNA content of samples. The rate of DNA synthesis is represented by measuring the ratios of ^{3}H counts per minute to ^{14}C counts per minute and

calculated as a percentage of irradiated cells over un-irradiated cells. The absence of this IR-induced S-phase arrest, referred to as radioresistant DNA synthesis (RDS), has been previously reported for cells deficient in key DNA damage response proteins such as ATM, NBS1, or BRCA1 [2, 3, 6, 8].

1. Culture cells in a 37 °C incubator. Pre-label cells with [^{14}C] thymidine by incubating exponentially growing cells in growth medium containing 10 nCi of [^{14}C]thymidine per mL for approximately 24 h. For culturing cells that require transfection, *see* **Note 4**. A control plate of cells that is only labeled with [^{14}C] is needed for correction of channel crossover (*see* **Note 5**).
2. Split cells into three dishes for triplicate analysis of the assay (*see* **Note 6**). Incubate cells in fresh normal nonradioactive medium for another 24 h.
3. Irradiate cells with different doses (e.g., 5, 10, 15, 20, and 25 Gy). Include a sample of mock-treated cells as a control (0 Gy) for comparison. Return cells to 37 °C and grow for 30 min.
4. Replace with medium containing 2.5 μCi/mL of [^{3}H]thymidine for 15 min (*see* **Note 7**). The control plate for [^{14}C] labeling only is set aside without [^{3}H] labeling.
5. Harvest cells by trypsinization. Place harvested cells immediately on ice.
6. Collect cell pellet by centrifugation at 220 × *g* for 5 min at 4 °C.
7. Wash cell pellet twice with cold 1× DPBS.
8. Resuspend the pellet in 300 μL of cold 1× DPBS. Fix cells by adding 700 μL ice-cold 100 % methanol (stored at −20 °C) dropwise. Mix it well by inverting the tube a couple of times. Incubate on ice for at least 30 min.
9. Spin down the fixed cells by centrifugation at 2,000 rpm in a microfuge for 5 min at 4 °C and wash once with 70 % methanol/DPBS.
10. Resuspend cell pellet in 200 μL of 70 % methanol/DPBS. The cell suspension is filtered through a GF/C (Whatman) filter placed on a Pyrex fritted funnel and rinsed sequentially with 1 mL of 70 % and 1 mL of 95 % methanol/DPBS.
11. Place the filter on a clear paper towel and air-dry.
12. Place the filter into a liquid scintillation vial. Add 5 mL scintillant, and read radioactivity with a scintillation counter. The resulting ratios of ^{3}H counts per minute to ^{14}C counts per minute, corrected for channel crossover, were calculated (*see* **Note 5**).
13. The DNA synthesis is measured by calculating the ratios of ^{3}H/^{14}C of cells irradiated at a certain dose as a percentage of un-irradiated cells.

3.3 G2/M Checkpoint Assay

The G2/M checkpoint prevents G2-phase cells with DSBs from entering into mitosis. The G2/M checkpoint assay assesses the progression of irradiated cells from G2 into mitosis. Phosphorylation at Ser10 of histone H3 is tightly correlated with chromosome condensation during mitosis [9, 10]; thus, an antibody that specifically recognizes the phosphorylated form of histone H3 (p-histone H3 Ser10) is used to identify mitotic cells. Co-staining of cells with propidium iodide (PI) and anti-p-histone H3 Ser 10 antibody distinguishes mitotic cells from G2 cells in a flow cytometry analysis [6]. This assay has been successfully applied to a number of different mammalian cell lines. It has been very consistent that 1.5–3 % of cells in mitosis are detected in the undamaged cell population. The percentage of cells in mitosis dramatically decreases to less than 0.2 % when cells with an intact G2/M checkpoint are treated with IR.

1. Culture cells in a 37 °C incubator. About 2×10^6 cells at exponentially growing phase are needed for this assay.
2. Irradiate cells with 2 Gy IR. Include a sample of mock-treated cells (un-irradiated) in the analysis as a control. Return cells to 37 °C and culture for 1 h.
3. Collect the medium, wash cells once with 1× DPBS, and collect the DPBS. Harvest cells by trypsinizing cells with 0.25 % trypsin–EDTA. Harvest floating cells as well (*see* **Note 8**).
4. Collect cells by centrifugation at 220 × *g* at 4 °C for 5 min. Keep the cell pellet on ice.
5. Wash cells once with cold 1× PBS and centrifuge at 220 × *g* at 4 °C for 5 min.
6. Resuspend the cell pellet in 300 μL of cold 1× DPBS, mix well, and transfer the mixture to a 1.5 mL Eppendorf tube.
7. Fix cells by adding 700 μL of ice-cold 100 % ethanol (stored at −20 °C). Mix well by inverting the tube a couple of times.
8. Place the tube in a −20 °C freezer for at least 1 h (*see* **Note 9**).
9. After fixation, pellet cells at 3,500 rpm in a microfuge at 4 °C for 2 min. Wash the pellet twice with 1 mL cold 1× DPBS. Resuspend cells completely in the second wash.
10. Add 1 mL ice-cold 0.25 % Triton X-100/PBS to permeabilize cells for 15 min on ice.
11. Pellet cells at 3,500 rpm in a microfuge at 4 °C for 3 min. Wash the pellet once with 1 mL of 1 % BSA/PBS. Resuspend cells completely and then centrifuge at 3,500 rpm in a microfuge at 4 °C for 3 min.
12. Resuspend the pellet in 100 μL of 1 % BSA/PBS containing 1:100 dilution of the anti-phospho-histone H3 Ser10 antibody.
13. Incubate for 1–3 h at room temperature with agitation using a rocker such that fixed cells are in suspension during incubation.

14. Pellet cells at 3,500 rpm in a microfuge at room temperature for 3 min. Wash the pellet twice with 300 μL of 1 % BSA/DPBS each time (*see* **Note 10**).
15. Resuspend the pellet in 100 μL of 1 % BSA/DPBS containing 1:100 dilution of Alexa 488-conjugated goat-anti-rabbit antibody.
16. Incubate for 0.5–1 h in the dark or in a rack wrapped with aluminum foil at room temperature.
17. Pellet cells at 3,500 rpm in a microfuge at room temperature for 3 min. Wash the pellet once with 300 μL 1 % BSA/DPBS, followed by a one-time wash with 1× DPBS at room temperature.
18. Pellet cells at 3,500 rpm in a microfuge at room temperature for 3 min. Resuspend the pellet in 1× DPBS containing propidium iodide (25 μg/mL) and 0.1 mg/mL RNase at 37 °C for 15 min.
19. Use flow cytometry to determine the percentage of cells in M phase. The cells can also be stored at 4 °C overnight for analysis the next day.

4 Notes

1. Do not resuspend the cell pellet directly in 70 % ethanol because cells will aggregate and make it difficult for single-cell analysis with flow cytometry.
2. Loosen the pellet by flicking the bottom of the Eppendorf tube before adding 4 N HCl.
3. After washing twice with 1× DPBS, the pH value should be above pH 6.5 (if pH is lower, repeat incubation with 1× DPBS).
4. For assaying cells that require transfection with plasmids or siRNAs, seed cells the day before transfection. Remove medium, and replace with medium containing [^{14}C]thymidine. Transfect cells with proper transfection methods and incubate in medium containing [^{14}C]thymidine for about 24 h.
5. A control plate that is labeled with [^{14}C]thymidine only is used for correcting channel crossover. Channel crossover is calculated using the counts from the control sample containing [^{14}C]thymidine only. The ratio of ^{3}H counts per minute to ^{14}C counts per minute, corrected for those counts per minute that are the result of channel crossover, is calculated as a measure of DNA synthesis.
6. When splitting cells, prevent cells from becoming too confluent. Exponentially growing cells respond well to pulse labeling with [^{3}H]thymidine treatment in the later step.

7. Medium containing [^{3}H]thymidine needs to be pre-warmed at 37 °C.
8. Cells in mitosis are often loosely attached to the plate; thus, it is necessary to collect floating cells as well. Collect the medium and the DPBS used for washing the cells before trypsinization, and combine these with the cells trypsinized off the plate.
9. Fixing at −20 °C for 1 h is enough for a successful staining. Fixing overnight may result in a failed staining with the p-H3Ser10 antibody.
10. Cell pellet is quite loose after this step. Be careful not to disturb the pellet after centrifugation. Use a pipet tip to carefully remove the supernatant after wash. Do not use vacuum.

Acknowledgements

This work was supported by NIH grant CA155025, the Mel Klein Family Fund, and start-up funds from the University of Texas MD Anderson Cancer Center.

References

1. Ciccia A, Elledge SJ (2010) The DNA damage response: making it safe to play with knives. Mol Cell 40(2):179–204
2. Lim DS, Kim ST, Xu B, Maser RS, Lin J, Petrini JH, Kastan MB (2000) ATM phosphorylates p95/nbs1 in an S-phase checkpoint pathway. Nature 404(6778):613–617
3. Shiloh Y (1997) Ataxia-telangiectasia and the Nijmegen breakage syndrome: related disorders but genes apart. Annu Rev Genet 31:635–662
4. Kastan MB, Onyekwere O, Sidransky D, Vogelstein B, Craig RW (1991) Participation of p53 protein in the cellular response to DNA damage. Cancer Res 51(23 Pt 1):6304–6311
5. Lowe SW, Ruley HE, Jacks T, Housman DE (1993) p53-dependent apoptosis modulates the cytotoxicity of anticancer agents. Cell 74(6):957–967
6. Xu B, Kim S, Kastan MB (2001) Involvement of Brca1 in S-phase and G(2)-phase checkpoints after ionizing irradiation. Mol Cell Biol 21(10):3445–3450
7. Wang B, Matsuoka S, Carpenter PB, Elledge SJ (2002) 53BP1, a mediator of the DNA damage checkpoint. Science 298(5597):1435–1438
8. Zhao S, Weng YC, Yuan SS, Lin YT, Hsu HC, Lin SC, Gerbino E, Song MH, Zdzienicka MZ, Gatti RA, Shay JW, Ziv Y, Shiloh Y, Lee EY (2000) Functional link between ataxia-telangiectasia and Nijmegen breakage syndrome gene products. Nature 405(6785):473–477
9. Goto H, Tomono Y, Ajiro K, Kosako H, Fujita M, Sakurai M, Okawa K, Iwamatsu A, Okigaki T, Takahashi T, Inagaki M (1999) Identification of a novel phosphorylation site on histone H3 coupled with mitotic chromosome condensation. J Biol Chem 274(36):25543–25549
10. Hendzel MJ, Wei Y, Mancini MA, Van Hooser A, Ranalli T, Brinkley BR, Bazett-Jones DP, Allis CD (1997) Mitosis-specific phosphorylation of histone H3 initiates primarily within pericentromeric heterochromatin during G2 and spreads in an ordered fashion coincident with mitotic chromosome condensation. Chromosoma 106(6):348–360

Chapter 16

Analyzing DNA Replication Checkpoint in Budding Yeast

Nicole Hustedt and Kenji Shimada

Abstract

Checkpoints are conserved mechanisms that prevent progression into the next phase of the cell cycle when cells are unable to accomplish the previous event properly. Cells also possess a surveillance mechanism called the DNA replication checkpoint, which consists of a conserved kinase cascade that is provoked by insults that block or slow down replication fork progression. In the budding yeast *Saccharomyces cerevisiae*, the DNA replication checkpoint controls the timing of S-phase events such as origin firing and spindle elongation. This checkpoint also upregulates dNTP pools and maintains the replication fork structure in order to resume DNA replication after replication block. Many replication checkpoint factors have been found to be tumor suppressors, highlighting the importance of this checkpoint pathway in human health. Here we describe a series of protocols to analyze the DNA replication checkpoint in *S. cerevisiae*.

Key words DNA replication checkpoint, Mec1, Rad53, Kinase assay, Budding yeast

1 Introduction

Cells are constantly exposed to DNA damage. DNA lesions can arise from either exogenous (e.g., DNA-damaging drugs) or endogenous (e.g., replication forks encountering barriers) agents [1]. To preserve the genetic information, cells have evolved mechanisms called DNA damage checkpoint that senses the damage, stops the cell cycle, and induces DNA repair pathways [2].

Depending on the cell cycle stage in which the damage occurs, cells arrest either in G1 (before starting DNA replication) or G2 (before entering mitosis) stages of the cell cycle. During S phase, cells have a mechanism called the DNA replication checkpoint that is provoked by the insults that block or slow down replication forks.

The checkpoint signaling cascades include the human PI3K-like (PIKK) kinases ATM and ATR and their homologs Tel1 and Mec1 in budding yeast, respectively (Fig. 1) [3]. ATR and Mec1 genes are essential for cell viability, although a Mec1 deletion mutant can be generated by simultaneously upregulating ribonucleotide reductase (e.g., by deleting the gene encoding the

Eishi Noguchi and Mariana C. Gadaleta (eds.), *Cell Cycle Control: Mechanisms and Protocols*, Methods in Molecular Biology, vol. 1170, DOI 10.1007/978-1-4939-0888-2_16,

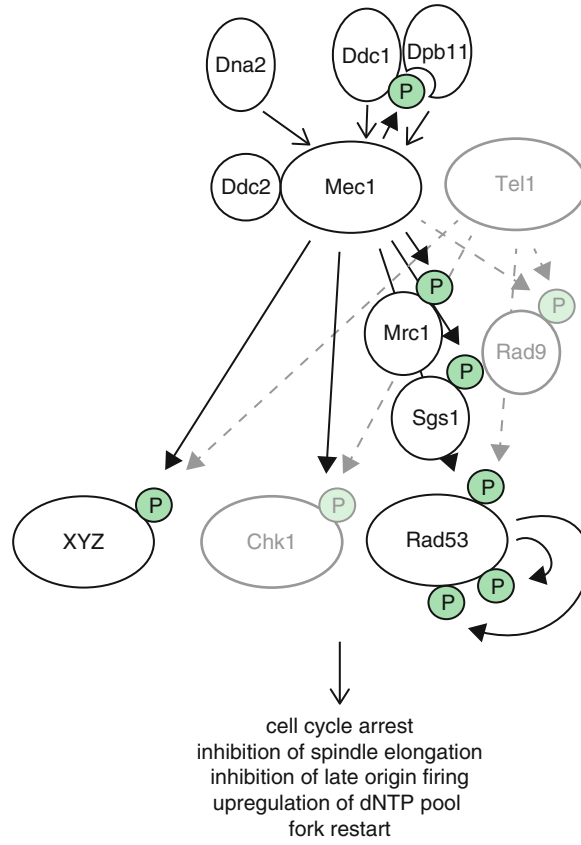

Fig. 1 Current model of the replication checkpoint in budding yeast. Ddc1, Dpb11, and Dna2 activate Ddc2–Mec1 when it is recruited to stalled replication forks. Phosphorylation of the downstream kinase Rad53 requires the checkpoint mediator Mrc1. Sgs1 also aids to activate Rad53. Tel1 can partially substitute for Mec1 in the activation of Rad53, as does Rad9 for Mrc1. Active Rad53 leads to its autophosphorylation, thus amplifying the checkpoint signal. The replication checkpoint suppresses late origin firing, inhibits spindle elongation, upregulates dNTP pools, and promotes recovery from the fork arrest

ribonucleotide reductase inhibitor *SML1*) in budding yeast. PIKKs are generally large proteins (about 2,500 amino acids in length) with a C-terminal kinase domain flanked by FRAPP ATM TRAPP (FAT) and FAT C-terminal (FATC) domains [3, 4]. Other members of this kinase family are mTOR kinases (budding yeast Tor1 and Tor2) and the catalytic subunit of DNA-PK [3].

While ATM becomes activated in response to DNA double-strand breaks (DSBs), ATR can sense a variety of lesions [3] that contain single-stranded DNA (ssDNA) coated by the single-strand DNA-binding protein replication protein A (RPA). ATR binds to these ssDNA-containing structures via its binding partner ATR-interacting protein (ATRIP, or Ddc2 in budding yeast) [5]. Experiments in *Xenopus* egg extracts indicated an additional

requirement of double-stranded DNA adjacent to the ssDNA stretch for ATR-dependent checkpoint activation [6]. The Rad17–RFC2-5 clamp-loading complex (Rad24–Rfc2-5 in budding yeast) recognizes such DNA structures and loads the 9-1-1 clamp (the Rad9–Rad1–Hus1 complex in *Schizosaccharomyces pombe* and metazoans, Rad17–Mec3–Ddc1 in budding yeast) [7]. Phosphorylation of the Rad9 (*Saccharomyces cerevisiae* Ddc1) subunit of 9-1-1 recruits TopBP1 (*S. cerevisiae* Dpb11) [8–10]. TopBP1 can activate ATR–ATRIP (*S. cerevisiae* Mec1–Ddc2) in vitro, and mutations that abolish the activation were mapped in both ATR and ATRIP [11].

In *S. cerevisiae*, Ddc1 not only recruits the TopBP1 homolog, Dpb11, but also enhances Mec1 kinase activity in certain conditions in vitro [7, 12]. A C-terminal unstructured region in both Ddc1 and Dpb11 was shown to activate Mec1, and it has been suggested that the mode of Mec1 activation depends on the cell cycle stage [12–15]. Recently, another protein, Dna2, has been reported to activate Mec1 specifically in S phase [16] (Fig. 1).

In the checkpoint cascade, Mec1 activation leads to phosphorylation of the downstream effector kinases Rad53 (human CHK2) and Chk1 (human CHK1) in budding yeast (Fig. 1) [2]. While Rad53 is commonly referred to as the CHK2 homolog, human CHK1 acts as the Rad53 functional homolog in the replication-associated checkpoint. Activation of those effector kinases requires mediator proteins [17, 18]. In the case of Mec1 activation in budding yeast, in response to DSBs or DNA adducts such as those caused by methyl methanesulfonate (MMS), the checkpoint protein Rad9 (human 53BP1) recruits Rad53 and facilitates its phosphorylation by Mec1 at the site of damage [19–21]. Once Mec1 has primed Rad53 for activation, Rad9 also provides a scaffold that accommodates Rad53 autophosphorylation, which is necessary for full Rad53 activation [19]. In this process, Rad53 becomes heavily phosphorylated, and this can be monitored by a band shift on Western blots. Alternatively, Rad53 activation can be monitored by testing its autophosphorylation capability. Rad9 has little role in Rad53 activation in response to fork-stalling agents such as hydroxyurea (HU) [17, 22]. Instead, the replication fork components Mrc1 and Sgs1 facilitate Rad53 phosphorylation in response to HU-induced replication stress [23–25]. Both Mrc1 and Rad9 enhance enzyme–substrate interaction rather than increasing enzymatic activity of Mec1 [20, 26]. Sgs1 contributes to Rad53 activation, both by regulating the amount of ssDNA at the fork (by reversing fold-back structures and aberrant annealing) and by directly binding to Rad53 [27]. Once activated, the replication checkpoint inhibits the firing of late origins [28, 29] and maintains replication fork integrity by preventing the conversion of forks into DSBs and/or by reducing recombination events [30, 31]. This checkpoint also upregulates dNTP pools [32] and suppresses spindle elongation [33] (*see* also review 34).

Besides the downstream kinases Chk1 and Rad53, Mec1/ATR phosphorylates multiple targets, many of which are replication proteins (*see* review 34). Therefore, a Mec1 in vitro kinase assay can be used to identify direct targets of Mec1.

Here, we describe a series of protocols to monitor replication checkpoint activation in *S. cerevisiae*. First we describe means to monitor the activation of the effector kinase Rad53, and then we describe three tractable readouts of the replication checkpoint: cell growth on HU (drop assay), recovery from fork arrest (colony-forming assay), and spindle elongation in response to HU. Finally, we provide a protocol to measure Mec1 kinase activity in vitro.

2 Materials

2.1 α-Factor Synchronization of Budding Yeast Cells

1. YPAD medium: 20 g/L Bacto peptone, 10 g/L yeast extract, 20 g/L dextrose, 25 mg/L adenine-hemisulfate salt. Dissolve in ddH_2O, and autoclave at 120 °C for 15 min.
2. Spectrophotometer to measure optical density (OD_{600}) of yeast culture or other cell-counting device.
3. YPAD medium pH 5.0: Adjust YPAD medium to pH 5.0 with HCl then autoclave at 120 °C for 15 min.
4. Sterile tubes with air-permeable lids (50 mL) or sterile (autoclaved) Erlenmeyer flasks (50–100 mL).
5. α-Factor stock solution: 5 mg/mL α-Factor in 10 mM HCl, 1 mM β-mercaptoethanol, 0.2 mM EDTA. Make aliquots, and store at −20 °C.
6. Light microscope with a 20× objective.
7. 1.5-mL tubes.
8. 70 % ethanol.
9. RNase A solution: 200 μg/mL RNase A, 50 mM Tris–HCl pH 7.5.
10. PI solution: 10 μg/mL propidium iodide, 50 mM citrate–acetate pH 7.0.
11. Pulse sonicator (550 Sonic Dismembrator, Fisher Scientific).
12. Flow cytometer (e.g., FACSCalibur, Becton Dickinson).

2.2 Phospho-Shift Analysis of Rad53 Phosphorylation

1. Cell culture tools, medium, and equipment as listed in Subheading 2.1 (**items 1–6**).
2. 15- and 50-mL tubes.
3. Hydroxyurea (*see* **Note 1**).
4. 2-mL tubes.
5. Microfuge (4 °C).
6. Solution I: 1.85 M NaOH, 7.4 % (v/v) β-mercaptoethanol (*see* **Note 2**).

7. Solution II: 50 % trichloroacetic acid (TCA).
8. Solution III: 80 % (v/v) acetone, 10 % (v/v) methanol, 10 mM Tris–HCl pH 7.5.
9. 1× NuPAGE LDS sample buffer (Life Technologies) supplemented with 50 mM dithiothreitol (DTT) freshly added (*see* **Note 3**).
10. Heating block.
11. 6 % acrylamide SDS-PAGE gels or commercially available low-percent gradient gels (e.g., NuPAGE 3–8 % Tris–acetate protein gels, Life Technologies).
12. SDS-PAGE gel-running apparatus.
13. Protein transfer apparatus.
14. PVDF (polyvinyl difluoride) or nitrocellulose membrane.
15. TEN + Tween-20 buffer: 50 mM Tris–HCl pH 7.5, 1 mM EDTA, 150 mM NaCl, 0.05 % Tween-20.
16. Blocking buffer: TEN + Tween-20 buffer supplemented with 5 % nonfat dry milk powder (skim milk).
17. Anti-Rad53 antibody (Santa Cruz, sc-6749).
18. Horseradish peroxidase-conjugated secondary antibody.
19. ECL-developing reagent.
20. Films and film-developing system or CCD camera-based detection system (e.g., ChemiDoc XRS system, Bio-Rad).

2.3 Rad53 Autophosphorylation by In Situ Kinase Assay

1. Cell culture tools, medium, and equipment as listed in Subheading 2.1 (**items 1–6**).
2. 10 % Acrylamide SDS-PAGE gels.
3. SDS-PAGE gel-running apparatus.
4. PVDF membrane.
5. Protein transfer apparatus.
6. Denaturing buffer: 7 M Guanidine–HCl, 50 mM Tris–HCl pH 8.0, 2 mM EDTA, 50 mM DTT (*see* **Note 4**).
7. Tris-buffered saline (TBS): 50 mM Tris–HCl pH 7.5, 150 mM NaCl.
8. Renaturing buffer: 10 mM Tris–HCl pH 7.5, 140 mM NaCl, 2 mM EDTA, 0.04 % w/v Tween-20, 1 % w/v bovine serum albumin (BSA), 2 mM DTT (*see* **Note 5**).
9. 30 mM Tris–HCl pH 7.5.
10. Kinase buffer: 40 mM HEPES–NaOH pH 8.0, 20 mM $MgCl_2$, 20 mM $MnCl_2$, 0.1 mM EGTA, 100 μM sodium orthovanadate, 1 mM DTT (freshly added from powder or 1 M –20 °C frozen stock).
11. γ-^{32}P-ATP (370 MBq (10 mCi)/mL).

12. 30 mM Tris–HCl pH 7.5, 0.01 % NP-40.
13. 1 M KOH.
14. 10 % TCA.
15. Plastic wrap (e.g., Saran wrap).
16. Phosphor-imaging system (e.g., Typhoon, GE Healthcare).

2.4 Testing Cell Sensitivity to DNA-Damaging Agents by Drop Assay

1. YPAD plates: 20 g/L Bacto peptone, 10 g/L yeast extract, 20 g/L dextrose, 25 mg/L adenine-hemisulfate salt, 20 g/L Bacto Agar. Suspend in ddH_2O, and autoclave at 120 °C for 15 min (*see* **Note 6**). Let it cool down about 50 °C, and pour about 20 mL in each petri dish.
2. Cell culture tools, medium, and equipment as listed in Subheading 2.1 (**items 1, 2 and 4**).
3. 96-well plates.
4. 8-channel pipette.
5. YPAD plates with DNA-damaging reagents: Autoclave YPAD-agar, cool down to about 50 °C, and then add DNA-damaging agents (HU, MMS, bleomycin, etc.) to the desired concentration. Pour about 20 mL in each petri dish in the ventilation hood.

2.5 Cell Recovery Assay

1. YPAD plates (*see* Subheading 2.4, **item 1**).
2. Cell culture tools, medium, and equipment as listed in Subheading 2.1 (**items 1–6**).
3. Hydroxyurea (*see* **Note 1**).

2.6 Monitoring Spindle Elongation

1. YPAD plates (*see* Subheading 2.4, **item 1**).
2. Cell culture tools, medium, and equipment as listed in Subheading 2.1 (**items 1–6**).
3. Budding yeast strain expressing the GFP-TUB1 fusion protein. If not available, wild-type cells can be used (*see* **Note 7**).
4. Hydroxyurea (*see* **Note 1**).
5. 20 % Paraformaldehyde solution: Dissolve 5 g of paraformaldehyde powder in 15 mL of H_2O, then add 25 μL of 10 N NaOH, and heat at 60 °C until the solution becomes clear. Add H_2O filling up to 25 mL, and keep at 4 °C.
6. Phosphate-buffered saline (PBS): 137 mM NaCl, 2.7 mM KCl, 8.1 mM Na_2HPO_4, 1.1 mM KH_2PO_4, pH 7.4.
7. 10 % Triton X-100.
8. (Optional) DAPI: 4′,6-Diamidino-2-phenylindole, dihydrochloride.
9. Fluorescent microscope and image analysis software (e.g., Image J).

2.7 In Vitro Mec1 Kinase Assay

1. Cell culture tools, medium, and equipment as listed in Subheading 2.4 (**items 1, 2 and 4**).
2. Budding yeast strain expressing the Ddc2–GFP fusion protein (*see* **Note 8**).
3. 500-mL Erlenmeyer flask.
4. PBS: 137 mM NaCl, 2.7 mM KCl, 8.1 mM Na_2HPO_4, 1.1 mM KH_2PO_4, pH 7.4.
5. 2-mL screw-cap tubes.
6. Liquid nitrogen.
7. Dynabeads Protein G (Life Technologies).
8. Lysis buffer: 50 mM HEPES–NaOH pH 7.5, 150 mM NaCl, 2 mM EDTA, 0.5 % (w/v) NP-40, protease inhibitor cocktail (complete, Roche).
9. Magnet tube holder (e.g., Dynamag, Life Technologies).
10. Anti-GFP antibody (Roche, 11814460001).
11. 0.5-mm Zirconia/silica beads.
12. FastPrep-24 cell disruptor system (MP Biomedicals).
13. 25-gauge needles.
14. 4× NuPAGE LDS sample buffer (Life Technologies) supplemented with 200 mM DTT (freshly added) or equivalent 4× SDS-PAGE sample buffer (*see* **Note 3**).
15. Heating block.
16. 10× Kinase buffer: 200 mM Tris–HCl pH 7.4, 100 mM magnesium acetate, 0.5 % (w/v) Tween-20, 40 mM $MnCl_2$, 1 mM DTT (freshly added from powder or 1 M –20 °C frozen stock).
17. 10 mM adenosine triphosphate (ATP).
18. γ-^{32}P-ATP (370 MBq (10 mCi)/mL).
19. Recombinant substrate (e.g., human EIF4EBP1 recombinant protein, Abnova, H00001978-P01) (*see* **Note 9**).
20. 300 mM caffeine.
21. 10 % SDS gels or commercially available gradient gels (e.g., 4–12 % Bis/Tris gels, Life Technologies).
22. SDS-PAGE gel-running apparatus.
23. Protein gel dye (e.g., Instantblue, Expedeon).
24. Gel-drying apparatus.
25. Phosphor-imaging system (e.g., Typhoon, GE Healthcare).
26. Protein transfer apparatus.

3 Methods

The activity of the effector kinase Rad53 is commonly used as readout of the activation of the replication checkpoint in budding yeast. As mentioned in Subheading 1, once activated, Rad53 undergoes autophosphorylation and becomes hyperphosphorylated (Fig. 1). Hyperphosphorylated Rad53 migrates more slowly than its less phosphorylated form in SDS-PAGE. In this section, we first describe how to synchronize budding yeast cells. We then describe two methods to monitor Rad53 activation and two different survival assays: drop assay and recovery assay, both of which reflect the activity of the replication checkpoint. In budding yeast, unlike other eukaryotes, microtubules (spindles) start to elongate in S phase, and the replication checkpoint inhibits, once activated, premature spindle elongation. We also describe a method to monitor spindle elongation in response to HU. Finally, we provide a protocol to test Mec1 kinase activity on a recombinant substrate in vitro.

3.1 α-Factor Synchronization of Budding Yeast Cells

We use α-factor to synchronize budding yeast cells in G1 phase. Efficacy of α-factor varies from one batch to the other. To ensure efficacy, every batch of α-factor should be tested to confirm its effect on cell synchronization. In this section, we provide a protocol to determine an optimal α-factor concentration.

3.1.1 α-Factor Treatment of Budding Yeast Cells

1. Culture MAT**a** yeast cells in 5 mL of YPAD medium overnight.
2. Dilute cells in 30 mL of YPAD (OD_{600} ~ 0.2) in a 250-mL flask, and then culture until an OD_{600} of 0.5–0.6 is achieved (*see* **Note 10**).
3. Centrifuge at 1,500 × *g* for 3 min at room temperature to collect cells, and resuspend cells in 30 mL of YPAD medium pH 5.0 (*see* **Note 11**).
4. Take 1 mL of cell culture for FACS analysis (random culture sample). Follow Subheading 3.1.2 for FACS analysis.
5. Distribute 5 mL of cell culture to 50-mL sterile tubes with air-permeable lids, and add different amounts of α-factor stock solution to each tube (e.g., 5, 2.5, 1, 0.5 μL to achieve final concentrations of 5, 2.5. 1, 0.5 μg/mL) (*see* **Note 12**).
6. Culture cells for 90 min at 30 °C.
7. Take 1 mL of each cell culture for FACS analysis (*see* Subheading 3.1.2). Also, monitor cell cycle arrest under the microscope (*see* **Note 13**).
8. Centrifuge the cultures at 1,500 × *g* for 2 min at room temperature, and remove the culture supernatant.
9. Suspend cells with 5 mL of YPAD and then spin at 1,500 × *g* for 2 min at room temperature to wash and collect cells.

10. Resuspend cells in 5 mL of YPAD and culture at 30 °C.
11. Take 1 mL of each cell culture at 15, 30, 45, and 60 min after release for FACS analysis (*see* Subheading 3.1.2).

3.1.2 FACS Analysis to Determine an Optimal α-Factor Concentration

1. Centrifuge cells at 1,500 × *g* for 2 min at room temperature to collect cells in a 1.5-mL tube.
2. Remove the medium from each sample, suspend cells in 500 μL of 70 % ethanol, and keep the samples at 4 °C for 30 min. The samples can be kept at 4 °C for several days.
3. Spin samples at 8,000 × *g* for 1 min at room temperature, and remove the ethanol.
4. Add 250 μL of RNaseA solution, and incubate at 37 °C for 2 h.
5. Spin samples at 8,000 × *g* for 1 min, remove supernatant, and add 250 μL of PI solution.
6. Pulse sonicate each sample for 1 s (*see* **Note 14**).
7. Dilute the samples by five- to tenfold, 50–100 μL of samples, in 500 μL of PI solution, and then analyze the cell-cycle profile by flow cytometry (*see* **Note 15**).
8. Determine the optimal α-factor concentration based on cell-cycle profiles of synchronized cells and cells released from the α-factor arrest (*see* **Note 16**).

3.2 Phospho-Shift Analysis of Rad53 Phosphorylation After Replication Stress

Rad53 activation can be monitored by its hyperphosphorylation. Hyperphosphorylated Rad53 migrates more slowly in an SDS-PAGE gel, resulting in a band shift (phospho-shift). This section describes a method to detect hyperphosphorylated Rad53 by Western blotting.

3.2.1 Synchronization and Hydroxyurea Treatment of Budding Yeast Cells

1. Streak yeast cells freshly on YPAD plates. Incubate for 1–2 days at 30 °C (*see* **Note 17**).
2. Inoculate a colony of yeast into 5 mL YPAD medium in a sterile (autoclaved) Erlenmeyer flask (50–100 mL) or into a sterile tube with air-permeable lids (50 mL). Shake the culture at 30 °C overnight.
3. Measure OD_{600} after overnight culture, and dilute the culture to an OD_{600} of 0.3 in 15 mL of YPAD in a sterile (autoclaved) Erlenmeyer flask (50–100 mL) or a sterile tube with air-permeable lid (50 mL); shake culture at 30 °C for about 3 h (*see* **Note 18**).
4. Measure OD_{600}, and transfer a culture volume equivalent to 15 mL of an OD_{600} 0.5 culture into a fresh 50-mL tube (*see* **Note 18**).
5. Spin at 1,500 × *g* for 2 min at room temperature.
6. Wash cells once with 15 mL of YPAD.
7. Resuspend in 15 mL of YPAD pH 5.0, and add the appropriate amount of α-factor.

8. Shake the culture at 30 °C for about 75 min, and check cells under the microscope for absence of small buds (*see* **Note 13**).
9. Spin at 1,500 × *g* for 2 min.
10. Wash cells once with 15 mL of YPAD.
11. Resuspend cells in 15 mL of YPAD supplemented with 0.2 M HU or intra-S damage checkpoint can be induced with other DNA-damaging drugs such as 0.03 % MMS. Culture cells at 30 °C.

3.2.2 Protein Sample Preparation by NaOH/ Trichloroacetic Acid Precipitation

1. Take 2 mL of the culture (*see* Subheading 3.2.1, **step 11**) after 0, 15, 30, 60, and 90 min of HU or MMS treatment into 2-mL tubes.
2. Spin at max speed in a microfuge for 1 min at 4 °C, remove the medium, and add 100 μL of ice-cold solution I.
3. Suspend cells, and keep the samples on ice for 10 min.
4. Add 100 μL of solution II, vortex to mix, and then keep samples on ice for 10 min. After adding solution II, samples can be kept on ice until the end of the time-course experiment (*see* **step 1**) and processed all together.
5. Spin down samples at max speed for 1 min at 4 °C in a microfuge, and remove supernatant.
6. Wash with 500 μL of solution III (do not disturb the pellet).
7. Spin at max speed for 1 min at 4 °C in a microfuge, and remove supernatant completely (*see* **Note 19**).
8. Let samples dry at room temperature with the tube lids open.
9. Resuspend samples in 50 μL of 1× NuPAGE sample buffer supplemented with 50 mM DTT (*see* **Note 3**).
10. Heat samples at 70 °C for 10 min (*see* **Note 3**).
11. Spin shortly, and store whole samples at −20 °C until SDS-PAGE and Western blot analysis. Repeat **step 10** and spin shortly just before loading sample on SDS-PAGE.

3.2.3 SDS-PAGE and Western Blotting

1. If samples were stored at −20 °C, heat samples at 70 °C for 10 min again (*see* **Note 3**).
2. Spin down briefly, load 2.5–5 μL of sample on a 6 % acrylamide SDS-PAGE gels, and perform electrophoresis according to standard procedures.
3. Transfer proteins to PVDF or nitrocellulose membrane according to the instructions for the protein transfer apparatus.
4. Block the membrane by incubating with blocking buffer for 30 min at room temperature (*see* **Note 20**).
5. Incubate the membrane with blocking buffer supplemented with the anti-Rad53 antibody (*see* **Note 21**) at room temperature for 1 h or at 4 °C overnight.

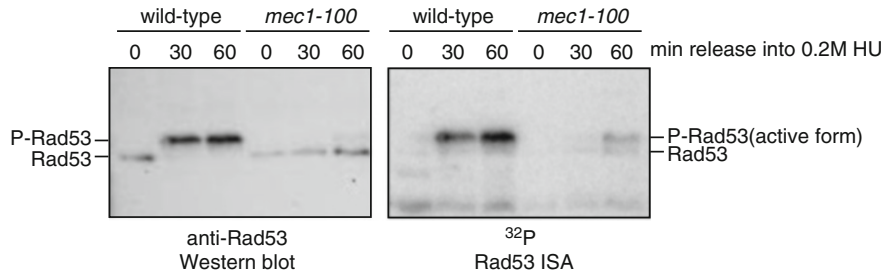

Fig. 2 Rad53 phospho-shift and Rad53-ISA. Wild-type and *mec1-100* cells were arrested in G1 phase with α-factor and released into YPAD medium supplemented with 0.2 M HU. Samples were taken at indicated time points, and proteins were extracted using TCA. Protein samples were subjected to SDS-PAGE and Western blot with anti-Rad53 antibody (*left*). An example of Rad53-ISA results is also shown (*right*)

6. Wash the membrane with TEN-Tween 20 buffer for 10–20 min at room temperature at least three times with buffer exchange.
7. Incubate the membrane with blocking buffer containing the secondary antibody for 30 min to 1 h at room temperature.
8. Wash the membrane with TEN-Tween 20 buffer for 5–10 min at room temperature at least five times with buffer exchange.
9. Detect Western blot signal using ECL-developing reagent on either films or a CCD camera-based system (Fig. 2).

3.3 Rad53 Autophosphorylation by In Situ Kinase Assay (ISA)

Rad53 activation can also be monitored by its autophosphorylation, which can be detected by an in situ kinase assay (ISA) described in this section. This procedure has ben adapted from a previously described method [22].

1. Follow all the steps in Subheadings 3.2.1 and 3.2.2.
2. Load 5–10 μL of sample on 10 % SDS-PAGE gel, and perform electrophoresis according to standard procedures.
3. Transfer proteins to PVDF membrane according to the instructions for the protein transfer apparatus (*see* **Note 22**).
4. Incubate membrane in denaturing buffer for 1 h at room temperature (*see* **Note 20**).
5. Wash membrane twice for 10 min in TBS.
6. Incubate membrane in renaturing buffer at 4 °C overnight. Change this buffer more than four times during the incubation.
7. Wash membrane in 30 mM Tris–HCl pH 7.5 for 30–60 min at room temperature.
8. Incubate membrane with kinase buffer for 30 min at room temperature.
9. Incubate membrane with kinase buffer supplemented with 0.37 MBq/mL (10 μCi/mL) of [γ-^{32}P]ATP for 1 h at room temperature (10 mL of kinase buffer is typically used for a mini-gel size of PVDF membrane, 10 × 8 cm).

10. Wash membrane with 30 mM Tris–HCl pH 7.5 twice for 10 min.
11. Wash membrane with 30 mM Tris–HCl pH 7.5 supplemented with 0.01 % NP-40 once for 10 min.
12. Wash membrane with 30 mM Tris–HCl pH 7.5 once for 10 min.
13. Wash membrane with 1 M KOH once for 10 min.
14. Rinse membrane with ddH_2O.
15. Wash membrane with 10 % TCA once for 10 min.
16. Rinse membrane with ddH_2O, and wrap it in plastic wrap.
17. Expose the membrane to a Phosphorimager screen overnight, and detect radioactivity by a phosphor-imaging system (*see* **Note 23** and Fig. 2).

3.4 Drop Assay to Test Cellular Sensitivity to DNA-Damaging Agents

1. Streak yeast cells fresh on YPAD plates. Incubate for 1–2 days at 30 °C (*see* **Note 17**).
2. Inoculate a colony of yeast into 5 mL of YPAD in a sterile (autoclaved) Erlenmeyer flask (50–100 mL) or a sterile tube with air-permeable lids (50 mL); shake the culture at 30 °C overnight.
3. Measure OD_{600} after overnight culture, and dilute all cultures to the same OD_{600} or cell number (e.g., OD_{600} 1.0) (*see* **Note 10**).
4. Prepare a tenfold serial dilution in a 96-well plate: Add 100 μL of cell density-adjusted cultures (e.g., OD_{600} 1.0) in the wells of the first column. Then, using an 8-channel pipette, add 90 μL of water in the wells of the second through the sixth columns (each column has 8 wells).
5. Using an 8-channel pipette, add 10 μL of cultures from the first column into the wells of the second column, and mix cells by pipetting up and down several times.
6. Repeat **step 5** until the sixth column (10 μL from the second to third, 10 μL from the third to fourth, and so on).
7. YPAD control plates and YPAD plates with DNA-damaging agent should be prepared the day before, and the surface should be free of water droplets. If you have water droplets, let plates dry in a fume hood or a laminar flow hood.
8. Drop 2–3 μL of the serially diluted cultures column by column on the YPAD plates using an 8-channel pipette (*see* **Note 24**). Finally, every row on the plate will show a tenfold serial dilution of cells of one strain.
9. Incubate plates at 30 °C for 2–3 days, and take pictures of the plates after incubation (Fig. 3a) (*see* **Note 25**).

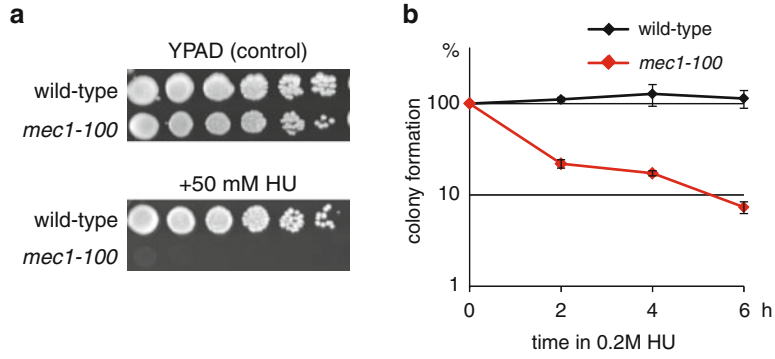

Fig. 3 HU sensitivity assays of budding yeast cells. (**a**) For drop assays, tenfold serial dilutions of wild-type and *mec1-100* cells were spotted and grown on YPAD-agar medium containing 0 (control) or 50 mM HU (*see* text for details). Pictures were taken after 2 days of incubation at 30 °C. (**b**) For cell recovery assays, wild-type and *mec1-100* cells were arrested in G1 phase with α-factor and released into YPAD medium containing 0.2 M HU. Samples were taken at 0, 2, 4, and 6 h after release from the α-factor arrest and subjected to colony-forming assay. Plating efficiency of each strain was normalized to samples at time 0 h. Error bar represents standard deviation of three independent experiments. Drop assay represents tolerance/outgrowth of cells on replication stress, whereas recovery assay reflects the replication fork stability/restart. The DNA replication checkpoint is important for both aspects

3.5 Cell Recovery Assay from HU Treatment

1. Follow Subheading 3.2.1 for synchronization and hydroxyurea treatment of budding yeast cells.
2. Determine cell density by a cell-counting device (can be done while cells are still in α-factor arrest).
3. Make dilutions of cells at 1×10^3 cells/mL, and plate 100–200 cells (100–200 μL) on three YPAD plates for each strain after 0, 2, 4, and 6 h of hydroxyurea treatment (*see* **Note 26**).
4. Incubate plates at 30 °C for 2–3 days before counting colonies.
5. Calculate average colony number of the three plates of each strain and each time point.
6. Calculate percentages of cell survival based on 0-h time point for each strain (Fig. 3b) (*see* **Note 27**).

3.6 Monitoring Spindle Elongation

1. Grow GFP-TUB1-expressing cells (*see* **Note 7**) to exponential phase, and treat cells with α-factor to induce G1 arrest in ~40 mL of YPAD (*see* Subheading 3.2.1 for details).
2. Take 1 mL of exponentially growing cells and α-factor-arrested cells for FACS analysis (*see* Subheading 3.1.2).
3. Release cells in ~40 mL of YPAD containing 0.2 M HU (*see* Subheading 3.2.1 for details).

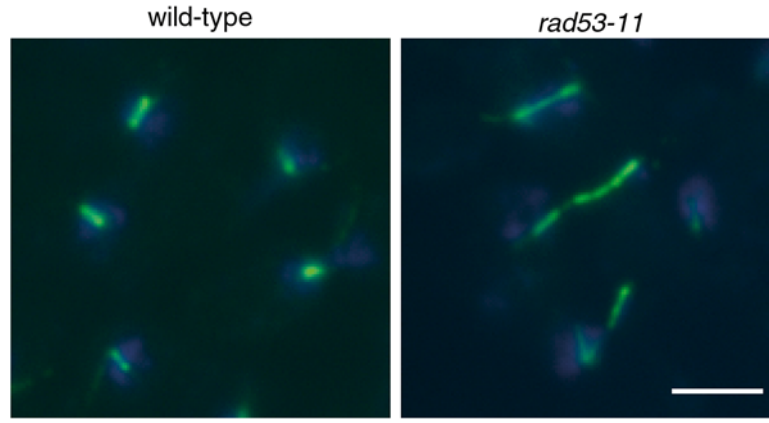

Fig. 4 Spindle elongation in checkpoint-deficient cells in response to HU. Wild-type and *rad53-11* cells were synchronized in G1 and released into S phase in YPAD medium supplemented with 0.2 M HU. Samples were taken after 4 h for immunofluorescence using TAT-1 that reacts with α-tubulin. DNA was counter-stained with DAPI. Scale bar, 5 μm. Checkpoint-deficient *rad53-11* cells exhibit an elongated spindle, while wild-type cells retain a short spindle

4. Take 5 mL of culture at 0, 1, 2, 3, 4, and 5 h after release from α-factor, and fix cells with 1 % paraformaldehyde (0.25 mL of 20 % paraformaldehyde solution) for 5 min at room temperature. Take also 1 mL of culture for FACS analysis at each time point to determine whether DNA synthesis is inhibited (*see* Subheading 3.1.2).
5. Spin fixed samples at 1,500 × *g* for 5 min at room temperature, and then remove the culture medium.
6. Add 5 mL of ice-cold PBS to wash the samples, and spin at 1,500 × *g* for 5 min at room temperature. Repeat this step once more.
7. (Optional) DAPI staining: Resuspend cells in 100 μL of PBS supplemented with 0.1 % Triton and 1 μg/mL DAPI and transfer to a 1.5-mL tube. Incubate for 5 min at room temperature, and then spin at 6,000 × *g* for 1 min at room temperature.
8. Resuspend cells in 100 μL of PBS, and keep the samples at 4 °C until analysis with a fluorescent microscope.
9. Take pictures with a fluorescent microscope, and measure the spindle length (Fig. 4) (*see* **Note 28**).

3.7 In Vitro Mec1 Kinase Assay

Immunoprecipitated Mec1–Ddc2 complex can be used to monitor its kinase activity on recombinant substrates. This protocol was adapted from a previously described assay [27].

3.7.1 Harvesting Cells

1. Streak yeast cells fresh on YPAD plates. Incubate overnight at 30 °C.
2. Inoculate a colony of Ddc2–GFP-expressing cells (*see* **Note 8**) into 5 mL YPAD in a sterile (autoclaved) Erlenmeyer flask (50–100 mL) or a sterile tube with air-permeable lid (50 mL); shake the culture at 30 °C overnight.
3. Measure OD_{600} of overnight culture, and dilute to an OD_{600} of 0.3 in 100 mL of YPAD in sterile (autoclaved) Erlenmeyer flasks (500 mL); shake the culture at 30 °C for about 2–3 h (*see* **Note 10**).
4. Measure OD_{600}, and harvest cells equivalent to 100 mL of an OD_{600} 0.5/mL culture (50 ODs, about 7×10^8 cells) by centrifugation at $1{,}500 \times g$ for 2 min at room temperature.
5. Resuspend cell pellets in 1 mL cold PBS, and transfer cells to 2-mL screw-cap tubes.
6. Spin at max speed in a microfuge for 1 min at 4 °C.
7. Remove supernatant. At this stage the cell pellet can be frozen in liquid nitrogen and stored at −80 °C.

3.7.2 Anti-GFP Bead Preparation

1. Transfer 50 μL of Dynabeads Protein G slurry per sample into a fresh 1.5-mL tube.
2. Wash beads twice with lysis buffer using a magnet tube holder. If necessary, centrifuge tubes only briefly.
3. Resuspend beads in 50 μL (original bead slurry volume) of lysis buffer, and add 5 μg of the anti-GFP antibody.
4. Incubate for 1 h at room temperature with rotation. In the meantime, extracts can be prepared (*see* Subheading 3.7.3).
5. Using a magnet tube holder, collect beads, remove supernatant, and wash beads twice with lysis buffer.
6. Wash beads once with lysis buffer supplemented with protease inhibitor cocktail.

3.7.3 Cell Extract Preparation

1. Resuspend the cell pellets (prepared in Subheading 3.7.1) in 200 μL ice-cold lysis buffer supplemented with protease inhibitor cocktail. Perform all the subsequent steps on ice.
2. Add ~200 μL of zirconia/silica beads.
3. Break cells using a FastPrep-24 system (*see* **Note 29**).
4. To separate zirconia/silica beads from crude cell extracts, make a hole at the tube bottom using a 25-gauge needle and assemble the tube onto a second tube. Spin at $1{,}500 \times g$ for 2 min at 4 °C, and collect the extracts in the second tube (*see* **Note 30**).
5. Transfer the crude extracts to a fresh 1.5-mL tube, and clarify the cell extract by spinning at max speed in a microfuge for 10 min at 4 °C.
6. Transfer the cleared supernatant into a fresh 1.5-mL tube.

7. Take 5 μL of cleared lysate (input sample), dilute into 40 μL lysis buffer, and add 15 μL 4× NuPAGE sample buffer supplemented with 50 mM DTT or equivalent. Heat sample for 10 min at 70 °C (*see* **Note 3**).

3.7.4 Immunoprecipitation

1. Using a magnet tube holder, remove the supernatant from the anti-GFP antibody-coupled magnetic beads (*see* Subheading 3.7.2), and directly add 200 μL of cleared lysates (*see* Subheading 3.7.3, **step 6**).
2. Incubate for 1 h at 4 °C with rotation.
3. Using a magnet tube holder, wash the immunoprecipitated beads three times for 10 min with lysis buffer supplemented with protease inhibitor cocktail.
4. Rinse beads two times with 1× kinase buffer.
5. Resuspend beads in 60 μL of 1× kinase buffer, and keep them on ice.

3.7.5 Kinase Assay

1. Prepare 5× master reaction mix (4 μL per reaction) containing 5× ATP (250 μM), 5× recombinant substrate (200 ng/μL), and 5× [γ-32P]ATP (9.25 kBq/μL = 0.25 μCi/μL) in 1× kinase buffer.
2. Prepare a dilution series of kinase: Add 3.5, 7, and 14 μL of the immunoprecipitated kinase sample (prepared in Subheading 3.7.4, **step 5**) to new tubes. Prepare the last one in duplicate: in one of these two tubes add 1.8 μL of caffeine stock solution for "plus caffeine" as a Mec1 inhibited control.
3. Add 1× kinase buffer to all samples filling up to 16 μL.
4. Add 4 μL of 5× master reaction mix, and then incubate for 30 min at 30 °C with gentle agitation.
5. Stop the reaction by adding 6 μL of 4× NuPAGE sample buffer supplemented with 200 mM DTT. Heat the sample for 10 min at 70 °C (*see* **Note 3**).
6. Load 10 μL of each sample on an SDS-PAGE gel, and follow standard SDS-PAGE procedures.
7. Stain the gel with protein gel stain according to the manufacturer's instructions, and check for equal amounts of substrate.
8. Dry the gel with a gel drying apparatus and expose to a phosphorimager screen to monitor the ^{32}P incorporation into the substrate (Fig. 5).
9. Denature by heating the residual immunoprecipitated kinase-bead sample (IP, *see* Subheading 3.7.4, **step 5**) with NuPAGE sample buffer for 10 min at 70 °C (*see* **Note 3**). Check the successful immunoprecipitation by Western blot of input (*see* Subheading 3.7.3, **step 7**) and IP sample.

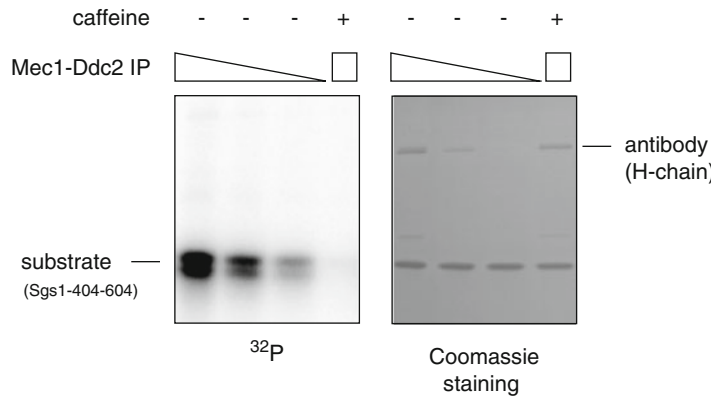

Fig. 5 In vitro Mec1 kinase assay. Cells expressing Ddc2–GFP were subjected to immunoprecipitation using the anti-GFP antibody. Immunoprecipitated Mec1–Ddc2–GFP complexes were transferred into kinase buffer, and kinase reactions were performed in twofold dilution series (*see* text for details). As a control, a reaction with the highest amount of Mec1–Ddc2–GFP was treated with 30 mM caffeine (Mec1 inhibitor). An Sgs1 peptide (amino acid 404–604) was used as a substrate [27]. Reactions were subjected to SDS-PAGE and Coomassie Brilliant Blue staining (*right*) and ^{32}P detection by a phosphorimager (*left*)

4 Notes

1. Hydroxyurea is hygroscopic and decomposes in the presence of moisture. Let vessel equilibrate to room temperature before opening. Weigh the amount needed, and dissolve directly in the culture medium.
2. Prepare solution I fresh before each experiment and keep it on ice.
3. We normally use 1× (or 4×) NuPAGE LDS sample buffer. However, regular 1× (or 4×) SDS-PAGE sample buffer (for 1×: 50 mM Tris–HCl pH 6.8, 10 % glycerol, 2 % SDS, 1 % β-mercaptoethanol, 0.01 % bromophenol blue) can also be used. Heat samples at 70 °C for 10 min with 1× NuPAGE LDS sample buffer or at 95 °C for 5 min with 1× SDS-PAGE sample buffer.
4. Weigh guanidine-HCl and dissolve directly in the buffer. Add DTT freshly from powder or from 1 M stock solution stored at −20 °C.
5. Weigh BSA and dissolve directly in the buffer. Add DTT freshly from powder or from 1 M stock solution stored at −20 °C.
6. Agar completely dissolves only during autoclaving.
7. The localization of the GFP-TUB1 fusion protein can be monitored by fluorescent microscopy described in this protocol. GFP-TUB1 yeast strain can be obtained from Life Technologies or upon request [35]. When using wild-type

cells, immunofluorescence with anti-TAT-1 antibody (anti-α Tubulin, Sigma 00020911) needs to be performed.

8. The budding yeast *DDC2–GFP* strain is available from Life Technologies or upon request.
9. We also use an Sgs1 peptide (amino-acid 404–604) as a Mec1 substrate [27].
10. Photometric measurements of OD_{600} are usually not linear at higher values. Overnight cultures should be diluted in such a way that the measured OD_{600} is below 1. The actual OD_{600} can be calculated as indicated below:

$$\text{Actual OD} = \text{Measured OD} \times \frac{\text{Final volume of diluted culture}}{\text{Volume of undiluted culture used for dilution}}$$

11. α-Factor arrest is more efficient in YPAD pH 5.0 than in standard YPAD because the secreted protease Bar1, which cleaves α-factor, is less active in low pH conditions.
12. To increase the efficiency of α-factor arrest, Bar1-deficient cells can be used. In this case, α-factor can be used at a 50–100 times lower concentration.
13. In budding yeast bud growth is coupled to cell cycle progression. G1-arrested cells should not contain small buds. Cells should be unbudded or arrested as two equal-sized cells that are attached together.
14. Output 1 using a 550 Sonic Dismembrator.
15. We use FACSCalibur. More information for flow cytometry conditions at http://www.bdbiosciences.com/instruments/facscalibur/.
16. After 90 min of α-factor treatment, cells should be arrested in G1. G1-arrested cells should not show small buds as can be seen by microscopic analysis. S or G2 populations should not be detected by flow cytometry. At 30–45 min after release from the α-factor arrest, the culture should be highly enriched with S-phase cells. At 60 min after the release, cells should reach G2 phase.
17. When using a temperature-sensitive strain, grow cells at 23 °C here and during the rest of cell culture steps in Subheading 3.2.1 before shifting up the temperature and inactivating a gene product.
18. An OD_{600} of 0.7 corresponds to roughly 1×10^7 cells/mL. Therefore, a 15 mL culture of OD_{600} 0.3 (4.5 ODs) and 0.5 (7.5 ODs) roughly corresponds to 6×10^8 and 1×10^8 cells, respectively.
19. If necessary, spin down once more in order to remove supernatant completely.

20. Submerge membrane in 10–20 mL buffer for each step, and gently agitate at room temperature unless otherwise indicated.
21. If the anti-Rad53 antibody is not available, use a strain that is engineered to express tagged Rad53 (e.g., Rad53-GFP is available from Life Technologies and Rad53-13myc is available upon request) [24]. Antibodies against those tags are available from various commercial sources.
22. A wet Transfer system is preferred in order to obtain consistent protein-transfer efficiency. It should also be considered to use slightly elevated amperage than usual to ensure most efficient transfer. We use 400–500 mA for this assay instead of the usual 200 mA.
23. Alternatively an X-ray film can be used to detect radioactive signals with a standard film developer.
24. Alternatively, a stamping device, such as a 48-pin replicator, can be used.
25. The drop assay scores the tolerance of cells typically on low dose of replication stress or DNA-damaging agents. In contrast, the cell recovery assay described in Subheading 3.5 reflects cell ability to restart and stabilize stalled replication forks.
26. Cell numbers refer to wild-type strains. Mutant strains might be more sensitive to DNA-damaging agents. In this case a higher number of cells can be plated.
27. Percentage of colony formation (plating efficiency) can be normalized to wild-type colony formation unit.
28. Checkpoint-deficient cells exhibit elongated mitotic spindles, which are typically more than 5 μm in length, while checkpoint-proficient cells keep the short spindle (<2 μm) (Fig. 4).
29. For Fast Prep-24, use the following settings: level 6.5, 60 s, three times with 5-min cooling on ice in between beating steps.
30. At this step the silica beads should stay in the 2-mL screw-cap tube. For collection of cells, FACS sample tubes (e.g., Semadeni, 3190; 10 mm × 54 mm length) or normal 1.5-mL tubes can be used depending on the size of the centrifuge used for collection.

Acknowledgements

We thank Dr. Susan M. Gasser for critical reading and helpful suggestions. Support was gratefully received from the Novartis Research Foundation, the Swiss Cancer League, and the FP7 Marie Curie Network, Imaging the DNA Damage Response (Image DDR).

References

1. Lambert S, Carr AM (2005) Checkpoint responses to replication fork barriers. Biochimie 87(7):591–602
2. Friedel AM, Pike BL, Gasser SM (2009) ATR/Mec1: coordinating fork stability and repair. Curr Opin Cell Biol 21(2):237–244
3. Cimprich KA, Cortez D (2008) ATR: an essential regulator of genome integrity. Nat Rev Mol Cell Biol 9(8):616–627
4. Bosotti R, Isacchi A, Sonnhammer EL (2000) FAT: a novel domain in PIK-related kinases. Trends Biochem Sci 25(5):225–227
5. Zou L, Elledge SJ (2003) Sensing DNA damage through ATRIP recognition of RPA-ssDNA complexes. Science 300(5625): 1542–1548
6. MacDougall CA, Byun TS, Van C, Yee MC, Cimprich KA (2007) The structural determinants of checkpoint activation. Genes Dev 21(8):898–903
7. Majka J, Niedziela-Majka A, Burgers PM (2006) The checkpoint clamp activates Mec1 kinase during initiation of the DNA damage checkpoint. Mol Cell 24(6):891–901
8. Delacroix S, Wagner JM, Kobayashi M, Yamamoto K, Karnitz LM (2007) The Rad9-Hus1-Rad1 (9-1-1) clamp activates checkpoint signaling via TopBP1. Genes Dev 21(12): 1472–1477
9. Furuya K, Poitelea M, Guo L, Caspari T, Carr AM (2004) Chk1 activation requires Rad9 S/TQ-site phosphorylation to promote association with C-terminal BRCT domains of Rad4TOPBP1. Genes Dev 18(10):1154–1164
10. Lee J, Kumagai A, Dunphy WG (2007) The Rad9-Hus1-Rad1 checkpoint clamp regulates interaction of TopBP1 with ATR. J Biol Chem 282(38):28036–28044
11. Mordes DA, Glick GG, Zhao R, Cortez D (2008) TopBP1 activates ATR through ATRIP and a PIKK regulatory domain. Genes Dev 22(11):1478–1489
12. Navadgi-Patil VM, Burgers PM (2009) The unstructured C-terminal tail of the 9-1-1 clamp subunit Ddc1 activates Mec1/ATR via two distinct mechanisms. Mol Cell 36(5):743–753
13. Navadgi-Patil VM, Burgers PM (2011) Cell-cycle-specific activators of the Mec1/ATR checkpoint kinase. Biochem Soc Trans 39(2): 600–605
14. Navadgi-Patil VM, Kumar S, Burgers PM (2011) The unstructured C-terminal tail of yeast Dpb11 (human TopBP1) protein is dispensable for DNA replication and the S phase checkpoint but required for the G2/M checkpoint. J Biol Chem 286(47):40999–41007
15. Puddu F, Piergiovanni G, Plevani P, Muzi-Falconi M (2011) Sensing of replication stress and Mec1 activation act through two independent pathways involving the 9-1-1 complex and DNA polymerase epsilon. PLoS Genet 7(3):e1002022
16. Kumar S, Burgers PM (2013) Lagging strand maturation factor Dna2 is a component of the replication checkpoint initiation machinery. Genes Dev 27(3):313–321
17. Emili A (1998) MEC1-dependent phosphorylation of Rad9p in response to DNA damage. Mol Cell 2(2):183–189
18. de la Torre-Ruiz MA, Green CM, Lowndes NF (1998) RAD9 and RAD24 define two additive, interacting branches of the DNA damage checkpoint pathway in budding yeast normally required for Rad53 modification and activation. EMBO J 17(9):2687–2698
19. Gilbert CS, Green CM, Lowndes NF (2001) Budding yeast Rad9 is an ATP-dependent Rad53 activating machine. Mol Cell 8(1): 129–136
20. Sweeney FD, Yang F, Chi A, Shabanowitz J, Hunt DF, Durocher D (2005) *Saccharomyces cerevisiae* Rad9 acts as a Mec1 adaptor to allow Rad53 activation. Curr Biol 15(15):1364–1375
21. Sun Z, Hsiao J, Fay DS, Stern DF (1998) Rad53 FHA domain associated with phosphorylated Rad9 in the DNA damage checkpoint. Science 281(5374):272–274
22. Pellicioli A, Lucca C, Liberi G, Marini F, Lopes M, Plevani P, Romano A, Di Fiore PP, Foiani M (1999) Activation of Rad53 kinase in response to DNA damage and its effect in modulating phosphorylation of the lagging strand DNA polymerase. EMBO J 18(22):6561–6572
23. Alcasabas AA, Osborn AJ, Bachant J, Hu F, Werler PJ, Bousset K, Furuya K, Diffley JF, Carr AM, Elledge SJ (2001) Mrc1 transduces signals of DNA replication stress to activate Rad53. Nat Cell Biol 3(11):958–965
24. Frei C, Gasser SM (2000) The yeast Sgs1p helicase acts upstream of Rad53p in the DNA replication checkpoint and colocalizes with Rad53p in S-phase-specific foci. Genes Dev 14(1):81–96
25. Bjergbaek L, Cobb JA, Tsai-Pflugfelder M, Gasser SM (2005) Mechanistically distinct roles for Sgs1p in checkpoint activation and

replication fork maintenance. EMBO J 24(2): 405–417

26. Chen SH, Zhou H (2009) Reconstitution of Rad53 activation by Mec1 through adaptor protein Mrc1. J Biol Chem 284(28):18593–18604
27. Hegnauer AM, Hustedt N, Shimada K, Pike BL, Vogel M, Amsler P, Rubin SM, van Leeuwen F, Guenole A, van Attikum H, Thoma NH, Gasser SM (2012) An N-terminal acidic region of Sgs1 interacts with Rpa70 and recruits Rad53 kinase to stalled forks. EMBO J 31(18):3768–3783
28. Zegerman P, Diffley JF (2010) Checkpoint-dependent inhibition of DNA replication initiation by Sld3 and Dbf4 phosphorylation. Nature 467(7314):474–478
29. Lopez-Mosqueda J, Maas NL, Jonsson ZO, Defazio-Eli LG, Wohlschlegel J, Toczyski DP (2010) Damage-induced phosphorylation of Sld3 is important to block late origin firing. Nature 467(7314):479–483
30. Cobb JA, Schleker T, Rojas V, Bjergbaek L, Tercero JA, Gasser SM (2005) Replisome instability, fork collapse, and gross chromosomal rearrangements arise synergistically from Mec1 kinase and RecQ helicase mutations. Genes Dev 19(24):3055–3069
31. Sogo JM, Lopes M, Foiani M (2002) Fork reversal and ssDNA accumulation at stalled replication forks owing to checkpoint defects. Science 297(5581):599–602
32. Chabes A, Georgieva B, Domkin V, Zhao X, Rothstein R, Thelander L (2003) Survival of DNA damage in yeast directly depends on increased dNTP levels allowed by relaxed feedback inhibition of ribonucleotide reductase. Cell 112(3):391–401
33. Krishnan V, Nirantar S, Crasta K, Cheng AY, Surana U (2004) DNA replication checkpoint prevents precocious chromosome segregation by regulating spindle behavior. Mol Cell 16(5): 687–700
34. Hustedt N, Gasser SM, Shimada K (2013) Replication checkpoint: tuning and coordination of replication forks in S phase. Genes 4(3): 388–434
35. Shimada K, Pasero P, Gasser SM (2002) ORC and the intra-S-phase checkpoint: a threshold regulates Rad53p activation in S phase. Genes Dev 16(24):3236–3252

Chapter 17

Analyzing Cell Cycle-Dependent Degradation and Ubiquitination in Budding Yeast

Dong-Hwan Kim and Deanna M. Koepp

Abstract

Cell cycle progression is tightly regulated to prevent uncontrolled growth and division. Specific cell cycle factors are responsible for driving the cell from one cell cycle stage to the next. Many of these proteins are targeted for degradation by the ubiquitin proteasome system when their function is no longer required or may disrupt cell cycle progression. Here we describe a series of experiments used to study the ubiquitin-mediated degradation of cell cycle proteins. This collection of assays may be used to determine the requirement for individual proteins in the degradation and ubiquitination of cell cycle proteins in *Saccharomyces cerevisiae*.

Key words Ubiquitin, Proteasome, Cell cycle, Protein stability assay, Degradation, Proteolysis

1 Introduction

When cells grow and divide, they follow a defined series of events. Specific cell cycle factors are responsible for driving the cell from one stage to the next. The activities of these factors are tightly regulated to prevent uncontrolled growth and division; many of these factors are controlled by ubiquitin-dependent proteolysis. For example, G1 and mitotic cyclins are regulated by proteolysis and disruption of their respective proteolytic pathways has deleterious ramifications for the cell, including defects in chromosome segregation [1–3]. Other cell cycle factors, including cyclin-dependent kinase inhibitors [4–6], transcription factors [7, 8], and phosphatases [9], are also regulated by ubiquitin-dependent proteolysis. In all cases, absence of this ubiquitination leads to defective cell growth and division. Thus, regulated proteolysis of cell cycle factors has emerged as an important mechanism to control cell division.

A major mechanism of regulated proteolysis inside the cell is through polyubiquitination. The formation of ubiquitin conjugates requires the activity of three enzymes [10]. An ubiquitin-activating

Eishi Noguchi and Mariana C. Gadaleta (eds.), *Cell Cycle Control: Mechanisms and Protocols*, Methods in Molecular Biology, vol. 1170, DOI 10.1007/978-1-4939-0888-2_17,

enzyme (E1) covalently attaches to the small polypeptide ubiquitin [11] and transfers it to an E2 or a ubiquitin-conjugating enzyme. The E2 transfers ubiquitin to a lysine residue in the substrate protein, often with a third enzyme, the ubiquitin ligase (E3). Multiple rounds of this cycle lead to polyubiquitination of the substrate protein [10, 12]. The primary means of specificity in this process is provided by the E3 ubiquitin ligase. As such, they are prime targets for regulation. Multiple ubiquitin ligases have roles in regulating cell cycle transitions. Two of the most significant ubiquitin ligases that function in cell cycle progression are the SCF family and the anaphase-promoting complex/cyclosome (APC/C) (reviewed in ref. 13). Several SCF complexes have been shown to function in the ubiquitination of cell cycle factors in G1 and S phase, while the APC/C has been implicated in the ubiquitination of mitotic and early G1 factors [14–25].

To be recognized and destroyed by the 26S proteasome, a protein must be modified with a chain of at least four ubiquitins [26]. Ubiquitin receptor proteins recognize ubiquitin chains and target the modified protein to the regulatory subunit of the 26S proteasome (reviewed in [27]). At the proteasome, ubiquitin chains are trimmed and cleaved by the action of de-ubiquitination enzymes. Then, the substrate protein is unfolded to enter the central core of the proteasome, which is composed of proteases that sever peptide bonds [27, 28]. The substrate protein is digested to short stretches of amino acids and released from the proteasome; these short peptides are eventually cleaved to free amino acids by isopeptidases in the cytosol [27, 29].

In this chapter, we describe a collection of experiments that we have used to investigate cell cycle proteins targeted for ubiquitination and degradation in *Saccharomyces cerevisiae*. These experiments include assays examining protein turnover, the isolation of proteins modified by ubiquitin, and generating an in vitro ubiquitination system.

2 Materials

2.1 Protein Stability Assays

1. YPD medium: 20 g/L Peptone, 10 g/L yeast extract, 20 g/L glucose.
2. Hemacytometer.
3. Cell cycle arrest agent: For G1: 5 mg/mL Alpha factor dissolved in water and stored at −20 °C (*see* **Note 1**). For early S: 1 M Hydroxyurea (HU) dissolved in water and used fresh. For G2/M: 5 mg/mL Nocodazole dissolved in DMSO and stored at 4 °C.
4. Cycloheximide: 100 mg/mL Dissolved in DMSO and stored at 4 °C.

5. 15 mL Conical tubes.
6. 20 % Trichloroacetic acid (TCA) solution, stored at 4 °C.
7. 2.0 mL Screw-cap tubes (cap with O-ring).
8. 0.5 mm Glass beads.
9. 5× SDS-PAGE sample buffer: 60 mM Tris–HCl pH 6.8, 25 % glycerol, 2 % SDS, 5 % beta-mercaptoethanol, 0.1 % bromophenol blue.
10. 1 M Tris base: Dissolved in water and stored at room temperature.
11. RC DC Protein Assay kit (Bio-Rad).
12. Nitrocellulose or PVDF membrane for Western blotting.
13. PBST buffer, pH 7.4: 137 mM NaCl, 2.7 mM KCl, 10 mM Na_2HPO_4, 2 mM KH_2PO_4, 0.1 % Tween-20.
14. Anti-HA antibody (Covance) and anti-Pgk1 antibody (Abcam).

2.2 Immunoprecipitation of Ubiquitin-Conjugated Proteins

1. 50 mM MG132 proteasome inhibitor: Dissolved in DMSO and stored at −20 °C.
2. 50 mL conical tubes.
3. RIPA lysis buffer: 1 % Triton X-100, 0.1 % SDS, 0.5 % deoxycholic acid, 20 mM Tris–HCl pH 7.5, 10 % glycerol.
4. Protease inhibitor cocktail (Hoffmann-La Roche): One tablet dissolved in 2.0 mL water and stored at −20 °C. Use this solution as 25×.
5. 2.0 mL Screw-cap tubes (cap with O-ring).
6. 0.5 mm Glass beads.
7. 25 gauge Needle.
8. 5 mL Centrifuge tubes.
9. Bio-Rad Protein Assay Reagent (Bio-Rad).
10. Anti-HA antibody (HA.11 monoclonal, Covance).
11. Protein A/G agarose.
12. 5× SDS-PAGE sample buffer: 60 mM Tris–HCl pH 6.8, 25 % glycerol, 2 % SDS, 5 % beta-mercaptoethanol, 0.1 % bromophenol blue.
13. Nitrocellulose or PVDF membrane for Western blotting.
14. Anti-ubiquitin antibody (PD41 monoclonal, Covance).

2.3 In Vitro Ubiquitination Assays

1. 4 L Culture flask.
2. YPD medium: 20 g/L Peptone, 10 g/L yeast extract, 20 g/L glucose.
3. 500 mL Centrifuge bottles.
4. Predigestion buffer: 100 mM Tris–HCl pH 9.2, 10 mM DTT.

5. 50 mL Conical tubes.
6. Digestion buffer: 1 M Sorbitol, 50 mM Tris–HCl pH 7.5, 50 mM $MgCl_2$, 50 mM $CaCl_2$.
7. Zymolyase 20T.
8. 1 and 2 M sorbitol solutions.
9. Yeast extraction buffer (YEB): 125 mM Potassium acetate, 30 mM HEPES–KOH pH 7.2, 3 mM EDTA, 3 mM EGTA, 2 mM DTT.
10. Mortar and pestle.
11. Liquid nitrogen.
12. Ultracentrifuge.
13. Ultracentrifuge tubes.
14. Bio-Gel P-6 DG desalting gel and empty columns (Bio-Rad): Soak Bio-Gel in sterile water overnight prior to use.
15. Desalting buffer: 50 mM Tris–HCl pH 7.5, 50 mM KCl, 0.5 mM DTT.
16. DEAE Sephacel (GE Healthcare Life Sciences).
17. Elution buffer: 50 mM Tris–HCl pH 7.5, 250 mM KCl, 0.5 mM DTT.
18. Bio-Rad Protein Assay Reagent (Bio-Rad).
19. Centricon concentrators (Millipore).
20. Recombinant GST-Cdc6 substrate protein, purified from insect cells using a baculovirus system (*see* **Note 2**).
21. Recombinant ubiquitin (Sigma-Aldrich): Resuspended in water and stored at −80 °C.
22. Recombinant E1 and E2 enzymes (Boston Biochem).
23. 10 mM ATP.
24. 10× Energy mix (10× EM): 10 mM ATP, 350 mM creatine phosphate, 20 mM HEPES–KOH, pH 7.2, 10 mM magnesium acetate, 500 μg/mL creatine kinase.
25. 5× SDS-PAGE sample buffer: 60 mM Tris–HCl pH 6.8, 25 % glycerol, 2 % SDS, 5 % beta-mercaptoethanol, 0.1 % bromophenol blue.
26. Nitrocellulose or PVDF membrane for Western blotting.
27. Anti-GST antibody (Santa Cruz).

3 Methods

Many proteins required for cell cycle progression are targeted for degradation at specific times in the cell cycle, presumably to prevent activity at sensitive times during cell division. Other proteins are

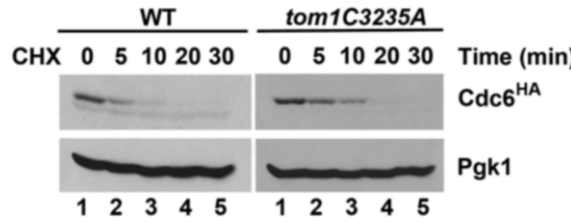

Fig. 1 The catalytic activity of the Tom1 E3 ubiquitin ligase is required for Cdc6 turnover. Wild-type and *tom1C3235A* strains arrested with alpha factor were used in protein stability assays. Samples were collected at indicated times after cycloheximide (CHX) addition. Pgk1 was used as a loading control. Modified from [34]

unstable throughout the cell cycle, but the rate of degradation fluctuates with cell cycle stage. For example, the ATPase Cdc6, which is required to load the MCM replicative helicase complex onto replication origins [30, 31], exhibits a markedly shorter half-life during the G1-to-S phase transition than during other parts of the cell cycle [32].

In this section, we describe the use of protein stability assays to evaluate whether a protein is degraded in a cell cycle-dependent manner. Observing protein turnover requires examining a population of protein that cannot be replenished by new synthesis. A simple approach to accomplish this is to treat cells with the translation inhibitor cycloheximide. Because cycloheximide will inhibit all protein synthesis and cell cycle progression, when examining the effect of cell cycle dependence on protein stability, cell cycle synchronization must be performed prior to the addition of the drug so that any inherent differences in cell cycle distribution in the strains do not affect the interpretation of the results.

Figure 1 exhibits the turnover of the Cdc6 protein during G1 phase in wild-type cells as well as in a strain in which the catalytic cysteine in the *TOM1* gene is defective (*tom1 C3235A*). Tom1 is a HECT domain ubiquitin ligase [33]. As shown, Cdc6 turnover is inhibited in the *tom1 C3235A* cells in this assay. Pgk1 is a stable protein that is used as a loading control. These results indicate that the catalytic function of Tom1 is important for the normal degradation of Cdc6. As Tom1 functions as an E3 ubiquitin ligase, these results suggest that Tom1 may be responsible for the ubiquitin-mediated degradation of Cdc6 in G1.

3.1 Protein Stability Assays

1. Inoculate 5 mL YPD with *S. cerevisiae* cells. Grow overnight at 30 °C with rotation or shaking.
2. Prepare a 1:20 dilution of culture (50 μL in 950 μL water), and use 10 μL of dilution to count cells in a hemacytometer.
3. Adjust cell density to 5×10^6 cells/mL in 25 mL of YPD. Incubate at 30 °C with shaking for 2–4 h until cell density reaches $1–2 \times 10^7$ cells/mL.

4. Perform cell cycle arrest as desired (*see* **Note 3**).
5. Add cycloheximide to the culture at a final concentration of 100 μg/mL. Immediately take out 5 mL aliquot for the first time point and transfer to a 15 mL conical tube.
6. Pellet cells for 2 min at 3,220 × *g*. Aspirate supernatant, and store cells on ice (*see* **Note 4**).
7. Continue to take aliquots for each desired time point, and pellet as described in **step 6**.
8. Add 2 mL of 20 % TCA to each pellet, vortex to resuspend the cells, and then pellet cells as described in **step 6**.
9. Aspirate supernatant, and resuspend pellet in 50 μL of 20 % TCA.
10. Transfer suspension to 2 mL screw-cap tubes with attached cap. Add 50 μL of glass beads, and vortex for 3–4 min at 4 °C (*see* **Note 5**).
11. Pellet at 835 × *g* for 10 min in a microfuge (*see* **Note 6**). Aspirate supernatant.
12. Add 50 μL sterile water, 20 μL 5× SDS sample buffer, and 30 μL 1 M Tris base to the pellet, and resuspend by vortexing. If the color of suspension is orange or yellow, continue to add water, 5× SDS sample buffer, and Tris base in the same proportions until suspension turns blue or purple.
13. Heat samples at 95 °C for 5 min, and then spin samples for 2 min at 835 × *g* in a microfuge.
14. Use RC DC Protein Assay kit to determine protein concentration of samples (*see* **Note 7**).
15. Load equal protein amounts for each sample on a 10 % SDS-PAGE gel.
16. Transfer proteins to nitrocellulose or PVDF membrane for Western blotting.
17. Perform Western blotting (*see* **Note 8**). Anti-Pgk1 antibodies are used to determine if equal protein was loaded in each sample. After probing with the antibody for the protein of interest, the blot may be re-probed with the anti-Pgk1 antibodies or the blot may be cut if the protein of interest is of significantly different size than Pgk1.

3.2 Immunoprecipitation of Ubiquitin-Conjugated Proteins

To determine if a ubiquitin ligase is required for the ubiquitination of a cell cycle protein, the generation of ubiquitin conjugates established in vivo or in vitro can be examined. The next two methods in this chapter outline approaches to examine in vivo or in vitro ubiquitination of a substrate protein.

The advantage of examining in vivo conjugates is that they are physiological and are not the result of a promiscuous ligase in an in vitro reaction. However, these conjugates are often very labile

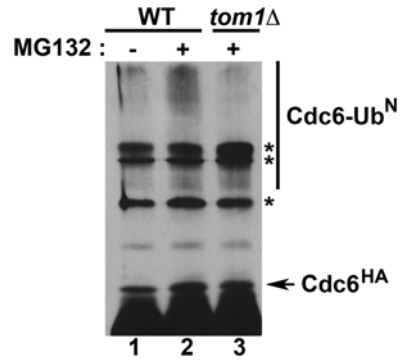

Fig. 2 Cdc6 ubiquitination is dependent on Tom1. Wild-type and *tom1*Δ strains were arrested with 200 mM hydroxyurea for 3 h and treated with DMSO (–) or 20 mM MG132 (+) for 5 h. Cdc6 protein was immunoprecipitated and visualized by immunoblot assays with anti-HA antibodies. The *asterisks* indicate nonspecific bands

and difficult to detect. To maximize the recovery of ubiquitinated proteins, cells are treated with the proteasome inhibitor MG132 and immunoprecipitation is used. Because ubiquitin conjugates are a heterogeneous mix of long and short chains, the ubiquitinated species are typically observed as a smear in the gel lane. As shown in Fig. 2, the presence of Cdc6 ubiquitin conjugates (or smear) is enhanced in the wild-type strain when MG132 is added. In contrast, substantially fewer Cdc6 ubiquitin conjugates are isolated from cells lacking the *TOM1* gene (*tom1*Δ), even though MG132 was added to the cells. These results indicate that Tom1 is required for the efficient formation of ubiquitin conjugates on Cdc6.

1. Prepare a log-phase culture of *S. cerevisiae* cells as described in Subheading 3.1.
2. Add MG132 to a final concentration of 50 μM, and incubate for 2 h (*see* **Note 9**).
3. Collect cells in a 50 mL conical tube, and spin for 2 min at 3,220×*g*.
4. Aspirate supernatant, and resuspend cells in 250 μL of RIPA lysis buffer containing 1× protease inhibitor cocktail. Transfer cell suspension to 2 mL screw-cap tubes.
5. Add 50 μL of glass beads, and vortex for 40 min at 4 °C.
6. Puncture a hole in the bottom of the tube with a 25 gauge hot needle.
7. Place the tube in a 5 mL centrifuge tube, and spin at 200×*g* for 1 min at 4 °C to collect the cell lysate in the 5 mL centrifuge tube.
8. Transfer the cell lysate in the 5 mL tube to a new microcentrifuge tube.

9. Spin samples at top speed in a microfuge for 15 min at 4 °C.
10. Transfer supernatant to a new microcentrifuge tube.
11. Determine the protein concentration using Bio-Rad protein assay.
12. Set up new microfuge tubes with 1–2 mg total protein. Adjust the volumes to equal concentration using RIPA lysis buffer with 1× protease inhibitor cocktail.
13. Add 1 μL of antibody against a protein of interest (e.g., anti-HA antibody for immunoprecipitation of HA-tagged Cdc6). Incubate with rotation at 4 °C overnight.
14. Add 20 μL of protein A/G agarose (previously washed with 10 volumes of lysis buffer plus protease inhibitors), and rotate at 4 °C for 1–2 h.
15. Pellet beads by spinning at 2,138 × *g* for 30 s in a microfuge. Aspirate supernatant, and wash three times with equal volume of lysis buffer containing protease inhibitors (*see* **Note 10**).
16. Resuspend beads in 20 μL of lysis buffer containing protease inhibitors, and add 5 μL of 5× SDS-PAGE sample buffer. Incubate samples at 95 °C for 5 min.
17. Load equal volumes for each sample on a 10 % SDS-PAGE gel.
18. Transfer proteins to nitrocellulose or PVDF membrane for Western blotting.
19. Perform Western blotting using anti-Ubiquitin antibody at 1:1,000 dilution (*see* **Note 8**).

3.3 In Vitro Ubiquitination Assays

Another approach to determine whether a ubiquitin ligase is required for the formation of ubiquitin conjugates on a substrate protein is to use an in vitro ubiquitination assay. This approach requires significant amounts of substrate protein, E1 and E2 enzymes, as well as ubiquitin. Thus, it is best to have access to recombinant protein or the ability to generate recombinant protein, particularly for the substrate protein. E1 and E2 enzymes, as well as ubiquitin, are commercially available. These proteins are mixed together with fractionated yeast extracts, which serve as the source for E3 enzymes, and ATP to promote the formation of ubiquitin conjugates on the substrate protein. With budding yeast, it is possible to make extracts from ubiquitin ligase mutants to determine if the ligase is important for the formation of ubiquitin conjugates on the substrate. As shown in Fig. 3, ubiquitin conjugates are observed on Cdc6 when wild-type cell extract is mixed with all reagents but reduced in the absence of E1 and E2. In contrast, Cdc6 ubiquitin conjugates are reduced in *tom1*Δ extracts, despite the addition of E1 and E2.

A primary advantage of the in vitro system is that the ubiquitination reaction can be modified by changes in incubation

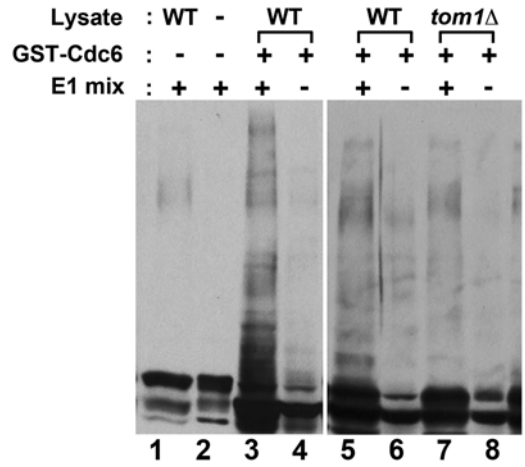

Fig. 3 In vitro ubiquitination of Cdc6. GST-Cdc6 protein expressed from baculovirus-infected insect cells was purified using glutathione-sepharose 4B beads. GST-Cdc6 protein was incubated with ubiquitin, E1, E2, ATP, an ATP regeneration system (Energy Mix), and fractionated yeast extracts purified from wild type or *tom1*Δ at 30 °C for 45 min. Samples were run on 6 % SDS-PAGE and immunoblotted with anti-GST antibodies

time, temperature, or amount of yeast extract to give the maximal ubiquitin conjugates on the substrate protein. The protocol given below outlines a standard assay that can be easily modified for specific situations.

1. Prepare 2 L culture of *S. cerevisiae* cells. Inoculate 50 mL YPD with *S. cerevisiae* cells and grow overnight at 30 °C. When cell density reaches $O.D._{600}$ of at least 1.0, add the culture to 2 L of YPD and continue to grow until $O.D._{600}$ reaches 1.0.
2. Collect cells in 500 mL centrifuge bottles, and pellet cells at 3,800 × *g* at 4 °C for 5 min.
3. Decant supernatant. Wash cells twice with 100 mL sterile water. Vortex to resuspend, and pellet cells as in **step 2**.
4. Decant supernatant. Resuspend the pellet in 50 mL of predigestion buffer and transfer to a conical tube. Incubate at room temperature for 15 min with rocking.
5. Pellet cells by spinning for 2 min at 3,220 × *g* and wash with an equal volume of sterile water. Vortex to resuspend, and pellet cells as before.
6. Aspirate supernatant. Determine the weight of cells using an empty tube to tare the balance.
7. Resuspend cells in 50 mL of digestion buffer, and add 1 g of Zymolyase 20T per gram of cells. Vortex to mix, and incubate with rocking at room temperature for 30–45 min.

8. Pellet cells as in **step 5**, and aspirate supernatant. Wash cells with 500 mL 1 M sorbitol and pellet as before.
9. Decant supernatant, and resuspend cells in 20 mL 1 M sorbitol. Gently layer the cell suspension onto a 400 mL cushion of 2 M sorbitol in a centrifuge bottle.
10. Spin cells through the sorbitol cushion for 5 min at 3,800 × *g* at 4 °C. Gently decant supernatant, and resuspend cells in 1 pellet volume of cold YEB (prepare only the volume that is needed, DTT added fresh each time).
11. Cool mortar and pestle with liquid nitrogen. Add liquid nitrogen half way to the top of mortar. Add cell suspension drop by drop to the liquid nitrogen. As liquid nitrogen evaporates, tap cell pellets to break and grind into powder. Add liquid nitrogen periodically to keep cold. Continue until all of the cell suspension has been ground into a powder.
12. Use a plastic spoon to transfer powder to a conical tube, and store at –80 °C.
13. Thaw cell lysate powder in ice bath.
14. Transfer lysate to ultracentrifuge tubes and spin at 541,000 × *g* at 4 °C for 30 min.
15. Transfer supernatant to a fresh tube.
16. Desalt on a Bio-Gel P-6DG desalting column. To prepare a column, soak Bio-Gel in sterile water overnight. Transfer three sample volumes of Bio-Gel to an empty column (e.g., if you have 10 mL cell lysate, load 30 mL Bio-Gel on column). Allow Bio-Gel to settle by gravity. Equilibrate column with 10 bed volumes of YEB. Load lysate onto the column.
17. Elute with 3 sample volumes of desalting buffer (prepare only the volume that is needed, DTT added fresh each time). Collect the last 2.5 volumes.
18. Centrifuge lysate at 11,000 × *g* at 4 °C for 30 min.
19. Transfer supernatant to a fresh tube (*see* **Note 11**).
20. Fractionate lysate on DEAE column. Prepare column by loading sufficient volume of DEAE Sephacel onto an empty column to give a 5 mL bed volume. Allow beads to settle by gravity. Equilibrate the column with 50 mL of desalting buffer.
21. Elute with four applications of 5 mL elution buffer. Collect each elution volume in a separate tube.
22. Measure protein concentration of each elution volume using Bio-Rad protein assay.
23. Combine elutions with maximum protein concentrations, and concentrate samples to 10–40 mg/mL using Centricon con-

centrators. Concentrated extracts may be flash frozen in liquid nitrogen and stored at –80 °C.

24. Prepare ubiquitination reactions by mixing 40 μg GST-Cdc6 (substrate protein) with 50 μg ubiquitin, 12 ng E1, 1.5 μg E2, 10 mM ATP, 1× EM, and 50 μg fractionated yeast extract. Use sterile water to bring the reaction volume to 20 μL. Incubate reactions at 30 °C for 45 min.
25. Add 5 μL of 5× SDS-PAGE sample buffer. Incubate samples at 95 °C for 5 min.
26. Load equal volumes for each sample on 10 % SDS-PAGE gel.
27. Transfer proteins to nitrocellulose or PVDF membrane for Western blotting.
28. Perform Western blotting using anti-GST antibody at 1:1,000 dilution (*see* **Note 8**).

4 Notes

1. If using a large amount of alpha factor, it is often more economical to have it synthesized by a peptide synthesis company.
2. We used GST-Cdc6 expressed and purified from insect cells using glutathione-Sepharose (GE Healthcare Life Sciences). Protein still bound to beads was added directly to ubiquitination reactions to reduce loss of the recombinant protein that may happen with elution. Insect cell expression systems have the advantage that posttranslational modifications, which may be necessary for ubiquitination, are often conserved.
3. Cell cycle arrests are performed as follows: (a) Alpha factor (if the strain is not defective for the *BAR1* gene): Transfer cells to YPD pH 3.9 medium, add 40 μL of 5 mg/mL alpha factor per 10 mL of culture, and after 1 h, add an additional 20 μL of alpha factor every 30 min until 90 % of cells exhibit shmoo morphology. Most strains reach this stage in 2–3 h. If the strain is defective for *BAR1*, regular YPD may be used and a final concentration of 5 μM alpha factor is sufficient to arrest 90 % of cells in 2–3 h. Strains must be mating type **a** for alpha factor arrest. (b) HU: Add HU to culture to give a final concentration of 200 mM. Incubate for 2–3 h until 90 % of cells are budded. (c) Nocodazole: Add nocodazole to culture to give a final concentration of 15 μg/mL. Incubate for 2–3 h until 90 % of cells are large budded. If necessary, a brief sonication pulse (2 s, 20 % output) can break up clumps of cells without lysing them to distinguish buds.
4. Flash freezing cell aliquots in liquid nitrogen and storing them at –80 °C prior to TCA precipitation can reduce nonspecific protein degradation.

5. To measure glass beads, we use a cutoff microfuge tube attached to a Pasteur pipet.
6. Separating the glass beads from the lysate by poking a hole in the bottom of the lysis tube with a hot needle and performing a 1-min spin at 200 × *g* prior to the 10-min centrifugation of the lysed cells prevents accidental pipetting of glass beads in later steps (*see* Subheading 3.2, **steps 6–8**).
7. We use the manufacturer's directions for micro samples, but use only 5 μL of the protein sample instead of 25 μL.
8. We block the membrane in PBST + 5 % nonfat dry milk for 20 min at room temperature prior to incubating with primary antibody (e.g., anti-HA at 1:1,000 dilution) in PBST + 5 % milk overnight at 4 °C. Wash membrane at least three times in PBST for 20–30 min each time. Secondary antibody incubation (e.g., HRP-conjugated anti-mouse at 1:5,000) in PBST + 5 % milk is for 1 h at room temperature followed by washing in PBST as after primary antibody.
9. MG132 inhibition works best in strains bearing deletions of the *RPN4* and *PDR5* genes to reduce new proteasome synthesis and export of the drug from the cells. Deletion strains are available from ATCC, Invitrogen, Open Biosystems, and EUROSCARF.
10. It is important to remove as much supernatant as possible without losing beads. We use a 0.25 mm diameter gel-loading tip attached to an aspirator. These tips can be inserted into the bead pellet without losing significant volume.
11. Crude yeast extracts may be concentrated and used in ubiquitination assays in Subheading 3.3, **step 25**, although a proteasome inhibitor such as MG132 should be added to these assays.

Acknowledgements

This work was supported in part by NIH grant GM076663 (D.M.K.).

References

1. Holloway SL, Glotzer M, King RW, Murray AW (1993) Anaphase is initiated by proteolysis rather than by the inactivation of maturation-promoting factor. Cell 73(7):1393–1402
2. Won KA, Reed SI (1996) Activation of cyclin E/CDK2 is coupled to site-specific autophosphorylation and ubiquitin-dependent degradation of cyclin E. EMBO J 15(16):4182–4193
3. Diehl JA, Zindy F, Sherr CJ (1997) Inhibition of cyclin D1 phosphorylation on threonine-286 prevents its rapid degradation via the ubiquitin-proteasome pathway. Genes Dev 11(8):957–972
4. Schneider BL, Yang QH, Futcher AB (1996) Linkage of replication to start by the Cdk inhibitor Sic1. Science 272(5261):560–562

5. Pagano M, Tam SW, Theodoras AM, Beer-Romero P, Del Sal G, Chau V, Yew PR, Draetta GF, Rolfe M (1995) Role of the ubiquitin-proteasome pathway in regulating abundance of the cyclin-dependent kinase inhibitor p27. Science 269(5224):682–685
6. Scheffner M, Werness BA, Huibregtse JM, Levine AJ, Howley PM (1990) The E6 oncoprotein encoded by human papillomavirus types 16 and 18 promotes the degradation of p53. Cell 63(6):1129–1136
7. Hofmann F, Martelli F, Livingston DM, Wang Z (1996) The retinoblastoma gene product protects E2F-1 from degradation by the ubiquitin-proteasome pathway. Genes Dev 10(23):2949–2959
8. Hateboer G, Kerkhoven RM, Shvarts A, Bernards R, Beijersbergen RL (1996) Degradation of E2F by the ubiquitin-proteasome pathway: regulation by retinoblastoma family proteins and adenovirus transforming proteins. Genes Dev 10(23): 2960–2970
9. Michael WM, Newport J (1998) Coupling of mitosis to the completion of S phase through Cdc34-mediated degradation of Wee1. Science 282(5395):1886–1889
10. Hershko A, Heller H, Elias S, Ciechanover A (1983) Components of ubiquitin-protein ligase system. Resolution, affinity purification, and role in protein breakdown. J Biol Chem 258(13):8206–8214
11. Wilkinson KD, Urban MK, Haas AL (1980) Ubiquitin is the ATP-dependent proteolysis factor I of rabbit reticulocytes. J Biol Chem 255(16):7529–7532
12. Ciechanover A, Elias S, Heller H, Hershko A (1982) "Covalent affinity" purification of ubiquitin-activating enzyme. J Biol Chem 257(5):2537–2542
13. Teixeira LK, Reed SI (2013) Ubiquitin ligases and cell cycle control. Annu Rev Biochem 82:387–414
14. King RW, Peters JM, Tugendreich S, Rolfe M, Hieter P, Kirschner MW (1995) A 20S complex containing CDC27 and CDC16 catalyzes the mitosis-specific conjugation of ubiquitin to cyclin B. Cell 81(2):279–288
15. Sudakin V, Ganoth D, Dahan A, Heller H, Hershko J, Luca FC, Ruderman JV, Hershko A (1995) The cyclosome, a large complex containing cyclin-selective ubiquitin ligase activity, targets cyclins for destruction at the end of mitosis. Mol Biol Cell 6(2):185–197
16. Cohen-Fix O, Peters JM, Kirschner MW, Koshland D (1996) Anaphase initiation in *Saccharomyces cerevisiae* is controlled by the APC-dependent degradation of the anaphase inhibitor Pds1p. Genes Dev 10(24): 3081–3093
17. McGarry TJ, Kirschner MW (1998) Geminin, an inhibitor of DNA replication, is degraded during mitosis. Cell 93(6):1043–1053
18. Carrano AC, Eytan E, Hershko A, Pagano M (1999) SKP2 is required for ubiquitin-mediated degradation of the CDK inhibitor p27. Nat Cell Biol 1(4):193–199
19. Skowyra D, Craig KL, Tyers M, Elledge SJ, Harper JW (1997) F-box proteins are receptors that recruit phosphorylated substrates to the SCF ubiquitin-ligase complex. Cell 91(2):209–219
20. Feldman RM, Correll CC, Kaplan KB, Deshaies RJ (1997) A complex of Cdc4p, Skp1p, and Cdc53p/cullin catalyzes ubiquitination of the phosphorylated CDK inhibitor Sic1p. Cell 91(2):221–230
21. Skowyra D, Koepp DM, Kamura T, Conrad MN, Conaway RC, Conaway JW, Elledge SJ, Harper JW (1999) Reconstitution of G1 cyclin ubiquitination with complexes containing SCFGrr1 and Rbx1. Science 284(5414):662–665
22. Koepp DM, Schaefer LK, Ye X, Keyomarsi K, Chu C, Harper JW, Elledge SJ (2001) Phosphorylation-dependent ubiquitination of cyclin E by the SCFFbw7 ubiquitin ligase. Science 294(5540):173–177
23. Strohmaier H, Spruck CH, Kaiser P, Won KA, Sangfelt O, Reed SI (2001) Human F-box protein hCdc4 targets cyclin E for proteolysis and is mutated in a breast cancer cell line. Nature 413(6853):316–322
24. Moberg KH, Bell DW, Wahrer DC, Haber DA, Hariharan IK (2001) Archipelago regulates Cyclin E levels in Drosophila and is mutated in human cancer cell lines. Nature 413(6853):311–316
25. Ayad NG, Rankin S, Murakami M, Jebanathirajah J, Gygi S, Kirschner MW (2003) Tome-1, a trigger of mitotic entry, is degraded during G1 via the APC. Cell 113(1):101–113
26. Piotrowski J, Beal R, Hoffman L, Wilkinson KD, Cohen RE, Pickart CM (1997) Inhibition of the 26S proteasome by polyubiquitin chains synthesized to have defined lengths. J Biol Chem 272(38):23712–23721
27. Finley D (2009) Recognition and processing of ubiquitin-protein conjugates by the proteasome. Annu Rev Biochem 78:477–513
28. Tomko RJ Jr, Hochstrasser M (2013) Molecular architecture and assembly of the eukaryotic proteasome. Annu Rev Biochem 82:415–445

29. Hershko A, Ciechanover A (1998) The ubiquitin system. Annu Rev Biochem 67:425–479
30. Donovan S, Harwood J, Drury LS, Diffley JF (1997) Cdc6p-dependent loading of Mcm proteins onto pre-replicative chromatin in budding yeast. Proc Natl Acad Sci U S A 94(11):5611–5616
31. Tanaka T, Knapp D, Nasmyth K (1997) Loading of an Mcm protein onto DNA replication origins is regulated by Cdc6p and CDKs. Cell 90(4):649–660
32. Drury LS, Perkins G, Diffley JFX (2000) The cyclin-dependent kinase Cdc28p regulates distinct modes of Cdc6p proteolysis during the budding yeast cell cycle. Curr Biol 10(5): 231–240
33. Saleh A, Collart M, Martens JA, Genereaux J, Allard S, Cote J, Brandl CJ (1998) TOM1p, a yeast hect-domain protein which mediates transcriptional regulation through the ADA/SAGA coactivator complexes. J Mol Biol 282(5):933–946
34. Kim DH, Zhang W, Koepp DM (2012) The hect domain E3 ligase Tom1 and the F-box protein Dia2 control Cdc6 degradation in G1 phase. J Biol Chem 287(53):44212–44220

Chapter 18

Imaging Analysis of Cell Cycle-Dependent Degradation of Cdt1 in Mammalian Cells

Yasushi Shiomi, Naohiro Suenaga, Miyuki Tanaka, Akiyo Hayashi, and Hideo Nishitani

Abstract

Numerous cell cycle-regulating proteins are controlled by protein degradation. Recent work shows that ubiquitination-dependent proteolysis plays an important role in once-per-cell cycle control of DNA replication. Cdt1 is a licensing factor essential for assembling the pre-replicative complex on replication origins. Cdt1 is present in G1 phase, but after S phase ubiquitin-mediated proteolysis maintains Cdt1 at low levels. This is important to prevent the re-replication of chromosomal DNA. The cell cycle-dependent degradation of Cdt1 can be monitored by dual staining of the cell nuclei with antibodies against Cdt1- and S/G2-phase marker proteins, such as cyclin A or geminin.

Key words Ubiquitin, Proteolysis, DNA replication licensing, Cdt1, Cyclin A, Geminin, $CRL4^{Cdt2}$, SCF^{Skp2}

1 Introduction

Periodic activation of cyclin-dependent kinases (CDKs) globally regulates the process by which chromosome duplication and subsequent sister-chromatid separation are faithfully performed during the cell cycle [1]. This regulation is achieved by controlling protein levels; inactivation of CDKs is accomplished by proteolysis of cyclin proteins in a ubiquitination-mediated process. Similarly, many cell cycle-regulating proteins are controlled by protein degradation during the cell cycle, ensuring that cellular events are spatially and temporarily coordinated [2, 3]. DNA replication is one of the major events in the cell cycle. To maintain genome integrity, chromosomal DNA must be correctly replicated in S phase, before entering mitosis. Furthermore, a control called *DNA replication licensing* ensures that no segment of DNA undergoes replication more than once in the same cycle [4–6]. Much work has been done to understand the replication licensing, and recent work demonstrates that ubiquitination-mediated proteolysis plays an essential role in this

Eishi Noguchi and Mariana C. Gadaleta (eds.), *Cell Cycle Control: Mechanisms and Protocols*, Methods in Molecular Biology, vol. 1170, DOI 10.1007/978-1-4939-0888-2_18,

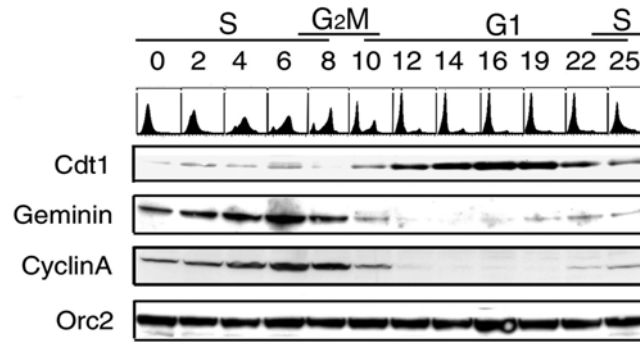

Fig. 1 Cdt1 expression during the cell cycle. Synchronized culture of HeLa cells was prepared after double-thymidine block. Cells in early S phase (0 h) were released and sampled every 2 or 3 h for Western blotting. Cdt1 levels increase as cells progress into G1 phase; levels then decrease as cells enter S phase (about 22 h after release). In contrast, cyclin A and geminin are present during S and G2/M phases but are targeted for degradation during M to G1 phases by APC/C. Orc2 is present throughout the cell cycle and can be used as a loading control. Adapted from Nishitani et al. [7] with permission

control. Cdt1 is one of the licensing factors, and its tight control is critical for once-per-cell cycle control of DNA replication. Cdt1 is present in G1 phase but is absent from the S phase to the G2/M phases because ubiquitin-mediated proteolysis regulates Cdt1 levels during the cell cycle (Fig. 1) [7]. In addition, Cdt1 is inactivated by binding to its inhibitor, geminin [8, 9].

Replication origins, bound by the origin recognition complex (ORC), are licensed for replication by assembly of the pre-replicative complex (pre-RC) at the end of mitosis and in the early G1 phase before S-CDK is activated. To assemble the pre-RC, Cdc6 and Cdt1 associate with ORC and then assist chromatin loading of the MCM2-7 complex [4–6]. MCM2-7 is a DNA helicase; however, it is inactive in G1 phase. Activation of pre-RC by the protein kinases S-CDK and DDK (Dbf4-dependent protein kinase) leads to origin firing and initiation of DNA replication. At this point, other essential replication factors, such as Cdc45 and GINS, associate with MCM2-7 to form an active helicase complex. This complex, which is termed the CMG complex, travels along the DNA at the head of the replication fork [10, 11]. At the same time, the origin shifts to a post-replicative state and cannot be licensed again owing to Cdt1 proteolysis after the onset of S phase. Even if Cdt1 is still present, geminin is able to inhibit Cdt1 [8, 9]. Thus, even a single origin is not reused in the same cycle.

In ubiquitin–proteasome-mediated proteolysis, the target proteins are polyubiquitinated by the repeated action of the group of enzymes E1, E2, and E3. E1 is a ubiquitin-activating enzyme and transfers ubiquitin to a ubiquitin-conjugating enzyme, E2.

Ubiquitin is then transferred to the target protein from the E2 ubiquitin conjugate in a reaction mediated by a substrate-recognizing E3 ubiquitin ligase. E3 is important for the timely and rapid degradation of target proteins. Two major multicomplex E3 ubiquitin ligases that function during the cell cycle have been identified [2, 3]. The first is anaphase-promoting complex/cyclosome (APC/C), operating from M phase to G1 phase. This E3 is required for the metaphase-to-anaphase transition to degrade securin and cyclin B. The other is the SCF ubiquitin ligase, which is composed of Skp1, cullin 1 (Cul1), Rbx1, and the variable F-box subunit. SCF is also called cullin-ring ligase 1 (CRL1). Cul1 is a scaffold protein that assembles the complex; the F-box protein is a substrate-recognizing subunit; and Skp1 is an adaptor protein connecting Cul1 and F-box protein. Rbx1 transfers ubiquitin from E2 to the substrate. The best known SCF is SCF^{Skp2}, which regulates the G1/S transition by targeting the CDK inhibitor p27 for degradation, leading to the activation of S-CDK. p27 is phosphorylated on T187 by cyclin E/Cdk2 and recognized by Skp2, a phosphodegron-recognizing subunit of SCF^{Skp2} [2, 3, 12, 13].

SCF^{Skp2} also targets Cdt1 for degradation. Concomitant with the onset of S phase, cyclin A/Cdk2 is activated and phosphorylates Cdt1 on T29. This phosphorylation creates a binding site, namely, a phosphodegron, for SCF^{Skp2}, which polyubiquitinates Cdt1 [14–16]. In addition, Cdt1 is redundantly targeted by another E3 ubiquitin ligase, $CRL4^{Cdt2}$, during S phase [17–21]. $CRL4^{Cdt2}$ is composed of the scaffold protein Cul4, the adaptor protein DDB1, Rbx1, and the substrate receptor Cdt2. $CRL4^{Cdt2}$ ubiquitinates Cdt1 when Cdt1 associates with proliferating cell nuclear antigen (PCNA) on the chromatin. PCNA is a sliding clamp, originally identified as an accessory factor for DNA polymerase δ [22]. When DNA replication is initiated, PCNA is loaded on chromatin and functions as a scaffold for many proteins involved in chromosome duplication [23]. Most of these proteins contain PCNA interaction protein motifs (PIP boxes), which directly bind to PCNA. Cdt1 also has a PIP box at the N-terminus. In addition, Cdt1 has a basic amino acid at a position 4 downstream from the PIP box, PIP-x-x-x-B. Both the PIP box and the basic amino acid are essential for degradation of Cdt1, and the motif (PIP-x-x-x-B) is called PIP degron [24, 25]. Cdt2 is a WD40 repeat-containing protein, which is thought to recognize the specialized protein domain that is created by binding between the PIP degron of Cdt1 and PCNA. While the PCNA-mediated Cdt1 degradation by $CRL4^{Cdt2}$ is conserved from yeast cells to mammalian cells, the SCF^{Skp2}-dependent ubiquitination of Cdt1 appears to be specific to mammalian cells. This means that Cdt1 degradation is regulated redundantly in mammalian cells. Thus, only when both SCF^{Skp2} and $CRL4^{Cdt2}$ are knocked down does Cdt1 protein become stable in mammalian cells [20]. After DNA replication is completed and

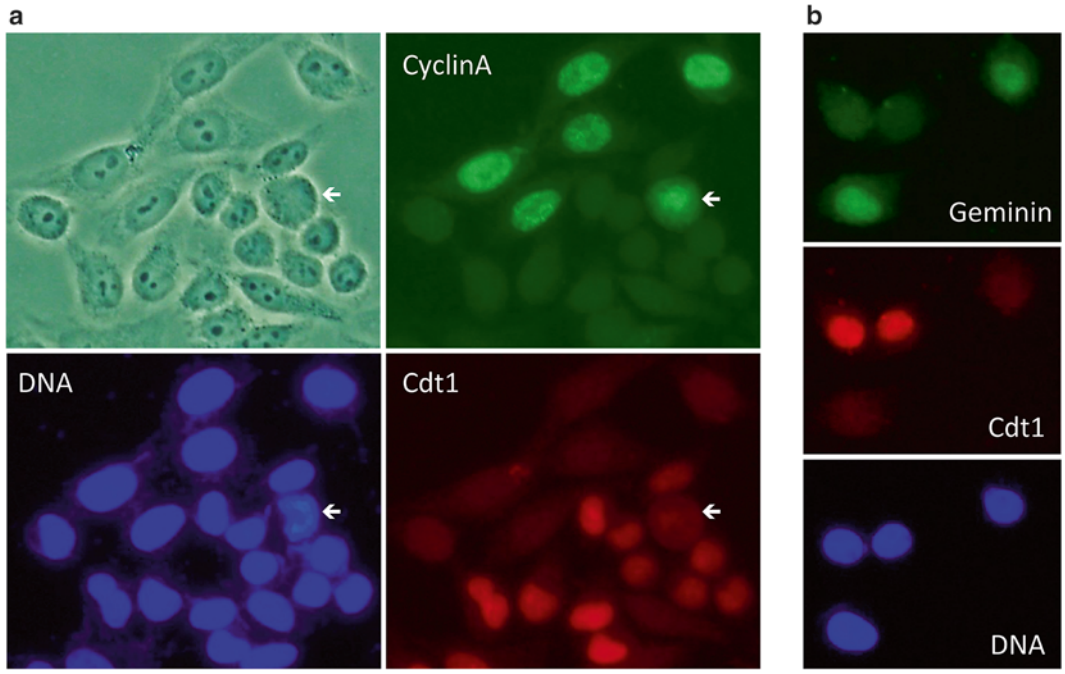

Fig. 2 Dual staining of asynchronous HeLa culture with antibodies against Cdt1 and cyclin A or geminin. (**a**) Both Cdt1 and cyclin A are localized in the nucleus, but they are present in different populations of cells. Cdt1 is detected in G1-phase cells but is absent in S–G2 (and early M) cells. Cyclin A is detected in the opposite manner. The cell labeled with an *arrow* is a mitotic cell. (**b**) Dual staining of Cdt1 and geminin

CDK is inactivated by degradation of cyclins during mitosis, ubiquitination activity on Cdt1 is turned off and Cdt1 levels again increase (Fig. 1).

In this chapter, we describe an immunostaining method needed to analyze the level of Cdt1 in asynchronous mammalian cell culture. Cdt1 is a nuclear protein that is present only in G1-phase cells. In contrast, S and G2 cells can be identified by staining with antibodies against cyclin A or geminin, which are also nuclear protein and present from the beginning of S phase until early M phase but are absent in late M phase and in G1 phase owing to APC/C-mediated proteolysis (Fig. 1). Dual staining with Cdt1 and cyclin A or geminin provides a simple method for analyzing a cell cycle-dependent degradation of Cdt1 [7, 20] (Fig. 2).

2 Materials

1. 35-mm Culture dish.
2. Glass cover slip, sterilized by baking in an oven at 180 °C for 2 h (*see* **Note 1**).
3. HeLa cells: Cultured in Dulbecco's modified Eagle's medium with 10 % fetal bovine serum supplemented with 100 units/mL

of penicillin and 0.1 mg/mL of streptomycin in a 5 % CO_2 atmosphere at 37 °C.

4. Phosphate-buffered saline (PBS): Dissolve 8 g of NaCl, 0.2 g of KCl, 1.44 g of Na_2HPO_4, and 0.24 g of KH_2PO_4 in 800 mL of H_2O. Adjust the pH to 7.4 with 1 N HCl. Add H_2O to 1 L.
5. 4 % Paraformaldehyde (PFA) (*see* **Note 2**): Dissolve 4 g PFA in about 90 mL PBS in a Pyrex or other appropriate containers with a stir bar. Heat to 60 °C, and add first 1 N and then 0.1 N NaOH dropwise until the solution becomes clear (*see* **Note 3**). Cool to room temperature. Adjust the pH to 7.4 with 0.1 N NaOH or 0.1 N HCl depending on the pH of the solution, and adjust the volume to 100 mL with PBS. Commercially available 4 % PFA phosphate buffer solution also works well.
6. PBS containing 0.25 % Triton X-100.
7. Pipette tip (200 μL) box with an empty tip holder (*see* **Note 4**): Used as a coverslip holder.
8. Blocking buffer: 3 % bovine serum albumin, 0.2 % Tween 20, and 0.02 % NaN_3 in PBS.
9. Primary antibodies and solution: Anti-Cdt1 antibody (rabbit, *see* **Note 5**), anti-cyclin A antibody (mouse, Thermo Scientific, Ab-6), and anti-geminin antibody (goat, Santa Cruz Biotechnology, N-19). Dilute anti-Cdt1 antibody at 1:200, anti-cyclin A antibody at 1:100, and anti-geminin antibody at 1:100 in blocking buffer.
10. Secondary antibodies and solution: For dual staining of Cdt1 and cyclin A: Alexa488-conjugated goat anti-mouse antibody and Alexa594-conjugated goat anti-rabbit antibody are diluted at 1:400 in blocking buffer. For dual staining of Cdt1 and geminin: Alexa488-conjugated donkey anti-goat antibody and Cy3-conjugated sheep anti-rabbit antibody are diluted at 1:400 in blocking buffer.
11. Hoechst solution: Stock solution (5–10 mg/mL Hoechst33258), dilute at 1 μg/mL in PBS for use.
12. Mounting medium: Vectashield Mounting Medium (VECTOR Laboratories) or equivalent.
13. Nail polish.
14. Fluorescence microscope.

3 Methods

Cdt1 is present throughout G1 phase; however, after the onset of S phase, Cdt1 is targeted for degradation by two independent E3 ubiquitin ligases in mammalian cells. The PIP box-dependent ubiquitination of Cdt1 by $CRL4^{Cdt2}$ is mediated by chromatin-bound

PCNA. Because PCNA is unloaded from chromatin in G2 phase, $CRL4^{Cdt2}$ operates only during S phase. In contrast, because cyclin A is present from G1/S phase to early M phase, SCF^{Skp2}-mediated degradation of Cdt1 operates for a longer period during the cell cycle. This implies that Cdt1 is degraded and not detected in cyclin A-expressing cells. Thus, when asynchronous cells are dually stained with antibodies for Cdt1 and cyclin A, both of which are nuclear proteins, they are detected in a mutually exclusive manner. Cells that are Cdt1 positive but cyclin A negative are identified as G1 cells, whereas cyclin A-positive but Cdt1-negative cells are identified as S-phase or G2/M-phase cells. This method provides a simple way to show Cdt1 degradation in a single cell during a cell cycle. In addition to cyclin A, the Cdt1 inhibitor geminin can be used as an S–G2/M-phase marker [7], because its levels are also controlled by APC/C, like cyclin A, in a cell cycle-dependent manner (Fig. 1). The combination of Cdt1 and cyclin A or geminin can also be used as a marker to follow the cell cycle position and was successfully used to develop a live imaging method, fluorescence ubiquitination cell cycle indicator (FUCCI), of the cell cycle by establishing a cell culture expressing mKO (Kusabira Orange)-tagged Cdt1 and GFP-tagged geminin [26].

1. Using sterile forceps, place a glass cover slip in a 35-mm tissue culture dish.
2. Plate the cell suspension into the dish ($1–2 \times 10^5$ HeLa cells in a 35-mm dish in a medium volume of 2 mL), let the cells adhere to the glass surface, and incubate for 1–2 days (*see* **Note 6**).
3. Remove the medium by aspiration, and wash the cover slip twice with PBS in the culture dish (*see* **Note 7**). All the steps hereafter are performed at room temperature unless otherwise indicated.
4. Fix cells in 4 % PFA solution for 10 min (*see* **Note 7**).
5. Wash the cover slip twice with PBS for 5 min each.
6. Permeabilize cells with PBS containing 0.25 % Triton X-100 for 2–3 min.
7. Wash cells three times with PBS for 5 min each.
8. Remove the cover slip from the dish (*see* **Note 8**), and place it on a pipette tip holder (*see* **Note 9**) with cell side up. Gently add 100 μL of blocking buffer to the 18 × 18 mm cover slip, and incubate for 1 h.
9. Remove blocking buffer (*see* **Note 10**).
10. Gently add 100 μL of primary antibody solution to the cover slip, and incubate for 1 h.
11. Wash three times for 5 min each with PBS (*see* **Note 11**). After the final wash, drain off the buffer (*see* **Note 10**).

12. Gently add 100 μL of secondary antibody solution, and incubate for 1 h (*see* **Note 12**).
13. Remove the secondary antibody solution.
14. (Optional) Add 100 μL of Hoechst 33258 solution (1 μg/mL), and incubate the cover slip for 5 min to stain DNA.
15. Wash three times for 5 min each with PBS, drain off buffer from the cover slip, and let it air-dry briefly.
16. Drop a mounting medium (approximately 5 μL) on a microscope slide, and place the cover slip on the mounting medium with the cell side down.
17. Seal cover slip with clear nail polish to prevent drying out and movement under microscope.
18. Store in the dark at 4 °C.

4 Notes

1. There are different sizes of cover slips. Either round (10–20 mm diameter) or square (18 × 18 mm) cover slips can be used. The thickness of cover slips is usually 0.12–0.17 mm. The steam autoclave is not suitable, because cover slips get stuck together.
2. PFA is very toxic. Work in the fume hood when preparing the solution. Do not inhale. Wear gloves.
3. Keep the solution at 60 °C in a water bath and be patient until the solution becomes clear.
4. Many tip manufacturers sell pipette tip refill systems. In these systems, the tip holder can be separated from the tip box. Flip the tip holder, and place it upside down on the tip box. We use this tip holder as a coverslip holder.
5. This antibody has been reported previously [7].
6. Let cells adhere to the cover slip at least for 20–24 h in a CO_2 incubator at an appropriate temperature, normally at 37 °C. Proper cell density is also critical for immunostaining. When cells are plated at a high density, cell proliferation may be compromised.
7. Washing and fixation of cells on the cover slip are performed in the culture dish by aspirating buffers from the dish and/or flooding the dish with solutions. Use caution when adding the solution. Flood slowly from the edge of the dish using a wide-mouth pipette. Do not add solution directly on the cells. For washing cells on a cover slip in a culture dish, put the dish on a shaker and gently shake. Keep the lid of the culture dish for the washing from **step 11**.

8. Remove the cover slip from the dish using fine-tipped forceps, and drain off the buffer by touching the edge of the cover slip on a paper towel.
9. We use a pipette tip rack as a coverslip holder. To keep the cover slips from drying up, put water in the bottom of the tip box and put the lid on.
10. Drain off the buffer by touching the edge of the cover slip on a paper towel.
11. Put the cover slips back into the lid of the culture dish for washing.
12. Be careful to use the right combination of secondary antibodies.

Acknowledgements

This work was financially supported by JSPS KAKENHI and MEXT KAKENHI, Grant in Aid from the Ministry of Education, Culture, Sports, Science, and Technology of Japan.

References

1. Nurse P (1994) Ordering S phase and M phase in the cell cycle. Cell 79(4):547–550
2. Nakayama KI, Nakayama K (2006) Ubiquitin ligases: cell-cycle control and cancer. Nat Rev Cancer 6(5):369–381
3. Petroski MD, Deshaies RJ (2005) Function and regulation of cullin-RING ubiquitin ligases. Nat Rev Mol Cell Biol 6(1):9–20
4. Bell SP, Dutta A (2002) DNA replication in eukaryotic cells. Annu Rev Biochem 71:333–374
5. Nishitani H, Lygerou Z (2002) Control of DNA replication licensing in a cell cycle. Genes Cells 7(6):523–534
6. Blow JJ, Dutta A (2005) Preventing re-replication of chromosomal DNA. Nat Rev Mol Cell Biol 6(6):476–486
7. Nishitani H, Taraviras S, Lygerou Z, Nishimoto T (2001) The human licensing factor for DNA replication Cdt1 accumulates in G1 and is destabilized after initiation of S-phase. J Biol Chem 276(48):44905–44911
8. Wohlschlegel JA, Dwyer BT, Dhar SK, Cvetic C, Walter JC, Dutta A (2000) Inhibition of eukaryotic DNA replication by geminin binding to Cdt1. Science 290(5500):2309–2312
9. Tada S, Li A, Maiorano D, Mechali M, Blow JJ (2001) Repression of origin assembly in metaphase depends on inhibition of RLF-B/Cdt1 by geminin. Nat Cell Biol 3(2):107–113
10. Ilves I, Petojevic T, Pesavento JJ, Botchan MR (2010) Activation of the MCM2-7 helicase by association with Cdc45 and GINS proteins. Mol Cell 37(2):247–258
11. Li Y, Araki H (2013) Loading and activation of DNA replicative helicases: the key step of initiation of DNA replication. Genes Cells 18(4):266–277
12. Carrano AC, Eytan E, Hershko A, Pagano M (1999) SKP2 is required for ubiquitin-mediated degradation of the CDK inhibitor p27. Nat Cell Biol 1(4):193–199
13. Tsvetkov LM, Yeh KH, Lee SJ, Sun H, Zhang H (1999) p27(Kip1) ubiquitination and degradation is regulated by the SCF(Skp2) complex through phosphorylated Thr187 in p27. Curr Biol 9(12):661–664
14. Li X, Zhao Q, Liao R, Sun P, Wu X (2003) The SCF(Skp2) ubiquitin ligase complex interacts with the human replication licensing factor Cdt1 and regulates Cdt1 degradation. J Biol Chem 278(33):30854–30858
15. Liu E, Li X, Yan F, Zhao Q, Wu X (2004) Cyclin-dependent kinases phosphorylate human Cdt1 and induce its degradation. J Biol Chem 279(17):17283–17288
16. Sugimoto N, Tatsumi Y, Tsurumi T, Matsukage A, Kiyono T, Nishitani H, Fujita M (2004) Cdt1 phosphorylation by cyclin A-dependent kinases negatively regulates its function with-

out affecting geminin binding. J Biol Chem 279(19):19691–19697

17. Higa LA, Wu M, Ye T, Kobayashi R, Sun H, Zhang H (2006) CUL4-DDB1 ubiquitin ligase interacts with multiple WD40-repeat proteins and regulates histone methylation. Nat Cell Biol 8(11):1277–1283
18. Jin J, Arias EE, Chen J, Harper JW, Walter JC (2006) A family of diverse Cul4-Ddb1-interacting proteins includes Cdt2, which is required for S phase destruction of the replication factor Cdt1. Mol Cell 23(5): 709–721
19. Arias EE, Walter JC (2006) PCNA functions as a molecular platform to trigger Cdt1 destruction and prevent re-replication. Nat Cell Biol 8(1):84–90
20. Nishitani H, Sugimoto N, Roukos V, Nakanishi Y, Saijo M, Obuse C, Tsurimoto T, Nakayama KI, Nakayama K, Fujita M, Lygerou Z, Nishimoto T (2006) Two E3 ubiquitin ligases, SCF-Skp2 and DDB1-Cul4, target human Cdt1 for proteolysis. EMBO J 25(5): 1126–1136
21. Senga T, Sivaprasad U, Zhu W, Park JH, Arias EE, Walter JC, Dutta A (2006) PCNA is a cofactor for Cdt1 degradation by CUL4/DDB1-mediated N-terminal ubiquitination. J Biol Chem 281(10):6246–6252
22. Prelich G, Tan CK, Kostura M, Mathews MB, So AG, Downey KM, Stillman B (1987) Functional identity of proliferating cell nuclear antigen and a DNA polymerase-delta auxiliary protein. Nature 326(6112):517–520
23. Moldovan GL, Pfander B, Jentsch S (2007) PCNA, the maestro of the replication fork. Cell 129(4):665–679
24. Havens CG, Walter JC (2009) Docking of a specialized PIP Box onto chromatin-bound PCNA creates a degron for the ubiquitin ligase CRL4Cdt2. Mol Cell 35(1):93–104
25. Michishita M, Morimoto A, Ishii T, Komori H, Shiomi Y, Higuchi Y, Nishitani H (2011) Positively charged residues located downstream of PIP box, together with TD amino acids within PIP box, are important for CRL4(Cdt2)-mediated proteolysis. Genes Cells 16(1):12–22
26. Sakaue-Sawano A, Kurokawa H, Morimura T, Hanyu A, Hama H, Osawa H, Kashiwagi S, Fukami K, Miyata T, Miyoshi H, Imamura T, Ogawa M, Masai H, Miyawaki A (2008) Visualizing spatiotemporal dynamics of multicellular cell-cycle progression. Cell 132(3): 487–498

Chapter 19

PCNA-Dependent Ubiquitination of Cdt1 and p21 in Mammalian Cells

Akiyo Hayashi, Naohiro Suenaga, Yasushi Shiomi, and Hideo Nishitani

Abstract

PCNA is a DNA clamp, acting on chromatin as a platform for various proteins involved in many aspects of DNA replication-linked processes. Most of these proteins have the PCNA-interaction protein motif (PIP box) that associates with PCNA. Recent works show that PCNA plays an important role as a matchmaker, connecting PCNA-interacting proteins to the ubiquitin ligase $CRL4^{Cdt2}$ for their degradation. Proteins degraded by $CRL4^{Cdt2}$ include Cdt1, p21, and Set8 in mammalian cells. These $CRL4^{Cdt2}$ substrates have a PIP degron that consists of the canonical PIP-box sequence and additional conserved amino acids required for ubiquitination. The degradation of these proteins is triggered when PCNA is loaded onto chromatin at the onset of S phase, and this process is important to prevent re-replication of DNA. These $CRL4^{Cdt2}$ substrates are also degraded through the same mechanism in response to DNA damage. In this chapter, we describe several approaches to investigate how PIP degron-containing proteins are degraded in a PCNA-dependent manner.

Key words Ubiquitin, Proteolysis, DNA replication, Chromatin, $CRL4^{Cdt2}$, PCNA, PIP degron, Cdt1, p21

1 Introduction

Proper progression of the cell cycle is driven by a controlled degradation of cell cycle-regulated proteins [1, 2]. The timely, specific, and rapid proteolysis is carried out by the ubiquitin–proteasome system. The target proteins are polyubiquitinated by the consecutive actions of a group of enzymes, E1 (ubiquitin-activating enzyme), E2 (ubiquitin-conjugating enzyme), and E3 (ubiquitin ligase), and are finally degraded by the 26S proteasome. The timely proteolysis during the cell cycle is normally dependent on the proper completion of a previous cell cycle event. For example, the polyubiquitination of securin by the APC/C^{Cdc20} for the separation of sister chromatids is activated when all kinetochores have been correctly attached to the mitotic spindles and all chromosomes are aligned on the metaphase plate. The ubiquitin–proteasome system

Eishi Noguchi and Mariana C. Gadaleta (eds.), *Cell Cycle Control: Mechanisms and Protocols*, Methods in Molecular Biology, vol. 1170, DOI 10.1007/978-1-4939-0888-2_19,

is also involved in the regulation of DNA replication. During each cell cycle, chromosomes are replicated once and only once before mitosis. Initiation of DNA replication is dependent on the prior formation of pre-replicative complex (pre-RC) on the replication origin, and this process is called origin licensing [3–5]. Replication origins are bound and marked by the origin recognition complex (ORC). Cdc6 and Cdt1 collaborate with ORC and load the MCM2-7 complex on origins, promoting pre-RC formation. MCM2-7 is a DNA helicase; however, it is inactive until it forms a complex with GINS and Cdc45 when S-CDK and DDK are activated [6, 7]. The resulting Cdc45–MCM2-7–GINS (CMG) complex acts as an active replicative DNA helicase, unwinds the double-helix DNA at the origin, and bidirectionally moves away from the origin, thereby functioning at the front of the replication fork for DNA synthesis. Once cells enter into S phase, licensing factors are inactivated, and thus origin licensing is inhibited. Therefore, by controlling the DNA replication licensing in the cell cycle, DNA is replicated precisely once in a cell cycle [8, 9].

Recent works demonstrated that PCNA coordinates $CRL4^{Cdt2}$-dependent polyubiquitination and degradation of Cdt1 in order to prevent re-replication of chromosomal DNA [10, 11]. PCNA, which forms a homo-trimeric ring-shaped complex and belongs to the family of DNA sliding clamps, encircles double-stranded DNA and slides freely along it. PCNA was originally identified as a cofactor for DNA polymerases [7, 12]. When DNA replication is initiated, the DNA polymerase α/primase complex synthesizes the primer, and PCNA is loaded at the end of the primer by a clamp loader, the replication factor C (RFC) complex. PCNA tethers DNA polymerases and enhances their processivity. PCNA is involved not only in DNA replication but also in many replication-linked processes. These processes include chromatin assembly and remodeling, epigenetic inheritance, sister-chromatid cohesion, and DNA damage repair. Therefore, PCNA acts as a platform that recruits and orchestrates the crucial players on the chromatin [13]. Many of these proteins have a PCNA-interaction motif called the PIP box (Q-x-x-[I/L/M/V]-x-x-[F/Y]-[F/Y]), which docks into a hydrophobic pocket of PCNA [14]. The replication-licensing factor Cdt1 also has a PIP box at the N-terminal end. However, in contrast to other PCNA-interacting proteins, PIP box-dependent interaction of Cdt1 with the chromatin-bound PCNA in S phase leads to Cdt1 degradation, which contributes to inhibition of origin licensing and thus prevention of re-replication [15–17]. This Cdt1 degradation is dependent on the ubiquitin ligase $CRL4^{Cdt2}$. Cullin ring ligase 4 (CRL4) is composed of Cul4, DDB1, and Rbx1. Cdt2 is a WD40-repeat protein thought to function as a substrate receptor of CRL4. Cdt1, in addition to the canonical PIP-box sequence, has TD amino acids within the PIP box and basic residue four amino acids downstream of the

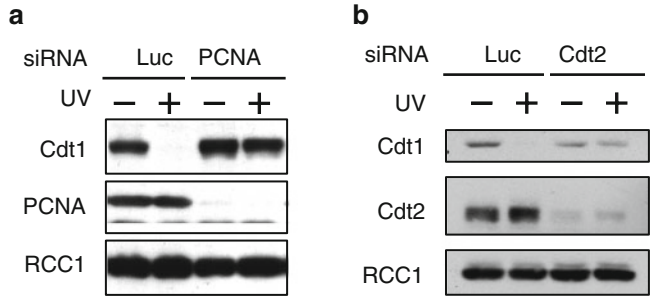

Fig. 1 PCNA and Cdt2 are required for Cdt1 degradation after UV irradiation. (**a**) HeLa cells were transfected with siRNA for PCNA or control siRNA. Cells were incubated for 3 days and were irradiated with UV at 50 J/m^2 (+) or not (–). Thirty minutes post-UV irradiation, cells were collected for Western blotting. (**b**) Same experiment was done with siRNA for Cdt2. RCC1 was used as a loading control

PIP box (Q-x-x-[I/L/M/V]-T-D-[F/Y]-[F/Y]-x-x-x-B, called PIP degron, a degradation signal) [18, 19]. In the case of human Cdt1, a basic residue three amino acid downstream of the PIP box is also required for efficient degradation of Cdt1 [19]. Cdt2 recognizes the PIP degron presented on the chromatin-bound PCNA. However, it is not known why only the chromatin-bound PCNA, but not the free PCNA, is capable of supporting CRL4^{Cdt2} activity.

The CRL4^{Cdt2}-mediated degradation of Cdt1 is also triggered by DNA damage following genotoxic stresses such as UV irradiation (Fig. 1) and the alkylating agent methyl methanesulfonate and is associated with DNA damage repair processes [20–24]. UV irradiation induces the formation of cyclobutane pyrimidine dimers and 6-4 photoproducts. These helix-distorting DNA damages are repaired by the nucleotide excision repair (NER). The NER accompanies the chromatin loading of PCNA for repair synthesis, and chromatin-bound PCNA appears to be connected to the rapid degradation of Cdt1 [25, 26].

Since the discovery of the PCNA-dependent proteolysis of Cdt1, additional targets of CRL4^{Cdt2} have been identified. These include the p21 CDK inhibitor and the Set8/PR-Set7 monomethyltransferase in mammalian cells [27–34]. Similar to Cdt1, both p21 and Set8/PR-Set7 have a PIP degron, which confer both S phase- and DNA damage-specific degradation of these proteins (Fig. 2a). However, PIP degron is placed at different positions in these proteins; the p21-PIP degron is located at the C-terminal end (Fig. 2b), the Set8/PR-Set7-PIP degron is located in the middle of the protein, and the Cdt1-PIP degron is located at the N-terminal end. Some evidences show that CRL4^{Cdt2}-mediated degradation of both p21 and Set8 contribute to prevention of re-replication [10, 11]. Failure of p21 degradation in *Caenorhabditis elegans* causes defect in the cytoplasmic export of Cdc6 in S phase

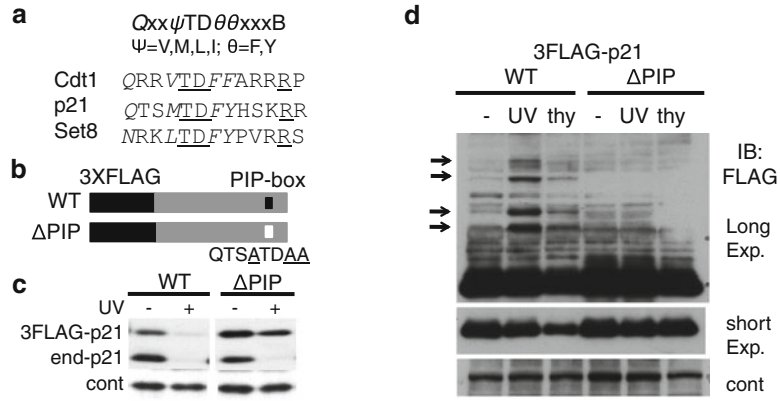

Fig. 2 PIP box-dependent polyubiquitination and degradation of p21. (**a**) PIP degron sequences of Cdt1, p21, and Set8. Consensus sequence is shown above them. PIP-box sequences are shown in *italics*. Amino acids, TD, and a basic amino acid of PIP degron are *underlined*. (**b**) Vector constructs expressing $p21^{3FLAG\text{-}WT}$ (WT) and $p21^{3FLAG\text{-}\Delta PIP}$ (ΔPIP). The position of the PIP box in the p21 protein is shown. In the ΔPIP mutant three amino acid residues within the PIP box were changed to alanine (*underlined*). (**c**) PIP box-dependent degradation of p21. After UV irradiation, both $p21^{3FLAG\text{-}WT}$ (WT) and endogenous p21 (end-p21) are degraded, whereas $p21^{3FLAG\text{-}\Delta PIP}$ (ΔPIP) is stably maintained. (**d**) PIP box-dependent in vivo polyubiquitination of p21. $p21^{3FLAG\text{-}WT}$- or $p21^{3FLAG\text{-}\Delta PIP}$-expressing cells were incubated with MG132 for 1 h, irradiated with UV (UV) or not (–), and incubated for another 1 h. The polyubiquitinated forms of p21 (indicated by *arrows*) were detected only in $p21^{3FLAG\text{-}WT}$-expressing cells. Also included in the Western blot is a sample prepared from thymidine-treated cells. Cells were arrested in S phase by 20 h of thymidine treatment and incubated in the presence of MG132 for 1 h (thy). The polyubiquitination-specific ladder was detected in $p21^{3FLAG\text{-}WT}$-expressing cells. Note that the level of $p21^{3FLAG\text{-}WT}$ is lower than that of $p21^{3FLAG\text{-}\Delta PIP}$ in thymidine-treated cells, reflecting that p21 degradation during S phase is also dependent on the PIP box

likely due to the inhibition of S-CDK [28]. Set8 is present in G2 and M phases and monomethylates histone H4 at lysine 20. The levels of methylation increase at the replication origins concomitant with the origin licensing. Indeed, studies found that expression of stable Set8 induces re-replication.

The $CRL4^{Cdt2}$ ubiquitin ligase contributes to genome integrity by tightly controlling the levels of cell cycle regulators as mentioned above. For this, cells have developed an elaborate mechanism that uses PCNA for the timely activation of $CRL4^{Cdt2}$ as fine-tuner of cell cycle transitions. During the cell cycle, chromatin association patterns of PCNA change. PCNA is dissociated from the chromatin in G1 phase, associated with chromatin in S phase, and again dissociated from chromatin in G2 phase. The change of chromatin association status of PCNA is nicely connected to the regulation of Cdt1 during the cell cycle. Thus, PCNA couples the

initiation of DNA replication with the inactivation of initiator proteins, creating an elegant feedback control for once-per-cell cycle control of DNA replication. In addition, the same degradation pathway operates in response to DNA damage. It is highly possible that there are multiple $CRL4^{Cdt2}$ targets waiting to be discovered. In this chapter, we describe methods to analyze how PIP degron-containing proteins are degraded by $CRL4^{Cdt2}$ in a manner dependent on the chromatin-bound PCNA.

2 Materials

2.1 PCNA-Dependent Degradation: Knockdown of PCNA with siRNA

1. HeLa cells: Cultured in Dulbecco's modified Eagle's medium (DMEM) with 10 % fetal bovine serum supplemented with 100 units/mL of penicillin and 0.1 mg/mL of streptomycin in a 5 % CO_2 atmosphere at 37 °C.
2. Culture medium: DMEM medium with 10 % fetal bovine serum without antibiotics.
3. 35-mm Dishes.
4. siRNA solution (50 μM):

   siRNA for PCNA: CGGUGACACUCAGUAUGUCdTdT.

   siRNA for Cdt2: CCAGGAGGUGAUAAACUUUdTdT.

   Control siRNA (siLuc known as GL2): CGUACGCGGAA UACUUCGAdTdT (Dharmacon).
5. Opti-MEM (Life Technologies).
6. Transfection reagents: Oligofectamine (Life Technologies) or HiPerFect (Qiagen) (*see* **Note 1**).
7. UV crosslinker (Stratagene or UVP).
8. 1.5-mL Microcentrifuge tubes.
9. Phosphate-buffered saline (PBS): Dissolve 8.0 g of NaCl, 0.2 g of KCl, 1.44 g of Na_2HPO_4, and 0.24 g of KH_2PO_4 in 800 mL of H_2O. Adjust the pH to 7.4 with HCl. Add H_2O to 1 L.
10. 1× SDS-PAGE sample buffer: 50 mM Tris–HCl pH 6.8, 10 % glycerol, 2 % SDS, 0.02 % bromophenol blue, 0.1 M dithiothreitol (DTT).
11. Antibodies against Cdt1 (Santa Cruz sc-28262 or Abcam ab70829), Cdt2 (Bethyl Laboratories A300-948A or BioAcademia 70-115), PCNA (Santa Cruz PC10), and RCC1 (*see* **Note 2**).

2.2 PIP Box-Dependent In Vivo Polyubiquitination of p21

1. HeLa cell lines stably expressing 3×FLAG-tagged wild-type p21 ($p21^{3FLAG\text{-}WT}$) or 3×FLAG-tagged PIP box-mutated p21 ($p21^{3FLAG\text{-}\Delta PIP}$) (*see* the constructs and sequence in Fig. 2a, b) (*see* **Note 3**).

2. 35-mm Dishes.
3. 1,000× Proteasome inhibitor MG132: 20 mM, dissolved in DMSO.
4. UV crosslinker (Stratagene or UVP).
5. 1.5-mL Microcentrifuge tubes.
6. Antibodies: FLAG (M2, Sigma), p21 (BD Pharmingen 556430).

2.3 Purification of $CRL4^{Cdt2}$ from Insect Cells and In Vitro Ubiquitination Assay

1. Baculoviruses: Recombinant viruses expressing HA-Cul4A, DDB1, Cdt2-3FLAG, or His-myc-Rbx1, generated using a kit from Clontech (*see* **Note 4**).
2. Insect cells: Sf9 (*Spodoptera frugiperda* 9), Sf21, and High Five (*see* **Note 5**).
3. Grace's Insect Cell Culture Medium (Life Technologies) supplemented with 10 % v/v fetal bovine serum and antibiotics (100 units/mL of penicillin and 0.1 mg/mL of streptomycin).
4. 150-mm Dishes.
5. Tubes: Conical tubes (15 and 50 mL), 1.5-mL microcentrifuge tubes, 10-mL ultracentrifuge tubes.
6. Swing rotor for 50-mL conical tubes.
7. PBS (*see* Subheading 2.1, **item 9**).
8. 50× PIC solution: Dissolve one tablet of Complete Protease Inhibitor Cocktail (Roche Applied Science) in 1 mL H_2O, make aliquots, and store at −20 °C.
9. Buffer B: 50 mM Tris–HCl pH 8.0, 1 mM EDTA, 10 % glycerol, 1 mM phenylmethylsulfonyl fluoride (PMSF), 2 μg/mL leupeptin, 0.5× PIC.
10. 0.1 M NaCl, 0.15 M NaCl, and 0.5 M NaCl buffer B: Buffer B containing 0.1, 0.15, and 0.5 M NaCl, respectively.
11. 10 % Nonidet P-40 (NP-40).
12. Sonicator.
13. 5 M NaCl.
14. DEAE column: Econo column (ID = 2.5 cm, L = 5 cm, BioRad) filled with 2 mL of DEAE sepharose fast flow (GE Healthcare) and equilibrated with 0.5 M NaCl buffer B.
15. Anti-FLAG antibody beads (ANTI-FLAG M2 Affinity Gel, Sigma-Aldrich).
16. Econo column (ID = 1.0 cm, L = 10 cm, BioRad).
17. Elution buffer: 200 μg/mL 3×FLAG peptide (Sigma-Aldrich) in 0.1 % NP-40 containing 0.1 M NaCl buffer B.
18. SDS-PAGE system.
19. Coomassie Brilliant Blue (CBB) solution for gel staining.

20. 100 ng/μL Cdt1 (*see* **Note 6**).
21. 200 ng/μL PCNA (*see* **Note 7**).
22. Calf thymus DNA, activated (Sigma-Aldrich): Phenol extracted and resolved in TE at ~10 ng/μL (*see* **Note 8**).
23. Ubiquitination reagents: 20 mg/mL Ubiquitin (BioMol), 0.1 mg/mL E1 (Wako), 1 mg/mL E2 (UbcH5c, BioMol).
24. 10× Ubiquitination buffer: 500 mM Tris–HCl pH 7.5, 100 mM $MgCl_2$, 50 mM DTT, 20 μM MG132.
25. 100 mM ATP.
26. 2× SDS-PAGE sample buffer: 100 mM Tris–HCl pH 6.8, 20 % glycerol, 4 % SDS, 0.04 % bromophenol blue, 0.2 M DTT.
27. Anti-Cdt1 antibody (*see* Subheading 2.1, **item 11**).

3 Methods

In mammalian cells, Cdt1, p21, and Set8 are degraded after polyubiquitination by $CRL4^{Cdt2}$, when PCNA is loaded on chromatin during S phase or in response to DNA damage. These substrate proteins have a PIP degron (Fig. 2a), through which they associate with PCNA and are recognized by $CRL4^{Cdt2}$. Therefore, proteins that contain a PIP degron or a similar motif are candidate $CRL4^{Cdt2}$ substrates. To confirm that the protein is substrate for this E3 ligase, several experiments can be conducted: (1) Downregulate a component of PCNA-$CRL4^{Cdt2}$-mediated ubiquitination (such as PCNA, its loader (RFC), or Cdt2), and determine whether the degradation of the substrate protein is blocked (Fig. 1). (2) Mutate the PIP box or basic amino acid of the PIP degron, and determine whether the degradation is blocked (Fig. 2c). (3) Analyze ubiquitination of the substrate protein in vitro (Fig. 3). When the first two experiments are conducted to investigate the proteolysis of the target protein in S phase, it is important to keep in mind that many of the $CRL4^{Cdt2}$ substrates are redundantly targeted by other ubiquitin ligases. For example, Cdt1 is also ubiquitinated by SCF^{Skp2} (also known as $CRL1^{Skp2}$) in S phase in human cells. SCF^{Skp2} detects a phospho-degron created by cyclin A–CDK2-dependent phosphorylation [16]. p21 is also targeted by SCF^{Skp2}, although $CRL4^{Cdt2}$ is the major ubiquitin ligase that operates on p21 in HeLa cells [29]. Therefore, to investigate the $CRL4^{Cdt2}$-dependent proteolysis of Cdt1 in normal S phase, the SCF^{Skp2} pathway needs to be inactivated. In contrast, SCF^{Skp2}-mediated protein degradation is not normally activated following UV irradiation. Therefore, the first two experiments can easily be conducted by examining the PCNA-$CRL4^{Cdt2}$-mediated degradation of substrate proteins following UV irradiation without downregulating SCF^{Skp2}.

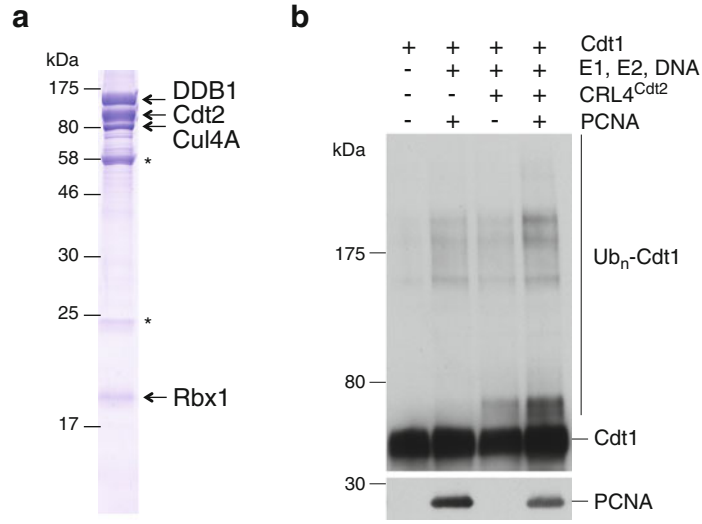

Fig. 3 In vitro ubiquitination assay of Cdt1 by $CRL4^{Cdt2}$. (**a**) The purified $CRL4^{Cdt2}$ complex from insect cells was analyzed by SDS-PAGE followed by CBB staining. *Asterisks* indicate contaminated protein, probably anti-FLAG antibodies. (**b**) PCNA-dependent ubiquitination of Cdt1. Cdt1 was incubated with indicated combination of proteins. Ubiquitinated forms of Cdt1 were detected by Western blotting with the anti-Cdt1 antibody

The dependence on PCNA for protein degradation can simply be examined by siRNA-mediated downregulation of PCNA (Fig. 1a), while the dependence on chromatin-loaded PCNA can be examined by downregulation of PCNA loaders. Eukaryotic cells have a canonical PCNA loader, Rfc1-RFC, and two RFC-like complexes (Ctf18-RFC and Elg1-RFC). Interestingly, downregulation of Rfc1 prevents UV-induced Cdt1 degradation, while depletion of Ctf18 prevents $CRL4^{Cdt2}$-dependent degradation of Cdt1 during S phase. These results suggest that different loader complexes operate during the different aspects of chromatin events [26]. Knockdown analyses of ubiquitin-conjugating enzymes, E2s, indicate that different E2s are separately used for the polyubiquitination of different substrates [35].

Although an in vitro ubiquitination assay using purified recombinant proteins and chromatin-loaded PCNA has not been established yet, $CRL4^{Cdt2}$ purified from baculovirus-infected cells shows ubiquitination activity on Cdt1 and p21 (Fig. 3).

3.1 PCNA-Dependent Degradation: Knockdown of PCNA with siRNA

1. For siRNA transfection with Oligofectamine (*see* **Note 1**), plate the cell suspension into the four dishes. Plate 1×10^5 HeLa cells in 2 mL DMEM medium without antibiotics (*see* **Note 9**) per 35-mm dish (*see* **Note 10**), and let the cells adhere for 20 h under regular growth conditions.

2. Two hours before transfection, remove medium and add 1 mL of fresh DMEM medium without antibiotics.
3. Prepare siRNA-transfection mixtures for two dishes with control siRNA and for two dishes with PCNA siRNA. For a single transfection with Oligofectamine, prepare the transfection mixture as follows. Add 2 μL of siRNA into 75 μL of Opti-MEM, and mix gently. Add 3–4 μL of Oligofectamine into 20 μL of Opti-MEM, mix gently, and incubate for 5 min at room temperature. Combine the two solutions, mix gently, and incubate for 20 min.
4. Add the siRNA-transfection mixture dropwise into the dish, mix gently by rocking the dish back and forth, and left and right (final siRNA concentration is 100 nM), and incubate cells overnight under regular growth conditions.
5. Next day, add 1 mL of DMEM medium to the dishes, and incubate cells for 1 or 2 days under regular growth conditions (*see* **Notes 11** and **12**).
6. Remove medium from all the four dishes. Place one control siRNA dish and one PCNA siRNA dish into a UV crosslinker. Irradiate cells with UV at 50 J/m^2 (*see* **Note 13**). Other two dishes of cells serve as controls (without UV treatment).
7. Add 1 mL of medium to all the four dishes, and incubate for 30 min to 1 h under regular growth conditions.
8. Scrape cells off the dishes, and transfer cells into 1.5-mL microcentrifuge tubes.
9. Spin down cells at 5,000 rpm (~2,000×*g*) for 3 min in a microfuge at 4 °C, and remove medium.
10. Resuspend cells in 1 mL of cold PBS, spin down cells as above, and remove medium. Repeat this washing step three times.
11. Add 50 μL of 1× SDS sample buffer to the cell pellets, and mix well by pipetting.
12. Boil the samples at 95–100 °C for 5 min, vortex, and boil for another 2 min.
13. Analyze the four samples by Western blotting using antibodies against Cdt1, Cdt2, PCNA, and RCC1: Lane 1, control siRNA-transfected cells, not UV irradiated (−UV); lane 2, control siRNA-transfected cells, irradiated with UV (+UV); lane 3, PCNA-siRNA-transfected cells (−UV); and lane 4, PCNA-siRNA-transfected cells (+UV) (Fig. 1a).

3.2 PIP Box-Dependent In Vivo Polyubiquitination of p21

1. Plate 2×10^5 cells per 35-mm dish with 2 mL of medium (two dishes of p21$^{3FLAG\text{-}WT}$-expressing cells and two dishes of p21$^{3FLAG\text{-}\Delta PIP}$-expressing cells), and let the cells adhere. Grow cells for 1 or 2 days under regular growth conditions.

2. Add 2 μL of MG132 (final concentration: 20 μM), and incubate cells for 10 min to 1 h under regular growth conditions (*see* **Note 14**).
3. Remove medium from all dishes.
4. Place one dish with $p21^{3FLAG\text{-}WT}$-expressing cells and one dish with $p21^{3FLAG\text{-}\Delta PIP}$-expressing cells into a UV crosslinker, and irradiate cells with UV at 50 J/m^2.
5. Add 1 mL of medium containing 20 μM MG132 to all dishes, and incubate cells for 30 min to 1 h under regular growth conditions.
6. Scrape cells off the plates, transfer cells into a 1.5-mL microcentrifuge, and prepare SDS-PAGE sample as described in Subheading 3.1, **steps 9–12**.
7. Run the samples for Western blotting using anti-FLAG and anti-p21 antibodies: $p21^{3FLAG\text{-}WT}$-expressing cells (−UV and +UV) and $p21^{3FLAG\text{-}\Delta PIP}$-expressing cells (−UV and +UV) (Fig. 2d).

3.3 Purification of $CRL4^{Cdt2}$ from Insect Cells and In Vitro Ubiquitination Assay

3.3.1 Purification of $CRL4^{Cdt2}$ from Insect Cells

1. Generate high-titer stocks of viruses for individual proteins (Cul4A, DDB1, Rbx1, and Cdt2) (*see* **Notes 4** and **5**).
2. Seed Sf21 insect cells (*see* **Note 5**) onto ten dishes (150 mm) at 1.5×10^7 cells/plate in 17 mL of Grace's Insect Cell Culture Medium supplemented with fetal bovine serum and antibiotics, and allow cells to adhere for 1 h at 27 °C (*see* **Note 15**).
3. To infect and express four proteins (Cul4A, DDB1, Rbx1, and Cdt2) in the same cell culture, prepare a virus solution mixture containing all four viruses in one tube by mixing the four high-titer virus stocks, about 40–80 μL of each virus stock (*see* **step 1** above, total MOI = 10), and then adding Grace's insect medium to the total of 3 mL (final volume) for infecting one dish of cells (i.e., 30 mL for ten dishes).
4. Remove medium from the dishes, add 3 mL of the virus solution mixture of four viruses to each dish, and incubate for 1 h for virus infection.
5. Add 14 mL of culture medium to each plate, and incubate at 27 °C for 48 h (*see* **Note 16**).
6. Scrape cells off the ten dishes, totaling around 170 mL of cell suspension, transfer to four 50-mL conical tubes (or larger tubes), and centrifuge at 750 × *g* for 5 min at 4 °C using a swing rotor.
7. Wash cells with 40 mL of ice-cold PBS per 50-mL conical tube (*see* **Note 17**). Pellet cells by centrifugation at 750 × *g* for 5 min at 4 °C. Resuspend the cell pellets in 10 mL of PBS in each tube, pool cell suspensions into one 50-mL conical tube, and centrifuge at 750 × *g* for 5 min at 4 °C with swing rotor. Remove the supernatant (*see* **Note 18**).

8. Suspend the cell pellet in 8 mL of 0.15 M NaCl buffer B containing 0.1 % NP-40, and sonicate the cell suspension with eight rounds of 10-s pulse (output 5.5, duty cycle 20 %) (*see* **Note 19**).
9. Add 0.4 mL of 10 % NP-40 (final concentration: 0.5 %) and 0.7 mL of 5 M NaCl (final concentration: 0.5 M) (*see* **Note 20**), and vortex vigorously for 30 s.
10. Transfer the lysate into a 10-mL ultracentrifuge tube and incubate for 20 min. Transfer 50 μL of lysate in a 1.5-mL tube as a whole-cell extract sample for protein analysis (*see* **Note 21**).
11. Ultracentrifuge at 120,000 × *g* for 20 min at 4 °C, and transfer the supernatant to a new 15-mL conical tube. Transfer 50 μL of supernatant in a 1.5-mL tube (*see* **Note 21**).
12. Apply the supernatant to a DEAE column slowly in order to remove nucleic acids from the lysate, and collect the flow-through fraction in a 15-mL conical tube.
13. Add the DEAE flow-through fraction to the anti-FLAG antibody beads (1 mL bed volume), which was equilibrated with 0.5 M NaCl buffer B in a 15-mL conical tube. Incubate the bead slurry at 4 °C with a gentle mixing on a tube rotator for 1 h (*see* **Note 22**).
14. Wash the beads once by centrifuging at 3,000 × *g* for 5 min at 4 °C, removing the supernatant, and then resuspending the beads in 10 mL of 0.5 M NaCl buffer B (*see* **Note 23**).
15. Transfer the bead slurry into an Econo column (ID = 1 cm, L = 10 cm).
16. Wash the beads (~1 mL bed volume) with 10 mL of 0.5 M NaCl buffer B and then with 2 mL of elution buffer without 3×FLAG peptide (*see* **Note 24**).
17. Using a stepwise elution approach, sequentially pass 250 μL of elution buffer through the column, and collect each eluted fraction in separate 1.5-mL tubes. Collect 20 fractions (20 tubes) to obtain about 5 mL (equivalent to 5 bed volumes) of protein in elution buffer (*see* **Note 25**).
18. Check each elution fraction for the $CRL4^{Cdt2}$ components (DDB1, Cdt2, Cul4A, and Rbx1) by running 5 μL of eluted samples on SDS-PAGE gel and staining the gel with CBB (*see* Fig. 3a and **Note 25**).
19. Combine the $CRL4^{Cdt2}$-containing fractions, make aliquots, and store at −80 °C.

3.3.2 In Vitro Ubiquitination Assay

1. Prepare PCNA and activated calf thymus DNA mixture (PCNA–DNA mixture). For one ubiquitination assay, mix 200 ng of PCNA and 25 ng of calf thymus DNA and incubate at 37 °C for 30 min.

2. In a 10 μL complete reaction, add PCNA–DNA mixture (*see* **step 1** above), 6 μg of ubiquitin, 100 ng of E1, 400 ng of E2, 330 ng of $CRL4^{Cdt2}$ (*see* Subheading 3.3.1, **step 19**), 150 ng of Cdt1, 1 μL 10× ubiquitination buffer, and then H_2O and NaCl to a final NaCl concentration of 0.1 M and to a total volume of 9.8 μL. Add 0.2 μL ATP, and mix gently.
3. Incubate at 37 °C for 1 h.
4. Stop reaction by adding 10 μL of 2× SDS-PAGE sample buffer and boil at 96 °C for 5 min.
5. Run the samples on an SDS-PAGE gel, and detect the ubiquitinated Cdt1 by Western blotting with the anti-Cdt1 antibody (Fig. 3b).

4 Notes

1. Many companies provide transfection reagents. Find out which are the best reagents for your cell line with a high knockdown efficiency and a low toxicity.
2. Cdt1, Cdt2, and RCC1 antibodies are also described in our previous studies [29, 36, 37]. RCC1 blotting is used as a loading control.
3. You may use cells transiently transfected with expression plasmids. However, the variability in transfection efficiency and expression levels of the transfected gene among the experiments makes it difficult to get reproducible results.
4. Baculovirus expression plasmids and viruses are prepared according to the manufacturer's instructions. We use a kit from Clontech which is provided with BacPAK6 virus genome DNA and the pBacPAK8 or 9 vector. The titers of virus stocks obtained for Cdt2, DDB1, Cul4A, and Rbx1 are 5×10^8–1×10^9 pfu/mL on plaque assay. Cdt2 is tagged with 3×FLAG at the C-terminus for purification using the anti-FLAG beads.
5. See the user manual provided by the company for the cell lines, Sf9, Sf21, and High Five (e.g., Growth and Maintenance of Insect cell Lines by Invitrogen). The Sf21 cell line is our first choice. Generally, High Five cells produce the protein at higher levels than other cells. However, we recommend a pilot experiment with different cell lines by checking the expression levels, stability, and solubility of your proteins in order to find a suitable cell line for your proteins (*also see* **Note 21**).
6. Cdt1 can be expressed and purified from insect cells as described for $CRL4^{Cdt2}$ protein purification. Since Cdt1 has a PIP degron at the N-terminal end, the 3×FLAG tag is fused to the C-terminus end.

7. PCNA can be expressed and purified from *E. coli* as described in previous studies [38, 39].
8. The DNA is prepared from calf thymus, treated briefly with DNase I (Sigma-Aldrich). This procedure generates nicks and short gaps in the DNA. This DNA is used in the DNA polymerase assay. It is also used to trap PCNA at the nicks, the sites where PCNA can be loaded, therefore providing chromatin-loaded PCNA for the ubiquitination assay.
9. Do not add antibiotics to media during transfection as this causes cell death.
10. Use exponentially growing cells for transfection. A 3-day-old cell culture is not recommended for obtaining a high transfection efficiency. The number of cells plated is also critical for knockdown efficiency via siRNA and for cell cycle analysis. When cells are plated at a high density, knockdown efficiency is reduced and cell proliferation may be compromised. Find a proper cell density for your cell line.
11. When you culture cells for 3 days after transfection, replace medium with 2 mL of fresh DMEM medium 1 or 2 days after transfection.
12. When the knockdown efficiency is low, we recommend performing a second transfection on the following day after the first transfection.
13. The dose of UV radiation (typically 5–100 J/m^2) should be optimized for individual experiments.
14. To detect a ladder of polyubiquitinated substrate on Western blotting, it is required to incubate cells with proteasome inhibitor, such as MG132.
15. It is important to make sure that cells have attached to the bottom of the plate before virus infection.
16. Incubation time is normally around 24–72 h and should be optimized by examining the expression levels, stability, and solubility of your proteins (*see* also **Note 21**).
17. All the processes after this step use ice-cold buffer and should be performed on ice.
18. Cell pellets can be stored at −80 °C for future use.
19. Sonication conditions should be optimized for each cell type and instrument.
20. NaCl is added to a final concentration of 0.5 M to dissociate proteins from DNA and to avoid binding of negatively charged proteins to DEAE.
21. Whole-cell extract, supernatant, and pellet fractions should be examined for the expression levels, stability, and solubility of your protein. This can be done by CBB staining of SDS-PAGE gels.

Western blotting may be appropriate if protein expression levels are low.

22. A longer incubation causes degradation of the Cdt2 protein.
23. This wash helps elution steps by preventing the protein from getting stuck on the column during the next step.
24. Before moving onto the elution step with 3×FLAG peptide (200 μg/mL)-containing elution buffer, you may wash the beads with elution buffer containing a low concentration of 3×FLAG peptide (5–20 μg/mL) to remove the nonspecific proteins bound on the beads.
25. The elution peaks of $CRL4^{Cdt2}$ components are around fractions 5–7. Run protein standards (0.1, 0.5, 1, 2 μg of bovine serum albumin) on the same SDS-PAGE gel in order to estimate the amounts of $CRL4^{Cdt2}$ in each fraction. From ten dishes (150 mm), about 0.5 mg of the $CRL4^{Cdt2}$ complex can be obtained.

Acknowledgements

This work was financially supported by JSPS KAKENHI and MEXT KKENHI, Grant in Aid from the Ministry of Education, Culture, Sports, Science, and Technology of Japan.

References

1. Nakayama KI, Nakayama K (2006) Ubiquitin ligases: cell-cycle control and cancer. Nat Rev Cancer 6(5):369–381
2. Petroski MD, Deshaies RJ (2005) Function and regulation of cullin-RING ubiquitin ligases. Nat Rev Mol Cell Biol 6(1):9–20
3. Bell SP, Dutta A (2002) DNA replication in eukaryotic cells. Annu Rev Biochem 71: 333–374
4. Nishitani H, Lygerou Z (2002) Control of DNA replication licensing in a cell cycle. Genes Cells 7(6):523–534
5. Blow JJ, Dutta A (2005) Preventing re-replication of chromosomal DNA. Nat Rev Mol Cell Biol 6(6):476–486
6. Ilves I, Petojevic T, Pesavento JJ, Botchan MR (2010) Activation of the MCM2-7 helicase by association with Cdc45 and GINS proteins. Mol Cell 37(2):247–258
7. Masai H, Matsumoto S, You Z, Yoshizawa-Sugata N, Oda M (2010) Eukaryotic chromosome DNA replication: where, when, and how? Annu Rev Biochem 79:89–130
8. Machida YJ, Hamlin JL, Dutta A (2005) Right place, right time, and only once: replication initiation in metazoans. Cell 123(1):13–24
9. Arias EE, Walter JC (2007) Strength in numbers: preventing rereplication via multiple mechanisms in eukaryotic cells. Genes Dev 21(5):497–518
10. Abbas T, Dutta A (2011) CRL4Cdt2: master coordinator of cell cycle progression and genome stability. Cell Cycle 10(2):241–249
11. Havens CG, Walter JC (2011) Mechanism of CRL4Cdt2, a PCNA-dependent E3 ubiquitin ligase. Genes Dev 25(15):1568–1582
12. Waga S, Stillman B (1998) The DNA replication fork in eukaryotic cells. Annu Rev Biochem 67:721–751
13. Moldovan GL, Pfander B, Jentsch S (2007) PCNA, the maestro of the replication fork. Cell 129(4):665–679
14. Gulbis JM, Kelman Z, Hurwitz J, O'Donnell M, Kuriyan J (1996) Structure of the C-terminal region of p21(WAF1/CIP1) complexed with human PCNA. Cell 87(2):297–306

15. Arias EE, Walter JC (2006) PCNA functions as a molecular platform to trigger Cdt1 destruction and prevent re-replication. Nat Cell Biol 8(1):84–90
16. Nishitani H, Sugimoto N, Roukos V, Nakanishi Y, Saijo M, Obuse C, Tsurimoto T, Nakayama KI, Nakayama K, Fujita M, Lygerou Z, Nishimoto T (2006) Two E3 ubiquitin ligases, SCF-Skp2 and DDB1-Cul4, target human Cdt1 for proteolysis. EMBO J 25(5):1126–1136
17. Senga T, Sivaprasad U, Zhu W, Park JH, Arias EE, Walter JC, Dutta A (2006) PCNA is a cofactor for Cdt1 degradation by CUL4/DDB1-mediated N-terminal ubiquitination. J Biol Chem 281(10):6246–6252
18. Havens CG, Walter JC (2009) Docking of a specialized PIP Box onto chromatin-bound PCNA creates a degron for the ubiquitin ligase CRL4Cdt2. Mol Cell 35(1):93–104
19. Michishita M, Morimoto A, Ishii T, Komori H, Shiomi Y, Higuchi Y, Nishitani H (2011) Positively charged residues located downstream of PIP box, together with TD amino acids within PIP box, are important for CRL4(Cdt2)-mediated proteolysis. Genes Cells 16(1):12–22
20. Higa LA, Wu M, Ye T, Kobayashi R, Sun H, Zhang H (2006) CUL4-DDB1 ubiquitin ligase interacts with multiple WD40-repeat proteins and regulates histone methylation. Nat Cell Biol 8(11):1277–1283
21. Hu J, McCall CM, Ohta T, Xiong Y (2004) Targeted ubiquitination of CDT1 by the DDB1-CUL4A-ROC1 ligase in response to DNA damage. Nat Cell Biol 6(10):1003–1009
22. Jin J, Arias EE, Chen J, Harper JW, Walter JC (2006) A family of diverse Cul4-Ddb1-interacting proteins includes Cdt2, which is required for S phase destruction of the replication factor Cdt1. Mol Cell 23(5):709–721
23. Sakaguchi H, Takami T, Yasutani Y, Maeda T, Morino M, Ishii T, Shiomi Y, Nishitani H (2012) Checkpoint kinase ATR phosphorylates Cdt2, a substrate receptor of CRL4 ubiquitin ligase, and promotes the degradation of Cdt1 following UV irradiation. PLoS One 7(9):e46480
24. Stathopoulou A, Roukos V, Petropoulou C, Kotsantis P, Karantzelis N, Nishitani H, Lygerou Z, Taraviras S (2012) Cdt1 is differentially targeted for degradation by anticancer chemotherapeutic drugs. PLoS One 7(3):e34621
25. Raman M, Havens CG, Walter JC, Harper JW (2011) A genome-wide screen identifies p97 as an essential regulator of DNA damage-dependent CDT1 destruction. Mol Cell 44(1):72–84
26. Shiomi Y, Hayashi A, Ishii T, Shinmyozu K, Nakayama J, Sugasawa K, Nishitani H (2012) Two different replication factor C proteins, Ctf18 and RFC1, separately control PCNA-CRL4Cdt2-mediated Cdt1 proteolysis during S phase and following UV irradiation. Mol Cell Biol 32(12):2279–2288
27. Abbas T, Sivaprasad U, Terai K, Amador V, Pagano M, Dutta A (2008) PCNA-dependent regulation of p21 ubiquitylation and degradation via the CRL4Cdt2 ubiquitin ligase complex. Genes Dev 22(18):2496–2506
28. Kim Y, Starostina NG, Kipreos ET (2008) The CRL4Cdt2 ubiquitin ligase targets the degradation of p21Cip1 to control replication licensing. Genes Dev 22(18):2507–2519
29. Nishitani H, Shiomi Y, Iida H, Michishita M, Takami T, Tsurimoto T (2008) CDK inhibitor p21 is degraded by a proliferating cell nuclear antigen-coupled Cul4-DDB1Cdt2 pathway during S phase and after UV irradiation. J Biol Chem 283(43):29045–29052
30. Abbas T, Shibata E, Park J, Jha S, Karnani N, Dutta A (2010) CRL4(Cdt2) regulates cell proliferation and histone gene expression by targeting PR-Set7/Set8 for degradation. Mol Cell 40(1):9–21
31. Centore RC, Havens CG, Manning AL, Li JM, Flynn RL, Tse A, Jin J, Dyson NJ, Walter JC, Zou L (2010) CRL4(Cdt2)-mediated destruction of the histone methyltransferase Set8 prevents premature chromatin compaction in S phase. Mol Cell 40(1):22–33
32. Jorgensen S, Eskildsen M, Fugger K, Hansen L, Larsen MS, Kousholt AN, Syljuasen RG, Trelle MB, Jensen ON, Helin K, Sorensen CS (2011) SET8 is degraded via PCNA-coupled CRL4(CDT2) ubiquitylation in S phase and after UV irradiation. J Cell Biol 192(1):43–54
33. Oda H, Hubner MR, Beck DB, Vermeulen M, Hurwitz J, Spector DL, Reinberg D (2010) Regulation of the histone H4 monomethylase PR-Set7 by CRL4(Cdt2)-mediated PCNA-dependent degradation during DNA damage. Mol Cell 40(3):364–376
34. Tardat M, Brustel J, Kirsh O, Lefevbre C, Callanan M, Sardet C, Julien E (2010) The histone H4 Lys 20 methyltransferase PR-Set7 regulates replication origins in mammalian cells. Nat Cell Biol 12(11):1086–1093
35. Shibata E, Abbas T, Huang X, Wohlschlegel JA, Dutta A (2011) Selective ubiquitylation of p21 and Cdt1 by UBCH8 and UBE2G ubiquitin-conjugating enzymes via the CRL4Cdt2 ubiquitin ligase complex. Mol Cell Biol 31(15):3136–3145
36. Nishitani H, Taraviras S, Lygerou Z, Nishimoto T (2001) The human licensing factor for DNA

replication Cdt1 accumulates in G1 and is destabilized after initiation of S-phase. J Biol Chem 276(48):44905–44911

37. Nishitani H, Ohtsubo M, Yamashita K, Iida H, Pines J, Yasudo H, Shibata Y, Hunter T, Nishimoto T (1991) Loss of RCC1, a nuclear DNA-binding protein, uncouples the completion of DNA replication from the activation of cdc2 protein kinase and mitosis. EMBO J 10(6):1555–1564
38. Fukuda K, Morioka H, Imajou S, Ikeda S, Ohtsuka E, Tsurimoto T (1995) Structure-function relationship of the eukaryotic DNA replication factor, proliferating cell nuclear antigen. J Biol Chem 270(38):22527–22534
39. Zhang P, Zhang SJ, Zhang Z, Woessner JF Jr, Lee MY (1995) Expression and physicochemical characterization of human proliferating cell nuclear antigen. Biochemistry 34(34):10703–10712

Chapter 20

Analyzing Cdc2/Cdk1 Activation During Stress Response in *Schizosaccharomyces pombe*

Miguel A. Rodríguez-Gabriel

Abstract

Stress leads to multiple changes in the physiology of the cell. One of the most important is the adaptation of the cell cycle to the changing conditions of the environment. Cellular responses after stress can be followed by cellular synchronization previous to the insult. In this chapter, we use centrifugal elutriation to synchronize *Schizosaccharomyces pombe* cells and outline methods to investigate the hallmarks of cell cycle progression upon stress. These include analyses of cyclin-dependent kinase phosphorylation and cell size change.

Key words Fission yeast, Cell cycle, Synchronization, Elutriation, Cdc2, Cdk

1 Introduction

In his historical book "What is life?" Erwin Schrödinger proposed that life itself is defined by the interaction between the "living matter" and the environment [1]. We, therefore, cannot understand cellular life without the exchange of matter, energy, and information with the extracellular milieu. One of these environmental changes that affect cellular life is stress, which is understood as the chemical or the physical changes that require an adaptative response in the cell. Such responses must be perfectly tuned to tackle multiple situations and include modifications in gene expression that lead to changes in cell division and growth.

In order to examine specific changes in the cell cycle, cellular size, or morphology upon stress in cell populations, it is necessary to synchronize cells. In this way, all the cells are in the same stage of cell cycle and respond in a similar way to stimuli.

A method to follow up cell cycle progression in *Schizosaccharomyces pombe* is tracking Cdc2 (*S. pombe* cyclin-dependent kinase, Cdk) phosphorylation at tyrosine 15 (Y15). Wee1 and Mik1 kinases phosphorylate this residue and inactivate Cdc2. The phosphate group is then removed by the Cdc25 phosphatase, leading to Cdc2 activation

Eishi Noguchi and Mariana C. Gadaleta (eds.), *Cell Cycle Control: Mechanisms and Protocols*, Methods in Molecular Biology, vol. 1170, DOI 10.1007/978-1-4939-0888-2_20,

which allows mitotic entry. Y15 phosphorylation is, therefore, an excellent readout of the cell cycle state of the cell and of the whole-cell population if cells are synchronized [2–4].

This chapter describes methods to synchronize cells and induce cellular stress. I also provide a collection of experiments that I have used to analyze cell cycle progression in *S. pombe*.

2 Materials

2.1 Cellular Synchronization

1. YE medium: 5 g/L Yeast extract, 30 g/L glucose.
2. Two plastic Fernbach 3-L flasks.
3. Elutriation system: JE 5.0 Rotor (Beckman Coulter, Brea, CA) for use with Avanti J-26S XP Series, Avanti J-26 XP Series, and J6-MI Centrifuges. More information at https://www.beckmancoulter.com/wsrportal/techdocs?docname=JE5-IM-13.
4. Bubble trap (*see* **Note 1**).
5. Peristaltic pump.
6. Spectrophotometer.

2.2 Stressing and Collecting Cells

1. Filtering system: Filter funnel manifold 3-place polyurethane (Pall).
2. 25-mm Cellulose ester filters (0.45 μm pore size).
3. 1.5-mL Screw-cap tubes.

2.3 Measuring Septation and Cell Size

1. Microscope (Nomarski optics).
2. Hemocytometer.
3. Slides and cover slips.
4. Digital camera (attached to the microscope).

2.4 Cdk Activation

1. Lysis buffer: 50 mM Tris–HCl pH 8.0, 150 mM NaCl, 5 mM EDTA, 10 % glycerol, 50 mM NaF, 1 mM Na_3VO_4, Complete protease inhibitor cocktail (Hoffmann-La Roche, Basel, Switzerland), 1 mM PMSF.
2. Fastprep (Bio101 Savant).
3. 0.4–0.6-mm Glass beads.
4. Needle (0.5 mm).
5. 1.5-mL Screw-cap tubes.
6. Spectrophotometer (A_{280} measurement).
7. 5× SDS loading buffer: 250 mM Tris–HCl pH 6.8, 10 % SDS, 30 % glycerol, 5 % beta-mercaptoethanol, 0.02 % bromophenol blue.
8. SDS-PAGE system (MiniProtean, BioRad).

9. Blotting system (BioRad).
10. PVDF membrane (Immobilon®-P, Millipore).
11. Ponceau solution: 0.2 % Ponceau S, 3 % v/v acetic acid.
12. Antibodies: Anti-phospho Cdc2 Tyr15 (Cell Signaling #9111), Anti-Cdc2 (Abcam #ab5467), Anti-rabbit IgG HRP-linked (Cell Signaling #7074), Anti-mouse IgG HRP-linked (Cell Signaling #7076).
13. TBS-T: 10 mM Tris–HCl pH 7.5, 150 mM NaCl, 0.5 % Tween 20.
14. TBS: 10 mM Tris–HCl pH 7.5, 150 mM NaCl.
15. Bovine serum albumin (BSA) fraction V.
16. HRP substrate (Immobilon Western, Millipore).
17. X-ray film.

3 Methods

3.1 Cellular Synchronization

There are several systems for synchronization of fission yeast cells. These include temperature-sensitive mutants, drug treatments, and elutriation. The last method is the choice for stress studies due to the unmodified state of the cells obtained. The elutriation process consists in the continuous centrifugation of a fission yeast culture through a chamber where cells will be separated according to their size: from smaller (recently divided G2 cells) to larger (septated, about to divide) cells.

Inside the elutriation rotor, separation takes place in a funnel-shaped elutriation chamber. Two opposing forces act upon cells: centrifugal force and fluid velocity (Fig. 1a).

During the first stage of elutriation, the balance of centrifugal force versus fluid velocity favors the accumulation of the cells inside the elutriation chamber. During the second stage of elutriation, the balance of centrifugal force versus fluid velocity favors the exit of cells from the elutriation chamber, with small G2 cells leaving the chamber first. Using this system it is possible to collect up to 5–10 % of the original cells, corresponding to an early G2 cell cycle stage. This method has been succinctly described before [5].

1. Grow fission yeast cells in 3 L YE medium at 30 °C until OD_{600} reaches 0.5–1.0.
2. Start pumping cells into the elutriation chamber through one of the inlet tubes (about 80–100 mL/min) (*see* **Note 2**). Outlet tubing should also be inside the culture flask in order to avoid losing culture volume or cells escaping from the system (Fig. 1a).

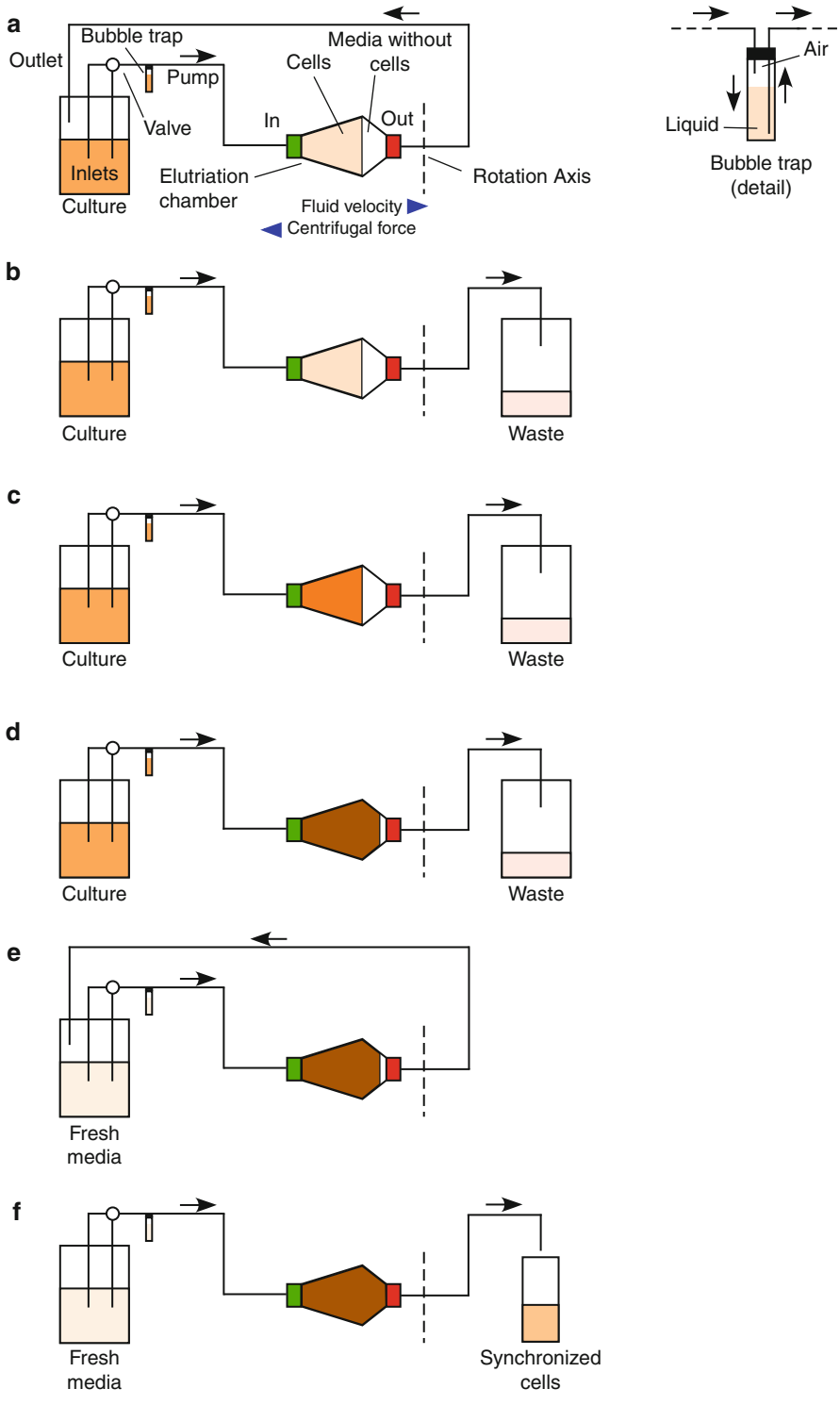

Fig. 1 Schematic view of the elutriation process. (**a**) The system starts. Cells start entering the system in a "closed circuit." (**b**) Net entry of cells into the chamber. (**c**, **d**) Chamber fills up. (**e**) Chamber is full. Start measuring exiting cells. (**f**) Collection of synchronized cells

3. Start centrifugation immediately (about 4,700 × *g* using the JE 5.0 Rotor). Select a temperature of 30 °C in the centrifuge settings. This temperature should be kept throughout the entire process of elutriation.
4. Remove all air bubbles present in the system using the bubble trap (*see* **Note 3** and Fig. 1a).
5. Look through the observation window in the centrifuge, and confirm that cell density starts increasing at the bottom of the elutriation chamber (*see* **Note 4** and Fig. 1a).
6. Measure the OD_{600} of the outgoing media. It should be close to 0, indicating that cells are entering the system but do not exit.
7. Once the outgoing medium is cell free, start discarding it in a separate flask or container (Fig. 1b). If the outgoing medium contains cells, increase centrifugation speed and/or decrease cell flow inside the chamber. Confirm that cells accumulate in the elutriation chamber (*see* **Note 5** and Fig. 1c).
8. Continue pumping in the cell culture until most of the elutriation chamber is filled with cells and they are closer to the top end (easy to observe through the centrifuge observation window) (Fig. 1d).
9. Move the inlet and outlet lines into fresh medium, and start pumping fresh media into the chamber (*see* **Note 6** and Fig. 1e).
10. Start the collection of the small cells. First, decrease the centrifugation speed very gradually (100 rpm each time with the JE 5.0 Rotor), making sure that cells inside the chamber do not reach the exit of the chamber.
11. Cells will start moving towards the exit of the elutriation chamber. Before they start to exit, stop decreasing centrifugation speed and start increasing the pumping speed. Measure OD_{600} of the outlet line. As the culture starts going out of the chamber, there is a small increase in OD_{600} of the outgoing medium (containing cells). An optimum OD_{600} should be about 0.1–0.2.
12. Check septation index of the outgoing cells (*see* Subheading 3.3).
13. If the septation is 0 (no post-mitotic cells), place the outlet line in a new flask and start collecting synchronized cells (Fig. 1f). It is possible to obtain about 500 mL of high-quality synchronized cells.
14. Once the cells have been collected, mix well and measure septation of the whole synchronized culture (*see* **Note 7**).
15. If the septation index is 0, the experiments described below should start immediately.
16. To stop elutriation, just stop centrifugation and let the cells be pumped out of the chamber.

3.2 Stressing and Collecting Cells

Once the cells have been collected, the experiment must start immediately. If the starting unsynchronized culture contained $1–5 \times 10^{10}$ cells, the synchronized culture may contain up to 10^9 cells. Considering that the number of cells used for the following experiments is about 5×10^7 cells per time point, it is possible to collect up to 20 time points, including non-stressed control.

1. Split the synchronized culture into as many flasks as needed for the experiment. In one simple experiment (one stress condition + non-stress control), it is possible to collect ten time points per condition (e.g., 0–90 min every 10 min) (*see* **Note 8**).
2. Once the synchronized culture is split into two (or more) flasks, add the stressor to the culture (KCl, H_2O_2, sorbitol, etc.), and set the cultures to grow at 30 °C (*see* **Note 9**).
3. Collect cells (about 5×10^7 cells) by filtration using the filter funnel manifold in 25-mm filters (0.45 μm pore size).
4. Remove the filter from the manifold, and transfer it into a 1.5-mL screw-cap tube containing 1 mL of ice-cold water.
5. Vortex to release the cells from the filter, discard the filter, and then centrifuge briefly to collect cells at the bottom of the tube.
6. Discard water, and snap freeze cells in liquid nitrogen. Follow the same process for all the time points under study.

3.3 Measuring Septation and Cell Size

In parallel with cell collection described above, it is necessary to measure the number of post-mitotic cells by determining the septation index (Fig. 2). Septation index is the percentage of cells that have gone through mitosis and is indicated by the ratio of cells with septum. As an option, it is possible to measure cell size using the microscopic observation. Septated cells can be used as a control

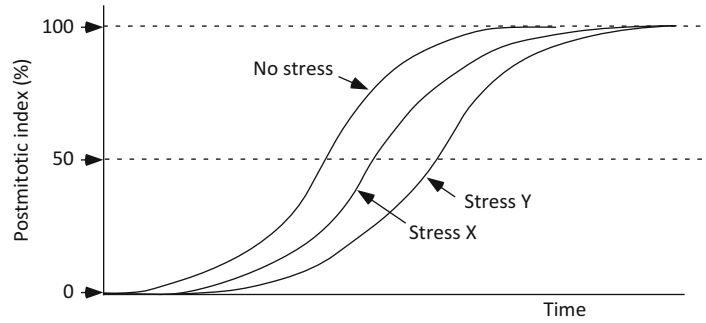

Fig. 2 Effect of stress on cell cycle advance in synchronized cells. Cells go through mitosis synchronously after elutriation. When cells are treated with different types of stress or different amounts of stress, mitosis is delayed

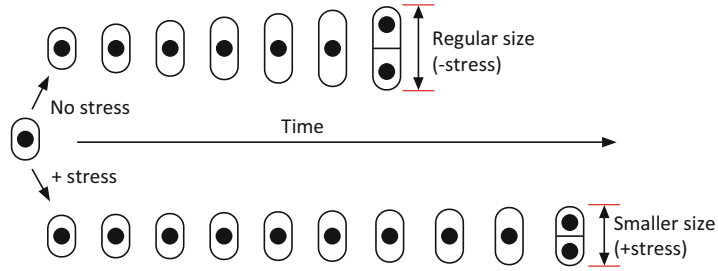

Fig. 3 Effect of stress on cell size. In a regular (no-stressed) cell cycle, G2 cells grow, enter mitosis, and septate at about 13–14 μm in length. When cells are stressed, entry into mitosis is delayed and they divide at smaller cell size (<13–14 μm)

for cell size analysis. On average, septum-containing non-stressed cells grown in rich media are 13–14 μM in length. Many stress conditions cause cells to divide at smaller sizes (Fig. 3).

1. At each time point, before collecting cells, transfer a small portion (100 μL) of cell culture to a microcentrifuge tube and keep on ice until the time course cell collection experiment is finished. Stress conditions affect cell cycle progression. The degree of cell cycle delay is dependent on stress types and stress amounts (Fig. 2).
2. Using Nomarski optics, determine the presence or the absence of septum in the fission yeast cells (*see* **Note 10**). Calculate the percentage of septated cells in the total population as a measure of the post-mitotic state of each cell.
3. Photograph control and treated cells using Nomarski optics, and digitally measure the cell length (*see* **Note 11**).

3.4 Cdk Activation

The most important biochemical hallmark of G2/M progression in fission yeast is Cdc2 (Cdk) phosphorylation at tyrosine 15 (Y15). Phosphorylation of Cdc2 by Wee1 and Mik1 blocks mitotic entry, while dephosphorylation by Cdc25 allows the cell entry into mitosis. Therefore, Y15 phosphorylation of Cdc2 is an excellent marker to determine cell cycle stage upon stress induction. This is especially relevant since elutriation synchronizes cells in early G2 phase (with phosphorylated Cdc2), and any change caused by stress on cell cycle progression will be readily visualized at the first mitotic entry.

1. Resuspend frozen cells prepared in Subheading 3.2 in 200 μL of lysis buffer.
2. Add glass beads, enough to reach the liquid surface.
3. Break cells using Fastprep at 4 °C (two cycles of 40 s, output 6.0).

4. Pierce the tube with a hot needle.
5. Place the pierced tube on top of a new 1.5-mL microcentrifuge tube and centrifuge (500 × *g* for 30 s) in order to collect cell lysate in the bottom tube.
6. Discard the tubes that contain the glass beads.
7. Add 100 μL of lysis buffer to the lysate.
8. Mix by vortexing.
9. Centrifuge at 15,000 × *g* for 15 min at 4 °C.
10. Transfer the supernatant to a new 1.5-mL microfuge tube.
11. Estimate protein concentration by A_{280} absorbance or any colorimetric method.
12. Take up to 20 μL of cellular lysate (20–50 μg of whole-cell extract).
13. Mix with appropriate volume of 5× SDS loading buffer.
14. Incubate for 5 min at 100 °C.
15. Mix by vortexing.
16. Load the sample in a 12–15 % SDS-PAGE gel, and perform electrophoresis.
17. Transfer proteins to PVDF membrane for Western blotting.
18. After transfer, wash the membrane with water.
19. Stain the membrane with Ponceau S for 1–2 min.
20. Destain the membrane with water, and observe equal protein loading in all lanes.
21. Block the membrane with 5 % BSA in TBS + Tween 20 for 1 h at room temperature.
22. Incubate the membrane with the anti-phospho Cdc2-Tyr15 antibody (diluted 1:1,000 in TBS-T containing 5 % BSA) for 2 h at room temperature or overnight at 4 °C (*see* **Note 12** for loading control).
23. Wash the membrane with TBS-T, for 10 min, three times.
24. Incubate the membrane with secondary antibody (anti-rabbit IgG HRP-linked diluted 1:5,000 in TBS-T containing 5 % BSA) for 1 h at room temperature.
25. Wash the membrane with TBS-T, for 10 min, three times.
26. Wash the membrane with TBS for 10 min.
27. Incubate the membrane with chemiluminescent HRP substrate for 1 min.
28. Expose the membrane to an X-ray film in a darkroom and develop.

4 Notes

1. The sample reservoir equipped with the JE 5.0 elutriation system serves as a bubble trap (Fig. 1).
2. When moving inlets from flask to flask, switch off the valve to that inlet. Move the "off" inlet to the new flask. Switch on again the inlet. Only one of the two inlet tubes works at any given time. Never close both inlets at the same time. One can be initially used for culture and the second one for fresh medium.
3. Set the bubble trap: pump medium into the bubble trap. Invert the tube to fill it up with liquid. From this moment, always keep the active inlet inside the culture or the fresh medium in order to prevent trapping air back in the system.
4. The centrifuge has a strobe flash lamp installed on the side of the rotation axis at the bottom of the centrifugation chamber. The flash lamp is covered by an opaque plastic window. During operation, a signal from the centrifuge spindle tachometer triggers the strobe once per revolution, allowing the observation of the transparent rotor chamber and the cell density inside through the centrifuge window.
5. Cells start accumulating in the centrifugation chamber because the system is introducing cell-containing medium through the inlet and discarding cell-free medium through the outlet (Fig. 1c). It may take about 30 min to introduce most cells in the elutriation chamber.
6. This step allows for keeping the flow without introducing additional cells in the elutriation chamber. Therefore, there is a stable, closed-circuit system where no new cells enter the system, and the culture inside the chamber has reached equilibrium (no net entry or exit) (Fig. 1e).
7. If collected cells are not well synchronized, they can be reintroduced in the rotor and restart the collection process.
8. We consider that all cells with a septum have finished mitosis (post-mitotic). When estimating post-mitotic cells, be careful with small G2 cells that appear after the first mitosis. They belong to a second mitotic cycle, originated from a single mother cell, so they should be counted as half-cells.
9. We describe a protocol where stress is induced at early G2 phase. By using this protocol it is also possible to induce stress at later time points, although it should be noted that synchrony fades away after one cycle.

10. The use of Nomarski optics is important because staining is not required. We counted a minimum of 200 cells per observation. We consider that about 1 % septation is acceptable to start the experiment.
11. A total of 50 septated cells should be measured to obtain average length. Software provided by the microscope camera provider was used, but other software could be used (Adobe Photoshop).
12. As a loading control, total Cdc2 may be monitored using a similar protocol but with the anti-Cdc2 antibody.

Acknowledgements

Research in MARG laboratory is supported by grant BFU2009-09116 awarded by MICINN/MINECO (Spanish Government).

References

1. Schrödinger E (1944) What is life? Cambridge University Press, Cambridge, UK
2. Russell P, Nurse P (1986) *cdc25*$^{+}$ functions as an inducer in the mitotic control of fission yeast. Cell 45(1):145–153
3. Russell P, Nurse P (1987) Negative regulation of mitosis by *wee1*$^{+}$, a gene encoding a protein kinase homolog. Cell 49(4):559–567
4. Gould KL, Nurse P (1989) Tyrosine phosphorylation of the fission yeast *cdc2*$^{+}$ protein kinase regulates entry into mitosis. Nature 342 (6245):39–45
5. Walker GM (1999) Synchronization of yeast cell populations. Methods Cell Sci 21(2–3): 87–93

Chapter 21

Analyzing Ras-Associated Cell Proliferation Signaling

Matthew C. Stout, Edgar Asiimwe, James R. Birkenstamm, Su Yeon Kim, and Paul M. Campbell

Abstract

Ras-dependent signaling is an important regulator of cell cycle progression, proliferation, senescence, and apoptosis. Several of the downstream effectors of Ras play dual roles in each of these processes. Under one set of conditions, they promote cell cycle progression and proliferation; yet, in a different paradigm, they drive cell cycle arrest and apoptosis. Furthermore, there is cross talk between certain downstream effectors of Ras including the PI3K–AKT and Raf–MEK–ERK pathways. Here we describe a series of experiments used to dissect the effect of different Ras-dependent signaling pathways on cell cycle progression, proliferation, senescence, and apoptosis. Furthermore, we highlight the importance of consistent growth conditions of cells in culture when studying Ras-dependent signaling as we show that the activation of downstream effectors of Ras changes with the confluency at which the cells are grown.

Key words Ras, Cell cycle, Proliferation, Senescence, Anoikis, Pulldown assay, Confluency

1 Introduction

Ras proteins (H-, K-, and N-Ras) are part of a superfamily of small GTPases, functioning as signaling nodes that convey extracellular stimuli into an intracellular response. They are targets of signaling cascades initiated by a variety of cell surface receptors and proteins, such as tyrosine kinases, integrins, and G protein-coupled receptors [1]. Once active, Ras activates numerous downstream effector pathways, which affect a variety of cellular functions including cell cycle regulation, proliferation, anoikis, and senescence [2–5]. Many signaling pathways are implicated in regulating these cellular functions but the most studied are the Raf–MEK–ERK, PI3K–AKT, and RalGEF–Ral pathways. Other important proteins investigated in these cellular functions include cyclin D1, CDK4, c-Myc, p16, p53, pRB, and BRAF. While Ras is a critical signaling node for normal cellular activity, we, like many others, tend to focus on the aspects of Ras biology that directly relate to cancer initiation and malignancy.

Eishi Noguchi and Mariana C. Gadaleta (eds.), *Cell Cycle Control: Mechanisms and Protocols*, Methods in Molecular Biology, vol. 1170, DOI 10.1007/978-1-4939-0888-2_21,

The Raf–MEK–ERK, PI3K–AKT, and RalGEF–Ral pathways have been well studied for their effects on cell cycle progression, cell survival, and proliferation. To date, the least studied pathway is the RalGEF–Ral pathway. However, studies investigating the role of RalA and RalB in these processes have shown opposing roles for RalA and RalB despite their gene and amino acid similarities [6, 7]. RalA is required for anchorage-independent proliferation, and RalB is required for suppression of apoptosis [6]. The Raf–MEK–ERK pathway has dual roles in that it can initiate cell survival leading to proliferation or it can initiate cell death. When activated by phosphorylation, ERK1/2 translocates to the nucleus and enhances the transcription of growth-related proteins including Elk1, Sap-1a, and TIF-IA [8–11]. Activated ERK1/2 also inactivates components of the cell death machinery such as FOXO transcription factors [12–14]. However, ERK1/2 can promote cell death by being sequestered in the cytoplasm by a variety of proteins like DAPK and activating autophagy and other death cascades [15]. The PI3K–AKT pathway is known as a cell survival pathway. It promotes progression through the cell cycle by phosphorylating forkhead transcription factors inactivating them, which promotes the expression of cyclin D1 [13, 16–18]. Also, activated AKT inhibits GSK3β by phosphorylation, which stabilizes cyclin D1 and c-Myc [19, 20], both of which are needed for cell cycle progression. To promote survival, AKT negatively regulates transcription factors that promote cell death, such as forkhead transcription factors FKHR, FKHRL1, and AFX, and it also upregulates anti-apoptotic genes IKK and CREB [21–25]. These three pathways highlight the complexity that governs the cellular processes of cell cycle progression, cell survival, and proliferation.

These pathways and cellular functions are studied using a variety of cell model systems, ranging from primary cells to immortalized and/or transformed cells to cancer cell lines. In addition, constitutively active or dominant negative mutants have been generated to help decipher the role of each pathway in each process. Furthermore, small-molecule inhibitors and shRNAs are used to knock down these proteins in cell model systems [26].

The usual readouts for experiments with these cell model systems are western blots for the presence or the absence of specific proteins. However, these experiments provide only a part of the story about how Ras affects cell cycle and proliferation. Additional experiments such as EMSA, BrdU incorporation, enzyme-linked immunosorbent assay (ELISA), fluorescence-activated cell sorting (FACS), or immunohistochemistry focus on the function of proteins or their interaction with other proteins or DNA and thus provide more useful information.

2 Materials

2.1 Electrophoretic Mobility Shift Assay

1. NPBT buffer: 10 mM Tris–HCl pH 7.4, 140 mM NaCl, 2 mM $MgCl_2$, 0.1 % Triton X-100, 1 mM dithiothreitol (DTT), 20 mM β-glycerophosphate, 100 μM sodium orthovanadate, 0.5 mM PMSF, 1 μg/mL of aprotinin, 1 μg/mL of leupeptin.
2. 50 % Sucrose cushion: 0.5 M Sucrose in NPB buffer (*see* below for recipe).
3. NPB buffer: 10 mM Tris–HCl pH 7.4, 140 mM NaCl, 2 mM $MgCl_2$, 1 mM DTT, 20 mM β-glycerophosphate, 100 μM sodium orthovanadate, 0.5 mM PMSF, 1 μg/mL of aprotinin, 1 μg/mL of leupeptin.
4. Microcentrifuge.
5. DC buffer: 20 mM HEPES–NaOH pH 7.9, 25 % glycerol, 420 mM NaCl, 1.5 mM $MgCl_2$, 0.2 mM EDTA, 1 mM DTT, 20 mM β-glycerophosphate, 100 mM sodium orthovanadate, 0.5 mM PMSF, 1 μg/mL of aprotinin, 1 μg/mL of leupeptin.
6. Binding buffer: 10 mM HEPES–KOH pH 7.9, 10 % glycerol, 50 mM KCl, 5 mM $MgCl_2$, 0.1 mM EDTA, 1 mM DTT, 2.5 μg of poly[d(I–C)].
7. 0.1 ng of ^{32}P-labeled oligonucleotide.
8. 6 % Non-denaturing polyacrylamide gel.
9. 0.25× TBE: Dilute 5× TBE (for 1 L dissolve 54 g of Tris base and 27.5 g boric acid in 900 mL of deionized water, add 20 mL of 0.5 M EDTA pH 8.0, bring total volume to 1 L by adding deionized water) with deionized water.

2.2 Detection of Senescence

1. 1× PBS, pH 7.4: 136.9 mM NaCl, 2.68 mM KCl, 8.1 mM Na_2HPO_4, 1.47 mM KH_2PO_4.

2.2.1 β-Galactosidase Staining

2. 3 % Formaldehyde.
3. Senescence-associated β-galactosidase stain solution: 1 mg of 5-bromo-4-chloro-3-indolyl β-galactosidase (X-Gal) per mL, 40 mM citric acid/sodium phosphate pH 6.0, 5 mM potassium ferrocyanide, 5 mM potassium ferricyanide, 150 mM NaCl, and 2 mM $MgCl_2$.
4. Dry incubator (no CO_2).
5. 70 % glycerol.
6. Bright-field microscope.

2.2.2 Bromo-Deoxyuridine Labeling

1. Growth medium containing 40 μM bromo-deoxyuridine (BrdU).
2. 1× PBS (*see* Subheading 2.2.1, **item 1**).

3. 4 % Paraformaldehyde.
4. Ice-cold methanol–acetone.
5. Anti-BrdU antibody (clone BU-33, Sigma).
6. Blocking buffer: 5 % Goat serum, 5 % horse serum, 0.2 % Tween 20 in 1× PBS.
7. 4′,6′-Diamidino-2-phenylindole (DAPI) in 1× PBS at 1:500.
8. Fluorescence microscope.

2.3 Detection of Anoikis

1. 20 mg/mL Poly-HEMA (2-hydroxyethyl methacrylate) solution: Dissolve poly-HEMA powder in 95 % ethanol.
2. 95 % Ethanol.
3. Sterile tissue culture (TC) dishes or plates.
4. Sterile 1× PBS.

2.3.1 Poly-HEMA-Coated Plates

2.3.2 Death Assay ELISA

1. Sterile TC dishes or plates.
2. Sterile TC dishes or plates coated with poly-HEMA.
3. 0.05 % Trypsin/EDTA (available from various commercial sources).
4. Cell Death Detection ELISA kit (Roche, 11-544-675-001) including incubation buffer, coating buffer, adhesive plate cover foils, washing buffer, conjugate solution (dilute 1 mL of anti-DNA-POD with 9 mL of incubation buffer), and substrate buffer.
5. Plate incubator at 15–25 °C.
6. 96-Well plates.
7. Plate shaker.
8. Microplate reader able to read 405 nm.

2.4 Flow Cytometry for Senescence and Anoikis

1. Sterile TC dishes or plates.
2. Sterile TC dishes or plates coated with poly-HEMA.
3. 0.05 % Trypsin/EDTA.
4. Cold saline GM solution: 6.1 mM Glucose, 1.5 mM NaCl, 5.4 mM KCl, 1.5 mM Na_2HPO_4, 0.9 mM KH_2PO_4, 0.5 mM EDTA.
5. 100 % ethanol.
6. 1× PBS supplemented with 5 mM EDTA.
7. Propidium iodide (PI) staining solution: 30 μg/mL PI, 300 μg/mL RNase A in 1× PBS.
8. 30 μm nylon mesh.

2.5 The Effect of Confluency on Ras-Dependent Signaling

2.5.1 Harvesting Mammalian Cells

1. Chilled non-sterile 1× PBS.
2. Chilled microcentrifuge tubes.
3. Microcentrifuge.
4. Cell scrapers.

2.5.2 Lysis of Cells

1. Magnesium lysis buffer (MLB) lysis buffer: 25 mM HEPES pH 7.5, 150 mM NaCl, 10 % NP-40, 0.25 % Na-deoxycholate, 10 % glycerol, 10 mM $MgCl_2$.
2. Protease and phosphatase inhibitor cocktail (Thermo Scientific Halt Combined Protease and Phosphatase Inhibitor Cocktail).
3. Microcentrifuge at 4 °C.
4. BCA Protein Quantification Assay Kit (Pierce, Thermo Scientific).

2.5.3 Ras-GTP or Ral-GTP Pulldown Assay

1. Centrifuges: Microcentrifuge (e.g., Eppendorf 5430R, rotor: FA-45-30-11), tabletop centrifuge (e.g., Eppendorf 5810R, rotor: A-4-62), and floor centrifuge (e.g., Sorvall RC 5C Plus, rotor: SLA-1500).
2. LB broth with ampicillin: Casein peptone 10 g/L, yeast extract 5 g/L, NaCl 10 g/L, ampicillin (final concentration 0.1 mg/mL).
3. LB broth without ampicillin: Casein peptone 10 g/L, yeast extract 5 g/L, NaCl 10 g/L.
4. pGEX-4T1, pGEX-Raf-1 RBD, and pGEX-RalBD constructs (*see* **Note 1**).
5. 0.1 M Isopropyl-β-D-thiogalactopyranoside (IPTG).
6. MTPBS-EDTA buffer: 4 mM $NaH_2PO_4{\cdot}H_2O$, 16 mM $Na_2HPO_4{\cdot}7H_2O$, 150 mM NaCl, 50 mM EDTA.
7. Protease and phosphatase inhibitor cocktail (Thermo Scientific Halt Combined Protease and Phosphatase Inhibitor Cocktail).
8. Sonicator.
9. 10 % (v/v) Triton X-100: 100 % Triton X-100 dissolved in deionized water.
10. Glutathione agarose beads (BD BaculoGold Glutathione Agarose Beads).
11. MLB lysis buffer: 25 mM HEPES, 150 mM NaCl, 10 % NP-40, 0.25 % Na deoxycholate, 10 % glycerol, 10 mM $MgCl_2$.
12. 1× Laemmli buffer: 100 mM 0.5 M Tris–HCl pH 6.8, 20 % glycerol, 4 % SDS, 0.2 % bromophenol blue, 200 mM β-mercaptoethanol.
13. SDS-PAGE gel and standard western blot materials.

3 Methods

3.1 Electrophoretic Mobility Shift Assay

The experiments described in this section focus on interaction of proteins with DNA. They allow us to decipher the signaling pathways, one intermediate at a time, in order to build an accurate understanding of how a cell responds to a particular stimulus and how that stimulus affects the cell cycle and subsequent proliferation. An electrophoretic mobility shift assay (EMSA) allows you to determine if transcription factors bind a particular sequence of DNA, typically transcription regulatory sequences.

In EMSA, protein–DNA complexes migrate more slowly than free DNA molecules in gel electrophoresis. The use of EMSA has provided valuable evidence that Ras is involved in many cell cycle regulatory pathways. Seminal work by Pestell showed that Ras can induce the cyclin D1 promoter in several different cell types [27]. In EMSA using nuclear extracts from cultured and primary cells, several heterodimeric AP-1 proteins (c-Jun, JunB, JunD, and c-Fos) bound the -954 region of the cyclin D1 gene promoter [27]. Furthermore, Vaque et al. showed using EMSA that c-Myc inhibits Ras-mediated AP-1 activity and c-Jun expression [28]. This work highlights just one aspect of the complex interaction of c-Myc with Ras signaling to promote cell cycle processes.

3.1.1 Nuclear Extract Preparation

1. Suspend $1–5 \times 10^7$ cells in 300 μL of NPBT buffer.
2. Incubate for 10 min on ice.
3. Recover nuclei by centrifugation through a 50 % sucrose cushion in NPB buffer for 10 min at $15{,}000 \times g$ at 4 °C (*see* **Note 2**).
4. Suspend nuclear pellets in 100–200 μL of DC buffer and rotate for 30 min at 4 °C.
5. Clarify nuclear extracts by centrifugation for 10 min at $15{,}000 \times g$ at 4 °C.

3.1.2 EMSA

1. In 20 μL volume reactions, mix 5–10 μg (protein amounts) of nuclear extract in binding buffer with 0.1 ng of ^{32}P-labeled oligonucleotide (*see* **Note 3**).
2. Incubate for 30 min at room temperature.
3. Resolve DNA–protein complexes and free probe at room temperature on a 6 % non-denaturing polyacrylamide gel with 0.25× TBE. Run gel at 4 °C at 180 V for 2–4 h. Dry gel and expose to autoradiographic film.

3.2 Detection of Senescence

Both senescence and anoikis (apoptosis which results from the loss of attachment to a substrate) represent phenotypes of normal cell biology that serve to remove cells from the mitotic population. While Ras signaling can initiate the former in normal cells, aberrant

Ras activation in tumor cells drives the escape from both of the phenotypes. Senescence-associated (SA) β-galactosidase staining and BrdU labeling are common techniques used to determine if cells have arrested their cell cycle and become senescent. BrdU labeling stains cells that are actively replicating their DNA, while β-galactosidase staining labels cells that have undergone senescence by quantifying SA β-galactosidase activity [29]. Furthermore, sorting cells by FACS allows one to accurately determine the percentage of the cell population that is proliferating, senescent, or apoptotic.

The use of these techniques has shown that oncogenic Ras provokes premature cell senescence associated with accumulation of p53 and $p16^{INK4a}$ [30]. Furthermore, results from these techniques have indicated that culture-imposed stress sensitizes cell to Ras-induced arrest [31]. Additionally, these techniques have helped decipher the complex interaction of Ras and c-Myc. Zhuang et al. [32] showed that c-Myc overexpression is required for continuous suppression of Ras-induced senescence in melanoma cells.

3.2.1 β-Galactosidase Staining

1. Grow cells in a 24-well plate. The starting number of cells varies depending on the exact experiment (duration, drug treatment, transduction or knockdown of ectopic genes, etc.).
2. Aspirate growth medium, and wash cells once with 1× PBS.
3. Fix for 3–5 min at room temperature in 250 μL of 3 % formaldehyde.
4. Wash two times with 500 μL 1× PBS, and add 250 μL of fresh senescence-associated β-Gal stain solution.
5. Incubate at 37 °C in a dry incubator (no CO_2) overnight.
6. Remove β-Gal stain solution. For long-term storage, overlay the cells with 250 μL of 70 % glycerol after removing the stain solution.
7. Count the number of β-galactosidase-positive cells (blue staining) under a bright-field microscope.

3.2.2 Bromo-Deoxyuridine Labeling

1. Incubate cells (here we describe parameters for 24-well plates) in growth medium supplemented with 40 μM BrdU for 4 h.
2. Aspirate growth medium containing BrdU and wash once with 1 mL of 1× PBS.
3. Fix cells in 500 μL of 4 % paraformaldehyde.
4. Permeabilize with 500 μL of ice-cold methanol–acetone.
5. Stain fixed cells for immunofluorescence by using the anti-BrdU antibody (1:1,000) in blocking buffer.

6. Stain nuclei with DAPI using 500 μL of 1:500 dilution (DAPI:PBS) in order to determine the total number of cells in a given field.
7. Photograph 100–500 nuclei per condition, and determine the percentage of BrdU-positive cells [31].

3.3 Detection of Anoikis

A fundamental technique used to study anoikis is the use of poly-HEMA-coated plates or low-attachment plates [33–36]. Cells cannot adhere to these plates, which will trigger anoikis in cells not resistant to it. This technique allows for the testing of different cell lines, mutants, or drugs in preventing anoikis or causing anoikis in resistant cells. With the utilization of poly-HEMA-coated plates and a death assay ELISA, McFall et al. [35] showed that oncogenic Ras blocks anoikis by activation of MEK independently of PI3K. Furthermore, using the same techniques, Ma et al. [36] showed that knockdown of $p66^{Shc}$ in normal epithelial cells leads to unrestrained Ras activation, preventing anoikis through downstream suppression of another Ras family small GTPase, RhoA. Conversely, lung cancer cell lines resistant to anoikis are made sensitive by re-expression of $p66^{Shc}$ [36]. In addition, Yu et al. have suggested that clusters of circulating tumor cells (CTCs) protect the inner cells from anoikis by providing cell–cell contact [37].

3.3.1 Poly-HEMA-Coated Plates

1. Make a 20 mg/mL solution of poly-HEMA (2-hydroxyethyl methacrylate) powder in 95 % ethanol, with mild heating and constant stirring overnight.
2. Coat sterile tissue culture dishes or plates with poly-HEMA solution and dry by evaporation from open plates in a sterile hood overnight (*see* **Note 4**).
3. Prior to use, surfaces should be washed twice with sterile 1× PBS.

3.3.2 Sample Preparation for Death Assay ELISA

1. Culture cells normally using testing conditions (mutants, drugs) on normal tissue culture-treated plates or poly-HEMA-coated plates (or low-attachment plates).

2 (a) To collect cells from normal tissue culture-treated plates, collect the growth medium (for floating cells) and transfer to a conical tube. Trypsinize the adherent cells as normal. Mix the trypsinized cells with the collected medium, and pellet the cells by centrifugation for 5 min at 200 × *g* at 4 °C.

2 (b) To collect cells from poly-HEMA-coated plates, collect all the growth medium into a conical tube and pellet the cells by centrifugation for 5 min at 200 × *g* at 4 °C.

3. Resuspend the cell pellets with 500 μL of incubation buffer and transfer to a clean microcentrifuge tube.

4. Mix thoroughly by combination of pipetting and vortexing.
5. To lyse cells, incubate the samples for 30 min at 15–25 °C.
6. Centrifuge the lysate for 10 min at 20,000 × *g* at 4 °C.
7. Carefully remove 400 µL of the supernatant (cytoplasmic fraction) (*see* **Note 5**).
8. Pre-dilute the resulting supernatant 1:10 with cold (2–8 °C) incubation buffer.

3.3.3 ELISA

1. Pipette 100 µL of coating buffer into each well of a 96-well plate (*see* **Note 6**).
2. Cover with an adhesive plate cover foil, and incubate for 1 h (alternately overnight at 2–8 °C).
3. Aspirate coating buffer from all wells.
4. Pipette 200 µL of incubation buffer into each well.
5. Cover with an adhesive plate cover foil, and incubate for 30 min.
6. Aspirate incubation buffer from all wells.
7. Rinse wells three times with 300 µL of washing buffer, and aspirate washing buffer between each wash.
8. Pipette 100 µL of conjugate solution into each well except for blank.
9. Cover with an adhesive plate cover foil, and incubate for 90 min.
10. Aspirate conjugate solution from all wells.
11. Rinse wells three times with 300 µL of washing buffer, and aspirate washing buffer between each wash.
12. Pipette 100 µL of substrate buffer into each well.
13. Incubate on a plate shaker at 250 rpm until color development is sufficient for a photometric analysis (10–20 min).
14. Using a microplate reader, read the wells at 405 nm (*see* **Note 7**).

3.4 Flow Cytometry for Senescence and Anoikis

1. Follow Subheading 3.3.2, **steps 1** and **2**.
2. Resuspend cell pellets in 1 mL of cold saline GM solution.
3. Add 3 mL of 100 % ethanol to fix cells overnight at 4 °C.
4. Pellet cells by centrifugation for 5 min at 200 × *g* at 4 °C.
5. Wash cells once with 1 mL of 1× PBS containing 5 mM EDTA.
6. Pellet cells by centrifugation for 5 min at 200 × *g* at 4 °C.
7. Resuspend cell pellet in 1 mL of PI staining solution.
8. Stain cells for 1 h at room temperature in the dark.
9. Filter the cell suspension through a 30 µm nylon mesh to remove aggregates. Sample is now ready to be sorted on flow cytometer.
10. Collect 10,000 events, and analyze PI intensity using FL2 channel for relative DNA content (*see* **Note 8**).

3.5 The Effect of Confluency on Ras-Dependent Signaling

Ras signaling is important for translating extracellular stimuli into cellular responses. Because cell–cell contact has an impact on several elements of intracellular signaling, including Ras-dependent cascades, when investigating Ras signaling pathways in culture, it is important to keep the culturing conditions as consistent as possible. This includes growing the cells to a consistent confluency for all experiments. If the confluency of the cells varies between experiments, there is the possibility that the cells are receiving different signals due to the different number of cells present in the dish, resulting in altered cell–cell contact signaling and secreted paracrine factors (growth factors, apoptotic signals, chemokines, etc.).

Our work here shows that the activity of both Ras and its downstream effectors that we have previously described as being critical for proliferation regulation varies between different confluences of the same cell line. We tested several pancreatic adenocarcinoma cell lines growing at three different confluences (60 %, which is representative of our standard log-phase conditions, 95 % and overconfluent). We collected lysates from each cell line at each confluency and performed western blots probing for Ras, phosphorylated MEK1/2 (pMEK1/2), phosphorylated ERK1/2 (pERK1/2), phosphorylated AKT (pAKT), RalA, and RalB. We performed pull-down assays for GTP-loaded (active) Ras, RalA, and RalB [38, 39] prior to running a western blot probing for Ras, RalA, and RalB. Our results show that these signaling pathways change with different confluences. These changes are not predictable or consistent, as we observe different protein expression and/or activation patterns among the cell lines. Indeed, even upstream K-Ras expression and activity change across variable culture conditions and cell lines (Fig. 1). Another example of this unpredictable inconsistency is seen in RalA expression and activation in T3M4 cells (Fig. 1). While there are relatively equal amounts of total RalA in the three conditions, RalA-GTP diminishes considerably as the cells become more tightly packed. A similar trend is observed for CFPac1 cells, but the opposite occurs for MiaPaCa2 cells, where there is a slight but distinct increase in RalA activation as confluency increases. Comparing pERK1/2 to total ERK in MiaPaCa2 and T3M4 cells in Fig. 2, we observe similar expression levels of total ERK1/2 in both cell lines but different levels of pERK1/2. For MiaPaCa2, the levels of pERK1/2 activation increase with an increase in confluency, whereas the T3M4 samples have equal levels of pERK1/2 activation across all three confluences. It should be noted that the trends seen in downstream effector pathways do not closely follow the levels of either K-Ras expression or GTP loading, indicating that cells recruit effectors differently when placed in crowded culture scenarios. These results highlight the importance of keeping the environment, including confluency, that cells grow in as constant as possible and consistent between experiments when investigating Ras-related proliferation and death.

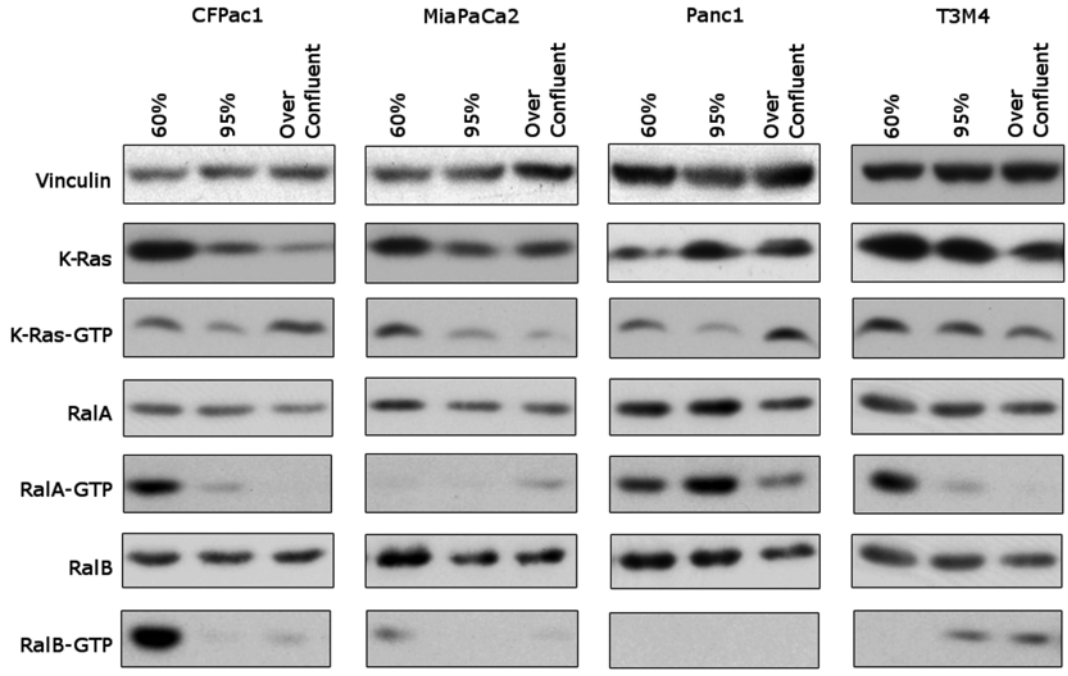

Fig. 1 Western blots of total and GTP-loaded K-Ras, RalA, and RalB in PDAC cell lines CFPac1, MiaPaCa2, Panc1, and T3M4. Samples were prepared from 60 %, 95 %, and over-confluent cell populations. Pulldowns were performed in order to blot for GTP-loaded proteins. Vinculin was used as a loading control

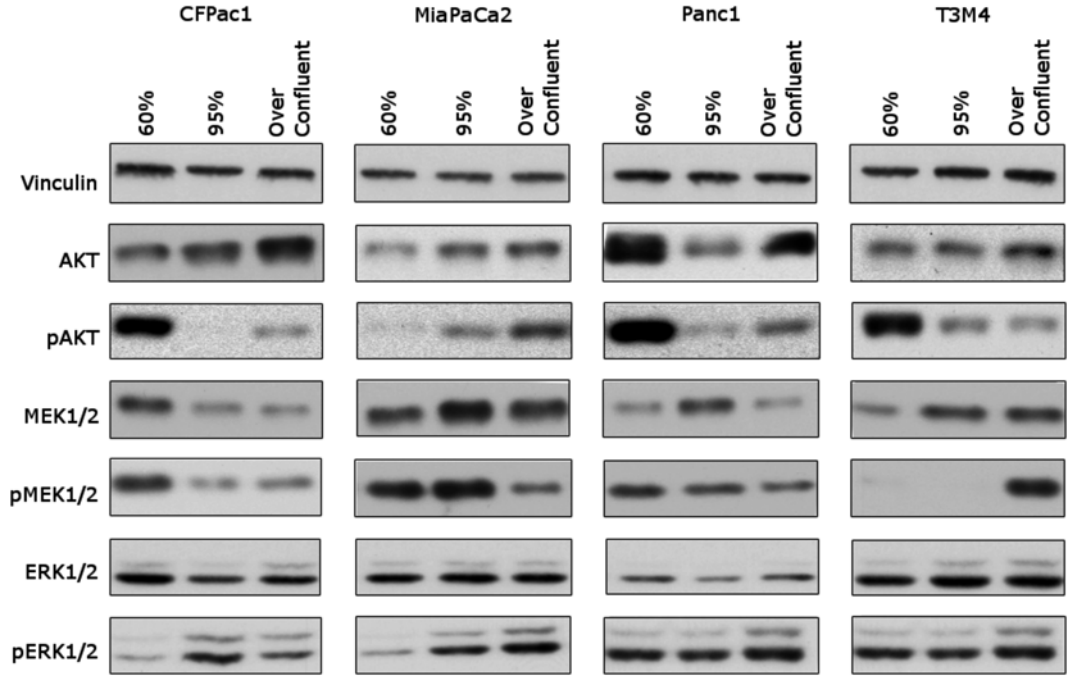

Fig. 2 Western blots of total and phosphorylated AKT, MEK1/2, and ERK1/2 in PDAC cell lines CFPac1, MiaPaCa2, Panc1, and T3M4. Samples were prepared from 60 %, 95 %, and over-confluent cell populations. Vinculin was used as a loading control. pAKT, phosphorylated AKT; pMEK1/2, phosphorylated MEK1/2; pERK1/2, phosphorylated ERK1/2

3.5.1 Harvesting Mammalian Cells

1. Chill non-sterile PBS on ice. Label appropriate microcentrifuge tubes. Chill microcentrifuge to 4 °C.
2. Remove plates of cells from the incubator and place on ice immediately (*see* **Note 9**). Aspirate medium, and rinse cells with 5 mL (for 10 cm plate) of ice-cold 1× PBS. Aspirate immediately (*see* **Note 10**).
3. Add 1 mL of 1× PBS to the first plate, and ensure that the cell surface is covered in PBS. Scrape cells with the blade of a cell scraper in a uniform fashion to pool the cells in the PBS. When the plate surface is cleared of cells, transfer the cell/PBS mixture with a pipette to the next plate, ensuring again that the cell surface is covered.
4. Repeat scraping, collecting, and transferring until all cells have been pooled into a single microcentrifuge tube. Transfer all to a chilled tube on ice.
5. When all the cells have been collected, spin tubes for 5 min at 200 × *g* at 4 °C in a microcentrifuge to pellet the cells. Aspirate the PBS completely and discard (*see* **Note 11**). Cells are ready to be lysed or frozen immediately at −80 °C.

3.5.2 Lysis of Cells

1. Add protease and phosphatase inhibitor cocktails to MLB buffer.
2. Resuspend cell pellet in appropriate volume of MLB buffer plus protease and phosphatase inhibitors by pipetting and vortexing (*see* **Note 12**).
3. Incubate on ice for 10 min.
4. Vortex for a few seconds.
5. Incubate on ice for 10 more min.
6. Centrifuge for 10 min at 21,000 × *g* at 4 °C in a microcentrifuge.
7. Transfer the supernatant to a new microcentrifuge tube (*see* **Note 13**).
8. Quantify protein concentration.
9. Use immediately or freeze at −80 °C for future use.

3.5.3 Ras-GTP or Ral-GTP Pulldown Assay

1. Inoculate 50 mL of LB-Amp cultures with glycerol stocks of *E. coli* containing either pGEX-Raf-1-RBD (*R*as-*b*inding *d*omain, for Ras-GTP pulldown), pGEX-RalBD (for Ral-GTP pulldown), or pGEX-4T1 (control vector). Grow overnight on shaker at 37 °C.
2. In the morning, add the 50 mL starter culture to 450 mL of sterile LB without Amp for each starter culture.
3. Grow for 1 h on shaker at 37 °C.
4. Induce by adding IPTG to a final concentration of 0.1 mM.

5. Grow for 2 h on shaker at 37 °C.
6. Centrifuge cells for 10 min at 5,500 × *g* at room temp.
7. Resuspend all cell pellets in 9 mL of MTPBS-EDTA plus inhibitor cocktail (freshly added).
8. Sonicate on ice at medium level, three times and 10 pulse cycles (50 % on/off), with about 10-s pausing between intervals to prevent warming (*see* **Note 14**).
9. Add 1 mL of 10 % Triton X-100 to make a final concentration of 1 %. Mix well.
10. Spin for 10 min at 3,200 × *g* at 4 °C.
11. Prepare glutathione beads (*see* **Note 15**). Use 5–15 μL of packed bead volume per experimental sample (*see* **Note 16**). First, quickly spin the beads down in a microcentrifuge and aspirate the supernatant (*see* **Note 17**). Wash the beads twice in 500 μL of MTPBS-EDTA plus inhibitors. Remove MTPBS-EDTA, and make a 1:1 slurry by adding a volume of MTPBS-EDTA plus inhibitors equal to the bead volume.
12. Transfer the supernatant of sonicated bacteria to a 15 mL tube, and add the washed glutathione beads (10–30 μL of the 1:1 slurry per experimental sample).
13. For Ras-GTP pulldown, rock the beads for 15 min at 4 °C. For Ral-GTP pulldown, rock beads for 10 min at room temperature.
14. Spin briefly to pellet beads.
15. Remove the supernatant and transfer to a new 15 mL tube (*see* **Note 18**).
16. Resuspend the beads in 500 μL of MTPBS-EDTA plus inhibitors and transfer to a microcentrifuge tube.
17. Wash two more times with 500 μL of MTPBS-EDTA plus inhibitors.
18. Wash once with 500 μL of MLB plus inhibitors.
19. Add a volume of MLB plus inhibitors equal to the bead volume to create a 1:1 slurry.
20. Use immediately or store on ice for use that day.
21. Thoroughly mix the prepared 1:1 slurry of beads containing the GST-RBD or GST-RalBD protein, and add 10–30 μL of the slurry to each experimental sample. The volume of each experimental sample should be equal to 100–250 μg (protein amounts) of lysate (prepared as in Subheading 3.5.2, **step 9**; *see* **Note 19**). Add 300–500 μL of MLB plus inhibitors to ensure that beads are free flowing. Set aside 10–20 μg (protein amounts) of lysate per sample in separate tubes to be run on the gel as a positive control for total Ras, RalA, and RalB proteins.

22. Tumble tubes for 30 min at 4 °C (*see* **Note 20**).
23. Collect beads by briefly centrifuging. Carefully aspirate as much liquid as possible.
24. Wash twice with cold MLB plus inhibitors by adding 500 μL and flicking the tube thoroughly.
25. Collect beads by briefly centrifuging, aspirate as much liquid as possible, and add 10–15 μL of 1× Laemmli buffer (*see* **Note 21**).
26. Load the entire volume of each sample, including the beads (*see* **Note 22**), onto an SDS-PAGE gel.
27. Perform western blot according to normal protocol.

4 Notes

1. The empty pGEX-4T-1 can be purchased from GE Healthcare Life Sciences or Addgene.
2. To recover the nuclei, add the cells resuspended in NPBT to a tube already containing NPB with the 50 % sucrose cushion. Centrifuge. Remove the supernatant, and resuspend the pellet (nuclei) in DC.
3. Some of the targets typically used are AP-1 proteins (such as c-Jun, JunB, JunD, and c-Fos), cyclin D, and c-Myc.
4. Coated plates are good for several weeks stored at room temperature and kept sterile. The volume of poly-HEMA varies depending on the size of the dish or the plate. It is important to use enough poly-HEMA to cover the surface of dishes or plates.
5. Cell pellet contains cell nuclei with high-molecular-weight, unfragmented DNA.
6. All incubation steps in Subheading 3.3.3 are at 15–25 °C. Samples should be done in at least duplicate. A negative control (untreated cells) should be analyzed, which allows calculation of an enrichment factor.
7. More information for this protocol is described in previous studies [36, 40].
8. Forward and side scatter gates and a doublet discrimination plot should be set to include whole- and individual cell populations, respectively. The resulting data should be analyzed to determine cell cycle distribution and sub-diploid/apoptotic cell fraction [41].
9. After removing cells from the incubator, all subsequent steps are done cold, either on ice or in a refrigerated centrifuge, with ice-cold reagents and tubes.
10. When collecting multiple plates into one microcentrifuge tube, be sure to aspirate as much of the PBS wash as possible.

If not enough of the PBS wash is aspirated, then the cell suspension might not fit in one microcentrifuge tube.

11. Using a needle and syringe to remove the PBS from the cell pellet allows for complete removal of the PBS without disrupting the cell pellet.
12. When pipetting to resuspend the cell pellet, wash the sides of the tube with the lysis buffer in order to collect the cells that might be on the sides of the tube instead of at the bottom with the pellet.
13. Keep lysates on ice at all times when working with them.
14. Sonication conditions may vary depending on the type of sonicator. These conditions may need to be optimized in each laboratory.
15. Make sure that the beads are resuspended well in the bottle before pipetting.
16. Prepare a larger volume (20–30 % more) of beads than needed per sample.
17. A needle and syringe work best for this. The fine tip of the needles allows you to get very close to the beads without aspirating the beads.
18. Save for future use as the bacterial lysate can be stored at 4 °C, usually for about a month, and reused to make additional GST-conjugated beads.
19. For Ras-GTP pulldown, 200–250 μg of lysate will be needed for each construct being tested and 10 μg of lysate for total protein (loading controls for western blot). For Ral-GTP pulldown, 100 μg of lysate will be needed for each construct being tested plus 10 μg for total RalA protein and 20 μg for total RalB protein.
20. Make sure that the total volume is larger enough so that the beads are free flowing and not staying in the bottom of the microcentrifuge tube.
21. The volume of 1× Laemmli buffer should be at least equal to the volume of beads.
22. Resuspend the beads in the Laemmli buffer just prior to loading to the gel so that the beads are completely suspended and all are loaded onto the gel. Flicking the tube or stirring with the pipet tip is the best way to resuspend the beads just prior to loading.

Acknowledgements

We would like to thank Channing J. Der for the kind gift of the GTPase-binding domain pGEX constructs used in the pulldown assays.

References

1. Malumbres M, Barbacid M (2003) RAS oncogenes: the first 30 years. Nat Rev Cancer 3:459–465
2. Mebratu Y, Tesfaigzi Y (2009) How ERK1/2 activation controls cell proliferation and cell death: is subcellular localization the answer? Cell Cycle 8(8):1168–1175
3. Kim JK, Diehl JA (2009) Nuclear cyclin D1: an oncogenic driver in human cancer. J Cell Physiol 220(2):292–296
4. Campisi J, d'Adda di Fagagna F (2007) Cellular senescence: when bad things happen to good cells. Nat Rev Mol Cell Biol 8: 729–740
5. Tokunaga E, Oki E, Egashira A, Sadanaga N, Morita M, Kakeji Y, Maehara Y (2008) Deregulation of the Akt pathway in human cancer. Curr Cancer Drug Targets 8(1):27–36
6. Chien Y, White MA (2003) RAL GTPases are linchpin modulators of human tumour-cell proliferation and survival. EMBO Rep 4(8): 800–806
7. Lim KH, O'Hayer K, Adam SJ, Kendall SD, Campbell PM, Der CJ, Counter CM (2006) Divergent roles for RalA and RalB in malignant growth of human pancreatic carcinoma cells. Curr Biol 16:2385–2394
8. Gille H, Sharrocks AD, Shaw PE (1992) Phosphorylation of transcription factor p62^{TCF} by MAP kinase stimulates ternary complex formation at c-*fos* promoter. Nature 358: 414–417
9. Lenormand P, Sardet C, Pages G, L'Allemain G, Brunet A, Pouyssegur J (1993) Growth factors induce nuclear translocation of MAP kinases (p42^{mapk} and p44^{mapk}) but not of their activator MAP kinase kinase (p45^{mapkk}) in fibroblasts. J Cell Biol 122(5):1079–1088
10. Chen RH, Sarnecki C, Blenis J (1992) Nuclear localization and regulation of erk- and rsk-encoded protein kinases. Mol Cell Biol 12(3):915–927
11. Zhao J, Yuan X, Frodin M, Grummt I (2003) ERK-dependent phosphorylation of the transcription initiation factor TIF-IA is required for RNA polymerase I transcription and cell growth. Mol Cell 11:405–413
12. Finnberg N, El-Deiry WS (2004) Activating FOXO3a, NF-kappaB and p53 by targeting IKKs: an effective multi-faceted targeting of the tumor-cell phenotype? Cancer Biol Ther 3(7):614–616
13. Burgering BM, Kops GJ (2002) Cell cycle and death control: long live Forkheads. Trends Biochem Sci 27(7):352–360
14. Dijkers PF, Medema RH, Pals C, Banerji L, Thomas NS, Lam EW, Burgering BM, Raaijmakers JA, Lammers JW, Koenderman L, Coffer PJ (2000) Forkhead transcription factor FKHR-L1 modulates cytokine-dependent transcription regulation of p27^{KIP1}. Mol Cell Biol 20(24):9138–9148
15. Chen CH, Wang WJ, Kuo JC, Tsai HC, Lin JR, Chang ZF, Chen RH (2005) Bidirectional signals transduced by DAPK-ERK interaction promote the apoptotic effect of DAPK. EMBO J 24(2):294–304
16. Schmidt M, Fernandez de Mattos S, van der Horst A, Klompmaker R, Kops GJ, Lam EW, Burgering BM, Medema RH (2002) Cell cycle inhibition by FoxO forkhead transcription factors involves downregulation of cyclin D. Mol Cell Biol 22(22):7842–7852
17. Burgering BM, Medema RH (2003) Decisions on life and death: FOXO Forkhead transcription factors are in command when PKB/Akt is off duty. J Leukoc Biol 73(6):689–701
18. Medema RH, Kops GJ, Bos JL, Burgering BM (2000) AFX-like Forkhead transcription factors mediate cell-cycle regulation by Ras and PKB through p27^{kip1}. Nature 404:782–787
19. Alt JR, Cleveland JL, Hannink M, Diehl JA (2000) Phosphorylation-dependent regulation of cyclin D1 nuclear export and cyclin D1-dependent cellular transformation. Genes Dev 14:3102–3114
20. Diehl JA, Cheng M, Roussel MF, Sherr CJ (1998) Glycogen synthase kinase-3B regulates cyclin D1 proteolysis and subcellular localization. Genes Dev 12:3499–3511
21. Biggs WH 3rd, Meisenhelder J, Hunter T, Cavenee WK, Arden KC (1999) Protein kinase B/Akt-mediated phosphorylation promotes nuclear exclusion of the winged heliz transcription factor FKHR1. Proc Natl Acad Sci U S A 96:7421–7426
22. Brunet A, Bonni A, Zigmond MJ, Lin MZ, Juo P, Hu LS, Anderson MJ, Arden KC, Blenis J, Greenberg ME (1999) Akt promotes cell survival by phosphorylating and inhibiting a Forkhead transcription factor. Cell 96:857–868
23. Rena G, Guo S, Cichy SC, Unterman TG, Cohen P (1999) Phosphorylation of the transcription factor forkhead family member FKHR by protein kinase B. J Biol Chem 274(24):17179–17183
24. Romashkova JA, Makarov SS (1999) NF-kB is a target of AKT in anti-apoptotic PDGF signaling. Nature 401:86–90

25. Du K, Montminy M (1998) CREB is a regulatory target for the protein kinase Akt/PKB. J Biol Chem 273(49):32377–32379
26. Campbell PM, Singh A, Williams FJ, Frantz K, Ulku AS, Kelley GG, Der CJ (2006) Genetic and pharmacologic dissection of Ras effector utilization in oncogenesis. Methods Enzymol 407:195–216
27. Albanese C, Johnson J, Watanabe G, Eklund N, Vu D, Arnold A, Pestell RG (1995) Transforming p21^{ras} mutants and c-Ets-2 activate the cyclin D1 promoter through distinguishable regions. J Biol Chem 270(40): 23589–23597
28. Vaque JP, Fernandez-Garcia B, Garcia-Sanz P, Ferrandiz N, Bretones G, Calvo F, Crespo P, Marin MC, Leon J (2008) c-Myc inhibits Ras-mediated differentiation of pheochromocytoma cells by blocking c-Jun up-regulation. Mol Cancer Res 6(2):325–339
29. Dimri GP, Lee X, Basile G, Acosta M, Scott G, Roskelley C, Medrano EE, Linskens M, Rubelj I, Pereira-Smith O et al (1995) A biomarker that identifies senescent human cells in culture and in aging skin *in vivo*. Proc Natl Acad Sci U S A 92:9363–9367
30. Serrano M, Lin AW, McCurrach ME, Beach D, Lowe SW (1997) Oncogenic *ras* provokes premature cell senescence associated with accumulation of p53 and p16I^{NK4a}. Cell 88: 593–602
31. Benanti JA, Galloway DA (2004) Normal human fibroblasts are resistant to RAS-induced senescence. Mol Cell Biol 24(7):2842–2852
32. Zhuang D et al (2008) C-MYC overexpression is required for continuous suppression of oncogene-induced senescence in melanoma cells. Oncogene 27:6623–6634
33. Frisch SM, Francis H (1994) Disruption of epithelial cell-matrix interactions induces apoptosis. J Cell Biol 124(4):619–626
34. Re F, Zanetti A, Sironi M, Polentarutti N, Lanfrancone L, Dejana E, Colotta F (1994) Inhibition of anchorage-dependent cell spreading triggers apoptosis in cultured human endothelial cells. J Cell Biol 127(2):537–546
35. McFall A, Ulku A, Lambert QT, Kusa A, Rogers-Graham K, Der CJ (2001) Oncogenic Ras blocks anoikis by activation of a novel effector pathway independent of phosphatidylinositol 3-kinase. Mol Cell Biol 21(16): 5488–5499
36. Ma Z, Liu Z, Wu RF, Terada LS (2010) p66^{Shc} restrains Ras hyperactivation and suppresses metastatic behavior. Oncogene 29: 5559–5567
37. Yu M, Stott S, Toner M, Maheswaran S, Haber DA (2011) Circulating tumor cells: approaches to isolation and characterization. J Cell Biol 192(3):373–382
38. Taylor SJ, Shalloway D (1996) Cell cycle-dependent activation of Ras. Curr Biol 6(12): 1621–1627
39. Campbell PM, Groehler AL, Lee KM, Ouellette MM, Khazak V, Der CJ (2007) K-Ras promotes growth transformation and invasion of immortalized human pancreatic cells by Raf and phosphatidylinositol 3-kinase signaling. Cancer Res 67(5):2098–2106
40. Ma Z, Myers DP, Wu RF, Nwariaku FE, Terada LS (2007) p66^{Shc} mediates anoikis through RhoA. J Cell Biol 179(1):23–31
41. Noonan EJ, Place RF, Basak S, Pookot D, Li LC (2010) miR-449a causes Rb-dependent cell cycle arrest and senescence in prostate cancer cells. Oncotarget 1(5):349–358

Chapter 22

Telomere Regulation During the Cell Cycle in Fission Yeast

Bettina A. Moser, Ya-Ting Chang, and Toru M. Nakamura

Abstract

The fission yeast *Schizosaccharomyces pombe* has emerged as a useful model organism to study telomere maintenance mechanisms. In this chapter, we provide detailed protocols for quantitative ChIP and BrdU incorporation analyses to investigate how fission yeast telomeres are regulated during the cell cycle by utilizing *cdc25-22* synchronized cell cultures.

Key words Cell cycle synchronization, *cdc25-22*, BrdU incorporation, Antibodies, Chromatin immunoprecipitation, Dot blot analysis, DNA hybridization, Real-time quantitative PCR

1 Introduction

Telomeres are the natural ends of eukaryotic chromosomes that must be protected from DNA repair enzymes and checkpoint response factors [1]. In most eukaryotic cells, telomeric DNA consists of G-rich repetitive sequences, and the telomere-specific reverse transcriptase known as telomerase is utilized to extend telomeric repeats to counteract loss of telomeric DNA during DNA replication by replicative DNA polymerases [2]. Telomeric repeat sequences provide binding sites for telomere-specific protective complexes, such as shelterin and CST (CTC1/Cdc13-Stn1-Ten1), which in turn regulate the accessibility of telomeres to DNA damage response factors and telomerase [3, 4]. While studies in the telomere field are often performed with asynchronous cell cultures, it is important to recognize that telomere maintenance mechanisms are carefully regulated during cell cycle, and in fact, recruitment of telomerase to telomeres has been found to be intimately linked to DNA replication [2, 5]. Therefore, in order to fully understand how cells ensure stable maintenance of telomeres, we must study them in the context of the cell cycle.

In recent years, the fission yeast *Schizosaccharomyces pombe* has emerged as an attractive model organism to study telomere biology, since it utilizes telomere factors that show high degree of

Eishi Noguchi and Mariana C. Gadaleta (eds.), *Cell Cycle Control: Mechanisms and Protocols*, Methods in Molecular Biology, vol. 1170, DOI 10.1007/978-1-4939-0888-2_22,

evolutionary conservation with mammalian telomere factors [4]. In this chapter, we describe our detailed protocol for chromatin immunoprecipitation (ChIP) assays on samples taken from synchronized cell cultures to characterize how the protein composition of telomeres is dynamically regulated during the cell cycle. While various ways to synchronize fission yeast cell cultures have been described [6, 7], we prefer the use of the temperature-sensitive *cdc25-22* allele, since no other method easily allows for collection of sufficient quantity of cells from synchronized cell cultures to carry out ChIP experiments. Cdc25 is a key regulator of cell cycle progression in fission yeast [8], and its inactivation causes cells to arrest in G2 phase. In addition, we describe our protocol for monitoring the replication timing of telomeric DNA by quantitatively determining the timing of BrdU incorporation after release from the *cdc25-22* cell cycle arrest in G2 phase.

Finally, both real-time quantitative PCR (qPCR)- and dot blot hybridization-based methods to analyze ChIP and BrdU incorporation experiments are described. While wild-type fission yeast cell telomeres are relatively short (~300 bp) and can be effectively characterized by both methods, the dot blot hybridization-based method should be carried out for mutant cells with longer (≥1 kb) telomeres. Although we only describe ChIP and BrdU incorporation protocols in this chapter, it should be noted that samples obtained from synchronized *S. pombe* cultures can also be used for other types of experiments, such as western blot analysis to monitor protein levels and/or protein modifications, co-immunoprecipitation analysis to monitor telomere complex formation, and Southern blot analysis to monitor telomere length variations. Thus, we hope that the protocols described here prove useful in elucidating cell cycle regulation of fission yeast telomeres in future studies.

2 Materials

2.1 Cell Cycle Synchronization of cdc25-22 Cells

1. YES medium: 5 g Yeast extract, 30 g glucose (dextrose), 100 mg leucine, 100 mg uracil, 100 mg histidine-HCl, and 100 mg Adenine per 1 L. Autoclave for 20 min.
2. Hydroxyurea (HU) stock solution: 1 M HU in ddH_2O. Filter-sterilize with a 0.22 μm filter, and store at −20 °C until use.

2.2 Chromatin Immunoprecipitation Analysis

1. Formaldehyde solution: 11 % Formaldehyde (v/v), 100 mM NaCl, 1 mM EDTA pH 8.0, 0.5 mM EGTA, 50 mM Tris–HCl pH 8.0.
2. 2.5 M glycine: Dissolve 93.8 g glycine in 500 mL ddH_2O, filter-sterilize, and store at room temperature.
3. Tris-buffered saline (TBS): 20 mM Tris–HCl pH 7.6, 150 mM NaCl. Store at 4 °C.

4. 0.5 mm Glass beads.
5. Fast Prep® FP120 (Qbiogene).
6. Misonix Sonicator 3000 with cup horn device.
7. Lysis buffer: 50 mM Hepes–KOH pH 7.5, 140 mM NaCl, 1 mM EDTA, 1 % (v/v) Triton X-100, 0.1 % (w/v) sodium deoxycholate, "Complete" protease inhibitor (Roche), 1 mM phenylmethylsulfonyl fluoride (PMSF). Prepare fresh on ice.
8. Lysis buffer 500: Replace 140 mM NaCl in lysis buffer (**item 7** above) with 500 mM NaCl and no protease inhibitors. Prepare fresh on ice.
9. Wash buffer: 10 mM Tris–HCl pH 8.0, 0.25 M LiCl, 0.5 % NP-40, 0.5 % sodium deoxycholate, 1 mM EDTA. Prepare fresh on ice.
10. TE buffer: 10 mM Tris–HCl, 1 mM EDTA pH 7.5. Store at 4 °C.
11. Antibodies: We commonly use monoclonal anti-myc (9B11, Cell Signaling 2276S) or anti-FLAG (M2, Sigma F1804) antibodies for myc- or FLAG-tagged proteins, respectively. Other antibodies that efficiently purify the protein of interest can also be used.
12. Dynabeads® Protein G (Life Technologies, 30 mg/mL).
13. Magnetic stand.
14. Chelex 100 Resin 10 %: 0.1 mg/mL in ddH_2O (BioRad). Prepare fresh.
15. Proteinase K: Dissolve Proteinase K (Invitrogen) at 10 mg/mL in 10 mM Tris–HCl pH 7.5, 20 mM calcium chloride, 50 % glycerol. Store at –20 °C.

2.3 Analysis of 5-Bromo-2-Deoxyuridine-Incorporated DNA

1. 5-Bromo-2-deoxyuridine (BrdU): 10 mM BrdU stock solution (3.07 mg/mL) in ddH_2O. Prepare fresh.
2. 1 M Sodium azide: Store at room temperature.
3. SP1 buffer: 1.2 M sorbitol, 50 mM sodium citrate, 50 mM sodium phosphate (Na_2HPO_4), 40 mM EDTA. Adjust pH to 5.6 using citric acid.
4. Zymolyase 100T (Amsbio).
5. 5× TE: 50 mM Tris pH 8.0, 5 mM EDTA.
6. 10 % Sodium dodecyl sulfate (SDS): 10 g SDS in 100 mL ddH_2O. Store at room temperature.
7. 5 M Potassium acetate: Dissolve 49.1 g KCH_3CO_2 in 100 mL ddH_2O. Autoclave, and store at room temperature.
8. Isopropanol.
9. DNase free RNase A (Fermentas).

10. Phenol: Equilibrated with 10 mM Tris pH 8.0, 1 mM EDTA.
11. Phenol, chloroform, and isoamyl alcohol mix (25:24:1), saturated with 10 mM Tris pH 8.0, 1 mM EDTA.
12. Chloroform and isoamyl alcohol mix (24:1).
13. Ethanol: Store at −20 °C.
14. 10 mM Tris–HCl pH 8.0: Store at room temperature.
15. Anti-BrdU antibody: 25 µg/mL (Becton Dickinson, 347580).
16. Dynabeads® Protein G: 30 mg/mL (Life Technologies).
17. Magnetic stand.
18. TBS: 20 mM Tris–HCl pH 7.6, 150 mM NaCl. Store at 4 °C.
19. 1× Phosphate-buffered saline (PBS): 8 g NaCl, 0.2 g KCl, 1.44 g Na_2HPO_4, 0.24 g KH_2PO_4 per 1 L ddH_2O. Dissolve components in 800 mL ddH_2O, adjust to pH 7.4 with HCl, and bring to 1 L with ddH_2O. Sterilize by autoclaving, and store at 4 °C.
20. IP buffer: Add 0.05 % Triton X-100 to 1× PBS.
21. TBSE: 10 mM Tris–HCl pH 7.5, 150 mM NaCl, 0.1 mM EDTA.
22. TBSE + Triton: TBSE + 1 % Triton X-100.
23. TE buffer: 10 mM Tris–HCl, 1 mM EDTA pH 7.5.
24. Chelex 100 Resin 10 %: 0.1 mg/mL in ddH_2O (BioRad). Prepare fresh.
25. Proteinase K: Dissolve Proteinase K at 10 mg/mL in 10 mM Tris–HCl pH 7.5, 20 mM calcium chloride, 50 % glycerol. Store at −20 °C.

2.4 Quantitative PCR Analysis

1. iQ SYBR Green Supermix (Bio-Rad).
2. PCR primers: jk380 (5′-TAT TTC TTT ATT CAA CTT ACC GCA CTT C-3′) and jk381 (5′-CAG TAG TGC AGT GTA TTA TGA TAA TTA AAA TGG-3′) [9].
3. iQ5 Real-Time PCR Detection System with iQ5 Optical Software (Bio-Rad).

2.5 Dot Blot Analysis

1. 1 M NaOH.
2. 500 mM EDTA.
3. Amersham Hybond-XL membrane (GE Healthcare).
4. Bio-Dot Microfiltration Apparatus (Bio-Rad).
5. 2× Saline sodium citrate (SSC): 300 mM NaCl, 30 mM Na citrate ($Na_3C_6H_5O_7{\cdot}2H_2O$).
6. UV Stratalinker 1800 (Stratagene).
7. Church buffer: 0.25 M Sodium phosphate buffer pH 7.2, 1 mM EDTA, 1 % BSA, 7 % SDS. Aliquot, and store at −20 °C.
8. Stratagene Prime It II Labeling Kit.

9. [α-^{32}P]-dCTP (3,000 Ci/mmol).
10. ProbeQuant G-50 Micro Columns (GE).
11. Telomeric probe template DNA: Gel purify a ~300 bp SacI-ApaI DNA fragment from pTELO plasmid and resuspend in 10 mM Tris, pH 8.5 (*see* **Note 1**).
12. 0.1× SSC, 0.1 % SDS.
13. PhosphorImager (Molecular Dynamics) and phosphorImager cassettes.

3 Methods

3.1 Cell Cycle Synchronization of cdc25-22 Cells

1. Grow a 500 mL culture of *cdc25-22* cells in YES medium overnight at 25 °C to OD_{600} = ~0.25 (early- to mid-exponential phase). Shift the cell culture to 36 °C for 3 h to arrest cells in G2 (*see* **Note 2**). Shift the culture back to 25 °C rapidly (*see* **Note 3**), incubate at 25 °C for the ongoing experiment, and take 30 mL aliquots every 20 min for 4 h (*see* **Note 4**).
2. In order to prevent telomere replication, HU can be added to the culture (15 mM final concentration) immediately after it has been shifted back to 25 °C. HU causes stalling of ongoing replication forks due to dNTP depletion and inhibits replication of late-replicating regions, including telomeres [5, 10].
3. Cell cycle progression should be monitored by measuring the septation index (% of cells with septum). *S. pombe* cells form a septum during G1/S phase, which can be easily monitored microscopically. The septation index should reach 60–80 % during S phase (Fig. 1). At every time point take ~5 μL culture to determine the septation index.

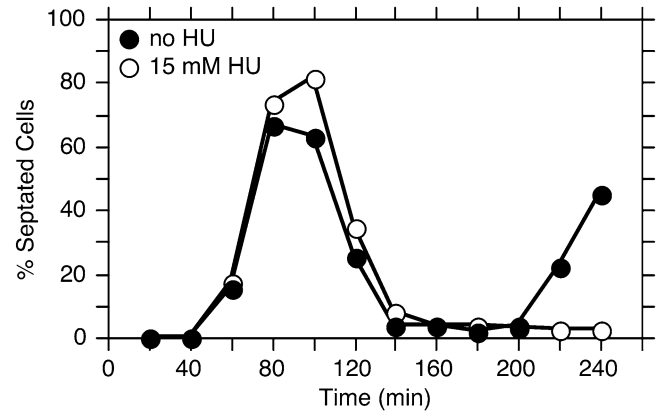

Fig. 1 Typical changes in the percentage of septated cells after release from a *cdc25-22* cell cycle arrest

3.2 Chromatin Immunoprecipitation Analysis

Cell cycle-regulated association of telomere proteins can be monitored by performing ChIP analysis of samples obtained from synchronized cell cultures (*see* Subheading 3.1). In ChIP analysis, proteins are first cross-linked to DNA with formaldehyde and then purified with protein-specific antibodies. DNA is recovered and analyzed for the presence of telomeric DNA sequences. While many ChIP protocols exist, we prefer a protocol that is short, is less toxic, and produces highly reproducible results by using Chelex 100 resin [11], rather than phenol–chloroform extraction or various commercially available spin columns designed to purify dsDNA to recover DNA (*see* **Note 5**).

1. Fix 30 mL aliquot samples (*see* Subheading 3.1) immediately with 1 % formaldehyde by adding 1/10 sample volume of formaldehyde solution and incubating for 20 min at room temperature by gently shaking.
2. Add 2.5 M glycine to a final concentration of 125 mM and incubate for 5 min at room temperature while shaking.
3. Collect cells by centrifugation (2,100 × *g* for 5 min) and transfer into a 1.5 mL screw top microcentrifuge tube.
4. Wash three times with 1 mL of TBS on ice (*see* **Note 6**). Snap-freeze the cell pellets in liquid nitrogen and store at −80 °C until further use (*see* **Note 7**).
5. Thaw cell pellets on ice. For all subsequent steps, work should be performed on ice or at 4 °C using ice-cold buffers.
6. Resuspend each cell pellet in 250 μL of lysis buffer, add glass beads, and lyse cells in Fast Prep® (*see* **Note 8**).
7. Recover lysate in a new microcentrifuge tube by punching a small hole into the bottom of the tube with a hot needle, putting the tube into a receiver tube (snap cap), and spinning at 376 × *g* for a few seconds in a microcentrifuge.
8. Sonicate lysate in an ice bath (Misonix Sonicator 3000 with cup horn device) to obtain DNA fragments ~500 bp (*see* **Note 9**). Centrifuge at 16,200 × *g* for 10 min at 4 °C. Recover supernatant.
9. Prepare 1–2 mg of lysate in 200 μL of lysis buffer for each ChIP (*see* **Note 10**). For input control, save 5 μL and process as described below. Until it is ready to be processed, it should be stored at −20 °C.
10. For ChIP samples, add 1 μg of antibody to the lysate and incubate with gentle rocking for 2 h at 4 °C.
11. Add 25 μL of Dynabeads® Protein G (*see* **Note 11**), and incubate for 1 h at 4 °C. Alternatively, preincubate the antibody with Dynabeads® Protein G for 1 h at 4 °C, wash the beads using the magnetic stand with 1 mL of lysis buffer to remove

excess antibody, add the beads to lysates, and incubate for 2–3 h at 4 °C. The amount of antibody and beads can be adjusted depending on the protein of interest and its epitope.

12. Using the magnetic stand, wash beads successively 2× with 1 mL of lysis buffer (*see* **Note 12**), 2× with 1 mL of lysis buffer 500, 2× with 1 mL of wash buffer, and 2× with 1 mL of TE buffer. For washing with lysis buffer 500 and wash buffer, samples should be incubated for 10 min at 4 °C on a rotating device. Remove all liquid after the final wash (*see* **Note 13**).
13. Add 100 µL of 10 % Chelex 100 Resin to input (*see* **step 9** above) and bead samples, mix, and boil for 15 min to reverse the formaldehyde cross-link in order to recover DNA (*see* **Note 14**).
14. Cool samples to room temperature, add 2 µL of Proteinase K, and incubate at 55 °C for 30 min while shaking.
15. Add an additional 100 µL of ddH_2O. Boil for 10 min, and recover 130 µL of supernatant (*see* **Note 14**). Store samples at −20 °C.
16. Samples are now ready for qPCR analysis (*see* Subheading 3.4) or dot blot analysis (*see* Subheading 3.5).

3.3 Analysis of BrdU-Incor-porated DNA

BrdU is a thymidine analog, and its incorporation into newly synthesized DNA during cell cycle progression allows for monitoring the progression of the DNA replication fork. Anti-BrdU antibodies can be utilized in immunoprecipitation to purify BrdU-labeled DNA from bulk DNA samples. The protocol described here has been used to determine the timing of replication at telomeres in our lab [5], but it can also be adapted to monitor replication timing of other genomic loci.

For this experiment, modified fission yeast cells carrying the human equilibrative nucleoside transporter 1 (*hENT1*) gene and the *Herpes simplex* virus thymidine kinase (*hsv-tk*) gene are used. Expression of hENT is required for efficient entry of BrdU into cells, and expression of TK is necessary to incorporate BrdU into DNA [12, 13].

1. Synchronize *cdc25-22 hENT hsv-tk* cells as described above (*see* Subheading 3.1).
2. After the arrested cell culture has been shifted back to 25 °C, add BrdU to the culture to a final concentration of 50 µM. Incubate cells at 25 °C, and take 30 mL of aliquots every 20 min.
3. Add sodium azide to each aliquot to a final concentration of 10 mM.
4. Spin at 2,100 × *g* for 5 min.
5. Wash pellets in 1 mL of SP1 buffer, transfer to a 1.5 mL microcentrifuge tube, and centrifuge to collect cells as pellets.

6. Snap-freeze the cell pellets in liquid nitrogen and store at −80 °C.
7. Thaw cell pellets on ice, resuspend each in 1 mL of SP1 buffer supplemented with 0.2 mg/mL Zymolyase 100T, and incubate at 37 °C for 30–60 min while shaking in order to obtain protoplasts by digesting the cell wall. To monitor completion of the cell wall digestion, mix 2 μL of the protoplasts and 2 μL of 2 % SDS, and then check under a phase-contrast microscope (*see* **Note 15**).
8. Gently spin the protoplasted cells in a microcentrifuge at 1,500 × *g* for 2 min, and resuspend them in 0.9 mL of 5× TE. Bring to 1 % SDS by adding 100 μL of 10 % SDS, and incubate at 65 °C for 15 min.
9. Add 306 μL of 5 M potassium acetate (1.17 M final), and incubate on ice for 10 min. Spin sample at 16,200 × *g* for 10 min at 4 °C, and recover 800 μL of supernatant.
10. Add 1 volume (800 μL) of isopropanol to each sample, and incubate on ice for 30 min.
11. Spin sample at 16,200 × *g* for 15 min at 4 °C. Remove all liquid, and air-dry pellet for 10–15 min. When the color of the pellet turns from white to clear, move on to the next step.
12. Resuspend each sample in 500 μL of 5× TE + RNaseA (20 μg/mL) and incubate at 37 °C for 2 h. Wrap samples in aluminum foil to minimize exposure of BrdU-labeled DNA to light.
13. Extract samples sequentially with phenol, phenol/chloroform/isoamyl alcohol, and chloroform/isoamyl alcohol (500 μL each), and recover aqueous (top) phase, which contains DNA (*see* **Note 16**).
14. Precipitate DNA by adding 2.5× volume of −20 °C ethanol and incubating at −20 °C for 30 min.
15. Spin at 16,200 × *g* for 15 min at 4 °C, and wash pellet with 500 μL of 70 % ethanol. Remove any residual liquid, and air-dry pellet for 10–15 min.
16. Resuspend pellet in 50 μL of 10 mM Tris pH 8.0, and measure DNA concentration (*see* **Note 17**). Samples can be stored at −20 °C.
17. Prepare 2 μg of each DNA sample in 50 μL 10 mM Tris pH 8.0.
18. Sonicate samples to obtain DNA fragments ~500 bp (*see* **Note 9**). Fragmentation of DNA should be verified by running 4 μL of sample on a 1.5 % agarose gel. Samples can be stored at −20 °C.
19. For every sample, preincubate 1 μg (40 μL) of the anti-BrdU antibody with 30 μL of pre-washed Dynabeads® Protein G at 4 °C overnight. This step should be scaled up for the number of samples (= *n*) for each experiment (*see* **Note 18**).

20. Next day, using the magnetic stand wash beads with 1 mL of TBS, resuspend in 1 ml of TBS, and split into *n* times aliquots. Remove all liquid from the beads and resuspend in 100 μL of IP buffer each.
21. Use 6 μL of sonicated sample (*see* **step 18**), and add 54 μL of IP buffer. Heat denature at 95 °C for 5 min (*see* **Note 14**), and put immediately on ice.
22. Add 50 μL of the sonicated and denatured DNA (*see* **step 21**) to the 100 μL of the anti-BrdU/beads/IP buffer (*see* **step 20**). Incubate at room temperature for 2 h with gentle rocking. Reserve the remaining sonicated and denatured DNA sample as input and store at −20 °C.
23. Using the magnetic stand, wash beads successively 2× with 1 mL of TBSE, 4× with 1 mL of TBSE + Triton, and 1× with 1 mL of TE buffer. For each wash, incubate the beads for 10 min at 4 °C on a rotating device. After the final TE buffer wash, remove all liquid and keep beads only.
24. To recover DNA, add 100 μL of 10 % Chelex 100 Resin to input (*see* **step 22**) and bead samples (*see* **step 23**), mix, and boil for 15 min (*see* **Note 14**). Cool samples to room temperature.
25. Add 2 μL of Proteinase K, and incubate at 55 °C for 30 min while shaking.
26. Add an additional 100 μL of ddH_2O, boil for 10 min (*see* **Note 14**), and using the magnetic stand, recover 130 μL supernatant. Store samples at −20 °C.
27. Samples are now ready for qPCR analysis (Subheading 3.4) or dot blot analysis (Subheading 3.5).

3.4 Quantitative PCR Analysis

In this analysis, we quantify the amount of telomeric DNA that has been coprecipitated with a given protein in ChIP or telomeric DNA that has been pulled down with the anti-BrdU antibody. Primers have been designed against a region within the subtelomere immediately adjacent to the G-rich telomeric repeat sequence, ~400 bp from the end of wild-type length telomeres. It would be difficult to provide a universal protocol that covers various real-time PCR setups available in other labs. Thus, we will only describe our protocol, which utilizes SYBR Green to quantify PCR products. However, we hope that the following protocol may serve as a useful guideline for researchers who wish to utilize other types of real-time PCR reagents.

1. Input samples should be diluted 1:100 in ddH_2O, while IP samples can be taken straight for qPCR analysis (*see* **Note 19**).
2. PCR reaction: 2 μL sample, 1× iQ SYBR Green Supermix, 0.3 μM primers (*see* **Note 20**). PCR condition: 3 min 95 °C, followed by 40 cycles [20 s 95 °C, 40 s 60 °C].

3. Calculate % of precipitated DNA values based on ΔCt between input and IP samples with the following formula: [% of Precip itated DNA] = [100 × $E\Delta^{Ct}$]/[$D \times R$], where E = amplification efficiency of primer pairs, ΔCt = [Ct Input] − [Ct ChIP], D = [dilution factor of ChIP]/[dilution factor of input], and R = [Sample volume used in IP]/[Sample volume set aside for input control] (*see* **Note 21**).

3.5 Dot Blot Analysis

Dot blot analysis is preferred over qPCR for fission yeast strains that carry significantly longer telomeres (≥1 kb) than wild-type cells. This is because telomeric ends may be too distant from the subtelomeric region that is amplified in our qPCR analysis.

1. Use 120 μL of DNA sample, and bring to 0.4 M NaOH and 10 mM EDTA in a total volume of 300 μL. Heat sample at 100 °C for 10 min (*see* **Note 14**), and rapidly cool on ice.
2. Pre-wet Hybond-XL membrane in ddH_2O for 15 min.
3. Set up the Bio-Dot Microfiltration Apparatus according to the manufacturer's instructions. Lay the membrane on the gasket in the apparatus so that it covers all the holes, and remove all air bubbles underneath. Place the sample template on top and screw into place. All sample wells that are not needed should be tightly taped off. Attach your vacuum source (house vacuum or pump).
4. Apply 500 μL of ddH_2O to all sample wells to rehydrate the membrane. Remove all ddH_2O gently by applying vacuum. Release the vacuum.
5. Apply 300 μL of denatured DNA (*see* **step 1** and **Note 22**) with the vacuum, wash wells with 500 μL of 0.4 M NaOH, and remove membrane from the blotting apparatus.
6. Rinse the membrane one time in 2× SSC, and allow to air-dry.
7. UV-cross link (Stratalinker, autocrosslink, 120 μJ/cm^2) samples to the membrane.
8. Hybridize membrane in Church buffer for 30 min at 65 °C.
9. To prepare the telomeric probe, we use the Stratagene Prime It II Labeling Kit according to the manufacturer's instructions. For removal of excess unincorporated [α-^{32}P]-dCTP, we use illustra ProbeQuant G-50 Micro Columns. Denature the double-stranded probe by heating at 100 °C for 5 min, and then cool rapidly on ice.
10. Add the telomeric probe to the Church buffer at 10^6 cpm/mL, and incubate for 24 h at 65 °C.
11. Wash membrane in 0.1× SSC and 0.1 % SDS for 30 min at 65 °C.
12. Expose membrane on a PhosphorImager cassette for 24–48 h.

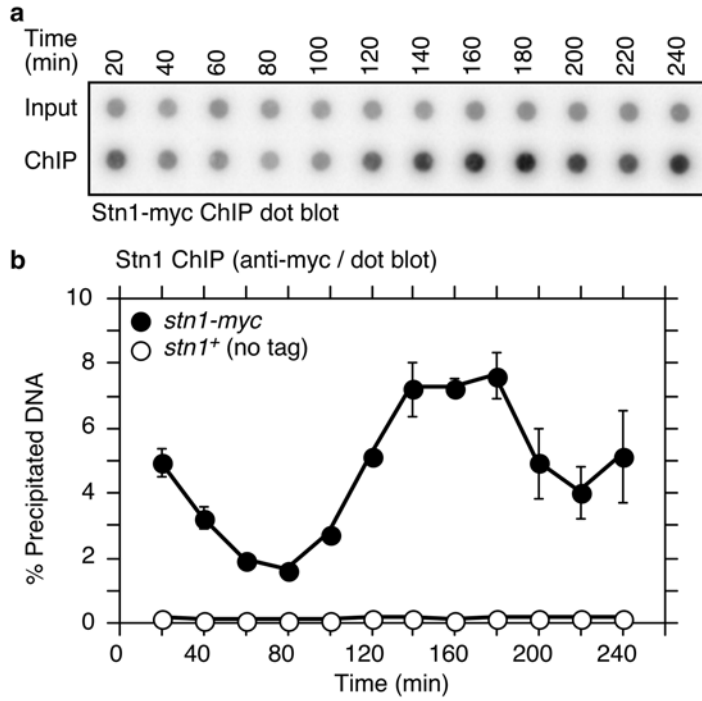

Fig. 2 Cell cycle ChIP analysis of the fission yeast shelterin subunit Stn1 by dot blot hybridization to a telomeric DNA probe. (**a**) Stn1-myc ChIP dot blot hybridized to telomere probe. (**b**) Cell cycle ChIP data (Stn1-myc and no tag control) obtained from *cdc25-22* synchronized samples. Error bars represent standard deviation

13. Quantify using ImageQuant software (GE Healthcare Life Sciences) or similar software. *See* Fig. 2 for an example of a dot blot-based cell cycle ChIP analysis.

4 Notes

1. The pTELO plasmid was generated by cloning ~300 bp SacI-ApaI telomere repeat DNA fragment from pNSU70 plasmid [14]. The pTELO plasmid is available upon request from our laboratory. Alternatively, pNSU70 can also be used to make a telomere repeat probe. While the pNSU70 plasmid was originally constructed by Dr. Neal Sugawara, it was only described in his Ph.D. thesis. However, the pNSU70 plasmid should be widely available from most laboratories that study fission yeast telomeres.
2. All cells should be elongated, and no septa should be visible after 3-h incubation at 36 °C. This can easily be determined by microscopic observation. If for any reason this is not the case, the culture can be incubated at 36 °C for an additional 30–60 min.

3. It is important that cell cultures are quickly equilibrated to their permissive temperature. To achieve this, we typically place our flasks in large 5 L autoclave pans filled with ice and water, and shake them gently by hand. Changes in temperature are carefully monitored by directly inserting a thermometer into the cell culture.
4. Although the cell cycle experiment can be performed for longer time periods, the synchrony of the culture will eventually diminish. Therefore, carrying out experiments beyond a second full round of cell cycle (~300 min after release from *cdc25-22* arrest) is not recommended. We have settled on 20-min time point intervals as it allows us to process samples for ChIP and determine the septation index. If shorter time intervals are required, it may be necessary to have two people to collect and process samples.
5. We found DNA purification columns that are often used in asynchronous ChIP protocols to be unsuitable for cell cycle ChIP for telomeres, as we are especially interested in localization of proteins during replication, and replication intermediates may purify differently from canonical dsDNA.
6. Between washes, perform low-speed spins at 1,500 × *g* for 30 s in a microcentrifuge to allow easy resuspension of pellets. After the final wash, perform a high-speed spin at 16,100 × *g* for 15 s and completely remove all excess liquid.
7. Since synchronization and sample collection require several hours, we usually collect and freeze samples at −80 °C in 1 day and perform ChIP and BrdU analysis on a later day. We found samples stored at −80 °C to be stable for at least several months.
8. When adding glass beads, we leave a little space at the top, so that the beads have room to move. Our FastPrep is set up in a 4 °C room. We usually perform lysis at setting 5.5 for 4× 15 s, with 2-min cooling intervals with an open lid. Other glass bead-based homogenizers may also work to lyse cells, but one should check carefully under a microscope to make sure that the majority of cells have been lysed.
9. Sonication conditions must be established depending on the sonicator used to ensure proper fragmentation of DNA. For ChIP analysis (*see* Subheading 3.2) using the Misonix Sonicator 3000 with cup horn device, we perform ten rounds of sonication for 15 s with 1-min cooling intervals at setting 5.0. For BrdU labeling (*see* Subheading 3.3) we perform six rounds of sonication for 15 s with 1-min cooling intervals at setting 6.0.
10. The amount of lysate used for ChIP might vary depending on the protein of interest, but 1–2 mg of lysate has worked well for us for most proteins we investigated.

11. We generally use 25 μL of Dynabeads® Protein G per ChIP sample. To prepare the beads, wash them with TBS and resuspend in lysis buffer. The use of magnetic beads is preferred over the use of Sepharose- or agarose-based beads, as magnetic beads result in significantly less background and therefore higher reproducibility. To wash and handle magnetic beads, we used a magnetic stand throughout our protocols. Magnetic stands are available from various vendors.
12. While the lysis buffer used to prepare the lysate should be supplemented with protease inhibitors, buffers used for sample washes do not require protease inhibitors.
13. As ChIP is a highly quantitative analysis, variation among samples has to be avoided. Therefore, it is important to avoid any loss of beads during the washes and to remove all liquid after the final wash.
14. It is important to avoid popping of tube lids during boiling, which would result in loss of sample. Use cap closures or a heavy weight to prevent the lids from popping.
15. Addition of SDS should cause protoplasted cells to lyse. Lysed cells will appear flat and less shiny (or dark) under a phase-contrast microscope.
16. The interface between the aqueous phase and the organic phase should become clear. If it is not, extra extraction steps must be carried out before moving on to the next step.
17. To measure DNA concentrations, we are currently using the Qubit® 2.0 Fluorometer from Life Technologies with dsDNA BR Assay Kit, which utilizes a fluorescent dye that only emits a signal when bound to DNA, even at low concentrations. This method is more reliable than measuring DNA concentration by UV absorbance at 260 nm and thus improved the reproducibility of our BrdU experiments by allowing us to more consistently utilize equal amounts of DNA across different time points.
18. To pre-wash, use *n* times 30 μL Dynabeads® Protein G in a 1.5 mL microcentrifuge tube, wash 2× with 1 mL TBS, and remove all liquid. Add *n* times 40 μL anti-BrdU antibody and *n* times 40 μL TBS. Incubate at 4 °C o/n.
19. When undiluted ChIP input samples are used for qPCR analysis, PCR reactions can be inhibited, possibly due to residual inhibitory factors in the sample. Therefore, we recommend performing an initial titration analysis of your samples to make sure that you are testing within the linear range.
20. While we are using SYBR Green for our qPCR analysis, conditions can be established based on your method of choice. Although most manufacturers recommend a reaction volume of 50 μL, we routinely perform 10 μL reactions, as we did not

find any noticeable difference in PCR results performed at either volume. For each time point, we set up triplicate PCR reactions to obtain average Ct values for input and IP samples.

21. For the ChIP protocol described in Subheading 3.2, $E=2$ (based on titration analysis, primer pairs jk380 and jk381 had ~100 % amplification efficiency), $D=1/0.01=100$ (ChIP samples are used undiluted, while input samples are diluted 1:100), and $R=195/5$ (195 μL extract was used in IP, while 5 μL extract was set aside as input control). These values should be adjusted if other primer pairs are used or protocols are modified. For example, if a new pair of primers is found to have only 80 % amplification efficiency, E should be 1.8.
22. During sample application, samples occasionally do not transfer well through the membrane although the vacuum is applied. In this case, carefully pipette the liquid in the well up and down a few times.

Acknowledgement

This work was supported by NIH grant GM078253 (to T.M.N.).

References

1. Lydall D (2009) Taming the tiger by the tail: modulation of DNA damage responses by telomeres. EMBO J 28(15):2174–2187
2. Verdun RE, Karlseder J (2007) Replication and protection of telomeres. Nature 447(7147): 924–931
3. Price CM, Boltz KA, Chaiken MF, Stewart JA, Beilstein MA, Shippen DE (2010) Evolution of CST function in telomere maintenance. Cell Cycle 9(16):3157–3165
4. Moser BA, Nakamura TM (2009) Protection and replication of telomeres in fission yeast. Biochem Cell Biol 87(5):747–758
5. Moser BA, Subramanian L, Chang YT, Noguchi C, Noguchi E, Nakamura TM (2009) Differential arrival of leading and lagging strand DNA polymerases at fission yeast telomeres. EMBO J 28(7): 810–820
6. Forsburg SL (2003) Growth and manipulation of *S. pombe*. Curr Protoc Mol Biol Chapter 13:Unit 13.16
7. Alfa C, Fantes P, Hyams J, McLoed M, Warbrick E (1993) Experiments with Fission Yeast. Cold Spring Harbor Laboratory Press, Cold Spring Harbor, NY
8. Russell P, Nurse P (1986) *cdc25*$^{+}$ functions as an inducer in the mitotic control of fission yeast. Cell 45(1):145–153
9. Kanoh J, Sadaie M, Urano T, Ishikawa F (2005) Telomere binding protein Taz1 establishes Swi6 heterochromatin independently of RNAi at telomeres. Curr Biol 15(20):1808–1819
10. Hayashi M, Katou Y, Itoh T, Tazumi A, Yamada Y, Takahashi T, Nakagawa T, Shirahige K, Masukata H (2007) Genome-wide localization of pre-RC sites and identification of replication origins in fission yeast. EMBO J 26(5):1327–1339
11. Nelson JD, Denisenko O, Bomsztyk K (2006) Protocol for the fast chromatin immunoprecipitation (ChIP) method. Nat Protoc 1(1):179–185
12. Sivakumar S, Porter-Goff M, Patel PK, Benoit K, Rhind N (2004) *In vivo* labeling of fission yeast DNA with thymidine and thymidine analogs. Methods 33(3):213–219
13. Hodson JA, Bailis JM, Forsburg SL (2003) Efficient labeling of fission yeast *Schizosaccharomyces pombe* with thymidine and BUdR. Nucleic Acids Res 31(21):e134
14. Sugawara NF (1988) DNA sequences at the telomeres of the fission yeast *S. pombe*. Ph.D. thesis. Harvard University, Cambridge, Massachusetts

Chapter 23

Detecting Senescence: Methods and Approaches

Elizabeth P. Crowe, Timothy Nacarelli, Alessandro Bitto, Chad Lerner, Christian Sell, and Claudio Torres

Abstract

The detection of senescent cells has become an important area of research in the aging field. Due to the complexity of the senescence program and the lack of a unique signature for senescence, the detection of these cells remains problematic. This is especially true for in vivo detection in aged or diseased tissue samples. This chapter outlines approaches for the detection of senescent cells based upon methods established for mesenchymal cells in culture. A stepwise approach to the detection of senescent cells using multiple techniques is provided.

Key words Aging, Cell cycle, Chromatin, Cytokine, p53, p16, SASP, Senescence

1 Introduction

Although the precise definition of cellular senescence is complex and varies according to cell type, the senescence phenotype is generally characterized by stable growth arrest, altered cell function, and morphology, which are driven by specific changes in gene expression and chromatin structure. Two broad issues complicate how senescent cells are detected and how the results of those assays are interpreted. First, no single marker is entirely sensitive for, or specific to, senescent cells; therefore, it is advisable to examine multiple markers that interrogate different aspects of the senescent phenotype. Secondly, as the senescence phenomenon is examined more closely in multiple cell types, it is becoming clear that certain aspects of the senescent phenotype are species, cell type, and senescence-inducing stimulus dependent [1]. For example, human and mouse cells differ in the underlying signaling pathways and manifestations of the senescence phenotype, specifically in terms of their telomeres [2] and the ability to form robust senescence-associated heterochromatin foci (SAHF) [3]. Furthermore, ectopic expression of the cyclin-dependent kinase inhibitor $p16^{INK4a}$ induces growth arrest without the senescence-associated secretory phenotype (SASP) [4].

Eishi Noguchi and Mariana C. Gadaleta (eds.), *Cell Cycle Control: Mechanisms and Protocols*, Methods in Molecular Biology, vol. 1170, DOI 10.1007/978-1-4939-0888-2_23,

For these reasons, the general markers of senescence that are outlined in this chapter should be evaluated in the context of the experimental paradigm or disease state that is being examined and those markers that are relevant should be employed, in addition to markers which may be specific to the cell type in question.

An issue that is fundamental to the study of the senescence arrest is growth state; it is essential to match growth states when examining senescence markers, comparing senescent cells with quiescent cells, rather than with actively proliferating cultures of early-passage cells. While this is elementary in conceptual terms, it is important to bear in mind during experimental design in order to avoid confusing differences in cell cycle (i.e., cycling versus non-cycling populations) with senescence-associated changes. Clearly, this consideration is important when working in vitro but must also be considered when interpreting results obtained from in vivo studies, which primarily involve immunostaining for senescent markers. In some instances, it is possible to analyze two markers of senescence simultaneously through the use of dual immunofluorescence, an approach particularly useful for in vivo analysis.

For the purposes of characterizing a cell type, an in vitro analysis to assess senescence of primary cell strains or tumor lines in response to specific stress or damage is best approached in a stepwise fashion. These steps should include examining growth arrest, cell cycle, expression of senescence-associated growth arrest proteins (p53, $p21^{Cip1/Waf1}$, $p16^{INK4a}$) [5], nuclear remodeling (chromatin remodeling, DNA damage response (DDR) activation), and altered secretory phenotype [6]. The precise set of markers to be employed is best determined by the individual investigator based upon the experimental paradigm and cell type involved. In this chapter, we describe assays for detecting senescent cells in vitro and, wherever applicable, we highlight potential pitfalls and indicate in which cases these methods have been used in tissues to detect senescent cells. The analysis of senescence in vivo is more limited regarding the ability to assess cell parameters. The primary assays employed are immunostaining approaches to detect changes in protein expression [7, 8].

2 Materials

2.1 Culturing Human Fibroblast Cells to Induce Senescence

1. Sterile 1× PBS.
2. Complete MEM growth medium (per 500 mL bottle): Add 1× MEM vitamins, 1× MEM amino acids, 1× penicillin–streptomycin solution (Corning cellgro, 10,000 IU penicillin, 10,000 μg/mL streptomycin), 2 mM L-glutamine, and 10 % fetal bovine serum (FBS) (v/v).
3. 1× Trypsin–EDTA (Corning cellgro).
4. Bright-field microscope.

2.2 Cryopreservation of WI-38 Cells

1. Materials for cell culture as indicated in Subheading 2.1.
2. Freezing medium: Complete MEM growth medium, 80 % FBS, 10 % DMSO.
3. Cryogenic vials.
4. Nalgene cell freezing container (Nalgene).
5. Liquid nitrogen storage system.

2.3 Cell Cycle Analysis of Senescent Growth Arrest

1. 60 mm Diameter dishes.
2. Materials for cell culture as indicated in Subheading 2.1.
3. 5-Bromo-2′-deoxyuridine (BrdU) Stock Solution (BdPharmingen): Prepare a 1 mM BrdU working solution in complete growth medium, which can be stored at −20 °C protected from light (*see* **Note 1**).
4. Ice-cold 100 % ethanol.
5. 2 N Hydrochloric acid (HCl).
6. 0.1 M $Na_2B_4O_7$, pH 8.5.
7. PBS–5%FBS: 5 % FBS in 1× PBS.
8. 20 % Tween-20.
9. Anti-BrdU monoclonal antibody: 1:100 dilution (eBiosciences, #14-6071).
10. Goat anti-mouse-Alexa Fluor 488 (Molecular Probes, Invitrogen).
11. 5 mg/L Propidium iodide (PI) (Sigma) or Guava Cell Cycle analysis reagent (Millipore).
12. Flow cytometer.
13. Guava system using the ExpressPlus program or a similar cell cycle analysis tool.

2.4 Colony-Forming Assay

1. Materials for cell culture as indicated in Subheading 2.1.
2. 10 % Crystal violet solution (w/v) in methanol.

2.5 Whole-Cell Protein Extract Preparation

1. 1× RIPA buffer: 50 mM Tris pH 8.0, 150 mM NaCl, SDS 0.1 % (w/v), 1 % NP-40 (v/v), 0.5 % sodium deoxycholate (w/v).
2. Protease Inhibitor Cocktail (Sigma Aldrich): To prepare a working stock of 10× protease inhibitor cocktail in ddH_2O, add 10 mL to the vial containing the lyophilized powder and prepare 500 µL aliquots to be stored at −20 °C.
3. Phosphatase inhibitor: 200 mM sodium orthovanadate (Na_3VO_4).
4. Phosphatase inhibitor: 200 mM sodium fluoride (NaF).
5. RIPA with protease and phosphatase inhibitors (for 5 mL): To 4.4 mL of 1× RIPA buffer, add 500 µL of 10× protease inhibi-

tor cocktail (1× final v/v), 50 μL Na_3VO_4 (1 mM final), and 50 μL 200 mM NaF (1 mM final).

6. Ice-cold 1× PBS.
7. Disposable cell scraper.
8. BCA protein quantification kit or a similar commercially available system.

2.6 Senescence-Associated β-Galactosidase

1. Fixative solution: 2 % Formaldehyde (v/v), 0.2 % glutaraldehyde (v/v) in 1× PBS.
2. pH 6.0 buffer: Prepared from 0.2 M sodium phosphate dibasic (Na_2HPO_4) solution and 0.1 M citric acid solution. For 100 mL of pH 6.0 buffer, combine 36.85 mL of 0.1 M citric acid with 63.15 mL of 0.2 M sodium phosphate dibasic (Na_2HPO_4) and check the pH of the solution (*see* **Note 2**).
3. 100 mM Potassium ferricyanide ($K_3Fe(CN)_6$).
4. 100 mM Potassium ferrocyanide trihydrate ($K_4Fe(CN)_6 \cdot 3H_2O$).
5. 5 M NaCl.
6. 1 M $MgCl_2$.
7. 50 mg/mL (w/v) 5-Bromo-4-chloro-3-indolyl-b-D-galactopyranoside (X-gal) in *N*,*N*-Dimethylformamide (DMF) (Sigma Aldrich) stored at −20 °C (*see* **Notes 3** and **4**).
8. Senescence-associated β-galactosidase (SA β-gal) stain: For 1 mL stain solution, mix 648 μL of MilliQ water, 200 μL of pH 6.0 buffer, 50 μL of 100 mM of potassium ferricyanide, 50 μL of 100 mM potassium ferrocyanide trihydrate, 30 μL of 5 M NaCl, 2 μL of 1 M $MgCl_2$, and 20 μL of 50 mg/mL (w/v) X-gal in DMF. Prepare fresh.
9. Air incubator without CO_2.

2.7 Immunofluorescence Detection of Proteins Enriched in SAHF

1. 12- or 24-Well plates containing cleaned, sterile glass cover slips (*see* **Note 5**).
2. 4 % Paraformaldehyde in 1× PBS, pH = 7.2 (*see* **Note 6**): For 100 mL of 4 % solution of paraformaldehyde in 1× PBS (w/v), add 4 g paraformaldehyde to 80 mL ddH_2O + 10 mL of 10× PBS. In order to get paraformaldehyde into solution, bring pH to approximately 11 using a concentrated solution of sodium hydroxide (NaOH). Once paraformaldehyde is dissolved, bring pH back down to 7.2 by adding HCl. Adjust final volume to 100 mL with ddH_2O.
3. Permeabilization solution: 1× PBS, 0.2 % Triton-X100 (v/v).
4. 0.1 % Bovine serum albumin (BSA) (w/v) in 1× PBS: For 1 L, add 1 g BSA to 1× PBS and bring volume to 1 L. This should be prepared fresh.

5. Blocking solution: 1× PBS, 0.1 % BSA, 5 % serum from the animal in which the secondary antibody was raised (*see* **Note 7**).
6. 1× PBS–0.1 % BSA.
7. Antibodies: Rabbit polyclonal anti-macroH2A1.2 1:100 (Cell Signaling cat# 4827), Mouse monoclonal anti-HP1β heterochromatin protein 1β 1: 40 (Millipore, cat# MAB 3448), Rabbit polyclonal anti-H3K9me3 (Abcam cat# 8898), Alexa Fluor 555 Donkey anti-Rabbit 1:500, and Alexa Fluor 488 Goat anti-Mouse 1:500 (Life Technologies).
8. Humidified chamber with staining apparatus (*see* **Note 8**).
9. DAPI working solution: Prepare DAPI working solution by diluting DAPI (50 μg/mL stock, Sigma) 1:5,000 with 1×PBS–0.1 %BSA.
10. Glass slides.
11. Vectashield fluorescence mounting media (Vector Laboratories).
12. Fluorescence microscope.
13. Image analysis software: ImageJ (NIH) or CellProfiler (Broad Institute).

2.8 Collection of Conditioned Medium for SASP Analysis

1. Materials for cell culture as indicated in Subheading 2.1.
2. Phosphate-buffered saline (1× PBS).
3. MCDB-105 (Sigma-Aldrich) or other appropriate serum-free media depending on cell type of interest (*see* **Note 9**).
4. 0.22 μm PVDF syringe filter or a similar low-protein-binding filter and a syringe with a volume capacity of the medium collected from cell culture vessel.
5. Collection tube for conditioned media (15 mL conical tube or similar).
6. Dry ice.

3 Methods

One of the major hallmarks of a senescent cell is a stable arrest of cell proliferation, the Hayflick limit [9, 10]. Growth arrest can be analyzed using simple cell number determination, cell cycle analysis, and analysis of DNA synthesis using incorporation of bromodeoxyuridine [11].

In order to examine growth arrest in a systematic manner, it is critical to maintain consistent cell culture conditions. We utilize a standard seeding protocol for all cell culture work to ensure reproducibility in terms of growth characteristics and cell responses [12]. Replicative senescence should be evaluated by population

doublings (i.e., cell division number) rather than passage. In our hands, a seeding density of $1 \times 10^4/cm^2$ for mesenchymal cells ensures consistency in growth state between experiments. A typical cell passage using a 3:1 dilution of the culture leads to a progressive reduction in seeding density as the growth of primary cells slows down creating additional stress on the cell population. Replicative senescence is defined as the observation of no population doubling in 2 consecutive weeks of culture. Senescence may also occur in post-mitotic, terminally differentiated cells exhibiting permanent cell cycle exit [13, 14]. An analysis of cell cycle and DNA synthesis in this setting has not been rigorously undertaken but is certain to provide crucial information regarding the relationship between cell cycle control and senescence.

3.1 Culturing Human Fibroblast Cells to Induce Senescence

The following steps should be performed 7–10 days following initial cell seeding.

1. Aspirate culture medium and wash one time with sterile 1× PBS.
2. Add 2 mL of trypsin–EDTA (*see* **Note 10**), and allow cells to detach in incubator for 3–5 min.
3. Inactivate trypsin–EDTA with 8 mL complete MEM growth medium.
4. Count cells and seed accordingly, calculating the change in population doubling (P.D.) as indicated below (*see* **Note 11** and Table 1):

Table 1
Growth area chart for commonly used tissue culture vessels

Culture vessel	Diameter (mm)	Area (cm^2)	Working volume (mL)
6 well	34.8	9.5	1.9–2.9
12 well	22.1	3.8	0.76–1.14
24 well	15.6	1.9	0.38–0.57
48 well	11.0	0.95	0.19–0.285
35 mm dish	35	9.0	1.8–2.7
60 mm dish	60	21	4.2–6.3
100 mm dish	100	55	10–15
25 cm^2 flask	–	25	5–7.5
75 cm^2 flask	–	75	15–22.5

Values are for Corning® tissue cultureware, although products from other manufacturers have similar surface areas

$$\text{Change in P.D.} = \frac{\log\left(\dfrac{\text{Number of cells harvested}}{\text{Number of cells seeded}}\right)}{\log 2}$$

5. Add this number to the current P.D. number to obtain the new P.D. Replicative senescence is achieved when less than one population doubling is observed after 2 weeks of culture growth (*see* **Note 12**).

3.2 Cryopreservation of WI-38 Cells

1. Trypsinize and count cells as described in Subheading 3.1.
2. Centrifuge cells at 500 × *g* for 5 min at 4 °C and resuspend in freezing medium at a concentration of 1×10^6 cells/mL (*see* **Note 13**).
3. Aliquot 1 mL of cell suspension per freezing vial.
4. Place vials at −80 °C in a Nalgene cell freezing chamber or a simple Styrofoam container to allow slow temperature equilibration (*see* **Note 14**).
5. Move cells to liquid nitrogen after 24 h (*see* **Note 15**).

3.3 Cell Cycle Analysis of Senescent Growth Arrest

1. Start with 60 mm diameter dishes, seeded at double density (2×10^4/cm^2) (*see* **Note 16**).
2. After a 24-h attachment period, add 1 mM BrdU working solution directly to the tissue culture medium to a final concentration of 10 μM.
3. Incubate the treated cells at 37 °C for the desired length of time (*see* **Note 17**).
4. After incubation, trypsinize and collect cells in 15 mL conical tubes.
5. Centrifuge cells at 1,000 × *g* for 10 min at 25 °C.
6. Remove supernatant, and resuspend cells by flicking the pellet sharply by hand.
7. Wash with 1× PBS once by adding 4–5 mL of 1× PBS to the resuspended pellet, and centrifuge at 1,000 × *g* for 10 min at 25 °C.
8. Resuspend cells as above in a small volume of 1× PBS (300 μL).
9. Add 0.7 mL of ice-cold 100 % ethanol dropwise while gently vortexing.
10. Centrifuge cells at 1,000 × *g* for 10 min at 4 °C.
11. Remove supernatant, and resuspend pellet by flicking tube with the fingers.
12. Add 500 μL 2 N HCl, and incubate for 30 min at room temperature for DNA denaturation.

13. Neutralize with 1 mL of 0.1 M $Na_2B_4O_7$ (pH 8.5), resuspend by flicking tube by hand, and spin down.
14. Wash twice with 1 mL of PBS–5 % FBS each time (*see* **Note 18**), and centrifuge at 1,000 × *g* for 5 min at 4 °C, resuspending each time by flicking the tube.
15. Add 50–100 μL of 1× PBS containing 0.5 % Tween-20 and anti-BrdU monoclonal antibody to the pellet.
16. Incubate for 30 min at room temperature.
17. Wash twice with PBS–5 % FBS as described in **step 14**.
18. Resuspend, and incubate in 100 μL of goat anti-mouse-Alexa Fluor 488 secondary antibody solution (diluted 1:100 in 1× PBS containing 0.5 % Tween-20) for 15–20 min at room temperature in the dark.
19. Wash twice with PBS–5 % FBS as described in **step 14**.
20. Resuspend the pellet in 200 μL of the Guava Cell Cycle solution warmed to room temperature. Incubate for 30 min at room temperature in the dark. Alternatively, a solution containing 5 mg/L PI in 1× PBS can be added to the pellet for 30 min at 37 °C in the dark.
21. Analyze samples on the Guava machine using the ExpressPlus program or a similar cell cycle analysis tool on a flow cytometer to look for red (cell cycle, PI emission 617 nm) and green (BrdU, Alexa Fluor 488 emission 518 nm) fluorescence. The percent of cells labeled with BrdU provides growth fraction, while cell cycle analysis can be performed following standard procedures.

3.4 Distinguishing Reversible and Irreversible Arrest: Colony-Forming Assay

Senescence is irreversible under physiologic conditions. A global genomic reprogramming via nuclear transfer to a germline environment or induction of pluripotency is required to reverse the senescence arrest [15–17]. Colony formation provides an assessment of single-cell growth and long-term viability within the population. A caveat of the assay is that primary cells have a low inherent ability to grow as single-cell colonies while this ability is relatively high in immortalized tumor lines. Nonetheless, colony formation can be used to verify that a permanent growth arrest has been induced.

1. Trypsinize and count cells as described in Subheading 3.1.
2. Seed cells at clonal density (i.e., a density at which each individual cell gives rise to a colony) in full growth medium. Generally, it is good practice to seed at least two densities, 500 cells/cm^2 and 50 cells/cm^2. If a stress agent has been used to induce senescence, it should be excluded during the colony formation assay.

3. Allow cell growth for 14–21 days, changing growth medium every 5–7 days.
4. Remove growth medium, and wash cells with 1× PBS two times.
5. Stain cells using a solution of 10 % crystal violet dissolved in methanol (*see* **Note 19**). 5–10 mL per 10 cm plate can be serially transferred between plates.
6. Rinse plates in tap water (*see* **Note 20**). A simple apparatus of an 8 in.×10 in. glass pan containing a beaker can be used. Allow water to run into the beaker at a slow rate so that the pan fills from the overflow. In this manner, the plates are not subjected to a strong water force during rinsing which can dislodge the colonies.
7. Count colonies either by eye or under a dissecting microscope. Plates can be stored almost indefinitely at room temperature.

3.5 Whole-Cell Protein Extract Preparation to Determine Activation of Tumor Suppressor Pathways

The growth arrest observed in senescent cells is best differentiated from a quiescent arrest due to the elevation of the cell cycle inhibitor $p16^{INK4a}$. When working in vitro, changes in protein levels are generally most accurately examined by immunoblot analysis. Total protein extracts can be obtained using standard procedures, typically by protein extraction using RIPA buffer. However, the subcellular localization of the protein should also be considered, and the lysis buffer should be modified accordingly. For example, histone proteins are not always extracted efficiently using RIPA buffer.

1. To cold RIPA buffer, add protease inhibitor cocktail and phosphatase inhibitors immediately prior to lysis.
2. Rinse cells growing on plates once with ice-cold 1× PBS. Drain excess PBS from the plates by tilting the plates, and place them on ice.
3. Add 500 µL of RIPA buffer (for 10 cm plates) (*see* **Note 21**) on an angle to cover the entire surface of the plate. Scrape cells using a disposable cell scraper. Pipette homogenate into a cold 1.5 mL microcentrifuge tube.
4. Incubate cells for 15–30 min on ice.
5. Centrifuge for 2 min at 14,000×*g* at 4 °C.
6. Remove supernatant (protein extract) and place in a new cold microcentrifuge tube. Store at –80 °C.
7. Protein concentrations can be determined using a number of commercially available kits. Our choice is the BCA method from Pierce®.
8. Immunoblot analysis can be carried out on protein lysates to examine senescence-associated changes in steady-state protein levels (*see* **Note 22**).

3.6 Senescence-Associated β-Galactosidase

The SA β-gal assay has been widely employed to detect senescent cells because it is easily implemented and not normally positive in reversibly arrested or terminally differentiated cells [18]. This distinction makes the SA β-gal assay an attractive choice as an initial screen for senescent cells; however, there are a few caveats to be aware of when performing the experiment and interpreting the outcome of this assay. First, SA β-gal activity is indicative of the increased lysosomal content, an activity characteristic of senescent cells [19] but not necessarily intrinsic to the development of the senescence phenotype [20]. Second, false positives can result when SA β-gal activity is measured in confluent cells. Finally, this assay should not be used in tissues that have been formalin-fixed or frozen for long periods, which unfortunately comprise most tissue specimens in pathology archives, because the β-galactosidase enzyme activity is destroyed [21]. Nevertheless, when performed under the proper conditions, the SA β-gal assay can be used to identify senescent cells in a variety of cell and tissue types from both model organisms and humans [18, 22–24]. Following cleavage of the exogenously applied substrate X-gal, cells that demonstrate SA β-gal activity will turn blue and can be easily quantified using a light microscope. Furthermore, SA β-gal staining can be combined with cell proliferation indices (e.g., BrdU/EdU labeling) to demonstrate multiple hallmarks of senescence (SA β-gal-positive/low proliferative index) in the same cell [25].

1. Aspirate cell culture media, and wash non-confluent cells two times with 1× PBS.
2. Fix cells with fixative solution for 3–5 min (*see* **Note 23**).
3. Prepare SA β-gal stain by combining solutions according to Subheading 2.6, **item 8**.
4. Wash cells two times with 1× PBS, and apply SA β-gal stain.
5. Incubate for 16 h to overnight at 37 °C in an incubator without CO_2 (*see* **Note 24**).
6. After incubation with SA β-gal stain, rinse plates with 1× PBS and quantify the percent of cells that exhibit a blue color (*see* **Note 25**).

3.7 Immunofluorescence Detection of Proteins Enriched in SAHF

Senescent cells undergo significant changes in chromatin structure, the most obvious example of which is the formation of SAHF [26, 27]. SAHF were originally described as nuclear foci that can be easily visualized by fluorescent DNA staining (e.g., DAPI) and are enriched with known markers of heterochromatin including heterochromatin protein 1 (HP-1), the histone variant macroH2A (mH2A), and methylation of histone H3 at lysine 9 (H3K9me2/3) [27, 28]. These regions of facultative heterochromatin contribute to the silencing of proliferation-promoting genes, whereas in the context of oncogene-induced senescence, SAHF restrain DDR

signaling in order to prevent apoptosis [29]. The formation of heterochromatin may be related to chromatin remodeling observed in malignant cells that have bypassed the senescence arrest [30]. SAHF formation requires the localization of histone chaperone HIRA to PML nuclear bodies [28] and depends on an intact p16–Rb pathway [27]. However, SAHF does not occur in reversibly arrested cells.

The presence of SAHF is highly dependent upon cell type and senescence-inducing stimulus and generally follows $p16^{INK4A}$ expression [1]. Although the discrete structures known as SAHF have been difficult to identify in tissues, the levels of SAHF components, such as macroH2A and HP1β, are elevated in tissues from aged mice and primates [13, 31]. Whether such enrichment of SAHF-associated proteins represents a *bona fide* senescence response in vivo remains to be determined and should be considered in the context of other senescence biomarkers.

1. On the day prior to fixation, plate cells on glass cover slips in 12- or 24-well plates at double the standard density (2×10^4/cm^2) (*see* **Note 26**).
2. Aspirate cell culture media, and wash cover slips in wells two times with 1× PBS (*see* **Note 27**).
3. Fix cells with 4 % paraformaldehyde in 1× PBS (w/v) for 10 min at room temperature.
4. Wash cover slips with 1× PBS three times for 5 min each (*see* **Note 28**).
5. Apply permeabilization solution for 15 min.
6. Repeat wash steps as directed in **step 4**.
7. Incubate cover slips with blocking solution for 2 h at room temperature.
8. Dilute primary antibody to desired final concentration (v/v) in 1× PBS + 0.1 % BSA. If performing dual immunofluorescence, primary antibodies can be mixed together at this step as long as they were raised in different species (*see* **Note 29**).
9. Place a drop (~50–70 μL for a 12-well cover slip) of primary antibody solution onto the parafilm in the humidified chamber (*see* **Note 8**).
10. Individually remove cover slips from wells, and invert onto the drop of primary antibody solution taking care to avoid moving cover slips once they have been inverted. Incubate at room temperature overnight.
11. Invert the cover slips back, transfer them to wells of cell culture plates, and wash them three times for 5 min each with 1× PBS.
12. Prepare secondary antibody at a final concentration of 1:500 in 1× PBS + 0.1 % BSA and protect from light.

13. Invert cover slips on secondary antibody solution as described in **steps 9** and **10**. Incubate for 1 h at room temperature in the dark.
14. Wash cover slips as directed in **step 11**.
15. While still in the wells of cell culture plate, cover slips can be incubated with DAPI working solution for 10 min at room temperature and protected from light.
16. Rinse cover slips at least three times with an excess volume of MilliQ ddH_2O.
17. Prepare glass slides with approximately 3–4 μL of fluorescent mounting media in a slide box protected from light.
18. Invert cover slip onto the mounting media present on slide and seal with nail polish.
19. Slides can be stored at 4 °C for several days.
20. Cells are scored for the senescence biomarker of interest using fluorescence microscopy (*see* **Note 30**).

3.8 Senescence-Associated Secretory Phenotype Analysis

In addition to cell-intrinsic changes in function, senescent cells perturb their microenvironment through an altered pattern of secretion termed the SASP [32]. Altered secretion patterns of insulin-like growth factor-binding proteins were initially identified in the 1990s through differential gene expression studies in normal human fibroblast cells and cells from patients suffering from Werner's syndrome [33, 34]. Although at that time the emphasis was on the control of growth within the culture population undergoing senescence, later work revealed that the SASP includes a number of pro-inflammatory cytokines including interleukin-6 (IL-6) and IL-8 [32]. It is this pro-inflammatory nature of the SASP that is currently the subject of intense study due to the potential connection with increased inflammation during aging, which is thought to contribute to the functional decline associated with aging [35].

The SASP develops as a consequence of altered gene expression and consists of milieu of proinflammatory cytokines, chemokines, proteases, and growth factors [36]. The production of these mediators is not an acute, transient response to the senescence-inducing insult, but rather a delayed and persistent response regulated by DDR and p38MAPK signaling [37, 38]. Several functions have been attributed to the SASP; whether these functions are beneficial or detrimental to the tissue microenvironment is often context dependent. The SASP reinforces growth arrest through both cell-autonomous and non-autonomous mechanisms [39, 40] and signals to cells of the immune system in order to facilitate clearance and proper wound repair [41, 42]; however, the SASP may also disrupt tissue homeostasis by creating a proinflammatory tumor-promoting microenvironment [6] and altering the stem cell niche [43].

The SASP in vitro is reminiscent of the low-level chronic inflammation characteristic of both age-related degenerative pathologies and cancers [8].

Although SASP constituents are relatively conserved across species [44], not all senescence-inducing stimuli result in a SASP [4], and variation exists among the SASPs from different cell types and senescence-inducing stimuli. Therefore, it is important to examine multiple potential SASP factors and to consider the experimental context. This type of approach is facilitated by antibody arrays for multiple inflammatory factors, which can be subsequently validated by individual enzyme-linked immunosorbent assays (ELISA) or at the mRNA level using qRT-PCR assays. Although sophisticated, unbiased approaches are useful for the full analysis of the SASP in a specific setting [45], an examination of most common elements of the SASP can be performed in the laboratory at relatively low cost, and this can serve as a further confirmation of the senescence phenotype when considered in conjunction with the other approaches outlined in this chapter.

Detection of SASP requires collection of conditioned medium from cultures with proliferative potential (i.e., pre-senescent) and senescent cultures. Obviously, if one is evaluating changes in non-dividing cultures, this distinction may not hold but a comparator is required.

1. Establish cultures of pre-senescent and senescent cells in stationary growth phase in full growth medium containing serum and growth factors if working with proliferating cultures. If working with primary cells, this is best performed by allowing cells to proliferate to high cell density (*see* **Note 31**).
2. Remove growth medium, and rinse two times with 1× PBS and one time with serum-free medium.
3. Add serum-free medium at 50 % of the normal volume used for the culture flask or dish that contains the cells of interest. Keep track of volume added.
4. Incubate cells in serum-free medium in cell culture incubator (37 °C, 5 % CO_2) for 24–48 h (*see* **Note 32**).
5. Collect conditioned medium from culture vessel and filter through 0.22 μm syringe filter to remove cell debris (*see* **Note 33**).
6. Place conditioned medium on dry ice immediately and store at −80 °C.
7. Trypsinize and count cells as described in Subheading 3.1. In order to normalize expression levels of SASP mediators, it is essential to determine the number of cells in the dish from which the conditioned medium was generated (i.e., cell number/[mL of conditioned medium]).

8. Analyze conditioned medium for SASP by ELISA (IL-6 or other specific cytokine markers) or using an antibody array according to the manufacturer's instructions (*see* **Note 34**).

4 Notes

1. BrdU is a potential mutagen; appropriate precautions should be taken. BrdU working solution can be stored at –20 °C, protected from light.
2. Confirming the pH of this solution is an important step to maintain suboptimal conditions for differential enzyme activity between senescent and non-senescent cells. A pH that is too low (increases enzyme activity) will result in false positives.
3. The concentration of X-gal in the staining solution may have to be titrated depending upon cell type and senescence-inducing stimulus; thus, it is essential to include any relevant positive and negative controls.
4. Use a wrapped tube protected from light. 50 mg/mL X-gal in DMF can be prepared ahead of time and stored at –20 °C for up to 1 month as long as the solution remains clear and colorless. DMF is hazardous and should be handled under the chemical fume hood with appropriate precautions taken to avoid inhalation or skin contact.
5. Clean cover slips by washing with a saturated solution of laboratory detergent (e.g., Alconox), followed by three rinses with MilliQ ddH_2O and one rinse in 70 % ethanol. Cover slips are then allowed to dry and autoclaved for sterilization.
6. Paraformaldehyde is an irritant. Care should be taken to avoid inhalation or skin/eye contact. Appropriate precautions and personal protective equipment should be employed while handling paraformaldehyde.
7. The type of serum used in the blocking solution is based on the secondary antibody used (e.g., for goat anti-rabbit secondary antibody, use 5 % goat serum in the blocking solution). If dual immunofluorescence is to be performed, 5 % serum final (v/v) for each type of animal used to generate the secondary antibodies should be included in this step (e.g., for goat anti-rabbit and donkey anti-mouse secondary antibodies, use 5 % goat serum and 5 % donkey serum in the blocking solution).
8. A humidified chamber containing a staining apparatus is constructed by placing a moistened paper towel/piece of filter paper at the bottom of a large box with a lid. This box should be large enough to accommodate a separate smaller lid or surface that has been covered with parafilm. Antibody solutions will be placed on the parafilm and cover slips placed on top

with the cell surface down. This allows the use of small volumes and prevents evaporation during the incubation steps.

9. For mesenchymal cells, MCDB-105 is a good choice as a serum-free medium. It has been formulated to sustain clonal growth of human cells, and we have used this medium to maintain human fibroblast cultures for up to 21 days without loss of viability [46, 47].
10. Carefully monitor cells during trypsin–EDTA treatment. Place cells in tissue culture incubator for ~5 min, and check under an inverted microscope for detachment. A vigorous tap or two against the side of the flask will often dislodge cells after a few minutes of exposure to trypsin. Do not allow cells to sit for long periods in trypsin solution or they will clump together and seeding efficiency will decrease. If not all cells detach within 10 min, the trypsin solution containing cells can be removed and placed into a centrifuge tube containing complete growth medium (FBS neutralizes trypsin) and a fresh aliquot of trypsin–EDTA added to the culture flask. Cells will rapidly detach in fresh trypsin solution.
11. Number of cells seeded is the number of cells required to reach standard density ($1 \times 10^4/cm^2$). It depends on the specific size of culture vessel used (*see* Table 1).
12. As cultures progress through their replicative life-span, the interval between passages can be increased from 7 to 14 days. Fresh medium should be provided to cells at 3–4-day intervals.
13. Cells become fragile in DMSO-containing media. Following centrifugation, it is advisable to gently dislodge the cell pellet after removal of growth media by flicking the tube prior to adding the freezing media containing DMSO.
14. Cells must be slowly brought to −80 °C for viability (optimally one degree decrease per minute), which has traditionally been performed using an automated system. The use of the Nalgene cryopreservation chambers circumvents the cost associated with such an apparatus, but optimal viability may not be obtained. If viability becomes an issue for a specific cell type, more sophisticated approaches should be explored.
15. Cells can remain at −80 °C for several weeks, but not all cells tolerate this condition.
16. Seeding density for BrdU assays can be varied according to the cell type. Cells should be in log-phase growth when BrdU is added; therefore, rapidly dividing cells may need to be seeded at a lower density, while slower growing cells may need to be seeded at a higher density to obtain sufficient cells for the assay.
17. The duration of incubation with BrdU is dependent on the cell division time. To determine the proliferating fraction in a cell

population, label for the length of an entire cell cycle. A crude assessment of cell cycle length can be made by dividing the number of hours in a week by the number of population doublings per week (e.g., 3 P.D. per week, $(7 \times 24)/3 = 168/3 = 56$ h). Assessment of senescence arrest is best performed using both a short and a long labeling period. This allows an assessment of both percent of cells in S phase at any point and the proliferating fraction of the population. Cells from the same population that are not stained with anti-BrdU serve as a negative control.

18. The addition of FBS in the wash step serves as a blocking agent for subsequent antibody staining. BSA or species-specific serum, depending upon the source of anti-BrdU antibody, can be substituted for FBS.
19. Crystal violet solution will stain everything it comes in contact with including lab benches, personnel, and even stainless steel sinks (although these will eventually come clean).
20. Label the bottom of the plates prior to rinsing!
21. Examine the level of cell confluence prior to lysis, and adjust the volume of lysis buffer accordingly.
22. We recommend the following antibodies: anti-p16 rabbit polyclonal antibody, Santa Cruz sc-468; anti-$p21^{WAF-1}$ (Ab-1) mouse monoclonal antibody (EMD Millipore, Ab-1, OP64), and anti-p53 (Ab-6) mouse monoclonal antibody (EMD Millipore, Ab-6, OP43). This list is based on our experience with the antibodies for immunoblotting on cell extracts prepared from human fibroblasts and astrocytes during senescence. The cyclin-dependent kinase inhibitor, $p16^{INK4a}$, is a key marker for senescence in multiple cell types. Unfortunately, antibodies are problematic. The INK4a locus is subject to complex regulation and alternative splicing [48, 49] which adds to the problems associated with the evaluation of changes in $p16^{INK4a}$ expression. Antibodies that react with human $p16^{INK4a}$ likely do not cross-react with mouse $p16^{INK4a}$. In addition, p16 antibodies for immunoblotting may not be suitable for immunohistochemistry. For a discussion of the difficulties with anti-$p16^{INK4a}$ antibodies *see* Sawicka et al. [50].
23. It is important to avoid over-fixation as it could compromise enzyme activity. A fixative prepared with commercially available 37 % formaldehyde works better than a fixative prepared from paraformaldehyde powder.
24. An incubator without CO_2 should be used because the CO_2 in most tissue culture incubators alters the pH of the assay.
25. The blue color in cells that are SA β-gal positive can be seen with a light microscope. Turning off phase contrast will enable the blue color to be seen more easily at the expense of visualizing cell morphology. We score SA β-gal-positive cells in

two categories, strongly positive and weakly positive. This distinction is important as one may find weak staining in control cultures and monitoring "blue" and "less blue" cells can be useful in the interpretation of the results. A strong stress may induce high SA β-gal positivity but only in a subset of the population. Noting whether the activity is high (as indicated by strong staining) can help to determine the percent of the cell population that has undergone a significant stress.

26. Depending on cell type, coating of glass cover slips may be required for cells to adhere. In our experience with both human fibroblasts and astrocytes, this is not necessary. As long as cover slips have been cleaned properly cells should adhere within 1 day of plating. Seeding density may need to be determined empirically, as it is important to avoid cell confluence when immunostaining.
27. In order to avoid dislodging cells from cover slips, solutions should not be pipetted directly onto the cover slips. Washes should be performed by pipetting solution against the wall of well containing the cover slip. Also, avoid letting cover slips dry out.
28. The protocol can be stopped at this point, and cover slips can be stored at 4 °C for future staining for up to 1 month.
29. Primary antibodies to be used in combination must be raised in different species in order to avoid cross-reactivity of the secondary antibodies. Secondary antibodies should also be carefully selected to avoid cross-reactivity with the other secondary antibody; for example, secondary antibodies raised in goat should not be used in combination with a primary antibody raised in the same species in order to avoid cross-reactivity with the anti-goat secondary antibody. A vast array of fluorescently tagged antibodies is available from several commercial providers; thus, we strongly encourage the user to invest in additional antibodies instead of relying on sequential staining and extra blocking steps to overcome this issue.
30. Depending on the senescence biomarker, cells can be scored as either positive or negative for the signal of interest, or the fluorescence intensity can be quantified with freely available image analysis software such as ImageJ or CellProfiler. Directions for quantification of nuclear staining intensity with ImageJ software can be found at http://digital.bsd.uchicago.edu/resources_files/Basic%20image%20quantification.pdf. Quantitative immunofluorescence to measure the nuclear staining intensity of SAHF-enriched heterochromatin-associated proteins (macroH2A1, HP1β) can be performed provided that the antibodies are used at saturating concentrations [31].

31. This induces growth arrest through contact inhibition and allows a comparison of pre-senescent cells in a nondividing state with senescent cells that are inherently nondividing. This important consideration for comparisons to senescent cells has been somewhat lost in recent years; but this was a very important aspect of the original gene expression comparisons that led to the discovery of the SASP.
32. Depending upon cell type, duration of incubation with serum-free medium may have to be empirically determined as some cell types may dedifferentiate in the absence of growth factors.
33. In order to remove cell debris that contains SASP mediators, filtration or centrifugation (500 × *g* for 10 min at 4 °C) should be performed.
34. We have used the IL-6 Quantikine Immunoassay (human IL-6) (R&D Systems, cat# D6050) and membrane-based cytokine antibody arrays (RayBiotech) with good success [51, 52], although other commercial producers exist and multiplex analysis using the Luminex technologies is a possibility depending upon cost considerations.

Acknowledgements

This work was supported by grants 1RO1NS078283 to C.T. and AG039799 to C.S., the Commonwealth of Pennsylvania Universal Research Enhancement Grant (CT), the Drexel University College of Medicine Research Program Planning Grant (CT), and the Drexel Aging Initiative. T.N. is the recipient of a fellowship from the Drexel Aging Initiative. Research reported in this publication is also supported by the National Institute on Aging of the National Institutes of Health under Award Number F30AG043307 (EPC). The content of this chapter is solely the responsibility of the authors and does not necessarily represent the official views of the National Institutes of Health.

References

1. Kosar M, Bartkova J, Hubackova S, Hodny Z, Lukas J, Bartek J (2011) Senescence-associated heterochromatin foci are dispensable for cellular senescence, occur in a cell type- and insult-dependent manner and follow expression of p16(ink4a). Cell Cycle 10(3):457–468
2. Wright WE, Shay JW (2000) Telomere dynamics in cancer progression and prevention: fundamental differences in human and mouse telomere biology. Nat Med 6(8):849–851
3. Kennedy AL, McBryan T, Enders GH, Johnson FB, Zhang R, Adams PD (2010) Senescent mouse cells fail to overtly regulate the HIRA histone chaperone and do not form robust Senescence Associated Heterochromatin Foci. Cell Div 5:16
4. Coppe JP, Rodier F, Patil CK, Freund A, Desprez PY, Campisi J (2011) Tumor suppressor and aging biomarker p16(INK4a) induces cellular senescence without the associated

inflammatory secretory phenotype. J Biol Chem 286(42):36396–36403
5. Itahana K, Dimri G, Campisi J (2001) Regulation of cellular senescence by p53. Eur J Biochem 268(10):2784–2791
6. Coppe JP, Desprez PY, Krtolica A, Campisi J (2010) The senescence-associated secretory phenotype: the dark side of tumor suppression. Annu Rev Pathol 5:99–118
7. Krishnamurthy J, Torrice C, Ramsey MR, Kovalev GI, Al-Regaiey K, Su L, Sharpless NE (2004) Ink4a/Arf expression is a biomarker of aging. J Clin Invest 114(9):1299–1307
8. Naylor RM, Baker DJ, van Deursen JM (2013) Senescent cells: a novel therapeutic target for aging and age-related diseases. Clin Pharmacol Ther 93(1):105–116
9. Hayflick L (1965) The limited *in vitro* lifetime of human diploid strains. Exp Cell Res 37: 614–636
10. Hayflick L, Moorhead P (1961) The serial cultivation of human diploid cell strains. Exp Cell Res 25:585–621
11. Eidukevicius R, Characiejus D, Janavicius R, Kazlauskaite N, Pasukoniene V, Mauricas M, Den Otter W (2005) A method to estimate cell cycle time and growth fraction using bromodeoxyuridine-flow cytometry data from a single sample. BMC Cancer 5:122
12. Gibson GE, Tofel-Grehl B, Scheffold K, Cristofalo VJ, Blass JP (1998) A reproducible procedure for primary culture and subsequent maintenance of multiple lines of human skin fibroblasts. Age (Omaha) 21(1):7–14
13. Jurk D, Wang C, Miwa S, Maddick M, Korolchuk V, Tsolou A, Gonos ES, Thrasivoulou C, Saffrey MJ, Cameron K, von Zglinicki T (2012) Postmitotic neurons develop a p21-dependent senescence-like phenotype driven by a DNA damage response. Aging Cell 11(6):996–1004
14. Besancenot R, Chaligné R, Tonetti C, Pasquier F, Marty C, Lécluse Y, Vainchenker W, Constantinescu SN, Giraudier S (2010) A senescence-like cell-cycle arrest occurs during megakaryocytic maturation: implications for physiological and pathological megakaryocytic proliferation. PLoS Biol 8(9): e1000476. doi:10.1371/journal.pbio.1000476, pii: e1000476
15. Lanza RP, Cibelli JB, Blackwell C, Cristofalo VJ, Francis MK, Baerlocher GM, Mak J, Schertzer M, Chavez EA, Sawyer N, Lansdorp PM, West MD (2000) Extension of cell lifespan and telomere length in animals cloned from senescent somatic cells. Science 288(5466):665–669
16. Niedernhofer LJ, Glorioso JC, Robbins PD (2011) Dedifferentiation rescues senescence of progeria cells but only while pluripotent. Stem Cell Res Ther 2(3):28
17. Banito A, Rashid ST, Acosta JC, Li S, Pereira CF, Geti I, Pinho S, Silva JC, Azuara V, Walsh M, Vallier L, Gil J (2009) Senescence impairs successful reprogramming to pluripotent stem cells. Genes Dev 23(18):2134–2139
18. Dimri GP, Lee X, Basile G, Acosta M, Scott G, Roskelley C, Medrano EE, Linskens M, Rubelj I, Pereira-Smith O et al (1995) A biomarker that identifies senescent human cells in culture and in aging skin in vivo. Proc Natl Acad Sci U S A 92(20):9363–9367
19. Kurz DJ, Decary S, Hong Y, Erusalimsky JD (2000) Senescence-associated (beta)-galactosidase reflects an increase in lysosomal mass during replicative ageing of human endothelial cells. J Cell Sci 113(Pt 20):3613–3622
20. Lee BY, Han JA, Im JS, Morrone A, Johung K, Goodwin EC, Kleijer WJ, DiMaio D, Hwang ES (2006) Senescence-associated beta-galactosidase is lysosomal beta-galactosidase. Aging Cell 5(2):187–195
21. Debacq-Chainiaux F, Erusalimsky JD, Campisi J, Toussaint O (2009) Protocols to detect senescence-associated beta-galactosidase (SA-betagal) activity, a biomarker of senescent cells in culture and in vivo. Nat Protoc 4(12):1798–1806
22. Donnini S, Solito R, Cetti E, Corti F, Giachetti A, Carra S, Beltrame M, Cotelli F, Ziche M (2010) Abeta peptides accelerate the senescence of endothelial cells in vitro and in vivo, impairing angiogenesis. FASEB J 24(7):2385–2395
23. Minamino T, Miyauchi H, Yoshida T, Ishida Y, Yoshida H, Komuro I (2002) Endothelial cell senescence in human atherosclerosis: role of telomere in endothelial dysfunction. Circulation 105(13):1541–1544
24. Cao L, Li W, Kim S, Brodie SG, Deng CX (2003) Senescence, aging, and malignant transformation mediated by p53 in mice lacking the Brca1 full-length isoform. Genes Dev 17(2):201–213
25. Wei W, Sedivy JM (1999) Differentiation between senescence (M1) and crisis (M2) in human fibroblast cultures. Exp Cell Res 253(2):519–522
26. Narita M, Narita M, Krizhanovsky V, Nunez S, Chicas A, Hearn SA, Myers MP, Lowe SW (2006) A novel role for high-mobility group a proteins in cellular senescence and heterochromatin formation. Cell 126(3): 503–514

27. Narita M, Nunez S, Heard E, Lin AW, Hearn SA, Spector DL, Hannon GJ, Lowe SW (2003) Rb-mediated heterochromatin formation and silencing of E2F target genes during cellular senescence. Cell 113(6):703–716
28. Zhang R, Chen W, Adams PD (2007) Molecular dissection of formation of senescence-associated heterochromatin foci. Mol Cell Biol 27(6):2343–2358
29. Di Micco R, Sulli G, Dobreva M, Liontos M, Botrugno OA, Gargiulo G, dal Zuffo R, Matti V, d'Ario G, Montani E, Mercurio C, Hahn WC, Gorgoulis V, Minucci S, d'Adda di Fagagna F (2011) Interplay between oncogene-induced DNA damage response and heterochromatin in senescence and cancer. Nat Cell Biol 13(3):292–302
30. Cruickshanks HA, McBryan T, Nelson DM, Vanderkraats ND, Shah PP, van Tuyn J, Singh Rai T, Brock C, Donahue G, Dunican DS, Drotar ME, Meehan RR, Edwards JR, Berger SL, Adams PD (2013) Senescent cells harbour features of the cancer epigenome. Nat Cell Biol 15(12):1495–1506
31. Kreiling JA, Tamamori-Adachi M, Sexton AN, Jeyapalan JC, Munoz-Najar U, Peterson AL, Manivannan J, Rogers ES, Pchelintsev NA, Adams PD, Sedivy JM (2011) Age-associated increase in heterochromatic marks in murine and primate tissues. Aging Cell 10(2):292–304
32. Coppe JP, Patil CK, Rodier F, Sun Y, Munoz DP, Goldstein J, Nelson PS, Desprez PY, Campisi J (2008) Senescence-associated secretory phenotypes reveal cell-nonautonomous functions of oncogenic RAS and the p53 tumor suppressor. PLoS Biol 6(12):2853–2868
33. Goldstein S, Moerman EJ, Baxter RC (1993) Accumulation of insulin-like growth factor binding protein-3 in conditioned medium of human fibroblasts increases with chronologic age of donor and senescence in vitro. J Cell Physiol 156(2):294–302
34. Thweatt R, Murano S, Fleischmann RD, Goldstein S (1992) Isolation and characterization of gene sequences overexpressed in Werner syndrome fibroblasts during premature replicative senescence. Exp Gerontol 27(4):433–440
35. Tchkonia T, Zhu Y, van Deursen J, Campisi J, Kirkland JL (2013) Cellular senescence and the senescent secretory phenotype: therapeutic opportunities. J Clin Invest 123(3):966–972
36. Freund A, Orjalo AV, Desprez PY, Campisi J (2010) Inflammatory networks during cellular senescence: causes and consequences. Trends Mol Med 16(5):238–246
37. Rodier F, Coppe JP, Patil CK, Hoeijmakers WA, Munoz DP, Raza SR, Freund A, Campeau E, Davalos AR, Campisi J (2009) Persistent DNA damage signalling triggers senescence-associated inflammatory cytokine secretion. Nat Cell Biol 11(8):973–979
38. Freund A, Patil CK, Campisi J (2011) p38MAPK is a novel DNA damage response-independent regulator of the senescence-associated secretory phenotype. EMBO J 30(8):1536–1548
39. Kuilman T, Michaloglou C, Vredeveld LC, Douma S, van Doorn R, Desmet CJ, Aarden LA, Mooi WJ, Peeper DS (2008) Oncogene-induced senescence relayed by an interleukin-dependent inflammatory network. Cell 133(6): 1019–1031
40. Acosta JC, Banito A, Wuestefeld T, Georgilis A, Janich P, Morton JP, Athineos D, Kang TW, Lasitschka F, Andrulis M, Pascual G, Morris KJ, Khan S, Jin H, Dharmalingam G, Snijders AP, Carroll T, Capper D, Pritchard C, Inman GJ, Longerich T, Sansom OJ, Benitah SA, Zender L, Gil J (2013) A complex secretory program orchestrated by the inflammasome controls paracrine senescence. Nat Cell Biol 15(8):978–990
41. Krizhanovsky V, Yon M, Dickins RA, Hearn S, Simon J, Miething C, Yee H, Zender L, Lowe SW (2008) Senescence of activated stellate cells limits liver fibrosis. Cell 134(4):657–667
42. Jun JI, Lau LF (2010) The matricellular protein CCN1 induces fibroblast senescence and restricts fibrosis in cutaneous wound healing. Nat Cell Biol 12(7):676–685
43. Severino V, Alessio N, Farina A, Sandomenico A, Cipollaro M, Peluso G, Galderisi U, Chambery A (2013) Insulin-like growth factor binding proteins 4 and 7 released by senescent cells promote premature senescence in mesenchymal stem cells. Cell Death Dis 4:e911
44. Coppe JP, Patil CK, Rodier F, Krtolica A, Beausejour CM, Parrinello S, Hodgson JG, Chin K, Desprez PY, Campisi J (2010) A human-like senescence-associated secretory phenotype is conserved in mouse cells dependent on physiological oxygen. PLoS One 5(2):e9188
45. Acosta JC, Snijders AP, Gil J (2013) Unbiased characterization of the senescence-associated secretome using SILAC-based quantitative proteomics. Methods Mol Biol 965:175–184
46. Lerner C, Bitto A, Pulliam D, Nacarelli T, Konigsberg M, Van Remmen H, Torres C, Sell C (2013) Reduced mammalian target of

rapamycin activity facilitates mitochondrial retrograde signaling and increases life span in normal human fibroblasts. Aging Cell 12(6):966–977

47. Bitto A, Lerner C, Torres C, Roell M, Malaguti M, Perez V, Lorenzini A, Hrelia S, Ikeno Y, Matzko ME, McCarter R, Sell C (2010) Long-term IGF-I exposure decreases autophagy and cell viability. PLoS One 5(9):e12592
48. Kim WY, Sharpless NE (2006) The regulation of INK4/ARF in cancer and aging. Cell 127(2):265–275
49. Gil J, Peters G (2006) Regulation of the INK4b-ARF-INK4a tumour suppressor locus: all for one or one for all. Nat Rev Mol Cell Biol 7(9):667–677
50. Sawicka M, Pawlikowski J, Wilson S, Ferdinando D, Wu H, Adams PD, Gunn DA, Parish W (2013) The specificity and patterns of staining in human cells and tissues of p16INK4a antibodies demonstrate variant antigen binding. PLoS One 8(1):e53313
51. Bhat R, Crowe EP, Bitto A, Moh M, Katsetos CD, Garcia FU, Johnson FB, Trojanowski JQ, Sell C, Torres C (2012) Astrocyte senescence as a component of Alzheimer's disease. PLoS One 7(9):e45069
52. Bitto A, Sell C, Crowe E, Lorenzini A, Malaguti M, Hrelia S, Torres C (2010) Stress-induced senescence in human and rodent astrocytes. Exp Cell Res 316(17):2961–2968

Part III

Protocols: Analyzing Cell Cycle Events and Molecules

Chapter 24

Analyzing RB and E2F During the G1–S Transition

Michael J. Thwaites, Matthew J. Cecchini, and Frederick A. Dick

Abstract

The G1/S-phase restriction point is an important landmark in the mammalian cell division cycle. The key regulator of the G1/S transition is the retinoblastoma gene product (pRB). It prevents the transcription of genes required for S-phase progression by repressing E2F transcription factors. An increase in Cdk phosphorylation of pRB causes the release of E2F transcription factors and advancement into S phase. Here we describe two simple techniques used to assess pRB phosphorylation and E2F transcription during G1/S progression.

Key words Retinoblastoma, Transcription, Phosphorylation, Gene expression, E2F

1 Introduction

The primary regulator of the G1/S-phase transition in mammalian cells is the retinoblastoma protein (pRB). It inhibits E2F transcription factors, thereby repressing the transcription of genes necessary for DNA replication and cell division [1]. When a cell is triggered to divide via mitogen stimulation, an increase in cyclin-dependent kinase activity in late G1 leads to the hyperphosphorylation of pRB [2]. This, in turn, causes a conformational change and the release of the bound E2F transcription factors, allowing for an upregulation of E2F target gene expression [3]. In mitosis, pRB returns to a hypophosphorylated state and represses E2Fs in the ensuing G1 phase [4].

As the RB pathway is vital to maintaining proliferative control, it is often the target for inactivation in cancer [5]. The majority of mutations affecting this pathway do not specifically target pRB; instead, they influence the phosphorylation status of pRB [6]. Two major indicators of the functionality of the pRB pathway are the phosphorylation status of pRB and the transcriptional activation of E2F target genes. Both the constitutive hyperphosphorylation of pRB and increased transcription of E2F target genes suggest a deficiency in the pRB pathway and a loss of G1 checkpoint control.

Eishi Noguchi and Mariana C. Gadaleta (eds.), *Cell Cycle Control: Mechanisms and Protocols*, Methods in Molecular Biology, vol. 1170, DOI 10.1007/978-1-4939-0888-2_24,

The abundance of E2F target genes [7] and numerous phosphorylation sites on pRB [4] both prevent a straightforward analysis of these parameters. Based on reliability of antibodies, we use phosphorylation of pRB at S807 and S811 to gauge phosphorylation status [8–10]. However, inactivation of pRB at S-phase entry is generally accompanied by phosphorylation of at least 12 sites. Consequently, we routinely supplement these blots with phospho-shift analysis to gain insight into a broader number of potential phosphorylation sites on pRB. Similarly, expression microarray and ChIP-chip or ChIP-sequence experiments suggest that an overwhelming number of genes are under the control of E2Fs [11–13]. This makes the analysis of single E2F targets anecdotal and incomplete, while microarray or RNA-sequence techniques are too cumbersome for rapid assessment of large numbers of samples. We have devised an approach using the Quantigene Plex 2.0 assay from Affymetrix to profile six common E2F targets that represent the major subclasses of E2F targets at the G1/S transition. These include genes encoding cell cycle regulators (cyclin E1, cyclin A2, and p107), nucleotide biosynthetic enzymes (thymidylate synthase), and DNA replication factors (MCM3 and PCNA). Taken together, these methods will allow investigators to assess G1/S regulation in synchronized cell culture experiments or in tissue extracts from genetically modified mice.

2 Materials

2.1 Immunoblotting

1. 8 % SDS-PAGE resolving gel: 8 % Acrylamide:bis-acrylamide (37.5:1), 375 mM Tris–HCl (pH 8.8), 0.1 % SDS, 0.05 % ammonium persulfate, 0.05 % TEMED.
2. 4 % SDS-PAGE stacking gel: 4 % Acrylamide:bis-acrylamide (37.5:1), 125 mM Tris–HCl (pH 6.8), 0.1 % SDS, 0.05 % ammonium persulfate, 0.2 % TEMED.
3. Mini PROTEAN® 3 System glass plates 0.75 mm (Bio-Rad, Hercules, CA) or an equivalent.
4. 5× SDS sample buffer: 312.5 mM Tris–HCl (pH 6.8), 25 % glycerol, 10 % SDS, 2.3 M β-mercaptoethanol, and bromophenol blue to desired color.
5. Precision Plus Protein™ Standards, Kaleidoscope™ (Bio-Rad) or an equivalent.
6. SDS running buffer: 25 mM Tris base, 192 mM glycine, 0.1 % SDS.
7. Hybond ECL nitrocellulose membrane (Fisher) or an equivalent.
8. Mini Trans-Blot® System (Bio-Rad) or an equivalent.
9. Transfer buffer: 50 mM Tris base, 386 mM glycine, 0.1 % SDS, 20 % methanol.

10. TBST: 20 mM Tris–HCl pH 7.5, 150 mM NaCl, 0.3 % Tween-20.
11. TBS: 20 mM Tris–HCl pH 7.5, 150 mM NaCl.
12. Skim milk powder.
13. Anti-pRB antibody (G3-245, BD Pharmingen, catalog # 554136).
14. Anti-phospho-Rb (Ser807/811Cell Signaling, catalog # 9308).
15. ECL anti-mouse IgG, HRP-linked whole Ab (from sheep, Fisher, catalog # NA931-1ML).
16. ECL anti-rabbit IgG, HRP-linked whole Ab (from donkey, Fisher, catalog # NA934-1ML).
17. ECL solution: 1.25 mM Luminol, 0.2 mM coumeric acid, 100 mM Tris–HCl pH 8.5.
18. Filter paper.
19. Autoradiographic film.

2.2 Expression of E2F Targets Using Quantigene Plex 2.0 Reagent System

2.2.1 RNA Purification

1. TRIzol® Reagent (Life Technologies).
2. 3 M Sodium acetate.
3. 100 % Ethanol.
4. 4 °C Microcentrifuge.
5. 75 % Ethanol in DEPC water.
6. RNase-free water.

2.2.2 Hybridization of Purified RNA Samples to Quantigene® Plex 2.0 Probe Set

1. RNase-free water.
2. 95 °C Heat block.
3. Quantigene® Plex 2.0 Reagent System (Affymetrix, catalog # QP01010) including Quantigene® Plex 2.0 Lysis Mixture, Quantigene® Plex 2.0 Capture Beads, and Quantigene® Plex Blocking reagent.
4. Quantigene® Plex 2.0 Probe set (Panel #21118, Affymetrix, catalog # 390000-109).
5. Hybridization plate, kit comes with one plate, if additional plates are required use 96-well cell culture cluster round bottom with lid.
6. 96-Well PCR Plate Sealing Mat (Bio-Rad) or an equivalent.
7. Rubber bands.
8. Labnet Vortemp56 Shaker or equivalent.

2.2.3 Hybridization of the 2.0 Preamplifier

1. 2.0 Wash buffer (for one full 96-well plate): 190 mL of nuclease-free water, 600 µL of wash buffer component #1, and 10 mL of wash buffer component #2. Wash buffer must be made fresh every time, and adjust volumes accordingly.

2. Preamplifier reagent: Add 36 µL of preamplifier to 12 mL of pre-warmed amplifier diluent. Invert to mix (*see* **Note 1**).
3. 100 mL Capacity reservoir.
4. 25 mL Capacity reservoir.
5. Multichannel pipette (p200).
6. MultiScreen® Filter plates (Multiscreen HTS BV, 1.2 µm, Millipore).
7. 96-Well plate to serve as a plate holder.
8. Foil plate sealer (included in Quantigene® Plex 2.0 Reagent System (Affymetrix catalog # QP01010)).
9. Aurum Vacuum manifold (Bio-Rad) or an equivalent.
10. Lint-free tissues.
11. Labnet Vortemp56 Shaker or an equivalent.
12. Centrifuge capable of spinning 96-well cell culture plates.

2.2.4 Hybridization of the 2.0 Amplifier

1. Amplifier reagent: Add 36 µL of amplifier to 12 mL of pre-warmed amplifier diluent. Invert to mix (*see* **Note 1**).
2. Aurum Vacuum manifold (Bio-Rad) or an equivalent.
3. Multichannel pipette (p200).
4. 2.0 Wash buffer (*see* Subheading 2.2.3).
5. 100 mL Capacity reservoir.
6. Lint-free tissues.
7. 25 mL Capacity reservoir.
8. Labnet Vortemp56 Shaker or an equivalent.

2.2.5 Hybridization of the Label Probe

1. Label probe reagent: Add 36 µL of label probe to 12 mL of label probe diluent and vortex for 15 s to mix (*see* **Note 1**).
2. Aurum Vacuum manifold (Bio-Rad) or an equivalent.
3. Multichannel pipette (p200).
4. 2.0 Wash buffer (*see* Subheading 2.2.3).
5. 100 mL Capacity reservoir.
6. Lint-free tissues.
7. 25 mL Capacity reservoir.
8. Labnet Vortemp56 Shaker or an equivalent.

2.2.6 Binding the Streptavidin and Phycoerythrin

1. Streptavidin and phycoerythrin (SAPE) reagent: Add 36 µL of SAPE to 12 mL of SAPE diluent, vortex for 15 s to mix, and protect from light by wrapping in aluminum foil (*see* **Note 1**).
2. Aurum Vacuum manifold (Bio-Rad) or an equivalent.
3. Multichannel pipette (p200).

4. 2.0 Wash buffer (*see* Subheading 2.2.3).
5. 100 mL Capacity reservoir.
6. Lint-free tissues.
7. 25 mL Capacity reservoir.
8. Aluminum foil.
9. Labnet Orbit P4 Shaker or an equivalent.

2.2.7 Signal Detection

1. Aurum Vacuum manifold (Bio-Rad) or an equivalent.
2. SAPE Wash buffer (included in Quantigene® Plex 2.0 Reagent System, Affymetrix).
3. 100 mL Reservoir.
4. Multichannel pipette (p200).
5. Lint-free tissues.
6. Aluminum foil.
7. Labnet Orbit P4 Shaker or equivalent.
8. BioPlex200 System (Bio-Rad) or an equivalent.

3 Methods

3.1 Immunoblotting to Determine the Ratio of Hyper- to Hypophosphorylated pRB

In this section we describe immunoblotting techniques that allow for the separation of hyper- and hypophosphorylated pRB despite the size difference being only a few kilodaltons. This can further be verified by the use of phosphorylation-specific antibodies. Figure 1 (top panel) shows an example immunoblot depicting the separation between hyper- and hypophosphorylated species of pRB. The lower blot shows an example immunoblot against pRB phosphorylated at

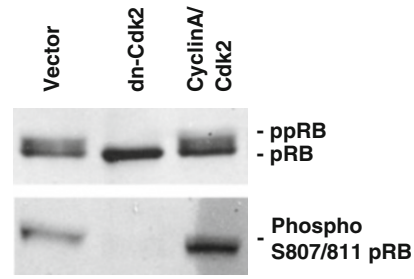

Fig. 1 Detection of hyperphosphorylated pRB. C33A cells were transfected with a CMV-RB expression vector along with an empty vector control or a CMV construct encoding dominant negative Cdk2 or cyclin A/Cdk2. The *upper blot* shows the migration positions of underphosphorylated or "hypophosphorylated" pRB as well as "hyperphosphorylated" ppRB. The *lower blot* shows phospho S807/811 detection of the same pRB species

serine residues 807 and 811, two representative phosphorylation sites (*see* **Notes 2–4**). Immunoblotting of pRB described here uses nuclear protein extract prepared as described previously [9].

1. Prepare duplicate 8 % SDS-PAGE resolving gels that are 0.75 mm thick using standard methods.
2. Once solidified, overlay with 4 % SDS-PAGE stacking gel and insert a 10-well comb.
3. Dilute 120 μg of nuclear protein extract with 5× SDS sample buffer so that samples are in 1× SDS sample buffer.
4. Boil samples at 95 °C for 5 min.
5. Load duplicate gels with 60 μg of nuclear protein extract for each sample. Load a 10 μL aliquot of protein standard ladder into a parallel lane.
6. Run gel(s) in SDS running buffer at 50–70 V at 4 °C until the 75 kDa marker has reached the bottom of the gel, approximately 6 h.
7. Transfer samples to GE Hybond ECL membrane with Mini Trans-Blot® System in transfer buffer for 1 h at 100 V at 4 °C.
8. Block membranes using TBST with 5 % skim milk powder for 1-h shaking at room temperature.
9. Make up primary antibody solutions. Anti-RB: Dilute 10 μg of BD Pharma anti-pRB antibody G3-245 in 10 mL of TBST containing 1 % skim milk powder. Anti-phospho-RB: Dilute 10 μg of cell signaling anti-phospho-RB (Ser807/811) antibody in 10 mL of TBST containing 1 % skim milk powder.
10. Incubate membranes with primary antibody solution, one with anti-RB antibody and the other with anti-phospho-RB antibody overnight at 4 °C while rocking.
11. Wash membranes three times with TBST at room temperature for 10 min.
12. Make up secondary antibody solutions by diluting ECL Anti-Mouse IgG-HRP-conjugated antibody 1:10,000 into 10 mL of TBST containing 1 % skim milk powder (use for anti-pRB blot). Dilute ECL Anti-Rabbit IgG-HRP-conjugated antibody 1:10,000 into 10 mL of TBST containing 1 % skim milk powder (use for anti-phospho-pRB blot).
13. Incubate membranes with appropriate secondary antibody solution at room temperature for 1 h while shaking.
14. Wash membranes three times with TBST at room temperature for 10 min.
15. Wash membranes once with TBS for 10 min at room temperature while shaking.

16. Prepare ECL solution immediately before use, and incubate membrane in ECL solution at room temperature for 2 min.
17. Remove excess ECL solution with filter paper and expose to film in darkroom.

3.2 Analysis of E2F Target Gene Expression Using Quantigene® Plex 2.0 Reagent System

A key function of pRB is the repression of E2F target genes to prevent S-phase entry [1]. Therefore, while the phosphorylation status of pRB is a good indicator of the functionality of pRB, determining E2F target gene message levels is an important companion to assessing its activity. Our system for analyzing E2F target gene transcription allows for the determination of relative quantities of various E2F target genes (Ccne1, Ccna2, Rbl1, Tyms, PCNA, and Mcm3) as well as three internal controls (Ppib, Rplp0, and Actb) in a single reaction. This confers a number of advantages over traditional qRT-PCR while providing equivalent accuracy. First, with each sample being internally controlled, the variability introduced through pipetting is dramatically reduced. Second, each reaction requires only 2 μg of RNA to analyze nine targets, the same amount of material required for one qRT-PCR reaction. Finally, it is cost effective compared to the reagents needed for nine separate qRT-PCR assays. In simple terms, this method measures the abundance of individual mRNA species akin to antibody detection of proteins in an ELISA, with captured mRNAs being adsorbed through hybridization. The adsorption occurs on different colored fluorescent beads such that quantities of mRNA, and identities of the mRNAs, are determined simultaneously through a two-color flow detection system in a Luminex bead reader. This protocol requires some knowledge of the Luminex system. Figure 2 demonstrates our approach to ensuring that hybridization plates remain sealed throughout the following procedures. Figure 3 shows sample data taken from WT and *Rb1* null fibroblasts to demonstrate defective E2F target gene repression.

3.2.1 RNA Purification (See **Note 5**)

1. Extract RNA using Trizol® Reagent according to the manufacturer's instructions.
2. To a high-quality RNA sample add 0.1 volumes of 3 M sodium acetate and 2.5 volumes of 100 % ethanol. Incubate overnight at −20 °C.
3. Spin samples at 10,000 × *g* for 10 min at 4 °C.
4. Discard supernatant, and wash pellet with 75 % ethanol made up in DEPC water.
5. Respin samples at 10,000 × *g* for 10 min at 4 °C.
6. Discard supernatant, and let pellets air-dry until residual ethanol has evaporated.
7. Resuspend pellets in 50 μL of RNase-free water and store at −80 °C for future use.

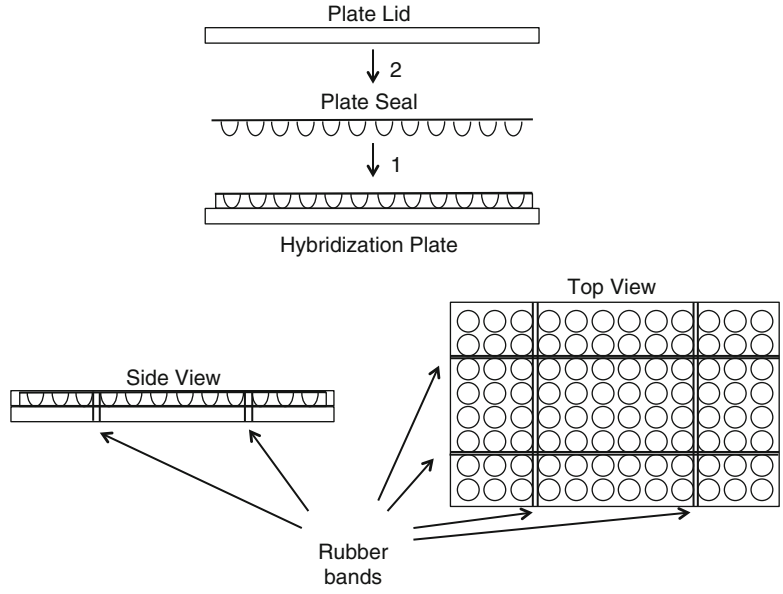

Fig. 2 Schematic representation of a 96-well plate setup for overnight hybridization of RNA samples to our Quantigene® Plex 2.0 probe set. Ensure that each well is sealed tightly with the PCR plate sealing mat before replacing the plate lid. Hold the entire assembly together with rubber bands as depicted

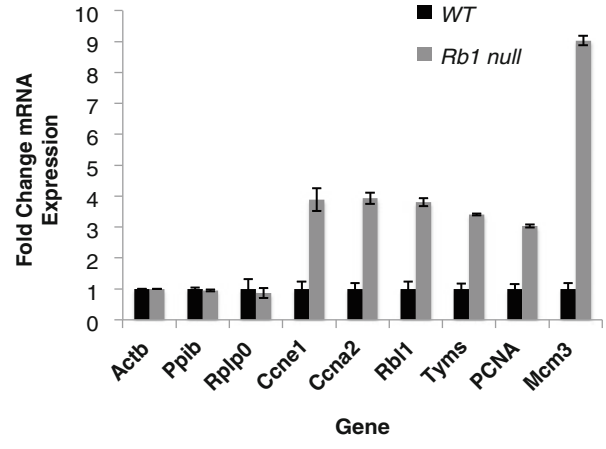

Fig. 3 Quantification of E2F target gene expression levels by Quantigene® Plex 2.0 Reagent system. mRNA was isolated from mouse embryonic fibroblasts after 60 h of serum deprivation to induce a cell cycle arrest. Relative expression of six E2F targets (Ccne1, Ccna2, Rbl1, Tyms, PCNA, and Mcm3) and three internal controls (Actb, Ppib, and Rplp0) was determined and normalized to Actb. Wild-type expression for each gene is scaled to 1 for comparison

Table 1
Hybridization master mix

Reagent	Volume per well (μL)
RNase-free water	38.7
Quantigene® Plex 2.0 Blocking reagent	2
Quantigene® Plex 2.0 Lysis Mixture	33.3
Quantigene® Plex 2.0 Capture Beads	1
2.0 Probe set	5
Total volume	80

3.2.2 Hybridization of Purified RNA Samples to Quantigene® Plex 2.0 Probe Set

1. Thaw purified RNA samples, and dilute samples in RNase-free water to 100 ng/μL in 75 μL aliquots. Keep on ice.
2. Pre-warm lysis mixture at 37 °C for 30 min.
3. Boil appropriate volume of probe set (7 μL per well) at 95 °C for 5 min using a heat block (*see* **Note 6**).
4. Make up hybridization master mix (*see* **Note 7** and Table 1). Add 80 μL of hybridization master mix and 20 μL of diluted RNA (2 μg total) to each well in the hybridization plate (*see* **Note 8**). Seal plate with 96-well plate sealing mat, lid, and hold it together with rubber bands as shown in Fig. 2.
5. Incubate for 16 h at 55 °C at 600 rpm in Labnet Vortemps56 shaker or an equivalent, protected from light.

3.2.3 Hybridization of the 2.0 Preamplifier

1. Next morning make up enough 2.0 Wash buffer for the number of wells being used.
2. Pre-warm amplifier diluent at 37 °C for 20 min.
3. Prepare preamplifier reagent.
4. Pour 2.0 Wash buffer into 100 mL capacity reservoir.
5. Using multichannel pipette, pre-wet Multiscreen® Filter plate by adding 100 μL of 2.0 Wash buffer to each well to be used and incubate for 1 min (*see* **Note 9**).
6. Seal plate using foil plate sticker, and carefully peal back seal to expose only the wells you will be using for samples.
7. Filter wash buffer using vacuum manifold (*see* **Note 10**).
8. Spin down hybridization plate in plate centrifuge at 240 × *g* for 1 min to ensure that liquid is at the bottom of each well.
9. Adjust plate shaker temperature to 50 °C. Using a multichannel pipette, pipette samples up and down five times to mix and transfer to filter plate.

10. Filter liquid through plate using vacuum manifold (*see* **Note 10**).
11. Using multichannel pipette, wash filter plate three times with 200 µL of 2.0 Wash buffer per well from 100 mL reservoir and filter liquid through after each wash using vacuum manifold (*see* **Note 10**).
12. Blot the bottom of the filter plate using lint-free tissues to remove any excess liquid.
13. Pour preamplifier reagent into 25 mL capacity reservoir.
14. Using multichannel pipette, add 100 µL of preamplifier reagent to each well.
15. Reseal plate and incubate at 50 °C shaking at 600 rpm for 1 h.

3.2.4 Hybridization of the 2.0 Amplifier

1. Prepare amplifier reagent.
2. Remove plate from plate shaker, carefully peal back plate seal, and filter the preamplifier reagent through the plate using vacuum manifold (*see* **Note 10**).
3. Using multichannel pipette, wash filter plate twice with 200 µL of 2.0 Wash buffer per well from 100 mL reservoir and filter liquid through after each wash using vacuum manifold (*see* **Note 10**).
4. Blot the bottom of the filter plate using lint-free tissues to remove any excess liquid.
5. Pour amplifier reagent into 25 mL capacity reservoir.
6. Using multichannel pipette, add 100 µL of amplifier reagent to each well.
7. Reseal the plate and incubate at 50 °C shaking at 600 rpm for 1 h.

3.2.5 Hybridization of the Label Probe

1. Prepare label probe reagent.
2. Remove plate from plate shaker, carefully peal back plate seal, and filter the amplifier reagent through the plate using vacuum manifold (*see* **Note 10**).
3. Using multichannel pipette, wash filter plate twice with 200 µL of 2.0 Wash buffer per well from 100 mL reservoir and filter liquid through after each wash using vacuum manifold (*see* **Note 10**).
4. Blot the bottom of the filter plate using lint-free tissues to remove any excess liquid.
5. Pour label probe reagent into 25 mL capacity reservoir.
6. Using multichannel pipette, add 100 µL of label probe reagent to each well. Reseal the plate and incubate at 50 °C shaking at 600 rpm for 1 h.

3.2.6 Binding the Streptavidin and Phycoerythrin

1. Prepare SAPE reagent.
2. Remove plate from plate shaker, carefully peal back plate seal, and filter the label probe reagent through the plate using vacuum manifold (*see* **Note 10**).
3. Using multichannel pipette, wash filter plate twice with 200 μL of 2.0 Wash buffer per well from 100 mL reservoir and filter liquid through after each wash using vacuum manifold (*see* **Note 10**).
4. Blot the bottom of the filter plate using lint-free tissues to remove any excess liquid.
5. Pour SAPE reagent into 25 mL capacity reservoir.
6. Using multichannel pipette, add 100 μL of SAPE reagent to each well. Reseal the plate, and wrap plate and plate holder in foil to protect from light. Incubate at room-temperature shaking at 600 rpm for 30 min using Labnet Orbit P4 Shaker or an equivalent.

3.2.7 Signal Detection

1. Remove plate from plate shaker, carefully peal back plate seal, and filter SAPE reagent through the plate using vacuum manifold (*see* **Note 10**).
2. Pour SAPE wash buffer into 100 mL capacity reservoir.
3. Using multichannel pipette, wash filter plate twice with 200 μL of SAPE wash buffer per well from 100 mL reservoir and filter liquid through after each wash using vacuum manifold (*see* **Note 10**).
4. Blot the bottom of the filter plate using lint-free tissues to remove any excess liquid.
5. Using multichannel pipette, add 130 μL of SAPE wash buffer, reseal plate, and rewrap filter plate and plate holder in aluminum foil to protect from light (*see* **Note 11**). Incubate at room temperature for 5 min on plate shaker, shaking at 600 rpm, and read immediately using Bioplex200 reader or an equivalent Luminex instrument.

3.2.8 Analysis of E2F Target Gene Expression

1. Subtract values from blank wells with water from unknown wells to remove background.
2. Identify the internal control whose value is closest to values of E2F target genes, and divide each well by the average of that internal control.
3. Average values for each gene in your untreated control.
4. Divide treatment values by average of untreated control for the corresponding gene to determine fold change relative to untreated.

5. Average triplicates of each gene to determine overall fold change and determine the standard deviation of the triplicate.
6. Sample processed data appears in Fig. 3.

4 Notes

1. This is enough for one plate. Adjust volumes according to the number of samples used.
2. Alternatively a single blot can be probed, stripped, and re-probed.
3. Following these procedures murine and human pRB will typically resolve into two bands. A standard 6 % SDS-PAGE and longer gel will allow human pRB to be resolved into as many as four bands, but we find these gels too soft to handle without frequent distortion of shape.
4. Phospho-specific antibodies against pRB rarely detect the upper, hyperphosphorylated band.
5. RNA purity can affect results. Ideal 260/280 and 230/260 ratios should be over 2.0. If ratios are lower, perform RNA purification step. If ratios are over 2.0, continue to hybridization of purified RNA samples to Quantigene® Plex 2.0 Probe set.
6. Quantigene® Plex 2.0 Reagent system panel # 21118 is specifically designed for murine target genes and is unlikely to cross-react with human.
7. We typically make up the hybridization mixture for the number of wells plus 20 % additional solution to ensure a sufficient supply. Vortex capture beads for 30 s prior to adding to mixture.
8. Make sure to prepare all samples in triplicate and include three blank wells with RNase-free water instead of RNA. Use multichannel pipette for all steps except while adding purified RNA samples to hybridization plate.
9. At no time can the filter plate make contact with another surface; use a 96-well plate to serve as a plate holder.
10. Ensure that flow is slow for all filtration steps, approximately 5–15 s to filter liquid through.
11. At this point the plate can be stored for up to 2 h at room temperature in the dark or 24 h at 4 °C in the dark.

References

1. Classon M, Harlow E (2002) The retinoblastoma tumour suppressor in development and cancer. Nat Rev Cancer 2:910–917
2. Sherr CJ, Roberts JM (2004) Living with or without cyclins and cyclin-dependent kinases. Genes Dev 18:2699–2711
3. Carrano AC, Eytan E, Hershko A, Pagano M (1999) SKP2 is required for ubiquitin-mediated degradation of the CDK inhibitor p27. Nat Cell Biol 1(4):193–199
4. Rubin SM (2013) Deciphering the retinoblastoma protein phosphorylation code. Trends Biochem Sci 38(1):12–19
5. Hanahan D, Weinberg RA (2011) Hallmarks of cancer: the next generation. Cell 144(5): 646–674
6. Sherr CJ, McCormick F (2002) The RB and p53 pathways in cancer. Cancer Cell 2(2): 103–112
7. Chen HZ, Tsai SY, Leone G (2009) Emerging roles of E2Fs in cancer: an exit from cell cycle control. Nat Rev Cancer 9(11):785–797
8. Francis SM, Bergsied J, Isaac CE, Coschi CH, Martens AL, Hojilla CV, Chakrabarti S, Dimattia GE, Khoka R, Wang JY, Dick FA (2009) A functional connection between pRB and transforming growth factor beta in growth inhibition and mammary gland development. Mol Cell Biol 29(16):4455–4466
9. Cecchini MJ, Dick FA (2011) The biochemical basis of CDK phosphorylation-independent regulation of E2F1 by the retinoblastoma protein. Biochem J 434(2):297–308
10. Hirschi A, Cecchini M, Steinhardt RC, Schamber MR, Dick FA, Rubin SM (2010) An overlapping kinase and phosphatase docking site regulates activity of the retinoblastoma protein. Nat Struct Mol Biol 17(9):1051–1057
11. Ren B, Cam H, Takahashi Y, Volkert T, Terragni J, Young RA, Dynlacht BD (2002) E2F integrates cell cycle progression with DNA repair, replication, and G(2)/M checkpoints. Genes Dev 16(2):245–256
12. Xu X, Bieda M, Jin VX, Rabinovich A, Oberley MJ, Green R, Farnham PJ (2007) A comprehensive ChIP-chip analysis of E2F1, E2F4, and E2F6 in normal and tumor cells reveals interchangeable roles of E2F family members. Genome Res 17(11):1550–1561
13. Fujiwara K, Yuwanita I, Hollern DP, Andrechek ER (2011) Prediction and genetic demonstration of a role for activator E2Fs in Myc-induced tumors. Cancer Res 71(5): 1924–1932

Chapter 25

Analyzing G1–S Transcriptional Control

Steffi Klier, Sarah Farmer, and Robertus A.M. de Bruin

Abstract

G1–S transcriptional control involves the coordination of the expression of a large set of co-regulated genes as a function of cell cycle progression (Bertoli et al., Nat Rev Mol Cell Biol 14:518–528, 2013). Confining transcription to the G1 phase of the cell cycle requires the regulation of specific transcription factor activity through either co-factors or regulation of promoter DNA binding. Therefore, the analysis of G1–S transcriptional control involves cell cycle synchronization and monitoring cell cycle synchrony, in order to establish DNA binding of G1–S transcription factors to G1–S promoters and to investigate changes in gene expression during the different phases of the cell cycle. Here, we describe a cell cycle synchrony method and ways to monitor synchrony. We also describe a chromatin immunoprecipitation (ChIP) method to locate G1–S transcription factor components to promoters and a quantitative PCR (qPCR) protocol to determine gene expression. Defining the binding dynamics of G1–S transcription factors and changes in gene expression during the cell cycle should provide new insights into the mechanism that control G1–S transcription and will allow for investigation of the biological relevance of confining gene expression to G1.

Key words G1–S transcription, DNA content, DNA–protein interaction, Cell cycle synchrony, Gene expression

1 Introduction

The primary regulation of cell proliferation in most eukaryotic cells is imposed during the G1–S transition of the cell cycle. Uncontrolled cell proliferation is an invariable characteristic of human cancer and is often associated with deregulated expression of G1–S cell cycle genes. Such deregulation, which is found in every type of cancer, allows cancer cells to sustain proliferation in the absence of growth factors and renders them insensitive to growth-inhibitory signals. Despite frequent lack of sequence homology, recent work has revealed that the basic molecular mechanisms involved are conserved from yeast to man [1]. This conservation of systems-level properties across eukaryotes is an emerging theme of cell cycle studies and suggests that particular network wiring is important for cell division control. Future work will provide a better understanding of

Eishi Noguchi and Mariana C. Gadaleta (eds.), *Cell Cycle Control: Mechanisms and Protocols*, Methods in Molecular Biology, vol. 1170, DOI 10.1007/978-1-4939-0888-2_25,

the role of the transcriptional networks during the G1 and S phases of the cell cycle, allowing for the investigation of the biological relevance of confining gene expression to G1.

For G1–S transcriptional analysis, both a high level of cell cycle synchrony in the culture and the ability to identify the stage of the cell cycle at any time point are very important. There are a number of methods for synchronizing budding yeast cultures (reviewed in ref. 2). Whilst elutriation is a very effective method for harvesting pure and, importantly, unperturbed cultures of G1 cells for study of the G1–S transition, gaining access to an elutriator may be a problem for many labs. In addition, with elutriation, it is difficult to obtain large volumes of synchronized budding yeast cells required for chromatin immunoprecipitation experiments at multiple time point. We therefore prefer to use a more accessible, routinely used method, which involves α-factor mating pheromone block and release, in order to synchronize cells in G1. This method is discussed in Subheading 3.1. To assess progression of the cell cycle during every experiment the analysis of DNA content by flow cytometry is a powerful and routine method for monitoring the population-wide progression of DNA replication in all cell types [3], and budding yeast is highly amenable to analysis in this way (*see* Subheading 3.2).

Establishing G1–S transcriptional control requires monitoring G1–S transcription factors binding to G1–S target promoters during the cell cycle. This will provide an insight into the mechanisms involved in G1–S transcriptional regulation. Chromatin Immunoprecipitation (ChIP) allows you to monitor Protein–DNA binding during the cell cycle. ChIP in budding yeast works very well with proteins fused to myc epitopes or TAP tag but works less well with proteins fused to HA tag (note that anti-HA probing of western blots of whole-cell extracts run on SDS-PAGE gels also reveals unspecific binding to untagged proteins). Although tagging yeast proteins is highly convenient (for example, using simple PCR-based methods [4], it is also possible to immunoprecipitate protein-bound chromatin using antibodies raised against the proteins themselves if the antibodies are sufficiently specific (ChIP-grade). Such protein-specific antibodies would be useful to investigate the chromatin binding of multiple proteins within the same culture [5]. In Subheading 3.3, we provide an example of ChIP analysis of the myc-tagged DNA-binding component of the G1–S transcriptional activator SBF, Swi4, during the cell cycle. Finally, cell cycle synchrony and transcription factor–promoter binding should be correlated to changes in gene expression. We describe expression analysis of G1–S transcripts using the gold standard quantitative PCR (qPCR) on cDNA generated by reverse transcriptase (RT) in Subheading 3.4.

2 Materials

2.1 Cell Cycle Synchronization of Budding Yeast Using Mating Pheromone

1. YPD (also YEPD, yeast extract, peptone, dextrose medium): 1 % yeast extract, 2 % peptone, 2 % glucose/dextrose.
2. 1.5-mL cuvettes.
3. Spectrophotometer.
4. 30 °C shaking incubator.
5. Light microscope.
6. Centrifuge (accommodating 50-mL tubes).
7. Microcentrifuge.
8. α-factor mating pheromone, yeast (GenScript).

2.2 Flow Cytometry for Monitoring S-Phase Entry in Budding Yeast

1. 99.9 % ethanol.
2. Saline sodium citrate buffer (SSC) pH 7: 150 mM NaCl, 15 mM sodium citrate (tribasic dihydrate).
3. RNase A.
4. Proteinase K.
5. SYTOX Green (Invitrogen).
6. Water bath sonicator.
7. FACS tubes.
8. Fluorescence activated cell sorter.

2.3 Chromatin Immunoprecipitation in Budding Yeast

1. 37 % formaldehyde solution.
2. 2.5 M glycine, filtered.
3. Tris-buffered saline (TBS).
4. 50-mL tubes.
5. 1.5-mL screw cap tubes.
6. Liquid nitrogen.
7. Centrifuge (accommodating 50-mL tubes).
8. Refrigerated microcentrifuge.
9. Lysis buffer A: 50 mM HEPES–KOH pH 7.5, 140 mM NaCl, 1 % Triton-X100, 0.1 % sodium-deoxycholate, 1 mM EDTA, complete mini protease inhibitor cocktail tablets (Roche Diagnostics).
10. Lysis buffer B: 50 mM HEPES–KOH pH 7.5, 500 mM NaCl, 1 % Triton-X100, 0.1 % sodium-deoxycholate, 1 mM EDTA.
11. Wash buffer: 10 mM Tris–HCl pH 8, 250 mM LiCl, 0.75 % NP-40, 0.75 % sodium deoxycholate, 1 mM EDTA.
12. TE: 1 M Tris–HCl pH 8, 0.5 M EDTA.

13. Elution buffer: 50 mM Tris–HCl pH 8, 10 mM EDTA, 1 % SDS.
14. 0.5-mm glass beads (Bio Spec Products).
15. Vortex mixer with microcentrifuge tube holders.
16. 25-Gauge needle.
17. Misonix Sonicator 3000.
18. Mouse IgG monoclonal anti-myc 9E10 antibody (Santa Cruz).
19. Protein A-Sepharose (lyophilized beads) from *Staphylococcus aureus* (Sigma Aldrich) (*see* **Note 1**).
20. 65 °C water bath shaker.
21. QIAquick PCR purification kit (Qiagen).
22. MESA Blue qPCR Mastermix (Eurogentec).
23. Oligonucleotide primer pairs for qPCR of the promoter regions of your transcripts of interest (*see* **Note 2**).
24. Real-time PCR thermal cycler.

2.4 Expression Analysis of G1–S Transcripts Using Reverse Transcriptase Quantitative PCR

1. Liquid nitrogen.
2. ß-Mercaptoethanol.
3. 0.5-mm glass beads (Bio Spec Products).
4. 25-Gauge needle.
5. Qiagen RNeasy PLUS kit (Qiagen).
6. RNase-free water.
7. NanoDrop spectrophotometer.
8. One Step MESA Green qRT-PCR Mastermix (Eurogentec).
9. Oligonucleotide primer pairs for qPCR of the open reading frames of your transcripts of interest and *ACT1* (*see* **Note 3**).
10. Real-time PCR thermal cycler.

3 Methods

3.1 Cell Cycle Synchronization of Budding Yeast Using Mating Pheromone

Here, we describe an α-factor mating pheromone block and release method to synchronize cells in G1 for routine experiments. It must be noted that only MATa strains can be arrested in this way. Furthermore, the method is much more effective in a *bar1*Δ background [6]. The *BAR1* gene encodes a protease, which cleaves and thus inactivates the α-factor mating pheromone. Wild-type (*BAR1*) strains can still be arrested by α-factor, but a higher concentration must be used, making the method less cost-effective, and the synchronization can also be less complete.

1. Inoculate 20 mL of YPD with your strain of interest and grow overnight at 30 °C in a shaking incubator. The next day, dilute the culture into the desired culture volume of YPD to OD_{600} ~0.1

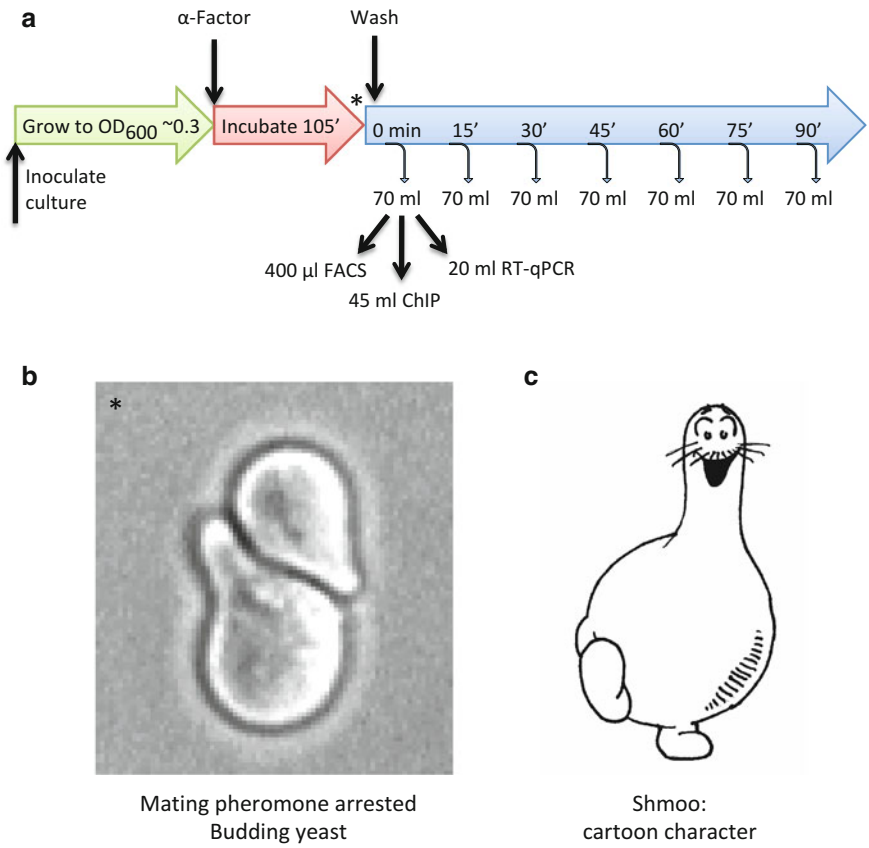

Fig. 1 Synchronization of budding yeast cells. (**a**) Overview of α-factor arrest and release time-course experiment. (**b**) Cells arrested in G1 with α-factor "shmoo-ing." Image was captured with a Hamamatsu Orca-ER camera attached to a Zeiss Axioskop microscope using a 40× objective. (**c**) The "shmoo" cartoon character. Image is inspired by the 1948 cartoon character originally created by Al Capp

and further incubate for 2–3 h until OD_{600} reaches 0.2–0.4 (*see* **Note 4** and Fig. 1a).

2. Add α-factor mating pheromone to each culture to a final concentration of 50 µM and incubate at 30 °C in a shaking incubator for 1 h 45 min to arrest the cells in G1. The efficiency of the arrest can be monitored by light microscope (*see* **Note 5**). >99 % of the cells should be without a bud and look like a so-called "shmoo" (*see* Fig. 1b, c). Take a G1 sample (0 min time point) at this point as described in the next step.
3. Centrifuge the G1-arrested cells at 3,700×*g* for 1–2 min and rapidly wash the cells with 50 mL of YPD by resuspending and re-centrifuging (*see* **Note 6**). Finally resuspend the culture into the original volume of YPD pre-warmed to 30 °C. Incubate at 30 °C in a shaking incubator. At appropriate time points (*see* **Note 7**) take 70 mL samples and rapidly process for flow cytometry, chromatin immunoprecipitation, and expression analysis in the manner outlined in Subheadings 3.2–3.4 (*see* Fig. 1a).

3.2 Flow Cytometry for Monitoring S-Phase Entry in Budding Yeast

Monitoring the cell cycle by flow cytometry can only be achieved retrospectively, however, we also find it useful to track the progression of a culture through the cell cycle (and therefore verify that the block and release has been efficient) during the time-course itself by determining the budding index at each time point. In this section, we show examples of budding index analysis, along with the flow cytometry analysis (*see* Fig. 2).

1. Add 400 μL of culture to 1.2 mL of cold 100 % ethanol and vortex cells to fix. The fixed cells can then be stored at 4 °C for at least several weeks (*see* **Note 8**).
2. Centrifuge for 2 min at 1,500 × *g* and resuspend cells in 1 mL SSC.

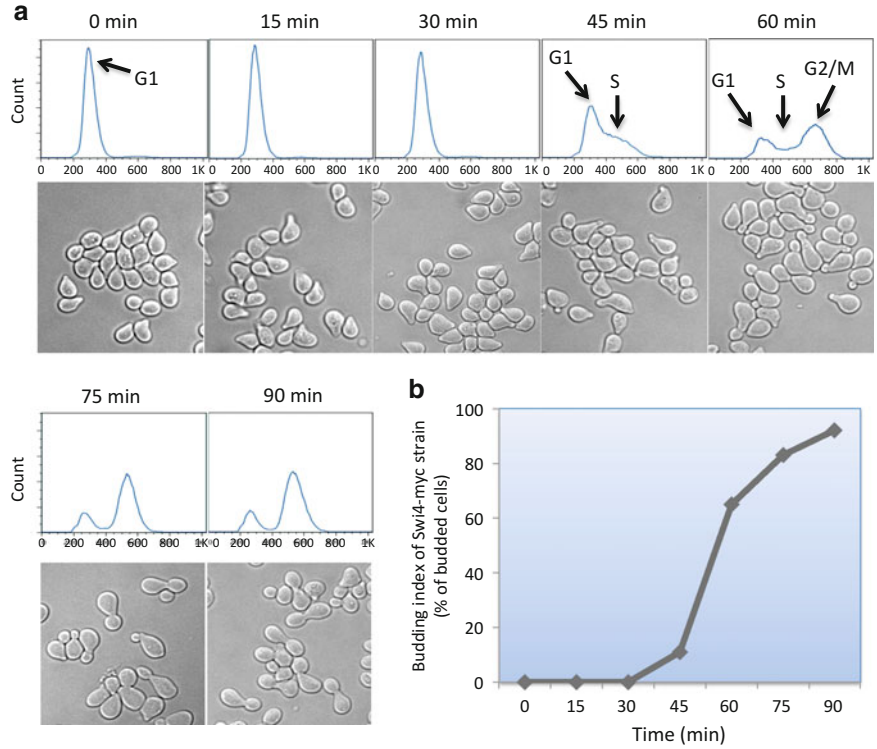

Fig. 2 Monitoring progression of the cell cycle in a *SWI4*-6xMyc culture synchronized by α-factor block and release. Minutes after removal of α-factor from the culture are indicated. (**a**) Analysis of DNA content by flow cytometry shows that bulk DNA replication can be observed 45 min after release from α-factor arrest when the arbitrary DNA amount (*Phycoerythrin* (*PE*) fluorescence, *X* axis) begins to increase from the 1 N peak (corresponding to G1) at ~300. A 2 N peak (corresponding to G2/M) at ~600 is visible after 60 min. From this point, G2 nuclei start dividing and thus 1 N peak reappear. It is important to note that the firing of origins and start of DNA replication (G1–S transition) occurs prior to the observation of bulk DNA replication at 45 min. Images of cells were also photographed when flow cytometry samples were collected, and budding index was measured. (**b**) Monitoring the budding index (% budded cells) of the culture is also an excellent way of tracking cell cycle in real time; the appearance of budded cells correlates with bulk DNA replication

3. Centrifuge for 2 min at 1,500 × *g* and resuspend cells in 250 μL SSC containing 0.2 mg/mL RNase A and incubate overnight at 50 °C.
4. Add 50 μL SSC containing 6 mg/mL proteinase K (for final concentration of 1 mg/mL) and incubate at 50 °C for 1 h.
5. Add 500 μL SSC containing 0.64 μM SYTOX Green (for final concentration of 0.4 μM) and incubate at 4 °C in the dark for at least 1 h (*see* **Note 9**).
6. Briefly sonicate the samples in a water bath sonicator (*see* **Note 10**) and transfer to FACS tubes.
7. Analyze each sample in a fluorescence activate cell sorter. SYTOX Green has a maximum excitation of 504 nm and a maximum emission of 523 nm. Therefore, a possible laser–collection filter combination can be a 488 nm excitation laser and a 510–545 nm filter.

3.3 Chromatin Immunoprecipitation in Budding Yeast

ChIP analysis allows for monitoring the binding dynamics of G1–S transcription factors to G1–S promoters during the cell cycle. An example of ChIP assays of the Swi4 protein at the *CLN2* promoter is shown in Fig. 3.

1. To 45 mL of culture, add 1.25 mL of 37 % formaldehyde solution (1 % final concentration) (*see* **Note 11**) to fix the cells and cross-link proteins onto DNA. Incubate for 20 min at room temperature on a rotation platform (*see* **Note 12**).

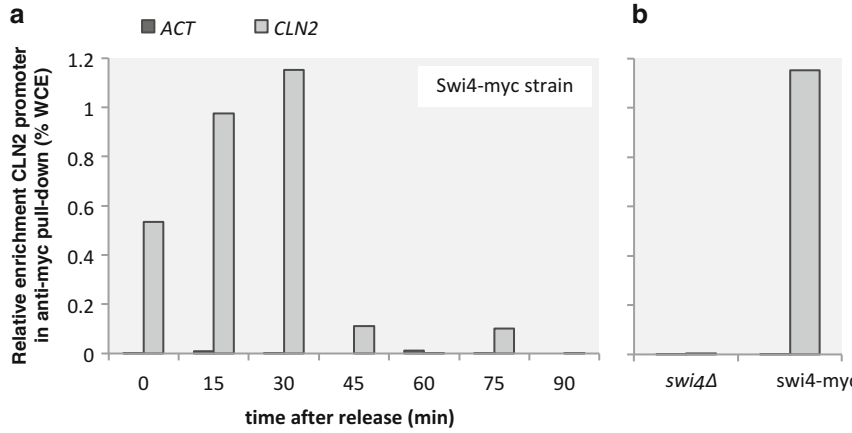

Fig. 3 ChIP assay of the Swi4 proteins at the *CLN2* promoter. (**a**) Cells were synchronized by α-factor and released into the cell cycle. Binding of Swi4 to the *CLN2* promoter was assessed by ChIP at 15-min intervals. Data show that Swi4 is bound to the *CLN2* promoter during early G1 and continue to be bound until the start of S phase when cells start to bud at 45 min. (**b**) ChIP analysis carried out on control *swi4*Δ and myc-tagged Swi4 cell lysates using anti-myc antibodies reveal the over background enrichment of the *CLN2* promoter in Swi4-myc pull-downs. Enrichment levels of pulled-down DNA were measured by qPCR and normalized to WCE signals (percentage of WCE). *ACT1* signals represent nonspecific background in each sample

2. Add 2.3 mL of 2.5 M glycine (0.125 M final concentration) and incubate for 5 min at room temperature on a rotation platform to stop the cross-linking.
3. Wash cells twice with 50 mL of ice-cold TBS.
4. Resuspend cells in 1 mL of ice-cold TBS and transfer to a microcentrifuge tube, centrifuge for 1 min at 20,000 × *g*, remove the supernatant, and snap-freeze the pellet in liquid nitrogen.
5. Store samples at –80 °C.
6. Resuspend the pellet in 500 µL of ice-cold lysis buffer A (*see* **Note 13**).
7. Add ~500 µL of 0.5 mm glass beads.
8. Vortex at maximum speed at 4 °C for 30 min (*see* **Note 14**).
9. Pierce the bottom of the tube and place over another 1.5-mL microcentrifuge tube (*see* **Note 15**). Centrifuge for a few seconds no higher than 1,200 × *g* to collect the sample in the lower tube and discard the upper tube (*see* **Note 16**).
10. Centrifuge the lysed cells for 15 min at 20,000 × *g* at 4 °C and discard the supernatant.
11. Resuspend the pellet (chromatin fraction) in 500 µL of ice-cold lysis buffer A (*see* **Note 17**).
12. Sonicate the samples at 4 °C in a Cup Horn Sonicator Misonix 3000: 30 s ON time, 2 min OFF time, output level 10, 5 min total ON time (*see* **Note 18**).
13. Centrifuge for 15 min at 20,000 × *g* at 4 °C. Transfer the supernatant to a clean 1.5-mL microcentrifuge tube.
14. Repeat **step 13** then add lysis buffer A to increase the sample volume to 505 µL (*see* **Note 19**).
15. Transfer 5 µL of each sample to a screw cap tube for whole-cell extract (WCE) referencing and store at –20 °C (*see* **Note 20**).
16. Add the appropriate antibody to the remaining 500 µL supernatant to immunoprecipitate (*see* **Note 21**).
17. Incubate overnight on a rotation platform at 4 °C.
18. Add 50 µL of ice-cold 50 % suspension of Protein A-Sepharose (*see* **Note 1**). Incubate for 3–4 h on a rotation platform at 4 °C.
19. Centrifuge at 4 °C for 1 min at 900 × *g* to collect the beads (*see* **Note 22**). Discard supernatant and wash beads with the following buffers, each for 15 min on a rotation platform at 4 °C, collecting the beads by centrifugation at 4 °C for 1 min at 900 × *g*:
    (a) 2 × 1 mL lysis buffer A (without protease inhibitors).
    (b) 2 × 1 mL lysis buffer B.

(c) 2 × 1 mL wash buffer.

(d) 1 × 1 mL TE.

20. After the last wash, remove supernatant completely and add 100 μL of elution buffer to each sample (*see* **Note 23**).
21. Incubate the samples for 30 min at 65 °C to reverse the cross-linking.
22. Centrifuge samples for 1 min at 20,000 × *g* and transfer 90 μL of supernatant to a new tube.
23. Add 95 μL of elution buffer to the WCE samples (*see* **step 15** above) and incubate all samples in the water bath shaker overnight at 65 °C.
24. Add 500 μL of PB buffer (supplied in the QIAquick PCR Purification kit) to each sample and load onto a QIAquick column.
25. Wash column-bound DNA with 750 μL of PE buffer (supplied in the kit) according to manufacturer's instructions.
26. Elute DNA with 100 μL of EB buffer (supplied in the kit) by centrifuging for 1 min at 20,000 × *g* to collect the immunoprecipitate (IP) (*see* **Note 24**).
27. Run real-time intercalating dye qPCR reactions (*see* **Note 25**) in triplicate for the WCE and IP samples using oligonucleotide primers to the promoter regions of your transcripts of interest.
28. Analyze qPCR data to calculate the percentage of chromatin-immunoprecipitated DNA (promoter region) over the total DNA in WCE (*see* **Note 26**).

3.4 Expression Analysis of G1–S Transcripts Using Reverse Transcriptase Quantitative PCR

To establish accurate expression levels, quantitative PCR (qPCR) on cDNA generated by reverse transcriptase (RT) is the gold standard. To minimize the experimental error, we recommend using Qiagen gDNA RNeasy columns for RNA isolation and one-step RT-qPCR reactions.

1. Centrifuge 20 mL culture for 2 min at 3,700 × *g* (*see* **Note 11**). Remove the supernatant, and resuspend the cell pellet in 1 mL of water and transfer to a clean 1.5-mL microcentrifuge tube. Centrifuge briefly at 20,000 × *g*, discard the supernatant, snap-freeze the cell pellet in liquid nitrogen, and store at −80 °C indefinitely (*see* **Note 27**).
2. Thaw the cell pellet on ice and resuspend in 500 μL of Qiagen RNeasy PLUS RLT buffer with freshly added 1 % ß-mercaptoethanol (*see* **Note 28**).
3. Add ~500 μL of 0.5-mm glass beads.
4. Vortex at maximum speed at 4 °C for 30 min (*see* **Note 14**).

5. Pierce the bottom of the tube and place over another 1.5-mL microcentrifuge tube (*see* **Note 15**). Centrifuge for a few seconds no higher than 1,200 × *g* to collect the sample in the lower tube and discard the upper tube containing the glass beads (*see* **Note 16**).
6. Spin for 2 min at 20,000 × *g*.
7. Add 350 μL of the supernatant to a Qiagen gDNA RNeasy column and follow the Qiagen RNeasy instructions until the elution step.
8. Transfer the RNeasy column into a new collection tube and elute the RNA by adding 100 μL RNase-free water to the column and centrifuging for 1 min at 20,000 × *g*.
9. Measure the RNA concentration (for example using a NanoDrop spectrophotometer) and adjust the RNA concentration to 20 ng/μL (*see* **Note 29**).
10. Run reverse transcription real-time intercalating dye qPCR reactions (*see* **Note 30**) in triplicate using primers for the open reading frames of your transcripts of interest and *ACT1* (*see* **Note 3**).
11. Analyze qRT-PCR data to calculate the levels of the transcripts of interest normalized to the actin transcript levels (*see* **Note 31**) (*see* Fig. 4).

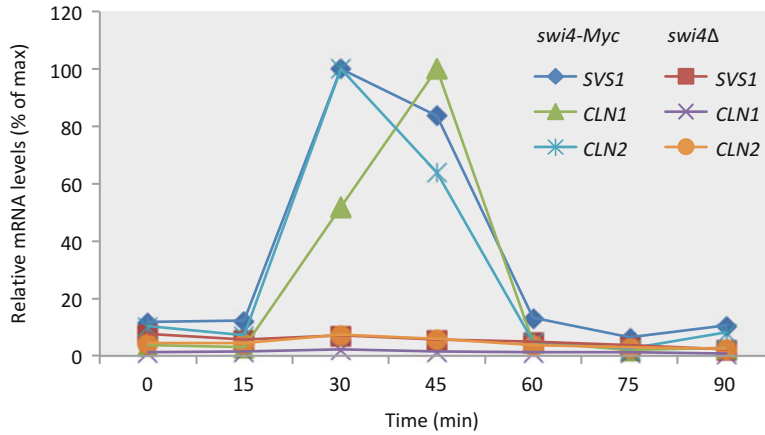

Fig. 4 Expression of G1–S genes. *swi4*Δ (control) and *swi4-Myc* cells were synchronized by α-factor, released into the cell cycle, and collected at 15-min intervals. Relative mRNA levels of *CLN1*, *CLN2,* and *SVS1* were determined by qPCR and normalized against *ACT1.* Expression levels are plotted as percentage of highest value detected in the experiment (100 %). After the release from α-factor arrest, relative mRNA levels of all tested genes peak at around 30–45 min when cells start entering S phase

4 Notes

1. Beads are hydrated in lysis buffer A (without protease inhibitors) for 20 min and then washed four times.
2. Promoter regions, when not identified in the literature, can be assumed to be contained within the 500 bp immediately upstream of the ATG. Additionally, chromatin is sheared into fragments larger than 500 bp. Therefore, the levels of immunoprecipitated promoters are accurately reflected by quantifying amplicons in this region (*see* **Note 3** for primer design).
3. Amplicons for qPCR should be <200 bp, preferably ~150 bp, and short (~20 bp) oligonucleotide primers flanking such regions should be identified according to the usual parameters for PCR primers. There are numerous free online tools to assist with this.
4. The purpose of this growth scheme is to obtain a mid-log phase culture; it is not just the OD_{600} that is important, but also that the culture has reached that density by growing in a good supply of nutrients for at least one cell division. Yeast should preferably be cultured in conical flasks of five times the volume of the culture for proper aeration.
5. Check with a light microscope whether shmoos have formed. These cellular bulges are a response to the mating pheromone and indicative of cell cycle arrest (*see* Fig. 1b, c).
6. The wash can be done with medium at room temperature. The time-course timer should be started at the moment the wash is started and the α-factor mating pheromone removed.
7. We take samples every 15 min to follow the cell cycle in our example described in Fig. 1a. However, once the normal cell cycle progression for your strain and conditions have been established, it may be more economical to use standard time points such as 0 min for G1 and 30 min for the beginning of S phase.
8. Some medium preparations can cause the precipitated cells to stick together during storage, but discoloration or clumping of the cells is remedied upon rehydration in SSC buffer in the following step.
9. Propidium iodide can be used instead of SYTOX Green (at 5 μg/mL for a final concentration of ~3 μg/mL) but it has been reported that SYTOX Green is preferable in several respects, including fluorescence correlation to DNA [7]. At this point, the stained cells can be stored for up to a month at 4 °C in the dark.
10. This is to disrupt cell clumps and may not always be necessary. A probe sonicator can also be used; however, SYTOX Green is toxic and precautions should be taken for its aerolization.

11. Due to different treatments and growth phenotypes, the amount of cells collected may vary a little. Slightly different amounts of starting material (and any resultant small differences in cell lysis efficiency) are not important since the end result is normalized to internal controls.
12. It has been reported that fixation times can vary depending on the protein but we have found 20 min to be adequate for the G1–S transcription factors we have studied.
13. Protease inhibitor cocktail tablets are dissolved in lysis buffer A fresh on the day.
14. This step can be accelerated by using screw-cap tubes in a FastPrep machine at 4 °C at speed 4.5 for 30 s four times with 3 min-rest between cycles, although this method also increases heating of samples.
15. This is most easily achieved by heating a 25-Gauge needle in a flame until red-hot and quickly pricking the bottom of the tube. Invert the tube and knock on the bench first to deposit the sample and beads to the lid-end of the tube.
16. Standard microcentrifuges allow this method if you do not add the lid.
17. Passing the liquid through a 25-Gauge needle three times makes it easier to resuspend the pellet. The importance of this step is to refresh the supply of protease inhibitors.
18. In these conditions DNA is sheared into 500–1,500 bp fragments. This may vary with different sonicators and should be optimized by individual laboratories.
19. This is most easily achieved by setting a pipette to 505 μL and aspirating the whole volume of WCE in a controlled fashion then completing the aspiration by moving the pipette tip to a small aliquot of lysis buffer A (which should then be discarded to avoid cross-contamination).
20. The 5 μL of WCE should be frozen at this point to be used at a later stage.
21. The amount of antibody added should be optimized for each antibody, but we have achieved good results using 3 μL anti-myc 9E10 mouse monoclonal IgG (Santa Cruz) for immunoprecipitation of myc-tagged proteins.
22. Wash supernatants should be removed leaving the bead pellet just covered with minimal buffer.
23. After the TE wash, the supernatant can be removed completely by using a gel-loading tip or syringe pushed into the bottom of the tube. Elution buffer should be added immediately to prevent bead dehydration.

24. This eluate can be further diluted, if many chromatin locations are to be analyzed.
25. We obtain consistent results with 10–20 μL reactions using MESA Blue qPCR Mastermix (Eurogentec) and 0.5 μM primers.
26. Convert mean triplicate ΔCT value to % of WCE by subtracting the mean triplicate ΔCT value of the corresponding WCE sample (1 %) using the formula: $\%\ \mathrm{WCE} = 0.5^{(\Delta\mathrm{CT\ ChIP}-\Delta\mathrm{CT\ WCE})} \times 1.1$. Note that the starting material WCE (5 μL) is only 1 % of the starting material IP sample (500 μL) while recovering only 90 % of the IP (*see* Subheading 3.3, **steps 15**, **16** and **22**).
27. Snap-freezing is important to prevent stress-induced transcription that can initiate very rapidly when the temperature of cells drops less quickly [8].
28. For RNA techniques, elimination of RNases from all steps is important; however we do not take any particular precautions above wearing gloves and other standard good laboratory practices (i.e., we do not use filter tips or "clean" hoods). We do not experience problems with sample degradation with our protocol.
29. RNA samples can be stored at −20 °C indefinitely.
30. We obtain consistent results with 10–20 μL reactions using One Step MESA Green qRT-PCR Mastermix (Eurogentec) and 0.5 μM primers.
31. To obtain relative gene expression first calculate the mean of triplicate ΔCT values and normalize value by subtracting the mean of triplicate ΔCT of a non cell cycle regulated control gene (generally actin) using the formula: Normalized ΔCT value = ΔCT gene of interest − ΔCT non cell cycle regulated control. To obtain relative gene expression as fold over arrested cells ($t = 0$) use the formula: Relative expression level over arrested cells $= 2^{(\text{normalized } \Delta\text{CT gene of interest at } t=0 - \text{normalized } \Delta\text{CT gene of interest at } t=x)}$. Alternatively, to obtain gene expression levels as a % of maximum (100 %) use the formula: Relative expression level over maximum $= 2^{(\text{normalized } \Delta\text{CT gene of interest with lowest } \Delta\text{CT} - \text{normalized } \Delta\text{CT gene of interest at } t=x)} \times 100$.

Acknowledgements

We are grateful to the de Bruin group for support and help. This work was supported by the MRC career development fellowship awarded to R.d.B. (G0800297).

References

1. Bertoli C, Skotheim JM, de Bruin RA (2013) Control of cell cycle transcription during G1 and S phases. Nat Rev Mol Cell Biol 14(8): 518–528
2. Manukyan A, Abraham L, Dungrawala H, Schneider BL (2011) Synchronization of yeast. Methods Mol Biol 761:173–200
3. DePamphilis ML, Bell SD (2011) Genome duplication: concepts, mechanism, evolution and disease, vol 1. Garland Science, Taylor and Francis Group, LLC. HEA Guide to Publications in the Physical Sciences 22(12):27
4. Longtine MS, McKenzie A 3rd, Demarini DJ, Shah NG, Wach A, Brachat A, Philippsen P, Pringle JR (1998) Additional modules for versatile and economical PCR-based gene deletion and modification in *Saccharomyces cerevisiae*. Yeast 14(10):953–961
5. Harris MR, Lee D, Farmer S, Lowndes NF, de Bruin RA (2013) Binding specificity of the G1/S transcriptional regulators in budding yeast. PLoS One 8(4):e61059
6. Chan RK, Otte CA (1982) Isolation and genetic analysis of *Saccharomyces cerevisiae* mutants supersensitive to G1 arrest by a factor and alpha factor pheromones. Mol Cell Biol 2(1): 11–20
7. Haase SB, Reed SI (2002) Improved flow cytometric analysis of the budding yeast cell cycle. Cell Cycle 1(2):132–136
8. Robert F, Pokholok DK, Hannett NM, Rinaldi NJ, Chandy M, Rolfe A, Workman JL, Gifford DK, Young RA (2004) Global position and recruitment of HATs and HDACs in the yeast genome. Mol Cell 16(2):199–209

Chapter 26

Analysis of Replication Timing Using Synchronized Budding Yeast Cultures

Jie Peng, M.K. Raghuraman, and Wenyi Feng

Abstract

Eukaryotic DNA replication exhibits at once extraordinary fidelity and substantial plasticity. The importance of the apparent presence of a replication temporal program on a population level has been the subject of intense debate of late. Such debate has been, to a great extent, facilitated by methods that permit the description and analysis of replication dynamics in various model organisms, both globally and at a single-molecule level. Each of these methods provides a unique view of the replication process, and also presents challenges and questions in the interpretation of experimental observations. Thus, wider applications of these methods in different genetic backgrounds and in different organisms would doubtless enable us to better understand the execution and regulation of chromosomal DNA synthesis as well as its impact on genome maintenance.

Key words Replication timing, Temporal program, Origins of replication, Density transfer, CsCl gradient, Microarray

1 Introduction

Eukaryotic chromosomal DNA replication, on a cell-population level, follows a temporal order, i.e., certain regions of the chromosome replicate before others during S phase of the cell cycle [1]. Because such a temporal order is readily observed from yeast to humans [2, 3], it is inferred that a well-executed temporal program of replication is crucial for the fidelity of chromosome maintenance and partition. Indeed, altered replication timing has been linked to increased genome instability in yeast [4–6] and, in metazoans, to transcription [7, 8], cell differentiation [4, 9–12], and cancer formation [13–15]. Thus, it is of great importance to understand how the replication temporal program is executed and regulated. The execution of this replication temporal program involves the coordination of hundreds to thousands of origins of replication in the genome, the sites where replication initiates [16, 17]. Therefore, the replication temporal program is a complex result of the many variables associated

Eishi Noguchi and Mariana C. Gadaleta (eds.), *Cell Cycle Control: Mechanisms and Protocols*, Methods in Molecular Biology, vol. 1170, DOI 10.1007/978-1-4939-0888-2_26,

with each origin location, efficiency of initiation, and the contentious intrinsic timing of initiation [18–20]. Naturally, in order to understand its function and regulation it is important to observe and describe the replication temporal program in experimental systems.

Genome-wide analyses of replication timing have been described in various eukaryotes from yeast to humans [21]. Here, we focus on a modified approach of the classic Meselson/Stahl density transfer coupled with microarray. This technique is based on the separation of replicated from unreplicated DNA in a density gradient and their subsequent labeling and co-hybridization on a microarray, in order to study replication timing of synchronized budding yeast cells (Fig. 1). Variations of this method have previously

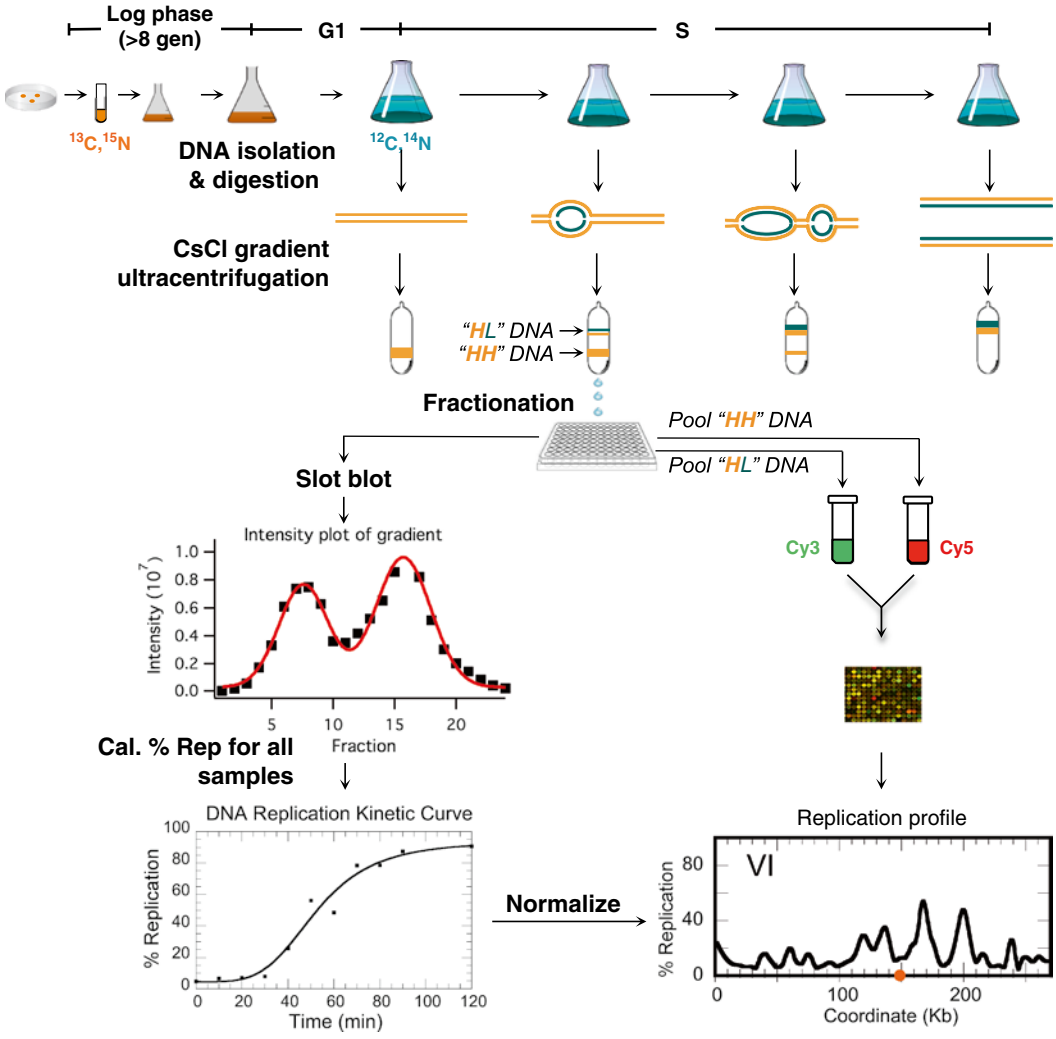

Fig. 1 Overview of procedures for density transfer coupled with microarray. Sample graphs for slot-blot, replication kinetics, and Chromosome VI replication profile are all derived from a W303 culture at 25 °C. The *dot* on the *x*-axis of the replication profile denotes the centromere. *% Rep* % replication

been applied in diverse genetic backgrounds to describe a variety of replication timing-associated phenotypes [4, 5, 19, 22–24]. Labeling DNA with dense-isotope-substituted nitrogen and carbon sources is deemed relatively less disruptive than labeling with nucleotide analogs such as BrdU [25], although not as benign as simply measuring the increase in copy number as different segments of the genome are replicated. On the other hand, the density transfer method may offer higher sensitivity and resolution than monitoring DNA copy number changes [26]. Thus, the density transfer method permits global analysis of replication timing in yeast strains of virtually any genetic background, though with greater ease in strains that are: (1) prototrophic for uridine and adenine synthesis, as mutations in these biosynthesis pathways lead to inefficient uptake of the substituted isotopes in genomic DNA, and (2) of the mating type *a* so as to facilitate cell cycle synchronization via the mating pheromone α-factor.

2 Materials

All solutions are autoclaved or filter sterilized unless otherwise noted.

2.1 Cell Culture Sample Collection

1. AGD H_2O (autoclaved glass-distilled H_2O). Prepare all solutions in AGD H_2O unless otherwise noted.
2. "-N" Medium: 1.61 g/L YNB (Yeast nitrogen base) without $(NH_4)_2SO_4$ and without amino acids, 94 mM succinic acid, 167 mM NaOH.
3. Dense Medium: 0.1 % D-Glucose-$^{13}C_6$ (Sigma) and 0.01 % Ammonium-$^{15}N_2$ sulfate (Sigma) in "-N" Medium (*see* **Note 1**). Supplement with required amino acids.
4. "Y complete" Medium, pH 5.8: 14.5 g/L YNB without $(NH_4)_2SO_4$ and without amino acids, 10 g/L succinic acid, 6 g/L NaOH, 5 g/L $(NH_4)_2SO_4$, 20 g/L glucose, 76.7 mg/L adenine, 76.7 mg/L histidine, 76.7 mg/L methionine, 76.7 mg/L uracil, 76.7 mg/L arginine, 191.8 mg/L phenylalanine, 230.1 mg/L lysine, 230.1 mg/L tyrosine, 306.8 mg/L tryptophan, 306.8 mg/L leucine, 306.8 mg/L isoleucine, 383.6 mg/L glutamic acid, 383.6 mg/L aspartic acid, 575.3 mg/L valine, 767.1 mg/L threonine, 1534.2 mg/L serine (*see* **Note 2**).
5. α-factor (peptide sequence: NH_2–WHWLQLKPGQPMY–COOH, custom synthesized by ThermoFisher at >70 % purity): Prepare as 200 μM or 3 mM stocks (1,000× stocks) for *bar1* and *BAR1* strains, respectively. Store at –80 °C.
6. Bioruptor Standard Model (Diagenode).

7. 500-mL centrifuge bottles.
8. Centrifuge with JA-10 and JA-17 rotors.
9. Pronase.
10. 10 % NaN_3.
11. 0.2 M EDTA pH 8.0.
12. Frozen (−20 °C) EDTA/NaN_3 Mix: 0.1 % NaN_3, 0.2 M EDTA pH 8.0 (*see* **Note 3**).
13. Nalgene 50-mL Oak Ridge high-speed centrifuge tubes.
14. 500-mL screw-cap centrifuge bottles.
15. Cold 100 % ethanol, stored at −20 °C.

2.2 Flow Cytometry

1. Cold AGD H_2O, stored at 4 °C.
2. 50 mM sodium citrate pH 7.4.
3. 1 mg/mL RNase A, stored at −20 °C.
4. 20 mg/mL proteinase K: 50 % Glycerol, 10 mM Tris–HCl pH 7.5, 19.73 μM $CaCl_2$, 20 mg/mL Proteinase K, stored at −20 °C.
5. 1 μM SYTOX Green in 50 mM sodium citrate, prepared fresh.
6. Bioruptor Standard Model (Diagenode).
7. BD flow cytometry tubes (Becton Dickinson): 5-mL polystyrene round-bottom tubes for flow cytometric acquisition.
8. BD LSRFortessa flow cytometry analyzer (Becton Dickinson).
9. FlowJo software (Tree Star, Inc.) for data analysis.
10. Microscope slides and cover glasses.

2.3 Genomic DNA Isolation, EcoRI Restriction Digestion, and Southern Hybridization

1. Glass beads, acid washed 425–600 μm (Sigma-Aldrich), autoclaved.
2. 25:24:1 phenol:chloroform:isoamyl alcohol, stored at 4 °C.
3. Lysis buffer: 10 mM Tris–HCl pH 8.0, 1 mM EDTA pH 8.0, 100 mM NaCl, 1 % SDS, 2 % Triton X-100.
4. 100 % ethanol, stored at room temperature.
5. Cold 70 % ethanol, stored at −20 °C.
6. $TE_{0.1}$: 10 mM Tris–HCl, 0.1 mM EDTA pH 8.0.
7. 1 mg/mL RNase A, stored at −20 °C.
8. 1 M Tris–HCl, pH 7.5.
9. 5 M NaCl.
10. 100 mM $MgCl_2$.
11. 1 % Triton X-100.
12. *EcoR*I.
13. 10× TBE: 850 mM Tris–Base, 890 mM boric acid, 30 mM EDTA pH 8.3.

14. 1× TBE: dilute from 10× TBE.
15. 0.8 % agarose gel: 8 g/L agarose and 0.3 μg/mL ethidium bromide in 1× TBE.
16. Electrophoresis buffer: 1× TBE, 0.3 μg/mL ethidium bromide.
17. Materials for standard Southern analysis.

2.4 CsCl Gradient Preparation by Ultracentrifugation, Fractionation, Slot-Blot Analysis, and Replication Kinetic Data Processing

1. $T_{10}E_{100}$ pH 7.5: 10 mM Tris–HCl, 100 mM EDTA, 75 mM NaOH, filter-sterilized (*see* **Note 4**).
2. CsCl solution: Weigh $T_{10}E_{100}$ pH 7.5 and CsCl powder at a ratio of 1:1.292 and dissolve the CsCl in $T_{10}E_{100}$ (*see* **Note 5**). Prepare fresh.
3. Refractometer (Zeiss or Bausch & Lomb).
4. 13×51 mm or 16×45 mm Quick-seal tubes (Beckman Z11207SCA or Z00729SCA), (*see* Subheadings 3.4.1 and 3.4.2).
5. Pasteur pipette.
6. Quick-Seal sealer (Beckman 358312).
7. Beckman VTi 65.2 or Ti 70.1 rotor.
8. Ultracentrifuge.
9. 96-well plates.
10. 1 M NaOH, stored in polypropylene containers at 4 °C.
11. Template Sealing Foil (Fisher Scientific).
12. 20× SCP: 600 mM Na_2HPO_4, 20 mM EDTA pH 8.0, 2 M NaCl pH 6.8.
13. 10× SCP: dilute from 20× SCP with AGD H_2O.
14. Multichannel pipette.
15. Minifold II Slot-Blot system (Schleicher & Schuell).
16. Whatman 3MM blotting paper (Whatman) for the Minifold II Slot-Blot system.
17. Genescreen™ Hybridization Transfer Membrane (Perkin Elmer), cut to the same size as the Whatman paper.
18. UV crosslinker (e.g., UVP HL-2000 HybriLinker™).
19. Radioisotope imaging and quantification system (e.g., Typhoon phosphorimager and storage phosphor screen).
20. IgorPro 6.3 software (WaveMetrics) or equivalent for data deconvolution.
21. Kaleidagraph 4.1 software (Synergy) or equivalent for replication kinetics curve fitting.

2.5 DNA Labeling and Microarray Hybridization

1. Cold 70 % ethanol, stored at −20 °C.
2. TE: 10 mM Tris–HCl, 1 mM EDTA pH 8.0.
3. 2.5× labeling reaction buffer: 125 mM Tris–HCl pH 6.8, 12.5 mM $MgCl_2$, 25 mM β-mercaptoethanol, 750 μg/mL random hexamers, stored at −20 °C.

4. 10× dNTP mix: 1.2 mM dATP, 1.2 mM dCTP, 1.2 mM dGTP, 0.6 mM dTTP, 10 mM Tris–HCl pH 8.0, stored at −20 °C.
5. 1 mM Cy5- and Cy3-dUTP (GE Healthcare).
6. 50,000 units/mL Klenow Fragment (3′–5′ exo-) (NEB).
7. QIAquick PCR Purification Kit (Qiagen).
8. Nanodrop ND-2000 spectrophotometer (Thermo Scientific).
9. Agilent 4×44K ChIP to chip yeast microarrays.
10. Feature Extraction software (Agilent).
11. Microarray hybridization and scanning facility.

2.6 Generation of Replication Profiles

1. A file containing a list of genomic coordinates (chromosome number and coordinate) for the microarray probes that will be used in the analysis (e.g., excluding probes corresponding to mitochondrial DNA). For convenience, we shall call this file "ProbeCoordinates.txt". The list should be sorted by ProbeID (ascending order), one line per probe, and saved preferably as a tab-delimited text file. Sorting by ProbeID should result in the list also being sorted by chromosome number and coordinate. To allow easy computer processing, chromosome numbers should be in Arabic numerals even though the convention for budding yeast is to use Roman numerals for chromosome numbers. This file needs to be prepared only once for each particular microarray platform, and can subsequently be used for all experiments using that platform. Typically, we prepare this list by performing a batch BLAST search of the yeast genome using the vendor-provided list of probe sequences, discarding all sequences that show either more than one match to the genome or less than a perfect match. From the BLAST results, we extract the chromosome number and coordinate for the left end of the probe. The first row of the file should have column headers. The columns for chromosome number, coordinate (kb), and coordinate (bp) should be labeled "Chr", "Coord_kb", and "Coord_bp" (without the quotes) to match the file manipulations in Subheading 3.6, **step 16**.
2. A file containing a list of probes to exclude from the final analysis (e.g., probes corresponding to Ty element sequences), formatted as above. Again, this file needs to be prepared only once for each microarray platform.
3. The statistical software package R, available online at <http://cran.r-project.org/>.
4. The following set of commands saved as a plaintext file to be run in R (*see* Subheading 3.6, **step 16**); name the file (for example) "rep_smoothing.R" (*see* **Note 6**):

```
# R script for loess smoothing of density transfer data
files <- list.files(path = "path_to_%replication_files", full.names =
    TRUE)
for(i in seq(along=files)) {
dataIn <- read.delim(files[i])
attach(dataIn)
rep.loess <- loess(Percent_rep ~ Coord_kb, dataIn, span =
    winSize/tail(Coord_kb, n=1))
rep.predict <- predict(rep.loess, Coord_kb)
dataOut <- data.frame(Chr, Coord_kb, Coord_bp, HLraw,
    HHraw, Percent_rep, Percent_rep_loess=rep.predict)
write.table(dataOut, files[i], quote=FALSE, sep="\t", eol="\r",
    row.names = FALSE)
detach(dataIn)
}
```

3 Methods

3.1 Sample Collection (Day 1)

1. Grow yeast cells in Dense Medium at 25 °C for at least eight generations. For kinetic measurements with slot-blot analysis only, each sample requires 20 mL of culture; samples for microarray analysis require >200 mL of culture (*see* **Note 7**).
2. Add α-factor to the log phase culture (at $OD_{660} = 0.25$) to a final concentration of 200 nM or 3 μM for *bar1* or *BAR1* strains, respectively.
3. Continue growing the cells until the percentage of unbudded cells reaches ≥90 % (*see* **Note 8**).
4. Transfer the cells into sterile 500-mL centrifuge bottles and centrifuge in a JA-10 rotor at 1,600 × *g* for 10 min at 25 °C to collect cell pellets (*see* **Note 9**).
5. Wash the cell pellets with appropriate volumes of "Y-complete" Medium containing 200 nM or 3 μM of α-factor for *bar1* or *BAR1* strains, respectively, and centrifuge again for 10 min.
6. Resuspend the cell pellets with "Y-complete" Medium with 200 nM or 3 μM of α-factor for *bar1* or *BAR1* strains, respectively, at a similar volume as that of the cell culture before centrifugation in **step 4**; continue culturing for another 30 min at 25 °C.
7. Add pronase to the culture at 0.02 mg/mL or 0.3 mg/mL for *bar1* or *BAR1* strains, respectively, to release cells from α-factor arrest (*see* **Note 10**).
8. Harvest cell samples at a series of time points: pour 20 mL or 200 mL (for slot-blot and microarray analysis, respectively) of

the culture into a clean graduated cylinder with 20 μL or 200 μL of 10 % NaN_3 already added, respectively. Quickly mix and transfer the cells onto frozen EDTA/NaN_3 Mix stored in either 50-mL Oak Ridge tubes or 500-mL bottles. Immediately vortex or shake to chill the cells.

9. Store the samples in an ice bath until all samples are collected and follow **steps 10–15** for further processing. Remove 1 mL from each sample for flow cytometry and budding index analysis and store in the ice bath until all samples are collected and follow **steps 16–18** for further processing.
10. Centrifuge the samples in either a JA-17 (50-mL Oak Ridge tubes) or JA-10 (500-mL bottles) at 1,600 × *g* for 10 min at 4 °C.
11. Wash the cells with 10 mL of cold AGD H_2O and centrifuge again.
12. Discard the supernatant and transfer the cell pellets with residual liquid into 1.5-mL microcentrifuge tubes or 50-mL tubes, for culture size of 20 or 200 mL, respectively.
13. Centrifuge in a table-top microcentrifuge at 2,500 × *g* or in a swinging bucket rotor at 2,500 × *g* for the microcentrifuge tubes or the 50-mL tubes, respectively, for 5 min at 4 °C.
14. Resuspend the cells in 1 or 10 mL of cold AGD H_2O, for culture size of 20 or 200 mL, respectively, and centrifuge again as described in **step 13** above.
15. Aspirate the supernatant and store the cell pellets at −20 °C until ready for DNA isolation.
16. For the 1-mL sample collected for FACS and budding index analyses (*see* **step 9** above), centrifuge at 2,500 × *g* in a microcentrifuge for 5 min at 4 °C.
17. Wash the cells in 1 mL of cold AGD H_2O and centrifuge again.
18. Add 300 μL of cold AGD H_2O to resuspend the cells, and then add 700 μL of cold 100 % ethanol, while vortexing slowly to mix (*see* **Note 11**). Store the samples at 4 °C.

3.2 Flow Cytometry and Budding Index Analyses

3.2.1 Flow Cytometry Analysis (Day 2–3)

1. Transfer 500 μL from the 1-mL cell sample (*see* Subheading 3.1, **step 18**) to a new 1.5-mL microcentrifuge tube and centrifuge at 5,000 rpm for 5 min at 4 °C.
2. Wash the cells in 1 mL of 50 mM sodium citrate pH 7.4 and centrifuge again.
3. Resuspend the cells in 1 mL of 50 mM sodium citrate pH 7.4 containing 50 μg/mL RNase A.
4. Incubate the cells for 1 h at 55 °C.
5. Add 50 μL of 20 mg/mL proteinase K to the cells and continue incubation for 1 h at 55 °C.
6. Centrifuge the cells at 2,500 × *g* for 5 min at 4 °C.

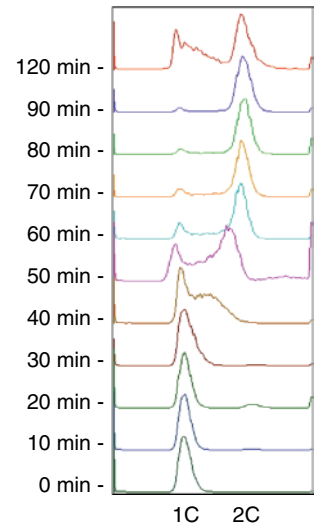

Fig. 2 Cell cycle progression of a synchronized W303 culture exiting from α-factor arrest at 25 °C analyzed by flow cytometry. Time after release from the block is indicated. "*1C*" and "*2C*" indicate positions of DNA contents in G1 and G2 cells, respectively

7. Add 1 mL of the 1 μM SYTOX green solution to resuspend the cells.
8. Incubate the cells in the dark overnight at 4 °C.
9. Sonicate the cells to reduce clumping by a Bioruptor Standard Model on "Low" setting, 30 s on and 30 s off, for two cycles at 4 °C in the dark. Probe sonicator is also acceptable, at a user-defined setting.
10. Transfer the cells to BD flow cytometry tubes and analyze samples on a BD LSRFortessa Flow Cytometry Analyzer, under the Blue Laser (488 nm excitation) with a BP filter at 530 nm emission. The user can also refer to instrument-specific flow cytometry procedures published elsewhere for data acquisition.
11. Analyze the data by FlowJo (Fig. 2) or equivalent.

3.2.2 Budding Index Analysis (Day 2)

1. Transfer 200 μL from the 1-mL cell sample (*see* Subheading 3.1, **step 18**) to a fresh 1.5-mL microcentrifuge tube and centrifuge at 2,500 × *g* for 5 min at 4 °C.
2. Resuspend the cells in 1 mL of AGD H_2O.
3. To eliminate cell clumping, sonicate them with a Bioruptor Standard Model on "Low" setting, 30 s on and 30 s off, for two cycles at 4 °C. Probe sonicator is also acceptable, at a user-defined setting.

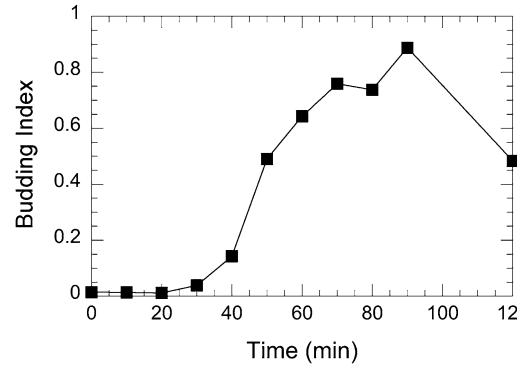

Fig. 3 Budding indices of a W303 culture exiting the G1 arrest by α-factor at the indicated times at 25 °C

4. Centrifuge the cells at 2,500 × *g* in a microcentrifuge for 5 min at 4 °C and aspirate most of the water (residual liquid should be less than 20 μL).
5. Resuspend the cells with the residual liquid.
6. Pipette 2 μL of cells and spot on a microscope slide, cover with a cover glass.
7. Count at least 200 cells and note the number of budded cells and unbudded cells.
8. Calculate the budding indices and plot as a function of time (Fig. 3):

   Budding Index = number of budded cells ÷ total number of cells.
9. The maximum budding index could be used to normalize microarray data (*see* Subheading 3.6).

3.3 Genomic DNA Isolation, EcoRI Restriction Digestion, and Southern Hybridization (Day 4–7)

The following steps are specific for cell pellets collected from 20-mL cell samples. Scale up by fivefold for 200-mL cell culture samples until **step 13** below. Perform restriction digestion in the same volume (100 μL) for the 200-mL culture samples as for the 20-mL culture samples.

1. Add 0.3 g of glass beads, 0.2 mL of lysis buffer, and 0.2 mL of 25:24:1 phenol:chloroform:isoamyl alcohol to each frozen cell pellet stored in a 1.5-mL microcentrifuge tube from Subheading 3.1, **step 15**.
2. Vortex at top speed for 3 min (*see* **Note 12**).
3. Add 0.2 mL of TE and vortex for 10 s at top speed.
4. Centrifuge at >17,000 × *g* in a microcentrifuge for 5 min at room temperature.
5. Transfer the upper aqueous phase to a fresh 1.5-mL microcentrifuge tube.

6. Add 0.2 mL of lysis buffer to the original tube and repeat **steps 2–4**.
7. Transfer and combine the upper aqueous phase with that collected in **step 5**.
8. Add two volumes of room temperature 100 % ethanol and mix thoroughly.
9. Centrifuge at >17,000 × *g* in a microcentrifuge for 5 min at room temperature and discard the supernatant.
10. If processing the samples (in 50-mL tubes) collected from 200-mL cultures, transfer 1 mL of the mix (*see* **step 8** above) to a 1.5-mL microcentrifuge tube and perform **step 9**. Transfer another 1 mL of the mix to the same tube and repeat **step 9** until the entire mix is processed. This step ensures maximum yield of genomic DNA.
11. Rinse the DNA pellets with 0.5 mL of cold 70 % ethanol by letting the liquid flow onto the pellet side of the tube slowly.
12. Centrifuge at >17,000 × *g* in a microcentrifuge for 5 s and discard the supernatant.
13. Leave the cap open and air-dry the DNA pellets at room temperature for ~20 min.
14. Dissolve DNA in 50 μL of $TE_{0.1}$ with 50 μg/mL of RNase A and incubate at 37 °C for 30 min. The DNA can be stored at 4 °C; or, continue to *Eco*RI digestion.
15. For each DNA sample (50 μL), make the *Eco*RI digestion reaction mix (total 50 μL for each DNA sample) by mixing 10 μL of 1 M Tris–HCl, pH 7.5, 1 μL of 5 M NaCl, 5 μL of 100 mM $MgCl_2$, 2.5 μL of 1 % Triton X-100, 20 U of *Eco*RI, and AGD H_2O to the final volume of 50 μL (*see* **Note 13**).
16. Add the 50-μL *Eco*RI digestion reaction mix to each of the 50-μL DNA samples.
17. Incubate the restriction digestion reaction overnight at 37 °C.
18. Add 1 μL of fresh *Eco*RI enzyme to the restriction digestion reaction and continue incubation for another 2 h.
19. Transfer the sample to 4 °C to stop the reaction.
20. Analyze 4 μL from the 100-μL restriction digestion reaction on a 0.8 % agarose gel in Electrophoresis buffer (Fig. 4a; *see* **Note 14**).
21. Use standard Southern blot procedures to check the level of digestion with an appropriate DNA probe hybridizing to an average size *Eco*RI fragment (~3 kb). If the digestion is incomplete, ethanol precipitate the DNA and repeat the restriction digestion until it reaches >90 % completion (Fig. 4b).

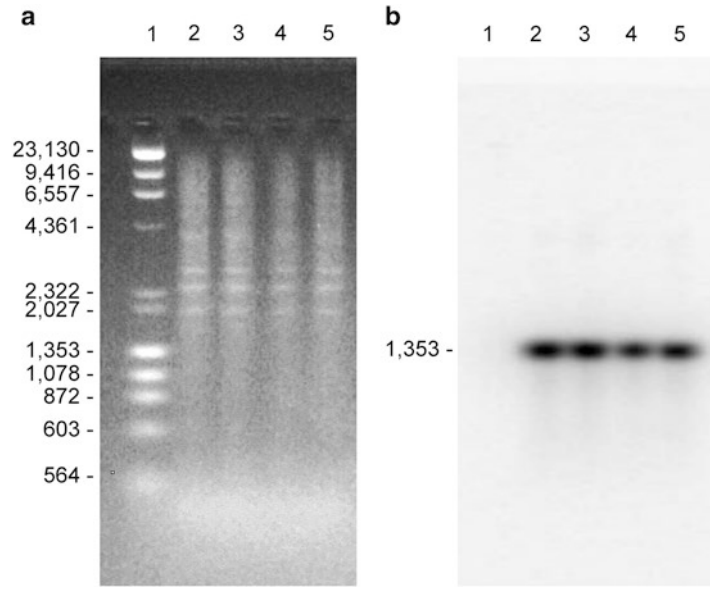

Fig. 4 Ethidium bromide-stained agarose gel and Southern analysis of *EcoRI-digested* genomic DNA. (**a**) Genomic DNA (*lanes* 2–5) isolated from 200 mL of W303 culture was digested with *EcoR*I and 0.5 % of the total DNA (0.5 μL from a 100 μL restriction digestion reaction) was separated on a 0.8 % agarose gel. *Lane 1*, λ/*Hind*III and ϕx174/*Hae*III DNA marker with sizes of DNA fragment in base-pair (bp) as indicated. (**b**) Southern analysis using the *TRP1* gene as a probe

3.4 CsCl Gradient Preparation, CsCl Gradient Fractionation, Slot-Blot Analysis, and Replication Kinetic Data Processing

3.4.1 CsCl Gradient Preparation by Ultracentrifugation Using the Vertical Rotor VTi 65.2 (Day 8–9)

Ultracentrifugation can be done in the vertical rotor VTi 65.2 (described in this section) or the fixed-angle rotor Ti 70.1 (described in Subheading 3.4.2). Comparison of CsCl gradient formation using these rotors is shown in Fig. 5.

1. Weigh 9.141 g CsCl solution in a 15-mL tube and mix with 90 μL of *Eco*RI restriction digestion reaction mix from Subheading 3.3, **step 19**.
2. Transfer the CsCl and DNA mix into a 13 × 51 mm Quick-seal tube with a Pasteur pipette and use "dummy digestion mix" (*Eco*RI digestion reaction mix without DNA, mixed with CsCl as described in **step 1**) to fill up the tube.
3. Seal the tube by a Quick-Seal sealer or a heated flat spatula.
4. Centrifuge at 275,444 × *g* for 18 h at 20 °C and then at 71,388 × *g* for 3.5 h at 20 °C, setting the deceleration at transition to "0" (no brakes) and at the end to "1" (transition speed 170 rpm).

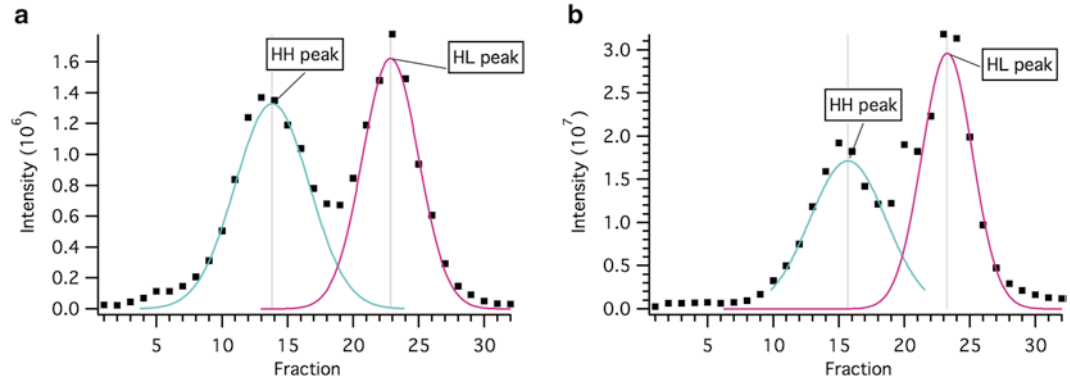

Fig. 5 Comparison of gradient formation of identical DNA samples isolated from a W303 culture at 90 min after release from α-factor arrest, through ultracentrifugation using two different Beckman rotors: the VTi 65.2 rotor (**a**) and the Ti 70.1 rotor (**b**). Centrifugation conditions are described in the protocol. Deconvoluted "HH" and "HL" DNA peaks from the slot-blot data are as shown

3.4.2 CsCl Gradient Preparation by Ultracentrifugation Using the Fixed-Angle Rotor Ti 70.1 (Day 8–9)

1. Weigh 10.97 g CsCl solution in a 15-mL tube and mix with 90 μL of *Eco*RI restriction digestion reaction mix from Subheading 3.3, **step 19**.
2. Transfer the CsCl and DNA mix into a 16 × 45 mm Quick-Seal tube with a Pasteur pipette and use "dummy digestion mix" to fill up the tube.
3. Seal the tube by Quick-Seal sealer or a heated flat spatula.
4. Centrifuge the DNA at 207,346 × *g* for 48 h at 20 °C, setting the deceleration to "1".

3.4.3 CsCl Gradient Fractionation, Slot-Blot Analysis, and Replication Kinetic Data Processing (Day 10–12)

1. Carefully remove samples from the centrifuge and the rotor.
2. Fractionate each gradient as follows. Secure the centrifuge tube in the fractionation apparatus. Slowly punch a hole at the bottom of the tube and let the gradient steadily drip into the wells of a 96-well plate with seven drops per well (approximately 170 μL/well) (Fig. 6a; *see* **Note 15**).
3. Transfer an appropriate volume of DNA (e.g., 42 μL for DNA from 20-mL cell samples and 2 μL for DNA from 200-mL samples) from each fraction into a new 96-well plate. Add 40 μL of AGD H_2O to the 2 μL DNA, bringing the final volume to 42 μL for the samples from 200-mL cultures.
4. Add 28 μL of 1 N NaOH to each fraction and mix.
5. Seal the 96-well plate with the Template Sealing Foil and incubate for 1 h at 65 °C.
6. Cool the plate to room temperature.

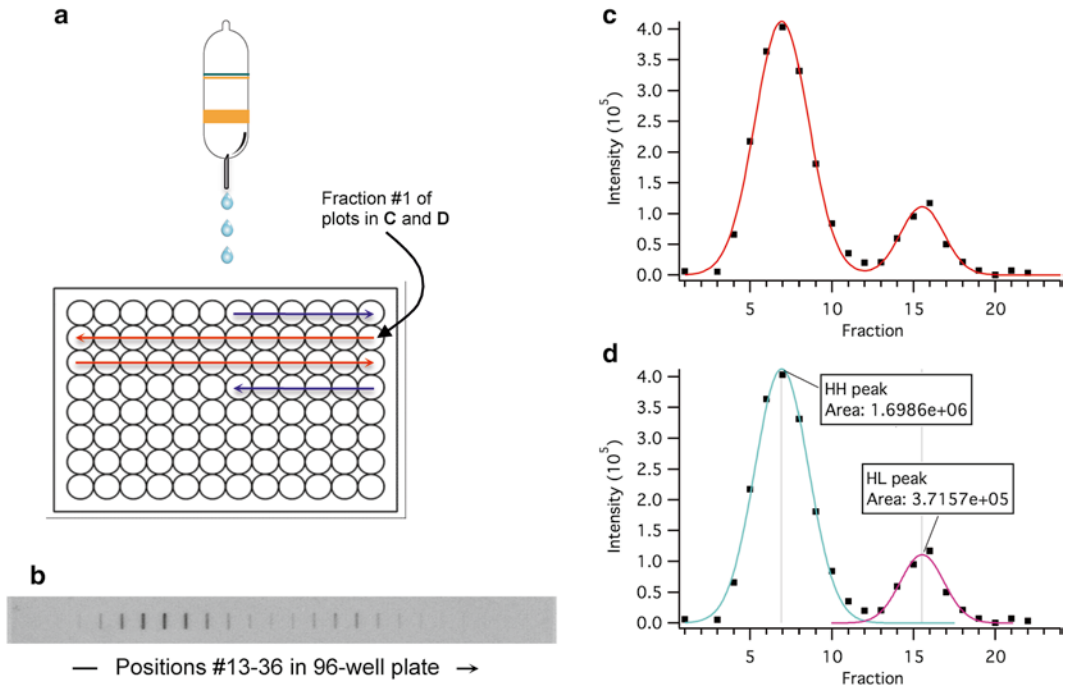

Fig. 6 Drip fractionation and slot-blot analyses for quantifying the "HH" and "HL" DNA. Examples of experimental results were obtained from a W303 strain at 50 min after release from α-factor arrest. (**a**) The gradient is fractionated by collecting seven drops in each well of a 96-well plate in a zig–zag fashion (shown by the *arrows* for direction of collection). (**b**) Slot blot image of the middle 24 fractions of the gradient indicated by *red arrows* in (**a**), probed with ^{32}P-dATP-labeled ARS609 DNA. A priori, all 36 fractions might be slot blotted. (**c**) "Multiple peak fitting" of the intensity plot of slot blot (**b**) by IgorPro: *black squares* represent raw data points. (**d**) Deconvoluted intensity plot in (**c**): "HH" and "HL" peaks and the values of the integrated area under the peaks are indicated

7. Add 70 μL of 20× SCP to each fraction and mix.
8. Pre-wet the Whatman paper and the membrane with 10× SCP and place them into the Minifold, using two layers of Whatman paper underneath the membrane.
9. Using a multichannel pipetter, pipette 140 μL of 10× SCP into each well of the Minifold first, ensuring sound vacuum-assisted flow, before pipetting the 140-μL samples into the wells, followed by 140 μL of 10× SCP to rinse (*see* **Note 16**).
10. Remove the membrane from the Minifold and crosslink DNA to the membrane with 1200 mJ of ultraviolet light in a Crosslinker.
11. Perform standard hybridization of a random-primed ^{32}P-labeled genomic DNA probe. An example of the blot is shown (Fig. 6b).
12. Perform image acquisition of the radioactively hybridized membrane. Quantify the intensity of each fraction as "total volume" by ImageQuant 5.1 or equivalent software and generate a gradient profile (Fig. 6c).

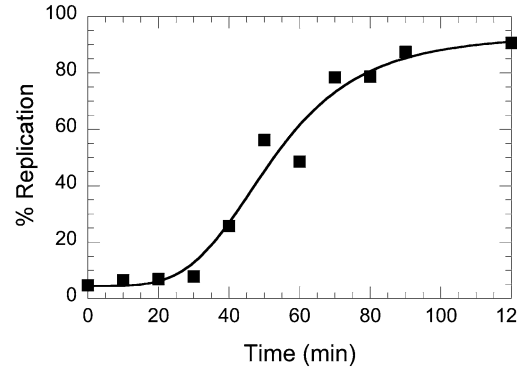

Fig. 7 Fitted replication kinetic curve of genomic DNA from a W303 culture at 25 °C

13. Deconvolute the twin peaks of signals representing the "HH" (unreplicated) and "HL" (replicated) DNA by using the "Multipeak fitting 2" function in IgorPro. Calculate the area under each of the twin peaks and record as "HH" and "HL", respectively (Fig. 6d).
14. Calculate the percentage of replication (% Replication) at each time point by the following formula: $\%\text{Replication} = 0.5 \times \text{"HL"} \div (\text{"HH"} + 0.5 \times \text{"HL"}) \times 100$.
15. Plot the % Replication value over the time with KaleidaGraph 4.1 and then fit the data using the "Sigmoidal" function ($m1 = 100$, $m2 = -4$, $m3 = 30$ and $m4 = 0.5$) to generate the replication kinetic curve (Fig. 7).
16. Calculate T_{rep} (the time at which half of the maximum percentage of replication is achieved) for the genomic DNA by using a genomic DNA probe.
17. The maximum percentage of replication will be used to normalize microarray data for f, the fraction of the cell population that was cycling—i.e., that actually entered S phase (*see* Subheading 3.6):

$$f = \frac{\text{Maximum \%Replication}}{100}.$$

3.5 DNA Labeling, Microarray Hybridization, and Data Extraction (Day 13–14)

1. Pool those fractions containing an estimated 80 % pure "HH" or "HL" DNA, with <20 % contaminations from each other, based on the gradient profile obtained with a genomic DNA probe. This results in a "HH" and a "HL" DNA sample from each original DNA sample collected at a discrete time. Transfer each of these samples, NOT mixing "HH" and "HL" DNA, into a 50-mL Oak Ridge tube (*see* **Note 17**).
2. Add three volumes of cold 70 % ethanol to each DNA sample and mix thoroughly by swirling.

3. Precipitate the DNA for 30 min at −20 °C.
4. Centrifuge at >12,000 × *g* for 30 min at 4 °C and discard the supernatant.
5. Wash the DNA pellet with 1 mL of cold 70 % ethanol by letting the liquid flow onto the pellet side of the tube slowly.
6. Centrifuge again and discard the supernatant.
7. Invert the tube and air-dry the DNA pellets for up to 16 h (overnight).
8. Add 50 μL of TE to dissolve the DNA and measure the concentration before storing at −20 °C.
9. Transfer 500 ng "HH" DNA and 500 ng "HL" DNA from each sample collected at a discrete time to a new 1.5-mL microcentrifuge tube. Adjust to a final volume of 21 μL with AGD H_2O.
10. Add 20 μL of 2.5× labeling reaction buffer and denature the DNA at 95–100 °C for 5 min.
11. Quick chill the DNA mix on ice and pulse centrifuge to collect condensation.
12. Add 5 μL of 10× dNTP mix, 3 μL of Cy5- or Cy3-dUTP for "HH" or "HL" DNA, respectively, and 1 μL of 50,000 units/mL Klenow Fragment (3′–5′ exo-).
13. Incubate the labeling reaction mix for 2–3 h at 37 °C in the dark.
14. Mix together the "HH" and "HL" samples for each sample collected at a discrete time and use a QIAquick PCR purification kit to clean up the DNA (follow the manufacturer's instructions), eluting with 45 μL of EB buffer.
15. Measure DNA concentration using a NanoDrop ND-2000 spectrophotometer.
16. Hybridize the labeled DNA onto Agilent ChIP to chip yeast microarray slides following manufacturer's instructions.
17. Extract data with the Feature Extraction software and save as a tab-delimited text file.

3.6 Generating a Replication Profile for Each Chromosome in the Yeast Genome

1. Duplicate the data file from Subheading 3.5, **step 17**. Leave the original file untouched as an archival copy; give the duplicate file a distinctive name and perform all further manipulations on this duplicate.
2. Open the file in Microsoft Excel (or equivalent) and delete the first rows of descriptors, if any, so that the row of column headers (ProbeID, ProbeName, etc.) becomes the first row.
3. Select all the data in the file and sort by ProbeID (ascending sort).

4. Delete the rows corresponding to hybridization control spots (rows 2–331 for Agilent 4×44 ChIP arrays).
5. Delete the rows corresponding to mitochondrial DNA probes (the rows at the end of the data table). *Important: Perform this step only if you have eliminated mitochondrial DNA probes from the list of probe coordinates in file ProbeCoordinates.txt (see Subheading 2.6, **item 1**). If you have retained mitochondrial DNA probe information in Subheading 2.6, **item 1**, you must retain the corresponding rows in the data file from **step 4** of this section*. At this point, the number of rows of data in this file should correspond exactly to the number of rows of probe coordinates in file ProbeCoordinates.txt.
6. Optional step: delete columns that you will not be using, so as to reduce the file size and speed subsequent manipulations. Typically, we only retain the following columns: ProbeName, gProcessedSignal, rProcessedSignal, gMedianSignal, rMedianSignal, gBGMedianSignal, and rBGMedianSignal.
7. With the data still sorted by ProbeID, insert the list of genomic locations (chromosome and coordinates, file ProbeCoordinates from Subheading 2.6, **item 1**) as the left-most columns in the table (i.e., after this step, the chromosome number will be in column 1 and coordinates as kb and bp will be in columns 2 and 3, respectively). Because the data file (*see* **step 6** above) and the list of coordinates (ProbeCoordinates.txt) were both sorted in ascending order by ProbeID, each row of microarray data is now identified by its genomic location. Save the file as tab-delimited text and continue.
8. Identify the "ProcessedSignal" columns corresponding to the HH-DNA and HL-DNA channels. For example, if HH-DNA was labeled with Cy3, the column corresponding to the HH-DNA signal will be the column labeled "gProcessedSignal". For convenience and for future manipulations, re-label these two columns in the file as "HHraw" and "HLraw".
9. Obtain the sum of all the HHraw values ("HHsum"). Likewise, get the sum of the HLraw values ("HLsum").
10. Calculate the normalization parameter γ as defined by the formula:

$$\gamma = \left(\frac{\mathrm{HL}}{\mathrm{HH}}\right) \div \left(\frac{\mathrm{HLsum}}{\mathrm{HHsum}}\right)$$

    where ***HH*** and ***HL*** are the areas under the HH-DNA and HL-DNA peaks obtained for that sample by slot-blot analysis in Subheading 3.4.3, **step 13** (Fig. 6d).
11. Create a new column in the worksheet. For each probe location i in the genome, obtain the corrected value $\%HL_{Corr(i)}$; i.e.,

the value of %HL for that location, corrected for signal differences between the Cy3 and Cy5 channels:

$$\text{RawRatio}_i = \frac{\text{HLraw}_i}{\text{HHraw}_i}.$$

$$\text{Ratio}_{\text{Corr}(i)} = \text{RawRatio}_i \times \gamma.$$

$$\%\text{HL}_{\text{Corr}(i)} = \left(\frac{\text{Ratio}_{\text{Corr}(i)}}{1 + \text{Ratio}_{\text{Corr}(i)}}\right)100.$$

12. Create a new column in the worksheet. Perform the final normalization step to account for *f*, the fraction of cells in the population that actually entered S phase (*see* Subheading 3.4.3, **step 17**). The maximum budding index observed in Subheading 3.2.2, **step 9** can be used as a substitute for f if necessary. For each probe location *i*, calculate $\%\text{HL}_{\text{Norm}(i)}$, the normalized %HL, and $\%\text{Replication}_{\text{Norm}(i)}$, the normalized value of % replication:

$$\%\text{HL}_{\text{Norm}(i)} = \left(\frac{\%\text{HL}_{\text{Corr}(i)}}{200f + (1-f)\%\text{HL}_{\text{Corr}(i)}}\right)200$$

$$\%\text{Replication}_{\text{Norm}(i)} = \left(\frac{\%\text{HL}_{\text{Norm}(i)}}{200 - \%\text{HL}_{\text{Norm}(i)}}\right)100$$

Label the column with the normalized percent replication values as "Percent_rep" (without the quotes). Save the file.

13. Use the exclusion list (*see* Subheading 2.6, **item 2**) to eliminate the rows corresponding to genomic locations you wish to exclude from the final output (*see* **Note 18**).
14. Split the file by chromosome; i.e., create a set of files, each containing the data for just one chromosome but retaining the column headers (Chr, Coord_kb, etc.) from the source file. Create a sub-folder and save each file as tab-delimited text within that folder. For clarity, save each file with a common base name, differing only in a numerical index indicating the chromosome corresponding to that file (e.g., chr01_rep.txt, chr02_rep.txt, etc.; *see* **Note 19**).
15. Using a text editor, open the text file "rep_smoothing.R" created in Subheading 2.6, **item 4**. In this file, replace "path_to_%replication_files" with the actual path to the folder containing the files saved after splitting the data by chromosome; retain the quotes surrounding the folder path.

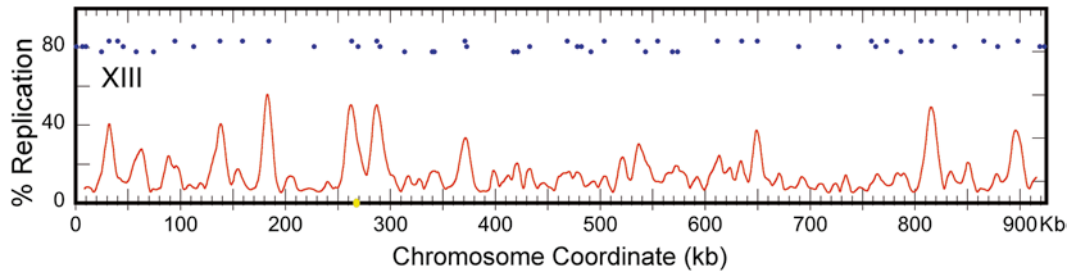

Fig. 8 Replication profile of chromosome XIII of a W303 culture at 30 min after exiting α-factor arrest at 25 °C. The *dots* (positioned from *high* to *low*) shown above the profile represent OriDB-curated (http://oridb.org) confirmed, likely and dubious origins, respectively

Replace "winSize" with the desired smoothing window in kb (but "winSize" should be replaced just by the numerical value of the desired window and should not contain the text "kb"). Typically, for density transfer profiles, we use a smoothing target window of 18 kb. Save the text file (*see* **Note 20**).

16. Smooth the percent replication data for each chromosome by running the following batch command in the unix shell after navigating to the folder/directory containing the file "rep_smoothing.R" (*see* **Note 21**): R CMD BATCH rep_smoothing.R. The command will invoke the R commands and apply loess smoothing to the data, appending a column of smoothed data values to the file for each chromosome. The column containing the smoothed % replication values will have the label, "Percent_rep_loess".
17. Using the graphing application of your choice, plot the data for each chromosome (Percent_rep_loess as a function of Coord_kb or Coord_bp). Set the *x*-axis dimension to some constant scaling factor (e.g., 1 cm = 100 kb) such that profiles for all chromosomes are on the same scale. For a sample plot *see* Fig. 8.

4 Notes

1. Filter-sterilize the medium.
2. All the amino acids are weighed and mixed to make an amino acids powder mix. The amino acids powder and glucose are supplemented after autoclaving or filter-sterilization.
3. For collecting a 20 mL sample, freeze 8 mL of the EDTA/NaN_3 mix in a 50-mL Oak Ridge centrifuge tube (Nalgene) at −20 °C; for collecting a 200-mL sample freeze 80 mL of the EDTA/NaN_3 mix in a 500-mL centrifuge bottle at −20 °C.
4. Before filter-sterilization, measure the refractive index of the buffer. The refractive index of $T_{10}E_{100}$, pH 7.5 should be

1.3395 (the refractive index of H_2O is 1.3330 at 25 °C). If it is too high, add 10 mM Tris–HCl pH 7.5 to adjust.

5. Dissolving CsCl in $T_{10}E_{100}$ pH 7.5 is an endothermic process. Cover the beaker containing the solution and measure the refractive index of the solution after the temperature of the solution has equilibrated to room temperature. The refractive index of the CsCl solution should be close to 1.4058. If it is too high, add $T_{10}E_{100}$, pH 7.5 to adjust.
6. Hanging indentations in the code text indicate text that belongs all on one line.
7. Inoculate the cells in 5 mL of Dense Medium and culture overnight. The culture may or may not reach saturation depending on the population doubling time of the strain and the culturing temperature. We typically employ 25 °C for wild-type yeast cultures. The user may determine the appropriate temperature depending on the yeast strain. Inoculate 25 mL of Dense Medium with the primary culture and measure the population doubling time. Based on the population doubling time and the cell density of the 25-mL culture, inoculate fresh Dense Medium with an appropriate volume of the 25-mL culture.
8. Transfer 1 mL of the culture into 1.5-mL microcentrifuge tube. Sonicate the culture by the Bioruptor Standard Model ("Low" setting, 30 s on and 30 s off, for two cycles). Pipette 2 μL of the culture onto a microscope slide and cover it with a cover glass. Then check the percentage of cells showing buds of any size.
9. We also use vacuum-assisted filtration to transfer cells from Dense Medium into "Y-complete" Medium if the culture volume is suitable. However, the filtration process might take too long to filter a large volume of culture.
10. Weigh the Pronase powder and dissolve in AGD H_2O before use. It can be temporarily stored on ice.
11. Add the AGD H_2O and ethanol slowly down the side of the tube and then vortex.
12. Vortex for 30 s and cool on ice for 30 s; repeat six times.
13. Make enough digestion reaction mix for all samples plus a "dummy digestion mix" without DNA. One could make the digestion mix by using the NEB 10× buffer for *Eco*RI instead.
14. For 200-mL cell culture samples, load 0.5–1 μL of the 100-μL restriction digestion mix on the agarose gel.
15. Be sure not to disturb the gradient. The speed of dripping should be fairly low, not higher than one drop per second.

16. Make sure the solution is aspirated completely through the vacuum before adding the sample, as well before washing.
17. Those fractions that contain significantly cross-contaminated "HH" and "HL" DNA are excluded from pooling and further analysis.
18. This step can be accomplished using a scripting language such as Perl or Python, or Microsoft Office VBA for Applications, depending on the investigator's skill/comfort with such languages. Alternatively, it can be accomplished using Microsoft Excel and Microsoft Word without any scripting. For example, each open reading frame (ORF) in the exclusion list can be converted to a pair of rows in the file: one row containing the chromosome number and start coordinate for that ORF and containing the word "START" as a third field in that row, and one row with the chromosome number and the end coordinate and containing the word "END" as the third field for that row. This list of start and end coordinates can be appended to the data file and whole file sorted by chromosome and coordinate and saved as a tab-delimited text file. Now, each set of probes to be excluded will be preceded by a row containing the word "START" and followed immediately by a row containing the word "END". Next, using the "Advanced Find and Replace" command with wild card searching enabled in Microsoft Word, the rows between each START…END pair can be deleted. Using Microsoft Excel again to sort the data, the lines containing START and END can be grouped and deleted, leaving just the desired microarray data.
19. The next step (the smoothing step) will result in alteration of the input file, so it would be a good idea to make an archival copy of the files before performing the smoothing operation.
20. Be aware that unix, Microsoft Windows, and Apple Macintosh files typically use different line delimiters. For example, Macintosh files typically use carriage returns (ASCII character 13) to signify line endings, while unix files use the "linefeed" character (ASCII character 10). So, some experimentation with line delimiters within the R script file and in the output files defined in the R script file may be necessary to find the appropriate format for the system being used. For example, the "eol" (end-of-line) definition in the R script (Subheading 2.6, **item 4**) can be changed from "\r" (carriage-return) to "\n" (linefeed).
21. The R batch command syntax is appropriate for unix-based systems, e.g., to be run in the Terminal application in Mac OS X. The same batch file (rep_smoothing.R) will work in Windows systems also, but the syntax to invoke the file will have to be modified appropriately.

Acknowledgements

This work was supported by NIH grant 4R00GM08137804 to W.F. and NIGMS grant 18926 to M.K.R.

References

1. Lucas I, Feng W (2003) The essence of replication timing: determinants and significance. Cell Cycle 2(6):560–563
2. Yaffe E, Farkash-Amar S, Polten A, Yakhini Z, Tanay A, Simon I (2010) Comparative analysis of DNA replication timing reveals conserved large-scale chromosomal architecture. PLoS Genet 6(7):e1001011
3. Muller CA, Nieduszynski CA (2012) Conservation of replication timing reveals global and local regulation of replication origin activity. Genome Res 22(10):1953–1962
4. McCune HJ, Danielson LS, Alvino GM, Collingwood D, Delrow JJ, Fangman WL, Brewer BJ, Raghuraman MK (2008) The temporal program of chromosome replication: genome-wide replication in clb5{Delta} *Saccharomyces cerevisiae*. Genetics 180(4):1833–1847
5. Feng W, Bachant J, Collingwood D, Raghuraman MK, Brewer BJ (2009) Centromere replication timing determines different forms of genomic instability in *Saccharomyces cerevisiae* checkpoint mutants during replication stress. Genetics 183(4): 1249–1260
6. Lengronne A, Schwob E (2002) The yeast CDK inhibitor Sic1 prevents genomic instability by promoting replication origin licensing in late G(1). Mol Cell 9(5):1067–1078
7. Schubeler D, Scalzo D, Kooperberg C, van Steensel B, Delrow J, Groudine M (2002) Genome-wide DNA replication profile for *Drosophila melanogaster*: a link between transcription and replication timing. Nat Genet 32(3):438–442
8. Woodfine K, Fiegler H, Beare DM, Collins JE, McCann OT, Young BD, Debernardi S, Mott R, Dunham I, Carter NP (2004) Replication timing of the human genome. Hum Mol Genet 13(2):191–202
9. Ryba T, Hiratani I, Sasaki T, Battaglia D, Kulik M, Zhang J, Dalton S, Gilbert DM (2011) Replication timing: a fingerprint for cell identity and pluripotency. PLoS Comput Biol 7(10):e1002225
10. Hiratani I, Ryba T, Itoh M, Yokochi T, Schwaiger M, Chang CW, Lyou Y, Townes TM, Schubeler D, Gilbert DM (2008) Global reorganization of replication domains during embryonic stem cell differentiation. PLoS Biol 6(10):e245
11. Hiratani I, Ryba T, Itoh M, Rathjen J, Kulik M, Papp B, Fussner E, Bazett-Jones DP, Plath K, Dalton S, Rathjen PD, Gilbert DM (2010) Genome-wide dynamics of replication timing revealed by in vitro models of mouse embryogenesis. Genome Res 20(2):155–169
12. Shufaro Y, Lacham-Kaplan O, Tzuberi BZ, McLaughlin J, Trounson A, Cedar H, Reubinoff BE (2010) Reprogramming of DNA replication timing. Stem Cells 28(3):443–449
13. De S, Michor F (2011) DNA replication timing and long-range DNA interactions predict mutational landscapes of cancer genomes. Nat Biotechnol 29(12):1103–1108
14. Liu L, De S, Michor F (2013) DNA replication timing and higher-order nuclear organization determine single-nucleotide substitution patterns in cancer genomes. Nat Commun 4:1502
15. Merrick CJ, Jackson D, Diffley JF (2004) Visualization of altered replication dynamics after DNA damage in human cells. J Biol Chem 279(19):20067–20075
16. Masai H, Matsumoto S, You Z, Yoshizawa-Sugata N, Oda M (2010) Eukaryotic chromosome DNA replication: where, when, and how? Annu Rev Biochem 79:89–130
17. Mechali M (2010) Eukaryotic DNA replication origins: many choices for appropriate answers. Nat Rev Mol Cell Biol 11(10):728–738
18. Friedman KL, Brewer BJ, Fangman WL (1997) Replication profile of *Saccharomyces cerevisiae* chromosome VI. Genes Cells 2(11):667–678
19. Raghuraman MK, Winzeler EA, Collingwood D, Hunt S, Wodicka L, Conway A, Lockhart DJ, Davis RW, Brewer BJ, Fangman WL (2001) Replication dynamics of the yeast genome. Science 294(5540):115–121
20. de Moura AP, Retkute R, Hawkins M, Nieduszynski CA (2010) Mathematical modelling of whole chromosome replication. Nucleic Acids Res 38(17):5623–5633
21. Gilbert DM (2010) Evaluating genome-scale approaches to eukaryotic DNA replication. Nat Rev Genet 11(10):673–684

22. Alvino GM, Collingwood D, Murphy JM, Delrow J, Brewer BJ, Raghuraman MK (2007) Replication in hydroxyurea: it's a matter of time. Mol Cell Biol 27(18):6396–6406
23. Vincent JA, Kwong TJ, Tsukiyama T (2008) ATP-dependent chromatin remodeling shapes the DNA replication landscape. Nat Struct Mol Biol 15(5):477–484
24. Lian HY, Robertson ED, Hiraga S, Alvino GM, Collingwood D, McCune HJ, Sridhar A, Brewer BJ, Raghuraman MK, Donaldson AD (2011) The effect of Ku on telomere replication time is mediated by telomere length but is independent of histone tail acetylation. Mol Biol Cell 22(10):1753–1765
25. Knott SR, Viggiani CJ, Tavare S, Aparicio OM (2009) Genome-wide replication profiles indicate an expansive role for Rpd3L in regulating replication initiation timing or efficiency, and reveal genomic loci of Rpd3 function in *Saccharomyces cerevisiae*. Genes Dev 23(9): 1077–1090
26. Yabuki N, Terashima H, Kitada K (2002) Mapping of early firing origins on a replication profile of budding yeast. Genes Cells 7(8): 781–789

Chapter 27

Analysis of ssDNA Gaps and DSBs in Genetically Unstable Yeast Cultures

Jie Peng, M.K. Raghuraman, and Wenyi Feng

Abstract

DNA replication defects are an underlying cause of genome instability, which could stem from alterations in replication intermediates such as extensive single-stranded DNA (ssDNA). Under replication stress, ssDNA is a precursor of the ultimate double-strand breaks (DSBs). Indeed, mutations that render the cell incapable of mediating and protecting the replication forks produce ssDNA genome-wide at high frequency and cause lethality when encountering DNA damage or replication perturbation. Here we describe two related microarray-based methods to query genetically unstable yeast cultures, such as the *mec1* and *rad53* mutants. These mutants are defective in central protein kinases in the checkpoint pathway. To induce ssDNA and DSB formation in these mutants, we utilize hydroxyurea, a drug that causes nucleotide shortage in the cell.

Key words DNA replication checkpoint, Replication stress, Single-stranded DNA, Double-strand break, Hydroxyurea, Origins of replication, Chromosome fragile sites

1 Introduction

Eukaryotic chromosomal DNA replication is a complex process that involves the activation, coordination, and resolution of hundreds to thousands of origins of replication. These are the sites where replication initiates in a bidirectional manner, forming the so-called replication bubbles. At either end of the replication bubble are the junctions of replicated and unreplicated DNA, also called replication forks. The replication forks are particularly vulnerable structures that when unprotected could generate extensive single-stranded DNA (ssDNA) gaps [1, 2] and ultimately double-strand breaks (DSBs) [3].

Observation of ssDNA formation near the origins of replication during hydroxyurea-induced nucleotide shortage was first made visually by microscopy [1] and later confirmed by genome-wide approaches [2], which are facilitated by the development of a microarray-based ssDNA labeling method. It was then proposed

Eishi Noguchi and Mariana C. Gadaleta (eds.), *Cell Cycle Control: Mechanisms and Protocols*, Methods in Molecular Biology, vol. 1170, DOI 10.1007/978-1-4939-0888-2_27,

that ssDNA formation at replication origins during nucleotide shortage caused by the treatment with hydroxyurea (HU, an inhibitor of the ribonucleotide reductase) is an evolutionarily conserved process and can be exploited in order to map origins of replication in diverse organisms. Indeed, HU treatment has been used to identify origins of replication in diverse yeast species such as *Schizosaccharomyces pombe* [2], *Lachancea waltii* [4], and *Saccharomyces bayanus* (G. Alvino, M. Dunham, B. Brewer, and M.K. Raghuraman, unpublished). We have also observed that other forms of replication inhibition also induce ssDNA formation (Feng W. unpublished data), suggesting that it is a general response elicited by the cell under replication stress. In an attempt to examine the fate of ssDNA formation, particularly in mutant backgrounds where such an event brings about the cell's demise, it was then demonstrated that persistent ssDNA indeed ultimately led to DSBs at the replication forks as previously postulated [3]. Again, such experimental evidence was facilitated by the development of a similar microarray-based method to query persistent DSBs in the yeast genome.

Here we describe the details of two microarray-based protocols related to the abovementioned methods in order to interrogate the yeast genome for ssDNA and DSBs under replication stress caused by HU in a synchronous yeast culture (Fig. 1). However, we envisage that both methods can be applied to query ssDNA and DSBs produced by other replication stress or indeed agents (chemicals or genetic mutations) that may very well be unrelated to the replication process. We have mapped both in vitro restriction digestion-induced DSBs as well as in vivo HO (endonuclease)-induced irreparable DSBs in the yeast genome using the DSB labeling method [3]. We also note that the two methods described in this chapter are readily adaptable to use with the more superior next-generation sequencing platforms in place of the microarray platform in order to achieve higher sensitivity and better coverage of the genome. With this adaptation, it is then also feasible to apply these methods to the vastly more complex mammalian genomes in order to identify important chromosomal landmarks such as origins of replication and fragile sites.

2 Materials

All solutions are autoclaved or filter sterilized unless otherwise noted.

2.1 Cell Culture Sample Collection

1. AGD H_2O (autoclaved glass-distilled H_2O): All solutions are prepared in AGD H_2O unless otherwise noted.
2. YPD medium: 10 g/L Yeast extract, 20 g/L Bacto Peptone, 20 g/L D-glucose.

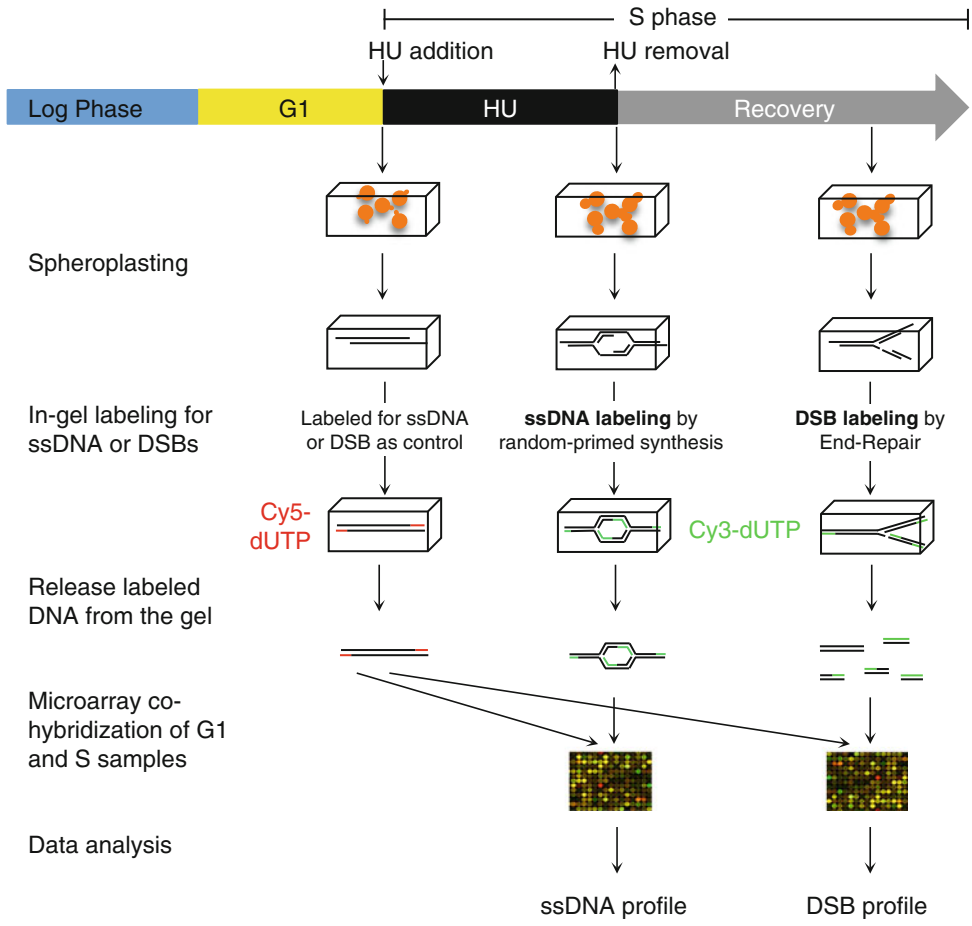

Fig. 1 Outline of procedures for cell culture collection followed by in-gel ssDNA and DSB labeling by random-primed synthesis via Klenow and by end repair via T4 DNA polymerase, respectively. These procedures were followed by microarray analysis. *HU* hydroxyurea. Note that significant DSBs were observed only during the "recovery" phase after transient exposure to HU in the *mec1* mutant [3]

3. α-Factor (peptide sequence: NH_2–WHWLQLKPGQPMY–COOH, custom synthesized by ThermoFisher at >70 % purity), prepared as 200 μM or 3 mM stocks (1,000× stocks) for *bar1* and *BAR1* strains, respectively, and stored at −80 °C.
4. 10 % NaN_3.
5. HU powder.
6. Pronase.
7. 15- and 50-mL tubes.

2.2 Preparation of Cells Embedded in Agarose Plugs

1. Centrifuge with swing bucket rotors (e.g., TX-750 rotor, Thermo Scientific).
2. 0.5 M EDTA, pH 8.0.
3. 50 mM EDTA, pH 8.0.
4. 1 % Low-melt agarose: 1 % InCert or NuSieve GTG agarose (Lonza) in 50 mM EDTA pH 8.0, melted and then cooled to 42 °C before use.
5. 50-Well disposable plug molds (Bio-Rad); can be washed and reused.
6. Six-well sterile tissue culture-treated plates with flat bottoms.
7. TE: 10 mM Tris–HCl, 1 mM EDTA pH 8.0.
8. 1 M Sorbitol.
9. 1 M Tris–HCl pH 7.5.
10. Spheroplasting solution: 1 M Sorbitol, 20 mM EDTA pH 8.0, 10 mM Tris–HCl pH 7.5, 14 mM β-mercaptoethanol, 0.5 mg/mL Zymolyase 20-T. Prepare fresh.
11. 1× Sodium dodecyl sulfate (SDS) solution for plugs: 10 mM Tris–HCl pH 8.0, 1 % SDS, 100 mM EDTA. Prepare from a 10× stock.
12. 5× NDS: 10 mM Tris–base pH 8.0, 0.5 M EDTA, 1 % Sarkosyl.
13. 1× NDS: Diluted from 5× NDS.

2.3 In-Gel Labeling for ssDNA or DSBs

1. 10× ssDNA labeling reaction buffer: 500 mM Tris–HCl pH 6.8, 50 mM $MgCl_2$, 100 mM β-mercaptoethanol. Store at –20 °C.
2. 1× ssDNA labeling reaction buffer, prepared fresh from the frozen 10× stock, and used to equilibrate agarose plugs prior to the labeling reaction.
3. $TE_{0.1}$: 10 mM Tris–HCl pH 8.0, 0.1 mM EDTA pH 8.0.
4. 10× dNTP mix: 1.2 mM dATP, 1.2 mM dCTP, 1.2 mM dGTP, 0.6 mM dTTP, and 10 mM Tris–HCl pH 8.0, stored at –20 °C.
5. 2.5× ssDNA labeling reaction buffer stock: 125 mM Tris–HCl pH 6.8, 12.5 mM $MgCl_2$, 25 mM β-mercaptoethanol, 750 μg/mL random hexamers (custom synthesized). Store at –20 °C.
6. 1 mM Cy5- and Cy3-dUTP (GE Healthcare).
7. 50,000 units/mL Klenow Fragment (3′–5′ exo-) (NEB).
8. 10× End-repair labeling reaction buffer: 330 mM Tris–acetate pH 7.8, 660 mM potassium acetate, 100 mM magnesium acetate, 5 mM dithiothreitol. Store at –20 °C.
9. 1× End-repair labeling reaction buffer, prepared fresh from the frozen 10× stock, and used to equilibrate agarose plugs prior to the labeling reaction.

10. End-It™ DNA End-repair kit (Epicentre).
11. 1× β-Agarase buffer: Diluted from 10× β-Agarase buffer (NEB) with AGD H_2O.
12. 1,000 units/mL β-Agarase (NEB).
13. Bioruptor (Diagenode Standard Model).
14. QIAquick PCR Purification Kit (Qiagen).
15. NanoDrop ND-2000 spectrophotometer (Thermo Scientific).

2.4 Microarray Hybridization

1. Agilent 4×44K ChIP-to-chip yeast microarrays.
2. Microarray hybridization facility and Agilent microarray scanner.

2.5 Generation of ssDNA/DSB Profiles

1. A file containing a list of genomic coordinates (chromosome number and coordinate) for the microarray probes that will be used in the analysis (e.g., excluding probes corresponding to mitochondrial DNA): For convenience, we shall call this file "ProbeCoordinates.txt." The list should be sorted by ProbeID (ascending order), one line per probe, and saved as a tab-delimited text file. Sorting by ProbeID should result in the list also being sorted by chromosome number and coordinate. To allow easy computer processing, chromosome numbers should be in Arabic numerals even though the convention for budding yeast is to use Roman numerals for chromosome numbers. This file needs to be prepared only once for each particular microarray platform and can subsequently be used for all experiments using that platform. Typically, we prepare this list by performing a batch BLAST search of the yeast genome using the vendor-provided list of probe sequences, discarding all sequences that either show more than one match to the genome or less than a perfect match. From the BLAST results, we extract the chromosome number and coordinate for the left end of each probe. The first row of the file should have column headers. The columns for chromosome number, coordinate (kb), and coordinate (bp) should be labeled "Chr," "Coord_kb," and "Coord_bp" (without the quotes) to match the file manipulations in Subheading 3.5, **step 12**.
2. A file containing a list of probes to exclude from the final analysis (e.g., probes corresponding to Ty element sequences), formatted as above: Again, this file needs to be prepared only once for each microarray platform.
3. The statistical software package R, available online at <http://cran.r-project.org/>.
4. The following set of commands saved as a plain-text file to be run in R (Subheading 3.5, **step 12**); name the file (for example)

"ssDNA_smoothing.R" (hanging indentations in the code text below indicate text that all belongs on one line):

```
# R script for loess smoothing of ssDNA/DSB data
files <- list.files(path = "path_to_ssDNA_or_DSB_files", full.
names = TRUE)
for(i in seq(along=files)) {
dataIn <- read.delim(files[i])
attach(dataIn)
Sphase_ratio_raw <- Sphase_raw/G1_raw
Sratio.loess <- loess(Sphase_ratio ~ Coord_kb, dataIn, span =
winSize/tail(Coord_kb, n=1))
Sratio.predict <- predict(Sratio.loess, Coord_kb)
dataOut <- data.frame(Chr, Coord_kb, Coord_bp, Sphase_
raw, G1_raw, Sphase_ratio_raw, Sphase_ratio_loess=Sratio.
predict)
write.table(dataOut, files[i], quote=FALSE, sep="\t",
eol="\r", row.names = FALSE)
detach(dataIn)
}
```

3 Methods

3.1 Cell Collection

1. Grow yeast cells in YPD medium at the appropriate temperature to log phase (at $OD_{660} = 0.25$) (*see* **Note 1**).
2. Add α-factor to the log-phase culture (at $OD_{660} = 0.25$) at 200 nM or 3 μM for *bar1* or *BAR1* strains, respectively.
3. Continue growing the cells until the percentage of unbudded cells reaches ≥90 % (*see* **Note 2**).
4. Collect an appropriate volume of cells as the G1 control sample by pouring the cells into an appropriate container, e.g., a 50-mL tube (for a small sample) or a 250-mL graduated cylinder (for a large sample), with 0.01 volumes of 10 % NaN_3 already added such that its final concentration would be 0.1 %. Store the G1 control sample on ice until further processing.
5. Add HU powder to the culture at 200 mM (*see* **Note 3**).
6. Add pronase to the culture at 0.02 mg/mL or 0.3 mg/mL for *bar1* or *BAR1* strains, respectively, to release cells from α-factor arrest (*see* **Note 4**).
7. Collect an appropriate volume of S-phase cells, typically after 1-h exposure to HU, similarly as described in **step 4** above. Multiple samples collected at other time intervals may be desired. Store the collected samples on ice until further processing.

3.2 Preparation of Genomic DNA in Agarose Plugs

3.2.1 Preparation of Cells Embedded in Agarose Plugs

1. Centrifuge the collected samples in swing bucket rotors (e.g., TX-750 rotor) at 2,500 × *g* for 10 min at 4 °C.
2. Wash the cell pellets with 10 mL of 50 mM EDTA and centrifuge again. Repeat once.
3. Resuspend the cell pellets with 1 mL of 50 mM EDTA and transfer to a 1.5-mL microcentrifuge tube.
4. Centrifuge in a tabletop microcentrifuge at ~2,500 × *g* for 5 min at 4 °C. Aspirate the liquid thoroughly, and resuspend the cells in 50 mM EDTA to a final concentration of 2×10^9 cells/mL. Measure the volume of cell suspension with a pipette.
5. Add equal volume of 1 % low-melt InCert agarose pre-warmed to 42 °C (*see* **Note 5**). Mix thoroughly, and quickly pipet 100 μL aliquots into each well of the plug molds to harden at room temperature (*see* **Note 6**).
6. Extrude each plug from the plug molds into a 6-well plate containing 6 mL of TE with a maximum of three plugs per 6 mL TE. The plugs can be stored at 4 °C for up to 48 h before spheroplasting.

3.2.2 Spheroplasting in Agarose Plugs

1. Make fresh spheroplasting solution.
2. Aspirate the TE buffer from the 6-well plates containing plugs, and add 6 mL of fresh spheroplasting solution to each well.
3. Incubate with gentle shaking for 4 h at 37 °C.
4. Aspirate off the spheroplasting solution, and add 6 mL of 1× SDS solution for plugs.
5. Incubate with gentle shaking for at least 15 min at 37 °C.
6. Exchange the 1× SDS solution with 6 mL of fresh 1× SDS solution.
7. Incubate with gentle shaking overnight at 37 °C.
8. Aspirate the 1× SDS solution.
9. Wash the plugs twice with 6 mL of 1× NDS solution with 30 min with gentle shaking at room temperature.
10. Wash the plugs three times with 6 mL of TE for 30 min with gentle shaking at room temperature.
11. Add 6 mL of fresh TE to each well. Cover the plate with plastic wrap. The samples can be stored at 4 °C for up to 6 months. Exchange with fresh TE periodically.

3.3 In-Gel Labeling of ssDNA or DSBs and DNA Extraction and Purification

3.3.1 In-Gel Random-Primed Labeling of ssDNA by Klenow Fragment (3′–5′ Exo-)

1. Make fresh 1× ssDNA labeling reaction buffer from 10× stock.
2. Transfer one plug from each sample collected at a specific time point to a well in a new 6-well plate, with one plug per well. Transfer the same number of plugs from the G1 control sample to the plate as well in order to pair each S-phase sample with a G1 control sample.
3. Wash the plugs twice with 5 mL of $TE_{0.1}$ per well for 15 min at room temperature with gentle shaking.
4. Wash the plugs twice with 5 mL of 1× ssDNA labeling reaction buffer per well for 30 min at room temperature with gentle shaking.
5. Assemble a small water chamber (to prevent desiccation of the agarose plugs) using an emptied 1-mL pipette tip box with approximately 50 mL AGD H_2O added to the bottom. Cut a piece of parafilm, and place it on the tip rack, marking the position/sample name on the edge of the parafilm to indicate where the plugs would be positioned.
6. During the last step of washing, prepare the ssDNA labeling reaction mix. For each plug (~50 μL), mix the following (*see* **Note 7**): 10 μL of 10× dNTP mix, 20 μL of 2.5× ssDNA labeling reaction buffer stock, 6 μL of Cy5- or Cy3-dUTP, 3 μL of 50,000 units/mL Klenow Fragment (3′–5′ exo-), and 11 μL of AGD H_2O.
7. Transfer the plugs onto the parafilm according to the arranged position with a clean spatula.
8. Pipet 50 μL of the ssDNA labeling reaction mix onto each agarose plug (generally Cy5 for G1-phase sample and Cy3 for S-phase sample).
9. Close the tip box, and incubate the reactions for 2–3 h in the dark at 37 °C.

3.3.2 In-Gel End Repair by the End-It™ Kit (T4 DNA Polymerase)

1. Prepare fresh 1× end-repair labeling reaction buffer from 10× stock.
2. Transfer one plug from each sample collected at a specific time point to a well in a new 6-well plate, with one plug per well. Transfer the same number of plugs from the G1 control sample to the plate as well in order to pair each S-phase sample with a G1 control sample.
3. Wash the plugs twice with 5 mL of $TE_{0.1}$ per well for 15 min at room temperature with gentle shaking.
4. Wash the plugs twice with 5 mL of 1× end-repair labeling reaction buffer per well for 15 min at room temperature with gentle shaking.
5. Assemble a small water chamber (to prevent desiccation of the agarose plugs) using an emptied 1-mL pipette tip box with

approximately 50 mL AGD H_2O added to the bottom. Cut a piece of parafilm, and place it on the tip rack, marking the position/sample name on the edge of the parafilm to indicate where the plugs would be positioned.

6. During the last step of washing, prepare the end-repair labeling reaction mix. For each plug (~50 μL), mix the following (*see* **Note 7**): 5 μL of 10× end-repair buffer (from the End-It™ end-repair kit), 10 μL of 10 mM ATP (from the End-It™ end-repair kit), 10 μL of 10× dNTP mix, 6 μL of Cy5- or Cy3-dUTP, 3 μL of End-It™ Enzyme mix, and 16 μL of AGD H_2O.
7. Transfer the plugs onto the parafilm according to the arranged position with a clean spatula.
8. Pipet 50 μL of the end-repair labeling reaction mix onto each agarose plug (generally Cy5 for G1-phase sample and Cy3 for S-phase sample).
9. Close the tip box, and incubate the reactions for 1–1.5 h in the dark at 25 °C.

3.3.3 Extract and Purify DNA from Agarose Plug

The following steps should be performed in dim light to prevent inactivation of the Cy dyes.

1. Transfer plugs from the parafilm into a new 6-well plate with one plug per well. Wrap the plate in aluminum foil to prevent light exposure; do likewise for the subsequent steps.
2. Wash the plugs twice with 5 mL of $TE_{0.1}$ for 15 min at room temperature with gentle shaking.
3. Equilibrate the plugs twice with 200 μL of 1× β-Agarase buffer for 30 min at 0–4 °C (by placing the 6-well plate on ice) with gentle shaking.
4. Transfer one G1- and one S-phase plug into the same 1.5-mL microcentrifuge tube with a clean spatula (*see* **Note 8**).
5. Melt the plugs for 10 min in a 65 °C water bath with occasional mixing to encourage melting (*see* **Note 9**).
6. Equilibrate the melted plugs for 10 min in a 42 °C water bath.
7. Add 2 μL of β-Agarase to each tube, and incubate for 1 h at 42 °C.
8. Centrifuge the mix in a tabletop microcentrifuge at >17,000 × *g* for 20 min at 4 °C.
9. Transfer the supernatant to a fresh 1.5-mL microcentrifuge tube.
10. Sonicate the mix to shear the DNA by Bioruptor ("low" setting, 30 s ON and 30 s OFF, 30 cycles, 4 °C).
11. Purify the DNA by the QIAquick PCR Purification Kit following the manufacturer's instructions.

12. Elute the DNA from each pair of pooled samples with 45 μL of EB buffer.
13. Measure the DNA concentration using a NanoDrop ND-2000 spectrophotometer (*see* **Note 10**). The labeled DNA is ready for hybridization or can be stored in the dark at 4 °C overnight.

3.4 Microarray Hybridization and Data Extraction

1. Hybridize the labeled DNA onto Agilent ChIP-to-chip yeast microarray slides following the manufacturer's instructions.
2. Extract data with the Feature Extraction software (Agilent).

3.5 Generating an ssDNA or a DSB Profile for Each Chromosome in the Yeast Genome

1. Duplicate the data file from Subheading 3.4, **step 2**. Leave the original file untouched as an archival copy; give the duplicate file a distinctive name, and perform all further manipulations on this duplicate.
2. Open the file in Microsoft Excel (or equivalent), and delete the first rows of descriptors, if any, so that the row of column headers (ProbeID, ProbeName, etc.) becomes the first row.
3. Select all the data in the file and sort by ProbeID (ascending sort).
4. Delete the rows corresponding to hybridization control spots (rows 2–331 for Agilent 4×44 ChIP arrays).
5. Delete the rows corresponding to mitochondrial DNA probes (the rows at the end of the data table). *Important: Perform this step only if you have eliminated mitochondrial DNA probes from the list of probe coordinates in file ProbeCoordinates.txt (see Subheading 2.5, **item 1**). If you have retained mitochondrial DNA probe information in Subheading 2.5, **item 1**, you must retain the corresponding rows in the data file from **step 4** above.* At this point, the number of rows of data in this file should correspond exactly to the number of rows of probe coordinates in file ProbeCoordinates.txt.
6. Optional step: Delete columns that you will not be using, so as to reduce the file size and speed subsequent manipulations. Typically, we only retain the following columns: ProbeName, gProcessedSignal, rProcessedSignal, gMedianSignal, rMedianSignal, gBGMedianSignal, and rBGMedianSignal.
7. With the data still sorted by ProbeID, insert the list of genomic locations (chromosome and coordinates, file ProbeCoordinates from Subheading 2.5, **item 1**) as the leftmost columns in the table (i.e., after this step, the chromosome number will be in column 1 and coordinates as kb and bp will be in columns 2 and 3, respectively). Because the data file (*see* **step 6** above) and the list of coordinates (ProbeCoordinates.txt) were both sorted in ascending order by ProbeID, each row of microarray data is now identified by its genomic location. Save the file as tab-delimited text, and continue.

8. Identify the "ProcessedSignal" columns corresponding to the G1-DNA and ssDNA or DSB-DNA channels. For example, if G1-DNA was labeled with Cy5, the column corresponding to the G1-DNA signal will be the column labeled "rProcessedSignal." For convenience and for future manipulations, re-label these two columns in the file as "G1_raw" and "Sphase_raw."
9. Use the exclusion list (Subheading 2.5, **item 2**) to eliminate the rows corresponding to genomic locations you wish to exclude from the final output (*see* **Note 11**).
10. Split the file by chromosome; that is, create a set of files, each containing the data for just one chromosome but retaining the column headers (Chr, Coord_kb, etc.) from the source file. Create a sub-folder, and save each file as tab-delimited text within that folder. For clarity, save each file with a common base name, differing only in a numerical index indicating the chromosome corresponding to that file (e.g., chr01_ssDNA.txt, chr02_ssDNA.txt) (*see* **Note 12**).
11. Using a text editor, open the text file "ssDNA_smoothing.R" created in Subheading 2.5, **item 4**. In this file, replace "path_to_ssDNA_or_DSB_files" with the actual path to the folder containing the files saved after splitting the data by chromosome; retain the quotes surrounding the folder path. Replace "winSize" with the desired smoothing window in kb (but "winSize" should be replaced just by the numerical value of the desired window and should not contain the text "kb"). Typically, for ssDNA and DSB DNA profiles, we use a smoothing target window of 6 kb. Save the text file (*see* **Notes 13** and **14**).
12. Smooth the ssDNA or DSB-DNA data for each chromosome by running the following batch command in the unix shell after navigating to the folder/directory containing the file "ssDNA_smoothing.R" (*see* **Note 15**):

    R CMD BATCH ssDNA_smoothing.R

    The command will invoke the R script and apply loess smoothing to the data, appending a column of raw S-phase/G1 ratios and a column of smoothed data values to the file for each chromosome. The columns with raw and smoothed S-phase/G1 ratios will have the labels, "Sphase_ratio_raw" and "Sphase_ratio_loess," respectively.
13. Using the graphing application of your choice, plot the data for each chromosome (Sphase_ratio_loess as a function of Coord_kb or Coord_bp). Set the *x*-axis dimension to some constant scaling factor (e.g., 1 cm = 100 kb) such that profiles for all chromosomes are on the same scale.
14. *See* Figs. 2 and 3 for a sample plot of ssDNA and DSB, respectively.

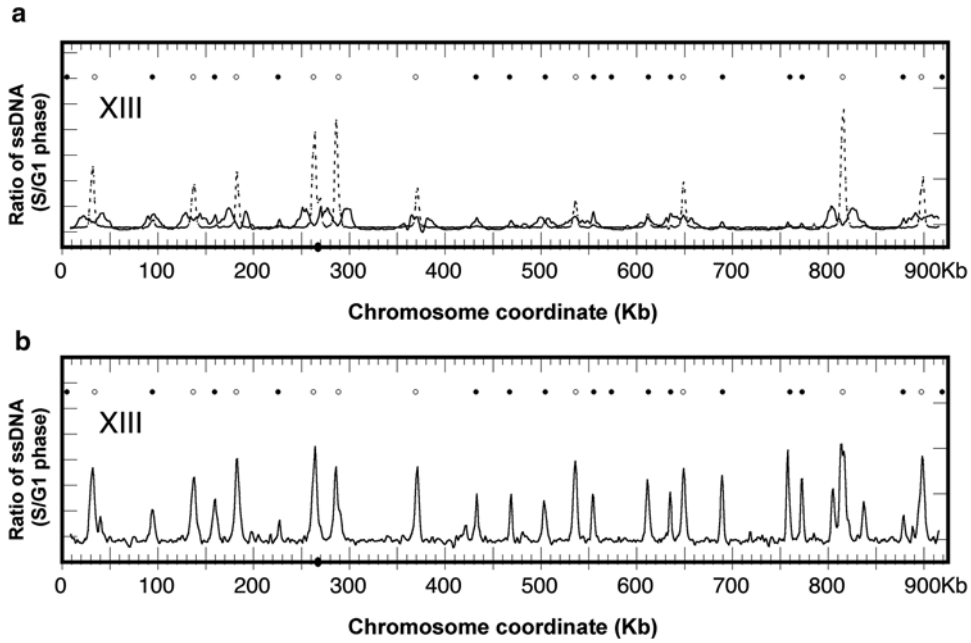

Fig. 2 ssDNA profiles of chromosome XIII. (**a**) ssDNA profiles for WT (W303) cells synchronously released into S phase in YPD containing 200 mM HU for 1 h (*dashed line*) and 3 h (*solid line*). ssDNA migrates away from the origins bidirectionally during the 2-h period between sample collections. (**b**) ssDNA profile for isogenic *rad53K227A* mutant cells [1] after synchronously released into S phase in YPD containing 200 mM HU for 1 h. In both plots, *solid* and *open circles* represent previously defined Rad53-checked and Rad53-unchecked replication origins, respectively [2]. The *dot* on the *x*-axis denotes the centromere

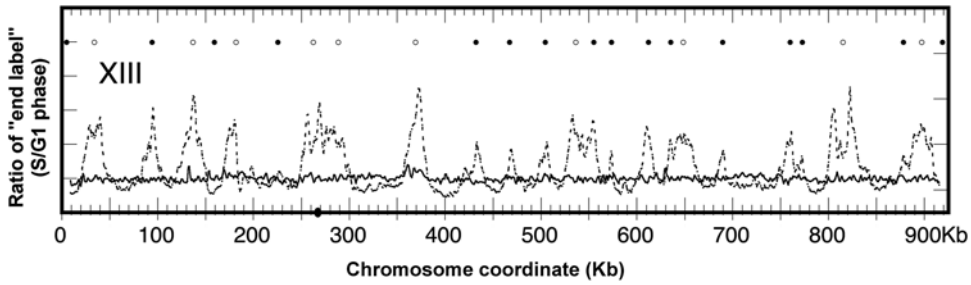

Fig. 3 DSB profiles of chromosome XIII for WT (A364a, *solid line*) and an isogenic *mec1-1 sml1-1* mutant (*dashed line*) after transient exposure to 200 mM HU for 1 h and recovery for 2 h, respectively. In both plots, *solid* and *open circles* represent previously defined Rad53-checked and Rad53-unchecked replication origins, respectively [2]. The *dot* on the *x*-axis denotes the centromere

4 Notes

1. Inoculate the cells in 5 mL of YPD medium and culture overnight. The culture may or may not reach saturation depending on the generation time of the strain at the chosen culturing temperature. Then, inoculate cells from the primary culture into 25 mL of YPD medium and measure the generation time. Based on the generation time and the cell density of the 25 mL culture, inoculate the cells from the 25 mL culture into fresh YPD medium with a volume that is appropriate for sample collection. Determine culture volume based on the number of agarose plugs per sample desired. We typically obtain three agarose plugs per 50 mL of culture at ~10^7 cells/mL. Bear in mind that each S-phase sample is to be paired with a G1 control sample for co-hybridization onto the microarray; therefore, one must collect a larger sample for the G1 control accordingly. The amount of ssDNA or DSBs in a given strain is also an important point for consideration, which might require experimental trials to determine the optimal amount of cells to utilize in the microarray analysis.
2. Transfer 1 mL of the culture to a 1.5-mL microcentrifuge tube. Sonicate the culture by Bioruptor ("low" setting, 30 s ON and 30 s OFF, two cycles). Pipet 2 μL of the culture onto a microscope slide, and cover it with a cover glass. Then count the number of budded cell in a minimum of total 200 cells counted.
3. Weigh HU and deliver into the culture via a weighing boat or a piece of folded weighing paper while tilting the culturing flask to prevent the powder from sticking to the neck of the vessel. Mix well by swirling the culture vigorously. HU should dissolve in 1–2 min.
4. Weigh the pronase powder and dissolve in AGD H_2O before use. It can be temporally stored on ice.
5. Melt the 1 % low-melt InCert or NuSieve agarose by heating in the microwave, taking precautions not to let the solution boil over. Equilibrate to 42 °C in a water bath for at least 1 h.
6. Hold the microcentrifuge tube containing the mix tightly to keep the mix warm, quickly pipet to mix, and then transfer into the plug mold. Avoid bubbles during pipetting.
7. The apparent final concentration of dNTP mix is 2×, but the final concentration is 1× considering further dilution from the gel volume (~50 μL) as the dNTP mix is not included in the equilibration step.
8. As the G1- and S-phase sample are subjected to co-hybridization onto the microarray, pooling them at this step is acceptable.

However, we recommend assessing the efficiency of DNA extraction from the gel from each independent sample first for quality control.

9. Longer incubation time might be necessary. Up to 20 min has been tested and proven acceptable.
10. The incorporation of Cy-dUTP using the ssDNA labeling method typically yields ~1.5 pmol/μL, while the incorporation of Cy-dUTP using the DSB labeling method is often tenfold lower. Scaling up the samples for each microarray labeling is recommended.
11. This step can be accomplished using a scripting language such as Perl or Python, or Microsoft Office VBA for Applications, depending on the investigator's skill/comfort with such languages. Alternatively, it can be accomplished using Microsoft Excel and Microsoft Word without any scripting. For example, each open reading frame (ORF) in the exclusion list can be converted to a pair of rows in the file: one row containing the chromosome number and start coordinate for that ORF and containing the word "START" as a third field in that row, and one row with the chromosome number and the end coordinate and containing the word "END" as the third field for that row. This list of start and end coordinates can be appended to the data file and whole file sorted by chromosome and coordinate and saved as a tab-delimited text file. Now, each set of probes to be excluded will be preceded by a row containing the word "START" and followed immediately by a row containing the word "END." Next, using the "Advanced Find and Replace" command with wild card searching enabled in Microsoft Word, the rows between each START…END pair can be deleted. Using Microsoft Excel again to sort the data, the lines containing START and END can be grouped and deleted, leaving just the desired microarray data.
12. The next step (the smoothing step) will result in alteration of the input file, so we recommend making an archival copy of the files before performing the smoothing operation.
13. Although the R script is called ssDNA_smoothing.R, the same script will work for smoothing DSB-DNA data also.
14. Be aware that unix, Microsoft Windows, and Apple Macintosh files typically use different line delimiters. For example, Macintosh files typically use carriage returns (ASCII character 13) to signify line endings, while unix files use the "linefeed" character (ASCII character 10). So, some experimentation with line delimiters within the R script file and in the output files defined in the R script file may be necessary to find the appropriate format for the system being used. For example, the

"end-of-line" (eol) definition in the R script (*see* **item 4** of Subheading 2.5) can be changed from "\r" (carriage-return) to "\n" (linefeed).

15. The R batch command syntax is appropriate for unix systems, e.g., to be run in the Terminal application in Mac OS X. The same batch file (ssDNA_smoothing.R) will also work in Windows systems, but the syntax to invoke the file will have to be modified appropriately.

Acknowledgements

This work was supported by NIH grant 4R00GM08137804 to W.F. and NIGMS grant 18926 to M.K.R.

References

1. Sogo JM, Lopes M, Foiani M (2002) Fork reversal and ssDNA accumulation at stalled replication forks owing to checkpoint defects. Science 297(5581):599–602
2. Feng W, Collingwood D, Boeck ME, Fox LA, Alvino GM, Fangman WL, Raghuraman MK, Brewer BJ (2006) Genomic mapping of single-stranded DNA in hydroxyurea-challenged yeasts identifies origins of replication. Nat Cell Biol 8(2):148–155
3. Feng W, Di Rienzi SC, Raghuraman MK, Brewer BJ (2011) Replication stress-induced chromosome breakage is correlated with replication fork progression and is preceded by single-stranded DNA formation. G3 (Bethesda) 1(5):327–335
4. Di Rienzi SC, Lindstrom KC, Mann T, Noble WS, Raghuraman MK, Brewer BJ (2012) Maintaining replication origins in the face of genomic change. Genome Res 22(10):1940–1952

Chapter 28

Chromatin Fractionation Analysis of Licensing Factors in Mammalian Cells

Hideo Nishitani, Masayuki Morino, Yusuke Murakami, Takeshi Maeda, and Yasushi Shiomi

Abstract

ORC, Cdc6, Cdt1, and MCM2-7 are replication-licensing factors, which play a central role in the once-per-cell cycle control of DNA replication. ORC, Cdc6, and Cdt1 collaborate to load MCM2-7 onto replication origins in order to license them for replication. MCM2-7 is a DNA helicase directly involved in DNA replication and dissociates from DNA as S phase progresses and each replicon is replicated. In the cell cycle, the loading of MCM2-7 is restricted during the end of mitosis and the G1 phase. Thus, the levels of chromatin-bound MCM2-7 and its loaders oscillate during the cell cycle. Chromatin association of these factors can be analyzed by separating a cell lysate into soluble and chromatin-enriched insoluble fractions in mammalian cells.

Key words Replication licensing, Pre-RC, Chromatin, Replication foci, MCM2-7, Cdt1, Cdc6, ORC, PCNA

1 Introduction

Chromosome replication is a major event in the cell cycle. Eukaryotic chromosomes are composed of multiple replication units, called replicons, each of which contains a replication origin. Before replication starts, MCM2-7 is loaded onto chromatin, and origins are licensed for replication [1–3]. MCM2-7, a hexamer composed of six Mcm proteins (Mcm2–Mcm3–Mcm4–Mcm5–Mcm6–Mcm7), is the DNA helicase complex essential for initiation of DNA replication. MCM2-7 is activated at the onset of S phase; DNA is unwound, and replication is then initiated. To ensure genomic integrity, the chromosome must replicate precisely, and replication must be restricted to occur once and only once in the cell cycle. If whole chromosomes are re-replicated more than once, the result is an increase in ploidy. Even re-replication from a single origin may cause genome instability. These abnormalities in replication can cause malignant transformation of cells.

Eishi Noguchi and Mariana C. Gadaleta (eds.), *Cell Cycle Control: Mechanisms and Protocols*, Methods in Molecular Biology, vol. 1170, DOI 10.1007/978-1-4939-0888-2_28,

To prevent such illegitimate chromosomal replication, origin licensing (i.e., chromatin loading of MCM2-7) is tightly controlled in the cell cycle such that it is allowed only during the end of mitosis and in the G1 phase [1–3].

Replication origins are bound by the origin recognition complex (ORC) to mark the replication initiation sites. Late in mitosis or early in the G1 phase of the cell cycle, Cdc6 and then Cdt1 are recruited to the ORC. They then load the MCM2-7 onto origins to assemble a pre-replicative complex (pre-RC), and thus origins are "licensed" for DNA replication [1–3]. Therefore, ORC, Cdc6, Cdt1, and MCM2-7 are all called DNA replication-licensing factors. When loaded, MCM2-7 is detected as a head-to-head double hexamer surrounding the DNA [4], but it is inactive as a DNA helicase until the onset of S phase. Activation of S-phase cyclin-dependent kinase (S-CDK) and DDK (Dbf4-dependent protein kinase, also known as the Cdc7 kinase) brings about the recruitment of Cdc45 and GINS to MCM2-7. The multiprotein complex thus formed, called the CMG complex, is now active as a replicative helicase [5–7].

Following its activation, the MCM2-7 complex functions as a core of the active CMG helicase complex, unwinding the double-helix DNA at the origin, and single-stranded DNA (ssDNA) is produced. DNA polymerase alpha/primase is recruited to the ssDNA to synthesize primer DNA. Proliferating cell nuclear antigen (PCNA) is loaded to the primer template junction and functions to tether and assist DNA Pol ε and DNA Pol δ for leading and lagging strand synthesis, respectively [8–10]. In this manner, DNA replication is initiated and the origin is "fired." After unwinding DNA at origin, the MCM2-7 complex moves away from the origin, continuing unwinding of the dsDNA at the front of the replication fork by translocating on the ssDNA in the 3′–5′ direction for chain elongation [11]. When each replicon is fully replicated, MCM2-7 is displaced from the DNA, and PCNA is also unloaded. On the other hand, once MCM2-7 leaves the origins, origins attain a post-replicative state and cannot be reloaded with MCM2-7 in the same cell cycle, because pre-RC assembly is prevented after the onset of S phase. This is the essence of the licensing control for the prevention of re-replication of DNA [12, 13]. In mammalian cells, Cdt1 is inactivated by multiple means, namely, ubiquitin-mediated proteolysis and geminin binding [12, 13]. Proteolytic control ensures that Cdt1 is present only from M phase and in G1 phase [14]. The Cdt1 inhibitor geminin accumulates from S phase and is present until M phase [14] (Fig. 1). Thus, as chromosomes are replicated during S phase, the levels of chromatin-bound MCM2-7 decrease. When DNA replication is completed, there is no MCM2-7 on chromatin in G2 cells. The new round of MCM2-7 loading is allowed only after the completion of mitosis.

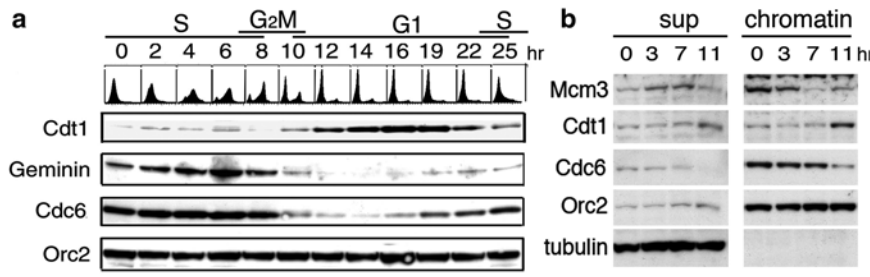

Fig. 1 Cell cycle-dependent association of licensing factors (synchronized cell culture prepared by double-thymidine block and release). (**a**) Oscillation of protein levels in a synchronized cell culture (adapted from ref. 14). (**b**) Cells at the indicated time points were harvested. Cell lysates were prepared and separated into soluble (sup) and chromatin-enriched pellet (chromatin). Most Mcm3 protein is present on chromatin in early S phase (0 h). Its levels on chromatin decrease as S phase progresses, because MCM2-7 dissociates from replicated chromatin regions. In G2 phase (7–8 h), Mcm3 was detected in the supernatant. When cells entered G1 phase (10 h), the chromatin levels of Mcm3 again increased owing to the next round of licensing event

On the other hand, control of chromatin association of ORC and Cdc6 is not well characterized in terms of the once-per-cell cycle control of replication. The ORC complex is composed of six subunits (Orc1–6). It appears that Orcs 2–5 are bound on chromatin throughout the cell cycle, but that Orc1 is degraded or dissociates from chromatin after the onset of S phase [15–17]. Thus, it is likely that Orc1 is also negatively regulated to prevent licensing during the S and G2 phases. Cdc6 is already associated with condensed chromatin during M phase, whereas Cdt1 interacts with chromatin as cells complete mitosis (Fig. 2) [18]. Curiously, Cdc6 is then degraded during early G1 phase by anaphase-promoting complex/cyclosome (APC/C)-dependent ubiquitination [19] (Figs. 1 and 2). Thus, licensing is performed in a small window between the end of mitosis and early G1 phase before Cdc6 is degraded [18] (Fig. 2c). Cdc6 starts to accumulate at a later stage in G1 phase and is present during the rest of the cell cycle. As cells enter into S phase, Cdc6 is phosphorylated by S-CDK. Part of Cdc6, probably in soluble form, is exported into the cytoplasm, while part remains associated with chromatin [15, 20]. Association of Cdt1 with chromatin starts as cells complete mitosis. Its levels on chromatin increase during G1 phase and then decrease after the onset of S phase owing to its proteolysis.

In this chapter, we describe a simple chromatin fractionation method to measure the chromatin-bound levels of licensing factors, mostly of MCM2-7, during the mammalian cell cycle. Cells are collected at specific stages, lysed, and separated into soluble and chromatin-containing insoluble pellet fractions after centrifugation. Similar methods can be used to investigate the behavior of other chromatin-binding factors.

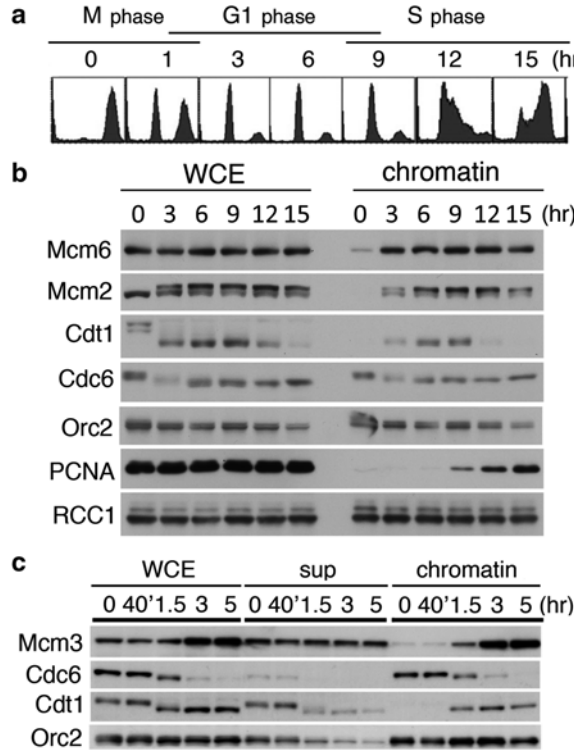

Fig. 2 Chromatin association of licensing factors in the cell cycle (synchronized cell culture from M phase). (**a**) Flow cytometry analysis of synchronized cell culture. HeLa cells were arrested in M phase with nocodazole treatment. Mitotic cells were collected, released synchronously after removal of nocodazole, and harvested at the indicated time points (in hours). Rough cell cycle positions are indicated. (**b**) As cells progress from M through G1 into S phase, levels of licensing factors oscillate. Flow cytometry analysis indicates that cells enter S phase about 9 h after release. Consistently, at this time point, the levels of chromatin-associated PCNA, a marker of DNA replication, started increasing. At 12 h when most cells have entered S phase, Cdt1 levels decreased owing to its degradation. As cells progress further into S phase, the chromatin levels of Mcm2 and Mcm6 also decreased owing to their dissociation from the replicated chromatin, whereas Orc2 and RCC1, which are used as controls, continuously stayed on the chromatin. Note that Cdt1 is highly phosphorylated in M phase (0 h) and migrates slowly. Cdc6 is also phosphorylated and migrates slowly in M phase. In contrast, phosphorylated Mcm2 migrates fast in M phase. (**c**) Licensing is established very early in G1 phase. Cells were collected at the indicated time points, and whole-cell extract (WCE) was prepared and separated into soluble (sup) and chromatin-containing pellet (chromatin) fractions. Levels of the indicated proteins were analyzed. Mcm3 was detected on the chromatin 1.5 h after release from M phase, indicating that licensing is established at the end of mitosis or early in G1 phase prior to the APC/C-dependent Cdc6 degradation. Note that Cdc6 is associated with chromatin from M phase (0 h), while Cdt1, phosphorylated and not associated with chromatin in M phase (0 h), is dephosphorylated as cells exit from M phase (1.5 h) and associates with chromatin

2 Materials

2.1 Synchronization of Mammalian Cells

1. HeLa cells: Cultured in Dulbecco's modified Eagle's medium with 10 % fetal bovine serum supplemented with 100 units/mL of penicillin and 0.1 mg/mL of streptomycin in a 5 % CO_2 atmosphere at 37 °C.
2. 0.1 M Thymidine: Dissolve 2.42 g thymidine in 100 mL distilled water. The solution must be sterilized through a 0.2-μm filter. Dispense 5–10 mL into sterilized tubes, and store them at −20 °C.
3. Phosphate-buffered saline (PBS): Dissolve 8 g of NaCl, 0.2 g of KCl, 1.44 g of Na_2HPO_4, and 0.24 g of KH_2PO_4 in 800 mL of H_2O. Adjust the pH to 7.4 with HCl. Add H_2O to 1 L.
4. 10 mg/mL Nocodazole: Dissolve in 1 mL of dimethyl sulfoxide, dispense in aliquots, and store at −20 °C.
5. Cell culture 60-mm dishes or 150-cm^2 culture flasks.
6. 15- and 50-mL conical tubes.

2.2 Fractionation Assay of Cell Lysate

1. PBS.
2. CSK buffer: 0.5 % Triton X-100, 0.1 M NaCl, 10 mM piperazine-N,N′-bis[2-ethanesulfonic acid] (PIPES) pH 7.0, 300 mM sucrose, 1 mM $MgCl_2$, 1 mM EDTA, 2 mM phenylmethylsulfonyl fluoride, 10 mM NaF, 20 mM β-glycerophosphate, 100 μM Na_3VO_4 (*see* **Note 1**), 1× complete protease inhibitor cocktail (Roche Diagnostics).
3. 2× Sodium dodecyl sulfate (SDS) sample buffer: 100 mM Tris–HCl pH 6.8, 4 % SDS, 0.02 % bromophenol blue, 20 % glycerol, 200 mM dithiothreitol.
4. Cell scraper.
5. 1.5-mL Tubes, 15-mL conical tubes.
6. Primary antibodies for Western blotting: Mcm2 (BD Transduction Laboratories, 610701), Mcm3 (Abcam, ab4460 and BD Pharmingen, 559543), Mcm6 (Santa Cruz Biotechnology, C-20), PCNA (Santa Cruz Biotechnology, PC-10), Orc2 (BD Pharmingen, 559266), Cdt1 (*see* **Note 2**), Cdc6 (Santa Cruz Biotechnology, 180.2, and Upstate (Millipore), DCS-180), RCC1 (*see* **Note 2**), α-tubulin (Sigma).

3 Methods

ORC, Cdc6, Cdt1, and MCM2-7 proteins are licensing factors for DNA replication. Among these, MCM2-7 is directly involved in DNA replication as a DNA helicase complex. MCM2-7 is present

throughout the cell cycle at almost constant levels [15, 21]; however, its chromatin association is tightly regulated in the cell cycle in order to initiate DNA replication at the proper time and also to prevent re-replication of DNA. This regulation is achieved mainly by controlling the MCM2-7 loader, Cdt1, as described in Subheading 1.

Chromatin association of licensing factors can be monitored by fractionating cell extracts by centrifuge. Chromatin-associated proteins are recovered in the insoluble pellet fraction. Using a synchronized cell culture, a change in the levels of licensing factors on the chromatin is determined by Western blotting.

3.1 Synchronization of Mammalian Cells

3.1.1 Preparation of Synchronized Cell Culture by a Double-Thymidine Block and Release (Fig. 1a)

1. Plate 3 mL of 4×10^5 HeLa cell suspension into the 60-mm dishes (*see* **Notes 3** and **4**), and let the cells adhere for 6–20 h at 37 °C.
2. Add 60 μL of 0.1 M thymidine to the culture medium dropwise (final 2 mM), mix well, and incubate for 15 h at 37 °C.
3. Wash cells with 3 mL of pre-warmed PBS two or three times.
4. Add 3 mL of pre-warmed fresh medium, and incubate for 9 h at 37 °C.
5. Add 60 μL of 0.1 M thymidine solution to the medium (final 2 mM), mix well, and incubate for 15 h (*see* **Note 5**). Cells are now synchronized at early S phase by the double-thymidine block.
6. Wash cells with 3 mL of pre-warmed PBS two or three times, and add fresh medium to release cells from the block synchronously into S phase (*see* **Note 4**).

3.1.2 Preparation of Synchronized Cell Culture by Nocodazole Arrest and Release (Fig. 2a)

1. Plate 1.5×10^6 of HeLa cells into a 150-cm^2 culture flask in 20 mL medium (*see* **Note 6**) and incubate for 6–20 h.
2. Add 400 μL of 0.1 M thymidine solution to the culture medium (final 2 mM), and incubate for 15–18 h to arrest cells in S phase.
3. Wash cells with 10 mL of pre-warmed PBS two or three times, and add 20 mL of pre-warmed medium.
4. After 2–3 h, add 20 μL of 0.1 mg/mL nocodazole (final concentration is 0.1 μg/mL) (*see* **Note 7**), and incubate for 8–12 h (cells are incubated for a total of 10–14 h after washing out thymidine).
5. Shake off mitotic cells by gently shaking or tapping the flask (*see* **Note 8**). Transfer cell suspension (around 20 mL) into a 50-mL conical tube.
6. Transfer a quarter of the mitotic cell suspension (about 5 mL) into a 15-mL conical tube, which is used for the fractionation assay to prepare mitotic cell samples (or "time 0 h" sample of

synchronized culture), and go to Subheading 3.2, **step 2** (*see* **Note 9**). The rest (three-quarters) of the cell suspension (about 15 mL in 50-mL conical tubes) is used to prepare synchronized cell cultures released from nocodazole arrest for the time points required for the research; then follow the next step.

7. Centrifuge the cells at 500 × *g* for 3 min.
8. Aspirate the medium, add 10 mL of fresh pre-warmed medium, suspend cells, and centrifuge again.
9. Aspirate the medium. Add 9 mL of pre-warmed medium, resuspend cells, and plate 3 mL of cell suspensions into three 60-mm dishes. Cells are now released synchronously from mitotic arrest into G1 phase, attach to the bottom of the dish, and then become flat. Incubate cells for desired time points (*see* **Note 6**).

3.2 Fractionation Assay

1. Scrape cells grown in a 60-mm dish (*see* **Note 10**), and collect cell suspension in a 15-mL tube. In the case of mitotic cell culture, cells are collected by shaking off as described in Subheading 3.1.2, **step 5**.
2. Centrifuge cells at 500 × *g* for 3 min.
3. Aspirate the medium. Add 3 mL of ice-cold PBS (*see* **Note 11**), resuspend the cells, and centrifuge as above. Repeat this cell-washing step once more.
4. Add 1 mL of PBS to the cell pellet, resuspend, and transfer the cell suspension into a 1.5-mL microfuge tube.
5. Centrifuge at 5,000 rpm (~2,000 × *g*) in a microfuge for 1 min, and remove the PBS (*see* **Note 12**).
6. Add 150 μL of CSK buffer, and lyse cells by pipetting up and down (*see* **Note 13**).
7. Keep on ice for 10–20 min while vortexing every 5 min.
8. After pipetting the lysate five more times, save 50 μL of lysate in a new tube as a whole-cell extract (WCE) sample.
9. Centrifuge the remaining lysate at 5,000 rpm (~2,000 × *g*) for 5 min in a microfuge (*see* **Note 14**).
10. Remove the supernatant, and transfer to a new tube (*see* **Note 15**). The pellet fraction is treated as described in the next step.
11. Add 200 μL of CSK buffer, and resuspend the pellet by pipetting (*see* **Note 16**).
12. Centrifuge at 5,000 rpm (~2,000 × *g*) for 5 min in a microfuge.
13. Remove the supernatant.
14. Resuspend the pellet in 100 μL CSK buffer and transfer 50 μL to a new tube (chromatin) (*see* **Note 17**).

15. Add 50 μL of 2× SDS sample buffer to the tube containing 50 μL WCE, and mix by pipetting up and down. Add 50 μL of 2× SDS sample buffer to the tube containing 50 μL of chromatin-containing fraction, and mix by pipetting up and down. When examining the soluble chromatin-unbound fraction, add 50 μL of 2× SDS sample buffer to the 50 μL of supernatant prepared in **step 10** of this section, and mix by pipetting up and down.
16. When sampling at different time points using synchronized cell culture, keep the tubes on ice until all the samples are prepared (*see* **Note 18**).
17. Heat the samples at 95–100 °C for 5 min, vortex, and heat for another 2 min.
18. Run the samples using SDS-PAGE (polyacrylamide gel electrophoresis) for Western blotting analysis.

4 Notes

1. CSK buffer is supplemented with phosphatase inhibitors NaF, β-glycerophosphate, and Na_3VO_4 because some licensing factors and their subunits are phosphorylated in a cell cycle-dependent manner. ATP may be included at 0.1–1 mM, because all subunits of MCM2-7, Cdc6, and some subunits of ORC are AAA^+ proteins.
2. The Cdt1 antibody described in [14] and the RCC1 antibody described in [22] are raised in rabbits in our laboratory.
3. Make sure that cells are plated evenly on the dish by shaking the dish slowly back and forth and left and right. Do not plate cells at high density; otherwise, cell cycle progression is altered.
4. Prepare dishes of cell cultures required for synchronous time course analysis. If samples will be prepared every 3 h over the course of a 12-h experiment, after the release from the block samples will be needed at 0, 3, 6, 9, and 12 h. Then, five dishes of synchronized cell culture are needed.
5. At this time, cells are arrested at early S phase ("time 0 h"). Cells are then released into S phase after removing thymidine as described in the next step (*see* Subheading 3.1.1, **step 6**). Instead of the second addition of thymidine, some researchers use aphidicolin, a DNA polymerase inhibitor, to more strictly arrest cells at the beginning of S phase. This alternative method is called thymidine–aphidicolin block.
6. Four dishes (60 mm) of mitotic cell cultures can be obtained from one 150-cm^2 flask. This allows for the collection of cells at four different time points, including 0 h. If more time points are needed, prepare more flasks of cells.

7. For HeLa cells, nocodazole can be added soon after washing out thymidine and incubated for 10–14 h. Nocodazole can be used at concentrations of about 0.04–0.4 μg/mL depending on the cell lines.
8. The mitotic HeLa cells become rounded up and detach easily from the dish. Normally, more than 80 % of cells are rounded up using the method described here. Instead of tapping, mitotic cells can be collected by gently washing the cells with the medium. The cells that remain attached to the dish are used as G2-phase cells.
9. The cell suspension prepared by mitotic shake-off as described here is used directly to prepare the mitotic cell sample for the fractionation assay. This is also a "time 0 h" sample of time course analysis when proteins are analyzed in the cell cycle using a synchronized cell culture made by nocodazole arrest and release. For fractionation, go to Subheading 3.2, **step 2**.
10. Synchronized cell cultures are prepared by a double-thymidine block or nocodazole arrest as described in this chapter. Cells can also be synchronized in G1 or G0 phase by incubation in growth medium with low serum.
11. All the processes after this step use ice-cold buffers and should be performed on ice.
12. When sampling at different time points using synchronized cell culture, the cell pellet can be kept frozen in liquid nitrogen until all the samples of time course analysis are prepared (all the cell pellets may be kept in a deep freezer for weeks). When all the samples have been collected, fractionation assays for all samples can be begun at the same time from Subheading 3.2, **step 6**.
13. Pipette up and down about 20 times. Be careful not to make air bubbles. Use the same number of pipetting strokes for all sample preparations. Make sure that there are no cell aggregates or cell debris. Cell lysis can be checked under a microscope.
14. This step is to separate the lysate into soluble supernatant and insoluble chromatin-enriched pellet. Chromatin-bound proteins are recovered in this pellet fraction.
15. The supernatant is used to prepare an SDS sample as a soluble protein fraction, which contains chromatin-unbound proteins.
16. Pipette up and down about ten times to resuspend and wash the pellet.
17. The method described here is for preparing chromatin-associated proteins by isolating the chromatin-enriched fraction in the pellet. The pellet also contains nuclear matrix proteins and protein aggregates. To make sure that the

protein of interest is actually associated with chromatin, the chromatin-bound protein may be released after DNase I treatment or micrococcal nuclease treatment as described elsewhere [16, 21].

18. As mentioned in **Note 12**, the cell pellets may be frozen after **step 5** (Subheading 3.2). **Step 6** can be started when all the samples for time course analysis have been prepared.

Acknowledgements

This work was supported by JSPS KAKENHI and MEXT KAKENHI, Grant in Aid from the Ministry of Education, Culture, Sports, Science, and Technology of Japan.

References

1. Bell SP, Dutta A (2002) DNA replication in eukaryotic cells. Annu Rev Biochem 71: 333–374
2. Nishitani H, Lygerou Z (2002) Control of DNA replication licensing in a cell cycle. Genes Cells 7(6):523–534
3. Blow JJ, Dutta A (2005) Preventing re-replication of chromosomal DNA. Nat Rev Mol Cell Biol 6(6):476–486
4. Remus D, Beuron F, Tolun G, Griffith JD, Morris EP, Diffley JF (2009) Concerted loading of Mcm2-7 double hexamers around DNA during DNA replication origin licensing. Cell 139(4):719–730
5. Ishimi Y (1997) A DNA helicase activity is associated with an MCM4, -6, and -7 protein complex. J Biol Chem 272(39): 24508–24513
6. Masai H, Arai K (2002) Cdc7 kinase complex: a key regulator in the initiation of DNA replication. J Cell Physiol 190(3):287–296
7. Ilves I, Petojevic T, Pesavento JJ, Botchan MR (2010) Activation of the MCM2-7 helicase by association with Cdc45 and GINS proteins. Mol Cell 37(2):247–258
8. Waga S, Stillman B (1998) The DNA replication fork in eukaryotic cells. Annu Rev Biochem 67:721–751
9. Masai H, Matsumoto S, You Z, Yoshizawa-Sugata N, Oda M (2010) Eukaryotic chromosome DNA replication: where, when, and how? Annu Rev Biochem 79:89–130
10. Leman AR, Noguchi E (2013) The replication fork: understanding the eukaryotic replication machinery and the challenges to genome duplication. Genes (Basel) 4(1):1–32
11. Fu YV, Yardimci H, Long DT, Ho TV, Guainazzi A, Bermudez VP, Hurwitz J, van Oijen A, Scharer OD, Walter JC (2011) Selective bypass of a lagging strand roadblock by the eukaryotic replicative DNA helicase. Cell 146(6):931–941
12. Machida YJ, Hamlin JL, Dutta A (2005) Right place, right time, and only once: replication initiation in metazoans. Cell 123(1):13–24
13. Arias EE, Walter JC (2007) Strength in numbers: preventing rereplication via multiple mechanisms in eukaryotic cells. Genes Dev 21(5):497–518
14. Nishitani H, Taraviras S, Lygerou Z, Nishimoto T (2001) The human licensing factor for DNA replication Cdt1 accumulates in G1 and is destabilized after initiation of S-phase. J Biol Chem 276(48):44905–44911
15. Mendez J, Stillman B (2000) Chromatin association of human origin recognition complex, cdc6, and minichromosome maintenance proteins during the cell cycle: assembly of pre-replication complexes in late mitosis. Mol Cell Biol 20(22):8602–8612
16. Mendez J, Zou-Yang XH, Kim SY, Hidaka M, Tansey WP, Stillman B (2002) Human origin recognition complex large subunit is degraded by ubiquitin-mediated proteolysis after initiation of DNA replication. Mol Cell 9(3):481–491
17. DePamphilis ML (2005) Cell cycle dependent regulation of the origin recognition complex. Cell Cycle 4(1):70–79

18. Clijsters L, Ogink J, Wolthuis R (2013) The spindle checkpoint, APC/CC(dc20), and APC/CC(dh1) play distinct roles in connecting mitosis to S phase. J Cell Biol 201(7): 1013–1026
19. Petersen BO, Wagener C, Marinoni F, Kramer ER, Melixetian M, Lazzerini Denchi E, Gieffers C, Matteucci C, Peters JM, Helin K (2000) Cell cycle- and cell growth-regulated proteolysis of mammalian CDC6 is dependent on APC-CDH1. Genes Dev 14(18):2330–2343
20. Saha P, Chen J, Thome KC, Lawlis SJ, Hou ZH, Hendricks M, Parvin JD, Dutta A (1998) Human CDC6/Cdc18 associates with Orc1 and cyclin-cdk and is selectively eliminated from the nucleus at the onset of S phase. Mol Cell Biol 18(5):2758–2767
21. Fujita M, Yamada C, Tsurumi T, Hanaoka F, Matsuzawa K, Inagaki M (1998) Cell cycle- and chromatin binding state-dependent phosphorylation of human MCM heterohexameric complexes. A role for cdc2 kinase. J Biol Chem 273(27):17095–17101
22. Nishitani H, Ohtsubo M, Yamashita K, Iida H, Pines J, Yasudo H, Shibata Y, Hunter T, Nishimoto T (1991) Loss of RCC1, a nuclear DNA-binding protein, uncouples the completion of DNA replication from the activation of cdc2 protein kinase and mitosis. EMBO J 10(6):1555–1564

Chapter 29

Imaging Analysis to Determine Chromatin Binding of the Licensing Factor MCM2-7 in Mammalian Cells

Masayuki Morino, Miyuki Tanaka, Yasushi Shiomi, and Hideo Nishitani

Abstract

S-CDK and DDK protein kinases initiate DNA replication at replication origins. Prior to the activation of these kinases, origins must become competent for replication by loading MCM2-7 DNA helicase on chromatin. This process is known as replication licensing or pre-replicative complex (pre-RC) formation. After the onset of S phase, however, licensing is inhibited to prevent re-replication of DNA. In this chapter, we describe a method to analyze origin licensing by imaging the chromatin-bound licensing factor MCM2-7. In a normal cell cycle, MCM2-7 is loaded at the end of mitosis or early G1 phase. As S phase progresses, MCM2-7 is dissociated from the replicated regions. When DNA replication is completed, cells in G2 phase have no chromatin-bound MCM2-7. The analysis of chromatin-bound MCM2-7 in each cell provides an insight into cell cycle stage and condition for cell cycle.

Key words Replication licensing, Pre-RC, Replication foci, MCM2-7, PCNA, Cdt1, Cell extraction, Fixation, Immunofluorescence

1 Introduction

Replication of chromosomes is a key event in the cell cycle. Chromosomes are replicated once and only once in a cell cycle to maintain genome integrity. This is achieved by the DNA replication licensing control, which regulates the loading of MCM2-7 DNA helicase in the cell cycle. Replication in eukaryotes is initiated from specific sites on the chromosomes called replication origins. The origins become licensed for replication when the pre-replicative complex (pre-RC) is assembled. Origins are bound by the origin recognition complex (ORC). At the end of mitosis or early G1 phase of the cell cycle, Cdc6 and Cdt1 associate with the ORC and then load the MCM2-7 complex on origins [1–3]. Before loading onto DNA, the MCM2-7 complex forms a single hexamer ring, which is composed of the MCM2 to MCM7 proteins [4, 5]. Once loaded, MCM2-7 is detected as a head-to-head double hexamer surrounding the DNA [6]. At this stage, origins are fully assembled

Eishi Noguchi and Mariana C. Gadaleta (eds.), *Cell Cycle Control: Mechanisms and Protocols*, Methods in Molecular Biology, vol. 1170, DOI 10.1007/978-1-4939-0888-2_29,

with the pre-RC and thus considered to be "licensed" for DNA replication. Therefore, ORC, Cdc6, Cdt1, and MCM2-7 are all called *DNA replication licensing factors*. Among them, MCM2-7 plays a key role during DNA replication. MCM2-7 is a DNA helicase, but it is inactive until the onset of S phase. Following the activation of S-phase CDK (S-CDK) and DDK (Dbf4-dependent protein kinase, also known as the Cdc7 kinase), Cdc45 and GINS associate with MCM2-7 to form the active replicative helicase complex termed the CMG complex [7–9].

MCM2-7, as a part of the active CMG complex, unwinds the double-helix DNA at the origin and produces single DNA strands, which act as templates for DNA polymerase α/primase. These events lead to DNA replication initiation, often known as "origin firing" [10–13]. Following initiation, MCM2-7 complexes move bidirectionally away from origin, acting as a replicative DNA helicase in the direction of 3′–5′ at the front of the replication fork for the process of elongation steps during DNA replication [14]. Once each replication unit (replicon) is fully replicated, MCM2-7 is displaced from the DNA. Conversely, MCM2-7 cannot be reloaded at origins, because pre-RC assembly is prevented during S phase. This is a key mechanism to prevent re-replication of DNA [1–3, 15, 16]. In metazoans, for example, Cdt1 is inactivated in 2 ways, ubiquitin-mediated proteolysis and geminin binding [15, 16]. Thus, MCM2-7 loaded on chromatin in G1 phase dissociates progressively from the chromatin as chromosomes are replicated during S phase.

S-phase cells can be identified by incorporation of thymidine analogues (such as 5-bromo-2′-deoxyuridine, BrdU) or by staining proliferating cell nuclear antigen (PCNA). Originally identified as a cofactor for DNA polymerases, PCNA is a homotrimer ring-shaped complex, belonging to the family of DNA sliding clamps. When double-stranded DNA is unwound and primer DNA is made on the single-stranded template DNA, PCNA is loaded at the primer-template junction by the clamp loader complex, replication factor C (RFC) complex [10]. When loaded on chromatin, PCNA encircles and freely slides along the DNA double helix, acting as a platform for a large number of proteins involved in chromosome duplication at the replication fork [17]. The nuclear sites detected with anti-BrdU antibodies after brief exposure to BrdU directly represent the DNA replication sites. The sites having chromatin-bound PCNA also represent the sites where DNA replication factories are present and normally overlap with BrdU staining [18].

All origins do not fire at the same time in S phase. Origins located at euchromatic regions normally fire early in S phase, while origins at heterochromatic regions fire late [19]. Thus, cells show typical nuclear staining patterns of BrdU and PCNA during the discrete stages of S phase, i.e., early, mid, and late S phases. Therefore, BrdU and PCNA are excellent markers not only for

detecting S-phase cells but also for identifying the stage of cells during S phase [19, 20].

In this chapter, we describe a simple imaging method to detect the distribution pattern of chromatin-bound MCM2-7 during the cell cycle by immunofluorescence. Presence of chromatin-bound MCM2-7 represents licensed replication origins in G1 phase, whereas in S phase, it represents ongoing replication sites and licensed origins that have not yet fired. Chromatin-bound MCM2-7 can be determined by immunolocalization of Mcm proteins after cells were pre-extracted, i.e., treated with detergent (such as Triton X-100) before fixation. The pre-extraction of cells removes most of the soluble proteins, but chromatin-bound proteins remain associated with the nucleus. Because this pre-extraction step also leaves chromatin-bound PCNA, PCNA staining can be used to identify S-phase cells and ongoing replication sites within S-phase nuclei. Thus, dual staining of cells with PCNA and Mcm proteins provides a useful analysis of licensed state for individual cells during cell cycle progression [21, 22].

2 Materials

1. HeLa cells: Cultured in Dulbecco's modified Eagle's medium (DMEM) with 10 % fetal bovine serum supplemented with 100 units/mL of penicillin and 0.1 mg/mL of streptomycin in a 5 % CO_2 atmosphere at 37 °C.
2. Sterile forceps: Sterilize by flaming forceps with gas burner before use.
3. Glass coverslip: Sterilize by baking in an oven at 180 °C for 2 h (*see* **Note 1**).
4. 35-mm culture dishes.
5. Phosphate-buffered saline (PBS). Dissolve 8 g of NaCl, 0.2 g of KCl, 1.44 g of Na_2HPO_4, and 0.24 g of KH_2PO_4 in 800 mL of H_2O. Adjust the pH to 7.4 with HCl. Add H_2O to 1 L.
6. CSK buffer: 0.1 M NaCl, 10 mM Pipes pH 7.0, 300 mM Sucrose, 1 mM $MgCl_2$, 1 mM EDTA, 2 mM phenylmethylsulfonyl fluoride, 10 mM NaF, 20 mM β-glycerophosphate, 100 μM Na_3VO_4, and 1× Complete protease inhibitor cocktail (Roche Diagnostics).
7. CSK buffer containing 0.25 % Triton X-100 (*see* **Note 2**).
8. 4 % Paraformaldehyde (*see* **Note 3**): Dissolve 4 g paraformaldehyde in about 90 mL PBS in a Pyrex or appropriate container with a stir bar. Heat to 60 °C and add first 1 N, then 0.1 N, NaOH drop wise until solution becomes clear (*see* **Note 4**). Cool to room temperature. Adjust the pH to 7.4 with 0.1 N NaOH or 0.1 N HCl depending on the original

pH and the volume to 100 mL with PBS. Commercially available 4 % paraformaldehyde PBS also works well.

9. Methanol (stored at −20 °C or −30 °C).
10. Blocking buffer: 3 % bovine serum albumin, 0.2 % Tween-20, and 0.02 % NaN_3 in PBS.
11. Primary antibodies and solution: mouse monoclonal PCNA antibody (PC-10, Santa Cruz Biotechnology) and rabbit Mcm3 antibody (ab4460, Abcam). Dilute anti-PCNA antibody at 1:200 and anti-Mcm3 antibody at 1:500 in blocking buffer or commercially available solution (e.g., Can Get Signal immunostain solution from Toyobo).
12. Secondary antibodies and solution: Alexa488-conjugated anti-mouse antibody and Alexa594-conjugated anti-rabbit antibody are diluted at 1:400 in blocking buffer.
13. Mounting medium: VECTASHIELD Mounting Medium (Vector Laboratories) or equivalent.
14. Nail polish.
15. Microscope slides.
16. Fluorescence microscope.

3 Methods

Although the levels of MCM2-7 associated with chromatin change during the cell cycle, the total cellular levels of MCM2-7 do not fluctuate, and MCM2-7 is present in the nucleus throughout the cell cycle in mammalian cells. Thus, when whole cell proteins are fixed and stained with antibodies against Mcm proteins, all cell nuclei are stained irrespective of the cell cycle stage, because both chromatin-bound and soluble fractions of MCM2-7 are detected (Fig. 1, upper panel). This is also the case for PCNA. A simple way to analyze the chromatin-bound MCM2-7 (and also PCNA) is to perform a pre-extraction treatment to remove soluble MCM2-7 proteins from the cell and then fix the remaining (chromatin-bound) proteins. When cells are treated in this way and stained with antibodies against Mcm proteins, only G1 phase and S phase cell nuclei are detected as positive for chromatin-bound MCM2-7 (Fig. 1, lower panel).

Dual staining with an S-phase marker helps to identify the cell cycle stage of each cell [21, 22]. As previous reports demonstrated, S-phase progression can be monitored by the PCNA staining patterns [19, 20] (Fig. 2). In Fig. 1 (lower panel), a dual staining of pre-extracted cells with Mcm3 and PCNA antibodies is shown. Unlike MCM2-7, PCNA is not loaded on chromatin during G1 phase. Therefore, G1-phase cells are identified as cells that are positive for

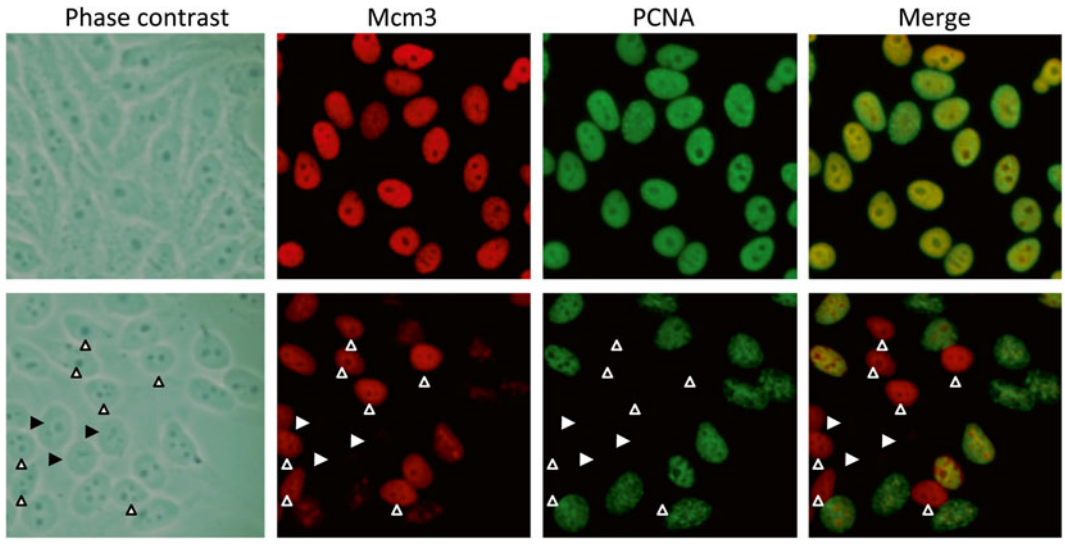

Fig. 1 Immunostaining of Mcm3 in HeLa cells. The cells are dually stained with antibodies for Mcm3, a component of licensing factor MCM2-7 and PCNA without (*upper panel*) or with (*lower panel*) detergent pre-extraction before fixation. Both MCM2-7 and PCNA are nuclear proteins and are present throughout the cell cycle. Thus, when fixed without pre-extraction, all cell nuclei are stained for both proteins (*upper panel*). Pre-extraction removes soluble fraction and retains Mcm3 and PCNA, which are bound to chromatin (*lower panel*). G1 cells (labeled with *open triangles*) are positive for Mcm3, but not for PCNA. G2 cells (labeled with *closed triangles*) are negative for both proteins. The rest of the cells are positive for PCNA, and thus, they are S-phase cells

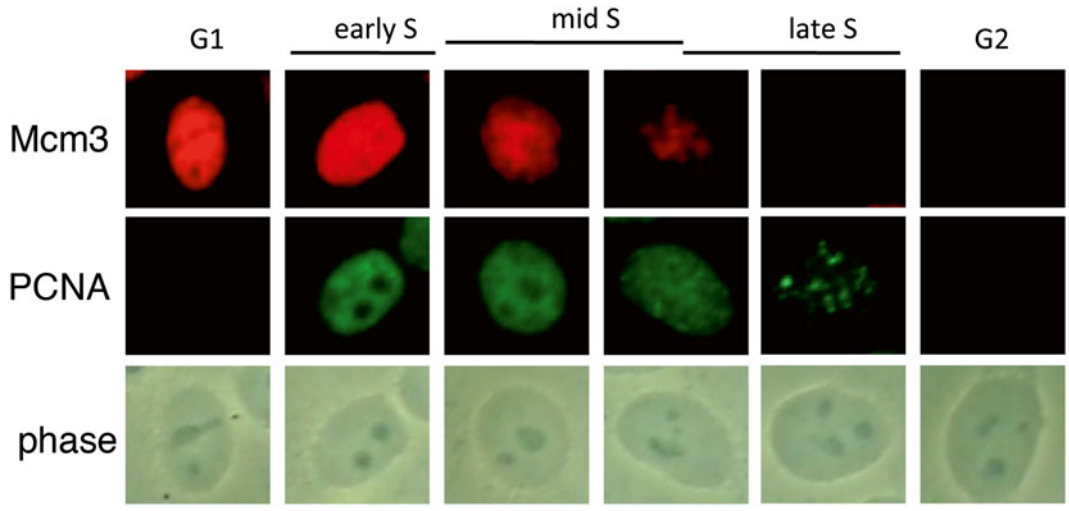

Fig. 2 Chromatin-associated Mcm3 protein during the cell cycle. HeLa cells are pre-extracted prior to fixation. Cell cycle positions are estimated by the PCNA staining pattern [19, 20]. G1 nucleus is stained intensely with Mcm3, but not with PCNA. During early S phase, Mcm3 staining is similar to that in G1 phase. PCNA is detected throughout the nucleoplasm, and PCNA foci are also observed. In mid S-phase cells, Mcm3 staining decreases and PCNA signal is observed surrounding the nucleolus. In late S phase, Mcm3 staining is negligible and large foci-like PCNA staining is observed. In G2 cells Mcm3 and PCNA staining are absent

MCM2-7 but not for PCNA (Fig. 1, lower panel: cell nuclei labeled by open triangles; also *see* Fig. 2). PCNA is loaded onto chromatin when DNA replication is started. At the beginning of S phase, MCM2-7 is detected within the whole nucleus, as in G1 phase. At this stage, however, the MCM2-7 complex activated at the early origins functions as a replicative helicase, whereas other MCM2-7 complexes remain inactive and located on the unfired late origins. PCNA is detected as foci that correspond to early-replicating chromosome regions. When the DNA replication of early replicating regions is completed, both MCM2-7 and PCNA are dissociated from those regions of DNA. As S phase progresses, PCNA-positive sites change from early- to late-replicating regions, while MCM2-7 signals are lost from the replicated regions. When DNA replication is completed, cells in G2 phase have no chromatin-bound MCM2-7 or PCNA signal (Fig. 1, lower panel: cell nuclei labeled with closed triangles; also *see* Fig. 2). This immunofluorescence method can also be applied to determine the cell cycle entry from G0 state.

1. Using sterile forceps, place the glass coverslip in an appropriate tissue-culture dish. Here, we use an 18×18 mm coverslip for a 35-mm culture dish.
2. Plate the cell suspension onto the dish (we normally plate $1–2 \times 10^5$ HeLa cells in a 35-mm dish with 2 mL medium) and let the cells adhere to the glass surface (*see* **Note 5**).
3. Remove the medium by aspiration and gently wash coverslip twice with 2 mL of PBS in culture dish (*see* **Note 6**). All the steps are performed at room temperature unless otherwise mentioned.
4. Pre-extract cells with 1–2 mL of 0.25 % Triton X-100 in CSK for 10 min on ice (*see* **Note 7**).
5. Gently wash twice with 2 mL of PBS.
6. Fix cells in 2 mL of 4 % paraformaldehyde solution for 10 min (*see* **Note 8**).
7. Wash the coverslip twice with PBS for 5 min each.
8. Fix in 2 mL of −30 °C methanol (*see* **Note 9**) for 10 min to visualize PCNA (*see* **Note 10**).
9. Wash 3 times with PBS for 5 min each.
10. Remove the coverslip from the dish (*see* **Note 11**) and place it on a pipette tip-rack (*see* **Note 12**). Gently add 100 μL of blocking buffer to the coverslip and incubate at room temperature for 1 h.
11. Remove blocking buffer (*see* **Note 13**).
12. Add 100 μL of primary antibody solution (*see* **Note 14**) to the coverslip and incubate for 1 h.

13. Wash 3 times for 5 min each with PBS (*see* **Note 13**).
14. Add 100 μL of secondary antibody solution (*see* **Note 14**) and incubate for 1 h (*see* **Note 15**).
15. Remove the secondary antibody solution.
16. Optional: Incubate the coverslip with Hoechst solution (*see* **Note 16**) for 5 min.
17. Wash 3 times for 5 min each with PBS, drain off buffer from the coverslip, and let it air-dry briefly.
18. Drop the mounting medium (approximately 5 μL) on a microscope slide, and place the coverslip on the mounting medium with the side that has cells facing down (*see* **Note 17**).
19. Seal coverslip with clear nail polish to prevent drying out and movement under microscope.
20. Store in dark at 4 °C.

4 Notes

1. There are different sizes of coverslips, round (10–20 mm diameter) and square (18 mm wide), of around 0.12–0.17 mm thick. The steam autoclave is not suitable, because coverslips get stuck together.
2. Depending on the cell type and cell density, cells may display sensitivity to detergents (Triton X-100). Detergent concentration (0.1–0.5 %), extraction time (1–10 min), and temperature (room temperature or on ice) should be optimized for your cell line.
3. Paraformaldehyde (PFA) is very toxic. Work in fume hood when preparing solution. Do not inhale. Wear gloves.
4. Be patient until the solution becomes clear. Keep the solution at 60 °C in a water bath or on a stirring hot plate.
5. Let the cells adhere to the coverslip for at least 20–24 h. Proper cell density is also critical for immunostaining. When the cells are plated at a high density, cell proliferation may be compromised.
6. Washing, extraction, and fixation of cells on the coverslip are performed in the culture dish by aspirating buffers from the dish and/or flooding the dish with solutions. Use caution when you add the solution. Flood slowly from the edge of the dish with a wide-mouth pipette. Do not add solution directly on the cell surface.
7. Instead of pre-extraction with 0.25 % Triton X-100 CSK buffer, treatment with 0.5 % Triton X-100 containing PBS for 5 min can be done. Because detergent-treated cells are very feeble, use great caution after detergent treatment. Aspirate off

the buffers slowly and flood the dish with the solution slowly from the edge of the dish to avoid disrupting the cell structure.

8. This paraformaldehyde fixation before methanol fixation in Subheading 3, **step 8** is recommended, because detergent-treated cells are very delicate when treated with organic solvents. Prior paraformaldehyde fixation somewhat protects cells from methanol-induced cell distortion.
9. Methanol stored at −20 °C or −30 °C can be added to the dish, and then the dish can be put into the freezer. As described in **Note 7**, add methanol slowly from the edge of the dish.
10. When the mouse monoclonal anti-PCNA antibody clone PC-10 is used to detect PCNA by immunofluorescence, the methanol fixation or treatment is essential. This clone, used by many researchers, works for methanol-fixed cells but does not work for paraformaldehyde-fixed cells. Thus, cells fixed with paraformaldehyde in Subheading 3, **step 6**, were further fixed in methanol.
11. Remove the coverslip from the dish using fine-tipped forceps and drain off the buffer by touching the edge of the coverslip on a paper towel.
12. We use a pipette tip rack as a coverslip holder (e.g., a Rainin 200-μL rack) with the tip holder bottom-side up. To prevent the coverslips from drying up, put water in the bottom of the rack and put on the lid. Instead of the rack, the coverslips can be placed on Parafilm.
13. After the last wash, drain off the buffer by touching the edge of the coverslip on a paper towel.
14. 100 μL of solution is enough to cover an 18 × 18 mm coverslip. When working with only a small amount of antibody, use a smaller coverslip with less solution.
15. To check the background staining of secondary antibody, a sample with no primary antibody may be included.
16. Hoechst solution: Dilute stock solution (5–10 mg/mL Hoechst33258) at 1 μg/mL in PBS for use. Hoechst or another dye is used to detect cellular DNA. By staining DNA, the outlines of nuclei in a population of cells can be determined, as well as the detained nuclear regions of single nuclei, where heterochromatic regions are stained more heavily than euchromatic regions, which helps to localize the Mcm- or PCNA-stained regions.
17. Place the coverslip slowly down from one edge to avoid air bubble formation.

Acknowledgements

This work was financially supported by JSPS KAKENHI and MEXT KAKENHI, Grant-in-Aid from the Ministry of Education, Culture, Sports, Science, and Technology of Japan.

References

1. Bell SP, Dutta A (2002) DNA replication in eukaryotic cells. Annu Rev Biochem 71: 333–374
2. Nishitani H, Lygerou Z (2002) Control of DNA replication licensing in a cell cycle. Genes Cells 7(6):523–534
3. Blow JJ, Dutta A (2005) Preventing re-replication of chromosomal DNA. Nat Rev Mol Cell Biol 6(6):476–486
4. Davey MJ, Indiani C, O'Donnell M (2003) Reconstitution of the Mcm2-7p heterohexamer, subunit arrangement, and ATP site architecture. J Biol Chem 278(7):4491–4499
5. Bochman ML, Bell SP, Schwacha A (2008) Subunit organization of Mcm2-7 and the unequal role of active sites in ATP hydrolysis and viability. Mol Cell Biol 28(19):5865–5873
6. Remus D, Beuron F, Tolun G, Griffith JD, Morris EP, Diffley JF (2009) Concerted loading of Mcm2-7 double hexamers around DNA during DNA replication origin licensing. Cell 139(4):719–730
7. Masai H, Arai K (2002) Cdc7 kinase complex: a key regulator in the initiation of DNA replication. J Cell Physiol 190(3):287–296
8. Ishimi Y (1997) A DNA helicase activity is associated with an MCM4, -6, and -7 protein complex. J Biol Chem 272(39):24508–24513
9. Ilves I, Petojevic T, Pesavento JJ, Botchan MR (2010) Activation of the MCM2-7 helicase by association with Cdc45 and GINS proteins. Mol Cell 37(2):247–258
10. Waga S, Stillman B (1998) The DNA replication fork in eukaryotic cells. Annu Rev Biochem 67:721–751
11. Masai H, Matsumoto S, You Z, Yoshizawa-Sugata N, Oda M (2010) Eukaryotic chromosome DNA replication: where, when, and how? Annu Rev Biochem 79:89–130
12. Leman AR, Noguchi E (2013) The replication fork: understanding the eukaryotic replication machinery and the challenges to genome duplication. Genes 4(1):1–32
13. Li Y, Araki H (2013) Loading and activation of DNA replicative helicases: the key step of initiation of DNA replication. Genes Cells 18(4):266–277
14. Fu YV, Yardimci H, Long DT, Ho TV, Guainazzi A, Bermudez VP, Hurwitz J, van Oijen A, Scharer OD, Walter JC (2011) Selective bypass of a lagging strand roadblock by the eukaryotic replicative DNA helicase. Cell 146(6):931–941
15. Machida YJ, Hamlin JL, Dutta A (2005) Right place, right time, and only once: replication initiation in metazoans. Cell 123(1): 13–24
16. Arias EE, Walter JC (2007) Strength in numbers: preventing rereplication via multiple mechanisms in eukaryotic cells. Genes Dev 21(5):497–518
17. Moldovan GL, Pfander B, Jentsch S (2007) PCNA, the maestro of the replication fork. Cell 129(4):665–679
18. Bravo R, Macdonald-Bravo H (1987) Existence of two populations of cyclin/proliferating cell nuclear antigen during the cell cycle: association with DNA replication sites. J Cell Biol 105(4):1549–1554
19. Gillespie PJ, Blow JJ (2010) Clusters, factories and domains: the complex structure of S-phase comes into focus. Cell Cycle 9(16): 3218–3226
20. Pope BD, Aparicio OM, Gilbert DM (2013) SnapShot: replication timing. Cell 152(6): 1390
21. Kimura H, Nozaki N, Sugimoto K (1994) DNA polymerase alpha associated protein P1, a murine homolog of yeast MCM3, changes its intranuclear distribution during the DNA synthetic period. EMBO J 13(18):4311–4320
22. Prasanth SG, Mendez J, Prasanth KV, Stillman B (2004) Dynamics of pre-replication complex proteins during the cell division cycle. Philos Trans R Soc Lond B Biol Sci 359(1441):7–16

Chapter 30

Chromatin Immunoprecipitation to Investigate Origin Association of Replication Factors in Mammalian Cells

Adam R. Leman and Eishi Noguchi

Abstract

A variety of DNA-binding proteins regulate DNA transactions including DNA replication and DNA damage response. To initiate DNA replication in S phase of the cell cycle, numerous replication proteins must be recruited to the replication origin in order to unwind and synthesize DNA. Some replication factors stay at the origin, while replisome components move with the replication fork. When the replisome encounters DNA damage or other issues during DNA replication, the replication fork stalls and accumulates single-stranded DNA that triggers the ATR-dependent replication checkpoint, in order to slow down S phase and arrest the cell cycle at the G2–M transition. It is also possible that replication forks collapse, leading to double-strand breaks that recruit various DNA damage response proteins to activate cell cycle checkpoints and DNA repair pathways. Therefore, defining the localization of DNA transaction factors during the cell cycle should provide important insights into mechanistic understanding of DNA replication and its related processes. In this chapter, we describe a chromatin immunoprecipitation method to locate replisome components at replication origins in human cells.

Key words Replication fork, Origin, Chromatin immunoprecipitation, ChIP, Replisome, Timeless, Cross-link, Fork protection complex, c-Myc origin

1 Introduction

Eukaryotic DNA replication begins at multiple replication origins, which are marked by the origin recognition complex (ORC). During late mitosis and G1 phase, Cdc6 and Cdt1 associate with origins and recruit the MCM (minichromosome maintenance proteins) DNA helicase complex, in order to assemble the pre-replication complex (pre-RC). However, to initiate DNA synthesis, additional factors are recruited at the origin for the unwinding of duplex DNA. These factors include Cdc45 and GINS, both of which associate with MCM to form the active DNA helicase known as the CMG complex. Once duplex DNA is unwound, the CMG complex moves with the replication fork together with DNA polymerases and other accessory factors, forming the replisome

Eishi Noguchi and Mariana C. Gadaleta (eds.), *Cell Cycle Control: Mechanisms and Protocols*, Methods in Molecular Biology, vol. 1170, DOI 10.1007/978-1-4939-0888-2_30,

complex, which is responsible for elongating DNA chains (reviewed in [1]). As DNA replication proceeds, the replisome complex may encounter a variety of obstacles including damaged template DNA, DNA secondary structures, and DNA binding proteins. Under these conditions, the replisome stalls, leading to accumulation of single-stranded DNA (ssDNA) at the replication forks and activation of the ATR-dependent replication checkpoint (reviewed in [2]). It is also possible that the replication fork collapses, generating DNA double-strand breaks (DSBs), which then induce a signal transduction cascade to activate the ATM-dependent DNA damage checkpoint. To properly activate these checkpoint pathways, which are essential for preservation of genomic integrity, numerous checkpoint proteins are recruited to stalled replication forks or at DSBs. These proteins sense the damage and send the checkpoint signal to arrest the cell cycle and coordinate with DNA repair pathways (reviewed in [3]). Therefore, to mechanistically understand DNA replication and DNA damage response mechanisms, it is important to investigate cell-cycle dependent localization of DNA transacting factors at specific sites of chromosomes. In this chapter, we describe a chromatin immunoprecipitation method to analyze origin association of replisome components during the cell cycle. Similar methods can also be used to investigate the localization of various DNA-binding factors, including damage response proteins and transcription factors, at specific chromosome loci.

2 Materials

2.1 Synchronization of HeLa Cells by a Double-Thymidine Block

1. HeLa cells cultured in growth medium in a 5 % CO_2 atmosphere at 37 °C.
2. Growth medium for HeLa cells: RPMI 1640 medium supplemented with 10 % calf serum, 10 mM HEPES–KOH pH 7.5, 100 units/mL penicillin, 100 μg/mL streptomycin.
3. 15-cm cell culture dishes.
4. 100 mM thymidine: Filter-sterilize with a 0.22 μm pore size membrane and store at −20 °C.
5. 1× PBS: 136.9 mM NaCl, 2.68 mM KCl, 8.1 mM Na_2HPO_4, 1.47 mM KH_2PO_4, pH 7.4.

2.2 Cross-linking Cells

1. 37 % formaldehyde.
2. 2.5 M glycine.
3. 1× PBS.
4. 15-mL conical tubes.

2.3 Cell Extract Preparation

1. ChIP lysis buffer: 50 mM Tris–HCl pH 7.5, 150 mM NaCl, 5 mM EDTA, 0.5 % NP-40, 0.1 % Triton X-100, 0.2 mM *p*-APMSF (4-amidinobenzylsulfonyl fluoride hydrochloride),

Roche Complete EDTA-free protease inhibitor cocktail. Prepare fresh and keep on ice.

2. 1.5-mL microcentrifuge tubes.
3. Misonix sonicator 3000 (Misonix).
4. 100-mL glass beaker.
5. Floating tube rack that fits in a 100-mL glass beaker (*see* **Note 1**).
6. Bio-Rad Protein Assay Dye Reagent Concentrate (Bio-Rad).

2.4 Immunoprecipitation

1. Protein A-Sepharose beads.
2. Anti-Timeless antibody or antibodies against other replisome components (*see* **Note 2**).

2.5 DNA Extraction

1. Chelex 100 resin (Bio-Rad).
2. 10 mg/mL proteinase K.

2.6 SYBR Green-Based Real-Time PCR Analysis

1. iQ SYBR Green Supermix (uses hot-start iTaq DNA polymerase, Bio-Rad, 170-8880).
2. 10 μM forward primer (*see* **Note 3**).
3. 10 μM reverse primer (*see* **Note 3**).

3 Methods

PCNA associates with chromatin and moves with the replication fork during S phase [4]. Therefore, S-phase cells can be identified as PCNA-positive cells in immunofluorescence microscopy. We also showed that the Timeless protein co-localizes with PCNA in S-phase cells, suggesting that Timeless is associated with replication forks [5]. Fork association of the protein can also be confirmed by examining physical association of the protein with a known replication fork component by immunoprecipitation. Indeed, PCNA was co-precipitated with Timeless using anti-Timeless antibodies [6]. However, these methods do not demonstrate the dynamics of protein movement along the chromosome during DNA replication. Accordingly, chromatin immunoprecipitation (ChIP) has been widely used to investigate direct association of replication factors with specific chromosome loci. Because cells are directly treated with formaldehyde to cross-link proteins onto DNA in a ChIP experiment, in vivo protein–chromatin association is preserved.

In this method, we describe a simple ChIP method to investigate the association of Timeless with a well-characterized replication origin at the *MYC* gene (c-Myc) region in human cells [5]. This method utilizes Chelex 100 resin, allowing for efficient ChIP experiments whereby a high reproducibility can be achieved [7]. We use HeLa cells synchronized at the beginning of S phase. Cells are treated with formaldehyde and released into the cell cycle.

DNA fragments precipitated with the anti-Timeless antibody are analyzed by quantitative PCR to monitor cell cycle-dependent association of Timeless with the MYC origin. The method described in this chapter is a typical ChIP assay that can be easily modified for detecting other chromatin-binding factors, such as replication and DNA damage response proteins.

3.1 Preparation and Synchronization of HeLa Cells by a Double-Thymidine Block and Release

1. Plate 4×10^6 cells in a 15-cm culture dish containing 20 mL growth medium (*see* **Note 4**). Multiple dishes are required depending on a time course schedule. For example, six culture dishes are required for 0-, 1-, 2-, 3-, 6-, and 9-h time points after the release from cell cycle arrest. Grow the cells overnight (16–24 h) at 37 °C to allow the cells to attach the dish surface.
2. Add 400 μL of 100 mM thymidine to the culture dish (final concentration is 2 mM), mix gently, and incubate the cells for 16–19 h.
3. Aspirate the medium, add 10 mL of 1× PBS, and gently shake the dish to wash the cells. Repeat this washing step once more with 10 mL of 1× PBS and once with 10 mL of fresh growth medium.
4. Aspirate the medium, add 20 mL of fresh growth medium to the dish, and grow the cells at 37 °C for 9 h.
5. Add 400 μL of 100 mM thymidine to the culture dish (final concentration is 2 mM), mix gently, and incubate the cells for 16 h.
6. Wash the cells as described in **step 3**.
7. Aspirate the medium, add 20 mL of fresh growth medium to the dish, and grow the cells for desired length of time (*see* **Note 5**) until cell fixation described in Subheading 3.2.

3.2 Cross-linking Cells

1. To fix the cells (1×10^7 cells), add 0.8 mL of 37 % formaldehyde (final concentration is 1.42 %) directly to the culture dish, mix the medium by gently shaking the dish, and incubate the cells for 15 min at room temperature.
2. To quench formaldehyde, add 1.1 mL of 2.5 M glycine (final concentration is 125 mM) directly to the dish, mix the medium by gently shaking the dish, and incubate the cells for 5 min at room temperature.
3. Aspirate the medium, add 10 mL of 1× PBS, and gently shake the dish to wash the cells. Repeat this washing step once more.
4. Aspirate the buffer, add 1 mL of 1× PBS, scrape the cells off the dish by an cell scraper, and transfer cell suspension to a 15-mL conical tube.
5. Centrifuge the cells at $800 \times g$ for 5 min at 4 °C.
6. Aspirate the buffer and immediately freeze the cell pellet at −80 °C (*see* **Note 6**).

3.3 Preparation of Cell Extract

1. Thaw cell pellets on ice, suspend the cells in 1 mL of ice-cold ChIP lysis buffer, and transfer the cell suspension to a 1.5-mL microcentrifuge tube.
2. Incubate the cell suspension on ice for 10 min.
3. Place the sample tube in a special float (*see* **Note 1**) that fits into a 100-mL glass beaker filled with ice water.
4. Sonicate the sample using a microtip: output 5, ON time of 1 s, OFF time of 5 s. The total ON time for each step is 15 s (15 cycles of 1 s ON, 5 s OFF).
5. Place the sample tube on a separate icebox, and perform **step 4** for all other samples (*see* **Note 7**).
6. Repeat **steps 4** and **5** for five times (*see* **Note 8**).
7. Centrifuge samples at the maximum speed in a microfuge at 4 °C.
8. Transfer the supernatant (cell extract) to a new 1.5-mL microcentrifuge tube and keep on ice.
9. Measure protein concentration using Bio-Rad Protein Assay Dye Reagent Concentrate.
10. Adjust protein concentration by diluting samples by ice-cold ChIP lysis buffer to the protein concentration of the lowest concentrated sample.
11. Transfer 10 μL of each extract to a new tube to use for the input control (*see* Subheading 3.4).
12. Perform immunoprecipitation with the rest of the cell extracts.

3.4 Immunoprecipitation

1. Prior to immunoprecipitation, prewash protein A-Sepharose beads (protein A beads) as follows: Use 50 μL (50 % slurry, 25 μL bead volume) of protein A beads for each sample. Transfer the required amount of beads to a 1.5-mL microcentrifuge tube, centrifuge briefly at 7,000 rpm in a microfuge, aspirate supernatant, and resuspend beads in 1 mL of ice-cold ChIP lysis buffer, in order to wash beads. Repeat this washing procedure two more times, and resuspend beads in ice-cold ChIP lysis buffer to obtain 50 % slurry of protein A beads. Keep on ice until needed (*see* **Note 9**).
2. Separate the cell extract obtained in Subheading 3.3 into two separate microcentrifuge tubes (450 μL each).
3. Add 7 μg of the anti-Timeless antibody to one tube and 7 μg of rabbit IgG to the other tube. Rotate samples overnight at 4 °C.
4. Add 50 μL of the pre-washed protein A beads to the samples. Rotate samples for 2 h at 4 °C.
5. To wash protein A beads, centrifuge briefly at 7,000 rpm in a microfuge, aspirate supernatant, and add 1 mL of ice-cold ChIP lysis buffer. Repeat this washing procedure five times, and aspirate supernatant (*see* **Note 10**).

3.5 DNA Extraction

1. Add 100 μL of Chelex 100 resin (10 % slurry in sterile H_2O) to the washed beads (*see* Subheading 3.4, **step 5**) and the input samples (*see* Subheading 3.3, **step 11**), mix well by vortex, and boil the samples for 10 min, in order to reverse cross-link and to extract DNA.
2. Cool samples to room temperature, add 2 μL of 10 mg/mL proteinase K, and incubate the samples at 55 °C for 30 min. Mix samples occasionally.
3. Boil the samples for 10 min to inactivate proteinase K.
4. Centrifuge the samples at the maximum speed in a microfuge at 4 °C for 1 min.
5. Carefully transfer 80 μL of supernatant (extracted DNA) to a new microcentrifuge tube (*see* **Note 11**).
6. Add 120 μL of ddH_2O to the beads, mix by vortexing.
7. Centrifuge the samples at maximum speed in a microfuge at 4 °C for 1 min.
8. Carefully transfer 120 μL of supernatant (extracted DNA) to the 80 μL previously collected (total 200 μL). Store the extracted DNA at −20 °C until needed for PCR (*see* **Note 11**).

3.6 PCR Using SYBR Green-Based Real-Time PCR Analysis

DNA immunoprecipitated by this protocol can be amplified and quantified using various PCR-based quantification methods. Below, we describe a simple quantification using the SYBR green-based real-time PCR. In our assay, we use primers that are designed to amplify the MYC replication origin region. This method can be applied to other chromosomal loci, in order to measure the quantity of DNA precipitated with antibodies. An example of this analysis is shown in our previous studies [5].

1. Mix the following PCR reagents for each reaction (*see* **Note 12**):
   (a) 3 μL of template DNA (input control or ChIPed DNA).
   (b) 5 μL of iQ SYBR Green Supermix.
   (c) 0.3 μL of Forward Primer (10 μM).
   (d) 0.3 μL of Reverse Primer (10 μM).
   (e) 1.4 μL of H_2O.
2. Perform PCR using the following cycles (*see* **Note 13**):
   (a) Denaturation of DNA and hot-start activation of iTaq DNA polymerase: 95 °C, 2 min.
   (b) Denaturation: 95 °C, 10 s.
   (c) Annealing: 55–60°, 30 s.
   (d) Extension: 72 °C, 30 s (perform SYBR Green detection here).
   (e) Go to (b)–(d), repeat for 39 additional cycles.

(f) To degrade the polymerase enzyme prior to melt curve analysis: 72°, 7 min.

(g) (Optional) Melting curve: 55–95 °C, (SYBR Green signal detection ever 0.5 °C) (*see* **Note 14**).

3. Obtain cycle threshold (Ct) values for each sample, IgG control, and input (*see* **Notes 15** and **16**).
4. After the Ct values have been ascertained, determine the relative enrichment of your protein of interest at a locus using the following equations:

(a) Protein occupancy = $2^{2.2\ \%\ \text{Input Ct} - \text{Timeless ChIP Ct}}$.

(b) Background correction = $2^{2.2\ \%\ \text{Input Ct} - \text{IgG ChIP Ct}}$.

(c) Background corrected occupancy = Protein occupancy − Background correction.

(d) The input sample must be corrected for the lower volume compared to the sample, in this case 2.2 % (10 μL of input/450 μL for the IP). Thus, Final Occupancy = (Background Corrected Occupancy)/45.

(e) To convert this number to the percentage of immunoprecipitated DNA from the total sample, multiple the Final Occupancy by 100 to obtain a percentage value.

4 Notes

1. For a floating rack, we use a thin Styrofoam plate cut into a circle to fit into a beaker. One hole is cut into the middle of the rack to hold 1.5-mL microfuge tubes above the ice water.
2. In this protocol, we use the anti-Timeless antibodies described in our previous studies [5, 8]. However, anti-Timeless antibodies are readily available from commercial sources. Also, antibodies specific to proteins of interest can be used to monitor their chromatin association.
3. Primers should be designed to amplify chromosome regions of interest. For SYBR-green based real-time PCR, the ideal amplicon size is between 80 and 200 bp, and amplicons over 300 bp are not recommended. To amplify the *MYC* (c-Myc) origin region, we use MYC11-F (5′-TAT CTA CAC TAA CAT CCC ACG CTC TG-3′) and MYC11-R (5′-CAT CCT TGT CCT GTG AGT ATA AAT CAT CG-3′) primers as described [5, 9]. Other defined origins we have used include *HHB* (β-globin), *LB2* (lamin B2) and *MCM4* (Mcm4) loci [9–11]. As a non-origin control, we use GACT-F (5′-GCT GTT CCA GGC TCT GTT CC-3′) and GACT-R (5′-ATG CTC ACA CGC CAC AAC ATG C-3′) primers to amplify the *ACTG1* (γ-actin) locus [11].

4. HeLa cells should be plated at approximately 25 % confluency considering that cells will be incubated further. This prevents cells from becoming confluent at the time of cell collection. Plating cell numbers need to be adjusted for each cell type.
5. We often take time points at 0, 1, 2, 3, 6, and 9 h after the release.
6. Use liquid nitrogen or dry ice–ethanol to snap-freeze cell pellets.
7. Continuous sonication of the same sample causes sample heating. To prevent this problem, sonication is performed at intervals.
8. This condition allows us to shear DNA into 500- to 700-bp fragments using our equipment. However, the sonication conditions should be optimized in individual laboratories by extracting and monitoring cross-linked DNA after sonication.
9. Prepare 20–30 % more pre-washed beads than needed.
10. Use caution not to aspirate any beads, as these contain the immunoprecipitated DNA.
11. At this point, a small volume of liquid will remain over the beads. This is normal, if Chelex 100 resin is transferred over to the new tube (for the final DNA sample), it will interfere with downstream amplification steps.
12. For consistent results, generate a master mix of all components minus the template DNA. As described in **Note 3**, to amplify the *MYC* origin, use MYC11-F and MYC11-R primers. As a control, use GACT-F and GACT-R primers to amplify the γ-actin gene region. Prepare excess master mix to ensure equal volumes in all PCR reactions.
13. Annealing temperature needs to be adjusted depending on the melting temperatures of the primers. For PCR conditions, see iQ SYBR Green Supermix supplier's instructions.
14. By running a melting curve analysis, one can determine the melting temperature of the PCR fragment generated during the PCR reaction. The melting temperature can be determined by the inflection point of the melting curve. It is important that only one inflection point is detected during melting curve analysis, indicating that only PCR product has been generated.
15. The method depends upon the software used and user preferences. For an accurate measurement of DNA precipitated by antibodies, it is vital to use a consistent method for Ct determination between the sample, IgG control, and input.
16. The efficiency of the PCR primer set can be determined experimentally using a standard curve. A variety of efficiency calculators are freely available online to determine the efficiency of the primer set. Using a value of 2 for the efficiency assumes a primer amplification efficiency of 100 %.

Acknowledgements

This work was supported in part by NIH grants (AG035480 to A.R.L. and GM0776043 to E.N.). We would like to thank Chiaki Noguchi for technical support and troubleshooting during protocol development.

References

1. Masai H, Matsumoto S, You Z, Yoshizawa-Sugata N, Oda M (2010) Eukaryotic chromosome DNA replication: where, when, and how? Annu Rev Biochem 79:89–130
2. Leman AR, Noguchi E (2013) The replication fork: understanding the eukaryotic replication machinery and the challenges to genome duplication. Genes 4(1):1–32
3. Hustedt N, Gasser SM, Shimada K (2013) Replication checkpoint: tuning and coordination of replication forks in S phase. Genes 4(3): 388–434
4. Moldovan GL, Pfander B, Jentsch S (2007) PCNA, the maestro of the replication fork. Cell 129(4):665–679
5. Leman AR, Noguchi C, Lee CY, Noguchi E (2010) Human timeless and tipin stabilize replication forks and facilitate sister-chromatid cohesion. J Cell Sci 123(Pt 5):660–670
6. Yang XH, Shiotani B, Classon M, Zou L (2008) Chk1 and Claspin potentiate PCNA ubiquitination. Genes Dev 22(9):1147–1152
7. Nelson JD, Denisenko O, Sova P, Bomsztyk K (2006) Fast chromatin immunoprecipitation assay. Nucleic Acids Res 34(1):e2
8. Leman AR, Dheekollu J, Deng Z, Lee SW, Das MM, Lieberman PM, Noguchi E (2012) Timeless preserves telomere length by promoting efficient DNA replication through human telomeres. Cell Cycle 11(12):2337–2347
9. Sibani S, Price GB, Zannis-Hadjopoulos M (2005) Decreased origin usage and initiation of DNA replication in haploinsufficient HCT116 Ku80+/– cells. J Cell Sci 118(Pt 15):3247–3261
10. Schaarschmidt D, Ladenburger EM, Keller C, Knippers R (2002) Human Mcm proteins at a replication origin during the G1 to S phase transition. Nucleic Acids Res 30(19):4176–4185
11. Tan BC, Chien CT, Hirose S, Lee SC (2006) Functional cooperation between FACT and MCM helicase facilitates initiation of chromatin DNA replication. EMBO J 25(17): 3975–3985

Chapter 31

Live-Cell Fluorescence Imaging for Phenotypic Analysis of Mitosis

Sushama Sivakumar, John R. Daum, and Gary J. Gorbsky

Abstract

Live-cell fluorescence microscopy is a powerful tool for characterizing aberrant mitotic phenotypes resulting from exposure to chemical inhibitors or after depletion of protein targets by RNA interference or other methods. Live imaging of cultured cells during mitotic progression presents challenges in maintaining optimal health of cells while achieving the temporal and spatial resolution to accomplish the goals of the study. We describe herein strategies to monitor and analyze mammalian cell mitosis with standard, inverted, fluorescence microscopy systems that are widely available.

Key words Fluorescence microscopy, Imaging, Mitosis, Cell division, Fluorescent protein, Microscope, RNAi

1 Introduction

1.1 Overview of Fluorescence Imaging and Mitosis

In the late 1800s Flemming, Van Beneden, and their contemporaries carried out the first studies of chromosome behavior in dividing cells in both living and fixed tissue using the available microscope methodology (reviewed in ref. 1). Since that time, tremendous advances in microscope technology and fluorescence imaging have greatly enhanced our ability to visualize mitotic progression with high spatial and temporal resolution. Modern fluorescence imaging and molecular biology techniques allow tracking of subcellular structures such as chromosomes, kinetochores, centrosomes, or microtubules during cell division with great detail. Specific proteins of interest may be fused with fluorescent proteins to enable study of their intracellular dynamics and localization throughout the cell cycle. By creating fluorescent fusion proteins varying in wavelength emission, one can further determine if proteins of interest co-localize or concentrate in specific subcellular compartments during mitosis. For the purposes of the assay described herein a cell line was employed that expresses Histone H2B fused to green fluorescent protein (GFP). Histone H2B is a component

Eishi Noguchi and Mariana C. Gadaleta (eds.), *Cell Cycle Control: Mechanisms and Protocols*, Methods in Molecular Biology, vol. 1170, DOI 10.1007/978-1-4939-0888-2_31,

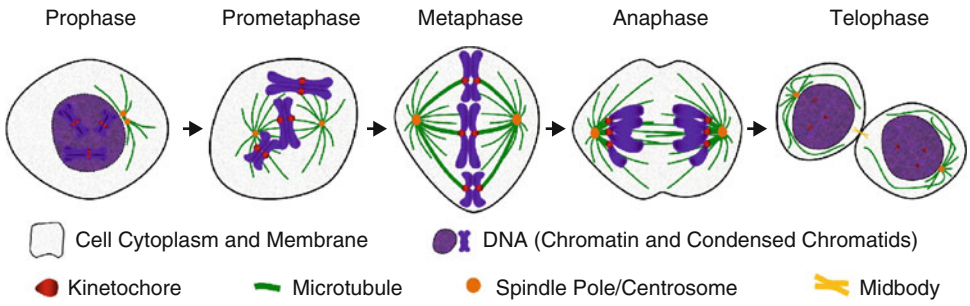

Fig. 1 Stages of mitosis are depicted by landmark events. In prophase the chromosomes condense within the nucleus. At prometaphase, the nuclear envelope breaks down and the kinetochores of the chromosomes interact with spindle microtubules. The chromosomes move to the spindle equator. At metaphase, the chromosomes are aligned at the spindle equator. At anaphase the sister chromatids separate and move to the spindle poles. The spindle poles also move apart. Cytokinesis is initiated. At telophase the mitotic spindle is disassembled, the chromatids decondense and the nuclear envelope reforms. Cytokinesis cleaves the cytoplasm in two until the daughter cells are connected only by the midbody

of nucleosomes, a repeating multi-protein unit of eukaryotic chromatin that localizes exclusively and stably to DNA. Thus, cells expressing Histone H2B-GFP permit observation of chromatin and condensed chromosomes throughout interphase and mitosis by fluorescence microscopy [2].

Mitosis in vertebrate cells proceeds through multiple stages, in which chromosomes exhibit differing physical states and undergo characteristic movements. In prophase, the first stage of mitosis, the duplicated sister chromatids condense to form the mitotic chromosomes within the nucleus (Fig. 1). During this time the spindle poles, also termed centrosomes, separate and begin to form the mitotic spindle composed of microtubules and accessory proteins. The chromosomes are released into the cytoplasm by the dissolution of the nuclear envelope, an event that marks the beginning of prometaphase. In the cytoplasm, the chromosomes interact with microtubules of the mitotic spindle through pairs of specialized multi-subunit substructures called the kinetochores, which power chromosome movements on the mitotic spindle. The sister kinetochores are arranged back to back on each chromosome and attach to spindle microtubules that emanate from opposite poles. The kinetochore interactions with the dynamic spindle microtubules move the chromosomes to the spindle equator. When all chromosomes have congressed to the spindle equator, the cell has reached metaphase. At the next stage, anaphase, the cohesions between sister chromatids are synchronously dissolved, and the separated chromatids move in opposite directions toward the spindle poles. In most cells the spindle poles also move apart. In the last stage of mitosis, called telophase, the mitotic spindle disassembles, the sister chromatids decondense,

and nuclear envelopes form around the spatially separated chromatin masses. Cytokinesis, initiated at anaphase onset, cleaves the cytoplasm until only a small bridge termed the midbody remains between the two daughter cells. With time, the midbody thins and is severed in a process called abscission, resulting in complete separation of the two daughter cells.

1.2 Live-Cell Imaging Considerations

1.2.1 Environment

Maintaining cell health is critical in live-imaging experiments. Mammalian cells must be viable and healthy during the imaging process to ensure that they will progress normally through the cell cycle. Important parameters that must be maintained include temperature, osmotic pressure and pH. Most human cells grow optimally in medium at 37 °C with an osmotic pressure range between 260 and 320 mOsm/kg and a pH range between 7.2 and 7.4. Temperature can be maintained by various strategies including objective heaters, stage heaters, and thermoregulated forced air. Evaporation must be avoided lest the medium become hypertonic. Typical bicarbonate-balanced media require proper control of CO_2 in the environment to maintain pH. Deviations from these optimum parameters may compromise cell viability and lead to arrest of cell cycle progression and cell division.

Use of one or a combination of methods is necessary to control these parameters. To control the incubation environment, the microscope or the microscope stage may be enclosed in commercially available or laboratory-constructed environmental chambers. This method is advantageous because the temperature, humidity, and CO_2 levels can be maintained using a single system. However, this strategy limits ready access to the cells. In addition, enclosures often expose microscope components to elevated humidity and temperature, which may be detrimental to the equipment. Alternatively, individual methods for the maintenance of temperature, pH, and osmotic pressure may be used. An objective heater (necessary for oil immersion objectives), a stage heater, or a system that maintains temperature by moving heated air across the culture vessel can be employed singly or in combination to maintain appropriate culture temperature. In order to maintain stable pH commonly used DMEM-based or other medium requiring 5 % CO_2 levels may be replaced with Leibovitz's L15-based media. Leibovitz's L15 is buffered by phosphates and free base amino acids instead of sodium bicarbonate and is suitable for culture of many cell lines. It is designed to maintain pH and support cell growth in environments without CO_2 equilibration. Both DMEM- and L15-based media provide an appropriate osmotic pressure near 290 mOsm/kg. To inhibit media evaporation and ensuing changes in osmotic pressure, sealed imaging chambers can be used. Alternatively, the culture media in imaging chambers can be overlaid with mineral oil.

1.2.2 Illumination and Fluorophores

Mammalian cells expressing fluorescent proteins are extremely sensitive to photo-damage from high intensity fluorescence light sources; minimization of illumination light helps maintain favorable growth and reduce fluorophore photobleaching. Settings for illumination intensity, duration, and intervals between image capture to achieve optimal results will vary with the light efficiency of the microscope system, fluorescent protein type and abundance, cell line, and the length of the experiment. It is necessary to carry out empirical trials to determine optimal settings for each parameter. If imaging parameters result in arrest or delay at any stage of the cell cycle, it is a strong indication that cell health has been compromised. Phenol red, a pH indicator that absorbs light and adds background fluorescence upon illumination, is commonly used in tissue culture medium, but it also interferes with the observation of certain fluorophores. Using medium lacking phenol red is recommended during fluorescence imaging to permit a reduction in the amount of illumination required to visualize the fluorescent protein of interest. One approach to minimize photo-damage and unnecessary photobleaching of target fluorophores is, wherever possible, to use transmitted light for focusing on cells and setting up experiments. Transmitted light can be used to identify cell or culture regions for image acquisition and for automated focusing protocols, thus reducing a cell culture's exposure to high intensity fluorescence illumination. In addition, it is often informative to monitor cytokinesis and other morphological changes by transmitted light as they may not be revealed by fluorescent Histone H2B-GFP or other fluorescent fusion proteins as cells progress through mitosis. Common bright-field methods include phase contrast and Nomarski *D*ifferential *I*nterference *C*ontrast (DIC). Although less phototoxic than fluorescence illumination, exposure to light commonly used for transmitted illumination should also be minimized to maintain cell health.

The constitutive expression and incorporation of H2B-GFP into the DNA of HeLa cells permits visualization of chromatin and condensed chromosomes for long periods without perturbing the cell cycle when environmental culture conditions are maintained and minimization of damaging light exposure is achieved. HeLa cells, commonly used in scientific research, are an immortal human cell line derived from cervical cancer cells. Histone H2B-GFP allows for effective monitoring of the various stages of mitosis by providing a clear indication of chromosome location, movements, and condensation state. Kinetochore proteins, tubulin subunits of microtubules, and other subcellular structures have also been expressed as fluorescent protein fusions and can be useful in studying mitotic progression. Although GFP remains one of the most commonly utilized fluorescent proteins, many other fluorescent proteins are available including photo-activatable and photo-convertible varieties. Co-expression of two or more proteins, each

tagged with fluorescent proteins of differing emission wavelengths, allows simultaneous tracking of multiple structures (e.g., chromosomes and microtubules) within the same cell. For simplicity in this example method, we examine mitotic progression by monitoring the status of a single fluorescent protein, Histone H2B-GFP, in HeLa cells.

In this section we describe a live-cell imaging approach to examine vertebrate mitosis using an automated, inverted fluorescence microscope. This method is particularly useful for identification and characterization of aberrant mitotic phenotypes. Under experimental conditions, these errors may be induced by exposure to chemical inhibitors or from protein depletion using RNAi or other methods to target suspected mitotic regulators.

2 Materials

The following materials are used to monitor mitotic progression using HeLa cells expressing Histone H2B-GFP fusion proteins. This cell line has been described in a previous study [2].

1. Automated inverted fluorescence microscope system (*see* **Note 1**).
2. Air Stream Stage Incubator (Model ASI400, NEVTEK) (*see* **Note 2**).
3. HeLa cell line expressing Histone H2B-GFP fluorescent protein fusion.
4. Leibovitz's L15 phenol red-free media supplemented with 10 % fetal bovine serum and antibiotics (penicillin and streptomycin solution).
5. Mineral Oil.
6. Culture chambers suitable for fluorescence imaging (*see* **Note 3**).
7. Taxol/paclitaxel (*see* **Note 4**).

3 Methods

The following procedure describes techniques to monitor chromosome location and analyze mitotic progression in HeLa H2B-GFP cells by live imaging using an inverted fluorescence microscope. In the examples we review, HeLa H2B-GFP cells were exposed to varying concentrations of Taxol, or depleted of either SKA3 (*S*pindle and *K*inetochore *A*ssociated *3*) [3] or MAD2 (*M*itotic *A*rrest *D*eficient *2*) [4] protein by RNAi (*see* **Note 5**). SKA3 and MAD2 are proteins that regulate proper mitotic progression, and depletion of these proteins emphasizes the detection and characterization of mitotic aberrations distinct from those induced by Taxol.

3.1 Cell Culture in Chambered Cover glasses

1. If RNAi experiments are to be done, transfect Hela H2B-GFP cells with the appropriate siRNA one or more days before the planned experiment (*see* **Note 6**).
2. The day before the planned experiment, transfer the cells into the cover-glass chambers. The cells should cover approximately 40 % of the available surface prior to initiating image acquisition (*see* **Note 7**).

3.2 Time-lapse Microscopy

1. Turn on the computer, microscope, and accessory devices. Accessory devices may include fluorescence illumination sources, shutters, filter wheels, and stage controllers.
2. Turn on the Air Stream Incubator and monitor temperature above the objective until a constant temperature of 37 °C is achieved (*see* **Note 8**).
3. Launch the software responsible for controlling the microscope system and define known parameters such as illumination wavelengths, time-lapse imaging frequency and duration, and the location for storage of the image acquisition files (*see* **Notes 9** and **10**).
4. Exchange the growth medium in the chambered cover glass using 37 °C Leibovitz's L15 phenol red-free supplemented media (*see* **Note 11**).
5. If chemical inhibitors are to be used, add to chambers immediately prior to imaging.
6. Overlay the L15 media with 37 °C mineral oil (*see* **Note 12**).
7. Mount the cover-glass chamber on the stage and ensure that it is firmly secured such that it does not shift with respect to the stage during movement of the stage.
8. Using transmitted light, select regions (imaging fields) with appropriate cell densities within cover-glass chambers. Instruct the microscope system's software to retain the selected field coordinates and to monitor correct focus at each position (*see* **Note 13**).
9. Define parameters for both transmitted light and GFP fluorescence imaging by experimenting with exposure times and light intensities at a few locations that will not be recorded during the experiment (*see* **Note 14**).
10. Once proper imaging and environmental parameters for the assay have been defined or achieved, initiate image acquisition.
11. At the end of the total imaging period, shut down the system and turn off all accessories.

3.3 Analysis

Captured images are examined to determine if perturbations in mitotic progression have occurred under experimental conditions and that control cells have progressed through mitosis normally.

Images can be assembled for analysis in convenient sequential series or time-lapse video records that display chronological events within single or multiple image fields. Several automated approaches have been described and applied to analyze fluorescence time lapse images of cells proceeding through mitosis that rely upon detection of various fluorescent fusion proteins. Many tools devoted to these goals are included in commercial microscopy software. However, it is important to analyze some of the results of this type of assay manually to ensure that criteria employed in automated analyses yield accurate results. Since automated systems and parameters vary widely and are specific to individual products, we describe a process for manual analysis that characterizes some general features of mitotic progression. We recommend this procedure be applied and results compared to those derived from automated data processing prior to relying upon the output from automated analyses.

Using the images acquired from this example assay, we measure multiple aspects of normal and perturbed mitotic progression. Failure to enter mitosis or aberrations that cause catastrophic errors in mitotic progression will be readily apparent and can be described accordingly. Phenotypic aberrations that are not as prevalent or penetrant can be revealed by careful examination of chromosome location and movements over time. For example, mitotic stressors can cause a normally bipolar spindle to become irregular or multipolar; these spindle alterations can often be inferred by chromosome movements and positioning during prometaphase congression. Less obvious but still measurable are perturbations that minimally alter the progression rate through mitotic stages. Convenient temporal landmarks include the release of condensed chromosomes into the cytoplasm at prometaphase, successful alignment of chromosomes at the spindle equator at metaphase, and the separation of sister chromatids as anaphase commences. Variances in the duration between periods marked by these landmarks can be compared to determine if experimental conditions have perturbed mitotic progression. Results are based upon examination of both phase contrast and fluorescence images, but the analysis described below emphasizes data obtained from Histone H2B-GFP fluorescence.

1. Prepare sets of individual image fields in sequential order so that cellular Histone H2B-GFP fluorescence can be examined as cells progress into and through mitosis.
2. Adjust the contrast and brightness, sometimes referred to as "scale" or "scaling," within the microscopy software so that captured fluorescence signals are displayed in a manner that applies the gray levels within the images (0–4,095 for 12 bit images) properly to the computer monitor. Details within nuclei and mitotic chromosome characteristics should be discernible (Fig. 2).

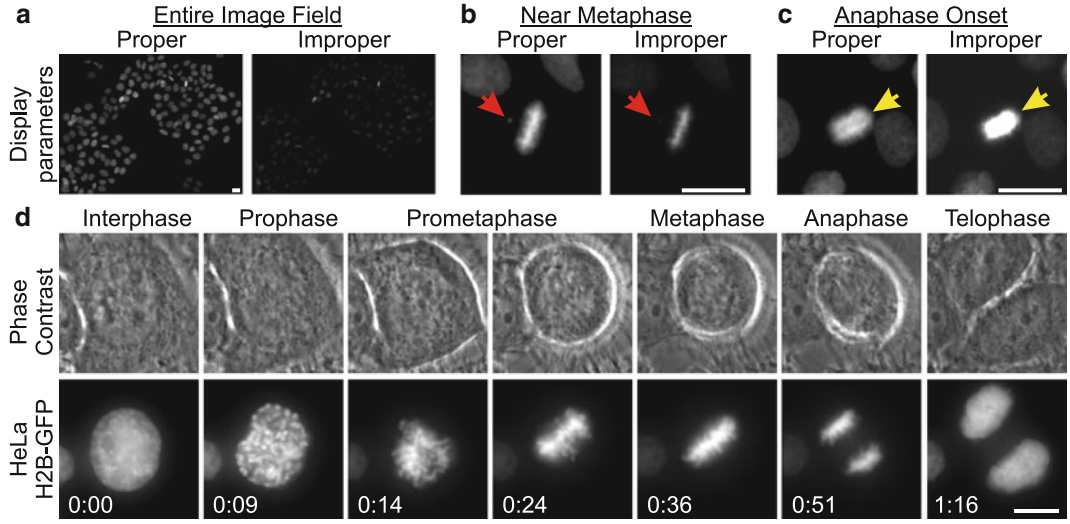

Fig. 2 Image display parameters and representative images from HeLa Histone H2B-GFP cell mitotic progression. (**a**) HeLa Histone H2B-GFP fluorescence images are presented with varying display characteristics demonstrating proper and improper scaling parameters. An entire image field acquired using a 20× objective is shown; proper scaling parameters reveal fluorescence signals within the DNA of all interphase and mitotic cells. (**b**) Properly displayed Histone H2B-GFP fluorescence reveals that the cell at the center of the image has not achieved complete metaphase; the *arrow* indicates the position of a chromosome that is not aligned with the majority of the chromosomes at the metaphase plate. (**c**) Proper display of the fluorescence signal from the mitotic cell reveals that it has entered anaphase (*arrow*); improper scaling limits the ability to resolve the two separating masses of chromatids. (**d**) Image panels showing phase contrast and GFP-fluorescence images of a HeLa-H2B GFP cell progressing through mitosis. Phase contrast and GFP-fluorescence images were acquired at 5-min intervals. Images representative of mitotic stages are shown. Scale bars = 10 μm

3. Beginning with a control sample, proceed sequentially through the images and record when individual cells enter prometaphase, reach metaphase, and initiate anaphase (*see* **Note 15**).
4. Make notations if abnormalities are observed, such as a failure of a subset of chromosomes to congress to the metaphase plate, an inferred multipolar spindle, or a failure of chromosomes to properly segregate during anaphase.
5. Process data from the various stage locations and experimental conditions. Image panels revealing examples of normal mitotic progression are shown in Fig. 2 (*see* **Note 16**).
6. Prepare graphical representations of the data to assess variances in mitotic progression under control conditions.
7. To determine if the culture conditions and imaging process negatively affect culture health and mitotic progression, create a plot that indicates the frequency of mitotic errors and variances in the time taken from prometaphase onset to the initiation of anaphase throughout the experimental period (Fig. 3) (*see* **Note 17**).

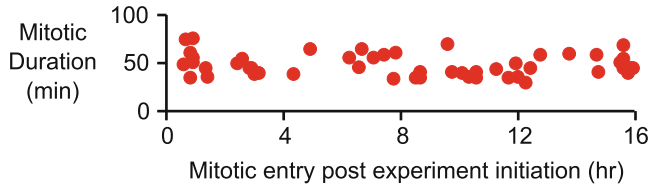

Fig. 3 Mitotic duration during the live-cell imaging process remains constant. HeLa H2B-GFP cells were imaged using an inverted fluorescence microscope system for 16 h. After image acquisition, the images were analyzed; onset of prometaphase and anaphase for every cell was established and mitotic duration was calculated by determining the difference between these two values. These durations were plotted against the time elapsed post initiation of the live-cell imaging process. Mitotic durations for the period of the assay were found to be consistent, indicating that the culture was healthy throughout the experiment

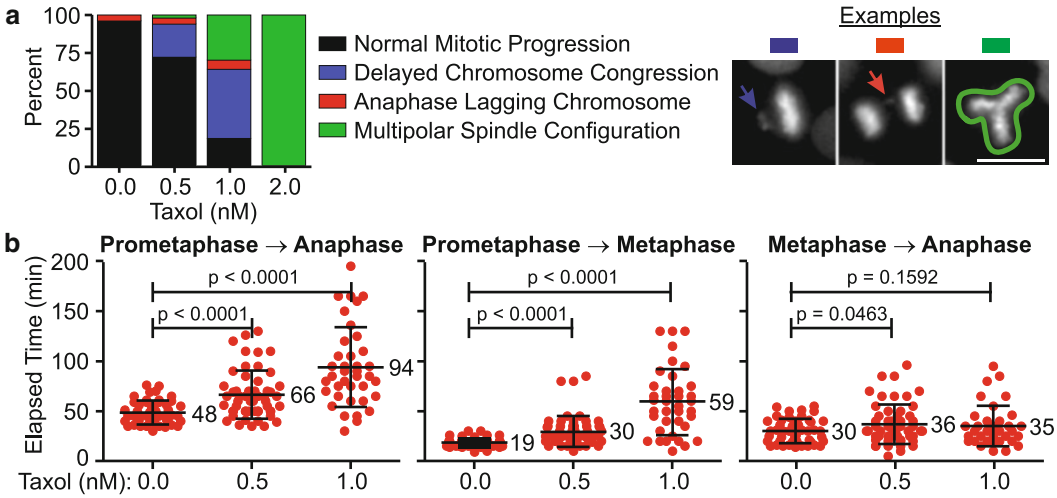

Fig. 4 Analysis of mitotic phenotypes upon Taxol treatment. HeLa Histone H2B-GFP cells were exposed to 0, 0.5, 1.0, or 2.0 nM Taxol and imaged with an inverted fluorescence microscope for 18 h. After image acquisition, the images were examined; mitotic defects and variances in mitotic duration were determined. (**a**) The percentage of cells exhibiting normal mitotic progression or mitotic defects is depicted in a column graph. Example images of defects are shown. With increasing concentrations of Taxol, the percentage of cells progressing normally through mitosis decreased, and the percentage of mitotic defects increased. Scale bars = 10 μm. (**b**) The elapsed time from prometaphase to anaphase onset, prometaphase to metaphase, and metaphase to anaphase onset was computed for cells progressing through mitosis in varying concentrations of Taxol. Results are plotted in a category scatter plot where data from each cell is depicted as a red circle. For each category the mean is labeled and the standard deviation is depicted by error bars. Statistical significance was calculated by performing an unpaired Student's *t*-test using data from control and experimental conditions; *p* values are indicated. With increasing concentrations of Taxol, the average time required to progress from prometaphase to anaphase increased. However, this increase was largely due to the increased duration taken from prometaphase to metaphase, as transition periods between metaphase and anaphase onset were largely unaffected

8. Prepare graphs using data from control and experimental conditions illustrating the type and frequency of mitotic errors. Since it is unlikely that the numbers of cells examined under each condition are equal, it is useful to display the frequency of mitotic errors as a percentage (Figs. 4a and 5a).

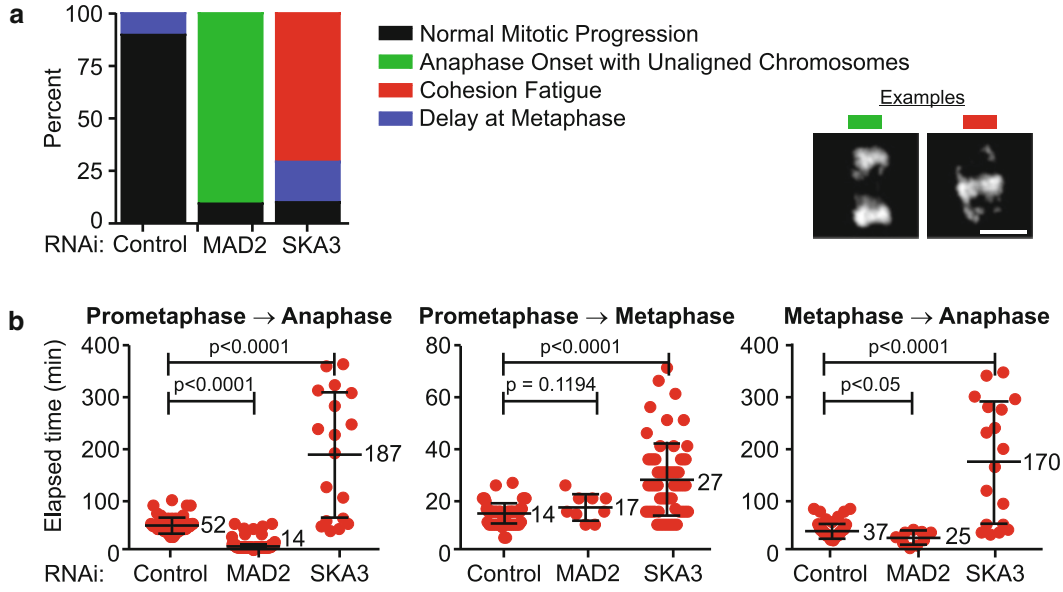

Fig. 5 Analysis of mitotic aberrations caused by MAD2 or SKA3 depletion by RNAi. HeLa H2B-GFP cells were transfected with control (non-targeting), MAD2 or SKA3 siRNA duplexes at 25 nM. Cells depleted of these proteins were imaged for 15 h. After image acquisition, the images were examined; mitotic defects and variances in mitotic duration were recorded. (**a**) Mitotic defects induced by different protein depletions were grouped into categories and are depicted in the column graph. Examples of observed defects are shown. The majority of control cells progressed normally through mitosis, but a large proportion of MAD2-depleted cells initiated anaphase with unaligned chromosomes. In contrast a majority of SKA3-depleted cells delayed at metaphase or underwent cohesion fatigue, a phenomenon whereby extended metaphase arrest causes asynchronous separation of sister chromatids without normal anaphase onset or mitotic exit cells due to persistent microtubule pulling forces [5]. Scale bars = 10 μm. (**b**) Mitotic duration from prometaphase to anaphase onset, prometaphase to metaphase, and metaphase to anaphase onset was determined for every observed cell in the different protein depletions. Results were plotted in a category scatter plot where cells are depicted as red circles. For each category the mean is labeled, and the error bars represent standard deviation. Statistical significance was calculated by performing an unpaired Student's *t*-test using data from control and experimental conditions; *p* values are indicated. The analysis indicates that MAD2-depletion decreases mitotic duration while SKA3-depletion increases mitotic duration. Time spent at metaphase decreases in MAD2-depleted cells as compared to control cells. The time taken to align chromosomes at the spindle equator and the metaphase duration increased in SKA3-depleted cells as compared to control cells

9. Prepare graphical representations of the data to assess and describe variances in mitotic progression between control and experimental conditions. Prepare scatter plots illustrating the time taken for cells to progress from prometaphase to anaphase, prometaphase to metaphase, and metaphase to anaphase (Figs. 4b and 5b) (*see* **Note 18**).

4 Notes

1. The system should include software that coordinates movements to and from assigned stage positions, that maintains focus, that regulates parameters of transmitted light and fluorescence illumination light exposures, and that controls digital image acquisition. The microscope should be designed for fluorescence microcopy with few optical elements in the light path in order to maximize the use of light; similarly, objectives should have a high numerical aperture (NA). In addition, the camera must be suitable for fluorescence microscopy. The more sensitive the detector of the camera, the lower the intensity of required illumination light. We use a Zeiss Axiovert 200 M microscope equipped with a Zeiss 20× Plan-NEOFLUAR infinity-corrected 0.50 NA objective, an appropriate excitation/dichroic/emission filter set for GFP fluorescence, and a Zeiss MCU28 motorized stage controller. The filter set is a BrightLine Basic™ single-band filter set, optimized for Green Fluorescent Protein and other like fluorophores (GFP-A-Basic-ZHE, Semrock). The camera is a Hamamatsu Orca ER. Illumination light is provided by a wide-field fluorescence microscope excitation light source (X-Cite 120Q, Lumen Dynamics). Microscope system components and digital image acquisition are managed by Metamorph software (Molecular Devices).
2. The Air Stream Stage Incubator has a regulated heating system that moves a curtain of thermoregulated air across the stage and culture. To ensure appropriate temperature regulation, a temperature probe is positioned adjacent to the culture chamber (digital thermometer model HH11, Omega).
3. We use Nunc Lab-Tek Chambered Cover glasses. These are polystyrene media chambers secured to a 1.0 Borosilicate chambered cover glass. One, 2, 4, or 8-well chambered cover glasses are available which permit up to 8 assay conditions per experiment.
4. Taxol/paclitaxel is a chemotherapeutic agent that inhibits normal microtubule dynamics by hyperstabilizing microtubules. Various other small molecular inhibitors that perturb mitotic progression are readily available. Inhibitors may interfere with microtubule dynamics, thus affecting the mitotic spindle, or inhibit kinases, phosphatases, and other proteins integral to mitotic progression.
5. RNA interference (RNAi) methods can be used to target message and prevent translation of known or proposed mitotic regulators. Mitotic proteins SKA3 and MAD2 were depleted by RNAi and effects on mitotic progression were determined.

6. The parameters for RNAi treatment will vary with the characteristics of the target protein. For instance, siRNA treatments for stable proteins may require 2–3 days for adequate depletion while other proteins that turnover rapidly or that reveal phenotypes when partially depleted may require that RNAi be carried out the day before imaging. Depletions that compromise mitosis often result in cell death, and therefore, parameters for RNAi-mediated depletion must be accurately established in preliminary experiments.
7. Ideally the cell culture will be at a density that accommodates the projected growth that will occur during image acquisition. Beginning an experiment at an appropriate cell density will help ensure the collection of interpretable images and provide sufficient space and nutrients for optimal cell proliferation.
8. Maintain this temperature for at least 30 min before imaging is initiated to ensure that the microscope stage and surrounding area has reached a temperature equilibrium that will be sustained by the Air Stream Incubator.
9. Usually we collect phase contrast and single plane GFP-fluorescence images at each stage location. For the 20× objective used in the above examples, a single image plane often provides sufficient depth for analysis. With the 20× objective each image filed contains many cells that can be analyzed as they enter and progress through mitosis. Acquisition of multiple focal planes at each location can be implemented to obtain additional information but this approach must be balanced with the necessity to avoid the phototoxic effects of fluorescence illumination.
10. The interval between image capture will determine the temporal resolution of the assay; the shorter the interval the greater the resolution. However, increase in the frequency of image capture, and therefore, exposure to fluorescence illumination will increase the chance for phototoxic effects. For most purposes, images of the HeLa H2B-GFP cells are collected at 5-min intervals. We find that acquisition frequencies near 5-min intervals are sufficient to detect most errors that may occur during mitotic progression without compromising the health of cells through phototoxicity.
11. Medium exchange can be achieved by aspiration of the existing medium and replacement with previously prepared and warmed replacement medium. To analyze effects of Taxol on HeLa cells, the Leibovitz's L15 medium was supplemented with Taxol ranging in concentrations between 0 and 2 nM during the imaging assay.
12. The L15 replacement medium volume and the mineral oil volume should be approximately 50 and 40 %, respectively of the

maximum volume recommended per chamber. The culture chamber's plastic cover may be absent during imaging; removing the cover often improves phase contrast or DIC images.

13. If the system relies upon the camera to set and test focus, it is preferable to use transmitted light rather than the fluorescence illumination.
14. The exposure times should be as short as is practical to produce an image with a reasonable signal to noise ratio and yet prevent photo-damage to the cell culture. These settings must be empirically determined based upon factors such as the efficiency of the microscope system and the fluorescent protein in use. In our system the camera contains a 12-bit digitizer that provides 4,096 gray levels. For phase contrast images we typically expose the cells for 150 ms to an intensity of transmitted light that results in an average intensity peak between 800 and 1,200; this is sufficient to visualize the location and shape of cells within the selected field. For Histone H2B-GFP fluorescence acquisition, we minimize illumination intensity and exposure duration to obtain images that enable both detection and characterization of interphase nuclei. Histone H2B-GFP fluorescence emission in condensed mitotic chromosomes is far greater per unit area than the intensities obtained from the chromatin present in interphase nuclei, so we set our parameters to suitably visualize these dimmer objects that are required for analysis within the experiment. In our system, the fluorescence illumination light source is limited to 12.5 % of maximum output and the exposure time is typically 40 ms. We aim to achieve average gray levels for interphase nuclei to be approximately twice that of the average background values, those areas lacking GFP fluorescence. This representative setting results in average Histone H2B-GFP nuclear fluorescence grayscale values between 300 and 400 with average background intensities near 200. With the same parameters, Histone H2B-GFP fluorescence from condensed mitotic chromosomes ranges between 800 and 2,000 gray levels. These intensities provide signal to noise capabilities sufficient for detecting single chromosomes within mitotic cells and observing cells for the duration of the experiment without causing phototoxicity.
15. The imaging software will have the capability to display the time at which images were acquired and/or display the elapsed time between images. The software may include functions to easily record these data points or the data may be entered manually into a separate spreadsheet application.
16. It is often advantageous to initially scan both control and experimental conditions to develop a catalog of frequent aberrations

(e.g., tripolar spindles, lagging chromosomes in anaphase) prior to analyzing the control and experimental samples in full.

17. Mitosis in HeLa cells is fallible, so one should expect a certain frequency of mitotic errors and variability in the duration of mitosis. However, these should not significantly increase with time on the microscope under control conditions. If significant increases in these categories occur as time progresses through the image acquisition period, then the overall health of the culture was likely challenged, and therefore, conclusions attributed to experimental conditions may be erroneous.
18. Numerical analyses can be applied to the data to determine if differences are statistically significant. Herein, a commonly applied statistical hypothesis test, the unpaired *t*-test, is applied to establish statistically relevant differences between experimental conditions. A p value of less than 0.05 returned by the test indicates a likely statistically significant variation. It indicates that there is a 95 % probability that control and experimental differences did not occur by chance.

References

1. Paweletz N (2001) Walther Flemming: pioneer of mitosis research. Nat Rev Mol Cell Biol 2(1):72–75
2. Kanda T, Sullivan KF, Wahl GM (1998) Histone-GFP fusion protein enables sensitive analysis of chromosome dynamics in living mammalian cells. Curr Biol 8(7):377–385
3. Daum JR, Wren JD, Daniel JJ, Sivakumar S, McAvoy JN, Potapova TA, Gorbsky GJ (2009) Ska3 is required for spindle checkpoint silencing and the maintenance of chromosome cohesion in mitosis. Curr Biol 19(17):1467–1472
4. Musacchio A, Salmon ED (2007) The spindle-assembly checkpoint in space and time. Nat Rev Mol Cell Biol 8(5):379–393
5. Daum JR, Potapova TA, Sivakumar S, Daniel JJ, Flynn JN, Rankin S, Gorbsky GJ (2011) Cohesion fatigue induces chromatid separation in cells delayed at metaphase. Curr Biol 21(12): 1018–1024

Chapter 32

Analyzing Sister Chromatid Cohesion in Mammalian Cells

Katherine M. Feeney, Laura McFarlane-Majeed, and Joanna L. Parish

Abstract

The metaphase chromosome spread technique and subsequent analysis of sister chromatid cohesion is used for (clinical) diagnosis of genetic abnormalities that can cause aberrant sister chromatid cohesion. In addition, the technique can be used to assess the contribution of novel genes to the cohesion establishment and maintenance pathways. Cells are swelled in a hypotonic solution and fixed in Carnoy's solution. Samples are then dropped onto glass slides, and the spread chromosomes are stained and visualized by microscopy. Defects in sister chromatid cohesion can be easily assessed using this method, examples of which are given.

Key words Cohesion, Metaphase, Sister chromatids, Chromosomes, Cohesin

1 Introduction

In order for normal cellular functions to be successfully carried out and for cells to survive and proliferate, it is essential that the integrity of the genome is maintained. Cells must succeed in passing on an accurate copy of their genetic material to each daughter cell during mitosis. Loss of genomic integrity in a cell can result in severely abnormal phenotypes and is associated with various human genetic disorders, including cancer [1, 2]. Consequently cells have evolved tightly regulated mechanisms to preserve genetic stability and to enable the consistently accurate transmission of genetic information to subsequent generations.

For cells to successfully undergo mitosis and produce two genetically identical daughter cells, there are several key processes that must first be carried out effectively and accurately. The first fundamental requirement of the cell cycle is that the cell must accurately synthesize exact copies of the DNA in each of its chromosomes to be passed on to its progeny during cell division. Subsequently, each of these replicated chromosomes, now termed sister chromatids, must be precisely segregated so that each daughter cell has the correct chromosomal complement following cytokinesis.

Eishi Noguchi and Mariana C. Gadaleta (eds.), *Cell Cycle Control: Mechanisms and Protocols*, Methods in Molecular Biology, vol. 1170, DOI 10.1007/978-1-4939-0888-2_32,

These two processes are intimately linked and tightly controlled by many cellular proteins ranging from those involved in the control of vital cellular checkpoints to the structural proteins responsible for holding sister chromatids together and subsequently allowing their separation. Establishment and termination of sister chromatid cohesion is a complex and highly ordered process that is vital for the maintenance of genome integrity [3].

During DNA replication, each newly replicated sister chromatid pair must be physically associated with each other until their separation at mitosis. Work carried out in yeast identified four genes which, when mutated, resulted in high-frequency chromosome loss. These included two *SMC* (Structural Maintenance of Chromosomes) family members as well as two uncharacterized genes which were named *SCC1* and *SCC3* (Sister Chromatid Cohesion) [4]. It was shown in later work that these four proteins are assembled as a large ring-like protein complex in cells, termed the cohesin complex, and that they facilitate the cohesion between newly synthesized sister chromatids by physically linking them together [5].

Although sister chromatid cohesion is established during DNA replication, studies have shown that cohesin actually becomes associated with DNA in G1 phase in the case of lower eukaryotes while in mammalian cells it has been observed that cohesin relocalizes to DNA towards the end of telophase [4, 6, 7]. Loading of cohesin onto DNA molecules is brought about by its interaction with another protein complex called the Scc2(NipBL)-Scc4 complex with the energy driving this process being generated by the ATPase activity of the SMC cohesin subunits, although the actual mechanism of cohesin loading is still unclear [8].

During replication, acetylation of SMC3 by Esco1/2 induces a conformational change in the cohesin ring which may permit passage of the replication fork and facilitate entrapment of both daughter DNA molecules [9–11]. The subsequent binding of Pds5 and sororin to cohesin ensure that the complex maintains a cohesive state [12]. Cohesion is maintained until prophase when chromosome arm cohesion is removed [13]. Prophase release is dependent on multiple mitotic kinases. Aurora B and Cdk1 phosphorylate sororin while Plk1 phosphorylates SA1/2, the human homologues of Scc3 [14, 15]. At the end of metaphase, dissolution of centromeric cohesion is triggered by separase-mediated cleavage of the Scc1 subunit [16]. Centromeric cohesion is protected by the combined action of Sgo1 and PP2a, which prevent phosphorylation of sororin, a process which is still poorly understood [17, 18].

Mutations in subunits of the cohesin complex or in cohesion-associated proteins can result in a variety of rare human diseases, known as cohesinopathies. Two of the best-characterized

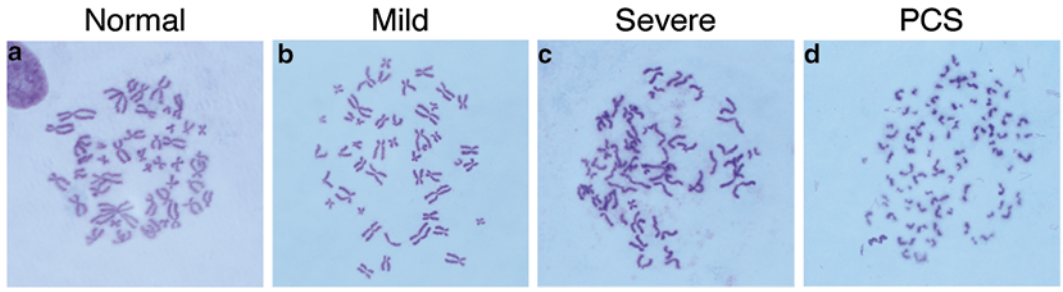

Fig. 1 Examples of metaphase spreads from cells with (**a**) normal sister chromatid cohesion; chromosomes are "X-shaped" with tight centromeric cohesion between all chromatid pairs. (**b**) Mild cohesion defects; some or all of the chromatid pairs have a "railroad" appearance with loss of centromeric cohesion, but chromosomes are loosely paired. (**c**) Severe cohesion defects; all chromosome pairs have lost centromeric cohesion and some chromosome pairs are no longer associated. (**d**) Premature chromatid separation (PCS); pairing of sister chromatids is completely absent

cohesinopathies are Roberts syndrome (RBS) and Cornelia de Lange syndrome (CdLS), both of which present as multisystem developmental disorders. The mitotic chromosomes of patients with these disorders show defects in sister chromatid cohesion with phenotypes including premature sister chromatid separation (PCS) and "railroad" chromosomes frequently observed (Fig. 1).

A new cohesinopathy called Warsaw breakage syndrome (WBS) has also been described which, like RBS and CdLS, is characterized by cohesion defects. However, cells from patients with WBS also show sensitivity to chemicals that induce replication stress, similar to those from patients with Fanconi anemia [19]. WBS is a recessive disorder caused by mutations in the *DDX11* gene that encodes the DNA helicase ChlR1. Chromosomes from these patients frequently have a railroad appearance, indicative of cohesion abnormalities. Indeed, experiments in mice and human cells have shown that loss of ChlR1 results in defects in sister chromatid cohesion [20, 21].

Abnormalities in sister chromatid cohesion are frequent in RBS, CdLS, and WBS, and assessment of chromatid cohesion in metaphase spreads is used as a diagnostic tool. In addition, determining whether novel genes are important in the establishment or maintenance of cohesion can be achieved by the examination of metaphase chromosomes. The preparation of metaphase spreads and analysis of sister chromatid cohesion is described below.

2 Materials

1. Colcemid solution: Gibco® KaryoMAX® Colcemid™ Solution in PBS (10 μg/mL).
2. Phosphate buffered saline (PBS): 1.06 mM KH_2PO_4, 2.97 mM Na_2HPO_4, 155 mM NaCl, pH 7.4.

3. 0.5 % Trypsin (if using adherent cells).
4. Hypotonic solution: 0.8 % w/v sodium citrate (*see* **Note 1**).
5. Carnoy's fixative: Mix three parts methanol with one part acetic acid, freshly prepared. Chill on ice before use.
6. Water bath, set at 37 °C.
7. Glass slides.
8. Giemsa solution: 1/20 dilution of Giemsa (Sigma) diluted in H_2O.
9. DPX mountant (Sigma).
10. Glass coverslips (40 × 22 mm).
11. Microscope fitted with a 63× or 100× objective.
12. Imaging software (e.g., Image J).

3 Methods

3.1 Metaphase Chromosome Preparation

1. Cells should be approximately 70 % confluent and growing in log phase. Contact inhibition of cells will dramatically reduce the number of metaphases obtained.
2. To each dish add 1/100 volume of colcemid solution (final concentration: 100 ng/mL) and return to incubator for 2–4 h (*see* **Note 2**). The volumes stated below are for a 10-cm tissue culture dish or a 25-cm^2 flask of suspension cells.
3. Harvest the cells.
   (a) *Adherent cells.* Wash the cells twice with 5 mL of PBS, add 1 mL 0.5 % trypsin and cover the cells by gentle rocking. Return the dish to 37 °C, and when the cells have detached (2–5 min, depending on cell type), suspend the cells in 10 mL of growth medium. When adherent cells are in mitosis they round up and detach from the culture plate. To minimize loss of detached cells, collect culture medium, PBS washes, and trypsinized cells into one sample tube. Pellet the cells by centrifugation for 5 min at 300 × *g*.
   (b) *Suspension cells.* Remove the cells from the culture flask and harvest by centrifugation for 5 min at 300 × *g*.
4. Remove the supernatant by pouring and gently wash the cells in 5 mL of ice cold PBS.
5. Centrifuge for 5 min at 300 × *g*. Pour off the supernatant and gently vortex to resuspend the pellet in the remaining solution (approximately 200 μL).
6. Slowly add 10 mL of hypotonic solution while gently vortexing.
7. Incubate at room temperature for 10 min (*see* **Note 3**).

8. Centrifuge for 5 min at 300×*g*. Pour off the supernatant and gently vortex to resuspend the pellet in the remaining solution (approximately 200 μL).
9. Slowly add 7 mL of ice-cold Carnoy's fixative while gently vortexing.
10. Incubate at room temperature for 10 min.
11. Repeat **steps 8–10** two more times.
12. Centrifuge for 5 min at 300×*g*. Pour off the supernatant and resuspend cells in 300 μL of Carnoy's fixative (*see* **Note 4**).

3.2 Preparing Slides

1. Thoroughly clean microscope slides with 100 % ethanol and lint free tissue.
2. Position the slides at ~45° angle in a warm humidified environment. For example, the slides can be placed on a tray lined with moist tissue with one end of the slide resting on the lip of the tray in a 37 °C water bath.
3. Pipette 2–3 drops of cell suspension onto microscope slide from a height of approximately 15 cm and leave to drain down the length of the slide. The fixative will evaporate as the drop travels down the slide.
4. Allow samples to air-dry.
5. Check density and quality of spreading by light microscopy (10× objective) before proceeding to slide staining (*see* **Note 5**).

3.3 Slide Staining and Mounting

1. Stain the slides with diluted Giemsa solution for 15 min (*see* **Note 6**).
2. Wash the slides in H_2O for 3 min.
3. Allow the slides to air-dry.
4. Apply several drops of DPX mountant to the slide.
5. Slowly apply a coverslip at an angle, avoiding the introduction of bubbles.
6. Cover the slide with tissue and gently press the coverslip to remove excess mountant.
7. Leave to set overnight at room temperature before analysis by microscopy.

3.4 Analysis

1. Once the mountant has set, slides can be imaged by conventional light microscopy using an upright microscope fitted with a 63× or 100× objective.
2. The data can be analyzed in two different ways.
   (a) Metaphases with normal versus abnormal sister chromatid cohesion can be counted and the percentage with railroad chromatids or PCS quoted.

(b) Digital images of the metaphases can be captured and the distance between each chromatid pair at the centromere can be measured using Image J software (or within the software used for the original image capture). When analyzing the images in this way, care must be taken to ensure that all images are taken using identical settings.

4 Notes

1. Alternatively, 0.075 M KCl may also be used.
2. Colcemid destabilizes microtubules and results in a prometaphase delay. Colcemid treatment will increase the number of mitotic cells; however, longer incubation times result in shorter and more condensed chromosomes. Therefore, the optimal incubation time in colcemid should be determined for each cell type used.
3. The incubation time may need to be optimized depending on cell type.
4. At this point, the samples can be stored at 4 °C for up to 4 weeks; however, it is best to drop onto slides promptly. If the samples have been stored for more than a day, two changes of fixative are recommended to remove esters and water formed in the fixative, which may inhibit spreading.
5. Sample density can be adjusted by altering the volume of fixative or the number of drops applied. Various techniques can be used to improve chromosome spreading. For example, use ice-cold slides, use wet slides, or apply fixative to slides and allow to partially dry before dropping samples.
6. The incubation time for Giemsa staining may need to be optimized, particularly if samples have been stored in fixative before dropping. Incubation in diluted Giemsa stain for up to 2 h is sometimes necessary.

Acknowledgements

JP is supported by a Royal Society University Research Fellowship (UF110010).

References

1. Ricke RM, van Ree JH, van Deursen JM (2008) Whole chromosome instability and cancer: a complex relationship. Trends Genet 24:457–466
2. Weaver BA, Cleveland DW (2006) Does aneuploidy cause cancer? Curr Opin Cell Biol 18: 658–667
3. Feeney KM, Wasson CW, Parish JL (2010) Cohesin: a regulator of genome integrity and gene expression. Biochem J 428:147–161
4. Michaelis C, Ciosk R, Nasmyth K (1997) Cohesins: chromosomal proteins that prevent premature separation of sister chromatids. Cell 91:35–45
5. Haering CH, Lowe J, Hochwagen A et al (2002) Molecular architecture of SMC proteins and the yeast cohesin complex. Mol Cell 9:773–788
6. Lengronne A, Katou Y, Mori S, Yokobayashi S et al (2004) Cohesin relocation from sites of chromosomal loading to places of convergent transcription. Nature 430:573–578
7. Darwiche N, Freeman LA, Strunnikov A (1999) Characterization of the components of the putative mammalian sister chromatid cohesion complex. Gene 233:39–47
8. Ciosk R, Shirayama M, Shevchenko A et al (2000) Cohesin's binding to chromosomes depends on a separate complex consisting of Scc2 and Scc4 proteins. Mol Cell 5:243–254
9. Kurze A, Michie KA, Dixon SE et al (2011) A positively charged channel within the Smc1/Smc3 hinge required for sister chromatid cohesion. EMBO J 30:364–378
10. Whelan G, Kreidl E, Peters JM et al (2012) The non-redundant function of cohesin acetyltransferase Esco2: some answers and new questions. Nucleus 3:330–334
11. Zhang J, Shi X, Li Y et al (2008) Acetylation of Smc3 by Eco1 is required for S phase sister chromatid cohesion in both human and yeast. Mol Cell 31:143–151
12. Nishiyama T, Ladurner R, Schmitz J et al (2010) Sororin mediates sister chromatid cohesion by antagonizing Wapl. Cell 143:737–749
13. Losada A, Hirano M, Hirano T (1998) Identification of Xenopus SMC protein complexes required for sister chromatid cohesion. Genes Dev 12:1986–1997
14. Nishiyama T, Sykora MM, Huis in't Veld PJ et al (2013) Aurora B and Cdk1 mediate Wapl activation and release of acetylated cohesin from chromosomes by phosphorylating Sororin. PNAS 110:13404–13409
15. Sumara I, Vorlaufer E, Stukenberg PT et al (2002) The dissociation of cohesin from chromosomes in prophase is regulated by Polo-like kinase. Mol Cell 9:515–525
16. Waizenegger IC, Hauf S, Meinke A et al (2000) Two distinct pathways remove mammalian cohesin from chromosome arms in prophase and from centromeres in anaphase. Cell 103:399–410
17. Liu H, Rankin S, Yu H (2013) Phosphorylation-enabled binding of SGO1-PP2A to cohesin protects sororin and centromeric cohesion during mitosis. Nat Cell Biol 15:40–49
18. Shintomi K, Hirano T (2010) Sister chromatid resolution: a cohesin releasing network and beyond. Chromosoma 119:459–467
19. van der Lelij P, Chrzanowska KH, Godthelp BC et al (2010) Warsaw breakage syndrome, a cohesinopathy associated with mutations in the XPD helicase family member DDX11/ChlR1. Am J Hum Genet 86:262–266
20. Inoue A, Li T, Roby SK, Valentine MB et al (2007) Loss of ChlR1 helicase in mouse causes lethality due to the accumulation of aneuploid cells generated by cohesion defects and placental malformation. Cell Cycle 6:1646–1654
21. Parish JL, Rosa J, Wang X et al (2006) The DNA helicase ChlR1 is required for sister chromatid cohesion in mammalian cells. J Cell Sci 119:4857–4865

Chapter 33

Affinity Purification of Protein Complexes from Drosophila Embryos in Cell Cycle Studies

Zoltan Lipinszki, Peng Wang, Rhys Grant, Catherine Lindon, Nikola S. Dzhindzhev, Pier Paolo D'Avino, Marcin R. Przewloka, David M. Glover, and Vincent Archambault

Abstract

The ability to identify protein interactions is key to elucidating the molecular mechanisms of cellular processes, including mitosis and cell cycle regulation. *Drosophila melanogaster*, as a model system, provides powerful tools to study cell division using genetics, microscopy, and RNAi. Drosophila early embryos are highly enriched in mitotic protein complexes as their nuclei undergo 13 rounds of rapid, synchronous mitotic nuclear divisions in a syncytium during the first 2 h of development. Here, we describe simple methods for the affinity purification of protein complexes from transgenic fly embryos via protein A- and green fluorescent protein-tags fused to bait proteins of interest. This in vivo proteomics approach has allowed the identification of several known and novel mitotic protein interactions using mass spectrometry, and it expands the use of the Drosophila model in modern molecular biology.

Key words Proteomics, Drosophila, Mitosis, Cell cycle, Embryos, Interactions, Protein complexes, Affinity purification

1 Introduction

Mitotic progression involves a complex and highly dynamic network of protein–protein interactions. The ability to dissect these associations is important to understand how specific proteins function relative to each other. The affinity purification of individual bait proteins, followed by the identification of associated factors by mass spectrometry, has allowed the detection of such networks involved in many cellular processes [1, 2]. However, in mitosis, many crucial interactions are restricted to a small time window or to discrete subcellular structures and often require specific posttranslational modifications. For this reason, mapping the mitotic protein interactome has proved challenging [3].

Eishi Noguchi and Mariana C. Gadaleta (eds.), *Cell Cycle Control: Mechanisms and Protocols*, Methods in Molecular Biology, vol. 1170, DOI 10.1007/978-1-4939-0888-2_33,

Proteins controlling cell division tend to be well conserved between species and have been studied in many model organisms. Yeast and vertebrate cells can be arrested and even synchronized in mitosis, in order to enrich for complexes of interest prior to their purification. This strategy has been successful, although it remains possible that an observed interaction does not reflect the normal physiology of the system, due to the artificial cellular state induced by the drug treatment. The fruit fly *Drosophila melanogaster* has contributed greatly to increasing our molecular understanding of mitosis. The genetic tools available in flies are extremely well developed for in vivo studies, and Drosophila cells in culture also offer several advantages. For example, we have previously developed protocols for the purification of protein complexes from Drosophila cultured cells [4], which have led to the identification of a number of new interactions and to the dissection of several molecular mechanisms of cell cycle regulation, mitosis, and cytokinesis [5–7]. Yet, these cells, such as Schneider (S2) or D.Mel-2 cells, are notoriously difficult to arrest and synchronize in mitosis, which limits the isolation and detection of transient, low-abundance complexes acting specifically during cell division. Moreover, cultured cell lines, adapted to grow in vitro by the process of immortalization, do not always accurately represent the in vivo physiology of the biological system. Therefore, the development of an in vivo proteomics methodology would add a new approach to the Drosophila toolbox and expand its value as a leading model organism in the field of mitosis.

We decided to exploit Drosophila early embryos as starting material for the identification of mitotic protein interactions. After fertilized eggs are laid, 13 rounds of rapid and synchronous mitotic divisions of nuclei in a syncytium take place before cellularization of the blastoderm occurs. This developmental stage relies on proteins and mRNAs that are maternally deposited in the egg. Divisions occur approximately every 10 min, where M phase and S phase alternate without intervening gap phases [8]. Therefore, embryos collected before 2 h of age constitute a starting material that is highly enriched in mitotic protein complexes.

We express proteins of interest (bait proteins) in fusion with a tag to facilitate their isolation by affinity purification. A single-step purification, which takes advantage of a high affinity between a tag and a resin, enormously simplifies the process of protein isolation, making it easy and straightforward even for an inexperienced biochemist. Moreover, a fast procedure increases the chances of preserving unstable protein complexes.

Here, we describe protocols and reagents that we have developed or adapted for the expression and purification of proteins fused to either protein A (PrA)- or green fluorescent protein (GFP)-tags. A transgene coding for the fusion protein expressed maternally in eggs results in the presence of the tagged protein in

the early embryos. This bait protein is incorporated into complexes with endogenous partner proteins. Following affinity purification of the bait, associated proteins can be identified by mass spectrometry. This method has been validated by the purification of several known and novel mitotic protein–protein interactions in our laboratories (unpublished). As expected, several of the associations identified in embryos were missed when Drosophila cultured cells were used, reflecting the importance of using embryos as a highly enriched mitotic source tissue. This approach also bears potential to probe interactions involved in other processes that occur in Drosophila early embryos.

2 Materials

2.1 Embryo Collection

1. Vials and bottles with standard Drosophila cornmeal food.
2. Transgenic flies expressing the bait protein: Few to tens of thousands of healthy and newly enclosed fruit flies.
3. From theses flies, 1 g of syncytial embryos per purification (*see* **Note 1**).
4. Embryo collection cages (Genesee Scientific) that can be fitted onto 100 mm-diameter plastic Petri dishes or large fly population cages (Genesee Scientific, cylindrical cages with 30 cm diameter and 60 cm length) suitable for large-scale embryo collections. Similar (homemade) cages made of plexiglass or durable acrylic can also be used. More information at: http://www.flystuff.com/general.php.
5. Grape juice agar (*see* **Note 2**): Dissolve 12.5 g sucrose and 11.25 g agar in 375 mL water. Boil until completely dissolved. Add 125 mL grape juice, allow to cool down, and distribute into plastic Petri dishes, which can be fitted onto embryo collection cages (100 mm-diameter), or into larger trays (e.g., 15 × 25 cm polystyrene trays) when using large fly population cages.
6. Yeast paste (*see* **Note 2**): Mix dry active yeast with distilled water until a homogenous paste with a consistency similar to peanut butter is obtained. Add water or yeast again as needed.
7. Sieves or mesh basket (Genesee Scientific) for small-scale embryo collections. For large-scale embryo collections, use large diameter (e.g., 10–20 cm) sieves (Endecotts Ltd, 70 μm pore size for embryo collection and 425 μm pore size for the collection of flies stuck to the yeast paste).
8. Paintbrushes: For embryo collection, normal soft paintbrushes can be used (size 3–6).
9. 50 % household bleach.
10. Distilled water.

11. Embryo wash solution (EWS): 0.7 % (w/v) NaCl and 0.05 % (w/v) Triton X-100.
12. Paper towels.
13. Flat-ended spatula.
14. Stereo microscope.
15. Benchtop micro centrifuge.
16. 1.5-mL microfuge tubes.
17. Analytical laboratory scale.
18. Liquid nitrogen.

2.2 Affinity Purification

We use rabbit IgG-coupled paramagnetic beads for PrA affinity purification. The detailed method for covalently coupling rabbit IgG to magnetic beads has been described previously [4]. For GFP affinity purification, we use the GFP-Trap system (ChromoTek GmbH).

2.2.1 Affinity Resins

1. Rabbit IgG-coupled paramagnetic beads for PrA affinity purifications: Home-made by covalently coupling rabbit IgG (MP Biomedicals) to Dynabeads® M-270 Epoxy (Life Technologies).
2. GFP-Trap system (*see* **Note 3**) (ChromoTek GmbH).

2.2.2 Solutions

1. Extraction Buffer (EB) for PrA or GFP-Trap purification: 20 mM Tris–HCl pH 7.5, 150 mM NaCl, 2 mM $MgCl_2$, 0.5 mM Na-EGTA pH 8.0, 1 mM dithiothreitol (DTT), 0.1 % NP-40, 5 % glycerol, 1 mM phenylmethanesulfonyl fluoride (PMSF), EDTA-free complete protease inhibitor cocktail (Roche) (*see* **Notes 4** and **5**).
2. Wash buffer (WB): Same as EB.
3. Final wash buffer (FWB): 20 mM Tris–HCl pH 7.5, 150 mM NaCl, 2 mM $MgCl_2$, 0.5 mM Na-EGTA pH 8.0, 1 mM DTT (*see* **Note 6**).
4. Elution solution: Elution of the PrA-baits requires a freshly made and filtered solution of 0.5 M NH_4OH and 0.5 mM EDTA.
5. 1× Laemmli sample buffer: 60 mM Tris–HCl pH 6.8, 2 % (w/v) SDS, 10 % glycerol, 5 % 2-mercaptoethanol, 0.01 % (w/v) bromophenol blue.

2.2.3 Tools

1. Prechilled plastic sample micropestles or 7/15-mL glass Dounce tissue grinder (*see* **Note 5**).
2. Prechilled 10 mL plastic syringes and 0.8 mm × 40 mm needles.
3. Prechilled plastic/glass funnel-filter device: Place a double-layer Miracloth filtering cloth (EMD Millipore) into the funnel.
4. Prechilled 1.5-mL microfuge tubes and 15-mL conical tubes.
5. Cell Culture microscope.

6. Refrigerated benchtop micro centrifuge.
7. Rotating wheel.
8. Magnetic stands (Promega) suitable for microfuge or larger tubes.
9. Aspirator.
10. Vacuum concentrator.
11. Heat block.
12. Apparatus suitable for conventional (denaturing) sodium dodecyl sulfate polyacrylamide gel electrophoresis (SDS-PAGE) and Western blotting. Use 4–12 % gradient SDS-polyacrylamide gels for optimal separation of small to large size proteins.
13. Silver-nitrate staining kit (Life Technologies).

3 Methods

3.1 Production of Embryos

3.1.1 Generation of Transgenic Flies with Embryonic Expression of the Bait Protein

Transgenic flies expressing the PrA- or GFP-tagged proteins can be generated by various methods including standard *P*-element random insertion in the embryonic germline or can be obtained from different laboratories or stock centers. We routinely use the Gateway system (Life Technologies) to generate recombinant plasmids suitable for the N- or C-terminal tagging of the bait protein (Table 1) [4]. When the endogenous promoter is used to drive the bait's expression, we use standard cloning [9]; the authentic promoter sequence is amplified by PCR and cloned upstream to the bait's CDS (previously fused in frame (5′ or 3′) with the affinity tag). Then the whole promoter-tag-CDS cassette is subcloned into the *pCaSpeR 4 P*-element vector lacking a general promoter followed by embryo injection using standard procedures [10].

Table 1
Vectors available for early embryonic expression of bait proteins of choice in fusion with GFP or PrA

Destination vector	Tag	Promoter	Source	cat #
pUGW	N-terminal GFP	*poly-ubiquitin promoter (U)*	DGRC	1283
pPGW	N-terminal GFP	*UASp*	DGRC	1077
pPWG	C-terminal GFP	*UASp*	DGRC	1078
pUASp_PrA_GW	N-terminal PrA	*UASp*	In-house	
pUASp_GW_PrA	C-terminal PrA	*UASp*	In-house	

All vectors allow insertion of the CDS of interest by an LR clonase-mediated recombination (Gateway) reaction [4], as well as *P*-element mediated random integration in the genome. Embryonic expression of *UASp*-controlled transgenes can be driven by Gal4 expressed from another transgene

We usually generate a stable population of transgenic flies (a stock) that can be expanded for the production of large amounts of embryos expressing the fusion protein of interest. We have experimented with the *poly-ubiquitin* promoter (*pUB*, ubiquitous expression), the *Maternal α-Tubulin* promoter (*MAT*, female germline expression), and the bait protein's own promoter for the immediate and constitutive expression of the bait protein. This strategy is often successful, but the (over)expression of the bait and/or the position of the tag can sometimes be toxic by interfering with oogenesis or early embryogenesis. In extreme cases, it is impossible to obtain a transgenic stock. In other cases, the stock is difficult to amplify due to few eggs laid and/or a low percentage of embryos hatching. This problem can be overcome by using an inducible promoter. We often make transgene encoding the tagged protein under the control of the inducible Gal4-UAS system [11]. Its expression can be driven in the female germline and in early embryos using a *Maternal α-Tubulin-Gal4-VP16* driver (we use an insertion of this transgene on chromosome II, which is homozygous viable and fertile; Bloomington stock 7062 or 7063). It is important to use the *UASp* variant because the more widely used UAS_T does not (or poorly) allow expression in the female germline [12, 13]. Other Gal4 drivers enable expression of the same bait protein in the same transgenic line in a variety of other tissues (providing tools also for genetic or biochemical experiments).

When using the Gal4-UASp system, a *Maternal α-Tubulin-Gal4-VP16; MKRS/TM6B* stock can be crossed to a *w*; *If/CyO; UASp-transgene/TM6B* stock to generate a *w; Maternal α-Tubulin-Gal4-VP16/CyO; UASp-transgene/TM6B* expression stock. The markers and balancer chromosomes as well as the localization of the driver and transgenic constructs may differ. Once generated, the stock can be easily amplified. The toxicity of the transgenes expressed will vary. In some cases, overexpression of the transgene greatly reduces fertility, and the stock tends to retain the balancers. In other cases, the expression stock tends to lose the balancers and becomes homozygous with two copies of the driver and/or two copies of the other transgene. This will not happen if a transgene insertion is homozygous lethal. The natural adaptation of the expression stock helps its rapid amplification and maximizes its fertility and the yields of embryo collections. In any case, several insertions of the transgene should be screened for health of the expression stock and levels of the bait protein. Expression can be tested by Western blot on protein extracts prepared from embryos or abdomens from well-fed females. We usually aim for the highest possible expression if the stock is healthy because low expression has been a limiting factor in complex purification, particularly for large bait proteins. However, if the amount of the protein is important, we choose the stock expressing the tagged protein at a similar level to the endogenous protein. Finally the expression level of

UASp transgenes can also be tuned by varying the temperature between 18 and 29 °C because the GAL4 driver is more active at higher temperatures.

3.1.2 Embryo Collection

1. Amplify the expression fly lines in vials or bottles containing standard Drosophila cornmeal food with yeast.
2. A few thousands (small cage) to tens of thousands of flies (large cage) should be added to an embryo collection cage, until they distribute individually on its walls, floor, and roof (*see* **Note 7**). The female to male ratio should be between 1 to 1 and 3 to 1. Flies should be no more than a few days old and need to be well fed for 1–2 days before maximum embryo production is reached. Maintain cages at 25 °C and at least 70 % humidity with controlled 12/12-h reverse light/dark cycles. Replace the food plates every 12 h, covering approximately one-third of the grape juice agar Petri dish with yeast paste.
3. When embryo production is maximal, begin collections in the morning. Replace the grape juice agar Petri dish with a fresh one, pre-warmed to room temperature for at least 30 min, containing yeast paste on roughly one-tenth of its surface, in the middle. Remove the Petri dish after 2 h and replace with a fresh food plate (*see* **Note 8**). After another 2 h, replace the food plates again, and collect embryos by washing the surface of the food plate with small amounts of distilled water and a paintbrush (*see* **Note 9**). In this process, resuspend the yeast paste on the surface of the food plate as it contains several embryos. Filter the suspension using a sieve and wash embryos thoroughly with distilled water to remove any remaining yeast. A sieve with larger pore size can be placed on top to collect the flies that were stuck to the plate, whilst letting the embryos through. Alternatively, flies can be removed with tweezers before filtration through the sieve.
4. Remove the chorion from embryos by soaking them in 50 % bleach for 2–5 min, with gentle agitation using a paint brush. Completion of dechorionation can be verified under a stereo microscope. Do not leave in bleach longer than necessary.
5. Thoroughly wash the embryos in distilled water followed by an EWS wash and place the sieve on a paper towel to remove the remaining liquid from the embryos.
6. Transfer the embryos to a 1.5-mL microfuge tube using a small, flat-ended spatula or a paintbrush with the tip dipped into distilled water.
7. Centrifuge at low speed for a few seconds to bring embryos to the bottom of the tube. Note the weight of the embryos and snap-freeze in liquid nitrogen. Dechorionated embryos can be stored at –80 °C for several months or years. Embryo collections

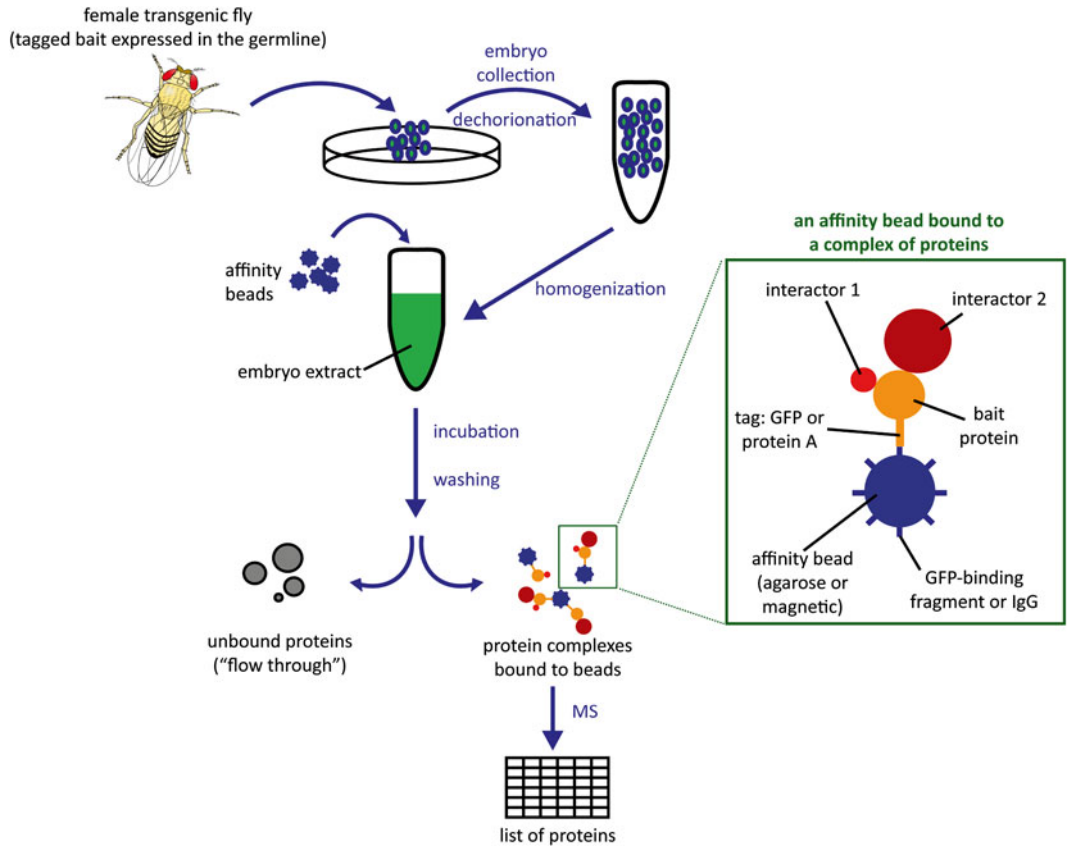

Fig. 1 In vivo proteomics and the rationale of affinity purification of protein complexes from Drosophila transgenic embryos. The flowchart demonstrates the major steps of the purification of tagged proteins along with their interactors, which are described in detail in Subheading 3. The *inset* illustrates how the bait protein, tagged either with PrA or GFP, binds to an affinity bead via direct interaction with IgG or GFP-binding domain, respectively. Proteins interacting with the bait protein co-purify on the affinity beads and are subsequently identified using mass spectrometry

can be repeated several times per day, for several days, until the desired amount of embryos is obtained or until embryo production has waned. Make sure to change the food plate at least once a day (ideally more) and change the cage itself when it becomes dirty.

3.2 Affinity Purification

3.2.1 Protein A Affinity Purification

This method has been designed with the ultimate goal of identifying co-purified proteins by mass spectrometry. The tag consists of two repeats of the immunoglobulin-binding domain of Protein A (PrA) from *Staphylococcus aureus*, and its purification takes advantage of the high binding affinity of PrA to rabbit IgGs. The principle is illustrated in Fig. 1. Because some proteins can stick nonspecifically to the affinity beads used or to the complex being purified, there is a need to compare the set of proteins detected in

any given purification with that obtained with an unrelated protein. For this control, we have been using a strain of flies that express PrA-GFP in embryos (*Maternal α-Tubulin-Gal4-VP16/CyO; UASp-PrA-GFP/TM6B*). The bait protein of interest and the control bait should be purified in parallel, under identical conditions. Proceed as follows:

1. Work at 4 °C throughout embryo lysis and purification (unless otherwise stated). Add 0.5 volume (relative to the weight of embryos) of EB to embryos while they are still frozen in 1.5-mL microfuge tubes. For example, for 1 g of embryos, add 0.5 mL of EB. The starting mass of embryos used may be adjusted depending on the bait protein and particular fly line (*see* **Note 1**).
2. Crush embryos thoroughly and for several seconds using prechilled plastic micropestles that fit a 1.5-mL microfuge tube. Alternatively, a Dounce tissue grinder can be used (*see* **Note 10**). Pool lysates at this point if they were initially contained in multiple tubes.
3. Add 4 volumes of EB (relative to the weight of embryos) after transferring to a larger tube and vortex for 10 s. If the protein is suspected to be associated with chromatin, add nuclease (*see* **Note 11**).
4. Pass lysates through a needle using a prechilled syringe. Repeat four times. However, this step may not be necessary if a Dounce homogenizer was used in **step 2**. The lysate can be checked under a cell culture microscope to ensure destruction of nuclei.
5. Centrifuge lysates at 4,000 × *g* for 20 min at 4 °C (*see* **Note 12**).
6. Transfer supernatant containing soluble proteins to a new tube, taking care to avoid the white, fatty layer, which is mainly composed of yolk, the nutritive droplets of the embryos. As it is sticky, it is important to remove as much yolk as possible to minimize the presence of nonspecific proteins in purification products (*see* **Note 13**).
7. A small fraction of the clarified supernatant can be taken for subsequent Western blot analysis ("soluble input"). The pellet can be resuspended in a volume of 1× Laemmli sample buffer equal to the volume of supernatant and a small fraction can be kept for Western Blot analysis ("pellet").
8. Before mixing with the extract, the required amount of IgG-conjugated magnetic beads (approximately 200 µL of bead suspension (20 mg of dry beads) per 1 g of embryos) is washed briefly in EB in separate tubes prepared for each sample (*see* **Note 14**).
9. Vortex the tubes gently and place them on a magnetic rack, wait for beads to settle and aspirate off or carefully remove the EB.

10. Resuspend beads with the protein extract's clarified supernatant and transfer to a new tube. Incubate on a rotating wheel at 4 °C from 30 min to 4 h (*see* **Note 15**).
11. Place tubes on the magnetic rack and wait until all beads have adhered to the side of the tube facing the magnet. A small fraction of the unbound supernatant can be taken for subsequent Western blot analysis ("unbound"). Discard the supernatant using an aspirator or pipette.
12. Add 1 volume of WB (relative to the original extract) and resuspend the beads by vortexing briefly. Place tubes on the rotating wheel and wash at 4 °C for 5 min. Place tubes on the magnetic rack and discard the WB. Repeat washes four times.
13. Perform two more washes with 1 volume of FWB (relative to the original extract) (*see* **Note 6**).
14. Transfer the suspension to new microfuge tubes attached on the magnetic rack, wait for beads to settle, and carefully remove all supernatant (*see* **Note 16**).
15. Add 0.5 mL freshly made Elution solution to each tube. Resuspend the beads by briefly vortexing and place the tubes on a rotating wheel for 5 min incubation at room temperature.
16. Insert the tubes in the magnetic rack and transfer supernatants (eluates) to new microfuge tubes.
17. Perform a second round of elution, pool the two eluates (total volume of 1 ml), place the tubes on the magnetic rack, and transfer eluates again to new tubes to remove any remaining magnetic particles.
18. Divide the combined eluates into two fractions of 100 μL (10 %) and 900 μL (90 %) and lyophilize both samples in a vacuum concentrator (*see* **Note 17**).
19. Keep the lyophilized 90 % fractions at −20 °C until sample preparation for mass spectrometric analysis.
20. Resuspend the precipitates from the 10 % fractions in 1× Laemmli sample buffer and boil for 5 min at 95 °C.
21. Visualize the eluted proteins by SDS-PAGE followed by silver-nitrate staining (Fig. 2), saving a small amount of the sample ("eluted from beads") for Western blot analysis (*see* **Note 18**).
22. If a purification product looks clean and reveals specific bands including a clear band at the expected molecular weight for the bait protein (as shown in Fig. 2), we generally proceed to gel-free mass spectrometric identification of purified proteins from the lyophilized precipitate obtained in **step 18**. This fraction can be processed and analyzed directly by most proteomics facilities.

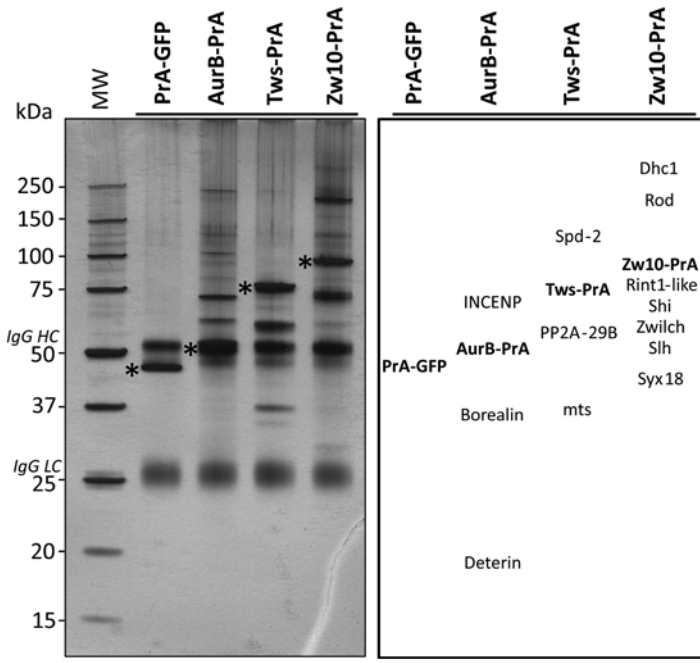

Fig. 2 Examples of protein complexes obtained by PrA affinity purifications from early embryos. A small fraction of the purification products were analyzed on a 4–12 % SDS polyacrylamide gel stained with silver nitrate. The bait proteins are indicated at the *top*. *Right*: specifically associated proteins identified by mass spectrometry are indicated at the level of their predicted molecular weight and under their respective bait protein. The main fraction of the purification products was analyzed without gel separation, and therefore we have no experimental positional information for the proteins labeled on the *right*. Purified bait proteins are marked by *asterisks* and indicated in *bold font names* in the *panel* on the *right*. *IgG HC* immunoglobulin G heavy chain, *IgG LC* immunoglobulin G light chain, *MW* molecular weight protein markers

3.2.2 GFP-Trap Affinity Purification

Over the past years, thousands of transgenic flies expressing proteins fused to a fluorophore, such as GFP and its variants, were established by different laboratories or consortia, in order to follow the localization and dynamics of the protein of interest by microscopy (fixed preparations or live imaging). Conveniently, the same fly lines can also be used for one-step affinity purifications against the GFP tag of the chimeric protein and its interacting factors from different ontogenetic stages or tissues for proteomic studies. Combined knowledge of localization and interactions is highly informative on a protein's function. Here we describe a general protocol for the GFP-Trap-based purification of GFP-fusions from Drosophila syncytial embryos. The general principle is similar to the PrA affinity purification and is illustrated in Fig. 1. We recommend purifying the bait protein of interest and the control GFP

bait (we made and used the *yw; Bc Gla/CyO, P[w+; Ub-GFP]* balancer stock that constitutively expresses GFP) in parallel, under identical conditions. The embryo lysis and soluble protein extract preparation is identical to the above procedure for PrA affinity purifications (*see* Subheading 3.2.1, **steps 1–7**). Follow these subsequent steps for the GFP-Trap purifications:

1. Pre-equilibrate GFP-Trap agarose beads: use 50–100 μL of the original GFP-Trap agarose suspension per sample (*see* **Note 19**) in 5 mL EB in 15-mL conical tubes.
2. Mix gently four times and sediment the beads by brief and slow centrifugation (e.g., for 3 min at 500 × *g*) with a slow deceleration speed in order to avoid turbulence.
3. Add the clarified supernatant of the embryo extract to the beads followed by incubation on a rotating wheel at 4 °C from 30 min to 2 h (*see* **Note 15**).
4. Sediment the beads and take a small fraction of the unbound supernatant for subsequent Western blot analysis. Carefully discard residual supernatant using an aspirator or pipette.
5. Wash the beads five times in 10 mL WB by gentle rotation at 4 °C for 5 min each time.
6. Sediment the beads and discard the supernatant.
7. Transfer the beads to a new 15-mL conical tube and wash two times in 10 mL FWB (*see* **Note 6**) by gentle rotation at 4 °C for 10 min.
8. Sediment the beads and discard the supernatant.
9. Transfer the beads to a microfuge tube and further wash two times for 2 min with FWB.
10. Sediment the beads and discard the supernatant.
11. Remove as much buffer as possible from the agarose beads; take 10 % of the beads for SDS-PAGE analysis using silver staining (load 9 % of the beads) and Western blotting (load 1 % of the beads). An example of a silver-stained gel of purification products is shown in Fig. 3.
12. Keep the rest of the beads (90 %) at 4 °C for subsequent on-beads tryptic digestion and mass spectrometric analysis (*see* **Note 20**).

4 Notes

1. The amount of embryos needed for affinity purification may be adjusted depending on the expression level of the bait protein. A method for very large-scale embryo production has been published previously in this series [14]. Overexpression of tagged proteins in transgenic embryos may be toxic or decrease fitness,

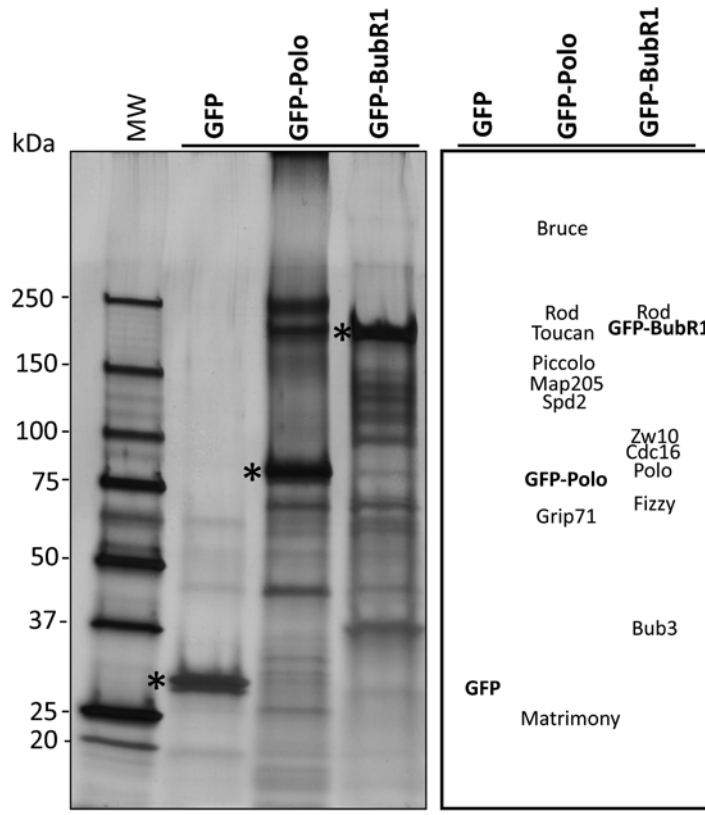

Fig. 3 Examples of affinity purification of three bait proteins using GFP-Trap. GFP alone, GFP-Polo [16], and GFP-BubR1 [17] fusions were purified from transgenic Drosophila syncytial embryos using GFP-Trap agarose beads. Small fractions of the preparations (9 %) were run on a 4–12 % SDS polyacrylamide gel and stained with silver nitrate (*left panel*), the remaining isolated material (90 %) was analyzed using mass spectrometry and examples of identified proteins are listed in the *panel* on the *right*. The main fraction of the purification products was analyzed without gel separation and therefore we have no experimental positional information for the proteins labeled on the *right*. Baits are marked by *asterisks* and indicated in *bold font names* in the *panel* on the *right*

leading to poor fertility and embryo production. In other cases, the expression of the bait protein may be extremely low, due to rapid degradation or transcriptional downregulation. Therefore, we recommend researchers to perform pilot experiments to observe the egg deposition rate in comparison to wild-type (e.g., Oregon-R) flies and to determine the overexpression level of the bait protein via Western blot. This approach should help evaluate the size of the population required to generate a sufficient amount of embryos. For protein identification by mass spectrometry, we use approximately 1 g of embryos per purification. It is recommended to collect embryos in a separate population

cage room, fly incubator, or chamber. To obtain a maximum yield of embryos, it is critical to maintain constant environmental conditions of 25 °C, at least 70 % relative humidity and controlled reverse light/dark cycles.

2. Flies are attracted to the acidic and aromatic smell of fruit juice, and they like to feed on yeast paste. Grape juice agar food plates/trays can be stored at 4 °C for several days. Prior to use, pre-warm the plates/trays to room temperature for 30 min. After initial mixing of the yeast paste, gas bubbles will form within a few hours. It is important to mix again to eliminate these bubbles as they can prevent firm adhesion of the yeast paste to the agar medium. Yeast paste can be stored at 4 °C for several days. Heat the yeast paste for a few seconds in microwave oven (do not let it melt) prior to spreading on agar, as lysed yeast cells are preferred by the flies.
3. The most common method for the affinity purification of GFP (and its variants)-tagged proteins is co-immunoprecipitation using antibodies recognizing the tag. However, the large immunoglobulin complexes, as major contaminants, cause "peptide masking" during mass spectrometric analysis, which may lead to the loss of important information about potential interactors or post-synthetic modifications. The GFP-Trap system instead utilizes the small 13 kDa intact GFP-binding domain of the special heavy-chain antibody of *Camelidae* to enable the rapid and efficient one-step isolation of GFP-tagged baits expressed in Drosophila embryos for subsequent analysis by mass spectrometry [15]. GFP-Trap is extremely stable with a high binding affinity to GFP. We recommend the agarose beads version of GFP-Trap as we found that the use of the magnetic beads version—although more convenient during washes—increases the background of nonspecific interactions with bait proteins. For the complete list of recognized fluorophores (RFP-Trap is also available) visit the FAQ section at www.chromotek.com.
4. The composition of the extraction buffer (EB) depends on a particular protein or complex to be purified. Proteins that are part of large organelles or subcellular structures may be extracted with higher salt and/or detergent; however the concentration of mild detergents should not exceed 0.5 % during the binding step. If the detergent concentration of the EB is higher than 0.5 %, it should be diluted prior to mixing with the beads (binding). Similarly, too much salt can slow down or prevent efficient binding of the bait protein to the beads. Chemical inhibitors of specific enzymatic activities can also be added to the EB at the extraction step, depending on the proteins to be purified and on the subsequent analysis. If the protein of interest is rapidly degraded by the 26S proteasome, use 25 μM

MG132 proteasome inhibitor in the EB and throughout the purification. If the bait protein is purified for mass spectrometry-based identification of potential posttranslational modifications (PTM) instead of for the identification of interactors, the stringency of the buffers can be increased (with more detergent or salt) and it is recommended to use specific phosphatase inhibitors, such as 50 nM okadaic acid (for PP2A-related phosphatases) or broader specificity phosphatase inhibitor cocktails (e.g., from Sigma or Roche) to preserve the phosphorylation state of proteins in the extract. For the inhibition of deubiquitylating enzymes (DUBs), use 10 mM of the sulfhydryl alkylating agent *N*-ethylmaleimide. Such inhibitors may also be used if the interaction between the bait protein and its partners is likely to be PTM-dependent.

5. Always use autoclaved or filter-sterilized ultra-pure water and stock solutions during the extraction and purification steps. Use properly cleaned and autoclaved microfuge and conical tubes, funnels, Dounce tissue grinder and micropestles, needles and syringes.
6. Final wash buffer (FWB) must not contain glycerol, protease inhibitors, or detergents, which may interfere with the trypsin digestion or other steps of sample preparation and analysis by liquid chromatography and mass spectrometry. If this problem persists, a protein precipitation step can be applied after elution (*see* **Note 17**).
7. Overcrowding of flies in the population cage will result in injury and stressing of the flies, leading to a reduced embryo yield.
8. The first collections of the day tend to yield fewer embryos than subsequent collections, and many of these embryos can be defective if they have been retained by the mothers for too long. Consequently, we recommend discarding the first plates.
9. During embryo collection, care should be taken not to stab the agar with the paintbrush, as agar flakes can clog the sieve used in later steps and are difficult to separate from the embryos. Around 100 mg of embryos is typically obtained from one good collection on a 100 mm-diameter Petri dish (significantly more in large cages from trays).
10. When using Dounce homogenizer, the initial lysis of the embryos can be done with a loose-fit pestle, and a finer homogenization step can be done with the tighter-fit pestle. Due to high backpressure, the initial strokes are usually difficult. Be careful to avoid "squirting up" of the homogenate; when there is resistance, release it by twisting the pestle left-and-right and continue pushing down gently.

11. If the bait and/or its interactors are likely to be chromatin associated, add 200 μg/mL (or 2,000 Kunitz units) final concentration of DNase I (Sigma DNEP dissolved in 150 mM NaCl, 4 mM $MgCl_2$ and pre-activated at 37 °C for 5 min, although other nucleases can also be used) to the lysate and incubate at 37 °C for 5 min, mix gently, and incubate for a further 10 min at room temperature prior to initial centrifugation. Alternatively the DNase I treatment may be performed at 4 °C for 1 h on a rotating wheel. DNA digestion can be monitored on an agarose gel after extraction of nucleic acids from lysates. For this, we found that DNazol (Life Technologies) gives a very good yield of DNA purification from extracts.
12. The duration and speed of centrifugations has to be optimized for different purifications. Large molecular complexes may be lost in the pellet after high-speed centrifugation.
13. To help remove the yolk, the homogenized lysate can be passed through a double layer of Miracloth (pre-equilibrated with EB and placed in a funnel). The supernatant can also be centrifuged once more to remove remaining yolk.
14. The ideal amount of beads used for purification depends mainly on the expression level of the bait protein to be purified.
15. A long incubation will favor a high yield of the bait protein while a short incubation will minimize the risk of disassembly of low affinity complexes.
16. It is important to transfer the samples to new tubes before the elution because some proteins from the extract stick on the walls of the tube and could be redissolved in presence of the elution solution, contaminating the purification product.
17. Alternatively, a protein precipitation step using methanol or acetone can be added to get rid of nonvolatile impurities that may remain in the eluted samples (even after lyophilization) and interfere with mass spectrometry. However, we find that it is usually not necessary.
18. The various small fractions kept during the procedure can be used for Western blot analysis to follow the path of the bait proteins purified during the preparation. We recommend loading equivalent fractions of the insoluble pellet, soluble input, unbound, eluates, and the bead fraction kept after elution (obtained by boiling the beads in 1× Laemmli sample buffer; load without bead particles). Use appropriate dilutions to ensure the loading of equal percentage of the total sample for every fraction. This analysis reveals if a protein has been efficiently expressed, extracted, bound, and eluted, and if it has been degraded or stayed intact (Fig. 4).

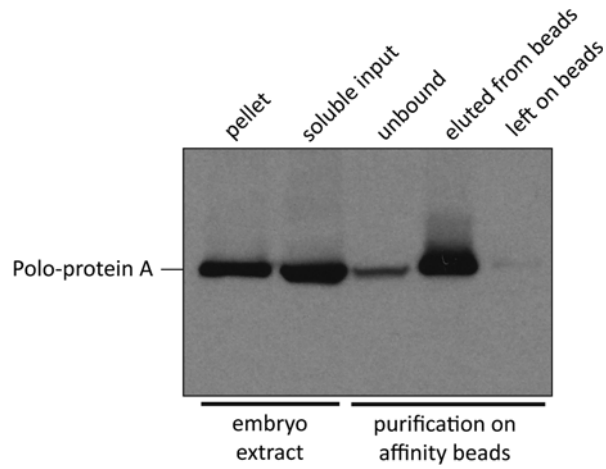

Fig. 4 Following the bait protein during the major steps of the affinity purification procedure. Polo-protein A fusion was purified from syncytial embryos using IgG-coupled magnetic Dynabeads. Small fractions were collected at different steps during the purification procedure. For each fraction, the same proportion of the total sample (0.1 %) was loaded on the gel, which was analyzed by Western blotting with HRP-conjugated rabbit IgG. This analysis reveals that Polo-protein A was incompletely extracted, efficiently bound to the beads, and efficiently eluted. No breakdown of the protein was detected

19. The binding efficiency of the GFP-Trap agarose beads is high. We found that 100 μL of original bead suspension is sufficient to bind 90–95 % of GFP alone prepared from 1.5 g syncytial embryos; however the binding to GFP-tagged proteins is less efficient.
20. Quantitative elution of the bait and its interactors from GFP-Trap is difficult due to the high affinity of the GFP-binding domain to GFP. However, we found that the elution of the purified proteins from beads is not necessary. The best results were obtained by direct tryptic digest of the material on beads followed by mass spectrometry. However, as an alternative, 0.3 M Glycine-HCl pH 2.5, 6 M Guanidine-HCl, or 1 M NH_4OH can be used for elution.

Acknowledgements

This work was supported by grants from the Canadian Institutes of Health Research (CIHR) and the Natural Sciences and Engineering Research Council of Canada (to V.A.) and by Cancer Research UK, Medical Research Council, and Biotechnology and Biological Sciences Research Council grants (to D.M.G.). V.A. holds a New Investigator Award from the CIHR. IRIC is supported in part by

the Canada Foundation for Innovation, and the FRQS. Z.L. holds the Long-term Fellowship of the Federation of European Biochemical Societies (FEBS). Some of the destination vectors for the Gateway cloning were obtained from the Drosophila Genomics Research Centre. We are grateful to Janusz Debski and Michal Dadlez (MS LAB, Institute of Biochemistry and Biophysics PAS, Warsaw, Poland) and Pierre Thibault and Éric Bonneil (IRIC, Université de Montréal) for mass spectrometric analysis.

References

1. Dunham WH, Mullin M, Gingras AC (2012) Affinity-purification coupled to mass spectrometry: basic principles and strategies. Proteomics 12(10):1576–1590
2. Walther TC, Mann M (2010) Mass spectrometry-based proteomics in cell biology. J Cell Biol 190(4):491–500
3. Archambault V (2005) Cell cycle: proteomics gives it a spin. Expert Rev Proteomics 2(4): 615–625
4. D'Avino PP, Archambault V, Przewloka MR, Zhang W, Laue ED, Glover DM (2009) Isolation of protein complexes involved in mitosis and cytokinesis from Drosophila cultured cells. Methods Mol Biol 545:99–112
5. Przewloka MR, Zhang W, Costa P, Archambault V, D'Avino PP, Lilley KS, Laue ED, McAinsh AD, Glover DM (2007) Molecular analysis of core kinetochore composition and assembly in Drosophila melanogaster. PLoS One 2:e478
6. Archambault V, D'Avino PP, Deery MJ, Lilley KS, Glover DM (2008) Sequestration of Polo kinase to microtubules by phosphopriming-independent binding to Map205 is relieved by phosphorylation at a CDK site in mitosis. Genes Dev 22(19):2707–2720
7. Montembault E, Zhang W, Przewloka MR, Archambault V, Sevin EW, Laue ED, Glover DM, D'Avino PP (2010) Nessun Dorma, a novel centralspindlin partner, is required for cytokinesis in Drosophila spermatocytes. J Cell Biol 191(7):1351–1365
8. Foe VE, Odell GM, Edgar BA (1993) Mitosis and morphogenesis in the Drosophila embryo: point and counterpoint. In: Bate M, Martinez Arias A (eds) The development of *Drosophila melanogaster*, vol 1. Cold Spring Harbor Laboratory Press, New York
9. Lipinszki Z, Klement E, Hunyadi-Gulyas E, Medzihradszky KF, Markus R, Pal M, Deak P, Udvardy A (2013) A novel interplay between the ubiquitin-proteasome system and serine proteases during Drosophila development. Biochem J 454(3):571–583
10. Ashburner M, Golic KG, Hawley RS (2005) Drosophila, a laboratory handbook, 2nd edn. Cold Spring Harbor Laboratory Press, New York
11. Duffy JB (2002) GAL4 system in Drosophila: a fly geneticist's Swiss army knife. Genesis 34(1–2):1–15
12. Rorth P (1998) Gal4 in the Drosophila female germline. Mech Dev 78(1–2):113–118
13. Brand AH, Perrimon N (1993) Targeted gene expression as a means of altering cell fates and generating dominant phenotypes. Development 118(2):401–415
14. Kunert N, Brehm A (2008) Mass production of Drosophila embryos and chromatographic purification of native protein complexes. Methods Mol Biol 420:359–371
15. Neumuller RA, Wirtz-Peitz F, Lee S, Kwon Y, Buckner M, Hoskins RA, Venken KJ, Bellen HJ, Mohr SE, Perrimon N (2012) Stringent analysis of gene function and protein-protein interactions using fluorescently tagged genes. Genetics 190(3):931–940
16. Moutinho-Santos T, Sampaio P, Amorim I, Costa M, Sunkel CE (1999) In vivo localisation of the mitotic POLO kinase shows a highly dynamic association with the mitotic apparatus during early embryogenesis in Drosophila. Biol Cell 91(8):585–596
17. Buffin E, Lefebvre C, Huang J, Gagou ME, Karess RE (2005) Recruitment of Mad2 to the kinetochore requires the Rod/Zw10 complex. Curr Biol 15(9):856–861

Chapter 34

Tracking Histone Variant Nucleosomes Across the Human Cell Cycle Using Biophysical, Biochemical, and Cytological Analyses

Marcin P. Walkiewicz, Minh Bui, Delphine Quénet, and Yamini Dalal

Abstract

Histone variants such as H3.3, macroH2A, H2A.Z, and CENP-A are important epigenetic modifiers of the chromatin state in eukaryotic genomes. The centromeric histone H3 variant CENP-A/CENH3 epigenetically marks centromeres and is required for assembly of the kinetochore complex, a region of the chromosome that is responsible for proper genome segregation during mitosis. Several diverse techniques using biochemical, cell biology, and biophysical approaches have been utilized to study the nature of the CENP-A nucleosome across the cell cycle. In this chapter, we describe methods for CENP-A nucleosome purification and separation of CENP-A from other core histones using traditional SDS-PAGE and more resolving techniques such as Triton acid urea (TAU) and two-dimensional gels. We also discuss methods for observation of CENP-A on chromatin fibers using immunofluorescence. Finally, we provide a detailed description of analysis of chromatin structures using atomic force microscopy.

Key words CENP-A, Histones, Cell cycle, SDS-PAGE, TAU, Western blotting, Chromatin fiber, Immunofluorescence, Atomic force microscopy, AFM

1 Introduction

Histone proteins are pivotal to the higher order organization of chromatin. Histones H3, H2A, H2B, and H4 form octameric nucleosomes that wrap around DNA [1]. This higher order organization regulates DNA compaction into fibers [2] and into chromosomes during cell division. Cell division is an important step that requires equal distribution of the genome amongst the daughter cells. For this to be accomplished, a region of the chromosome, known as the centromere, is the most important domain that is targeted by the microtubules for chromosomal segregation. This centromeric domain is epigenetically marked by a variant of histone H3 found in all eukaryotes, known collectively as CENP-A/CenH3 [3, 4]. Understanding the structural composition and dynamics of all the nucleosomes across the cell cycle, including the

Eishi Noguchi and Mariana C. Gadaleta (eds.), *Cell Cycle Control: Mechanisms and Protocols*, Methods in Molecular Biology, vol. 1170, DOI 10.1007/978-1-4939-0888-2_34,

CENP-A nucleosome, is a goal of many researchers. Although the structural composition of the CENP-A nucleosome is still under experimental investigation, the techniques we present in this work provide a comprehensive foundation to study chromatin across the cell cycle and are applicable to all histones and nucleosomes.

In a recent study by our group, CENP-A nucleosome structure and dynamics were determined over the cell cycle using human cells that were synchronized using a double thymidine block. Cells from the various cell cycle stages were harvested, and CENP-A proteins were enriched by immunoprecipitation using a CENP-A-specific antibody [5]. CENP-A dynamics were observed, including the notable depletion of its own chaperone called Holliday junction recognition protein (HJURP) from the centromeres during S-phase or DNA replication. Atomic force microscopy (AFM) studies performed on CENP-A nucleosomes derived from different stages of the cell cycle have also revealed that HJURP depletion marked a critical point of transition of CENP-A stable tetramers to stable octamers, in vivo [5].

With the exception of a few histone variants, CENP-A and the other histones are small, highly positively charged proteins, ranging from 14 to 18 kDa. They are found associated with each other on chromatin, and can be purified and studied using traditional biochemical and cell biology techniques. Such methods include SDS-PAGE or, for higher separation of the different histone species and modified forms, Triton acid urea (TAU) gel electrophoresis approach. This form of electrophoresis is capable of separating low to medium weight histones based on their charge and hydrophobicity, because the Triton X-100 detergent is capable of binding to the hydrophobic regions of proteins, allowing further retardation and separation [6–8]. This approach is also useful for studying multi-acetylated forms of histones [9], such as histone H3, and is a powerful tool for downstream applications such as Western blotting (WB) and mass spectrometric (MS) analyses.

Biochemical approaches are important for understanding the nature of a protein, as well as the composition of a complex when the protein associates with other partners. However, a different approach is required to assess protein localization and to achieve further insight into its function in a cellular context. Traditional cell biology techniques use fluorescently tagged proteins or antibodies (hence immunofluorescence or IF) to visualize where the protein is localized. Certain drawback with fluorescently tagged histones is that the tags are often much larger than the histones themselves, which could result in aberrant histone localization affecting its function. One study shows that GFP-tagged CENP-A mutants were more sterile than their untagged counterparts, suggesting the large fluorescent tag may contribute to chromatin

instability [10]. To alleviate that issue, specific antibodies have been produced to target the protein of interest, and small but unique peptide tags can also be cloned in frame and covalently attached to the protein to facilitate detection. These materials have provided cell biologists with useful tools to study protein localization, and allowed for such methods as DNA fluorescent in situ hybridization (FISH). Similar to SDS-PAGE gels, which later evolved to TAU gels, wherein proteins and their modifications could be definitively resolved, combined IF/FISH methods allow specific protein or histone recognition on chromatin fibers. Indeed, using high resolution imaging of chromatin fibers coupled to IF techniques, it was shown that within centromeres, domains of CENP-A alternate with domains of H3 di-methylated at lysine (H3K4Me2) [11, 12].

Another tool for chromatin and nucleosome imaging involves the use of an AFM. This technology dates back to the 1980s, and is commonly used in the fields of physics and materials chemistry, but has slowly gained acceptance over the past two decades as a robust method to study chromatin and nucleosome structure. AFM is a form of scanning probe microscopy (SPM) where the sample's surface is probed by an extremely small tip moving over it in a scanning fashion [13]. The tip, mounted on the end of a flexible cantilever and most often composed of silicon or silicon nitride, is approximately 2–10 nm in diameter and interacts with the sample within a short range of repulsive (Coulombic) and attractive (van der Waals) atomic forces. Over the last 30 years, AFM has been used for a broad variety of physical and electronic applications, but it has proven particularly useful for observation and analysis of biological molecules, including chromatin. The main advantage of AFM is that it allows for sample imaging with resolution akin to electron microscopy but with minimal processing, making it both an excellent analytical (high precision measurements of nucleosome dimensions) and preparative (quick determination of chromatin quality) technique [5, 14, 15].

Here, we provided detailed protocols on how to purify quantitative amounts of native nucleoprotein complexes from human cells for analysis on an SDS-PAGE or high-resolution protein gels for WB and MS, how to visualize such nucleosomes bound to other protein components on extracted chromatin fibers by IF, and how to analyze nucleosome dimensions and chromatin fiber folding using AFM. These methods have been used successfully by our lab for the study of low abundance (1–5 % of total) histone variants such as CENP-A and macroH2A from mouse, Drosophila, and human cells in culture, as well as from small amounts of tumor tissues. Consequently, the collection of techniques described herein should generally be applicable to any nucleoprotein complexes present as a small fraction of the total genome.

2 Materials

2.1 Nuclei Preparation, Chromatin Digestion, Extraction, and Immunoprecipitation

1. 1× PBS: 137 mM NaCl, 2.7 mM KCl, 1.5 mM KH_2PO_4, 8.1 mM Na_2HPO_4 pH 7.2.
2. Cold 1× PBS-T: PBS supplemented with 0.1 % Tween-20.
3. Cold TM2 buffer: 20 mM Tris–HCl pH 8.0, 2 mM $MgCl_2$.
4. Nonidet P40 (NP40) or Nonidet P40 Substitute (Fluka Analytical).
5. 0.1 M TE: 10 mM Tris–HCl pH 8.0, 0.2 mM EDTA, 100 mM NaCl.
6. Micrococcal Nuclease (MNase, Sigma Aldrich).
7. 100 mM $CaCl_2$.
8. MNase quenching solution: 500 mM EGTA pH 8.0.
9. Low-salt extraction buffer (LSEB): 0.5× PBS, 5 mM EGTA.
10. 100 mM phenylmethanesulfonylfluoride (PMSF): dissolved in ethanol.
11. Anti CENP-A antibody (Santa Cruz Biotechnology, Inc., Cat #sc-22787).
12. Protein A/G PLUS-agarose beads (Santa Cruz Biotechnology).
13. 0.2 M glycine pH 6.5.
14. 2× Laemmli sample buffer: 65.8 mM Tris–HCl pH 6.8, 2.1 % SDS, 26.3 % (w/v) glycerol, 0.01 % bromophenol blue.

2.2 Histone Extraction with Hydroxylapatite

1. 50-mL conical tubes with small stir bars.
2. 0.35 M NaCl PBS, 0.2 mM EDTA: 1× PBS containing a total of 0.35 M NaCl and 0.2 mM EDTA.
3. Hydroxylapatite.
4. 100 mM stock solution of phenylmethanesulfonylfluoride (PMSF) in ethanol.
5. 2 M NaCl PBS, 0.2 mM EDTA: 1× PBS containing a total of 2 M NaCl and 0.2 mM EDTA.
6. 15-mL conical tube.
7. 2.8 M NaCl PBS, 0.2 mM EDTA: 1× PBS containing a TOTAL of 2.8 M NaCl and 0.2 mM EDTA.
8. Amicon Ultra-4 Centrifugal Filter Unit with Ultracel-3 membrane (Millipore).
9. Slide-A-Lyzer Dialysis Cassette, 7K MWCO (Thermo Scientific).
10. Low-salt extraction buffer (LSEB): 0.5× PBS, 5 mM EGTA.

2.3 Casting Long TAU (L-TAU) Gels

1. 250-mL vacuum filter flask.
2. Urea.
3. 40 % acrylamide solution: acrylamide/bis-acrylamide (37.5:1).
4. Glacial acetic acid.
5. *N*,*N*,*N*′,*N*′-tetramethyl-ethylenediamine (TEMED).
6. 0.3 M Triton X-100: dissolved in dH_2O.
7. PROTEAN II xi Cell electrophoresis setup (BioRad) with proper combs and accessories.
8. 10 % Ammonium persulfate (APS); dissolved in dH_2O.
9. Butanol.

2.4 Running Long TAU (L-TAU) Gels and Immunoblotting

1. Triton X-100.
2. TAU Running Buffer: 65 mL glacial acetic acid, 1.3 mL Triton X-100, add water to a total of 1,300 mL.
3. Cysteamine Pre-run Solution: 3.84 g urea, 0.57 g cysteamine or β-mercaptoethanol, 430 µL glacial acetic acid, 160 µL 0.3 M Triton X-100, a pinch of pyronin Y (for tracking), add water to a total of 8 mL. Store at room temperature.
4. 2-L graduated cylinder.
5. 2× Sample Running Dye: 9.6 g urea, 750 µL β-mercaptoethanol, 750 µL glacial acetic acid, a pinch of pyronin Y (for tracking), add water to a total of 15 mL. Store at room temperature.
6. TAU Equilibrating Solution: 50 mM glacial acetic acid, 0.5 % SDS.
7. Transfer Buffer in 20 % ethanol (1× Tris-glycine transfer buffer): 25 mM Tris–HCl pH 8.0, 192 mM glycine, 20 % ethanol.
8. Transfer-Blot Turbo Transfer Pack: midi format, 0.2 µm nitrocellulose (BioRad).
9. Transfer-Blot Turbo Transfer System (BioRad).
10. 1× PBS: 137 mM NaCl, 2.7 mM KCl, 1.5 mM KH_2PO_4, 8.1 mM Na_2HPO_4 pH 7.2.
11. PBS-T: 1× PBS supplemented with 0.1 % Tween-20.
12. Membrane Blocking Buffer: 5 % nonfat dry milk solubilized in 1× PBS.
13. TAU Hybridization Buffer: 3 % BSA solubilized in PBS-T.
14. Antibodies: CENP-A antibody—ChIP grade (Abcam, Cat #ab13939), H2A (Abcam, Cat #ab18255), and H4 (Abcam, Cat #10158).
15. Plastic hybridization bag.
16. Heat bag sealer.

17. IRDye secondary antibodies (LI-COR Biosciences) or other secondary antibodies.
18. LiCor Odyssey Imaging System (LI-COR Biosciences) or other imaging/developing system.

2.5 Preparation of Chromatin Fibers

1. 1× PBS: 137 mM NaCl, 2.7 mM KCl, 1.5 mM KH_2PO_4, 8.1 mM Na_2HPO_4 pH 7.4.
2. Hemocytometer.
3. Hypotonic solution: 75 mM KCl diluted in sterilized distilled water.
4. CytoSpin 4 centrifuge (Thermo Scientific).
5. Shandon Single Cytofunnels with White Filter Cards (Thermo Scientific).
6. Shandon Cytoclips Stainless-Steel Slide Clip (Thermo Scientific).
7. Microscope slides.
8. Coplin jars.
9. Fiber lysis buffer: 2.5 mM Tris–HCl pH 7.5, 0.5 M NaCl, 1 % Triton X-100, 0.4 M urea.
10. Fixation buffer: 4 % formaldehyde, 1× PBS.
11. Permeabilization buffer: 1× PBS, 0.1 % Triton X-100.

2.6 Chromatin Fiber Immunofluorescence

1. Blocking buffer: 1× PBS, 0.5 % Bovine Serum Albumin (BSA), 0.01 % Triton X-100.
2. Wash solution: 1× PBS, 0.05 % Tween-20.
3. CENP-A primary antibody: mouse monoclonal [3–19] CENP-A antibody—ChIP grade (Abcam, Cat #ab13939) dilution 1:200 in blocking solution complemented with 1 % normal goat serum.
4. Secondary antibody: goat anti-mouse conjugated to Alexa Fluor 488 or Alexa Fluor 568 (Life Technologies, Cat #A11001 and Cat #A11004, respectively) dilution 1:500 in blocking solution complemented with 1 % normal goat serum.
5. 4′,6-Diamidino-2-phenylindole (DAPI) solution: dissolve 1 μg/μL DAPI in 1× PBS, 50 % glycerol. Store at −20 °C. Dilute 1:5,000 in 1× PBS to prepare a working solution.
6. 1× PBS.
7. Mounting Mowiol solution: add 2.4 g of anti-fading reagent MOWIOL 4-88 (Sigma-Aldrich, #81381) to 6 g of glycerol, stir to mix. Add 6 mL of distilled water and mix at room temperature for minimum 2 h. Add 12 mL of 0.2 M Tris pH 8.5, and heat to 50 °C for 30 min with occasional mixing. Clarify by centrifugation at 2,800×*g* for 20 min. Add to 2.5 % (w/v) 1,4,-diazobicyclo-[2.2.2]-octane (DABCO 33-LV, Sigma-Aldrich, #290734). Aliquot and store at −20 °C.

2.7 DNA FISH with an α-Satellite Probe

1. Coplin jars.
2. Crosslinking buffer: 8 % formaldehyde diluted in distilled water.
3. 1× PBS containing 0.5 % Tween-20.
4. Salmon sperm DNA.
5. Biotin-labeled DNA probe against centromeric α-satellite sequence: This labeling is performed by nick translation using a homemade plasmid containing repeats of centromeric α-satellite sequence (*see* **Note 1**). Mix 2 μg of DNA with 10 μL 10× nick translation buffer (0.5 M Tris–HCl pH 8.0, 50 mM $MgCl_2$, 0.5 mg/mL BSA), 10 μL of a solution containing 0.5 mM dATP, 0.5 mM dCTP, 0.5 mM dGTP and 0.1 mM dTTP, 10 μL 0.1 M β-mercaptoethanol, 4 μL 1 mM biotin-16-dUTP for a total volume of 100 μL after addition of DNA Polymerase I and DNase I. Vortex, centrifuge, and place on ice. Add 2 μL DNA Polymerase I (Invitrogen Cat #18010-025) and 5 μL DNase I (diluted 100× in sterile water, Invitrogen Cat #AM2235), flick gently and incubate for 90 min at 15 °C. Using 5 μL of the sample, check on 2 % agarose gel the length of the DNA, it should be between 300 and 600 bp. If DNA fragments are too long, add more DNase I and incubate for additional 30 min. Stop the reaction with 1 μL 0.5 M EDTA, incubate 10 min at 55 °C, then store at −20 °C.
6. 3 M sodium acetate pH 5.2.
7. 100 % ethanol.
8. 70 % ethanol.
9. Hybridization buffer: 20 % dextran sulfate, 4× SSC.
10. Denaturing solution: 70 % formamide, 2× SSC.
11. 12 × 12 round coverslips.
12. Rubber cement.
13. Wash solution 1: 50 % formamide, 2× SSC solution.
14. Wash solution 2: 2× SSC, 0.05 % Tween-20.
15. Blocking solution: 4× SSC, 0.1 % Tween-20, 3 % BSA.
16. Secondary antibody: dilution 1:300 diluted in blocking buffer.
17. Wash solution 3: 4× SSC, 0.1 % Tween-20.
18. DAPI solution (*see* Subheading 2.6, **item 5**).
19. 1× PBS.
20. Mounting Mowiol solution (*see* Subheading 2.6, **item 7**).

2.8 AFM

All buffers and washes should be prepared using ultrapure MilliQ filtered water. All materials listed in Subheading 2.1 are also required. For AFM, muscovite mica, grade V-1 or V-2, is recommended. This can be purchased in large sheets or pre-cut to desired dimension (discs, squares) and is available from several suppliers, including Structure Probe, Inc. and Electron Microscopy Sciences. However, untreated mica surface has a negative charge; therefore, to improve protein binding to the mica surface, a fresh, positively charged mica surface is required. Mica preparation methods have been described previously for (3-Aminopropyl)triethoxysilane (APTES)-mica (AP-mica) [16] and 1-(3-aminopropyl)silatrane (APS)-treated mica (APS-mica) [16–18].

1. AP-mica.
2. APS-mica.
3. Protease inhibitor cocktail.
4. 10× PBS pH 7.4, filtered, sterile.
5. 1 M $MgCl_2$ filtered, sterile.
6. AFM scanning system (Agilent AFM 5500, Bruker MultiMode 8, or equivalent).
7. Gwyddion software: free and open source software for SPM analysis (other analysis software is also acceptable, provided it has the capability to export raw data as ASCII text file; however, instructions in this chapter will be provided for Gwyddion only). More information at: www.gwyddion.net.
8. ImageJ software: free and open source software for image processing and analysis in Java (for automated analysis of nucleosomes). More information at: rsbweb.nih.gov/ij.

3 Methods

3.1 Nuclei Preparation, Chromatin Digestion, Extraction, and Immunoprecipitation

Human cells (e.g., HeLa) are synchronized with a double thymidine block and each cell cycle stage confirmed by FACS analysis [5]. It is important to determine if synchronization protocol results in DNA damage, especially if the complexes being studied are normally involved in such mechanisms. In this scenario, it may be preferable to isolate cells at different phases of the cell cycle using flow cytometry [19] or centrifugal elutriation [20] instead. Cells are then trypsinized, washed once with 1× PBS, once with cold 1× PBS-T, and kept on ice until ready to proceed onto nuclear preparation and chromatin extraction. Make sure centrifuges are cooled to 4 °C ahead of time.

1. Prepare 10 mL of TM2 solution supplemented with 0.5 % NP40/NP40 substitute (*see* **Note 2**) for each sample and add the solution to the broken up cell pellet (*see* **Note 3**). Incubate on ice for 2 min and centrifuge at 230 × *g* for 5 min at 4 °C.

2. Carefully remove solution/supernatant, leaving the pellet containing nuclei behind. Gently loosen the released nuclear pellet (*see* **Note 3**) and wash with cold TM2 (NP40 free). Centrifuge at 230×*g* for 5 min at 4 °C.
3. Carefully remove solution/supernatant, and loosen the nuclear pellet and add 2 mL of 0.1 M TE. Incubate tube(s) in the 37 °C water bath for about 5 min (*see* **Note 4**).
4. Add 0.4 U of MNase (*see* **Note 5**) to the top and side wall of the tube (*see* **Note 6**) and 30 μL of 100 mM $CaCl_2$ (to achieve final concentration of 1.5 mM) to the opposite wall of the tube. Gently rotate the tube to mix the enzyme and catalyst ($CaCl_2$) and start timer.
5. At the end of the chromatin digestion period, quench the reaction by adding 40 μL of 500 mM EGTA (to achieve final concentration of 10 mM). Gently rotate the tube to mix the quenching agent and place tube on ice until the next step.
6. Centrifuge samples at 230×*g* for 5 min at 4 °C and carefully remove supernatant not to disrupt the digested nuclear pellet. Gently loosen the pellet and add 1 mL of LSEB solution to the tube. Gently break up the pellet in the LSEB solution by flicking the tube. Cut pipette tip to widen the point of entry (*see* **Note 7**) and transfer nuclear pellet/LSEB slurry to a microcentrifuge tube.
7. Add 5 μL of 100 mM PMSF (final concentration of 0.5 mM) (*see* **Note 8**) and rotate samples for at least 6 h to overnight at 4 °C to extract chromatin.
8. Cut the pipette tip before any of the following steps (*see* **Note 7**). After extraction, save 5 % for input samples (store at –20 °C until use) and/or AFM analysis (*see* **Note 9**). Transfer the rest of the extract to a new tube.
9. Add 12 μL CENP-A antibody (or preferred target antibody) and rotate for at least 4 h to overnight at 4 °C.
10. Add 30 μL Protein A/G PLUS-agarose beads and let sample(s) rotate for another 2 h at 4 °C.
11. Centrifuge to pellet the beads, antibody, and immunoprecipitated target protein complex at 1,503×*g* for 5 min in a refrigerated microfuge. Save a small portion of the supernatant (5 %) as unbound sample, and discard the rest.
12. Gently wash the beads with the 1 mL LSEM buffer, and rotate for 5 min.
13. Centrifuge to pellet the beads, antibody, and immunoprecipitated target protein complex at 1,503×*g* for 5 min in a refrigerated microfuge.

14. Discard the supernatant and add fresh 1 mL LSEM buffer to wash the beads again, and rotate for 5 min. A third wash is also recommended.
15. Transfer the wash and bead/antibody/target protein complex to a new, clean tube using a cut tip.
16. Centrifuge to pellet the beads, antibody, and immunoprecipitated target protein complex at 1,503 × *g* for 5 min in a refrigerated microfuge.
17. Discard the wash solution, leaving just the beads behind and very little residual LSEM buffer (if any). If the ChIP'ed samples will be imaged by AFM, perform a gentle elution by adding 10 volumes of 0.2 M glycine pH 6.5 with end-over-end rotator for 1 h at room temperature. Otherwise, for gel electrophoresis, proceed to the next step.
18. Add the 2× Laemmli sample buffer directly to the beads and boil sample(s) if performing traditional SDS-PAGE analysis. If sample(s) will be analyzed by TAU gel electrophoresis, dissolve in 2× Sample Running Dye (*see* Subheading 3.4, **step 8**), and proceed with the TAU gel protocol.

3.2 Histone Extraction with Hydroxylapatite

Five to ten confluent flasks of human cells are synchronized with a double thymidine block as above [5]. Cells are then trypsinized and washed at least once with 1× PBS, cold 1× PBS-T, and kept on ice until ready to proceed onto histone extraction in 50-mL conical tubes.

1. Perform **steps 1–2** as outlined in Subheading 3.1.
2. Carefully remove supernatant not to disturb the nuclear pellet, and then flick tube to disperse the nuclei. To the 50-mL conical tubes, add 10 mL of the 0.35 M NaCl PBS, 0.2 mM EDTA (*see* **Note 10**), 1 g of hydroxylapatite (to achieve final concentration of 10 %), 0.5 mM PMSF, and a small stir bar that can stir freely in the tube.
3. Place tube(s) upside down in a thin wall plastic container, and stir overnight with a magnetic stirrer. The hydroxylapatite slurry will attach to DNA while the 0.35 M NaCl PBS, 0.2 mM EDTA will release the soluble proteins.
4. The next day, centrifuge the hydroxylapatite/chromatin and soluble protein mixture at 500 × *g* for 5 min at 4 °C and wash it twice with fresh 0.35 M NaCl PBS, 0.2 mM EDTA. This removes the excess soluble proteins, leaving the chromatin bound to the hydroxilapatite behind. Add 6 mL of 2 M NaCl PBS, 0.2 mM EDTA to the slurry (*see* **Note 10**), and magnetically stir for at least another 2–4 h. At 2 M NaCl, the majority of the histones or nucleosomes should be detached from DNA (*see* **Note 11**).

5. Centrifuge slurry, collect and transfer supernatant to a new 15-mL conical tube. Store samples at 4 °C until use.
6. To the hydroxylapatite slurry, add 4 mL of 2.8 M NaCl PBS, 0.2 mM EDTA and magnetically stir for another 2–4 h (*see* **Note 12**).
7. Centrifuge the slurry and pool the supernatants from the 2.8 M NaCl and 2.0 M NaCl PBS-containing solutions. Centrifuge at 900 × *g* for 5 min at 4 °C to sediment residual hydroxylapatite.
8. Transfer as much clear supernatant as possible to an Amicon Ultra Centrifugal Filter unit, and centrifuge at 2,000 × *g* at 4 °C until sample has been concentrated to ~0.5 mL (*see* **Note 13**).
9. Once samples are concentrated, dialyze sample(s) overnight at 4 °C in a beaker filled with LSEB, covered with plastic wrap, and stirred with a magnetic bar.
10. The following day, dialyzed samples are recovered and can be saved at −20 °C until ready to be run on a Long TAU gel and for WB.

3.3 Casting Long TAU (L-TAU) Gels

The following conditions are optimized for a 20 cm long gel that is 0.5–0.75 mm thick. For gels that are of a different size, scale the components up or down, as needed.

1. To a 250-mL vacuum filter flask, add the following to make the running gel: 12 g Urea, 5.6 mL 40 % acrylamide, 1.25 mL Glacial Acetic Acid, 125 µL TEMED, 0.5 mL 0.3 M Triton X-100, 7.6 mL dH_2O (to 25 mL total).
2. Gently stir without creating bubbles until urea is completely dissolved (*see* **Note 14**).
3. Degas for 10 min with a vacuum hose attached to the flask.
4. Properly assemble glass plates and clamps that will house the TAU gel according to BioRad's PROTEAN II xi Cell recommendations (http://www.bio-rad.com/webroot/web/pdf/lsr/literature/M1651801.pdf) or your manufacturer's recommendations.
5. Add 300 µL 10 % APS to the flask containing the contents in **step 1**, gently swirl to mix and pipette in between the glass plates, leaving about 3 cm at the top to allow room for the stacking gel and comb.
6. Cover the top of the gel by adding butanol or dH_2O to one side of the gel, which will slowly migrate to the opposite side, forming a uniformed monolayer that prevents the gel from over-drying.
7. Allow the gel to set for at least 30 min.

8. Prepare the stacking gel by adding the following to another 250 vacuum filter flask: 4.8 g Urea, 1.2 mL 40 % acrylamide, 500 μL Glacial Acetic Acid, 100 μL TEMED, 200 μL 0.3 M Triton X-100, 4.5 mL dH_2O.
9. Gently stir without creating bubbles until urea is completely dissolved (*see* **Note 14**).
10. Degas for 10 min with a vacuum hose attached to the flask.
11. Take assembled glass plates with solidified TAU gel to the sink, and wash off butanol and any unpolymerized acrylamide with dH_2O (*see* **Note 15**).
12. Assemble solidified gel/glass plate back on the gel stand, making sure the gel is leveled.
13. Add 250 μL 10 % APS to stacking gel mixture in flask, swirl to mix, and pipette into the top layer until it fills the lower glass plate.
14. Gently push comb of desired lane width in between the glass plates and allow stacking gel to set for at least 30 min to an hour (*see* **Note 16**).

3.4 Running L-TAU Gels and Western Blot

1. Assemble L-TAU gel apparatus in the electrophoretic unit according to BioRad's PROTEAN II xi Cell recommendations or your manufacturer's recommendations.
2. Fill the upper chamber with the TAU Running Buffer, allowing it to spill over into the outer chamber and cover the bottom of the assembled glass plates.
3. Pipette each lane of the gel several times to remove any unpolymerized material and debris (*see* **Note 17**).
4. Perform a Blank Pre-run for at least an hour without anything loaded into the wells, at a constant 15 mA. Make sure to reverse polarity of the cables (*see* **Note 18**).
5. Pipette each lane of the gel several times again to remove any unpolymerized material and debris (*see* **Note 17**).
6. Pipette 20–30 μL of the Cysteamine Pre-run Solution into each lane and electrophorese at a constant 15 mA for 16–22 h (*see* **Note 19**).
7. Make a fresh batch of the TAU Running Buffer, allowing it to stir with a magnetic stir bar in a 2 L graduated cylinder at room temperature overnight. This ensures the buffer is well mixed prior to next day's sample run.
8. The next day, dissolve the sample(s) in the 2× Sample Running Dye, making it 1× (*see* **Note 20**). Pipette up and down a few times to mix the sample with Sample Running Dye.
9. The dye from the Cysteamine Pre-run Solution should have run out into the outer chamber, giving it a slight pink hue.

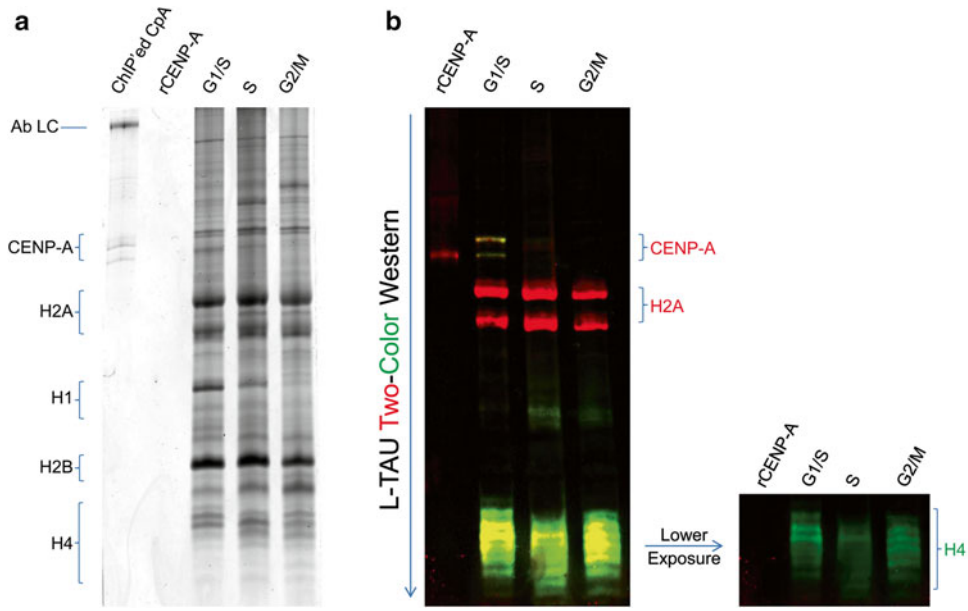

Fig. 1 L-TAU gel and Western Blot of histones purified from human cells across the cell cycle. (**a**) Coomassie stained L-TAU gel. (**b**) Two-Color Western Blot of L-TAU gel transferred onto nitrocellulose membrane. CENP-A (*red*), H2A (*red*), and H4 (*green*) histones were probed. *Ab LC* antibody light chain, *rCENP-A* recombinant CENP-A

Pipette each lane of the gel several times to remove any unpolymerized material and debris (*see* **Note 17**).

10. Load the appropriate amount of each sample that was dissolved in the 2× Sample Running Dye (*see* **step 8**) into their respective lanes and run at 15 mA for 4–5 h (*see* **Note 21**).
11. Once sample(s) are done migrating, disassemble the L-TAU gel and perform a quick wash (less than 5 min) with dH_2O in a clean container (*see* **Note 22**).
12. For Coomassie staining, fix the gel and proceed with Coomassie stain (*see* Fig. 1a). For WB, proceed as described in the next step.
13. Cut the gel to size, and equilibrate the L-TAU gel twice for 20 min each time with TAU Equilibrating Solution, under gentle shaking conditions (*see* **Note 23**).
14. Equilibrate and wash the L-TAU gel twice for 20 min each with Transfer Buffer, with gentle shaking (*see* **Note 23**).
15. Assemble the filter paper, membrane, and gel sandwich with the midi-format Transfer-Blot Turbo Transfer Pack.
16. Transfer with the preset BioRad's High Molecular Weight (MW) setting (2.5 A, 25 V) for 20 min total using Transfer-Blot Turbo Transfer System.

17. Disassemble the sandwich and wash the membrane with 1× PBS with gentle shaking to remove residual ethanol.
18. Block membrane for 30 min with Membrane Blocking Buffer at room temperature (RT).
19. Dilute the primary antibody to the recommended concentration with the TAU Hybridization Buffer (*see* **Note 24**).
20. Perform a quick rinse of the blocked membrane with PBS-T and assemble into a hybridization bag. Seal three sides of the bag with a heat bag sealer, leaving one side unsealed.
21. Add the antibody diluted in the TAU Hybridization Buffer to the unsealed side, and gently massage out the bubbles (*see* **Note 25**).
22. Seal the last side and gently rock the membrane overnight at 4 °C.
23. The next day, pour out the primary antibody solution, gently place membrane into a clean container, and perform two washes 5 min each with PBS-T.
24. Dilute the secondary antibody to the manufacturer's recommendations with the TAU Hybridization Buffer (*see* **Note 26**).
25. Repeats **steps 20–22** in Subheading 3.4 with the secondary antibody, and incubate with gentle rocking for an hour.
26. Wash the membrane twice with PBS-T with gentle rocking and image with LiCor Odyssey's supplied imaging software (*see* Fig. 1b) or with the preferred method of detection.

3.5 Preparation of Chromatin Fibers

This protocol was adapted from Sullivan [12] for HeLa cells, normal colon EpiCM cells, and colon cancer SW480 cells.

1. Trypsinize cells and wash once with 1× PBS in 50-mL conical tubes.
2. Count cells using a hemocytometer and resuspend in hypotonic buffer (final concentration 300,000 cells per mL). Incubate at RT for 10 min for HeLa cells and 30 min for normal colon EpiCM or tumor colon SW480 cells.
3. Using Cytofunnels, spin 200 μL of cells per slide for 10 min at 400 rpm in Cytospin 4. Mark with a permanent pen the circular area containing cells.
4. Remove slide(s) from the cytoclip and immerse them in Coplin jars filled with freshly prepared fiber lysis buffer for 15 min at RT. Do not move or agitate the slide(s) during this and the following incubation to avoid the formation of a bundle or tangle of fibers (*see* Fig. 2 and **Note 27**).
5. Slowly and gently pull slide(s) up and out, remaining vertical, and transfer to fixation buffer. Fix for 10 min at RT (*see* **Note 27**).

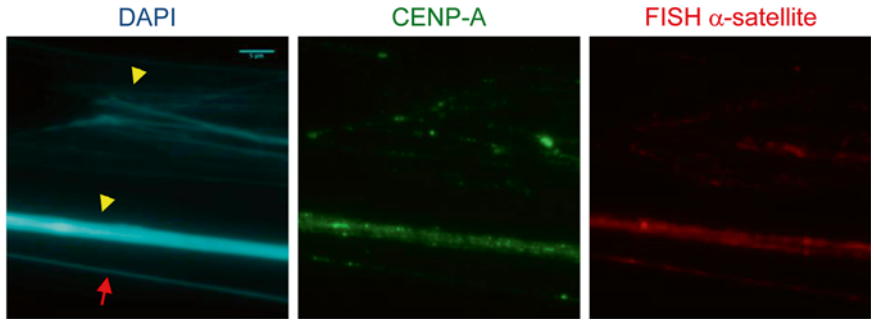

Fig. 2 Chromatin fiber stained with CENP-A antibody and FISH α-satellite probe on HeLa cells. Three types of fibers are visible. Fiber indicated with *arrow* represents a homogeneous diameter and nice shape, revealing the co-localization of CENP-A and α-satellite DNA probe. Fibers designated by *arrowheads* are either a bundle or a tangle of fibers obstructing a clear view of the co-localization of CENP-A onto the centromeric DNA

6. Gently transfer slide(s) from fixation buffer to permeabilization buffer to extract fibers for 7 min at RT (*see* **Note 27**).
7. If FISH or IF cannot be performed the same day, store slide(s) in 1× PBS at 4 °C for a maximum of 2 weeks.

3.6 Chromatin Fiber Immunofluorescence

1. Block slide(s) for 30 min in Blocking buffer at RT or overnight at 4 °C.
2. Incubate with primary antibody diluted in blocking solution complemented with 1 % normal goat serum overnight at 4 °C in a humidified chamber.
3. Wash slide(s) three times for 5 min each in wash solution. Do not agitate slide(s) (*see* **Note 27**).
4. Incubate with secondary antibody diluted in blocking solution complemented with 1 % serum for 1–2 h at RT in a humidified chamber in the dark.
5. Wash slide(s) three times for 5 min in wash solution.
6. Perform two more washes in 1× PBS for 2 min each at RT. Make sure slide(s) has limited exposure to light from this point onward (*see* **Note 28**).
7. For co-staining, repeat immunofluorescence from Subheading 3.6, **step 1** using a different primary and secondary antibody. For DNA FISH, go to Subheading 3.7. Otherwise, continue with the next steps.
8. Incubate with DAPI solution for 15 min at RT in the dark.
9. Wash slide(s) three times for 5 min in 1× PBS and mount coverslip with Mowiol solution. Make sure slide(s) is kept in the dark (*see* **Note 28**).

3.7 DNA FISH with an α-Satellite Probe

1. Crosslink antibody-protein complexes by immersing slide(s) in a Coplin jar containing crosslinking buffer for 10 min at RT.
2. Store slide(s) in 1× PBS, 0.5 % Tween-20 until FISH is performed. Slide(s) may be stored at 4 °C for up to 1 week.
3. Precipitate 100–150 ng of biotin-labeled DNA from Subheading 2.7, **item 5** with the addition of 1 μg of salmon sperm DNA, 1/10 volume of 3 M sodium acetate, and 3 volumes of 100 % ethanol per slide.
4. Centrifuge 30 min at 18,407 × *g* in a refrigerated microfuge. Wash the pellet with 70 % ethanol and centrifuge again for 5 min at 9,391 × *g* in a refrigerated microfuge. Resuspend the dry pellet with 5–6 μL of hybridization buffer.
5. Pre-warm denaturing solution in Coplin jar by successive incubations in 37 and 42 °C water baths for 10–15 min, before finally placing it into a 80 °C water bath (*see* **Note 29**).
6. Remove slide(s) from jar containing 1× PBS, 0.5 % Tween-20. Quickly wipe the slide(s) to remove excess solution using folded delicate task wipes or lint-free tissues, but avoid wiping the circular area containing the fibers (*see* Subheading 3.5, **step 3**).
7. Place slide(s) in denaturing solution for 8–10 min. During this time, place a tube containing biotin-labeled probe dissolved in hybridization buffer in 78 °C water bath to denature DNA for 9 min, and then place it on ice.
8. Remove the slide(s) from denaturing solution, wipe it, and add the entire denatured probe dissolved in hybridization buffer from **steps 3** to **4** above to the circular area containing fibers.
9. Carefully and quickly cover each circular area with a 12 × 12 round coverslip, seal with Rubber cement, and incubate slide(s) in humidified chamber at 37 °C incubator for 16–48 h in the dark (*see* **Note 28**).
10. Wash slide(s) three times for 5 min each, at 45 °C with wash solution 1.
11. Wash slide(s) four times for 5 min each, at 45 °C with wash solution 2.
12. Block for 30 min at RT with blocking solution.
13. Incubate slide(s) with the secondary antibody at 37 °C for 2 h.
14. Wash slide(s) four times for 5 min each, at 45 °C with wash solution 3.
15. Incubate with DAPI solution for 15 min at RT in the dark (*see* **Note 28**).
16. Wash slide(s) four times for 3 min with 1× PBS, and mount coverslip with Mowiol solution. Store slide(s) in the dark at 4 °C until ready for imaging (*see* **Note 28**).

3.8 AFM

AFM can operate in several modes, each resulting in different type of information being collected. The most suitable modes for chromatin imaging are tapping (frequency slightly lower than cantilever resonance) and noncontact mode (frequency slightly higher than cantilever resonance), which generate a detailed three-dimensional image of the sample surface. Each of these modes relies on the tip rapidly oscillating up-and-down within a close proximity to the sample surface but with little to no direct contact, thereby minimizing the risk of damage or disruption of the chromatin.

Any substrate could theoretically be used for sample deposition for the AFM, as long as it could provide a very flat and uniform surface. Freshly cleaved mica has been traditionally used as it has an atomically flat sheet surface, creating a perfect background for AFM imaging. Untreated, the surface of mica has a negative charge [16, 21] and can effectively bind DNA molecules, provided that salt concentration is low and divalent cations are added to the buffer to bridge the electrostatic interaction with negatively charged phosphate backbone of the DNA. However, under most physiological conditions it does not bind proteins very well. In order to improve protein deposition, mica can be treated with APTES {(3-Aminopropyl)triethoxysilane} or APS {1-(3-aminopropyl)silatrane} silica compounds that give it a positive surface charge by functionalizing with amino groups [16, 21]. The choice between these two reagents should be determined experimentally, as well as based on feasibility at one's facility. APTES mica is generally more consistent from batch to batch, but it also has the propensity to bind soluble proteins better, resulting in higher background from samples of lesser purity (*see* Fig. 3a). APS tends to have higher variability from one preparation to another (and therefore each batch needs to be checked prior to sample deposition), but when the surface is sufficiently flat the images are generally much cleaner and better looking (*see* Fig. 3b).

Another important consideration is the tip selection, as it will impact the quality of data acquired. Super sharp tips with diameters of ~2 nm (such as Bruker TESP-SS or Nanosensors SSS-SEIH) provide superior resolution and data quality, but are also costly and fragile during repeated use. Good quality, lower cost tips (such as Bruker OTESPA/Olympus AC160TS-10) can be a very good compromise, as they are much more affordable and robust while still being sharp enough to acquire good quality data.

Finally, a method of data analysis must be carefully considered. Automated analysis of surface features can be tempting, as it guarantees large number of data points with good statistical significance. However, unless the sample is exquisitely pure and all chromatin arrays are flat and evenly distributed, automated analysis can result in counting background particles in no way associated with DNA arrays (Fig. 4c). Furthermore, APS surface can degrade over time, resulting in formation of a maze of hills and valleys on a

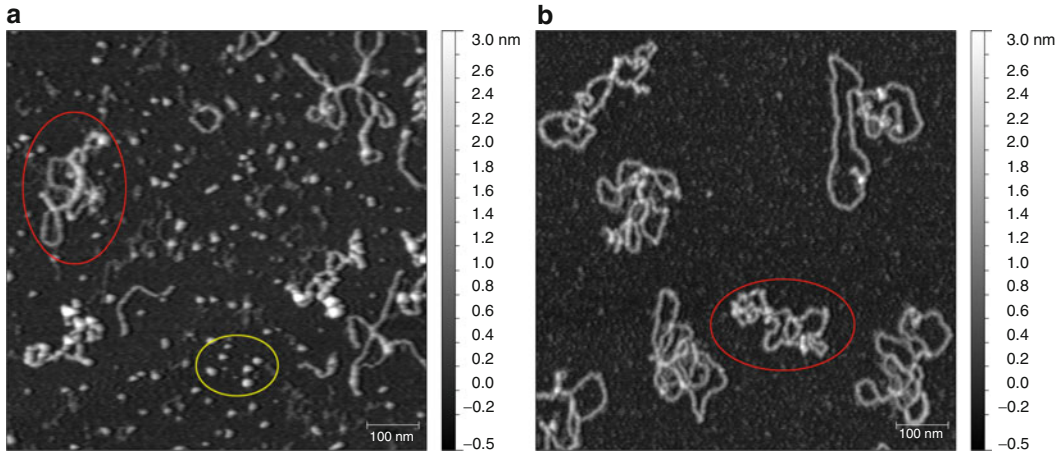

Fig. 3 Comparison of chromatin deposited on either APTES or APS surface. (**a**) Partial chromatin reconstitution was deposited on a fresh APTES surface in the presence of 2 mM $MgCl_2$. Notice the unincorporated histone proteins (*bottom oval*) bound all over the sample surface in between chromatin arrays (*left oval*). (**b**) Same sample as in (**a**) but deposited on freshly prepared APS surface in the presence of 2 mM $MgCl_2$. Unincorporated histones no longer contaminate the background between chromatin arrays (*oval*). Grayscale on the *right* represents approximate heights in nm; scale bar represents 100 nm

previously uniform background. This does not affect the values for nucleosome height or diameter but may interfere with the automated algorithm. Therefore, in most cases, manual evaluation of particles of interest is recommended to assure accuracy. We will discuss both analysis methods below, along with sample preparation and common scanning conditions.

3.8.1 AFM Sample Preparation

1. Prepare a fresh, positively charged mica surface (*see* Subheading 2.8).
2. Follow the chromatin extraction protocol as outlined in Subheading 3.1, **steps 1–8**. Use protease inhibitor cocktail in addition to PMSF (*see* **Note 8**).
3. Dilute the extracted chromatin sample in the appropriate buffer to the final concentration of ~5–10 μg/mL (the dilution buffer is the same as the buffer used for chromatin extraction but supplemented with 1–2 mM $MgCl_2$, e.g., 0.5× PBS 1 mM $MgCl_2$ for LSEB extracted chromatin) (*see* **Note 30**).
4. Deposit 5–10 μL of the diluted chromatin in the center of the AP(S)-mica surface. Cover sample with a petri dish lid to protect it from dust, and incubate for 10 min at RT.
5. Rinse the sample with 400 μL of ultrapure water, dripping 3–4 drops at a time and gently shaking it while holding the sample with tweezers.
6. Dry the sample under light vacuum (*see* **Note 31**).

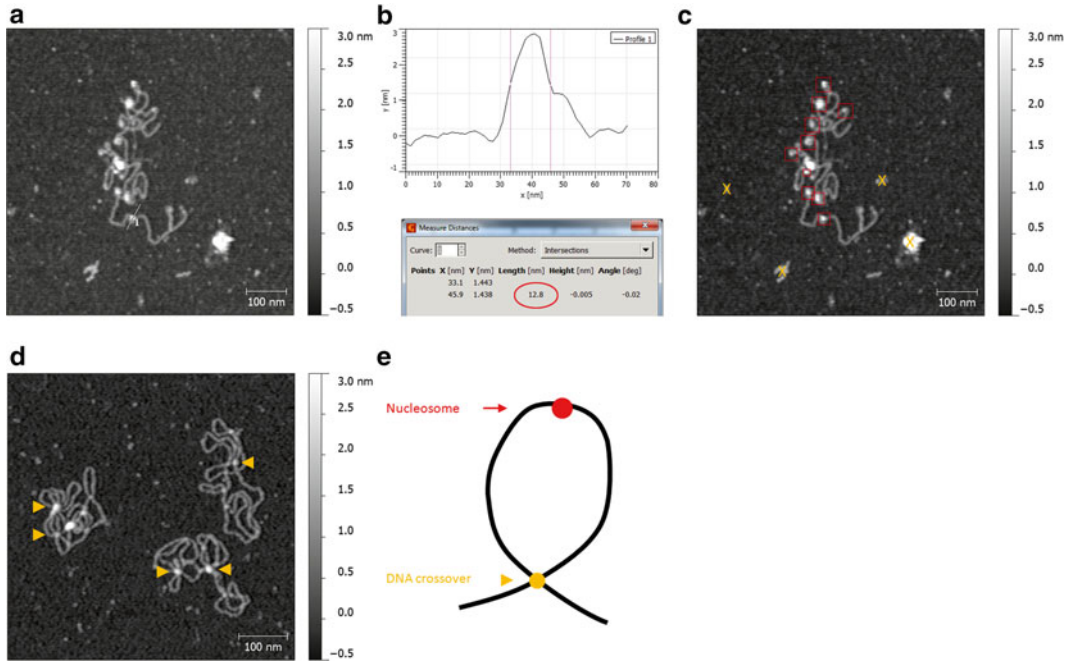

Fig. 4 Accurate identification of nucleosome features in AFM images. (**a**) Immunoprecipitated chromatin from cancer cells were deposited on APS-mica in the presence of 1 mM $MgCl_2$. Nucleosome arrays as well as features not associated with DNA are visible. Straight line represents a profile shown in (**b**). (**b**) *Top*: profile extraction graph of a nucleosome from (**a**); *vertical lines* denote the diameter of the nucleosome measured at half-height. *Bottom*: readout of the distance between the lines with the nucleosome diameter highlighted with the *oval*. (**c**) Same as in (**a**), but with *boxes* indicating the positively identified nucleosomes and "X" marking irrelevant background features that would still be included in the automated analysis. (**d**) Failed nucleosome reconstitution. The *arrowheads* indicate the spots where plasmid DNA crosses on top of itself resulting in a feature that resembles a nucleosome, but should not be counted as one. Notice lack of nucleosomes on free stretches of DNA and "false-nucleosome" features only occurring at DNA crossovers. (**e**) A *cartoon* indicating how the position of the feature on the DNA can aid in distinguishing between nucleosome and DNA crossover

3.8.2 AFM Scanning Conditions

1. Scan the sample either in tapping or noncontact mode (*see* **Note 32**). Contact mode should not be used as the tip dragging across the sample will easily disrupt chromatin complexes.
2. Use low force for scanning by setting a low free amplitude using the drive control (3–6 V on Agilent systems, 200–400 mV on Veeco/Bruker microscopes).
3. Adjust the setpoint as light as possible, but low enough to avoid the "comet tail" artifact (*see* Fig. 5a, b). This usually means a setpoint ~85–90 % of free amplitude for the tapping mode or 75–80 % for noncontact mode.
4. Scan with low speed (0.5–1 line/s) and capture a large (5 μm × 5 μm), high resolution (4096 × 4096) image. This will make the analysis easier and assure that a large number of nucleosomes can be measured under the same conditions.

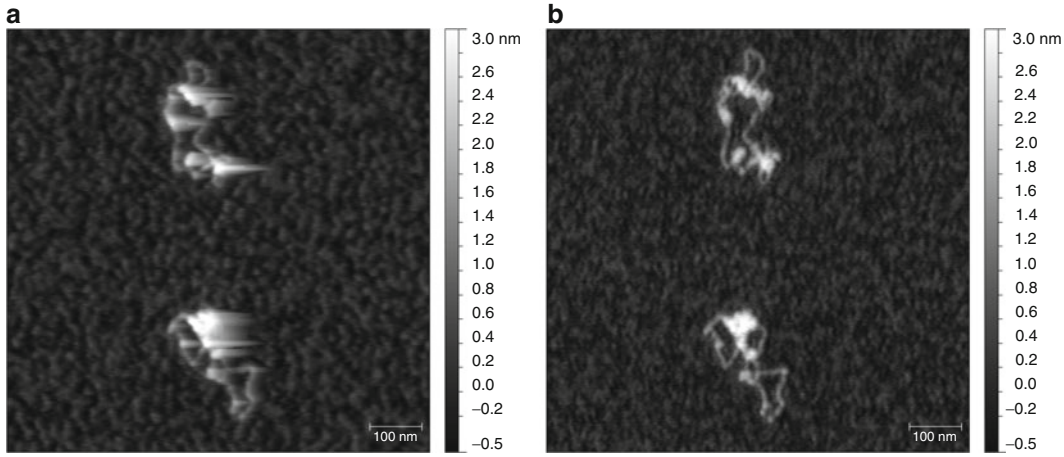

Fig. 5 Example of a "comet tail" artifact in AFM images. (**a**) One week-old chromatin was scanned in tapping mode with a set point of ~98 % free amplitude, resulting in elongated tracks in the direction of the trace scan (left-to-right) resembling a tail of a comet. (**b**) Same sample as in (**a**) was scanned with a lower set point of ~90 % free amplitude, resulting in clear shape outlines and no "comet tail" artifact

3.8.3 AFM Data Analysis

Data analysis consists of two major steps: preparing the image for analysis and performing the actual analysis.

1. Open the image in Gwyddion.
2. Click "Level data by mean plane subtraction."
3. Click "Correct lines by matching height median."
4. Click "Correct horizontal scars (strokes)."
5. Click "Remove polynomial background"; verify that both horizontal and vertical polynomial degree is set to "3." If large background structures are present in the image they may result in incorrect leveling. In that case, mask them out before subtracting polynomial background using "Mark with mask" option (*see* **Note 33**).
6. Verify that the image is properly leveled. Using the "Extract profiles" function, draw two long, intersecting, and roughly perpendicular lines spanning the entire sample. The extracted profiles should show a flat baseline, centered at the "zero" mark. If the baseline is curved then masking was not done correctly and some of the tall and/or deep features were included in the background subtraction calculation. If the baseline is flat but not centered at "zero," adjust it using the "Read value under mouse cursor" function (*see* **Note 34**).

   At this point the sample is ready for analysis. To analyze it manually continue reading from **step 7**. For automated analysis skip to **step 10**.

7. To analyze the sample manually, use the "Crop" function in Gwyddion to zoom in on each feature and study it carefully for presence of artifacts or contaminants. Identify nucleosomes by their characteristic round shape and association with DNA. Make sure not to confuse nucleosomes with DNA crossovers, which appear similar in height but only occur where two or more DNA strands intersect (*see* Fig. 4d).
8. To measure the exact height of each nucleosome, use the "Statistical quantities" function. Draw a square around the nucleosome and read the value corresponding to "Maximum" height.
9. To measure the diameter of each nucleosome, use the "Extract profiles" function. Draw a line dissecting the nucleosome at its highest point and click "Apply." Click "Measure distances in graph" and, knowing the height of the nucleosome, mark two positions intersecting the graph on both sides of the nucleosome at exactly half of its maximum height. Read the value of "Length (nm)" as the diameter of the nucleosome (*see* Fig. 4a, b).
10. To analyze the sample automatically, it must first be exported in a numerical (ASCII) format. To save the flattened image as ASCII, click "File" → "Save As." Type in the desired file name with ".txt" extension, select "File type" as "ASCII data matrix", and click "Save." In the dialog box uncheck "Add informational comment header" and select desired precision (default setting is "5").
11. Exported file contains the height data as units of meters, and needs to be converted to nanometers before it can be processed with ImageJ. Open the ASCII file in MS Excel, create a new sheet, and type in "1e9" (or 1,000,000,000) in the first cell. Select that cell and click "Copy." Go back to the sheet with ASCII data and select all cells (Ctrl + A). Open the "Paste" dialog box, select "Paste special" followed by "Multiply." This should result in all the values converting from meters to nanometers. Delete the created sheet (containing "1e9" in the first cell) and save the converted file.
12. Open the ASCII file in ImageJ using the following set of commands: "File" → "Import" → "Text Image." Perform the operation twice resulting in two identical images being open (this is important for the analysis **step 16** later). Keep track of which image was opened first (Image 1) and which was second (Image 2).
13. Click "Analyze" → "Set Scale." Input the correct dimensions for the image. For example, if the image acquired was 5 μm × 5 μm and the resolution was 4096 × 4096, input "4096" for "Distance in pixels," "5000" for "Known distance," and "nm" as "Unit of length." Check "Global" to apply the settings to both open pictures.

14. Brightness and contrast can be adjusted to change the image appearance. However, it will have no effect on the underlying data.
15. Set the threshold on Image 1 to average half-height of the nucleosomes in that image. Click "Image" → "Adjust" → "Threshold." Set the upper slider ("minimum") to the half-height value for the image (usually 1.2–1.3 nm) and the lower slider ("maximum") all the way to the right (*see* **Note 35**).
16. Click "Analyze" → "Set Measurements" and check the following options: "Area," "Min & max gray value," "Shape descriptors," "Integrated density," "Mean gray value," and "Perimeter." Also, in the "Redirect to" field select the Image 2 as the target.
17. To analyze the image open "Analyze" → "Analyze particles." Set "Size (pixel^2)" at "100–400" (the "perfect" nucleosome should be ~11 nm × 11 nm = 121 nm^2, or ~ $\pi^*(6\,nm)^2 = 113\,nm^2$) and "Circularity" at "0.8–1" (for less-than-perfect spheres set "0.7–1"). Also, select "Show: Outlines" and check "Display results," "Summarize," "Exclude on edges," and "Include holes."
18. Using the generated "Outlines" image verify that the structures analyzed are indeed nucleosomes.
19. Save the results as an ".xls" file and analyze it in MS Excel or any other statistical analysis software. "Max" column represents nucleosome height and "IntDen" represents volume of hypothetical sphere. Cylinder volume can be calculated using "Area" and "Max" values, and the nucleosome diameter can be calculated using the "Area" value.

4 Notes

1. Centromeric α-satellite sequence was based on a consensus sequence from human α-satellite DNA derived by Waye and Willard based on 130 independent monomers from at least 14 different human chromosomes [22].
2. NP40/NP40 substitute is difficult to get into solution. It is recommended that the pipette tip be cut to accommodate the viscous solution, and pipette around the edge of the TM2 solution, prior to vortexing to properly mix. While vortexing the TM2 + NP40 solution, bubbles will form. Continue vortexing until the NP40 is completely dissolved and not floating in the TM2, which can take several minutes.
3. Once the TM2/NP40 mixture is added to the cells, the cell membrane will lyse, leaving the nuclei behind. At this stage, the nuclei should be treated gently. Make sure to break up the

pellet by flicking the tubes. DO NOT vortex from this point forward.

4. During the 37 °C incubation period, set up all necessary materials such as pipettes, tips, MNase enzyme, $CaCl_2$, and EGTA solutions. Have a timer set to the preferred amount of time required for digestion. If long arrays are preferred (such as for AFM analysis), a 1–2 min MNase digestion should be sufficient. For chromatin of monomeric length, >8 min incubation is recommended.
5. Variability between the different brands and batches of MNase is likely to be expected. Thus, it is suggested that each batch of enzyme be optimized and quality control be maintained throughout the batches to maintain consistency in chromatin length.
6. The MNase and $CaCl_2$ catalyst should be added towards the top and opposing sides of the round bottom tube. When ready, the tube is gently rotated to mix the two and the timer is started at that time.
7. It is strongly recommended that the pipette tips be cut to widen the point of entry to prevent shearing of the nuclei and maintain chromatin integrity.
8. PMSF should be sufficient to prevent protein degradation. However, a protease inhibitor cocktail may be the preferred choice, especially for overnight chromatin extraction and downstream applications such as AFM analysis.
9. For AFM samples, cut the tip of a 10 μL pipette tip and transfer to a new tube. Store at 4 °C, but samples should be imaged within a day to prevent protein degradation.
10. 1× PBS already contains 137 mM NaCl; therefore, make sure one accounts for this NaCl concentration when preparing the 1× PBS with varying concentrations of NaCl.
11. The 0.35 M NaCl PBS, 0.2 mM EDTA washes will remove excess soluble proteins that are not bound to DNA, like histones. Additional washes may be necessary, especially for larger nuclei pellets. The 2 M NaCl PBS, 0.2 mM EDTA solution will release the majority of bound histones.
12. The extra 2.8 M NaCl PBS, 0.2 mM EDTA step with the very high salt concentration will release any leftover histones that were still bound to the chromatin after the previous 2 M NaCl PBS, 0.2 mM EDTA step. This step is optional but it does significantly increase the yield of released histone proteins.
13. If samples become over-concentrated, histones will start to precipitate during the process. To avoid over-concentrating, periodically check the sample with UV-spectrophotometer set at 280 nm to assure the OD is no more than 1.

14. Urea is difficult to get into solution. It is recommended that the flask be gently stirred while slightly immersed in a 37–45 °C water bath. The heat will help speed up the dissolution of the urea.
15. After washing the residual butanol and unpolymerized material, it is recommended that any excess water be removed by aspiration, prior to addition of the stacking gel.
16. If made properly, the bottom of each lane should be uniform and straight. The bottom should not be scraggly or dented, which could cause the bands to appear dented or scraggly as well.
17. It is important to remove any residual unpolymerized material from the lanes to prevent poor running and banding pattern aberrations that may make the gel look unsightly.
18. Because of the addition of acetic acid, the polarity of the protein migration will be reversed compared to traditional SDS-PAGE gel electrophoresis.
19. The BioRad PROTEAN II xi Cell apparatus is composed of large vertical electrophoresis cell that can be filled with water. This allows the glass plates and gels to remain slightly cooled. It is recommended that this chamber be filled for these long runs at room temperature, which could cause some overheating.
20. Unlike the traditional SDS-PAGE loading buffer like Laemmli sample buffer, the 2× Sample Running Dye for TAU gels DOES NOT need to be boiled. Pipetting up and down to mix and then directly loading into the wells is sufficient due to the presence of urea.
21. The sample run time of 4–5 h is generally sufficient to resolve all the histones for almost the entire length of the 20 cm L-TAU gel. However, it is recommended that run times and conditions be optimized for other protein running setups or for cases where the smaller histones (e.g., histone H4) are not needed and better resolution is required for the larger hydrophobic proteins (e.g., histone H3 or CENP-A).
22. This water wash will remove some residual 2× Sample Running Dye. The wash will appear slightly pink, which is normal. After all the subsequent washes, the pink hue on the gel should be mostly cleared. It is suggested that a corner of the gel be cut or marked so researcher knows which end is left or right.
23. Equilibration of the L-TAU gel with TAU Equilibrating and Transfer Buffer Solutions is essential for the removal of the Triton X-100, which will interfere with the transfer onto the membrane. These are the minimum steps and times, but more washes are advised, especially if the gel is still bright pink.

24. For CENP-A WB, a dilution of 1:2,000 is suggested. For detection of histones H4 and H2A, a dilution of 1:3,000 is suggested.
25. Gently massage the bubbles out of the top of the hybridization bag and seal it with a heat bag sealer. To ensure that remaining micro-bubbles do not interfere with the hybridization, it is best to orient the membrane with the transferred protein side facing down so that the bubbles float to the back of the membrane while on the rocker.
26. LiCor Odyssey's IRDye secondary antibodies are recommended at the dilution of 1:20,000. For other detection systems and secondary antibodies (e.g., horseradish peroxidase), secondary antibody concentrations must be optimized by the individual.
27. Care must be taken to not agitate the slides and when transferring from one buffer to the next. A slow pulling up motion is critical for proper fiber formation.
28. Keeping slides in the dark will prevent photo-bleaching of the secondary signal.
29. Check the temperature of denaturing solution inside the Coplin jar to ensure that it is 78 °C before proceeding with denaturation of chromatin fibers.
30. Prepare the dilution carefully. Dilute in small steps and gently flick the tube to mix content (e.g., 1:400 dilution should be broken down into two 1:20 dilutions). DO NOT pipette the solution up-and-down as this will shear the chromatin and disrupt nucleosome arrays.
31. Small desiccator or a petri dish lid over the sample with vacuum line connected to the lid work best. The sample can still dry without the vacuum, but will take significantly longer.
32. In tapping mode, when the frequency is set to slightly below resonance ("left of the peak") the tip makes very intermittent contact with the sample ("tap"). This results in sharper images but also usually more scars/background and shorter tip life. In noncontact mode, when the frequency is set to slightly above resonance ("right of the peak") the tip relies solely on atomic repulsion and does not contact the sample. This generates a cleaner image with less interference, but the features can have less sharp and slightly blurry outlines.
33. If large particles and/or deep strokes are present in the image to be analyzed, it is best to mask them out before subtracting the polynomial background. To do so, click "Data Process" → "Mask" → "Mark With." Select "Add mask" and "Data: Topography." Adjust "Minimum" to exclude any deep scars and trenches. Adjust "Maximum" to exclude any features

above surface (including objects of interest, such as DNA). What should remain marked is only the surface of the substrate to be leveled. Remove polynomial background as described but make sure that "Include only masked region" option is checked.

34. Sometimes leveling will result in a flat background surface but centered above or below zero. In that case read from the scale where the baseline is centered (e.g., –0.04 nm) and using "Read value under mouse cursor" option find a spot reading the opposite "Z value" of 0.04 nm and set it at zero by clicking "Set Zero." Verify on the extracted profiles that the baseline now centers around the "zero" mark.
35. It is important to select the threshold value that will be as close to the nucleosome half-height as possible, but that will also allow for a clear separation between nucleosomes. Thresholded nucleosomes that are "touching" will not be recognized as independent circular structures and will be excluded from measurement. Only single nucleosomes with clear outline will be measured.

Acknowledgements

We thank Dr. Rajbir Gill for expert advice on chromatin extraction, TAU gel preparation, and FISH protocols, and Dr. Emilios Dimitriadis for helpful advice on automated AFM image analysis.

References

1. Thomas JO, Kornberg RD (1975) An octamer of histones in chromatin and free in solution. Proc Natl Acad Sci U S A 72(7):2626–2630
2. Woodcock CL, Frado LL, Rattner JB (1984) The higher-order structure of chromatin: evidence for a helical ribbon arrangement. J Cell Biol 99(1 Pt 1):42–52
3. Palmer DK, O'Day K, Wener MH, Andrews BS, Margolis RL (1987) A 17-kD centromere protein (CENP-A) copurifies with nucleosome core particles and with histones. J Cell Biol 104(4):805–815
4. Earnshaw WC, Migeon BR (1985) Three related centromere proteins are absent from the inactive centromere of a stable isodicentric chromosome. Chromosoma 92(4):290–296
5. Bui M, Dimitriadis EK, Hoischen C, An E, Quenet D, Giebe S, Nita-Lazar A, Diekmann S, Dalal Y (2012) Cell-cycle-dependent structural transitions in the human CENP-A nucleosome in vivo. Cell 150(2):317–326
6. Shechter D, Dormann HL, Allis CD, Hake SB (2007) Extraction, purification and analysis of histones. Nat Protoc 2(6):1445–1457
7. Zweidler A (1978) Resolution of histones by polyacrylamide gel electrophoresis in presence of nonionic detergents. Methods Cell Biol 17:223–233
8. Waterborg JH (2002) Acid-urea-triton polyacrylamide gel electrophoresis of histones. In: Walker JM (ed) The protein protocols handbook. Springer, New York, pp 113–123
9. Earley KW, Shook MS, Brower-Toland B, Hicks L, Pikaard CS (2007) In vitro specificities of Arabidopsis co-activator histone acetyltransferases: implications for histone hyperacetylation in gene activation. Plant J 52(4):615–626
10. Ravi M, Shibata F, Ramahi JS, Nagaki K, Chen C, Murata M, Chan SW (2011) Meiosis-specific loading of the centromere-specific histone CENH3 in *Arabidopsis thaliana*. PLoS Genet 7(6):e1002121

11. Blower MD, Sullivan BA, Karpen GH (2002) Conserved organization of centromeric chromatin in flies and humans. Dev Cell 2(3):319–330
12. Sullivan BA (2010) Optical mapping of protein-DNA complexes on chromatin fibers. Methods Mol Biol 659:99–115
13. Binnig G, Quate CF, Gerber C (1986) Atomic force microscope. Phys Rev Lett 56(9): 930–933
14. Bui M, Walkiewicz MP, Dimitriadis EK, Dalal Y (2013) The CENP-A nucleosome: a battle between Dr. Jekyll and Mr. Hyde. Nucleus 4(1):37–42
15. Dimitriadis EK, Weber C, Gill RK, Diekmann S, Dalal Y (2010) Tetrameric organization of vertebrate centromeric nucleosomes. Proc Natl Acad Sci U S A 107(47):20317–20322
16. Lyubchenko YL, Gall AA, Shlyakhtenko LS (2001) Atomic force microscopy of DNA and protein-DNA complexes using functionalized mica substrates. Methods Mol Biol 148: 569–578
17. Shlyakhtenko LS, Gall AA, Lyubchenko YL (2013) Mica functionalization for imaging of DNA and protein-DNA complexes with atomic force microscopy. Methods Mol Biol 931:295–312
18. Shlyakhtenko LS, Gall AA, Filonov A, Cerovac Z, Lushnikov A, Lyubchenko YL (2003) Silatrane-based surface chemistry for immobilization of DNA, protein-DNA complexes and other biological materials. Ultramicroscopy 97(1–4):279–287
19. Juan G, Hernando E, Cordon-Cardo C (2002) Separation of live cells in different phases of the cell cycle for gene expression analysis. Cytometry 49(4):170–175
20. Pretlow TG II, Pretlow TP (1979) Centrifugal elutriation (counterstreaming centrifugation) of cells. Cell Biophys 1(2):195–210
21. Quenet D, Dimitriadis EK, Dalal Y (2012) Atomic force microscopy of chromatin. In: Atomic force microscopy investigations into biology—from cell to protein Rijeka, Croatia: InTech 195–218
22. Willard HF, Waye JS (1987) Hierarchical order in chromosome-specific human alpha satellite DNA. Trends Genet 3(7):192–198

Index

Eishi Noguchi and Mariana C. Gadaleta (eds.), *Cell Cycle Control: Mechanisms and Protocols*, Methods in Molecular Biology, vol. 1170, DOI 10.1007/978-1-4939-0888-2, © Springer Science+Business Media New York 2014

D

E

F

G

H

I

K

L

M

N

O

P

Q

R

S

T

U

V

W